

AD-A113 708

SOUTHEASTERN CENTER FOR ELECTRICAL ENGINEERING EDUCAT--ETC F/G 5/1
USAF SUMMER FACULTY RESEARCH PROGRAM. 1981 RESEARCH REPORTS. VO--ETC(U)
OCT 81 W D PEELE F49620-79-C-0038

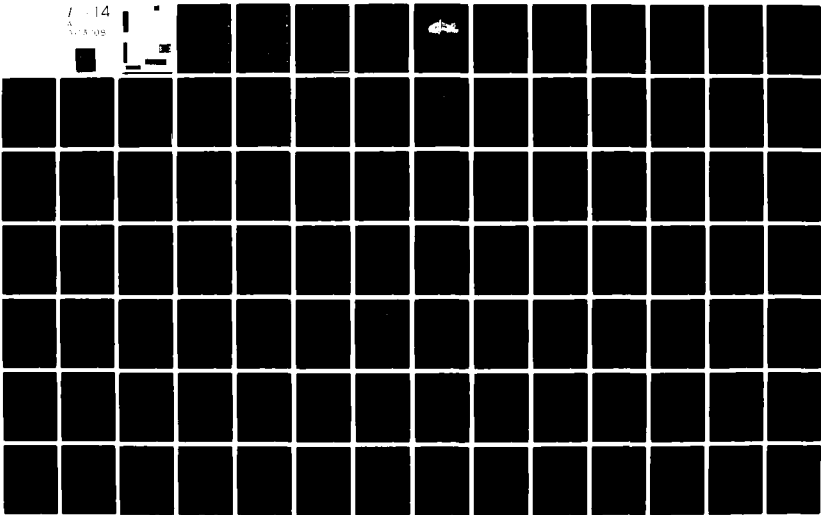
UNCLASSIFIED

AFOSR-TR-82-0227

NL

F-14

303 08



UNCLASSIFIED

SECURITY CLASSIFICATION OF THIS PAGE (When Data Entered)

REPORT DOCUMENTATION PAGE		READ INSTRUCTIONS BEFORE COMPLETING FORM
1. REPORT NUMBER AFOSR-TR- 82-0227	2. GOVT ACCESSION NO.	3. REPORT'S CATALOG NUMBER
4. TITLE (and Subtitle) USAF SUMMER FACULTY RESEARCH PROGRAM (VOL 1)	5. TYPE OF REPORT & PERIOD COVERED FINAL	
7. AUTHOR(s) PROF. WARREN D. PEELE	8. CONTRACT OR GRANT NUMBER(s) F49620-79-C-0038	
9. PERFORMING ORGANIZATION NAME AND ADDRESS SOUTHEASTERN CENTER FOR ELECTRICAL ENGINEERING EDUCATION 11th AND MASSACHUSETTS AVT. ST. CLOUD, FLORIDA 32769	10. PROGRAM ELEMENT, PROJECT, TASK AREA & WORK UNIT NUMBERS 61102F 2305/D5	
11. CONTROLLING OFFICE NAME AND ADDRESS AFOSR/XOT BOLLING AFB, DC 20332	12. REPORT DATE OCTOBER 1981	13. NUMBER OF PAGES 1328
14. MONITORING AGENCY NAME & ADDRESS (if different from Controlling Office)	15. SECURITY CLASS. (of this report) UNCLASSIFIED	
16. DISTRIBUTION STATEMENT (of this Report) APPROVED FOR PUBLIC RELEASE; DISTRIBUTION UNLIMITED		
17. DISTRIBUTION STATEMENT (of the abstract entered in Block 20, if different from Report)		
18. SUPPLEMENTARY NOTES		
19. KEY WORDS (Continue on reverse side if necessary and identify by block number)		
20. ABSTRACT (Continue on reverse side if necessary and identify by block number) The United States Air Force Summer Faculty Research Program (USAF-SFRP) is a program designed to introduce university, college, and technical institute faculty members to Air Force research. This is accomplished by the faculty members being selected on a nationally advertised competitive basis for a ten week assignment during the summer intercession to perform research at Air Force Laboratories/centers. Each assignment is in a subject area and at an Air Force facility mutually agreed upon by the faculty member and the Air Force. In addition to compensation and travel expenses, a cost of -		

DD FORM 1473

JAN 73

EDITION OF 1 NOV 65 IS OBSOLETE

UNCLASSIFIED

SECURITY CLASSIFICATION OF THIS PAGE (When Data Entered)

UNCLASSIFIED

SECURITY CLASSIFICATION OF THIS PAGE(When Data Entered)

20. Cont.

Living allowance is also paid. The USAF-SFRP is sponsored by the Air Force Office of Scientific Research/Air Force Systems Command, United States Air Force, and is conducted by the Southeastern Center for Electrical Engineering Education, Inc.

The following captioned papers with abstracts.



RE: Classified References, Distribution Unlimited
No change in distribution statement per Ms. Christiani, AFOSR/XOPD

Accession For	
NTIS GRA&I	<input checked="" type="checkbox"/>
DTIC TAB	<input type="checkbox"/>
Unannounced	<input type="checkbox"/>
Justification	
PER CALL JC	
By	
Distribution/	
Availability Codes	
Dist.	Avail and/or Special
A	



UNCLASSIFIED

SECURITY CLASSIFICATION OF THIS PAGE(When Data Entered)

AFOSR-TR- 82 - 0 2 2 7

AIR FORCE OFFICE OF SCIENTIFIC RESEARCH (AFSC)

NOTICE OF TRANSMITTAL TO DTIC

**This technical report has been reviewed and is
approved for public release IAW AFR 190-12.**

Distribution is unlimited.

MATTHEW J. KERPER

Chief, Technical Information Division

**Approved for public release;
distribution unlimited.**

**1981 USAF/SCEEE SUMMER FACULTY
RESEARCH PROGRAM**

Conducted by

Southeastern Center for

Electrical Engineering Education

under

USAF Contract Number F49620-79-C-0038

RESEARCH REPORTS

Volume I of II

Submitted to

Air Force Office of Scientific Research

Bolling Air Force Base

Washington D.C.

by

**Southeastern Center for
Electrical Engineering Education**

October 1981



SCEE
©
1981

PREFACE

The United States Air Force Summer Faculty Research Program (USAF-SFRP) is a program designed to introduce university, college, and technical institute members faculty members to Air Force research. This is accomplished by the faculty members being selected on a nationally advertised competitive basis for a ten-week assignment during the summer intercession to perform research at Air Force laboratories/centers. Each assignment is in a subject area and at an Air Force facility mutually agreed upon by the faculty member and the Air Force. In addition to compensation and travel expenses, a cost of living allowance is also paid. The USAF-SFRP is sponsored by the Air Force Office of Scientific Research/Air Force Systems Command, United States Air Force, and is conducted by the Southeastern Center for Electrical Engineering, Inc.

The specific objectives of the 1981 USAF-SFRP are:

- (1) To develop the basis for continuing research of interest to the Air Force at the faculty member's institution.
- (2) To further the research objectives of the Air Force.
- (3) To stimulate continuing relations among faculty members and their professional peers in the Air Force.
- (4) To enhance the research interests and capabilities of scientific and engineering educators.

In the 1979 summer program, 70 faculty members participated, and in the 1980 and 1981 programs, 87 faculty members participated. These researchers were assigned to 25 USAF laboratories/centers across the country. This two volume document is a compilation of the final reports written by the assigned faculty members about their summer research efforts.

1981 USAF/SCEEE SUMMER FACULTY RESEARCH PROGRAM

LIST OF PARTICIPANTS

Page 1

NAME/ADDRESS	DEGREE, SPECIALTY, LABORATORY ASSIGNED
<p>Dr. Milton J. Alexander Professor Auburn University Management Department Auburn University, AL 36849 (205) 826-4730</p>	<p><u>Degree:</u> D.B.A., Management Science, 1968 <u>Specialty:</u> Management Information Systems <u>Assigned:</u> LMC</p>
<p>Dr. David W. Allender Associate Professor Kent State University Dept. of Physics Kent, OH 44242 (216) 672-2816</p>	<p><u>Degree:</u> PhD, Physics, 1975 <u>Specialty:</u> Condensed Matter Theory <u>Assigned:</u> AL</p>
<p>Dr. Martin D. Altschuler Associate Professor SUNY/Buffalo Dept. of Computer Science 4226 Ridge Lea Campus Amherst, NY 14226 (716) 831-3065</p>	<p><u>Degree:</u> PhD, Physics and Astronomy, 1964 <u>Specialty:</u> Robot Vision, Surface Mapping, Internal Mapping <u>Assigned:</u> SAM</p>
<p>Dr. Aloysius A. Beex Assistant Professor VPI & SU Dept. of Electrical Engineering Blacksburg, VA 24061 (703) 961-6307</p>	<p><u>Degree:</u> PhD, Electrical Engineering, 1979 <u>Specialty:</u> Signal Analysis and Signal Processing <u>Assigned:</u> RADC (Griffiss)</p>
<p>Dr. Jay B. Benziger Assistant Professor Princeton University Dept. of Chemical Engineering Princeton, NJ 08544 (609) 452-5416</p>	<p><u>Degree:</u> PhD, 1979 <u>Specialty:</u> Surface Science and Catalysis <u>Assigned:</u> RPL</p>
<p>Dr. Albert W. Biggs Professor University of Kansas Dept. of Electrical Engineering 2026 Learned Hall Lawrence, KS 66045 (913) 864-4615</p>	<p><u>Degree:</u> PhD, Electrical Engineering, 1965 <u>Specialty:</u> Electromagnetics, Radar, Micro- waves, Antennas <u>Assigned:</u> WL</p>
<p>Dr. William G. Bradley Assistant Professor University of AL/Huntsville Electrical Engineering Dept. Huntsville, AL 35899 (205) 895-6139</p>	<p><u>Degree:</u> PhD, Electrical Engineering, 1973 <u>Specialty:</u> Communication and Radar Systems and Digital Design <u>Assigned:</u> RADC (Hanscom)</p>

1981 USAF/SCEEE SUMMER FACULTY RESEARCH PROGRAM

LIST OF PARTICIPANTS

Page 2

NAME/ADDRESS

DEGREE, SPECIALTY, LABORATORY
ASSIGNMENT

Dr. Jerome D. Braverman
Professor & Chairman
Rider College
Dept. of Decision Science & Computers
Lawrenceville, NJ 08648
(609) 896-5124

Degree: PhD, Statistics, 1966
Specialty: Statistical Inference,
Statistical Decision Theory,
Quality Control & Reliability
Assigned: RADC (Griffiss)

Dr. Louis W. Buckalew
Assistant Professor
Alabama A & M University
Dept. of Psychology
Box 200
Normal, AL 35762
(205) 859-7451

Degree: MS, General Experimental Psychology
1969
Specialty: Physiological Psychology
Assigned: AMRL

Dr. Gale H. Buzzard
Assistant Professor
Duke University
Dept. of Mechanical Engineering and
Material Science
Durham, NC 27706
(919) 684-2832

Degree: PhD, Mechanical Engineering, 1966
Specialty: Fluid Mechanics, Heat Transfer,
System Dynamics
Assigned: RPL

Dr. David A. Carlson
Assistant Professor
University of Massachusetts/Amherst
Dept. of Electrical & Computer Engineering
Amherst, MA 01003
(413) 545-0973

Degree: PhD, Computer Science, 1980
Specialty: Computer Science, Design &
Analysis of Algorithms
Assigned: HRL (Lowry)

Dr. Robert E. Carlson
Assistant Professor
Kent State University
Dept. of Biological Science
Kent, OH 44242
(216) 672-2266

Degree: PhD, Ecology & Limnology, 1975
Specialty: Ecology, Aquatic Biology
Assigned: ESC

Dr. Junho Choi
Assistant Professor
Florida Institute of Technology
Dept. of Electrical Engineering
University Boulevard
Melbourne, FL 32901
(305) 723-3701 X 430

Degree: PhD, Control Systems & Signal
Processing, 1978
Specialty: Modern & Conventional Control
Systems
Assigned: ESMC

1981 USAF/SCEE SUMMER FACULTY RESEARCH PROGRAM

LIST OF PARTICIPANTS

Page 3

NAME/ADDRESS

DEGREE, SPECIALTY, LABORATORY
ASSIGNMENT

Dr. Hugh W. Coleman
Associate Professor
Mississippi State University
Dept. of Mechanical Engineering
P.O. Drawer ME
Mississippi State, MS 39762
(601) 325-3260

Degree: PhD, Mechanical Engineering, 1976
Specialty: Turbulent boundary layers -
Fluid Mechanics & Heat Transfer
Assigned: AD

Dr. David L. Cozart
Associate Professor
The Citadel
Dept. of Mathematics
Charleston, SC 29409
(803) 792-7896

Degree: PhD, Mathematics, 1973
Specialty: Programming languages, Statistics
Assigned: AL

Dr. Robert W. Cunningham
Associate Professor
Kent State University
Dept. of Physics
University Drive, NE
New Philadelphia, OH 44663
(216) 339-3391

Degree: PhD, Physics, 1969
Specialty: Solid State Physics
Assigned: ML

Dr. Larry R. Dalton
Associate Professor
SUNY/Stony Brook
Dept. of Chemistry
Long Island, NY 11794
(516) 246-8601/5068

Degree: PhD, Chemistry, 1972
Specialty: Physical Chemistry, Electronics
& Instrumentation Microwaves
Assigned: FJSRL

Dr. Charles B. Davis
Assistant Professor
University of Toledo
Dept. of Mathematics
Toledo, OH 43606
(419) 537-2297/2568

Degree: PhD, Statistics, 1976
Specialty: Mathematical & Applied Statistics
Assigned: SAM

Dr. Carol A. Deakyne
Assistant Professor
College of the Holy Cross
Chemistry Dept.
Worcester, MA 01610
(617) 793-3367

Degree: PhD, Theoretical Chemistry, 1976
Specialty: Applications of Molecular Orbital
Theory
Assigned: GL

Dr. Donald W. Emerich
Professor
Mississippi State University
Chemistry Dept.
P.O. Box CH
Mississippi State, MS 39762
(601) 325-3584

Degree: PhD, Chemistry, 1951
Specialty: Analytical Chemistry, Classical
Electro-analytical Chemistry
Assigned: RPL

1981 USAF/SCEEE SUMMER FACULTY RESEARCH PROGRAM

LIST OF PARTICIPANTS

Page 4

NAME/ADDRESS	DEGREE, SPECIALTY, LABORATORY ASSIGNMENT
Dr. Chris W. Eskridge Assistant Professor University of NB/Lincoln Dept. of Criminal Justice 103 Brace Laboratory Lincoln, NB 68588 (402) 472-3677	<u>Degree:</u> PhD, Public Administration, 1978 <u>Specialty:</u> Public Administration, Police Organization & Management <u>Assigned:</u> LMDC
Dr. Glenn E. Fanslow Associate Professor Iowa State University Electrical Engineering Dept. Coover Hall Ames, IA 50011 (515) 294-6576/2663	<u>Degree:</u> PhD, Electrical Engineering, 1962 <u>Specialty:</u> Applications of Microwave Power <u>Assigned:</u> APL
Dr. William A. Feld Assistant Professor Wright State University Dept. of Chemistry Dayton, OH 45433 (513) 873-2511	<u>Degree:</u> PhD, Chemistry, 1971 <u>Specialty:</u> Synthetic Organic & Polymer Chemistry <u>Assigned:</u> ML
Dr. John A. Fleming Assistant Professor Texas A & M University Dept. of Electrical Engineering College Station, TX 77843 (713) 845-7441 X 66	<u>Degree:</u> PhD, Electrical Engineering, 1977 <u>Specialty:</u> Electrical Systems <u>Assigned:</u> AL
Dr. Dennis R. Flentge Assistant Professor Cedarville College Dept. of Mathematics & Science Box 601 Cedarville, OH 45314 (513) 766-2211 X 311	<u>Degree:</u> PhD, Physical Chemistry, 1974 <u>Specialty:</u> Physical Chemistry, Catalysis, IR & EPR Spectroscopy <u>Assigned:</u> APL
Dr. Harold W. Fox Professor Ball State University Dept. of Business Muncie, IN 47306 (317) 285-5244	<u>Degree:</u> PhD, Economics, 1967 <u>Specialty:</u> Business Administration <u>Assigned:</u> BRMC
Dr. Peter Freymuth Associate Professor University of Colorado Aerospace Engineering Science Dept. Campus Box 429 Boulder, CO 80309 (303) 492-7611	<u>Degree:</u> PhD, Aerospace Engineering, 1965 <u>Specialty:</u> Turbulence, Thermal Anemometry, Stability <u>Assigned:</u> FJSRL

1981 USAF/SCEEE SUMMER FACULTY RESEARCH PROGRAM

LIST OF PARTICIPANTS

Page 5

NAME/ADDRESS	DEGREE, SPECIALTY, LABORATORY ASSIGNMENT
<p>Dr. Joel R. Fried Assistant Professor University of Cincinnati Chemistry Engineering Dept. Mail Location #171 Cincinnati, OH 45221 (513) 475-3500</p>	<p><u>Degree:</u> PhD, Polymer Science & Engineering, 1976 <u>Specialty:</u> Mechanical Properties, Calorimetry & Rheology of Polymer Blends <u>Assigned:</u> ML</p>
<p>Dr. David E. Greene Assistant Professor Texas A & M University Industrial Engineering Dept. College Station, TX 77840 (713) 845-5531</p>	<p><u>Degree:</u> PhD, Applied Mathematics, 1973 <u>Specialty:</u> Control Theory, Man Machine Systems, Biological Regulation, PDE, DE <u>Assigned:</u> SAM</p>
<p>Dr. Gurmohan S. Grewal Professor Southern University/Baton Rouge Dept. of Electrical Engineering P.O. Box 11060 Baton Rouge, LA 70813 (504) 771-2317</p>	<p><u>Degree:</u> PhD, Electrical Engineering, 1969 <u>Specialty:</u> Control Systems, Simulation, State Estimation <u>Assigned:</u> AL</p>
<p>Dr. Paul B. Griesacker Associate Professor Gannon University Dept. of Physics Erie, PA 16508 (814) 871-7338</p>	<p><u>Degree:</u> PhD, Physics, 1963 <u>Specialty:</u> Physical Optics, Coherent Radiation <u>Assigned:</u> RADC (Griffiss)</p>
<p>Dr. Vijay K. Gupta Assistant Professor Central State University Dept. of Chemistry Wilberforce, OH 45384 (513) 376-6423</p>	<p><u>Degree:</u> PhD, Chemistry, 1968 <u>Specialty:</u> Physical Chemistry, Physical Organic Laboratory, Physical Science, General Chemistry <u>Assigned:</u> APL</p>
<p>Dr. Kenneth R. Hall Associate Professor Mississippi State University Aerospace Engineering Dept. P.O. Drawer A Mississippi State, MS 39762 (601) 325-3623</p>	<p><u>Degree:</u> PhD, Aerospace Engineering, 1973 <u>Specialty:</u> Simulation, Flight Dynamics, Control, Optimization <u>Assigned:</u> AD</p>
<p>Dr. Robert M. Harnett Associate Professor & Director Clemson University System Engineering Dept. Clemson, SC 29631 (803) 656-3375</p>	<p><u>Degree:</u> PhD, Industrial & Systems Engineering, 1974 <u>Specialty:</u> Operations Research, Optimi- zation <u>Assigned:</u> AD</p>

1981 USAF/SCEEE SUMMER FACULTY RESEARCH PROGRAM

LIST OF PARTICIPANTS

Page 6

NAME/ADDRESS	DEGREE, SPECIALTY, LABORATORY ASSIGNMENT
<p>Dr. Ronney D. Harris Professor Utah State University Dept. of Electrical Engineering UMC 41 Logan, UT 84321 (801) 750-2973</p>	<p><u>Degree:</u> PhD, Electrical Engineering, 1964 <u>Specialty:</u> Aeronomy - Atmospheric Radiation Transfer <u>Assigned:</u> GL</p>
<p>Dr. Franklin D. Hill Professor Grambling State University Chemistry Dept. Grambling, LA 71245 (318) 247-8397</p>	<p><u>Degree:</u> PhD, Biochemistry, 1960 <u>Specialty:</u> Lipid Metabolism <u>Assigned:</u> AMRL</p>
<p>Dr. Francis J. Jankowski Professor Wright State University Dept. of Engineering Dayton, OH 45434 (513) 873-2079/2403</p>	<p><u>Degree:</u> ScD, Physics, 1949 <u>Specialty:</u> Systems Engineering, Nuclear Engineering, Mechanical Engin- eering, Human Factors Engineering <u>Assigned:</u> WL</p>
<p>Dr. Stanley E. Jones Associate Professor University of Kentucky Engineering Mechanics Lexington, KY 40506 (606) 258-2719</p>	<p><u>Degree:</u> PhD <u>Specialty:</u> Applied Mathematics, Nonlinear Mechanics <u>Assigned:</u> AD</p>
<p>Dr. Paul R. Kalata Assistant Professor Drexel University Dept. of Electrical & Computer Engineering 32nd & Chestnut Street Philadelphia, PA 19104 (215) 895-2251</p>	<p><u>Degree:</u> PhD, Electrical Engineering, 1974 <u>Specialty:</u> Control Theory, Estimation Theory <u>Assigned:</u> WL</p>
<p>Dr. Richard Y.C. Kwor Assistant Professor University of Notre Dame Dept. of Electrical Engineering Notre Dame, IN 46556 (219) 283-6269</p>	<p><u>Degree:</u> PhD, Electrical Engineering, 1976 <u>Specialty:</u> Electrical Engineering <u>Assigned:</u> AL</p>
<p>Dr. Richard C. Liu Associate Professor Purdue University Dept. of Industrial Engineering Grissom Hall W. Lafayette, IN 47907 (317) 749-2948</p>	<p><u>Degree:</u> PhD, IE (Manufacturing), 1973 <u>Specialty:</u> Manufacturing Engineering <u>Assigned:</u> ML</p>

1981 USAF/SCEEE SUMMER FACULTY RESEARCH PROGRAM

LIST OF PARTICIPANTS

Page 7

NAME/ADDRESS	DEGREE, SPECIALTY, LABORATORY ASSIGNMENT
Dr. William S. McCain Assistant Professor Tennessee State University Mechanical Engineering 3500 Centennial Blvd. Nashville, TN 37203 (615) 320-3555	<u>Degree:</u> PhD, Metallurgical Engineering, 1973 <u>Specialty:</u> Aluminum alloys, fabrication & heat treatments of aerospace alloys, rolling, forging, extrusion x-ray diffraction <u>Assigned:</u> ML
Dr. William S. McCormick Associate Professor Wright State University Engineering Dept. Dayton, OH 45435 (513) 873-2403	<u>Degree:</u> PhD, Electrical Engineering, 1967 <u>Specialty:</u> Electrical Engineering <u>Assigned:</u> AL
Dr. Donald F. McCoy Associate Professor University of Kentucky Dept. of Psychology Lexington, KY 40506 (606) 258-8589/5601	<u>Degree:</u> PhD, Experimental Psychology, 1966 <u>Specialty:</u> Learning, Operant Conditioning, Animal Performance <u>Assigned:</u> AMRL
Dr. Henry A. McGee, Jr. Professor & Dept. Head VPI & SU Chemistry Engineering Dept. Blacksburg, VA 24061 (703) 961-6631	<u>Degree:</u> PhD, Chemical Engineering, 1955 <u>Specialty:</u> Cryogenics, Molecular Phenomena & Processes <u>Assigned:</u> WL
Dr. Patrick J. McKenna Assistant Professor University of Florida Mathematics Dept. Gainesville, FL 32611 (904) 392-6721	<u>Degree:</u> PhD, Mathematics, 1976 <u>Specialty:</u> Partial Differential Equations <u>Assigned:</u> FDL
Dr. John R. McNeil Assistant Professor New Mexico State University Dept. of Electrical & Computer Engineering Las Cruces, NM 88003 (505) 646-3115	<u>Degree:</u> PhD, Electrical Engineering, 1977 <u>Specialty:</u> High Energy Laser Optics, Ion Beam Applications <u>Assigned:</u> WL
Dr. Louis A. Martin-Vega Associate Professor University of Florida Industrial & Systems Engineering Dept. Gainesville, FL 32611 (904) 392-1464 X 35	<u>Degree:</u> PhD, Industrial & Systems Engineering, 1975 <u>Specialty:</u> Scheduling, Applied IE & OR <u>Assigned:</u> LMC

1981 USAF/SCREE SUMMER FACULTY RESEARCH PROGRAM

LIST OF PARTICIPANTS

Page 8

NAME/ADDRESS	DEGREE, SPECIALTY, LABORATORY ASSIGNMENT
Dr. Kishan G. Mehrotra Professor Syracuse University Dept. of Computer & Information Science 313 Link Hall Syracuse, NY 13210 (315) 423-2811	<u>Degree:</u> PhD, Statistics, 1971 <u>Specialty:</u> Discriminant Analysis, Non- parametric Reliability <u>Assigned:</u> SAM
Dr. David F. Miller Assistant Professor Wright State University Mathematics Dept. Dayton, OH 45435 (513) 873-2068/2785	<u>Degree:</u> PhD, Applied Mathematics, 1979 <u>Specialty:</u> Optimization Theory, Optimal Control <u>Assigned:</u> FDL
Dr. Levon Minnetyan Assistant Professor Clarkson College Dept. of Civil & Environmental Engineering Potsdam, NY 13676 (315) 268-4432	<u>Degree:</u> PhD, Structural Mechanics, 1974 <u>Specialty:</u> Nonlinear Structural Analysis, Structural Dynamics <u>Assigned:</u> FDL
Dr. Rex C. Moyer Director & Associate Professor Trinity University Thorman Cancer Laboratory Box 191, 715 Stadium Drive San Antonio, TX 78218 (512) 736-7231/7235	<u>Degree:</u> PhD, Microbiology, 1965 <u>Specialty:</u> Oncology, Microbiology, Virology, Tissue Culture <u>Assigned:</u> SAM
Dr. Steven B. Newman Assistant Professor Central Community State College Physics Dept. 1615 Stanley St. New Britain, CT 06050 (203) 827-7341	<u>Degree:</u> PhD, Atmospheric Sciences, 1978 <u>Specialty:</u> Cloud & Precipitation Physics, Analysis & Forecasting <u>Assigned:</u> GL
Dr. Eugene E. Niemi Jr. Associate Professor University of Lowell Mechanical Engineering Dept. One University Ave. Lowell, MA 01854 (617) 452-5000 X 2768/2312	<u>Degree:</u> PhD, Mechanical & Aerodynamic Engineering <u>Specialty:</u> Aerodynamics, Fluid Mechanics, Thermodynamics <u>Assigned:</u> AEDC
Dr. Samuel Noodleman Adjunct Professor University of Arizona Dept. of Electrical Engineering Tucson, AZ 85721 (602) 626-5210	<u>Degree:</u> B.S., Electrical Engineering, 1937 <u>Specialty:</u> Electric Machines, Rare Earth Magnet Materials <u>Assigned:</u> APL

1981 USAF/SCEEE SUMMER FACULTY RESEARCH PROGRAM

LIST OF PARTICIPANTS

Page 9

NAME/ADDRESS	DEGREE, SPECIALTY, LABORATORY ASSIGNMENT
<p>Dr. William N. Norton Assistant Professor Southeastern LA University Biology Department Box 335 Hammond, LA 70402 (504) 549-2173</p>	<p><u>Degree:</u> PhD, Entomology, 1975 <u>Specialty:</u> Electron Microscopy, Insect Physiology, Cell Biology, Histology <u>Assigned:</u> AMRL</p>
<p>Dr. Alan H. Nye Assistant Professor Rochester Institute of Technology Mechanical Engineering Dept. 1 Lomb Memorial Drive Rochester, NY 14623 (716) 475-6663</p>	<p><u>Degree:</u> PhD, MEchanical & Aerospace Science, 1975 <u>Specialty:</u> Solar Magnetohydrodynamics <u>Assigned:</u> GL</p>
<p>Dr. Thomas E. Nygren Assistant Professor Ohio State University Dept. of Psychology 404C W. 17th Avenue Columbus, OH 43210 (614) 422-2935</p>	<p><u>Degree:</u> PhD, Quantitative Psychology, 1975 <u>Specialty:</u> Measurement & Scaling; Mathe- matical Models of Decision Making <u>Assigned:</u> AMRL</p>
<p>Dr. William W. Payne Associate Professor Virginia Military Institute Civil Engineering Dept. Lexington, VA 24450 (703) 463-6331</p>	<p><u>Degree:</u> PhD, Civil Engineering, 1976 <u>Specialty:</u> Structural Design & Analysis <u>Assigned:</u> ESC</p>
<p>Dr. John E. Powell Professor University of South Dakota School of Business Dept. of Mathematics Vermillion, SD 57069 (605) 677-5231</p>	<p><u>Degree:</u> DEA, Quantitive Business Analysis, 1972 <u>Specialty:</u> Computer Applications to Business <u>Assigned:</u> LC</p>
<p>Dr. Robert H. Puckett Professor Indiana State University Dept. of Political Science Terre Haute, IN 47809 (812) 232-6311 X 2591</p>	<p><u>Degree:</u> PhD, Political Science, 1961 <u>Specialty:</u> US Foreign Policy; American National Security Policy <u>Assigned:</u> AL</p>
<p>Dr. G. Frederic Reynolds Professor Michigan Technological University Dept. of Chemical & Chemical Engineering Houghton, MI 49931 (906) 487-2054</p>	<p><u>Degree:</u> PhD, Chemistry, 1959 <u>Specialty:</u> Physical Chemistry (Spectroscopy) of Organic Molecules <u>Assigned:</u> FJSRL</p>

1981 USAF/SCEEE SUMMER FACULTY RESEARCH PROGRAM

LIST OF PARTICIPANTS

Page 10

NAME/ADDRESS	DEGREE, SPECIALTY, LABORATORY ASSIGNMENT
Dr. Richard O. Richter Assistant Professor Washington University Civil & Environmental Engineering Pullman, WA 99164 (509) 335-2147/3175	<u>Degree:</u> PhD, Chemistry, 1959 <u>Specialty:</u> Physical Chemistry (Spectroscopy) of Organic Molecules <u>Assigned:</u> ESC
Dr. John J. Riggs Assistant Professor Tuskegee Institute Dept. of Pharmacology School of Veterinary Medicine Tuskegee Institute, AL 36088 (205) 727-8471	<u>Degree:</u> PhD, Pharmacology, 1976 <u>Specialty:</u> Cardiovascular Pharmacology <u>Assigned:</u> AMRL
Dr. Edward J. Rinalducci Professor GIT Dept. of Psychology Atlanta, GA 30332 (404) 894-4260/2680	<u>Degree:</u> PhD, Experimental Psychology, 1966 <u>Specialty:</u> Vision & Visual Perception, Engineering Psychology <u>Assigned:</u> HRL (Williams)
Dr. John M. Roberts Professor Rice University Dept. of Mechanical Engineering & Mathematical Science P.O. Box 1892 Houston, Texas 77001 (713) 527-8101 X3590	<u>Degree:</u> PhD, Metallurgical Engineering, 1960 <u>Specialty:</u> Elastic-Anelastic & Plastic Deformation of Materials <u>Assigned:</u> APL
Dr. Thomas A. Roth Associate Professor Kansas State University Dept. of Chemical Engineering Durland Hall Manhattan, KS 66506 (913) 532-5584	<u>Degree:</u> PhD, Metallurgical Engineering, 1967 <u>Specialty:</u> Metallurgical Engineering <u>Assigned:</u> ML
Dr. Charles D. Sanders Professor Coppin State College Dept. of Psychology 2500 W. North Ave. Baltimore, MD 21216 (301) 383-7410	<u>Degree:</u> PhD, Education & Counseling Psychology <u>Specialty:</u> Psychological Measurement & Evaluation <u>Assigned:</u> HRL (Williams)
Dr. Sarwan S. Sandhu Assistant Professor University of Dayton Chemical Engineering Dept. 300 College Park Ave. Dayton, OH 45469 (513) 229-2627	<u>Degree:</u> Chemical Engineering, Combustion, 1973 <u>Specialty:</u> Combustion, Heat Transfer, Effect Electrical Fields on Heat Transfer Kinetics, Thermodynamics & Laser Interferometry <u>Assigned:</u> APL

1981 USAF/SCEEE SUMMER FACULTY RESEARCH PROGRAM

LIST OF PARTICIPANTS

Page 11

NAME/ADDRESS

Degree, Specialty, Laboratory
Assignment

Dr. Gerald W. Simla
Assistant Professor
California State University/Northridge
Dept. of Geological Science
18111 Nordhoff St.
Northridge, CA 91330
(213) 885-3541

Degree: PhD, Geophysics, 1980
Specialty: Seismology
Assigned: WL

Dr. Vina Y. Sloan
Professor
Eastern Washington University
Accounting & Decision Science Dept.
201 Kingston Hall
Cheney, WA 99004
(509) 359-7972

Degree: MS, Industrial Engineering, 1981
Specialty: Operations Research Techniques;
Corporate Planning
Assigned: HRL (Williams)

Dr. Russell W. Smith
Assistant Professor
N. Texas State University
Political Science Dept.
Box 5338, NT Station
Denton, Texas 76203
(817) 788-2321/2356

Degree: PhD, Political Science/Public Admin-
istration, 1976
Specialty: Management
Assigned: RPL

Dr. Stanley L. Spiegel
Assistant Professor
University of Lowell
Mathematical Dept.
One University Ave.
Lowell, MA 01854
(617) 452-5000 X 2512

Degree: PhD, Physics, 1966
Specialty: Numerical Modeling & Computer
Simulation
Assigned: GL

Dr. Alan K. Stiffler
Associate Professor
Mississippi State University
Dept. of Mechanical Engineering
Drawer ME
Mississippi State, MS 39762
(601) 325-3260

Degree: PhD, Mechanical Engineering, 1971
Specialty: Fluid Mechanics
Assigned: AD

Dr. Lawrence Suchow
Professor
NJ Institute of Technology
Dept. of Chemistry
323 High Street
Newark, NJ 07102
(201) 645-5389

Degree: PhD, Chemistry, 1951
Specialty: Solid State Inorganic Chemistry
Assigned: RADC (Hanscom)

Dr. Patrick J. Sweeney
Associate Professor
University of Dayton
Engineering Management Dept.
KL 361 300 College Park
Dayton, OH 45469
(513) 229-2238

Degree: PhD, Mechanical Engineering, 1977
Specialty: OPS Research, Quality, Statistics
Assigned: BRMC

1981 USAF/SCEEE SUMMER FACULTY RESEARCH PROGRAM

LIST OF PARTICIPANTS

Page 12

NAME/ADDRESS

DEGREE, SPECIALTY, LABORATORY
ASSIGNED

Dr. Charles J. Teplitz
Assistant Professor
SUNY/ALBANY
Dept. of Operations Management
School of Business
Albany, NY 12222
(518) 457-4951

Degree: DBA, Decision Science, 1980
Specialty: Operations Management & Physical
Distribution
Assigned: HRL (Wright-Patterson)

Dr. Albert N. Thompson
Assistant Professor
Fayetteville State University
Dept. of Chemistry
Fayetteville, NC 28301
(919) 486-1684

Degree: PhD, Inorganic Chemistry, 1978
Specialty: Porphyrins & Metalloporphyrins
Assigned: SAM

Dr. Arthur R. Thorbjornsen
Associate Professor
University of Toledo
Dept. of Electrical Engineering
2801 W. Bancroft Street
Toledo, OH 43606
(419) 537-2406/2638

Degree: PhD, Electrical Engineering, 1972
Specialty: Computer aided design of integrated
circuits, IC device modeling
Assigned: AL

Dr. Richard M. Van Slyke
Professor
Stevens Institute of Technology
Dept. of Electrical Engineering &
Computer Science
Hoboken, NJ 07030
(201) 420-5606

Degree: PhD, Operations Research, 1965
Specialty: Information Systems
Assigned: ESD

Dr. Venugopal S. Veerasamy
Assistant Professor
Tennessee State University
Dept. of Mechanical Engineering
Downtown Campus
Nashville, TN 37203
(615) 251-1513

Degree: PhD, Mechanical Engineering, 1980
Specialty: Propulsion Engineering, Thermal
Sciences, Aeroacoustics
Assigned: AEDC

Dr. M.C. Wang
Associate Professor
Pennsylvania State University
Civil Engineering Dept.
212 Sackett Building
University Park, PA 16802
(814) 863-0026

Degree: PhD, Geotechnical Engineering, 1968
Specialty: Geotechnical Engineering & Pave-
ment Design
Assigned: ESC

Dr. Alice Ward
Assistant Professor
Southern University/Baton Rouge
Dept. of Biology
P.O. Box 11068
Baton Rouge, LA 70813
(504) 771-5210

Degree: PhD, Cellular, Molecular, & Develop-
mental Biology, 1975
Specialty: Cell Biology
Assigned: SAM

1981 USAF/SCREE SUMMER FACULTY RESEARCH PROGRAM

LIST OF PARTICIPANTS

Page 13

NAME/ADDRESS

DEGREE, SPECIALTY, LABORATORY
ASSIGNED

Dr. Brenton J. Watkins
Assistant Professor
University of Alaska
Geophysical Institute
Fairbanks, AK 99701
(907) 479-7479

Degree: PhD, Geophysics, 1976
Specialty: Troposphere & Stratosphere
turbulence studies with high power
radar also incoherent scatter radar
ionospheric research
Assigned: GL

Dr. Hsi-Han Yeh
Associate Professor
University of Kentucky
Dept. of Electrical Engineering
Lexington, KY 40506
(606) 258-4649

Degree: PhD, Electrical Engineering, 1967
Specialty: Modern Control Theory
Assigned: FDL

Dr. Robert L. Yolton
Assistant Professor, Director
Pacific University
Dept. of Optometry
Forest Grove, OR 97116
(503) 357-6151 X 272

Degree: PhD, Psychology, 1975
Specialty: Visual System Function & Analysis
Assigned: SAM

Dr. Poh Shien Young
Associate Professor
Mississippi State University
Physics Dept.
Mississippi State, MS 39762
(601) 325-2806

Degree: PhD, Physics, 1966
Specialty: Sparse Physics, Cosmic Rays,
Mathematical Physics, Orbital
Determination, Optimal Control
Assigned: AD

PARTICIPANT LABORATORY ASSIGNMENT

1981 USAF/SCEEE SUMMER FACULTY RESEARCH PROGRAM

APL

AERO PROPULSION LABORATORY

(Wright-Patterson Air Force Base)

1. Dr. Glenn Fanslow - Iowa State University
2. Dr. Dennis Flentge - Cedarville College
3. Dr. Vijay Gupta - Central State University
4. Dr. Samuel Noodleman - University of Arizona
5. Dr. John Roberts - Rice University
6. Dr. Sarwan Sandhu - University of Dayton

AMRL

AEROSPACE MEDICAL RESEARCH LABORATORY

(Wright-Patterson Air Force Base)

1. Dr. Louis Buckalew - Alabama A & M University
2. Dr. Franklin Hill - Grambling State University
3. Dr. Donald McCoy - University of Kentucky
4. Dr. William Norton - Southern Louisiana University
5. Dr. Thomas Nygren - Ohio State University
6. Dr. John Riggs - Tuskegee Institute

AD

ARMAMENT DIVISION

(Eglin Air Force Base)

1. Dr. Hugh Coleman - Mississippi State University
2. Dr. Kenneth Hall - Mississippi State University
3. Dr. Robert Harnett - Clemson University
4. Dr. Stanley Jones - University of Kentucky
5. Dr. Alan Stiffler - Mississippi State University
6. Dr. Poh Shien Young - Mississippi State University

AEDC

ARNOLD ENGINEERING DEVELOPMENT CENTER

(Arnold Air Force Station)

1. Dr. Eugene Niemi - University of Lowell
2. Dr. Venugopal Veerasamy - Tennessee State University

AL

AVIONICS LABORATORY

(Wright-Patterson Air Force Base)

1. Dr. David Allender - Kent State University
2. Dr. David Cozart - The Citadel
3. Dr. John Fleming - Texas A & M University
4. Dr. Gurmohan Grewal - Southern University/Baton Rouge
5. Dr. Richard Kwor - University of Notre Dame
6. Dr. William McCormick - Wright State University
7. Dr. Robert Puckett - Indiana State University
8. Dr. Arthur Thorbjornsen - University of Toledo

BRMC

BUSINESS RESEARCH MANAGEMENT CENTER

(Wright-Patterson Air Force Base)

1. Dr. Harold Fox - Ball State University
2. Dr. Patrick Sweeney - University of Dayton

ESMC

EASTERN SPACE & MISSILE CENTER

(Patrick Air Force Base)

1. Dr. Junho Choi - Florida Institute of Technology

PARTICIPANT LABORATORY ASSIGNMENT (Continued)

ESD **ELECTRONIC SYSTEMS DIVISION**
(Hanscom Air Force Base)
1. Dr. Richard Van Slyke - Stevens Institute of Technology

ESC **ENGINEERING & SERVICES CENTER**
(Tyndall Air Force Base)
1. Dr. Robert Carlson - Kent State University
2. Dr. William Payne - Virginia Military Institute
3. Dr. Richard Richter - Washington State University
4. Dr. M. C. Wang - Pennsylvania State University

FDL **FLIGHT DYNAMICS LABORATORY**
(Wright-Patterson Air Force Base)
1. Dr. Patrick McKenna - University of Florida
2. Dr. David Miller - Wright State University
3. Dr. Levon Minnetyan - Clarkson College
4. Dr. Hsi-Han Yeh - University of Kentucky

FJSRL **FRANK J. SEILER RESEARCH LABORATORY**
(USAF Academy)
1. Dr. Larry Dalton - SUNY/Stony Brook
2. Dr. Peter Freymuth - University of Colorado
3. Dr. Frederic Reynolds - Michigan Technological University

GL **GEOPHYSICS LABORATORY**
(Hanscom Air Force Base)
1. Dr. Carol Deakne - College of the Holy Cross
2. Dr. Ronney Harris - Utah State University
3. Dr. Steven Newman - Central Community State College
4. Dr. Alan Nye - Rochester Institute of Technology
5. Dr. Stanley Spiegel - University of Lowell
6. Dr. Brenton Watkins - University of Alaska

HRL/ASD **HUMAN RESOURCES LABORATORY/ADVANCED SYSTEMS DIVISION**
(Wright-Patterson Air Force Base)
1. Dr. Charles Teplitz - SUNY/Albany

HRL/FTD **HUMAN RESOURCES LABORATORY/FLYING TRAINING DIVISION**
(Williams Air Force Base)
1. Dr. Edward Rinalducci - Georgia Institute of Technology
2. Dr. Charles Sanders - Coppin State College
3. Dr. Vina Sloan - Eastern Washington University

HRL/PRD **HUMAN RESOURCES LABORATORY/PERSONAL RESEARCH DIVISION**
(Brooks Air Force Base)

HRL/TTD **HUMAN RESOURCES LABORATORY/TECHNICAL TRAINING DIVISION**
(Lowry Air Force Base)
1. Dr. David Carlson - University of Massachusetts/Amherst

LMDC **LEADERSHIP & MANAGEMENT DEVELOPMENT CENTER**
(Maxwell Air Force Base)
1. Dr. Chris Eskridge - University of Nebraska/Lincoln

PARTICIPANT LABORATORY ASSIGNMENT (Continued)

- LC LOGISTICS COMMAND
(Wright-Patterson Air Force Base)
1. Dr. John Powell - University of South Dakota
- LMC LOGISTICS MANAGEMENT CENTER
(Gunter Air Force Base)
1. Dr. Milton Alexander - Auburn University
2. Dr. Louis Martin-Vega - University of Florida
- ML MATERIALS LABORATORY
(Wright-Patterson Air Force Base)
1. Dr. Robert Cunningham - Kent State University
2. Dr. William Feld - Wright State University
3. Dr. Joel Fried - University of Cincinnati
4. Dr. Richard Liu - Purdue University
5. Dr. William McCain - Tennessee State University
6. Dr. Thomas Roth - Kansas State University
- RPL ROCKET PROPULSION LABORATORY
(Edwards Air Force Base)
1. Dr. Jay Benziger - Princeton University
2. Dr. Gale Buzzard - Duke University
3. Dr. Donald Emerich - Mississippi State University
4. Dr. Russell Smith - North Texas State University
- RADC ROME AIR DEVELOPMENT CENTER
(Griffiss Air Force Base)
1. Dr. Aloysius Beex - Virginia Polytechnic Institute &
State University
2. Dr. Jerome Braverman - Rider College
3. Dr. Paul Griesacker - Gannon University
- RADC/ET ROME AIR DEVELOPMENT CENTER/ELECTRONICS TECHNOLOGY
(Hanscom Air Force Base)
1. Dr. William Bradley - University of Alabama/Huntsville
2. Dr. Lawrence Suchow - New Jersey Institute of Technology
- SAM SCHOOL OF AEROSPACE MEDICINE
(Brooks Air Force Base)
1. Dr. Martin Altschuler - SUNY/Buffalo
2. Dr. Charles Davis - University of Toledo
3. Dr. David Greene - Texas A & M University
4. Dr. Kishan Mehrotra - Syracuse University
5. Dr. Rex Moyer - Trinity University
6. Dr. Albert Thompson - Fayetteville State University
7. Dr. Alice Ward - Southern University/Baton Rouge
8. Dr. Robert Yolton - Pacific University
- WL WEAPONS LABORATORY
(Kirtland Air Force Base)
1. Dr. Albert Biggs - University of Kansas
2. Dr. Francis Jankowski - Wright State University
3. Dr. Paul Kalata - Drexel University
4. Dr. Henry McGee - Virginia Polytechnic Institute &
State University

PARTICIPANT LABORATORY ASSIGNMENT (Continued)

WL

**WEAPONS LABORATORY (Continued)
(Kirtland Air Force Base)**

- 5. Dr. John McNeil - New Mexico State University**
- 6. Dr. Gerald Simla - California State University/Northridge**

RESEARCH REPORTS

1981 USAF-SCEEE SUMMER FACULTY RESEARCH PROGRAM

<u>Volume I</u> <u>Report No.</u>	<u>Title</u>	<u>Research Associate</u>
1	The Determination of Input Data Accuracy in the Maintenance Data Collection System	Dr. Milton J. Alexander
2	Superconducting Pair Binding Energy in Degenerate Fermi Systems	Dr. David W. Allender
3	Software for Rapid Remote 3-D Mapping of an Arbitrarily-Complex Object	Dr. Martin D. Altschuler
4	Enhanced Scene Resolution: 2-D Spectral Estimator Approaches	Dr. A.A. Beex
5	Decomposition of Nitromethane Over Metal Oxide Catalysts	Dr. Jay B. Benziger
6	Interaction Between an Electromagnetic Pulse and a Metal Cylinder Connected to a Parallel Plate Guide by a Wire	Dr. Albert W. Biggs
7	Electromagnetic Scattering From Dielectric and Composite Bodies	Dr. William G. Bradley
8	An Investigation of Nonparametric Maintainability and Reliability Test Procedures	Dr. Jerome D. Braverman
9	Environmental Effects on Affect and Psychomotor Performance	Dr. Louis W. Buckalew
10	Thermal Analysis of a Rocket Engine Altitude Test Facility Diffuser	Dr. Gale H. Buzzard
11	Rehosting the Advanced Instructional System	Dr. David A. Carlson
12	The Biological Degradation of Spilled Jet Fuels; A Literature Review	Dr. Robert E. Carlson
13	On-Axis Kalman Tracking Filter for H.S. Vandenberg Aris Systems	Dr. Junho Choi
14	Rough Surface Effects on Turbulent Boundary Layers	Dr. Hugh W. Coleman
15	Interpolation and Approximation Techniques for Gridded Terrain Data	Dr. David L. Cozart
16	Epitaxial Layer Evaluation of III-V Semiconductor Materials	Dr. Robert W. Cunningham

RESEARCH REPORTS (Continued)

<u>Report No.</u>	<u>Title</u>	<u>Research Associate</u>
17	(A) Spectroscopic Analysis and Optimization of the Oxygen/Iodine Chemical Laser and (B) Aluminum-27 NMR of Dialkylimidazolium Chloroaluminate Molten Salts	Dr. Larry R. Dalton
18	Some Aspects of Cardiac Risk Evaluation at the USAF School of Aerospace Medicine	Dr. Charles B. Davis
19	A Molecular Orbital Study of $\text{NO}_3^- \cdot \text{H}_2\text{O}$, $\text{OH}^- \cdot \text{HNO}_3$, AND $\text{H}^+(\text{H}_2\text{O})_m(\text{CH}_3\text{CN})_k$ Cluster Ions	Dr. Carol A. Deakyne
20	Analysis of Several Solid Propellant Stabilizers by DC Polarographic Techniques	Dr. Donald W. Emerich
21	The Impact of Background Characteristics on OAP Test Scores: Developing Baseline Information	Dr. Chris W. Eskridge
22	Radiation Signatures From a Space Power System	Dr. Glenn E. Fanslow
23	Acetylene Terminated Systems: Quinoxalines and Isomeric Sulfones	Dr. William A. Feld
24	A Simulation Framework for the Evaluation of Terrain Following and Terrain Avoidance Techniques	Dr. John A. Fleming
25	Voltametric Studies of the Lithium/Vanadium Oxide Electrochemical Cell	Dr. Dennis R. Flentge
26	Project IMP: Institutionalization Methods and Policies at the Business Research Management Center	Dr. Harold Fox
27	Some Problems of Laser Velocimetry and Unsteady Aerodynamics of Current Interest to the Frank J. Seiler Research Laboratory	Dr. Peter Freymuth
28	Effects of Cloth Substrate and Finish on the Nitrogen Cure of Acetylene Terminated Sulfone (ATS) by Torsion Impregnated Cloth Analysis (TICA)	Dr. Joel R. Fried
29	Application of Conjoint Measurement Theory to the Quantification of Subjective Ratings	Dr. David E. Greene
30	Sensor Noise and Kalman Filter for Aided Inertial Navigation System	Dr. Gurmohan S. Grewal
31	Calibration of Wideband Optical Signal Processor	Dr. Paul B. Griesacker
32	Corrosion Studies of Calcium-Thionyl Chloride Electrolyte Systems	Dr. Vijay K. Gupta

RESEARCH REPORTS (Continued)

<u>Report No.</u>	<u>Title</u>	<u>Research Associate</u>
33	An Investigation Into State Estimation for Air-to-Air Missiles	Dr. Kenneth R. Hall
34	Optimal Recovery From Cratering Attacks on Airbase Prepared Surfaces	Dr. R. Michael Harnett
35	Infrared Clutter: Effects of Air Motion Produced by Auroral Zone Joule Heating	Dr. Ronney D. Harris
36	Catabolism of Toluene in the Bluegill Sunfish	Dr. Franklin D. Hill
37	Studies of the Engineering Design Process: Design of Explosively Driven Generators; Human Factors in Hazardous Activities	Dr. Francis Jankowski
38	Impact of Cylindrical Rods on Rigid Boundaries	Dr. Stanley E. Jones
39	An Information-Theoretic Approach to Target Estimation of a Conical Scan Controlled Laser Radar Tracking System	Dr. Paul Kalata
40	Electrical Characterization of Ion Implantation in GaAs	Dr. Richar Kwor
41	A Review of Current Data Base Systems for Flexible Manufacturing	Dr. Richard Liu
<u>Volume II</u>		
42	Homogeneous Compression of Rapidly Solidified Alumina, Powder Alloy Billets	Dr. William S. McCain
43	Imaging Radar Autofocus Update of an Inertial Navigation System by Means of a Kalman Filter	Dr. William S. McCormick
44	The Utility of the Animal Model Concept	Dr. Donald F. McCoy
45	Vibration-Rotation Relaxation in the HF Laser	Dr. Henry McGee
46	Appropriate Far-Field Boundary Conditions for the Numerical Solution of the Navier-Stokes Equations	Dr. Patrick J. McKenna
47	Constituent Monitoring of Evaporation Source Plumes	Dr. J. R. McNeil
48	Development of a Computer Assisted Aircraft Load Planning Model	Dr. Louis A. Martin-Vega
49	A Model for Cath Data and Some Results on the Arbitrary Right Censored Data	Dr. Kishan G. Mehrotra
50	A Direct State Space Approach to the Control of Sampled-Data Systems	Dr. David F. Miller

RESEARCH REPORTS (Continued)

<u>Report No.</u>	<u>Title</u>	<u>Research Associate</u>
51	Transient Analysis of Structures with Distinct Nonlinearities	Dr. Levon Minnetyan
52	Plasmid Fingerprints of Staphylococcus Aureus Strains Isolated From a Toxic Shock Syndrome Female Patient	Dr. Rex C. Moyer
53	An Investigation Into the Nature of the Melting Layer in Stratiform Clouds	Dr. Steven B. Newman
54	Jet Simulation Parameters for Wind Tunnel Model Thrust Reverser Testing	Dr. Eugene E. Niemi, Jr.
55	Analysis of the 60 KVA Permanent Magnet Alternator and a New Rotor Concept for these Type Machines	Dr. Samuel Noodleman
56	The Effects of JP-4 Aviation Fuel on Specific Internal Organs of the Fat-Head Minnow, Pimphale Promelus	Dr. William N. Norton
57	Observations of Sunspot Dynamics and Theoretical Effects of Inhomogeneities in the Solar Convection Zone	Dr. Alan H. Nye
58	Development of a Manual of use for Conjoint Scaling Techniques	Dr. Thomas E. Nygren
59	Evaluation of Nastran to Predict the Dynamic Response of Reinforced Concrete	Dr. William W. Payne, Jr.
60	An Analysis of the Availability, Accessibility and Timeliness of Cost Data Associated with the AFLC Aircraft Modification System with Emphasis on Class IV Modifications	Dr. John E. Powell
61	The Air Force Wright Aeronautical Laboratories Research and Development Planning Process	Dr. Robert H. Puckett
62	Coupling Reactions and Rearrangements of 1,3,5-Triazines	Dr. G. Frederic Reynolds
63	Adsorption of Trichloroethylene by Soils from Dilute Aqueous Systems	Dr. Richard O. Richter
64	The Effects of 2,3,7,8-Tetrachlorodibenzo-p-Dioxin (TCDD) Triiodothyronine (T ₃) Binding to Rat Isolated Hepatic Nuclei	Dr. John J. Riggs
65	Visual Cues in the Simulation of Low Level Flight	Dr. Edward J. Rinalducci

RESEARCH REPORTS (Continued)

<u>Report No.</u>	<u>Title</u>	<u>Research Associate</u>
66	A Metallurgical Investigation of the Internal Bronze Manufacturing Process of NB_3Sn Superconducting Wire	Dr. John M. Roberts
67	Investigation of the Mechanical Properties of Less Than 100% Dense Titanium Powder Metallurgy Compacts	Dr. Thomas Roth
68	Application of Task Analytic Techniques to the Design of a Flight Simulator Instructor/Operator Console	Dr. Charles D. Sanders
69	Study of Dynamic Behavior of a Bluff-Body Diffusion Flame in the APL Combustion Tunnel Facility	Dr. Sarwan S. Sandhu
70	Shear-Wave Velocity Structure Determined From Analysis Rayleigh-Wave Group-Velocity Dispersion	Dr. Gerald W. Simila
71	Operating Various Subsystems of the Total Simulation Systems for Flight Training	Dr. Vina Sloan
72	Enhancing Career Development at the Air Force Rocket Propulsion Laboratory	Dr. Russ Smith
73	Development of a Computer Algorithm for the Automatic Determination of Space Vehicle Potential Utilizing Electrostatic Analyzer Measurements	Dr. Stanley L. Spiegel
74	Plastic Rotating Band Loads and Sliding Resistance Forces	Dr. A. Kent Stiffler
75	Binary and Ternary Compositions and their Physical Properties	Dr. Lawrence Suchow
76	A System Dynamics Model of the Acquisition Process	Dr. Patrick J. Sweeney
77	Analysis of Maintenance Decisions at Lower Echelon Levels Involving Jet Aircraft Engines	Dr. Charles J. Teplits
78	A Study of the Interaction of Hydrazine Methylhydrazine and Unsymdimethylhydrazine with Porphyrins, Metalloporphyrins, and some Metal Coordination Compounds	Dr. Albert N. Thompson
79	GaAs Mesfet Modeling	Dr. Arthur A. Thorbjornsen
80	Covering Problems in C^3I Systems	Dr. Richard Van Slyke
81	Effects of Acoustic Disturbances on the Boundary-Layer Transition in AEDC Wind Tunnels	Dr. Venugopal Veerasamy

RESEARCH REPORTS (Continued)

<u>Report No.</u>	<u>Title</u>	<u>Research Associate</u>
82	An Evaluation of Air Force Pavement Non-Destructive Testing Method	Dr. M.C. Wang
83	The Effect of One Hundred Percent Oxygen at One ATA and Increased Pressure on the Metabolism of an Organophosphate (Parathion) in the Rat	Dr. Alice Ward
84	Measurements of Turbulence in the Troposphere and Lower Stratosphere using the Millstone Hill 440 MHz Radar	Dr. Brenton J. Watkins
85	Optimal Design of Digital Flight Control Systems Following an Analog Model	Dr. Hsi-Han Yeh
86	Amplitude Variability of the Steady State Visual Evoked Response	Dr. Robert L. Yolton
87	New Tests of Theories on Shaped Charge	Dr. Poh Shien Young

1981 USAF - SCEEE SUMMER FACULTY RESEARCH PROGRAM

Sponsored by the

AIR FORCE OFFICE OF SCIENTIFIC RESEARCH

Conducted by the

SOUTHEASTERN CENTER FOR ELECTRICAL ENGINEERING EDUCATION

FINAL REPORT

THE DETERMINATION OF INPUT DATA ACCURACY

IN THE MAINTENANCE DATA COLLECTION SYSTEM

Prepared by: Dr. Milton J. Alexander
Academic Rank: Professor
Department and University: Management Department
Auburn University
Research Location: Air Force Logistics Management Center
Directorate of Maintenance
USAF Research Colleague: Lt Col David A. Dietsch
Date: September 7, 1981
Contract No: F49620-79-C-0038

THE DETERMINATION OF INPUT DATA ACCURACY

IN THE MAINTENANCE DATA COLLECTION SYSTEM

by

Milton J. Alexander

ABSTRACT

The question of input data accuracy in the maintenance data collection system is investigated. It is shown that the level of input data accuracy is subject to two different types of errors - data which should have been entered into the MDCS (Type I errors) and erroneous data which was entered into the MDCS (Type II errors). Techniques were developed to measure both types of errors and field tested on a TAC unit. The two error types may be combined as a joint probability to provide a measure of input data accuracy. When field test data was substituted in the mathematical formulation, the computed input data accuracy level was about one percent, i.e., only about one maintenance action in 100 was being correctly reported into MDCS. Suggestions for improving input data accuracy as well as further research in this area are offered.

ACKNOWLEDGEMENTS

The author would like to thank the Air Force Logistics Management Center (AFLMC) and the Southeastern Center for Electrical Engineering Education for providing him with the opportunity to spend a very worthwhile and interesting summer at the AFLMC, Gunter AFS, Alabama. He would like to acknowledge, in particular, Capt Lindel Thompson for his assistance and collaboration on this project. Finally, he would like to thank Lt Colonel David A. Dietsch and other members of the AFLMC staff for their patient assistance on this project.

I. INTRODUCTION

The Maintenance Data Collection System (also known as MDCS or MDC System) was initially implemented throughout the USAF in 1957-58. The principal objective of the MDCS was, and still largely remains, to collect raw aircraft and ground support equipment maintenance data for subsequent use in other base level and AFLC electronic data processing systems.

The basic operation of the MDCS has also remained much the same since its inception. Essentially, MDCS is designed to collect certain data from every maintenance action, transcribe the data to 80 column punch cards and prepare magnetic tape transcription files for entry to other higher level computerized information systems. The only major modification to the system occurred in 1968 when the currently used multi purpose source document form (AFTO Form 349) was adopted to replace the original source document forms (AFTO Forms 992, 210, 211 and 212). At the same time, the number of data item inputs required for entry by maintenance personnel was reduced to the present level.

Almost from its inception, personnel associated with MDCS realized that the information generated by the system was highly suspect and full of errors. A worldwide meeting in 1959 of MDCS associate personnel was the first large scale effort to correct MDCS deficiencies. Other major MDCS investigations have followed through the years:

- (1) The RAND investigations in the mid-1960's (RM-4985-PR, RM-4778-PR and RM-4849-PR).
- (2) The Artronic Information Systems, Inc. study in 1976 (Contract No. F49642-76-90743).
- (3) The Desmatics, Inc. study in 1979 (Contract No. MDA903-78-C-0234).

Other investigations of a more limited scope have also taken place in the intervening years. All of the system improvement efforts notwithstanding, MDCS has remained an intractable giant spewing out huge volumes of very dubious quality information.

II. OBJECTIVES

The initial objectives of the research effort may be summarized as follows:

- (1) To review USAF literature on the MDC System.
- (2) To review academic literature concerning accuracy in the data collection process.
- (3) To develop method(s) for evaluating the accuracy of MDCS data collection.
- (4) To conduct a field test to check the method(s) efficacy.

Once the project was begun, it became apparent that some modification of the objectives would be necessary. The first objective was extended to include documentation of the MDCS in both SAC (66-1) and TAC (66-5) organizations with information systems flowcharts. In this way all of the raw data entry points could be readily identified and an organized analysis of MDCS operations performed.

The second objective was reduced in importance when a cursory review of the academic literature failed to yield any significant information which could be applied to the MDCS. The third and fourth objectives were retained intact.

III. DETERMINATION OF CURRENT MDCS CONFIGURATION AND STATUS

The MDCS was originally designed in 1957 - 58. Electronic data

processing technology was, of course, just beginning to develop at that time. The original MDCS design incorporated the best data processing technology then available. Raw data was collected in code form on source documents, keypunched to 80 column cards, then batch computer processed.

The same basic data processing techniques are still being used today in the MDCS. The only significant system modifications have been changes in the responsibility for source document preparation and additional information outputs for other information systems and users.

The first major task undertaken in this portion of the project was the determination of the actual information (document) flows in the MDCS. A systems investigation including field studies at Warner Robins AFB (SAC) and Moody AFB (TAC) was performed. Information system flowcharts for both 66-1 (SAC) and 66-5 (TAC) organizations were prepared and are shown as Exhibits 1 through 11. The generally small differences in MDCS structure between the two organizational unit types largely reflect their different operating environments.

AFTO Form 349 is the source document for all data entered into the MDCS. The data transcribed to the Form 349 is either the data used to initiate maintenance action or data needed to close out a maintenance action. Activity initiating data comes from several different organizational sources - Debriefing, Job Control, Work Centers, Plans and Scheduling, and Quality Verification. The actual number of data entries, however, is relatively small (3 to 6) and the data is readily available in unambiguous form. Nearly all data entry errors associated with Form 349 initiation will be quickly discovered by subsequent Form 349 users.

The data required to close out an open Form 349 (or complete a specific job identified by a Job Control Number (JCN)) is a completely different matter. The maintenance personnel who actually perform the maintenance tasks are responsible for entering raw data about the work performed. There is no separate verification of data accuracy, only a manual/computer edit process. Though the number of separate data entries is not large (3 to 6), the data collection process is subject to many difficulties related primarily to the personnel responsible for data entry and the physical environment in which they function.

The following observations and conclusions were derived from the analysis of the information systems flowcharts.

- (1) There is no control over the issuance of Job Control Numbers (JCN's).
Though there is a pattern for all JCN's, various individuals in all of the organizational units can issue JCN's as they deem necessary.
- (2) There is no organizational unit responsible for the administration of JCN's.
- (3) Data accuracy in JCN initiation does not appear to be a significant problem because any input errors will be discovered later by Work Center personnel.
- (4) There is no organizational unit responsibility for the reconciliation of completed Forms 349 with JCN's issued.
- (5) There is no data feedback or information availability to any of the data initiators.

IV. DETERMINATION OF DATA INPUT ACCURACY

Computerized information systems may produce unreliable and, hence, scarcely useable information due to input data errors arising from two

different sources. The determination of input data accuracy requires that both error types be examined and evaluated with respect to their influence on data reliability.

The first type of error (Type I error) occurs when data exists but is not entered into the information system. The resulting information generated by the computerized information system is incomplete and may provide an unsatisfactory or undesirable base for decision making.

Type I errors could exist in the MDCS when no Form 349 is ever prepared and yet maintenance activities are still performed. Since maintenance activity is a response to a perceived systemic dysfunction, work center personnel cannot respond unless they are somehow notified that a failure or problem discovered by another organizational unit exists. Thus, this specific type of data omission can only occur when work center personnel discover problems and immediately apply corrective action with no JCN ever being initiated. Because these special circumstances would tend to occur only infrequently and usually be restricted to minor repairs, no attempt was made to determine the frequency of Type I errors in Form 349 initiation.

The major source of Type I errors takes place when required maintenance actions are noted and documented on Form 349s in Debriefing, Job Control, Plans and Scheduling and Quality Verification, and no corresponding maintenance action is reported to the MDCS. The maintenance work was done, but the paperwork wasn't.

Most of the Type I errors can be identified with a special computer reconciliation program. The great majority of required maintenance actions are noted by Debriefing and the corresponding Form 349s are prepared. All

discrepancies which change aircraft flight status are automatically reported to MDCS. Thus, the MDCS files list virtually all of the significant required maintenance actions for each aircraft. On the other hand, the MDCS lists all of the completed Form 349s. When the two lists are reconciled, the maintenance actions which were not closed out with a completed Form 349 may be readily identified. The JCNs which have not been closed out for some valid reason, such as awaiting replacement parts, may be found on the Equipment Verification Listing and manual corrections made on the reconciliation report.

The second type of error (Type II error) stems from erroneous data being entered into the MDCS. A work sampling study conducted by Desmatics, Inc. in 1979 concluded that work time reported was about twice the actual time spent performing the work. Unfortunately, work time is not the only data item reported by work center personnel. How/mal and action taken codes must also be entered into MDCS. Both of these codes require reference to a thick code book to determine the proper codes.

The questionnaire technique was adopted to provide an indication of employee data entry performance. This technique was selected because it is direct, amenable to statistical analysis and requires modest time and effort to conduct the study. The final questionnaire design was actually a joint effort by several staff members of the AFLMC. The questionnaire used in the field test is shown in appendix 1.

The questionnaire included several questions (nos. 6 and 8 in particular) to cross check the Type I error results from the computer reconciliation report and provide some validation of the questionnaire data. In addition there were several key questions designed to assess data accuracy with respect

to Type II errors. Question #12, for example, provides a direct measure of input data accuracy for job time. Questions #13, 14 and 15 taken together provide a subjective measure of how/mal code input data accuracy.

Input data accuracy may be formulated as a joint probability function.

That is,

$$[1 - P(\text{Type I error})] \times [1 - P(\text{Type II error})] = \text{Data Accuracy.} \quad (1)$$

Data accuracy may be further defined as the probability that all data pertaining to a given activity or transaction will be input correctly to a computerized information system.

The mathematical formulation of data accuracy given above must be expanded somewhat in order to be applied to the MDCS. Three particular input data items are required on all Form 349s - time spent, how/mal code and action taken codes. The second term in the equation above then becomes

$$\begin{aligned} [1 - P(\text{Type IIa error})] \times [1 - P(\text{Type IIb error})] \\ \times [1 - P(\text{Type IIc error})] = [1 - P(\text{Type II error})] \end{aligned} \quad (2)$$

The complete mathematical formulation for the determination of MDCS input data accuracy therefore is

$$\begin{aligned} [1 - P(\text{Type I error})] \times [1 - P(\text{Type IIa error})] \\ \times [1 - P(\text{Type IIb error})] \times [1 - P(\text{Type IIc error})] \\ = \text{MDCS input data accuracy.} \end{aligned} \quad (3)$$

V. DATA RELIABILITY FIELD TEST

A field test using both data reliability study methods was conducted at a TAC Air Force base in August, 1981. The goals of the field test were (a) to examine the applicability of both study methods in a real world setting and (b) to obtain data for the evaluation of MDCS data reliability.

The first study method (Type I errors) required a computer run reconciling the open JCN's according to MDCS and the incomplete JCNs according to MILAP. Accordingly a representative time period (Feb 1 to Feb 15, 1981) was selected for the reconciliation run. The resulting report listed a total of 997 JCN's which had been submitted. Of these, 481 JCN's were listed as completed and 516 JCN's had not been closed out for a 48% submission rate. A subsequent search of open JCN's in the EVL for the current period did not disclose a single one of those JCN's as still active, i.e., a delayed discrepancy. Inasmuch as many of these discrepancies could be sufficient cause for grounding the aircraft, it is safe to assume that the maintenance work was performed but simply never reported to the MDCS.

The second portion of the field test required the administration of a questionnaire to maintenance personnel. Capt Lindel Thompson administered the questionnaire to 187 maintenance personnel (total population, 1020). Since questionnaire completion was strictly voluntary, many individuals declined to participate. The questionnaire results are shown in Appendix 2.

Several conclusions can be drawn from a cursory analysis of the completed questionnaires. First, accurate work time data is being input less than 25% of the time. Second, accurate and descriptive how/mal codes are difficult to determine and may very well not exist at all. Finally, while action taken codes are more easily determined, there are apparently overlaps and voids in this code structure.

The observed or inputted values from the field test are:

P(Type I error) = .52

P(Type IIa error) = .75

P(Type IIb error) = .7

P(Type IIc error) = .7

These values may be substituted in the MDCS input data accuracy equation as

$$(1 - .52) \times (1 - .75) \times (1 - .7) \times (1 - .7) \quad \text{or} \\ .48 \times .25 \times .3 \times .3 = .0108.$$

According to the field test data, a given maintenance activity will be input correctly into the MDCS only about one time in 100.

The data accuracy value determined above is subject to certain restrictions and considerations.

- (1) Type IIb and Type IIc error rates were inputted and not measured directly.
- (2) The field test data sample (4 squadrons at one AFB during a particular two week period) was quite small relative to the whole population and could, therefore, be an exceptional condition.
- (3) The Type II error portion of the MDCS input data accuracy calculation assumes that the three data inputs are statistically independent. It is likely, however, that conscientious individuals will enter accurate data for all input data items. In this case the data items would not be statistically independent.
- (4) Only the major input error sources have been included in this study; other minor error sources have been ignored.
- (5) A high level of input data accuracy may not be necessary for all subsequent users of MDCS data. This area has not been explored.

VI. RECOMMENDATIONS

The field test results seem to confirm the grave reservations many MDCS users have long expressed. A conclusive statement about MDCS data input accuracy, however, can only be made after the questionnaire has been improved and a larger sample has been studied. The extension of this investigation technique is a necessary step to fully establish the magnitude of the input data accuracy problem.

A second area for investigation concerns information utility. The level of required input data accuracy is dependent upon the uses to which the resulting information (system outputs) is being applied. Thus, the various information systems which utilize MDCS data must be examined to determine both their specific information requirements and the necessary input data accuracy level.

Finally, after these two investigatory phases have been completed, the examination of alternative means to accomplish the desired ends may be rationally undertaken.

APPENDIX 1

INTRODUCTION

1. The purpose of this Questionnaire is to help determine the level of data accuracy on AFTO Forms 349 submitted to data automation. We realize there are limitations associated with requiring maintenance technicians to complete AFTO Forms 349 since many factors contribute to either intentional or unintentional erroneous reporting of data. Your candid responses to the questions will make the results of our analysis more meaningful.
2. Completion of this Questionnaire is strictly voluntary. We hope, of course, that you will cooperate by answering the questions to the best of your ability. Many of the questions call for estimates of one sort or another. Please base your responses on your personal work experiences.
3. The completed Questionnaire will be kept confidential and will not be released to anyone. No attempt will be made to use your responses in evaluating your job performance or your unit's job performance. Further, this study is not a part of an IG inspection or similar investigation. It will be used for research purposes only.
4. In order to keep your responses to the questions totally anonymous your name and Social Security Number are not required. We would like you to complete the sex, age, pay grade, primary AFSC and duty AFSC portions of the response sheet. Insert your work center code in the work group code space and leave the supervisors code space blank.

QUESTIONNAIRE

1. My total time in my present duty AFSC is:
 - a. Less than 6 months
 - b. At least 6 months but less than 1 year
 - c. At least 1 year but less than 2 years
 - d. At least 2 years but less than 3 years
 - e. At least 3 years but less than 5 years
 - f. At least 5 years but less than 10 years
 - g. 10 years or more

2. During a typical work day, I will work on _____ Job Control Numbers that require an AFTO Form 349 be completed.
 - a. 0-3
 - b. 4-5
 - c. 6-7
 - d. 8-9
 - e. 10-12
 - f. 13-15
 - g. More than 15

3. When working jobs requiring a crew or assistance, I am responsible for completing the AFTO Form 349 for _____ of the jobs.
 - a. Less than 20%
 - b. At least 20% but less than 40%
 - c. At least 40% but less than 60%
 - d. At least 60% but less than 80%
 - e. At least 80% but less than 100%
 - f. 100%
 - g. Don't know

4. Of the job control numbers I work on in a typical day, _____ are TCTO's, Time Change Items, Special Inspections, Cannibalizations or some combination of these categories.
 - a. Less than 10%
 - b. At least 10% but less than 20%
 - c. At least 20% but less than 30%
 - d. At least 30% but less than 40%
 - e. At least 40% but less than 50%
 - f. 50% or more
 - g. Don't know

5. I have adequate time to carefully research the -06 Code Book and properly complete for AFTO Forms 349 I submit for JCNs in Question #4 for _____ of the jobs.
 - a. Less than 20%
 - b. At least 20% but less than 40%
 - c. At least 40% but less than 60%
 - d. At least 60% but less than 80%
 - e. At least 80% but less than 100%
 - f. 100%
 - g. Don't know

6. I complete AFTO Forms 349 for _____ TCTO's, Time Change Items, Special Inspections, and Cannibalization jobs.
 - a. Less than 50%
 - b. At least 50% but less than 60%
 - c. At least 60% but less than 70%
 - d. At least 70% but less than 80%
 - e. At least 80% but less than 90%
 - f. At least 90% but less than 100%
 - g. 100%

7. For JCNs other than TCTO's, Time Change Items, Special Inspections, and Cannibalizations, I have adequate time to research the -06 Code Book and properly complete the AFTO Forms 349 for _____ of the jobs.
 - a. Less than 50%
 - b. At least 50% but less than 60%
 - c. At least 60% but less than 70%
 - d. At least 70% but less than 80%
 - e. At least 80% but less than 90%
 - f. At least 90% but less than 100%
 - g. 100%

8. For JCNs other than TCTO's, Time Change Items, Special Inspections, and Cannibalizations, I complete the AFTO Form 349 for _____ of the jobs.
 - a. Less than 50%
 - b. At least 50% but less than 60%
 - c. At least 60% but less than 70%
 - d. At least 70% but less than 80%
 - e. At least 80% but less than 90%
 - f. At least 90% but less than 100%
 - g. 100%

9. I usually complete the AFTO Form 349:
 - a. Immediately after I finish the job
 - b. As soon as I get some free time
 - c. At the end of my shift
 - d. First thing on the next work day
 - e. When reminded by my supervisor
 - f. At some other time
 - g. Never

10. What is the most important reason that you do not complete all AFTO Forms 349?
 - a. No AFTO Form 349 was received
 - b. It is too hot, cold, noisy and/or dirty
 - c. It takes too much time and effort
 - d. No one asked for the AFTO Form 349
 - e. I forgot it
 - f. There are no acceptable reasons for all AFTO Forms 349 not being completed
 - g. Some reason other than a through f

11. What is the second most important reason that you do not complete all AFTO Forms 349?
- a. No AFTO Form 349 was received
 - b. It is too hot, cold, noisy and/or dirty
 - c. It takes too much time and effort
 - d. No one asked for the AFTO Form 349
 - e. I forgot it
 - f. There are not acceptable reasons for all AFTO Forms 349 not being completed
 - g. Some reason other than a through f
12. On the average for all jobs, the time I report on the AFTO Form 349 compared to actual time spent on the job is:
- a. About 50% of actual time
 - b. About 70% of actual time
 - c. Time reported equals time spent
 - d. About 125% of actual time spent
 - e. About 150% of actual time spent
 - f. About twice as much as time spent
 - g. Don't know
13. How often do you refer to the -06 Code Book to determine the appropriate How/Mal Code?
- a. Never
 - b. Less than 25% of the time
 - c. At least 25% but less than 50% of the time
 - d. At least 50% but less than 75% of the time
 - e. At least 75% but less than 90% of the time
 - f. At least 90% but less than 100% of the time
 - g. 100%
14. How accurately do How/Mal Codes listed in -06 Code Book describe what is wrong with the equipment?
- a. Never
 - b. Less than 25% of the time
 - c. At least 25% but less than 50% of the time
 - d. At least 50% but less than 75% of the time
 - e. At least 75% but less than 90% of the time
 - f. At least 90% but less than 100% of the time
 - g. 100%
15. When entering the How/Mal Code on an AFTO Form 349:
- a. I try very hard to find the most accurate code
 - b. I try to find a good, close code
 - c. I try to find a reasonable code
 - d. I use any one of several codes that I know and will not reject

16. The most important reason I do not enter the most accurate How/Mal Code is:

- a. Too much trouble
- b. Code books aren't readily available
- c. Code book is hard to use
- d. No appropriate code in the code book
- e. I always enter the most appropriate code.

17. What is the second most important reason that I do not enter the most accurate How/Mal Code:

- a. Too much trouble
- b. Code books aren't readily available
- c. Code book is too hard to use
- d. No appropriate code in the code book
- e. I always enter the most appropriate code.

18. When entering the Work Unit Code on an AFTO Form 349:

- a. I try very hard to find the most accurate code
- b. I try to find a good, close code
- c. I try to find a reasonable code
- d. I use any one of several codes that I know and will not reject

19. The most important reason I do not enter the most accurate Work Unit Code is:

- a. Too much trouble
- b. Code books aren't readily available
- c. Code book is too hard to use
- d. No appropriate code in the code book
- e. I always enter the most appropriate code.

20. What is the second most important reason that I do not enter the most accurate Work Unit Code:

- a. Too much trouble
- b. Code books aren't readily available
- c. Code book is too hard to use
- d. No appropriate code in the code book
- e. I always enter the most appropriate code.

21. When entering the Action Taken Code on an AFTO Form 349:

- a. I try very hard to find the most accurate code
- b. I try to find a good, close code
- c. I try to find a reasonable code
- d. I use any one of several codes that I know and will not reject

22. The most important reason I do not enter the most accurate Action Taken Code is:

- a. Too much trouble
- b. Code books aren't readily available
- c. Code book is too hard to use
- d. No appropriate code in the code book
- e. I always enter the most appropriate code.

23. What is the second most important reason that I do not enter the most accurate Action Taken Code:

- a. Too much trouble
- b. Code books aren't readily available
- c. Code book is too hard to use
- d. No appropriate code in the code book
- e. I always enter the most appropriate code.

APPENDIX 2

RESULTS FROM QUESTIONNAIRE

1.	(a) 9 (b) 24 (c) 23 (d) 38 (e) 32 (f) 34 (g) 20 (h) 5	2.	(a) 77 (b) 54 (c) 21 (d) 12 (e) 7 (f) 6 (g) 7	3.	(a) 43 (b) 16 (c) 31 (d) 18 (e) 16 (f) 36 (g) 20 (h) 3	4.	(a) 114 (b) 37 (c) 9 (d) 4 (e) 8 (f) 5 (g) 4 (h) 2
5.	(a) 34 (b) 15 (c) 13 (d) 14 (e) 31 (f) 53 (g) 21 (h) 2	6.	(a) 119 (b) 20 (c) 6 (d) 6 (e) 3 (f) 6 (g) 20 (h) 3	7.	(a) 44 (b) 10 (c) 8 (d) 8 (e) 13 (f) 28 (g) 40 (h) 6	8.	(a) 71 (b) 21 (c) 10 (d) 7 (e) 17 (f) 17 (g) 32 (h) 8
9.	(a) 43 (b) 47 (c) 61 (d) 8 (e) 10 (f) 3 (g) 11	10.	(a) 12 (b) 3 (c) 17 (d) 9 (e) 21 (f) 61 (g) 51 (h) 8	11.	(a) 11 (b) 4 (c) 13 (d) 14 (e) 21 (f) 51 (g) 59 (h) 9	12.	(a) 33 (b) 26 (c) 45 (d) 23 (e) 15 (f) 25 (g) 11 (h) 5
13.	(a) 13 (b) 28 (c) 27 (d) 31 (e) 23 (f) 32 (g) 25	14.	(a) 2 (b) 12 (c) 19 (d) 25 (e) 40 (f) 60 (g) 24 (h) 2	15.	(a) 68 (b) 44 (c) 24 (d) 17 (e) 5	16.	(a) 17 (b) 7 (c) 3 (d) 55 (e) 89 (f) 11 (g) 1

17. (a) 18
(b) 19
(c) 9
(d) 54
(e) 74
(f) 8
(g) 1

18. (a) 130
(b) 32
(c) 12
(d) 8
(e) 1

19. (a) 9
(b) 5
(c) 5
(d) 40
(e) 114
(f) 10

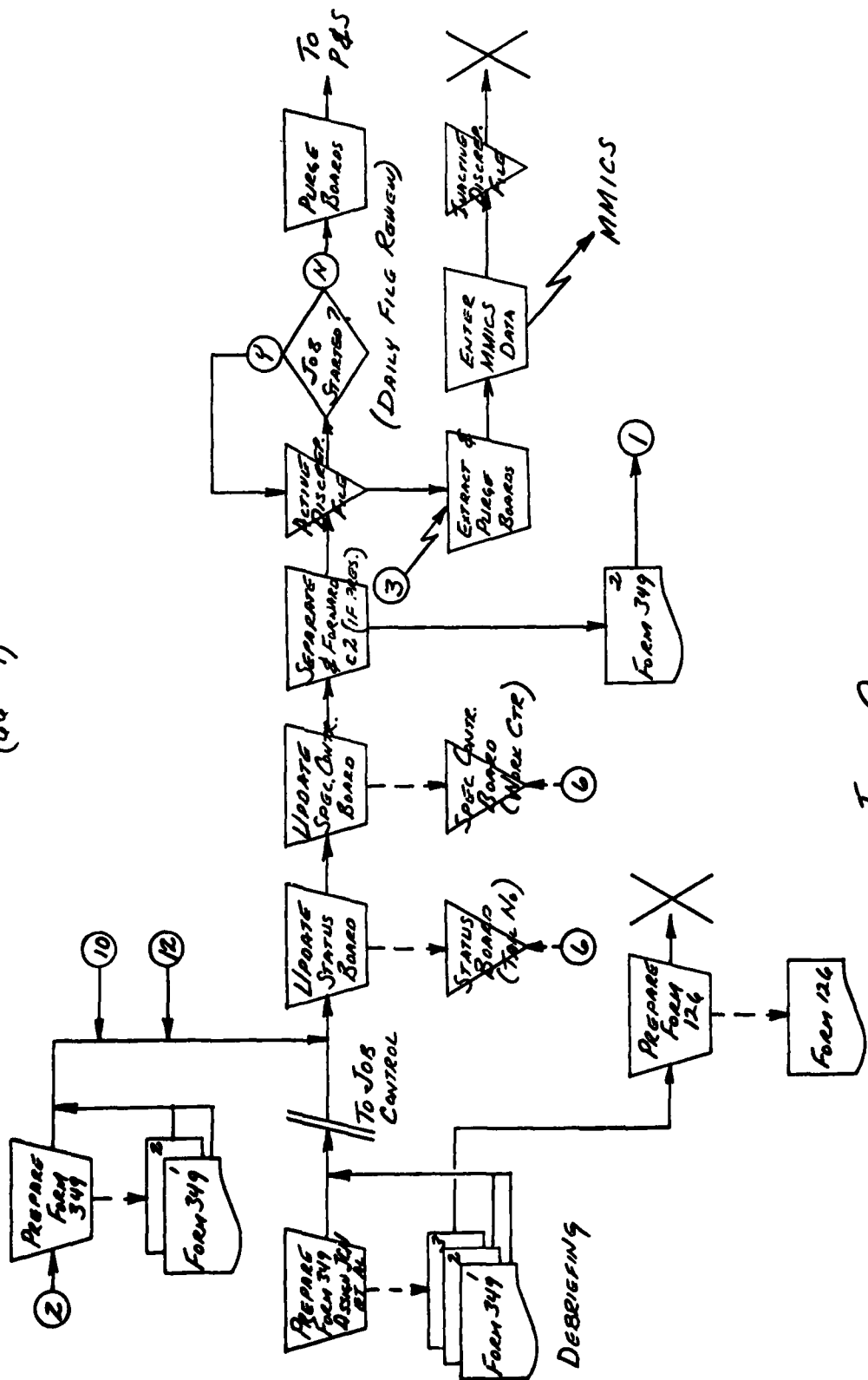
20. (a) 15
(b) 16
(c) 6
(d) 33
(e) 107
(f) 5
(g) 1

21. (a) 104
(b) 45
(c) 16
(d) 17
(e) 1

22. (a) 15
(b) 3
(c) 11
(d) 37
(e) 107
(f) 9

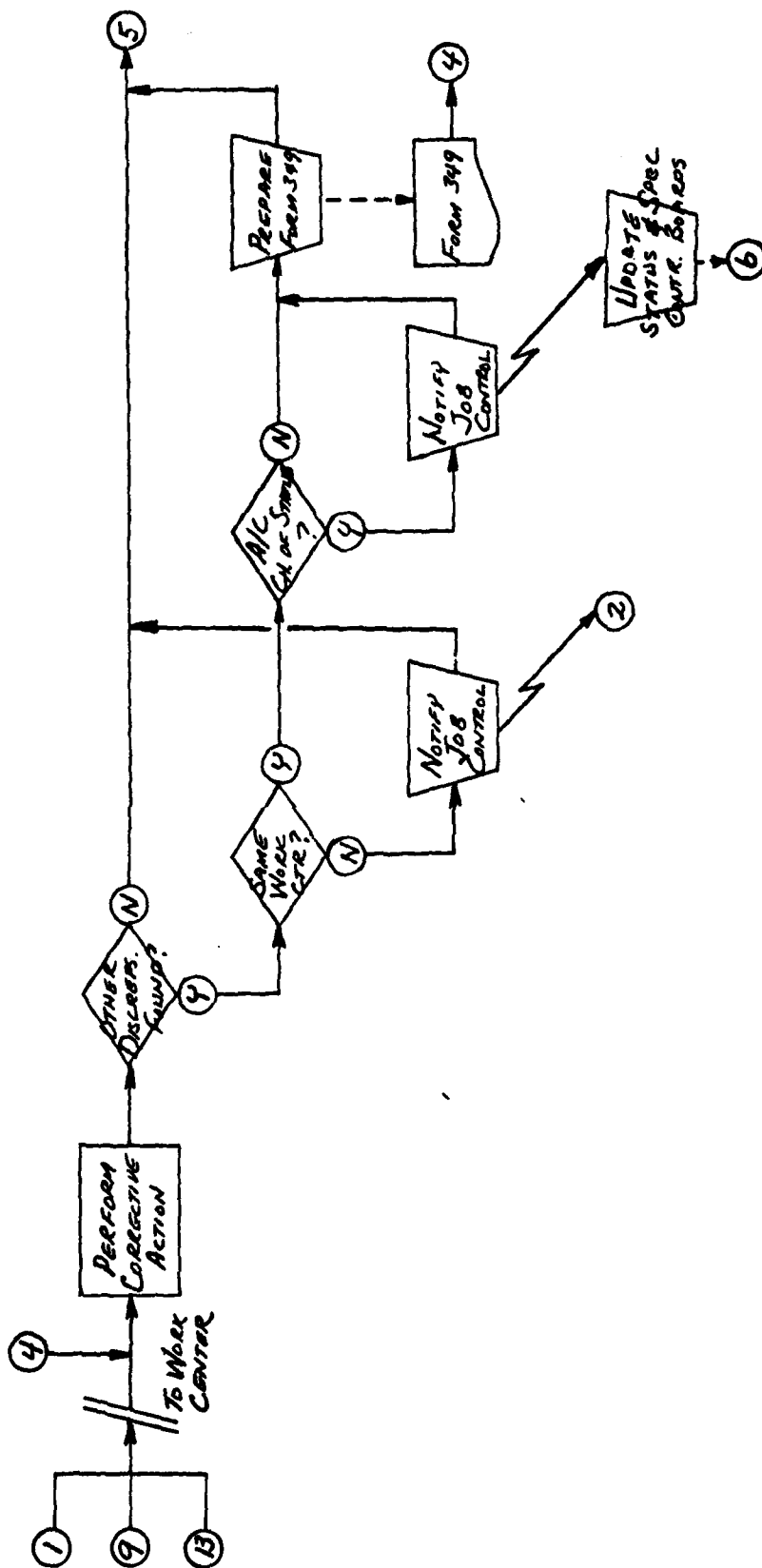
23. (a) 15
(b) 15
(c) 11
(d) 44
(e) 96
(f) 2

SYSTEMS FLOWCHART - 1
 MAINTENANCE DATA COLLECTION SYSTEM
 (66-1)



JOB CONTROL

SYSTEMS FLOWCHART - 2
 MAINTENANCE DATA COLLECTION SYSTEM
 (66-1)

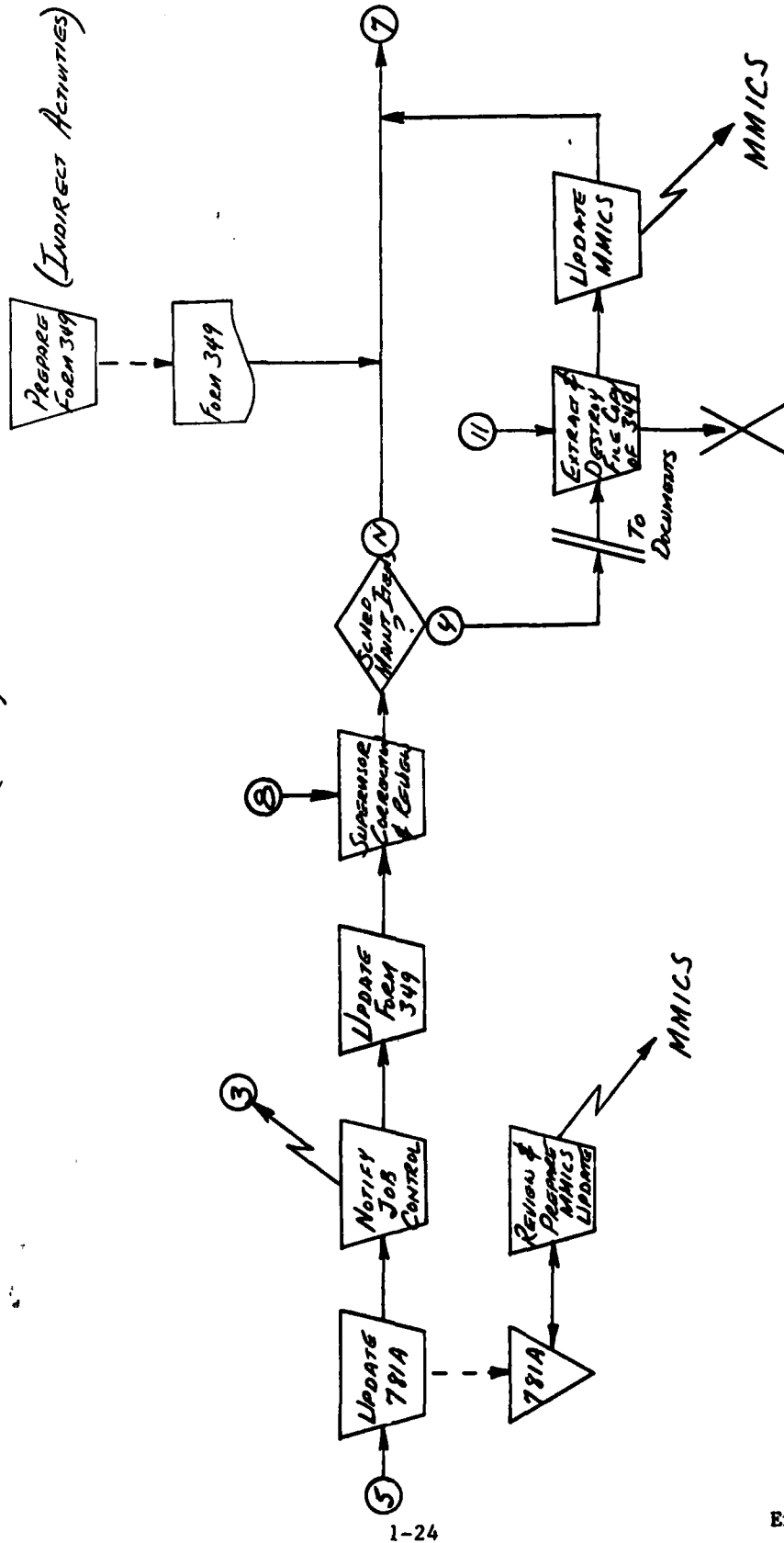


WORK CENTER

SYSTEMS FLOWCHART - 3

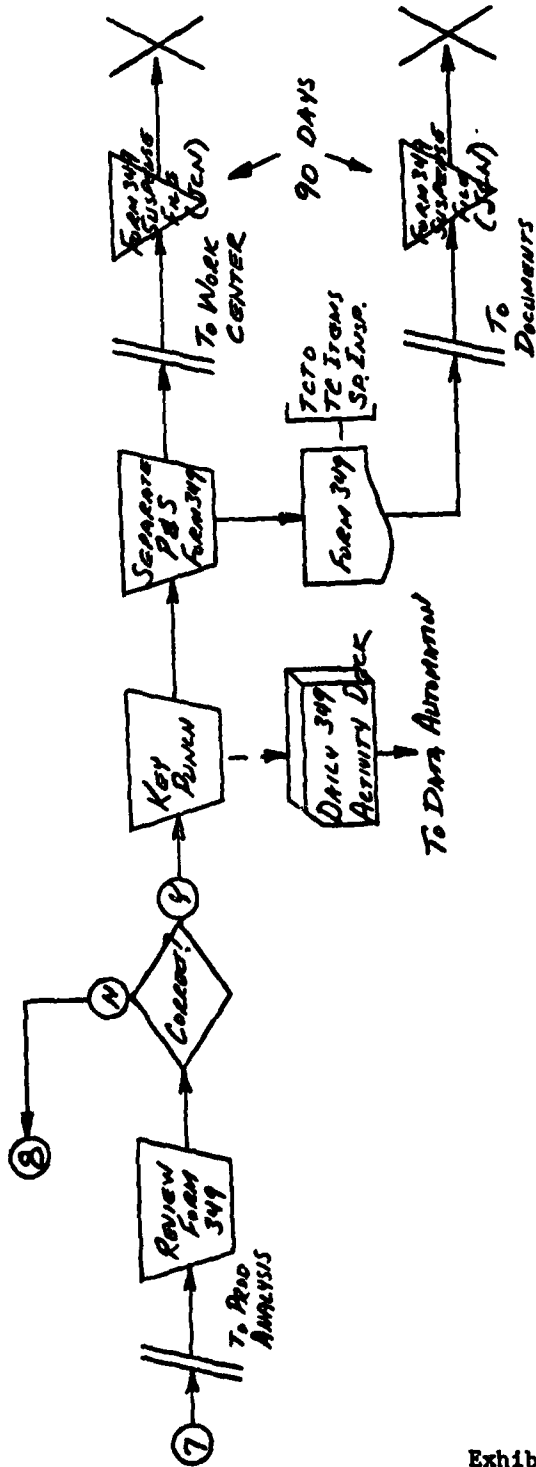
MAINTENANCE DATA COLLECTION SYSTEM

(66-1)



WORK CENTER

SYSTEMS FLOWCHART - 4
 MAINTENANCE DATA COLLECTION SYSTEM
 (66-1)

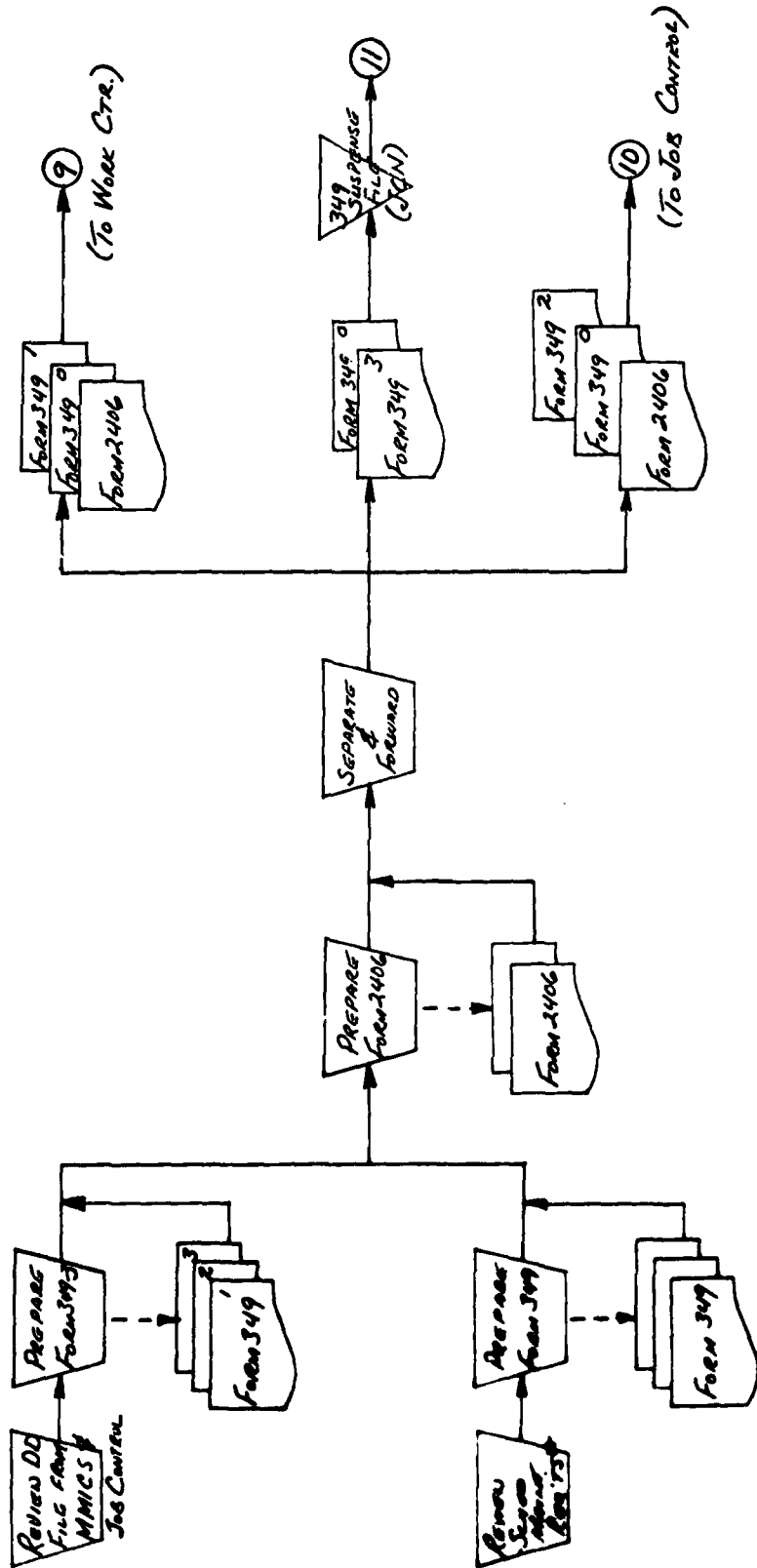


PRODUCTION ANALYSIS

Exhibit 4

SYSTEMS FLOWCHART - 5

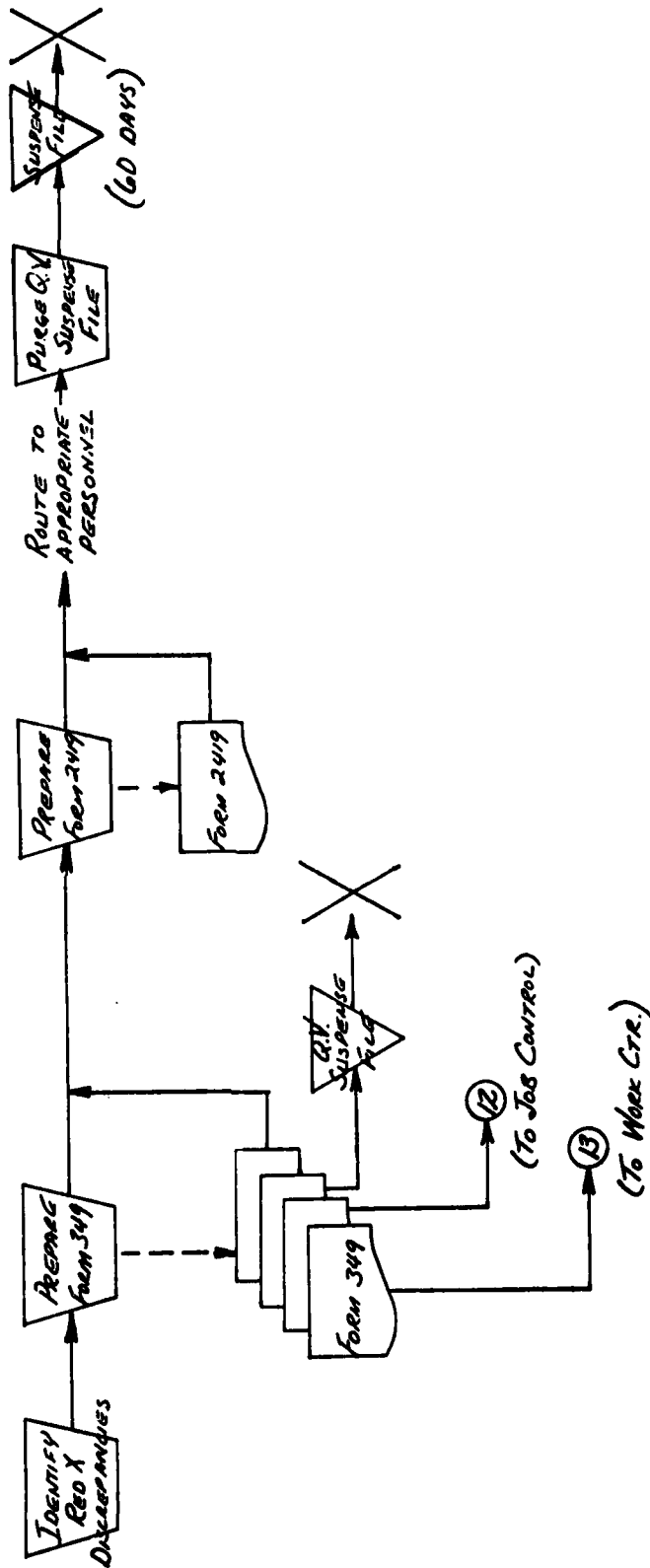
MAINTENANCE DATA COLLECTION SYSTEM (66-1 & 66-5)



* TCTO's, TIME CHANGE ITEMS
AND SPECIAL INSPECTIONS

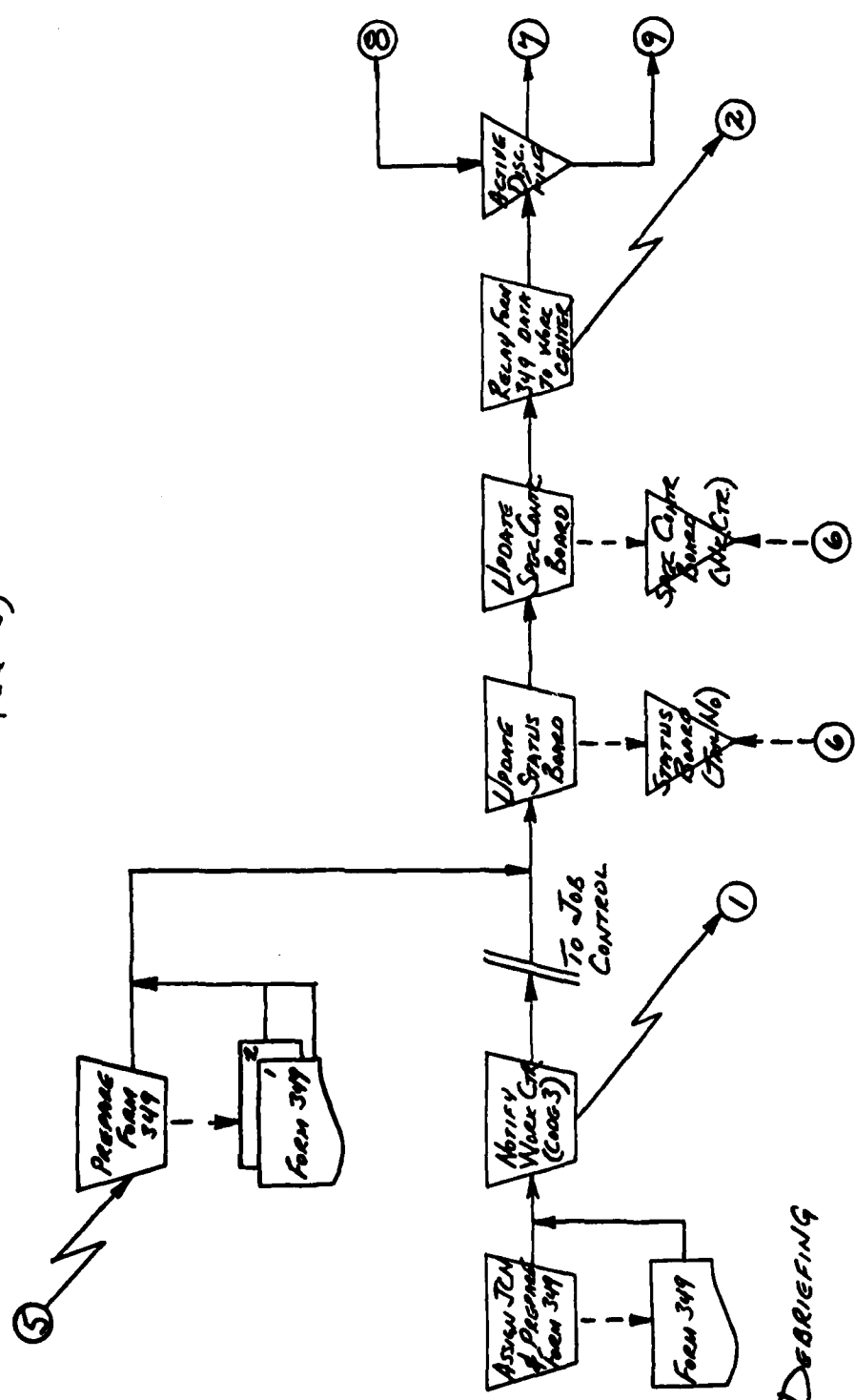
PLANS & SCHEDULING

SYSTEM FLOWCHART--6
 MAINTENANCE DATA COLLECTION SYSTEM
 (66-1 & 66-5)



QUALITY VERIFICATION

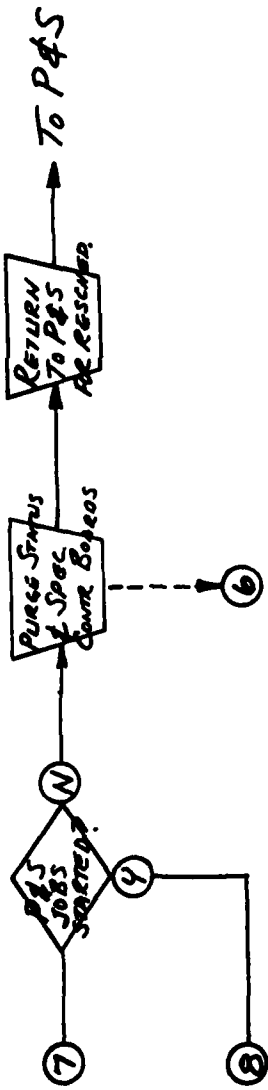
SYSTEMS FLOWCHART - 7
 MAINTENANCE DATA COLLECTION SYSTEM
 (66-5)



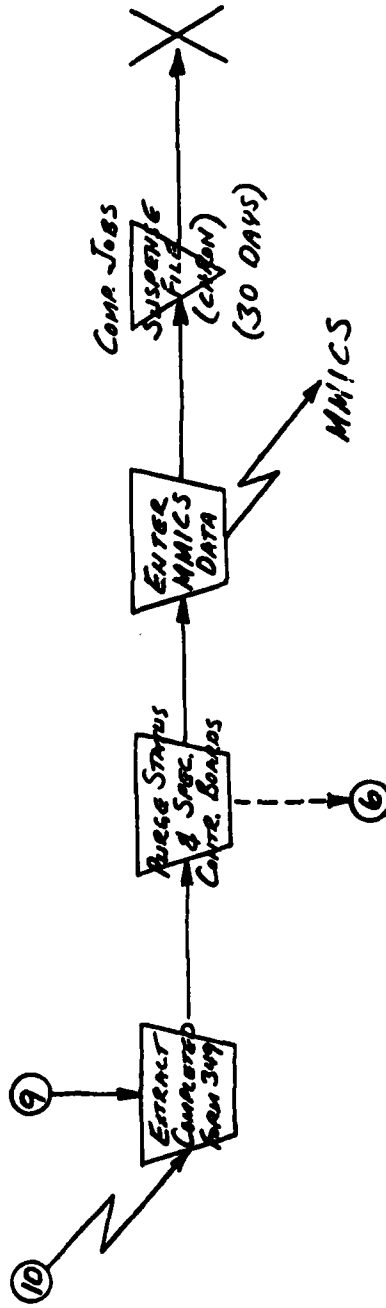
DEBRIEFING

JOB CONTROL

SYSTEMS FLOWCHART - 8
 MAINTENANCE DATA COLLECTION SYSTEM
 (66-5)



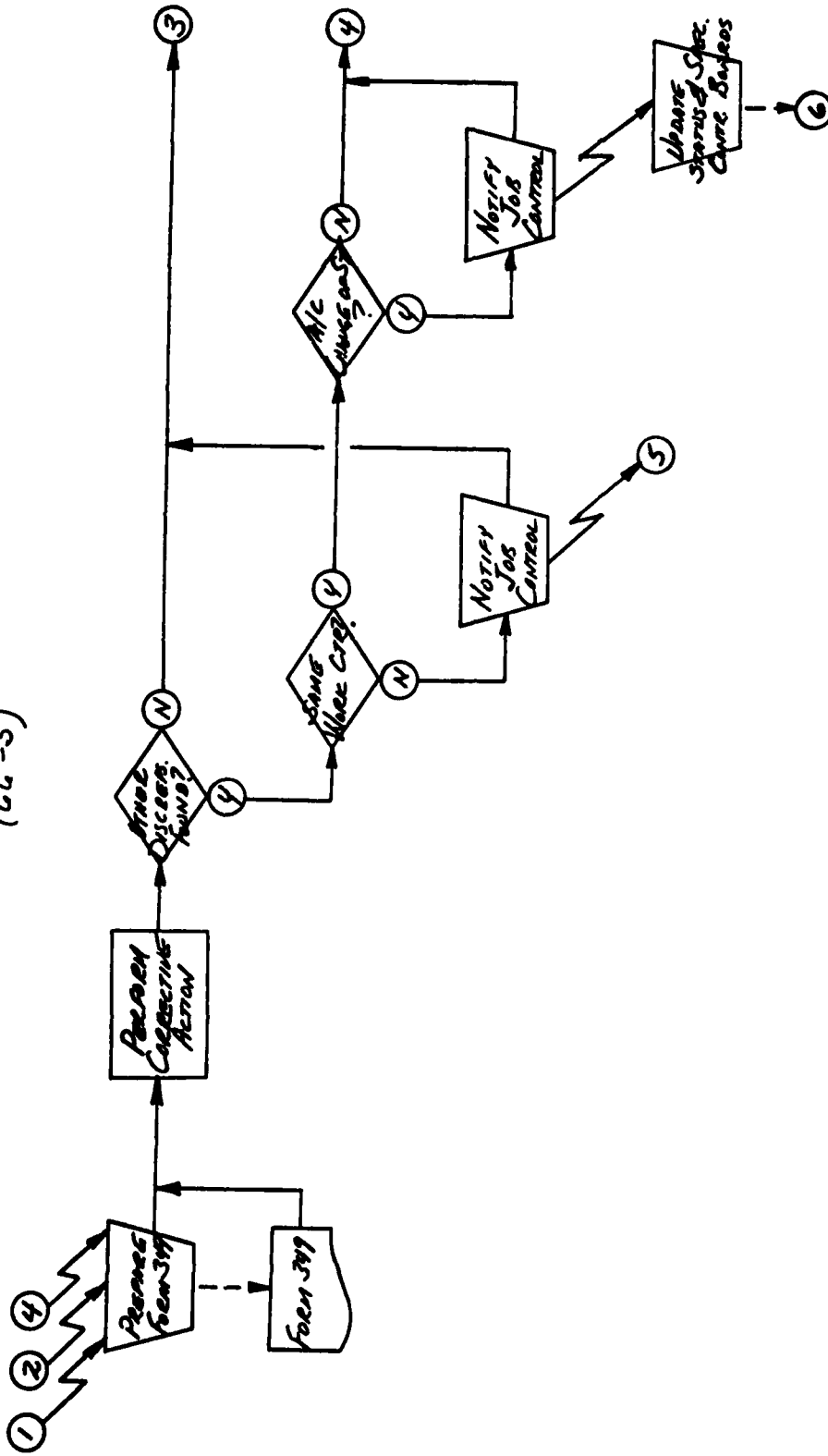
(DAILY P&S FORM 349 REVIEW)



JOB CONTROL

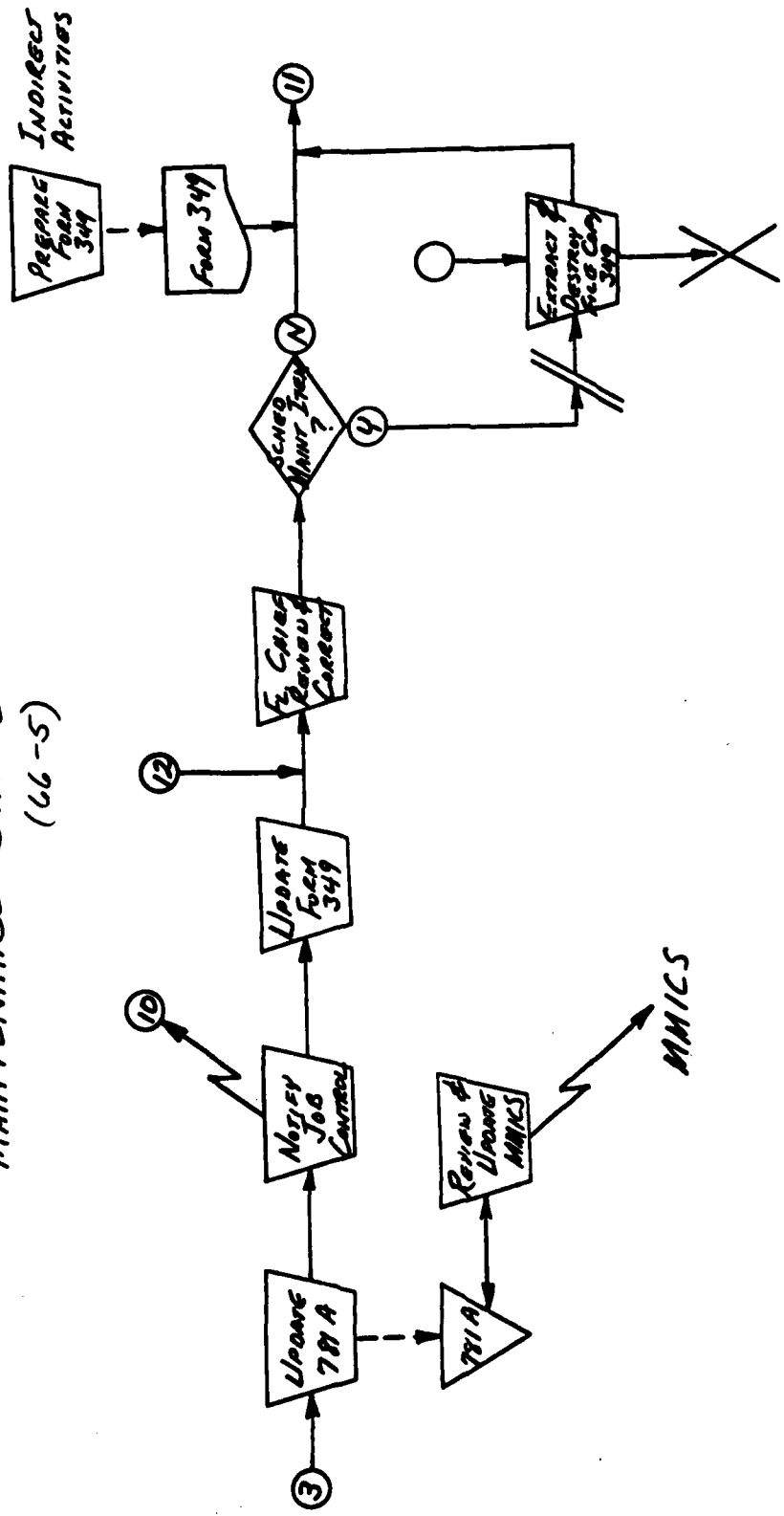
SYSTEMS FLOWCHART - 9

MAINTENANCE DATA COLLECTION SYSTEM
(66-5)



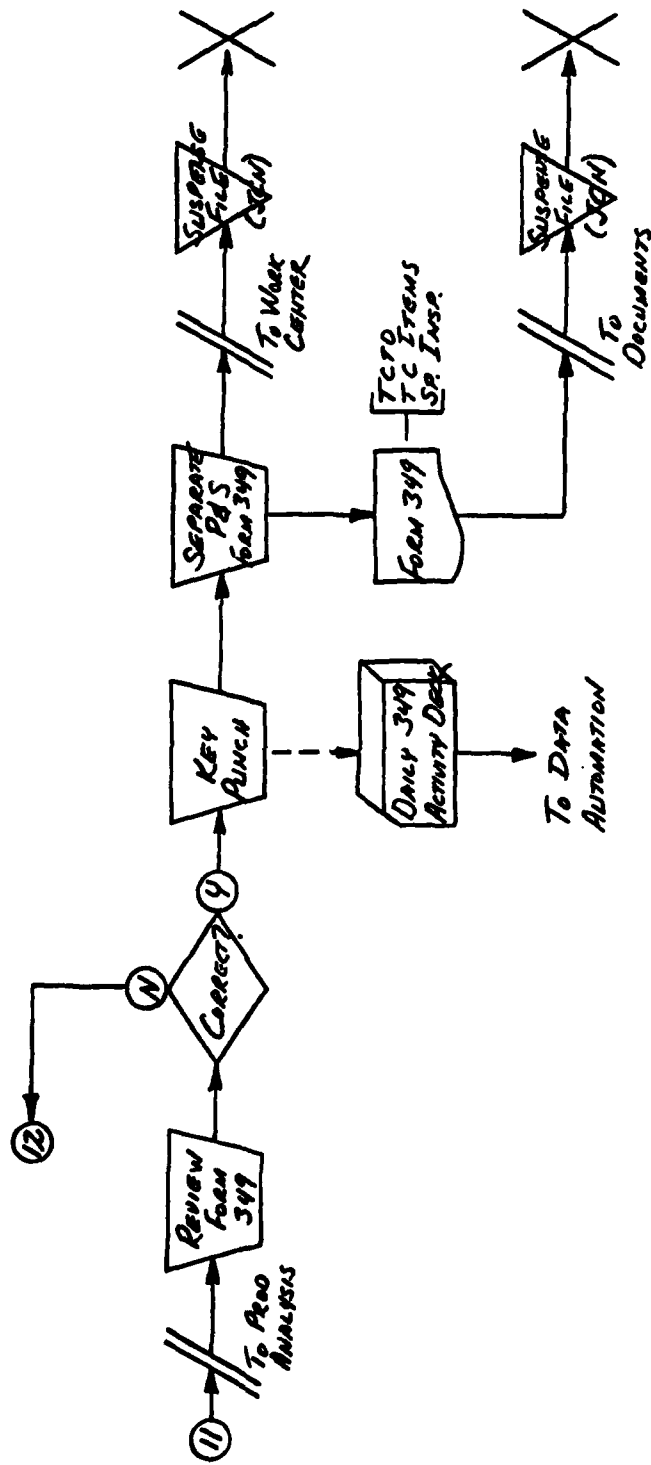
WORK CENTER

SYSTEMS FLOWCHART-10
 MAINTENANCE DATA COLLECTION SYSTEM
 (66-5)



WORK CENTER

SYSTEMS FLOWCHART - 11
 MAINTENANCE DATA COLLECTION SYSTEM
 (66-5)



PRODUCTION ANALYSIS

1981 USAF - SCEEE SUMMER FACULTY RESEARCH PROGRAM

Sponsored by the

AIR FORCE OFFICE OF SCIENTIFIC RESEARCH

Conducted by the

SOUTHEASTERN CENTER FOR ELECTRICAL ENGINEERING EDUCATION

FINAL REPORT

SUPERCONDUCTING PAIR BINDING ENERGY IN DEGENERATE FERMI SYSTEMS

Prepared by: Dr. David W. Allender
Academic Rank: Associate Professor
Department and University: Department of Physics
Kent State University
Research Location: Air Force Wright Aeronautical Laboratories, Avionics
Laboratory, Electronics Research Branch
USAF Research Colleague: D. C. Reynolds
Date: August 10, 1981
Contract No: F49620-79-C-0038

SUPERCONDUCTING PAIR BINDING ENERGY

IN DEGENERATE FERMI SYSTEMS

by

David W. Allender

ABSTRACT

The binding energy of Cooper pairs in degenerate Fermi systems in one and three dimensions is examined as a function of the carrier density, the cut-off energy of the attractive interaction, and the momentum of the pair. It is found that when the cut-off energy is sufficiently small compared to the effective BCS interaction parameter, the binding energy as a function of momentum, q , has two relative maxima: one at $q = 0$ and one at q greater than twice the Fermi momentum in a one dimensional system. Thus a metastable state is predicted. Large momentum pairing in three dimensions is also examined. Results are related to experimental observations and recommendations are made for further research.

Acknowledgement

The author would like to sincerely thank the Air Force Systems Command, the Air Force Office of Scientific Research and the Southeastern Center for Electrical Engineering Education for their support which enabled him to spend this past summer at the Air Force Wright Aeronautical Laboratories, Wright-Patterson Air Force Base, Dayton, Ohio. A special debt of gratitude is owed to P. E. Stover, Branch Chief of the Electronics Research Branch of the Avionics Laboratory; to D. C. Reynolds, and to S. B. Nam. Their efforts, support, and encouragement have made this research possible.

I. INTRODUCTION

Ever since the discovery of superconductivity by Kamerlingh Onnes in 1911, physicists have continued to search for new and different materials which exhibit this effect. Of particular interest has been the search to observe the phenomenon at increasingly high temperatures. This search has led to the observation in recent years of some highly unusual behavior in samples of quenched CdS¹ and CuCl² under high pressures. The effect is present at liquid nitrogen temperatures (i.e. 77K). The Air Force, as well as the Army, has carried out experiments on these materials and is interested in elucidating the nature of the cooperative behavior in such materials, while it must be noted that it is still unsettled and speculative whether the behavior is related to actual superconductivity or not.

The author's past experience in studying, from a theory standpoint, the possibility of unusual mechanisms of superconductivity, coupled with the Air Force's interest in these materials made our collaboration a natural one.

II. OBJECTIVE

The primary objective of the research was discussed by D. C. Reynolds and the author during a visit which occurred last spring. It was agreed that the objective would be to extend the theory of superconductivity³ in an attempt to explain the behavior of CdS and CuCl. During the course of the summer, this objective was further refined and better defined, resulting in a concise statement of the problem to be solved: examine the stability of Cooper pairs in degenerate Fermi systems as a function of three variables - 1) the cut-off energy, ω_c , characteristic of the attractive interaction between carriers, 2) the Fermi momentum, k_F , describing the density of carriers, and 3) the momentum, q , of the pairs.

The remainder of this report details how this study was carried out and presents the results.

III. CALCULATIONS

Our starting point is the binding energy equation⁴,

$$1 = v_{BCS} \sum_k \frac{1}{(\omega + \epsilon_1 + \epsilon_2)} \quad (1)$$

where $\epsilon_{1,2} = (\frac{1}{2} q \pm k)^2/2m - k_F^2/2m$, and ω is the binding energy

with $k_F < |\frac{1}{2} q \pm k| < K_F = (2m \omega_c + k_F^2)^{1/2}$.

To carry out the integration of Eq. (1), it is convenient to consider six separate regions on the $k_F - q$ plane. These six regions are shown in Fig. 1.

In one dimension, we find, by integrating Eq. (1),

$$1/K_5 = F_1 = (1/2K_6) \ln[(K_1 - K_6)(k_2 + K_6)/(K_1 + K_6)(k_2 - K_6)],$$

for $q \leq K_F - k_F, 2k_F$;

$$1/K_5 = F_2 = 0, \text{ for } K_F - k_F \leq q \leq 2k_F;$$

$$1/K_5 = F_3 = (1/K_7) \{ \tan^{-1}(K_1/K_7) - \tan^{-1}(k_1/K_7) - \tan^{-1}(k_2/K_7) \},$$

for $2k_F \leq q \leq K_F - k_F$;

$$1/K_5 = F_4 = (1/K_7) \tan^{-1}(-k_1/K_7), \text{ for } K_F - k_F \leq q \leq K_F + k_F;$$

$$1/K_5 = F_5 = (1/K_7) \tan^{-1}(K_1/K_7), \text{ for } K_F + k_F \leq q \leq 2K_F;$$

$$1/K_5 = F_6 = 0, \text{ for } 2K_F \leq q; \quad (2)$$

where $K_5 = mV_{BCS}/\hbar$, $K_1 = K_F - q/2$,

$$k_1 = k_F - q/2, \quad k_2 = k_F + q/2,$$

$$K_6^2 = k_F^2 - m \omega - q^2/4 = -K_7^2$$

By studying the functions F_1 , one finds the desired objectives. These results are illustrated in Fig. 1. For the case of $q = 0$, we find that the binding energy of a zero-momentum pair decreases as carrier density increases. On the other hand, we find that the binding energy in region 4 increases as q increases for given k_F and ω_c ,

$$(d\omega/dq)_{k_F, \omega_c} > 0, \text{ for } k_m \leq k_F \leq k_M, \quad (3)$$

near $q \geq 2k_F$, but in region 5, for all q ,

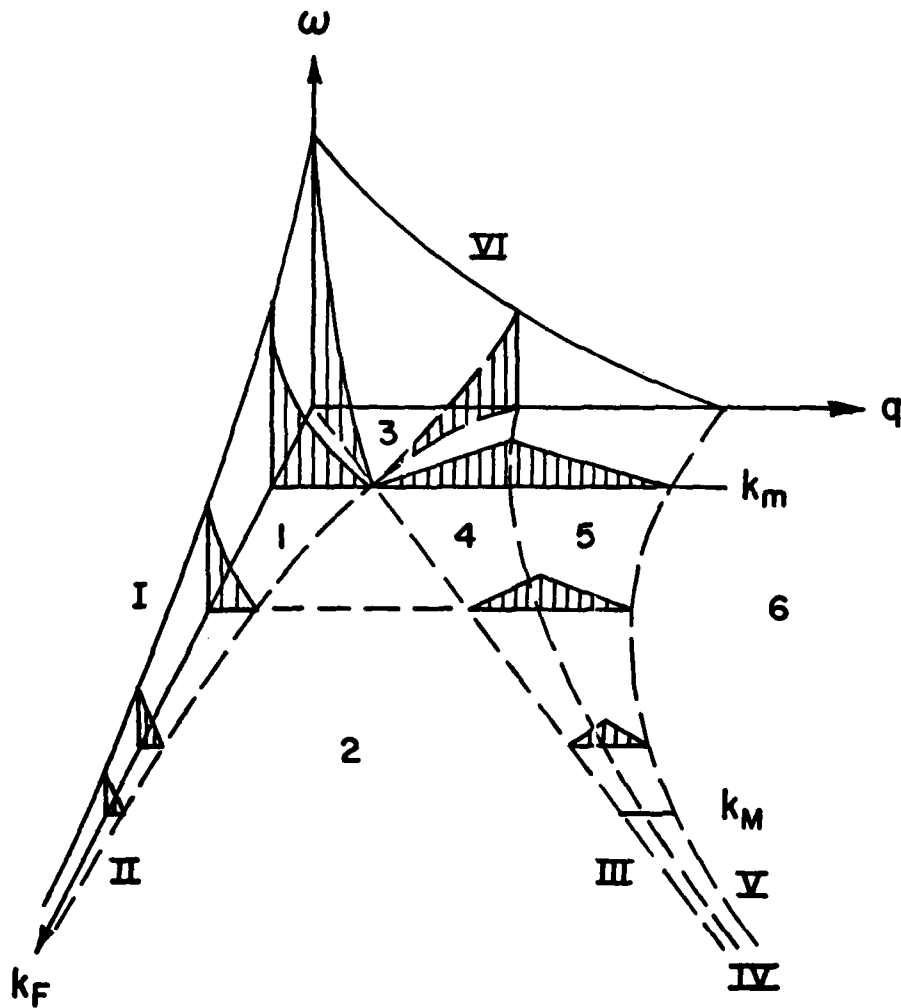


FIGURE 1 - THE BINDING ENERGY OF A PAIR OF CARRIERS IN A ONE DIMENSIONAL SYSTEM, AT FIXED ω_c .

$$(d\omega/dq)_{k_F, \omega_c} < 0. \quad (4)$$

Thus, pairs which have some value of q between $2k_F$ and $2K_F$ have a relative maximum binding energy. The binding energy of a pair in region 4 is found to decrease with respect to k_F , and to vanish at $k_F = K_M = K_S/2$ as shown in Fig. 1. Now the condition for having two regions of q where pairs have finite binding energies is simply given as $K_F - k_F \leq 2k_F$, or $k_F \geq k_m = (m\omega_c)^{1/2}/2$.

For the three dimensional system, we carry out the same calculations as in the one dimensional case. The results are shown in Fig. 2. One can get the corresponding functions F_i in the six separate regions of the $k_F - q$ plane. The condition for a pair of $q \geq 2K_F$ having a finite binding energy is determined from the corresponding function F_3 in the limit $\omega \rightarrow 0$ and $k_F \rightarrow 0$,

$$F_3 = 2K_0 = x^{1/2} - \frac{1}{2} q - \frac{1}{2} \pi q - (x/q) \ln\{1 - q(x^{1/2} - \frac{1}{2} q)/x\}, \quad (5)$$

where $x = 2m \omega_c$.

This equation has a solution for q only when $\omega_c \geq K_0^2/2m$.

For pairs with $q \leq 2k_F$, the upper bound of q for pairs having finite binding energies is determined from the corresponding functions F_1 and F_2 in the limit $\omega \rightarrow 0$. We find

$$\begin{aligned} F_1 = 2K_0 &= K_F - k_F - q - (x/q) \ln(1 - qK_1/x) \\ &\quad + k_0 \ln\{x - qK_1\} (k_2 + k_0)^2 / (qk_2)(K_1 + k_0)^2\}, \\ F_2 = 2K_0 &= (x/q) \ln 2, \end{aligned} \quad (6)$$

where $k_0 = (k_F^2 - q^2/4)^{1/2}$.

From the above equation, we find the upper bound of q for pairs having finite binding energies is

$$q \leq q_1 \text{ for } k_F \leq K_A - q_c \text{ and } q \leq q_c \text{ for } k_F \geq K_A - q_c, \quad (7)$$

where q_1 is a solution from F_1 as shown in Fig. 2.

In this case, for given k_F , the pair has a finite binding energy in one region $q < q_1, q_3, q_4, q_5, q_c$, where q_i are determined from the corresponding functions F_i in the limit $\omega \rightarrow 0$. All q_i are less than q_c . In particular, we

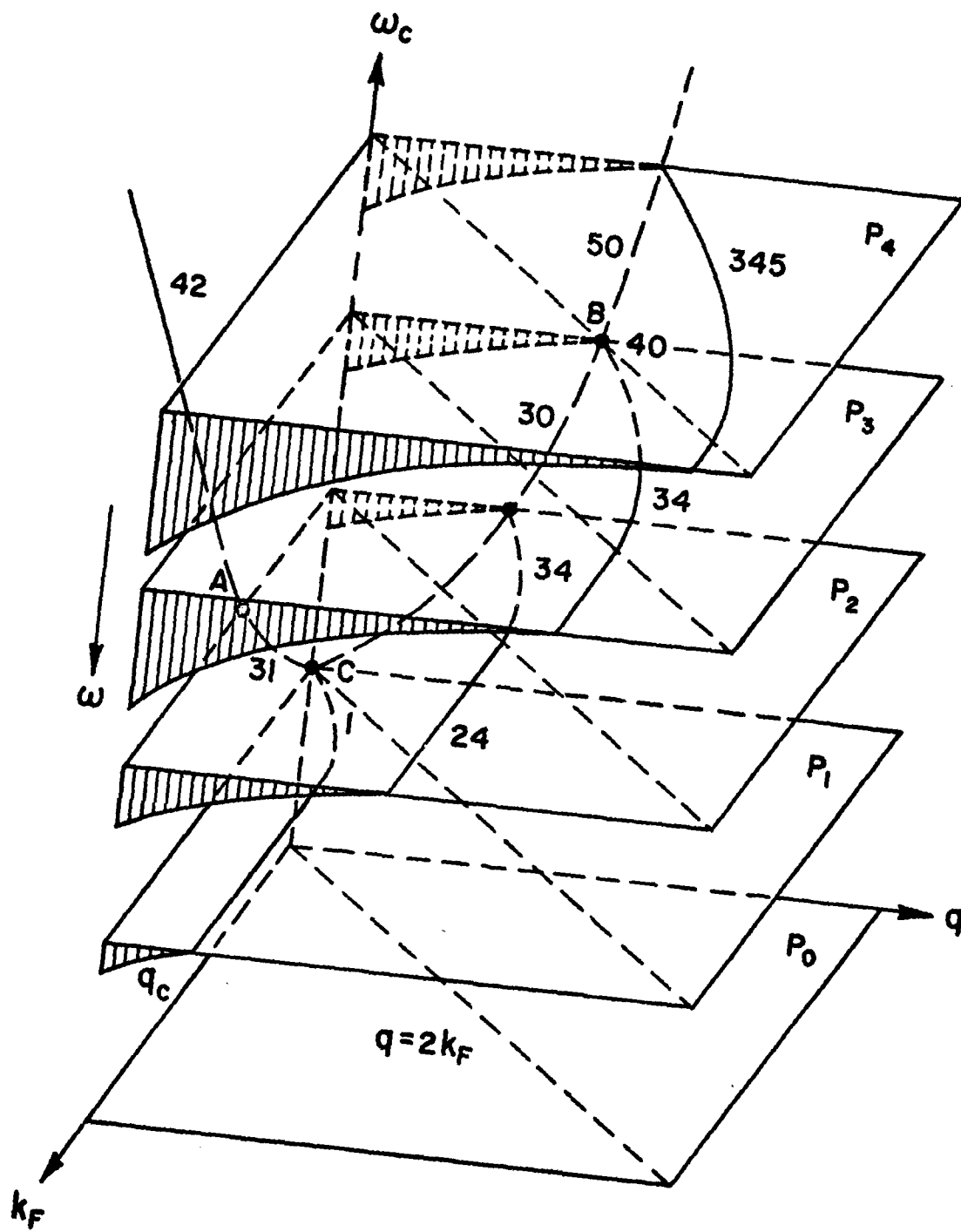


FIGURE 2 - THE BINDING ENERGY OF A PAIR OF CARRIERS IN THE THREE DIMENSIONAL SYSTEM.

find that for given k_F and ω_c the binding energy of a pair decreases as q increases as shown in Fig. 2. The binding energy goes to zero as q reaches the upper bound with a zero slope with respect to q .

We conclude that in a one dimensional system a pair of carriers with momentum $q > 2k_F$ can be locally stable, or metastable. The material parameters required to permit the occurrence of such pairs appear to be not very restrictive. Therefore, these pairs would play a role in quasi-one dimensional materials such as organic superconductors and superconducting polymers. Furthermore, it is very interesting to note that filamentary structures have been observed in high pressure quenched CdS⁵, and CuCl, and CuBr⁶ under high pressure, which are suggestive of quasi-one dimensional behavior.

However, in the three dimensional case, the condition to have pairs of momentum $q \geq 2k_F$, namely $\omega_c \geq K_0^2/2m$, is unlikely to be met for ordinary metals where the cut-off energy is determined by phonon frequencies. On the other hand, for degenerate semiconductors, the Fermi momentum may be sufficiently small so that the required condition might be satisfied.

IV. RECOMMENDATIONS

The work that has been carried out predicts that Cooper pairs having momentum greater than twice the Fermi momentum are metastable when the cut-off energy is sufficiently less than the effective BCS interaction constant. This result was unexpected and exciting, so a manuscript was prepared by S. B. Nam and the author and submitted for publication to a professional journal. Although we feel that significant progress has been made, we also feel that it is only a beginning and that this work should be continued and extended. Specifically, the following recommendations are made.

- (1) The equations for the superconducting energy gap, Δ , ought to be generalized to include the effect of the predicted metastable, large momentum pairs. Studies should be done to determine the resultant transition temperature, T_c .
- (2) Recently some investigators⁷ have suggested that negative U centers ought to be important in determining the effective BCS coupling constant in materials like CdS and CuCl. It therefore appears to be appropriate to incorporate the effect of U-centers into the equations mentioned in the previous recommendation.

- (3) Various properties, such as the magnetic susceptibility, should be calculated in order to carry out a comparison with experimental observations.
- (4) The consequences of having degenerate bands, permitting inter-band as well as intra-band pairing should be examined. (This work has already begun.)

The author hopes to continue to participate in carrying out these recommendations by submitting a proposal for a mini-grant to AFOSR on the subject.

REFERENCES

1. E. Brown, C. G. Homan, and R. K. MacCrone, Phys. Rev. Lett. 45, 478 (1980). C. G. Homan, and R. K. MacCrone, J. Non-Crystalline Solids, 40, 369 (1980). C. G. Homan, D. K. Kendall, and R. K. MacCrone, Solid State Comm. 32, 521 (1979).
2. C. W. Chu, A. P. Rusakov, S. Huang, S. Early, T. H. Geballe, and C. Y. Huang, Phys. Rev. B 18, 2116 (1978); and T. H. Geballe and C. W. Chu, Comments Solid State Phys. 9, 115 (1979).
3. J. Bardeen, L. N. Cooper, and J. R. Schrieffer, Phys. Rev. 108, 1175 (1957).
4. J. R. Schrieffer, Theory of Superconductivity (W. A. Benjamin, Inc. Press, New York, 1964) p33.
5. S. B. Nam, Y. Chung, and D. C. Reynolds, (unpublished) have observed the filamentary structures in high pressure quenched CdS.
6. S. Ves, D. Gloetzel, M. Cardona, and H. Overhof, preprint.
7. C. S. Ting, K. L. Ngai, and C. T. White, Phys. Rev. B 22, 2318 (1980).

1981 USAF - SCEEE SUMMER FACULTY RESEARCH PROGRAM

Sponsored by the

AIR FORCE OFFICE OF SCIENTIFIC RESEARCH

Conducted by the

SOUTHEASTERN CENTER FOR ELECTRICAL ENGINEERING

FINAL REPORT

SOFTWARE FOR RAPID 3-D MAPPING OF AN ARBITRARILY-COMPLEX OBJECT

Prepared by:	Dr. Martin D. Altschuler
Academic Rank:	Research Professor
Department and University:	Department of Radiation Therapy Hospital of the University of Pennsylvania
Research Location:	School of Aerospace Medicine Brooks Air Force Base
USAF Research Colleagues:	Mr. Bruce Montague Lt. Col. (Dr.) Bruce R. Altschuler
Date:	August 1, 1981
Contract No.:	F49620-79-C-0038

1/1/83

SOFTWARE FOR RAPID REMOTE 3-D MAPPING OF AN
ARBITRARILY-COMPLEX OBJECT

by

Martin D. Altschuler

ABSTRACT

The development of interactive software for dependable remote nondestructive 3-D surface mapping of an arbitrarily-complex object in real time is well under way. Hardware/software techniques and trade-offs have been investigated for the rapid (in parallel) laser illumination, imaging, and triangulation of 16,000 points of an unknown surface. To produce an operational device for real-time anthropometric measurement (for example, to measure real-time changes in human-body anatomy and work motions in a zero-gravity space environment) requires developing, implementing, testing, and packaging optimal algorithms for (1) multi-directional laser-array illumination, (2) multi-directional imaging, and (3) rapid dependable calibration of cameras and laser arrays. Needed resources are an interactive raster graphics facility and a compatible host computer. If funding is available, an operational real-time surface mapping system can be produced within two years.

Acknowledgement

I would like to thank the Air Force Office of Scientific Research and the Southeastern Center for Electrical Engineering Education for the opportunity to spend the summer working with top-notch people at the USAF School of Aerospace Medicine, Brooks AFB, Texas. In particular, I am indebted to Col. R. DeHart the school commander for his full support, to Dr. B. Hartman for his efficient administration, to the librarian and staff of the Aerospace Medical Library, to Dr. H. Hughes the chief of the USAFSAM Computer Division, and to the entire staff of the USAFSAM computer operations for their cheerful efficiency and continual assistance. One man, Mr. Bruce Montague, worked with me long hours day and night to guide me through the subtleties and potentialities of the DEC operating system. I am also indebted to my colleague Dr. B. Altschuler (USAFSAMNGD) for hours of augmentation concerning the best hardware/software image processing methods to extract geometric information from laser reflection images. I performed this work without salaried compensation and received only reimbursement for expenses, as agreed.

I. INTRODUCTION:

Since 1977 I have been working informally with USAFSAMNGD to develop a technology for rapid remote high-resolution 3-D numerical mapping of unknown arbitrarily-complex surfaces¹⁻⁴. Such a technology would allow real-time measurement of biomedical surfaces, in particular measurement of changes and distortions of the human body under high-gravity or zero-gravity forces. Other potential applications are: the rapid mapping of facial, dental, and limb topography for automated manufacturing of prostheses; anatomical documentation for surgery and radiation therapy; and real-time environmental mapping to assist the blind⁵. Industrial applications would include assembly-line inspection and control, computer-aided manufacturing, robot vision, mapping of machine parts and castings, etc.

The technique we developed determines the spatial locations of 128 x 128 sample points on a surface. The procedure involves (1) optically transforming a single laser beam into an array of 128 x 128 individual laser beams, (2) illuminating the surface of interest with this array of 128 x 128 (simultaneous) laser beams, (3) using a programmable electro-optic modulator to switch on and off very rapidly specified subsets of laser beams and thereby to illuminate the surface of interest with a rapid sequence of mathematical patterns (spacecode), (4) image recording each of the mathematical patterns as they reflect off the surface using (a) a wavelength-specific optically-filtered video camera positioned at a suitable perspective angulation and (b) appropriate image memory devices, (5) analyzing the stored images to obtain the 3-D locations of each of the 128 x 128 illuminated points on the surface which are visible to the camera or imaging device, (6) determining which of the laser beams in the array do not provide reflections visible to the imaging device.

Spacecoding of the light beams allows automatic correlation of the camera image (of the spot pattern reflected by the surface) with the projected laser-beam array, thus enabling triangulation of each illuminated surface point. Whereas ordinary laser rangefinders aim and project one

laser beam at a time and expect to receive one laser-beam reflection (bright-dot image) at a time, the present system is optical (non-mechanical and vibration-free) and collects all the data needed for high-resolution 3-D topographic mapping (of the 128 x 128 sample surface points) with the projection of as few as $1 + \log_2 128 = 8$ light patterns. In some applications involving a rapidly-changing time-dependent environment, these eight light patterns can be projected simultaneously in different wavelengths to allow virtually instantaneous data collection for a surface topography.

Conceptually, the laser-beam array acts as a reverse (or inverse) camera, with rays emanating from a focus and diverging out into the scene. Thus the technology we are developing can be viewed mathematically as a form of stereophotogrammetry, but now there are one active and one passive camera rather than two passive cameras. The active/passive system allows automatic stereo correlation and triangulation of many points in the passive image at the same time. The mathematical ideas have been discussed in detail in the references¹⁻⁵.

By May 1981, the beginning of the AFOSR/SCEEE summer faculty contract, the hardware and software were sufficiently developed to permit us to step through the surface mapping technique from data acquisition to 3-D numerical results. Although everything apparently worked correctly, including the rapid interactive calibration scheme, the need for several improvements was already becoming apparent. For example, my initial software used a global threshold to filter out unwanted noise (background reflections and ambient light). As a result, intense noise (background laser reflections) seen in some areas of the raster (passive) image exceeded the global threshold and could not be filtered out, whereas faint signal (from laser-illuminated space points) was filtered out (see discussion of objective 2 below).

An additional problem we faced in May 1981 was that the data collection camera, the data (digitizing) processor, the main processor, and the graphics display processor were all using different operating systems

and/or locally-developed systems languages. This situation arose because limited funding required purchasing the least expensive hardware, with little regard for software compatibility, and then implementing improvised interfaces.

II. OBJECTIVES:

When the opportunity of the AFOSR/SCEEE award for the summer of 1981 became available, I decided to use the time to work with USAFSAMNGD to achieve the following objectives:

- (1) Modify the higher-level software to be compatible with the widely-used DEC RSX-11M operating system (hence also with the VAX-VMS operating system).
- (2) Replace the arbitrary global threshold for pixel gray levels with local thresholds determined automatically.
- (3) Implement local thresholding and other image processing with a graphics display processor.
- (4) Fragment the software into a sequence of independent programs linked only through data files on a disk.
- (5) Allow the software options to be controlled simply and interactively by a physician (or operator) who does not have special training in software languages.

The reasons for these objectives are now described in turn.

Objective 1:

The DEC RSX-11M operating system was chosen for use in all further development of the biomedical surface mapping project. The reasons for this choice were (1) the in-house availability of DEC hardware by those researchers involved in the project, (2) the ability to use RSX-11M on several different DEC computers (in particular the LSI 11-23, PDP 11-34, PDP 11-70), (3) the upward compatibility of the RSX-11M with the (DEC) VAX-VMX operating system, so that software developed on RSX-11M can be run without further development on a VAX, (4) the widespread availability, support, and documentation of the RSX-11M system, and (5) the proven dependability of the system.

Objective 2:

The global threshold algorithm to distinguish the images of the laser beam reflections from the images of the ambient light background in the raster (TV) camera was not completely satisfactory. Although the brightest pixels seen in the raster image did correspond to laser-beam reflections from the surface of interest, it was nevertheless possible for unwanted ambient light and background reflections to appear brighter in the raster image than actual laser beams reflected from a surface whose normal was inclined significantly relative to the direction of the TV camera. Thus a global threshold value could not detect the raster image locations of all the laser beam reflections without also detecting background reflections and ambient light. This meant that noise separation would require manual preprocessing (an operator to work interactively with the graphics display to separately threshold each image region before data processing) or manual postprocessing (setting a low global threshold and letting the user manually separate the good results from the bad).

Objective 3:

At the time the AFOSR/SCEEE contract began, the image processing software was being implemented by the main CPU. Each digitized image was transferred (one raster line at a time) from the disk memory to the CPU, processed, and transferred back to the disk. Several minutes were required per image for each of the eight images. Almost all this time was spent transferring data between disk and CPU. Since most of the image processing (adding or subtracting images and masks) involved simple arithmetic operations repeated for each of the 256 x 256 pixels in each of the raster images, it should speed up the software implementation considerably if we perform the image processing in a display processor which can store several complete images and do the simple operations of image processing in parallel --- essentially a whole image at a time.

Objective 4:

The software development of the biomedical surface mapping involves a number of logically separate tasks. These include (1) specifying the physical parameters of the camera and shutter, (2) obtaining the scene-to-raster (TV image) transformation, (3) obtaining the scene-to-shutter

(laser-beam-array) transformation, (4) processing a set of digitized images to determine thresholds (local or global), the spacecode, filters, etc., (5) obtaining the numerical 3-D locations of the 128 x 128 sample points, (6) processing the 3-D sample point locations to achieve specific application goals and output displays.

To develop large multi-task software systems, one can structure each task as a subroutine (procedure) in a large program and use overlaying to manage the CPU core memory, or else one can write a separate program for each task, use the operating system command language to chain the sequence of programs, and use disk files to hold the intermediate results generated by each program. During the stages of logical design, algorithm development, algorithm implementation, and testing, the latter method of completely independent programs communicating through data files is most efficacious. Only the input and output of each program module need concern the developer. Thus software debugging, modifications, and testing can be done quickly and without chain reaction.

Objective 5:

Most users of the surface mapping software will not know the particular programming language or operating system in which the system is implemented. Consequently, it is often convenient to transfer the necessary information for a surface mapping task by having the computer interactively interrogate the user in simple English. The individual programs can request numerical information from the user for the parameters and for the calibration of the system. (Interactive capability is particularly important in the calibration phase when the user defines the three-dimensional coordinate system by a raster graphics display of a known block inserted into the scene.) The operating system on the other hand can request from the user the status of the project and enable the proper sequence of programs to be run.

III. APPROACHES AND RESULTS

Objective 1 --- to modify the surface mapping software for compatibility with the DEC RSX-11M operating system --- was accomplished. The previous software, which runs on a Data General Eclipse S-200, was modified for the DEC system. Some of the programs that ran on the Eclipse, however, did not fit on the PDP 11-34 and had to be fragmented into smaller programs (see also objective 5 below).

Objectives 2 and 3 --- to replace global thresholding for pixel gray levels with automatic thresholding of each pixel, and to implement this thresholding together with other image processing on a graphics display processor --- were investigated theoretically and a new hardware/software design was conceived. By adding an extra light pattern to the spacecode illumination sequence, we can determine for each raster pixel the difference in gray level intensity between the on and off states of the laser beam array. This change of gray level intensity can provide a local threshold for each pixel. Once the local threshold is known, the sequence of spacecoded images can be processed to obtain a spacecode for each pixel.

The new illumination pattern is the reverse of the on-off-on-off ... shutter pattern in the spacecode illumination sequence. Thus those pixels of the raster image which do not contain a laser-beam image would show only a small relative change of gray-level intensity when the laser beams are turned on and off. Such background pixels could then be eliminated by another criterion based on thresholding relative changes of gray level intensity. In this way, we can improve the detection of the coded laser-beam reflections in the image and distinguish them from background (noise) reflections.

Because the display processor works in parallel (virtually on an entire image at a time) and is so much faster than transferring digitized images between CPU and disk, it is faster and more reliable to detect the laser reflections in the image after determining the spacecode at each pixel. Thus whereas at present we transfer image data between disk and CPU, determine the peaks (highest gray levels) in the image, use a global threshold to remove those peaks due to background reflections, and then

find the spacecode for the bright peaks of the laser-beam reflections, we can with the new concept use the display processor and an extra image in the spacecode illumination sequence to determine the local threshold of each pixel of the image, determine the spacecode at each pixel, and finally, with another criterion, eliminate the background. The new approach uses the display processor and its image memories to do in parallel (and in a few seconds or less) the simple operations which threshold, spacecode, and detect the relevant laser reflection peaks in the image. Moreover, as mentioned earlier, local thresholding should improve the likelihood of detecting real but faint laser-beam images in the overall raster image. The design for the new hardware/software system was accomplished during the AFOSR/SCEEE contract in collaboration with USAFSAMNGD.

Objective 4 --- to fragment the surface mapping software into a sequence of independent programs linked only through data files on a disk --- was achieved during the AFOSR/SCEEE contract. The logically independent tasks of surface mapping were separated into different programs or sets of programs each of which reads the data files created by previous programs in the sequence and creates a file for the next program. These files document intermediate results of the surface mapping procedure (such as parameter values, calibration points, transformation matrices, etc.) and allow interruption and restart of the procedure at several stages. The precise sequence of programs is determined interactively by the user through the system command language. Different program sequences can be generated depending on how much information has been previously calculated and stored on intermediate files. For example, for a single viewing direction the calibration need be done only once; unknown objects can then be placed in the field of view and mapped.

The independent tasks of the software are:

Task 1: Parameter file generation (1 program, 4 subroutines)

EITHER

Accept old parameter file name and verify its existence;

Check the validity of the parameter values on file.

OR

Accept new parameter file name;

Accept new parameter values for laser-beam array and raster (TV) image;
Check the validity of the parameter values;
Create new parameter file.

Switch: If calibration is already on file, go to task 5.

Task 2: Interactive calibration data (1 program, 2 subroutines)

Display known calibration object;

Use trackball or joystick to record the raster image position of each of
six known points of the calibration object;

Enter the 3-D (x,y,z) position of each of the six points. (This procedure
in effect defines the 3-D coordinates of the scene);

Generate a file for the scene and image positions of the six calibration
points.

Task 3: Scene-to-image transformation matrix (1 program, 10 subroutines)

Read the file of task 2;

Calculate the T_{ij} parameters¹⁻⁵ for the scene-to-image transformation;

Calculate the focal distance for the imaging camera;

Generate a file for the calculated results.

Task 4: Scene-to-shutter (laser beam array) transformation matrix (2 programs,
9 and 11 subroutines)

Read data files of previous tasks;

EITHER

Individually project six laser beams of the array onto the calibration
object;

Calculate the 3-D (x,y,z) locations of the beam intersections with the
known calibration object;

Calculate the L_{ij} parameters¹⁻⁶ for the scene-to-shutter transformation;

Generate a file for the calculated results.

OR

Project a sequence of spacecoded images onto the calibration object;

Obtain spacecodes and raster positions of each laser reflection;

From known surfaces of calibration block, calculate the 3-D (x,y,z) positions
of each laser-illuminated point in the scene;

Use least-squares to determine the L_{ij} values;

Generate a file for the calculated results.

Task 5: Regular mapping run for unknown object (1 program, 8 subroutines)

Read in results of previous files;

Read in digitized data for spacecoded image sequence of unknown object;

Calculate set of (x,y,z) positions (3-D) for each laser-beam intersection with the unknown object whose image is visible on the raster image;

Methods: At present, only a global thresholding algorithm is

implemented for detecting laser-beam reflections in the image.

As discussed earlier (objectives 2 and 3), this algorithm will be replaced by a local thresholding algorithm.

One calibration is needed for each (laser-camera) perspective. An additional camera can be added and automatically calibrated without user interaction provided there is some overlap of the field of view with that of the first camera. (This follows because the 3-D locations of several points on a surface can be determined by triangulating with the laser-beam array and the first camera.)

During the AFOSR/SCEEE contract period, there was insufficient time to set up the interactive raster graphics. No in-house interactive raster graphics and display processor was available. A Grinnell display processor was loaned by the company and installed only two weeks before the end of the contract period. The display processor configuration did not seem to be compatible with that described in the documentation and no useful images could be processed. Consequently those (three) software modules which required interactive raster graphics (and which previously ran on an Eclipse S-200 with a Comtal display processor) have not yet been transferred to the DEC PDP 11-34. However, the other software modules were successfully tested on the DEC computer by inserting numerical values previously obtained on the Eclipse/Comtal system. Completion of the DEC-compatible software system requires the testing of only three modules with an operational interactive raster graphics display processor.

Objective 5 --- to set up an interactive language which would allow lay users (medical personnel, technicians, etc.) to operate the surface mapping procedure without special training in computers --- was achieved

during the AFOSR/SCEEE contract. The different programs are now linked through the operating system command language. After each program is run, the command language asks the user if he wants to continue or exit. The user can exit after certain disk files are created and later resume at that point (after the program verifies the parameter file).

The first program asks the operator to provide a project name. It then (task 1) creates and/or recalls the parameter file and verifies the validity of all the parameters. All data files related to the project are named automatically by appending letters to the project name. Thus bookkeeping by the user is eliminated. After the first (mandatory) program is completed and the parameter file either verified or shown to have errors, the command language provides the user a menu of options -- create a new parameter file, continue, or exit. Another menu then allows the operator to go directly to the calculation of the unknown surface (if calibration was done previously) or to the last program completed. Thus the user needs no more than a few minutes of instruction to learn to operate the system, and no knowledge of the DEC Fortran language or the operating system.

A small amount of training may be needed to use the interactive graphics for calibration. The interactive graphics module asks the user to locate six known calibration points on the viewing screen with a trackball or joystick. The user must then enter the 3-D coordinates of each known point by the keyboard.

IV. RECOMMENDATIONS:

During the AFOSR/SCEEE contract period, previously-tested software for biomedical surface mapping was fragmented into DEC-compatible user-interactive software which can be operated by non-experts in computers. The software developed up to now, however, provides only a feasibility study of the surface mapping technique. It demonstrates that the basic mathematics, the spacecoding, the triangulation of many points at the same time, and the simple calibration procedure all work as expected.

The task now is to produce a truly operational surface mapping device that works reliably in real time. For this development, better hardware and

software are required. The development of the hardware and software should be done concurrently and interactively to achieve the best trade-offs in speed, accuracy, and cost. As an example of this interaction, the concept of using an extra image in the spacecoding sequence together with a display processor for image analysis should provide a very significant increase in the speed of the surface mapping program as well as a significant improvement in separating laser peak images from noise reflections (see objectives 2 and 3).

Based on the feasibility studies so far accomplished, my general recommendations are as follows:

1. Begin the development of a truly operational surface-mapping system of the type described. With proper support, a device (hardware/software system) could be constructed within two years which would permit remote 3-D numerical mapping of 16,000 points of an unknown arbitrarily-complex surface in a few seconds, with data acquisition in real time (less than one second).
2. Permit the development of hardware and software to proceed interactively.
3. Provide interactive raster graphics capability to support the higher-level software development of the system.

Specific recommendations for follow-on research to develop software for an operational surface-mapping device are as follows:

1. Develop a phantom-generating software system that will allow generation of artificial data for use in simulating and testing new hardware/software methods in remote surface mapping.
2. Test the efficacy of different image-processing algorithms to determine the best way to extract information in parallel from many targets (laser beam images) in the image.
3. Develop and test algorithms for multi-camera/multi-laser systems to achieve integrated 3-D measurements of an object from all directions.
4. Develop and test algorithms for the generation of surface patches from the 16,000 measured surface sample points.

5. Develop and test application software, namely algorithms for anthropometric measurement and documentation of (1) real-time human body changes (surface and volume) in zero-gravity environment and/or under physiological stress and (2) long-term anatomical changes.

REFERENCES

1. M. D. Altschuler, B. R. Altschuler, and J. Taboada, "Measuring Surfaces Space Coded by a Laser-Projected Dot Matrix," SPIE, Vol. 182, Imaging Applications for Automated Industrial Inspection and Assembly, pp. 187-191, 1979.
2. B. R. Altschuler, J. Taboada, and M. D. Altschuler, "Laser Electro-Optic System for Three-dimensional (3-D) Topographic Mensuration," SPIE, Vol. 182, Imaging Applications for Automated Industrial Inspection and Assembly, pp. 192-196, 1979.
3. M. D. Altschuler, B. R. Altschuler, and J. Taboada, "A Laser Electro-Optic System for Rapid 3-D Topographic Mapping of Surfaces," *Medical Image Processing Group (S.U.N.Y. at Buffalo, Dept. of Computer Science)*, Technical Report No. MIPG 51, February 1981 (to be published in *Optical Engineering*, Nov.-Dec. 1981).
4. M. D. Altschuler, J. L. Posdamer, G. Frieder, B. R. Altschuler, and J. Taboada, "The Numerical Stereo Camera," SPIE, Vol. 283, 3-D Machine Perception, 1981, in press.
5. M. D. Altschuler, J. L. Posdamer, G. Frieder, M. J. Manthey, B. R. Altschuler, and J. Taboada, "A Medium-Range Vision Aid for the Blind," *Proc. International Conference on Cybernetics and Society (ISSN 0360-8913)*, pp. 1000-1002, October 1980.

1981 USAF - SCEEE SUMMER FACULTY RESEARCH PROGRAM

Sponsored by the

AIR FORCE OFFICE OF SCIENTIFIC RESEARCH

Conducted by the

SOUTHEASTERN CENTER FOR ELECTRICAL ENGINEERING EDUCATION

FINAL REPORT

ENHANCED SCENE RESOLUTION: 2-D SPECTRAL ESTIMATOR APPROACHES

Prepared by: Dr. A. A. (Louis) Beex
Academic Rank: Assistant Professor
Department and University: Department of Electrical Engineering
Virginia Polytechnic Institute and State University
Research Location: Rome Air Development Center
Surveillance Division
Surveillance Technology Branch
Signal Processing Section
USAF Research Colleague: Mr. Paul Van Etten
Date: August 21, 1981
Contract No: F49620-79-C-0038

ENHANCED SCENE RESOLUTION: 2-D SPECTRAL ESTIMATOR APPROACHES

by

A.A. (Louis) Beex

ABSTRACT

In this report, an initial performance evaluation is presented for two modern spectrum estimators, used in the context of resolution enhancement in scenes with limited support. This is to identify the potential these methods may have in a practical environment.

The availability of limited sets of observations has spurred procedures for extending data beyond the observation limits, in order to defeat the classical Rayleigh resolution. The one-step extrapolator /2/ is one such approach, that is extended and implemented in the 2-D setting. The potential of this one-step extrapolator is demonstrated, but also the enormous sensitivity to any type of noise, which renders this particular extrapolation algorithm of low practical value.

A different approach is to assume a parametric model for the stochastic process that underlies the data. The 2-D autoregressive moving average (ARMA) model is rather general, and leaves one with a difficult parameter estimation problem. The difficulty of implementation pays off in a high resolution property for certain classes of signals, and a relative robustness in the presence of noise.

ACKNOWLEDGEMENTS

The author would like to thank the Air Force Systems Command, the Air Force Office of Scientific Research, Rome Air Development Center, and the Southeastern Center for Electrical Engineering Education for providing the opportunity to carry out the research described in this report.

Special acknowledgement is made to Mr. Paul Van Etten of RADC for discussions and guidance, which helped make the author's stay a worthwhile and instructive experience. Appreciation is also due to Mr. Haywood Webb, Mr. Russell Brown, and Mr. John Huss, all of RADC, for their most helpful discussions, software development, and logistical support.

My final commendation goes to Prof. Warren Peele for providing a well-organized program in which to participate.

I. INTRODUCTION

One of the most intriguing and important problems, in many different disciplines, is the recovery of signals that underwent some type of a distortion. Moreover, the observations of the distorted signal are often limited in scope. In the system identification discipline we are often interested in the input signal to a system, and have only the output of the system available for measurements. The limited scope of these measurements compounds the problem. Applications of tomographic imaging are another example. Here we try to reconstruct images from a limited number of its projections as in computerized X-ray tomography, or for nuclear reactor core examination.

Our specific problem originates in the physical setting of a space-based infrared sensor. Such a sensor consists of a Fourier transforming lens with a lightshade at the front end, and a photodetector array in its focal plane /4/. Such a physical setting warrants the assumption that the front end scene has a finite support. This continuous scene is transformed by the lens into its continuous Fourier transform. The latter has infinite support due to the limited support of the scene. The photodetector array then samples the continuous transform over a finite support. It is the latter operation which yields the data set from which the Air Force must draw inference on the front end scene with finite support. Let us identify the problem in mathematical terms.

If x denotes the front end scene with finite support S_x , and Y denotes the continuous Fourier transform over the infinite support S_y , the following relationship is valid:

$$y(f) = \int_{S_x} x(u) e^{-j2\pi f' u} du \quad \forall f \in S_y \quad (1)$$

Note that the respective variables are defined over 2-D fields. Substitution of the inverse Fourier transform relationship for $x(u)$, and subsequent interchange of integration operations, yields:

$$\begin{aligned}
 Y(f) &= \iint_{S_x S_y} X(v) e^{j2\pi v'u} dv e^{-j2\pi f'u} du = \\
 &= \int_{S_y} X(v) \int_{S_x} e^{-j2\pi(f-v)'u} du dv \quad \forall f \in S_y \quad (2)
 \end{aligned}$$

The support of the front end scene is not only limited, but also known, and the inner integral in (2) can be evaluated analytically. This yields the kernel $h(f-v)$ of the linear integral operator \mathcal{L} on $X(v)$, which results in $Y(f)$. As our knowledge of $Y(f)$ is limited to its samples over the data region, say S_d (where S_d is a subset of S_y with finite support), we find from (2):

$$Y(f) = \int_{S_y} X(v) h(f-v) dv \quad \forall f \in S_d \quad (3)$$

As x is a function with finite support, it can be represented by the samples of its Fourier transform, provided we have all samples, and provided the sampling theorem is satisfied. Our first problem is that we do not have all samples available, and due to the infinite extent of the Fourier transform the missing sample values are not all equal to zero. A second problem is that our observations are likely to be corrupted by noise.

There are several approaches towards the solution of the problem. As our scene has finite support, and is assumed to have finite energy, its Fourier transform is analytic over S_y [5]. Knowing $Y(f)$ over some region of finite, nonzero, support allows one, in principle, to apply the concept of analytic continuation. Theoretically there is a basis for the belief that our observations contain sufficient information to somehow extend these observations beyond the finite observation support. This signal extrapolation in the transform domain would then result in the scene domain in resolution beyond the Rayleigh limit (so-called super-resolution). Analytic continuation requires higher order deriva-

tives which are increasingly sensitive to noise, rendering the approach practically useless.

Several other methods for extrapolation of band-limited signals (the dual of our problem) have been reported recently. Most often these procedures observe a band-limited function over a continuous support. One can expand this known portion in an orthonormal series of prolate spheroidal wave functions, and the expansion coefficients are then valid in a series expansion for the entire signal /6/. More recent methods are generalizations and variations of the iterative algorithm due to Gerchberg /7/. In this algorithm the known finite portion of the spectrum is Fourier transformed, subsequently limited to its known extent, and another transform yields a spectrum which is corrected in the observed portion. And so the iterations continue by again Fourier transforming, limiting to the known extent, etc. Various proofs for the convergence of this, and more general, iterative projection algorithms have been given /8,9/. Recently a fast optical implementation of Gerchberg's algorithm, in 2-D, has been reported /10/.

In the problem setting as outlined, the observations are available on a discrete set of finite support. From the iterative procedure an efficient one-step extrapolation method has been derived. Specific examples given illustrate the potential use of the one-step algorithm by successfully extrapolating to a twenty times larger support /11/. Encouraged by these results we will in Section III, give an alternative derivation of this one-step extrapolator, and extend it to 2-D. Subsequently an empirical investigation will be made of its potential performance with respect to the desired enhancement of resolution in the scene with limited support.

The second algorithm we will subject to closer investigation is based on a rather different approach. We already referred to the fact that the scene with limited support will facilitate a proper sampling rate for the Fourier transform. Our scene has another property resulting from the physical constraint that light intensity is a nonnegative quantity. The function representing the scene, has therefore all the

properties of spectral density function associated with a wide sense stationary stochastic field /16/. High resolution in our scene domain should therefore be expected from the application of so-called super resolution spectrum estimators /17/.

Our observations are samples of the Fourier transform of the scene, which by the Wiener-Khinchine relationship, corresponds to the autocorrelation function. Direct or indirect extrapolation of a finite set of autocorrelation samples is the main thrust in modern spectrum estimators. In the method made popular by Burg /12,13/, the autocorrelation extension is such that the resulting spectrum has the maximum entropy of any power spectrum, while being consistent with the measured data. The resulting all-pole, or autoregressive (AR) model is stable, and can therefore be used to extrapolate the known segment of the autocorrelation function to an infinite extent. The associated high resolution spectrum can be evaluated from the parametric model without actually performing the extrapolation. In order to place confidence in the spectral estimate so derived, one must have infinite confidence in the parametric model. A more appropriate measure of confidence may be expressed by performing the extrapolation over a comparatively extended, but finite, support. Many different methods are available, and some comparative analyses have been reported /14/.

Most of the activity has been in 1-D spectral analysis but extensions to 2-D have recently become available. An application of the maximum entropy method in image reconstruction, was fairly successful in reconstructing a "stacked blocks" phantom from a relatively small number of 2-D frequency domain samples /15/. As in the 1-D case, there are reasons one might attempt to use a pole-zero, or autoregressive-moving average (ARMA), model. With the same number of parameters one may represent certain spectra more accurately /18/. It is much more difficult, however, to evaluate these parameters, and to guarantee a non-negative spectral density. In Section IV we will briefly introduce one such 2-D ARMA spectral estimator, for which a FORTRAN IV package was made available to us /1/.

AD-A113 708

SOUTHEASTERN CENTER FOR ELECTRICAL ENGINEERING EDUCAT--ETC F/G 5/1
USAF SUMMER FACULTY RESEARCH PROGRAM. 1981 RESEARCH REPORTS, VO--ETC(U)
OCT 81 W D PEELE F49620-79-C-0038

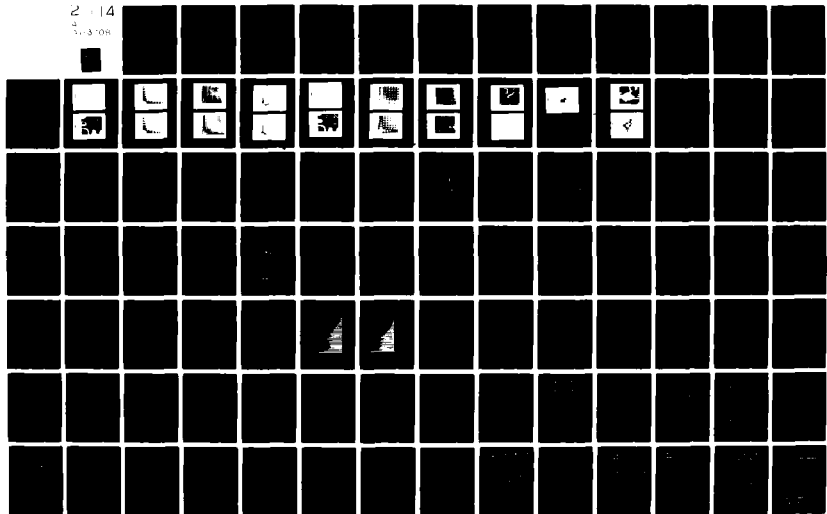
UNCLASSIFIED

AFOSR-TR-82-0227

NL

2 14

3 3 08



II. OBJECTIVES OF THE RESEARCH EFFORT

The objective of this research effort was to show the feasibility of some of the most recently developed spectral estimation techniques, for enhancement of resolution in 2-D scenes with finite support. Specific algorithms to be implemented and investigated are a parametric ARMA 2-D spectral estimator /1/, and a signal extrapolator for signals with finite support /2/. The latter requires the development of an extension to 2-D.

It is a further objective of the present research to identify improvements or new techniques that will lead to increased performance in terms of resolution and/or algorithm implementation considerations.

III. THE EXTRAPOLATOR APPROACH

In general /19/, we may state our problem in terms of a distortion operator \mathcal{D} on the signal, resulting in the observation Y :

$$y = \mathcal{D}X \quad (4a)$$

In addition, we may have some a priori knowledge that puts a constraint on the Fourier transform of the scene X . This constraint is expressed by the constraint operator \mathcal{C} :

$$X = \mathcal{C}X \quad (4b)$$

Substitution of (4b) into (4a), yields:

$$y = \mathcal{D}\mathcal{C}X \quad (5)$$

From (4b) and (5), we can therefore also write the following equality:

$$X = \mathcal{C}X + \mu (Y - \mathcal{D}\mathcal{C}X) \quad \forall \mu \quad (6)$$

Or, in general:

$$X = \mathcal{F}X \quad (7a)$$

$$= \mu Y + (\mathcal{I} - \mu \mathcal{D})\mathcal{C}X \quad (7b)$$

$$= \mu Y + \mathcal{G}X \quad (7c)$$

where \mathcal{I} denotes the identity operator. A classical approach to finding a solution X (a so-called fixed point of the operator \mathcal{F}), is the method of successive approximations. In the right hand side of (7) we substitute an approximation X_k , to yield a new approximation at step $k+1$:

$$X_{k+1} = \mathcal{F}X_k = \mu Y + \mathcal{G}X_k \quad (8)$$

This brings us to the important issue of when the iterative algorithm of (8) converges. According to the contraction mapping theorem /3/, (7a) has a unique solution, the fixed point X , if \mathcal{F} is a contraction in some subspace. More importantly, for every starting point X_0 in that subspace, the corresponding successive approximation sequence converges to X . An equivalent requirement for convergence, is that \mathcal{G} is a contraction. The latter translates into the requirement that the operators $(\mathcal{I} - \mu \mathcal{D})$ and \mathcal{P} are nonexpansive, and at least one of these is a contraction. If both operators are merely nonexpansive, many solutions could exist and convergence of the iterative algorithm may or may not occur.

Our scene has limited support, and satisfying the sampling theorem, it is completely determined by all its samples. We can only observe a limited number of these samples, as expressed by the truncation operator \mathcal{T} .

$$y = \mathcal{T}X \quad (9)$$

The scene support S_x , and the data support S_d are rectangular,

$$S_x = \left\{ x: -T_1 \leq x_1 \leq T_1, -T_2 \leq x_2 \leq T_2 \right\} \quad (10a)$$

$$S_d = \left\{ n: \frac{\Omega_1}{2\pi} \leq n_1 \leq N_1 \frac{\Omega_1}{2\pi}, \frac{\Omega_2}{2\pi} \leq n_2 \leq N_2 \frac{\Omega_2}{2\pi} \right\} \quad (10b)$$

where Ω denotes the sampling interval. As a constraint we use the fact that our scene is space limited, and denote this by the operator \mathcal{B} .

$$X = \mathcal{B}X \quad (11)$$

Starting with our finite set of observations, this leads to the following iterations:

$$X_0 = Y \quad (12a)$$

$$X_{k+1} = Y + (I - \mu \mathcal{T}) \mathcal{B} X_k \quad (12b)$$

Note that the second term on the right hand side of (12b) is a correction term to the known samples. Over S_d we do not want any correction, and express this by choosing $\mu = 1$. One can then show /19/, that $(I - \mathcal{T})$ and \mathcal{B} are nonexpansive operators. For the continuous case the operator $(I - \mathcal{T}) \mathcal{B}$ can be shown to be strictly nonexpansive, thereby guaranteeing the convergence of the iterative process in the continuous case. In the discrete case the operator $(I - \mathcal{T}) \mathcal{B}$ is not strictly nonexpansive, so that convergence of the iterative algorithm cannot be guaranteed.

Let us suppose that the iterative process converges to a solution X_∞ . From (12b) we then have, with $\mu = 1$,

$$X_\infty = Y + (I - \mathcal{T}) \mathcal{B} X_\infty \quad (13)$$

The solution satisfies the constraint, so that

$$Y = \mathcal{T} \mathcal{B} X_\infty \quad (14a)$$

$$= \mathcal{B} \mathcal{T} X_\infty \quad (14b)$$

We should therefore find a solution $\mathcal{T} X_\infty$ that satisfies (14b). For the particular case we are dealing with:

$$Y(n) = \sum_{m \in S_d} \mathcal{T} X_\infty(m) \prod_{i=1}^2 2T_i \frac{\rho_i}{2\pi} \text{sinc} 2T_i \frac{\rho_i}{2\pi} (n_i - m_i) \quad \forall n \in S_d \quad (15)$$

This same relationship can be used then to extrapolate, by replacing $Y(n)$ by $X(n)$ and executing (15) $\forall n \in S_d$. Note that $Y(n)$ represents a 2-D array that is known. Let us define the 2-D array $Z(m)$ as follows:

$$Z(m) = 2T_1 \frac{\Omega_1}{2\pi} \cdot 2T_2 \frac{\Omega_2}{2\pi} \cdot \mathcal{F}X_{\infty}(m) \quad (16)$$

Expression (15) can then be represented in matrix formulation

$$Y = S_1 Z S_2' \quad (17a)$$

$$\triangleq S_1 Q \quad (17b)$$

where

$$\text{col}_i(S_1) = \left\{ \text{sinc } 2T_1 \frac{\Omega_1}{2\pi} (n_1 - i) \right\}_{n_1=1}^{N_1} \quad \forall i=1, \dots, N_2 \quad (17c)$$

$$\text{col}_i(S_2) = \left\{ \text{sinc } 2T_2 \frac{\Omega_2}{2\pi} (n_2 - i) \right\}_{n_2=1}^{N_2} \quad \forall i=1, \dots, N_1 \quad (17d)$$

the matrixes S_1 and S_2 are symmetric and Toeplitz, so that (17b) can be solved efficiently for Q , by solving

$$\text{col}_j(Y) = S_1 \text{col}_j(Q) \quad (18)$$

for each column of Q /20/. Knowing Q we then have the following from (17a/b):

$$Q' = S_2 Z' \quad (19)$$

This system is then solved, in the same efficient manner, by solving

$$\text{row}_j(Q) = \sum_2 \text{row}_j(Z) \quad (20)$$

for each row of Z . The solution Z , if it exists, can then be used to extrapolate beyond the finite data support. This system of symmetric, Toeplitz solvers was implemented in FORTRAN IV, and results are reported in Section V.

IV. THE PARAMETRIC APPROACH

We referred to several parametric approaches that could be taken. The one implemented was somewhat dictated by the availability of the corresponding FORTRAN code, and its reported promise for resolution enhancement. In the 2-D setting, ARMA spectral estimation assumes the following model to underly the wide sense stationary data process:

$$\sum_{k \in K} a_k x(n-k) = \sum_{l \in L} b_l \varepsilon(n-l) \quad (21)$$

where a_k and b_l are 2-D arrays and $K = \{k: 0 \leq k_1 \leq p_1, 0 \leq k_2 \leq p_2\}$ and $L = \{l: 0 \leq l_1 \leq q_1, 0 \leq l_2 \leq q_2\}$. Again, the data is available over a finite support $1 \leq n_1 \leq N_1$ and $1 \leq n_2 \leq N_2$ say. The excitation process ε is assumed to be white. With the process x is associated a spectral density function, given by

$$S_x(\omega) = \sum_{n \in \mathbb{I}} R_x(n) e^{-j n' \omega} \quad (22a)$$

Where \mathbb{I} denotes the set of all integers, and R_x denotes the autocorrelation function, defined by

$$R_x(n) = \mathcal{E} \left\{ x(k+n) x^*(k) \right\} \quad (22b)$$

In order to get the spectral density function all of the samples of the autocorrelation function are needed. A finite data set does not generally contain sufficient information to determine the entire correlation function. One can alternatively evaluate the spectral density function from the parameters in (21), as follows /16/:

$$S_x(\omega) = \frac{\left| \sum_{l \in L} b_l e^{-j l' \omega} \right|^2 \cdot \sigma^2}{\left| \sum_{k \in K} a_k e^{-j k' \omega} \right|^2} \quad (23)$$

where σ^2 is the variance of the excitation process.

In his particular method, Cadzow defines in an ad hoc manner his "basic error terms" by multiplying (21) by $x^*(n-m)$:

$$e(m,n) = \sum_{k \in K} a_k x(n-k) x^*(n-m) \quad (24a)$$

$$= \sum_{l \in \Pi} b_l \varepsilon(n-l) x^*(n-m) \quad (24b)$$

The index set for m is taken such that the random variables

$\varepsilon(n-l) x^*(n-m)$ are uncorrelated. The zero mean excitation then renders the "basic error terms" to be zero mean random variables.

By minimizing a weighted squared error criterion, (24a) yields an estimate for the autoregressive coefficients via the solution of a linear system of equations, much like the modified least squares or linear predictive coding algorithms. Substitution of the a_k array in the difference equation satisfied by the half plane causal correlation function, readily yields a representation for the power spectral density /24/.

We note here that the coefficient arrays a_k and b_l are estimated, and no constraint is incorporated to guarantee that the estimated spectral density function is nonnegative. The corresponding estimated scene would have a negative light intensity over some subset of its support. In Section V we will give the details and results of the APMA scene estimator.

V. NUMERICAL EXAMPLES

The ARMA FORTRAN code was first transcribed to the RADC Signal Processing Lab's computer, and its computational speed increased. This process took significantly longer than anticipated. The ARMA package operates on an array of real data, so that our data generator has to generate a real data array. For convenience of generation the scene was chosen to be separable, and took the following form in each of its directions:

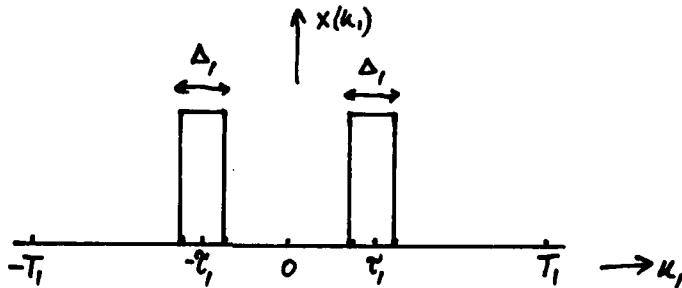


Figure 1. One Dimensional Phantom Scene.

Analytical evaluation of the Fourier transform yields

$$X(f_1) = 2 \cos 2\pi f_1 \tau_1 \cdot \Delta_1 \cdot \text{sinc } f_1 \Delta_1 \quad (25)$$

To satisfy the Nyquist sampling rate we choose the frequency sampling interval equal to:

$$\Delta f_1 = \frac{\Omega_1}{2\pi} = \frac{1}{2T_1 j_1} \quad (26)$$

where $j_1 > 1$ is the factor by which we over-sample. Due to the linearity of the Fourier transform, the data field is also separable and given by:

$$X(f) = X(f_1) \cdot X(f_2) \quad (27)$$

In order to synthesize a more complex phantom scene, up to three of these rectangular phantoms can be added, each parametrized by its own τ , Δ , and amplitude. Due to the symmetry of the resulting scene, its Fourier transform is real, with the same type of symmetry. With such symmetry only the NE quadrant will be displayed. We note here that the real data requirement is not essential for the extrapolator approach. Due to the symmetric limited support assumption, the matrices S_1 and S_2 in (17) are real. If the data array were complex, this would translate to parallel extrapolators, the one for the real part independent from the one for the imaginary part. As we will use real data, the extrapolator for the imaginary part becomes the zero operator.

Given a specific data array the extrapolator approach consists of two steps:

- i) determine the extrapolator matrix, i.e. find a solution to (17). (64 bit wordlength used)
- ii) use that solution to extend the data array as in (15). (32 bit wordlength used)

As it is rather difficult to get a reasonable idea of the resolution enhancement from a direct comparison of the extrapolated and analytically determined arrays, this comparison is visualized by displaying the FFT of these arrays after zero-padding to a 128 x 128 array. The resulting display is affected by aliasing due to the truncation of the data array. It is however a perfectly valid way of comparison due to the fact that the FFT operator is one-to-one.

For the following choice of parameters, a phantom scene was Fourier transformed and then sampled:

$$\begin{aligned}
 T_1 = T_2 &= 128 \\
 \Delta_1 = \Delta_2 &= 1 \\
 \tau_1 = \tau_2 &= 55 \\
 \delta_1 = \delta_2 &= 6
 \end{aligned}
 \tag{28}$$

Samples of the original scene are displayed in Figure 2. Taking a 3×3 data array, the classical processing procedure zero-pads and takes an FFT, the result of which is displayed in Figure 3. Visualize the other three quadrants and notice that one big blur is produced by this classical processing method. We actually have four little phantoms. The same 3×3 data array is next extrapolated to an 8×8 array, and compared to the 8×8 analytical array. The results are shown for comparison in Figures 4a and 4b respectively. Note that the blur has become smaller, and also that the extrapolated and analytical data are virtually the same. Next we extrapolate the 3×3 data array to a 16×16 , and 32×32 array respectively, and perform the respective FFT operations. The results are shown in Figures 5 and 6 respectively. In Figure 5 we start to resolve the four phantoms, but we also note that the extrapolator starts to deviate from the analytical data. Extrapolating even further yields a larger discrepancy as shown in Figure 6.

Let us now add another phantom with equal amplitude, $\Delta_1 = \Delta_2 = 1$, and $\tau_1 = \tau_2 = 110$. The sampled original scene is shown in Figure 7, and the classical approach of zero-padding the 3×3 observations leads to Figure 8. We then extrapolate to an 8×8 , and 16×16 array respectively. A comparison can be made from Figures 9 and 10 respectively, and shows that the extrapolator deviates increasingly from the analytical data. These results show that the extrapolator, as implemented here, can work. The author does not intend to call these results "typical", however, as attempts to start from larger data arrays, as 8×8 , do not yield a solution for the extrapolator array. This is due to the ill-conditioned nature of the matrix operators S_1 and S_2 /22/. Another approach would be to start with a 3×3 array but with a faster sampling rate. This, again, leads to the ill-conditioning problem /22/. In hindsight, these problems might have been anticipated, as it is noted in /2/, that generally a subset of band-limited signals exists for which the one-step extrapolator problem does not have a solution. In the author's experience arbitrary band-limited signals fall in the disclaimed class with high probability.

Due to the extreme sensitivity to any type of noise, the practicality of the one-step extrapolator is rendered nil. The principle of extrapolation remains fully valid, however, and emphasis must be directed towards different procedures and algorithms. Recall that in the successive approximation approach a constraint operator was introduced. Such a constraint limits the number of solutions one may find. The ill-conditioning effect is really an expression of the existence of many solutions. This suggests investigating the iterative approach with more constraints. A natural constraint we have not used is the positivity constraint. It could easily be incorporated in the iterative approach, in addition to other constraints, as long as the set of constraints is compatible /21/.

The scene in Figure 7 generates a 32 x 32 data array, on which we now operate with the ARMA scene estimator. The model orders in (21) have been fixed at $p_1 = p_2 = q_1 = q_2 = 6$. Computational requirements limit the flexibility to increase the model orders, and we note that an order of 6 is fairly restrictive. Some processes can be modeled well, others only poorly with such low order. The required system memory for the ARMA package, limits the order to 6 for the RADC Signal Processing Lab's computer, unless special arrangements are made. Figure 11 then shows fairly good resolution for the general location of the phantoms, even though the data is oversampled considerably (a necessity in the extrapolator approach). This result should be compared again to the classical approach, as depicted in Figure 12. Note that we have far better resolution indeed, by using the ARMA method. In essence, this is the type of data for which the ARMA model is well suited, as the scene approximates a scene of impulses. It was for sinusoids in relatively low level noise that encouraging results were reported /1/.

The next phantom is determined by the parameters

$$\begin{aligned}
 T_1 = T_2 &= 128 \\
 \Delta_1' = \Delta_2' &= 25 & \Delta_1^2 = \Delta_2^2 &= 15 & \Delta_1^3 = \Delta_2^3 &= 5 \\
 \tau_1' = \tau_2' &= 50 & \tau_1^2 = \tau_2^2 &= 61 & \tau_1^3 = 70 & \tau_2^3 = 90 \quad (29) \\
 f_1 = f_2 &= 1
 \end{aligned}$$

each of equal amplitude. The sampled scene is shown in Figure 13, and the ARMA scene estimate and the classical estimate are given in Figure 14. We note that the classical approach does a reasonable job here, as no high resolution is required. Furthermore, the jargon super-resolution has always pertained to resolving closely spaced peaks, as opposed to resolving closely spaced nulls. Note that the ARMA scene estimator is fairly robust, in the sense that its estimate does in some sense reflect the phantom. It is here the estimator that is constrained so much by the low model order, that it cannot represent the particular phantom more accurately. The ARMA scene estimator is quite promising therefore if higher model orders can be implemented in a computationally efficient manner.

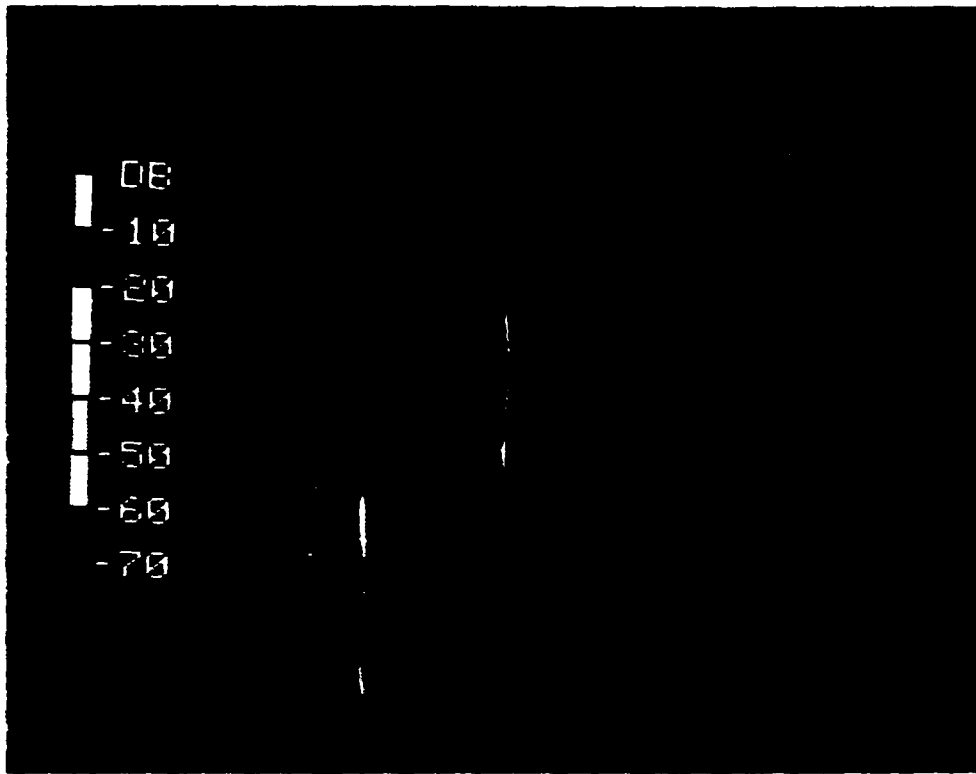


Figure 2. Original Phantom I (28).

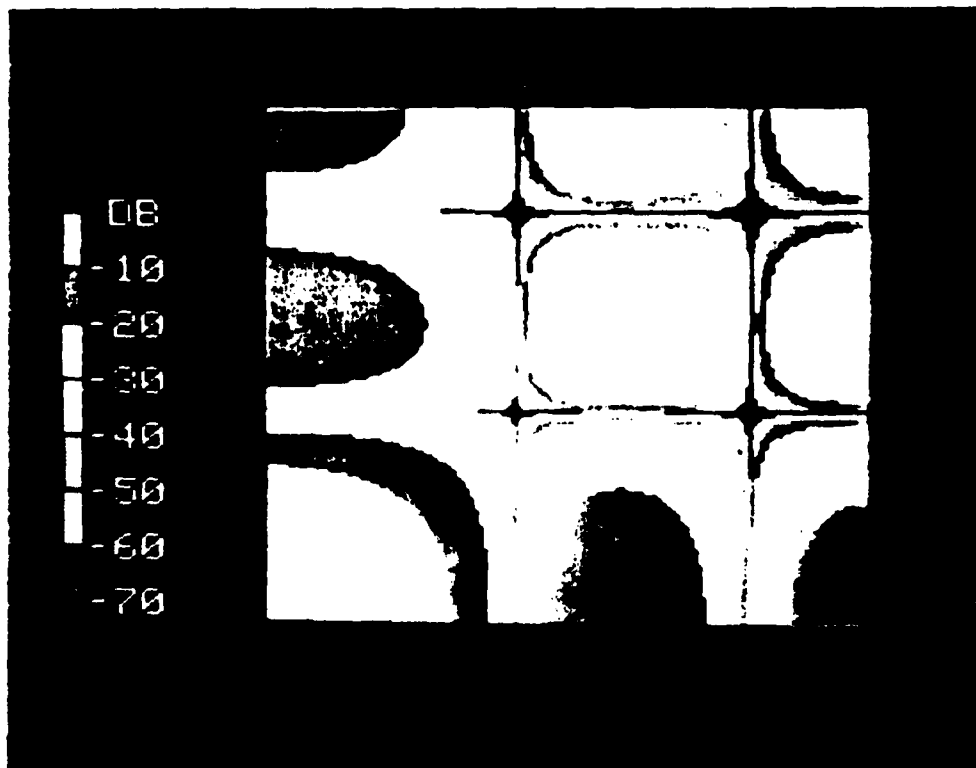


Figure 3. After Classical Processing of 3x3 Data.

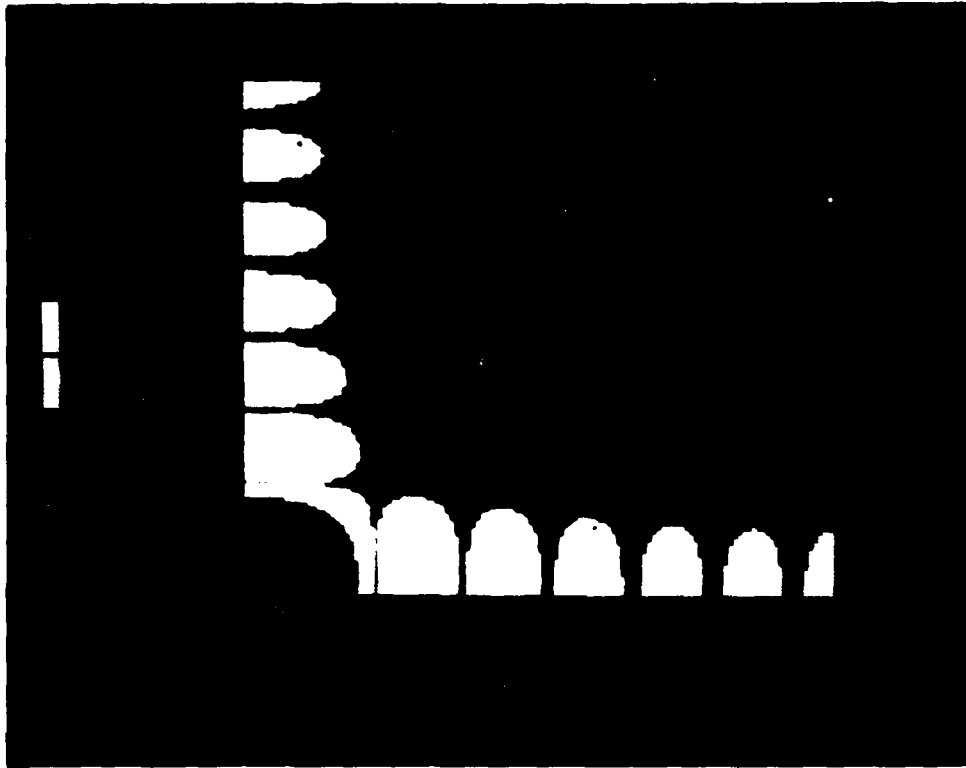


Figure 4a. After Processing of 8x8 Extrapolated Data.

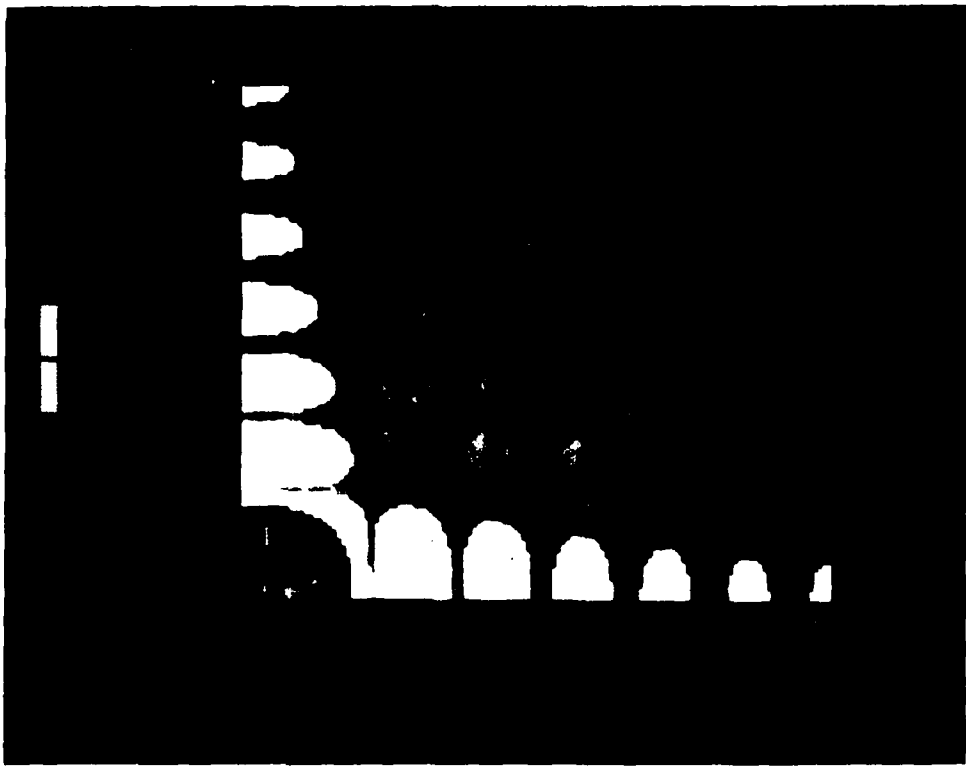


Figure 4b. After Processing of 8x8 Analytical Data.

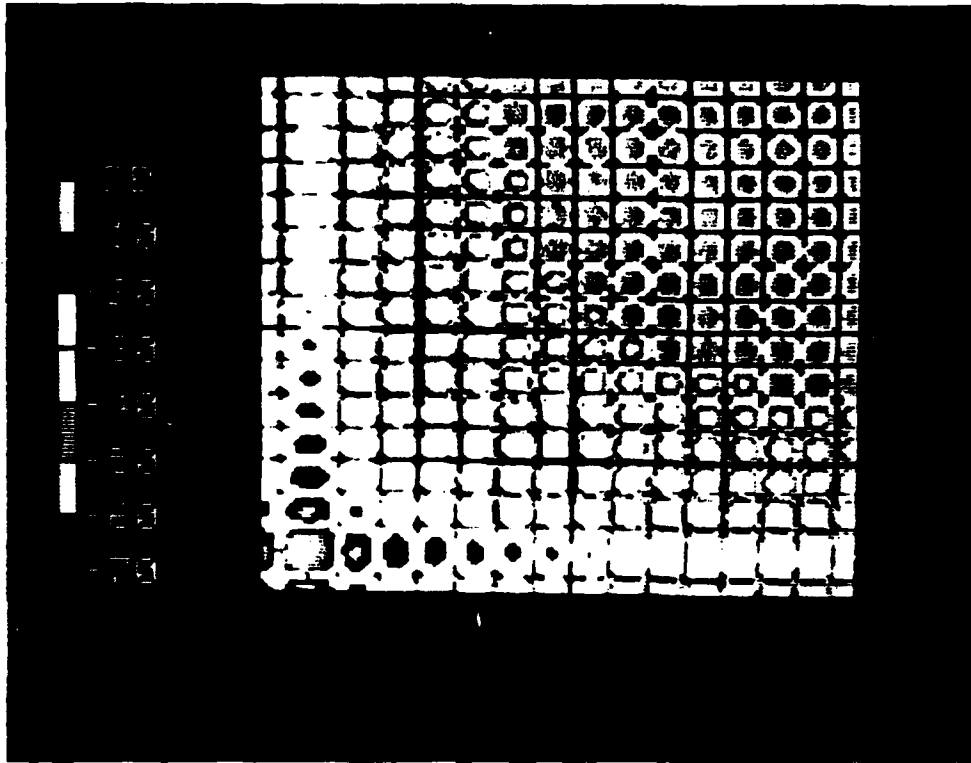


Figure 5a. After Processing of 16x16 Extrapolated Data.

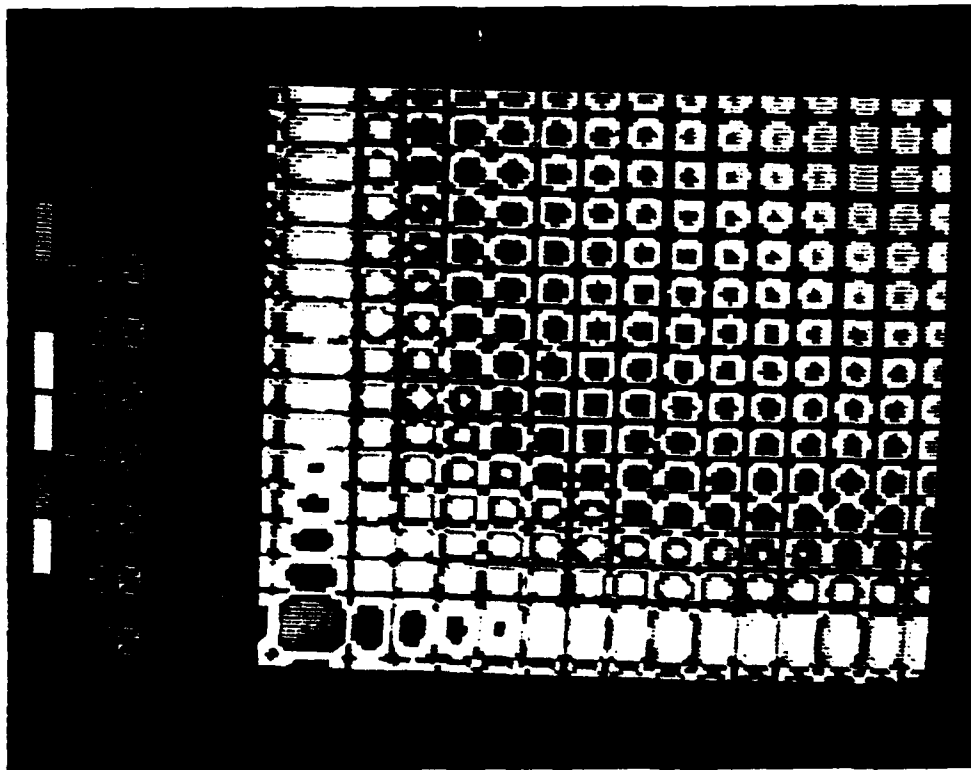


Figure 5b. After Processing of 16x16 Analytical Data.

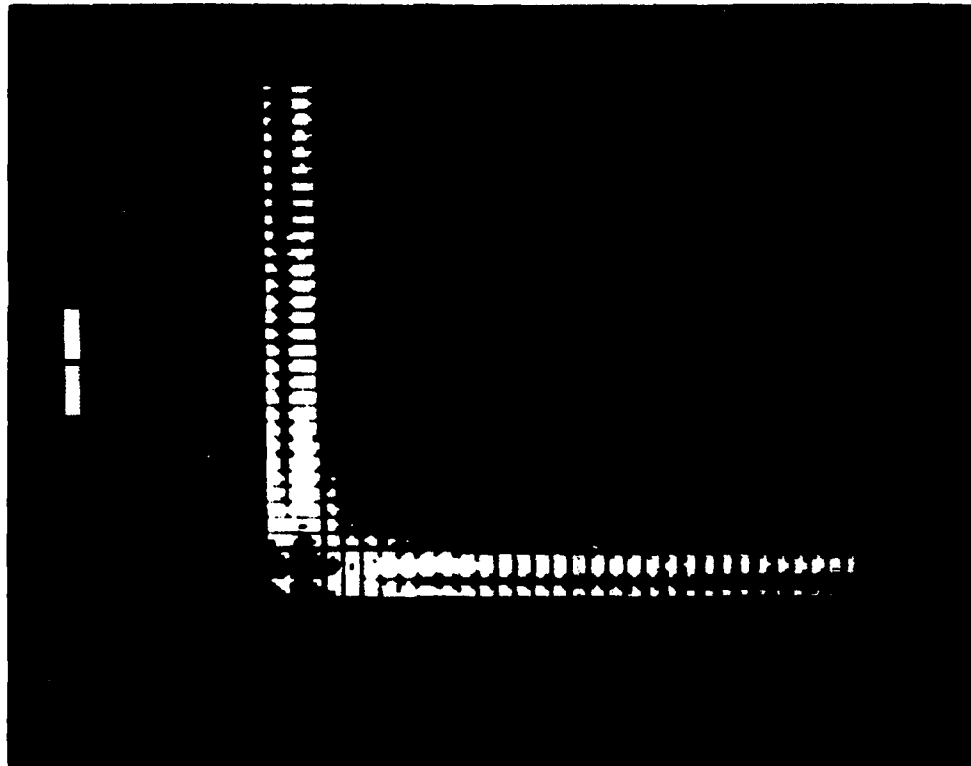


Figure 6a. After Processing of 32x32 Extrapolated Data.

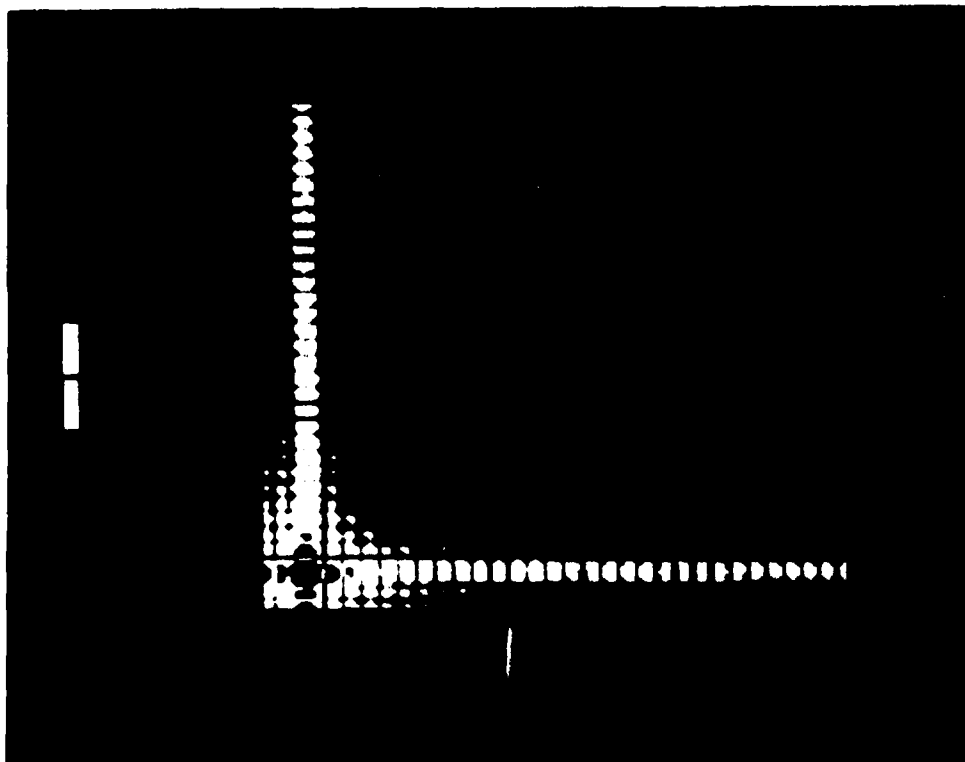


Figure 6b. After Processing of 32x32 Analytical Data.

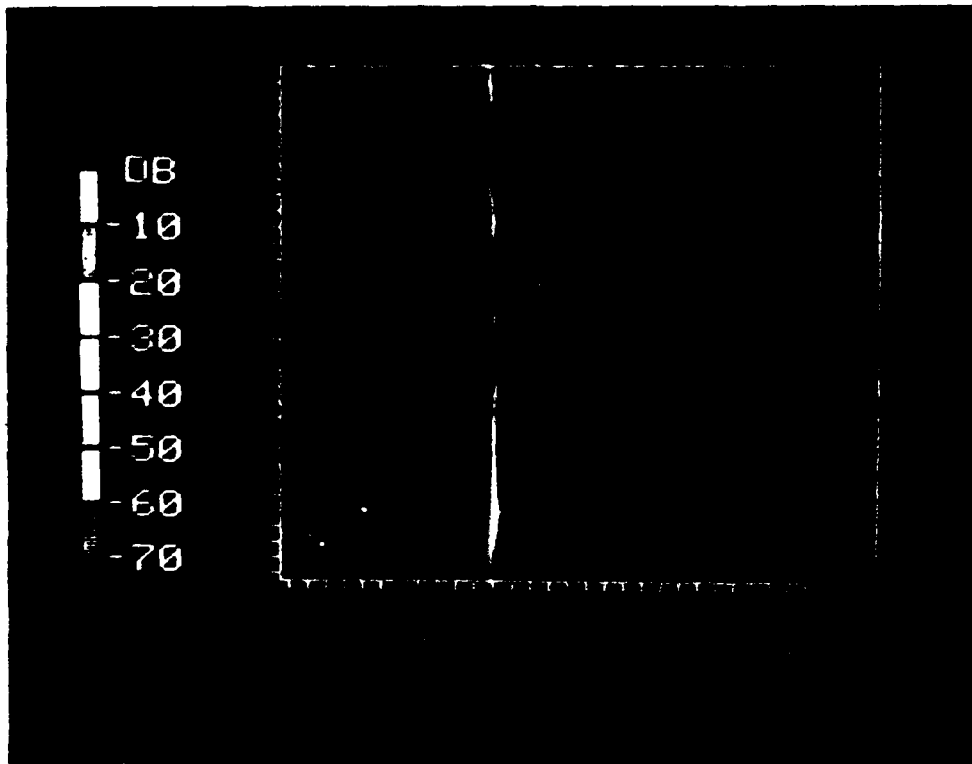


Figure 7. Original Phantom II.

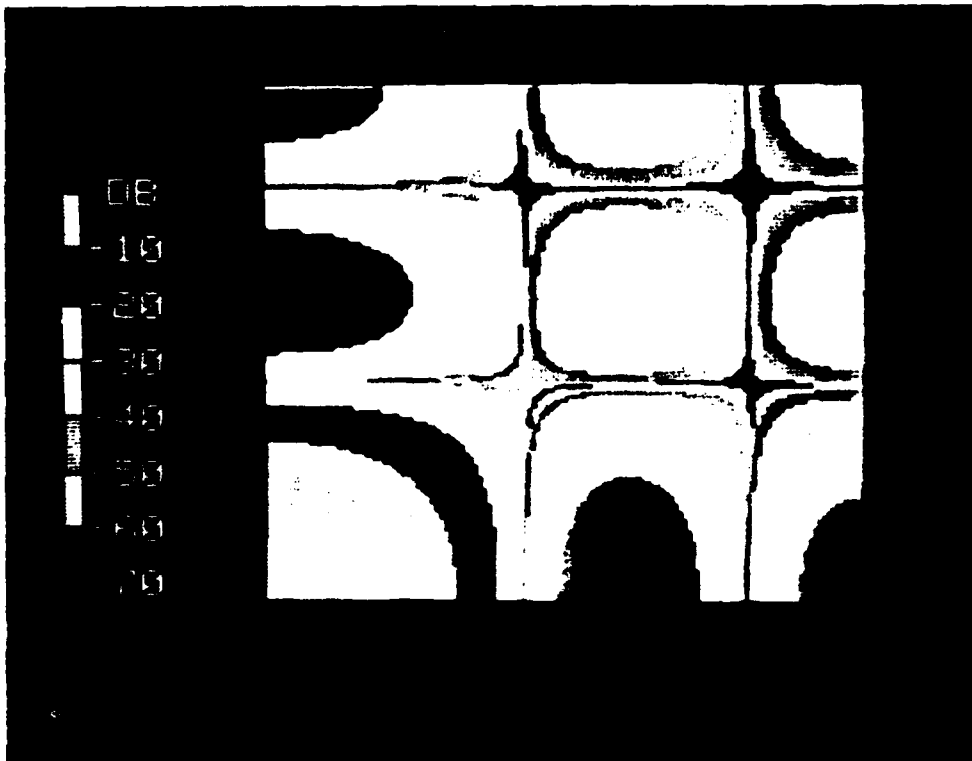


Figure 8. After Classical Processing of 3x3 Data.

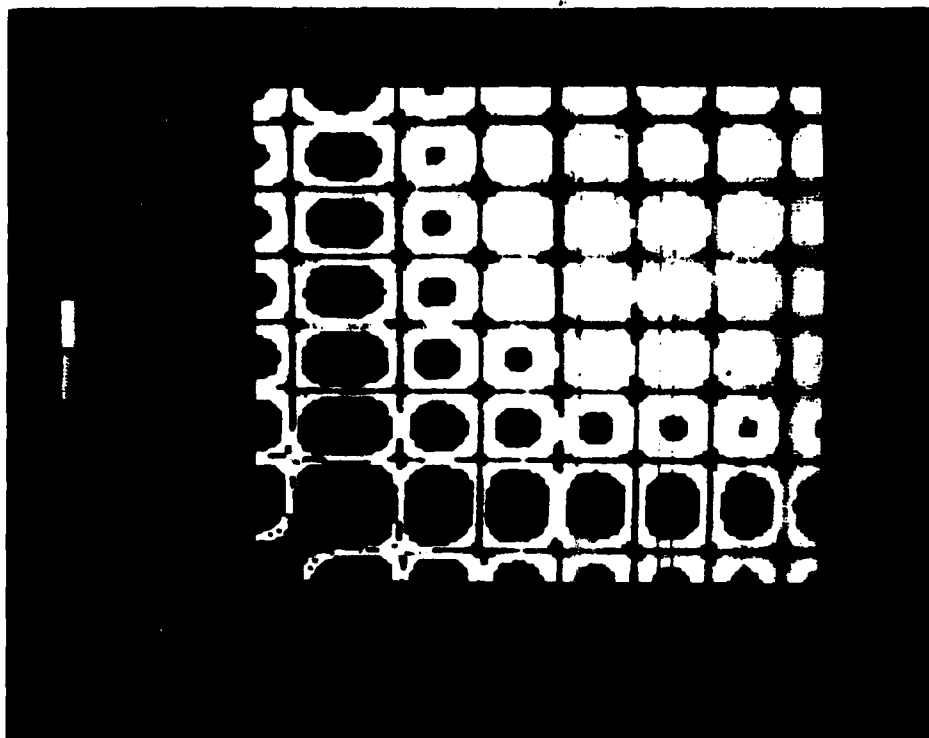


Figure 9a. After Processing of 8x8 Extrapolated Data.

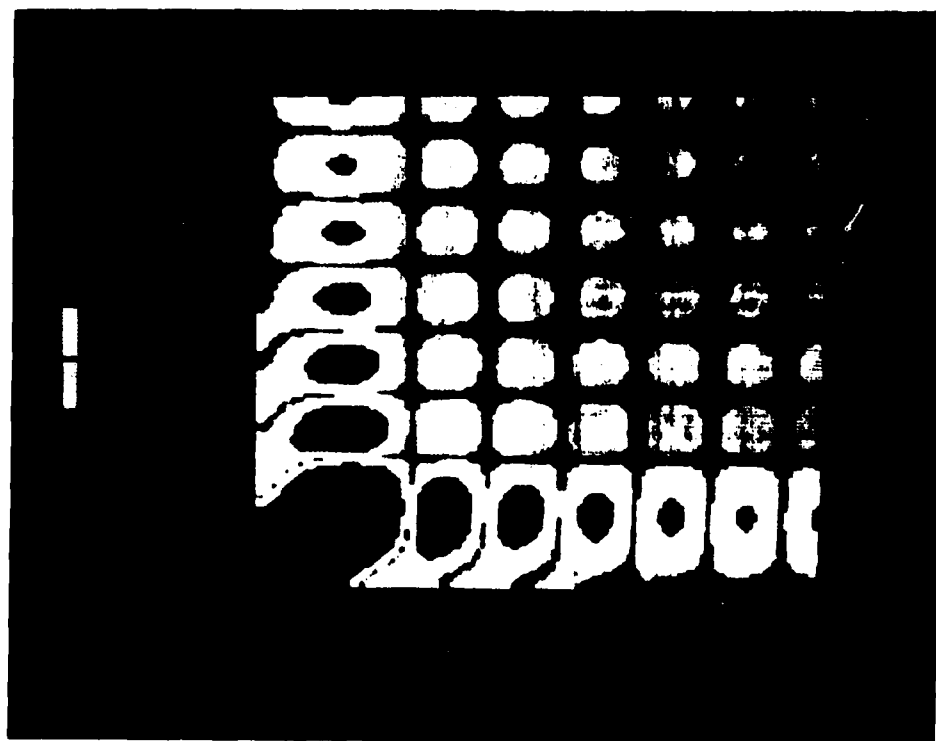


Figure 9b. After Processing of 8x8 Analytical Data.

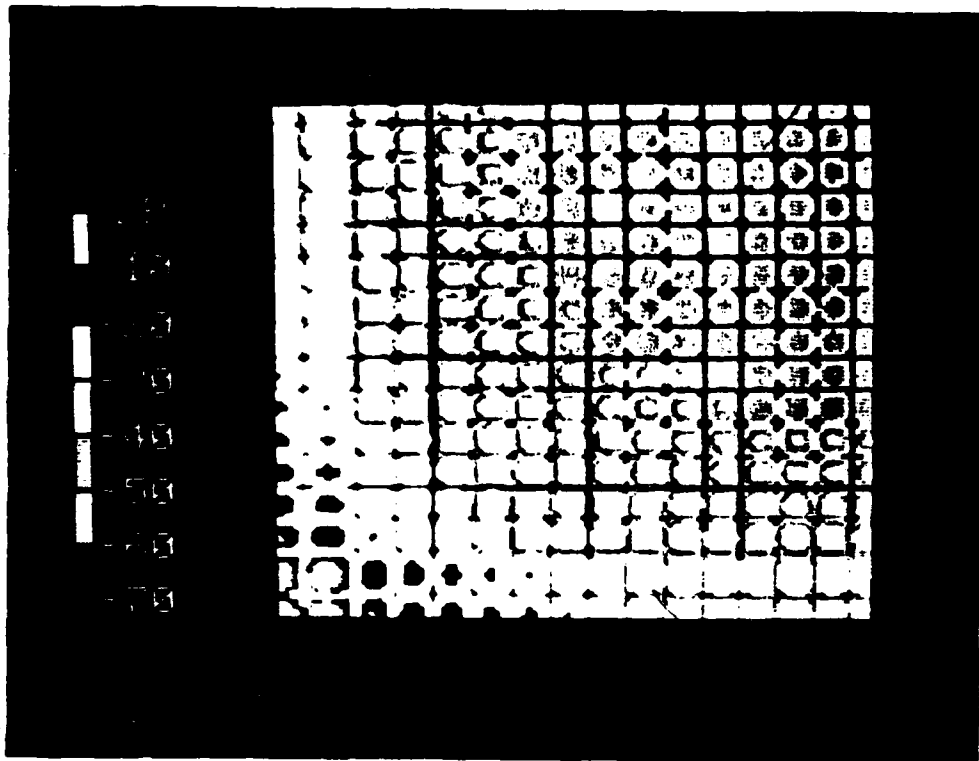


Figure 10a. After Processing of 16x16 Extrapolated Data.

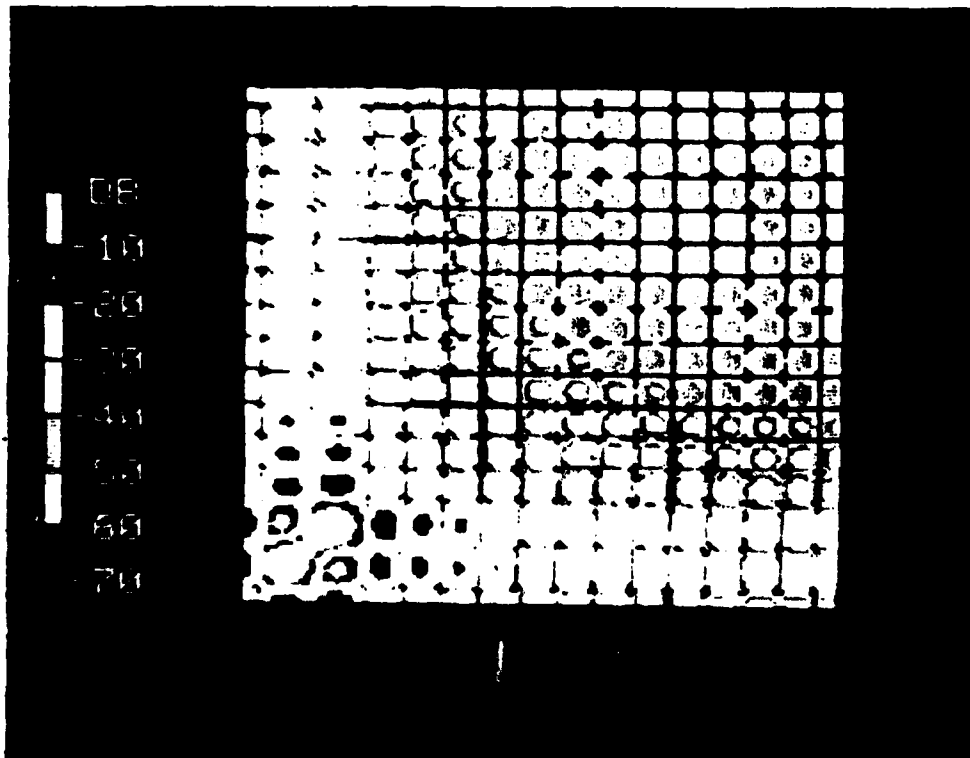


Figure 10b. After Processing of 16x16 Analytical Data.

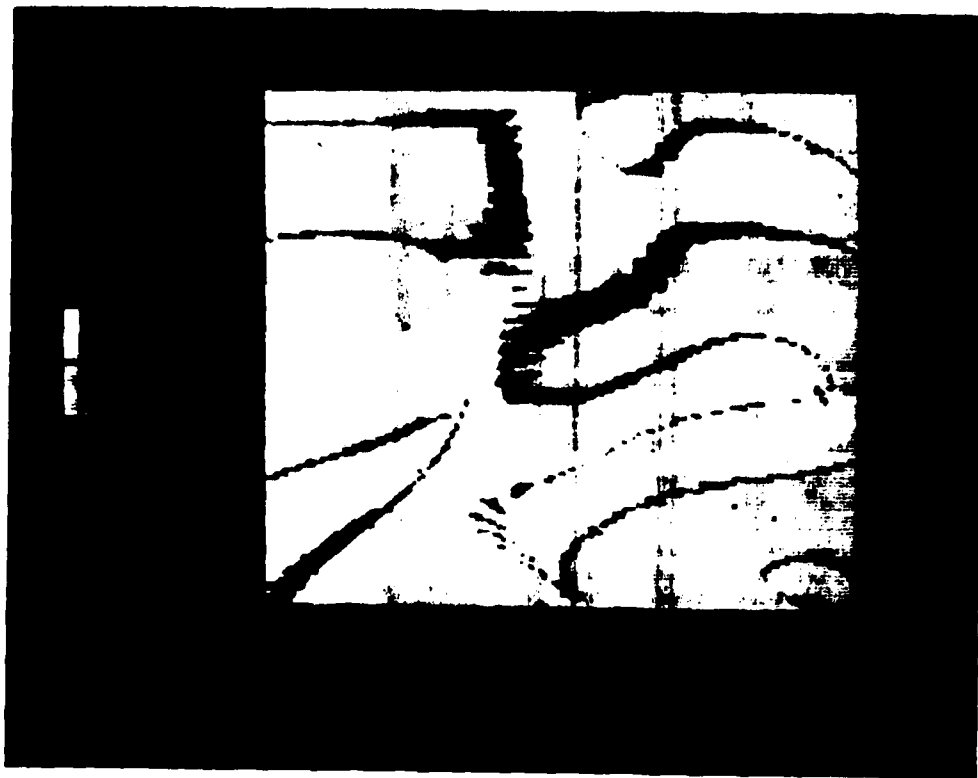


Figure 11. ARMA (6,6,6,6) Scene Estimate from 32x32 Data.

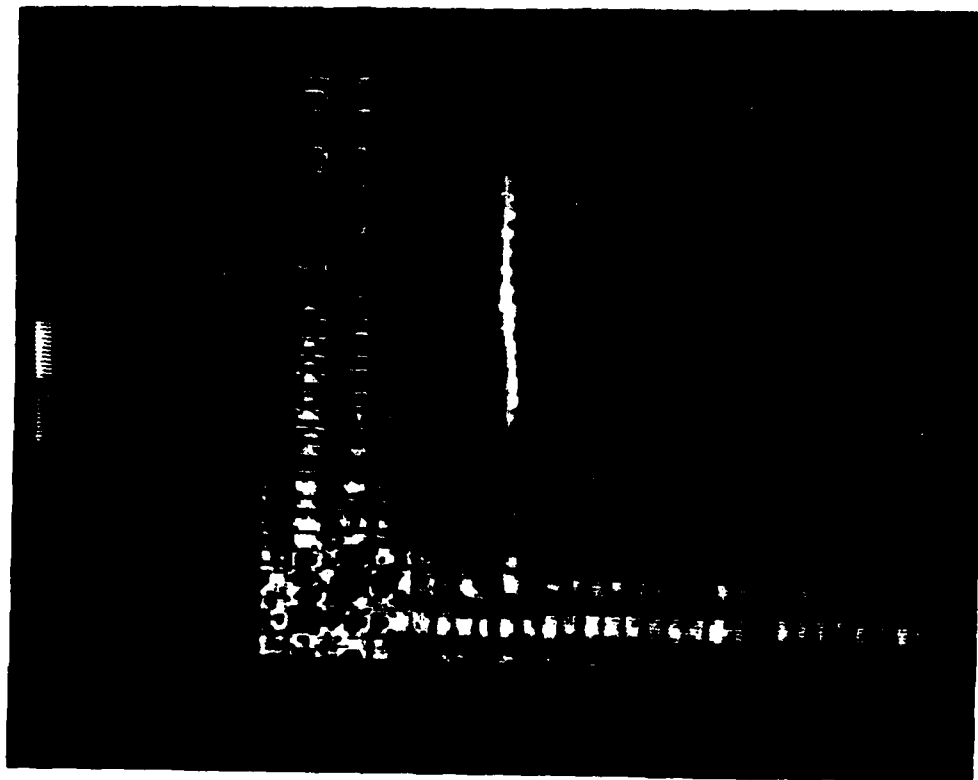


Figure 12. After Classical Processing of 32x32 Data.

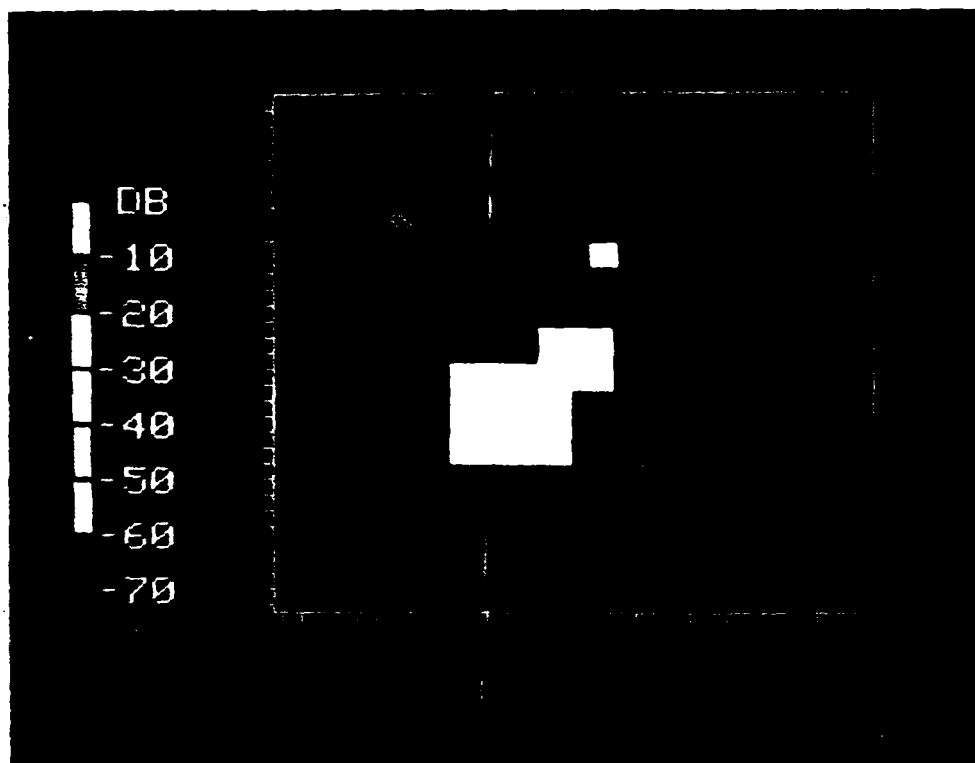


Figure 13. Original Phantom III (29).



Figure 14a. ARMA (6,6,6,6) Scene Estimate from 32x32 Data.

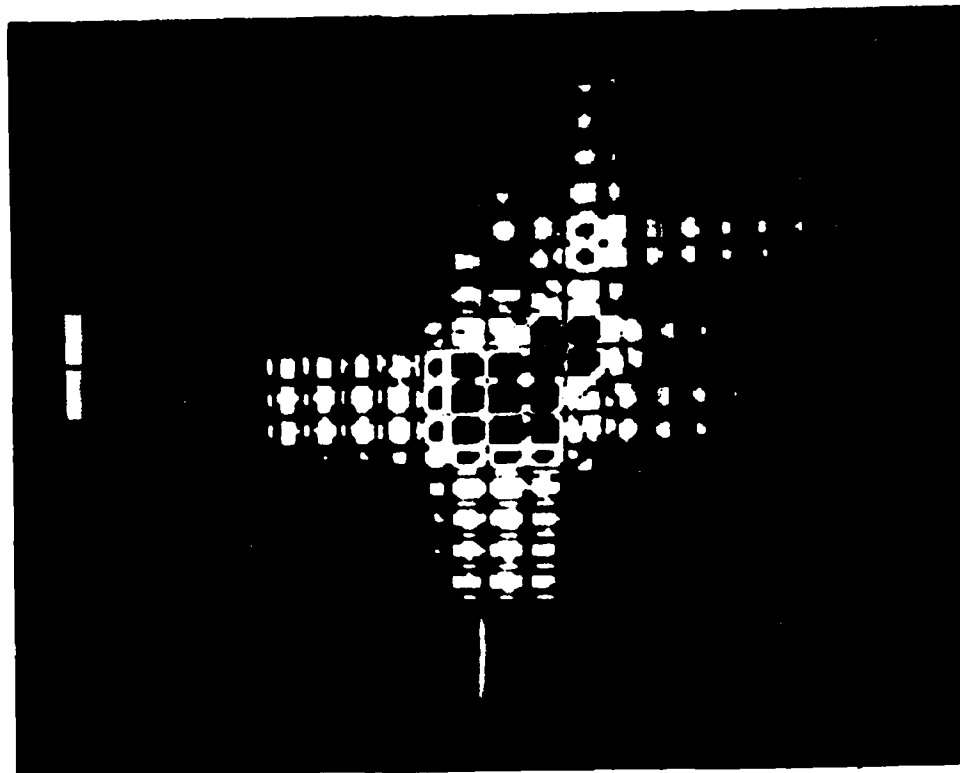


Figure 14b. After Classical Processing of 32x32 Data.

VI. RECOMMENDATIONS

Our experiments show that the one-step 2-D extrapolator can work in principle. Its relatively simple implementation, however, is extremely sensitive to any type of noise not satisfying the limited support assumption. This non-robustness renders the technique of low value in practical situations.

The emphasis should be on recursive techniques for signal extrapolation, as these are less prone to accumulation of errors. It is easier, in addition, to incorporate many different constraints, thereby shrinking the number of possible solutions of the ill-conditioned system of equations to be solved. The constraints may be of a probabilistic nature to handle measurement noise.

Recall that in the continuous problem we need to solve a first order Fredholm integral equation (3), and that this problem has a unique solution. It is the discretization process that transforms a well-conditioned problem into an ill-conditioned one. A recent suggestion /23/ is to pay more attention to this discretization process. Properties of the known kernel of the Fredholm integral equation can lead to a non-uniform sampling scheme, that results in a well-conditioned system of equations for the discrete case.

The ARMA scene estimator gives promising results for pointlike scenes, as these can be represented by a small number of ARMA parameters. To represent more complex scenes, a large number of ARMA parameters is necessary, which presently leads to "the curse of dimensionality" for the required computational burden. Truly computationally efficient algorithms for ARMA modeling need to be developed. ARMA order determination procedures should form an integral part of such algorithms.

Another approach is to limit the class of scenes one wants to represent. This would hopefully lead to a specialized class of basis functions for such scenes, thereby reducing the number of parameters necessary for its representation.

As a scene has all properties of a spectral density function, the measured Fourier transform data are samples of a correlation function, rather than the underlying process itself. It seems more rational, and appropriate, to direct the parametric modeling towards covariance sequence modeling /25/.

REFERENCES

1. Cadzow, J. A., Ogino, K., "Two-Dimensional Spectral Estimation," IEEE Trans. on Acoustics, Speech, and Signal Processing, ASSP-29, No. 3, June 1981, pp. 396-401.
2. Cadzow, J. A., "An Extrapolation Procedure for Band-Limited Signals," IEEE Trans. on Acoustics, Speech, and Signal Processing, ASSP-27, No. 1, February 1979, pp. 4-12.
3. Luenberger, D. G., Optimization by Vector Space Methods, (John Wiley & Sons, Inc., New York, 1969.) pp. 272-277.
4. Cagliardi, R. M., Karp, S., Optical Communications, (John Wiley & Sons, Inc., New York, 1976) pp. 43.
5. Papoulis, A., Signal Analysis, (McGraw-Hill, Inc., New York, 1977) pp. 184-186.
6. Slepian, D., Landau, H. J., Pollack, H. O., "Prolate Spheroidal Wave Functions, Fourier Analysis and Uncertainty Principle I and II," Bell Syst. Tech. J., Vol. 40, No. 1, 1961, pp. 43-84.
7. Gerchberg, R. W., "Super-resolution through error energy reduction," Optica Acta, Vol. 21, No. 9, 1974, pp. 709-720.
8. Papoulis, A., "A New Algorithm in Spectral Analysis and Band-limited Extrapolation," IEEE Trans. on Circuits and Systems, CAS-22, No. 9, September 1975, pp. 735-742.
9. Youla, D., "Generalized Image Restoration by the Method of Alternating Orthogonal Projections," IEEE Trans. on Circuits and Systems, CAS-25, No. 9, September 1978, pp. 694-702.
10. Marks, R. J., "Coherent optical extrapolation of 2-D band-limited signals: processor theory," Applied Optics, Vol. 19, No. 10, 15 May 1980, pp. 1670-1672.
11. Cadzow, J. A., "An Extrapolation Procedure for Band-Limited Signals," IEEE Trans. on Acoustics, Speech, and Signal Processing, ASSP-27, No. 1, February 1979, pp. 4-12.
12. Burg, J. P., "Maximum Entropy Spectral Analysis," Proc. 37th Meeting of the Society of Exploration Geophysicists, 1967. (Also See /17/)
13. Burg, J. P., "A New Analysis Technique for Time Series Data," NATO Adv. Study Inst. on Sign. Proc., Aug 12-23, 1968. (Also See /17/)

14. Frost, O. L., Sullivan, T. M., "High-Resolution Two-Dimensional Spectral Analysis," Proc. ICASSP'79: 1979 IEEE Intn'l. Conf. on Acoustics, Speech, and Signal Processing, Washington, D.C., April 1979, pp. 673-676.
15. Wernecke, S. J., D'Addario, L. R., "Maximum Entropy Image Reconstruction," IEEE Trans. Comput., C-26, April 1977, pp. 351-364. (Also See /17/).
16. Koopmans, L. H., The Spectral Analysis of Time Series, (Academic Press, Inc., New York, 1974), pp. 30-35.
17. Childers, D. G., ed., Modern Spectrum Analysis, (IEEE Press, IEEE Inc., New York, 1978)
18. Gutowski, P. R., Robinson, E. A., Treitel, S., "Spectral Estimation: Fact or Fiction," IEEE Trans. Geosci. Electron., GE-16, April 1978, pp. 80-84. (Also see /17/)
19. Schafer, R. W., Mersereau, R. M., Richards, M. A., "Constrained Iterative Restoration Algorithms," Proc. IEEE, Vol. 69, No. 4, April 1981, pp. 432-450.
20. Zohar, S., "Fortran Subroutines for the Solution of Toeplitz Sets of Linear Equations," IEEE Trans. on Acoustics, Speech, and Signal Processing, ASSP-27, No. 6, December 1979, pp. 656-658.
21. Stark, H., Cahana, D., Webb, H., "Restoration of Arbitrary finite-energy optical objects from limited spatial and spectral information," Jrnl. Opt. Soc. Am., Vol. 71, No. 6, June 1981, pp. 635-642.
22. Jain, A. K., Ranganath, S., "Extrapolation Algorithms for Discrete Signals with Application in Spectral Estimation," IEEE Trans. on Acoustics, Speech, and Signal Processing, ASSP-29, No. 4, August 1981, pp. 830-845.
23. Hagin, F., "A Stable Approach to Solving One-Dimensional Inverse Problems," SIAM J. Appl. Math., Vol. 40, No. 3, June 1981, pp. 439-453.
24. Cadzow, J. A., "High Performance Spectral Estimation - A New ARMA Method," IEEE Trans. on Acoustics, Speech, and Signal Processing, ASSP-28, No. 5, October 1980, pp. 524-529.
25. Beex, A. A., "Covariance Sequence Approximation With Applications to Spectrum Analysis and Digital Filter Design," Ph.D. dissertation Colorado State University, Fort Collins, Colorado, Summer 1979.

ROME AIR DEVELOPMENT CENTER
GRIFFISS AIR FORCE BASE, NEW YORK 13441

August 21, 1981

Professor Warren Peele
SCEEE SFRP Office
1101 Mass. Ave.
St. Cloud, FL 32769

Dear Professor Peele:

This is to certify my approval of the final report, "Enhanced Scene Resolution: 2-D Spectral Estimator Approaches," as submitted by Dr. Louis Beex.

Sincerely,



Paul Van Etten
Effort Focal Point
USAF/RADC/OCTS

AUG 23 1981

JH

1981 USAF - SCEEE SUMMER FACULTY RESEARCH PROGRAM

Sponsored by the

AIR FORCE OFFICE OF SCIENTIFIC RESEARCH

Conducted by the

SOUTHEASTERN CENTER FOR ELECTRICAL ENGINEERING EDUCATION

FINAL REPORT

DECOMPOSITION OF NITROMETHANE OVER METAL OXIDE CATALYSTS

Prepared by: Jay B. Benziger
Academic Rank: Assistant Professor
Department and University: Department of Chemical Engineering
Princeton University
Research Location: Air Force Rocket Propulsion Laboratory
USAF Research Colleague: Capt Scott A. Shackelford
Date: August 4, 1981
Contract No: F49620-79-C-0038

DECOMPOSITION OF NITROMETHANE
OVER METAL OXIDE CATALYSTS

by
Jay B. Benziger

ABSTRACT

In the course of this work, the reaction of nitromethane over NiO/alumina and Cr₂O₃/alumina catalysts was examined to determine the feasibility of developing a nitromethane based monopropellant system. The kinetics of nitromethane decomposition over those two catalysts were found to be adequately represented by Langmuir-Hinshelwood expressions

$$r = -k_s C_s \frac{K_e P}{1 + K_e P}$$

under conditions $T = 100 - 300^\circ\text{C}$, $P = 1 - 100$ torr. The kinetic parameters $k_s C_s$ and K_e were measured and used to fit the data over the entire temperature range. It was found that nitromethane decomposition caused catalyst deactivation due to carbon deposition, which was due to the fuel rich nature of the nitromethane. The rate of deactivation was found to increase with decreasing temperature. Lastly, a reactor model was presented to display the qualitative features of operation of a monopropellant system. Catalyst bed length and preheat temperature and feed temperature were identified as the important parameters in determining system response time.

Acknowledgement

The author would like to thank the Air Force Systems Command, the Air Force Office of Scientific Research, and the Southeastern Center for Electrical Engineering Education for providing him the opportunity to participate in the Summer Faculty Research Program at the Air Force Rocket Propulsion Laboratory, Edwards Air Force Base, California. He would like to acknowledge the cooperation of the Liquid Rocket Division in providing the stimulus for this work. Particular thanks are due to Captain S.A. Shackelford for his suggestion of this project, Mr. B. Goshgarian for his cooperation in setting up the experimental equipment, Dr. W. Hoffman for performing the BET analyses, Mr. H. Martens for performing the x-ray diffraction analysis, and Mr. T. Owens for taking scanning electron micrographs.

I. INTRODUCTION

Small rocket thrusters and demand gas generators utilizing monopropellants are extremely important in rocket technology. Hydrazine is extensively used as a monopropellant for small attitude control thrusters and is currently the most important monopropellant. However, hydrazine has recently been identified as a suspected carcinogen which has prompted efforts to identify new monopropellant systems.

Nitromethane has been identified as a possible replacement for hydrazine as a monopropellant. It has a theoretical specific impulse greater than hydrazine. In a study performed by the Acurex Corporation for the AFRPL, several nitromethane based propellants were examined (1). They examined several metal oxide catalysts with nitromethane/1,7-octadiene, nitromethane/cyclohexane, and nitromethane/o-xylene mixtures in a packed bed reactor in an effort to identify an optimal system. The hydrocarbon was added in an amount of 4-6 wt % to desensitize the nitromethane to detonation and to act as a diluent reducing the adiabatic reaction temperature. The main results from the Acurex report are summarized below:

1) Two catalysts - NiO/alumina and Cr_2O_3 /alumina were identified as having the highest catalytic activity for nitromethane decomposition.

2) The catalyst activity declined with time as evidenced by an increase in the lightoff temperature and a longer response time required to achieve steady state temperature and pressure.

3) Of the three hydrocarbon desensitizers 1,7-octadiene yielded the best performance when judged with respect to its influence on catalytic activity.

The report also concluded that surface area was important in the catalytic activity; the study cited results showing crushed catalyst pellets displaying greater catalytic activity than uncrushed pellets. It will be shown below that this result is the result of diffusional limitations in the catalyst pores rather than being due to surface area.

II. OBJECTIVES

The purpose of the present study is to examine the catalytic decomposition of nitromethane over NiO/alumina and Cr₂O₃/alumina catalysts in order to assess their performance in nitromethane based monopropellant systems. Particular attention has been given to the reaction products and reaction kinetics for the heterogeneous catalytic reaction. A flow reactor has been used in conjunction with a mass spectrometer to experimentally measure reaction kinetics and the reaction products. This information has been used to evaluate the behavior of nitromethane based monopropellant systems.

III. EXPERIMENTAL PROCEDURE

The experiments were performed on a Finnigan 400 GC/MS. The gas chromatograph was modified to serve as a flow reactor, while the mass spectrometer was used to monitor the reactor effluent. A schematic of the apparatus is shown in Figure 1. Helium (99.999%) was metered through a flow meter and bubbled through nitromethane (Eastman spectrograde) in a constant temperature bath. The helium, saturated with nitromethane, flowed through the reactor maintained at a constant temperature in the GC oven. A glass leak was used to sample the reactor effluent. The sampled gas was stripped of helium using a jet separator before introduction to the mass spectrometer.

Quantitative analysis of the mass spectral data was performed by experimentally determining the relative sensitivities of the reactor effluents sampled by the mass spectrometer. The mass spectrometer was run at an electron ionization energy of 25 volts to reduce fragmentation. Relative ionization probabilities for different gases were measured at a known pressure. The enrichment by the jet separator as a function of mass was given by the manufacturer (2). The relative sensitivities (with CO₂ as a reference) are given in Table 1. Usually, the nitromethane pressure in the reactor feed was known giving a calibration point. An additional calibration was provided by adding a known Argon leak to the Helium to provide a constant reference pressure.

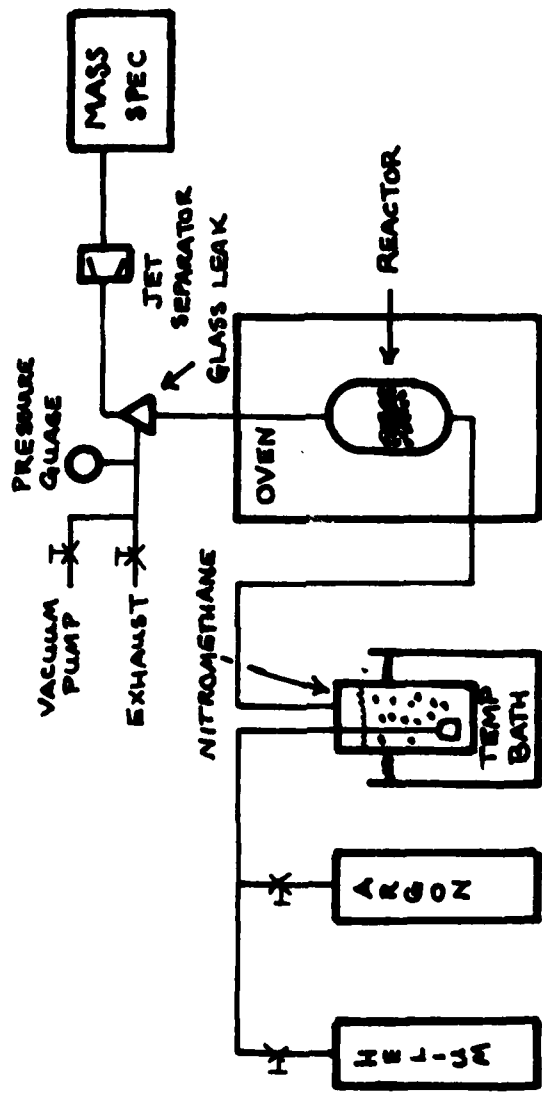


FIGURE 1
SCHEMATIC OF THE APPARATUS

TABLE I
RELATIVE SENSITIVITIES FOR REACTOR EFFLUENTS

<u>SPECIES</u>	<u>IONIZATION PROBABILITY</u>	<u>JET SEPARATOR ENRICHMENT</u>	<u>RELATIVE SENSITIVITY</u>
NH ₃ (m/e 17)	0.53	0.58	0.91
H ₂ O (m/e 18)	0.85	0.59	1.45
HCN (m/e 29)	0.69	0.73	0.94
CO (m/e 28)	1.2	0.75	1.6
N ₂ (m/e 28)	1.3	0.75	1.7
CH ₃ CN (m/e 41)	0.89	0.95	0.93
CO ₂ (m/e 44)	1.0	1.0	1.0
CH ₃ NO ₂ (m/e 61)	0.96	1.27	0.77

Note that hydrogen is removed by the jet separator and cannot be detected as a reaction product.

The reactor was a glass tube, 1 cm in diameter with a glass frit on the bottom to support the catalyst bed. The catalyst bed was 0.6 cm deep. The temperature of the bed was monitored by a chromel-alumel thermocouple attached to the outside of the reactor. Pressure was measured by a diaphragm gauge located downstream of the reactor. Total pressure in the reactor was maintained of 1 atm. A blank run of nitromethane flowing through the reactor with no catalyst showed no activity up to 300°C, which was the maximum temperature used in these studies.

A typical experiment consisted of outgasing the catalysts to 275°C under vacuum for 30 min. and then allowing them to cool to 100°C while still under vacuum. Gas flow was started with a helium flow rate of 70 cm³/min (measured at STP). The nitromethane pressure was fixed by choosing the temperature of the temperature bath containing the nitromethane. The reactor temperature was ramped up to 270°C at a rate of 2°C/min and a mass spectrum of the reactor effluent was recorded every 15 sec. After reaching the final temperature the reactor temperature was held constant, and mass spectra continued to be recorded. A typical set of spectra for the ammonia product are shown in Figure 2. Similar results are obtained for all reaction products with the exception of hydrogen. The ordinate is scan number, which corresponds to



FIGURE 2
AMMONIA PRODUCT YIELD FROM
NITROMETHANE DECOMPOSITION
OVER NiO/ALUMINA CATALYST

time. The rising portion of the curve, from scan 100 to 350 corresponds to heating of the reactor from 145 to 270°C. The kinetic parameters (activation energy and pre-exponential factors) may be evaluated from this data. The falling portion of the curve from scans 350 to 600 corresponds to the isothermal reaction rate during which catalyst deactivation is occurring. The rate of catalyst deactivation may be determined from this data.

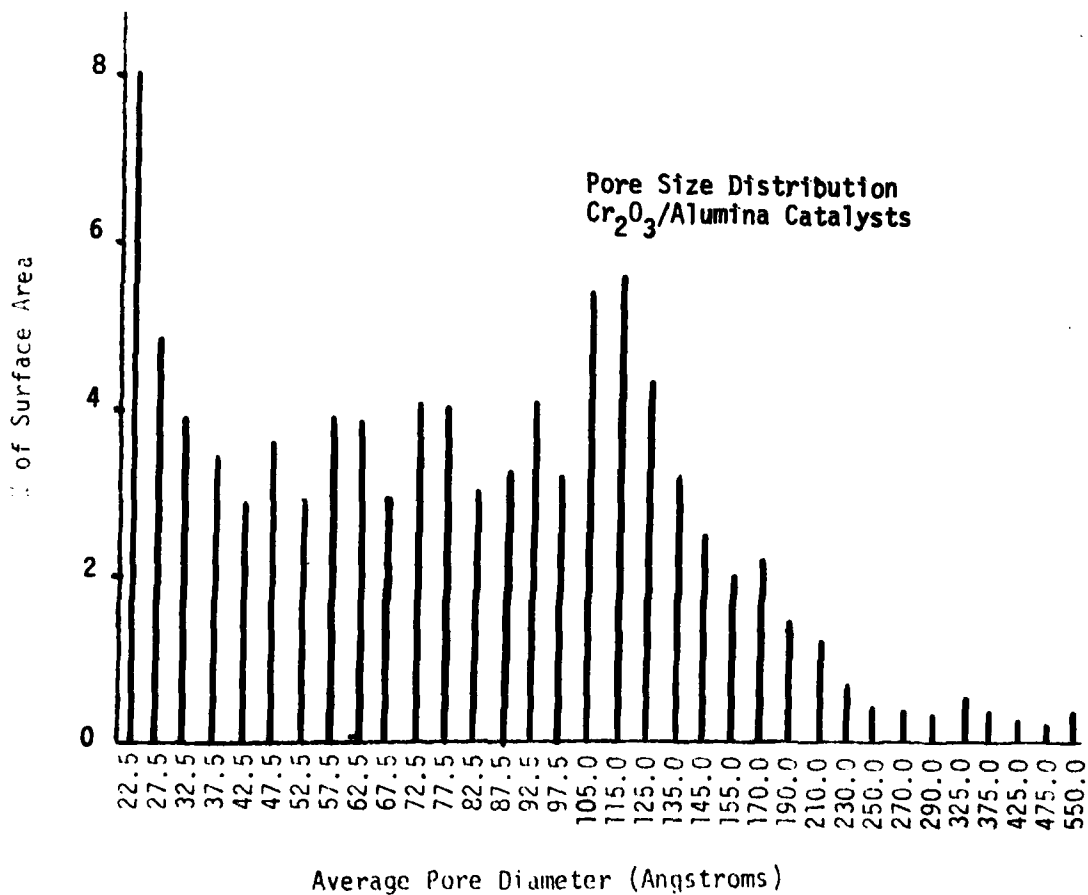
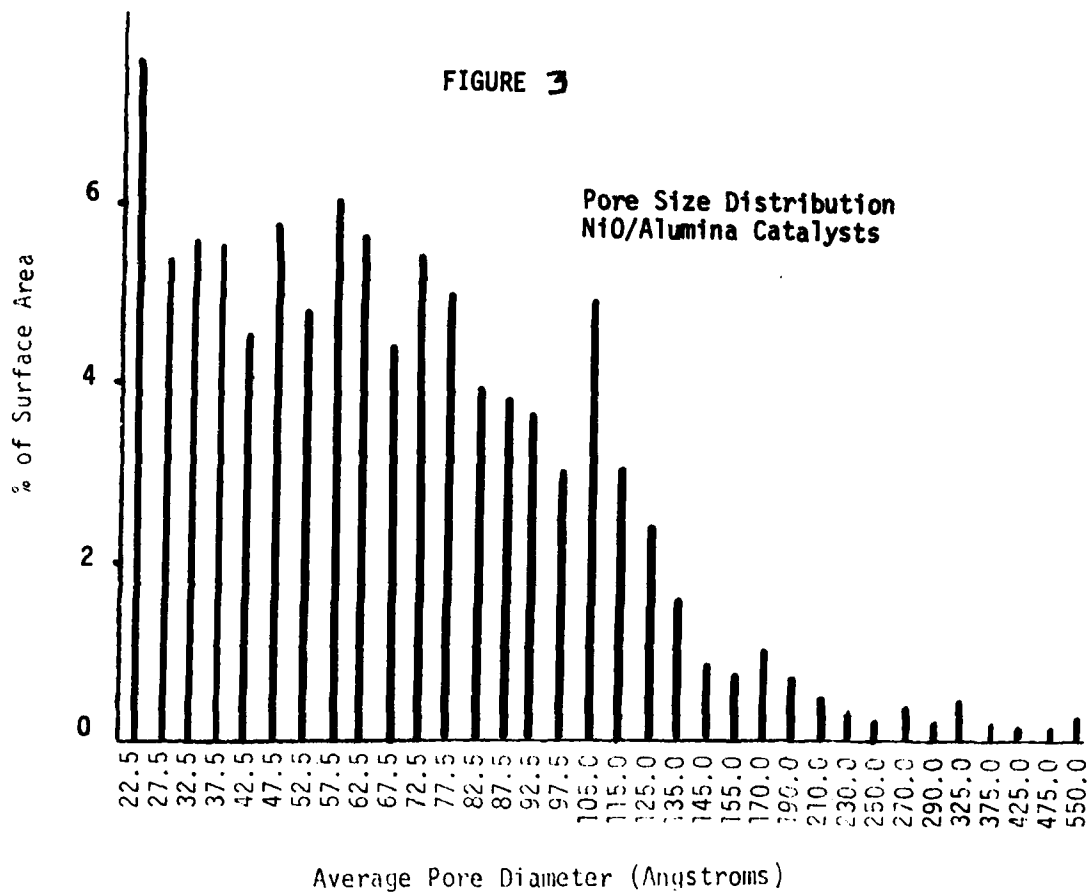
A second type of experiment that was performed was to vary the nitromethane pressure while maintaining the reactor temperature fixed. In this experiment, the temperature of the nitromethane bath was increased gradually by heating a water bath from 0°C to 35°C, which caused a variation of the nitromethane pressure from 8 torr to 60 torr. The reactor temperature and helium flow were maintained fixed at 264°C and 70 cm³/min, respectively. A fixed Argon leak was added to the Helium flow to calibrate the reactor pressure. Reactor effluents were monitored every 10 sec, which corresponded to every 1 torr increase in feed pressure at 50 torr.

The catalysts used in these experiments were obtained from Alfa Products. They were both 3 mm pellets with a nominal surface area of 70 m²/g. The NiO/alumina catalysts were 42% NiO by weight and the Cr₂O₃/alumina catalysts were 15% Cr₂O₃ by weight. X-ray diffraction analysis showed no crystallinity for either catalyst. BET analyses were performed with a Micromeritics Digisorb 2500. Surface area and pore volume distributions were obtained on the pellets and <160 mesh powder. The surface area results given in Table II showed little effect due to crushing. Pore size distributions for the two catalysts are given in Figure 3.

TABLE II
BET SURFACE AREA OF CATALYSTS

<u>Catalyst</u>	<u>Surface Area (m²/g)</u>
Cr ₂ O ₃ /alumina Pellet	61.0
Cr ₂ O ₃ /alumina Crushed	61.3
NiO/alumina Pellet	75.1
NiO/alumina Crushed	80.7

FIGURE 3

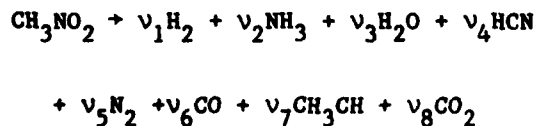


IV. IDENTIFICATION OF REACTION PRODUCTS

The reaction products from nitromethane decomposition were determined from their mass fragmentation patterns. Listed in Table III are the mass spectra for various possible reaction products. Table IV lists the mass spectra for the reactor effluent with Cr_2O_3 /alumina and NiO/alumina catalysts. The reaction products identified were NH_3 , H_2O , HCN, CO and N_2 , CH_3CN and CO_2 . In addition, H_2 was determined to be a product, although it could not be detected in these experiments.

Several other species could be eliminated as significant reaction products. The m/e: 17 m/e 16 ratio corresponded to that for NH_3 , indicating that the m/e 16 fragment in the reactor effluent spectra was due to NH_3 and not CH_4 . The results also indicated that the NO_x products were also insignificant as the m/e 30: m/e 46: m/e 61 ratio was the same during reaction as found for pure nitromethane.

From the experimental results, it was impossible to separate the CO and N_2 products directly, and any H_2 product could not be detected. It was possible to separate out these products from the data by using mass balances in conjunction with the experimental results. For the chemical reaction



four mass balances may be written for the four atomic species. In addition, the stoichiometric coefficients for NH_3 , H_2 , HCN, CH_3CN , and CO_2 were directly available from the experimental results; they were computed as

$$\nu_i = \frac{P_{i,\text{effluent}}}{P_{\text{NM, inlet}} - P_{\text{NM, effluent}}} = \frac{(m/e)_i}{(m/e)_{61}^0 - (m/e)_{61}} * \frac{R_i}{R_{\text{NM}}}$$

where

$(m/e)_i$ is the magnitude of the product peak

TABLE III

FRAGMENTATION OF SPECIES AT 25eV

	m/e fragment	(Relative Magnitude)		
CH ₄	16(100)	15(40)		
NH ₃	17(100)	16(35)		
H ₂ O	18(100)	17(8)		
HCN	27(100)	28(2)		
CO	28(100)			
N ₂	28(100)			
NO	30(100)	14(6)		
CH ₃ CN	41(100)	40(45)	14(8)	42(5)
CO ₂	44(100)			
NO ₂	30(100)	46(80)	16(8)	
CH ₃ NO ₂	30(100)	61(58)	15(40)	46(35)

TABLE IV

MASS SPECTRA OF REACTOR EFFLUENT

m/e	RELATIVE MAGNITUDE	
	Cr ₂ O ₃ /Alumina Catalyst	NiO/Alumina Catalyst
15	38.02	40.35
16	19.73	20.17
17	54.32	64.12
18	58.75	26.45
27	41.64	0.89
28	17.90	8.96
29	3.82	1.79
30	80.28	100.00
40	2.41	1.06
41	8.45	4.93
43	4.42	1.79
44	100.00	83.85
45	4.42	1.79
46	30.38	35.42
61	46.27	54.70

$(m/e)_{61}^0 - (m/e)_{61}$ is the change in magnitude of the nitromethane parent peak due to reaction

R_i is the relative sensitivity given in Table I.

The known stoichiometric coefficients were substituted into the mass balances to determine the stoichiometric coefficients for H_2 , N_2 , and CO . The reaction stoichiometries for nitromethane decomposition over Cr_2O_3 /alumina and NiO /alumina at 10 torr and $260^\circ C$ are summarized in Table V.

The influences of temperature, pressure, and catalyst deactivation on the reaction stoichiometry were also examined. The effects of temperature and pressure on reaction stoichiometry are shown in Figures 4 and 5. For both catalysts, it was found that hydrogenation activity increased with increasing pressure and decreasing temperature. Hence, the relative amount of H_2O and NH_3 products increased with increasing pressure, while CO_2 , N_2 , and H_2 products decreased. Hydrogenation activity also showed a slight increase with time on stream while total catalyst activity decreased. Tables VI and VII compare the reaction stoichiometries for fresh catalysts and after 90 minutes on stream. The NH_3 product showed an increase in relative yield while CO_2 and N_2 showed decreases in their relative yields.

A cautionary note should be raised at this point. The quantitative aspects of these results rely on the assumption that instrument sensitivity is independent of pressure and gas composition. This assumption is only approximately true so that the stoichiometries reported should be viewed as being accurate to within $\pm 10\%$. Furthermore, changes in stoichiometry with pressure and temperature should be viewed only as indicating the direction of change, and the quantitative aspects should be viewed with caution.

V. KINETICS OF THE HETEROGENEOUS DECOMPOSITION

The reactor configuration was such that it was most appropriately modelled as a well mixed vessel. The rate of reaction was then given by the difference of the molar flow rates in and out of the reactor. As helium was always in a great excess it was reasonable to assume that the total molar flow rate was constant, equal to the helium flow. The nitromethane flow into the reactor (F_i) is given by

TABLE V

REACTION STIOCHIOMETRY

Species	Homogeneous Reaction*	Over Cr ₂ O ₃ /Alumina ⁺	Over NiO/Alumina ⁺
H ₂	0.003	0.10	0.06
CH ₄	0.26		
NH ₃		0.33	0.66
H ₂ O	0.60	0.69	0.33
HCN	0.10	0.25	0.01
CO	0.37		0.03
N ₂	0.06	0.18	0.12
C ₂ H ₄	0.01		
H ₂ CO	0.12		
NO	0.74		
C ₂ H ₆	0.01		
CH ₃ OH	0.07		
CH ₃ CN		0.05	0.07
CO ₂	0.05	0.66	0.82
N ₂ O	0.02		
NO ₂	0.01		

* Taken from ref. 8

+ At a nitromethane pressure of 10 torr

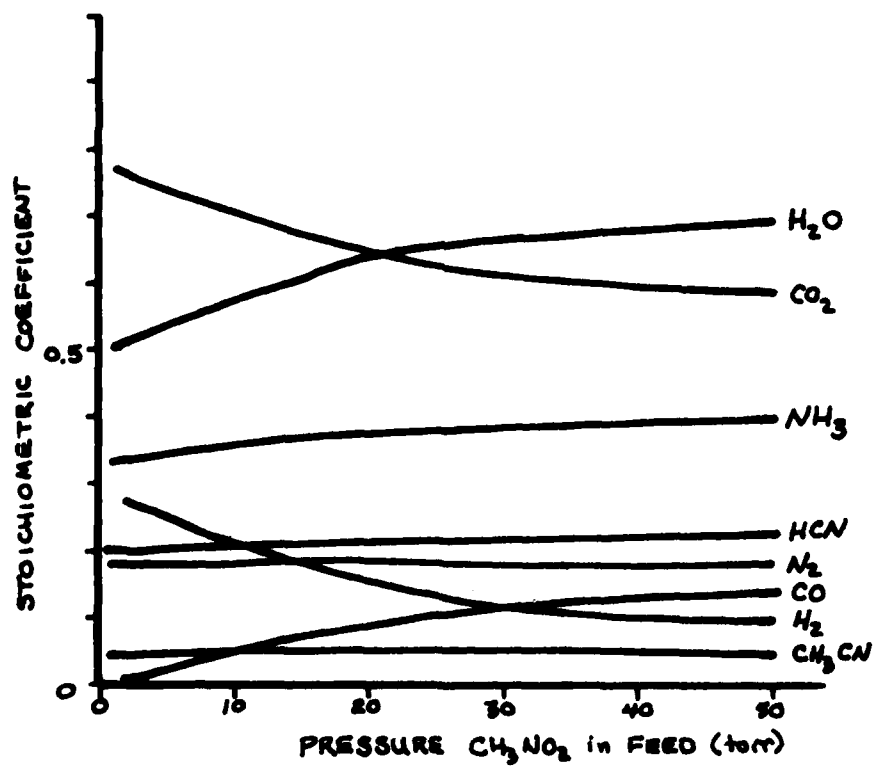
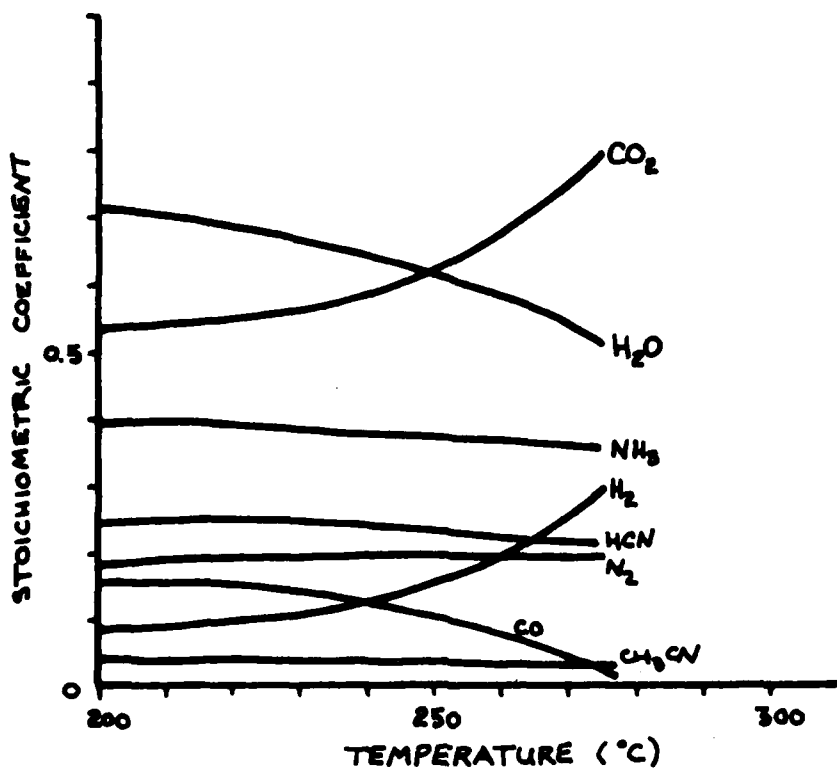


FIGURE 4
 TEMPERATURE AND PRESSURE EFFECT ON
 REACTION STOICHIOMETRY ON C₂O₃/alumina

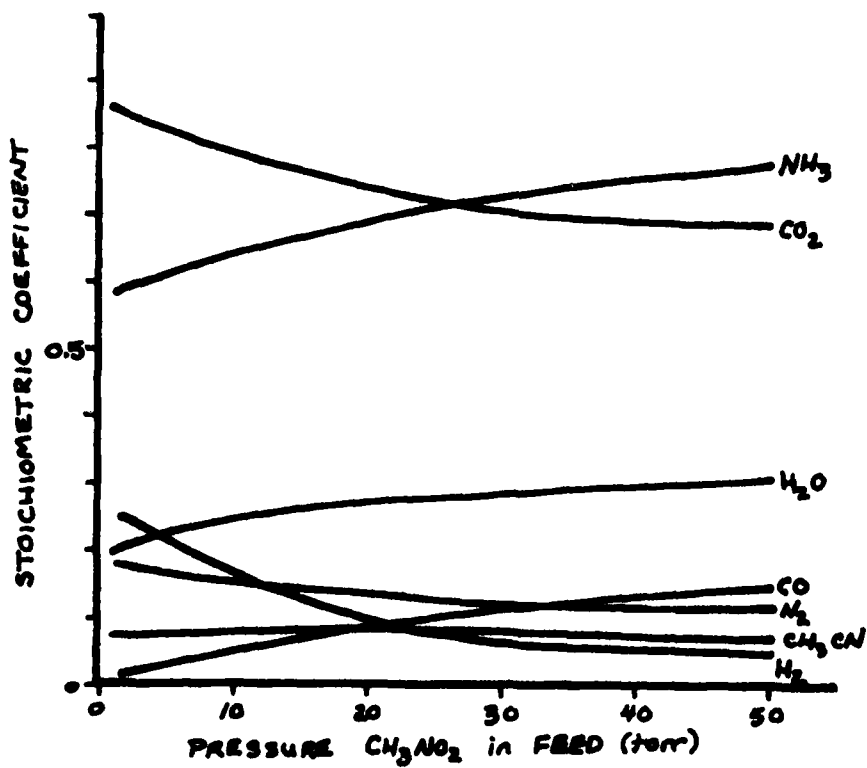
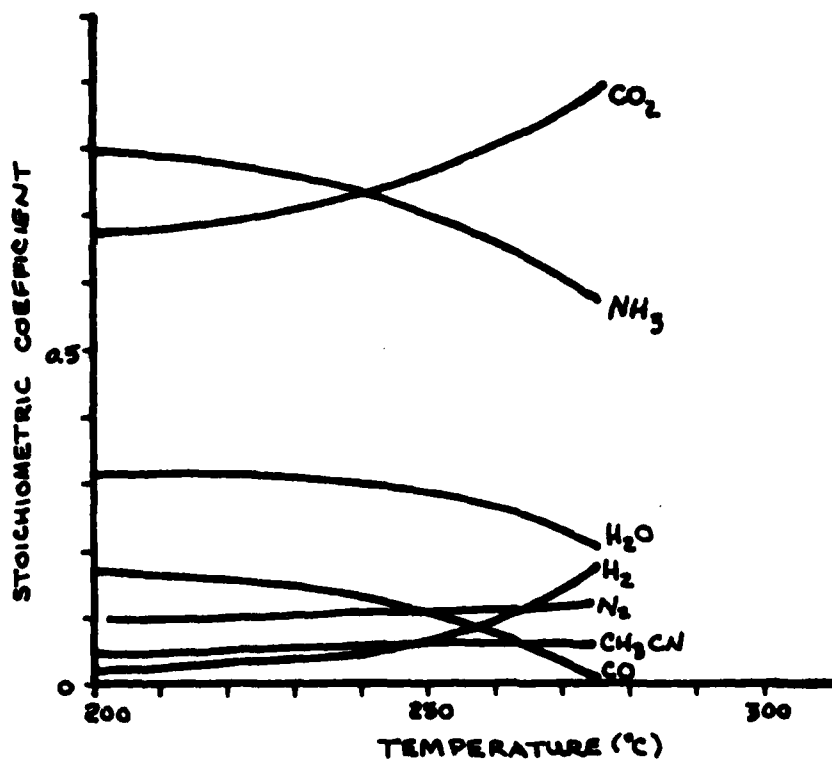


FIGURE 5
TEMPERATURE AND PRESSURE EFFECT ON
REACTION STOICHIOMETRY ON NiO/alumina

TABLE VI

INFLUENCE OF CATALYST DEACTIVATION ON
REACTION STIOCHIOMETRY - $\text{Cr}_2\text{O}_3/\text{Alumina}$ T = 265°C P_{CH₃NO₂} = 10 torr

SPECIES	FRESH CATALYST	90 MINUTES ON STREAM
H ₂	0.10	0.12
NH ₃	0.33	0.36
H ₂ O	0.69	0.67
HCN	0.25	0.28
N ₂	0.18	0.17
CO	----	0.01
CH ₃ CN	0.05	0.03
CO ₂	0.66	0.66

TABLE VII

INFLUENCE OF CATALYST DEACTIVATION ON
REACTION STIOCHIOMETRY - NiO/AluminaT = 265°C P_{CH₃NO₂} = 10 torr

SPECIES	FRESH CATALYST	90 MINUTES ON STREAM
H ₂	0.06	0.02
NH ₃	0.66	0.71
H ₂ O	0.33	0.31
HCN	0.01	----
N ₂	0.12	0.09
CO	0.03	0.10
CH ₃ CN	0.07	0.03
CO ₂	0.82	0.79

$$F_i = q(4.06 \times 10^{-2} \text{ gmol/cm}^3) \frac{P^0}{760}$$

where

q = helium flow measured by the flow meter in $\text{cm}^3 \text{min}^{-1}$

P^0 = nitromethane vapor pressure in torr at the bath temperature.

The molar flow of reaction products in the reactor effluent (F_{oi}) was determined from

$$F_{oi} = q (4.06 \times 10^{-2}) \frac{(m/e)_i}{(m/e \ 61)} *S* \frac{P^0}{760}$$

where

$(m/e)_i$ = mass spectrometer signal of product i

$m/e \ 61$ = mass spectrometer signal of CH_3NO_2 with no reaction

S = sensitivity of reaction product relative to nitromethane

The rate of reaction is given by the difference in the molar flow rates. Reaction rates between 10^{-6} gmol/s to 10^{-4} gmol/s were measured. Specific rates were obtained by dividing the measured rates by the catalyst surface area. The influence of diffusional limitations on the reaction kinetics may be ascertained using the Weisz-Prater criteria (3). The Weisz ϕ parameter may be estimated assuming an effective diffusion coefficient of $10^{-2} \text{ cm}^2/\text{s}$.

$$\phi = \frac{(r_v)_{\text{obs}} L^2}{D_e C}$$

where

$(r_v)_{\text{obs}}$ = observed reaction rate per unit volume of catalyst

L = characteristic particle dimension

D_e = effective diffusion coefficient

C = concentration in reactor

For the observed reaction rates it was found that

$$10^{-1} < \phi < 10$$

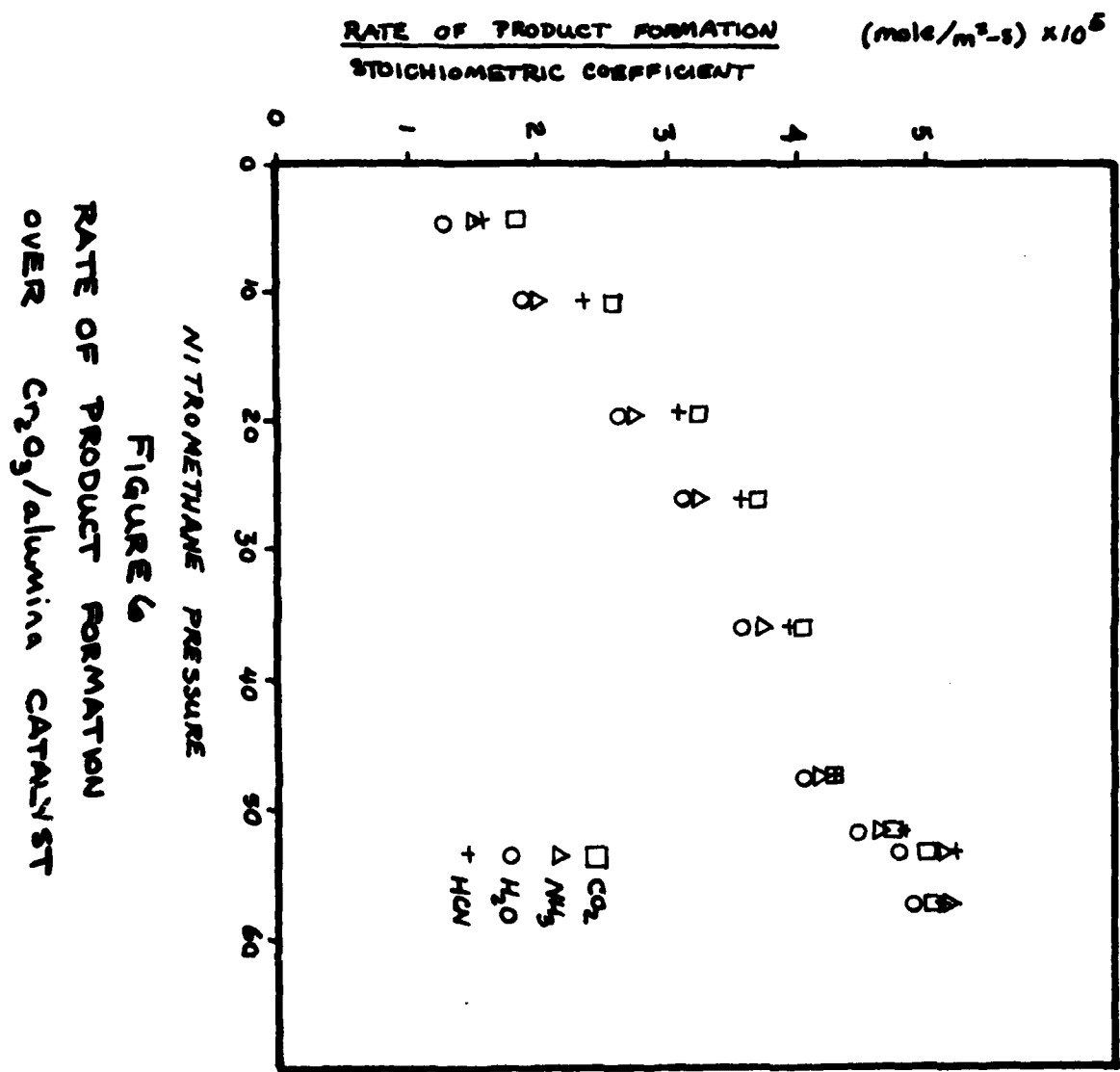
This represents an intermediate regime in which diffusional effects may or may not be important. It is inconvenient to ignore diffusional limitations in the kinetic analysis. We shall return to this assumption after developing a kinetic model.

The rate of formation of the various reaction products from nitromethane decomposition over a Cr_2O_3 /alumina catalyst as a function of pressure is shown in Figure 6. The rates of formation of various products as a function of temperature are shown in Figure 7 for scans 0-250, and the rates of formation of the products as a function of catalyst activity are shown in Figure 7 for scans 250-370. These results show that except for minor variations all the reaction products are formed at the same relative rates indicating a single rate limiting step in the reaction sequence. Similar results were obtained for the NiO/alumina catalyst.

The existence of a single rate limiting step considerably simplifies the kinetic analysis as it will suffice to consider a single reaction product. For kinetic analysis, it was decided to follow the CO_2 product as it represented the most significant product over both catalysts. The rate of CO_2 formation as a function of nitromethane pressure in the reactor over the Cr_2O_3 /alumina and NiO/alumina catalysts are shown in Figures 8 and 9, respectively. The observed behavior, an increasing rate at low pressures approaching an asymptotic limit at higher pressures, suggested a Hougen-Watson type of rate expression (4)

$$r_s = v_{\text{CO}_2} k_s C \frac{K_e P}{1 + K_e P}$$

where



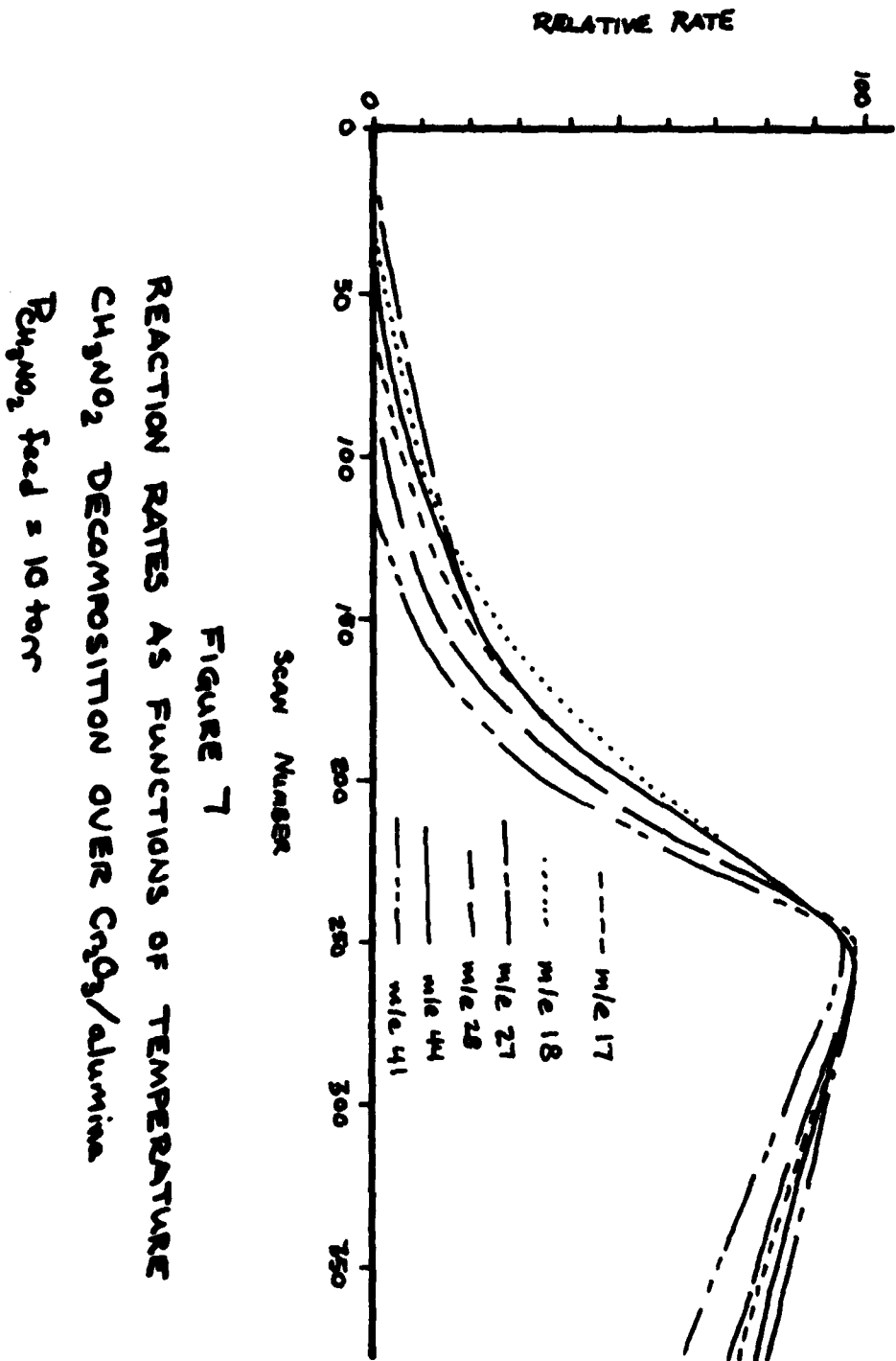


FIGURE 7

REACTION RATES AS FUNCTIONS OF TEMPERATURE
 CH_4NO_2 DECOMPOSITION OVER C_2O_3 /ALUMINA

$P_{\text{CH}_4\text{NO}_2}$ FEED = 10 Torr

v_{CO_2} is the stoichiometric coefficient for CO_2 formation

k_s is the rate constant for the rate limiting decomposition step

C_s is the number of surface adsorption sites

K_e is the equilibrium constant for nitromethane adsorption

P is the nitromethane pressure

It should be noted in passing that the term $C_s \frac{K_e P}{1 + K_e P}$ represents the number of nitromethane molecules adsorbed on the catalyst surface.

In the rate expression given above, both k_s and K_e are exponential functions of temperature. The surface rate constant k_s may be written as

$$k_s = A e^{-E/RT}$$

where

A is a preexponential factor

E is the activation energy of the rate limiting surface reaction

R is the gas constant

T is the absolute temperature

The adsorption equilibrium constant may be written as

$$K_e = e^{-\Delta G/RT} = e^{\Delta S/R} e^{-\Delta H/RT}$$

where

ΔG is the free energy change for adsorption

ΔS is the entropy of adsorption

ΔH is enthalpy of adsorption

All the kinetic parameters may be estimated from an appropriate choice of experiments. At low pressure and high temperature, the rate expression may be approximated by

$$r_s \approx v_{CO} k_s C_s K_e P$$

A plot of $\ln r/P$ versus $1/T$ has a slope of $-(E + \Delta H)/R$, and an intercept of $\ln(v_{CO} AC_s) + \frac{\Delta S}{R}$. At high pressures the rate asymptotically approaches a constant

$$r_s \approx v_{CO_2} k_s C_s$$

At high pressure, a plot of $\ln(r)$ versus $1/T$ has a slope of $-E/R$ and an intercept of $\ln(v_{CO_2} AC_s)$. Combining the high and low pressure limits with the known stoichiometry one can obtain E , ΔH , ΔS , and AC_s . The values obtained in these experiments are listed in Table VIII. These kinetic parameters have been used to calculate the isothermal reaction rates as functions of pressure and the results are compared with the experimental data in Figures 8 and 9.

VI. CATALYST DEACTIVATION

It was observed that the catalytic activity for nitromethane decomposition significantly declined with time on stream. This was observed with both the Cr_2O_3 /alumina and NiO/alumina catalysts. The catalyst deactivation on Cr_2O_3 /alumina catalysts is shown in Figure 7. Scans 250-370 are the isothermal catalytic activities as functions of time for the various reaction products over a period of 30 minutes at $265^\circ C$. It is convenient to introduce the activity function defined as

$$\zeta = \frac{\text{rate at time } t}{\text{rate at time } 0}$$

The rate of deactivation was measured at three different reactor temperatures by plotting $\ln \zeta$ versus time, consistent with first order kinetics. Attempts to fit the data with zero and second order kinetics were unsuccessful. The rate constants are summarized in Table IX. It should be noted that the rate of deactivation decreased with increasing temperature.

TABLE VIII

KINETIC PARAMETERS FOR
NITROMETHANE DECOMPOSITION

	Cr ₂ O ₃ /Alumina	NiO/Alumina
Activation Energy (kJ/mole)	164	175
Adsorption Enthalpy (kJ/mole)	-82	-92
Pre-exponential Factor AC _s (mole/m ² - s)	1.0 x 10 ¹²	2.9 x 10 ¹²
Adsorption Entropy (J/mole ^o K)	-119	-133

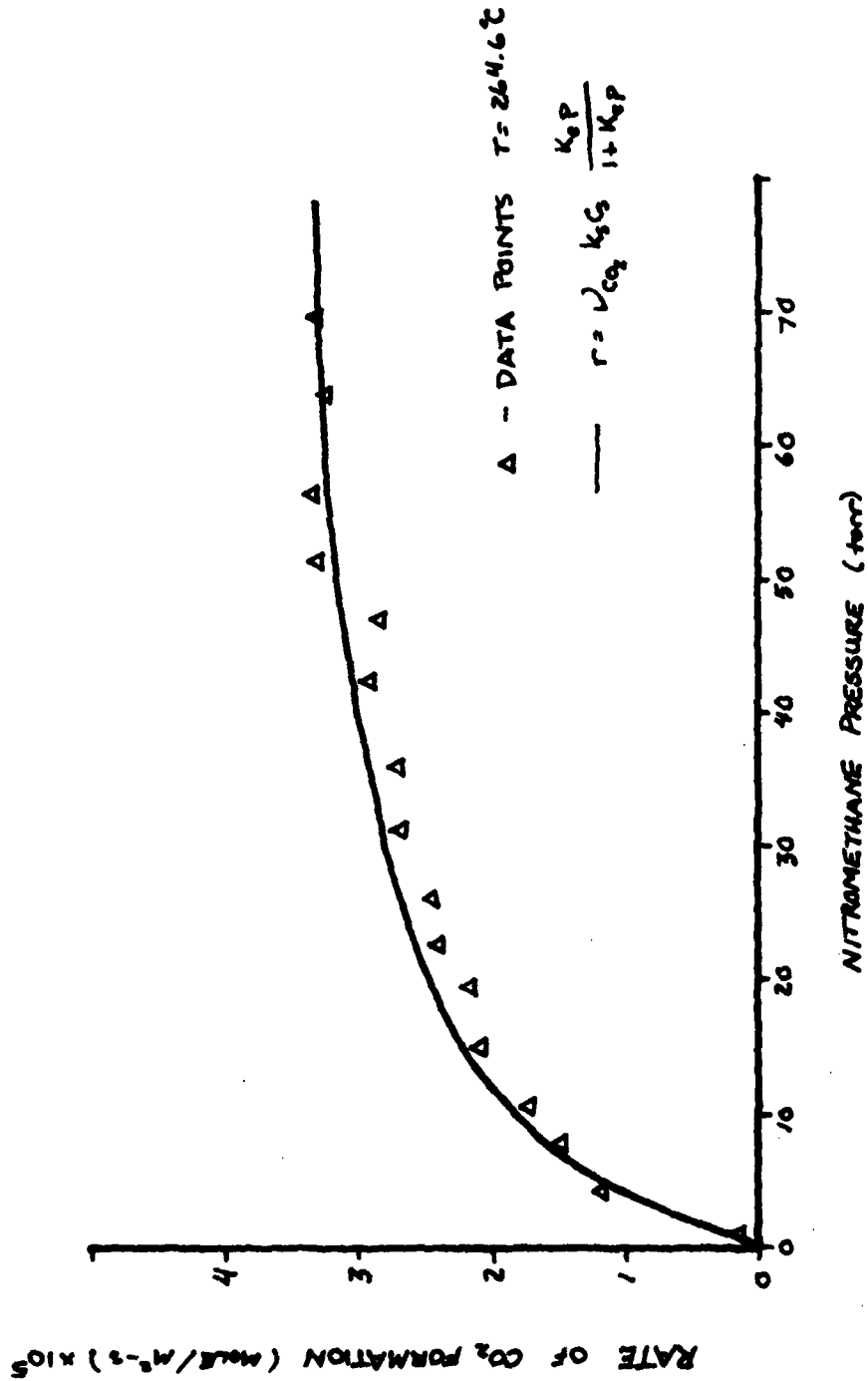


FIGURE 8
RATE OF CO₂ FORMATION FROM CH₃NO₂ DECOMPOSITION
AS A FUNCTION OF PRESSURE OVER CsO₃/alumina

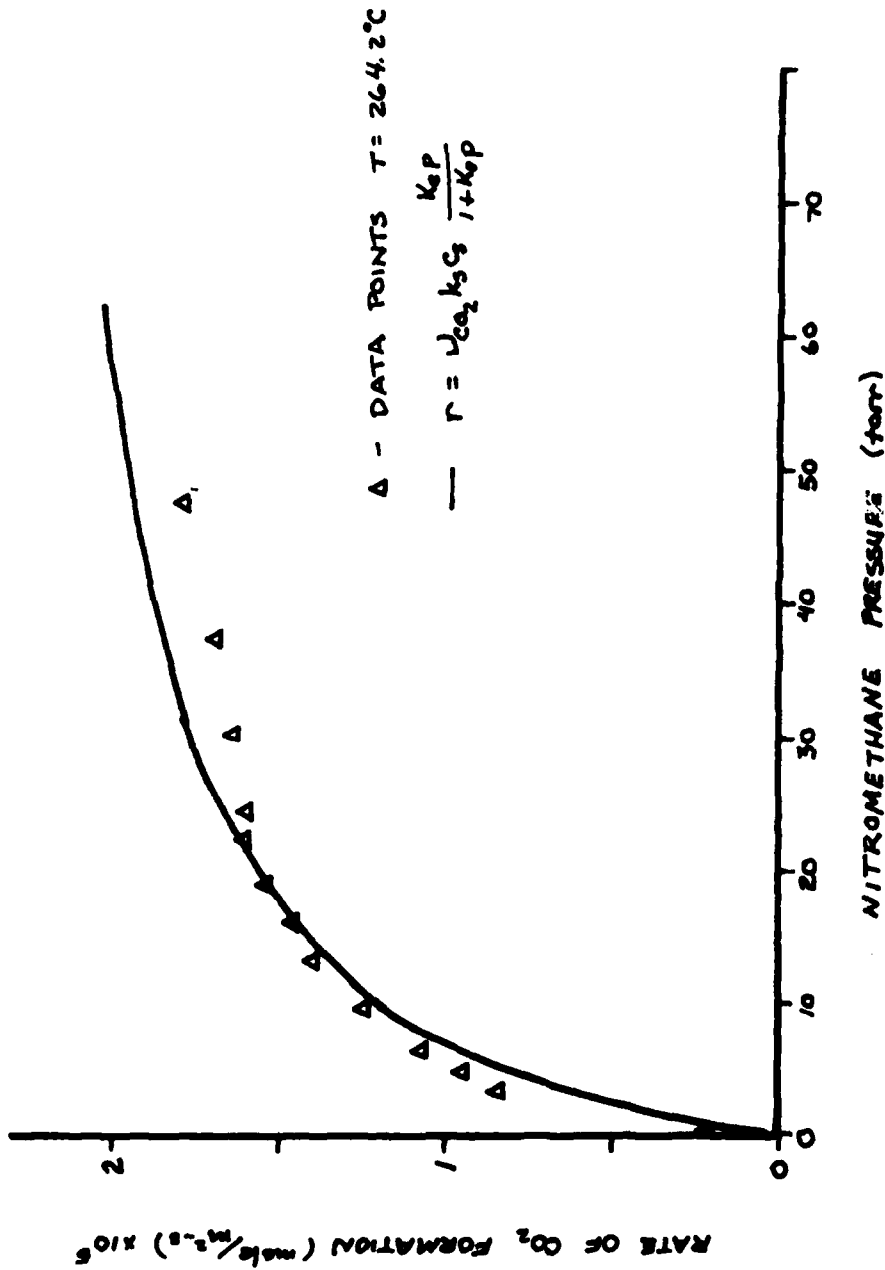


FIGURE 9
RATE OF CO₂ FORMATION FROM CH₃NO₂ DECOMPOSITION
AS A FUNCTION OF PRESSURE OVER NiO/alumina

TABLE IX

RATE FOR CONSTANTS FOR CATALYST DEACTIVATION

Temperature	Rate Of Cr ₂ O ₃ /Alumina Deactivation	Rate of NiO/Alumina Deactivation
250°C	0.017 min ⁻¹	0.016 min ⁻¹
265°C	0.0078 min ⁻¹	0.013 min ⁻¹
280°C	0.0046 min ⁻¹	0.0094 min ⁻¹

The used catalysts were characterized by a darker color compared to the fresh catalyst. BET analyses were also performed on the used catalysts. A comparison of the surface area on the new and used catalysts is given in Table X; there was approximately a 10% decrease in surface area after 90 minutes on stream at 265°C. The pore size distributions shown in Figures 10 and 11 indicate a substantial shift in the average pore size to smaller pores on the spent catalysts. Scanning electron microscopy was also used to look at the catalysts, but no significant features were noted.

VII. DISCUSSION OF EXPERIMENTAL RESULTS

The catalytic decomposition of nitromethane has not received much attention in the past. Hermoni and Salmon (5) studied the catalytic decomposition of nitromethane over various metal oxides and established an activity sequence based on the lightoff temperatures in a flow reactor. This sequence showed NiO and Cr₂O₃ to be among the most active for catalyzing nitromethane decomposition. It was also established in that study that the nitromethane partially reduced the catalyst. No detailed kinetics or product analyses were performed in that study.

The homogeneous gas phase decomposition of nitromethane has received much more attention than the heterogeneous reaction (6-9). The homogeneous decomposition has been found to be first order and produce NO, H₂O, CO and CH₄ as the main reaction products. A recent study looked at the reaction mechanism in detail and found the reaction to be first order with a rate constant $k = 10^{11} e^{(-44500/RT)} s^{-1}$, and the stoichiometry given in Table V (8,9).

From the results in Table V, it is clear that the heterogeneous reaction is substantially different from the gas phase reaction. The most noteworthy differences are the NH₃ and CO₂ products from the catalytic decomposition, which are insignificant in the homogeneous reaction, and the absence of CH₄ and NO_x products from the heterogeneous reaction.

These differences suggest substantially different reaction mechanisms. The gas phase reaction is known to proceed by the initial breaking of the C-N

TABLE X

COMPARISON OF SURFACE AREAS FOR
NEW AND USED CATALYSTS

CATALYST	SURFACE AREA (m^2/g)
$\text{Cr}_2\text{O}_3/\text{alumina}$ new ($\zeta = 1$)	61.0
$\text{Cr}_2\text{O}_3/\text{alumina}$ used ($\zeta = 0.58$)	53.2
$\text{NiO}/\text{alumina}$ new ($\zeta = 1$)	75.0
$\text{NiO}/\text{alumina}$ used ($\zeta = 0.49$)	70.9

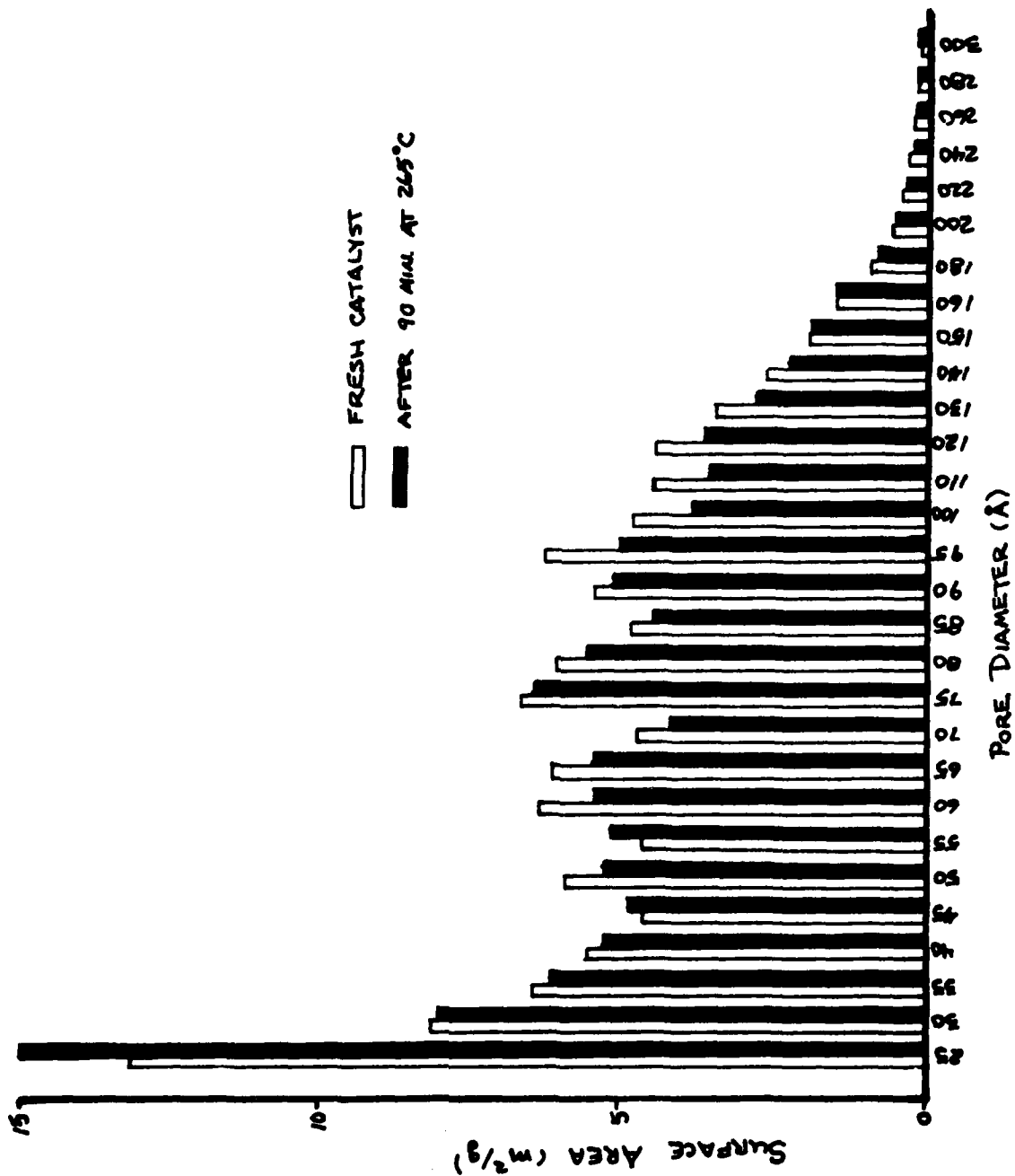


FIGURE 10
 PORE SIZE DISTRIBUTIONS
 Cr₂O₃/alumina CATALYSTS

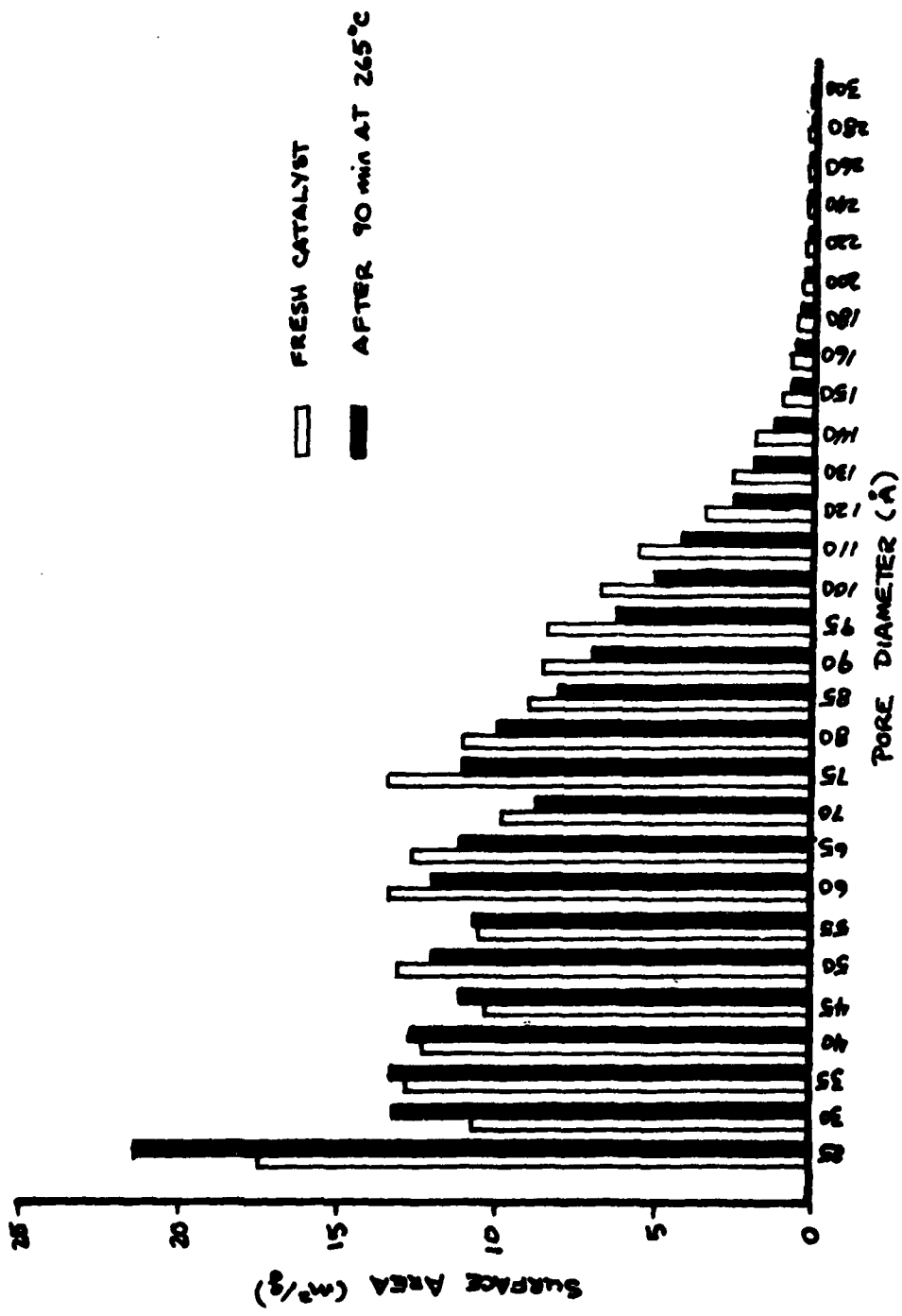
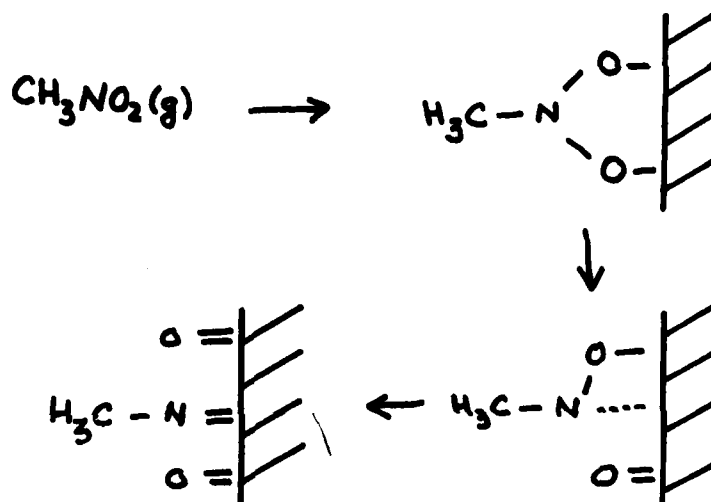


FIGURE 11
 PORE SIZE DISTRIBUTIONS
 NiO/alumina CATALYSTS

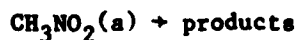
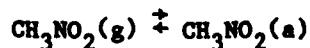
bond to give NO_2 and CH_3 (9). The NO_2 is subsequently degraded to NO , while the methyl radicals are either oxidized or abstract hydrogen to make methane. The heterogeneous reactions show substantial HCN and CH_3CN products, and no NO_x or CH_4 products. This suggests that breaking the C-N bond is not a prerequisite to reaction. A more reasonable alternative is the breaking of the N-O bonds as rate limiting. A possible mechanism based on this assumption is shown below. The bonding to the surface is shown to occur via the oxygens, and may be envisioned to occur at anion vacancies in the metal oxide lattice.



Many other possibilities can be suggested for the reaction mechanism, and from the available data it is impossible to make any more definitive statement. We did attempt to identify a possible kinetic isotope effect using CD_3NO_2 ; however, the reaction rates for the deuterated nitromethane were not substantially different than the normal species to draw any conclusions.

Another noteworthy feature illustrated in Table V was the difference in reaction products for the Cr_2O_3 and NiO catalysts. The NiO catalysts form much more NH_3 product and much less HCN product. This suggests that NiO is much more effective at breaking the C-N bond and is a better ammonia synthesis catalyst.

The kinetics for the heterogeneous decomposition of nitromethane suggest the reaction proceeds by a classic Langmuir-Hinshelwood reaction.



Adsorption equilibrium is established and the adsorbed nitromethane undergoes a unimolecular surface decomposition as the rate limiting step. The kinetic parameters that were determined for this mechanism give an adequate fit to the data, although the error limits on these values are fairly significant. There are two sources of error in the calculation of the kinetic parameters. First is the presence of diffusion limitations (10). For reaction in a porous catalyst the observed rate is related to the actual rate by an effectiveness factor (η)

$$r_{\text{obs}} = \eta r_{\text{act}}$$

The effectiveness factor is a function of the Thiele modulus (ϕ)

$$\phi = L \sqrt{k_v/D_e}$$

where

L is the characteristic particle dimension

k_v is the effective homogeneous rate constant

D_e is the effective diffusion coefficient

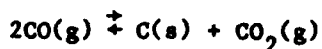
Using the kinetic parameters and rate expression determined here, the effectiveness factor ranged between 0.4 and 1.0 for the experimental conditions encountered. The value of the effectiveness factor decreased with increasing temperature. The diffusional limitations to reaction result in low estimates for the activation energy of the surface reaction and the heat of adsorption. The second source of error was the assumption that the rate of reaction was described by certain asymptotic limits of the rate expression.

This assumption should lead to a low estimate of the activation energy for surface reaction and a high estimate for the heat of adsorption. It is estimated that these two sources of error lead to overall error limits of ± 15 kJ/mole on the kinetic parameters. Further experiments are called for using finely crushed catalyst to avoid diffusional limitations. Additional experiments at higher temperatures and pressures would also be useful for more accurate kinetic parameter determination.

It is interesting to note that diffusional effects were observed by Acurex in their study, although they failed to recognize them as such. They observed that crushing the Cr_2O_3 /alumina catalysts reduced the minimum light-off temperature, which they attributed to an increase in surface area. As we have shown crushing did not significantly alter the surface area; however, the smaller catalyst particles would offer substantially less diffusional resistance resulting in a greater observed reaction rate. The diffusional resistances are of particular importance as the temperature increases and hence are magnified in the Acurex study where temperatures up to 1700K were achieved.

Diffusional limitations are extremely important for optimal design of a catalyst bed in a monopropellant engine. Large pellets are desirable from the viewpoint of reducing the pressure drop which accompany the high gas throughput, while small particles are desirable to achieve high reaction rates and fast response time. Obviously, a tradeoff must be made to optimize the engine performance. Monolithic catalysts also offer a reasonable alternative for monopropellant systems. By using an appropriate washcoat, this type of catalyst can be designed to have high surface areas with short diffusion lengths, and at the same time the pressure drop can be kept low.

Perhaps the most significant problem with developing a nitromethane based monopropellant system is the deactivation of the catalyst. Acurex reported that carbonaceous deposits built up on the catalyst with continued use. The extent of the carbon deposit was observed to be less for continuous operation than for intermittent operation. In the present studies, we studied the rate of catalyst deactivation at various temperatures. It was found that the rate of deactivation decreased with increasing temperature. This is consistent with carbon deposition being thermodynamically controlled. The formation of graphite can be described by the Boudouard reaction



This reaction is exothermic ($\Delta H = -170\text{kJ/mole}$), so that the amount of carbon deposition decreases with increasing temperature. Acurex observed the intermittent operation to be more detrimental because the cold starts resulted in more operating time at low temperatures where carbon deposition is preferred.

The deposition of carbon appears to deactivate the catalyst by blocking sites for reaction. Site blockage occurs in two ways; first, carbon is deposited on the metal oxide so that nitromethane can no longer adsorb on the metal oxide. Second, carbon deposits can block pores so that nitromethane can no longer diffuse into the pores, thus reducing the available surface area for reaction. Pore blockage appears to be significant as it was found that surface area as determined from N_2 adsorption decreased with time on stream. The pore distributions also showed a significant decrease in the amount of surface area associated with 50-200A pores. This range represents the most significant pore sizes for reaction as the surface area in this range is substantial and diffusional limitations are much less significant than in the smaller pores.

Carbon deposition is a major problem with nitromethane as a monopropellant. Nitromethane is fuel rich and will tend to reduce the catalyst and/or deposit carbonaceous material. In looking for desensitizers for nitromethane, Acurex further aggravated the problem by adding unsaturated hydrocarbons, making the feed even more fuel rich. To overcome the problem of carbon deposition on the metal oxide catalyst it would be desirable to have oxidant rich feeds. Some possibilities might be mixed fuels of nitromethane and nitroform, tetranitromethane, or hydrogen peroxide. In choosing desensitizers, it is worthwhile noting that carbon deposition usually proceeds via aromatic rings, which are known to form graphite on acidic metal oxides (11). This accounts for the observation that Acurex made showing the rate of carbon deposition decreased through the series o-xylene > cyclohexane > octadiene. Therefore, in choosing desensitizers one should avoid materials that can readily form aromatics.

VIII. REACTOR ANALYSIS FOR MONOPROPELLANT SYSTEMS

The ultimate goal in developing a kinetic model for nitromethane decomposition is its use in the design and analysis of a reactor for small space thrusters. It is instructive to present a model for the reactor and identify the important parameters effecting the performance. The simplest model for the reactor is shown below. It assumes plug flow of the gas phase through the reactor, with no mass transfer limitations between the bulk fluid and the catalyst. The heat of reaction is released in the solid catalyst phase. Heat transfer between the catalyst and gas is described by a heat transfer coefficient. The model also includes the effect of heat conduction through the solid. The four independent variables are the total pressure (p), nitromethane concentration (C_A), gas phase temperature (T), and catalyst temperature (T_s). All of these quantities are functions of position down the reactor bed (Z) and time (t). The descriptive equations are

$$\frac{\partial p}{\partial Z} = \frac{Z f \rho_g}{g d_p}$$

$$\frac{\partial C_A}{\partial t} = \frac{\partial (u C_A)}{\partial Z} - r_A$$

$$\frac{\partial T}{\partial t} = -u \frac{\partial T}{\partial Z} + \frac{h a}{C_p} (T_s - T)$$

$$\frac{\partial T_s}{\partial t} = \frac{(-\Delta H) r_A}{C_p^s} - \frac{h a}{C_p^s} (T_s - T) + \frac{k_e}{C_p^s} \frac{\partial^2 T_s}{\partial Z^2}$$

$$u = u_o \left(1 + \delta \left(1 - \frac{C_A}{C_{A0}} \frac{T_o}{T} \right) \right)$$

with boundary conditions

$$t = 0$$

$$T_s = T_a$$

$$T = T_a$$

$$C_A = 0$$

$$P = 0$$

$$z = 0, t > 0$$

$$T = T_o$$

$$C_A = C_{A0}$$

where the parameters in the above equation are

f is the friction factor for packed beds given by correlations

ρ_g is the gas phase density

u is the superficial fluid velocity

d_p is the catalyst particle diameter

r_A is the rate of reaction at C_A, T_s

h is the gas-solid heat transfer coefficient

a is the interfacial area for heat transfer

C_p is the gas phase heat capacity

C_p^s is the catalyst heat capacity

K_e is the thermal conductivity of the catalyst

u_o is the inlet gas velocity

T_a is the cold bed temperature

T_o is the inlet gas temperature.

From examination of these model equations it is possible to show some of the characteristic behavior of a monopropellant thruster. Figure 12 shows the response of a reactor as a function of time. The sequence of events may be described as follows

i) Pre-heated catalyst bed heats up cold nitromethane feed.

ii) Lightoff occurs and the exothermic reaction heats the catalyst bed. The heat generated is transferred to the gas which carries it downstream to heat the end of the reactor bed.

iii) Heat conduction through the solid heats up the upstream portion of the bed causing the point where lightoff occurs to move upstream.

From the model the following design parameters can be identified as having the most significant impact on the response time of monopropellant thrusters.

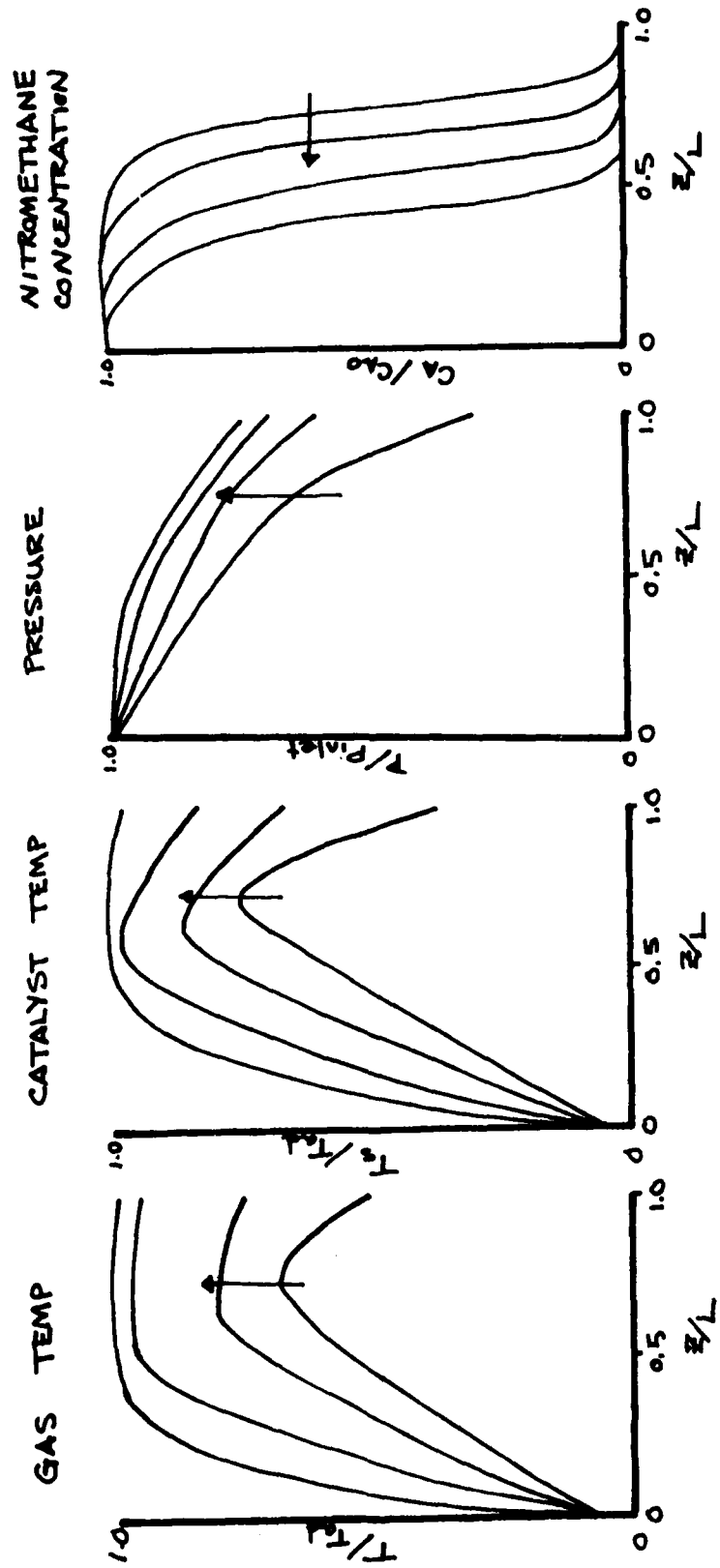


FIGURE 12
 REACTOR BED PROFILES

T_{ad} = Adiabatic decomposition temperature
 → denotes increasing time

- 1) bed length
- 2) feed temperature
- 3) bed preheat temperature

The bed length becomes important because making a bed too short can cause the cold feed to cool the bed too much preventing lightoff; on the other hand, too long a bed causes much of the heat generated to be lost to the catalyst bed downstream of where lightoff occurred. The feed temperature is important as it determines the necessary bed preheat temperature to achieve lightoff. Increasing the feed temperature above that where lightoff is achieved will result in a faster response time. The bed preheat temperature coupled with the feed temperature determines the necessary conditions to achieve lightoff and the response time. In the case where liquid propellants are used the heat contained in the catalyst bed must be sufficient to vaporize the liquid and still be at a sufficient temperature to achieve lightoff.

The model presented here is useful in understanding the results obtained by Acurex. That study measured transient temperature and pressure responses for nitromethane decomposition in a catalyst bed. As a measure of temperature they took an average along the length of the reactor. The temperature transient they determined was not representative of the response time of the system as the system will achieve maximum thrust as soon as the exit temperature is raised to the adiabatic decomposition temperature. This mistake in identifying the proper response was verified by the observation that the downstream pressure response was much faster than the temperature response (1).

Even the pressure response studies in the Acurex investigation showed an extremely long response time. Several things can be done to improve the response of this system. A shorter bed along with a heated vaporized feed would be capable of delivering full thrust with a short response time. Such configurations deserve serious consideration in developing nitromethane based monopropellants.

IX. RECOMMENDATIONS

Based on the work presented here, it may be concluded that nitromethane based monopropellant systems using hydrocarbon desensitizers and metal oxide catalysts are not feasible due to catalyst deactivation. The problem of catalyst deactivation must be overcome to develop a feasible monopropellant system. Three possible approaches are:

- 1) Identify catalyst materials that are active for nitromethane decomposition and resistant to carbon deposition. The probability of success is not very great, though zeolites or metal carbides may offer some possibilities.

- 2) Develop an insitu catalyst regeneration scheme using an oxidant to remove carbon deposits intermittently. This is an awkward system but may be feasible since most aircraft are equipped with oxidants for main engines.

- 3) Develop an oxidant rich monopropellant. Mixtures of nitromethane and hydrogen peroxide, tetranitromethane, or nitroform are a few possibilities. This approach offers the best chance for success.

To facilitate the development of a nitromethane-based monopropellant fundamental work on the reaction mechanism and kinetics would be useful in providing insight as to what materials would be catalytically active for nitromethane decomposition, and how are these material poisoned by carbon deposition. We propose to initiate such studies at Princeton University using surface science techniques. The kinetics of absorption and surface reaction can be studied on well defined surfaces elucidating the fundamental reaction mechanism and kinetics.

References

1. K.D. Seifert, S.J. Anderson, M. Friedman, and E. Turner - Tamiyasu, "Nitromethane-Based Monopropellants" Technical Report AFRPL-TR-81-17, Prepared for AFRPL by Acurex Corp., May 1981.
2. Finnigan 4000 GC/MS Systems Operation Manual, Finnigan Corp., 1976.
3. P.B. Weisz and C.D. Prater, Adv. Catal., Vol 6, p. 143, 1954.
4. O.A. Hougen and K.M. Watson, Chemical Process Principles, Vol III, Wiley, New York, 1947.
5. A. Harmoni and A. Salmon, Chem. Ind. (London), Vol 41, p. 1265, 1960.
6. T.L. Cottrell, T.E. Graham, and T.J. Reid, Trans. Far. Soc., Vol 47, p. 584, 1951.
7. P. Gray, A. Voffe, and L. Roselaar, Trans. Far. Soc., Vol. 51, p. 1489, 1955.
8. A. Perche, J.C. Tricot, and M. Lucquin, J. Chem. Res. (M) 1979, p. 1555.
9. A. Perche, J.C. Tricot, and M. Lucquin, J. Chem Res. (M) 1979, p. 3219.
10. E.W. Thiele, Ind. Eng Chem., Vol 31, p. 163, 1939.
11. J.R. Katzer, B.C. Gates, and G.C.A. Schuit, The Chemistry of Catalytic Processes, McGraw-Hill, New York, 1979.

1981 USAF - SEEE SUMMER FACULTY RESEARCH PROGRAM

Sponsored by the

AIR FORCE OFFICE OF SCIENTIFIC RESEARCH

Conducted by the

SOUTHEASTERN CENTER FOR ELECTRICAL ENGINEERING EDUCATION

FINAL REPORT

Prepared by: Dr. Albert W. Biggs
Academic Rank: Professor
Department and University: Department of Electrical Engineering
University of Kansas
Research Location: Air Force Weapons Laboratory, Applied Physics
Division, Electromagnetics Branch
USAF Research Colleague: Dr. Jerrold S. Shuster, Major, USAF
Date: 14 August 1981
Contract No: F49620-79-C-0038

INTERACTION BETWEEN AN ELECTROMAGNETIC PULSE AND A
METAL CYLINDER CONNECTED TO A PARALLEL PLATE GUIDE BY A WIRE

by

Albert W. Biggs

ABSTRACT

The interaction between an electromagnetic pulse (EMP) and a metallic cylinder, connected to one side of a parallel plate guide by a wire, is analyzed. The axes of the cylinder are collinear and perpendicular to the walls of the guide. The EMP is a transverse electromagnetic (TEM) wave with the electric field intensities of the frequency components being perpendicular to the guide walls. The surface currents and charges induced on the cylinder and wire surfaces are dependent upon the geometry or spatial dimensions of the structure normalized with respect to the width of the guide.

Acknowledgment

The author would like to thank the Air Force Systems Command, the Air Force Office of Scientific Research and the Southeastern Center for Electrical Engineering Education for providing him with the opportunity to spend a very worthwhile and interesting summer at the Air Force Weapons Laboratory, Kirtland AFB, NM. He would like to acknowledge the laboratory, in particular the Electromagnetics Branch of the Applied Physics Division, for its hospitality and excellent working conditions.

Finally, he would like to thank Dr. Jerrold S. Shuster for suggesting his area of research and for his collaboration and guidance, and he would like to acknowledge many helpful discussions with Drs. Carl E. Baum and Kenneth C. Chen.

I. INTRODUCTION:

In addition to thermal, blast, and radiation phenomena, nuclear explosions are also sources of electromagnetic pulses (EMP's). The interactions between the electromagnetic fields of a transient EMP and either airborne or ground-based systems induced surface current and surface charge distributions on these systems. The resulting currents and voltages may be coupled into the interiors of aircraft or ground-based communication terminals, where they may damage electronic components or create error signals in critical computers and microprocessors. Although component damage may not be present, error signals can cause premature launch of an air cruise missile or ignition of explosive squibs in areas such as the crew and pilot compartments. Sparks induced by large transient currents in electrical cables connected to fuel gauge indicators can ignite partially filled fuel tanks.

This analysis will consider currents induced on a cylinder which simulates the fuselage of a B-52 airplane or a KC-135 refueling tanker. The cylinder will be relatively thick, with a ratio of length to diameter of 10 or less. It will be assumed to have perfect conductivity. The top and bottom will consist of perfectly conducting disks. If experimental verifications were to be conducted, this cylinder could be represented by a closed metallic can. A thin, perfectly conducting cylinder or wire, with its axis collinear with that of the cylinder, extends from the thick cylinder to one side of a perfectly conducting parallel plate waveguide. The cylinder axes are perpendicular to the guide wall.

The EMP propagates in the parallel plate guide in the transverse electromagnetic (TEM) mode. Although transverse magnetic (TM) or transverse electric (TE) modes, or both, might be present in an experimental configuration, neither would be encountered in actual practice. The electric field will be parallel to the cylinder axes, and normal to the sides of the parallel plate guide. Realistic simulation is achieved with only the TEM mode. The wire simulates a trailing wire antenna or a refueling boom.

II. OBJECTIVES

Four methods are presented for resolution of the field perturbations created by and the currents induced on these collinear cylinders. The first method is a two dimensional solution of Laplace's equation by numerical

approximation. This method is useful for solving many electromagnetic field problems which have geometrical shapes not amenable by rigorous mathematical techniques. It is a scheme of replacing differential equations by difference equations.

The second method introduces an analytical formulation to conformal mapping. It deforms a two dimensional region into the upper half of the complex plane bounded by the real axis. The boundary of the region becomes the real axis. The expressions which map the boundaries of the region, usually a geometrical shape formed by straight line segments, provide formulations of the electric field and potential contours.

However, the above methods only provide two dimensional results which do not generally apply to actual phenomena in three dimensions. An example is a metal sphere in free space. A plane wave incident upon the sphere is reflected in spherical waves which have the form:

$$j_n(r) = \left(\frac{\pi}{2r}\right)^{\frac{1}{2}} J_{n+\frac{1}{2}}(r), \quad (1)$$

$$n_n(r) = \left(\frac{\pi}{2r}\right)^{\frac{1}{2}} N_{n+\frac{1}{2}}(r), \quad (2)$$

where $j_n(r)$ and $n_n(r)$ are spherical Bessel functions. These may be combined to form spherical Hankel functions $h_n^{(1)}(r)$ and $h_n^{(2)}(r)$,

$$h_n^{(1)}(r) = \left(\frac{\pi}{2r}\right)^{\frac{1}{2}} \left[J_{n+\frac{1}{2}}(r) + j N_{n+\frac{1}{2}}(r) \right] \quad (3)$$

$$h_n^{(2)}(r) = \left(\frac{\pi}{2r}\right)^{\frac{1}{2}} \left[J_{n+\frac{1}{2}}(r) - j N_{n+\frac{1}{2}}(r) \right], \quad (4)$$

and these half order Bessel functions for the first few orders are

$$\begin{aligned} j_0(r) &= \frac{1}{r} \sin r, & n_0(r) &= -\frac{1}{r} \cos r, \\ j_1(r) &= \frac{1}{r} \left[\frac{\sin r}{r} - \cos r \right], \\ n_1(r) &= -\frac{1}{r} \left[\frac{\cos r}{r} + \sin r \right], \end{aligned} \quad (5)$$

while a plane wave incident upon a cylinder is reflected in cylindrical waves which have the form

$$J_n(r) \approx \sqrt{\frac{2}{\pi r}} \cos\left(r - \frac{\pi}{2} - \frac{n\pi}{2}\right),$$

(6)

$$N_n(r) \approx \sqrt{\frac{2}{\pi r}} \sin\left(r - \frac{\pi}{2} - \frac{n\pi}{2}\right),$$

(7)

where the asymptotic form is used to indicate the form of the sinusoids and the decay with distance of the two wave forms.

Other examples are available to illustrate the differences in two and three dimensional scattering and reflections. The two dimensional results are valuable when the shape of the reflecting obstacle is cylindrical or when the wave is confined to the plane of symmetry of the obstacle. For example, ray tracing can be used for spheres when the plane through the sphere center is in the plane of incidence, and the plane of incidence is normal to the cylinder axis.

The third method is an analytical formulation of the current induced on the cylinder and wire (or smaller cylinder) by the scattered vector potential on the surfaces of the cylinders. The vector potential is divided into separate segments for the top of the cylinder, the sides of the cylinder except for the junction of the wire and cylinder, and the wire. The vector potentials are represented as integral expressions of current distributions on an infinite array of dipoles in free space. The dipoles are collinear and are formed by two infinitely conducting cylinders, equal in length and radius, connected by an infinitely conducting wire. As indicated earlier, the EMP source is a transient plane wave with the electric field components parallel to the axes of the cylinder. The method of moments is introduced to solve the integral equations.

The fourth method will obtain the cylinder currents with the magnetic field component of the incident EMP plane wave. This is obtained from the use of modified Green's functions and surface current densities in the integral expressions for the top, bottom, and side surfaces of the cylindrical obstacles.

III. NUMERICAL APPROXIMATIONS FOR CONFORMAL MAPPING

Figure 1 represents the coordinate system for the interaction of an EMP wave with two collinear cylinders. This coordinate system is also applicable to the other three methods described in successive sections. The $Z = 0$, or x - y plane, represents one side of a perfectly conducting parallel plate guide. The other side is represented by the $Z = S$ plane. The incident EMP wave is traveling in the positive x direction, with only Z - components of the electric field and y -components of the magnetic field. The radius of the larger cylinder is $r = a$, while radius of the smaller cylinder or wire is $r = b$. The lengths of each are L_1 and L_2 for cylinder and wire, respectively. The gap between the top of the upper cylinder and the upper guide wall is D .

If the cylinder is replaced by a strip, with width $2a$ and infinite in length in the y direction, and having infinite conductivity, and the wire is replaced by an infinitely conducting strip, also infinite in length in the y direction, then the problem becomes two dimensional. If the image of this configuration is introduced, then the lower guide plate is replaced by the image seen in Figure 2 because of the symmetry present. Although the two dimensional model does have limitations discussed in Section I, it has some value in providing areas of high field intensities. These occur at edges and corners of the scattering structure in the two dimensional case, and rims or circular corners in the three dimensional case. The analytical formulation for two dimensional geometries is given by Laplace's equation.

Laplace's equation can be solved in a number of ways. The most attractive solution is an exact mathematical formulation¹ with tabulated or calculable functions such as cosines, hyperbolic sines, and Bessel functions of integer or fractional orders. It is an unfortunate fact that many real applications²⁻⁵ that arise in engineering practice cannot be solved by rigorous mathematics or analytical techniques. One possibility in these applications is to introduce numerical approximations. The method is tedious and the results have a slow convergence, and at times a slight divergence, but the results provide a

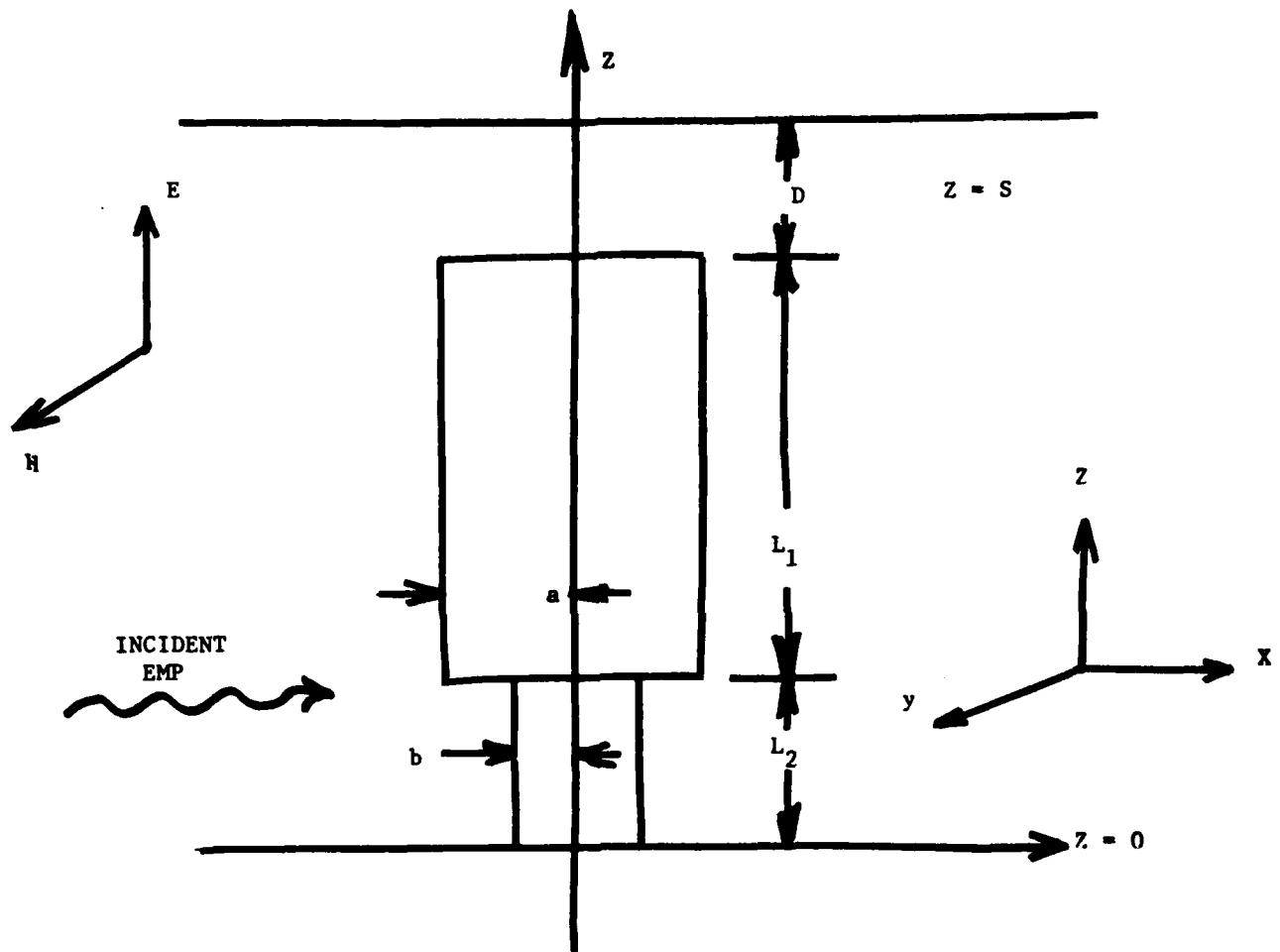


FIGURE 1 - CYLINDER AND FAT WIRE CONFIGURATION IN A PARALLEL PLATE GUIDE

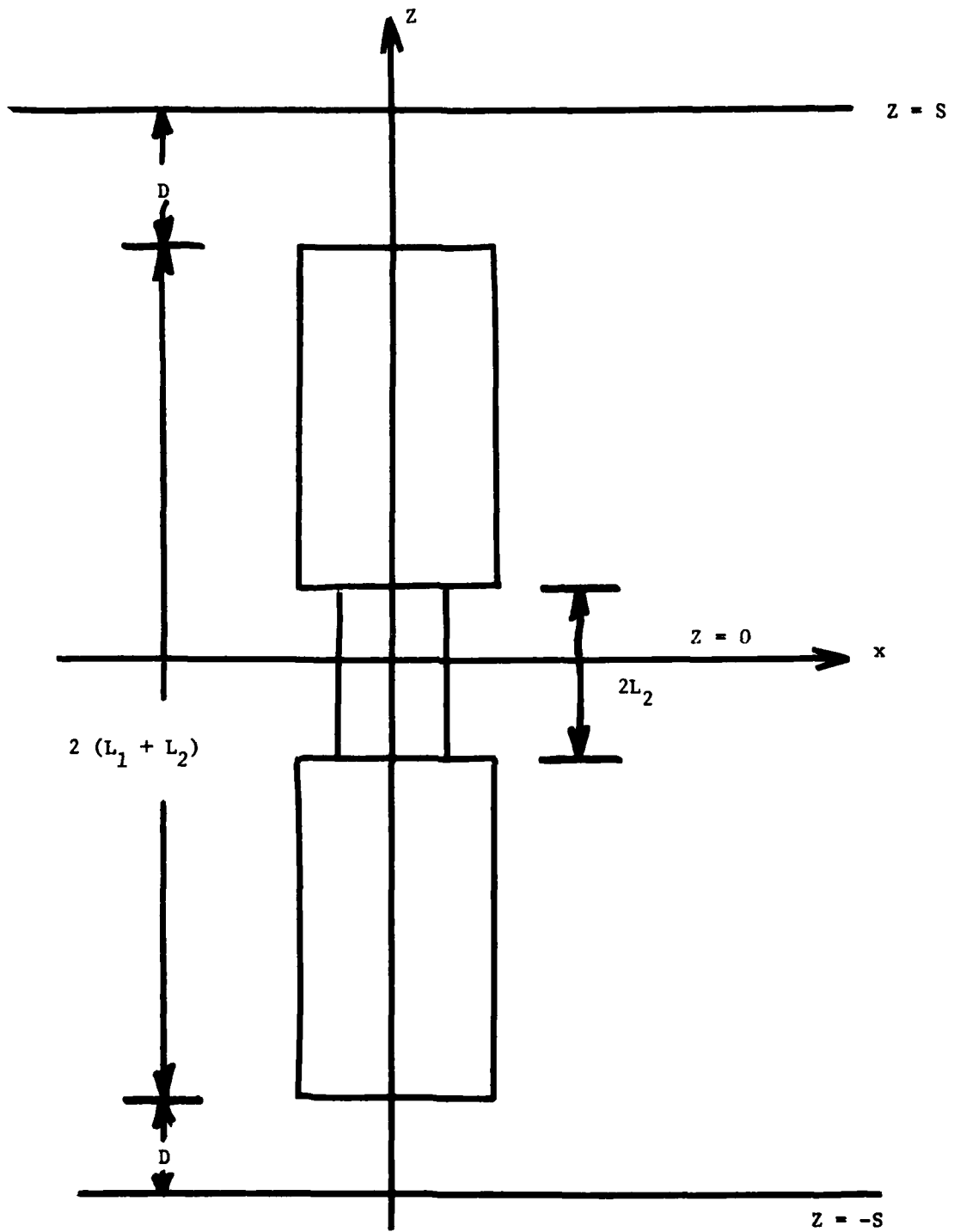


FIGURE 2 - REPLACEMENT OF THE ORIGINAL PAIR OF CYLINDERS BY THEIR IMAGES IN THE LOWER HALF PLANE

valuable picture of potential distributions around unusual shaped conductors. Interest in this method has increased because of the introduction of computer programs which remove human drudgery and transfer it to computer drudgery. Several circuit and conformal mapping problems have been solved by the currently popular "relaxation method."

The relaxation method⁶ is almost as old as differential equations. It is a scheme for replacing differential equations by difference equations. John Bernoulli used the concept in 1728, Jacobi⁷ in 1844, and many others in the intervening years.

The numerical approximation method⁸⁻⁹ consists in replacing the smooth potential variation by a set of discrete values at the intersection of a grid. In Figure 3, the potential is given on the path C, and the solution of Laplace's equation is to be found for the enclosed region. A rectangular mesh with arbitrary spacing h is superposed on the region. The potential is found at the intersecting points of the mesh.

The potential at the point 0 will be found as an example of this method. The true value of $\partial\phi/\partial x$ is approximated by the grid values

$$\left. \frac{\partial\phi}{\partial x} \right|_{10} \approx \frac{\phi_1 - \phi_0}{h}, \quad (8)$$

$$\left. \frac{\partial\phi}{\partial x} \right|_{03} \approx \frac{\phi_0 - \phi_3}{h}, \quad (9)$$

which apply at points a and b, respectively. The second derivative becomes

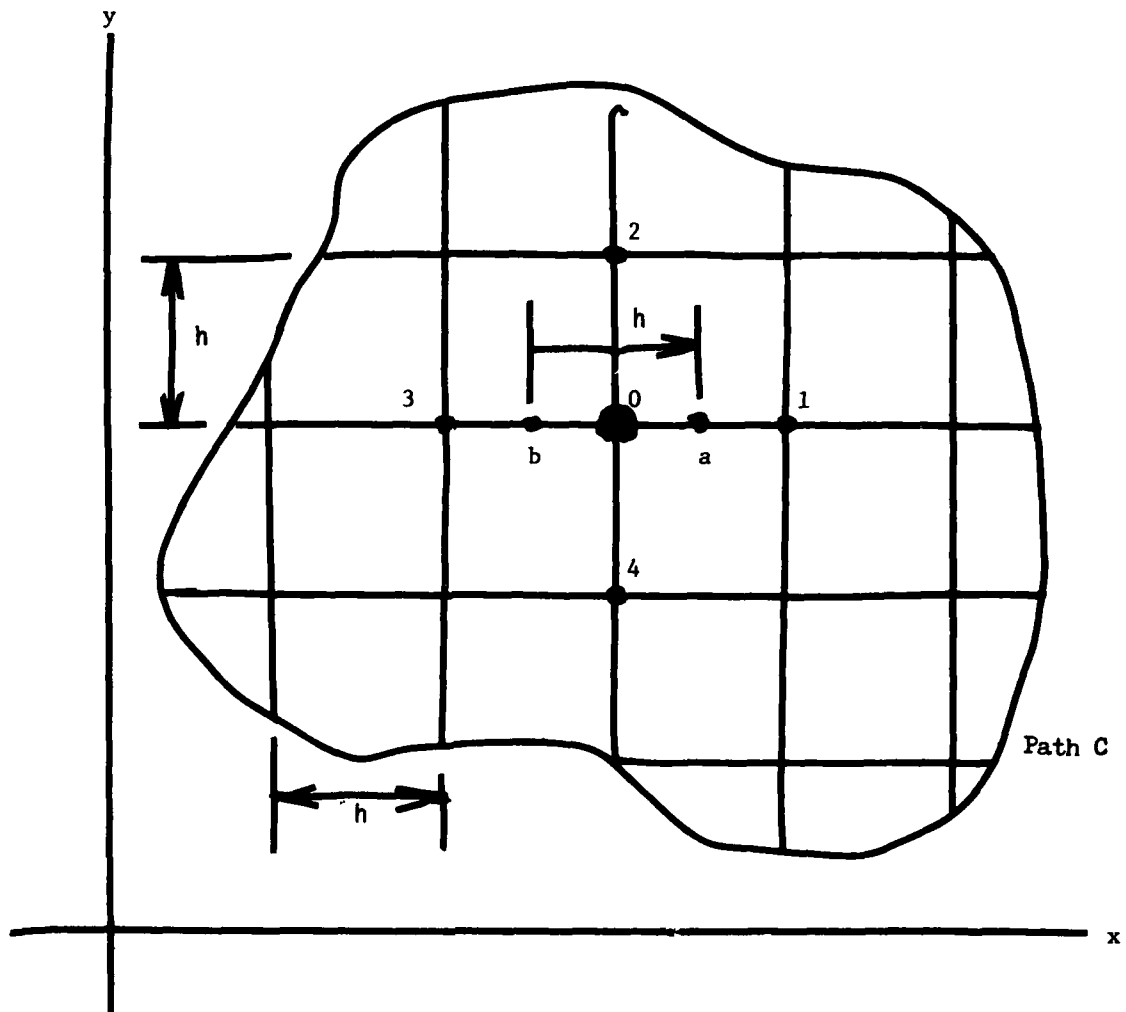


FIGURE 3 - SQUARE GRID SUPERPOSED ON A REGION IN WHICH THE POTENTIAL DISTRIBUTION IS TO BE OBTAINED BY THE NUMERICAL APPROXIMATION METHOD .

$$\begin{aligned}
\frac{\partial^2 \phi}{\partial x^2} &\approx \frac{1}{h} \left[\left(\frac{\partial \phi}{\partial x} \right)_{10} - \left(\frac{\partial \phi}{\partial x} \right)_{03} \right] \\
&\approx \frac{1}{h^2} [(\phi_1 - \phi_0) - (\phi_0 - \phi_3)] \\
&= \frac{1}{h^2} [\phi_1 + \phi_3 - 2\phi_0],
\end{aligned} \tag{10}$$

$$\frac{\partial^2 \phi}{\partial y^2} \approx \frac{1}{h^2} [\phi_2 + \phi_4 - 2\phi_0], \tag{11}$$

so that the Laplacian becomes

$$\begin{aligned}
\frac{\partial^2 \phi}{\partial x^2} + \frac{\partial^2 \phi}{\partial y^2} &\approx \frac{1}{h^2} [\phi_1 + \phi_2 + \phi_3 + \phi_4] \\
&\quad - \frac{1}{h^2} [4\phi_0] = 0,
\end{aligned} \tag{12}$$

so that the potential ϕ_0 at the center is the average potential at the surrounding points.

$$\phi_0 = \frac{1}{4} [\phi_1 + \phi_2 + \phi_3 + \phi_4].$$

(13)

The potential lines for a two dimensional cylinder and wire are calculated in this section. Subsequent to these results is a simple example to illustrate the method. In Figure 4, a square region is grounded on three sides at zero potential, while the potential on the fourth side is

$$\phi = 1000 \sin \left(\frac{\pi x}{a} \right).$$

(14)

A square grid is drawn as shown in Figure 4 with h chosen as $a/4$. With symmetry about the vertical center line, only half the region need be considered.

A set of potentials are arbitrarily chosen at points A, B, C, . . . G, H, and I. The potentials along the boundary points 0, 707, 1000, 707, 0, 0, etc., are part of the boundary conditions. The final results are independent of the assumed values. The convergence increases when they are closer to the true potentials. We now proceed in an orderly manner, starting with point A and making the potential at each point equal to the average of the four surrounding points in accord with Eq. (13).

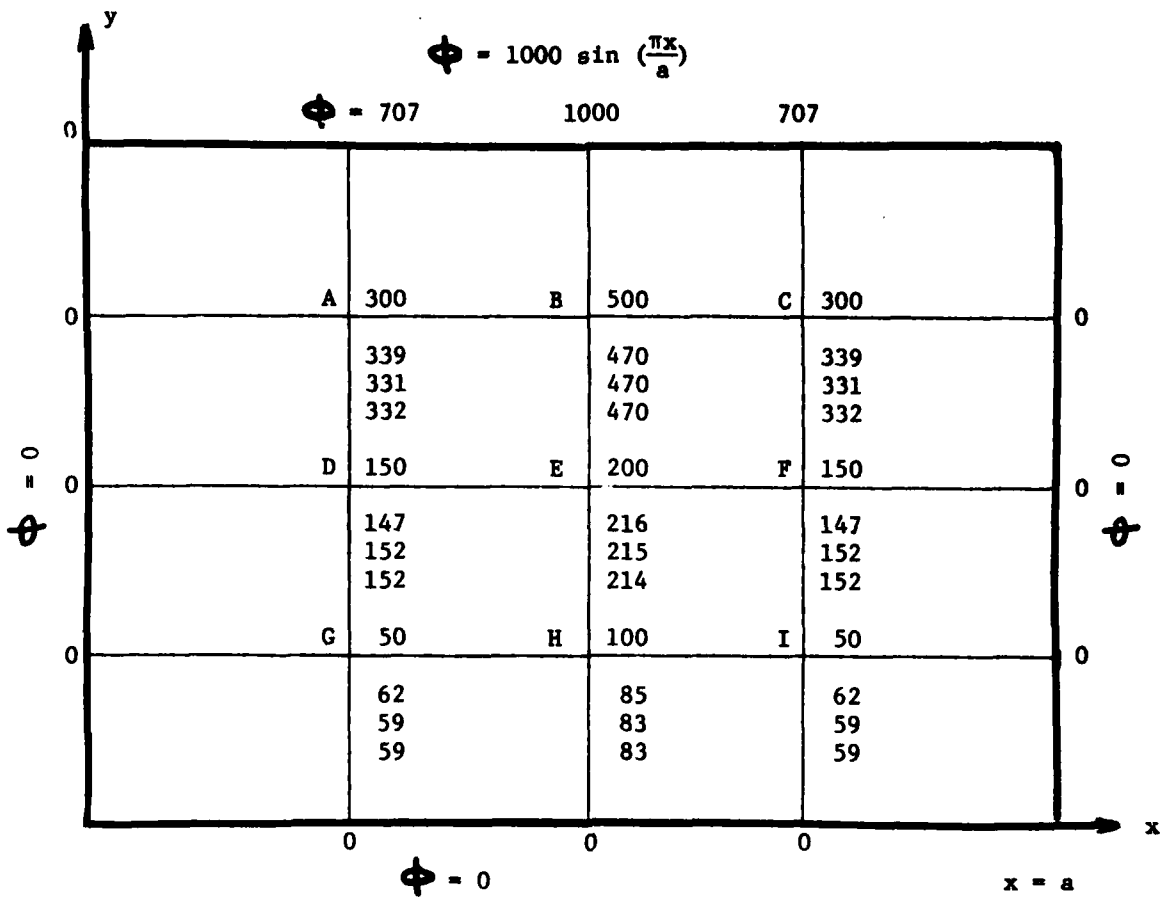


FIGURE 4 - POTENTIAL DISTRIBUTION WITH ASSUMED POTENTIAL VALUES AND SUCCESSIVE APPROXIMATIONS WITH $h = a/4$

The next potential at point B is then calculated with the new potentials at points A and C. Symmetry preordains the potential at point C when that at point A is calculated. The next potential is calculated for point D (and decreed at point F) with the new potentials from point A and the assumed potentials at points E and G. The results are listed in Table 1.

The new values are written below the old values in Figure 4. Each sum includes all corrected values currently available. The process continues until convergence is obtained within the necessary engineering accuracy. If desired, a finer mesh can later be chosen with a continuation of the process. This interaction process, known as the Liebmann method, always converges.

It is preferable to commence with a very coarse grid or net, even when a fine mesh is ultimately desired. The coarse division provides converging values which are then chosen as reference values for the next subdivision. The Liebmann method is then employed to obtain another set of potentials.

A second example in Figure 5 has one side at 1000 volts and the other three sides of a square at zero volts. Nine approximations were made in this configuration. If desired, a finer mesh can be formed with these values as boundary conditions.

Figure 6 represents a perfectly conducting cylinder connected to one plate of a parallel plate guide by a perfectly conducting wire. The cylinder has a length of $9D$, where D is the cylinder diameter, and the wire has a length of $2D$. The separation between cylinder top and the top plate is $3D$. The top plate is at a potential of 1400 volts and the lower plate is at a potential of zero volts.

The numbers indicate the final approximations, made after twelve intermediate successive approximations. As additional approximations are made, convergence increases.

IV. SCHWARZ-CHRISTOFFEL TRANSFORMATION

The Schwarz-Christoffel transformation is a conformal transformation¹⁰ which will map the real axis in the complex z -plane into a general polygon in the complex w -plane. The upper half of the z -plane maps into the interior region of the polygon. The mapping function is

Point	Assumed	First Approx	Final
A	300	339	332
B	500	470	470
C	300	339	332
D	150	147	152
E	200	216	214
F	150	147	152
G	50	62	59
H	100		
I	50	62	59

Table 1 - Results of solution by successive approximation.

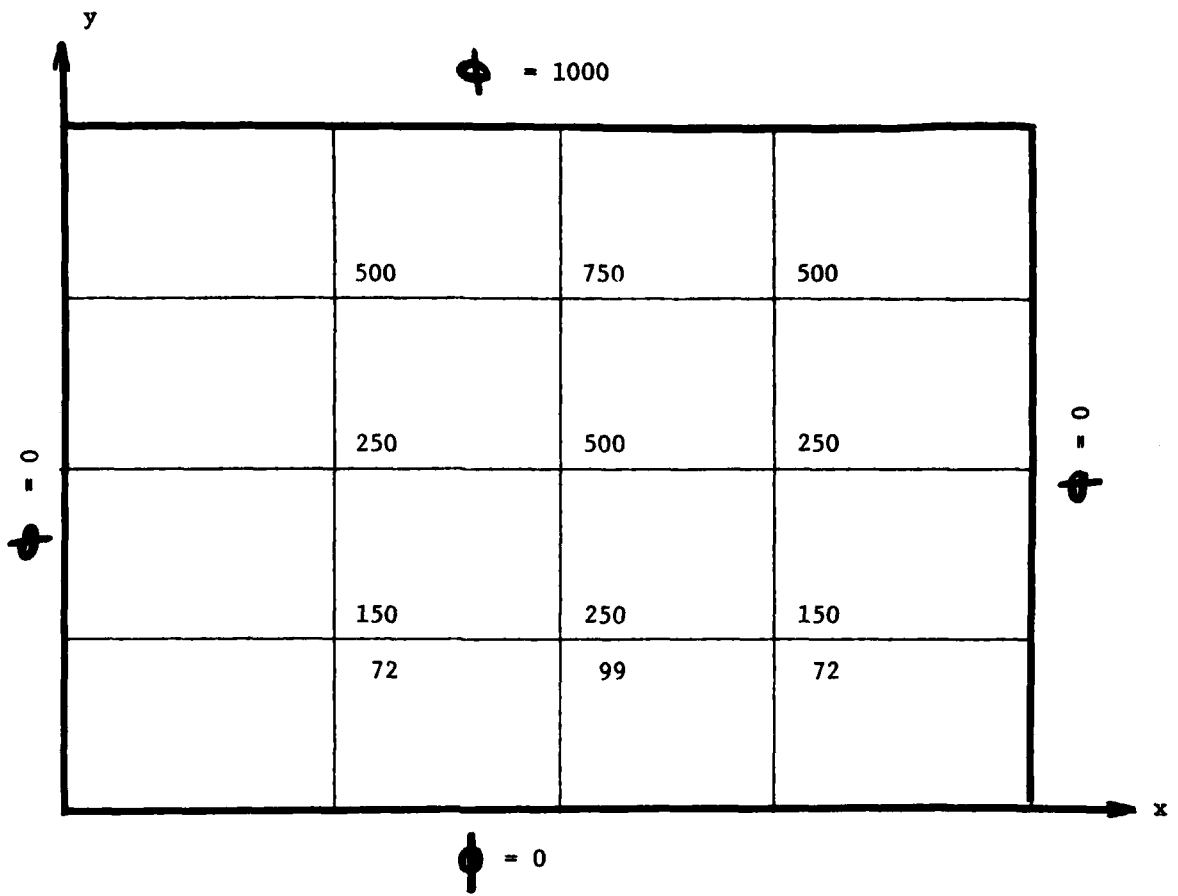


FIGURE 5 - POTENTIAL DISTRIBUTION WITH ASSUMED AND FINAL POTENTIALS.

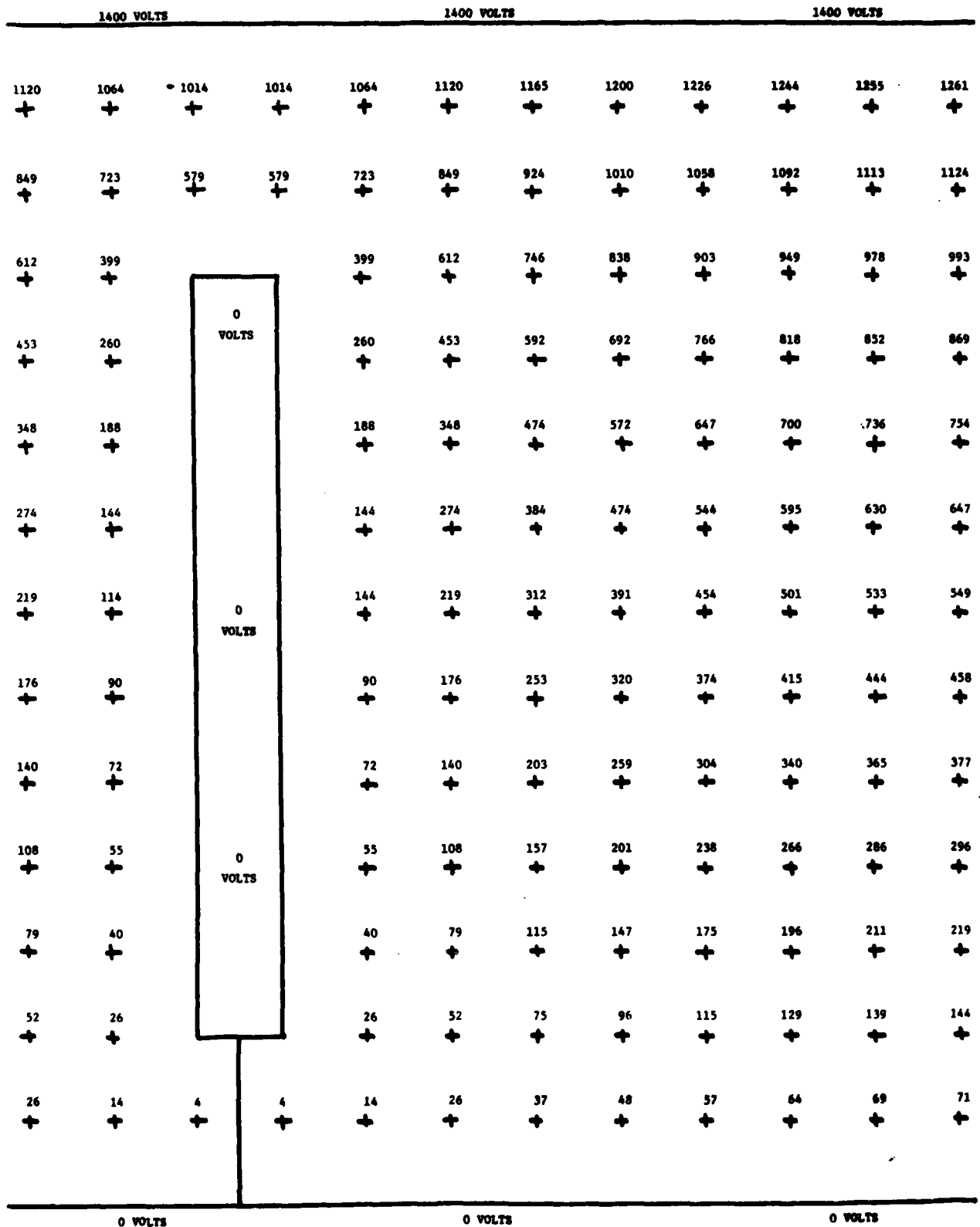


FIGURE 6 - TWO-DIMENSIONAL POTENTIAL DISTRIBUTION FOR WIRE AND CYLINDER IN A PARALLEL PLATE GUIDE

$$\frac{dw}{dz} = A(z-x_1)^{\frac{\alpha_1}{\pi}-1} (z-x_2)^{\frac{\alpha_2}{\pi}-1} (z-x_3)^{\frac{\alpha_3}{\pi}-1},$$

(14)

where the points x_1 , x_2 , and x_3 to be mapped into the points W_1 , W_2 , and W_3 , or $W_1 = f(x_1)$, $W_2 = f(x_2)$, and $W_3 = f(x_3)$. The direction of each patch follows the increasing subscripts 1, 2, and 3.

In Figure 7, as each point x_i is passed in the z -plane, the angle changes by α_i in the w -plane. The integral in Eq. (14) becomes

$$w = A \int (z-x_1)^{\frac{\alpha_1}{\pi}-1} (z-x_2)^{\frac{\alpha_2}{\pi}-1} \cdot (z-x_3)^{\frac{\alpha_3}{\pi}-1} dz + B,$$

(15)

where A and B are to be found from boundary conditions.

Representation of the cylinder and wire is shown in Figure 8. The two-dimensional polygon representing the cylinder and wire in the w -plane, its mapping along the x -axis in the z -plane, and the desired mapping in the w' -plane are identified by corresponding points in each plane. The purpose of the w' -plane is to provide a two bar transmission line for electric field and potential mapping. The electric field lines in the w' -plane are vertical lines parallel to the v' -axis, and the potential lines are horizontal lines parallel to the u' -axis. The electric field lines are sketched for the three planes in Figure 9.

The transformation between the w - and z -planes is given by

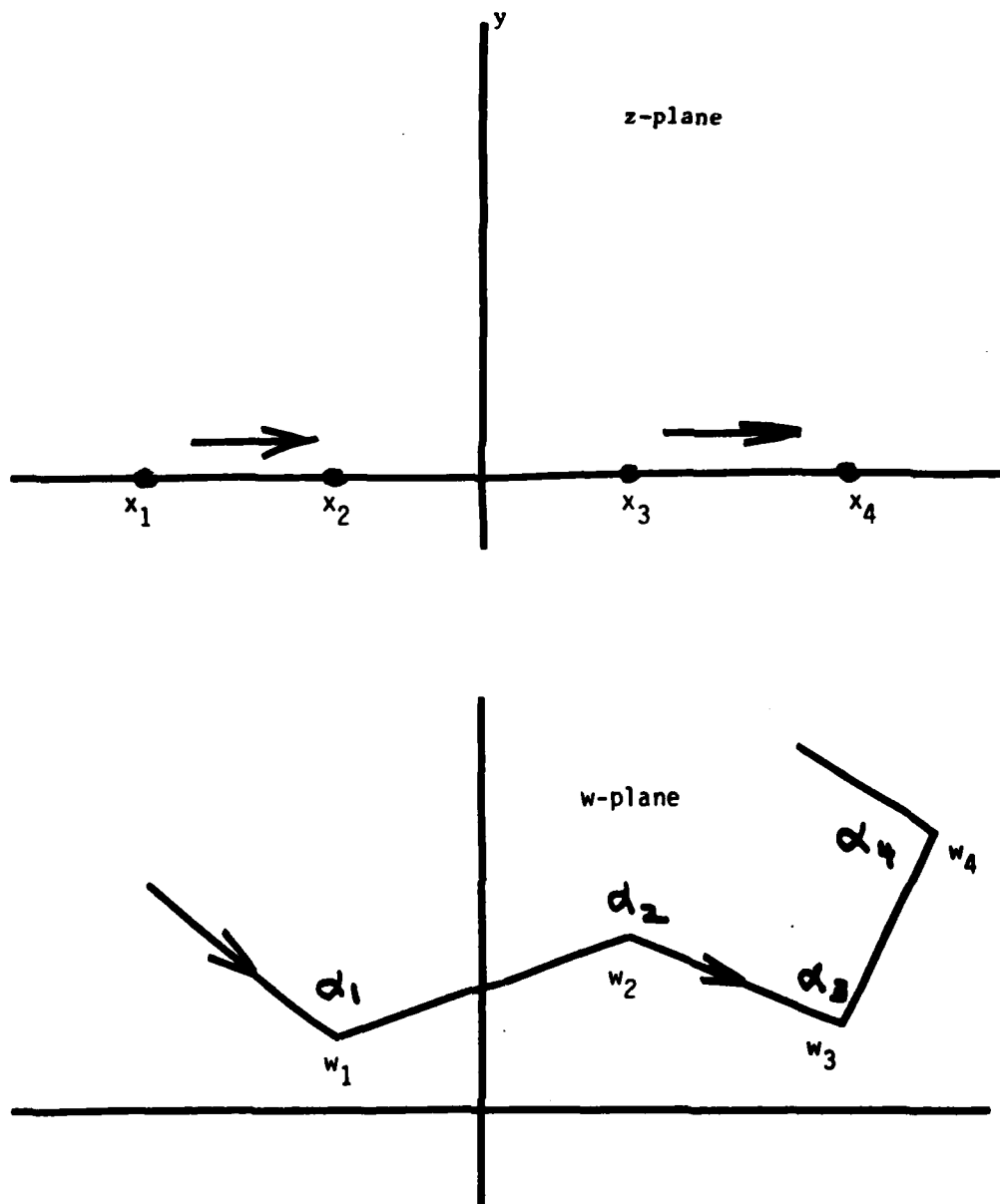


FIGURE 7 - THE SCHWARZ-CHRISTOFFEL TRANSFORMATION

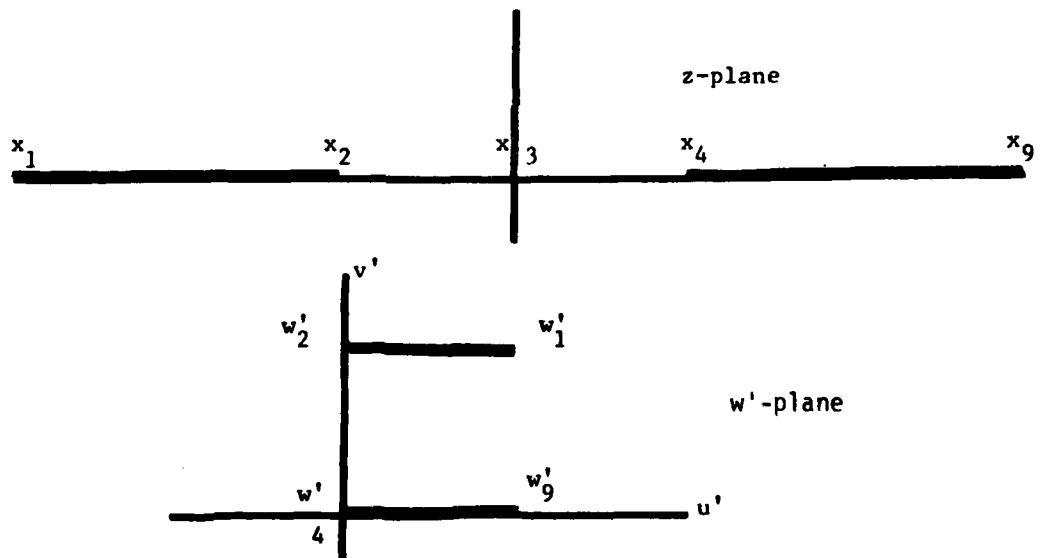
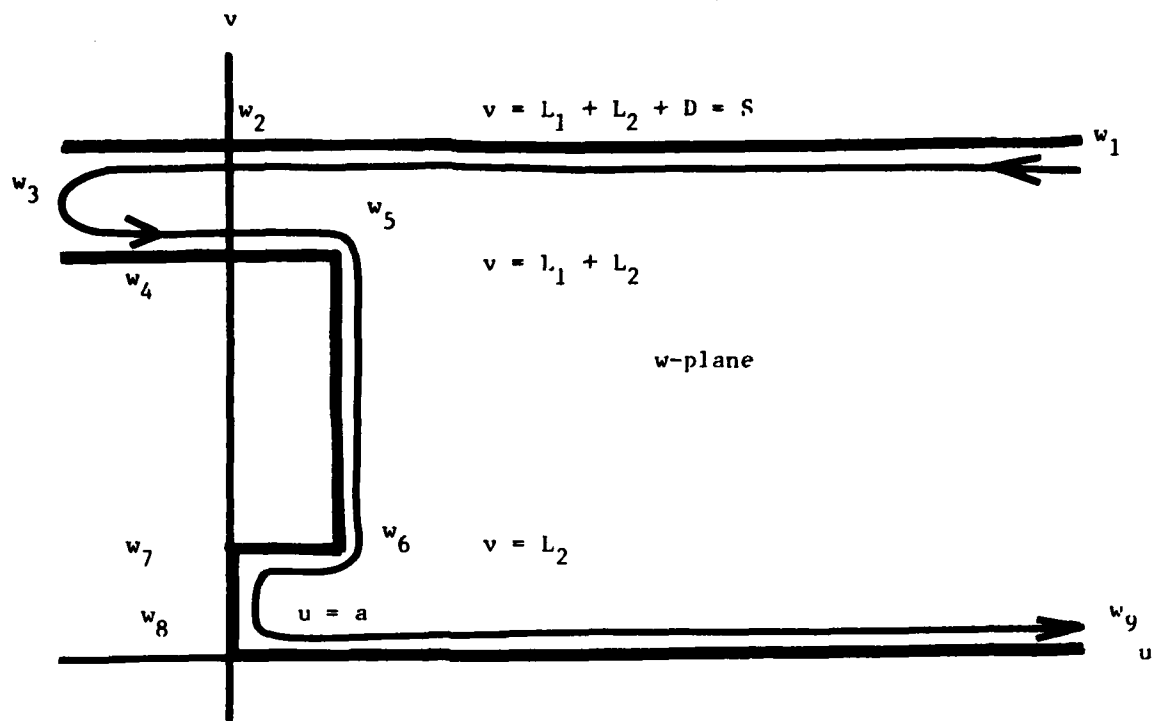


FIGURE 8 - MAPPING IN THE w -, z -, AND w' - PLANES

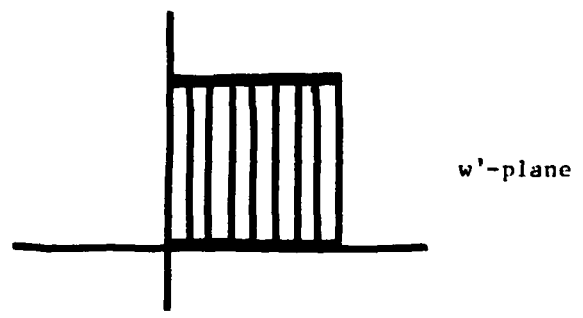
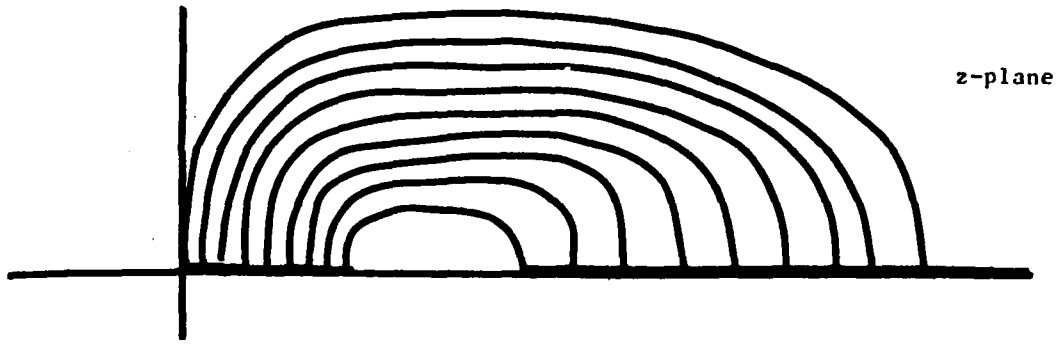
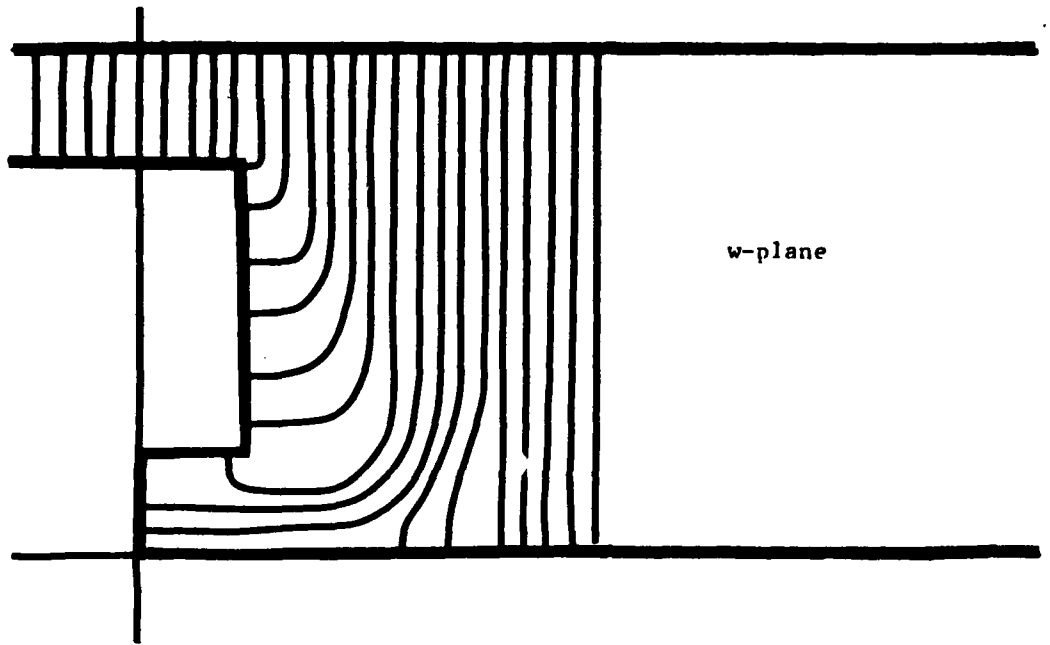


FIGURE 9 - ELECTRIC FIELD LINES IN THE THREE PLANES

$$\begin{aligned} \frac{dw}{dz} = & A (z-x_3)^{\frac{\alpha_3}{\pi}-1} (z-x_5)^{\frac{\alpha_5}{\pi}-1} \\ & \cdot (z-x_6)^{\frac{\alpha_6}{\pi}-1} (z-x_7)^{\frac{\alpha_7}{\pi}-1} \\ & \cdot (z-x_8)^{\frac{\alpha_8}{\pi}-1}, \end{aligned} \quad (16)$$

where $\alpha_3, \alpha_5, \alpha_6, \alpha_7$, and α_8 are $0, 3\pi/2, 3\pi/2, \pi/2$, and $\pi/2$, respectively, so that the expression for w is

$$\begin{aligned} w = & A \int \frac{\sqrt{(z-x_5)(z-x_6)}}{(z-x_3)\sqrt{(z-x_7)(z-x_8)}} dz \\ & + B, \end{aligned} \quad (17)$$

where the integrand is rearranged as

$$\frac{(z-x_5)(z-x_6)}{(z-x_3)\sqrt{(z-x_5)(z-x_6)(z-x_7)(z-x_8)}} \quad (18)$$

and a change of variable,

$$x = z - x_3, \quad z = x + x_3, \quad (19)$$

results in the integrand

$$\begin{aligned} & \frac{(x - [x_5 - x_3])(x - [x_6 - x_3])}{x \sqrt{(x - [x_5 - x_3])(x - [x_6 - x_3])} \cdot \frac{1}{(x - [x_7 - x_3])(x - [x_8 - x_3])}} \\ &= \frac{x}{\sqrt{(x - [x_5 - x_3])(x - [x_6 - x_3])} \cdot \frac{1}{(x - [x_7 - x_3])(x - [x_8 - x_3])}} - \frac{x_6 + x_5 - 2x_3}{\sqrt{(x - [x_5 - x_3])(x - [x_6 - x_3])} \cdot \frac{1}{(x - [x_7 - x_3])(x - [x_8 - x_3])}} \\ & \quad + \frac{(x_5 - x_3)(x_6 - x_3)}{\sqrt{(x - [x_5 - x_3])(x - [x_6 - x_3])} \cdot \frac{1}{(x - [x_7 - x_3])(x - [x_8 - x_3])}} \end{aligned} \quad (20)$$

The integrals in Eq. (20) are evaluated in the ranges

$$\begin{aligned}
 d > y > 0, & & a > y > b \\
 c > y > d, & & y > a, \\
 b > y > c, & &
 \end{aligned}
 \tag{21}$$

where $a > b > c > d$. In terms of x_1 to x_8 , these points are

$$\begin{aligned}
 a &= x_8 - x_3, & c &= x_6 - x_3 \\
 b &= x_7 - x_3, & d &= x_5 - x_3,
 \end{aligned}
 \tag{22}$$

so that the ranges corresponding to Eq. (21) are

$$\begin{aligned}
 x_5 > z > 0, & & x_8 > z > x_7, \\
 x_6 > z > x_5, & & z > x_8 \cdot \\
 x_7 > z > x_6
 \end{aligned}
 \tag{23}$$

The first interval becomes, for $d > y > 0$ or $x_5 > z > 0$ ¹¹,

$$\begin{aligned}
 & \int_0^z \frac{dt}{\sqrt{(a-t)(b-t)(c-t)(d-t)}} \\
 &= g [F(\phi_0, k) - F(\phi_4, k)],
 \end{aligned}
 \tag{24}$$

where $F(\phi, k)$ is the normal elliptic integral of the first kind, and g ,

ϕ_4, ϕ_0 , and k are

$$g = \frac{2}{\sqrt{(a-c)(b-d)}}$$

$$\sin^2 \phi_4 = \frac{(a-c)(d-y)}{(a-d)(c-y)} = \frac{(x_8-x_6)(x_5-z)}{(x_8-x_5)(x_6-z)},$$

$$\sin^2 \phi_0 = \frac{(a-c)d}{(a-d)c} \quad (25)$$

$$= \frac{(x_8-x_6)(x_5-x_3)}{(x_8-x_5)(x_6-x_3)},$$

$$k^2 = \frac{(b-c)(a-d)}{(a-c)(b-d)} = \frac{(x_7-x_6)(x_8-x_5)}{(x_8-x_6)(x_7-x_8)},$$

and in the range $c > y \geq d$ or $x_6 > z \geq x_5$,

$$\int_d^y \frac{dx}{\sqrt{(a-x)(b-x)(c-x)(x-d)}}$$

$$= g [F(\phi_d, k) - F(\phi_5, k)], \quad (26)$$

where ϕ_5, ϕ_d , and k are

$$\begin{aligned} \sin^2 \phi_5 &= \frac{(b-d)(c-y)}{(c-d)(b-y)} \\ &= \frac{(x_7 - x_5)(x_6 - z)}{(x_6 - x_5)(x_7 - z)}, \end{aligned}$$

$$\begin{aligned} \sin^2 \phi_d &= \frac{(x_7 - x_5)(x_6 - x_5)}{(x_6 - x_5)(x_7 - x_5)} \\ &= 1, \end{aligned} \tag{27}$$

$$k^2 = \frac{(a-b)(c-d)}{(a-c)(b-d)} = \frac{(x_8 - x_7)(x_6 - x_5)}{(x_8 - x_6)(x_7 - x_5)},$$

and in the range¹¹ $b > y \geq c$, or $x_7 > z \geq x_6$,

$$\begin{aligned} &\int_c^y \frac{dx}{\sqrt{(a-x)(b-x)(x-c)(x-d)}} \\ &= g [F(\phi_c, k) - F(\phi_b, k)], \end{aligned} \tag{28}$$

where ϕ_b, ϕ_c , and k are

$$\sin^2 \phi_b = \frac{(a-c)(b-y)}{(b-c)(a-y)} = \frac{(x_8-x_6)(x_7-z)}{(x_7-x_6)(x_8-z)},$$

$$\sin^2 \phi_c = \frac{(a-c)(b-c)}{(b-c)(a-c)} = 1, \quad (29)$$

$$k^2 = \frac{(b-c)(a-d)}{(a-c)(b-d)} = \frac{(x_7-x_6)(x_8-x_5)}{(x_8-x_6)(x_7-x_5)},$$

and in the range¹¹ $a > y \geq b$, or $x_8 > z \geq x_7$,

$$\int_b^y \frac{dx}{\sqrt{(a-x)(x-b)(x-c)(x-d)}}$$

$$= g[F(\phi_b, k) - F(\phi_7, k)], \quad (30)$$

where ϕ_7 , ϕ_b , and k are

$$\sin^2 \phi_7 = \frac{(b-d)(a-y)}{(a-b)(y-d)} = \frac{(x_7-x_5)(x_8-z)}{(x_8-x_7)(z-x_5)},$$

$$\sin^2 \phi_b = \frac{(b-d)(a-b)}{(a-b)(b-d)}$$

$$= 1,$$

(31)

$$k^2 = \frac{(a-b)(c-d)}{(a-c)(b-d)}$$

$$= \frac{(x_8-x_7)(x_6-x_5)}{(x_8-x_6)(x_7-x_5)},$$

and in the range $y > a$, or $z > x_8$,

$$\int_a^y \frac{dt}{\sqrt{(t-a)(t-b)(t-c)(t-d)}}$$

$$= g [F(\phi_b, k)]$$

(32)

where ϕ_8 and k are given by

$$\sin^2 \phi_8 = \frac{(b-d)(y-a)}{(a-d)(y-b)} = \frac{(x_7-x_5)(z-x_8)}{(x_8-x_5)(z-x_7)}, \quad (33)$$

$$k^2 = \frac{(b-c)(a-d)}{(a-c)(b-d)} = \frac{(x_7-x_6)(x_8-x_5)}{(x_8-x_6)(x_7-x_5)}.$$

The second integral is also described over the ranges¹¹ in Eqs. (21) and (22), so that for $d > y > 0$, or $x_5 > z > 0$,

$$\int_0^y \frac{x dx}{\sqrt{(a-x)(b-x)(c-x)(d-x)}} = dg \left[\frac{\alpha_4^2 - \alpha_{14}^2}{\alpha_4^2} \left\{ \pi(\phi_0, \alpha_4^2, k) - \pi(\phi_4, \alpha_4^2, k) \right\} + \frac{\alpha_{14}^2}{\alpha_4^2} \{ u_0 - u_4 \} \right], \quad (34)$$

where $\Pi(\phi, \alpha^2, k)$ is the normal elliptic integral of the third kind, in the form

$$\begin{aligned} \Pi(\phi, \alpha^2, k) &= \int_0^\phi \frac{dt}{(1-\alpha^2 t^2)\sqrt{(1-t^2)(1-k^2 t^2)}} \\ &= \int_0^\phi \frac{d\theta}{(1-\alpha^2 \sin^2 \theta)\sqrt{1-k^2 \sin^2 \theta}} \\ &= \int_0^{u_1} \frac{du}{(1-\alpha^2 \sin^2 u)} = \Pi(u_1, \alpha^2). \end{aligned} \quad (35)$$

The parameters ϕ_4, ϕ_0 and k appear in Eq. (25). The others are

$$\begin{aligned} \alpha_4^2 &= \frac{x_8 - x_5}{x_8 - x_6}, \\ \alpha_{14}^2 &= \alpha_4^2 \frac{c}{d} = \frac{(x_8 - x_5)(x_6 - x_3)}{(x_8 - x_6)(x_5 - x_3)}. \end{aligned} \quad (36)$$

The functions u_0 and u_4 are

$$u_4 = \sin^{-1}(\sin \phi_4), \quad u_0 = \sin^{-1}(\sin \phi_0). \quad (37)$$

In the range $c > y \geq d$ or $x_6 > z \geq x_5$,

$$\int_d^y \frac{t dt}{\sqrt{(a-t)(b-t)(c-t)(t-d)}}$$

$$= cg \left[\frac{\alpha_s^2 - \alpha_{1s}^2}{\alpha_s^2} \left\{ \Pi(\phi_d, \alpha_s^2, k) \right. \right.$$

$$\left. \left. - \Pi(\phi_s, \alpha_s^2, k) \right\} + \frac{\alpha_{1s}^2}{\alpha_s^2} \left\{ u_d - u_s \right\} \right], \quad (38)$$

where ϕ_s, ϕ_d , and k appear in Eq. (27), and

$$\alpha_s^2 = \frac{c-d}{b-d} = \frac{x_6 - x_5}{x_7 - x_5},$$

$$\alpha_{1s}^2 = \frac{b(c-d)}{c(b-d)}$$

$$= \frac{(x_7 - x_3)(x_6 - x_5)}{(x_6 - x_3)(x_7 - x_5)}, \quad (39)$$

$$u_d = \operatorname{sn}^{-1}(\operatorname{sn} \phi_d) = \frac{\Pi}{2},$$

and in the range $b > y \geq c$, or $x_7 > z \geq x_6$,

$$\int_c^y \frac{t dt}{\sqrt{(a-t)(b-t)(t-c)(t-d)}}$$

$$= bg \left[\frac{\alpha_b^2 - \alpha_{1b}^2}{\alpha_b^2} \{ \Pi(\phi_c, \alpha_b^2, k) - \Pi(\phi_b, \alpha_b^2, k) \} + \frac{\alpha_{1b}^2}{\alpha_b^2} \{ u_c - u_b \} \right], \quad (40)$$

where ϕ_b, ϕ_c , and k appear in Eq. (29), and

$$\alpha_b^2 = \frac{b-c}{a-c} = \frac{x_7 - x_6}{x_8 - x_6},$$

$$\alpha_{1b}^2 = \frac{a(b-c)}{b(a-c)}$$

$$= \frac{(x_8 - x_3)(x_7 - x_6)}{(x_7 - x_3)(x_8 - x_6)}, \quad (41)$$

$$u_c = \operatorname{sn}^{-1}(\sin \phi_c),$$

and in the range $a > y \geq b$, or $x_8 > z \geq x_7$,

$$\int_b^y \frac{x dx}{\sqrt{(a-x)(x-b)(x-c)(x-d)}}$$

(42)

$$= ag \left[\frac{\alpha_7^2 - \alpha_{17}^2}{\alpha_7^2} \left\{ \Pi(\phi_b, \alpha_7^2, k) - \Pi(\phi_7, \alpha_7^2, k) \right\} + \frac{\alpha_{17}^2}{\alpha_7^2} \left\{ u_b - u_7 \right\} \right],$$

where ϕ_7, ϕ_b , and k appear in Eq. (31), and

$$\alpha_7^2 = \frac{b-a}{b-d} = \frac{x_7 - x_8}{x_7 - x_5} < 0,$$

$$\alpha_{17}^2 = \frac{(b-a)d}{(b-d)a}$$

$$= \frac{(x_7 - x_8)(x_5 - x_3)}{(x_7 - x_5)(x_8 - x_3)},$$

(43)

$$u_b = \operatorname{sn}^{-1}(\operatorname{sn} \phi_b),$$

and in the range $y > a$, or $z > x_8$,

$$\int_a^y \frac{x dx}{\sqrt{(x-a)(x-b)(x-c)(x-d)}}$$

$$= ag \left[\frac{\alpha_8^2 - \alpha_{18}^2}{\alpha_8^2} \Pi(\phi_8, \alpha_8^2, k) \right. \\ \left. + \frac{\alpha_{18}^2}{\alpha_8^2} u_8 \right], \quad (44)$$

where ϕ_8 and k are given by Eq. (33),

$$\alpha_8^2 = \frac{a-d}{b-d} = \frac{x_8 - x_5}{x_7 - x_5} > 1,$$

$$\alpha_{18}^2 = \frac{(a-d)b}{(b-d)a} \\ = \frac{(x_8 - x_5)(x_7 - x_3)}{(x_7 - x_5)(x_8 - x_3)}. \quad (45)$$

The third integral¹¹ is also described over the ranges in Eqs. (21) and (22). In the range for $d > y > 0$,

$$\begin{aligned}
 & \int_0^y \frac{dt}{t \sqrt{(a-t)(b-t)(c-t)(d-t)}} \\
 &= \frac{g}{a} \left[\frac{\alpha_{14}^2 - \alpha_4^2}{\alpha_{14}^2} \left\{ \Pi(\phi_0, \alpha_{14}^2, k) \right. \right. \\
 & \quad \left. \left. - \Pi(\phi_4, \alpha_{14}^2, k) \right\} \right. \\
 & \quad \left. + \frac{\alpha_4^2}{\alpha_{14}^2} \{ u_0 - u_4 \} \right], \tag{46}
 \end{aligned}$$

where $\phi_0, \phi_4, \alpha_4^2, \alpha_{14}^2, u_0$, and u_4 are defined in Eqs. (25) and (36). The remaining expressions are, for $c > y > d$,

$$\begin{aligned}
 & \int_0^y \frac{dt}{t \sqrt{(a-t)(b-t)(c-t)(t-d)}} \\
 &= \frac{g}{c} \left[\frac{\alpha_{15}^2 - \alpha_5^2}{\alpha_{15}^2} \left\{ \Pi(\phi_d, \alpha_{15}^2, k) \right. \right. \\
 & \quad \left. \left. - \Pi(\phi_5, \alpha_{15}^2, k) \right\} + \frac{\alpha_5^2}{\alpha_{15}^2} \{ u_d - u_5 \} \right], \tag{47}
 \end{aligned}$$

and for $b \gg y \gg c$,

$$\int_c^y \frac{dt}{t \sqrt{(a-t)(b-t)(t-c)(t-d)}}$$

$$= \frac{g}{b} \left[\frac{\alpha_{16}^2 - \alpha_6^2}{\alpha_{16}^2} \left\{ \Pi(\phi_c, \alpha_{16}^2, k) - \Pi(\phi_b, \alpha_{16}^2, k) \right\} + \frac{\alpha_6^2}{\alpha_{16}^2} \{u_c - u_b\} \right], \quad (48)$$

and for $a \gg y \gg b$,

$$\int_b^y \frac{dt}{t \sqrt{(a-t)(t-b)(t-c)(t-d)}}$$

$$= \frac{g}{a} \left[\frac{\alpha_{17}^2 - \alpha_7^2}{\alpha_{17}^2} \left\{ \Pi(\phi_b, \alpha_{17}^2, k) - \Pi(\phi_7, \alpha_{17}^2, k) \right\} + \frac{\alpha_7^2}{\alpha_{17}^2} \{u_b - u_7\} \right], \quad (49)$$

and for $y > a$,

$$\int_a^y \frac{dt}{t \sqrt{(t-a)(t-b)(t-c)(t-d)}}$$

$$= \frac{q_1 q_2}{q_3} \left[\frac{\alpha_{18}^2 - \alpha_8^2}{\alpha_{18}^2} \Pi(\phi_8, \alpha_{18}^2, k) + \frac{\alpha_8^2}{\alpha_{18}^2} u_8 \right], \quad (50)$$

where the parameter ϕ_4 to ϕ_8 , u_4 to u_8 , ϕ_a to ϕ_d , α_4 to α_8 , and k are defined in even numbered equations from Eqs. (25) to (32) and Eqs. (37) to (45).

Since the integral in Eq. (20), written as

$$\frac{(t-d)(t-c)}{t \sqrt{(t-d)(t-c)(t-b)(t-a)}}, \quad (51)$$

the evaluation of the integral is made over intervals because, as t passes from the region $t < d$ to $t = d$ to $t > d$, the integral becomes imaginary until the point c is reached. The further division into three integrals yields various form of elliptic functions. The values of each integral for the different ranges are necessary because the value of the function at a given

point depends on the results of preceding integrations. Thus, at $y = d$, c , b , and a , respectively, the integrations in Eqs. (24) to (30) are

$$\begin{aligned}
 g[F(\phi_0, h) - F(\phi_4, h)] &= g F(\phi_0, h), \\
 jg[F(\phi_d, h') - F(\phi_5, h')] &= jg K(h'), \\
 g[F(\phi_c, h) - F(\phi_6, h)] &= g K(h), \\
 jg[F(\phi_b, h') - F(\phi_7, h')] &= jg K(h'),
 \end{aligned} \tag{52}$$

while the integrations in Eqs. (34) to (42) at these points are

$$\begin{aligned}
 [\Pi(\phi_0, \alpha_4^2, h) - \Pi(\phi_4, \alpha_4^2, h)] &= \Pi(\phi_0, \alpha_4^2, h), \\
 u_0 - u_4 &= u_0, \\
 [\Pi(\alpha_5^2, h') - \Pi(\phi_5, \alpha_5^2, h')] &= \Pi(\alpha_5^2, h'), \\
 u_d - u_5 &= \frac{\Pi}{2} - u_5 = \frac{\Pi}{2}, \\
 [\Pi(\alpha_6^2, h) - \Pi(\phi_6, \alpha_6^2, h)] &= \Pi(\alpha_6^2, h), \\
 u_c - u_6 &= \frac{\Pi}{2} - u_6 = \frac{\Pi}{2}, \\
 [\Pi(\alpha_7^2, h') - \Pi(\phi_7, \alpha_7^2, h')] &= \Pi(\alpha_7^2, h'), \\
 u_b - u_7 &= \frac{\Pi}{2} - u_7 = \frac{\Pi}{2},
 \end{aligned} \tag{53}$$

with corresponding results for Eqs. (46) to (49).

The expressions for $w(z)$ in the preceding ranges are

$$\begin{aligned}
 w(z) = & A \left\{ (c+d) F(\phi_4, k) \right. \\
 & + (c-d) \Pi(\phi_4, \alpha_4^2, k) \\
 & \left. - (c-d) \Pi(\phi_4, \alpha_{14}^2, k) - (c+d) u_4 \right\} \\
 & + B, \quad y < d \text{ or } z < x_5,
 \end{aligned}$$

(54)

$$\begin{aligned}
 w(z) = & A \left\{ j(c+d) [F(\phi_5, k') - K(k')] \right. \\
 & + j(b-c) [\Pi(\phi_5, \alpha_5^2, k') - \Pi(\alpha_5^2, k')] \\
 & + j \frac{d(b-c)}{b} [\Pi(\alpha_{15}^2, k') - \Pi(\phi_5, \alpha_{15}^2, k')] \\
 & \left. + j(b + \frac{cd}{b}) \left[\frac{\Pi}{2} - u_5 \right] \right\} + B, \\
 & d < y < c \text{ or } x_5 < z < x_6,
 \end{aligned}$$

(55)

$$\begin{aligned}
w(z) = A & \left\{ (c+d) \left[F(\phi_6, k) - j K(k') \right. \right. \\
& \left. \left. - K(k) \right] + \left[(a-b) \Pi(\phi_6, \alpha_6^2, k) \right. \right. \\
& \left. \left. + j(b-c) \Pi(\alpha_5^2, k') - (a-b) \cdot \right. \right. \\
& \left. \left. \cdot \Pi(\alpha_6^2, k) \right] - \left[\frac{dc(a-b)}{ab} \Pi(\phi_6, \alpha_{16}^2, k) \right. \right. \\
& \left. \left. - j \frac{d(b-c)}{b} \Pi(\alpha_{15}^2, k') - \frac{dc(a-b)}{ab} \cdot \right. \right. \\
& \left. \left. \cdot \Pi(\alpha_{16}^2, k) \right] + j \left(b + \frac{cd}{b} \right) \frac{\pi}{2} \right. \\
& \left. + \left(a + \frac{cd}{a} \right) \left[\frac{\pi}{2} - u_6 \right] \right\} + B, \\
& c < y < b \quad \text{or} \quad x_6 < z < x_7
\end{aligned}$$

(56)

$$\begin{aligned}
w(z) = A & \left\{ (c+d) \left[j F(\phi_7, k') \right. \right. \\
& \left. \left. - j 2K(k') - K(k) \right] - \left[j(a-d) \cdot \right. \right. \\
& \left. \left. \cdot \Pi(\phi_7, \alpha_7^2, k') + j(b-c) \Pi(\alpha_5^2, k') \right. \right. \\
& \left. \left. + (a-b) \Pi(\alpha_6^2, k) - j(a-d) \cdot \right. \right. \\
& \left. \left. \cdot \Pi(\alpha_7^2, k') \right] + \left[j \frac{(a-d)c}{a} \cdot \right. \right. \\
& \left. \left. \cdot \Pi(\phi_7, \alpha_{17}^2, k') + j \frac{d(b-c)}{b} \Pi(\alpha_{15}^2, k') \right. \right. \\
& \left. \left. + \frac{dc(a-b)}{ab} \Pi(\alpha_{16}^2, k) - j \frac{(a-d)}{a} \cdot \right. \right. \\
& \left. \left. \cdot \Pi(\alpha_{17}^2, k') \right] + \left(a + \frac{cd}{a} \right) \frac{\Pi}{2} \right. \\
& \left. + j \left(b + \frac{cd}{b} \right) \frac{\Pi}{2} + (d+c) \left[\frac{\Pi}{2} - u_7 \right] \right\} \\
& + B, \quad b < y < a \quad \text{or} \quad x_7 < z < x_8,
\end{aligned}$$

(57)

$$\begin{aligned}
w(z) = A \{ & -(c+d) [F(\phi_8, k) + j 2K(k') \\
& + K(k)] + [(a-b) \Pi(\phi_8, \alpha_8^2, k) \\
& - j(b-c) \Pi(\alpha_5^2, k') - (a-b) \cdot \\
& \cdot \Pi(\alpha_6^2, k) + j(a-d) \Pi(\alpha_7^2, k')] \\
& - \left[\frac{(a-b)dc}{ab} \Pi(\phi_8, \alpha_{18}^2, k) - j \frac{(b-c)d}{b} \cdot \right. \\
& \cdot \Pi(\alpha_{15}^2, k') - \frac{dc(a-b)}{ab} \Pi(\alpha_{16}^2, k) \\
& \left. + j \frac{(a-d)c}{a} \Pi(\alpha_{17}^2, k') \right] \\
& + (a + \frac{cd}{a}) \frac{\Pi}{2} + j(b + \frac{cd}{b} + d + c) \frac{\Pi}{2} \\
& \left. + (b + \frac{cd}{b}) u_8 \right\} + B, \quad y > a \\
& \text{or } z > x_8,
\end{aligned}$$

(58)

and, after seeing these complete elliptic integrals of the third kind, one recalls, "Double, double, toil and trouble," from Macbeth.

If we refer to Figure 8, the expression for $w(z)$ maps points along the x -axis into a polygon in the w -plane. Corresponding points are

$$x_1, w_1 = \infty,$$

$$x_2, w_2 = j(L_1 + L_2 + D) = jS,$$

$$x_3, w_3 = -\infty,$$

$$x_4, w_4 = j(L_1 + L_2),$$

$$x_5, w_5 = a + j(L_1 + L_2),$$

(59)

$$x_6, w_6 = a + jL_2,$$

$$x_7, w_7 = jL_2,$$

$$x_8, w_8 = 0,$$

$$x_9, w_9 = \infty.$$

The conditions at x_1 , x_3 , and x_9 are satisfied because the normal elliptic integral of the third kind becomes logarithmically infinite for

$$\sin^2 \phi = \frac{1}{\alpha^2},$$

(60)

which, from Eq. (36), occurs at

$$\begin{aligned}\sin^2 \phi &= \frac{(x_8 - x_6)(x_5 - z)}{(x_8 - x_5)(x_6 - z)} \\ &= \frac{1}{d_1 z} \\ &= \frac{(x_8 - x_6)(x_5 - x_3)}{(x_8 - x_5)(x_6 - x_3)},\end{aligned}$$

(61)

or $z = x_3$ for $\pi(\phi, d_1^2, k)$, and at

$$\begin{aligned}\sin^2 \phi &= \frac{(x_8 - x_6)(x_5 - z)}{(x_8 - x_5)(x_6 - z)} \\ &= \frac{1}{d^2} \\ &= \frac{(x_8 - x_6)}{(x_8 - x_5)},\end{aligned}$$

(62)

or $z = \pm \infty$.

In Figure 8, in the z -plane, x_3 is chosen to be 0. With these values, the mapping between the z -plane and the w' -plane is found with

$$w' = A' \int \frac{dz}{\sqrt{(z+x_2)(z-x_4)}} + B', \quad (63)$$

where the interior angles α_2 and α_4 are equal to $\frac{\pi}{2}$. The integral in Eq. (63) is

$$w' = A' \ln(z + \sqrt{z^2 - x_2^2}) + B', \quad (64)$$

with $x_4 = -x_2$ for symmetry and improved integrability. The constants A' and B' are found with

$$w_4' = A' \ln x_2 + B' = 0, \quad B = -A' \ln x_2,$$

$$w_2' = j V_0 + A' \ln(-1) = j \frac{\pi}{2}, \quad A' = \frac{2V_0}{\pi}$$

$$w' = \frac{V_0}{\pi} \ln \frac{z + \sqrt{z^2 - 1}}{z - \sqrt{z^2 - 1}}$$

$$= \frac{V_0}{\pi} \cosh^{-1} z,$$

(65)

which satisfies the conditions at x_1 and x_3 , and x_2 and x_4 are equal to minus and plus one. The relationships between V_0/π and the dimensions of the two dimensional cylinder are found from Eqs. (47) to (52) for the appropriate range of z . The greatest effort in this method was found in BRIEF ENCOUNTERS OF THE THIRD KIND of elliptic integrals.

The mapping from the w plane to the w' plane allows the potential lines, horizontal in the w plane, to be found in the original coordinate system. In conformal mapping, "Plus ca change, plus c'est la meme chose." (from Alphonse Karr).

V. VECTOR POTENTIAL METHOD

When the lower conducting plane in Fig. 1 is removed, the image of the collinear cylinders appears in Fig. 2 as part of two thick cylinders connected by one thin cylinder. If the original "dumbbell" dipole in Fig. 2 was the initial scatterer, then symmetry considerations allow placing a conducting ground plane at the plane of symmetry. Additional images of dipoles appear as the newly created image ground planes are removed. Eventually, as more image ground planes are replaced by even more dipole images, an infinite array of collinear dumbbell dipoles in free space represents the original collinear cylindrical monopole above one side of a parallel plane guide.

Figure 10 is a coordinate system for the collinear dipole array with currents in a typical dipole n . The current in the thick cylindrical arms is $I_{an}(z')$. The current in the thin cylinder is less than that in the thick cylinder by the ratio.

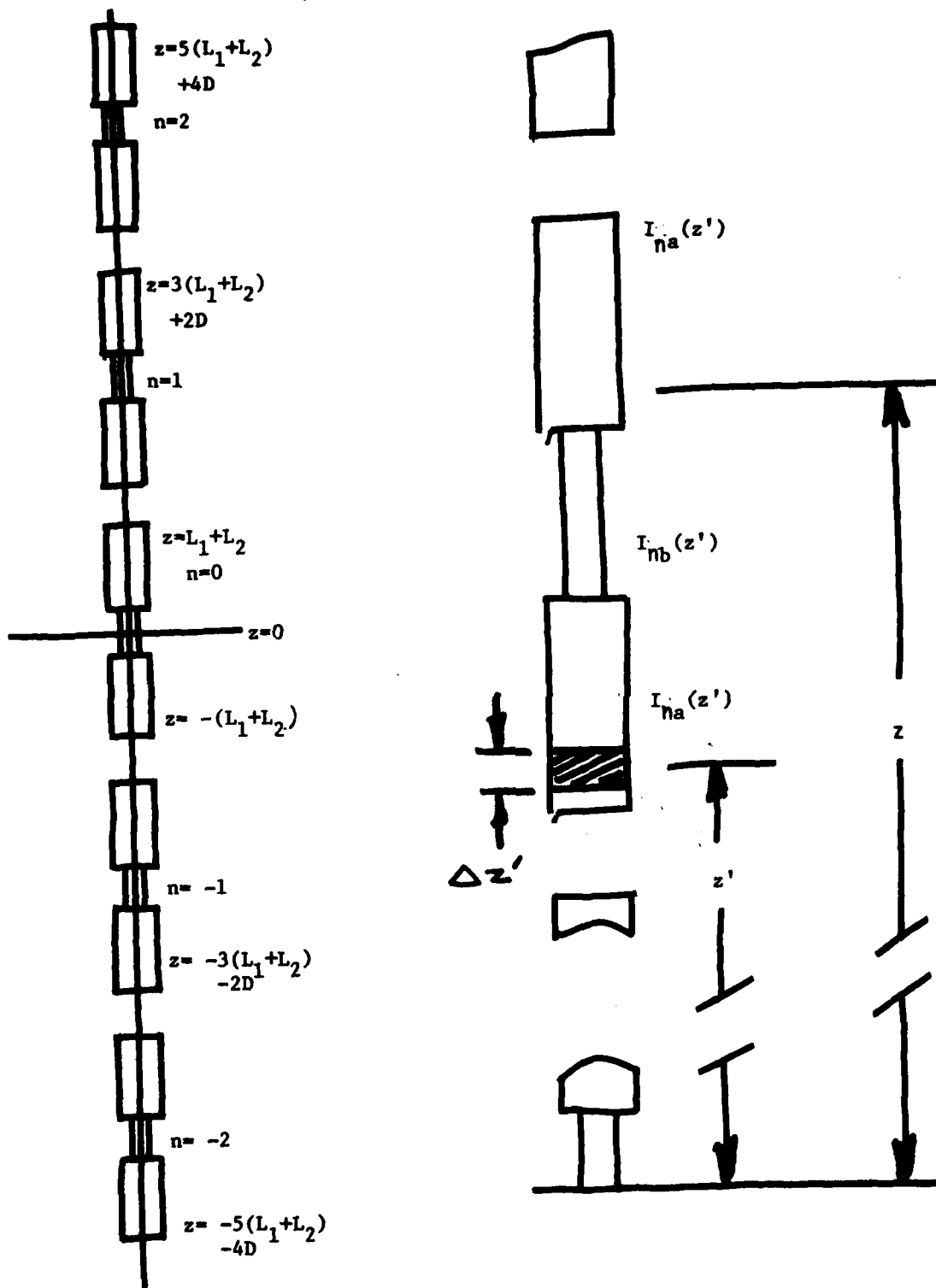


FIGURE 10 - COLLINEAR IMAGE CONFIGURATIONS FOR DUMBELL DIPOLES.

where the radius dependent scale factors are

$$\begin{aligned}\Psi_a &= 2[\ln(2/\beta a) - \gamma], \\ \Psi_b &= 2[\ln(2/\beta b) - \gamma],\end{aligned}\tag{67}$$

with $\gamma = 0.5772$. The scale factors are associated with tapered antennas and junctions of unequal radius cylinders or wires. The effects of these associations are the constancies of the products of the charge per unit length q_i and the expansion parameter Ψ_i along a wire or cylinder. The parameters a , b , and β are the radii of the two wires and the phase constant. Thus, in addition to Kirchhoff's current law, the following conditions must be met at several junctions of n conductors with different radii,

$$q_1 \Psi_1 = q_2 \Psi_2 = \dots = q_n \Psi_n,\tag{68}$$

where the currents I_i are related to the charge per unit length q_i by

$$\frac{dI_i}{ds} + j\omega q_i = 0,\tag{69}$$

which is the continuity equation with time dependence $\exp(j\omega t)$. This time dependence is also applicable to subsequent expressions. The variable s is the coordinate along the conductor axis. The major importance of the constancy in Eq. (68) is the charge concentration at the intersection of the wire and cylinders. The charge concentration creates a high concentration of electric field lines at the junctions of wires and cylinders. This electric field concentration was also present in the two dimensional models in the preceding sections on difference equations and conformal mapping.

The coordinates for the n th dumbbell dipole, which will be utilized in the method of moments later in this section and in expressions for current flow at different points are

$$\begin{aligned}
z' &= (2n+1)(L_1+L_2) + 2nD, \text{ top,} \\
&= (2n-1)(L_1+L_2) + 2nD, \text{ bottom,} \\
&= 2\pi(L_1+L_2) + L_2 + 2nD, \text{ wire-cyl top,} \\
&= 2\pi(L_1+L_2) - L_2 + 2nD, \text{ wire-cyl bot,}
\end{aligned}
\tag{70}$$

where n is positive for dipoles above and negative for dipoles below the $z' = 0$ plane.

The scattered vector potential at the surface of the cylinders satisfies the following differential equations,

$$\left\{ \frac{\partial^2}{\partial z^2} + \beta^2 \right\} A_z(a, z) = -j \frac{\beta^2}{\omega} E^{inc}, \tag{71}$$

$$\left\{ \frac{\partial^2}{\partial z^2} + \beta^2 \right\} A_z(b, z) = -j \frac{\beta^2}{\omega} E^{inc}, \tag{72}$$

for the cylindrical sections with radii a and b , where $a > b$. The incident electric field E^{inc} has only one component in the positive z -direction. The phase constant β and radian frequency ω provide frequency components over the complete spectrum of the EMP. The incident magnetic field H^{inc} has only one component in the negative y -direction. The electric field has collinear images which form an electric field. The electric and magnetic field images are components of a plane electromagnetic wave incident upon an infinite array of dipoles.

The solutions to Eqs. (71) and (72) are ¹²

$$A_z(a, z) = C_1 e^{z\beta} - j \frac{\beta}{\omega} U, \tag{73}$$

$$A_z(b, z) = C_2 e^{z\beta} - j \frac{\beta}{\omega} U, \tag{74}$$

where U is E^{inc}/β , and C_1 and C_2 are arbitrary constants.

Another representation for the vector potentials is presented in the following integrals. The radial current flowing from the center of the bottom face of the n^{th} cylindrical dipole at $\rho = 0$ to the rim at $\rho = a$ produces radial components of the vector potential. Since these components are not ϕ -dependent, the total ρ -component is zero. (For a given ϕ , the ρ -com-

ponent is cancelled by the ρ - component at $\phi + \pi$.) Similar radial currents also create a total radial vector potential equal to zero. If the radius were greater than a wavelength, there would be a ϕ - dependence in the radial current distribution. However it is neglected here. The first integral represents the axial component of the vector potential for the current flowing on the surface of the lower cylinder. The second integral represents the axial current along the wire between the two cylinders. The third integral represents the current flow along the upper cylinder.

$$A_{z1}(a, z) = \frac{\mu_0}{4\pi} \sum_{n=-\infty}^{\infty} \int_{2n(L_1+L_2)-L_2+2nD}^{2n(L_1+L_2)+L_2+2nD} I_{na}(z') K_a(z, z') dz', \quad (75)$$

$$A_{z2}(b, z) = \frac{\mu_0}{4\pi} \sum_{n=-\infty}^{\infty} \int_{2n(L_1+L_2)+L_2+2nD}^{2n(L_1+L_2)-L_2+2nD} I_{nb}(z') K_b(z, z') dz', \quad (76)$$

$$A_{z3}(a, z) = \frac{\mu_0}{4\pi} \sum_{n=-\infty}^{\infty} \int_{2n(L_1+L_2)+L_2+2nD}^{(2n+1)(L_1+L_2)+2nD} I_{na}(z') K_a(z, z') dz', \quad (77)$$

where $K_a(z, z')$ and $K_b(z, z')$ are

$$K_a(z, z') = \frac{e^{-j\beta\sqrt{(z-z')^2+a^2}}}{\sqrt{(z-z')^2+a^2}}, \quad (78)$$

$$K_b(z, z') = \frac{e^{-j\beta\sqrt{(z-z')^2+b^2}}}{\sqrt{(z-z')^2+b^2}}. \quad (79)$$

The expressions for currents at the four interfaces in Eq. (70) are

$$I_{n1}(\rho) = I_{na} (2n-1) [L_1 + L_2] + 2nD \cdot \left\{ 1 - \left(1 - \rho^2/a^2 \right)^{2/3} \right\}, \quad (80)$$

$$I_{n3}(\rho) = I_{na} (2n[L_1 + L_2] - L_2 + 2nD) \cdot \left\{ 1 - \frac{I_{na} (2n[L_1 + L_2] - L_2 + 2nD)}{I_{nb} (2n[L_1 + L_2] - L_2 + 2nD)} \cdot \frac{I_{na} (2n[L_1 + L_2] - L_2 + 2nD)}{I_{na} (2n[L_1 + L_2] - L_2 + 2nD)} \right\} \cdot \left[1 - \left(\frac{\rho-b}{a-b} \right)^2 \right]^{2/3} \}, \quad (81)$$

$$I_{n5}(\rho) = I_{na} (2n[L_1 + L_2] + L_2 + 2nD) \cdot \left\{ 1 - \frac{I_{na} (2n[L_1 + L_2] + L_2 + 2nD)}{I_{nb} (2n[L_1 + L_2] + L_2 + 2nD)} \cdot \frac{I_{na} (2n[L_1 + L_2] + L_2 + 2nD)}{I_{na} (2n[L_1 + L_2] + L_2 + 2nD)} \right\} \cdot \left[1 - \left(\frac{\rho-b}{a-b} \right)^2 \right]^{2/3} \}, \quad (82)$$

$$I_{n1}(\rho) = I_{na} ([2n+1][L_1 + L_2] + 2nD) \cdot \left\{ 1 - \left(1 - \rho^2/a^2 \right)^{2/3} \right\},$$

(83)

where the currents such as

$$I_{na} ([2n-1][L_1 + L_2] + 2nD)$$

(84)

and similar currents are not products, but represent currents at the point

$$z' = [2n-1][L_1 + L_2] + 2nD,$$

(85)

where the axial current at the bottom of the lower cylinder equals the radial current at the rim of the bottom disk of this cylinder. For example, at $\rho = a$,

$$I_{n1}(a) = I_{na} ([2n-1][L_1 + L_2] + 2nD),$$

(86)

from Eq. (80). It is of interest to note, at the same point in Eq. (85), that the current at $\rho = 0$ in Eq. (80) is

$$I_{n1}(0) = I_{na} ([2n-1][L_1 + L_2] + 2nD) \cdot \{0\} = 0,$$

(87)

so that the current vanishes at the lower end of this dipole. The vanishing of the current at the center is similar to that of a long dipole antenna. The center of the disk is like the apex of a degenerate cone. The flat cone approaches a thin needle as the cone angle approaches zero.

At another point,

$$z' = 2n[L_1 + L_2] - L_2 + 2nD,$$

(88)

the lower cylinder axial current equals the radial current at the upper rim of the lower cylinder at $\rho = a$,

$$I_{na}(2n[L_1+L_2] - L_2 + 2nD) = I_{nz}(a), \quad (89)$$

and at $\rho = b$,

$$I_{nb}(b) = I_{nb}(2n[L_1+L_2] - L_2 + 2nD). \quad (90)$$

Similar expressions relate to the top of the cylinder where the current vanishes at $\rho = 0$.

Each dipole in the array is illuminated equally by the electric field, which, like the dipole images, is infinite in coverage. Therefore the current distributions are equal, or

$$I_{na}(z') = I_{0a}(z' - 2n[L_1+L_2+D]), \quad (91)$$

$$I_{nb}(z') = I_{0b}(z' - 2n[L_1+L_2+D]), \quad (92)$$

for the axial currents. The radial currents become¹⁶

$$I_{01}(\rho) = I_{0a}(-L_1-L_2) \left\{ 1 - \left(1 - \rho^2/a^2 \right)^{2/3} \right\}, \quad (93)$$

$$I_{03}(\rho) = I_{0a}(-L_2) \left\{ 1 - \frac{I_{0a}(-L_2) - I_{0b}(-L_2)}{I_{0a}(-L_2)} \cdot \left[1 - \left(\frac{\rho-b}{a-b} \right)^2 \right]^{2/3} \right\}, \quad (94)$$

$$I_{05}(\rho) = I_{0a}(L_2) \left\{ 1 - \frac{I_{0a}(L_2) - I_{0b}(L_2)}{I_{0a}(L_2)} \cdot \left[1 - \left(\frac{\rho - b}{a - b} \right)^2 \right]^{2/3} \right\}, \quad (95)$$

$$I_{07}(\rho) = I_{0a}(L_1 + L_2) \left\{ 1 - \left(1 - \rho^2/a^2 \right)^{2/3} \right\}. \quad (96)$$

Since the relationship between I_{0a} and I_{0b} is described in Eqs. (66) to (69), the radial currents are not necessary for evaluating the expressions for axial currents. They are included here because relationship between current and surface charge density,

$$\nabla \cdot \vec{K} - \frac{\partial \sigma}{\partial x} = 0, \quad (97)$$

over the disks on the ends of the dipoles or on the interfaces between wires and cylinders is

$$\frac{d I_{n1}(\rho)}{d \rho} = 2 \pi \rho \frac{\partial \sigma_{n1}}{\partial x}, \quad (98)$$

where σ_{n1} is the surface charge density in coulombs per square meter. The surface charge density is a measure of the total electric field on a perfect conductor. This relationship is

$$E_{n1} = \frac{\sigma_{n1}}{\epsilon_0}, \quad (99)$$

where E_{n1} is the electric field originating from the surface charge density σ_{n1} , where E_{n1} is normal to the surface. A plot of the radial current appears in Fig. 11. Curves for four ratios of I_{0a} to I_{0b} are plotted, with the extrema for $I_{0a} = I_{0b}$ (same wire radii) and $I_{0b} = 0$ (wire radius $b = 0$).

When the variable z' is changed to a new variable u with

$$u = z' - 2n[L_1 + L_2 + D], \quad (100)$$

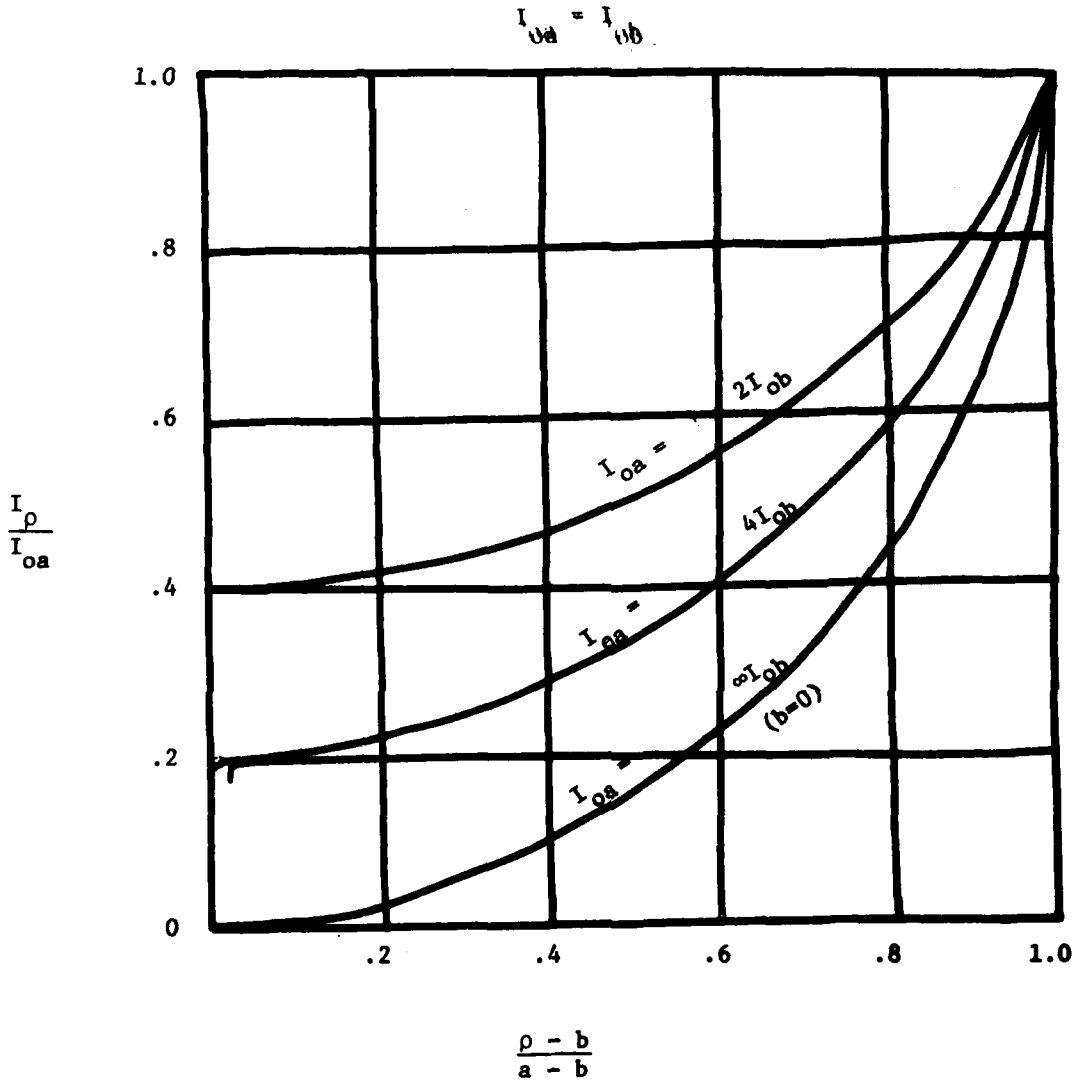


FIGURE 11 — RATIO OF CURRENTS FOR UNEQUAL WIRES OR CYLINDERS

the axial vector potential components in Eqs. (75) to (77) become

$$A_{z1}(a, z) = \frac{\mu_0}{4\pi} \int_{-(L_1+L_2)}^{-L_2} I_a(u) \bar{K}_a(z, u) du, \quad (101)$$

$$A_{z2}(b, z) = \frac{\mu_0}{4\pi} \int_{-L_2}^{L_2} I_b(u) \bar{K}_b(z, u) du, \quad (102)$$

$$A_{z3}(a, z) = \frac{\mu_0}{4\pi} \int_{L_2}^{L_1+L_2} I_a(u) \bar{K}_a(z, u) du, \quad (103)$$

where the zero subscript for current was dropped to simplify notation and

$$\bar{K}_a(z, u) = \sum_{n=-\infty}^{\infty} K_a(z, u + 2n[L_1 + L_2 + D]), \quad (104)$$

$$\bar{K}_b(z, u) = \sum_{n=-\infty}^{\infty} K_b(z, u + 2n[L_1 + L_2 + D]). \quad (105)$$

When Eqs. (71) and (72) are combined with Eqs. (101) to (103), the resulting expressions are

$$\begin{aligned} & \int_{-(L_1+L_2)}^{-L_2} I_a(u) \bar{K}_a(z, u) du \\ & + \int_{L_2}^{L_1+L_2} I_a(u) \bar{K}_a(z, u) du \\ & = \frac{4\pi}{\mu_0} C_1 \cos \beta z - \frac{4\pi}{\mu_0} U, \end{aligned}$$

$$\int_{-L_2}^{L_2} I_b(u) \bar{K}_b(z, u) du = \frac{4\pi}{\mu_0} C_2 \cos \beta z - j \frac{4\pi}{\eta_0} U,$$

(106)

where η_0 is the characteristic impedance of free space and the constant C_1 and C_2 may be found from matching radial and axial currents at the ends and interfaces of the dumbbell dipole. With Eqs. (93) and (95), the axial currents at the ends are

$$I_{01}(a) = I_a(-L_1 - L_2),$$

$$I_{05}(a) = I_a(L_1 + L_2).$$

(107)

The numerical solution of Eq. (106) is obtained from two finite sums N_1 and N_2 over an interval of N different points with the method of moments. The increment Δ between adjacent points is

$$\Delta = \frac{L_1 + L_2}{N}, \quad N = \frac{L_1 + L_2}{\Delta},$$

(108)

with N_1 and N_2 determined by L_1 , L_2 , and Δ ,

$$N_1 = \frac{L_1}{\Delta} = \frac{L_1}{L_1 + L_2} N,$$

$$N_2 = \frac{L_2}{\Delta} = \frac{L_2}{L_1 + L_2} N.$$

(109)

The integrals for the first and third terms in Eq. (106) are combined as

$$\begin{aligned}
& \int_{-L_2}^{-L_1+L_2} I_a(u) \bar{K}_a(z, u) du \\
& + \int_{L_2}^{L_1+L_2} I_a(u) \bar{K}_a(z, u) du \\
& = \int_{L_2}^{L_1+L_2} I_a(u) [\bar{K}_a(z, u) + \bar{K}_a(z, -u)] du,
\end{aligned}$$

(110)

and the second term becomes

$$\begin{aligned}
& \int_{-L_2}^{L_2} I_b(u) \bar{K}_b(z, u) du \\
& = \int_0^{L_2} I_b(u) [\bar{K}_b(z, u) + \bar{K}_b(z, -u)] du.
\end{aligned}$$

(111)

In the method of moments, the integral in Eq. (110) is approximated by a finite sum over N_1 different points,

$$\begin{aligned}
& \int_{L_2}^{L_1+L_2} I_a(u) [\bar{K}_a(z, u) + \bar{K}_a(z, -u)] du \\
& = \int_{L_2}^{L_2+\Delta} I_a(L_2) [\bar{K}_a(z, u) + \bar{K}_a(z, -u)] du
\end{aligned}$$

$$\begin{aligned}
& + \int_{L_2+\Delta}^{L_2+2\Delta} I_a(L_2+\Delta) [\bar{K}_a(z,u) + \bar{K}_a(z,-u)] du \\
& \dots + \int_{L_1+L_2-\Delta}^{L_1+L_2} I_a(L_1+L_2-\Delta) [\bar{K}_a(z,u) + \bar{K}_a(z,-u)] du,
\end{aligned}
\tag{112}$$

with a similar expression for Eq. (111), for N_2 points,

$$\begin{aligned}
& \int_0^{\Delta} I_b(0) [\bar{K}_b(z,u) + \bar{K}_b(z,-u)] du \\
& + \int_{\Delta}^{2\Delta} I_b(\Delta) [\bar{K}_b(z,u) + \bar{K}_b(z,-u)] du \\
& + \int_{L_2-\Delta}^{L_2} I_b(L_2-\Delta) [\bar{K}_b(z,u) + \bar{K}_b(z,-u)] du.
\end{aligned}
\tag{113}$$

The first terms in Eqs. (112) and (113) are similarly divided,

$$\begin{aligned}
& \int_{L_2}^{L_2+\Delta} I_a(u) [\bar{K}_a(z,u) + \bar{K}_a(z,-u)] du \\
& = \int_{L_2}^{L_2+\Delta} I_a(u) [\bar{K}_a(0,u) + \bar{K}_a(0,-u)] du
\end{aligned}$$

$$\begin{aligned}
& + \int_{L_2}^{L_2+\Delta} I_a(u) [\bar{K}_a(\Delta, u) + \bar{K}_a(\Delta, -u)] du \\
& + \dots + \int_{L_2}^{L_2+\Delta} I_a(u) [\bar{K}_a(N\Delta, u) + \bar{K}_a(N\Delta, -u)] du
\end{aligned}$$

$$\begin{aligned}
& \int_0^{\Delta} I_b(u) [\bar{K}_b(z, u) + \bar{K}_b(z, -u)] du && (114) \\
& = \int_0^{\Delta} I_b(u) [\bar{K}_b(0, u) + \bar{K}_b(0, -u)] du \\
& + \int_0^{\Delta} I_b(u) [\bar{K}_b(\Delta, u) + \bar{K}_b(\Delta, -u)] du \\
& + \dots + \int_0^{\Delta} I_b(u) [\bar{K}_b(N\Delta, u) + \bar{K}_b(N\Delta, -u)] du,
\end{aligned}$$

(115)

with similar divisions for subsequent terms.

Rearrangements of the preceding equations are made in the partial sums

$$\begin{aligned}
& \int_{L_2+\Delta}^{L_2+\Delta} I_a(u) [\bar{K}_a(0,u) + \bar{K}_a(0,-u)] du \\
& + \int_{L_2+\Delta}^{L_2+2\Delta} I_a(u) [\bar{K}_a(0,u) + \bar{K}_a(0,-u)] du \\
& + \dots + \int_{L_2+\Delta}^{L_1+L_2} I_a(u) [\bar{K}_a(0,u) + \bar{K}_a(0,-u)] du \\
& = \sum_{m=N_2+1}^N I_a(z_{am}) \pi_{amp},
\end{aligned}$$

(116)

where z_{am} and π_{amp} are

$$z_{am} = (m-1)\Delta + L_2,$$

$$m = N_2+1, N_2+2, \dots, N-1, N,$$

(117)

$$\begin{aligned}
\pi_{amp} = & \int_{(m-1)\Delta+L_2}^{m\Delta+L_2} [\bar{K}([p-1]\Delta, u) \\
& + \bar{K}([p-1]\Delta, -u)] du, \\
p = & 1, 2, 3, \dots, N-1, N.
\end{aligned}$$

(118)

Another change of variables,

$$v = u - (m-1)\Delta,$$

(119)

in the square root term in Eq. (78) creates, with z equals $[\rho - 1]\Delta$,

$$\begin{aligned} & \sqrt{(z-z')^2 + a^2} \\ &= \sqrt{(z-u-2n[L_1+L_2+D])^2 + a^2} \\ &= \sqrt{([\rho-1]\Delta-u-2n[L_1+L_2+D])^2 + a^2} \\ &= \sqrt{([\rho-m]\Delta - [v+2n(L_1+L_2+D)])^2 + a^2}, \end{aligned}$$

(120)

and for $-u$ instead of $+u$, this last term is

$$\sqrt{([\rho+m-2]\Delta - [v+2n(L_1+L_2+D)])^2 + a^2},$$

(121)

so that $\bar{K}_a(z, u)$ and $\bar{K}_a(z, -u)$ become

$$\begin{aligned} \bar{K}_a(z, u) &= \sum_{n=-\infty}^{\infty} K_{an}(z, u + 2n[L_1+L_2+D]) \\ &= \sum_{n=-\infty}^{\infty} K_{an}([\rho-1]\Delta, v + [m-1]\Delta \\ & \quad + 2n[L_1+L_2+D]) \end{aligned}$$

$$= \sum_{n=-\infty}^{\infty} K_{an}([p-m]\Delta, v+2n[L_1+L_2+D]),$$

(122)

$$\begin{aligned} & \bar{K}_a(z, -u) \\ &= \sum_{n=-\infty}^{\infty} K_{an}([p+m+2]\Delta, -v+2n[L_1+L_2+D]). \end{aligned}$$

(123)

In Eqs. (122) and (123), we can write

$$\pi_{amp} = g_a(p-m) + g_a(p+m-2), \quad (124)$$

where $g_a(m)$ is $L_2 + \Delta$

$$g_a(m) = \int_{L_2}^{\infty} \sum_{n=-\infty}^{\infty} K_{an}(m\Delta, v+2n[L_1+L_2+D]) \cdot dv. \quad (125)$$

For the center wire, the similar set of expressions are

$$\sum_{m=1}^{N_2} I_b(z_{bm}) \pi_{bmp}, \quad (126)$$

where

$$z_{bm} = (m-1)\Delta,$$

$$\pi_{bmp} = g_b(p-m) + g_b(p+m-2),$$

(127)

where, as in Eq. (125), $g_b(m)$ is

$$g_b(m) = \int_0^{\Delta} \sum_{n=-\infty}^{\infty} K_{bn}(m\Delta, v + 2n[L_1 + L_2 + D]) \cdot dv,$$

(128)

Equations (116) and (126), combined with Eqs. (73) and (74) yield

$$\sum_{m=1}^{z_2} I_b(z_{bm}) \pi_{bmp} = \frac{4\pi}{\mu_0} C_1 \cos \beta z_p - j \frac{4\pi}{\eta_0} U,$$

$$\sum_{m=N_2+1}^z I_a(z_{am}) \pi_{amp} = \frac{4\pi}{\mu_0} C_2 \cos \beta z_p - j \frac{4\pi}{\eta_0} U,$$

(129)

where $z_p = (\rho - 1)\Delta$. The combined system of equations has N unknowns and N equations. The $N \times N$ matrix must be inverted to find values for $I_a(z_{am})$ and $I_b(z_{bm})$. Accuracy of results increases with larger values of N , but computer time also increases.

VI. GREEN'S FUNCTION

The preceding section introduced the method of moments to find the currents induced on two collinear cylinders in a parallel plane waveguide. The source was the incident electric field corresponding to one of the frequency components of the EMP. This section introduces the azimuthal component, or ϕ -component, of the incident magnetic field corresponding to one of the frequency components of the EMP. Instead of the functions $K(z, z')$, which are similar to Green functions, the Green functions $G(\rho, z | \rho', z')$ are also introduced in the form of Green's second identity.

If V is a closed region of space bounded by a regular surface S , and ψ and Φ are two scalar functions of position which are continuous together with their first and second derivatives in V and on S , then the divergence theorem applied to the vector $\psi \nabla \Phi$ gives

$$\int \nabla \cdot (\psi \nabla \Phi) dV = \int (\psi \nabla \Phi) \cdot \vec{n} dS, \quad (130)$$

and expansion of $\nabla \cdot (\psi \nabla \Phi)$ gives

$$\nabla \cdot (\psi \nabla \Phi) = \nabla \psi \cdot \nabla \Phi + \psi \nabla^2 \Phi, \quad (131)$$

and with the dot product of the gradient of Φ and the unit vector along the outward going normal,

$$\nabla \Phi \cdot \vec{n} = \frac{\partial \Phi}{\partial n}, \quad (132)$$

George Green's first identity is obtained,

$$\int \nabla \psi \cdot \nabla \Phi dV + \int \psi \nabla^2 \Phi dV = \int \psi \frac{\partial \Phi}{\partial n} dS. \quad (133)$$

George Green's second identity is found by interchanging ψ and Φ in Eq. (133) and then finding the difference,

$$\int \{ \nabla \cdot (\Phi \nabla \psi) - \nabla \cdot (\psi \nabla \Phi) \} dV = \int \{ \Phi \nabla^2 \psi - \psi \nabla^2 \Phi \} dV = \int \{ \psi \frac{\partial \Phi}{\partial n} - \Phi \frac{\partial \psi}{\partial n} \} dS, \quad (134)$$

where the normal n is now directed inward to represent the inside surface of the parallel plate guide.

If Ψ is the Green's function G , where

$$\Psi = G = \frac{e^{-j\beta|r-r'|}}{4\pi|r-r'|} \quad (135)$$

$$|r-r'| = \sqrt{\rho^2 + \rho'^2 - 2\rho\rho'\cos(\phi-\phi') + (z-z')^2}, \quad (136)$$

and ϕ is the source,

$$\Phi = u(\rho, z) \cos \phi, \quad (137)$$

then ϕ satisfies the Helmholtz equation in cylindrical coordinates,

$$\begin{aligned} & \left\{ \frac{1}{\rho} \frac{\partial}{\partial \rho} \left(\rho \frac{\partial}{\partial \rho} \right) + \frac{1}{\rho^2} \frac{\partial^2}{\partial \phi^2} + \frac{\partial^2}{\partial z^2} + \beta^2 \right\} u \cos \phi \\ &= \left\{ \frac{\partial^2}{\partial \rho^2} + \frac{1}{\rho} \frac{\partial}{\partial \rho} - \frac{1}{\rho^2} + \frac{\partial^2}{\partial z^2} + \beta^2 \right\} u \\ &= 0. \end{aligned} \quad (138)$$

If $\Psi = G$, where G is a function of $\rho, \rho', z, z', \phi, \phi'$, and ϕ is $u \cos \phi$, where u is a function of ρ and z , then Eq. (134) becomes

$$\begin{aligned} & \int \{ u \cos \phi \nabla^2 G - G \nabla^2 (u \cos \phi) \} dV' \\ &= \int \left\{ G \frac{\partial}{\partial n'} (u \cos \phi) - u \cos \phi \frac{\partial G}{\partial n'} \right\} ds', \end{aligned} \quad (139)$$

where $dv' = \rho' d\phi' dz'$ and

$$(\nabla^2 + \beta^2)G = \frac{-\delta(\rho')\delta(\phi')\delta(z')}{\rho'} \quad (140)$$

with δ equal to the Dirac delta function, named after the infinitely known Paul Andre Maurice Dirac. Substitution of Eq. (140) into (139) yields

$$u(\rho, z) \cos \phi = \int \left\{ u \cos \phi' \frac{\partial G}{\partial n'} - G \frac{\partial}{\partial n'} (u \cos \phi') \right\} \cdot ds' \quad (141)$$

where $ds' = \rho' d\phi' dz'$. Multiplying Eq. (141) by $\cos \phi$ and integrating with respect to ϕ creates

$$\begin{aligned} \int_0^{2\pi} u(\rho, z) \cos^2 \phi d\phi &= \pi u(\rho, z) \\ &= \int_0^{2\pi} \cos \phi d\phi \int \left\{ u \cos \phi' \frac{\partial G}{\partial n'} - G \cos \phi' \frac{\partial}{\partial n'} u \right\} ds' \end{aligned} \quad (142)$$

If a function $F(\phi)$ is an even and periodic function, then $F(\phi) = F(-\phi)$ and $F(\phi) = F(2\pi + \phi)$, then

$$\begin{aligned} &\int_0^{2\pi} \cos \phi d\phi \int_0^{2\pi} F(\phi - \phi') \cos \phi' d\phi' \\ &= \int_0^{2\pi} d\phi \int_0^{2\pi} \frac{1}{2} \{ \cos(\phi' + \phi) + \cos(\phi' - \phi) \} \cdot F(\phi' - \phi) d(\phi' - \phi) \end{aligned}$$

$$\begin{aligned}
&= \pi \int_0^{2\pi} F(\phi' - \phi) \cos(\phi' - \phi) d(\phi' - \phi) \\
&= \pi \int_0^{2\pi} F(\psi) \cos \psi d\psi,
\end{aligned}$$

(143)

with the orthogonality of $\cos \psi$ being introduced. The function $F(\psi)$, where $\psi = \phi' - \phi$, could be expanded into an infinite Fourier series, but only $a_1 \cos \psi$ would remain. Since G and $\frac{\partial G}{\partial n}$ are similar to $F(\psi)$,

$$u(\rho, z) = \int \left\{ u \frac{\partial G^{(1)}}{\partial n'} - G^{(1)} \frac{\partial u}{\partial n'} \right\} \rho' dz',$$

(144)

where

$$G^{(1)}(\rho, z | \rho', z') = \int_0^{2\pi} \cos \psi \phi \cdot$$

$$\cdot \frac{e^{-\frac{1}{2}\beta \sqrt{(z-z')^2 + \rho^2 + \rho'^2 - 2\rho\rho' \cos \psi}}}{4\pi \sqrt{(z-z')^2 + \rho^2 + \rho'^2 - 2\rho\rho' \cos \psi}} d\psi,$$

(145)

which satisfies

$$\begin{aligned}
&\left\{ \frac{1}{\rho} \frac{\partial}{\partial \rho} \rho \frac{\partial}{\partial \rho} - \frac{1}{\rho^2} + \frac{\partial^2}{\partial z^2} + \beta^2 \right\} G^{(1)} \\
&= -\delta(z-z') \frac{\delta(\rho-\rho')}{\rho'}.
\end{aligned}$$

(146)

When u is the ϕ - component of the magnetic field, and is equal to u , and the volume V is the pair of collinear cylinders, with

$$j\omega\epsilon E_{\rho} = -\frac{\partial}{\partial z} H_{\phi},$$

$$j\omega\epsilon E_z = \left(\frac{\partial}{\partial \rho} + \frac{1}{\rho}\right) H_{\phi},$$

(147)

we have from Eq. (144),

$$H_{\phi} = \int (\vec{n}' \cdot \vec{e}_z) \left\{ H_{\phi} \frac{\partial}{\partial z'} G^{(1)} + j\omega\epsilon E_{\rho} G^{(1)} \right\} \rho' d\rho'$$

$$+ \int \left\{ H_{\phi} \frac{\partial}{\partial \rho'} (\rho' G^{(1)}) - j\omega\epsilon \rho E_z G^{(1)} \right\} \cdot dz'.$$

(148)

When this equation is applied to the two cylinders in Fig. 1, with boundary conditions

$$\frac{\partial}{\partial z} G = 0, \quad z = 0, S,$$

(149)

and with the integration path along the cylinder surfaces, end or top, and interface between wire and cylinder, E_{ρ} and E_z are tangent to the conducting surfaces and are zero. The expression for the total magnetic field (ϕ - component) is

$$\begin{aligned}
H_{\phi}(p, z) = & H_{\phi}^{inc}(p, z) \\
& + \int_0^{L_2} [H_{\phi} \frac{\partial}{\partial p'}(p'G)]_{p'=b} dz' \\
& + \int_b^a [H_{\phi} \frac{\partial}{\partial z'} G]_{z'=L_2} p' dp' \\
& + \int_{L_2}^{L_1+L_2} [H_{\phi} \frac{\partial}{\partial p'}(p'G)]_{p=a} dz' \\
& + \int_a^{\rho} [H_{\phi} \frac{\partial}{\partial z'} G]_{z'=L_1+L_2} p' dp',
\end{aligned}$$

(150)

where the first term is the incident magnetic field, the second is for the axial current induced on the wire (or thin cylinder), the third is for the radial current induced on the interface between wire and cylinder, the fourth is for the axial current induced on the cylinder, and the last is for the current induced on the top of the cylinder.

The incident magnetic field

$$\vec{H}^{inc} = -\vec{a}_y H_0 e^{-j\beta z},$$

(151)

and if the waves are incident on cylindrical structures, a representation of plane waves in a cylindrical coordinate system is required. A Fourier series in ϕ is represented as

$$H^{inc} = -2H_0 \sum_{n=0}^{\infty} j^n J_n(\beta\rho) \cos n\phi,$$

(152)

and the axi-symmetric mode of the incident magnetic field is, for $n = 1$,

$$\begin{aligned} H_{\phi}^{inc}(\rho) &= \frac{1}{2\pi} \int_0^{2\pi} \vec{a}_{\phi} \cdot \vec{H}^{inc} d\phi \\ &= -\frac{1}{2\pi} \int_0^{2\pi} H^{inc} \cos\phi d\phi \\ &= \frac{H_0}{2\pi} \sum_{n=0}^{\infty} j^n J_n(\beta\rho) \int_0^{2\pi} \cos\phi \cos n\phi d\phi \\ &= j \frac{H_0}{\pi} J_1(\beta\rho) \int_0^{2\pi} \cos^2\phi d\phi = j H_0 J_1(\beta\rho), \end{aligned}$$

(153)

where all $J_n(\beta\rho)$ terms vanish except $n = 1$ because of orthogonality.

In terms of currents on the cylinders and cylinder faces, with axial currents related to magnetic fields by

$$\begin{aligned} \Gamma_a(z') &= 2\pi a H_{\phi}(a, z'), \\ \Gamma_b(z') &= 2\pi b H_{\phi}(b, z'), \end{aligned} \quad (154)$$

and with $K(\rho, z|a, z')$ and $K(\rho, z|b, z')$ related to the Green's function by

$$K_a(\rho, z|a, z') = -\frac{\partial}{\partial \rho'} (\rho' G) \Big|_{\rho'=a},$$

$$K_b(\rho, z|b, z') = -\frac{\partial}{\partial \rho'} (\rho' G) \Big|_{\rho'=b},$$

(155)

the expression for current becomes

$$I_a(z) + \int_{L_1+L_2}^{L_2} K_b(b, z|b, z') I_b(z') dz'$$

$$+ \int_{L_2} K_a(a, z|a, z') I_a(z') dz'$$

$$= j 2\pi a H_0 J_1(ka)$$

$$+ a \int_b^a I_{05}(\rho') \left[\frac{\partial G}{\partial \rho'} \right]_{z'=L_2} d\rho'$$

$$+ a \int_0^b I_{07}(\rho') \left[\frac{\partial G}{\partial z'} \right]_{z'=L_1+L_2} d\rho',$$

(156)

where $I_{05}(\rho')$ and $I_{07}(\rho')$ are identical to expressions in Eqs. (95) and (96) in the last section. The currents I_{0a} and I_{0b} correspond to I_a and I_b in this section.

The Green's function G is found with the theory of images and with Eq. (145),

$$G(\rho, z | \rho', z') = \sum_{n=-\infty}^{\infty} \int_0^{2\pi} \left\{ \frac{e^{j\beta R_{n0}}}{R_{n0}} + \frac{e^{j\beta R_{n1}}}{R_{n1}} \right\} \cos \phi \, d\phi, \quad (157)$$

where R_{n0} and R_{n1} are the images,

$$R_{n0} = \sqrt{(2nS + z + z')^2 + \rho^2 + \rho'^2} \quad (158)$$

$$-2\rho\rho' \cos \phi,$$

$$R_{n1} = \sqrt{(2nS - z + z')^2 + \rho^2 + \rho'^2}$$

$$-2\rho\rho' \cos \phi.$$

(159)

The method of moments, applied to this formulation, will yield better results than the preceding section because it has better coverage of the end and interface of the cylinders. Numerical integration is more suitable here.

Another method related to conformal mapping was brought into consideration, but time constraints intervened. It is described below (from the Snark Hunt by Lewis Carroll).

You boil it in sawdust;
 You salt it in glue;
 You condense it with locusts and tape;
 Still keeping one principal object in view,
 To preserve its symmetrical shape.

VII. RECOMMENDATIONS

Four methods to find the currents and charge distributions on a cylinder connected by a wire to one side of a parallel plate guide indicate an interesting phenomena in the wire-cylinder interface. The concentration of electric field lines at this interface is accompanied by an increase in electric charge density. The decrease in current from the cylinder to the wire appears in the displacement current originating from the increase in charge density.

Follow-on research can follow two related paths. One path is a computer-aided evaluation of the results described in the last three methods. Another path is an experimental evaluation of currents induced on a metal cylinder connected to one side of the TRESTLE or ALECS EMP facility. The cylinder could be connected with short, intermediate, and long (compared with cylinder length) wires. Current measurements should be made at the junction and intermediate points. The displacement current should also be monitored, especially in the junction of wire and cylinder vicinity.

REFERENCES

1. H. Kober, Dictionary of Conformal Representation, 2nd edition, Dover Publications, New York, 1957.
2. H. H. Meinke, "Ein Allgemeines Lösungsverfahren für inhomogene Zylindersymmetrische Wellenfelder," Zeitschrift für angewandte Physik, Vol. 1, pp. 509-516, 1949.
3. "A Survey on the Use of Conformal Mapping For Solving Wave-Field Problems," Proceedings of a Symposium on Electromagnetic Theory and Antennas, pp. 1113-1124, Copenhagen, Denmark, June 1962.
4. R. Piloty, "Das Feld in inhomogenen Rechteckrohren bei Anregung mit der H_{10} - Welle," Zeitschrift für angewandte Physik, Vol. 1, pp. 490-497, 1949.
5. R. Piloty, "Die Anwendung der konformen Abbildung auf die Feldgleichungen in inhomogenen Rechteckrohren," Zeitschrift für angewandte Physik, Vol. 1, pp. 441-448, 1949.
6. R. V. Southwell, Relaxation Methods in Theoretical Physics, Oxford University Press, 1946.
7. C. G. J. Jacobi, "Über eine neue Auflösungsart der bei der Methode der kleinste Quadrate vorkommenden linearen Gleichungen," Astron. Nachr., Vol. 22, No. 523, 1844; Ges. Werke (Georg Reimer, Berlin, 1884, Vol. III, p. 467).
8. P. Moon and D. E. Spencer, Field Theory for Engineers, D. Van Nostrand, Princeton, NJ, 1961, pp. 1-41.
9. H. L. Liebmann, Die angenäherte Ermittlung harmonischer Funktionen und konformer Abbildung, Sitzber. math.-physik. Kl., Bayer Akad. Wiss., p. 385, 1918.
10. R. V. Churchill, Introduction to Complex Variables and Applications, McGraw-Hill, New York, 1948.
11. P. F. Byrd and M. D. Friedman, Handbook of Elliptic Integrals for Engineers and Scientists, Springer-Verlag, Berlin, 1971.

12. C. D. Taylor and G. A. Steigerwald, "On the Pulse Excitation of a Cylinder in a Parallel Plate Waveguide," Sensor and Simulation Note No. 99, Air Force Weapons Laboratory, Kirtland AFB, NM, March 1970.
13. T. T. Wu and R. W. P. King, "The Tapered Antenna and Its Application to the Junction Problem for Thin Wires," IEEE Trans. on Antennas and Propagation, Vol. AP-24, pp. 42-45, January 1976.
14. Roger F. Harrington, Field Computation by Moment Methods, Macmillan, NY, 1968.
15. R. W. Latham and K. S. H. Lee, "Electromagnetic Interaction Between a Cylindrical Post and a Two-Parallel-Plate Simulator," Sensor and Simulation Note 111, Air Force Weapons Laboratory, Kirtland AFB, NM, July 1970.
16. R. W. Sassman, K. S. H. Lee, and R. W. Latham, "Minimization of Current Distributions on a Cylindrical Post Piercing a Parallel-Plate Waveguide," Sensor and Simulation Note No. 93, Air Force Weapons Laboratory, Kirtland AFB, NM, September 1969.

1981 USAF - SCEE SUMMER FACULTY RESEARCH PROGRAM

Sponsored by the

AIR FORCE OFFICE OF SCIENTIFIC RESEARCH

Conducted by the

SOUTHEASTERN CENTER FOR ELECTRICAL ENGINEERING EDUCATION

FINAL REPORT

ELECTROMAGNETIC SCATTERING FROM DIELECTRIC

AND COMPOSITE BODIES

Prepared by: Dr. William G. Bradley
Academic Rank: Assistant Professor
Department and Department of Electrical Engineering
University: University of Alabama in Huntsville
Research Location: Rome Air Development Center, Hanscom AFB,
Electromagnetic Sciences Division, EM Techniques
Branch, Targets and Environment Section
USAF Research Dr. Ronald G. Newburgh
Colleagues:
Date: August 19, 1981
Contract No: F46920-79-C-0038

ELECTROMAGNETIC SCATTERING FROM
DIELECTRIC AND COMPOSITE BODIES

by

Dr. William G. Bradley

ABSTRACT

The methods of computing scattered fields from dielectric bodies are reviewed. The procedure that is required to extend some of these methods to include the computation of bistatic cross sections is considered. A literature search showed that little work has been done on scattering from composite bodies. Carbon composites are of particular interest, and experimental and analytic work is proposed. The possibility of controlling the scattering cross sections by the design of special composite materials is considered. Specifically, it may be possible to construct a composite with $\mu_r = \epsilon_r$. This is relevant to the theory of absorbers in scattering where additional work is proposed.

I. INTRODUCTION: The Electromagnetic Sciences Division has been involved with Electromagnetic Scattering for many years. They presently are constructing a new scattering range that will be capable of measuring backscatter and bistatic radar cross sections of a wide range of targets, and planning analytical studies of scattering problems. Since the author's Ph.D thesis was in the area of scattering from dielectric bodies, he was asked to review the literature on scattering from dielectrics, and suggest ways of extending the previous work to other cases and other materials. The research reported in this paper is intended to support and help in the planning of the scattering program.

II. OBJECTIVES: The primary objectives of this present were:

- a. Review the literature and study the various methods of calculating the scattered fields from dielectric bodies.
- b. Present a seminar on scattering from dielectric bodies.
- c. Collect information on composite and other materials that may be important to radar scattering.
- d. Recommend future measurements that could be done at the scattering range and analytical work that will support and measured results.

III. SCATTERING FROM DIELECTRIC BODIES: The topic of electromagnetic scattering from dielectric bodies has received a considerable amount of attention for many years. However, there are many unanswered questions of current interest.

Logan¹ did an extensive review of the early work on scattering from spheres. He indicates that Clebsch² solved the elastic wave equations for a spherical obstacle in 1863. Many other researchers worked on the problem and Mie³ (1908) extended the work of earlier papers. His paper was used as the basis for much of the later work. Stratton⁴ (1941) included Mie's work in his text.

Even though Mie's results were available as early as 1908, it was not practical to compute numerical solutions for wide ranges of parameters until high speed digital computers became available. Aden⁵ (1951) used the equations in Stratton's text, with minor modifications, to compute the backscatter areas of metal and water spheres. Atlas et al⁶ (1963) computed the backscatter area of ice spheres. King and Harrison⁷ (1971) computed a comprehensive set of results for a wide range of frequencies and complex dielectric constants.

It is possible to compute the scattered fields from a few non-spherically shaped bodies by a method of separation of variables similar to that used for a sphere. Specifically, the surface of the scatterer must be a constant coordinate surface in an appropriate coordinate system. This method was applied to a perfectly conducting prolate spheroid, with nose-on incident wave, by Siegel et al⁸ (1956). The results were in terms of an infinite series of prolate spheroidal harmonics. Ritter⁹ explains the considerable computational effort required to obtain numerical results. Dodge¹⁰ (1980) calculated the scattered fields from a thin metallic disk with arbitrary angle of incidence. The analytical and computational difficulties have prevented the widespread application of this method to dielectrics. However, Assano and Yamamoto¹¹ succeeded in deriving the equations and computing numerical results for dielectric prolate and oblate spheroids. The elegance of the analytic solutions is impressive. However, the computation time required to obtain numerical results from the equations may be comparable to that required for some of the numerical methods to be considered later.

Since general analytic solutions of the scattering problem are complex, and are available for only a few simple shapes, both high and low frequency approximation methods have been developed. High frequency approximation methods apply to bodies that are large compared to a wavelength. They involve application of geometric and/or physical optics methods. These methods work best for convex metal objects. Dielectric and concave metal objects require tracing rays through multiple reflections. See for example, Van Bladel¹² Chapter 9 for an introduction to high frequency methods and the review article by Kouyoumian.¹³

Rayleigh¹⁴ (1897) developed a low frequency method which can be applied to bodies that are small compared to a wavelength, and he used it for spheres. If the dimensions of the body are small compared to a wavelength, the field is approximately uniform across the body. Therefore, on an instantaneous basis, the field can be considered constant, allowing static field techniques to be used. Many analytic as well as numerical techniques are available for mapping the static fields. Kleinman¹⁵ reviewed the low frequency approximation techniques.

The resonance region is the frequency range where the dimensions of the scatterer are of the order of a wavelength. Neither the high frequency nor low frequency approximations are adequate in the resonance region. Maxwells

equations or equations derived from them must be solved for the fields.

There have been several attempts to extend the Rayleigh approximation into the lower part of the resonance region. Stevenson¹⁶ derived the first three terms of a series solution. The Rayleigh approximation corresponds to the first of the series terms, Stevenson¹⁷ applied his method to a dielectric ellipsoid. However, Greenberg et al¹⁸ obtained disappointing results with the Stevenson method when they compared it and the Rayleigh approximation to the exact results for the sphere. Kleinman¹⁹ reduced the problem of finding the first few series terms for perfectly conducting scatterers to a series of scalar potential problems each of which probably could be solved numerically. These series methods probably deserve more attention than they have received in recent years.

Perturbation and point matching methods have been developed as a means of extending the exact solution for a sphere to obtain approximate solutions for non-spherical bodies. Oguchi^{20,21} obtained an approximate solution for slightly non-spherical bodies by means of a first order perturbation on the shape of a sphere. Oguchi²², and Morrison and Cross²³ assumed a solution in the form of the spherical wave functions that are exact for the sphere, and then adjusted the coefficients such that the boundary conditions are satisfied at a series of points on the surface of the scatterer. Morrison and Cross also used a least square technique to improve the match at the boundary.

Integral equation methods, with numerical solutions, have proven to be among the most efficient techniques for use in the resonance region with non-spherical scatterers. Edwards and Van Bladel²⁴ (1965) derived an integral equation for the scalar potential on the surface of a dielectric body in a static field. Waterman²⁵ indicates that Mave derived an integral equation and an integro-differential equation, either of which can be used to determine the surface currents on a perfectly conducting scatterer. The integral equation is included in Val Bladel's¹² text. Waterman²⁵ derived an alternate but similar integral equation. Several papers that apply the integral equation method were reviewed by Richmond²⁶ and Waterman²⁷.

Andreason²⁸ determined the surface current and the scattered fields for a perfectly conducting body of revolution. He derived an integral equation, which he approximated with a matrix equation that was solved on a digital com-

puter. The dimensions of the matrix equation were reduced by expanding the incident field in cylindrical modes and solving for the fields on a mode by mode basis.

Rhodes²⁹ derived an integral equation for scattering from a dielectric body. However, in practice, solution of his equation by numerical methods is limited by the fact that it includes both an integral over the surface of the scatterer and an integral over the interior volume of the scatterer. Harrington³⁰ includes an integral equation which contains only a volume integral. This equation is very powerful in that it can be applied to dielectric bodies with complex dielectric constants, as well as non-homogeneous bodies. However, when the integral equation is approximated by a matrix equation, the accuracy is severely limited by the size of the matrices which can be handled on available computers. Several methods have been developed which use only surface integrals. However, these methods are limited to homogeneous bodies.

Surface integral equations were derived by use of the equivalence theorem, which states that sources inside a closed surface may be replaced with equivalent electric and magnetic current sheets on the surface.³¹ Outside the surface, the fields due to the equivalent current sheet $J_g = n \times H_g$ and the magnetic current sheet $M_g = -n \times E_g$ are equivalent to the fields due to the integral sources. Bradley³² used the equivalence theorem to derive integral equations for the internal fields inside the scatterer in terms of the tangential components of the scattered fields at the surface. For bodies of revolution, the incident fields were expanded into cylindrical modes and the fields were determined on a mode by mode basis. The surface was divided into subsections and the method of subsections with point matching was used to approximate the integral equations with matrix equations. The matrix equations were then solved for several bodies of revolution.

The approach used by Bradley is limited to lossless dielectric bodies because the induced currents in lossy dielectric would violate the assumption that the internal fields can be expressed in terms of the surface fields with no internal sources. Barber and Yeh³³ used a method originally proposed by Waterman³⁴ to remove the requirement that the dielectric constant be real. They used the equivalence the internal field in terms of spherical harmonics with point matching at the boundary. Their expansion of the internal fields

in spherical harmonics works best for bodies that are not too far from spherical. However, I recommend their method of solving for the scattered fields from homogeneous bodies of revolution with complex dielectric constant.

The unimoment method as developed by Mei³⁵ is an application of the finite element method. Mei restricted his equations to bodies of revolution where the elements are rings and the variation around each ring is known for any given mode. Even with this restriction, the number of elements is large resulting in large matrices. However, the matrices contain many zeros and the equations that must be solved for each element are relatively simple. A major advantage of this method is that in principle it can be applied to inhomogeneous bodies. Practical limitations may require that ϵ and μ be constant around each elemental ring, thus requiring that the body be rotationally symmetric with no variations in ϵ and μ about an axis of symmetry. Also, if the inhomogeneous material extends throughout the body, the number of elements will be very large because Mei's method of terminating the finite elements on a sphere and continuing the solution throughout the sphere may not be applicable.³⁶ However, the application of finite element and/or finite difference methods to electromagnetic fields problems appears to be a very productive area of research, especially with inhomogeneous or anisotropic media.

IV. BISTATIC CROSS SECTION: Most of the papers referred to in the previous section compute the backscatter cross section and/or the extinction cross section. However, there is current interest in calculating the effective cross sectional area for signals reflected in directions other than directly back toward the transmitting antenna. Computation of these "bistatic" cross sections presents no theoretical difficulties. In most of the computational methods discussed in the previous section, the tangential components of the scattered electromagnetic fields are computed as an intermediate step in the backscatter computations. With the tangential components of the electric and magnetic fields on the scatterer surface known, a straight forward application of the equivalence theorem yields the E and H fields in any desired direction. Bradley³² explains the details of this computation in the backscatter direction, and a similar procedure can be used to compute the bistatic cross section in any desired direction. This will require an integration over the surface of the scatterer. The

receiving antenna normally will be in the far field of the scattered radiation, hence only the $1/R$ terms must be included in the integral equation. If the computer programs that were used to compute backscatter area are still available, it may be possible to modify them to compute bistatic cross sections. Only a modest amount of programming and some additional computer time would be required to compute a series of bistatic cross sections. Probably many of the published computations of backscatter area should be extended to include bistatic cross sectional area for a range of bistatic angles.

VI. COMPOSITES: There are two primary areas of interest involving scattering from composites. First, large amounts of composite materials are being used in aircraft and other radar targets. For example, Aviation Week and Space Technology, in the concluding article in a feature on advanced materials, predicts all composite fighters,³⁷ Thus, it is important to know the scattering properties of the various composite materials that are being used as structural components. Second, it may be possible to control the scattering properties of objects by the design of the composite materials from which they are constructed.

Composites consist of one or more distinct materials. For example, one definition is: "Composites consist of one or more discontinuous phases embedded in a continuous phase. The discontinuous phase is usually harder and stronger than the continuous phase and is called the reinforcement or reinforcing material, whereas the continuous phase is called the matrix."³⁸

Materials that fit this definition have been around since ancient times. For example the ancients used straw as reinforcement in their bricks, and the Eskimos used moss to strengthen ice. However, the advanced composites that are used in aircraft and space applications have been developed more recently. As explained in references 38 and 39, most materials have measured strengths two or more orders of magnitude less than theoretical. Various defects cause the discrepancy between theoretical and measured strengths. Whiskers are single crystals that are almost completely free of defects. Whiskers of graphite, Al_2O_3 , SiC etc are used for reinforcing plastics. However, due to the short length of the whiskers, they are not as good reinforcing material as fibers. Fibers of materials such as glass, kevlar, boron and carbon can be made relatively free of defects and are commonly used as reinforcing materials. Among these, the

carbon fibers (due to the high strength of the covalent carbon bond, and good high temperature performance) appear to be preferred for advanced composites.

Matrix materials include plastics, metals, and ceramics. Metal matrix materials have some interesting properties, but are of little interest in the scattering field because usually a radar will see only the conducting metal matrix. Ceramic matrix materials are used primarily for high temperature applications.⁴⁰ Several polymers have been used as matrix materials. Among these, epoxy matrixes are most commonly used with carbon fibers, at temperatures below about 250°C.

Hybrid composites containing two or more different types of fibers are sometimes used to improve the performance or reduce the cost relative to a composite containing a single type of fiber. For example, carbon fiber composites are very strong but brittle. Glass and Kevlar composites are not as strong, but much less brittle. It has been found that introduction of glass and/or Kevlar fibers into carbon composites significantly increases the impact strength without reducing the maximum strength.⁴¹

VI. SCATTERING FROM CARBON COMPOSITES: Since increasing amounts of carbon composites are being used in aircraft and other radar targets, the scattering properties of carbon composites are important. A search of the open literature did not locate any articles on scattering from carbon composites. A large number of books and articles have been published which deal primarily with the mechanical properties of composites. One handbook on the Electronic Properties of Composite Materials,⁴² which was sponsored by the U.S. Defense Supply Agency contains some relevant information. However, it does not consider scattering and the electrical information on carbon composites is somewhat limited without much background explanation. One problem is the considerable variation in electrical properties of various carbon fibers. For example resistivities ranging from $.83 \times 10^{-3}$ to 7×10^{-3} ohm-cm are given for various carbon fibers. The electrical properties of the composite material depends upon the orientation of the fibers and the percentage of fibers in the composite, as well as the conductivity of the fibers themselves. The fiber orientation may be unidirectional, bidirectional, or random. Also, the fibers may be oriented for maximum strength of complex parts.

The simplest possible model for composite material is unidirectional conducting fibers imbedded in a dielectric matrix with the fibers separated from each other by dielectric. When this composite is in an electric field, the author would expect it to behave much like a perfect conductor when the electric field is polarized parallel to the conducting fibers and much like a dielectric when the electric field is polarized perpendicular to the fibers. Composite material with bidirectional conducting fibers should behave much like a conductor regardless of the polarization. The author suggests that these theories be tested by constructing circular disks of unidirectional and bidirectional composite sheets. The disks could be placed in the scattering chamber and the backscatter area measured as the disk is rotated from parallel to perpendicular polarization. Dodge¹⁰ computed the backscatter area of circular metallic disks and his results could be compared with the measured results for the composite disks.

An analytical model also could be developed for scattering from unidirectional composite. I suggest starting with geometric optics and Rayleigh approximations and proceeding to the more difficult resonance region if preliminary results indicate that the effort is justified.

VII. DESIGN OF SPECIAL COMPOSITES: A considerable amount of effort has gone into the design of composites to optimize various mechanical properties. However, apparently little effort has gone into the design of composites with desired scattering parameters. Allen and McCormick⁴³ constructed a dielectric material that closely matched the dielectric constant of ice. They increased the dielectric constant of a plastic matrix by adding titanium dioxide powder.

One simple procedure would be to create conducting paths in glass or kevlar composites by replacing the non-conducting fibers in certain areas with conducting fibers such as baron or carbon. These conducting paths could be used as antennas, or to change the radar signature of the composite objects.

Weston⁴⁴ and Wagner and Lynch⁴⁵ have shown that a body of revolution constructed of material with $\mu_r = \epsilon_r$ will have identically zero backscatter area when viewed from the nose-on direction. It now appears possible to design a composite material with $\mu_r = \epsilon_r$ for some range of frequencies. If this can be done, spherical satellites would be invisible to radars whose oper-

ating frequency is in the range where $\mu_r = \epsilon_r$. One limitation is the fact that the dielectric constant is a function of both frequency and temperature. Specifically, the author believes such a composite could be constructed by starting with a polymer matrix such as epoxy and adding a powder with a high dielectric constant such as titanium dioxide and another powder with high permeability. For example, 2-81 moly permalloy powder has $\mu_r = 125$ and carbonyl iron powder has $\mu_r = 60^{45}$, and titanium dioxide has ϵ_r in the range of 85 to 170 depending upon the orientation of the crystals⁴⁶. The resulting composite could be used as a layer on the surface of a sphere. Aden⁴⁷ includes equations that could be used to compute the scattered fields from two concentric spheres.

VIII. RECOMMENDATIONS: Several recommendations have been included in the body of the report. Some specific recommendations are:

1. Compute bistatic cross sections for some of the dielectric bodies whose backscatter area has previously been computed. One possible starting point is to take the numerical method used by Barber and Yeh³³, and extend it to compute bistatic cross sections.
2. Construct circular disks with unidirectional carbon fiber composite and bidirectional carbon fiber composite. Measure the backscatter area of the disk as the disk is rotated. Compare the results with Dodge's¹⁰ computed results for circular metallic disks. Start with disks that are large compared to a wavelength, and then use disks of the order of a wavelength and small compared to a wavelength.
3. Develop an analytical model for scattering from simple shapes constructed of unidirectional carbon composite. Start with high and low frequency approximations and proceed to the resonance region if preliminary results indicate that the effort is justified.
4. Experiment with the design of various composite materials. A composite with $\mu_r = \epsilon_r$ appears to be possible for some range of frequency.

ACKNOWLEDGEMENTS

The author would like to thank the Air Force Systems Command, the Air Force Office of Scientific Research, and the Southeastern Center for Electrical Engineering Education for providing him with the opportunity to spend a very worthwhile and interesting summer at the Rome Air Development Center, Hanscom AFB, MA. In particular, he would like to thank the Electromagnetic Sciences Division for the opportunity to work in an area that is closely related to his Ph.D thesis, and hopes to continue work in this area.

He would especially like to thank Dr. Ronald Newburgh for his collaboration and guidance. Also, he would like to acknowledge several very interesting discussions and assistance from Philipp Blacksmith.

REFERENCES

1. Logan, N.A., "Survey of Some Early Studies of the Scattering of Plane Waves by Spheres," Proc. IEEE, Vol. 53, August 1965, pp. 773-785.
2. Clebsch, A., "Ueber die Reflexion an Einer Kugelflache," J. fur Math., Vol. 61, 1863, pp. 195-262.
3. Mie, G., "Beitrage Zur Optic Truber Median, Speziell Kolloidar Metallosungen," Ann. d. Physik, Vol. 25, 1908, pp. 377-442.
4. Stratton, J.A., Electromagnetic Theory, New York, McGraw Hill, 1941.
5. Aden, A.L., "Electromagnetic Scattering from Spheres with Sizes Comparable to the Wavelength," J. of Applied Physics, Vol. 22, May 1951, pp. 117-132.
6. Atlas, D., Battan, L.J., Harper, W.G., Herman, M.M., Kerker, M. and Matijeuc, "Back-scatter by Dielectric Spheres (Refractive Index 1.6)," IEEE Trans. Ant. and Prop., January 1963, pp. 68-72.
7. King, R.W.P. and Harrison, C.W., "Scattering by Imperfectly Conducting Spheres," IEEE Trans. Ant. and Prop., Vol, AP-19, March 1971, pp. 197-207.
8. Siegel, K.M., Schultz, F.V., Gere, B.H., and Sleater, F.B., "The Theoretical and Numerical Determination of the Radar Cross Section of a Prolate Spheroid," IEEE Trans Ant. and Prop., Vol AP-4, July 1956, pp. 266-275.
9. Ritter, E.K., "Solution of Problems in Electromagnetic Wave Theory on a High Speed Digital Calculating Machine," IEEE Trans. on Ant. and Prop., Vol AP-4, July 1956, pp. 266-276.
10. Dodge, D.B., "Scattering by Circular Metallic Disks," IEEE Trans. on Ant. and Prop., Vol AP-28, Sepebmer 1980, pp. 707-712.
11. Asano, S., and Yamamoto, G., "Light Scattering by a Spheroidal Particle," Appl. Opt., Vol 14, 1975, pp. 29-49.
12. Van Bladel, J., Electromagnetic Fields, McGraw Hill, New York, 1963.
13. Kouyoumjian, R.G., "Asymptotic High-Frequency Methods," Proceedings IEEE, Vol. 53, August 1965, pp. 864-876.
14. Rayleigh, Lord, Phil. Mag., Vol. 44, p. 28.
15. Kleinman, R.E., "The Rayleigh Region," Proceedings IEEE, Vol. 53, August 1965, pp. 848-856.
16. Stevenson, A.F., "Solution of Electromagnetic Scattering Problems as Power Series in the Ratio (Dimension of Scatterer)/Wavelength," Journal of Appl. Physics, Vol. 24, September 1953, pp. 1134-1142.

17. Stevenson, A.F., "Electromagnetic Scattering by an Ellipsoid in the Third Approximation," J. of Appl. Physics, Vol. 24, September 1953, pp. 1143-1151.
18. Greenbern, J.M., Libelo, L., Lind, A., and Wang, R.T., "Scattering by Non-spherical Particles Whose Size is of the Order of the Wavelength," Electromagnetic Theory and Antennas, Edited by E.C. Jordans, MacMillan, New York, 1963, pp. 81-92.
19. Kleinman, R.E., "Low Frequency Solution of Electromagnetic Scattering Problems," Electromagnetic Wave Theory, ed. J. Brown, Pergamon Press, 1967, pp. 891-905.
20. Oguchi, T., "Attenuation of Electromagnetic Wave due to Rain with Distorted Raindrops," J. of the Radio Research Lab., (Tokyo), Vol. 7, September 1960, pp. 467-485.
21. Oguchi, T., "Attenuation of Electromagnetic Wave due to Rain with Distorted Raindrops (Part II)," J. of the Radio Research Lab. (Tokyo), Vol. II, January 1964, pp. 19-44.
22. Oguchi, T., "Attenuation and Phase Rotation of Radio Waves Due to Rain: Calculations at 19.3 and 34.8 GHz," Radio Science, Vol. 8, January 1973, pp. 31-38.
23. Morrison, J.A. and Cross, M.J., "Scattering of a Plane Electromagnetic Wave by Axisymmetric Raindrops," Bell System Technical Journal, Vol. 53, January 1974, pp. 955-1019.
24. Edwards, T.W., and Van Bladels, J., "Electrostatic Dipole Moment of a Dielectric Cube," Applied Science Research, Se et. B, Vol. 9, pp. 151-155.
25. Waterman, P.C., "Matrix Formulation of Electromagnetic Scattering," Proceedings IEEE, Vol. 53, August 1965, pp. 805-812.
26. Richmond, J.H., "Digital Computer Solutions of the Rigorous Equations for Scattering Problems," Proceedings IEEE, Vol. 53, August 1965, pp. 796-804.
27. Waterman, P.C., "Symmetry, Unitarity, and Geometry in Electromagnetic Scattering," Physical Review D, Vol. 3, February 15, 1971, pp. 825-839.
28. Andreason, M.G., "Scattering from Bodies of Revolution," IEEE Trans. on Ant. and Prop., Vol. AP-13, March 1965, pp. 303-310.
29. Rhodes, D.R., On the Theory of Scattering by Dielectric Bodies, Engineering Report 475-1, Ohio State University Research Foundation, Columbus 10, Ohio, July 1953.
30. Harrington, R.F., Field Computation by Moment Methods, MacMillan, New York, 1968, pp. 97-98.

31. Jordan, E.G. and Balmain, K.G., Electromagnetic Waves and Radiating Systems, Prentice Hall, Englewood Cliffs, N.J., 1968, pp. 485-488.
32. Bradley, W.G., Electromagnetic Scattering from Dielectric Bodies in the Resonance Region, Ph.D. Thesis University of Vermont, Burlington, Vermont, 1973.
33. Barber, P. and Yeh, C., "Scattering of Electromagnetic Waves by Arbitrarily Shaped Dielectric Bodies," Appl. Opt., Vol 14, December 1975, pp. 2864-2872.
34. Waterman, P.C., and McCarthy, C.V., "Numerical Solution of Electromagnetic Scattering Problems," Mitre Corporation, Bedford, MA, Report MTP-74 (N69-31912), June 1968.
35. Mei, K.K., "Unimoment Method of Solving Antenna and Scattering Problems," IEEE Trans. on Ant. and Prop., Vol. AP-22, November 1974, pp. 760-766.
36. Chang, S. and Mei, K.K., Electromagnetic Scattering by Targets Over a Real Earth, Final Report RADC Contract No. F19628-78-C-0090, EMtec, Berkley, CA 94701, 1981.
37. "All Composite Fighter Design Foreseen," Aviation Week and Space Technology, January 26, 1976, pp. 130-131.
38. Ararwal, B.D., and Broutman, L.J., Analysis and Performance of Fiber Composites, New York, Wiley, 1980, p. 2.
39. Tewary, V.K., Mechanics of Fiber Composites, New York, Wiley, 1978.
40. Davis, L.W. and Bradstreet, S.W., Metal and Ceramic Matrix Composites, Cahners Publishing Co., Boston, 1970.
41. Ref. 38, pp. 264-268.
42. Leeds, M.A., Electronic Properties of Composite Materials, IFI/Plenum, New York, 1972.
43. Allen, L.E., and McCormick, G.C., "Measurements of the Backscatter Matrix of Dielectric Spheroids," IEEE Trans Antennas and Propagation, Vol AP-26, pp. 579-587, July 1978.
44. Weston, V.H., "Theory of Absorbers in Scattering," IEEE Trans. Antennas and Propagation, Vol. AP-11, 1963, pp. 578-584.
45. McGraw Hill Encyclopedia of Science and Technology, Vol. 8, 1977.
46. Kraus, J.D., Antennas, McGraw Hill, New York, 1950.
47. Aden, A.L., and Kerker, M., "Scattering of Electromagnetic Waves from Two Concentric Spheres," J. of Applied Physics, Vol 22, October 1951, pp. 1242-1246.

1981 USAF - SCEE SUMMER FACULTY RESEARCH PROGRAM

Sponsored by the

AIR FORCE OFFICE OF SCIENTIFIC RESEARCH

Conducted by the

SOUTHEASTERN CENTER FOR ELECTRICAL ENGINEERING EDUCATION

FINAL REPORT

AN INVESTIGATION OF NONPARAMETRIC MAINTAINABILITY AND RELIABILITY

TEST PROCEDURES

Prepared by: Dr. Jerome D. Braverman

Academic Rank: Professor

Department and University: Department of Decision Sciences and Computers
Rider College

Research Location: Rome Air Development Center
Reliability and Compatibility Division
Engineering Branch

USAF Research Colleague: Mr. Jerome Klion

Date: August 14, 1981

Contract No: F49620-79-C-0038

AN INVESTIGATION OF NONPARAMETRIC MAINTAINABILITY AND
RELIABILITY TEST PROCEDURES

by

Jerome D. Braverman

ABSTRACT

A wide body of nonparametric statistical tests was investigated to determine which, if any, are applicable, either as described or with modifications, to the maintainability/reliability demonstration problem. The nonparametric tests having the greatest potential for this application belong to the category of one-sample tests of location. Of these, the sign test and the Wilcoxon signed rank test appear to be directly applicable to the maintainability demonstration problem as alternatives to the currently used parametric tests, particularly when sample sizes are small and/or parametric assumptions cannot be validated.

A group of tests called "normal scores tests" also appear to be applicable to the maintainability demonstration problem while the "exponential scores test" may be applicable to the reliability demonstration problem. These tests should be the subject of future research effort. It is also recommended that further research into the general area of order statistics, a class to which the previous tests belong, be continued.

ACKNOWLEDGEMENT

The author would like to thank the Rome Air Development Center and especially the personnel of the Engineering Branch of the Reliability and Compatibility Division for their hospitality and support. Special thanks are due to Mr. Jerome Klion for his suggestions regarding the area of research and for his support and assistance.

In addition, the author would like to acknowledge the sponsorship of the Air Force Systems Command, the Air Force Office of Scientific Research, and the Southeastern Center for Electrical Engineering Education who made this research effort possible.

AN INVESTIGATION OF NONPARAMETRIC MAINTAINABILITY AND RELIABILITY
TEST PROCEDURES

I. INTRODUCTION

MIL-STDS 471A and 781B list currently used maintainability and reliability demonstration test procedures. With a few exceptions, the procedures used are the classical parametric statistical tests common in most types of testing situations. These tests impose requirements either on the type of population distribution involved, i.e., exponential, normal, log-normal, etc., or on known values of population parameters such as the variance, or on both. When large samples are possible, central limit theorems obviate exact adherence to the requirements of the parametric tests but nevertheless do not entirely eliminate problems associated with a lack of conformance to these requirements. And since these central limit theorems apply only to large samples, problems arise when samples of sufficient size may simply not be available or possible.

According to Bradley (2), central limit theorems have usually dealt with linear functions of a large number of variates, and under various assumptions have proved convergence to normality as that number increases. For a large, but fixed number, the approximation of the distribution to normality is typically close within a restricted portion of its range, but bad in the tails. Yet it is the tails that are used in tests of significance, and the statistic used for a test is seldom a linear function of the observations. Furthermore, these theorems apply strictly only to $n \rightarrow \infty$. When in application we take n to mean large, even very large, the fit between the true distribution of \bar{X} , for example, and the approached normal distribution tends to worsen rapidly at a given n , at increasingly remote tail regions. Unfortunately, this qualification is rarely mentioned in the statistical literature where extravagant claims about the rapidity of approach to the normal distribution are commonplace. It does not follow logically that approximate normality and homogeneity insure approximate validity of a test which assumes exact normality and exact homogeneity. It

has become apparent that under violation of assumptions, normal-theory statistics are in fact approximate tests. In a surprising number of cases the approximation is excellent, in many cases the approximation is fair to good, but that in some perfectly realistic cases it is so bad as to be unacceptable.

It would be advantageous to determine if alternate tests can be obtained from the large body of procedures called nonparametric or distribution free that require no, or at least fewer and/or weaker, assumptions about population distributions and parameters. These nonparametric methods use nominal and ordinal data, categorizations and ranks, instead of the interval and ratio scaled data used in most parametric tests.

Classical statistics typically use the mean and variance as measures of location and dispersion. This is because it was mathematically convenient to do so rather than because the mean and variance are any truer measures of location and dispersion than many others. A good, though debateable case can be made for means and variances as indices of location and dispersion when the normality assumption holds; the argument loses much of its force, however, when that assumption fails. The medians interquartile ranges, etc., used in nonparametric statistics have certain unique advantages even under normality and may be far more appropriate when the sampled population is nonnormal.

The efficiency of nonparametric methods relative to classical tests has been investigated under common nonparametric conditions and the nonparametric tests have often proved superior to their parametric counterparts. Consequently, the preference for classical tests over nonparametric tests in situations where distribution and parameter assumptions cannot be demonstrated appears to be unjustified while reliance on central limit theorems may not lead to any better results.

The investigations of nonparametric alternatives to current maintainability and reliability tests could result in more accurate, i.e., smaller risks, tests in situations where sample sizes are small and distribution and parametric assumptions cannot be validated.

II. OBJECTIVES

The principal objective of this research originally was to determine which, if any, types of nonparametric methods are applicable to maintainability and reliability demonstration. A secondary objective was to analyze the applicable nonparametric methods and determine how they compare with the present classical tests with respect to power, risk, cost, and robustness. An additional objective which should be added to these is to determine and recommend the most promising course of future research into nonparametric methods for maintainability and reliability demonstration.

In order to accomplish these objectives it was necessary to perform the following tasks:

1. Survey the tests currently being used.
2. Search the nonparametric literature to determine which of the many types of nonparametric tests have potential for application to maintainability and reliability demonstration.
3. Select from the appropriate categories of test procedures those specific tests that appear to be most applicable to the problem.
4. Demonstrate the use of the selected nonparametric tests in the required application areas.
5. Develop comparative measures of effectiveness for these tests vis a vis present test methods.

Due to time constraints, tasks (2) through (5) could only be partially accomplished during this period and the objectives only partially achieved. However, recommendations for continuing this research and achieving its objectives have been formulated and appear in the appropriate section of this report.

III. SUMMARY OF CURRENT MAINTAINABILITY/RELIABILITY DEMONSTRATION TESTS

The appropriate MIL-STDs list eleven test methods for maintainability demonstration and a series of sequential and fixed sample test plans for reliability demonstration. The reliability tests fall into two classes, sequential and fixed sample plans, and within each class the tests are similar and differ primarily with respect to the risk levels and discrimination ratio. None of these reliability tests are nonparametric and all assume the underlying failure distribution to be exponential. In fact, Handbook H108 states, "It is important to note that the life test sampling plans of this chapter are not to be used indiscriminately simply because it is possible to obtain life test data. Only after the exponential assumption is deemed reasonable should the sampling plans of this chapter be used."*

The maintainability test methods are tests of means and/or percentiles. Two of these are based on a log-normal assumption for the underlying distribution and one of these requires a known prior estimated variance. Five test methods depend on the central limit theorem and large samples. Only two appear to be truly nonparametric. These are method #2 which utilizes a test (sign test) based on binomial probabilities and #8 utilizing a sequential test of proportions again based on binomial probabilities.

The most likely test situations which appear to lend themselves to the use of nonparametric methods are test methods 1, 2, 4, 5, and 7 where the demonstration of maintainability requirements is limited to a single parameter. With regard to reliability, it would appear that this area is wide open for the application of nonparametric methods.

*H108 Sampling Procedures and Tables for Life and Reliability Testing, Office of the Assistant Secretary of Defense (Supply and Logistics), Washington, D.C., 21 April 1961.

IV NONPARAMETRIC STATISTICAL METHODS

In 1962 a bibliography of nonparametric methods listed about 3000 different procedures.* Twelve years later, in 1974, E. L. Lehman (11) estimated that that number had approximately doubled. A detailed survey and review of such a large body of procedures would obviously be very time consuming, though possibly worthwhile, and would obviously delay any practical application of pertinent techniques to the problems at hand for an unacceptable period of time. Fortunately, nonparametric methods can be categorized into general types of tests and only those categories investigated which appear to contain procedures of the type that are applicable to the maintainability/reliability demonstration problem. This is the procedure that was adopted during this research effort and although applicable techniques may possibly have been overlooked in eliminating whole categories of procedures without detailed investigation, this appears to be the most practical way of achieving results within the shortest time period.

Although classification schemes differ, a simple categorization of non-parametric tests that is useful in the context of this research is as follows:

- (1) Tests for randomness
- (2) Tests for independence or correlation
- (3) Tests for goodness-of-fit
- (4) Tests for comparing two treatments or populations - two sample tests
- (5) Tests for comparing multiple treatments or populations - multiple sample tests
- (6) One sample tests of location.

It is the tests that fall within category (6) which appear to have the greatest potential for application to the maintainability/reliability demonstration problem and it is this group of tests that have been the subject of this research.

*Savage, I.R., Bibliography of Nonparametric Statistics, Cambridge MA, Harvard University Press, 1962.

I. R. Savage places the true beginning of nonparametric statistics in 1936 although tests of this type date back to the year 1710. However, it is from 1936 that nonparametric statistics began to take the form of a separate discipline. In this new discipline no attempt is made to identify or specify the exact form of the sampled population. Emphasis is placed instead on the characteristics of the observed sample.

Nonparametric statistics generally do not utilize the actual magnitudes of the sample observations. Instead, they use frequencies or order relationships such as ranks. Although it may appear that the information that is inherent in the value of the magnitude of an observation is wasted when nonparametric techniques are used, actually the utilization of this additional sample information is only made possible by the population information embodied in the parametric tests' assumptions. Therefore the nonparametric test is wasting information only if the assumptions necessary for the parametric test are known to be true.

This leads to a consideration of the relative efficiency of nonparametric tests with respect to their parametric counterparts. The general conception is that nonparametric tests are less efficient and less powerful than parametric tests. However, studies of test effectiveness which led to this conclusion were apparently conducted under conditions meeting all of the assumptions of the latter type of test. Under those ideal conditions the parametric test was always found to be more efficient than the nonparametric. Frequently, however, the difference in efficiency was quite small. However, as mentioned above, when comparisons are made under less than ideal conditions, that is when the parametric assumptions are not valid, the nonparametric tests are usually equal or superior in efficiency.

The sample size is also an important factor in determining the relative merits of nonparametric and classical tests. When only small samples are available nonparametric tests are easier to use and only slightly less efficient even if all of the requirements of the parametric test have been met. When samples are large, some nonparametric tests will still compare favorably with their parametric counterparts. In many cases, however,

their efficiency relative to the parametric test may drop appreciably. On the other hand, violations of the parametric assumptions can be compensated for at large sample sizes due to the effect of the central limit theorem. Consequently, when samples can be large, although either type of test may be superior, circumstances become more favorable to the parametric test. Nevertheless, since population distributions and parameters are generally not shown in maintainability/reliability demonstration situations it would seem that a body of nonparametric tests should provide a viable alternative to classical tests.

V. APPLICABLE NONPARAMETRIC TESTS

A. Sign Test

The sign test is one of the simplest nonparametric tests based on the binominal distribution and uses nominally scaled data. It can be used to test three essentially different hypotheses. These are:

(1) If Z_1, \dots, Z_n are independently distributed according to a common continuous distribution L , it can be used to test that L is symmetric about zero or any given point.

(2) If it is known only whether each Z_i is positive or negative and if we let $p = P(Z_i > 0)$ it can test the hypothesis that $p = 1/2$ against the alternatives $p \neq 1/2$, $p < 1/2$, or $p > 1/2$.

(3) In case 1 the sign test can test the broader hypothesis that the median of L has a specified value.

Referring to category (3), suppose we wish to test the hypothesis that the median M of a continuously distributed population has the value M_0 . The outcome of randomly drawing a single observation X from the population can be dichotomized into $X > M_0$ and $X < M_0$, or $X - M_0$ is positive and $X - M_0$ is

negative. If the null hypothesis is true then M_0 divides the population in half and if $p = P(X > M_0)$, $p = 1/2$. Drawing an observation from the population is a single Bernoulli trial and the number r of the X 's which fall into a given category is a binomially distributed variate with $p = .5$.

That is,

$$P(r \leq c) = \sum_{r=0}^c \binom{n}{r} p^r (1-p)^{n-r} \quad (1)$$

The hypothesis that $M = M_0$ can be tested by counting the number of $X - M_0$ differences being of one algebraic sign and using either equation (1) or the tables of the cumulative binomial distribution. The counting of signs is the same as counting the number of values of $X > M_0$ or $X < M_0$.

The test is also applicable to hypotheses about any other percentile such as $X_{.75} = X_0$. In this case if $p = P(X > X_0)$, $p = .25$.

Test method #3 from MIL-STD-471A called a Test on Critical Maintenance Time or Manhours applies the rationale of the Sign Test. This test is of the hypothesis

$$\begin{aligned} H_0: T &= X_{p_0} \\ H_1: T &= X_{p_1} \end{aligned}$$

The values n and c , sample size and acceptance number, are obtained using either the normal or Poisson approximation to the binomial distribution. A decision rule of the form accept H_0 if $r \leq c$ otherwise reject is formulated where r represents the number of observation with a value greater than T .

B. A Nonparametric Sequential Test for Test Method #3

The fixed sample nonparametric test procedure used in Test Method #3 of MIL-STD-471A could be converted to a sequential probability ratio test

which will on the average result in a reduction in the sample size necessary to reach a decision. The hypothesis, as stated in the standard

$$\begin{aligned} H_0: T &= X_{p_0} \\ H_1: T &= X_{p_1} \end{aligned}$$

is equivalent to the following hypothesis:

$$\begin{aligned} H_0: p &= p_0 \\ H_1: p &= p_1 \end{aligned}$$

and a standard sequential test of a proportion is applicable.

Such a test is designed so that sample observations are made one at a time and a decision to accept, reject, or sample one more unit is made after each observation. The test can be designed so that an accept or reject decision cannot be made before some minimum number of items is sampled.

The decision criteria are as follows:

- if $p_1/p_0 \leq \beta/1-\alpha$, accept H_0 ;
- if $p_1/p_0 \geq 1-\beta/\alpha$, reject H_0 ;
- if $\beta/1-\alpha < p_1/p_0 < 1-\beta/\alpha$, continue sampling.

For the example given in the standard, the fixed sample test plan requires a sample of $n = 23$. Under a sequential test plan with the same α and β , the average sample number at $p = p_0$ is about 13 and at $p = p_1$ is about 14. The ASN reaches a maximum for some value of p between p_0 and p_1 . For the example this maximum ASN is approximately 18. The formulas for the accept/reject criteria and ASN can be found in Dixon & Massey (5).

C. Signed Rank Test

One of the simplest nonparametric methods which can be applied to tests of location (means, medians) is the Wilcoxon signed rank test. This test was originally designed as a two sample test for identical populations and was applied to the difference scores $X_1 - Y_1$ obtained from the sample. However, there is no need for the variate to be a difference score in order to

use this test. It can be applied to n observations of X_i to test whether or not every X_i was drawn from a population that is symmetric about zero. Therefore, if M is the median of the X population, the variate $X-M=Z$ will be symmetric about zero. So if we hypothesize that M_0 is the median of the X population, subtract M_0 from each X_i and apply the signed rank test to the n values of $X_i - M_0$, we are testing the hypothesis that the median of the symmetric X population has the value M_0 . The signed rank test should be applicable as a substitute for test methods 1, 4, 5, and 7 from MIL-STD-471A.

The assumption necessary for this test is that X_i , is a continuous random variable with a symmetric distribution. Conover (3) defines symmetry as follows:

The distribution of a random variable X is symmetric about a line $X=c$ for some constant c if the probability of $X \leq c-x$ equals the probability of $X \geq c+x$ for each possible value of x .

Even though the exact distribution of a random variable may not be known, it may be reasonable to assume that its distribution is symmetric. Such an assumption is not as restrictive as the assumption of normality since while all normal distributions are symmetric not all symmetric distributions are normal.

There are in fact a large number of symmetric, non-normal distributions which include:

1. The Continuous Uniform Distribution
2. The Cauchy Distribution
3. The Logistic Distribution
4. The Double Exponential Distribution
5. The LaPlace Distribution
6. Student's t Distribution

If a distribution is symmetric then the mean coincides with the median and any inferences concerning the median are also valid statements about the mean.

The consequences of using the signed rank test under minor violations of the assumption of symmetry are not known and would warrant investigation.

Let Z_1, \dots, Z_n be a random sample from a continuous distribution that is symmetric about zero. Actually, the point of symmetry could be any known value. If X is symmetrically distributed about θ_0 , $Z = X - \theta_0$ is symmetrically distributed about 0. Let $\omega_i = \omega(Z_i)$

where $\omega_i = 1$ if $Z_i > 0$ and $\omega_i = 0$ if $Z_i \leq 0$.

For the random variables Z_1, \dots, Z_n , arranged in ascending order of magnitude, the absolute rank of Z_i , which specifies that it is the i th smallest observation in terms of its absolute value is denoted by R_i . The signed rank of Z_i is then $\omega_i R_i$. Consequently, the signed rank of a positive observation is simply its absolute rank while the signed rank of a nonpositive observation is zero.

Let X_1, \dots, X_n be a random sample from a continuous distribution that is symmetric about an unknown median, θ . Consider testing

$$H_0: \theta = \theta_0$$

against any one of three alternatives,

$$H_1: \theta \neq \theta_0$$

$$H_1: \theta > \theta_0$$

$$H_1: \theta < \theta_0$$

Let $Z_i = X_i - \theta_0$, $i = 1, \dots, n$ and let ${}_i R_1, \dots, {}_n R_n$ be the signed ranks of Z_1, \dots, Z_n respectively. Using the alternative hypothesis $\theta > \theta_0$ as an example, it is necessary to determine an appropriate rejection region for the test. The rejection region for this alternative should correspond

to many positively signed ranks. The statistic proposed by Wilcoxon is

$$W = \sum_{i=1}^n \omega_i R_i \quad (2)$$

where W is the sum of the signed ranks. Large values of W lead to rejection of the null hypothesis in favor of the alternative hypothesis $\theta > \theta_0$. The critical point at a significance level of α is equal to the 100 α th percentile of the null distribution of W for a sample of size n . This distribution has been tabled for various values of n .

For $n > 15$ the normal approximation can be used for the distribution of W . $P(W \leq k)$ is approximately the area under the unit normal curve below $[(k + 1/2) - \mu] / \sigma$ where

$$\mu = \frac{n(n+1)}{4} \quad (3)$$

$$\sigma = \sqrt{\frac{n(n+1)(2n+1)}{24}} \quad (4)$$

When zeros occur among the observations, that is $X_{-0} = 0$, the usual practice is to discard them and proceed with the number of nonzero observations as n .

If there are ties among the absolute values, the tied ranks are replaced by their average (mean) rank. When using the normal approximation, in the event of ties, the standard deviation of W should be computed from

$$\sigma = \sqrt{\frac{3n(n+1)^2 + n^3 - D}{48}} \quad (5)$$

where D is the sum of the cubes of the total number of scores within each tie among the absolute values. Equation 5 is provided by Kraft and VanEeden (11).

The most common index of efficiency for nonparametric tests is the asymptotic relative efficiency, abbreviated A.R.E. The A.R.E. of the

Wilcoxon signed rank test is .955 relative to the one-sample t test for an hypothesized population mean and an A.R.E. of 1.50 relative to the sign test for the median according to Bradley (2). This is in the case of a normally distributed population, a requirement necessary for the t test. Under these conditions, as the sample size diminishes from infinity toward zero the efficiency of the signed rank test relative to the t test increased from .955 and approaches 1.00. If the population is symmetric and continuous, conditions required for the signed rank test, but its exact shape is unspecified, the A.R.E. of the signed rank test relative to the t test cannot drop below .864, therefore .864 is the lower bound for the A.R.E. over the class of continuous symmetric populations.*

Lehmann (12) provides a sample size formula for the Wilcoxon signed rank test for a given α and β .

$$n \approx \frac{\pi \sigma^2 (Z_\alpha + Z_\beta)}{3 \Delta^2} \quad (6)$$

where $\Delta = M_1 - M_0$ and σ^2 must be estimated. Using this formula and data given in examples for Test Methods 1B and 5 from MIL-STD-471A, the comparable samples required are as follows:

To test:

$$\begin{array}{ll} H_0: \mu = 30 & \alpha = \beta = 0.05 \\ H_1: \mu = 45 & \sigma^2 = 900 \end{array}$$

Test Method 1B, n = 43

Signed Rank Test, n = 46

To test:

$$\begin{array}{ll} H_0: M = 2.0 & \alpha = \beta = 0.10 \\ H_1: M > 2.0 & \Delta = M - M_0 = 0.30 \end{array}$$

Test Method 5, n = 73

Signed Rank Test, n = 30

*Hodges, J. L. and E. L. Lehmann, "The Efficiency of Some Nonparametric Competitors of the t Test," Annals of Mathematical Statistics, Vol 27, pp 324-335, 1956.

D. Normal Scores Tests

There exists a body of tests which can be grouped under the general category of normal scores tests. These tests involve transforming ranks of observations to values obtained from the standard normal distribution. All of these normal scores tests are similar in principle and all require a transformation that cannot be made without reference to tables. In fact, the use of the normal scores tests requires two transformations. First, a transformation from observed values to ranks, then a transformation from the ranks to a normal score. These tests compete extremely well in terms of efficiency with other comparable tests both parametric and nonparametric. However, the extra statistical efficiency is bought by sacrificing the simplicity that is inherent in other nonparametric tests such as the signed rank test. Nevertheless this group of tests warrants investigation as alternatives to the present maintainability demonstration tests.

There are three basic categories of tests of this type. These are:

- (1) The random normal scores transformation
- (2) The expected normal scores transformation
- (3) The inverse normal scores transformation

(1) The Random Normal Scores Transformation

According to Walsh (17) many different kinds of values can be used to represent the ranks of a set of univariate observations. The principal requirement is that the ranks have the same ordering, with respect to algebraic value, as the corresponding observations. That is, the smallest of the set of rank values is the rank of the smallest observation, etc. In

particular, the values used for a set of ranks could be obtained as a random sample from some completely specified univariate populations. Rank values obtained in this way are called random ranks.

The use of random ranks to obtain significance tests, rather than ranks with fixed values has both advantages and disadvantages. For many situations where the use of random ranks is appropriate, the null hypothesis implies that replacement of each observation by its rank results in the ranks being a random sample from the population which yielded their values. That is, the properties of the experiment, in combination with the random method used to obtain the set of ranks, are such that this situation occurs. In particular, if the observations are ordered in some manner that does not depend on their values, so that the corresponding ordering is obtained for the ranks of these observations, this ordering has no conditional effect on the joint distribution of the ranks. This random sample property of the ranks allows an approximate null distribution for a test statistic to be determined without much difficulty when the number of observations is not too small.

The principle behind this test is to use order statistics from normally distributed random samples instead of ranks. That is, instead of using the rank i where the ranks range from 1 to n , use the i th smallest observation from n random normal deviates. The arithmetic of the test is performed on the order statistics in the same way that it would be performed on the ranks in the rank tests or on the original observations in the parametric tests.

The test is accomplished by entering a table of random values for the standard normal variate, randomly selecting n values from the table then for every value of X , the original observations, replacing the i th smallest by the i th smallest of the n random values of the standard normal variate. This transformation completely meets the normality requirements of the t and F tests provided that the null hypothesis is true. In such cases, the classical, parametric tests can be used in the usual way.

The random normal scores tests has the disadvantage that the test statistic depends not only on the ranks of the observations but also on the particular set of normal deviates selected. This introduces additional variation into the data. There has apparently been no study of the amount of variation that different sets of random normal deviates introduce into the test statistic. A further disadvantage of this test is that additional effort is required to determine the values assigned to the ranked observations.

From the standpoint of efficiency, according to Conover (3) the A.R.E. of this test is 1 when compared with the usual parametric tests in situations where the parametric test is appropriate. If the normality assumptions underlying the parametric test are not satisfied, then the A.R.E. of this test is greater than 1. The A.R.E. of this test relative to the signed rank test discussed previously is approximately the same when the underlying distribution is close to normal. For non-normal distributions the normal scores test is superior.

(2) The Expected Normal Scores Transformation

Fisher and Yates* suggested that when original observations were in the form of ranks, the ranks might be replaced by appropriate expected normal scores and the resulting data could then be analyzed by performing conventional parametric tests such as the t test. The appropriate expected normal score for an observation that received a rank from 1 to n, say i, is the expected value of the observation having a rank of i in a random sample of n observations from a normal distribution with zero means and unit variance.

Extensive tables of expected normal scores are provided by Harter (7).

*Fisher, R.A., and F. Yates, Statistical Tables for Biological, Agricultural and Medical Research, 3rd Edition, New York, NY, Hafner Publishing Company, 1949

The test statistic is:

$$S = \sum_{i=1}^n E_{NR_i} \quad (7)$$

where E_{NR_i} represents the expected normal score of the observation with rank i .

S approaches a normal distribution for large values of n with a mean of zero and a variance of approximately

$$\frac{(n/2)^2}{n(n-1)} \sum_{i=1}^n (E_{NR_i})^2 \quad (8)$$

(3) The Inverse Normal Scores Transformation

Consider a random sample of n observations drawn from a continuous but otherwise unspecified population of Z 's. Let Z_i be the i th smallest observation in the sample. Then the expected proportion of the population that lies below Z_i is $i/(n+1)$. This is also the expected proportion of a standard normal distribution that lies below the i th smallest of n observations randomly drawn from it. The inverse normal scores transformation is accomplished by entering a table of lower-tail cumulative probabilities of the standard normal distribution, finding the value of the variate whose cumulative probability is $i/(n+1)$, and substituting that value for Z_i . Thus one replaces the i th smallest of n sample observations with the population quantile of which it would be an estimate if the sampled population were standard normal. The advantage of the inverse normal scores transformation over the expected normal scores transformation is that it requires only the tables of the standard normal distribution which are generally more extensive and more easily available than tables of expected normal scores.

The test statistic is

$$V = \sum_{i=1}^n \Phi^{-1}\left(\frac{i}{n+1}\right) \quad (9)$$

where $\Phi^{-1}(z)$ denotes that number x for which $\Phi(x) = z$. No tables of V have been located. However it is known that V approaches a normal distribution for large n with a mean of zero and a variance of approximately

$$\frac{(n/2)^2}{n(n-1)} \sum_{i=1}^n \left[\Phi^{-1}\left(\frac{i}{n+1}\right) \right]^2 \quad (10)$$

The normal scores tests apparently have an A.R.E. of one or greater relative to the parametric t test, the exact value depending upon the underlying population.

The direct applicability of these tests to the maintainability/reliability demonstration problem has not yet been determined. It appears that because of their high efficiencies and their immunity to the normality assumptions required by the comparable parametric tests, these tests would provide powerful alternatives to the present tests. Further study of these tests and their applicability is certainly warranted.

E. Exponential Scores Test

The applicability of the exponential scores test to the one sample reliability demonstration test has not yet been determined. The procedure is related to the normal scores tests of the previous section but the values substituted for the ranks are expected exponential scores obviating the requirement for an underlying exponential distribution. Some modification to the test as described in Lehmann (12) and Hajek (6) may result in an applicable nonparametric test for reliability. The test was designed for the hypothesis:

$$\begin{aligned} H_0: \theta_0 &= \theta_1 \\ H_1: \theta_0 &< \theta_1 \end{aligned}$$

when two independent random samples are tested for time to failure. The classical test for these hypotheses rejects H_0 when

$$\frac{\sum y_j}{\sum x_i} \geq c$$

To make the test less sensitive to the assumption of underlying exponential distributions for X and Y the observations are replaced by their ranks

which are in turn replaced by expected exponential scores, $E[Z_i]$. That is, the i th smallest observation is given rank R_i and R_i receives a score $E[Z_i]$ which is the expected value of the i th smallest observation drawn from an exponential distribution with $\theta = 1$.

The expected exponential scores are equal to

$$Z_i = \frac{1}{n} + \frac{1}{n-1} + \dots + \frac{1}{n-i+1}$$

Tables for $n \leq 120$ are provided by Harter (7).

The test is then performed using the expected exponential scores instead of the original observations.

An adaptation of this test to single sample situations designed to demonstrate that $\theta = \theta_0$ versus an appropriate alternative seems to be feasible and would provide a nonparametric alternative to the tests described in MIL-STD-781B.

V Order Statistics

Several of the tests described in the previous section belong to a general category of order statistics tests. That is, the actual values of observations are replaced by scores assigned on the basis of the order or rank of the observation. This class of tests based on order statistics appears to have a significant potential for providing nonparametric alternatives to classical maintainability and reliability test procedures.

If X_1, \dots, X_n are n observations with cdf F , then if $X_{(1)} \dots X_{(n)}$ denotes these observations arranged in ascending order of magnitude, $X_{(1)}, \dots, X_{(n)}$ are the order statistics and $X_{(i)}$ is called the i th order statistic.

$X_{(i)}$ has a probability density given by

$$n \binom{n-1}{i-1} F(x)^{i-1} [1-F(x)]^{n-i} f(x) \quad (11)$$

Let Y_i equal the probability to the left of the i th order statistic. The probability density function of Y is

$$n \binom{n-1}{i-1} \gamma^{i-1} (1-\gamma)^{n-i} \quad (12)$$

which is the probability density of the beta distribution with parameters i and $n-i+1$.

When i and n grow large so that $0 < i/(n+1) < 1$, Y_i is approximately normally distributed with

$$E(Y_i) = \frac{i}{n+1} \quad (13)$$

$$\text{Var}(Y_i) = \frac{i(n-i+1)}{(n+1)^2(n+2)} \quad (14)$$

Order statistics have been used to find tolerance intervals, confidence intervals on medians and other percentiles, and to test hypotheses about medians and other percentiles. Further investigation of the practical application of order statistics could lead to additional procedures that might prove superior in power and efficiency to the nonparametric tests described in Section IV of this report.

VI RECOMMENDATIONS

Certain of the following recommendations apply to the present tests listed in MIL-STD-471A. The others are for continuation of the research effort in those areas that appear to be particularly promising. With respect to present maintainability and reliability demonstration tests:

(1) A nonparametric sequential probability ratio test is suggested in Section IV as an alternative to test method #3 in MIL-STD-471A. The

sequential test should reduce the amount of sampling required to reach an accept/reject decision. Such a test can be established to require some minimum amount of sampling before an accept/reject decision can be made.

(2) The Wilcoxon Signed Rank Test described in Section IV.C. should be adopted as a nonparametric alternative to maintainability demonstration tests where the parameter to be tested is a mean or median. This test should compete extremely well with the classical tests particularly when sample sizes are small.

Recommendations for continuing study center on the general area of order statistics and particularly on that group of tests called Normal and Exponential Scores Tests. These types of tests should be studied to determine their applicability to reliability (for the exponential) and maintainability (for the normal) testing.

For those specific tests, determined to be applicable, including the signed rank test recommended previously, additional effort should be made to determine their relative efficiency with respect to the competing parametric tests at various levels of sampling.

Finally, and with lower priority, a more extensive survey of the non-parametric area should be conducted to determine if any other category or categories of the tests have applicability to the maintainability/reliability test problem.

REFERENCES

1. Bell, C. B., and K. A. Doksum, "Some New Distribution-Free Statistics," Annals of Mathematical Statistics, Vol 36, pp 203-214, 1965.
2. Bradley, James V., Distribution-Free Statistical Tests, Englewood Cliffs, NJ, Prentice-Hall, Inc., 1968.
3. Conover, W. J., Practical Nonparametric Statistics, New York, NY, John Wiley & Sons, Inc., 1971.
4. Davies, Robert B., "Rank Tests for Lehmann's Alternative," Journal of the American Statistical Association, Vol 66, pp 879-882, 1971.
5. Dixon, W. J. and F. J. Massey, Introduction to Statistical Analysis, New York, NY, McGraw-Hill Book Company, Inc., 1957.
6. Hajek, J., Nonparametric Statistics, San Francisco, CA, Holden-Day, Inc., 1969.
7. Harter, H. Leon, Order Statistics and Their Use in Testing and Estimation Volumes 1 and 2, Wright-Patterson Air Force Base, Ohio, Aerospace Research Laboratories, U.S. Air Force, 1969.
8. Hollander, Myles and D. A. Wolfe, Nonparametric Statistical Methods, New York, NY, John Wiley & Sons, Inc., 1973.
9. Klotz, J., "Small Sample Power and Efficiency for the One Sample Wilcoxon and Normal Scores Tests," Annals of Mathematical Statistics, Vol 34, pp 624-628, 1963.
10. Klotz, J., "Alternative Efficiencies for Signed Rank Tests," Annals of Mathematical Statistics, Vol 36, pp 1759-1766, 1965.
11. Kraft, C. H., and C. VanEeden, A Nonparametric Introduction to Statistics, New York, NY, The MacMillan Company, 1968.

12. Lehmann, E. L., Nonparametrics: Statistical Methods Based on Ranks, San Francisco, CA, Holden-Day, Inc., 1975.
13. Lloyd, D. K. and Myron Lipow, Reliability, Management, Methods and Mathematics, Englewood Cliffs, NJ, Prentice-Hall, Inc., 1962.
14. Mosteller, Frederick and R.E.K. Rourke, Sturdy Statistics, Reading, MA, Addison-Wesley Publishing Company, 1973.
15. Puri, M. L. and P. K. Sen, Nonparametric Methods in Multivariate Analysis, New York, NY, John Wiley & Sons, Inc., 1971.
16. Randles, Ronald H. and Douglas A. Wolfe, Introduction to the Theory of Nonparametric Statistics, New York, NY, John Wiley & Son, Inc., 1979.
17. Walsh, John E., Handbook of Nonparametric Statistics, Princeton, NJ, D. VanNostrand Company, Inc., 1962.

1981 USAF - SCEE SUMMER FACULTY RESEARCH PROGRAM

Sponsored by the

AIR FORCE OFFICE OF SCIENTIFIC RESEARCH

Conducted by the

SOUTHEASTERN CENTER FOR ELECTRICAL ENGINEERING EDUCATION

FINAL REPORT

ENVIRONMENTAL EFFECTS ON AFFECT AND PSYCHOMOTOR PERFORMANCE

Prepared by: L. W. Buckalew

Academic Rank: Assistant Professor

Department and University: Department of Psychology
Alabama A & M University

Research Location: Air Force Aerospace Medical Research
Laboratory, Human Engineering Division,
Workload and Ergonomics Branch

USAF Research Colleague: LT Anthony Rizzuto and CPT George Wolf

Date: July 28, 1981

Contract No: F49620-79-C-0038

ENVIRONMENTAL EFFECTS ON AFFECT AND PSYCHOMOTOR PERFORMANCE

by

L. W. Buckalew

ABSTRACT

Scientific and public information sources have suggested or alluded to beneficial effects to humans of exposure to negative air ions. Claims include improved performance, reduced anxiety and depression, increased attention level, and enhanced physiological condition. While some evidence does support some of these claims, the clarity, validity, and reliability of findings are clouded by methodological problems of control and a lack of standardization in treatment and equipment, with particular problems in too narrow a spectrum of response considerations. This study investigated the effects of negative air ions, as produced by commercially available air purification/negative ion generation instrumentation, on a wide range of affective, cognitive, psychomotor, and physiological measures. Dependent variables included anxiety, grip magnitude, digit symbol coding, motor dexterity, reaction time, tracking, pulse, blood pressure, and temperature. Two groups of 12 subjects, similar in age, sex, education, and physical condition, were subjected to either 6 continuous hours of negative ion exposure or 'normal' ion exposure. Repeated measures (0,3,6 hours) on each of 10 variables were obtained for each subject. MANOVA comparisons of each group's change scores (0 vs 3, 0 vs 6, 3 vs 6 hour) revealed no significant differences between groups, and consideration of group differences on individual variables for both 0 vs 3 hour and 0 vs 6 hour change reflected no significance for any variable. It was concluded that the air ion condition resulting from treatment with air purifiers/negative ion generators did not produce any generalized effect or alteration of specific affective, performance, or physiological measures.

AD-A113 708

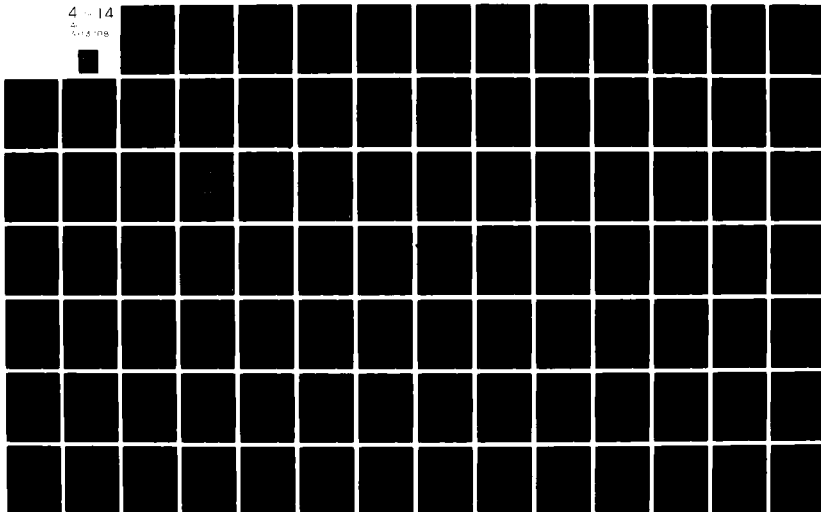
SOUTHEASTERN CENTER FOR ELECTRICAL ENGINEERING EDUCAT--ETC F/6 5/1
USAF SUMMER FACULTY RESEARCH PROGRAM. 1981 RESEARCH REPORTS, VO--ETC(U)
OCT 81 W D PEELE F49620-79-C-0038

UNCLASSIFIED

AFOSR-TR-82-0227

NL

4 - 14
4
4



ACKNOWLEDGMENTS

This Research Associate wishes to extend grateful appreciation to the Air Force Systems Command, Air Force Office of Scientific Research, the Air Force Aerospace Medical Research Laboratory, and the Southeastern Center for Electrical Engineering Education for providing an opportunity to engage in a worthwhile summer research experience. This experience has appreciably contributed to the personal and professional development of this researcher, and it is sincerely hoped that the Air Force finds this research effort as one which meaningfully serves their interests and supports the Air Force mission.

Any research effort typically entails the cooperation and support of many individuals. This summer effort, without qualification, could not have been conducted and completed without the generous contribution of time and effort from the personnel of AMRL/HEG and Systems Research Laboratories support personnel. In particular, special recognition is due Mr. Charles Clauser, Research Physical Anthropologist, and Ms. Julie Klug, On-site SRL Project Manager, for their voluntary and tireless efforts, both administrative and physical. The physical efforts of LT Anthony Rizzuto were indispensable to the efficacious conduct of this research, and his contribution is greatly appreciated. Also, Mr. Robert Love and Mr. David Grooms of SRL were instrumental in providing technical and physical support essential for research conduct. In essence, this research effort constituted a laboratory team effort of military, civilian, and contractor personnel which was in the highest tradition of professional cooperation.

I. INTRODUCTION:

The public media and scientific literature have given increasing attention to the possible physiological and psychological benefits of exposure to charged air ions. Historically, air ion research was formalized by experimentation in Russian laboratories in 1933, and Germany experimented with the use of negative ion generators in submarines during World War II. Present popularization of air ion interest is largely due to the publicity and claims made or implied by manufacturers of air cleaning devices which rely on the production of negative air ions for efficacy. Such claims beyond the purification of air, fueled by public interests, have included mood elevation, improved cognitive functioning, increased attentional posture, reduced healing time and bacteria level, and improved capacity for work endurance and efficiency.^{1,2,3} Federal agencies, such as the FDA and FTC, suggest a cautious approach to accepting such claims, and have warned manufacturers of negative ion generators to exercise restraint in implying or suggesting any supplemental benefits in excess of air purification until such claims can be scientifically documented and replicated. Relative to Air Force interests, if claims of improved cognitive, affective, physiological, and performance capabilities were shown to be empirically based, the scientific utilization of this source of negative air ions might support and enhance the mission of the Air Force and its personnel.

Air ions have been considered biologically active,⁴ with the suggestion that concentrated research of their effects might prove both practical and relevant to psychology.^{5,6,7,8} Comprehensive reviews and discussion of air ion effects are offered by several authors,^{4,6,9} and the literature suggests particular interest in the effects of negative air ions on learning.^{5,10,11,12} However, the relevance and validity of air ion activity or effect on many behaviors has been questioned.^{6,13} Little scientific evidence^{8,13} is available which

is specifically dedicated to determining the effects of charged air ions on a range of basic human abilities and response modes. Of particular interest to present considerations of air ions are early studies conducted by the Air Force^{14,15} which suggested that ionized air, both positive and negative, had no effect on specific measures of attitude, vigilance, or complex (cognitive) tasks which involved learning.

Given the appreciable amount of air ion research, much of which incorporates inconsistencies in findings suggesting a lack of replicability or reliability in effects, it is not presently justified to draw definitive conclusions as to the effects of air ions on human affect and performance. In particular, a recent review⁴ cited an uneven quality of reported research, with specific reference to faulty experimental design permitting the impact of environmental elements other than air ions on results attributed to ions. Particular concern was voiced for the use of corona discharge ion generators which produce ozone and nitrogen oxides, temperature, and humidity. Even recent, well controlled studies⁸, while suggesting that the ion content of air may exert an influence on human behavior, admit that much more work needs to be done on the industrial application of findings and the mechanism by which air ions exert their effects. What appears needed is a study of solid experimental design which incorporates appropriate controls and uses a representative range of relevant affective, cognitive, psychomotor, and physiological measures. Ideally, and responsive to public interests and stated or implied manufacturer claims, such a study should deliberately use readily available and commercially produced air ion generation devices.

II. OBJECTIVES:

An appreciable amount of negative ion research data is simply observational and/or inferred. Of existing empirical evidence, some data are methodologically confounded. Further,

few studies offer scientifically sound investigation of more than a few variables, inclusive of previous Air Force research efforts.^{14,15} Also, accepting the possible effect of ionized air on specific indices of human performance, questions remain as to relationships between effects and longevity of exposure and the amount of negative ions necessary for any effect. Lastly, it would be desirable to investigate specific effects of negative ion exposure on affective and performance indices which are specifically relevant to Air Force interests and which serve as substrate behaviors related to the overall work-related efficiency of personnel.

It was the purpose of this study to determine the effects, if any, of exposure, over time, to negatively ionized air on a representative sample of affective, cognitive, performance, and physiological measures. Inherent within this purpose was the assurance of appropriate methodological controls so as to support the elimination of learning, fatigue, psychological, and environmental variables as potential alternative explanations for findings. This study was, by design, restricted to consideration of commercially available ion generators which typify air purification units commonly marketed.

This study sought to be responsive to the presence or absence of a negative ion effect, to include the potential relationship between any such effect and length of exposure time. Methodological controls were instituted to protect against the contaminating influence of mental or physical fatigue, learning phenomena, individual differences, placebo effects, and other environmental variables. To facilitate the least restrictive opportunity for any ion effects, and respecting the relevance and nature of variables selected for study,^{8, 16,17} a wide range of dependent variables was used, inclusive of anxiety level, digit-symbol coding, body temperature, blood pressure, pulse, grip magnitude, small parts dexterity, reaction time, and tracking. The study sought to determine any negative ion effect collectively or individually on these

measures using subjects as their own controls as well as a separate control group, and was designed to be responsive to cumulative exposure effects.

While no specific hypotheses were stated, reflecting a nonjudgmental stance on the possibilities of negative ion effects and the exploratory nature of this study, data analysis was conducted under a statistical format which provided maximum opportunity for realization of any effect, i.e. statistical testing for individual variable response regardless of whether any collective effect was manifested.

III. SUBJECTS:

Volunteer subjects were recruited through the media of AFAMRL Information Letter, ASD Bulletin, and SRL Insider. Also, bulletin board announcements soliciting volunteers were placed in various building locations of Wright State University. Recruitment efforts resulted in obtaining 24 volunteers who met the requirements of male, between 20 and 30 years of age, good physical condition, and non-smoker. Subjects were informed of the general nature of the experiment and of the 7 hour confinement necessitated in their service. Subjects volunteered for one of two different days of service. The mean age of subjects was 22.8, with no significant difference in age between groups. For each of the two groups, 11 subjects were paid civilians and 1 subject was military. All subjects signed informed consent forms, though information was not provided as to under which experimental condition they would serve. They were simply informed that they may be serving in a negative, positive, or uncharged environment condition.

IV. APPARATUS AND MATERIALS:

With the exception of the negative ion generators, all equipment used was either available or produced by AMRL/HEG or was loaned by Alabama A & M University. Two negative ion generators (Air Care II) were obtained from DEV Industries of

Boulder, Colorado. Based on manufacturer literature and specifications, each negative ion generator had an area of maximum effectiveness extending in a radius of 8 feet, facilitating an area of maximum coverage of approximately 200 square feet. The test chamber encompassed approximately 400 square feet of area. The generators produced only insignificant amounts of ozone due to a multiple brush electrode system, as opposed to the contaminating amount of ozone potentially produced by corona discharge systems. These generators, which had detachable test lights for validating ion output, were placed at table top height, approximately 12 feet apart and in the center area of the controlled environment test chamber.

The wide range and nature of dependent variables used in this study necessitated appreciable instrumentation and materials. The Taylor Manifest Anxiety Scale (TMAS) was used to measure and record differences in anxiety level. The digit-symbol coding task from the Weschler Adult Intelligence Scale served as a measure of cognitive/perceptual motor performance. A hand dynamometer¹⁸ was used to measure grip magnitude. The Crawford Small Parts Dexterity Test (Psychological Corporation), simple visual reaction time apparatus (Lafayette Instruments) with a chronometer calibrated in 100ths of a second (Lafayette Instruments) and a programmed tracking apparatus with an 11 inch diagonal video screen (Keyser Video) served as measures of perceptual motor performance. A standard sphygmomanometer, stethoscope, and thermometers were used, respectively, to measure systolic and diastolic blood pressure, pulse rate, and temperature.

The test environment chamber was located in Building 33, Wright-Patterson AFB, and was a vault of approximately 400 square feet lined with plasterboard walls. The chamber had no windows and was electronically monitored for temperature by a self-contained system which activated or deactivated based on a preset temperature level. The facility contained padded wood chairs for all subjects and two large conference tables.

Cards, magazines, newspapers, and a variety of games were provided subjects for their entertainment between testing sessions of the 7 hour confinement. Additionally, subjects were allowed to bring work or reading material with them, and were informed to bring any food or nonalcoholic beverages they desired, as the experimental confinement included a dinner hour.

V. METHOD AND PROCEDURE:

As all subjects met the criteria specified for participation, the two groups could be considered matched on variables of education, sex, age, physical condition, and smoking habit. The physiological measures of temperature, blood pressure, and pulse rate confirmed good physical health claims. Also, while subjects could volunteer for a specific day (Thursday, July 2 or Saturday, July 11), some were shifted from one day (group) to the other to insure equality of group size. Hence, a degree of randomness was present. All subjects reported for service at 1 PM and served until 8 PM, and all civilian subjects (11 per group) were paid \$35 for their service. Military persons (1 per group) were unpaid but provided letters of appreciation sent to their superiors. While subjects were told the possible general effects of negative and positive ions, they were also told that the study had three conditions (negative, positive, or neutral) of exposure and that the condition under which they would serve was unknown. At Appendix A is the consent form addendum which explained possible conditions and effects which might be anticipated. None of the research personnel were aware of the condition operating for either group (negative or neutral). Hence, the study was conducted under a double blind condition, and only after data analysis had begun was it made known as to what condition was operable for a given group.

On the assigned day and time, subjects entered the test chamber and were allowed to leave only to use nearby bathroom

facilities. Prior to arrival of subjects or experimenters, a non-involved individual instituted the appropriate experimental condition. Ion generators were set up two hours in advance of subject arrival, with indicators of operation masked, to include visual access to the wall electrical socket. The ion generators used had no moving parts and made no noise or vibration during operation.

After signing consent forms, subjects were assigned code numbers under which all data was collected to insure anonymity. With the exception of the anxiety and coding measures, subjects were tested individually and were not allowed any information about their performance until all data from both groups had been collected. The same order of subject testing was maintained during all three testing sessions (0, 3, 6 hours), and the sequence of tasks was standardized both within and between groups. This sequence was: grip magnitude, motor dexterity, reaction time, tracking, anxiety, coding, temperature, pulse, and blood pressure. During the time subjects were not being tested, they were allowed to socialize with other subjects, participate in the games provided, read the materials provided, or otherwise use their free time. The total testing time for each subject was approximately 45 minutes.

For each task, subjects were read printed instructions and given an opportunity to ask questions. At Appendix B are the specific instructions given for each task which serve to operationally define that task. In summary, grip magnitude was presented as a single trial concerted effort to evidence maximum strength. The motor dexterity task required that as many pegs as possible be placed in holes using tweezers. Subjects were allowed 30 seconds of time for this effort, though not informed of this time restraint. Reaction time presented a white light stimulus to be responded to as quickly as possible, with a randomized 1 to 5 second foreperiod warning for each of 10 announced trials, and only trials 3 through 8 were used to calculate a mean RT to eliminate warm-up and end spurt

effects.¹⁹ For the tracking task, subjects were ask to hold a horizontally moving dot on a stationary dot or to minimize deviation from this dot. An announced tracking time of 45 seconds was allowed, and the number of times the moving dot was allowed to leave the screen was recorded as control losses. For both the reaction time and tracking tasks, on the first test session (0 hour), subjects were allowed 1 practice trial. For the anxiety measure, subjects were given the TMAS and allowed to complete it on an untimed basis as a group, though they were cautioned not to discuss any item or response with any other subject. The group-administered coding task was a 90 second timed effort. All physiological measures were individually obtained using a conventional procedure, as appropriate, for each measure.

All subjects of each group were tested beginning immediately after admission to the environmental chamber. This data baseline constituted the 0 hour measures. Repeated measures (test sessions) were obtained with the third and sixth hour of service. Due to the physical arrangement of data collection stations, it was possible to test two subjects at the same time though on different tasks. The last subject tested in any of the three test sessions had, at most, approximately one hour more of exposure time than did the first subject tested. However, as the same subject order was used for all test sessions, this exposure effect was standardized. While learning, fatigue, boredom, general environment, and confinement were free to influence any subject/task, both groups (negative and control) had systematically similar treatments and opportunities. This experimental situation made it possible to compare directly groups for any measure, as the only difference between groups was that of air ion condition. Further, this design allowed the direct comparison of changes within groups over time, collectively or for specific variables. Hence, the repeated measures, matched/randomized groups experimental design allowed consideration of within (time) and between

(ion condition) group comparisons, statistical equalizing of groups to compensate for any preexisting differences, and statistical considerations of groups in terms of change scores.

VI. RESULTS:

Each subject of each group was measured 3 times on each of 10 variables. For each group, performance means were computed on each variable for each of the testing sessions. The resulting descriptive statistics for the control and negative ion groups are presented in Tables 1 and 2.

For each testing session, the two groups were compared in terms of the amount of change, i.e. 0 vs 3 hours, 0 vs 6 hours, and 3 vs 6 hours, collectively over all 10 variables. This comparative data is presented in Table 3. To accomplish this comparison, which collectively considers dependent variables, the BMD 12V computer program for MANOVA was applied to the data. This program automatically accounts for relationships (covariances) between variables and yields an approximate F statistic for the amount of change within groups compared to the amount of change differences between groups. The resulting comparison for differential amount of change from hour 0 to hour 3 was $F = .336$, $df = 10,13$, and $p > .05$. For the similar comparison of change from hour 0 to hour 6, $F = 1.483$, $df = 10,13$, and $p > .05$. For the comparison considering change differences from hour 3 to hour 6, $F = .769$, $df = 10,13$, and $p > .05$. These nonsignificant MANOVA findings indicate no differences between groups, corrected for covariation of variables, regardless of length of exposure when considering all variables collectively. There was no general effect of negative ion exposure.

Given these findings, and assuming that longer exposure times would be most likely to facilitate any effect of negative ion exposure, groups were compared in terms of performance change from hour 0 to hour 6 on individual variables. Table 4 reflects this comparison. It may be seen that there were no

significant differences between groups on any of the 10 variables individually considered. While significant changes within groups were found for variables of anxiety, coding, motor dexterity, pulse rate, and temperature, no differences between groups in the amount of change was found for any of the 10 variables. Similar statistical consideration of the hour 0 vs hour 3 data indicated significant changes within groups on anxiety, coding, pulse rate, and temperature measures, but no significant differences between groups in the amount of change for any of the 10 variables. Regardless of length of exposure, there was no differential effect of negative ions on any variable.

TABLE 1

Group Means on Measured Variables for the Control Condition

Variable	0 Hour	3 Hour	6 Hour
Anxiety	14.5	13.0	13.3
Coding	60.1	67.2	70.9
Reaction Time	.205	.213	.208
Tracking	23.8	23.1	26.8
Grip Magnitude	603.3	592.5	555.0
Motor Dexterity	6.6	6.8	7.9
Pulse Rate	64.8	61.0	61.3
Temperature	98.7	97.8	97.7
Systolic Pressure	118	114	119
Diastolic Pressure	72	73	69

TABLE 2

Group Means on Measured Variables for the Negative Condition

Variable	0 Hour	3 Hour	6 Hour
Anxiety	11.1	9.8	9.0
Coding	55.1	61.3	62.7
Reaction Time	.222	.216	.222
Tracking	21.3	22.9	20.6
Grip Magnitude	600.8	609.2	605.8
Motor Dexterity	7.3	8.4	8.8
Pulse Rate	61.3	56.3	54.7
Temperature	97.9	97.4	97.2
Systolic Pressure	112	108	114
Diastolic Pressure	63	62	67

TABLE 3

Mean Change on Variables for Control and Negative Conditions

Variable	Group	Hour 0 vs 3	Hour 0 vs 6	Hour 3 vs 6
Anxiety	C	-1.50	-1.25	.25
	N	-1.25	-2.08	-.83
Coding	C	7.08	10.83	3.75
	N	6.25	7.58	2.17
Reaction Time	C	-.007	-.002	.005
	N	.006	.000	-.006
Tracking	C	-.75	2.92	5.83
	N	1.58	-.75	-2.33
Grip Magnitude	C	-10.8	-48.3	-37.5
	N	8.3	5.0	-3.3
Motor Dexterity	C	.25	1.33	1.08
	N	1.08	1.50	.42
Pulse Rate	C	-3.83	-3.50	.33
	N	-5.00	-6.67	-1.67
Temperature	C	-.95	-.98	-.03
	N	-.47	-.62	-.15
Systolic Pressure	C	-3.4	1.2	4.6
	N	-4.3	1.8	6.2
Diastolic Pressure	C	.8	-3.2	-4.0
	N	-1.5	3.6	5.1

TABLE 4
 Analysis of Negative Ion Exposure Effects
 on Individual Variables

Variables	Mean Change (0vs6)		Mean Squares		ANACOVA
	Control	Negative	Within	Between	F
Anxiety	-1.250	-2.083	5.871	4.167	.710
Coding	10.833	7.583	31.845	63.375	1.990
Reaction Time	-.002	-.000	.001	.000	.030
Tracking	2.917	-.750	329.961	80.664	.245
Grip Magnitude	-48.333	5.000	5721.19	17066.63	2.983
Motor Dexterity	1.333	1.500	5.076	.167	.033
Pulse Rate	-3.500	-6.667	67.076	60.167	.897
Temperature	-.983	-.617	.942	.807	.857
Systolic Pressure	1.167	1.833	219.242	2.664	.012
Diastolic Pressure	-3.167	3.583	109.117	273.375	2.505

VII. DISCUSSION AND CONCLUSIONS:

Results indicated no generalized effect, collectively considering the 10 variables measured, of the negative ion exposure condition when using a 'normal' environment control condition as a standard of comparison. This finding was evidenced in the 0 vs 3 hour, 0 vs 6 hour, and 3 vs 6 hour between group comparisons. When ANACOVA was applied to test for negative ion effects on individual variables for both the 0 vs 3 hour and 0 vs 6 hour situations, no single variable was shown to differentially respond to the negative ion treatment. It must be noted that the application of ANACOVA to this data of change scores automatically adjusted for potential contamination of data by any covariate, such as learning, fatigue, boredom, confinement, or other environmental influence. Indeed, the only variables even remotely suggesting any differential influence were diastolic blood pressure and grip magnitude.

Previous evidence⁸ from a well controlled study indicated a highly significant increase in performance in a negative ion exposed group for mirror drawing, rotary pursuit, and reaction time tasks. However, a significant interaction between group and time of day was also found, suggesting that this effect was related to time of day. There was no attempt reported to standardize testing times and task sequences, and there is the possibility that these tasks were influenced by a covariate. Further, a corona discharge ionizer was used which has been criticized⁴ due to the ozone and nitrogen oxides it produces which may act as influences on performance. Other studies^{14,15} which sought to determine ion effects under carefully controlled conditions reported no differences between control and negative ion groups on a complex mental task and several indices of vigilance.

Results of the present study are in agreement with some earlier findings^{14,15} and contradiction to others.⁸ This situation is typical of the current status of air ion research on humans, with few if any clearcut answers. Pervasive problems of lack of standardized ion-generating equipment, different exposure lengths and ion concentrations, lack of directly comparable measures, and potentially inadequate monitoring of ion levels continue to exist and detract from the comparability of different studies. Also, there are some differences between studies in what constituted a control condition, i.e. a balanced ion environment or a slightly positive environment which typifies modern energy-efficient buildings. Until such time as these methodological inconsistencies and problems are resolved, this research area is likely to remain confused.

Based on data from the present study, the conclusion of no generalized negative ion effect is warranted. Considering between group comparisons of individual variables following 6 hours of exposure (Table 4), no measure was found responsive to negative ion treatment, a finding also reflected in similar analysis of the 3 hour exposure data. As previously noted,

only the grip magnitude and diastolic blood pressure measures were even remotely responsive to negative ion treatment. It is of speculative note that, given the serotonin hypothesis of ion action⁴ which has been gaining support,^{5,6,8,20,21} these measures might be more likely affected than those of cognitive or psychomotor natures. However, were serotonin clearly active in this study, systolic blood pressure, pulse rate, and body temperature measures should have been at least equally influenced. Reference to Table 4 does not support this phenomenon.

Irrespective of effect substrates or mediation, present results clearly support the conclusion that exposure of up to six hours in a negative ion charged environment, using commercially available ion generators such as marketed for air purification in the manner prescribed by the manufacturer:

- 1) does not alter affect (anxiety),
- 2) does not alter low level cognitive functioning (coding),
- 3) does not alter basic psychomotor performance (motor dexterity, tracking),
- 4) does not alter vigilance/attention (reaction time),
- 5) does not alter the basic physiological condition of the organism (grip magnitude, pulse, temperature, blood pressure).

The findings and conclusions of this study must be weighed in terms of inherent reservations and limitations, mostly methodological, imposed on and by conduct of this research. It is important to respect that these limitations essentially only apply to the generalization of findings, and are not suggested as jeopardizing the validity of specific conclusions presented.

This study deliberately used negative ion generators which were commercially available and marketed as air cleaning devices. Hence, statements about negative ion effects must be limited to ion concentrations typical of these devices, used in the manner prescribed by the manufacturer. Further, while the negative ion production of these generators was validated,

no systematic attempt was made to periodically sample the ion content of the test chamber air during the study. Also, the test chamber did contain some exposed metal instrumentation, unrelated to the research, and a powerful battery used as part of a security system. These pieces of equipment may have altered the concentration of negative ions. Further, the ion condition of air in the test chamber was not checked or monitored for the control condition. This condition sought to replicate the 'normal' ion condition, thought to be slightly positive, of an energy-efficient enclosure. While no specific consideration was given individual differences in circadian rhythm, the hours of service were the same for all subjects and measures were obtained from both groups at the same times during service. Lastly, though of incidental nature, there was the possibility that two subjects in the control group learned of their group identity due to the box hiding the wall socket becoming loose from the wall late in the experiment. This situation was unknown to the experimenters and apparently to other subjects, as a non-involved monitor noted the condition and restored the damage. While subjective, and respecting the blind experimenter condition, it was felt that subjects who, it was later learned, served as the negative ion exposure group seemed more sociable and interactive than did control condition subjects.

VIII. RECOMMENDATIONS:

Results of this study lend no support to the suggestion that this level and length of negative ion exposure enhances emotional state, physiological condition, cognitive ability, or perceptual motor performance. Given stated reservations and limitations on findings, any decision to purchase or install similar ion generators in buildings for any reason other than air purification is not warranted. While evidence does exist suggesting the beneficial influence of negative ion exposure, it must be regarded in light of the confusion in consulting different authorities and sources precipitated by

methodological differences and the incomparability of efforts. Data of the present study clearly support a 'no effect' hypothesis of negative ion action, both collectively and for individual variables. Present data offer no support (note F values very close to unity in Table 4) for the biological or psychological action of conventional air ion generator treatment.

There remain several possibilities for future research considerations. As shown, measures of human condition and performance may not be responsive to the levels of negative ions produced by air cleaning types of ion generators. There remains the possibility of ion effects in higher concentration exposure conditions. However, any attempt to study the systematic increase of negative ion concentration must be cognizant of and responsive to possible side effects. This is particularly relevant when recognizing that the entire neural system of the body operates on an electrical substrate, and even the skin is differentially responsive to electrical conductivity.

The serotonin hypothesis of air ion action appears to have appreciable support, at least to the point that negative ion exposure can decrease brain serotonin levels. Serotonin has been shown to be related to affect, sleep, and physiological condition. It would seem potentially informative to determine the variability in brain serotonin concentration in response to systematic variations of negative ion concentrations in the environment. Additionally, and related, a well controlled study of negative ion effects on bacteria and healing time might prove valuable, as claims or suggestions of a decrease in both have been made or alluded to in the public media and scientific literature.

REFERENCES

1. "Negative Ions Enhance Environment," Rocky Mountain Journal, September 28, 1977.
2. Voisinet, R., "Ionization as a Socially Useful Technology in a Co-Evolving Man-Environment System," Journal of Environmental Sciences, Vol. 21, pp. 28-29, 1978.
3. Finley, L. S., "Get Ionized: Discovery of Happy-Making Generators Provides Proof that Negatives Attract," Washington Post, July 11, 1981.
4. Krueger, A. P., and E. J. Reed, "Biological Impact of Small Air Ions," Science, Vol. 193, pp. 1209-1213, 1976.
5. Lambert, J-F., and J-M. Olivereau, "Single-Trial Passive Avoidance Learning by Rats Treated with Ionized Air," Psychological Reports, Vol. 47, pp. 1323-1330, 1980.
6. Olivereau, J-M., "Atmospheric Ionization and its Effects on the Behavior of Animals and Man," Annee Psychologique, Vol. 76, pp. 213-244, 1976.
7. Rim, Y., "Psychological Test Performance of Different Personality Types on Sharav Days in Artificial Air-Ionization," International Journal of Biometeorology, Vol. 21, pp. 337-340, 1977.
8. Hawkins, L. H., and T. Barker, "Air Ions and Human Performance," Ergonomics, Vol. 21, pp. 273-278, 1978.
9. Krueger, A. P., "Preliminary Consideration of the Biological Significance of Air Ions," Scientia, Vol. 104, pp. 1-17, 1969.
10. Falkenberg, V., and R. E. Kirk, "Effects of Ionized Air on Early Acquisition of Sidman Avoidance Behavior by Rats," Psychological Reports, Vol. 41, pp. 1071-1074, 1977.
11. Gavalas-Medici, R., and S. R. Day-Masdaleno, "Extremely Low Frequency, Weak Electric Fields Affect Schedule-Controlled Behavior of Monkeys," Nature, Vol. 261, pp. 258-259, 1976.
12. Duffee, R. A., and R. H. Koontz, "Behavioral Effects of Ionized Air on Rats," Psychophysiology, Vol. 1, pp. 347-359, 1965.

13. Charry, J. M., "Meteorology and Behavior: The Effects of Positive Air Ions on Human Performance, Physiology, and Mood," Dissertation Abstracts International, Vol. 37, pp. 4751, 1977.
14. Chiles, W. D., and J. M. Cleveland, A Study of the Effects of Ionized Air on Behavior, WADD Technical Report 60-598, Wright Air Development Division, Wright-Patterson Air Force Base, Ohio, November 1960, pp. 1-17.
15. Chiles, W. D., Effects of Ionized Air on Decision Making and Vigilance Performance, MRL-TDR-62-51, Aerospace Medical Division, Wright-Patterson Air Force Base, Ohio, May 1962, pp. 1-9.
16. Lehmann, H. E., and D. A. Knight, "Placebo-Proneness and Placebo-Resistance of Different Psychological Functions," Psychiatric Quarterly, Vol. 34, pp. 505-516, 1960.
17. O'Donnell, R. D. Contributions of Psychophysiologic Techniques to Aircraft Design and Other Operational Problems, AGARDograph No. 244, North Atlantic Treaty Organization Advisory Group for Aerospace Research and Development, 1979.
18. Petrofsky, J. S., and A. R. Lind, "Aging, Isometric Strength and Endurance, and the Cardiovascular Responses to Static Effect," Journal of Applied Physiology, Vol. 38, pp. 91-95, 1975.
19. Buckalew, L. W., "An Analysis of Experimental Components in a Placebo Effect," Psychological Record, Vol. 22, pp. 113-119, 1972.
20. Frey, A. H., "Modification of the conditioned emotional response by treatment with small negative air ions," Journal of Comparative and Physiological Psychology, Vol. 63, pp. 121-125, 1967.
21. Gilbert, G. O., "Effects of negative air ions upon emotionality and brain serotonin level in isolated rats," International Journal of Biometeorology, Vol. 17, pp. 267-275, 1973.

APPENDIX A

Consent Form Addendum

You are invited to participate in a study entitled Environmental Effects on Affect and Psychomotor Performance. In this study, we intend to investigate the effects of negative, positive, and neutrally charged environments.

If you decide to participate, you will be asked to spend up to 6 hours in a room which will be charged either with negative ions, positive ions, or will have no charge at all. A negative ion environment is similar to that felt after a thunderstorm or near a waterfall. You may experience a feeling of well being, an elevated mood, improved cognitive functioning and attention, and increased work capacity and efficiency.

A positive ion environment is felt in centrally heated buildings in the wintertime. Here, one may experience reduced alertness, increased irritability and anxiety, and diminished work capability.

During the 7 hour period, you will be asked to undergo various tests and measurements, such as: a) tracking a target on a television screen, b) a measure of your reaction time, c) moving and placing pegs on a pegboard, d) answering a true and false test, e) solving a series of codes, f) measuring your maximum hand grip, g) blood pressure, h) temperature, i) pulse, and j) EMG.

You will be asked to bring your own food you expect to eat during the period. We hope to have various leisure activities such as card games, reading material, and the like to help occupy your time when actual measurements are not being taken. Since this will amount to about 6 hours, you may bring your own reading material or office work. You will be asked to participate for one day for up to 7 hours: 6 hours in the room plus

up to one hour preliminary and post exposure measurements. You will not be told which environment you will be exposed to until after completion of the entire study. Your confidentiality as a participant will be protected. Your name will not be revealed without your permission. Statistical data collected during this study may be published in scientific literature without identifying the subjects.

Your decision not to participate will not prejudice your future relations with the Air Force Aerospace Medical Research Laboratory. If you decide to participate, you are free to withdraw your consent and to discontinue participation at any time without prejudice. If you have any questions, we expect you to ask us. If you have any additional questions later, Louis Buckalew or Capt George Wolf (255-2558) will be happy to answer them.

You will be given a copy of this form to keep.

Date

Initials

APPENDIX B

Task Instructions

TMAS: You have been given a psychological instrument designed to find out how you feel. There are no right or wrong answers or trick questions on this test, and there is no time limit. As your responses will be confidential, please be open and honest in responding to each item.

In the upper left hand corner of your paper, please enter your assigned code number. In the upper right hand corner, please enter trial number . You are to respond to each item in terms of how true or false it is of you. Simply enter either a "T" or "F" on each blank provided, depending on whether the statement is true or false of you. Again, please be open and honest in responding. You may take as much time as you need.

CODING: This is a coding task designed to find how quickly and accurately you can work. Each of you should have a coding sheet and pen or pencil. Please enter your assigned code number in the space provided at the top left of this sheet. At the top right, please enter on the trial blank the number .

You will notice a series of boxes across the top of your sheet. Each box contains a number, 1 through 9, and the code symbols to be matched with each number. Your task is to enter in the small box below each number the correct code symbol for that number. This is a timed task which you will likely not finish, but you should work as quickly and rapidly as possible.

GRIP MAGNITUDE: This piece of equipment is a hand dynamometer. It measures the strength of your grip. You should grasp the two handles with your preferred hand, and get as comfortable a grip as possible. You may wish to remove any rings from this hand. After getting a good grip, squeeze the handles as hard as you can. Your arm may be placed however it is comfortable

for you. Go ahead and get a good grip. Squeeze as hard as you can, and release your grip when you have applied maximum pressure.

MOTOR DEXTERITY: In front of you is a test of perceptual motor dexterity or ability. This test is a measure of how rapidly you can place each of the pegs in the holes provided. However, you may not use your fingers to accomplish this task. You must use the tweezers to remove each peg from the upper right containment area and place it in a hole. You will be timed for your performance, so work as quickly and carefully as possible. If you should drop a peg, do not retrieve it. Simply get another from the containment area. Remember to work as carefully and quickly as you can.

REACTION TIME: This task measures the length of time it takes for you to respond to a visual stimulus. Your job is to press the large flat button marked "response" as soon as possible after the white light comes on. You should use a finger of your preferred hand, and you may rest it on the response button. I will let you know about when the light will come on by saying "ready." Then, within five seconds, the white light will come on. Only the white light will be used. The time it takes you to respond to this light is recorded, and this is your reaction time.

You will be given one practice trial to make sure you understand the task. (1st test session only)

Now, you will have 10 trials. Try to do your best.

TRACKING: There are two pieces of equipment in front of you. One is a small television screen which operates much like a video game. In the middle of the screen is a small, lighted stationary square called the target. There is another small,

lighted square moving horizontally across the screen. You will be able to control this moving square by manipulating, either to the left or right, the lever or "stick" in front of you. Your task is to try and keep the moving square on top of or as close to as possible the target square.

To get the feel of the "stick," you may have some practice time. (1st test session only)

You will now be allowed 45 seconds of tracking time. Do your best, and try to keep the moving square on target.

1981 USAF - SCEEE FACULTY RESEARCH PROGRAM

Sponsored by the

AIR FORCE OFFICE OF SCIENTIFIC RESEARCH

Conducted by the

SOUTHEASTERN CENTER FOR ELECTRICAL ENGINEERING EDUCATION

FINAL REPORT

THERMAL ANALYSIS

OF A

ROCKET ENGINE ALTITUDE TEST FACILITY DIFFUSER

Prepared by:	Gale H. Buzzard
Academic Rank:	Assistant Professor
Department and University:	Department of Mechanical Engineering and Materials Science Duke University
Research Location:	Air Force Rocket Propulsion Laboratory Propulsion Analysis Division Plume Technology Branch Edwards Air Force Base, CA 93523
USAF Research Colleagues:	Dr T. Dwayne McCay, Lt Martin Trout and Dr David Mann
Date:	24 August 1981
Contract No:	F49620-79-C-0038

THERMAL ANALYSIS
OF A
ROCKET ENGINE ALTITUDE TEST FACILITY DIFFUSER

by

Gale H. Buzzard

ABSTRACT

Simulated altitude testing of a rocket engine places a severe thermal load upon whatever device is used to contain the rocket engine exhaust plume and maintain the simulating low pressure. Analysis of the problem is considerably complicated for the complex two phase exhaust flow resulting from the combustion of high energy, metallized solid propellants. Such a propellant exhausts large quantities of very energetic solid particles. The thermal load imposed as these particles impinge upon the containment of the exhaust plume is capable of exceeding that of the convective load from the plume. One means of containing the exhaust plume under these conditions is a water cooled diffuser. Models for the heat loads on such a diffuser are discussed and recommendations are made for implementing a computational capable of predicting the maximum wall and coolant temperatures under test conditions.

Acknowledgement

The author would like to thank the Air Force Systems Command, the Air Force Office of Scientific Research, and the Southeastern Center for Electrical Engineering Education for providing him with the opportunity to spend an interesting and rewarding summer at the Air Force Rocket Propulsion Laboratory, Edwards Air Force Base, California. He would like to acknowledge the Laboratory and, in particular the Plume Technology Branch of the Propulsion Analysis Division, for having made him feel welcome and providing a very enjoyable and comfortable environment.

He would like to thank Dr T. Dwayne McCay, Lt Martin Trout and Dr David Mann for their collaboration and guidance in this effort.

I. INTRODUCTION

In the testing of a space motor under simulated altitude conditions, it is necessary to contain the motor within a low pressure facility and provide for the containment and removal of the exhaust plume. In the case of the Air Force Rocket Propulsion Laboratory's altitude test facility 1-42, the containment of the exhaust plume is accomplished by means of a water cooled diffuser which is evacuated by three large steam ejectors.

The thermal load on the diffuser can be quite large dependent upon the type engine and the duration of the burn. Faced with the need to test larger and more energetic motors, it became apparent to the Laboratory that there was a need for a quantitative engineering model that could be used in assessing the thermal load that a given test would place upon the diffuser of this facility.

Approximately one year ago, the decision was made to initiate a thermal analysis of the diffuser which would culminate in a computer code capable of predicting the maximum temperatures imposed upon the coolant water and the diffuser wall. The scope of the problem is vastly complicated by the requirement to test high energy, metallized solid propellants. These propellants result in a two phase exhaust plume containing large quantities of metallic oxide in solid particulate form. These solid particles possess large quantities of kinetic and thermal energy and impinge upon the diffuser wall in concentrated areas. This impingement heat load is capable of being greater than the convective heat load from the plume. The complex two phase flow within the diffuser and the largely unknown interaction between the particulate debris layer and the wall make this a very significant problem of thermal and fluid mechanics, one for which detailed modeling has as yet not been accomplished.

A significant inroad into the problem had been made by Trout and McCay (1) as of the time of my arrival, and I was asked to review what had been accomplished and to make further refinements in the thermal modeling of the problem.

II OBJECTIVES

The principal objective of this project was to review and refine the thermal code that had been implemented by Trout. The gas side fluid

mechanics of the problem is handled by several standard codes and therefore the objectives of this investigation were directed at the modeling of the diffuser wall heat transfer and the handling of the interaction between the particles and the wall. The potential heat load from impingement is quite serious and the radiant load from the particles is small but not negligible.

The original objectives of the project were to run the code in its preliminary form as delivered by Trout and to use experimental data in conjunction with what is known about debris layers to formulate a simple model of the particle impingement heat load. Unfortunately, a delay in the delivery of one of the standard codes and the lack of experimental data precluded this. What follows is a recommendation as to a second generation code for this problem. The expectation is that a follow on effort will implement this code and attack the original problem of particle impingement.

III. STATEMENT OF THE PROBLEM

Shown in Figure 1 is a schematic of the diffuser. The inlet section has a uniform diameter of 55 inches and is 30 inches long. Following the inlet section is a uniformly convergent section 47.5 inches long followed by an exit section with a uniform diameter of 45 inches. The overall length of the diffuser is 380 inches. The diffuser is fabricated from 1/4 inch mild carbon steel with an inner wall that contains the rocket engine plume and an outer wall that serves as a containment for the water jacket. The water jacket is pressurized and comprised of three parallel helical channels, each of which is 5 inches wide and 1.5 inches high. These channels are formed by 1.5 inch diameter rods that were wrapped around the inner wall during the course of fabrication.

The heat load upon the diffuser wall is comprised of the convective load from the hot gases, the thermal and kinetic energy of the particles impinging upon the wall, and the radiation flux from the particles and gases comprising the flowfield. In performing the thermal analysis of the diffuser wall, the particulate data necessary for evaluating these terms is available from standardized codes. Formulating a successful model for the interaction between the impinging particles and the diffuser wall remains the most significant obstacle within the overall problem. The gas

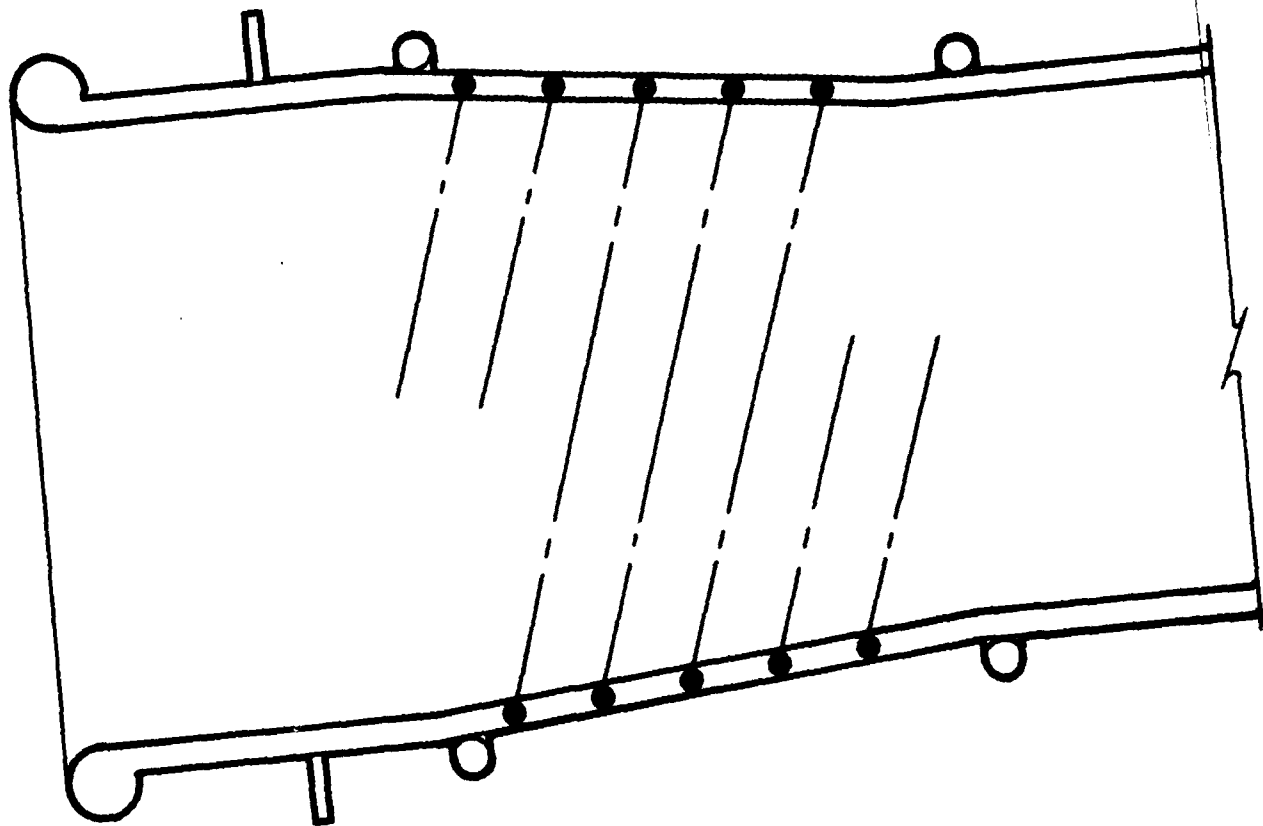


FIGURE 1. DIFFUSER

and particle properties at the exit plane of the rocket engine nozzle are supplied by SPP, the AFRPL Solid Performance Program (2). The two phase flowfield within the diffuser is supplied by SPF, the JANNAF Standardized Plume Flowfield Model (3,4). The gas side heat transfer coefficient is determined using TBL, the Inter-agency Chemical Rocket Propulsion Group Turbulent Boundary Layer Code (5).

The diffuser wall temperature must obey the unsteady heat equation. Trout and McCay cast their model in axisymmetrical coordinates. The computer code implemented by Trout is a very expensive code to run, requiring twenty minutes of computer time on the AFRPL CTC 6600 to model a 40 second motor burn. This twenty minute run time is exclusive of the roughly 10 minutes required to run the peripheral codes. Considering the geometry of the diffuser wall, it seems wasteful not to take advantage of the simplicity of modeling the conduction in two dimensional cartesian coordinates and use

$$\frac{\partial^2 T}{\partial x^2} + \frac{\partial^2 T}{\partial y^2} = \frac{\rho c}{k} \frac{\partial T}{\partial \tau} \quad (1)$$

where x will be taken axially and y will be taken radially. Trout and McCay simplify their model by assuming the temperature gradient to be negligible in the radial direction. Examination of the water side film coefficients which will run between 1500 and 3000 B/hr-ft²-F and the reciprocal of the thermal resistance of the 1/4 inch steel wall which will run approximately 1500 B/hr-ft²-F will show that this simplification is not justified in the light of temperature differentials across the water side boundary layer which are typically between 100 to 200 F deg. The need to include a two dimensional model for conduction within the diffuser wall dictates either streamlining the model wherever possible or incurring incredible run times on the code. The model implemented by Trout included axial conduction along the outer wall of the water jacket and assumed the outer surface of this outer wall to be adiabatic. There is no heat load on this outer wall and it seems quite reasonable to assume that it will float very close to the water temperature. It is proposed to delete this conduction path and to assume that the outer wall is an adiabatic surface.

The water jacket temperature is assumed to obey a one dimensional transient model with negligible axial conduction and satisfy the following energy equation

$$U \frac{\partial T}{\partial x} + \frac{2\pi R h}{\rho C A} (T - T_{\text{wall}}) = - \frac{\partial T}{\partial \tau} \quad (2)$$

where U is the axial velocity of the coolant, R is the outer radius of the inner wall of the diffuser, ρ is the mass density of the water, C is the specific heat of the water, and A is the axial cross sectional flow area of the water jacket. The water side film coefficient, h , is evaluated using the following temperature compensated correlation presented by Marks (6)

$$h' = 160(1 + 0.006(T_{\text{wall}} - T_b))V^{4/5}D'^{-1/5} \quad (3)$$

where D' is the hydraulic diameter of the rectangular channel (4 times the flow area divided by the wetted perimeter), T_b is the average bulk temperature of the coolant, and V is the coolant velocity. This value of the film coefficient is modified by the following empirical expression which compensates for the curvature of the channel

$$h = h'(1 + 3.5(D'/D_c)) \quad (4)$$

where D_c is twice the radius of curvature of the channel.

Solution of equation (1) and (2) by finite difference techniques is a very straightforward procedure. The necessary equations for handling these equations and the boundary conditions on the diffuser wall will be set up in SECTION V.

IV. PARTICLE RELATED HEAT FLUXES

Radiation

The radiation flux from the gas borne particles to the diffuser wall is a relatively minor but not negligible flux which may account for approximately five percent of the total load upon the diffuser wall. To handle this flux in a rigorous manner would present a very difficult

problem. Trout and McCay present a rather simplistic but adequate model which will be used here. They assume the flow to be transparent to the radiation and that all radiation originating within a cross sectional element of length dz falls upon the peripheral area $2\pi R dz$ associated with the element. This is admittedly an overly simplistic model but it is reasonable and does concentrate the radiant load in the proximity of the greatest radiation source. Assuming an emissivity of ϵ for the particles and that all radiation incident upon the diffuser is either absorbed or reflected and then absorbed, the radiant flux per unit may be approximated by

$$\frac{6\pi\sigma\epsilon}{r_i} \int_0^R \frac{K_i^4 \rho_i}{\rho_s} r dr \quad (5)$$

where T_i , ρ_i , and r_i are the temperature, particle cloud density, and particle radius of particle group i , ρ_s is the mass density of the particle, and σ is the Stefan-Boltzman constant. This assumes that the solid particles fall into several groups of uniform diameter particles and equation (5) must be summed over this series of particle groups.

Particle Impingement

Trout and McCay present a relatively simple model that appears to be a reasonable starting point. They model the particle as carrying thermal energy relative to the diffuser wall temperature in the amount $C_p(T_p - T_{wall})$, axial kinetic energy in the amount $U_p^2/2$, and radial kinetic energy in the amount of $V_p^2/2$, and radial kinetic energy in the amount of $V_p^2/2$. Each of these terms is multiplied by the mass flux of particles impinging upon the diffuser wall and the accommodation coefficient C_T , C_U , or C_V which accounts for the manner in which the particle interacts with the wall and partitions its energy. Written on an energy flux density basis, this gives rise to the following expression.

$$q_{imp} = \rho_p V_p (C_p(T_p - T_{wall}) + C_U U_p^2/2 + C_V V_p^2/2) \quad (6)$$

V. NUMERICAL ANALYSIS

Figure 2 shows the finite difference grid system that is proposed for use in solving for the temperature distribution within the wall of the

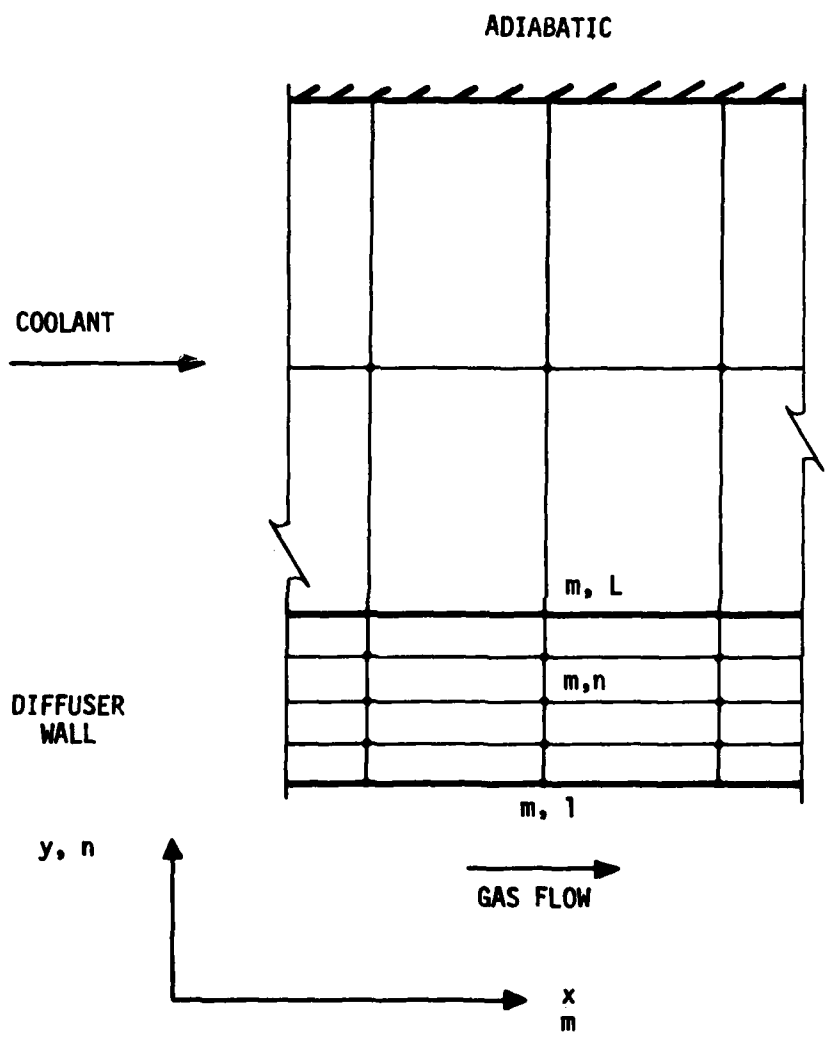


FIGURE 2. GRID SYSTEM

diffuser and within the water jacket. Equation (1) may be formulated in several different fashions. A totally explicit formulation approximates the spatial derivatives with central difference representations evaluated at time τ and approximates the temporal derivative with a forward difference representation. This gives rise to

$$\frac{T_{m-1,n} - 2T_{m,n} + T_{m+1,n}}{(\Delta x)^2} + \frac{T_{m,n-1} - 2T_{m,n} + T_{m,n+1}}{(\Delta y)^2} = \frac{T_{m,n}^+ - T_{m,n}}{\alpha \Delta \tau} \quad (7)$$

where α is the thermal diffusivity of the diffuser wall and the superscript $+$ indicates temperature evaluated at time $\tau + \Delta \tau$. Equation (7) may be solved for $T_{m,n}^+$ and rewritten as

$$T_{m,n}^+ = (T_{m,n-1} + T_{m,n+1} + \zeta^2 T_{m-1,n} + \zeta^2 T_{m+1,n} + (M - (2 + 2\zeta^2))T_{m,n})/M \quad (8)$$

where $M = (\Delta y)^2 / \alpha \Delta \tau$ and $\zeta = \Delta y / \Delta x$. In this form, the temperatures at time $\tau + \Delta \tau$ may be solved for one by one in terms of a known temperature distribution existing at time τ . This apparent simplicity is often negated by the fact that equation (8) will be unstable unless M is greater than or equal to $2(1 + \zeta^2)$. This in turn puts an upper bound on $\Delta \tau$. Assuming $\Delta x = 1.0$ inches, $\Delta y = 0.0625$ inches, and for mild carbon steel $\alpha = 1.9 \times 10^{-4}$ ft²/sec, this will require that $\Delta \tau$ be 71 msec or less. This is the criteria for stability. It may be necessary to use an even smaller $\Delta \tau$ in order to obtain a convergent solution. The model implemented by Trout is an explicit formulation, uses a nominal time step of 0.005 seconds and requires large amounts of computer time.

One may use a totally implicit formulation which employs a central difference representation for the spatial derivatives evaluated at time $\tau + \Delta \tau$ and a backward difference representation for the temporal derivative. This gives rise to the following formulation.

$$T_{m,n}^+ = (T_{m,n-1}^+ + T_{m,n+1}^+ + \zeta^2 T_{m-1,n}^+ + \zeta^2 T_{m+1,n}^+ + M T_{m,n}) / (2 + 2\zeta^2 + M) \quad (9)$$

Solving for the temperature distribution at time $\tau + \Delta\tau$ now requires the solution of a large set of simultaneous equations but the implicit formulation is known to be stable for all $\Delta\tau$. This set of equations lends itself to solution by a Gauss-Siedel iteration and may very well be a faster solution than the explicit formulation. The only restriction placed upon $\Delta\tau$ is that it be small enough to give convergence.

Probably the most desirable approach is to use a Crank-Nicholson formulation. In this case, the spatial derivatives are evaluated as an average of the central differences taken at time τ and the central differences taken at time $\tau + \Delta\tau$. It is then academic to argue whether the temporal derivative is a forward or backward form. This method is known to be stable for all sizes of time step and is very plausible from the point of view that the conduction terms are approximated at the midpoint of the time step. The Crank-Nicholson method gives rise to the following equation.

$$T_{m,n}^+ = (T_{m,n-1}^+ + T_{m,n+1}^+ + \zeta^2(T_{m-1,n}^+ + T_{m+1,n}^+) + T_{m,n-1} + T_{m,n+1} + \zeta^2(T_{m-1,n} + T_{m+1,n}) + (2M - 2(1 + \zeta^2))T_{m,n}) / (2M + 2(1 + \zeta^2)) \quad (10)$$

with no stability requirement.

In arriving at a formulation for node $m,1$ it is convenient to forsake the mathematical elegance of finite difference forms and to perform a heat balance on the element. Note that in terms of thermal capacity, node $m,1$ is only one-half an element. Done in explicit fashion this takes the following form

$$h_m \Delta x (TAW_m - T_{m,1}) + \frac{k\Delta y}{2\Delta x} (T_{m-1,1} - T_{m,1}) + \frac{k\Delta y}{2\Delta x} (T_{m+1,1} - T_{m,1}) + \frac{k\Delta x}{\Delta y} (T_{m,2} - T_{m,1}) + QPT_m \Delta x (TP_m - T_{m,1}) + QPI_m \Delta x + QPR_m \Delta x = \frac{\rho C \Delta x \Delta y}{2\Delta\tau} (T_{m,1}^+ - T_{m,1}) \quad (11)$$

where h is the gas side film coefficient, TAW is the adiabatic wall temperature of the gas, OPT is the thermal impingement flux coefficient, QPI is the inertial impingement heat flux per unit length and QPR is the

radiant heat flux per unit length. Equation (11) may be rewritten as follows

$$T_{m,1}^+ = (2T_{m,2} + 2N T_{AWm} + \zeta^2(T_{m-1,1} + T_{m+1,1}) + 2QPT_m \Delta y TP_m + 2(QPI_m + QPR_m) \Delta y + (M - (2 + 2\zeta^2 + 2N + 2QPT_m \Delta y))T_{m,1})/M \quad (12)$$

where $N = h_m \Delta y / k$. The stability criteria for the explicit form demands that the coefficient of $T_{m,1}$ be greater than or equal to zero. For the same assumed data as for equation (8) plus an estimated gas side film coefficient of 0.005 B/sec-ft²-F and QPT_m of 0.06 B/sec-ft²-F, M must be greater than or equal to 2.09 and $\Delta \tau$ must be less than or equal to 68 msec. Here again a Crank-Nicholson formulation could be used and there would be no limitation placed upon $\Delta \tau$ by stability.

Node m, J can be handled in a similar fashion to node $m, 1$ and will give rise to the following formulation

$$T_{m,L}^+ = (2T_{m,L-1} + 2N TC_m + \zeta^2(T_{m-1,L} + T_{m+1,L}) + (M - 2(1 + \zeta^2 + N))T_{m,L})/M \quad (13)$$

where TC is the coolant temperature and $N = h_m \Delta y / k$ is based on the water side film coefficient. For the same data assumed earlier and an estimated water side film coefficient of 1.0 B/sec-ft²-F, M must be greater than or equal to 2.633 and $\Delta \tau$ must be less than or equal to 54 msec. Here again one may wish to use a Crank-Nicholson formulation and avoid the restrictions imposed by stability.

Equation (2) may be formulated in an explicit fashion to give the following formulation

$$TC_m^+ = (T_{m,L} + \frac{\rho U A C}{4\pi R h_m \Delta x} (TC_{m-1} - TC_{m+1}) + (M' - 1)TC_m)/M' \quad (14)$$

where $M' = \rho CA / 2\pi R h_m \Delta \tau$. Stability will demand that M' be greater than or equal to unity. Typically h_m may run as large as 1.0 B/sec-ft²-F and the formulation will be stable for $\Delta \tau$ less than or equal to 8 seconds.

This is not restrictive and there is no advantage to an implicit formulation for this equation.

VI. RECOMMENDATIONS

It is recommended that as an initial step the explicit formulations set forth in SECTION V be implemented and their efficiency be explored. If an acceptable run time can be realized within the context of an explicit formulation, the simplicity of the explicit form has much to recommend it. Several aspects of the problem itself may be helpful. The stability criteria of 54 msec on $\Delta \tau$ is not prohibitive, and the very nature of the problem does not demand a totally convergent solution. As a means of predicting peak temperatures within the diffuser, if the solution is out of register by half a second timewise it is of little consequence. Also, the results predicted by Trout's model indicate that all but the coolant temperature has reached steady state conditions within 5 seconds so that one is almost looking for a steady state rather than a transient solution.

If it is impossible to set up an explicit formulation with a reasonable run time, then the problem should be programmed using Crank-Nicholson formulations on all but the water jacket nodes. The resulting set of equations should be solved using a Gauss-Seidel iteration and as large a step time wise as will give reasonable convergence.

A third possibility exists that is very intriguing and should not be overlooked. If the above Crank-Nicholson method is used and if the diffuser wall is broken into elements with $\Delta x = 1$ inch and $\Delta y = 0.0625$ inches, one will be faced with solving 1900 simultaneous equations at each step of the integration. This is possible with a Gauss-Seidel iteration, but it is a sizeable task. For this problem the temperature gradients in the radial direction are much greater than those in the axial direction and the thermal resistances are much greater in the axial direction than in the radial direction. In short, it is reasonable to expect the axial conduction to be less than one percent of the total heat flux. As such it may be possible to ignore the axial conduction terms. If so, one is faced with the fairly simple task of solving 380 sets of 5 equations each. If the water jacket nodes were set up in implicit form they would couple these 380 sets, but if they are set up in explicit form then the 380 sets are uncoupled and readily solved.

Once this part of the model is on firm ground the model must be compared with experimental data and an effort made to better understand the behavior of the particles as they interact with the wall. Hopefully, a combined theoretical and experimental approach to this problem can be used to refine the accomodation coefficients and yield a useful engineering tool.

REFERENCES

1. Trout, M. J. and McCay, T. D., "A Computational Model for Diffuser Heat Transfer Analysis," AIAA 16th Thermophysics Conference, Palo Alto, CA, June 1981.
2. Nickerson, G. R., Coats, D. E., and Hermsen, R. H., "A Computer Program for the Prediction of Solid Propellant Rocket Motor Performance," Interim Technical Report, Software and Engineering Associates, Inc., Santa Ana, CA, and Chemical Systems Division United Technologies, Sunnyvale, CA, AFRPL-TR-80-34, December 1980.
3. Dash, S. M., Pergament, H. S., Thorpe, R. D., Abuchowski, S. A., and Hussain, J. C., "Operational Instructions for a Preliminary Version of the JANNAF Standard Plume Flowfield Model (SPF/1)," Aeronautical Research Associates of Princeton, Inc., Princeton, NJ, A.R.A.P. Report No. 415, June 1980.
4. Dash, S. M., "A Two-Phase Flow Version of SCIPPY for the Analysis of Supersonic Exhaust Plumes, Nozzles, and Diffusers," Aeronautical Research Associates of Princeton, Inc., Princeton, NJ, A.R.A.P. Report No. 426, September 1980.
5. Weingold, H. D., "The ICRPG Turbulent Boundary Layer Reference Program," Pratt and Whitney Aircraft, East Hartford, CN, July 1968.
6. Marks, L. S., Standard Handbook for Mechanical Engineers, 7th ed., McGraw-Hill Book Company, New York, 1967, Section 4.

1981 USAF - SCEEE SUMMER FACULTY RESEARCH PROGRAM

Sponsored by the

AIR FORCE OFFICE OF SCIENTIFIC RESEARCH

Conducted by the

SOUTHEASTERN CENTER FOR ELECTRICAL ENGINEERING EDUCATION

FINAL REPORT

REHOSTING THE ADVANCED INSTRUCTIONAL SYSTEM

Prepared by: Dr. David A. Carlson

Academic Rank: Assistant Professor

Department and University: Department of Electrical and Computer Engineering
University of Massachusetts

Research Location: Air Force Human Resources Laboratory,
Logistics and Technical Training Division,
Technical Training Branch

USAF Research Colleague: Mr. Alan P. Marshall

Date: August 28, 1981

Contract No: F49620-79-C-0038

REHOSTING THE ADVANCED INSTRUCTIONAL SYSTEM

by

David A. Carlson

ABSTRACT

This report investigates a number of issues involving the rehosting of a computer-based instructional system from its present hardware configuration to a more affordable one. Specifically, four alternative approaches to the rehosting effort are analyzed in terms of their cost-effectiveness, and the problems that will occur in the transformation of the system's database are discussed. The report offers a set of general guidelines to be followed during the rehosting effort along with suggestions of areas where further study is required.

Acknowledgement

At this time, I would like to take the opportunity to thank the Air Force Systems Command, the Air Force Office of Scientific Research, and the Southeastern Center for Electrical Engineering Education for providing me with the chance to spend a worthwhile and stimulating summer at the Air Force Human Resources Laboratory, Lowry AFB, CO. In particular, I appreciate the efforts of Mr. Alan P. Marshall for providing a pleasant working environment and guidance concerning project goals. I also acknowledge the many helpful discussions about the Advanced Instructional System with Lt. William Greene.

1. Introduction.

The Advanced Instructional System (AIS) is a computer-based instructional system currently operational at Lowry Air Force Base, Colorado. It was developed as part of a large scale effort by the Air Force Training Command to improve technical training efficiency through the use of computer technology. At the present time, an effort is underway to rehost the system on a modern, "state-of-the-art" computer, with the goal being to provide a functionally equivalent system that other service branches interested in computer-based instruction can afford to purchase. This report outlines a set of alternatives for performing the rehosting effort, and also addresses specific problems associated with transporting the system's database to a different computer installation.

The AIS, as implemented at Lowry AFB, provides individualized, self-paced instruction of four technical training courses to approximately 2500 students simultaneously. The primary means by which these services are provided is computer-managed instruction (CMI), in which the computer prescribes instructional packages to students based on both past and predicted performances. In this mode of instruction, the computer handles much of the administrative overhead associated with a course, such as keeping detailed records of student performance and resource availability, while the student's instructional activities are done largely without computer interaction. The AIS also provides a facility for computer-assisted instruction (CAI), in which the student is able to take selected lessons interactively, obtaining responses directly from the computer.

A Control Data Corporation CYBER 73-16 is currently being used to host the AIS. This machine supports a set of software programs and a database of course and student related information that are used to

control a student's progress through a computer-based instructional sequence. Most of the software is written in the CAMIL programming language, which was developed to support both CMI and CAI applications. Students access the system primarily in a remote fashion, submitting forms for evaluation and obtaining instructional prescriptions as responses. However, interactive use of the system is available for CAI purposes.

The effort to rehost the AIS is motivated by the fact that the current hardware configuration is very expensive to purchase and maintain, which prohibits other organizations desiring a computer-based instructional system from obtaining AIS in its present state. Thus, after selection of a powerful but fairly inexpensive computer system (the choice now seems to be leaning towards Digital's VAX 11/780 as a target machine), the AIS will be transported to the new machine. This will involve translating present portions of the software from the CAMIL language into a programming language supported by the target machine (most likely DOD's ADA language), and transforming the database from its present format into a format that allows access by the target machine's operating system.

Rehosting the AIS is a non-trivial task, and this report attempts to isolate problems that will arise during the process, pose different methods for solving these problems, and give an analysis of the approaches suggested. The focal point of the report deals with the AIS database, since it is assumed that converting CAMIL source language programs to ADA (or another language) can be accomplished using standard techniques. Alternative approaches that can be taken in the rehosting effort as a whole are also discussed and evaluated, and suggestions are given as to whether different components of the system should be

redesigned, kept as is, or discarded.

2. Objectives.

The main objective of this project was to investigate the problems associated with rehosting the AIS. Rather than attempting to study the system in great detail, the project concentrated on providing a set of general guidelines for the rehosting effort. More specifically, the project's objectives were:

- (1) To present alternative approaches to the rehosting effort, providing an analysis of the advantages and disadvantages of each approach.
- (2) To identify and pose solutions to problems associated with transforming the AIS database from its present format to a format compatible with the system's new hardware environment.

3. The Rehosting Effort In General.

In this section, four alternatives to rehosting the AIS are proposed and analyzed. To provide the necessary background, we begin with a description of the system as it is presently configured.

3.1. Detailed Description of the AIS.

The hardware environment of the AIS consists of a Control Data Corporation CYBER 73-16 central processor connected to a network of plasma display terminals and intelligent student management terminals. The display terminals are used interactively for maintenance of the system's database, software development, course and instructional materials development, and CAI applications. Student management terminals (optical forms reader, printer, Digital PDP 11/05) are the means by which students submit information to and receive prescriptions from the central processor when taking lessons in a computer-managed instructional mode.

The software subsystem supported under this hardware configuration is made up of six different components: (1) Computer Assisted/Managed Instruction Language (CAMIL) component; (2) Information Management component; (3) Time-Sharing Operating System component; (4) Student Evaluation and Adaptive Model component; (5) Applications Programs component; and (6) CAI component. The CAMIL programming language was developed to support both CMI and CAI capabilities for the AIS. It is a high-level, general purpose programming language that has been used to write a large portion of the AIS software, including the adaptive model and CAI support software. The Information Management component provides access to the AIS database and consists of a file manager facility along with a set of editors for maintaining database files. The Time-Sharing Operating System component is a modification of the CDC Scope operating system that allows interactive access to AIS resources.

Student progress through an AIS course is monitored by the Student Evaluation and Adaptive Model component. It includes procedures for course registration, test scoring, and prediction of future performance. It also maintains detailed records of student, resource, and course related data on the system database. Coordination of most student activity makes it a major component of the AIS. The Applications Programs component is a set of programs that (1) assemble reports for the purpose of evaluating the degree of difficulty of tests and course segments, and (2) provide an on-line monitor of system performance. The CAI component consists of an editor for use in authoring lessons intended for CAI presentation, a program that presents such lessons interactively to the student (records of performance are maintained on the system database), and programs for generating reports detailing student performance in CAI lessons.

Before discussing alternative approaches to the rehosting effort, an evaluation of the present AIS should be made in order to identify features of the system that are or are not candidates for transformation. Obviously, both the Information Management and Time-Sharing Operating System components need not be converted in the rehosting effort, since it is assumed that the operating system available on the target machine will offer a time-sharing environment along with extensive file management capabilities. These file management capabilities should include at a minimum a choice of file organizations (to be discussed further in Section 4) and a powerful editing facility for maintaining system software (possibly useful for text processing also). One of the benefits to be derived under this new arrangement is the elimination of the segregation that currently exists between the AIS and other activities supported on the host CYBER.

It is also assumed that the CAMIL component of the AIS will be replaced with an environment enabling the creation and modification of software using a programming language such as ADA or PASCAL. This will be an improvement over the present programming support environment since it will undoubtedly offer better debugging aids (probably interactive in nature), more efficient compilation of source program code, more efficient execution of compiler generated code (at the machine level vs. the interpretive mode now used to execute most CAMIL programs), and elimination of CAMIL's reliance on machine dependent features. Perhaps the biggest benefit of converting AIS software to ADA or PASCAL will be the ease of performing future rehosting efforts. Whereas CAMIL is available only under the present AIS configuration, PASCAL is available on many different computer systems with only slight variations between versions, and it is anticipated that a standard version of ADA will

become available on most modern computers. This eliminates the need of developing a compiler for a new target machine, which would be required if the CAMIL language were to be retained.

The features of the AIS that are unique, and thus must be transported in some form, are the portions of the system that provide instructional services to students: the Student Evaluation and Adaptive Model, Applications Programs, and CAI components. The desired capabilities of the rehosted AIS must be considered before these components are converted so that new capabilities (if wanted) can be realized by redesigning the proper component. Through this process, it may be possible to learn from mistakes made in the initial AIS design, thus creating substantial improvements in the services that the AIS system currently provides. For example, it may be desirable (or be deemed a requirement) to convert the system into one in which CAI plays much more dominant role and is better integrated with the CMI component. These are decisions that depend largely on what course is to be taken in the rehosting effort, and will be discussed in the presentation of alternative approaches. Appendix A contains an evaluation of the AIS in its present state, with examples of both good and bad features.

3.2. Alternative Approaches to the Rehosting Effort.

At this point, we present a number of different ways in which rehosting the AIS can be done. The alternatives range from a simple conversion of necessary features to a major redesign of the system. An attempt is made to evaluate each approach in terms of costs, advantages and disadvantages, degree of difficulty, and probability of success.

3.2.1. Alternative 1: A Simple Conversion.

The AIS can be rehosted with a minimum of effort by simply translating the appropriate AIS software components (see Section 3.1)

from CAMIL source code into ADA (or any other programming language deemed suitable) and reformatting the system database to be compatible with the target machine's operating system. The translation process could be done using automatic means, which would require the development of a source-to-source translator program. Problems involving the software subsystem's dependence on hardware features would have to be reconciled during this process, with perhaps the best solution being to move these hardware dependencies away from the AIS into the target machine's compiler and operating system. A similar problem is that the CAMIL language provides access to system-wide global variables, which among other things, encouraged the design of programs that provide certain users a "privileged" execution mode. Issues involving the system database can be resolved using methods discussed in Section 4.

This approach to the rehosting effort would require no redesign of existing software programs; they would simply be transported to the target machine after their translation, and would retain their original control structures. The AIS would provide much of the same capabilities and interfaces to users after the conversion as before. The advantages to this alternative are that it is both time and cost effective. The AIS could be rehosted in a short period of time with a minimal expenditure of capital; both factors dependent primarily on the development of a translator program. The disadvantage is that the converted AIS will still contain many of the faults of the original system, and new system capabilities, if desired, would not be provided.

The faults of the AIS in its present state lie mainly in the design of its software. Existing software was not designed in a modular fashion, perhaps due partially to the restriction on segment and procedure size in CAMIL (see Appendix A for further explanation). Thus,

it is hard to maintain AIS software, and even harder for uninitiated programmers to understand it (this was discovered by painful experience!). Also, there seems to be a large number of programs that perform essentially the same task that could be combined into a smaller set of more general purpose programs. For example, a different editor exists for maintaining each individual file of the system database. These faults would not be corrected if a "quick-and -dirty" rehosting effort were to be performed, and their existence in the converted AIS may cause considerable dissatisfaction in procurers of the system.

3.2.2. Alternative 2: Redesigning System Software.

A significant improvement can be made in the quality of the AIS system by redesigning the software that is to be rehosted. This would involve rewriting AIS programs so that they are modular and well-structured, machine independent (relying on target machine provided packages for machine dependent features such as input and output), and general purpose in nature. For most AIS programs, this could be achieved without altering the basic control structure of the program, but for some, a radical redesign may be necessary. The main philosophy behind this activity should be to create an equivalent (performs the same function) but improved version of the original program.

The benefits to be derived from this approach include ease of maintenance throughout the system's lifetime, flexibility in changing system capabilities through ease of reprogramming, and a reduction in system size and apparent complexity as viewed by users. There would be considerable amount of effort required to rewrite the necessary AIS programs, but in comparison to alternative 1, a translator program would not have to be developed, which may make the two approaches similar in time and cost efficiency. Assuming that the two methods require about

the same amount of overhead to implement, alternative 2 should be the approach taken due to the improved quality of the resulting system.

3.2.3. Alternative 3: Redesigning System Capabilities.

Rehosting the AIS provides an opportunity to implement changes in the system's capabilities, since it would be more cost effective to make any desired changes during the rehosting effort rather than at a later date. Such a redesign could be made in order to correct flaws present in the existing AIS, or to incorporate new requirements made by future users of the system. For example, although CAI is available, the AIS in its present state is primarily a CMI based system. This could be interpreted as a design flaw, or a requirement could be made to provide a richer CAI environment in the converted system (perhaps allowing students to take entire courses in a CAI mode). Also, the AIS currently collects an enormous amount of data for report generation. Some of this data may be repetitious or rarely used, in which case it could be eliminated from the system database.

The author of this report is not an expert on computer-based instructional strategies; thus, no recommendations are given here as to what AIS capabilities should be modified. However, the rehosting effort does provide a means of implementing such changes, even though the overhead may be high (a significant redesign of system software and database organization may be required, depending on the changes to be made). Therefore, the recommendation made here is to identify candidates for redesign (AIS weaknesses, new capabilities desired by future users) before the rehosting effort is begun. Then, decisions on whether to implement these modifications can be made in terms of a benefit vs. cost tradeoff curve.

3.2.4. Alternative 4: A Major Redesign.

A major redesign of the AIS would be necessary only if it were to be determined that the present system provides very few of the services required of the rehosted system. For example, future users may demand a total CAI environment with a natural language dialogue between the computer and the student. Such requirements would warrant an almost complete redesign of all aspects of the AIS, which would be very costly in terms of time and capital. Because of the high overhead involved, this alternative is not recommended. In the author's opinion, the AIS, although it may be lacking in some respects, provides a reasonable alternative to computer-based instruction. The rehosting effort can result in an improved version of the AIS if the proper steps are taken, but a major redesign is not necessary in order to realize this goal.

3.3. Summary.

In summary, the AIS rehosting effort can be performed in a number of different ways, all of which have their advantages and disadvantages. The factors influencing the choice of an alternative are its associated costs and the characteristics of the resulting system, with the cost of rehosting being roughly proportional to the improvements made in the AIS. The conversion process should be approached by first determining how the revised system should be reconfigured; taking into account suggestions made by potential users, an evaluation of the strengths and weaknesses of the existing AIS, and the feasibility of making any desired modifications. This should result in some form of documentation describing the planned configuration of the rehosted system. Such a design-driven approach would provide a close match between user wants and actual system capabilities, and would also provide a strict set of guidelines for implementing the revised AIS system. Then, the rehosting effort can be carried out, with its goal being to produce the system

defined by the above procedure.

4. AIS Database Issues.

As mentioned earlier, the AIS rehosting effort involves translating selected portions of the software subsystem from CAMIL to another programming language, and transforming the system database from its present format into one compatible with the target machine's operating system. This section concentrates on the latter conversion process by outlining solutions to the problems that can be expected to arise when AIS database files are transported from one environment to another. Three problem areas are discussed in detail: (1) converting character data residing in AIS files, (2) the machine dependent layout of records in AIS files, and (3) selecting file organizations for the new environment. Suggestions are also made concerning space efficiencies in the AIS database that can be achieved during the conversion process. Appendix A outlines AIS database features, and Appendix B sketches the present structure of the AIS database.

4.1. Converting Character Oriented Data.

Character data in the AIS is represented by a 12 bit code designed to reflect the large number of keypresses available on the plasma display terminal used to gain interactive access to the system. It is expected that the target machine will store information in the standard ASCII code, so that character data residing in AIS database files will have to be converted into the ASCII code in order to allow transportation to the target machine. This conversion procedure should not be difficult to implement, and is not discussed here. However, it should be noted that character conversion need only be done for a rehosted AIS that "teaches" the same courses currently in use. If new courses are to be developed for instruction under a rehosted AIS system,

then course and student related information will be created upon system initialization instead of being converted from already existing data.

4.2. Record Formats.

AIS database files contain records that store information about a single entity, such as a particular student or a version of a course. The data structures representing these records were designed to hold as much information in as little space as possible (the CAMIL language has facility for creating a "packed" record), and to be compatible with the storage word size of the CYBER, which is 60 bits per word. Both of these factors must be taken into account when the database is transported to a new machine. The ADA language allows the programmer explicit control over the layout and storage size of the data fields of record data structure. In PASCAL, packed records can be specified in a program, with the compiler allocating storage as densely as possible. Thus, a packed record format can be preserved during the rehosting effort.

The fact that many of the data fields of an AIS record data structure are aligned so as to occupy 60 bit words will cause problems in converting the database, since the storage word size of the target machine will most likely be either 16 or 32 bits per word. The difference between a 32 bit and a 60 bit word would cause the data fields of a record to cross word boundaries instead of being properly aligned in the rehosted system. It would then be more inefficient to access the data in a record. For example, there may be data fields occupying two words (due to misalignment) that could be contained in one word, so that access to the data field may require two memory references instead of one. Also, storage inefficiencies may result due to a data field crossing a word boundary, because of the tendency to align the

next data field on the following word, which leaves a gap of unused storage between the data fields.

In order to alleviate the problems associated with an AIS record's dependence on 60 bit word size, it is recommended that all record data structures be rewritten in the target language so that either data fields are aligned with 32 bit word boundaries or no dependence on a particular hardware architecture remains. Such a change will only affect the portion of an AIS program where variables and data structures are defined and declared, since executable code accesses data fields through a field specification name, with the record's structure being hidden. Eliminating machine dependence would make future rehosting efforts easier, but may lead to increased storage requirements in the resulting system because of the inability to pack data as densely as possible.

An example of converting an AIS record is shown in Figure 1. Three data structure definitions are given for a record contained in the AIS Resource Type Descriptor file. The first is the record's definition in CAMIL as it now exists on the AIS. The second is a machine independent version written in ADA, and the third is an ADA representation specification written for a 32 bit architecture. This example shows that, through the use of the ADA programming language, a machine independent template for a record data structure can be created, and different layouts for the same record can then be specified for different machine architectures. The actual data residing in these structures would either be created upon initialization of the rehosted AIS, or would be transported using the methods for character data conversion outlined in Section 4.1.

4.3. Converting to a New File Organization.

In its present format, the AIS database is made up primarily of files having an indexed sequential organization. This type of file organization provides access to records in either a random or sequential mode. Each record is accessed through the use of an associated key, which forms one of the data fields of the record. Fast access to a randomly specified record is implemented through the use of an auxiliary set of tables, which store in order, key values paired with a database address of either another table or the corresponding record. The auxiliary tables can be searched for a key value much faster than the entire collection of records, and the use of such tables narrows the range of records that are searched in an average access operation. Figure 2 shows an example of an indexed sequential file organization.

An indexed sequential organization is a powerful method for gaining access to the data in a file, and as such, will probably be supported under the target machine's operating system. For example, the VMS operating system of Digital's VAX 11/780 supports indexed sequential files, and while the present definition of the ADA programming language does not provide input-output facilities for this type of organization, it is expected that software packages providing such facilities will allow programs written in ADA to access indexed sequential files. However, the target machine's operating system may not support an indexed sequential organization, in which case an alternative file organization must be found for all AIS files currently organized in such manner. Even if an indexed sequential organization is available, it may be desirable to convert certain AIS files to a different organization in order to gain more efficient access to the records in the file and eliminate the space associated with index tables.

Sequential and relative file organizations are currently supported by most computer operating systems. In a sequential organization, all records up to the total number in the file are always present (deletions are prohibited), read operations occur in a sequential manner (one after the other), and additions can be made only at the end of the file. A relatively organized file consists of a sequence of fixed length cells, each of which may or may not contain a record. Records can be accessed randomly by specifying their position within the file (the primary reason for using a relative organization), unused cells can accept newly created records, and records can be deleted from any cell in the file. Figure 3 shows, in general, a relative file organization.

If an indexed sequential file organization is not made available by the target machine's operating system, a relative organization should be chosen for files whose records are accessed randomly by AIS software components, so that random access to records in these files is preserved in the revised system. The difference between a relative and an indexed sequential organization lies in the keys used to access a record: in an indexed sequential file the key is actually part of the record and must be found in order to access the record's other data fields, whereas in a relatively organized file, the key is simply the record's position in the file. Converting a file from an indexed sequential to a relative organization involves either changing the file's key structure or somehow simulating an indexed sequential organization with a relative one. The former approach changes a file user's view of the database, while the latter approach requires significant overhead to implement, and both can provide more efficient access to the data within a file if implemented properly. The following two subsections discuss how these two approaches can be implemented, along with their advantages and

disadvantages.

4.3.1. Changing a File's Key Structure.

The key associated with a record of an indexed sequential file is usually a unique identifier for that record; for example, the AIS Student Data Profile (SDP) file uses a student's social security number as a record's key. If such a file is converted to a relative organization, it would not be wise to let the same key values refer to positions within the file. In the context of the above example, if social security numbers were to refer to a record's position in a file, as many as one billion storage cells (the total number of possible ssns) would be contained in the file, with very few actually being occupied for a typical AIS configuration of about 2500 students. A solution to this problem is to redefine the key used to access records in the file. Continuing the given example, a student could be assigned a unique number as he/she enters the AIS, which would serve as the student's key value throughout his/her lifetime on the system. The range of assignable numbers should be chosen to reflect the maximum enrollment in AIS courses (in order to provide enough, but not too much space), and each number would refer to a position within the SDP file. The system could easily keep track of available numbers, since they correspond to empty records in a relative file organization.

The advantage of this approach to file organization conversion is that it requires very little overhead to implement, and can provide significant improvements in efficiency. Faster access to the records in a file would be possible since the search process in a relative organization involves only a calculation based on a given position in the file (versus searching a set of index tables in an indexed sequential organization). Also, the space associated with the index

tables (possibly quite large) is not required by such an organization. The target machine's operating system would provide all the procedures necessary for processing a relatively organized file (presumably also available in any supported language). All that has to be done to convert a file is to change calls to file access procedures contained in AIS software programs. The file's original key can be deleted (which saves space), or it can be retained as an additional data field.

In many cases, the file's new key is just as natural a way to refer to individual records as the original key was. However, it may be difficult for users of certain files to adapt to referring to records by their positions. For instance, AIS files containing course related information have an associated key consisting of the course number and optionally the course version, block number, and lesson number. Users familiar with this type of protocol may have trouble adapting to a positional scheme, since in their thought processes, a course segment is represented by the original key value. In this situation, if file organization conversion must be performed, it may be worthwhile to try to preserve the original key structure during the conversion process. This is the topic of the next subsection.

4.3.2. Preserving a File's Key Structure.

Converting a file from an indexed sequential to a relative organization can be accomplished by simulating the properties of an indexed sequential file within the context of a relative organization. The ability to search for a record given its associated (non-positional) key must be compensated for, since it is not provided by a relative organization. This requires developing a search algorithm and organizing the data within the file to make the search algorithm as efficient as possible.

An indexed sequential file organization allows fairly efficient access to the records in a file based on their associated keys, since it sharply reduces the size of the subfile to be searched. However, for large files, the search process can require a number of comparisons before the desired key is located. The efficiency of the search process required in such an organization can be significantly improved by employing a method referred to as hashing. At the heart of this method is a function that converts a key drawn from a large range of values into an integer within a limited range. Under ideal conditions, no two keys will "hash" to the same integer value, so that this integer value can be interpreted as the associated record's position within a relatively organized file. However, since the range of possible keys is much larger than the range of integers, it is impossible to guarantee that no two keys will have the same hash value. Such a situation is called a hash collision and must be resolved when it occurs, since it is obvious that two records cannot occupy the same position within a file. A hash function should minimize the number of collisions and spread records uniformly throughout a file. In support of this, it is desirable to have a file size larger than the expected number of records, so as to lessen the likelihood of collisions.

The simplest way to resolve hash collisions is called linear probing, and operates by placing the conflicting record in the next available position in the file. Linear probing is an example of a more general method of resolving collisions called rehashing, in which a second hash function successively accepts and produces an integer file position until an available position is found. Another approach to collision resolution is called chaining, and involves maintaining a linked list of all records whose keys have the same hash value. An

array of header nodes called buckets is used, where bucket[i] points to the list of all records whose keys hash to the integer i. This method is illustrated in Figure 4.

Rehashing may not be an adequate way of dealing with hash collisions when the number of records grows beyond the range of the hash function (which is the file size). When this occurs, a record cannot be inserted into the file unless the file size is increased and hash values of the keys of all records in the file are recomputed using a new hash function with a larger range. Deleting records from such a file can also cause problems, since subsequent searches for records that collided with the deleted one may run afoul. Chaining offers solutions to these problems at the expense of the extra space required for the buckets and pointers in the the linked lists. Chaining can also employ a hash function more limited in range than rehashing, since it is not catastrophic if the number of records grows beyond the range of the hash function (certain linked lists will just grow longer). However, when the lists become overly long, the purpose of hashing (direct calculation of a record's position based on its key value) is defeated, and search efficiency is decreased.

While hashing does provide an efficient way to simulate an indexed sequential file, it must be emphasized that a significant amount of effort is required to implement the necessary software. To reduce development costs, if such an implementation is needed, it should take the form of a general purpose software package (ADA provides a facility for this type of software design), which can then be adapted to provide record access by key value for a specific file.

Summarizing Section 4.3, in order to gain efficiency or compensate for the lack of an indexed sequential organization, files presently

organized in this manner can be converted to a relative organization, with random access preserved. The conversion process can be done most easily by redefining the key structure of a file so that the new key refers to a position within the file. This essentially eliminates the search process and index tables required by an indexed sequential organization. Access to records in the file is thus much more efficient, and a modest savings in space can be achieved. Gains in space efficiency are dependent on the amount of variation in record size, since an indexed sequential organization allows truly variable length records, while a relative organization does not (record length may be variable, but the size of the cells they are stored in is not).

When the definition of a new key is unnatural to use, and conversion to a relative organization is deemed necessary (indexed sequential not available or efficiency desired), the ability to search for a record based on its key value can be preserved by using hashing techniques. Such an implementation is the most efficient general-purpose method of providing this service. Hashing allows much faster access to the records in a file as long as file size remains proportional to the range of the hash function. Index tables are replaced with hash tables, and again, variations in record length influence any possible gains in space efficiency, since a relative organization does not allow variable length records.

It should be noted here that there may be situation specific methods of implementing a search function more efficiently than hashing. For example, consider a file containing course related information whose records are accessed by a key specifying the course and version numbers. A position can easily be calculated from the above key by the formula: $(\text{course num.} - 1) * (\text{max. num. versions}) + (\text{version num.})$. This provides

access to records via a key value without the added overhead of a search operation, but may be somewhat space inefficient if most courses have only a few versions (records must be defined for all possible versions if the formula is to produce a relative position). The above example points out the fact that decisions regarding how and when to convert an indexed sequential file to a relative file organization should be made based on a file's individual characteristics. Such a decision should be influenced by the ease of implementation, the ease of access to the resulting file's records, and the possible gains in both access time and space efficiency.

4.4. Restructuring Information in the Database.

As discussed in Section 3, the rehosting effort provides an opportunity to make significant changes in the characteristics of the AIS. This statement also holds true for the structure of the AIS database. Such changes are, in large part, dependent on changes made to either software components or high level characteristics of the AIS. For example, if it is determined that a number of the data collection programs are not necessary, then the corresponding data fields contained within AIS files can be eliminated, possibly providing a sizeable reduction in space requirements.

The AIS database can also be restructured in various ways that leave it functionally the same, but provide better efficiency in terms of space. A notable example concerns the regression equation data fields contained within every module record of the AIS Lesson file. Regression equations are used to predict a student's performance within a lesson module, and it seems reasonable that a standard set of regression equations could be developed to reflect the conditions imposed by different lesson environments. A separate file of regression equations

could then be created, and the data field within the module record could be replaced by an index to the appropriate record in the regression equation file. Since there are a large number of module records in the Lesson file, and assuming the number of regression equations could be reduced to a small set, a significant savings in space could be achieved. This example is explained in more detail in Appendix A along with other ways of restructuring the AIS database. In order to identify further possible reductions in space, a more detailed study of the AIS database and its interaction with AIS software components than that conducted by the author should be made.

Restructuring the AIS database during the rehosting effort involves an effort parallel to that required in redesigning the system. First of all, the needs of potential users, an evaluation of database strengths and weaknesses, and the costs of making any desired changes should be combined to form a blueprint of how the database should be restructured. Then, worthwhile modifications to the database can be implemented in conjunction with other AIS modifications.

5. Recommendations.

Rehosting the Advanced Instructional System represents an attempt to provide an affordable computer-based instructional system to other service branches. It also provides an opportunity to make significant improvements in the current system's characteristics. This report has outlined a number of different ways to carry out the rehosting effort, along with more specific details concerning problems to be encountered during transformation of the AIS database.

While implementation of any of the alternatives discussed earlier in Section 3 will produce a system functionally equivalent to the AIS in its present state, it should be emphasized that the proper approach to

the rehosting effort is to first determine and document the capabilities of the revised system before any implementation work is done. This design process should take into account input from potential users of the revised AIS, an evaluation of how AIS can be improved upon, and the costs associated with changing system capabilities; and it should result in documentation describing in detail the future configuration of the system after rehosting is completed. The benefits of this approach are that a system will be developed closely matching the expectations of potential users, and implementation of the rehosting effort can proceed according to a well-defined set of guidelines.

In the author's opinion, the rehosting effort should at least include an attempt to rewrite AIS software components in a well-structured, machine independent form. This would allow for easier maintenance of the revised system, and would also make it easier to implement extensions of system capabilities at a later date. Maintenance and extensibility should be important considerations in the rehosting effort, since such work will have to be performed throughout the lifetime of the new AIS.

Problems concerning the transformation of the AIS database also should be solved before implementation begins in order to present a clear picture of database access protocols to potential users. The major problem to be addressed is how to maintain random access to a file's records based on an associated key if more efficient access to the file's records is required or a file organization providing this facility is not available in the target environment. There are other topics concerning the AIS database that should be investigated in more detail before the rehosting effort is begun. There is a large amount of data presently stored in the database, and it should be determined

exactly what data the AIS requires and uses frequently. It would also be worthwhile to study alternative ways of organizing the database that have special properties such as more efficient data access or more powerful queries of statistical information. For example, it may be possible to organize the database using a relational scheme, which allows the user to make a wide range of queries concerning the data in the database.

In conclusion, if approached properly, the AIS rehosting effort will result in a computer-based instructional system with many desirable properties that is adaptable to a large number of instructional situations. The approach to take is to first determine the capabilities of the revised system, and then implement these capabilities in the target computer system environment.

REFERENCES

1. "Reference Manual for the ADA Programming Language - Proposed Standard Document," United States Department of Defense, July 1980.
2. "CAMIL Reference Manual," AIS 3.8-1674, Lowry AFB, CO: Technical Training Division, Air Force Human Resources Laboratory, September 1979.
3. Wirth, N., "The Programming Language PASCAL," Acta Informatica, Volume 1, Number 1, pp. 35-63, 1971.
4. Lintz, L. M., Tate, T., Pflasterer, D. C., Nix, C. J., Klem, T. G., & Click, L. E., "Low-Cost Computer-Aided Instruction/Computer-Managed Instruction (CAI/CMI) System: Feasibility Study," AFHRL-TR-79-42, Lowry AFB, CO: Technical Training Division, Air Force Human Resources Laboratory, December 1979.
5. Montgomery, A. D., & Judd, W. A., "Computer-Assisted Instruction in the Context of the Advanced Instructional System: Authoring Support Software," AFHRL-TR-79-12, Lowry AFB, CO: Technical Training Division, Air Force Human Resources Laboratory, September 1979.
6. McDonnell Douglas Astronautics Co. - St. Louis, "Part II Specification, Student Evaluation and Adaptive Model Components, Advanced Instructional System," DD1017F023, Lowry AFB, CO: Technical Training Division, Air Force Human Resources Laboratory, September 1979.
7. McDonnell Douglas Astronautics Co. - St. Louis, "Computer Program Product Specification for the Computer-Assisted Instructional Component of the Advanced Instructional System," CAI-AS-020, Lowry AFB, CO: Technical Training Division, Air Force Human Resources Laboratory, September 1978.
8. McDonnell Douglas Astronautics Co. - St. Louis, "Part II Specification, Applications Programs Component, Advanced Instructional System," DD1017F023, Lowry AFB, CO: Technical Training Division, Air Force Human Resources Laboratory, August 1979.
9. McDonnell Douglas Astronautics Co. - St. Louis, "Part II Specification, Information Management Component, Advanced Instructional System," DD1017F020, Lowry AFB, CO: Technical Training Division, Air Force Human Resources Laboratory, September 1979.
10. McDonnell Douglas Astronautics Co. - St. Louis, "TSOS Part II Specification DD1017F022, Lowry AFB, CO: Technical Training Division, Air Force Human Resources Laboratory, July 1979.
11. McDonnell Douglas Astronautics Co. - St. Louis, "Advanced Instructional System CMI Database Administrator Manual," Lowry AFB, CO: Technical Training Division, Air Force Human Resources Laboratory, August 1979.
12. Digital Equipment Corp., "VAX-11 Record Management Services Reference Manual," AA-D031B-TE, Maynard MA, February 1979.

Appendix A: AIS Features.

This appendix outlines meaningful features of the AIS software components and the AIS database. Examples are given of good features that should be preserved in the rehosting effort, and of bad features that should not be carried over to the revised system.

AIS Software.

Good Features:

1. Computer-Aided Support Software (CASS) Editor.
The CASS Editor provides a convenient and time-saving way of creating and maintaining course related material on the AIS.
2. CAI Presentation Program.
The CAI Presentation Program is fairly modular in nature, containing two major loops for processing objectives within a lesson and frames within an objective. It also interfaces with the Adaptive Model software component to obtain prescriptions when a student has finished a CAI lesson. Combined with the CASS Editor, it forms a convenient way for personnel having little experience with computer programming to create and present instructional materials in a CAI mode.
3. CMI Instructional Strategy.
The Adaptive Model component has the ability to prescribe instructional strategies based on a student's past and predicted performances.
4. Library Procedures.
Library procedures can be defined and accessed in the CAMIL language component, which is a step towards modularity and machine independence. For example, many CAMIL programs access system-defined libraries to obtain definitions for common data types. Libraries should be used to provide access to commonly used utility programs and machine dependent routines.
5. Interactive Access to System Resources.
This AIS feature can be taken for granted, but should be preserved in the rehosting effort.

Bad Features:

1. Non-Modularity of AIS Software Components.
Source data for CAMIL programs is maintained in the Source Program Library, which is comprised of modules containing different CAMIL constructs such as segments and procedures. Due to the restriction on module size in the SOURCELIB file (which contains source data for all CAMIL programs on the AIS), logically distinct processing units in many CAMIL programs have been split up into a number of different segments. For example, the portion of the Adaptive Model component that prescribes instructional strategies has been written using eight separate CAMIL segments, instead of being one processing unit. There are also many examples of bad programming

style in existing CAMIL programs. For instance, many CAMIL programs open files that may be used during program execution when the program is initialized. In some cases, the files are never accessed, so that the overhead of file opening was unnecessary. Additionally, goto statements are heavily used in many CAMIL programs, which results in unstructured programs.

2. Machine Dependence of CAMIL Programs.
Many CAMIL programs access system-wide global variables and contain code dependent on machine features. For example, the CASS Editor allows users with certain system IDs (obtained from a system-wide global variable) special access privileges.
3. Non-Existence of General-Purpose Programs.
There are many programs in the AIS that perform essentially the same task. For example, separate editors exist for maintaining each CMI database file. If these could be combined into a general-purpose program, significant savings in system resources could be achieved (a shared copy of such a program could be accessed simultaneously by a number of users).
4. Menu-Driven Editors.
This design philosophy can cause confusion to editor users when menus (choices of editor functions) are too large. Editors should accept and parse a relatively small set of user entered commands.
5. CAI Capabilities.
AIS in its present state does not allow entire courses to be taken in a CAI mode.
6. CMI Capabilities.
The Adaptive Model component randomly assigns a course version to a student upon entry to a course. Course versions should be assigned to students based on predicted performance, not randomly.
7. Execution of the Adaptive Model Component in Background Mode.
The Adaptive Model (AM) component currently executes at a simulated terminal location (background mode). This is a drain on system resources, since a CPU time-slice must be continually allocated to the AM, even if it is not performing any useful computation. Unless the overhead to initialize the AM is prohibitively high, it should execute in the same mode as a widely-used editor: as a shared procedure accessible by a number of different users (here, users are remote terminals requesting analysis of student performance data).
8. Debugging Features of the CAMIL Language.
Hopefully this will improve with the support of better language features in the target environment.

AIS Database.

Good Features:

1. Logical Separation of Information.
The data contained in the AIS database is separated along file boundaries into course related data, resource related data, and student related data.
2. Indexed Sequential Organization.
Files whose data is accessed randomly are organized in an indexed sequential manner, which provides fairly efficient access to the records in a file based on an associated key.

Bad Features:

1. Too Much Data.
The AIS database stores an enormous amount of data concerning student performance histories. Much of this data may be collected for no good reason, and its elimination would cause a dramatic drop in the space requirements of the AIS.
2. Space Inefficiency.
Certain files in the AIS database could be restructured in order to create savings in space. For example, each module record of the AIS Lesson file contains five regression equations, each requiring 37 words of storage. If a file could be created containing a standard set of say 100 regression equations, a substantial savings in space could result, since the present database has upwards of 100K words of storage devoted to regression equations alone (4 courses, up to 16 blocks per course, up to 98 lessons per block, a number of modules per lesson, 5*37 words per module record). The regression equation data fields in the module records would simply be replaced with an index or key for the proper record in the newly created regression equation file. This replacement process may not exactly duplicate the original regression equation, but it is assumed that a close match can be found from the standard set contained in the new file.
3. Possible Overlaps in Information Stored in the Database.
Course related information exists in a Course file, a Hierarchy file, a Lesson file, and a Cross Reference file. Some of this information may be duplicated in two or more of these files.
4. Fixed Length Records.
While an indexed sequential organization allows variable length records in a file, all AIS database files organized in such a manner contain fixed length records. In some instances, these records contain arrays of data (such as absence transactions within a Student Data Profile record), so that the use of variable length records would provide a significant savings in space.

Appendix B: AIS Database Structure.

Course Related Files:

1. Course file.
Contains information pertaining to a course as a whole. Accessed by the Adaptive Model on every transaction.
2. Hierarchy file.
Contains information defining the structure of each version of a course. Accessed by the Adaptive Model when an assignment is made.
3. Lesson file.
Contains information regarding the individual lessons and modules (lesson alternatives) in a course. Accessed by the Adaptive Model when a lesson assignment is made.
4. Cross Reference file.
Contains information tying together the Hierarchy and Lesson files. Accessed by the Adaptive Model when an assignment override request is made.
5. Test Key file.
Contains information about the various tests administered by the Adaptive Model. Accessed by the Adaptive Model when a test is scored.
6. Test Item Text file.
Contains the text for tests that can be administered interactively. Not accessed by the Adaptive Model.

Resource Related Files:

1. Learning Center file.
Contains information concerning each distinct learning center. Accessed by the Adaptive Model when a student enters or leaves a learning center.
2. Resource Class file.
Contains information about the instructional resources managed by the Adaptive Model. Accessed by the Adaptive Model to determine if resources are available for a specific module assignment.
3. Resource Type Descriptor file.
Establishes a correspondence between resource type numbers and their English language names.
4. Calendar file.
Contains information defining the days on which a course is taught.
5. Variable Definition file.
Contains information defining the characteristics of student performance variables employed by the AIS. Accessed by the Adaptive Model to determine when to store a variable from a test.

Student Related Files:

1. Student Data Profile file.
Contains information regarding individual students registered for AIS courses. Accessed by the Adaptive Model for every transaction concerning the student. Contains the following types of records:
Status record: one for each student.
Module Completion record: one for each block a student has begun.
Testing record: one for each student who has been administered an on-line test.
Absence record: one for each block in which a student has been absent.
Restart record: one for each student restarting a CAI lesson.

CAI Related Files:

1. CAI file.
Contains information describing CAI lessons. Accessed by the CAI Presentation Program when a CAI lesson is presented.
2. TEXT file.
Contains the material to appear on the terminal screen in the presentation of a CAI lesson.
3. COMTEXT file.
Contains reviewer entered comments.
4. CAIDATA/CAIDEC file.
Contains response and decision point data for data analysis report generation.
5. Student Data Profile file.
Same as above.

CAMIL definition:

```
TYPE PACKED RECORD
  (I4B class;
   I8B rec_no) RTD_key_type;
TYPE PACKED RECORD
  (CHARACTER PACKED ARRAY (20) character) res_name_type;
TYPE PACKED RECORD
  (RTD_key_type key;
   res_name_type PACKED ARRAY (200) res_name) RTD_type; -- word 1
                                                         -- words 2 - 80;
```

ADA definition:(machine independent):

```
type RTD_KEY_TYPE is record
  CLASS : INTEGER range 1 .. 3;
  REC_NO : INTEGER range 0 .. 255;
end record;
type RES_NAME_TYPE is record
  CHARACTERS : array(1 .. 20) of CHARACTER; -- or STRING(1 .. 20)
end record;
type RTD_TYPE is record
  KEY : RTD_KEY_TYPE;
  RES_NAME : array(1 .. 200) of RES_NAME_TYPE;
end record;
```

ADA representation specification:

```
BYTE : constant := 8; -- 8 bits per byte
WORD : constant := 4; -- storage unit is byte, 4 bytes (32 bits) per word
for RTD_KEY_TYPE use record
  CLASS at 0*WORD range 0 .. 3;
  REC_NO at 0*WORD range 4 .. 11;
end record;
for RTD_TYPE use record
  KEY at 0*WORD range 0 .. 31; -- word 1
  RES_NAME at 1*WORD range 0 .. 31999; -- words 2 - 1001
end record;
```

-- or equivalently:

```
for RTD_KEY_TYPE'SIZE use 4*BYTE;
for RES_NAME_TYPE'SIZE use 20*BYTE;
for RTD_TYPE'SIZE use 4004*BYTE;
```

Figure 1: Resource Type Descriptor file record.

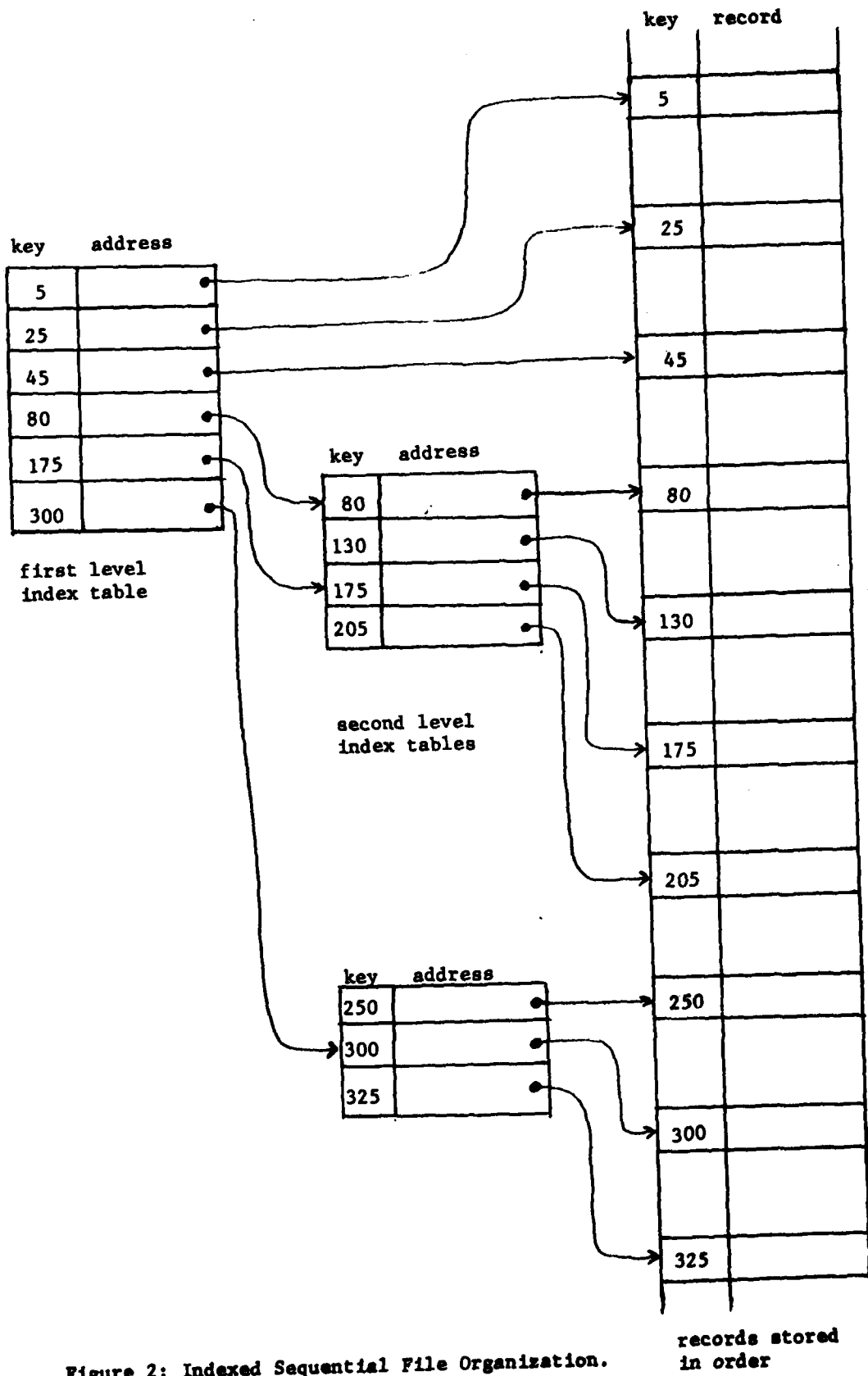


Figure 2: Indexed Sequential File Organization.

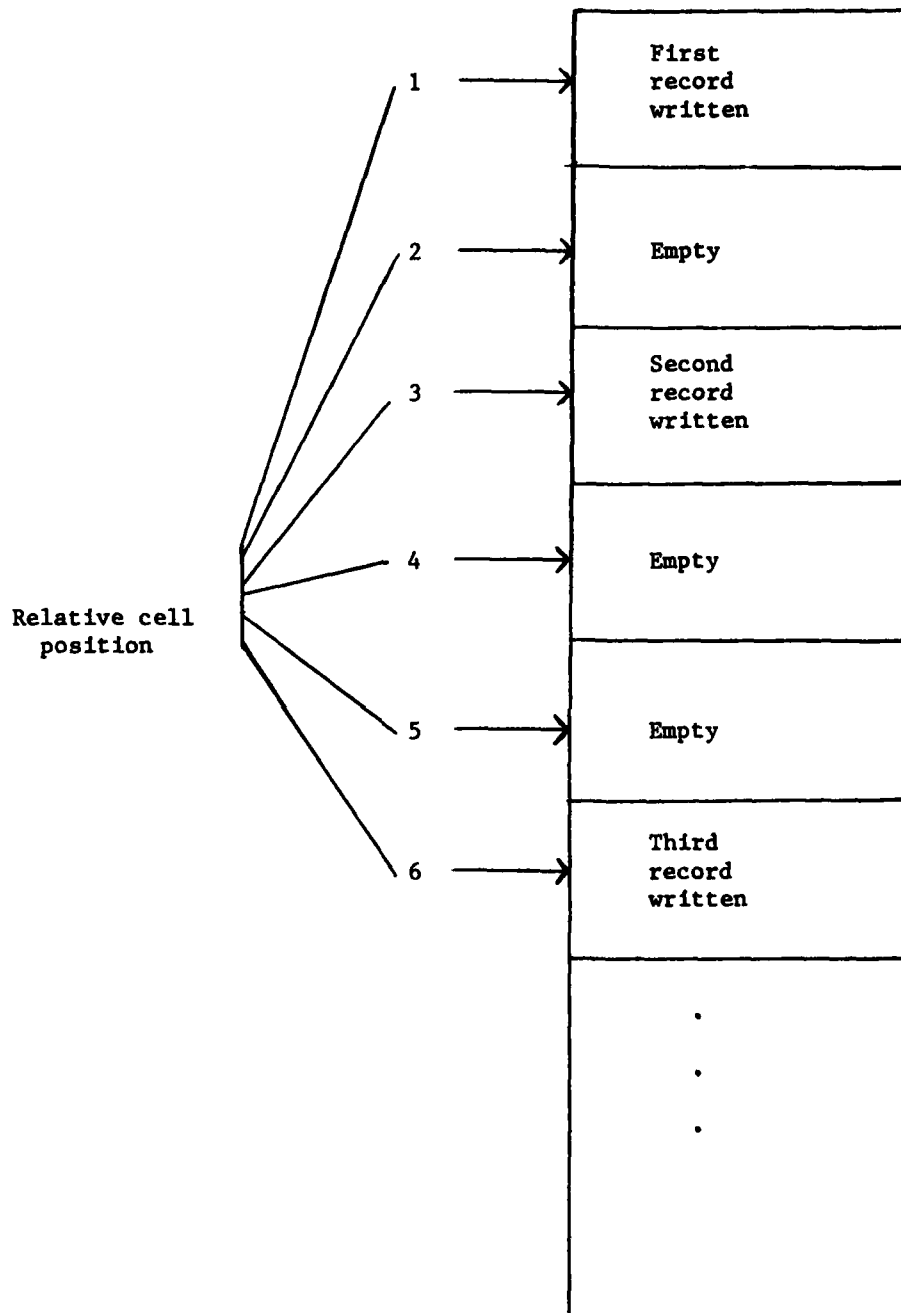
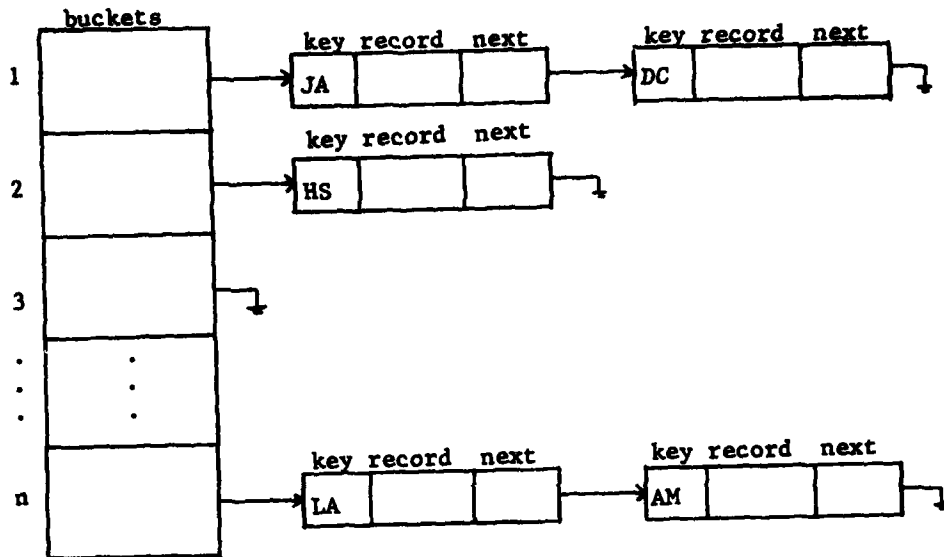


Figure 3: Relative File Organization.

Abstract version:



File contents:

bucket file	
1	1
2	5
3	nil
.	.
.	.
.	.
n	4

File storing records:

pos.	key	record	next
1	JA		3
2			
3	DC		nil
4	LA		6
5	HS		nil
6	AM		nil
			⋮

Figure 4: Hashing implemented using chaining to resolve collisions.

1981 USAF - SCEEE SUMMER FACULTY RESEARCH PROGRAM

Sponsored by the

AIR FORCE OFFICE OF SCIENTIFIC RESEARCH

Conducted by the

SOUTHEASTERN CENTER FOR ELECTRICAL ENGINEERING EDUCATION

FINAL REPORT

THE BIOLOGICAL DEGRADATION OF SPILLED JET FUELS: A LITERATURE REVIEW

Prepared by: Dr. Robert Carlson

Academic Rank: Associate Professor

Department and
University: Kent State University

Research Location: Air Force Engineering and Services Center,
Environics Division, Environmental Chemistry
Branch

USAF Research
Colleague: Mr. Thomas Stauffer

Date: August 11, 1981

Contract No: F49620-79-C-0038

THE BIOLOGICAL DEGRADATION OF SPILLED JET FUELS:
A LITERATURE REVIEW

by

Robert E. Carlson

ABSTRACT

Biodegradation of many of the components of Air Force fuels does occur, although most studies have been done under laboratory conditions, and the extrapolation of the findings to natural rates of biodegradation is premature. Many factors affect biodegradation rates, including the nature and concentration of the specific hydrocarbon compound, the species of bacteria present and their quantity, and environmental factors such as nutrient availability, temperature, and oxygen concentrations. Initial concerns should be first, the determination of the importance of biodegradation relative to other loss factors such as volatilization and sediment sorption, and second, the determination of the ultimate fate of recalcitrant compounds and their metabolites.

ACKNOWLEDGEMENT

I would like to thank the Air Force Systems Command, the Air Force Office of Scientific Research, and the Southeastern Center for Electrical Engineering Education for providing the opportunity to spend a worthwhile summer at the Air Force Engineering and Services Center, Tyndall AFB, Florida. I would like to thank the Center, particularly the Environics Division, for its hospitality and support this summer.

I especially want to thank Mr. Thomas Stauffer for his suggestions and guidance in the research and his efforts to make the summer enjoyable for me and my family. I would also like to acknowledge the help and advice given me by Captain Joseph Zirrolli and the other members of the Environics Division.

I. INTRODUCTION:

Accidental spills or leakage of commercial or Air Force jet fuels into surface waters or ground water have happened and will happen again. Jet fuels contain a number of highly toxic and even carcinogenic compounds and their potential effect on natural ecosystems and water supplies could be serious. Research is presently underway to broaden the specifications of the currently used jet fuels so that alternate sources such as shale oil and coal could be used. These alternate source fuels may have as much as 10 percent more aromatic hydrocarbons than present fuels, some of which will be polycyclic aromatic hydrocarbons (PAH). Several PAH are potent carcinogens. The fate in and effect on the environment of the present and proposed jet fuels is currently being investigated by the Air Force.

As most of the constituents of jet fuel have a limited solubility in water and are volatile, it might be expected that evaporation from the water surface may be the major mode of loss of a spilled fuel. However, a finite amount of many of the compounds may enter the water, either as small droplets or in solution. The fate of these compounds is the concern of this review.

Soluble hydrocarbons may sorb onto the surface of any organic particle in the water.¹ Some of these organic surfaces will be suspended and settled sediments, while other surfaces will be living: bacteria, algae, invertebrates, and fish. To some of these organisms the hydrocarbons will be toxic, affecting behavior, growth, reproduction and survival. Other organisms will utilize the hydrocarbons as a source of energy and carbon, degrading the compounds into simpler organic molecules, and ultimately into carbon dioxide and water.

Volatilization, abiotic and biotic sorption, and degradation are probably the major pathways of removal of jet fuel hydrocarbons from the open water. Of these, only volatilization and biodegradation represent true losses from the aquatic habitat. Sorbed hydrocarbons, unless sorbed irreversibly, may continue to be released into the water for some time, especially if initially

buried in the sub-surface sediments by burrowing invertebrates and bottom-feeding fish. The ability of the biota of aquatic environments to degrade hydrocarbons is therefore an important consideration in the possible effect of spilled fuels.

II. OBJECTIVES

The objective of this study is to review the literature pertaining to the factors influencing the rate of degradation of jet fuels by living organisms. It became apparent early in the study that no research has been done specifically with jet fuels, and only a limited number of studies have dealt with fuel components such as gasoline, kerosene, and diesel fuel. The vast majority of the research has been done using crude and refined oils. Research has also largely been confined to studies on marine bacteria and fungi. Little work has been done in fresh water, and the possibility that organisms other than bacteria may contribute to degradation has been virtually ignored. Finally, a wide diversity of methods has been used to study biodegradation, making comparison of degradation rates obtained in separate studies impossible. For these reasons, the following was done:

1. A review of the methodologies used in biodegradation research in order to provide a perspective of the methodological problems and possible solutions.

2. A review of the factors that have been identified as affecting the rate of biodegradation. From this review, the dominant factors are identified and areas where limited knowledge is available are identified.

The review does not cover all of the vast amount of literature on hydrocarbon biodegradation, but it reviews a sampling of the relevant literature published in English in the past five years.

III. THE METHODOLOGY OF BIODEGRADATION

Microcosms

In 1941 hydrocarbons were believed to be biologically inert or highly refractory to enzymatic attack.² By 1972 ZoBell² could report that virtually all kinds of hydrocarbons were susceptible to microbial degradation. In the 31 years since 1941 a great deal of research had been done on microbial degradation of hydrocarbons, much of it being the tedious task of demonstrating degradability of each individual hydrocarbon and then isolating and identifying the degrading organism. It is now obvious from ZoBell's 1972 review that although biodegradation of hydrocarbons had been adequately demonstrated, considerable research was needed in elucidating the factors that affected degradation rates. At the same symposium, Floodgate³ lamented the lack of an ecological approach to degradation research. He decried the tendency to use biochemical approaches to basically ecological problems. His paper is a discussion of the problems and of the possibilities that would allow the microbial ecologist to "mimic the natural environment as closely as possible."

Considering the complexity of the natural environment relative to the simplicity of the uni-species laboratory cultures, the transferral of laboratory data to field situations should be viewed with suspicion. The microcosm is one approach to providing some measure of the complexity of the natural system while maintaining the control obtainable in the laboratory environment. Although some would regard both the uni-species flask and the mathematical model as forms of microcosms,⁴ the definition of a microcosm is better limited to living multi-species micro-systems. The microcosm is used because it allows for species interactions, the one factor that cannot be obtained with a single species culture. It is also used because all possible interactions cannot be known and therefore cannot be modeled mathematically. The microcosm is a living model of a natural system. It is assumed that a multi-species system will exhibit a behavior which is a function of the quantity and quality of species within the system. Therefore the more species and functional groups represented, the more the microcosm behavior would deviate from the unispecies culture, and the more it would mimic the behavior of the natural world.

The utility of multi-species cultures is essential in measuring biodegradation because the complete degradation of some hydrocarbons cannot be accomplished unless several microbial species are present.^{3,4,5} In such cases a uni-species culture would give an erroneous picture of the microbial community's capability to degrade the compound.

Microcosms can be classified either on the basis of their openness to inputs and outputs of nutrients and water or on the basis of the degree of definition of the species within.⁷ A closed or static system assumes that the internal recycling of nutrients will provide adequate nutrients to maintain the system for the duration of the experiment. It is equivalent to a batch culture. In open systems nutrients and water are added and removed either continuously or discontinuously. The characteristics of the static and continuous-flow systems will be discussed later.

An undefined microcosm may be no more than a grab sample of water and mud from a pond,^{8,9} while in a defined system the species are all known and were deliberately added to the system. The assumption of the undefined microcosm is that knowledge of all possible species interactions in a system is impossible, and therefore a sample of the natural system, containing as complete a community as deemed necessary will be the best laboratory representation of the natural ecosystem. Often knowledge of the species or their interactions within the microcosm is de-emphasized, and the microcosm is treated as a black box, with an emphasis on total system function rather than on component behavior.⁹ Critics of this approach consider the undefined microcosms to be "dirty aquaria," where the sacrifice of knowledge of specific mechanisms and interactions is not compensated by the system's naturalness.

The defined microcosm usually has a different research purpose than the undefined system. It may be a closed micro-ecosystem, open only to light and gas exchange, or it may represent only a portion of a system, as for example, a model predator-prey system. It is not meant to be a mimic of any specific natural system and is therefore often used to explore general ecosystem behavior. Since all the components are known, the system can be constructed at any time. It also has the major advantage of a reproducible behavior. It

can and has been used to predict the effects of xenobiotics on system behavior and can provide valuable information on the possible toxicity responses of a multi-species system. As such it can be a powerful screening technique for possible toxic substances. Because it does not mimic any particular system and because its bacterial community is probably limited in numbers of species, it has little use in estimating natural degradation rates.

In biodegradation research microcosms used range in size from 20 ml scintillation vials¹⁰ to 1500 liter plastic bags.¹¹ The systems themselves may consist of grab samples of mud and/or water or may be attempts to take intact segments of the natural system.¹² Many studies use only the water or sediment-water components, while others attempt to include as much of natural system as possible.⁹ The exclusion of fish and invertebrates may be justified as they are thought to not contribute significantly to the total biodegradation of hydrocarbons, but restriction to small volumes simply because bacteria are small could increase the variability of replicate microcosms and miss some possible system matrix effects.

Although microcosms theoretically provide unique information because of the potential for interspecific interactions, microcosms at present have certain drawbacks that require that caution be taken when attempting to extrapolate microcosm-derived data to field situations. Some of the problems of the use of microcosms are listed below:

1. Microcosm results are specific to the type of microcosm used.⁴ Microcosms have inherent design features (size, S/V ratio, use of sediments, etc.¹³) that will affect the outcome of the experiment. The use of reference compounds would allow comparisons to be made between different microcosms.⁴ Certainly this problem is no different from the lack of uniformity between natural ecosystems, and is an implicit recognition that the problems of microcosm design are similar to those of field comparisons. The use of microcosms simply has not advanced to the state where the effect of microcosm design is considered.

2. A microcosm should give reproducible data within a given set of experiments.⁴ This requirement is achievable in defined microcosms, but in

these systems replicability is gained at the expense of the ability to extrapolate the findings to any specific ecosystem. Replicability is difficult to achieve in an undefined microcosm. Species in natural systems change both spatially and temporally, and a microcosm may not respond in exactly the same manner if the initial samples are taken on different days¹¹ or at different locations within the same ecosystem. Bourquin et al.¹⁴ achieved replicable microcosms by first mixing estuarine sediments in an aquarium and then sampling from this homogeneous system. In field work variability is handled by the use of multiple samples, both spatially and temporally. Such replication becomes logistically difficult with microcosms. Without at least temporal replication, extrapolation of microcosm results will be difficult.

3. When microcosms are used to mimic natural systems, there is a problem of scaling.⁴ If the assumption is that the richer the biotic community, the better the duplication of real-world events, then the inclusion of all or most of the natural functional groups should be necessary. To achieve this goal without putting large organisms into small microcosms, microcosms have grown in size, becoming field ecosystems in themselves. De Kreuk and Hanstveit¹¹ found, for example, higher degradation rates of 4-chlorophenol in larger enclosures because of the presence of a richer bacterial flora. With the achievement of the reality assumed to be gained with increasing enclosure size, comes a loss in the amount of control over and understanding of the dynamics of individual components. A trade-off exists between "reality" and control over the system.

4. In attempts to make microcosms more realistic, the use of a continuous culture system has been recommended.^{3,15} This provides a semblance of realism in regard to nutrient input, but ignores the importance of species introductions.¹¹ Natural systems have continual inputs of species as well as nutrients and these inputs may be responsible for the observed species richness. Cessation of immigration could result in an increasingly simpler community. This consideration becomes especially important when microcosms are used to screen toxic substances. The initial contact with a toxic compound may cause species extinctions. The resulting recovery-response trajectory of the microcosm may differ considerably from an open-species system. If realism is

desired, periodic re-seeding with field samples is recommended. Experiments where continual re-seeding was done are those of Horowitz and Atlas¹⁶ and of de Kreuk and Hanstveit.¹¹

Continuous Flow and Static Cultures

A static culture is open only to inputs of light and gasses. No effort is made to replenish nutrients or to remove metabolic by-products. Typically the growth within such a system would be initially a sigmoidal increase in biomass, followed by a definite period of relatively stable biomass, followed by a gradual decline of the system as nutrients become sequestered in internal sinks. The period of stable biomass is dependent on the degree of internal nutrient re-cycling. The advantage of the batch system is its simplicity; it requires little equipment other than the culture container, and it requires little or no maintenance once the experiment is initiated. Its disadvantages include (1) a lack of reality with the exclusion of inputs and outputs, (2) the possible buildup of toxic metabolic intermediates, (3) the time dependence of the results, and (4) the difficulty of monitoring changes over time.^{3,15}

The alternative to the static system is the continuous culture system, where inputs of water and nutrients enter and leave the reaction vessel. A specialized form of the continuous flow system is the chemostat, where the growth of the culture is limited by the rate of input of a nutrient. In the chemostat the growth rate can be regulated by varying the dilution rate of the system.

The claim that continuous flow techniques produce more realistic systems is lessened by the use of unrealistic dilution rates. At the dilution rates usually used, nutrient inputs and dilution losses are much higher than found in lentic ecosystems, and the system selects for species growing at the rate of dilution. Slower growing species are washed out of the cultures.¹¹ Pritchard and Starr¹⁵ found that manipulation of the dilution rate selected for different species of bacteria that degraded octane at different rates

(57.1 and 16.5 ug/hr). Such selection would seriously hinder the extrapolation of the results to natural systems. As mentioned earlier, most existing lentic continuous flow systems do not continuously introduce species to the microcosm. The exceptions are many lotic microcosms. In these systems, often the input water is natural stream water, allowing a continual seeding of species. In these systems, the organisms usually are attached to the substrate, minimizing the effect of dilution rate on species selection, although it is still possible that the assemblage that is established will be a function of the flow rate.

A major drawback of the continuous flow system is the amount of ancillary apparatus needed to maintain a constant flow through the system. The expense and maintenance time involved with the continuous flow systems limit the number of replications that can be done at one time. This could add substantially to the expense of the project. De Kreuk and Hanstveit¹¹ found that, although continuous flow systems appeared theoretically to be a better approach to replicating the real environment, test results obtained in both systems were very similar. The choice between the systems for them was guided on the basis of the relative simplicity of the method or the requirements dictated by the analytical procedures.

Biodegradation Techniques

Although biochemical oxygen demand,¹⁷ manometric respirometry, as well as the increase in optical density of a fat soluble dye¹⁵ have been used to measure hydrocarbon degradation, the most common techniques are the direct measurement of hydrocarbon loss, usually using gas liquid chromatography as the analytical technique, or the measurement of carbon dioxide evolution, often using a ¹⁴C-labeled compound.

Direct measurement of hydrocarbon loss involves the inoculation of the culture or microcosm with a hydrocarbon or hydrocarbon mix and subsequent measurement of changes in concentration with time. If samples are repeatedly taken from the same culture vessel, Mrsny et al.¹⁸ recommended the addition of a non-biodegradable internal standard, hexachloroethane, to correct for

sampling error. Prior to analysis the hydrocarbons are extracted from the water medium with hexane,¹⁹ diethyl ether,²⁰ carbon tetrachloride,²¹ or Freon 113.²² The extracts are concentrated, dried and either directly subjected to analysis by gas chromatography or other appropriate techniques, or a further separation may be used prior to analysis. Horowitz and Atlas¹⁶ used a silica-alumina gel column to separate the hydrocarbons from Prudhoe crude oil into saturates, monoaromatics, diaromatics and polycyclic aromatic fractions. Atlas et al.²³ used a mixture of methylene chloride and methanol (9:1) to extract oil hydrocarbons from sediments and subsequently fractionated the extract into aliphatic and aromatic fractions in an silica-alumina gel column using hexane and hexane-methylene chloride elutants.

The advantage of using chemical analysis lies in its directness of approach. Change in the absolute concentration can be measured, and if there are metabolic by-products, they can be quantified and identified if necessary. The technique is also amendable to the use of hydrocarbon mixes such as jet fuels, and if the analytical technique is sufficiently sensitive, degradation rates can be simultaneously obtained for each compound within the mix.

The problems with the technique are those related to the sensitivity of the analytical techniques involved. Biologically significant concentrations of hydrocarbons may be less than 100 ug/l and the normal lower limits of detection of gas chromatography may be 4 to 10 times higher. Some concentration step is usually necessary which adds to the time of analysis and to the variability of the results. As a considerable amount of hydrocarbon will be necessary for analysis, either whole microcosms would have to be sacrificed or large containers used to accommodate repeated sampling. Interference of hydrocarbons present initially in the sample or those produced by the organisms themselves may also be a problem.

The measurement of carbon dioxide release represents a measure of the complete degradation of the original compound to carbon dioxide and water, not just the loss of the original compound,²⁴. This distinction is important because (1) CO₂ release is not necessarily related to the original substrate degradation by a 1:1 relationship, as the method does not account for the

production of other non-biodegradable metabolic by-products or incorporation of the labeled carbon into cellular material (yield), and (2) the loss of the original substrate does not necessarily mean that all toxic forms have been removed. The metabolic breakdown products may be more toxic than the original substrate. Both breakdown rate of the original substrate and the evolution of CO₂ are important and not necessarily correlated measurements.

In measuring CO₂ evolution, a ¹⁴C-labeled substrate is often used. The technique involves the injection of the labeled substrate into a culture vessel or microcosm, and, after a time, the sacrifice of the culture and the subsequent counting by liquid scintillation of the radioactivity of the labeled CO₂ produced, and, in some cases the radioactivity of all the components of the system. Usually a control, killed by sterilization, formaldehyde, or mercuric chloride, is used to measure volatilization losses and abiotic uptake of the compound. Often the experiments are performed in sealed containers, and no volatilization is permitted. In these cases, the rates obtained represent biodegradation only, and not rates of total loss found in open containers. Carbon dioxide is captured in KOH, NaOH, phenethylamine,^{17,25,26,27} hyamine hydroxide,²⁰ ethanalamine,²⁸ ethanalamine and methanol,²⁹ or Oxiflor-CO₂.²³ CO₂ trapping, especially with the organic solvents, may also capture volatilized initial substrates or metabolic by-products. This possibility is either corrected using the measurement of apparent CO₂ trapped in the poisoned control or the insertion of an organic trap such as a cold Tenax column³⁹ or XAD resin,¹² or a vial containing a toluene or xylene base scintillation cocktail.²⁶ Removal of the CO₂ from the culture usually is accomplished by the addition of a small amount of acid, but Walker and Colwell²⁷ found that acidification caused the release of the label from the cells. Rather than acidification, stripping the CO₂ from the water with nitrogen gas³⁰ or air^{12,25} may be a more benign removal technique. The technique of air stripping of CO₂ also allows for continual CO₂ measurements without the sacrifice of the culture.

If other radioactive system components are counted, this is usually accomplished by extraction of the remaining hydrocarbons and the subsequent measurement of the radioactivity in the extract. Hexane or diethyl ether are

commonly used as a solvent,^{16,27} although ethyl acetate²⁴ has been used. Herbes and Schwall¹⁰ first used acetone to extract the labeled compounds from sediments and then combusted the sediments to obtain a bound-¹⁴C fraction. They used thin layer silica gel chromatography on the acetone extract to separate polar ¹⁴C compounds from the unaltered substrates. Herbes et al.²⁴ and Herbes and Schwall¹⁰ used silica gel column chromatography on ethyl acetate extracts evaporated to near dryness and subsequently redissolved in benzene to separate metabolites from unaltered PAH substrates.

There are several advantages to using a radio-labeled substrate.

1. Using labeled compounds with high specific activities, very small concentrations of the hydrocarbon can be detected without the analytical problems associated with direct chemical analysis.
2. Compounds can be added and detected at levels that would actually be found in the environment. There is no need to use high concentrations simply to make the procedure analytically tractable. High concentrations may activate dormant bacteria, be toxic, or mask cometabolic reactions,³¹ and should be avoided if the concentrations would not be found in either natural or spill conditions.
3. As only the original compound and its metabolic by-products will be labeled, the fate of the compound can be traced throughout the system without interference from naturally occurring hydrocarbons.
4. If parts of the system, including outputs, are sampled, a mass balance can be calculated, identifying both problems of technique and ultimate fate of the compound.
5. The sensitivity of the technique allows the measurement of small changes in substrate or CO₂ concentrations, allowing both the study of degradation over very short intervals of time and the measurement of extremely low degradation rates.²⁴

6. Labeled CO₂ evolution avoids possible errors associated with enhancement of microbial respiration and consequent increased unlabeled CO₂ evolution by hydrocarbon addition, and, if all the labeled CO₂ is driven from the water by acidification or air stripping, problems related to CO₂ incorporation into the bicarbonate system.³²

The technique does have some drawbacks.

1. As compounds can only be individually labeled and each is labeled with ¹⁴C, the degradation of only one compound can be studied at a time, although it should be possible to study its degradation within a hydrocarbon mix.

2. As the ¹⁴C atom occupies a specific site on the hydrocarbon molecule, the apparent degradation of the molecule will be a function of the ease with which that labeled location on the molecule comes under enzymatic attack.³⁰ The substrate-CO₂ balance could give the impression that the compound was completely degraded while in truth its breakdown products could still be within the system.

3. Because the labeled carbon can be incorporated into bacterial cellular material and the ¹⁴CO₂ can be taken up by algae, the tracer can remain in the system long after the original substrate is degraded and its metabolic by-products metabolized. This could give a false impression of resistance to degradation.

The Units of Degradation

One of the most frustrating aspects of this review was the impossibility of comparing degradation rates gathered in separate studies. This is largely because of a lack of uniformity in the units used to report degradation rates. Below are the enumerated and evaluated the units commonly used.

1. "Amount/unit volume/time" is a commonly used unit, especially when the methodology involves direct analysis of the hydrocarbon loss. A similar measure is "Amount/time" which is more an indicator of how fast an initial

dose or spill would last in the environment. These units assume a linear (zero-order) decrease in concentration with time. This assumption may be incorrect except at higher hydrocarbon concentrations and probably incorrect at concentrations of biological interest. If incorrect, the error will be greatest at the lower concentrations where the accuracy is necessary.

2. A variation of #1 is the use of the fraction degraded or the percent degraded per time. This is computed using the initial and final hydrocarbon concentrations, or the fraction of the initial labeled substrate evolved as labeled¹⁴ CO₂ at the termination of the experiment, or it may be a least square fit from a series of measurements over time. When the percentage is calculated using only initial and final values, a zero-order decay is still being assumed. As shown by Walker et al.³³ this assumption may be correct for saturated hydrocarbons, as least at the concentrations that he was using.

3. Degradation potential or heterotrophic potential are terms commonly used to report degradation as the percentage of radioactivity in the original substrate that is recovered as CO₂. As mentioned in a previous section CO₂ evolution is not necessarily a measure of substrate loss, although it is sometimes reported as such. Only Button et al.³⁰ have compensated for cellular incorporation in order to use CO₂ data to calculate substrate loss.

4. If degradation rates are assumed or found to be substrate concentration dependent, then a first-order decay rate is used. The rate constant (1/time) is reported in the same units as #2, but the decrease in concentration is assumed to be exponential. Some papers reported degradation rates in terms of half-life, the time necessary for one-half of the original substrate to be degraded.

5. The fraction of original substrate degraded per unit time is termed turnover rate.³⁴ Both uptake rate and substrate concentration affect turnover rates,³⁵ but it is a convenient measure if the naturally occurring concentration cannot be determined. The inverse of turnover rate is termed turnover time. Uptake rate (or negative degradation rate) is calculated by multiplying the turnover time by the concentration. If the labeled substrate is added in

very small quantities relative to the naturally occurring substrate, the natural uptake rate and the natural turnover times can be calculated.³⁵ In the case of hydrocarbon additions, the naturally occurring concentrations may not be a significant consideration except in polluted areas, and degradation rates could be calculated using only the added concentrations.

6. Since the degradation rate should be a function of the number or activity of the bacteria in the environment, it is quite possible that the degradation rate is second-order rather than first-order decay. If the incubation time is short relative to the growth rate of the bacteria, the number of bacteria may be relatively constant and a first-order rate may be obtained. In this case, the degradation rate obtained will be dependent on the number of bacteria present, and the rate constant should be standardized to the number of degraders present, termed the specific degradation rate. Paris et al.³⁶ have shown that the use of the specific degradation rate can produce similar decomposition rates over widely varying first-order constants. The use of these units assumes that an accurate method exists to quantify the number of degraders present.

7. Kinetic models assume that degradation rate is dependent on the concentration of the substrate relative to the uptake abilities of the bacteria. Bacterial uptake and growth is often represented by a Monod equation, and the kinetic variables measured are V_{max} , the maximum uptake rate, and k_s , the concentration of substrate at $1/2 V_{max}$. Paris et al.³⁶ have shown that at substrate concentrations less than k_s , uptake is a linear function of concentration, and a second order decay rate should be expected, which would produce a pseudo-first-order decay constant if the bacteria numbers are constant. At concentrations greater than k_s , the decay will be zero-order with respect to substrate concentration if the bacterial numbers are constant. Obtaining kinetic parameters requires the calculation of uptake or degradation at several substrate concentrations. The validity of the use of kinetic variables obtained from mixed bacterial populations has been questioned.³⁷

8. Representing the decomposition rate from cultures containing sediments is a special problem. Roubal and Atlas²⁰ added volumetric amounts of diluted

sediments to their culture vessels as did Wyndham and Costerton²⁹. Wyndham and Costerton²⁹ reported their results as ug degraded/ml of sediment/day. Herbes and Schwall¹⁰ reported PAH degradation in sediments as rate constants (1/hr), turnover time (hr) (both of which are dependent on the concentration of sediment used), and transformation rate (ug PAH degraded/gm sediment/hr). Representation of rates per gram sediment may not be appropriate unless the sediments are completely stirred. If the sediments are allowed to settle, only a small fraction of the sediments will actually be in contact with the hydrocarbons and the degradation rate will be underestimated. In this case, representation of the rates on an areal basis (amt degraded/cm² of sediment/time) would seem more appropriate.

All of the above units and more are found in the degradation literature, making comparison of rates between studies impossible. Certainly each study had its own objectives and therefore used appropriate techniques and terminology, but the lack of conformity has led to duplication of effort. Some possibilities do exist to bring about some conformity.

1. As CO₂ evolution is not necessarily equivalent to substrate loss, both should be measured. If only CO₂ is measured, the results should be corrected for non-CO₂ losses if the data is used to represent degradation rate.

2. Degradation rate will probably be a function of substrate concentration and bacterial numbers, and a second-order decomposition model should be assumed unless demonstrated otherwise. Results should be standardized to the number of degraders present.

3. Because of the non-linearity of uptake kinetics, the degradation rate per bacterium may be zero-order at high concentrations, changing to first-order as the concentration falls below k_s . Obtaining kinetic parameters would be desirable, but the necessity of using several substrate concentrations for each compound would make the work difficult, unless k_m and V_{max} can be calculated from time course data.³⁸

4. The introduction of spilled hydrocarbons will be largely a surface phenomenon. No matter where the point of entry, the majority of the fuel will

be at the water surface. An areal rather than volumetric degradation rate may be appropriate. If settled sediments or intact cores are used, again an areal representation of degradation could be used.

Probably no single unit of degradation will be appropriate in every study, but units should be used that could be utilized in a degradation model. If rate constants were used, comparisons could be made not only with other degradation studies but also with studies of volatilization and sorption losses. It is quite possible that different models are appropriate for different hydrocarbons.³³

Enumeration of Microorganisms

If it is necessary to obtain decomposition rates specific to the number of active degrading bacteria, then sensitive and accurate estimates of bacterial numbers are needed. Various techniques are used to enumerate the bacteria responsible for hydrocarbon degradation. It has been suggested that the ratio of hydrocarbon degraders to total heterotrophs is a better indicator of the hydrocarbon pollution in any environment than is the count of hydrogen degraders alone,³⁹ and usually both total heterotrophic bacteria and hydrocarbon-degrading bacteria are counted.

Total heterotrophic bacteria are usually enumerated with a plate count method using a wide variety of freshwater and marine media. Most probable number (MPN) techniques are occasionally used. Because of the selective nature of plate culturing, alternative techniques such as direct counting using epifluorescence have been recommended.⁴⁰ Epifluorescence counts however do not distinguish between living, dormant, and dead bacteria,³⁵ and autoradiography could be combined with the counts to determine activity.⁴¹

Hydrocarbon degrading bacteria are usually enumerated using a plate count technique in which a specific hydrocarbon or hydrocarbon mixture has been added as the sole carbon source. Recently a MPN technique using radiolabeled hydrocarbon substrates has been tried.^{20,29} The labeled $^{14}\text{CO}_2$ evolved is used

as the indicator of bacterial activity. Lehmicke et al.³¹ advocate this technique because it uses substrate concentrations much closer to natural levels, thus avoiding errors associated with high substrate levels such as toxicity, or the activation of dormant bacteria or enzymes. The technique, however, is specific to the one labeled substrate, and could be difficult to use in a mix unless the single labeled compound was an adequate indicator of bacterial activity on the total hydrocarbon mix or unless a number of labeled compounds were used simultaneously.

IV. FACTORS AFFECTING BIODEGRADATION

Many factors can affect degradation rates. Rates can be affected by (1) the nature and concentration of the specific hydrocarbon, (2) the species and quantity of the bacteria present in a given environment, (3) environmental factors that affect the metabolism and the growth rate of the bacteria, and (4) indirect effects such as the presence of other toxics, alternate carbon sources and cometabolic substrates. This section is a summary of some of the research related to the effect of these factors on hydrocarbon degradation.

Hydrocarbon Type and Concentration

Considerable research has been done on the relative degradability of various hydrocarbon compounds, and the bulk of this literature is not reported here. Degradability appears to be related to the cyclicity of the compound, the degree of branching, and the particular arrangement of the carbon atoms attached to a ring.

According to Bartha and Atlas⁴² the following summary can be made of the relative biodegradability of hydrocarbons.

1. n-Alkanes, especially those between C10 and C25, are the most widely and readily utilized hydrocarbons.

2. Iso-alkanes are generally degraded slower than n-alkanes, especially if branching is extensive or creates quaternary carbon atoms.

3. Olefins are less readily utilized than alkanes.

4. Low-molecular-weight aromatic hydrocarbons can be metabolized when present in low, non-toxic concentrations.

5. Polycyclic aromatic hydrocarbons are metabolized only rarely and at low rates.

6. Cycloalkanes serve as growth substrates for isolated organisms only in exceptional cases, but may be degraded by cometabolism.

This summary is illustrated by the work of Walker et al.³³ In this study it was shown that the degradability of cyclic alkanes and cyclic aromatics decreased with each additional ring on the structure. Herbes and Schwall¹⁰ found that benz(a)pyrene was degraded nearly 5,000 times slower than naphthalene in an oil-contaminated stream. In arctic marine samples, biodegradation potential of 4 ¹⁴C-labeled compounds followed the order naphthalene > hexadecane > pristane > benzantracene, with the potential for pristane and benzantracene often being zero. When nitrogen and phosphorus were added to the cultures, the order was altered to hexadecane > naphthalene >> pristane > benzantracene.²⁰ Roubal and Atlas²⁰ suggested that in the first experiments naphthalene and hexadecane degradation rates were nutrient limited, and the addition of nitrogen and phosphorus removed this limitation. They suggested that pristane and benzantracene were limited by available degradative enzyme systems and the addition of nutrients could not stimulate degradation.

When gasoline was exposed to a mixed bacterial flora for 192 hours, the highest degradation was found for benzene, ethyl benzene, toluene, and xylene, while the least degraded were iso-alkanes.²² They suggested that many of the degraded compounds may have been degraded by co-oxidation. Kappeler and Wuhrmann⁵ found that similar compounds differing only in the arrangement of the carbon atoms attached to the benzene ring could differ significantly in their degradation rates. Rates for 1,2,4, tri-methylbenzene were much higher than for 1,2,3 tri-methylbenzene or 1,3,5 tri-methylbenzene. Ortho-xylene degraded much slower than m- and p-xylene.

Degradability is also related to hydrocarbon concentration. If degradation is a first- or second-order function, then a rate changing as a function of concentration would be expected. However, at high concentrations the compounds or their metabolic intermediates may be toxic⁴² and therefore inhibit degradation. Photosynthesis in the marine diatom Cyclotella cryptica is stimulated at low concentrations of aromatics from North Sea crude oil, but is inhibited at concentrations greater than 1 mg/l.⁴³ Similar results of concentration-dependent stimulation or inhibition has been found in algae by others.^{44,45,46}

When hydrocarbon concentrations are low, biodegradation may also cease. Boethling and Alexander⁴⁷ found little degradation of 2,4-dichlorophenoxyacetate and 1-naphthyl-N-methylcarbamate occurring if the initial concentrations were less than 2-3 ug/l. McCarty et al.⁴⁸ determined the minimum concentration of acetate that would support growth to be 0.66 mg/l. Both Boethling and Alexander⁴⁷ and McCarty et al.⁴⁸ suggested that below these limiting concentrations, insufficient energy is extracted to offset these energy demands. McCarty et al.⁴⁸ suggested a compound might be degraded at concentrations below the minimum concentration if the concentration is fluctuating (non-steady state) or if the compound were degraded by cometabolism. Spain et al.⁴⁹ found that the duration of time before a given bacterial flora began to degrade p-nitrophenol was dependent on substrate concentration. At initial level below 0.43 uM, adaptation did not occur.

Number and Species of Bacteria

Over 200 species of bacteria, yeasts, and filamentous fungi have been shown to degrade one or more hydrocarbon compounds.⁵⁰ One alga, Protothoa zophi, has been shown to degrade hydrocarbons,⁵¹ but the number of reports of stimulation of algal growth^{44,46,51} when hydrocarbons are added suggest that algae may also contribute to its degradation. Algae, however, are not thought to contain the proper oxidases to permit hydrocarbon metabolism.⁵² Other organisms, zooplankton, amphipods, crabs, and fish have been shown to degrade hydrocarbons to some extent.⁵² Bacteria are probably considered to be the primary degraders of hydrocarbons not only because of their heterotrophic

existence, but also because of their high surface area relative to their volume.

Not all bacteria degrade hydrocarbons. The most common genera of hydrocarbon-degraders are Pseudomonas, Achromobacter, Arthrobacter, Micrococcus, Nocardia, Vibrio, Acinetobacter, Brevibacterium, Corynebacterium, and Flavobacterium.⁴² Each species may not be able to degrade all hydrocarbon compounds. Nocardia is probably responsible for n-alkane degradation while Pseudomonas degrades aromatics.²² Jamison et al.²² reported that gasoline could only be completely degraded by a mixed bacterial flora, not by isolated species. Similarly, Kappeler and Wuhmann⁵ found that 12 out of 30 isolated bacterial strains degraded gas-oil, but also found that there were only 4 metabolically different strains represented in those 12 species. Complete degradation of the gas-oil required the combined presence of 3 or those 4 strains.

The rate at which a hydrocarbon will disappear in a given environment will depend in part on the number of hydrocarbon degrading bacteria present. Identification and enumeration of all the possible hydrocarbon-degrading species would be tedious, and simpler indices have been advocated. As the isolation of hydrocarbon-degraders is possible by the plating of water samples with hydrocarbons used as the sole carbon source, it has been possible to enumerate the total number of hydrocarbon degraders without further identification. Some studies have found relationships between the number of hydrocarbon-degraders and the amount of hydrocarbons in the environment^{16,19,53} but better correlations have been found between concentration and the ratio of hydrocarbon-degraders to the total number of heterotrophic bacteria.^{39,53,54} Others have found little relationship between either total hydrocarbon degraders^{29,55} or hydrocarbon-degrader/total heterotroph ratios.^{17,56} Attempts at correlations of numbers of hydrocarbon-degraders or ratios with the heterotrophic activity have also gotten mixed results. Studies by Wyndham and Costerton,²⁹ Ward and Brock,¹⁷ Roubal and Atlas,²⁹ and Herbes⁵⁵ found no relationships, but Seki,²⁸ Caparello and LaRock,²⁵ and Walker and Colwell²⁷ did. In the study of Herbes⁵⁵ there was no relationship of heterotrophic potential with ambient PAH or with bacterial numbers, but higher degradation

rates were found at sites that were formerly polluted. He suggested that either the PAH degraders remained longer than the ambient PAH or that PAH concentrations were sufficiently high to maintain the degrading enzymes in the population. There appear to be several instances where there are higher degradation potentials in polluted environments than in pristine environments, although the difference is not seen in the number of degraders. This may be a result of the techniques used for the isolation and enumeration of these bacteria. If accurate bacterial numbers are needed to obtain number-specific degradation constants, the methodology should be examined carefully.

Prior History of Hydrocarbon Contamination

In several instances, including the findings of Herbes,⁵⁵ mentioned in the last section, there are instances where the degradation rate of hydrocarbons is higher if the environment has been previously exposed to hydrocarbons. Roubal et al.⁵⁷ reported that gasoline was not detected in the sediments 48 hours after a major gasoline spill in the Ohio River. They attributed the rapidity of the loss of gasoline to the degrading bacteria already being present because of a prior spill. The idea that degradation rate is dependent on the prior activation of hydrocarbon-degrading bacteria fits into the larger subject category of the causes of time lags in hydrocarbon degradation.

It has been noticed in a number of studies that a period of time often passes before degradation commences. This time lag may last from a few hours to a few days. According to Spain et al.⁴⁹ these lags may be the result of the time necessary to (1) induce or de-repress specific enzymes not present before exposure, (2) select new metabolic capabilities produced by genetic changes, and (3) increase the number of organisms able to catalyze a particular transformation. Caparello and LaRock²⁵ determined that the duration of the time lag was dependent on the initial size of the inoculum, although the final extent of degradation was not affected. Ward and Brock¹⁷ and Kappeler and Wuhrmann⁵⁸ observed that the initiation of decomposition commenced with the increase in bacterial numbers. Pritchard and Starr¹⁵ found that degradation of octane commenced when one bacterial species comprised 90 percent of the total bacterial numbers. Spain et al.⁴⁹ found that adaptation (a change

in degradation rate) would not occur if the substrate were below some threshold concentration, or if the proper bacteria were not present in the environment.

The duration of time lags can be altered in a number of ways. Spain et al.⁴⁹ found that prior exposure to p-nitrophenol would significantly decrease the time lag on re-exposure to the chemical. Volatile compounds of oils are toxic, and a temperature-dependent lag period can be produced until these compounds evaporate.⁴² Soto et al.⁵⁹ demonstrated that the volatile compounds in crude oil extracts inhibited the growth of the alga, Chlamydomonas angulosa. The toxic effect was maintained as long as the culture flasks were stoppered. When unstoppered, the toxics evaporated and algal growth commenced.

The effect of other organic substrates on time lags is more difficult to interpret. Ward and Brock¹⁷ found that the addition of glucose prolonged the time before hexadecane was degraded. When the glucose was consumed, hexadecane degradation began. They suggested that hydrocarbon-degrading enzymes were suppressed during growth on a preferred substrate. In a later experiment they found that if the samples were aged to remove BOD, the time lag was shortened. Walker and Colwell²⁷ found a time lag in the uptake of glucose that they suggested was the result of the preferential utilization of hydrocarbons before switching to alternate substrates. Gusev et al.²¹ found that the addition of glucose to diesel fuel extracts shortened the time lag for diesel fuel degradation, but had no effect on the degradation rate of diesel fuel. Both substrates were utilized simultaneously.

Nutrient Limitation

Since the work of Atlas and Bartha⁶⁰ it has been generally recognized that the addition of nitrogen and phosphorus will often stimulate the degradation rate of hydrocarbons.³² Nitrogen and phosphorus concentrations are the most significant factor in degradation of diesel oil.²¹ Horowitz and Atlas¹⁶ found that nitrogen and phosphorus additions gave 10 percent higher losses of crude oil than did the control, but if oleophilic fertilizers (paraffinized urea and octyl-phosphate) were used, a 15 percent higher degradation loss was obtained.

Dibble and Bartha¹⁹ have shown that the addition of iron together with nitrogen and phosphorus further stimulated degradation, but only in clean, iron-depleted waters. They also found that degradation was largely restricted to the n-alkane peaks if only nitrogen and phosphorus were added, but if iron were also supplemented, the unresolved envelope was also degraded. This may mean that only some of the bacterial species were iron-limited, but the activity of these species was necessary for the complete degradation of the oil.

In a detailed study of the nutrient limitation of hexadecane and mineral oil degradation in Wisconsin lakes, Ward and Brock¹⁷ found that nitrogen and phosphorus additions stimulated degradation rates in all of the nutrient-poor lakes studied. Degradation rate was a hyperbolic function of phosphorus concentration. Half-saturation concentrations for growth rates on mineral oil and hexadecane were approximately 20 ug of phosphorus and 50 ug of nitrogen per liter. They suggested that nutrient limitation of biodegradation is a widespread occurrence in freshwater systems.

A distinct seasonal pattern of degradation rate that suggests the dual control of temperature and nutrient limitation has also been noted.^{11,17} Decomposition rates are typically low in the winter, rising as the temperature increases in the spring. In mid-summer degradation rates decrease, following drops in soluble nitrogen and phosphorus concentrations. Apparently from mid-July to late fall, degradation rate is limited by nutrient supply.

Limitation of biodegradation by nutrients is not only important in the actual degradation of hydrocarbons in the field, but also in the estimation of degradation rates in the laboratory. In batch systems, where nutrient inputs are absent, nutrient limitation may reach levels far above that observed in the field. The experiments performed on such system may indicate far less degradation potential than is actually found in the field. Supplementing the cultures with nitrogen and phosphorus may give an artificially high degradation potential relative to the natural system, but at least it could be used as an index of potential degradation. Approximations of real-world values might require either short-term incubations (<24 hours) or the use of large flow-through systems where the enclosure effects are minimized and natural nutrient inputs are simulated.

Temperature

As mentioned earlier, temperature can have an important seasonal effect on the biodegradation rate of hydrocarbons. As might be expected for a factor that affects metabolic activity, degradation rate increases with a rise in temperature. Atlas and Bartha⁶¹ reported that degradation rate roughly doubled with each 5°C temperature increase in the 5° to 20° range. Usually, the temperature response curve is sigmoidal, with the maximum rates being reached between 20° and 25°,^{17,62,63} although inhibition can be sometimes seen at higher temperatures.¹⁷ Ward and Brock¹⁷ found that temperature response curves were similar in both summer and winter samples, suggesting that there is little low temperature adaptation.

The percentage of the initial substrate degraded to CO₂ is also dependent on temperature. Dibble and Bartha⁶³ found that the percent of original substrate (oil sludge) evolved as CO₂ increased as a function of temperature, but Walker and Colwell²⁷ found that although the percentage of hexadecane degraded increased with temperature, the fraction converted to CO₂ decreased. Increased time lags at low temperatures have also been described.^{17,61,63} Atlas and Bartha⁶¹ showed that the lag periods were caused by inhibitory volatile components in crude oil and that volatilization rates of these toxics were less at lower temperatures.

pH

It is generally believed that there is an optimum pH over and under which decomposition will decrease. Hambrick⁶⁴ found that the mineralization rates of naphthalene were highest at pH 8.0, lowest at pH 5.0. Dibble and Bartha⁶³ found that raising the pH from 5 to 7.8 increased the mineralization rate of oil sludge. One could conclude from studies such as these that the lowest degradation rates might be found in acid environments such as strip-mine impoundments, bogs, and poorly buffered lakes stressed by acid rain. The accuracy of this conclusion depends on the assumption that no adaptation or species replacements occur in low pH environments. My laboratory has isolated species of algae that grow at pH 3.2 as rapidly as the bioassay organism,

Selanastrum capricornutum does at pH 7. This suggests that producing pH curves from samples taken from one environment should not be used to predict the degradation rates in environments of different pHs. In-situ studies within each environment may be a better approach.

Oxidation-Reduction Conditions

Most biological degradation of hydrocarbons involves metabolic reactions that require oxygen; anaerobic degradation is negligible.⁴² Hambrick et al.⁶⁴ found decreasing rates of decomposition of naphthalene and octadecane as the Eh values decreased. If hydrocarbons are somehow displaced into anaerobic hypolimnia or sediments, they probably will not be degraded further. During periods of turnover in lakes, both the hypolimnetic waters and sediments could be mixed with oxygenated waters, releasing the hydrocarbons for further degradation. With each seasonal mixing event, further release and degradation would occur, producing an "echo effect" (A. Carlson, personal communication).

Salinity

Few papers have been written on the biodegradation of hydrocarbons in freshwater,¹⁷ and even fewer have examined rates as a function of the salinity of the parent environment. Ward and Brock⁶⁵ showed that the degradation of hexadecane and mineral oil decreased with increasing salinity in the Great Salt Lake; however their lower salinity was greater than the salinity of the oceans. Caparello and LaRock²⁵ reported hexadecane mineralization in freshwater samples to be greater than in estuarine and marine samples. Spain et al.⁴⁹ found that a riverine sediment degraded p-nitrophenol much faster than an estuarine sediment. They suggested that the differences were not so much the effect of salinity itself as much as the degrading ability of the natural flora. One study¹¹ found the relative rates of degradation in marine or freshwater environments to be dependent on the compound.

V. ULTIMATE FATE

Many factors, both abiotic and biotic, can affect biodegradation rates of hydrocarbons. The environments where biodegradation rates are potentially the

lowest can be approximated by superimposing each of factors that have been reviewed here. Degradation would be low in environments where there are few degrading organisms (which may be related to the lack of prior exposure to spills), high salinities, and cold temperatures. Such a superimposition would fit a pristine, arctic marine environment. Certainly the emphasis on possible environmental effects of oil spills in the arctic reflect such a reasoning. In temperate freshwater habitats the pristine acid bogs, as well as lakes already stressed by acid rain, may have problems degrading hydrocarbons. The interesting point of the above comparisons is that those habitats that may degrade hydrocarbons the slowest are those thought to be most ecologically susceptible to hydrocarbon toxicity.

The two other major pathways of hydrocarbon loss from the water column are volatilization and sediment sorption. Sorption by the sediments may be a complicating factor in the biodegradation of hydrocarbons. In a real sense, sediments act as competitors with the microbial flora for soluble hydrocarbons. The greater the concentration and sorption capacity of the sediments, the lower the concentration of the hydrocarbons in the water, and perhaps the greater the absolute amount of hydrocarbon that will be solubilized. As volatilization and biodegradation are concentration dependent, the net effect of sediment sorption will be a lower absolute rate of hydrocarbon loss from the water. As the hydrocarbons are lost by biodegradation and volatilization, they will be replaced to an extent by desorption from the sediments. Thus the organisms in the water will be exposed to a lower concentration than they would if sediments were not present, but the exposure will be for a longer period of time. To further complicate matters, if sediment sorption decreases the concentration below the minimum concentration for biodegradation, volatilization would be the only mode of hydrocarbon loss, further extending the exposure time of organisms to the fuel components.

It has been commonly observed that the fraction of a ^{14}C -labeled hydrocarbon that is mineralized to $^{14}\text{CO}_2$ is often much less than 100 percent. The fate of the remainder of the labeled carbon may be reversible or irreversible sorption onto the sediments, the formation of recalcitrant metabolic intermediates, or incorporation into cellular carbon. In an open system the

eventual loss of the material as CO₂ would be expected, but the studies so far reveal that these bound materials or metabolic intermediates are not easily metabolized. It may be that the hydrocarbons or their metabolic by-products, once spilled, will be around for a long time.

VI. RECOMMENDATIONS

As no research has been done so far by the Air Force in the area of the biodegradation of jet fuel components, certain priorities can be set based on existing knowledge of hydrocarbon biodegradation. The following research concerns could be considered.

1. Biological effect rather than analytical limitations must set the minimum hydrocarbon concentrations to which their biodegradation is observed. If such concentrations cannot be ascertained from existing research, then sensitive and unambiguous measures of effect should be developed.

2. The importance of biodegradation should be studied in relation to losses by volatilization. If biodegradation of hydrocarbons cannot be shown to contribute significantly to fuel component losses, it may cease to be a research concern of the Air Force.

3. The possible persistence of certain fuel components or their metabolic by-products weeks or even months after the initial spill should be investigated. The location and chemical characterization of these compounds should be studied, as well as their toxicological importance. The possible interaction with sediment sorption may play a role in the persistence of these compounds.

4. Previous experiments have been performed in the laboratory on relatively few environments. The findings of any laboratory studies should be tested in much larger field enclosures where a more complex interaction with the natural biota can be simulated. I value the use of large enclosures over the use of an entire pond, because enclosures can mimic most of the responses

of the pond, but allow replication. Enclosures can also be utilized on several types of environments, whereas the use of ponds limits the extrapolation of data to other environments.

5. Biodegradation rates have been shown to be a function of many factors. Extrapolation from a few laboratory studies to all the possible natural environments would be unwise. Manipulation of temperature, pH, or other variables on microbial samples from a single environment may produce response curves that bear little resemblance to the response of a microbial community taken from environments where those extreme conditions actually exist. An abbreviated methodology such as heterotrophic potential could be used to rapidly census a number of environments for their relative degradation rates. Special attention should be given to small, freshwater habitats because their small size relative to the size of a spill makes them more susceptible to fuel effects.

REFERENCES

1. G.L. Baughman and D.F. Paris, "Microbial Bioconcentration of Organic Pollutants from Aquatic Systems - A Critical Review," Crit. Rev. in Microbiol., Vol. 8, pp. 205-228, 1981.
2. C.E. ZoBell, "Microbial Degradation of Oil: Present Status, Problems, and Perspectives," The Microbial Degradation of Oil Pollutants, D.G. Ahearn and S.P. Meyers, Eds., Center for Wetland Resources, Louisiana State University Publ. No. LSU-SG-73-01, pp. 3-16, 1973.
3. G.D. Floodgate, "A Threnody Concerning the Biodegradation of Oil in Natural Waters," The Microbial Degradation of Oil Pollutants, D.G. Ahearn and S.P. Meyers, Eds., Center for Wetland Resources, Louisiana State University Publ. No. LSU-SG-73-01, pp. 17-24, 1973.
4. F. Matsumura, "Task Group IV: Microcosms," Microbial Degradation of Pollutants in Marine Environments, A.W. Bourquin and P.H. Pritchard, Eds., U.S. Environmental Protection Agency Publ. No. EPA-600/9-79-012, pp. 520-524, 1979.
5. Th. Kappeler and K. Wuhrmann, "Microbial Degradation of the Water-Soluble Fraction of Gas Oil - II. Bioassays with Pure Strains," Water Res., Vol. 12, pp. 335-342, 1978.
6. J.H. Slater, "Microbial Community Structure," Microbial Degradation of Pollutants in Marine Environments, A.W. Bourquin and P.H. Pritchard, Eds., U.S. Environmental Protection Agency Publ. No. EPA-600/9-79-012, pp. 283-295, 1979.
7. J. Ringelberg and K. Kersting, "Properties of an Aquatic Micro-Ecosystem: I. General Introduction to the Prototypes," Arch. Hydrobiol., Vol. 83, pp. 47-68, 1978.
8. G.D. Cooke, "The Pattern of Autotrophic Succession in Laboratory Microcosms," BioScience, Vol. 17, pp. 717-721, 1967.

9. J.M. Giddings, B.T. Walton, G.K. Eddlemon, and K.G. Olson, "Transport and Fate of Anthracene in Aquatic Microcosms," Microbial Degradation of Pollutants in Marine Environments, A.W. Bourquin and P.H. Pritchard, Eds., U.S. Environmental Protection Agency Publ. No. EPA-600/9-79-012, pp. 312-320, 1979.
10. S.E. Herbes and L.R. Schwall, "Microbial Transformation of Polycyclic Aromatic Hydrocarbons in Pristine and Petroleum-Contaminated Sediments," Appl. Environ. Microbiol., Vol. 35, pp. 306-316, 1978.
11. S.F. de Kreuk and A.O. Hanstvert, "Determination of the Biodegradability of the Organic Fraction of Chemical Wastes," Chemosphere, Vol. 10, pp. 561-573, 1981.
12. A.W. Bourquin, R.L. Garnas, P.H. Pritchard, F.G. Wilkes, C.R. Cripe, and N.I. Rubinstein, "Interdependent Microcosms for the Assessment of Pollutants in the Marine Environment," Intern. J. Environmental Studies, Vol. 13, pp. 131-140, 1979.
13. P.H. Pritchard, A.W. Bourquin, H.L. Frederickson, and T. Maziarz, "System Design Factors Affecting Environmental Fate Studies in Microcosms," Microbial Degradation of Pollutants in Marine Environments, A.W. Bourquin and P.H. Pritchard, Eds., U.S. Environmental Protection Agency Publ. No. EPA 600/9-79-012, pp. 251-272, 1979.
14. A.W. Bourquin, M.A. Hood, and R.L. Garnas, "An Artificial Microbial System for Determining Effects and Fate of Toxicants in a Salt-Marsh Environment," Dev. Ind. Microbiol., Vol. 18, pp. 185-191, 1977.
15. P.H. Pritchard and T.J. Starr, "Microbial Degradation of Oil and Hydrocarbons in Continuous Culture," The Microbial Degradation of Oil Pollutants, D.G. Ahearn and S.P. Meyers, Eds., Center for Wetland Resources, Louisiana State University Publ. No. LSU-SG-73-01, pp. 39-45, 1973.

16. A. Horowitz and R.M. Atlas, "Continuous Open Flow-Through System as a Model for Oil Degradation in the Arctic Ocean," Appl. Environ. Microbiol., Vol. 33, pp. 647-653, 1977.
17. D.M. Ward and T.D. Brock, "Environmental Factors Influencing the Rate of Hydrocarbon Oxidation in Temperate Lakes," Appl. Environ. Microbiol., Vol. 31, pp. 764-772, 1976.
18. R.J. Mersny, R.W. Barles, D. Chin, K.C. Enevold, B.R. Thomas, and M.L. Wheelis, "Use of an Internal Standard in Monitoring the Bacterial Degradation of Crude Oil," Appl. Environ. Microbiol., Vol. 36, pp. 776-779, 1978.
19. J.T. Dibble and R. Bartha, "The Effect of Iron on the Biodegradation of Petroleum in Seawater," Appl. Environ. Microbiol., Vol. 31, pp. 544-550, 1976.
20. G. Roubal and R.M. Atlas, "Distribution of Hydrocarbon-Utilizing Microorganisms and Hydrocarbon Potentials in Alaskan Continental Shelf Areas," Appl. Environ. Microbiol., Vol. 35, pp. 897-905, 1978.
21. M.V. Gusev, T.V. Koronelli, V.N. Maximov, V.V. Il'inskii, and V.T. Zakharov, "Study of Microbiological Oxidation of Diesel Fuel Using the Method of a Complete Factorial Experiment," Mykrobiologiya, Vol. 49, pp. 25-30, 1980.
22. V.W. Jamison, R.L. Raymond, and J.O. Hudson, "Biodegradation of High Octane Gasoline," Proc. 3rd International Biodegradation Symposium, J.M. Sharpley and A.M. Kaplen, Eds., Appl. Sci. Publ., pp. 187-196, 1976.
23. R.M. Atlas, P.D. Boehm, and J.A. Calder, "Chemical and Biological Weathering of Oil, From the Amoco Cadiz Spillage, Within the Littoral Zone," Estuarine and Coastal Mar. Sci., In Press, 1981.

24. S.E. Herbes, L.R. Schwall, and G.A. Williams, "Rate of Microbial Transformation of Polycyclic Aromatic Hydrocarbons: A Chromatographic Qualification Procedure," Appl. Environ. Microbiol., Vol. 34, pp. 244-246, 1977.
25. D.M. Caparello and P.A. LaRock, "A Radioisotope Assay for the Quantification of Hydrocarbon Biodegradation Potential in Environmental Samples," Microb. Ecol., Vol. 2, pp. 28-42, 1975.
26. A.C. Marinucci and R. Bartha, "Apparatus for Monitoring the Mineralization of Volatile ^{14}C -Labeled Compounds," Appl. Environ. Microbiol., Vol. 38, pp. 1020-1022, 1979.
27. J.D. Walker and R.R. Colwell, "Measuring the Potential Activity of Hydrocarbon Degrading Bacteria," Appl. Environ. Microbiol., Vol. 31, pp. 189-197, 1976.
28. H. Seki, "Method for Estimating the Decomposition of Hexadecane in the Marine Environment," Appl. Environ. Microbiol., Vol. 31, pp. 439-441, 1976.
29. R.C. Wyndham and J.W. Costerton, "Heterotrophic Potentials and Hydrocarbon Biodegradation Potentials of Sediment Microorganisms Within the Athabasca Oil Sands Deposit," Appl. Environ. Microbiol., Vol. 41, pp. 783-790, 1981.
30. D.K. Button, D.M. Schell, B.R. Roberson, "Sensitive and Accurate Methodology for Measuring the Kinetics of Concentration-Dependent Hydrocarbon Metabolism Rates in Seawater by Microbial Communities," Appl. Environ. Microbiol., Vol. 41, pp. 936-941, 1981.
31. L.G. Lehmicke, R.J. Williams, and R.L. Crawford, " ^{14}C -Most-Probable-Number Method for Enumeration of Active Heterotrophic Microorganisms in Natural Waters," Appl. Environ. Microbiol., Vol. 38, pp. 644-649, 1979.

32. G.D. Floodgate, "Nutrient Limitation," Microbial Degradation of Pollutants in Marine Environments, A.W. Bourquin and P.H. Pritchard, Eds., U.S. Environmental Protection Agency Publ. No. EPA-600/9-79-102, pp. 107-118, 1979.
33. J.D. Walker, R.R. Colwell, and L. Petrarkis, "Biodegradation Rates of Compounds of Petroleum," Can. J. Microbiol., Vol. 22, pp. 1209-1213, 1976.
34. E.P. Odum, Fundamentals of Ecology, 3rd Ed., Philadelphia, Penn., W.B. Saunders Co., 1971.
35. R.T. Wright, "Measurement and Significance of Specific Activity in the Heterotrophic Bacteria of Natural Waters," Appl. Environ. Microbiol., Vol. 36, pp. 297-305, 1978.
36. D.F. Paris, W.C. Steen, G.L. Baughman, and J.T. Barnett Jr., "Second Order Model to Predict Microbial Degradation of Organic Compounds in Natural Waters," Appl. Environ. Microbiol., Vol. 41, pp. 603-609, 1981.
37. F. Azam and O. Holm-Hansen, "Use of Tritiated Substrates in the Study of Heterotrophy in Seawater," Mar. Biol., Vol. 23, pp. 191-196, 1973.
38. G.H.M. Counotte and R.A. Prins, "Calculations of K_m and V_{max} from Substrate Concentration Versus Time Plot," Appl. Environ. Microbiol., Vol. 38, pp. 758-760, 1979.
39. J.D. Walker and R.R. Colwell, "Enumeration of Petroleum-Degrading Microorganisms," Appl. Environ. Microbiol., Vol. 31, pp. 198-207, 1976.
40. S.E. Hobbie, R.J. Daley, and S. Jasper, "Use of Nucleopore Filters for Counting Bacteria by Fluorescence Microscopy," Appl. Environ. Microbiol., Vol. 33, pp. 1225-1228, 1977.

41. L. Meyer-Reil, "Autoradiography and Epifluorescence Microscopy Combined for the Determination of Number and Spectrum of Actively Metabolising Bacteria in Natural Waters," Appl. Environ. Microbiol., Vol. 36, pp. 506-512, 1978.
42. R. Bartha and R.M. Atlas, "The Microbiology of Oil Spills," Adv. Appl. Microbiol., Vol. 22, pp. 225-266, 1977.
43. M. Karydis and G.E. Fogg, "Physiological Effects of Hydrocarbons on the Marine Diatom Cyclotella cryptica," Microb. Ecol., Vol. 6, pp. 281-290, 1980.
44. W.M. Dunstan, L.P. Atkinson, and J. Natoli, "Stimulation and Inhibition of Phytoplankton Growth by Low Molecular Weight Hydrocarbons," Mar. Biol., Vol. 31, pp. 305-310, 1975.
45. T.L. Butl and K. Rogenmuser, "Effects of No. 2 Fuel Oil, Nigerian Crude Oil, and Used Crankcase Oil on Attached Algal Communities: Acute and Chronic Toxicity of Water-Soluble Constituents," Appl. Environ. Microbiol., Vol. 36, pp. 673-682, 1978.
46. T.R. Parsons, W. Li, and R. Waters, "Some Preliminary Observations on the Enhancement of Phytoplankton Growth by Low Levels of Mineral Hydrocarbons," Hydrobiologia, Vol. 51, pp. 85-89, 1976.
47. R.S. Boethling and M. Alexander, "Effect of Concentration of Organic Chemicals on Their Biodegradation by Natural Microbial Communities," Appl. Environ. Microbiol., Vol. 37, pp. 1211-1216, 1979.
48. P.L. McCarty, R. Reinhard, and B.E. Rittmann, "Trace Organics in Groundwater," Environ. Sci. and Technol., Vol. 15, pp. 40-51, 1981.
49. J.C. Spain, P.H. Pritchard, and A.W. Bourquin, "Effects of Adaptation on Biodegradation Rates in Sediment/Water Cores From Estuarine and Freshwater Environments," Appl. Environ. Microbiol., Vol. 40, pp. 726-734, 1980.

50. R.E. Jordan and J.R. Payne, Fate and Weathering of Petroleum Spills in the Marine Environment, Ann Arbor, Michigan, Ann Arbor Science Publishers, 1980.
51. M.J. Masters and J.E. Zajic, "Myxotrophic Growth of Algae on Hydrocarbon Substrates," Dev. Ind. Microbiol., Vol. 12, pp. 77-86, 1971.
52. U. Varanasi and D.C. Malins, "Metabolism of Petroleum Hydrocarbons: Accumulation and Biotransformation in Marine Organisms," Effects of Petroleum on Arctic and Subarctic Marine Environments and Organisms, Vol. II. Biological Effects, D.C. Malins, Ed., New York, New York, Academic Press, 1977.
53. A. Horowitz and R.M. Atlas, "Response of Microorganisms to an Accidental Gasoline Spillage in an Arctic Freshwater Ecosystem," Appl. Environ. Microbiol., Vol. 33, pp. 1252-1258, 1977.
54. M.A. Hood, W.S. Bishop Jr., S.P. Meyers, and T. Whelan III, "Microbial Indicators of Oil-Rich Salt Marsh Sediments," Appl. Microbiol., Vol. 30, pp. 982-987, 1977.
55. S.E. Herbes, "Rates of Microbial Transformation of Polycyclic Aromatic Hydrocarbons in Water and Sediments in the Vicinity of a Coal-Coking Wastewater Discharge," Appl. Environ. Microbiol., Vol 41, pp. 20-28, 1981.
56. E.N. Buckley, R.L.B. Jonas, and Pfaender, "Characterization of Microbial Isolates from an Estuarine Ecosystem:" Relationship of Hydrocarbon Utilization to Ambient Hydrocarbon Concentrations," Appl. Environ. Microbiol., Vol. 32, pp. 232-237, 1976.
57. G. Roubal, A. Horowitz, and R.M. Atlas, "Disappearance of Hydrocarbons Following a Major Gasoline Spill in the Ohio River," Dev. Ind. Microbiol., Vol. 20, pp. 503-507, 1979.

58. Th. Kappeler and K. Wuhrmann, "Microbial Degradation of the Water-Soluble Fraction of Gas Oil - I.," Water Res., Vol. 12, pp. 327-333, 1978.
59. C. Soto, J.A. Hellebust, T.C. Hutchinson, and T. Sawa, "Effect of Naphthalene and Aqueous Crude Oil Extracts on the Green Flagellate Chlamydomonas angulosa. I. Growth," Can. J. Bot., Vol. 53, pp. 109-117, 1975.
60. R.M. Atlas and R. Bartha, "Degradation and Mineralization of Petroleum in Seawater: Limitation by Nitrogen and Phosphorus," Biotechnol. Bioeng., Vol. 14, pp. 309-318, 1972.
61. R.M. Atlas and R. Bartha, "Stimulated Biodegradation of Oil Slicks Using Oleophilic Fertilizers," Environ. Sci. Technol., Vol. 7, pp. 538-541, 1973.
62. R.M. Atlas and R. Bartha, "Biodegradation of Petroleum in Seawater at Low Temperatures," Can. J. Microbiol., Vol. 18, pp. 1851-1855, 1972.
63. C.F. Gibbs and S.J. Davis, "The Rate of Microbial Degradation of Oil in a Beach Gravel Column," Microbial Ecol., Vol. 3, pp. 55-64, 1976.
64. J.T. Dibble and R. Bartha, "The Effect of Environmental Parameters on the Biodegradation of Oil Sludge," Appl. Environ. Microbiol., Vol. 37, pp. 729-739, 1979.
65. G.A. Hambrick, R.D. DeLune, and W.H. Patrick Jr., "Effect of Estuarine Sediment pH and Oxidation-Reduction Potential on Microbial Hydrocarbon Degradation," Appl. Environ. Microbiol., Vol. 40, pp. 365-369, 1980.

1981 USAF - SCEEE SUMMER FACULTY RESEARCH PROGRAM

Sponsored by the

AIR FORCE OFFICE OF SCIENTIFIC RESEARCH

Conducted by the

SOUTHEASTERN CENTER FOR ELECTRICAL ENGINEERING EDUCATION

FINAL REPORT

ON-AXIS KALMAN TRACKING FILTER FOR H.S. VANDENBERG ARIS SYSTEMS

Prepared by: Dr. Junho Choi
Academic Rank: Assistant Professor
Department and University: Department of Electrical and Computer Engineering, Florida Institute of Technology
Research Location: Eastern Space and Missile Center Range Systems and Navigation
USAF Research Colleague: Mr. Charles D. Miller
Date: September 2, 1981
Contract No: F49620-79-C-0038

ON-AXIS KALMAN TRACKING FILTER FOR H.S. VANDENBERG ARIS SYSTEMS

by

Junho Choi

ABSTRACT

The Metric Accuracy Improvement Program (MAIP) has been rigorously studied during the last couple of decades at the Eastern Test Range, Patrick Air Force Base in Florida for the Advanced Range Instrumentation Ships (ARIS). To improve the accuracy, several approaches have been launched on a modernization program aimed at upgrading various systems such as computer hardware, calibration, timing systems, etc. In this work on-axis tracking algorithm was proposed through a several possible extended Kalman filter along with the brief review of the present tracking technique and coordinate algorithm.

Simulation was conducted on two-states Kalman filter and six-states Kalman filter to observe the feasibility of on-axis tracking purpose. Results indicate that the initializations are very important on the basis of the need for updating the measurement statistics of the maneuvering target which can effectively correct the differences between the measurement and filtering estimates.

Several areas for additional and continuing work are suggested to achieve the goals.

ACKNOWLEDGEMENTS

The author would like to thank the Air Force Systems Command, the Air Force Office of Scientific Research and the Southeastern Center for Electrical Engineering Education for providing him with the opportunity to spend a worthwhile and interesting summer at the Division of Ships Engineering, Patrick Air Force Base, Florida.

He would like to thank the people at ESMC/RSN, Technical Lab Library, and RCA for their hospitality, in particular to Charles D. Miller at RSN, Hank Henry, P. Utecht, L. Flowers and C. Welsh at RCA for their help and collaboration.

He would like to acknowledge Jay Boyd and Steve Thomas at RCA for their help in programming the simulation study during the period of this research.

Finally, the author would like to thank Mrs. Maggie Nagel for typing this report.

I. INTRODUCTION

With the extended use of overwater ranges and the emergency of a strong national space program, an urgent and continuing requirement arose for ship-based down-range instrumentation sites. In addition to the normal complement of problems associated with the establishment of land-based tracking stations, the added unknowns of platform stabilization, navigation, extreme long-distance time-correlation, etc., should be counted during the mission.

There are certain distinct advantages to be realized in the employment of the Advanced Range Instrumentation ships. A few of the more obvious benefits are ¹:

1) For purposes of increased range safety, the recovery of space vehicles is best accomplished over water.

2) The mobility of the instrumentation station allows the two distinct functions of tracking and recovery to be performed by a single vessel.

3) Since oceans cover almost 71% of the earth's surface, tracking ships can be located over a wide range of positions. It is therefore possible to incorporate a considerable degree of flexibility in mission planning and, at the same time, be assured of optimum station coverage.

4) The ability to vary the base-line geometry between pairs of tracking ships allows the test range to utilize multi-static range and range rate tracking systems which are inherently capable of providing extremely accurate target position and velocity data.

5) The political problem of establishing tracking sites on foreign soil is eliminated through the use of ships, since the use of the seas is relatively unrestricted.

The development of range instrumentation ships has been largely tied to measurement requirements of the supported user vehicle.

The USNS General H.H. Arnold and USNS General H.S. Vandenberg, operated by the Air Force Systems Command, Eastern Space and Missile

Center (ESMC), are two Advanced Range Instrumentation Ships (ARIS) designed to gather precision data on missile reentry vehicles (RV) and penetration aids with additional on-axis tracking missions.

Those ARIS systems are divided into eight major subsystems:

- 1) Radar subsystems.
- 2) Telemetry Data-Acquisition system.
- 3) Communications Subsystems.
- 4) Data handling subsystems.
- 5) Timing subsystems.
- 6) Meteorological subsystem.
- 7) Optical subsystem.

Because of the increasing speed, accuracy, and mission requirements by the users, the Metric Accuracy Improvement Program (MAIP) has been continuously launched during the last decade at ESMC, Eastern Test Range (ETR), Division of Range Systems Engineering (RSN).

When a range ship (ARIS) performs a tracking function, the most discussed problems are accuracy. The question like "Is the tracking accuracy of the shipboard tracker the same as the land-based tracker?" has been frequently asked. The answer of this question has long been in question in this particular program (MAIP). However, a remarkable progress has been achieved in this question in spite of several causing error factors such as ²:

- 1) Electromagnetic EM - Log errors due to:
 - a) Calibration errors.
 - b) Turbulence errors.
 - c) Dynamics errors.
 - d. Salinity errors.
 - e. Transmission errors generated by turbulence, ship-bottom roughness and motion factors. This causes the range-rate measurement errors.
- 2) Timing error effect.
- 3) Shipboard vibration (i.e., flexure).

4) Navigation-error problem.

5) Stabilization errors (i.e., coordinate transformations), etc.

The accuracy requirement by the users is still far-reaching in comparison with a land-based system because of those mentioned factors above.

To achieve the goals (metric accuracy requirement), several approaches have been launched on a modernization program aimed at upgrading various systems on ARIS such as the computer hardware, timing system, communication and so on.

Error models for range instrumentation ships differ from one another in form and degree of completeness. When the combined effects of errors in ship position, stabilization, and radar outputs are examined, each error source contribution to the total position tracking error depends upon the range to the target. It is thus very important to obtain the accurate position and velocity of the RV during the missions. As a part of MAIP project on H.S. Vandenberg, a feasibility study by Dr. Vemuri had been performed during the Summer 1980 and has been continued to develop the sub-optimal tracking algorithm.

Without improving the quality of data obtained on-board, the success of overall MAIP project might be jeopardized because of the creation of erroneous results and information for the users as reported in Appendix of Metric Accuracy Improvement Quarterly Report on H.S. Vandenberg on July 10, 1981 by the author.

In this context, the author of this report was asked to continue developing an optimal tracking algorithm (Kalman Tracking Filter) and simulate the algorithm to show the feasibility against the present auto-tracking system for the possible permanent software development on the new system, U1600 by Sperry.

II. OBJECTIVE

The main objective of this project was to develop an efficient radar data processing algorithm as a part of Metric Accuracy Improve-

ment Program under the development at Eastern Space and Missile Center/
Directorate of Range Systems/Ships Engineering Division.

As described in the introduction, this area represents a vital function to an automatic detection radar which provides discrimination against extraneous targets false alarms and the necessary low-bandwidth target reports and associated estimated target parameters to enable the use of the derived radar information in an overall system. Instead of pursuing the development of the suboptimal algorithm ($\alpha - \beta$ on-axis tracking algorithm), the more accessible and feasible Kalman tracking filter, to meet the future requirements without changing the major system configuration, had been developed and tested through the computer simulation. To complete this goal, several alternative features for the varying environments and demands had been suggested and derived in this report. In the computer simulation, we chose the rather simple cases, leaving the more complicated cases for later investigations.

Our specific objectives were:

- 1) To develop an efficient algorithm for the on-axis tracking purpose.
- 2) To determine the optimum methods to achieve the goals under development.
- 3) To suggest the right direction to attack the present problems in this data processing area.

It should be noted that the choice of the proper filter for a particular application is a function of the available computational resources, the number of targets expected, the target's dynamic characteristics, the parameters of the sensor radars, and system accuracy requirements.

In spite of some disadvantages of the Kalman filter tracking like computational load, this algorithm is more accessible to the future mission requirements and changing environments by modifying the algorithm such as adaptive or extended approach.

III. MATHEMATICAL FORMULATION

In an automatic detection radar system, the processing can be divided into two broad classifications -- signal processing and data processing. Signal processing is performed on a radar sweep-by-sweep basis and generally employs dedicated special purpose hardware capable of handling the high through-put data rate associated with this type of processing. The signal processor forms target reports (sometimes called plots) which are applied to the data processor where target tracks are formed. The relatively slow scan-to-scan processing is generally performed in a special purpose computer like U1600-Sperry.

When data processing is employed with continued scanning radar systems, the combination is called a Track-While-Scan (TWS) system. The data processing portion of TWS radar system performs a number of valuable functions³:

- 1) It complements the signal processing function by removing both the residual stationary clutter and the false target reports which are present at the output of any practical signal processor.
- 2) It provides a more accurate determination of the target's position and velocity vector that can be determined from single scan data.

The netting of several radars or the use of multisensor data also provides several distinct advantages such as:

- 1) Smooth out target fades.
- 2) Reduce target glint.
- 3) Minimize terrain shadowing effects, etc.

This combination of TWS single radar and netting of several radars or sensors could make a remarkable improvement in the accuracy if it could be feasible in the future.

The operation of a TWS system can be separated into the following distinct stages¹⁹:

- 1) Track initiation.
- 2) Track filtering and prediction.
- 3) Maneuver - following logic.
- 4) Correlation logic.

The development and concentration of first two steps are the main goals of this project to enhance the efficient operation of the TWS radar system through the basic steps of system analysis such as modeling, formulation, and analysis.

III. 1. Modeling:

One of the most important processes among the system analysis is the system modeling which can result in obtaining the better or worse information depending on the closeness of the model against the real system behavior. Fortunately enough, the tracking prediction and smoothing models have shown the great success in this aerospace area since Sklansky²⁰. In this section, the mathematical development of the tracking system dynamic model will be investigated in detail.

The radar system transmits a very large-amplitude and narrow-bandwidth pulsed sinusoid and received the reflected pulse energy with a total Δt seconds travel time. Since the pulse propagates at a speed of C -meters/sec. in space, the range can be easily determined by

$$X(t) = C \cdot \Delta t / 2 \quad (1)$$

For very accurate range determination, one usually makes periodic measurements of the travel time which amounts to periodically transmitting pulses every T seconds and obtaining measurements of range which are the data-processed to yield an accurate estimation of range.

If we assume that the radar moved only radially outward along the radar line of sight (boresight) so that only the single vector $X(t)$ is considered, then the motion of the reentry vehicle (RV) is assumed

to be described by Taylor series expansion at the next sampling instant, ⁴

$$X(t + T) = X(t) + T \dot{X}(t) + (T^2/2) \ddot{X}(t) \quad (2)$$

and the range rates are

$$\dot{X}(t + T) = \dot{X}(t) + T \ddot{X}(t) \quad (3)$$

and further the acceleration in case of powered flight is given by

$$\ddot{X}(t + T) = \ddot{X}(t) \quad (4)$$

In the matrix format,

$$\begin{bmatrix} \dot{X}_1 \\ \dot{X}_2 \\ \dot{X}_3 \end{bmatrix} = \begin{bmatrix} 1 & T & T^2/2 \\ 0 & 1 & T \\ 0 & 0 & 1 \end{bmatrix} \begin{bmatrix} X_1 \\ X_2 \\ X_3 \end{bmatrix} \quad (5)$$

$$\begin{aligned} \text{Where } \dot{X}_1(t) &= X(t + T) & \text{and } X_1(t) &= X(t) \\ \dot{X}_2(t) &= \dot{X}(t + T) & X_2(t) &= \dot{X}(t) \\ \dot{X}_3(t) &= \ddot{X}(t + T) & X_3(t) &= \ddot{X}(t) \end{aligned}$$

This is called a tracking equation which is the main dynamic model to be studied in this report.

To achieve the major goal of tracking accuracy, many suggestions and implementation of the above equation have been published through the filtering, smoothing, and prediction technique. Because of the tracking nature, several prediction algorithms have been developed as ¹⁹

- 1) Wiener filtering.
- 2) Fading-memory polynomial filtering.
- 3) Expanding-memory polynomial filtering.
- 4) Kalman filtering.
- 5) Bayes filtering (maximum likelihood).
- 6) Least squares filtering.
- 7) Benefict-Bordner filtering.
- 8) Lumped filtering.

The α - β filter (or g-h filter) ((1), (2), (3), (6), (7)) and Kalman and Bayes filtering ((4), (5)) will be mainly focused in this study since those techniques have been frequently adopted and used with the satisfactory performance.

1. α - β tracking filter 5, 6, 7, 8

This filter is designed to minimize the simple linear least squared error in the estimated position and velocity of a target under the assumption of a constant velocity target; thus it ends up with the suboptimal estimation. The general α - β - γ tracking and predicting equations are ⁴

$$\begin{aligned} \dot{X}_e(k) &= \dot{X}_p(k) + \alpha [X_m(k) - X_p(k)] \\ \ddot{X}_e(k) &= \ddot{X}_p(k) + \frac{\beta}{T} [X_m(k) - X_p(k)] \\ \ddot{X}_e(k) &= \ddot{X}_p(k) + \frac{2\gamma}{T^2} [X_m(k) - X_p(k)] \end{aligned} \quad (6)$$

where

$$X_p(k) = X_m(k) + TX_m(k) + \frac{T^2}{2} \ddot{X}_m(k) = \text{prediction of range}$$

$$\alpha = 1 - B^3$$

$$\beta = \frac{3}{2} (1-B)^2 (1+B) \quad (6-1)$$

$$\gamma = \frac{1}{2} (1-B)^3 \quad \text{for } 0 < B < 1.0$$

$\dot{X}_e(k)$: estimate of range

$\ddot{X}_e(k)$: estimate of range rate

$\ddot{X}_e(k)$: estimate of range acceleration

$X_m(k)$: measurement of range at time k

and if the velocity is constant (free-flight)

$$\ddot{X}_e(k) = 0$$

thus, the so-called α - β tracking equations are

$$\begin{aligned} \dot{X}_e(k) &= \dot{X}_p(k) + \alpha [X_m(k) - X_p(k)] \\ \ddot{X}_e(k) &= \ddot{X}_p(k) + \frac{\beta}{T} [X_m(k) - X_p(k)] \end{aligned} \quad (7)$$

For the critically damped case of this dynamic model, the coefficients are

$$\begin{aligned}\alpha &= 1 - B^2 \\ \beta &= (1 - B)^2 \\ B &= 0.96 - 0.992^{21}\end{aligned}\tag{8}$$

This filter has the advantage of very simple implementation using fixed parameters, and it provides good performance for non-maneuvering, constant velocity targets. Specially, if the filter parameters are adjusted for $(\beta = \alpha^2 / (2 - \alpha))$ this α - β filter provides the best transient following capability while simultaneously providing the best minimum variance estimate of position and velocity of any fixed parameter filter (steady-state Kalman filter).

The disadvantages of α - β filter is ³

- 1) Design implies a compromise between good noise smoothing operation (small α, β).
- 2) Good maneuver following capability (large α, β).

These problems can be corrected by adjusting the α, β parameters in accordance with the measured maneuver properties of the target. This approach was introduced by Singer, et al, and later Schooler, and currently Rao Vemuri is working with this approach.²²

However, in general, this α - β filter provides a poor performance against accelerating or maneuvering targets based on the land based antenna.

2. Kalman tracking filter: 9, 10, 11, 12, 13

The Kalman filter is the optimal filter for performing the tracking when the equations of target motion are known.

The quantities to be estimated by the Kalman filter are called states which describe the target dynamics in terms of the state vectors.

This state equation is driven by both the deterministic target dynamics and a random process which accounts for the inexactness of the difference equations used to describe the dynamics and to allow

for other sources of error.

The system states are observed through an observation equation which is corrupted by measurement noise. In contrast with the α - β filter, the Kalman filter accounts the perturbation (or random noise) in both tracking and observation, which is more accessible to the mobile antenna case than the fixed (or stationary) case.

The Kalman filter algorithm provides the optimal linear minimum error - variance unbiased estimate of the state of the linear (possibly time varying) dynamic system described by the state equations of the target motions. In addition, the Kalman filter algorithm also estimates the covariance matrix of the errors involved in the estimate, and hence provides a method for adapting the filter to changing target dynamics. ³

The disadvantages of this filter are

- 1) Heavy computational load.
- 2) Divergence of covariance matrix when the filter is not tuned to the proper target.

Either the dimensional reduction of the state equation, or the increase of the computational capability may solve the first problem and the better calibration may easily improve the second problem or by developing adaptive and compensation algorithm.

Because of gyro shift problems in a mobile tracking station (ARIS), periodic updating must be performed to remove position errors and calibrate the gyro drifts.

This results in attacking the major problems of Metric Accuracy Improvement Problems (MAIP) by adopting on-axis tracking technique.

Rewriting equation (5), the general random system dynamic models are:

$$\begin{bmatrix} X_1(k+1) \\ X_2(k+1) \\ X_3(k+1) \end{bmatrix} = \begin{bmatrix} 1 & T & T^2/2 \\ 0 & 1 & T \\ 0 & 0 & 1 \end{bmatrix} \begin{bmatrix} X_1(k) \\ X_2(k) \\ X_3(k) \end{bmatrix} + \Gamma w(k) \quad (9)$$

$$z(k) = [100] M(k) x(k) + Gv(k) \quad (10)$$

Where

- Γ : coefficient matrix correlated with the perturbation of each states.
- $w(k)$: additive state noise with zero mean and variance matrix R.
- $v(k)$: additive observation noise with zero mean and variance Q.
- G : coefficient of observation errors.
- M(k) : coordinate transformation matrix.

It is noted that the observation equation is different from the normal random dynamic system not only because of the free-moving platform (mobile antenna), but also because cartesian may offer the better all around solution particularly when implemented in a Kalman filter.

Many different possible approaches can be deduced from the equations (9) and (10) depending upon the particular applications and assumptions. Only two-dimensional spherical and cartesian coordinates Kalman tracking filter will be investigated because of the limited computational time and efforts. However, fully three-dimensional spherical coordinates Kalman filtering could be easily extended for further improvement and accuracy purpose.

Before we develop the Kalman filtering technique, the coordinate transformation will be addressed because of the serious movement and turbulence on the ship which is quite contrary to the land based antenna case.

III. 2. Coordinate Transformation

The most coordinate transformation has been currently applied after the mission except very few cases. With the consideration of uncertainty in range, velocity, bearing, elevation, and radar itself, on-axis coordinate transformation should be applied to enhance and correct the metric accuracy of the overall range systems.¹⁴

1) Space-to-space angle transformation

$$\begin{aligned} X_s &= r \cos \theta \cos \Theta \\ Y_s &= r \sin \theta \sin \Theta \\ Z_s &= -r \sin \theta \end{aligned} \quad (11)$$

where the negative sign in Z_s implies toward the earth center.

2) Space-to-deck transformation

$$\begin{pmatrix} X_D \\ Y_D \\ Z_D \end{pmatrix} = \begin{pmatrix} \cos P \cos H & \cos P \sin H & \sin P \\ \cos R \sin P \cos H & \sin R \sin P \sin H & -\sin R \\ +\cos R \sin H & +\cos R \cos H & -\cos P \\ -\cos R \sin P \cos H & -\cos R \sin P \sin H & \cos R \\ -\sin R \sin H & +\sin R \cos H & \cos R \\ & & \cos P \end{pmatrix} \begin{pmatrix} X_s \\ Y_s \\ Z_s \end{pmatrix} \quad (12)$$

where P : pitch angle of ships, R : roll angle of ships

H : yaw angle (or heading) of ships

subscript D denotes deck and S denoted space

and for the simplification, the computer coordinate system is equal to the ship's coordinate (i.e., SINS) without loss of generality, and the mount coordinate-to-the computer transformation is also neglected

3) Deck-to-mount transformation

$$\begin{pmatrix} X_m \\ Y_m \\ Z_m \end{pmatrix} = \begin{pmatrix} \cos E_p \cos B_p & \cos E_p \sin B_p & -\sin E_p \\ -\sin B_p & \cos B_p & 0 \\ \sin E_p \cos B_p & \sin E_p \sin B_p & \cos E_p \end{pmatrix} \begin{pmatrix} X_D \\ Y_D \\ Z_D \end{pmatrix} \quad (13)$$

where E_p : the primary axis deck elevation from the deck upward
 B_p : the primary axis deck bearing from the bow toward
 starboard, subscript m denotes mount of the antenna.

4) Mount-to-mount angle transformations

$$\begin{aligned} Y_m &= -\sin E_m \\ Y_m &= \sin A_m \cos E_m \\ Z_m &= -\cos A_m \cos E_m \end{aligned} \tag{14}$$

where A_m is measured from $-Z_m$ toward Y_m (from upward toward
 starboard when $E_p = B_p = 0$)

E_m is measured from $Y_m - Z_m$ plan away from X_m
 the los (antenna line of sight) coincides with $-Z_m$ when

$$\begin{aligned} A_m &= E_m - 0 \text{ and} \\ A_m &= \tan^{-1} \frac{Y_m}{Z_m} \\ E_m &= -\sin^{-1} \frac{X_m}{R} \\ R &= \sqrt{X_m^2 + Y_m^2 + Z_m^2} \end{aligned} \tag{15}$$

Because of the nonlinearity of this transformation matrix and
 the complexity, the application of this transformation should be
 seriously considered to save the computational and operational load.

Without considering the coordinate system, the radar data
 signal processing consists of seven states -- range, range rate,
 bearing, bearing rate, elevation, elevation rate, and drag ratio,
 which aids in deciding whether the object is authentic or a decoy.
 If we consider those seven states in the spherical coordinates
 system, the dynamic model system's matrix will have 11×11 matrix
 instead of 7×7 matrix. It is impossible to exploit all those
 seven states with spherical coordinates system Kalman tracking filter
 within the current computational facility unless the larger memory
 computer is provided.

The most important factors in radar data signal processing,
 however, is range, range rate, and bearing or elevation. Only these

parameters will be thus investigated in this study for both spherical and cartesian coordinates system.

III. 3. Kalman tracking filter formulation

1) Two State Dynamic Model (Range and Range Rate)

One of the simplest ways to formulate is a separate approach, but results in the inaccurate information and the ignorance of the correlation between tracking parameters. From equation (5), the range and range rate equations are

$$\begin{aligned} \begin{bmatrix} X_1(k+1) \\ X_2(k+1) \end{bmatrix} &= \begin{bmatrix} 1 & T \\ 0 & 1 \end{bmatrix} \begin{bmatrix} X_1(k) \\ X_2(k) \end{bmatrix} + \begin{bmatrix} T^2/2 \\ T \end{bmatrix} w(k) \\ Y(k) &= \begin{bmatrix} 1 & 0 \end{bmatrix} \begin{bmatrix} X_1(k) \\ X_2(k) \end{bmatrix} + \begin{bmatrix} 1 \\ 0 \end{bmatrix} v(k) \end{aligned} \quad (16)$$

However, the range position is not greatly affected by the acceleration of the RV, but the velocity is. With consideration of this fact, rewriting equation (16), we have

$$\begin{aligned} X(k+1) &= \Phi x(k) + \Gamma w(k) \\ Y(k) &= H X(k) + G v(k) \end{aligned} \quad (17)$$

where $\Phi = \begin{bmatrix} 1 & T \\ 0 & 1 \end{bmatrix}$ $\Gamma = \begin{bmatrix} 0 \\ 1 \end{bmatrix}$

$$H = \begin{bmatrix} 1 & 0 \end{bmatrix} \quad G = \begin{bmatrix} 1 \\ 0 \end{bmatrix}$$

T = sampling interval

w(k) and V(k) are white gaussian noise with zero mean and variance Q and R respectively.

In the spherical coordinates systems,

$$\begin{bmatrix} X_1x(k+1) \\ X_2x(k+1) \\ X_1y(k+1) \\ X_2y(k+1) \\ X_1z(k+1) \\ X_2z(k+1) \end{bmatrix} = \begin{bmatrix} 1 & T & 0 & 0 & 0 & 0 \\ 0 & 1 & 0 & 0 & 0 & 0 \\ 0 & 0 & 1 & T & 0 & 0 \\ 0 & 0 & 0 & 1 & 0 & 0 \\ 0 & 0 & 0 & 0 & 1 & T \\ 0 & 0 & 0 & 0 & 0 & 1 \end{bmatrix} \begin{bmatrix} X_1x(k) \\ X_2x(k) \\ X_1y(k) \\ X_2y(k) \\ X_1z(k) \\ Z_2z(k) \end{bmatrix} + \begin{bmatrix} 0 \\ 1 \\ 0 \\ 1 \\ 0 \\ 1 \end{bmatrix} w(k) \quad (18)$$

$$\begin{bmatrix} Yx(k) \\ Yy(k) \\ Yz(k) \end{bmatrix} = \begin{bmatrix} 1 & 0 & 0 & 0 & 0 & 0 \\ 0 & 0 & 1 & 0 & 0 & 0 \\ 0 & 0 & 0 & 0 & 1 & 0 \end{bmatrix} \begin{bmatrix} X_1x(k) \\ X_2x(k) \\ X_1y(k) \\ X_2y(k) \\ X_1z(k) \\ Y_2z(k) \end{bmatrix} + \begin{bmatrix} 1 \\ 1 \\ 1 \end{bmatrix} v(k) \quad (19)$$

or simply

$$\begin{aligned} X(k+1) &= \phi X(k) + \Gamma w(k) \\ Y(k) &= H x(k) + G v(k) \end{aligned} \quad (20)$$

where

$$\phi = \begin{bmatrix} 1 & T & 0 & 0 & 0 & 0 \\ 0 & 1 & 0 & 0 & 0 & 0 \\ 0 & 0 & 1 & T & 0 & 0 \\ 0 & 0 & 0 & 1 & 0 & 0 \\ 0 & 0 & 0 & 0 & 1 & T \\ 0 & 0 & 0 & 0 & 0 & 1 \end{bmatrix} \quad \Gamma = \begin{bmatrix} 0 \\ 1 \\ 0 \\ 1 \\ 0 \\ 1 \end{bmatrix}$$

$$H = \begin{bmatrix} 1 & 0 & 0 & 0 & 0 & 0 \\ 0 & 0 & 1 & 0 & 0 & 0 \\ 0 & 0 & 0 & 0 & 1 & 0 \end{bmatrix} \quad G = \begin{bmatrix} 1 \\ 1 \\ 1 \end{bmatrix}$$

Of course, the coordinate transformation matrix $M(k)$ in equation (10) is not considered here. If we compare the equations (16) and (18), the size and complexity are increased geometrically as a price of accuracy improvement mentioned earlier. Specifically, the ARIS system is required to use equation (18) because of changing environments in comparison with equation (17) which is proper for the land based system. The bearing and elevation model follow the exact equation. Figure 1. shows the block diagram to solve sequentially the above difference equation through Kalman Filter ¹⁵.

The solution of equations (17) and (20) is well known as a standard discrete Kalman filter equation ^{16, 17}.

smoothing: $\hat{X}(k+1) = \phi \hat{X}(k) + K(k+1)(Y(k+1) - H\phi \hat{X}(k))$ (21)
 (state estimate of filter)

prediction: $\hat{X}(k+1) = \phi \hat{X}(k)$ (22)
 (state estimate of prediction)

gain matrix; $K(k+1) = P(k+1)H^T(HP(k+1)H^T + R)^{-1}$ (23)

predictor equation: $M(k+1) = \phi P(k) \phi^T + \Gamma Q \Gamma^T$ (24)
 (covariance of prediction) (for the convenience of notation)

corrector equation: $P(k+1) = (M^{-1}(k+1) + H^T R^{-1} H)^{-1}$ (25)
 (covariance of filter)

or $= M(k+1) - M(k+1)H^T(HM(k+1) + H^T R^{-1} HM(k+1))^{-1} HM(k+1)$ (26)

or $= (I - K(k+1)H^T)P(k+1) M(k+1)$ (27)

where

$P(k) = E((X(k) - \hat{X}(k))(X(k) - \hat{X}(k))^T)$: covariance matrix and the utilization of $X(k)$ is generated by the first observation, $X(0) = X(1)$.

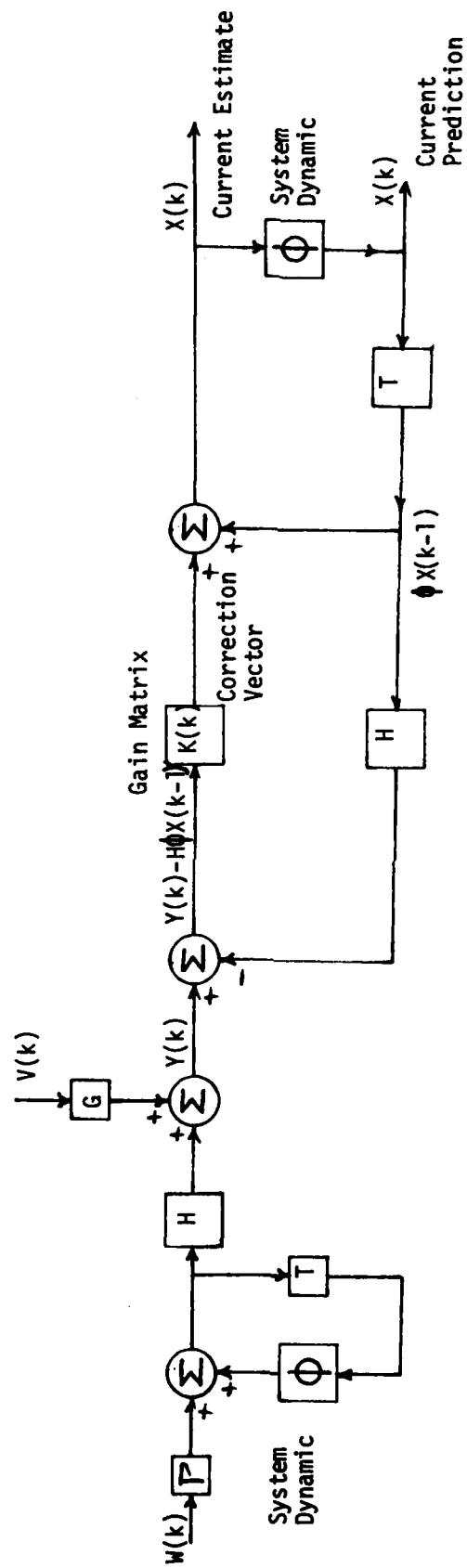


Fig. 1 Simultaneous Estimation and Prediction of Kalman Filtering

Q and R can be stored before the mission according to the information from the previous statistics.

Note that the dimension of the matrix inversion for equation (23) and (26) is as large as (3 x 3) matrix which reduces dramatically the computational complexity and time.

Similarly, the spherical coordinate system can be directly obtained along with equations (28) and (29). As mentioned earlier, this model should give a better information about the behavior of the tracking radar rather than the accuracy. The dimension of this model increases from 2 x 2 and 6 x 6 to 3 x 3 and 9 x 9 matrix respectively for both directional and spherical coordinates.

The solution of this approach is same as in equations (21) thru (27) except for the coefficients matrices.

3) Two states dynamic systems (range, range rate) with Cartesian coordinates.

To reduce the computational load, if Z-axis can be reasonably well adjusted to the reference axis, the Cartesian coordinate system may be applied to the ARIS system with reasonable accuracy

From equation (18),

$$\begin{bmatrix} X1x(k+1) \\ X2x(k+1) \\ X1y(k+1) \\ X2y(k+1) \end{bmatrix} = \begin{bmatrix} 1 & T & 0 & 0 \\ 0 & 1 & 0 & 0 \\ 0 & 0 & 1 & T \\ 0 & 0 & 0 & 1 \end{bmatrix} \begin{bmatrix} X1x(k) \\ X2x(k) \\ X1y(k) \\ X2y(k) \end{bmatrix} + \begin{bmatrix} 0 \\ 1 \\ 0 \\ 1 \end{bmatrix} w(k) \quad (30)$$

$$\begin{bmatrix} Y1x(k) \\ Y1y(k) \end{bmatrix} = \begin{bmatrix} 1 & 0 & 0 & 0 \\ 0 & 0 & 1 & 0 \end{bmatrix} \begin{bmatrix} X1x(k) \\ X2x(k) \\ X1y(k) \\ X2y(k) \end{bmatrix} + \begin{bmatrix} 1 \\ 1 \end{bmatrix} v(k) \quad (31)$$

There are several other alternative expressions which can be obtained depending upon the different point of calibration and environments. One of the most feasible simplest model may be directional three dimensional (range, bearing, elevation) dynamic model which can be written as

$$\begin{bmatrix} X_R(k+1) \\ X_\theta(k+1) \\ X_\phi(k+1) \end{bmatrix} = \begin{bmatrix} 1 & 0 & 0 \\ 0 & 1 & 0 \\ 0 & 0 & 1 \end{bmatrix} \begin{bmatrix} X_R(k) \\ X_\theta(k) \\ X_\phi(k) \end{bmatrix} + w(k) \quad (32)$$

or

$$Y(k) = X(k) + w(k)$$

The solution of this model may be obtained through the recursive estimation techniques as ¹⁸

$$\text{1st } Y(k-1) = X(k-1) + v(k-1) \quad (33)$$

$$Y(k) = X(k) + v(k)$$

$$\text{and } R = \begin{bmatrix} R_{(k-1)} & 0 \\ 0 & R(k) \end{bmatrix} \quad (34)$$

then

$$\hat{X}(k) = \hat{X}(k-1) + K(k) [Y(k) - \hat{X}(k-1)] \quad (35)$$

$$\text{where } K(k) = P(k-1) [P(k-1) + R_{(k)}]^{-1}$$

$$P(k) = (I - K(k))P(k-1)$$

$$\text{or } = (P(k-1)^{-1} + R_{(k)}^{-1})^{-1}$$

$$\text{or } = P(k-1) - P(k-1)(P(k-1) + R(k))^{-1}P(k-1),,$$

As an alternative expression. The estimate $X(k)$ is given by

$$X(k) = P(k)R^{-1}Y(k),, \quad (36)$$

which is similar to the α - β tracking system, but it is very rough estimation, in comparison with the previous approach.

4) Three Dimensional Cartesian Coordinate Kalman Filter.

To improve this problem, it can be extended to the following:

$$\begin{bmatrix} X_R(k+1) \\ \dot{X}_R(k+1) \\ X\theta(k+1) \\ \dot{X}\theta(k+1) \\ X\phi(k+1) \\ \dot{X}\phi(k+1) \end{bmatrix} = \begin{bmatrix} 1 & T & 0 & 0 & 0 & 0 \\ 0 & 1 & 0 & 0 & 0 & 0 \\ 0 & 0 & 1 & T & 0 & 0 \\ 0 & 0 & 0 & 1 & 0 & 0 \\ 0 & 0 & 0 & 0 & 1 & T \\ 0 & 0 & 0 & 0 & 0 & 1 \end{bmatrix} \begin{bmatrix} X_R(k) \\ \dot{X}_R(k) \\ X\theta(k) \\ \dot{X}\theta(k) \\ X\phi(k) \\ \dot{X}\phi(k) \end{bmatrix} + \begin{bmatrix} 0 & 0 & 0 \\ 1 & 0 & 0 \\ 0 & 0 & 0 \\ 0 & 1 & 0 \\ 0 & 0 & 0 \\ 0 & 0 & 1 \end{bmatrix} \begin{bmatrix} w1(k) \\ w2(k) \\ w3(k) \end{bmatrix} \quad (37)$$

$$\begin{bmatrix} Y1(k) \\ Y2(k) \\ Y3(k) \end{bmatrix} = \begin{bmatrix} 1 & 0 & 0 & 0 & 0 & 0 \\ 0 & 0 & 1 & 0 & 0 & 0 \\ 0 & 0 & 0 & 0 & 1 & 0 \end{bmatrix} \begin{bmatrix} X_R(k) \\ \dot{X}_R(k) \\ X\theta(k) \\ \dot{X}\theta(k) \\ X\phi(k) \\ \dot{X}\phi(k) \end{bmatrix} + \begin{bmatrix} 1 & 0 & 0 \\ 0 & 1 & 0 \\ 0 & 0 & 1 \end{bmatrix} \begin{bmatrix} v1(k) \\ v2(k) \\ v3(k) \end{bmatrix} \quad (38)$$

which are almost exactly same as the equations (18) and (19) except for the different coordinate systems. Should only range and bearings be considered, the size of the above model will be reduced to 4 x 4 matrix instead of 6 x 6 matrix.

The solution will be followed exactly same as the equations (21) - (27).

Special attention should be emphasized when the coordinate transformation is applied to the data processing. Since the range, elevation, and azimuth are highly correlated, the covariance matrix should take into account of those matters. This implies that the matrix Q and R are no longer diagonal matrix. In addition, the covariance matrix of state vectors should also be modified along with the coordinate transformation in order to weigh correctly. This

further development and study should be performed before applying to the real systems.

Notice also that the state transition matrix is almost diagonal matrix and this results in simplifying the computational procedures. Those mentioned techniques and procedures can be applied both land-based and any other ARIS range systems to improve the performance and the accuracy.

III. 4. Simulation

Two states Kalman filter with maneuvering target was examined to study the problems of tracking algorithm for further development of the on-axis tracking application to the ARIS system and possible extension to the land-based and any other radar systems. During the mission, the covariance matrix can be separately computed from the filtering procedure as shown in Figure 2.

The incorrect information of the acceleration and sampling rate (or traveling time) would create a false prediction and eventually lose the tracking the target as shown in Figure 3 and 4, on the other hand, the proper adjustment of parameter initialization would give a better performance for both errors and tracking purposes as shown in Figure 5 and 6. This implies the update corrections of the measurement error and acceleration errors are necessary for the accurate tracking. The further detailed investigation of the divergence of the covariance matrix and sensitivity of the filtering parameters is essential for the successful accomplishment of the MAIP goals.

Six states Kalman filter with real satellite tracking data was studied to investigate the real feasibility of the use of U1600 computer.

Figure 7, 8, and 9 show the diagonal element only of the 6 states covariance matrix case for each coordinate range by assuming that there is no correlation between range, range rate, azimuth, and elevation.

Figure 10, 11, and 12 show the errors between the actual measurement-extrapolation, actual measurement-filtered prediction, and the pure extrapolation-filtered prediction value respectively for each coordinate component of the real vectors.

Similarly, the case with the consideration of correlation between range, range rate, bearing, and elevation is shown in Figure 13 through 18.

As can be seen in the figure, the off-diagonal (with consideration of correlation) case performs better, but does not guarantee the convergence of the Kalman filter gain matrix. The diagonal only case, however, performs worse, but guarantees the convergence of the covariance matrices. Further details of this correlation factor should be extended to the real situation when it applies to the on-axis tracking mode.

As a conclusion, the feasibility of on-axis tracking algorithm for the ARIS systems had been shown within the current computational facility with an efficient data processing algorithm development (to be continued in future) which guarantees the acceptable performance.

IV. RECOMMENDATIONS.

Five different areas would be proposed to improve the present metric accuracy requirements.

1. Extended Kalman tracking filtering: the following items should be further investigated to access for the on-axis tracking purpose;

a. The development of an efficient covariance matrix computation algorithm for both spherical and Cartesian coordinate transformation approach because of their correlation between range, azimuth, and elevation .

b. A comparison between single dimensional spherical (x, y, z) coordinate system and two-dimensional Cartesian coordinate (x, y) Kalman filtering technique should be studied to choose the simplest and most efficient algorithm.

c. A comparison between four, six, seven, eight and nine states Kalman filtering techniques would be done before adopting some particular algorithm for the optimum and efficient operation.

d. Study the possible application to both land-based and any other current existing ARIS systems.

2. Netting Algorithm: A combination of several radar measurement, optics, and telemetry system measurement would be beneficial to enhance the accuracy of metric measurement;

a. A development of a netting algorithm will be very beneficial to improve the metric accuracy as mentioned in Section III.

b. A development of a technique, which can combine the information from both the netting of several radars and TWS system algorithm, will be a great milestone in correcting and improving the metric measurement.

3. Design of a Digital Controller: This technique is far from this project, but it could be much more beneficial to launch this problem;

The main idea of this proposal is to stabilize a present auto-tracking radar servo system using a computer along with a coordinate transformation correction. In case of on-axis tracking system failure, this technique can still track the RV with better accuracy than the present tracking system.

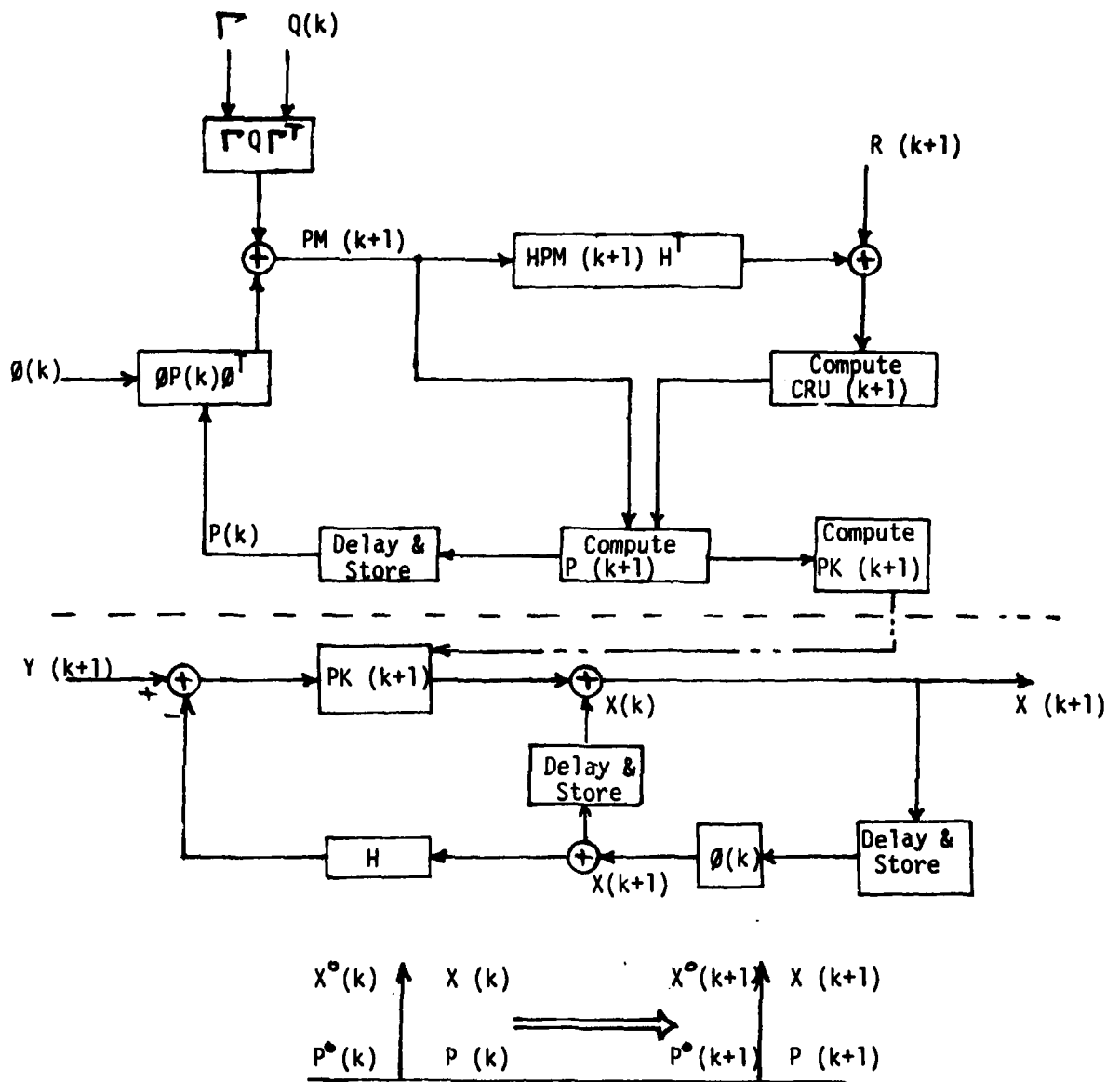
4. Further review and study of the data processing and reduction:

The present algorithm for the data processing and reduction is to be entirely reviewed and studied by adopting the on-axis tracking algorithm. This could result in improving the accuracy and reducing the computational load and related manpower.

5. Perturbation approach:

Because of the changing environment, a new technique may be more attractable to the ARIS systems by adopting a perturbation approach for developing a tracking algorithm in the future.

Those five areas of interests could be applicable and acceptable to the present computational facilities and the author strongly recommends the on-axis tracking algorithm and subsequent task forces to finish successfully for the major goals of MAIP program.



Where
$$CRU(k+1) = PM(k+1) H^T (HPM(k+1) H^T + R)^{-1} H PM(k+1)$$
or
$$= PK(k+1) H^T P(k+1) PM(k+1).$$

Fig. 2 Flow Diagram of Estimator and Computation Timing for Kalman Tracking Filter

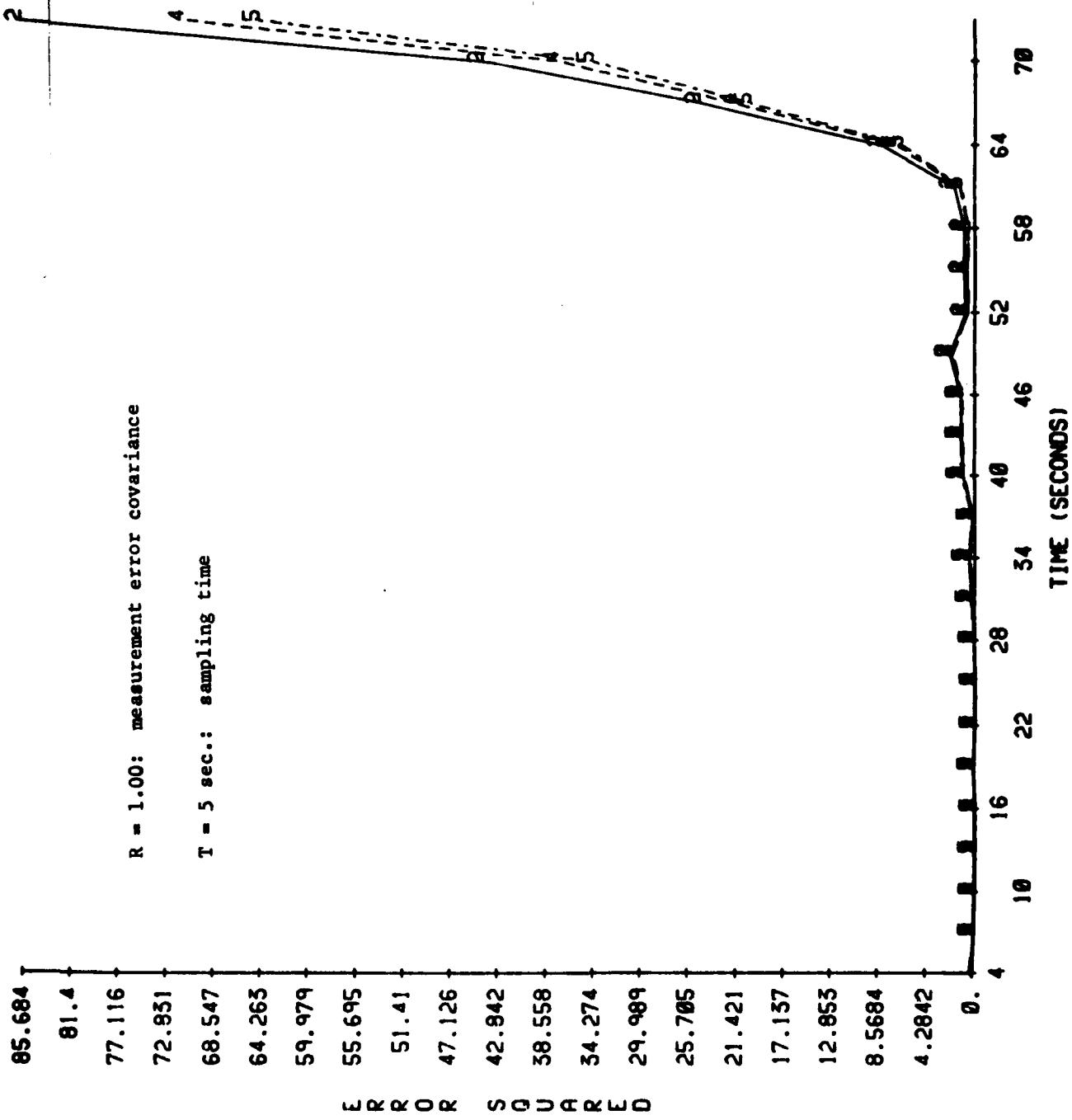
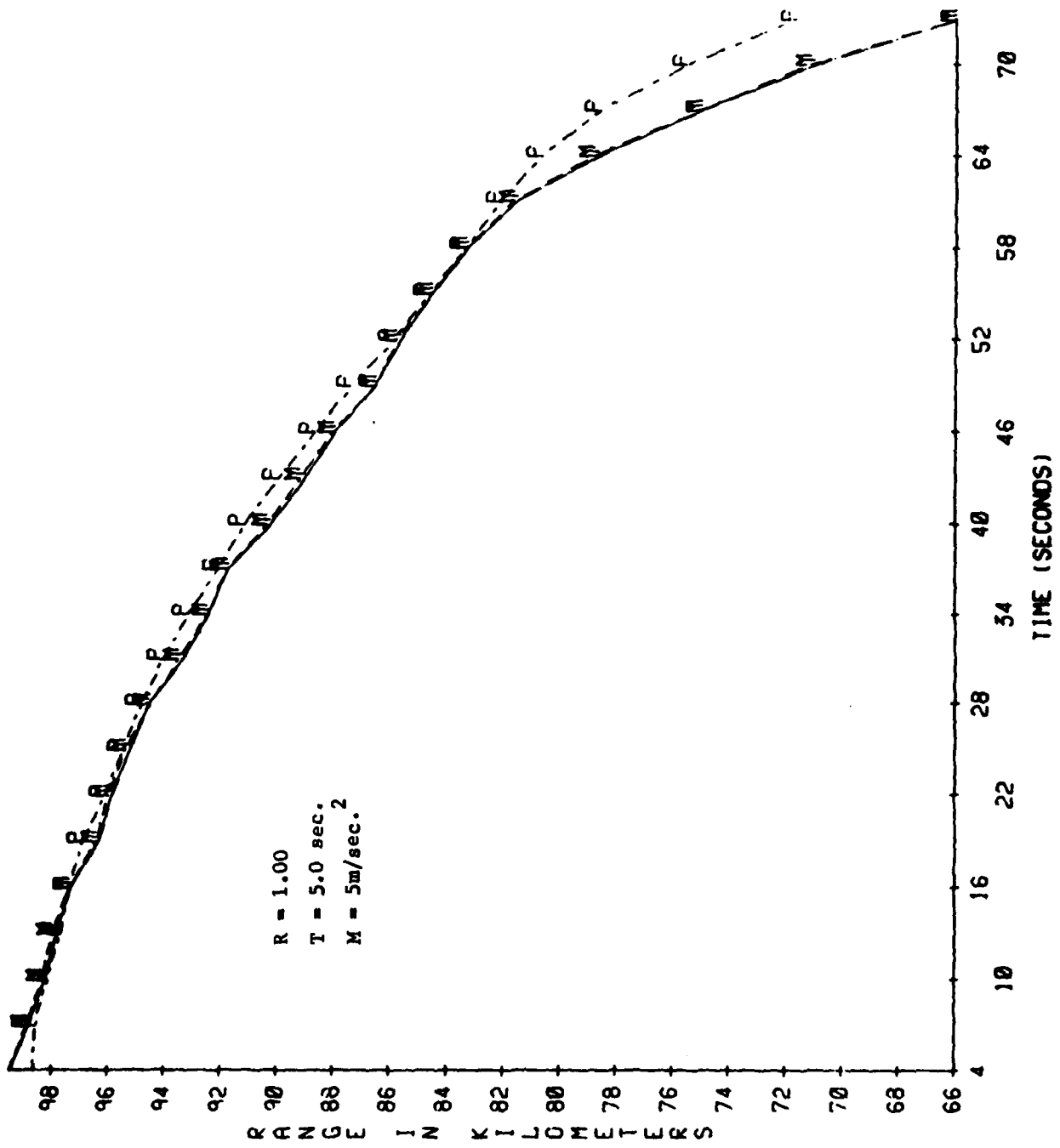
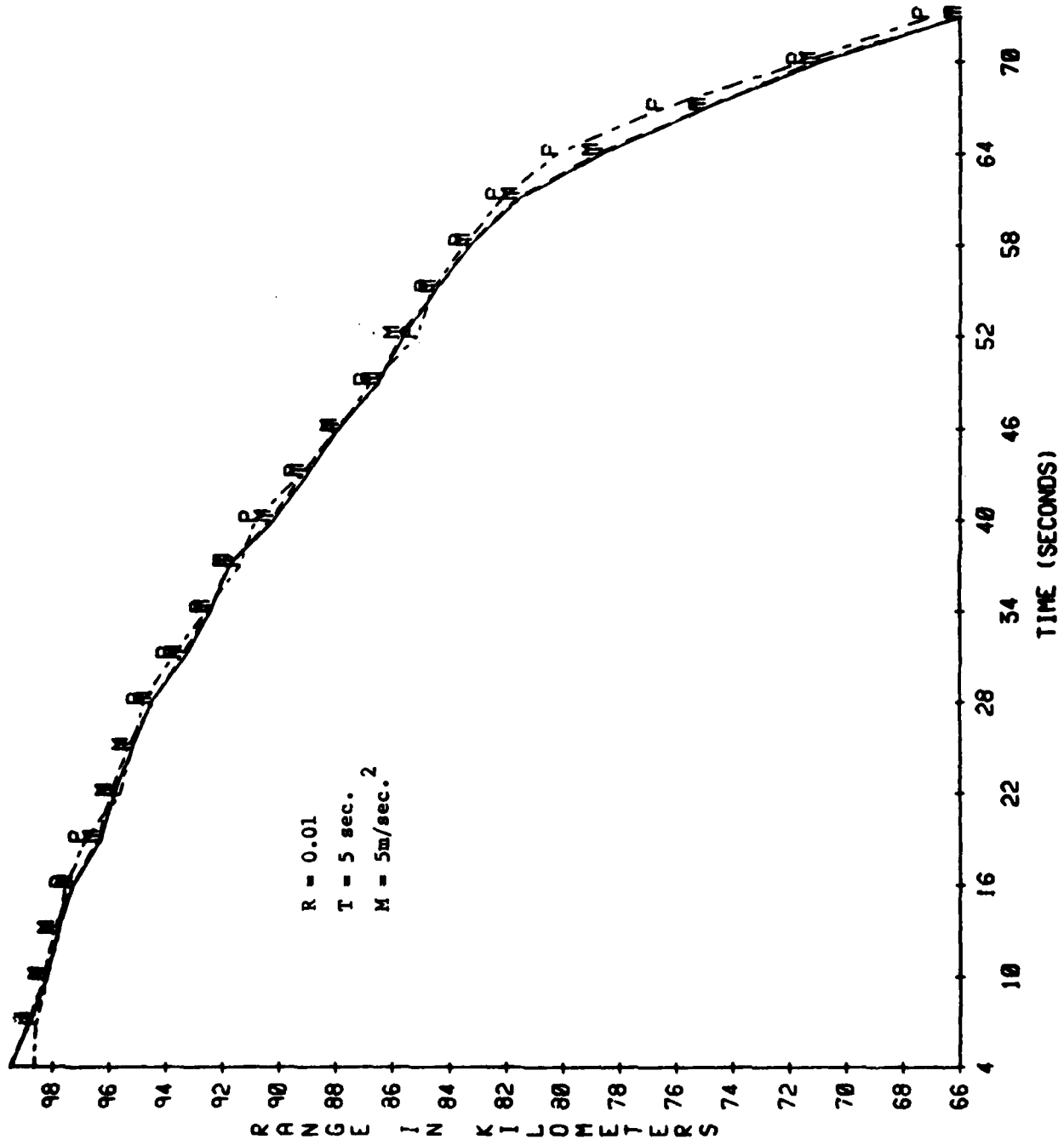


FIGURE 3. Error Square for different acceleration, M.



T-TRUE, M-MEASURED, P-PREDICTED

FIGURE 4. Tracking of a Target.



T-TRUE, M-MEASURED, P-PREDICTED

FIGURE 5. Tracking of a Target.

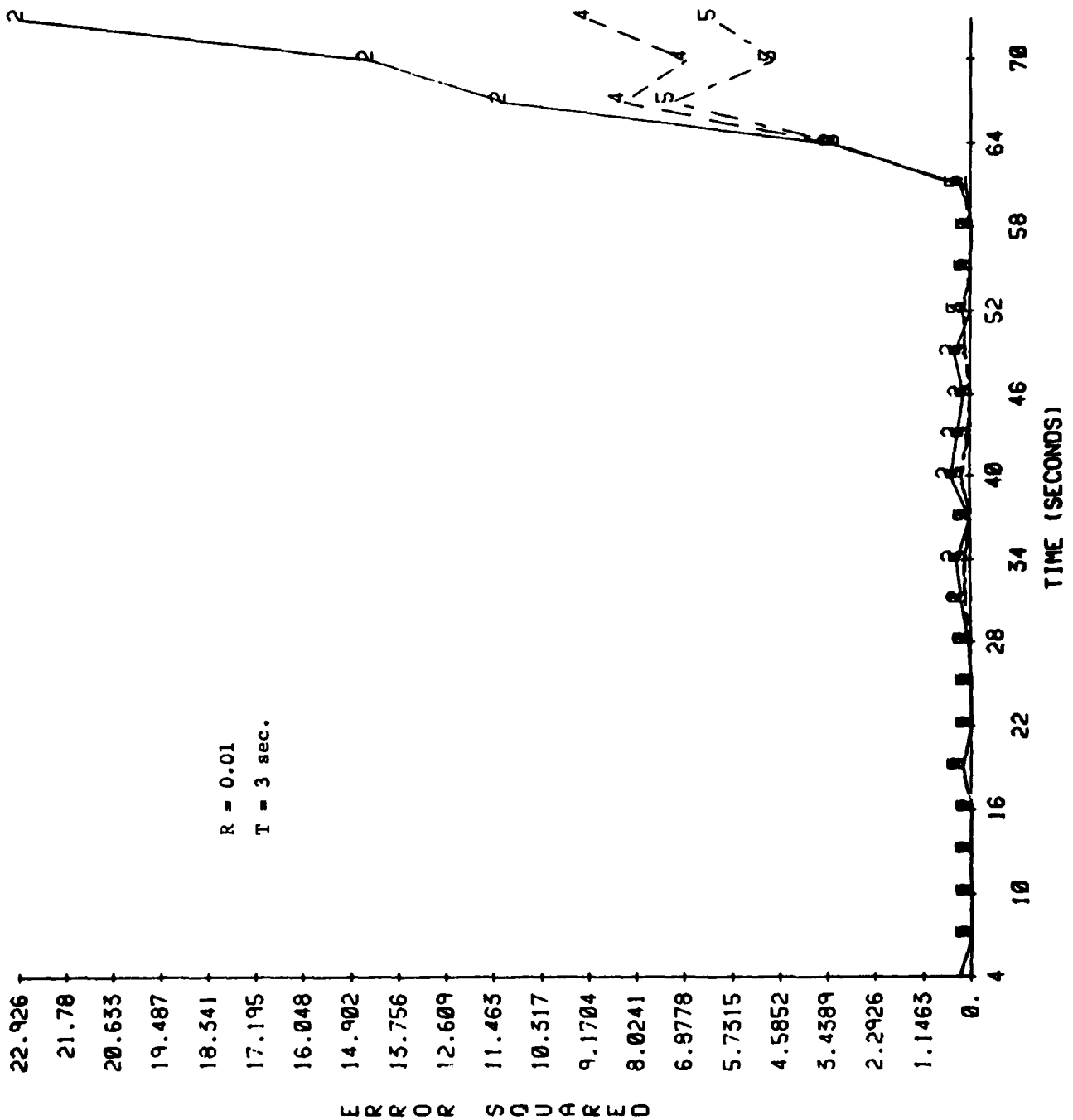
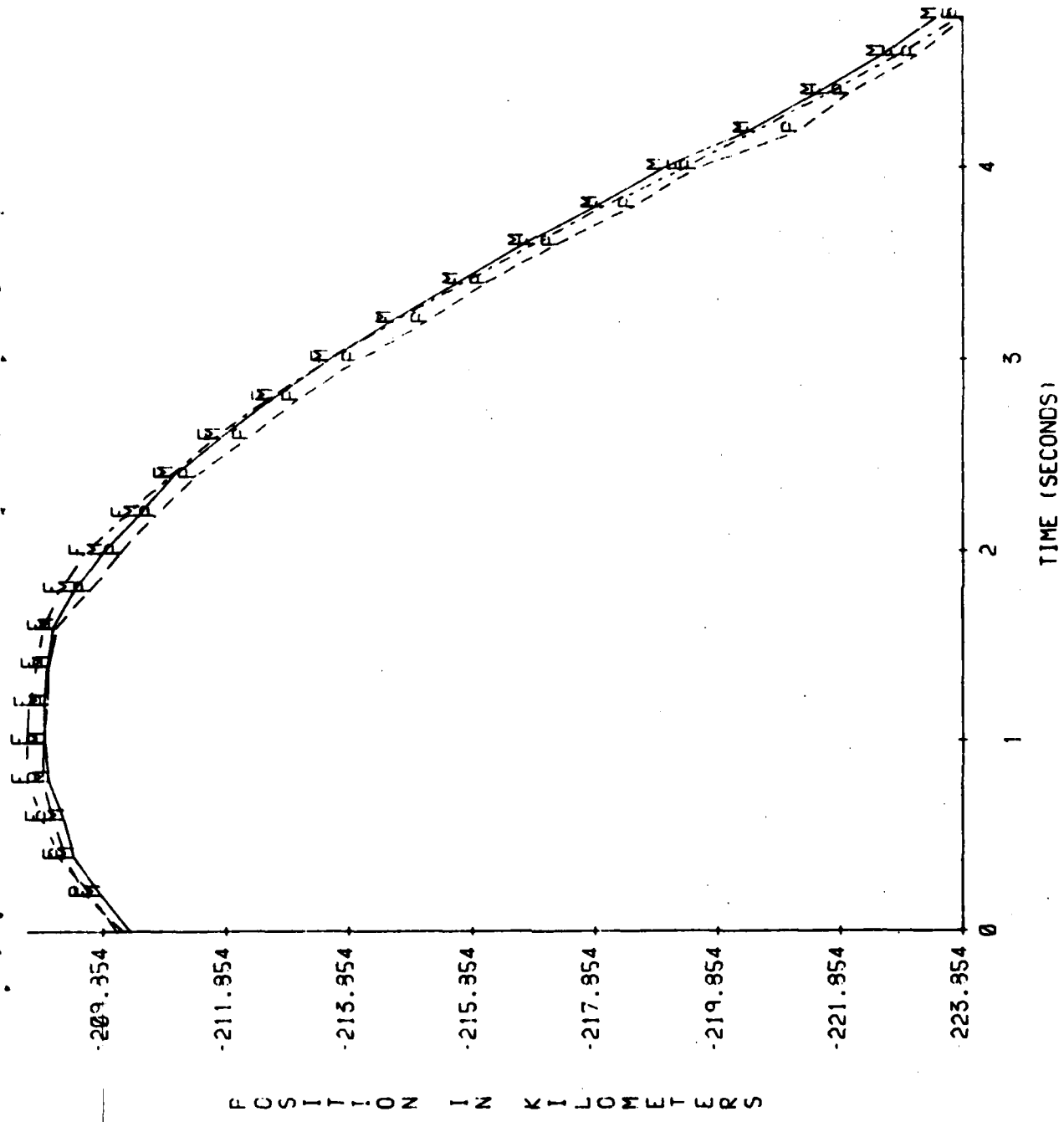


FIGURE 6. Error Square for different acceleration, M.



M-MEASURED, P-PREDICTED, F-FILTERED

FIGURE 7. X - coordinate tracking with diagonal only.

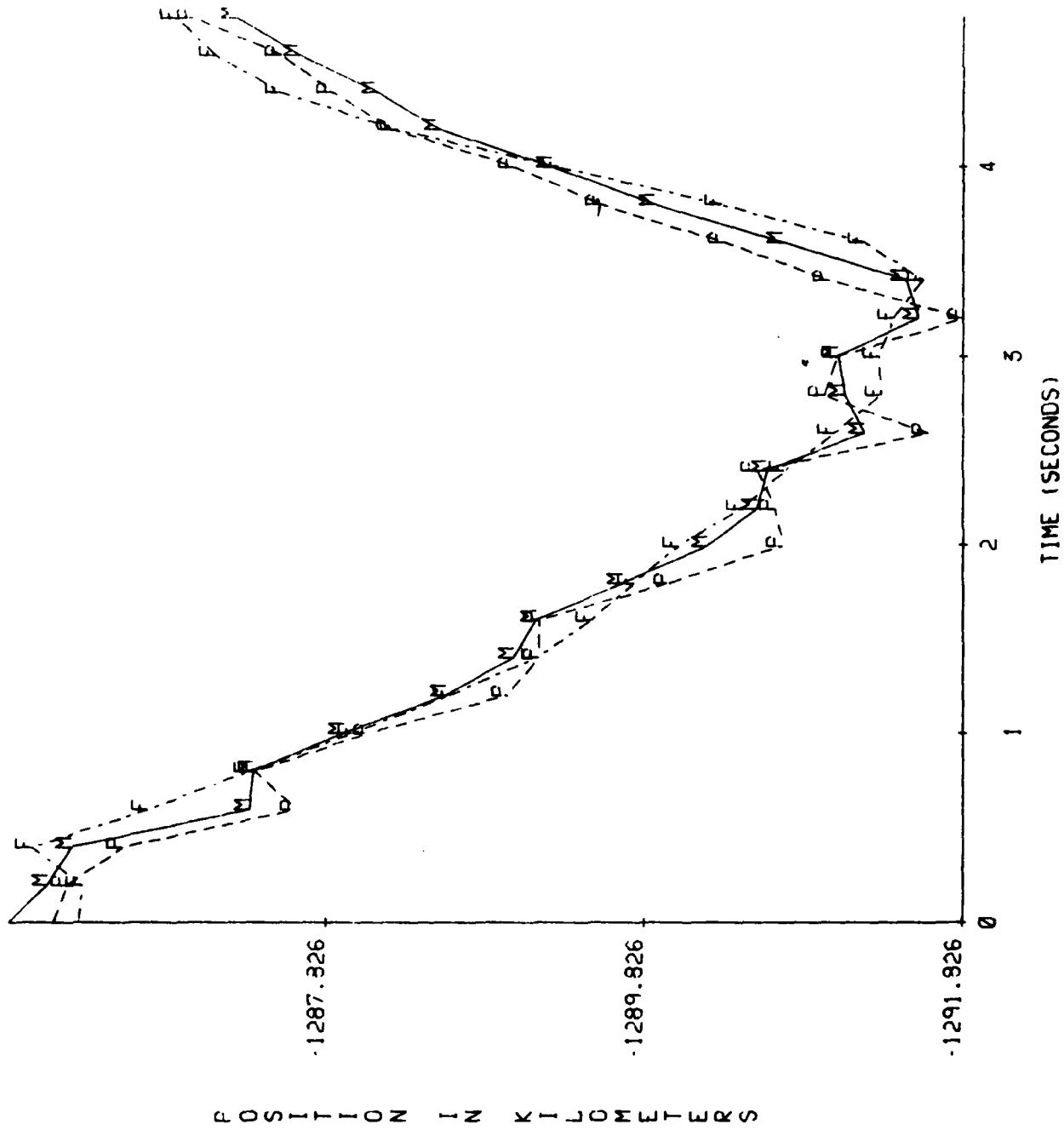


FIGURE 8. Y - coordinate tracking with diagonal only.

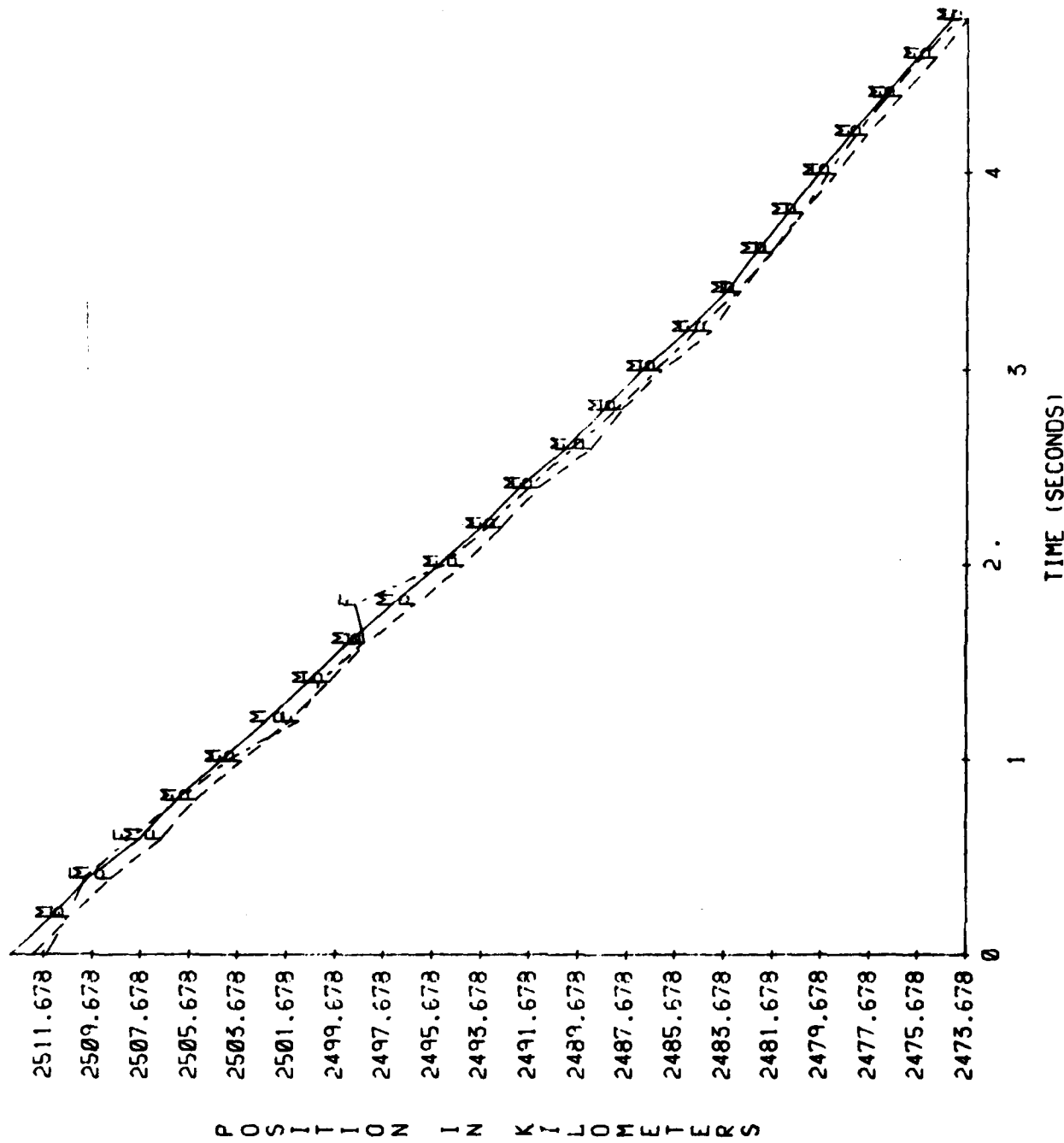
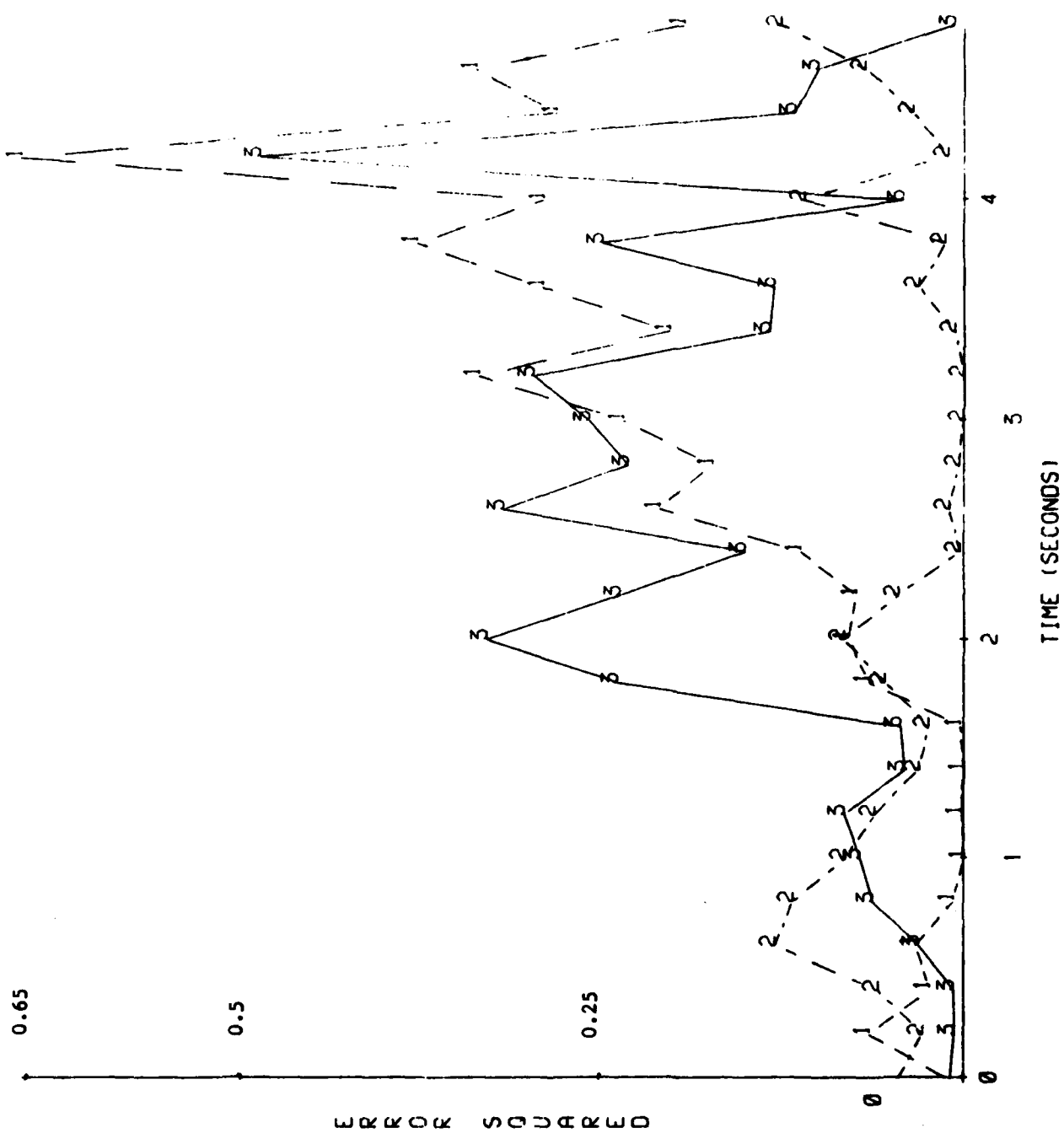


FIGURE 9. Z - coordinate tracking with diagonal only.
 M-MEASURED, P-PREDICTED, F-FILTERED



1-EXTRAPOLATION, 2-FILTER, 3-PREDICTION

FIGURE 10. Error square of X-coordinate tracking.

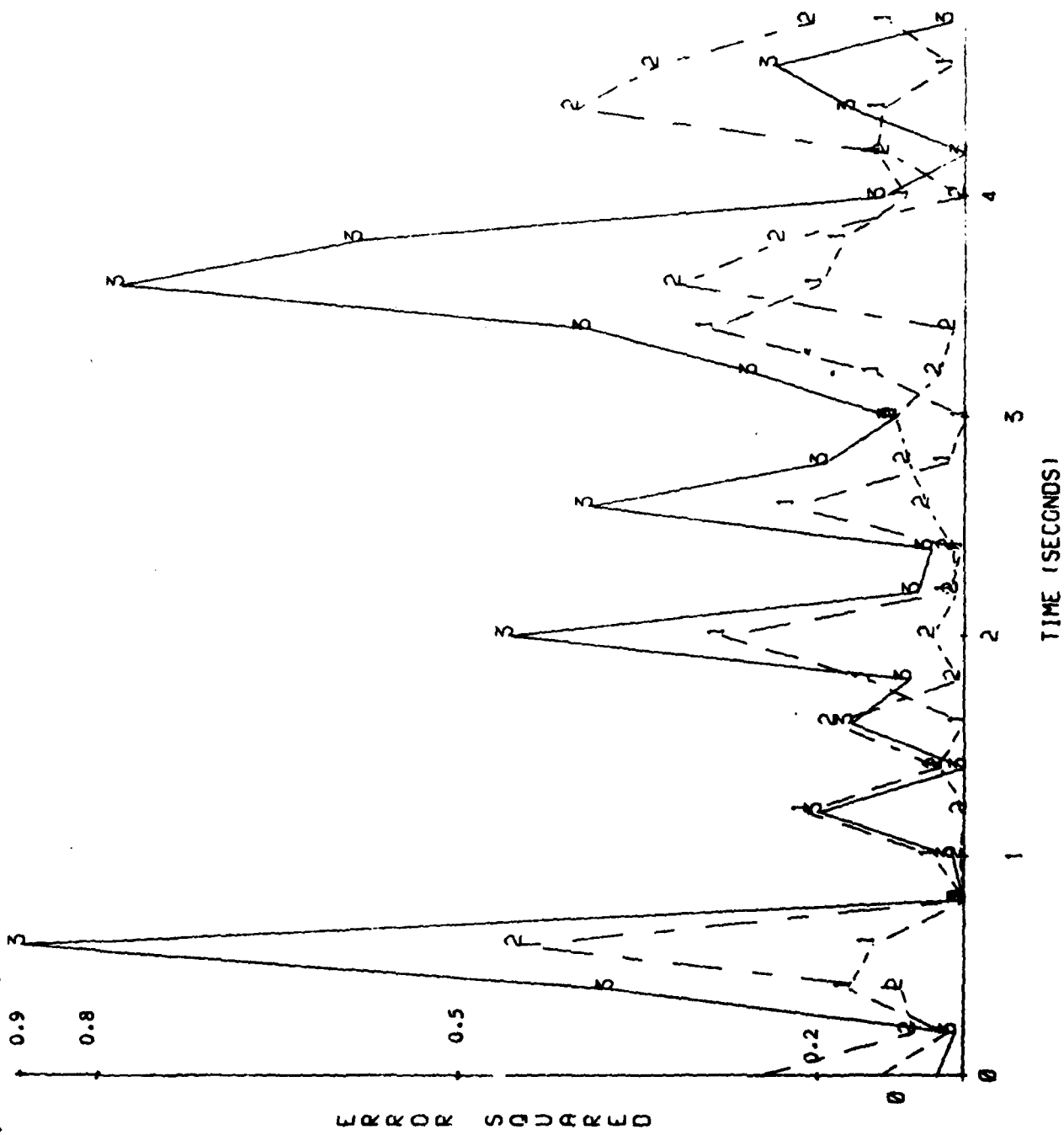


FIGURE 11. Error square of Y-coordinate tracking.
 1-EXTRAPOLATION, 2-FILTER, 3-PREDICTION

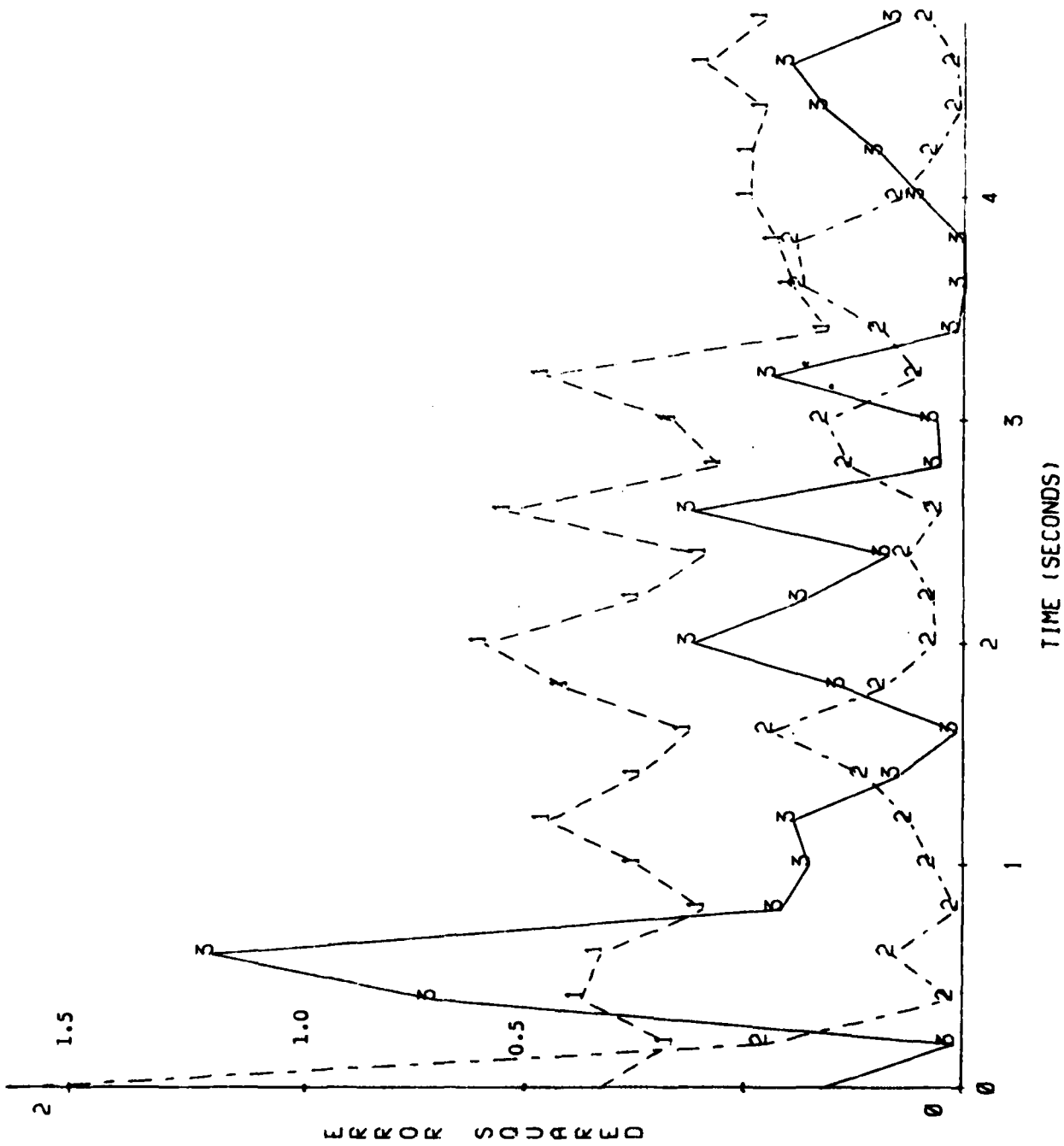


FIGURE 12. Error square of Z-coordinate tracking.
 1-EXTRAPOLATION, 2-FILTER, 3-PREDICTION

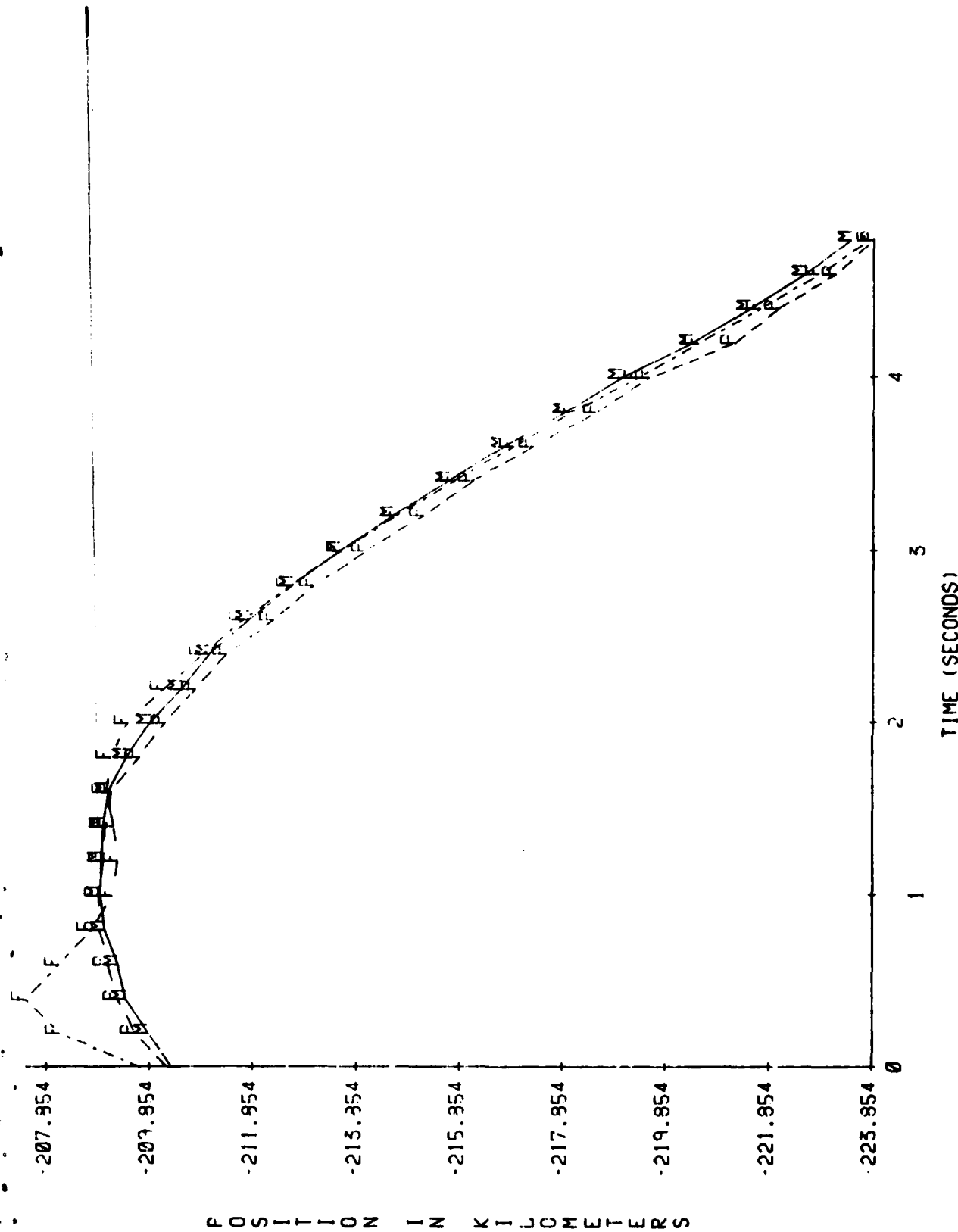
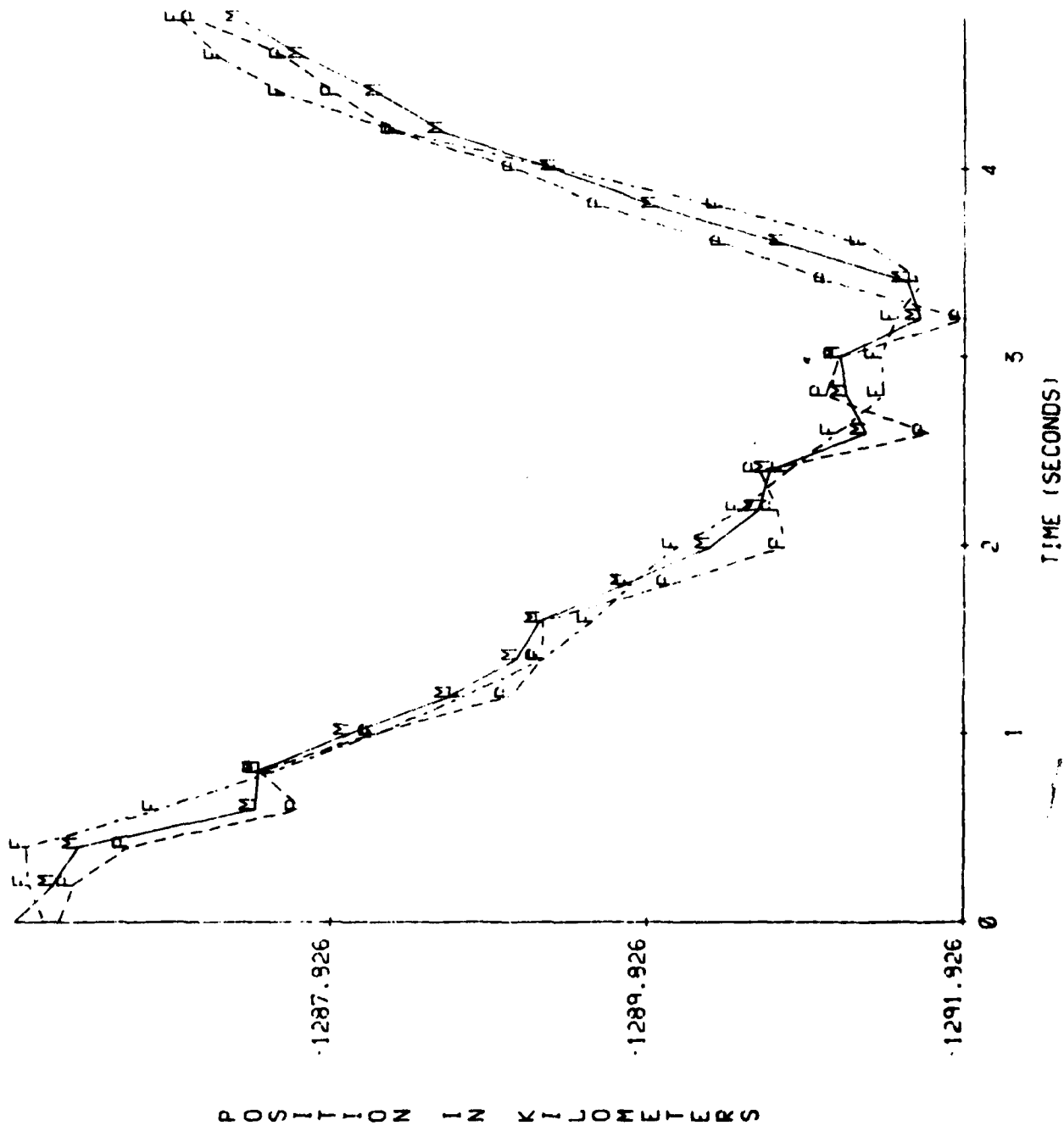
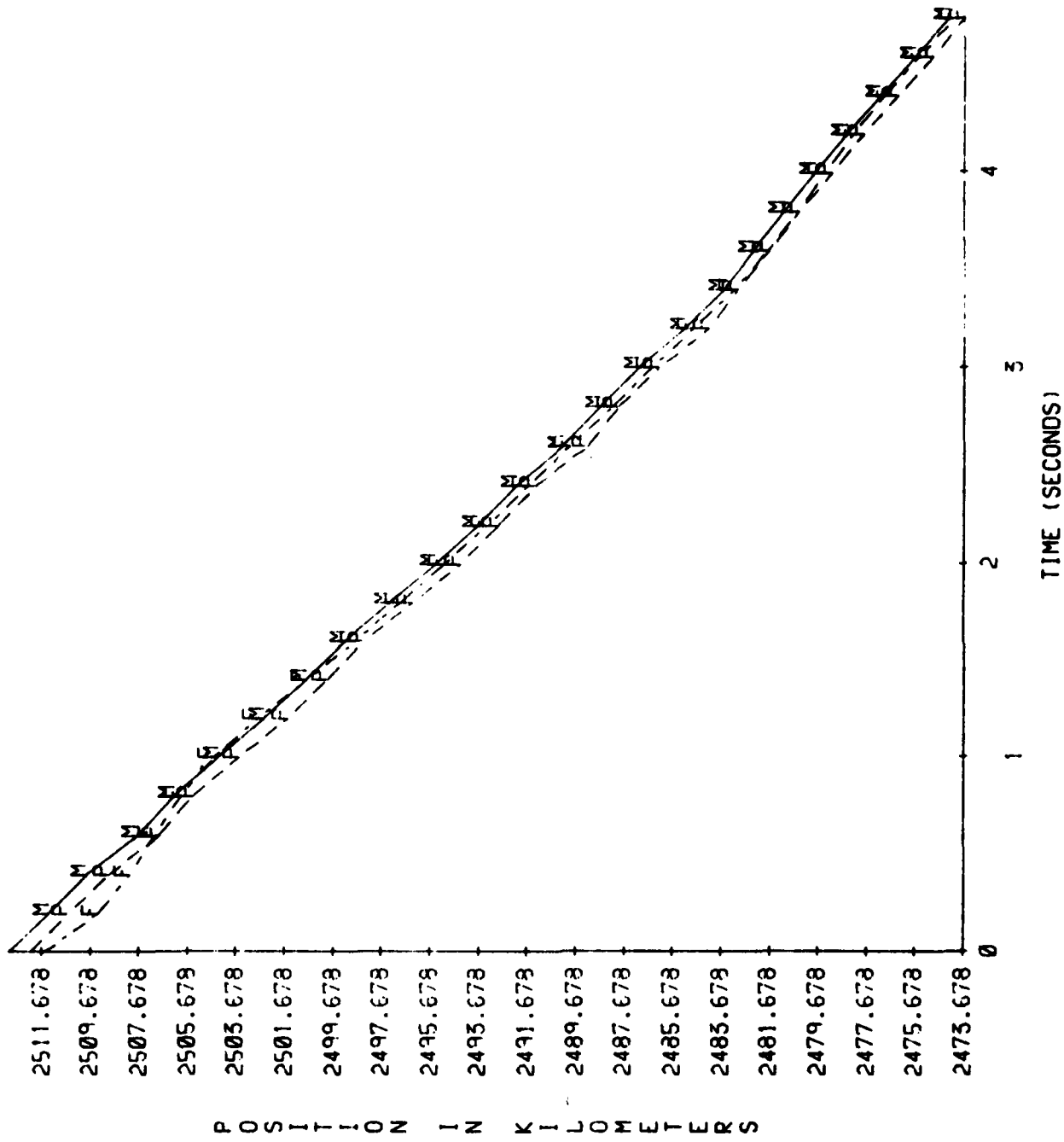


FIGURE 13. X-coordinate tracking with off-diagonal.
 M-MEASURED, P-PREDICTED, F-FILTERED



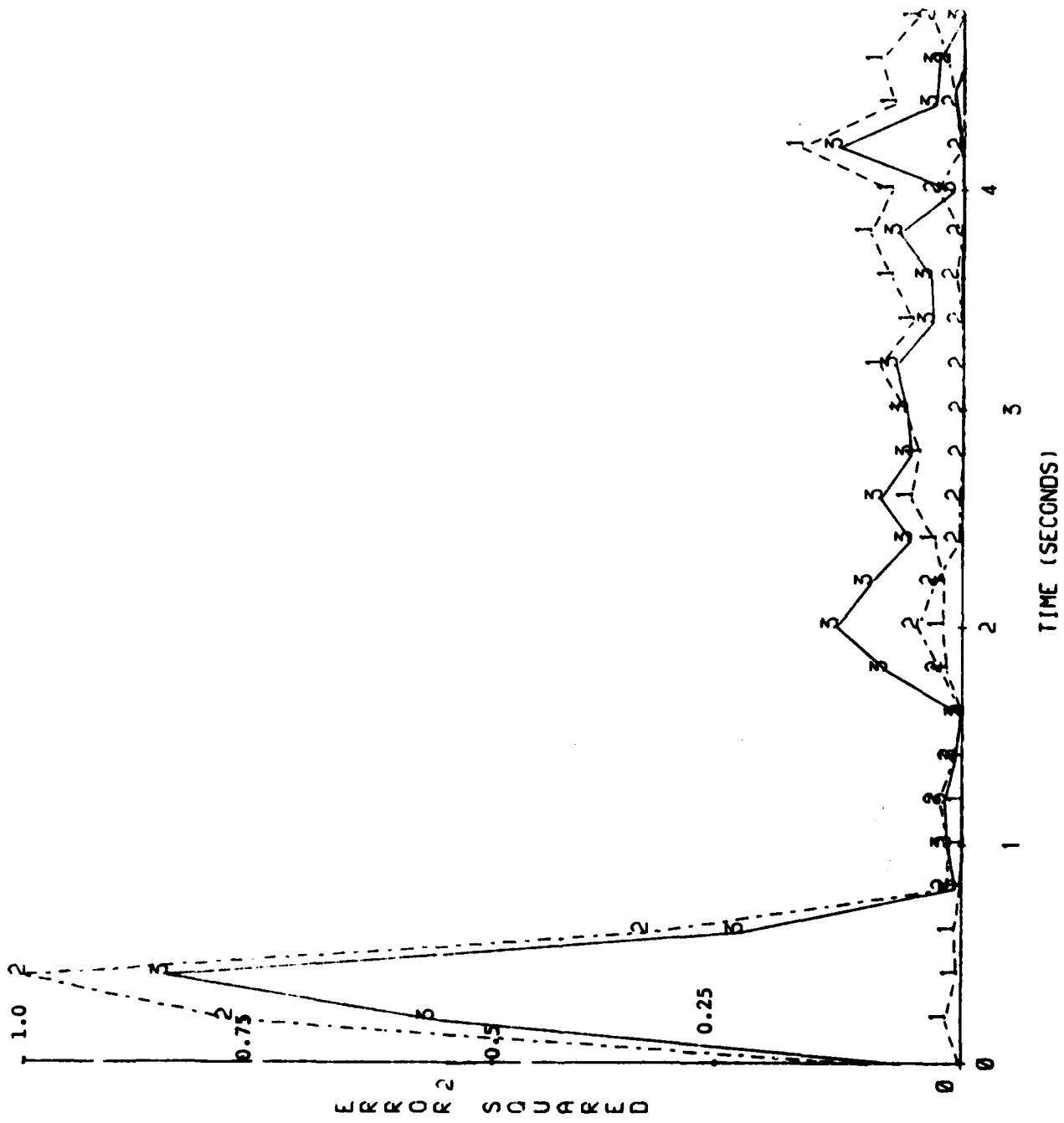
M-MEASURED, P-PREDICTED, F-FILTERED

FIGURE 14. Y-coordinate tracking with off-diagonal.



M-MEASURED, P-PREDICTED, F-FILTERED

FIGURE 15. Z-coordinate tracking with off-diagonal.



1-EXTRAPOLATION, 2-FILTER, 3-PREDICTION

FIGURE 16. Error square of X-coordinate tracking.

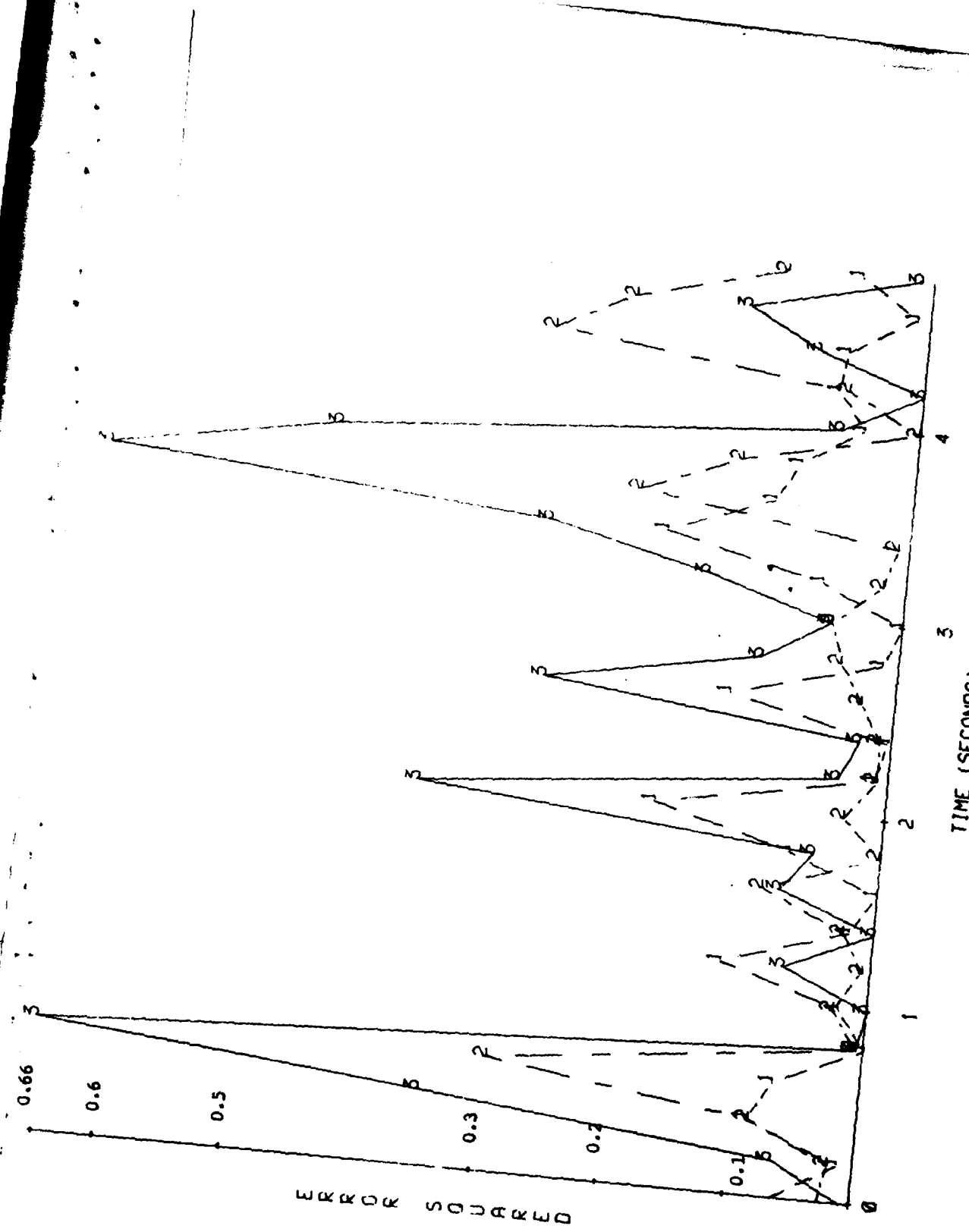
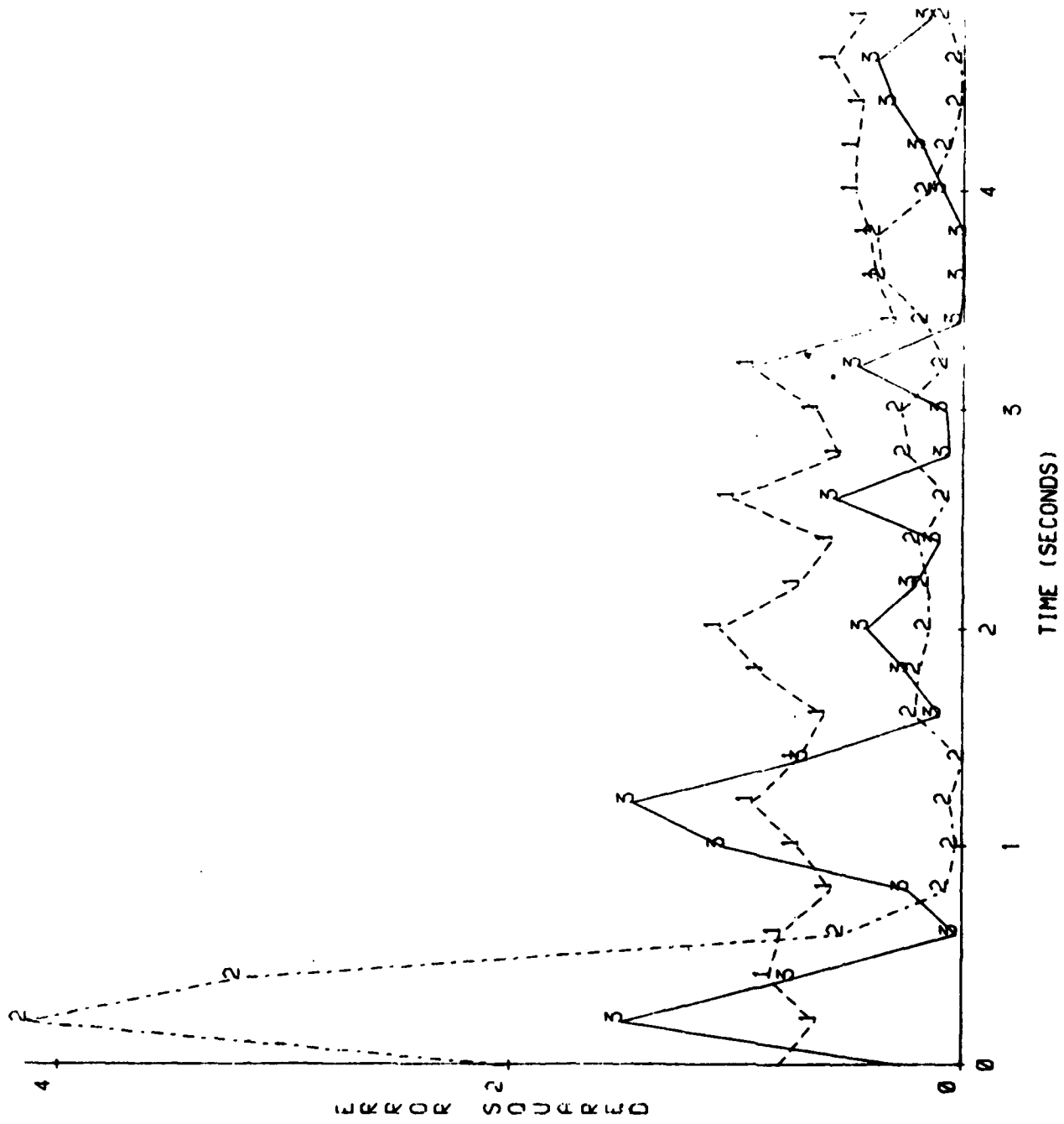


FIGURE 17. Error square of Y-coordinate tracking.
 1-EXTRAPOLATION, 2-FILTER, 3-PREDICTION



1-EXTRAPOLATION, 2-FILTER, 3-PREDICTION

FIGURE 18. Error square of X-coordinate tracking.

REFERENCES

1. Ehling, E.H., "Range Instrumentation" Prentice-Hall Englewoods, N.J., 1967.
2. Ships Accuracy Improvement Plan, USNS Vandenberg, ESMC/RSN Internal Technical Memo, 5 Dec 1978 for ASOAR Tests of C-Band.
3. Schleher, D. Curtis, "Automatic Detection and Radar Data Processing", Artech House, Inc., Mass 1980.
4. Morrison, N., "Introduction to Sequential Smoothing and Prediction", McGraw-Hill, New York, 1969.
5. Benedict, T.R. and Bordner, G.W. "Synthesis of an Optimal Set of Radar Track-While-Scan Smoothing Equations", IRE Transactions on Automatic Control Vol. AC-7 pp. 27-32, July 1962.
6. Singer, R.A. "Estimating Optimal Tracking Filter Performance for Manned Maneuvering Targets" IEEE Transactions on Aerospace and Electronic Systems, Vol. AES-6, No. 4 pp. 473-483, July 1970.
7. Singer, R.A. and Behnke, K.W., "Real-Time Tracking Filter Evaluation and Selection for Tactical Applications", IEEE Transaction on Aerospace and Electronic Systems Vol. AES-7, No. 1, pp. 100-110, Jan 1971.
8. Schooler, C.C., "Optimal α - β Filters for Systems with Modeling Inaccuracies", IEEE Transactions on Aerospace and Electronic Systems, Vol. AES-11, No. 6, pp. 1300-1306, Nov 1975.
9. Castella, F.R. and Dunnebacke, F.G., "Analytical Results for the X, Y Kalman Tracking Filter", IEEE Transaction on Aerospace and Electronic Systems, Vol. AES-10, No. 6, pp. 891-895, Nov 1974.
10. Gholson, N.H. and Moose, R.L., "Maneuvering Target Tracking Using Adaptive State Estimation", IEEE Trans. on Aerospace and Electronic Systems, Vol. AES-13, No. 3, pp. 310-317, May 1977.
11. Kamachandra, K.V. and Srinivasan, V.S., "Steady State Results for the X, Y, Z Kalman Tracking Filter", IEEE Trans. on Aerospace and Electronic Systems, Vol. AES-13, No. 4, pp. 419-423, July 1977.

12. Chang, C.B. and Dunn, K.P., "Kalman Filter Compensation for a Special Class of Systems", IEEE Transactions on Aerospace and Electronic Systems, Vol. AES-13, No. 6, pp. 700-706, Nov 1977.
13. Fauqi, F.A. and Davis, R.C., "Kalman Filter Design for Target Tracking", IEEE Trans. on Aerospace and Electronic Systems, Vol. AES-16, No. 4, pp. 500-508, July 1980.
14. O'Connor, J. J., "Transformations Applicable to Missile and Satellite Trajectory Computations", AFETR-TR-75-29, Patrick AFB, Fla. 32925.
15. Bozic, S.M., "Digital and Kalman Filtering", Halsted Press Book, John Wiley Sons Inc., New York, 1979.
16. Gelb, Arthur, "Applied Optimal Estimation", MIT Press, MA 1974.
17. Castella, F.R., "An Adaptive Two-Dimensional Kalman Tracking Filter", IEEE Trans. on Aerospace and Electronic Systems, Vol. AES-16, No. 6, pp. 822-829, Nov 1980.
18. Genin, Y., "Further Comments on the Derivation of Kalman Filters, Section II: Gaussian Estimates and Kalman Filtering", AGARDO graph 139, C.T. Leondes edited, NATO Advanced Groups for Aerospace R&D, 1970. pp. 55-63.
19. Brookner, Ali, "Radar Technology", Artech House, Inc., MA, 1979.
20. J. Sklansky, "Optimizing the Dynamic Parameters of a Track-While-Scan System", RCA Review, June 1957.
21. Proceedings for On-Axis Software Conference at Patrick Air Force Base, Florida, Technical Report No. ETR-TR-74-01, Directorate of Range Operations, Sep 1974.
22. Vemuri, Rao, "Improvement of Trajectory Tracking Accuracy of Instrumentation Ships: A Feasibility Study", Final Report, 1980 USAF SCEEE Summer Faculty Research Program.

1981 USAF - SCEEE SUMMER FACULTY RESEARCH PROGRAM

Sponsored by the

AIR FORCE OFFICE OF SCIENTIFIC RESEARCH

Conducted by the

SOUTHEASTERN CENTER FOR ELECTRICAL ENGINEERING EDUCATION

FINAL REPORT

ROUGH SURFACE EFFECTS ON TURBULENT BOUNDARY LAYERS

Prepared by: Dr. Hugh W. Coleman

Academic Rank: Associate Professor

Department and University: Department of Mechanical and Nuclear Engineering
Mississippi State University

Research Location: Air Force Armament Laboratory
Munitions Division
Aircraft Compatibility Branch
Aerodynamics Section

USAF Research Colleague: Dr. Lawrence E. Lijewski

Date: July 24, 1981

Contract No: F49620-79-C-0038

ROUGH SURFACE EFFECTS ON
TURBULENT BOUNDARY LAYERS

by

Hugh W. Coleman

ABSTRACT

The prediction of the fluid dynamic and thermal behavior of a turbulent boundary layer on a surface of arbitrary roughness is considered. The equivalent sand-grain roughness concept is examined in some detail, and it is concluded that (1) assumptions inherent in the concept are not supported by recent data, (2) there is currently no acceptable method for determining the equivalent sand-grain roughness for a general rough surface on which no skin friction data are available, and (3) experimental data and physical arguments indicate that heat transfer probably does not scale with equivalent sand-grain roughness. Brief comments on a discrete element approach to the problem are presented, and suggestions for further research are made.

ACKNOWLEDGEMENTS

The author wishes to thank the Air Force Systems Command, the Air Force Office of Scientific Research, the Southeastern Center for Electrical Engineering Education, and the Air Force Armament Laboratory, Eglin AFB, FL. for a professionally rewarding experience during the Summer Faculty Research Program.

Special thanks for their help, encouragement, and hospitality go to Dr. Don Daniel, Mr. Charles Mathews, Dr. Larry Lijewski, and Mr. Tom Durrenberger. The exceptionally competent help of the Eglin Technical Library staff (particularly Mrs. June Stercho and Mrs. Mary Weston) is gratefully acknowledged. Finally a sincere thanks to Mrs. B. Hinely, who typed this report and always cheerfully accepted the almost indecipherable pages of the rough draft.

I. INTRODUCTION:

Wall roughness can cause significant increases in drag and heat transfer on a surface exposed to a turbulent boundary layer. These effects have serious implications on the design and performance of such Air Force systems as reentry vehicles, missiles, and stores carried externally on high performance aircraft. Such effects are also important in such diverse areas as the design of ships, gas turbines, heat exchangers and piping systems and the modeling of atmospheric flows. Thus an attempt to understand and predict fluid dynamics and heat transfer in roughness-influenced turbulent flows can be viewed as a basic research problem with far-ranging applications rather than as a system-related problem.

The present effort is closely related to a research program outlined by the author and Dr. B. K. Hodge, a colleague at Mississippi State University. This program is described in a research proposal entitled "Generalized Roughness Effects on Turbulent Boundary Layer Heat Transfer" which was submitted to the Air Force Armament Laboratory prior to the author's participation in the Summer Faculty Research Program. The objective of the proposed research program is the prediction of fluid dynamics and heat transfer in turbulent boundary layer flows over general rough surfaces using an approach independent of the equivalent sand-grain roughness concept, which is described below.

Roughness effects on a turbulent boundary layer have traditionally been divided into three regimes of flow: hydraulically smooth, transitionally rough, and fully rough. The boundaries of these regimes are usually related to the magnitude of the roughness Reynolds number

$$k_s^+ = k_s U^* / \nu \quad (1)$$

where k_s is a roughness length scale called the "equivalent sand-grain roughness", U^* is the friction velocity ($= \sqrt{\tau_w / \rho}$), ν is the kinematic viscosity, τ_w is the wall shear stress, and ρ is the fluid density. In the hydraulically smooth regime the roughness is so small compared to the viscous sublayer that no appreciable effects of the roughness are evident. In the transitionally rough regime, the roughness elements protrude through the viscous sublayer and form drag on the elements becomes a significant contribution to the wall shear stress. As k_s^+ becomes larger ($> 55-70$) the

elements destroy the viscous sublayer, the form drag on the elements becomes the predominant contribution to the wall shear stress, and the skin friction coefficient

$$C_f = 2 \tau_w / (\rho U_\infty^2) \quad (2)$$

becomes independent of the flow Reynolds number. This state is the fully rough regime.

The above description is based on the behavior of the wall shear stress (or C_f). When one considers the heat transfer behavior, the situation is complicated by the fact that there is no thermal equivalent to the form drag contribution to the force on the wall. The heat transfer between the fluid and the wall is by molecular conduction and thus remains a function of both Reynolds number and Prandtl number even in the fully rough regime. The validity of the Reynolds analogy between the momentum and energy fields, which is widely used for zero pressure gradient smooth wall flows (for Prandtl and turbulent Prandtl numbers equal to one), is therefore extremely doubtful for flows influenced by roughness.

In order to predict the thermal and momentum fields using the Reynolds-averaged, boundary layer differential equations for continuity, momentum and energy (see Ref. 1, for example) one must model the turbulent shear stress ($-\rho \overline{u'v'}$) and turbulent heat flux ($-\rho C_p \overline{v't'}$) terms. Suppose, for the sake of argument, that this is done using the eddy diffusivity for momentum (E_m), turbulent Prandtl number (Pr_t), and k_s concepts. Then a turbulence model giving E_m and Pr_t as functions of k_s^+ is required for closure of the problem (see Healzer, et.al.², Cebeci and Chang³, and Ligrani⁴ for recent examples). Once closure is achieved, some numerical method for integrating the set of governing equations is used to determine the solution in terms of velocity and temperature profiles, C_f , and Stanton number, St , which is a non-dimensional heat transfer coefficient.

From the above discussion, one can see the steps or elements required to obtain a prediction of C_f and St for a given rough surface using this approach:

- (1) some means must be available to determine the equivalent sand-grain roughness k_s of the particular surface,
- (2) a turbulence model which incorporates roughness effects through a functional dependence on k_s must be available for closure of the equation set, and

(3) a numerical integration method must be available to solve the equations.

Item (3) will not be considered in this report - efficient numerical schemes are now in common use in boundary layer calculations. Items (1) and (2) were the areas of interest in the current study, with emphasis on the former.

II. OBJECTIVES:

As noted in the previous section, the primary objective of the long range research program proposed by the author and Hodge is the prediction of the fluid dynamics and heat transfer in turbulent boundary layer flows over general rough surfaces using an approach independent of the equivalent sand-grain roughness concept. The reason for this approach is the perceived inadequacy of the sand-grain concept in representing the physics of the thermal and fluid dynamic behavior in the boundary layer. This point will be investigated in some detail in the following sections.

The objectives of the ten-week long Summer Faculty Research Program effort were two-fold:

(1) To conduct a critical evaluation of the sand-grain equivalency concept and previously published efforts (such as those of Dvorak⁵, Dirling⁶, and Simpson⁷) at formulating models to determine k_s for a general rough surface.

(2) To conduct a literature survey in order to identify and obtain pertinent references which are not available in the open literature, i.e., documents with distribution limited to government agencies and/or which have been recently declassified.

The second objective was satisfied with the excellent help of the Technical Library staff at Eglin AFB and will not be explicitly discussed any further.

III. THE SAND-GRAIN EQUIVALENCY CONCEPT

The basis of all sand-grain equivalency analyses is the work reported by Nikuradse⁸ published in 1933. He measured C_f and velocity profiles in fully developed flow in pipes roughened with sand. The "ordinary building sand" was sifted through sieves to achieve a tight size distribution and was attached to the interior surfaces of the pipes using lacquer. The pipe Reynolds number range investigated covered the hydraulically smooth, transitionally rough, and fully rough regimes.

The concept of sand-grain equivalency was first proposed by Schlichting⁹ in 1936. He used a fully developed channel flow to investigate the C_f and velocity profile behavior for flow over surfaces roughened with uniform height elements spaced uniformly in staggered arrays. Surfaces with different element spacing were used to investigate the effects of roughness element density. The effect of roughness element shape was determined by using spheres, cones, spherical segments, short and long angles, and "Hamburg sand" on different test surfaces. The test conditions were such that the flow was in the fully rough state for all test points.

The primary results of this effort were presented as the ratio of an equivalent sand-grain roughness, k_s , to the height, k , of the roughness elements for each surface configuration. Schlichting defined^(9,10) k_s as that value which gives the actual coefficient of resistance when inserted into the equation found by Nikuradse⁸ to describe his results for fully rough flow

$$4C_f = (2 \log (R/k_s) + 1.74)^{-2} \quad (3)$$

where R is the radius of the pipe or hydraulic radius of the channel. The magnitude of k_s is the arithmetic mean height of the sand grains in Nikuradse's experiment, but it is not related in any unique manner to the height of the roughness elements on any other surface, even if the elements are grains of sand. It is also defined solely based on the fully rough regime.

The results of a critical evaluation of the k_s concept will be discussed below. First, however, it is probably worthwhile to answer the following question: "Why bother reanalyzing work which has been accepted as a standard for over 40 years?". Three points are necessary in answer.

First, the k_s approach has been used for years, primarily for skin friction predictions, but no physical basis for its applicability to modeling the thermal behavior of a turbulent flow has been established. If one's objective is to predict the heat transfer on a rough wall whose roughness characteristics are known but on which no data are available, then this applicability must be logically examined rather than being blindly accepted.

Second, the k_s concept and the k_s/k results of Schlichting⁹ have been used inconsistently from author to author and without an awareness of the assumptions in and the limitations on the approach. This situation has occurred because Schlichting defined the k_s concept and summarized his k_s/k results in two paragraphs and one figure in his book¹⁰ (first German edition 1951, first English edition 1955). Authors of later work have referenced (and evidently used) the book¹⁰ rather than the detailed 59-page report⁹. Some examples are Hama¹¹ in 1954, Dvorak⁵ in 1967, Dirling⁶ and Simpson⁷ in 1973, Denman¹² in 1976, and Cebeci and Chang³ in 1978.

Third, in the past decade or so much more detailed data on the structure of turbulent boundary layers over rough surfaces has been obtained (Blake¹³, Grass¹⁴, Pimenta¹⁵, Coleman¹⁶, and Ligrani⁴) than was available in the earlier efforts^{8,9,11,17} which reported and/or used only mean velocity profiles and skin friction coefficients. These more recent data sets call into question some of the assumptions made in earlier methods of analysis of rough wall flows.

IV. DETERMINATION OF k_s AND ITS USE:

One very revealing set of data were presented by Schlichting in his report⁹ but not his book¹⁰. As mentioned previously, he tested a surface roughened with "Hamburg sand" as distinguished from the "Gottingen sand" used by Nikuradse⁸. The results were a value of $k_s/k = 1.64$ for the Hamburg sand, i.e., the effective size of the Hamburg sand was 64% larger than the physical size. This result cannot be attributed to different methods of application of the sand to the test surface - Schlichting also tested a surface roughened with the same sand used by Nikuradse and obtained values of C_f "differing from those found by Nikuradse by 1 to 2 percent".

To the knowledge of this author, the Hamburg sand result has never been quoted, acknowledged, or used in any published work other than Reference 9. This may explain the erroneous but widely-held belief that for surfaces densely roughened by sand or which appear sand-grain-like to the eye (such as grit-blasted surfaces), k_s may be taken as the height of the roughness elements.

Powars¹⁸, in analyzing tests conducted in the Passive Noretip Technology (PANT) Program, noted that "review of the roughness fabrication process originally employed by Nikuradse indicates that the brazed particle models

have essentially a classic sand grain type roughness character". After observing a prediction of k_s/k of about 4 for the same surfaces using Dirling's⁶ correlation (to be discussed later), he stated that "this is in contradiction to the observation...that the brazed particle roughnesses were fabricated in a fashion analogous to Nikuradse's lacquered sand grain roughness which would imply a k_s/k of about unity".

Dahm¹⁹ reported an analysis of heat transfer and shear data from roughened surface tests conducted in the Reentry Vehicle Technology (REV-TECH) Program. Six types of rough surface were used - bonded grit, grit blasted, and four different chemically milled patterns. For the chemically milled patterns, k_s was determined from Dirling's correlation. However, for the bonded grit and grit blasted surfaces k_s was taken to be twice the mean RMS roughness height. Thus the implicit assumption was made that those two rough surfaces were equivalent to Gottingen sand applied to the surfaces using Nikuradse's technique. This assumption is highly questionable considering Schlichting's results on the Hamburg sand and his results for the spherical elements, for example. For the spherical elements, in one instance a 50% decrease in spacing resulted in a factor of 3.7 increase in k_s/k , while in another a 40% decrease in spacing resulted in a factor of 6 decrease in k_s/k (the change in k_s/k obviously being very dependent on the magnitude of the spacing to height ratio).

Since k_s/k is a function of (at least) the height, spacing, and shape of the roughness elements, a fair amount of effort has been reported on attempts to correlate k_s/k (or the shift in the mean velocity profile, which is a slightly different but essentially equivalent way of viewing the problem) with some parameter which takes this into account. Dvorak⁵, Simpson⁷, and Dirling⁶ have all presented such correlations. That of Dirling, which is the most widely used at present, is shown in Figure 1, where k_s/k is plotted against a "roughness density", λ , defined by

$$\lambda = (l_r/k) (A_s/A_p)^{4/3} \quad (4)$$

The mean roughness height is denoted by k , l_r is the mean center to center roughness spacing, A_p is the projected element area in the flow direction, and A_s is the windward surface area of the element seen by the flow.

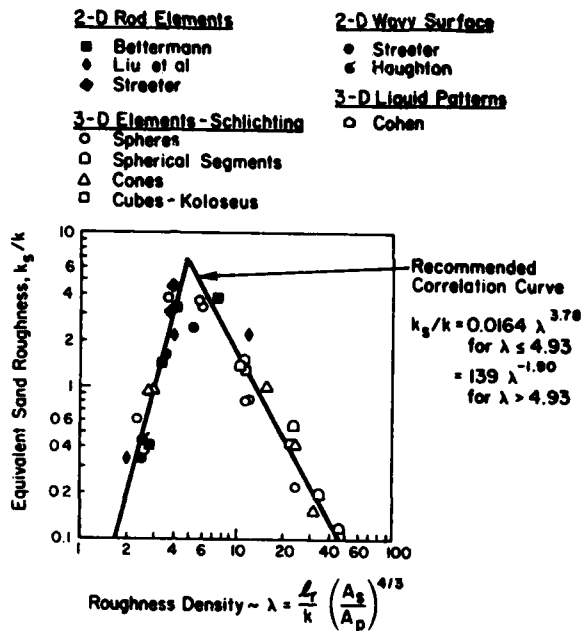


FIGURE 1. Effective sand-grain roughness correlation of Dirling (Reference 6).

This correlation collapses the available data better than any attempt published so far. Several points should be considered in evaluating the information shown in the figure. First, for a given value of roughness density, λ , the data points show values of k_s/k which differ by about a factor of 3. Second, for a surface with randomly sized and shaped roughness, different authors evaluate k , l_r , A_s and A_p differently since there is no one agreed-upon "correct" way. King, et. al.^{20p}, recently presented a discussion of this problem, but unfortunately offered no definite way to resolve it. Third, the correlation attempts to collapse the data from both two-dimensional (transverse bar roughness) and three-dimensional (distributed roughness) geometries. The physical characteristics of the flow around the two geometries are quite different. Perry, et. al.²¹, found that for transverse bar roughness the roughness effects on C_f scale with k for certain ranges of k/l_r , but not for other ranges.

The Dirling correlation has given poor results when compared with data recently reported by various investigators. In his work with transverse bar roughness at Cal Tech, Berg²² found the correlation gave k_s/k three times larger than his experimentally determined value. Denman^{12s}, in his work with grit blasted surfaces at Ohio State, found "the Dirling roughness density correlation also predicts very low rough surface skin friction and heat transfer". Dahm¹⁹, in his previously mentioned analysis of the REV-TECH data, observed that "the only thing conclusive about the results is that the heat transfer data do not rank according to Dirling's correlation of effective sand grain roughness". He did not fault the correlation, but reasoned that "the heat transfer characteristics do not scale with equivalent sand grain roughness for non-sand-grain surfaces".

At this time, it appears that there is no successful model to determine the equivalent sand-grain roughness of an arbitrary surface. Indeed, considering Schlichting's⁹ result for Hamburg sand, the k_s value for a sand-grain surface cannot be predicted without data on the particular surface being available. In addition, the most recent work¹⁹ reported on heat transfer on rough surfaces agrees with the author's tentative conclusion that the thermal behavior of a roughwall turbulent boundary layer does not scale with equivalent sand-grain roughness.

In the following section, an examination of the details of the sand-grain equivalency concept is presented which indicates some reasons why attempts to find a k_s/k correlation for general rough surfaces have not produced satisfactory results.

V. ROUGHNESS AND THE LAW OF THE WALL:

It is necessary to discuss the law of the wall - the logarithmic region of the mean velocity profile - because assumptions regarding its use are embedded in the data analyses which have led to k_s/k values reported for various surfaces. The assumptions required and the specifics of its use have been the source of misunderstandings between various researchers (see, for example, the recent acerbic exchange between Mills²³ and Cebeci and Chang²⁴ in the AIAA Journal).

For turbulent flows on smooth walls it has been shown both analytically and experimentally that there exists a region in the mean velocity profile described by

$$U^+ = B \log Y^+ + A \quad (5)$$

or, equivalently

$$U^+ = (1/\kappa) \ln Y^+ + A \quad (6)$$

where $U^+ = U/U^*$, $Y^+ = U^*Y/\nu$, κ is called the Karman constant, and obviously B and κ are related by

$$B = 2.303/\kappa \quad (7)$$

The Karman constant is considered to be a universal constant with a magnitude of about $\kappa=0.40$. We will not consider the arguments over the value or the constancy of κ for smooth wall flows here, but will accept the value of 0.40 (or $B=5.75$) and $A=5.5$ for purposes of this discussion.

For flow over rough walls, it has been postulated and/or assumed by many workers that the effect of roughness is to shift the velocity profile given by (5) downward on a semilogarithmic plot so that¹⁷

$$U^+ = B \log Y^+ + A - \Delta U^+(k_s^+) \quad (8)$$

where ΔU^+ is the amount of the shift and is a function of the equivalent sand-grain roughness. This effect can also be expressed in the form⁸

$$U^+ = B \log (Y/k_s) + A'(K_s^+) \quad (9)$$

where comparison of (8) and (9) shows that

$$A'(k_s^+) = B \log k_s^+ + A - \Delta U^+ \quad (10)$$

It can be shown¹¹ from consideration of (8), the experimentally-determined universal character of the velocity-defect law, and the definitions of U^* and C_f , that for the same magnitude of the displacement thickness Reynolds number

$$\Delta U^+ = (2/C_{f,smooth})^{1/2} - (2/C_{f,rough})^{1/2} \quad (11)$$

This direct relationship between the rough wall skin friction and ΔU^+ indicates the reason so much effort in the past has been directed at finding the function $\Delta U^+(k_s^+)$.

It is instructive to consider equations (5) through (11) from the viewpoint that a velocity profile U vs. Y has been measured and we wish to use

the equations and data to determine other flow parameters and variables. For a smooth wall, equation (5) applies with A and B being known constants so that U^* is the only unknown. Clauser²⁵ proposed a method for determining C_f from measured velocity profiles using the above observation and the fact that

$$C_f/2 = (U^*/U_\infty)^2 \quad (12)$$

where U_∞ is the freestream velocity at the boundary layer edge.

For a rough wall flow, equations (8) - (10) apply and the situation becomes more complicated. If only a velocity profile U vs. Y is known, then the unknowns can be considered to be U^* , Y , B , A , and k_s (or ΔU^+). The distance normal to the wall, Y , is unknown because the apparent wall location ($Y=0$) which gives a straight line in U^+ , $\log Y^+$ coordinates generally lies somewhere between the crests and valleys of the roughness elements and does not correspond to the distance Y used in an experimentally determined profile, which is usually arbitrarily referenced to the plane of the crests of the roughness elements. The values of B and A are usually taken as the smooth wall values; however, the arguments used to support this are not verified by experimental data and will be discussed below. The difficulty of determining k_s (or equivalently, ΔU^+) for a surface has been discussed in the previous section.

Both Nikuradse⁸ and Schlichting⁹ used equation (9) in their data analysis. Nikuradse determined C_f independently by measuring the pressure drop in his fully developed pipe flow; thus, U^* was known. He assumed the value of B was the same as that for smooth walls, and found for the fully rough regime that $A' = 8.48$ fit his data well. However, he never explicitly defined the $Y=0$ position which he used. The best inference which one can make is that he used the same definition as that of Schlichting⁹, who defined Y as "equal to the distance from a hypothetical smooth wall that replaces the rough wall in such a manner as to keep the fluid volume the same".

Schlichting⁹ determined the k_s/k ratios for his test surfaces in the following manner. He used the expression given by Nikuradse for fully rough flow

$$U/U^* = 5.75 \log (Y/k_s) + 8.48 \quad (13)$$

and assumed that his data for a surface of roughness elements of uniform height k could be fit by the expression

$$U/U^* = 5.75 \log (Y/k) + A^* \quad (14)$$

where U^* was essentially determined independently by using pressure drop measurements. Now if one defines the k_s for a particular surface to be that which causes equations (13) and (14) to be equal at a given value of Y , then one finds

$$5.75 \log (k_s/k) = 8.48 - A^* \quad (15)$$

or

$$k_s/k = 10^{(8.48 - A^*)/5.75} \quad (16)$$

Schlichting determined the average value of A^* using the velocity profiles (having approximately ten points each) on a given surface plotted in the form of equation (14). He then calculated k_s/k from equation (16). These k_s/k values are the basis of most of the arbitrary rough surface boundary layer work performed since 1937, and remain the primary data base for the k_s/k correlation schemes proposed to date^{5,6,7,12}.

The present author¹⁶ took fully rough regime velocity and skin friction measurements (among others) on a surface identical to Schlichting's⁹ Plate V - spheres packed in the densest pattern. Shown in Figure 2 is a typical velocity profile¹⁶ plotted in U^+ , $\log (Y/k)$ coordinates with three assumed effective wall locations $\Delta Y = 0, 0.2, \text{ and } 0.4 k$ below the plane of the spherical element crests. The $\Delta Y = 0.4k$ wall location is that which is obtained using Schlichting's⁹ definition given above. The $\Delta Y = 0.2k$ location is that obtained by assuming, since the spheres are packed so densely, the flow only "sees" the upper half of each spherical element. Thus for this case one assumes a surface of hemispheres of height $k/2$, and application of Schlichting's definition of wall location yields $\Delta Y = 0.2k$.

Several points should be noted from this analysis. First, for each effective wall location a logarithmic region can be discerned in the velocity profile; however, the slope B of these "log" regions varies with Y and is not equal to 5.75 for the ΔY 's used. Second, determination of k_s/k using

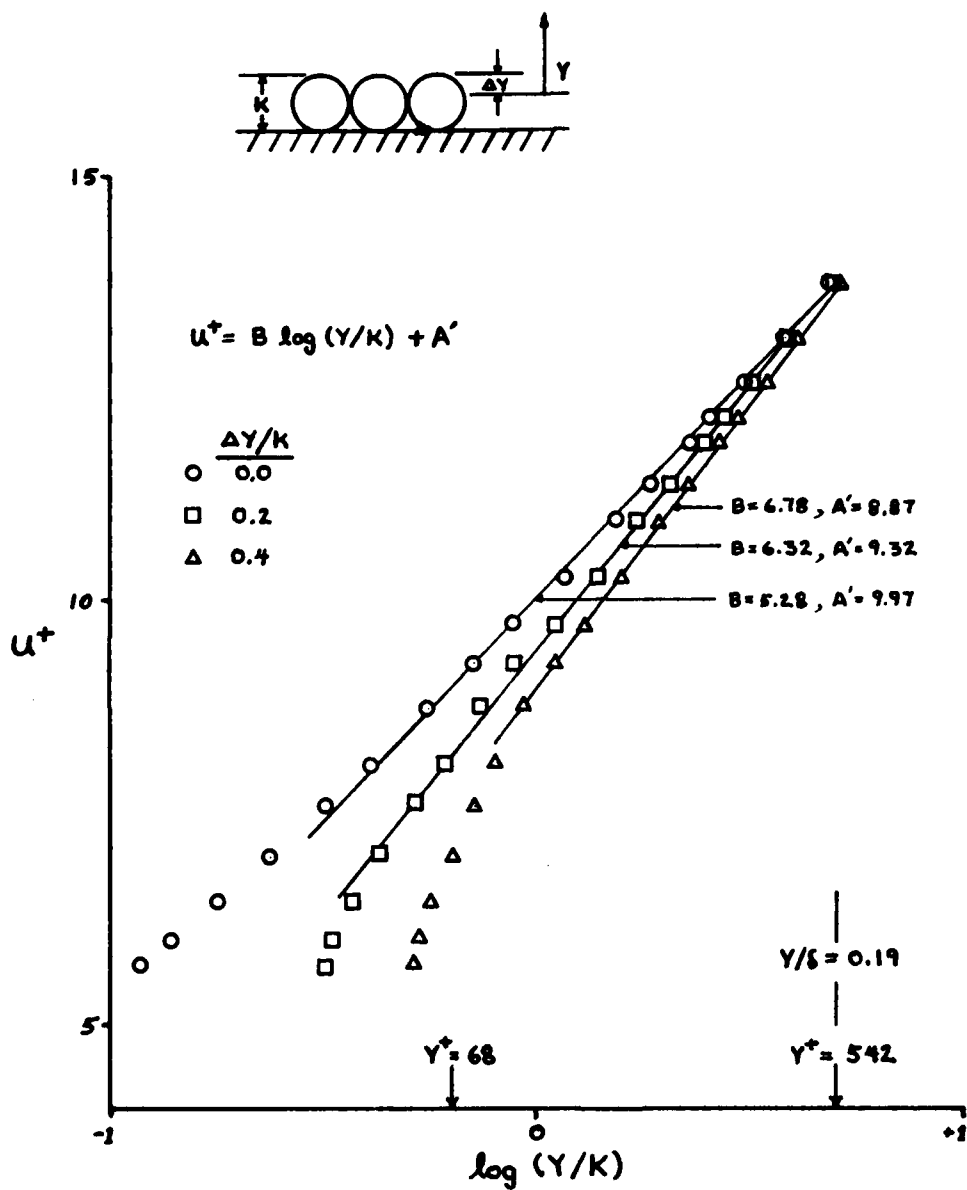


FIGURE 2. Typical Velocity Profile for Fully Rough Turbulent Boundary Layer in Zero Pressure Gradient (Reference 16).

exactly the same procedure as that used by Schlichting gives values of 0.519, 0.717, and 0.833 respectively for $\Delta Y = 0, 0.2 k$, and $0.4 k$. These values should be compared to the $k_s/k = 0.626$ value reported by Schlichting⁹.

A more detailed look at the data⁹ reported for Plate V shows that, for this particular surface, Schlichting did in fact assume the flow saw only the upper half of the spheres and he used $\Delta Y = 0.2 k$ rather than the $0.4 k$ value which would be obtained using his stated definition (and which was used for the other sphere spacings). If his stated definition of effective wall location is used, re-analysis of his data gives a value for k_s/k equal to 0.662, rather than the value of 0.626 he reported.

The discussion above shows that the k_s concept is intimately connected to the law of the wall concept with the slope B taken as the smooth wall value, and with the effective wall location being treated somewhat inconsistently. Note that the constant $A' = 8.48$ for fully rough flow was also determined using the same assumptions.

The argument that the log law applies to rough surfaces with the same slope B as for smooth surfaces has been based on the assertion that roughness effects are confined to a thin near-wall region and result therefore only in a shift in the intercept A. This argument was based only on C_f and mean velocity profile data. More extensive measurements over the past dozen years have shown that roughness effects are present throughout the boundary layer and are not confined only to a region near the wall. Blake¹³, Pimenta¹⁵, and Coleman¹⁶ observed increased turbulent kinetic energy across the entire layer, and the degree of anisotropy among the components of the turbulent kinetic energy was also changed by the wall conditions^{15,16}. Grass¹⁴ observed differences in the bursting behavior between smooth and rough wall flows in his flow visualization study. Ligrani⁴ concluded from his spectral measurements that more energy exists at higher frequencies in rough surface flows and that the magnitude of the Kolmogorov length scale for his rough surface flow was approximately half the magnitude for smooth wall flow.

In view of the above, one should be surprised if the slope B of the log region remained the same as in smooth wall flow, not vice-versa. In a very recent paper, Uram²⁶ addressed the question of the value of B for flow over various kinds of rough surfaces. He examined data for which C_f was determined independently of wall law assumptions, used the technique described by Perry

and Joubert²⁷ to find the effective wall location, and found values of B which varied from approximately 4 to 9 for wire mesh, right circular cylinder segment, and irregular ship hull roughness. This result, taken together with the others discussed above, must raise serious doubts about the validity of assuming a constant slope for the wall law over both smooth and rough surfaces.

VI. SUMMARY OF EVALUATION OF SAND-GRAIN EQUIVALENCY CONCEPT:

Since the definition of the equivalent sand-grain roughness concept by Schlichting⁹ in 1936, it has been misinterpreted and applied inconsistently from author to author. A surface roughened by application of sand grains in a dense pattern generally does not have a k_s/k of one - this is shown by Schlichting's results for Hamburg sand. There is certainly no basis for assuming that $k_s/k = 1$ if a surface "appears sand-grain-like" to the eye.

As shown in the previous section, the definition of k_s and the values reported by Schlichting (which still form the basis of much rough wall boundary layer analysis) are intimately tied to an assumed wall location and to a value of slope, B, for the law of the wall which is assumed to be the same as that in smooth wall flows. The fully rough regime wall law intercept ($A' = 8.48$) reported by Nikuradse⁸ and used by Schlichting is also tied to the same assumptions. As previously discussed, more recent experimental data and analyses indicate that the wall law slope is in fact influenced by wall roughness, with values of B from 4 to 9 being reported. This is not surprising since data on the structure of the turbulence field indicate roughness effects are not confined to the near wall region, but influence the turbulence across the entire boundary layer.

The effective wall location as defined by Schlichting is not consistent with his assumption of the wall law constants and was evidently used inconsistently in his determination of k_s/k values. This was shown by reanalysis of his data for spherical roughness elements arranged in the most dense pattern. Effective wall locations determined by other investigators (Pimenta¹⁵ and Perry, et. al.²¹, for example) using an assumed wall law slope equal to the smooth wall value have deviated significantly from the locations which would be found using Schlichting's definition. Perry, et.al.²¹, actually found effective wall locations 1.5 to 2 roughness heights below the roughness crests for transverse bar elements in an adverse pressure gradient.

There is currently no acceptable method for determining the equivalent sand-grain roughness, k_s , for a general rough surface on which no skin friction data are available. (Even if skin friction data are available, the k_s determination is subject to the ambiguities discussed above.) The most widely used correlation, that of Dirling⁶, has been found to give unacceptable results by various researchers^{12,22}. Data correlated using this technique⁶ give k_s/k values which can differ by a factor of 3 for a given value of "roughness density", λ .

It appears that k_s would be a poor choice on which to try to model roughness effects on turbulent heat transfer. Dahm¹⁹ found that the rough wall heat transfer data from the REV-TECH program do not scale with equivalent sand-grain roughness. Consideration of the physics of the flow field seems to support this conclusion. Since there is no thermal equivalent to the form drag contribution to the wall skin friction, the increases in heat transfer and skin friction due to roughness are caused by processes which are not analogous.

VII. COMMENTS ON A DISCRETE ELEMENT APPROACH:

An alternative to modeling roughness effects on the turbulent boundary layer with the sand-grain equivalency concept is to consider the momentum and energy transport processes on the collection of individual roughness elements - the so-called discrete element approach. This is not a new way of viewing the problem. Schlichting⁹ presented a brief analysis of the drag on individual roughness elements in analyzing the effect of roughness element density on skin friction. Liepmann and Goddard²⁸ also took this viewpoint, as did Lewis²⁹.

Calculation methods for skin friction and heat transfer on rough surfaces based on the discrete element approach have been reported by Finson and co-workers^{30,31}, Hodge and Adams³², and Lin and Bywater³³. The model of Hodge and Adams relies in some aspects on the k_s concept. Lin and Bywater state that they use an unpublished mixing length model by Dahm - they do not give details of the model, but this author surmises from Dahm's published work that the model is based on the k_s concept. The approach of Finson does not rely on the equivalent sand-grain concept, but only 3-D roughness elements of a uniform height and spacing are assumed. He uses the mean values of element height and spacing in calculations for non-uniform rough walls, and evidently

uses a single value of C_D , the drag coefficient, regardless of element shape or Reynolds number. The three techniques also differ in the extent of roughness effects present in the energy equation, and this difference must be resolved.

This author has concluded, based on his and Hodge's work over the last few years, that the most promising approach to calculating the fluid dynamics and heat transfer in a turbulent boundary layer influenced by roughness is a discrete element approach which accounts for the non-uniformity of the roughness elements found on most rough surfaces and which is free of any dependence on sand-grain equivalency concepts. Such a model will probably, in final form, be based on the means and standard deviations of both the roughness element height and spacing and will use a roughness element drag coefficient which is dependent on element shape.

The two most basic reasons for modeling the deviations of the actual elements from the mean height and spacing are their influence on the extent of the transitionally rough regime and on the sink term in the momentum equation, which takes the pressure drag into account. Ligrani⁴ discusses the effect of roughness height uniformity on the transitionally rough regime - essentially, the smaller the variability of height, the shorter the transitionally rough region (in terms of roughness Reynolds number). The importance in the momentum sink term arises because the term depends on velocity squared and velocity varies with distance from the wall.

VIII. RECOMMENDATIONS:

The inadequacies of the sand-grain equivalency concept and some of the reasons for them were examined in the previous sections, and the discrete element approach was commented upon in Section VII. This author recommends that the research program proposed by himself and Hodge and which was referred to in Section I be pursued. This program proposes (1) the development of a generalized mathematical description of roughness which will allow for non-uniform element height and spacing, (2) the formulation of a discrete element turbulence model which will account for the effects of non-uniform roughness elements on the fluid dynamics and heat transfer, and (3) the development/modification of a computational procedure capable of accurately predicting the fluid dynamics and heat transfer in a turbulent boundary layer flow over a prescribed rough surface.

REFERENCES

1. White, F.M., Viscous Fluid Flow, McGraw-Hill, New York, 1974.
2. Healzer, J. M., Moffat, R. J., and Kays, W. M., "The Turbulent Boundary Layer on a Rough, Porous Plate: Experimental Heat Transfer with Uniform Blowing," Report HMT-18, Thermosciences Division, Dept. of Mech. Eng., Stanford University, 1974. (Also Ph.D. Dissertation, 1974).
3. Cebeci, T., and Chang, K. C., "Calculation of Incompressible Rough-Wall Boundary-Layer Flows," AIAA Journal, Vol. 16, pp. 730-735, 1978.
4. Ligrani, P. M., "The Thermal and Hydrodynamic Behavior of Thick, Rough-Wall, Turbulent Boundary Layers," Ph.D. Dissertation, Dept. of Mech. Eng., Stanford Univ., 1979. (Also Report HMT-29).
5. Dvorak, F. A., "Calculation of Turbulent Boundary Layers on Rough Surfaces in Pressure Gradient," AIAA Journal, Vol. 7, pp. 1752-1759, 1969.
6. Dirling, R. B., Jr., "A Method for Computing Roughwall Heat Transfer Rates on Reentry Nosetips," AIAA Paper No. 73-763 presented at the AIAA 8th Thermophysics Conference, Palm Springs, Calif., July 16-18, 1973.
7. Simpson, R.L., "A Generalized Correlation of Roughness Density Effects on the Turbulent Boundary Layer," AIAA Journal, Vol. 11, pp. 242-244, 1973.
8. Nikuradse, J., "Laws for Flows in Rough Pipes," VDI-Forschungsheft 361, Series B, Vol. 4, 1933; NACA TM 1292, 1950.
9. Schlichting, H., "Experimental Investigation of the Problem of Surface Roughness," Ingenieur-Archiv, Vol VII, No. 1, 1936. (NACA TM 823, 1937).
10. Schlichting, H., Boundary Layer Theory, 7th Edition, McGraw-Hill Book Co., Inc., New York, 1979.
11. Hama, F. R., "Boundary Layer Characteristics for Smooth and Rough Surfaces," Trans. SNAME, Vol. 62, pp 333-358, 1954.
12. Denman, G. L., "Turbulent Boundary Layer Rough Surface Heat Transfer on Blunt Bodies at High Heating Rates," Ph.D. Dissertation, Dept. Mech. Eng., Ohio State Univ., 1976.
13. Blake, W. K., "Turbulent Boundary-Layer Wall-Pressure Fluctuations on Smooth and Rough Walls," Jn. Fluid Mech., Vol. 44, pp. 637-660, 1970.

14. Grass, A. J., "Structural Features of Turbulent Flow over Smooth and Rough Boundaries," Jn. Fluid Mech., Vol. 50, pp. 233-256, 1971.
15. Pimenta, M. M., "The Turbulent Boundary Layer: An Experimental Study of the Transport of Momentum and Heat with the Effect of Roughness," Ph.D. Dissertation, Dept. Mech. Eng., Stanford Univ., 1975. (Also Report HMT-21).
16. Coleman, H. W., "Momentum and Energy Transport in the Accelerated Fully Rough Turbulent Boundary Layer," Ph.D. Dissertation, Dept. Mech. Eng., Stanford Univ., 1976. (Also Report HMT-24).
17. Clauser, F. H., "The Turbulent Boundary Layer," Advances in Applied Mechanics, Vol. IV, pp. 1-51, Academic Press, New York, 1956.
18. Powars, C. A., "Passive Nosedip Technology (PANT) Program: Surface Roughness Effects - Roughness Augmented Heating Data Correlation and Analysis," SAMSO-TR-74-86-Vol. 3-Pt 2, 1974. (Declassified Dec. 31, 1980; Distrib. limited to U.S. Gov't. agencies.)
19. Dahm, T. J., "Analysis of AEDC Heat Transfer and Shear Data from Roughened RV Nosedip Models in Hypersonic Flow," Air Force Ballistic Missile Office Report BMO/TR-80-52-Vol III-Part IV, 1980. (Distrib. limited to U.S. Gov't agencies.)
20. King, M. J., et.al., "Roughness Characteristics of Plane Surfaces Based on Velocity Similarity Laws," ASME Paper 81-FE-34, 1981.
21. Perry, A. E., Schofield, W. H., and Joubert, P. H., "Rough Wall Turbulent Boundary Layers," Jn. Fluid Mech., Vol. 27, pp. 383-413, 1969.
22. Berg, D. E., "Surface Roughness Effects on the Hypersonic Turbulent Boundary Layer," Ph.D. Dissertation, Graduate Aeronautical Laboratories, Cal. Tech., 1977.
23. Mills, A. F., "Comment on 'Calculation of Incompressible Rough-Wall Boundary-Layer Flows'," AIAA J., Vol. 17, pp. 220-221, 1979.
24. Cebeci, T., and Chang, K. C., "Reply by Authors to A. F. Mills," AIAA J., Vol. 17, pp 221-222, 1979.
25. Clauser, F. H., "Turbulent Boundary Layers in Adverse Pressure Gradients," Jn. Aero. Sci., Vol. 21, pp. 91-108, 1954.
26. Uram, E. M., "Analysis of the Roughness Function and Wall Law Slope for Rough Surface Turbulent Boundary Layers," ASME Paper 81-FE-36, 1981.

27. Perry, A. E., and Joubert, P. N., "Rough-Wall Boundary Layers in Adverse Pressure Gradients," Jn. Fluid Mech., Vol. 17, pp. 193--211, 1963.
28. Liepmann, H. W., and Goddard, F. E., "Note on the Mach Number Effect Upon the Skin Friction of Rough Surfaces," J. Aeronautical Sci., Vol. 24, p. 784, 1957.
29. Lewis, M. J., "An Elementary Analysis for Predicting the Momentum and Heat Transfer Characteristics of a Hydraulically Rough Surface," J. Heat Transfer, Vol. 97, pp. 249-254, 1975.
30. Finson, M. L., "A Reynolds Stress Model for Boundary Layer Transition with Application to Rough Surfaces," AFOSR-TR-0322, 1975.
31. Finson, M. L., and Clarke, A. S., "The Effect of Surface Roughness Character on Turbulent Reentry Heating," AIAA Paper 80-1459, 1980.
32. Hodge, B. K., and Adams, J. C., "The Calculation of Compressible Transitional, Turbulent, and Relaminarizational Boundary Layers over Smooth and Rough Surfaces Using an Extended Mixing-Length Hypothesis," AEDC-TR-77-96, 1978.
33. Lin, T. C., and Bywater, R. J., "The Evaluation of Selected Turbulence Models for High-Speed Rough-Wall Boundary Layer Calculations," AIAA Paper 80-0132, 1980.

1981 USAF - SCEEE SUMMER FACULTY RESEARCH PROGRAM

Sponsored by the

AIR FORCE OFFICE OF SCIENTIFIC RESEARCH

Conducted by the

SOUTHEASTERN CENTER FOR ELECTRICAL ENGINEERING EDUCATION

FINAL REPORT

INTERPOLATION AND APPROXIMATION TECHNIQUES FOR GRIDDED TERRAIN DATA

Prepared by: Dr. David L. Cozart

Academic Rank: Associate Professor of Mathematics

Department and University: Department of Mathematics and Computer Science
The Citadel, Charleston, South Carolina

Research Location: Avionics Laboratory, System Avionics Division,
Support Systems Branch, Systems Projects and
Simulation Group, Wright Patterson Air Force
Base, Dayton, Ohio

USAF Research Colleague: Nelson N. Estes

Date: August 14, 1981

Contract No: F49620-79-C-0038

INTERPOLATION AND APPROXIMATION TECHNIQUES
FOR GRIDDED TERRAIN DATA

By

David L. Cozart

ABSTRACT

Various interpolation and approximation techniques which are applicable to terrain data defined on a square grid are described. Most of these techniques have the potential for data compaction, i.e., effectively representing the given data using less computer memory than required by the raw data. The amount of compaction obtained depends upon 1) the technique used, 2) the allowable error in representing the data, 3) the grid spacing, and 4) the raw data values. Some of the methods are two stage processes involving both approximation and interpolation. For each technique, the advantages and disadvantages of the method are discussed. One two stage technique is proposed for further research. A method of comparing the different techniques is also described.

ACKNOWLEDGEMENT

The author wishes to thank the Air Force Systems Command, the Air Force Officer of Scientific Research and the Southeastern Center for Electrical Engineering Education for the opportunity of spending ten weeks at the Avionics Laboratory, Wright Patterson Air Force Base, Dayton, Ohio. Special thanks are extended to members of the Systems Projects and Simulation Group for their hospitality and help.

Finally, the author is indebted to Nelson N. Estes for his guidance and suggestions during this research project.

I. INTRODUCTION

The Air Force is engaged in a project to develop techniques for out-the-window scene generation utilizing the digitized terrain elevation data supplied by the Defense Mapping Agency. The data is to be used to generate a terrain surface appropriate for simulation of actual terrain as seen from a low flying aircraft. The data is defined on a rectangular grid with a grid point separation of three seconds. A method of data compaction is sought which will allow rapid access to the data and then immediate display of the terrain.

Some techniques for surface generation from DMA data have already been considered by James Jancaitis for the U.S. Army Engineer Topographic Laboratories. Jancaitis replaces the original data with local least-square polynomial approximations which overlap. These local approximations are then combined using weighting functions to produce a smooth global approximation to the initial data. The global approximation is then used to visually display the data. This method has been applied to terrain data and the results have been compared with results obtained by using the conventional matrix format storage of data. This comparison of methods was done by Robert Jablinske for the Topographic Laboratories. The results indicate that the Jancaitis method may introduce too much error into the surface for certain types of terrain and that other surface generation techniques work just as well in terms of compaction and error.

II. OBJECTIVES

The main objective was to determine a compaction technique for the storage of terrain data and the display of out-the-window scenes. The specific goals are listed below:

- (1) Conduct a literature search for data compaction techniques.
- (2) Consider modifications to existing compaction techniques.

For example, with the Jancaitis approach, error is introduced into the final global approximation by the local approximations as well as by the weighting functions. Thus,

different local approximations and weighting functions yield different results. Jablinske uses a different local approximation since it yields a slightly lower value for the standard deviation from the mean error.

- (3) Determine a foundation for comparison of different compaction techniques. The methods should be compared in terms of data storage requirements, retrieval efficiency and data accuracy.

III. METHOD OF JANCAITIS

The gridded data is organized as shown in Figure 1. Each "•" indicates the location of a given z-value. A linear transformation has been used to scale the data to a unit square. The value of NFF is chosen first. Then NFF is chosen to correspond to the NFF value. The maximum NFF value is

$$NFF_{\max} = 2 NFF - 1 \quad (1)$$

and the minimum NFF value is

$$NFF_{\min} = \begin{cases} NFF & \text{if } NFF \text{ is odd} \\ NFF-1 & \text{if } NFF \text{ is even} \end{cases} \quad (2)$$

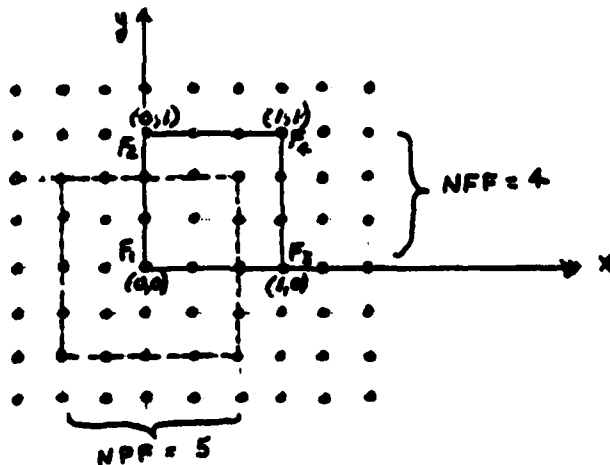


FIGURE 1 - METHOD OF JANCAITIS

Four polynomials F_1 , F_2 , F_3 and F_4 are obtained, each of which is of the form

$$a_0 + a_1x + a_2y + a_3xy \quad (3)$$

Each of these polynomials is centered at the corner point indicated in Figure 1. For example, F_1 is obtained by using all the z-values that fall in the square in Figure 1 with the broken line as boundary. A

weighted least squares method is used where the corner point (0,0) is weighted most heavily. The resulting F_1 interpolates to the data value given at (0,0).

The four F polynomials are combined as follows:

$$\begin{aligned} f(x,y) = & F_1(x,y) \cdot w_1(x,y) + F_2(x,y) \cdot w_2(x,y) \\ & + F_3(x,y) \cdot w_3(x,y) + F_4(x,y) \cdot w_4(x,y) \end{aligned} \quad (4)$$

where the w 's are weighting functions given by:

$$\begin{aligned} w_1(x,y) &= (1-x)^2(1-y)^2/D \\ w_2(x,y) &= (1-x)^2y^2/D \\ w_3(x,y) &= x^2(1-y)^2/D \\ w_4(x,y) &= x^2y^2/D \end{aligned} \quad (5)$$

with

$$D = [x^2 + (1-x)^2][y^2 + (1-y)^2] \quad (6)$$

The resulting global surface obtained from the $f(x,y)$ functions is continuous and smooth (belongs to C^1). Complete details of this technique are given by Jancaitis.²⁹ For any compaction to occur, the value of NFF must be greater than four.

Jablinske^{27,28} compares the above compaction technique with the technique of regridding and thus eliminating some of the data. Different terrains are used for comparison of the techniques in terms of storage requirements, retrieval efficiency, and data accuracy. The results of the study indicate that just as accurate interpolation results are obtained by eliminating every other gridded data point and then using a simple linear interpolation involving the four corner points of the cell in which the point (x,y) in question belongs. The compaction obtained for the different terrains using this method compares favorably with the compaction obtained using the Jancaitis method.

IV. BICUBIC SPLINE INTERPOLATION

The gridded data is organized as shown in Figure 2.

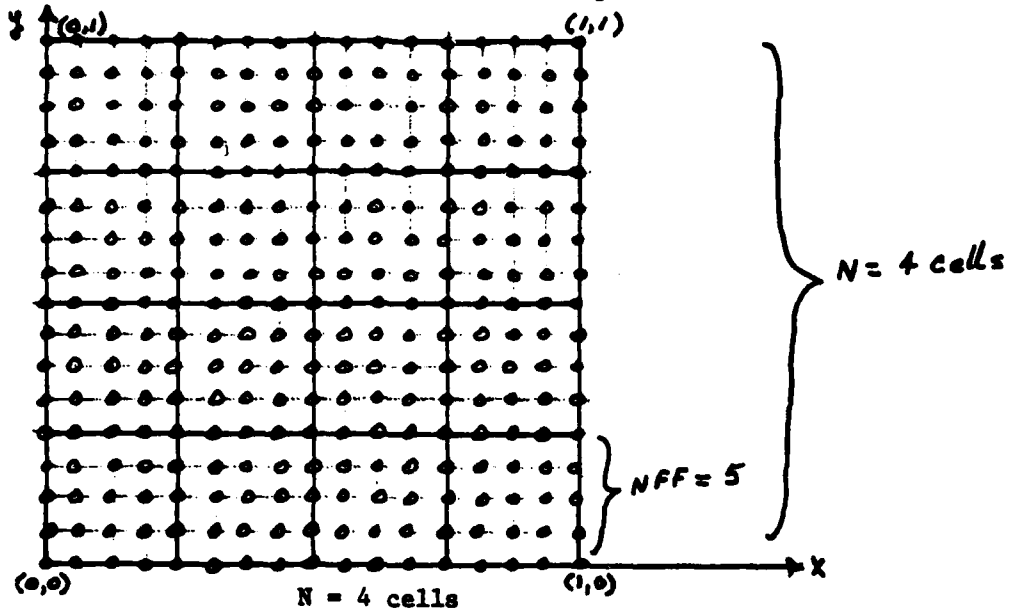


FIGURE 2 - DATA ORGANIZATION FOR SPLINE INTERPOLATION

NFF determines the size of each cell upon which a bicubic polynomial is to be defined, while N determines the number of cells which are considered as a unit. Only those values that fall on the corner of a cell are used in calculating the bicubic spline. The region may be scaled so that the corner points for the entire area are (0,0), (0,1), (1,1) and (1,0). For any compaction to take place, NFF must be greater than 4. This technique involves finding, for each cell with lower left corner point denoted by (x_m, y_n) , a bicubic polynomial of the form:

$$f_{mn}(x,y) = \sum_{i=0}^3 \sum_{j=0}^3 a_{ij}^{m,n} (x - x_m)^i (y - y_n)^j \quad (7)$$

These bicubic polynomials assume the given value at the corner points of the cell and they fit together on cell boundaries so that a surface is obtained over the entire area which is continuous and smooth (belongs to C^1). This is the case because values of f , f_x , f_y and f_{xy} are required to agree at corner points of adjacent cells. The value of f at corner points is given, but the values for f_x , f_y and f_{xy} must be determined. After these values have been obtained, the method of

determining $f(x,y)$ is identical to the method of local bicubic interpolation which is described in part VI. To determine the values of f_x , f_y and f_{xy} at corner points, the above continuity and smoothness conditions are assumed together with the following boundary conditions⁹:

$f_{xx} = 0$ at all corner points which fall on
vertical boundary lines of unit square.

$f_{yy} = 0$ at all corner points which fall on horizontal (8)
boundary lines of unit square.

$f_{xy} = 0$ at the four corner points of the unit square.

These boundary conditions together with the continuity and smoothness conditions completely determine the coefficients of each bicubic defined on the cells forming the unit square. Three tridiagonal systems of simultaneous linear equations are obtained, each of which has a unique solution obtainable through Gaussian elimination^{9,16,41}.

The above spline is called the natural bicubic spline. A FORTRAN subroutine which calculates natural bicubic splines is found in the IMSL Library²⁶. One disadvantage of this spline is that a flat spot is generated at a point where the second derivative is assumed to be zero. This problem may be overcome by specifying low-order derivative values on the boundary of the unit square instead of using the natural boundary conditions. A FORTRAN program for bicubic splines which requires input of low-order derivatives is given by Koelling and Whitten³¹. Also, using the natural cubic spline method, the global surface is continuous but the surface is not necessarily smooth on the boundaries of the unit square where the splines meet. Smoothness is obtain by specifying the low-order derivatives at grid points along the boundary of the unit square

This technique of compaction is very similar to the method of local bicubic interpolation, but there is one significant difference. Bicubic spline interpolation is not local in the sense that interpolation at a point (x,y) does not only depend upon the given f values at the corner points of the cell in which (x,y) belongs, but depends upon the f value at all corner points of Figure 1. Because of this, Birkhoff and

AD-A113 708

SOUTHEASTERN CENTER FOR ELECTRICAL ENGINEERING EDUCAT--ETC F/6 S/1
USAF SUMMER FACULTY RESEARCH PROGRAM. 1981 RESEARCH REPORTS, V6--ETC(U)
OCT 81 W D PEELE F49620-79-C-0038

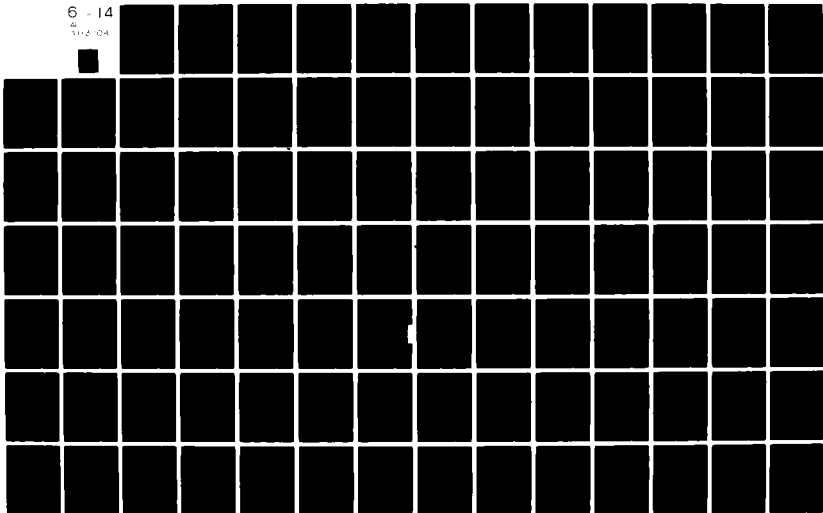
UNCLASSIFIED

AFOSR-TR-82-0227

NL

6 - 14

4
11-2-04



and DeBoor¹⁰ suggest that local bicubic interpolation is preferable. Another criticism of this method is the fact that the f values other than those that occur at the corner points of cells are completely ignored. Thus these non-corner f values provide no information in determining the final surface.

V. LEAST SQUARES APPROXIMATION

The gridded data is organized as shown in Figure 3.

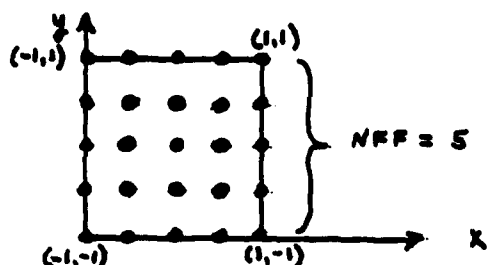


FIGURE 3 - ORGANIZATION OF DATA

Each "*" again indicates the location of a data value. The z -values have been scaled as indicated in Figure 3. All the z -values are used in obtaining a surface which approximates the given z -values.

This technique involves finding a polynomial

$$f(x,y) = \sum_{i=0}^k \sum_{j=0}^m b_{i,j} x^i y^j \quad (9)$$

defined on the entire grid of Figure 3 which best approximates the given z -values in the sense that the function $f(x,y)$ obtained minimizes

$$S^2 = \sum (f(x,y) - z_{xy})^2 \quad (10)$$

where the summation is taken over the entire grid.

This technique is not proposed as a compaction technique by itself, but as a part of a two step process to be described in Part XI. The least squares method cannot be used alone as a compaction technique because the global surface obtained is not continuous.

The above minimization requirement of Equation 10 leads to a set of simultaneous normal equations²³ which must be solved to obtain $f(x,y)$. This system theoretically has a solution, but the system is difficult to solve accurately. This problem is overcome^{23,24} by using orthogonal polynomials as basis elements instead of powers of x and y .

In this method, the form of the function $f(x,y)$ in Equation 9 is assumed to be known. However, the above technique may be used to determine the correct form of $f(x,y)$. The process involves determining Equation 9 for every degree up to a certain arbitrary degree. In each case, the value of J^2 of Equation 10 is considered. Often, this value decreases and then levels off when the correct form of $f(x,y)$ is obtained. Also, there is a standard statistical test to determine if the correct form of $f(x,y)$ has been obtained ²³.

The method of least squares approximation is important because this technique determines the underlying "trend" of the data. Trend of the data is important for data compaction. Once the trend surface is known, then a second stage process may be applied.

VI. DIRECT POLYNOMIAL TECHNIQUES ON SQUARE CELLS

In all of the following techniques, the gridded data is organized as shown in Figure 4.

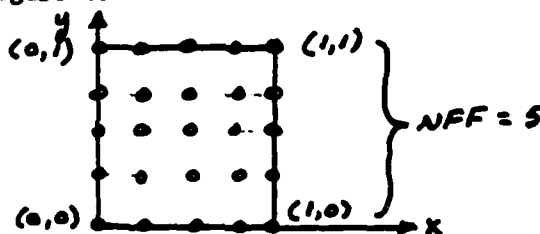


FIGURE 4- ORGANIZATION OF DATA

Each "•" corresponds to the location of a given z-value. The NFF value determines the number of data values to be grouped together and considered as a unit. In Figure 4, $NFF = 5$, so 25 z-values are used. Without loss of generality, these values are scaled to fit into a unit square. The distance between consecutive data values on the x or the y axis is referred to as "h".

4 Term Bilinear Polynomial

The function

$$f(x,y) = a_{00} + a_{10}x + a_{01}y + a_{11}xy \quad (11)$$

is obtained⁴³ which passes through the four z-values at the corner points of the unit square in Figure 4. The surface reduces to a straight line on each side of the unit square. This technique may be applied to each unit square of interest. The f-functions of Equation 11 fit together to

form a continuous surface, but the surface is not smooth on boundary lines.

The z-values which are given at non-corner points of the unit square are not used in determining $f(x,y)$. Thus, this information is essentially discarded. Also, the function $f(x,y)$ of Equation 11 is not sufficiently flexible to approximate various types of terrain.

Compaction occurs when NFF is greater than two.

8 Term Biquadratic Polynomial

The function

$$\begin{aligned} f(x,y) = & a_{00} + a_{10}x + a_{01}y + a_{20}x^2 + a_{11}xy + a_{02}y^2 \\ & + a_{21}x^2y + a_{12}xy^2 \end{aligned} \quad (12)$$

is obtained⁴³ which passes through the four z-values at the corner points of the unit square as well as the z-values at the midpoint of each side of the unit square. If the z-values at the midpoints of the sides are not given, they may be obtained by using the four nearest points on the grid line on which the point is located. A cubic polynomial may be fitted through these four points, and this polynomial is used for interpolation at the midpoint. The total surface is continuous, but it is not smooth at any points along the boundary⁴³.

The coefficients of $f(x,y)$ in Equation 12 may be obtained easily through the use of matrices⁴³. This polynomial gives more flexibility in representing various types of surfaces than does the bilinear polynomial. Some of the z-values which occur at non-corner points in Figure 4 may be used in the calculation of the z-values at the midpoints, but none of the z-values at interior points of the unit square affect the surface which is obtained. Thus this technique is not appropriate for general, varying terrain surfaces. Compaction occurs when NFF is greater than two.

12 Term Bicubic Polynomial

The function

$$\begin{aligned} f(x,y) = & a_{00} + a_{10}x + a_{01}y + a_{20}x^2 + a_{11}xy + a_{02}y^2 \\ & + a_{30}x^3 + a_{21}x^2y + a_{12}xy^2 + a_{03}y^3 \\ & + a_{31}x^3y + a_{13}xy^3 \end{aligned} \quad (13)$$

is obtained⁴³ by using the values z , z_x and z_y at each corner point of the unit square. The resulting surface passes through the given z -value at each corner point as well as assumes the specified derivatives, z_x and z_y , at these points. The total surface is globally continuous but may not be smooth at boundary points of the square other than at the corner points⁴³.

Leberl³⁵ calculates the z_x and z_y values in two different ways. One way is to use the method of weighted least squares using 16 z -values at 16 grid locations which surround the point in question. A bicubic polynomial is used in this process. The z_x and z_y values are then obtained from the bicubic surface generated. The second technique involves using the z -value itself together with two other z -values in the required direction. The average of the two slopes is then used to estimate the derivative.

This method continues the trend of using more of the non-corner z -values in determining the surface which represents the data. The global surface obtained is continuous⁴³, but is smooth only at the corner points of Figure 4. Compaction occurs when NFF is greater than three.

16-Term Bicubic Interpolation

We seek a bicubic polynomial

$$f(x,y) = \sum_{i=0}^3 \sum_{j=0}^3 a_{ij} x^i y^j \quad (14)$$

that agrees with z , z_x , z_y and z_{xy} at the four corner points of Figure 4.

For compaction to take place, the value of NFF must be greater than 4 since $f(x,y)$ contains 16 coefficients.

To obtain the coefficients a_{ij} , $i = 0,1,2,3$, $j = 0,1,2,3$ the problem may be formulated using matrices as shown below:

$$H = XAY^T \quad (15)$$

where

$$H = \begin{bmatrix} H_{00} & H_{10} \\ H_{01} & H_{11} \end{bmatrix} \quad (16)$$

with

$$H_{km} = \begin{bmatrix} z(x_k, y_m) & z_x(x_k, y_m) \\ z_y(x_k, y_m) & z_{xy}(x_k, y_m) \end{bmatrix} \quad (17)$$

for $k = 0, 1$, $m = 0, 1$.

Also,

$$X = Y = \begin{bmatrix} 1 & 0 & 0 & 0 \\ 0 & 1 & 0 & 0 \\ 1 & 1 & 1 & 1 \\ 0 & 1 & 2 & 3 \end{bmatrix} \quad (18)$$

and

$$A = \begin{bmatrix} a_{00} & a_{01} & a_{02} & a_{03} \\ a_{10} & a_{11} & a_{12} & a_{13} \\ a_{20} & a_{21} & a_{22} & a_{23} \\ a_{30} & a_{31} & a_{32} & a_{33} \end{bmatrix} \quad (19)$$

Solving Equation 15 for A, we obtain

$$A = X^{-1} H (Y^{-1})^T \quad (20)$$

where

$$X^{-1} = Y^{-1} = \begin{bmatrix} 1 & 0 & 0 & 0 \\ 0 & 1 & 0 & 0 \\ -3 & -2 & 3 & -1 \\ 2 & 1 & -2 & 1 \end{bmatrix} \quad (21)$$

Thus the bicubic $f(x,y)$ is easily determined once the values z , z_x , z_y and z_{xy} are known at the corner points. These derivatives may be obtained in several ways:

- (1) Formula method: Both three-point and five-point formulas are available for approximating z_x and z_y .
For example,

$$z_x(0,0) = \frac{1}{12h} [z(-2h,0) - 8z(-h,0) + 8z(h,0) - z(2h,0)] \quad (22)$$

$$z_y(0,0) = \frac{1}{12h} [z(0,-2h) - 8z(0,-h) + 8z(0,h) - z(0,2h)]$$

where h is the scaled distance between grid points on the x -axis.

Akima² uses the following formula to calculate $z_x(0,0)$:

$$z_x(0,0) = \frac{w_{x1} \left[\frac{z(0,0) - z(-h,0)}{h} \right] + w_{x2} \left[\frac{z(h,0) - z(0,0)}{h} \right]}{w_1 + w_2} \quad (23)$$

where

$$w_{x1} = \left| \frac{z(2h,0) - z(h,0)}{h} - \frac{z(h,0) - z(0,0)}{h} \right| \quad (24)$$

and

$$w_{x2} = \left| \frac{z(0,0) - z(-h,0)}{h} - \frac{z(-h,0) - z(-2h,0)}{h} \right| \quad (25)$$

Similar type formulas are available for calculating $z_{xy}(0,0)$ ^{2,10}. Birkhoff and DeBoor use the following formula¹⁰:

$$z_{xy}(0,0) = w \left[\frac{z_x(0,h) - z_x(0,-h)}{2h} \right] + (1-w) \left[\frac{z_y(h,0) - z_y(-h,0)}{2h} \right] \quad (26)$$

with $0 \leq w \leq 1$.

(2) Method of interpolatory bicubic spline

To find $z_x(0,0)$, $z_y(0,0)$ and $z_{xy}(0,0)$, a natural bicubic spline as described in Part IV is obtained using a certain number of designated points which surround $(0,0)$. The points chosen should form a complete rectangular grid with $(0,0)$ as one of the grid points. The size of the grid depends upon the NFF value used. A logical grid size to use is n^2 , where

$$n = \begin{cases} \text{NFF} & \text{if NFF is odd} \\ \text{NFF}-1 & \text{if NFF is even} \end{cases} \quad (27)$$

The bicubic which has the point $(0,0)$ as its lower left corner point is used to determine z_x , z_y and z_{xy} . An IMSL subroutine²⁷ is available which uses this method of determining the derivatives.

(3) Methods of least squares

Using the fifteen closest points to (0,0) together with (0,0), fit a bicubic polynomial to these data points using the method of weighted least squares as described in Part IV. The point (0,0) is weighted the most and points further away from (0,0) are weighted less.

The method of local bicubic interpolation yields a global surface that is continuous and smooth (belongs to C^1)⁴³. Birkhoff and DeBoor¹⁰ indicate that this method is superior to the bicubic spline interpolation of Part IV because the local bicubic interpolation is local in nature. Only the values z , z_x , z_y and z_{xy} at the corner points are required to obtain an interpolated value. In cubic spline interpolation, an interpolated value depends upon the z -values at all the corner points and hence is not a local procedure. Also, many of the z -values which occur at interior points affect the shape of the surface obtained. This is particularly true if method 2 or method 3 is used for determining z_x , z_y , and z_{xy} .

VII. DIRECT POLYNOMIAL TECHNIQUES ON TRIANGULAR CELLS

For all the following techniques, the gridded data is organized as in Figure 5.

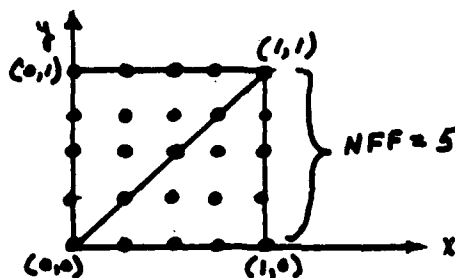


FIGURE 5 - ORGANIZATION OF DATA

The value of NFF in Figure 5 is 5. A polynomial surfaces is obtained for each of the triangles in Figure 5. For some terrain data, triangular shaped cells are advantageous because such a shape allows the surface generated to better conform to the terrain data. Much more flexibility is obtained if the size and even the shape of the triangles are allowed to vary. However, in the following techniques, it is assumed that the

size and shape of all the triangles are fixed according to the NFF value chosen.

3 Term Bilinear Polynomial

A polynomial

$$f(x,y) = a_0 + a_1x + a_2y \quad (28)$$

is sought which passes through the three z-values of the triangle in Figure 5 with corner points (0,0), (1,0) and (1,1). $f(x,y)$ forms a flat surface and this surface restricted to the above triangle forms a triangular surface. For any compaction to occur, NFF must be greater than two.

The global surface generated by this technique is continuous but it is not smooth. With only three parameters the surface has little flexibility.

Leberl³⁵ uses a modification of the above technique which is referred to as double linear interpolation. Suppose the z-value at the point "■" in Figure 6 is needed.

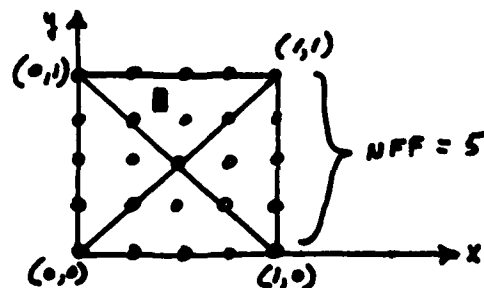


FIGURE 6 - DOUBLE LINEAR INTERPOLATION

Triangle 1 has corner points (0,0), (1,1) and (0,1). Triangle 2 has corner points (1,0), (1,1) and (0,1). Two z-values are obtained using the technique above applied to triangle 1 and to triangle 2. These two values are then averaged and the resulting value is used as an approximation to the z-value at "■".

Clough - Tocher Triangle

The triangle in Figure 5 with corner points (0,0), (1,0) and (1,1) is further divided into three triangles as shown in Figure 7.

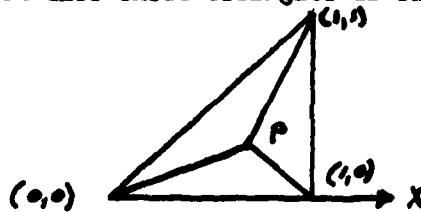


FIGURE 7 - SUBDIVISION OF TRIANGLE

The point P is the centroid of the large triangle.

In each subtriangle, a function of the form

$$\begin{aligned}
 f(x,y) = & a_{00} + a_{01}y + a_{02}y^2 + a_{03}y^3 \\
 & + a_{10}x + a_{11}xy + a_{12}xy^2 \\
 & + a_{20}x^2 + a_{21}x^2y + a_{30}x^3
 \end{aligned} \tag{29}$$

is obtained by using z , z_x and z_y at the corner points of the subtriangle. The values of z_x and z_y at a point P are obtained through the method of weighted least squares using up to 16 z -values given at surrounding grid points. A six-parameter biquadratic polynomial is used in this process. The z -value at P is weighed most heavily so the biquadratic passes through this z -value³⁴.

The resulting surface is continuous and smooth (belongs to C^1) over the boundaries of the subtriangles as well as over the boundaries of the larger triangle. Biquadratic surfaces are reproduced exactly by this method. Lawson³⁴ applies this technique to several sets of surface data. For any compaction to take place, the NFF value must be larger than seven.

21 Parameter Quintic Polynomial

A polynomial of the form

$$f(x,y) = \sum_{j=0}^5 \sum_{k=0}^{5-j} a_{jk} x^j y^k \tag{30}$$

is obtained using the values $z, z_x, z_y, z_{xx}, z_{yy}$ and z_{xy} at each of the vertices (0,0), (1,0) and (1,1) of the triangle in Figure 5 together with the normal derivatives at the midpoint of each edge of

this triangle. These normal derivatives may be eliminated resulting in an 18 parameter model⁸.

The resulting surface is continuous and smooth (belongs to C^1). For compaction to occur, NFF must be larger than 6. This technique has potential use for compaction of terrain data. There is some freedom in where the vertices of the triangles are to be placed. The placement of the vertices should be determined so that the sum of the squared differences between the given z-values and predicted z-values is minimized.

VIII. A STATISTICAL METHOD

A statistical approach^{5,32,43} is available for interpolation. Each z-value is assumed to be composed of a "trend" random variable and an "error" random variable. An estimate of the trend surface is obtained through the method of least squares using a polynomial of order 0 or 2. Higher order polynomials do not substantially improve the interpolation³⁵. The trend surface is obtained using n reference points. The residual values are the terms obtained from subtracting the trend values from the n z-values at the reference points. These residuals are used in the interpolation process.

Kraus³² uses an isotropic correlation function of the form

$$w(d) = c/\exp(-k^2 d^2) \quad (31)$$

Using Equation 31, the following covariance matrix is obtained from the n reference points:

$$Q = \begin{bmatrix} 1 & w(d_{12}) & w(d_{13}) & \dots & w(d_{1n}) \\ w(d_{21}) & 1 & w(d_{23}) & \dots & w(d_{2n}) \\ \vdots & & & & \\ w(d_{n1}) & w(d_{n2}) & w(d_{n3}) & \dots & 1 \end{bmatrix} \quad (32)$$

In Equation 32, d_{ij} represents the distance between the i^{th} and j^{th} reference points. For a new point (x,y) at which the z-value is desired, a covariance vector q is defined as follows:

$$q = [w(d_1), w(d_2), \dots, w(d_n)] \quad (33)$$

where d_i represents the distance between the i^{th} reference point and the new point (x,y) . The new z -value at (x,y) is then obtained by

$$z = t(x,y) + q \cdot Q^{-1} \cdot \Delta Z^T \quad (34)$$

where $t(x,y)$ is the z -value given by the trend surface at (x,y) and ΔZ represents the residuals obtained from subtracting the trend z -values from the original z -values.

This method is the most accurate of all the methods considered by Leberl³⁵. He uses an n value of sixteen. This n value corresponds to an NFF-value of four. No compaction occurs using this technique since the values of the covariance matrix in Equation 34 need to be retained as well as all original z -values for use in calculating the terms of the vector in Equation 33.

IX. ERROR ANALYSIS

Error analysis for interpolating and approximating functions of one variable is extensive^{12,18}. Most results involve the modulus of continuity or a high order derivative. Very few results were found for functions of two variables^{6,7,37}.

X. COMPARISON OF TECHNIQUES

With the small amount of error analysis found for techniques involving functions of two variables, no comparison of the techniques in terms of accuracy is possible. The accuracy of the technique may be determined however by applying the method to different terrain data. This is the approach taken by Leberl³⁵. Seven different interpolation techniques are applied to various types of terrain data. The techniques are compared in terms of storage requirements, retrieval time and data accuracy. Accuracy of the technique may be compared by checking the predicted z -value against the given z -value at numerous points. Jablinske^{27,28} compares two different interpolation techniques using actual data. There should also be some standard method with which to compare a given technique. The following standard method is used by Jablinske^{27,28}. Assume the data is organized as in Figure 8 and that

the NFF value has been chosen. We assume that the NFF value is odd.

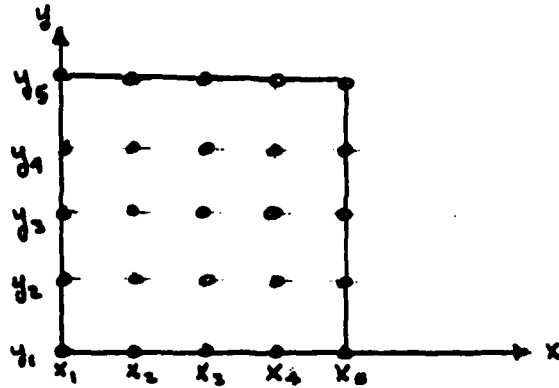


FIGURE 8 - DATA ORGANIZATION

If every other grid point is removed, the resulting grid appears in Figure 9.

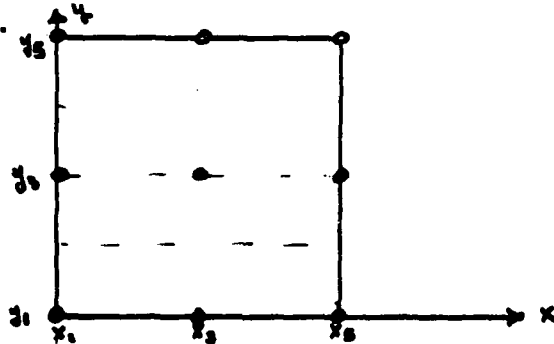


FIGURE 9 - RESULT OF REGRIDDING

The 4 term bilinear polynomial is then determined for each cell in Figure 8. The technique in question is then compared against this standard method in terms of compression and accuracy. For the technique in question to be acceptable, it should be superior to the above standard method of regridding. The process of regridding may continue so that two out of every three points are deleted. This process may continue until all grid points in Figure 8 are deleted except those that fall on the boundary. Another minimal requirement is that the technique in question should yield more accurate results than those obtained by using only the 4 corner points in Figure 8 together with the 4 term bilinear polynomial technique of Part VI.

XI. FURTHER RESEARCH

To compare the compaction techniques described in this report, they should be applied to various types of terrain data. I propose to concentrate on two of these techniques using the plan outlined below:

- (1) Using actual terrain data, apply the method of least squares approximation to the data in order to determine the underlying "trend" surface. Statistical tests will be used to determine which polynomial terms to include in the trend surface. The goal is to make NFF as large as possible while at the same time keep the number of terms in the "trend" surface small. Thus the terrain data will be classified for each NFF as to what the "trend" surface actually is. Values of NFF from 4 to 10 will be considered.
- (2) From Step 1, determine the largest NFF value for which the bicubic or smaller degree polynomial is the correct "trend" surface. This property must hold over a relatively large region D. Trend surfaces containing one or two terms whose degree is larger than three may be acceptable, since such terms may be approximated sufficiently close by lower power terms using Chebyshev economization.
- (3) Using the NFF value from Step 2, fit each square in region D with a local bicubic polynomial. Preprocessing will be required to obtain z_x , z_y and z_{xy} at each corner point. The resulting global surface is continuous and smooth on D.
- (4) Determine if the surface is sufficiently close to the given z-values on D. If there is too much error in the model, then some of the model parameters must be adjusted. The local bicubic polynomial contains 16 parameters: z , z_x , z_y and z_{xy} at each corner point of the cell. An interactive graphics package similar to that used by Barnhill⁶ is proposed. By means of a stylus on a tablet, these parameters may be modified. Simultaneously, the error and statistical data for the current model may be displayed. Thus the surface is modified until it is sufficiently close to the terrain data.

REFERENCES

1. Ahlin, A.C., "A Bivariate Generalization of Hermite's Interpolation Formula," Math. Comp., Vol. 18, pp.264-273, 1964.
2. Akima, H., "A Method of Bivariate Interpolation and Smooth Surface Fitting Based on Local Procedures," Communications of the ACM, Vol. 17, No. 1, pp. 18-20, 1974.
3. Akima, H., "Algorithm 474, Bivariate Interpolation and Smooth Surface Fitting Based on Local Procedures," Communications of the ACM, Vol. 17, No. 1, pp.26-31, 1974.
4. Akima, H., "A Method of Bivariate Interpolation and Smooth Surface Fitting for Irregularly Distributed Data Points," ACM Transactions on Mathematical Software, Vol. 4, No. 2, pp. 148-159, 1978
5. Arthur, D.W.G., "Interpolation of a Function of Many Variables," Photogrammetric Engineering and Remote Sensing, Vol. 31, No. 2, pp. 348-349, 1965.
6. Arthur, D.W.G., "Multivariate Spline Functions. II. Best Error Bounds," Journal of Approximation Theory, Vol. 15, pp. 1-10, 1975.
7. Barnhill, R.E., "Error Bounds for Smooth Interpolation in Triangles," Journal of Approximation Theory, Vol. 11, pp. 306-318, 1974
8. Barnhill, R.E., "Representation and Approximation of Surfaces," in Mathematical Software III, edited by J.R. Rice, (Academic Press, New York, 1977), pp. 69-120.
9. Bhattacharyya, B.K., "Bicubic Spline Interpolation as a Method for Treatment of Potential Field Data," Geophysics, Vol. 34, pp. 402-423, 1969.
10. Birkhoff, G. and C. DeBoor, "Piecewise Polynomial Interpolation and Approximation," in Approximation of Functions, edited by H. L. Garabedian, (Elsevier, New York, 1965), pp. 164-190.
11. Bosman, E.R., D. Eckhart and K. Kubik, "Delft-A Programme System for Surface Approximation," The Canadian Surveyor, Vol. 30, No. 5, pp. 13-20, 1976.
12. Burden, R.L., J.D. Faires and A.C. Reynolds, Numerical Analysis, (Prindle, Weber and Schmidt, Boston, 1978), 579 pages.

13. Clenshaw, C.W., "The Polynomial and Rational Approximation of a Function of one Variable," in Numerical Approximation to Functions and Data, edited by J.G. Hayes, (Athlone Press, Univ. of London, 1970), pp. 16-27.
14. Coons, S.A., "Surface Patches and B-Spline Curves," in Computer Aided Geometric Design, edited by R.E. Barnhill and R.F. Riesenfeld, (Academic Press, New York, 1974), pp. 1-16.
15. Cox, M.G., "A Survey of Numerical Methods for Data and Function Approximation," in The State of the Art in Numerical Analysis, edited by D. Jacobs, (Academic Press, New York, 1977), pp. 627-668.
16. Davis, M.W.D. and M. David, "Generating Bicubic Spline Coefficients on a Large Regular Grid," Computers and Geosciences, Vol. 6, pp. 1-6, 1980.
17. DeVore, R.A., "Degree of Approximation," in Approximation Theory II, edited by G.G. Lorentz, (Academic Press, New York, 1976), pp. 117-161.
18. Feinerman, R.P. and D.J. Newman, Polynomial Approximation, (Williams and Wilkins, Baltimore, 1974), pp. 13-107.
19. Gordon, W.J. and R.F. Riesenfeld, "B-Spline Curves and Surfaces," in Computer Aided Geometric Design, edited by R.E. Barnhill and R.F. Riesenfeld, (Academic Press, New York, 1974), pp. 95-126.
20. Gregory, J.A., "Smooth Interpolation Without Twist Constraints," in Computer Aided Geometric Design, edited by R.E. Barnhill and R.F. Riesenfeld, (Academic Press, New York, 1974), pp. 71-87.
21. Hall, C.A., "Bicubic Interpolation Over Triangles," Journal of Mathematics and Mechanics, Vol. 19, No. 1, pp. 1-11, 1969.
22. Hall, C., "Spline Blended Approximation of Multivariate Functions," in Polynomial and Spline Approximation, Theory and Applications, edited by B.N. Sahney, (D. Reidel Publishing, Boston, 1979), pp. 17-34.
23. Hayes, J.G., "Curve Fitting by Polynomials in One Variable," in Numerical Approximation to Functions and Data, edited by J.G. Hayes, (Athlone Press, Univ. of London, 1970), pp. 43-59.

24. Hayes, J.G., "Fitting Data in More Than One Variable," in Numerical Approximation to Functions and Data, edited by J.G. Hayes, (Athlone Press, Univ. of London, 1970), pp. 84-97.
25. Hulme, B.L., "A New Bicubic Interpolation over Right Triangles," Journal of Approximation Theory, Vol. 5, pp. 66-73, 1972.
26. IMSL library, "International Mathematical and Statistical Libraries, Inc.," Houston, Texas.
27. Jablinske, R.J., "Polynomial Modeling Versus Conventional Matrices in Terrain Data Applications," Consulting Report #ECAC-CR-79-040, for U.S. Army Engineer Topographic Laboratories, Fort Belvoir, Virginia, April, 1979, 38 pages.
28. Jablinske, R.J., "Investigations in Polynomial Modeling and Gridded Arrays as Applied to Digital Array Models," Final Report #ECAC-CR-80-017, for U.S. Army Engineer Topographic Laboratories, Fort Belvoir, Virginia, 1979.
29. Jancaitis, J.R., "Modeling and Contouring Irregular Surfaces Subject to Constraints," Final Technical Report #ETL-CR-74-19, for U.S. Army Engineer Topographic Laboratories, Fort Belvoir, Virginia, January, 1975, 171 pages.
30. Jancaitis, J.R. and J.L. Junkins, "Modeling Irregular Surfaces," Photogrammetric Engineering and Remote Sensing, Vol. 39, No. 4, pp. 413-420, 1973.
31. Keoiling M.E.V., and E.H.T. Whitten, "Fortran IV Program for Spline Surface Interpolation and Contour Map Production," Geocomprograms, Vol. 9, pp. 1-12, 1973.
32. Kraus, K. and E.M. Mikhail, "Linear Least - Squares Interpolation," Photogrammetric Engineering and Remote Sensing, Vol. 38, No. 10, pp. 1016 - 1029, 1972.
33. Kubik, K., "Approximation of Measured Data by Piecewise Bicubic Polynomial Functions," Rijkswaterstaat Communications, No. 12, pp. 34-51, 1971.
34. Lawson, C.L., "Software for C^1 Surface Interpolation," in Mathematical Software III, edited by J.R. Rice, (Academic Press, New York, 1977), pp. 161-194.
35. Leberl, F., "Interpolation in Square Grid DTM," ITC Journal, Vol. 5, pp. 756 - 807, 1973.

36. Lorentz, G.G., "Russian Literature on Approximation in 1958 - 1964," in Approximation of Functions, edited by H.L. Garabedian, (Elsevier, New York, 1965), pp. 191-215.
37. Mansfield, L.E., "Optimal Approximation and Error Bounds in Spaces of Bivariate Functions," Journal of Approximation Theory, Vol. 5, pp. 77-96, 1972.
38. Powell, M.J.D., "Piecewise Quadratic Surface Fitting for Contour Plotting," in Software for Numerical Mathematics, edited by D.J. Evans, (Academic Press, New York, 1974), pp. 253-271.
39. Powell, M.J.D. and M.A. Sabin, "Piecewise Quadratic Approximations on Triangles," ACM Transactions on Mathematical Software, Vol. 3, No. 4, pp. 316-325, 1977.
40. Rivlin, T.J., An Introduction to the Approximation of Functions, (Blaisdell Publishing, Waltham, Mass., 1969), pp. 11-65.
41. Schumaker, L.L., "Fitting Surfaces to Scattered Data," in Approximation Theory II, edited by G.G. Lorentz et. al., (Academic Press, New York, 1976), pp. 203-268.
42. Schut, G.H., "Two Interpolation Methods," Photogrammetric Engineering and Remote Sensing, Vol. 40, No. 12, pp. 1447-1453, 1974.
43. Schut, G.H., "Review of Interpolation Methods for Digital Terrain Models," The Canadian Surveyor, Vol. 30, No. 5 pp. 390 - 412, 1976.

1981 USAF - SCEEE SUMMER FACULTY RESEARCH PROGRAM

Sponsored by the

AIR FORCE OFFICE OF SCIENTIFIC RESEARCH

Conducted by the

SOUTHEASTERN CENTER FOR ELECTRICAL ENGINEERING EDUCATION

FINAL REPORT

EPITAXIAL LAYER EVALUATION OF III-V SEMICONDUCTOR MATERIALS

Prepared by: Dr. Robert W. Cunningham

Academic Rank: Associate Professor

Department and University: Department of Physics
Kent State University, Tuscarawas Campus

Research Location: Air Force Wright Aeronautical Laboratories,
Materials Laboratory

USAF Research Colleague: Dr. Patrick Hemenger

Date: August 4, 1981

Contract No: F49620-79-C-0038

EPITAXIAL LAYER EVALUATION OF III-V SEMICONDUCTOR MATERIALS

by

Robert W. Cunningham

ABSTRACT

Problems associated with the electronic evaluation of epitaxial layers on substrates have been studied. Two models for the measurable resistivity voltage of van der Pauw type specimens have been investigated to determine the importance of both the epi layer and substrate. A simple circuit model indicates the epi layer resistivity may be determined with negligible error under conditions that may be obtained in the laboratory. When the model is applied to the Hall effect an identical result is obtained. A more sophisticated model for the resistivity voltage is suggested but detailed solution has not been completed. Electrical measurements on several specimens are reported and the data is in reasonable agreement with other specimens. Suggestions for continued work are offered.

ACKNOWLEDGEMENTS

The author would like to thank the Air Force Systems Command, The Air Force Office of Scientific Research, The Southeastern Center for Electrical Engineering Education, and The Air Force Wright Aeronautical Laboratories for the opportunity to spend a very worthwhile summer at the Materials Laboratory, Wright Patterson AFB, Ohio. The working conditions and professional treatment were excellent.

Special thanks are due Dr. Patrick Hemenger for suggesting this work and for his collaboration and help at various stages. Thanks are also due Airman Kenneth Beasley who did most of the specimen preparation and equipment operation. Lt. Kenneth Bradley also made several helpful suggestions. Mr. Steven Smith also provided me with his standard computer routines for data analysis.

I. INTRODUCTION: Epitaxial layers on semiconductor materials are increasing in importance in modern semiconductor technology. The Materials Laboratory of AFWAL has for some years had an excellent facility for the evaluation of high purity silicon materials. Recently this laboratory began studies of silicon on sapphire thin layers, ion implanted layers, and epitaxial layers on InAs, a III-V compound.

The InAs epi layers are being prepared under contract by the Electrical Engineering Department of North Carolina A & T University by a current controlled technique.¹ Once epitaxial layers of InAs are received the Materials Laboratory of AFWAL needs to evaluate and characterize the material. It is therefore necessary to know something about InAs and methods to evaluate the epi layer. Since InAs is a narrow band gap material similar to InSb, experience with InSb should carry over to InAs. The band gap for InSb is 0.258 eV,² and for InAs it is 0.378 eV.³

Evaluation of an epi layer on a substrate is a problem because the layer and substrate interact electrically. Unless the substrate can be electrically isolated from the layer in some way⁴ the interaction of the layer and substrate must be accounted for. One method is by resistor network simulation similar to that used to simulate critical phenomena⁵ and disordered media.⁶

Models have often been used in the past to aid in the understanding of a complex phenomenon. For example, semiconducting platelets have been simulated with resistor networks and finite difference equations to study the effect on measurements of contact size and placement.⁷

This report will first consider a simple network model to simulate the resistivity voltage and Hall voltage when both the epi layer and substrate interact. A condition will be obtained which will allow the effect of the substrate to be ignored with negligible error. A more general network model will be suggested which should provide a better simulation of the epi layer and substrate. Although the solution is not fully developed, methods of solution are suggested, a numerical simulation using SPICE⁸ has been obtained. Several specimens of InAs and GaAs have been used to learn the processing techniques required to handle epi layers on substrates. Detailed measurements on an InAs substrate

and a GaAs epi layer and substrate have been carried out. Measurements on other specimens of GaAs epi layers have been initiated but are not complete. Finally, recommendations for future work are made.

II. OBJECTIVES: The main objective of this work was to help the Materials Laboratory group extend their experience into the measurement and characterization of III-V compounds and epitaxial layers on such compounds using the standard transport measurements currently in use. The investigation concentrated on (1) measurable quantities (resistivity and Hall voltages) in the presence of both an epitaxial layer and a substrate, and (2) measurements on epitaxial layers and substrates of III-V compounds. A third goal was to provide some evaluations of InAs specimens prepared under contract by North Carolina A & T University.

III. LAYER AND SUBSTRATE MODELING: A simple circuit model can be used to study the influence of the substrate on the electronic properties of a layer. This model will be introduced and used to estimate layer resistivity and carrier concentration (actually the Hall coefficient) and then the model will be criticised.

(a) Resistivity Voltage

Consider first the standard van der Pauw specimen as sketched in Fig. 1. A current I is injected into and extracted from a pair of

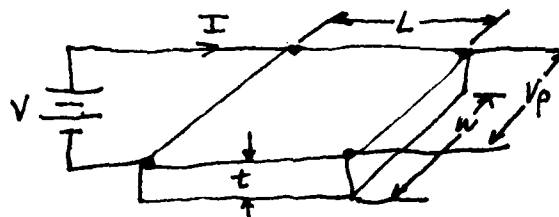


Fig. 1

adjacent contacts on one surface of the specimen, and the resistivity voltage is measured (open circuit) at the two adjacent contacts on the opposite side of the same face. The resistivity resistance R_p is then given by

$$R_p = \frac{V_p}{I} \quad (1)$$

It is assumed that V_p and I are experimentally determined quantities.

The resistivity is then found from the van der Pauw equation⁹ as

$$\rho = KR_{\rho}t, \quad (2)$$

where K is a numerical constant that depends on specimen dimensions.

This work will be concerned only with determination of Eq(1).

Equation (1) may be interpreted as a circuit model as sketched in Fig. 2. Here V_p is a controlled source, R_p is the controlled source resistance, and I is the current controlling the source. R_I is the

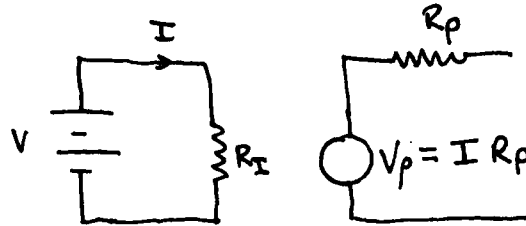


Fig. 2

Thevenin resistance obtained from the open circuit voltage - short circuit current theorem as seen at the voltage probes. Note that R_I does not equal R_p in general. In terms of Fig. 1 R_I is the resistance between the current contacts.

The model can now be generalized to a number of units similar to Fig. 1 interconnected in some way in order to form an epi layer on a substrate. One simple method assumes the applied voltage is the same for each layer and there is only one pair of resistivity contacts. Layers then interact through contact connections. This is shown in Fig. 3. Each independent voltage source and its R_{Ii} segment has been deleted to simplify the figure. The controlled voltage sources V_{pi} are given

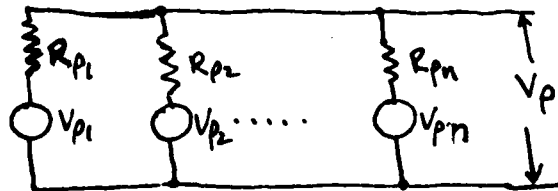


Fig. 3

by $V_{pi} = I_i R_{pi}$. Solution for V_p is given by Millman's Theorem¹⁰ as

$$V_p = \frac{\sum V_{pi} G_i}{\sum G_i}, \quad (3)$$

where $G_i = 1/R_i$ is the conductance of the i th layer Thevenin resistance.

Now the resistivity resistance is

$$R_p = \frac{V_p}{I} = \frac{\sum V_{pi} G_i}{I \sum G_i}$$

and I is

$$I = \sum I_i \quad (4)$$

so that

$$R_p = \frac{\sum V_i G_i}{(\sum I_i)(\sum G_i)} \quad (5)$$

If it may be assumed that $V_i = R_{pi} I_i$, Eq (5) reduces to

$$R_p = \frac{1}{\sum G_i} \quad (6)$$

Note that the bold assumption $R_{pi} = 1/G_i$ reduces R_p to the reciprocal of a simple sum. Physically this result implies the layers are all in parallel.

The material properties of each layer may be incorporated into Eq (6). Since $G_i = \sigma_i A_i / L_i$, A_i is the specimen cross section,

$$G_i = \sigma_i \frac{A_i}{L_i} = C \sigma_i \frac{w t_i}{L_i} \quad (7)$$

where C is a dimensionless constant that properly scales the conductance and is similar to the constant K of Eq (1). Then G_i becomes

$$G_i = C \frac{w}{L} \sigma_i t_i = n_i \mu_i t_i \quad c w / L \quad (8)$$

and R_p becomes

$$R_p = \frac{1}{C \frac{w}{L} \sum n_i \mu_i t_i} \quad (9)$$

Here e is the magnitude of the electronic charge. In the limit of very thin layers the sum becomes an integral and n_i and μ_i become functions of the position. Thus

$$R_p = 1 / \int_0^L \left(\frac{C w}{L} \right) e n(x) t(x) dx \quad (10)$$

Now consider a simple two component structure, a layer and substrate, each with uniform properties. For simplicity also assume $C w / L = 1$. Then Eq (6) becomes

$$R_p = \frac{1}{\sigma_s t_s + \sigma_e t_e} = \frac{1}{\sigma_e t_e \left(1 + \frac{\sigma_s t_s}{\sigma_e t_e} \right)}$$

or

$$R_p = \frac{\rho_e t_e}{\left(1 + \frac{\sigma_s t_s}{\sigma_e t_e} \right)} = \frac{R_R}{\left(1 + \frac{\sigma_s t_s}{\sigma_e t_e} \right)} \quad (11)$$

where R_R is the resistivity resistance of the layer.

Eq (11) may be used to set limits on σ_s and σ_e for small measurement error. Assume an error of less than 1% desired. Then

$$\sigma_s t_s \leq .01 \sigma_e t_e$$

or

$$\rho_s \geq 100 \rho_e \left(\frac{t_s}{t_e} \right).$$

For a layer 4% of the substrate thickness, ρ_s must be

$$\rho_s \geq 2500 \rho_L \quad (12)$$

(b) Hall Voltage

So far only a single resistivity model has been assumed. The same model, with some modifications, applies to the Hall effect. The Hall effect contact configuration and specimen dimensions are sketched in Fig. 4. As usual the Hall coefficient R_H is given by

$$R_H = \frac{V_H t}{I B} \quad (13)$$

where V_H is the Hall Voltage as given in Fig. 4, t is the specimen

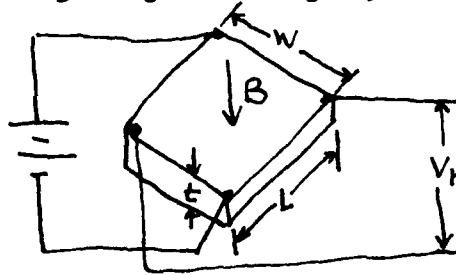


Fig. 4

thickness, I the current into the specimen, and B the magnetic field through the specimen thickness. Solution for V_H yields

$$V_H = \frac{R_H I}{t B} \quad (14)$$

Equation (14) suggests a simple circuit model similar to Fig. 2. Such a model is sketched in Fig. 5.

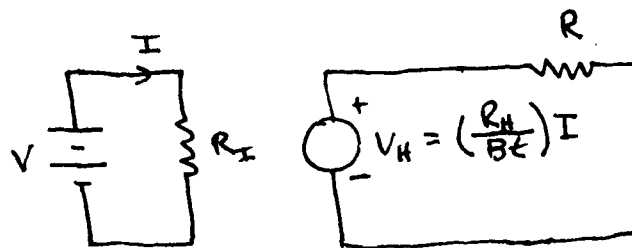


Fig. 5

Here R_I is the resistance seen by the source V and R is the Thevenin resistance seen from the Hall contacts. Both R_I and R may be functions of B and specimen dimensions.

The Hall effect model may be generalized in the same way as the resistivity model and is sketched in Fig. 6. Application of Millman's Theorem leads to

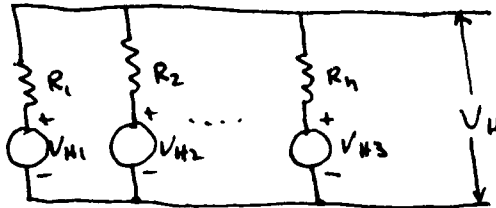


Fig. 6

$$V_H = \frac{\sum V_{Hi} G_i}{\sum G_i} \quad (15)$$

where G_i is the conductance $1/R_i$ and the subscript i refers to the i th layer. When Eq (15) is written in terms of the individual Hall coefficients, V_H becomes

$$V_H = \frac{\sum V_{Hi} G_i}{\sum G_i} = \frac{\sum R_{Hi} I_i G_i B / t_i}{\sum G_i}$$

As before, $I = \sum I_i$, and $I_i = V G_i$, so that R_H becomes

$$R_H = \frac{t \sum R_{Hi} G_i^2 / t_i}{(\sum G_i)^2} \quad (16)$$

Here t is the total specimen thickness.

Eq (16) is basically different from Eq (6) because R_H is not a resistance.

If G_i can be written in the form $G_i = F \left(\frac{w}{t} \right) t_i \sigma_i$, R_H simplifies to

$$R_H = \frac{t \sum R_{Hi} \sigma_i^2 t_i}{(\sum \sigma_i t_i)^2} \quad (17)$$

A further simplification occurs if $R_{Hi} = 1/n_i e$ and n_i is the carrier concentration of the i th layer. Then Eq (16) becomes

$$R_H = \frac{t \sum n_i \mu_i^2 t_i}{e (\sum n_i \mu_i t_i)^2} \quad (18)$$

For vanishingly thin layers the sums may be replaced by integrals so that R_H becomes

$$R_H = \frac{t \int_0^t n(x) \mu(x)^2 dx}{e \left(\int_0^t n(x) \mu(x) dx \right)^2} \quad (19)$$

Equation (19) is often quoted in the literature as the equation to use

for a continuous distribution or a concentration profile.¹¹

For a simple layer-substrate two component system Eq (18) yields

$$R_H = \frac{t(n_a \mu_a^2 t_a + n_s \mu_s^2 t_s)}{e(n_a \mu_a t_a + n_s \mu_s t_s)^2}$$

or

$$R_H = \frac{(t/t_a)}{e n_a} \left[\frac{1 + \frac{n_s t_s \mu_s^2}{n_a t_a \mu_a^2}}{\left(1 + \frac{n_s t_s \mu_s}{n_a t_a \mu_a}\right)^2} \right]$$

(20)

In terms of the layer conductivities R_H is

$$R_H = \frac{(t/t_a)}{e n_a} \left[\frac{1 + \frac{\sigma_s \mu_s t_s / \sigma_a \mu_a t_a}{1 + \sigma_s t_s / \sigma_a t_a}}{\left(1 + \sigma_s t_s / \sigma_a t_a\right)^2} \right]$$

If the mobilities are equal

$$R_H = \frac{t/t_a}{e n_a} \frac{1}{1 + \sigma_s t_s / \sigma_a t_a}$$

(21)

Once again an error less than 1% for R_H will occur if

$$\sigma_s t_s < .01 \sigma_a t_a$$

which is just the condition used for the resistivity determination with the same result.

Before leaving Eq (20) or Eq (21), it is appropriate to note both may be written in terms of R_{HL} , the Hall coefficient of the layer. The layer Hall coefficient is

$$R_{HL} = \frac{(t/t_a)}{e n_a}$$

(22)

where the factor (t/t_a) corrects the calculation of Eq (16) to the thickness of the layer. Now the factors involving carrier densities or conductivities are recognized as correction factors to account for the substrate.

(c) Criticism and Assumptions

A number of assumptions have been used in the derivations above that severely limit the applicability of the final equations and each is listed below.

1. Each layer has the same voltage applied to its current connections.
2. The resistances of each layer only depend on the bulk properties of that layer.
3. The current density of each layer is obtained from the current

in that layer by the same geometrical factor, and specimen dimensions except for the thickness.

4. Magnetoresistance does not occur for the Hall effect layer resistance.

Assumptions 1-3 are valid for standard Hall bars when contacts are made over the total thickness of the specimen, and assumption 4 is valid for vanishingly small magnetic fields. However, for square van der Pauw specimen configurations with contacts only on a surface (usually the epi layer) the first three assumptions have questionable validity. Assumption 4 in any case is rather restrictive and may never be a good approximation. In general it assumes a Hall factor of 1.0 independent of magnetic field.

One useful result of the above is that Eqns (11) and (21) represent worst case analyses. Thus, the actual error in analysis of data by these two equations should be less than 1% if Eq (12) is obeyed.

IV. MORE REALISTIC RESISTIVITY VOLTAGE MODEL: In order to construct a more realistic resistivity model and eliminate some of the objections raised above, a resistor array structure was developed. The simplest such model contains 12 resistors with three different values, and is sketched in Fig. 7. Once again the van der Pauw contact configuration is assumed. Resistors with subscript L make up the layer, resistors

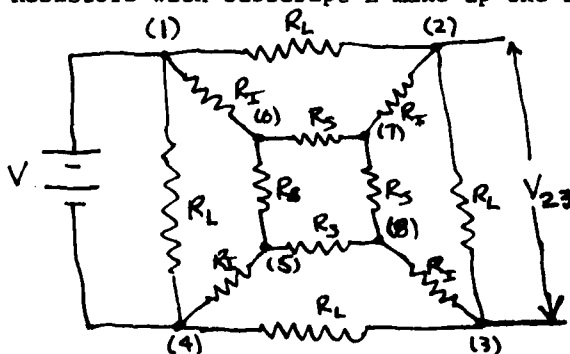


Fig. 7

with subscript S make up the substrate, and resistors with subscript I are interface resistors connecting the layer and substrate. Numbers in parenthesis designate a node. The problem then is to find the voltage V_{23} in terms of V and the resistor values.

Circuit theory shows that the left most resistor R_L may be removed

without changing V_{23} . Furthermore, if the value of either or both R_s and R_I is large V_{23} is simply $(1/3)V$. Thus if the substrate and layer are ideally isolated V_{23} will only be determined by the layer. In general this will not be true.

General solution for V_{23} can be obtained from Kirchhoff's current law (KCL) applied to each node. Since V is a constant voltage supply, nodes (1) and (4) may be eliminated if node (4) is assumed to be the datum node. By straight forward application of KCL to nodes (2), (3), (5), (6), (7), and (8), the voltages at these nodes can be obtained from the solution of the matrix equation

$$\begin{bmatrix} A & B & 0 & 0 & C & 0 \\ B & A & 0 & 0 & 0 & C \\ 0 & 0 & D & E & 0 & E \\ 0 & 0 & E & D & E & 0 \\ E & 0 & 0 & E & D & E \\ 0 & C & E & 0 & E & D \end{bmatrix} \begin{bmatrix} V_2 \\ V_3 \\ V_5 \\ V_6 \\ V_7 \\ V_8 \end{bmatrix} = \begin{bmatrix} -VB \\ 0 \\ -VC \\ 0 \\ 0 \\ 0 \end{bmatrix} \quad (23)$$

where

$$\begin{aligned} A &= 2G_L + G_I & E &= -G_s \\ B &= -G_L & G_L &= 1/R_L \\ C &= -G_I & G_s &= 1/R_s \\ D &= 2G_s + G_I & G_I &= 1/R_I \end{aligned}$$

In principle Cramers rule can be used to solve for V_2 and V_3 and $V_{23} = V_2 - V_3$ is found by subtraction. However, solution of a 6X6 determinate is not trivial. Numerical solution by the SOR technique¹² is also possible. Fortunately a network solution computer program package called SPICE is available at AFVAL and V_{23} was found by its use.¹³ The solutions show that V_{23} is within 2% of its true single layer value when $R_I = 10R_L$ and $R_s \geq 10R_L$. This indicates the interface resistance is more important than the substrate resistance and should be the quantity of greatest importance. Thus, any diode isolation such that the diode is not biased above the forward direction knee should provide adequate isolation between the substrate and the epi layer.

V. MEASUREMENT RESULTS: One of the primary goals of this work was

to help develop experience with III-V compounds within the AFWAL Materials Laboratory. Toward this end specimens of InAs and GaAs were obtained.

Two substrates of InAs and three current controlled growth of InAs epitaxial layers on InAs substrates were obtained from North Carolina A&T University as part of a contract obligation. The InAs specimens were found to be quite brittle and to cleave readily. Initial measurements indicated satisfactory contacts to either the layer or the substrate could be made by standard soldering techniques. Unfortunately the layer could not be distinguished from the substrate since the layer and substrate were the same conductivity type. That is, there was little or no isolation between the layer and substrate. Because of this evaluation of epitaxial layers for these specimens was impractical.

Optical evaluation of InAs epi layer and substrate surfaces showed many interesting features. However the quality of the layers and substrates was so poor that correlation of surface features to electrical properties was not practical.

Electronic transport data for the best InAs substrate was obtained for the temperature range $4.2K \leq T \leq 380K$. The substrate was found to be n-type, showed very little change in carrier concentration and differed only slightly from data reported over 20 years ago.¹⁴ The mobility showed a transition from lattice to impurity scattering with the peak at about 110K. Typical effects due to degeneracy¹⁵ were apparent and no indication of carrier freeze out was observed. Similar results were reported by the A&T group during a recent visit.

Three specimens of GaAs epi layers on semi insulating GaAs were received from the Avionics Laboratory group. After considerable effort a technique for placing good contacts on the epi layer seemed to be obtained. Pure indium solder placed on the surface with a soldering iron was annealed at 300°C to 400°C for one to three minutes. During the learning process one of the semi insulating substrates converted to lower resistance. Data was obtained for both the layer and substrate of this specimen over the temperature range $4.2K \leq T \leq 380K$. The specimen was n-type at all temperatures and showed a typical mobility-temperature curve with a transition from lattice to impurity scattering with a peak at 60K. Analysis of the low temperature data for one side indicated a compen-

sated acceptor density of $9.4 * 10^{14} \text{ cm}^{-3}$, a donor density of $1.1 * 10^{15} \text{ cm}^{-3}$ and an energy level 0.0044eV below the conduction band. Data for the other specimen side was similar but the mobility was lower and the carrier concentration was higher. The data was somewhat erratic at low temperatures but the donor energy level seemed to agree with the initial side data.

The specimen thickness that must be used in the analysis of both the Hall effect and resistivity is a problem. Direct measurement of the total thickness $t_2 + t_3 = t$ is straight forward. However measurement of t_2 is difficult. Staining and optical observation are both useful if a calibrated reticle eye piece is available for a microscope. An etch-weigh-back calculate technique has been used for ion implanted layers,¹⁶ but the technique is laborious and requires many hours of work. For epi layers on isolated substrates the capacitance-voltage technique may be useful since it yields the carrier concentration as a function of distance from the surface. At some distance the carrier concentration changes rapidly, and this should be the layer thickness.

The specimens of GaAs received for the work reported here were also provided with carrier concentration vs. thickness data and the thickness of the layer taken from this data was used in the calculation of the Hall coefficient and resistivity.

Agreement between the carrier concentrations obtained from C-V data, independent Hall data, and data reported here seems to be consistent. The carrier concentration n at 300K for these experiments was $n = 2.2 * 10^{14} \text{ cm}^{-3}$, for C-V data $n = 3.2 * 10^{14}$, and by independent Hall measurement $n = 9.4 * 10^{13} \text{ cm}^{-3}$. Thus our experiments are between two other measurements.

Further comparison of our transport data to the independent transport data is probably not appropriate since data was not taken on the same specimen and little is known about the layer homogeneity.

VI. RECOMMENDATIONS: The information reported above is a short resume of epitaxial layer evaluation. There is clearly much more that can be done. It is suggested that the same specimen be used in both the Avionics Lab Hall effect equipment and in the Materials Lab equipment to be sure both pieces of equipment yield consistent information. A second exper-

imental problem is to develop a good reliable way to determine an epi layer thickness. It seems reasonable that the C-V technique should be investigated as a tool for this measurement, perhaps in conjunction with staining.

It is also recommended that the simulation model be continued and expanded. The simulation could include the effect of a concentration gradient along the thickness as well as a more realistic model in three space of the layer and substrate. Also, with some changes the simulation can be applied to hopping conduction and critical phenomena.

The current controlled liquid phase epitaxial layers of InAs received so far can not be evaluated because the epi layer and the substrate are not electrically isolated. It is recommended that North Carolina A&T develop a means to grow p-Type epi layers. The technique they now use to produce the layer melt does not seem like a satisfactory method since only metallurgical grade "6-nines" indium and arsenic of unknown purity are used to form the melt with no further refining. It is suggested that high purity zone refined InAs including a p-Type dopant be used to form the epitaxial layer melt. If layer charge is known to be p-type InAs it seems reasonable that a p-Type epi layer would result.

REFERENCES

1. Abul-Fadl, A., and E. K. Stefanakos, "Current Controlled Growth of InP", Journal of Crystal Growth, Vol. 39, pp. 341-345, 1977.
2. Cunningham, R. W., and J. B. Gruber, "Intrinsic Concentration and Heavy-Hole Mass in InSb", Journal of Applied Physics, Vol. 41, pp. 1804-1809, 1970.
3. This value was calculated from Hall data, Dixon, Jack R., "Anomalous Electrical Properties of p-Type Indium Arsenide", Journal of Applied Physics, Vol. 30, pp. 753-759, 1959.
4. Cunningham, R. W., "Surface Photoconductivity of Gold Doped Germanium", Thesis, Purdue University, 1959, unpublished.
5. Kirkpatrick, S., - , Physical Review Letters, Vol. 27, pp. 1722-1725, 1971; Seager, C. H., and G. E. Pike, "Percolation and Conductivity: A Computer Study. II", Physical Review, Vol B 10 pp. 1435-1446, 1974.
6. Cunningham, R. W., "Unpublished Research".
7. White, D. J., M. L. Knotek, and M. H. Ritchie, "Application of Difference Equations to a Square Hall Plate with Finite Interior Driving and Hall Electrodes", Journal of Applied Physics, Vol. 44, pp. 1870-1877, 1973.
8. SPICE is one of a number of readily available network solution programs used in Electrical Engineering.
9. van der Pauw, L. J., "A Method of Measuring Specific Resistivity and Hall Effect of Discs of Arbitraru Shape", Philips Research Reports, Vol. 13, pp. 1-9, 1958.
10. O'Malley, John R., Circuit Analysis, (Prentice-Hall, Englewood Cliffs, N. J., 1980), p. 149.
11. Mayer, James W., Lennart Eriksson, and John A. Davies, Ion Implantation in Semiconductors, (Academic Press, New York, 1970) p. 190.
12. Young, David M., Iterative Solution of Large Linear Systems, (Academic Press, New York, 1971).
13. The author is indebted to Dr. Arthur Thorbjornsen, SCEEE Summer Faculty at AFWAL, 1981, for programming and running the network using SPICE.
14. Harada, Roy H., and Alan J. Strauss, "Preparation and Properties of Indium Arsenide", Report No. CML-TN-p108-14; 31 Jul 58, 23 p. Contract AF 18 (603) 9. ASTIA AD-202 311, Chicago Midway Labs, University of Chicago, Ill.

15. Putley, E. H., "The Hall Effect and Related Phenomena", (Butterworths, London, 1960) p. 150
16. See ref. 11, p. 192 ff.

1981 USAF - SCEE SUMMER FACULTY RESEARCH PROGRAM

Sponsored by the

AIR FORCE OFFICE OF SCIENTIFIC RESEARCH

Conducted by the

SOUTHEASTERN CENTER FOR ELECTRICAL ENGINEERING EDUCATION

FINAL REPORT

(A) SPECTROSCOPIC ANALYSIS AND OPTIMIZATION OF THE OXYGEN/

IODINE CHEMICAL LASER AND (B) ALUMINUM-27 NMR OF DIALKYL-

IMIDAZOLIUM CHLOROALUMINATE MOLTEN SALTS

Prepared by: Larry Raymond Dalton

Academic Rank: Professor

Department and University: Department of Chemistry
State University of New York at Stony Brook

Research Location: Frank J. Seiler Research Laboratory/NC
United States Air Force Academy, Colorado

USAF Research Colleagues: Major Chester A. Dymek and Dr. John S. Wilkes

Date: August 21, 1981

Contract No: F49620-79-C-0038

(A) SPECTROSCOPIC ANALYSIS AND OPTIMIZATION OF THE OXYGEN/
IODINE CHEMICAL LASER AND (B) ALUMINUM-27 NMR OF DIALKYL-
IMIDAZOLIUM CHLOROALUMINATE MOLTEN SALTS

by

Larry R. Dalton

ABSTRACT

The development of a computer correlated electron paramagnetic resonance/optical emission spectrometric/mass spectrometric (EPR/OES/MS) facility was undertaken for the analysis of the gas-phase chemical reactions in the oxygen/iodine chemical laser. The objective was EPR detection of the $O_2(^3\Sigma)$, $O_2(^1\Delta)$, $I(^2P_{3/2})$, $I(^2P_{1/2})$ and $I_2(^3\Pi)$ species with simultaneous EPR/OES monitoring of the $O_2(^1\Delta)$ and $I(^2P_{1/2})$ species. Failure by Varian Associates to complete upgrading of the EPR facility prevented realization of the original objectives although the feasibility of OES detection within a microwave cavity was demonstrated. Aluminum-27 NMR spin-spin and spin-lattice relaxation measurements were carried out on dialkylimidazolium chloroaluminate molten salts. NMR linewidths measured at ambient temperatures employing a WT-150 spectrometer varied from 60 Hz to 11 Hz in going from $AlCl_3$ concentrations of 0.3 to 0.5N and from 11 Hz to greater than 2000 Hz in going from 0.5N to 0.7N. In the former region linewidths were observed to exhibit a minimum with temperature while in the latter region linewidths were observed to monotonically decrease with increasing temperature. These measurements may permit a fast, non-invasive characterization of molten salt solutions.

Acknowledgement

The author would like to thank the Air Force Systems Command, the Air Force Office of Scientific Research and the Southeastern Center for Electrical Engineering Education for providing him with the opportunity to spend a very worthwhile and stimulating summer at Frank J. Seiler Research Laboratory, United States Air Force Academy, Colorado. He greatly acknowledges the stimulating scientific conversations, laboratory assistance and good fellowship of his colleagues and the entire staff at FJSRL. He particularly expresses his appreciation for the opportunity to associate with two outstanding scientists, Major Chester A. Dymek and Dr. John S. Wilkes. The research associate will definitely be a better researcher and teacher for this experience.

The use of the Regional NMR Center at Fort Collins is gratefully acknowledged as is the assistance of Dr. Fyre of the Center staff.

I. INTRODUCTION

Accurate identification of reacting chemical species and accurate determination of rate constants for the gas-phase chemical reactions involved in the oxygen/iodine chemical laser are necessary to model and optimize this laser device. Because of the recognized complexity and multi-variable nature of this system, simultaneous monitoring of many species is necessary in order to reliably characterize this system. Optical emission spectroscopy (OES) affords excellent sensitivity and is useful for detecting and monitoring the excited state species $O_2(^1\Delta)$ and $I(^2P_{1/2})$. Unfortunately OES does not permit direct quantitative determination of emitting species concentrations nor does this technique permit monitoring of ground state species. Electron paramagnetic resonance (EPR) spectroscopy on the other hand does permit quantitative measurement of at least four species, namely, $O_2(^1\Delta)$, $I(^2P_{1/2})$, $I(^2P_{3/2})$ and $O_2(^3\Sigma)$. However, the $I(^2P_{1/2})$ species is detected with rather poor signal-to-noise and an independent measurement of the reaction kinetics of this species is desirable. Performance of simultaneous EPR and OES measurements permits a cross check on the determination of reaction kinetics with EPR providing quantification at high concentrations and OES permitting the kinetics to be followed over a substantial range of concentrations. Mass spectrometric techniques permit the monitoring of ground state species particularly those such as Cl_2 , H_2O_2 , etc. involved in $O_2(^1\Delta)$ generation which are not detected by EPR or OES.

An as yet undetected intermediate, $I_2(^3\Pi_{2u})$, has been suggested as playing an important role in the reaction scheme of this laser system. This optically dark species should be EPR active and its potential importance in the reaction scheme suggest a need for a thorough search by EPR for its existence.

The research associate is an experienced spectroscopist possessing the necessary skills to modify the existing experimental apparatus for simultaneous OES/EPR/MS detection and the EPR spectrometer (once an upgrade by Varian was complete) for a high field and high sensitivity search for $I_2(^3\Pi_{2u})$. Improvement of the $O_2(^1\Delta)$ generator and iodine injection system was also necessary and was to be undertaken by highly qualified Air Force chemists (Maj. Chester A. Dymek and Capt. Larry P. Davis).

rate constants.

(6) Conduct an EPR search for the $I_2(^3\Pi_{2u})$ species.

(7) As a UTI model 100C mass spectrometer became available, interface this system to the laser model system working with Maj. Dymek and MSgt. Scott.

B. ^{27}Al Studies of Molten Salt Solutions. Objectives include measurement of the linewidths of ^{27}Al signals for molten salt AlCl_3 compositions ranging from 0.3 to 0.7N, measurement of the temperature dependence of linewidths for selected samples and the preliminary measurement of spin-lattice relaxation times.

III. PROGRESS REPORT FOR THE OXYGEN/IODINE LASER WORK

Objectives (1) through (4) were accomplished. Pole caps were added to the 15" electromagnet. A plate with optical stack was designed and constructed which replaced the front plate of the Varian TE_{102} cavity. The cavity with this plate in place yielded a sensitivity of 75% of that of the conventional cavity. This is in good agreement with theory for the Q degradation associated with microwave perturbation from the presence of an optical stack. A 19" light pipe was constructed by treading optical fibers through 3/8" Tigon tubing. A surgical scapel was used to cut the fibers and provide reasonably smooth end faces. Use of the light pipe (for providing transmission from the region of the flow stream contained in the microwave cavity to a Wang detector positioned above the electromagnet) with operation of the $\text{O}_2(^1\Delta)$ chemical generator demonstrated that this arrangement yielded adequate signal-to-noise sensitivity for monitoring the chemical kinetics of $\text{O}_2(^1\Delta)$. It follows from a consideration of the emission intensities (transition moments) of $\text{O}_2(^1\Delta)$ and $\text{I}(^2P_{1/2})$ that this OES detection scheme will be adequate for monitoring the chemical kinetics of $\text{I}(^2P_{1/2})$.

Working with Maj. Dymek and MSgt. Scott several designs for iodine injection into the reactant flow stream were developed. The research associate then participated in the testing of these designs which was directed by Maj. Dymek. The essential conclusion derived was that insertion of a glass iodine injector into the flow stream caused appreciable deactivation of $\text{O}_2(^1\Delta)$. The amount of deactivation is prohibitive for a 1/2" diameter flow tube but within acceptable limits for a 1" diameter flow

The second project area concerns the characterization of the composition and determination of the physical properties of dialkyl-imidazolium chloride/aluminum chloride molten salt solutions. Current techniques to determine composition are tedious, time consuming and difficult. Preliminary ^1H NMR studies by Wilkes and coworkers suggest that NMR can provide a fast, accurate and non-invasive means of characterizing the composition of molten salt solutions. Moreover, NMR may suggest structures for the solution species. The project pursued by the research associate was the use of ^{27}Al NMR as a companion technique to ^1H , ^{13}C , and ^{15}N NMR studies. Moreover, it is suggested that by performing spin-lattice (T_1) as well as spin-spin (T_2) relaxation measurements, the relative contributions of rotational diffusion and chemical exchange in determining individual relaxation times may be determined. Also variable temperature measurements are suggested as a means of assigning chemical shifts to individual aluminum species and of measuring activation energies for chemical exchange and rotational diffusion.

II. OBJECTIVES

A. Oxygen/Iodine Laser Project. The objectives of this project are as follows:

- (1) Working with Maj. Dymek and Capt. Davis optimize the efficiency of the $\text{O}_2(^1\Delta)$ chemical generator.
- (2) Working with Maj. Dymek develop an iodine injection system and optimize the efficiency of this system.
- (3) Install pole caps on the 15" electromagnet system to permit realization of magnetic fields of at least 20,000 Gauss.
- (4) Design and construct a system permitting simultaneous optical and EPR detection at the same point in the gas stream. This involves adding an optical port to a Varian TE₁₀₂ cavity and constructing a light pipe (optical guide) extending from the optical port to a Wang detector positioned above the magnet yoke.
- (5) Carry out OES and EPR measurements (as well as pH, chloride ion, etc. monitoring of the $\text{O}_2(^1\Delta)$ generator; temperature and pressure monitoring at various points) on a model laser system in an effort to measure relevant

tube. The flow tube was correspondingly redesigned to narrow from 1" to 1/2" only in the vicinity of the EPR cavity.

Preliminary consideration was given to the interface of the UTI mass spectrometer to the flow stream and detailed design was carried out by Maj. Dymek and MSgt. Scott. The utilization of the UTI mass spectrometer for other projects prohibited implementation of this interface during the summer 1981.

Near the end of July it was realized that Varian Associates would not complete the interface of the existing magnet power supply to the E-line magnet field controller. Without this interface, EPR measurements were impossible so a decision was made to discontinue work on the oxygen/iodine laser model system and to concentrate efforts on the ^{27}Al NMR studies of molten salt solutions.

IV. PROGRESS REPORT ON ^{27}Al NMR STUDIES OF DIALKYLIMIDAZOLIUM CHLOROALUMINATE MOLTEN SALTS

Initial ^{27}Al NMR measurements were conducted at 39 MHz on samples characterized by AlCl_3 concentrations ranging from 0.3 to 0.7N employing a Nicolet NT-150 NMR spectrometer located at the Regional NMR Center, Colorado State University, Fort Collins, Colorado. Each sample yielded a single resonance line with no significant chemical shift differences observed among the various samples. However, substantial linewidth variations were observed among the various samples. These are summarized in Table I.

Table I. Ambient Temperature ^{27}Al NMR Linewidths of 1-Methyl-3-Ethyl-imidazolium chloride : Aluminum Chloride Molten Salt

<u>Sample</u>	<u>N AlCl_3</u>	<u>Linewidth, Hz</u>
E	0.3157	60
C	0.3562	46
A	0.3987	34
1	0.4201	30
3	0.4573	14
6	0.5156	11
7	0.5392	425
8	0.5537	650
9	0.5805	1000
10	0.5936	1200
11	0.6130	1505
12	0.6806	2300

Two mechanisms are likely to dominate ^{27}Al spin-spin relaxation and hence NMR linewidths. The first of these is modulation of the ^{27}Al nuclear quadrupolar interaction by rotational diffusion. This mechanism yields a contribution to the NMR linewidth which monotonically decreases with increasing temperature.

The second mechanism is chemical exchange which can result either in line broadening or line narrowing with increasing temperature depending upon whether the exchange frequency is in the slow or fast exchange regions.

Nuclear quadrupolar relaxation is independent of spectrometer frequency while chemical exchange relaxation will depend upon spectrometer frequency if chemical shifts are modulated by the exchange. Modulation of nuclear dipolar or quadrupolar interactions by chemical exchange yields a frequency-independent contribution to the linewidth.

An important distinction between the above two mechanisms, in addition to the aforementioned temperature and spectrometer frequency dependence, is the different effect of these mechanisms upon nuclear spin-lattice relaxation. In the fast motion region, quadrupolar relaxation results in equal spin-lattice and spin-spin relaxation times while chemical exchange is, in general, not an efficient spin-lattice relaxation mechanism. Thus if chemical exchange is dominant, one might expect T_1 to be longer than T_2 .

To attempt to discriminate between quadrupolar and chemical exchange relaxation contributions to linewidths, spin-lattice as well as spin-spin relaxation measurements were performed and linewidth measurements as a function of temperature were carried out. The results are summarized in Tables II and III.

The effective equality of T_1 and T_2 evident in Table III suggests that quadrupolar relaxation may be the dominant relaxation mechanism. This conclusion is also supported by the partial resolution of two ^{27}Al transitions observed at 73 degrees centigrade for samples 7 and 9. The resolution of these transitions, which are likely due to the AlCl_4^- and Al_2Cl_7^- species, indicate that chemical exchange between the chloroaluminate species is in the slow exchange region. The decrease in linewidth with increasing temperature observed for samples of AlCl_3 concentrations greater than 0.5N is thus assignable to motionally narrowing by rotational diffusion of the

Table II. ^{27}Al NMR Linewidths as a Function of Temperature of 1-Methyl-Ethylimidazolium Chloride: Aluminum Chloride Molten Salt

Sample	N AlCl_3	^{27}Al NMR Linewidth, Hz				
		t = -10 °C	t = 12 °C	t = 26 °C	t = 48 °C	t = 73 °C
E	0.3157	294	220	58	59	158
32	0.423	150	34	22	44	78
4	0.4805		17	16	24	41
5	0.4955		15	13	16	23.5
7	0.5392		665	390	228	144
9	0.5805	5000	2005	1130	730	500
34	0.638		3177	1660	1234	950
36	0.659		5437	2200	1400	970

Table III. ^{27}Al Spin-Lattice and Spin-Spin Relaxation Times Determined For Selected Samples of 1-Methyl-Ethylimidazolium: Aluminum Chloride Molten Salt

Sample	Temperature, °C	T_1 (msec)	T_2 (msec)
E	26	6	5.5
5	26	31	24.5
36	26	0.14	0.14
5	73	15	13.6
7*	73	2.5	2.2

*For sample 7 two resonances are resolved. The resonance tentatively assigned to AlCl_4^- yielded a T_1 of 2.5 msec while the resonance tentatively assigned to Al_2Cl_7^- yielded a T_1 of 3.0 msec. It is not clear at this time if these differences are meaningful.

^{27}Al quadrupolar interaction. The magnitude of the decrease goes as the ratio of viscosity to temperature in degrees Kelvin.

The temperature dependence of the linewidths in the basic region (AlCl_3 concentrations less than 0.5) is more complicated. Indeed, the linewidths go through a minimum with changing temperature. The low temperature region likely reflects quadrupolar relaxation domination with this contribution decreasing with increasing temperature. The above-ambient temperature linewidth behavior most likely reflects the onset of

chemical exchange between the chloroaluminate species. An alternate but less plausible explanation of the unusual temperature dependence of the linewidths in the basic region in a spin-rotation relaxation mechanism.

V. RECOMMENDATIONS

A. Oxygen/Iodine Model System. The scheme developed for simultaneous EPR/OES detection is unique. Optical detection within a microwave cavity cannot be accomplished using the TE_{011} mode cavity employed by other workers studying the oxygen/iodine laser system. We recommend that this system be utilized as soon as the EPR is made operational by Varian.

We would also suggest an additional scheme for searching for the $I_2(^3\pi)$ species. We suggest irradiating the reaction stream with a tunable laser and monitoring the effect on the species detected by OES and EPR. The idea is that by optically pumping the $I_2(^3\pi)$ state one may perturb the concentrations of species detected by OES and EPR.

Optically pumping of other species is also desirable to elucidate details of the kinetics and to check the assignment of rate constants. A pulsed laser is most desirable for such studies.

The effects of spin polarization should be considered and ELDOR type (including pulsed ELDOR) studies may prove useful in elucidating the kinetics in a manner analogous to that discussed for optical pumping.

B. Molten Salt Studies. The present work clearly proves the hypothesis of Wilkes concerning the utility of NMR for characterizing molten salt solutions. A meeting was held with Dr. Wilkes at which a comprehensive program for the quantitative analysis of molten salt solutions by NMR was defined.

The recommendations listed below are an outgrowth of that meeting although the recommendations listed here were not the only studies defined.

First of all, it is suggested that ^{27}Al NMR measurements be conducted at temperatures between 50 and 75 degrees centigrade employing 400 MHz and possibly 600 MHz NMR spectrometers. For samples in the acidic region ($AlCl_3$ concentrations greater than 0.5) this would permit resolution of the two resonances associated with the chloroaluminate species. Such measurements would permit determination of both the equilibrium constant and kinetic rate for the equilibrium $AlCl_4^- \rightleftharpoons Al_2Cl_7^- + Cl^-$

Moreover, correlation of 150 and 400 MHz NMR data would permit determination of the contribution of chemical exchange to linewidths since quadrupolar relaxation is frequency-independent.

Viscosities of solutions should be measured. Such data could be used to rule out the possibility of a spin-rotation contribution to linewidths and could be used to further define the contribution of nuclear quadrupolar relaxation.

Proton NMR measurements should be carried out at 600 MHz to further refine measurement of the effect of molten salt composition upon cation environment.

It is proposed to carry out the above NMR measurements working in collaboration with Dr. Wilkes utilizing NMR spectrometers at Bruker Billerica and at Carnegie Mellon University.

¹⁵N and ¹³C NMR measurements should be conducted to define the effect of solution composition upon the cation.

Also a measurement of ²⁷Al quadrupolar coupling constants should be attempted by examining frozen solutions (glasses).

With the above data a quantitative modeling of the systems is not only possible but parameters can be overdetermined.

1981 USAF - SCEEE BUTLER FACULTY RESEARCH PROGRAM

Sponsored by the

AIR FORCE OFFICE OF SCIENTIFIC RESEARCH

Conducted by the

SOUTHEASTERN CENTER FOR ELECTRICAL ENGINEERING EDUCATION

FINAL REPORT

SCFE ASPECTS OF CARDIAC RISK EVALUATION
AT THE USAF SCHOOL OF AEROSPACE MEDICINE

Prepared by: Dr. Charles B. Davis
Academic Rank: Assistant Professor
Department and University: Department of Mathematics
University of Toledo
Research Location: USAF School of Aerospace Medicine,
Data Sciences Division,
Biomathematical Modelling Branch
USAF Research Colleague: Dr. Joel E. Michalek
Date: September 2, 1981
Contract No: F49620-79-C-0038

SOME ASPECTS OF CARDIAC RISK EVALUATION
AT THE USAF SCHOOL OF AEROSPACE MEDICINE

by

Charles B. Davis

ABSTRACT

Various statistical and biometrical aspects of coronary artery disease screening at the USAFSAAM are investigated, including the following: the selection of an appropriate data base from which to estimate risk functions; the missing data inherent in any such data base assembled over years, and procedures for using incomplete records in estimation; a multivariate binary/normal distribution suited for those missing data procedures; and the construction of statistical models incorporating measures of disease severity, including two-stage (latent and acute) models of the disease process. The data base constructed as suggested is described, and specific guidance for fitting the proposed models is offered.

ACKNOWLEDGEMENT

I would like to thank the Air Force Systems Command, the Air Force Office of Scientific Research, and the Southeastern Center for Electrical Engineering Education for providing this opportunity to work in the Biomathematical Modelling Branch, Data Sciences Division, USAFSAM, Brooks AFB, TX. The Branch and Division have been most helpful in allowing me the use of their excellent resources and support personnel.

In particular, I wish to acknowledge the discussions on matters statistical and biomathematical with Dr. Joel Michalek and Dr. Richard Albanese of USAFSAM and Dr. Dan Mihalko and Dr. Kishan Mehrotra, also visiting USAFSAM. The very willing and knowledgeable programming support given by Mr. Tom White greatly eased many of my tasks this summer, and the patient cooperation of Mr. Bill Besich and Mr. Bill Nixon in creating a data file to my specifications from the archives at USAFSAM was invaluable.

Also, I wish to acknowledge the several interesting discussions with Dr. James R. Hickman and Dr. Gil D. Tolan of the Clinical Sciences Division, USAFSAM, concerning the nature of coronary artery disease and its measurement, and with Mr. Robert Dedecke and Mr. William G. Jackson of the Data Sciences Division for freely given advice on the nature of the data available at USAFSAM.

I. INTRODUCTION:

Coronary artery disease (CAD) is a major public health problem, both because of its high incidence rate and because early detection is often difficult. In the general population it has been estimated¹ that one third of all males will have some major incapacitating cardiovascular problem; that one fifth of all males will have heart attacks before age 60; and that 65% of heart attacks will be "unexpected" (i.e., not preceded by warnings of CAD). In fact, in about one in five heart attacks, death is the major presenting symptom. The classical symptoms of CAD, such as angina pectoris, are often not evident until serious impairment of cardiac function is present. Findings from routine physical examinations, particularly electrocardiographic (ECG) studies, can point to cardiac function alteration and impairment, but not completely reliably and not before damage has been done.

Accordingly, much effort has been expended in identifying subsets of the population at greater than usual risk of developing heart disease. We will not attempt here to review the large and rapidly expanding literature on this subject, except to note that various authors have shown that CAD incidence can be related to age², serum cholesterol and systolic blood pressure³ or diastolic blood pressure⁴, personality type or behavior pattern⁵, smoking history⁶, relative weight⁷, family history of heart disease, and, more recently, the relative amounts of high density lipids (HDL) and low density lipids (LDL)⁸. Other studies have examined the best use of diagnostic tools such as the ECG⁹ and exercise testing^{10,11}. Most of these studies use as their endpoint clinically manifest heart disease; some use angiographically determined evidence of CAD, including some measurement of the severity of the disease along with the fact of its occurrence^{12,13}. Angiographic determinations

are available only on subjects suspected of having CAD, because of the expense and the risk involved in the catheterization procedure; studies using only such subjects are working with a selected high-risk subset of the population, an important point which will be discussed later.

The consequences of sudden incapacitation among aircrew, both civilian¹ and military^{14,15,16,17}, are exceptionally serious, and with high performance aircraft, pilots are subjected to greater stress than the population at large. Consequently, the USAF as well as other military and civilian aviation authorities are quite concerned with the problem of screening aircrew for potential CAD problems. In the absence of clinical symptoms, although the usual risk factors do differ significantly between groups with and without CAD, the current error rate (particularly, false positive rate, since the screening procedure is necessarily conservative) in screening procedures is not yet acceptable¹⁵.

Statistical methods used in epidemiological investigations of CAD have ranged from simple tabulation to discriminant analysis^{2,3}, logistic risk function analysis^{5,6}, and more sophisticated models for the progression of risk factors in time and the occurrence of acute cardiovascular events¹⁸. Discriminant analysis¹⁹ and regression analysis¹² have been used to deal with measures of disease severity, with varying degrees of success. Information-theoretic methods have been employed to describe the usefulness of stress testing²⁰.

A major problem in this field is that data bases are built up over years, during which knowledge about CAD changes. Each era in each study, therefore, uses a different set of risk factors, and it is often difficult to relate results from different investigations. Within one investigation, different subsets of potentially useful variables will be recorded on different subjects, creating technical problems in analysis.

It should be mentioned here that thallium-201 scintigraphy is a promising new non-invasive diagnostic tool^{15,21}, which is likely to add a new, effective step to the screening process, although its complexity and expense will not obviate the need for better screening procedures based on traditional measurements.

II. OBJECTIVES:

Based on initial discussions with persons in the Data Sciences and Clinical Sciences Divisions of USAFSAM, I decide that the initial stage of the summer's effort should involve literature review, particularly with an aim towards the mechanisms of CAD origin and development, and the role played by various interacting variables. It soon became clear that this area is not sufficiently well understood to allow for specific probabilistic modelling, so I went on to the following specific subproblems:

- (1) the role which measurements of the severity of CAD could play in the risk assessment problem, including a study of the types of measurements to be made and the measurement error involved therein;
- (2) the missing data problem;
- (3) the appropriate data base to use in developing screening procedures for USAFSAM use, and construction and checking of that data base; and
- (4) discrepancies between previous USAFSAM results and other published results in the cardiovascular risk literature.

III. THE ORIGIN AND DEVELOPMENT OF CORONARY ARTERY DISEASE:

Mechanisms and processes by which CAD begins and develops are not well understood at present, largely due to difficulties in observing the disease process at work. Also, there are undoubtedly stochastic elements involved in parts of the process, which will increase the difficulty in discovering the

mechanisms involved. In section VIII a simple, general model is presented which seems likely to be able to handle and even elucidate this problem somewhat.

An extremely interesting set of observations on the growth of CAD is that reported by Osborne²², involving necropsy studies of coronary arteries in over a thousand subjects. Some of his conclusions are:

- (1) newborn infants are free of CAD, but significant lesions can develop as early in life as ten weeks;
- (2) lipids are often but not necessarily found in lesions;
- (3) it is not clear that lipids do or do not have a role in causing lesions to form, or in fact what mechanism(s) are responsible for initiating lesions; and
- (4) lesions grow in stages (irritation, growth, and healing over), and routinely form over previously healed lesions.

On the basis of his observations, he forms the hypothesis that any person whose coronary arteries are free of disease at age 20 will not suffer from the disease before age 60. This conjecture, even if only partially true, has interesting implications for the type of models to be fitted to the CAD process, as well as for screening and prevention.

In the absence of sufficiently specific modelling information, we are left with a list such as that given in section I above of "risk factor variables" known to be associated statistically with the presence of CAD. These relationships put constraints on the nature of the disease mechanism, but so far the constraints are not at all strict.

IV. THE USAFSAM DATA BASE:

It will be useful at this point to discuss the nature of the data base available at the USAF School of Aerospace Medicine. The USAFSAM acts as a repository for results of annual physical examinations performed on aircrew, and as a medical consulting service. In particular, some 32000

ECG's arrive annually at the Central ECG Library; these are reviewed, and additional studies are requested on about 2.5% of the subjects involved¹⁵. Many of these subjects are referred to SAM (perhaps 150 new referrals per year) for cardiac evaluation, of whom about 35% undergo catheterization at SAM, resulting in the detection of about 20 flyers annually; with previously undiscovered CAD.

Since the installation of the Catheterization Laboratory in 1971, there have been changes, additions, and deletions to the various diagnostic procedures employed: the treadmill stress test protocol has changed, as has the serum cholesterol measurement procedure; HDL measurements were added in 12/77; and body fat, cortisol, and personality type are available only during certain periods. At my request a reasonably clean data base has been constructed, consisting of 1540 persons referred to SAM for cardiac evaluation for the first time between 1971 and 1980; this data base will be updated early in 1981, to add early years of pulmonary measurements, follow-up data on the subjects' CAD status, and laboratory measurement data from 1980, as well as to correct bad data which will be discovered between now and then. The current version of that file was made available to me only 8/30/81, so much work remains to be done in checking for internal consistency and erroneous values, before other use is made of the data. Appendix A contains a listing of the variables included in that data base, along with the particular repository from which that variable was taken.

USAF aircrewmembers are different from the general population in several relevant respects. They are male, mostly between the ages of 25 and 55. Because of their annual physical examinations, they can be expected to be generally more healthy than the general population. We expect aircrew not to be risk-averse persons, which is reflected in the fact

that nearly all flyers offered the choice of catheterization or disqualification from flying status choose the former. They work in similar environments and are similar with regard to intelligence and educational background. Most of the referral subjects are asymptomatic aside from ECG reports.

Because of these differences, it is likely that some of the usual risk factors will be less useful as predictors of CAD within the referral groups, due to its homogeneity and to the fact that the group was screened on the basis of ECG's (or, occasionally, other criteria). Conversely, risk profiles developed for this group will be directly applicable only to this group; in particular, it would be inappropriate to apply these profiles even to an unscreened population of aircrew. On the other hand, since the aim of the program is to improve the screening process, it is equally inappropriate to include in the study group only those patients known to have CAD, or only those who had been offered catheterization on the basis of the present screening procedure, since these are a further selected subset of the population of interest. (The statistical lore is full of misleading conclusions arrived at by applying the best of procedures to the wrong populations.) We have been careful to select our study group on the basis of first referral to AAF for Cardiac evaluation in order to ensure that it is as appropriate for our purpose as possible.

A major technical difficulty with this group is that angiographic determination of CAD status is available on only 25% of the subjects involved. It may be reasonable to simply assume that those not offered catheterization were free of CAD, since the consulting cardiologists estimate a false negative rate of less than 1% for their decisions on recommending or not recommending catheterization¹⁵, and the common statistical procedures (discriminant analysis and

logistic regression) tolerate such errors reasonably well²³. A hazard in this approach is that, conceivably, the disease rate in the non-catheterization group could be rather higher than assumed; this could result in the current catheterization criteria receiving greater weight than they deserve. A more sophisticated approach might involve putting a weak but not non-informative prior distribution on the incidence of CAD, based on values of risk variables, and performing a Bayesian analysis. In this approach, angiographic data, where available, would overwhelm the prior distribution, but the posterior distribution would be the prior distribution where no sample data is available. The prior distribution could be literature based (as was done in (20)), or could be based on expert opinion elicited from cardiologists familiar with the SAA aircrew referral population, in a sort of Delphi procedure.

The analysis using only subjects on whom angiographic endpoints are available will very likely show the catheterization criteria to be less useful than they actually are, simply because the study group will be rather homogeneous with respect to those criteria.

V. ANGIOGRAPHIC MEASUREMENTS OF DISEASE SEVERITY:

The statistical effects of errors in measurement of the various risk factors are reasonably well understood, and the usual risk function procedures as well as regression are reasonably well behaved in this regard²³.

Of greater interest for the study of CAD formation, development, and diagnosis is the accuracy of the coronary angiogram as a measurement of the extent of CAD, or as a measurement of the prognostic severity of the disease, or as a measurement of the degree of cardiac impairment already present. The differences between these are important, in that angiographically derived measures which are easier to predict may not be those with the greatest prognostic

significance, or those corresponding to the most easily diagnosed disease states.

A basic problem here is the relationship between angiographically determined degree of stenosis (maximal diameter reduction) of the artery, the flow reduction resulting from the stenosis, and the cardiac function limitation resulting. Biophysics does not help much here, as the geometry of the artery wall (lumen) remaining after the lesion has grown is rarely tractable, and blood is not a homogeneous fluid.

Based on photographs presented by Osborne²² and Isner et al.²⁴, and sketches presented by Osborne, a simulation experiment was conducted, using computer-generated geometries of initial and final lumen shapes as shown in Figure 1, in a wide range of amounts of occlusion. After eliminating configurations with residual area equal to zero, a relationship of the form

$$\log\left(\frac{\text{residual area}}{\text{initial area}}\right) = k \cdot \log\left(\frac{\text{min. residual diameter}}{\text{initial diameter}}\right) \quad (1)$$

was fit by least squares; exponentiating, this gives the relationship

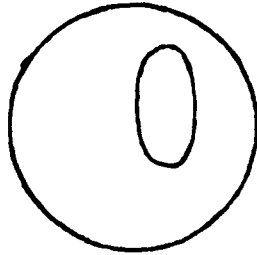
$$\left(\frac{\text{residual area}}{\text{initial area}}\right) = \left(\frac{\text{min. residual diameter}}{\text{initial diameter}}\right)^k$$

For circular lumens, k will be 2, and this value is often used regardless of shape. For the various shapes shown in Figure 1 and in the photographs cited, the best overall values of k are given below:

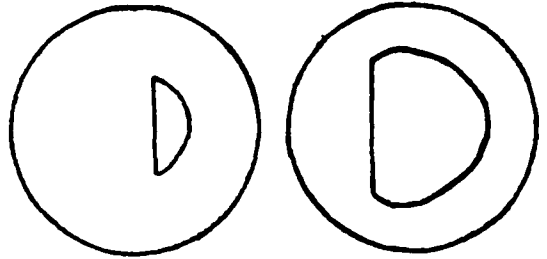
<u>Shape</u>	<u>k</u>
ellipse	1.27
segment	1.39
arc	1.91
triangle	1.68
rectangle	1.16
actual	1.63

FIGURE 1

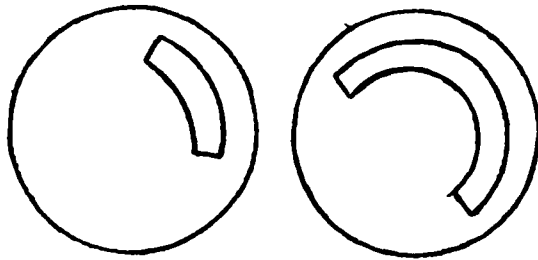
ELLIPSE



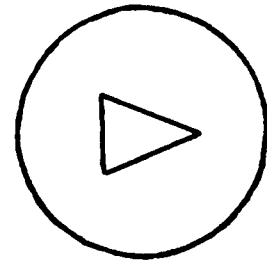
SEGMENT



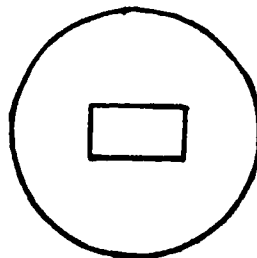
ARC



TRIANGLE



RECTANGLE



The weighted average of these values, weighted by the relative frequencies of the shapes as they appear in the photographs of Osborne, is 1.46.

Before constructing an index of the amount of lesion volume present, there is still the matter of the relative size of the various coronary vessels. A certain amount of examination of the photographic atlas of the heart by McAlpine²⁵ convinced me that the schematic drawings given by Froelicher et al.¹⁴ are reasonably accurate in this regard, at least relative to expected person-to-person variation. After allowing for artery wall thickness, the following rough "average" relative diameters were obtained for the various segments, using the nomenclature of Froelicher et al.¹⁴:

<u>Vessel</u>	<u>Segment</u>	<u>Relative diameter</u>	
LMCA	A,B	6	
	LAD	C	4
		F	2
LCA	G,H,D ₁ ,...,E	1	
	I	3	
	K	2	
	L,J ₁ ,...,N,1,2,3	1	
RCA	M,O	5	
	P	4	
	S	3	
	Q	2	
	Q ₁	2	
	Q ₂ ,...,R,T,U,1,2,4,5	1	

From these, an index of the volume of any one lesion was constructed as

$$V^3 \cdot (1 - (1 - D)^{1.46})^{1.5}, \quad (2)$$

where V is the relative diameter from the table above and D is the proportional reduction observed in diameter. This is summed over lesions observed to form an index of the total volume of lesion present.

To measure the resistance to blood flow due to one or more stenoses in series, we rely on the experiments of Gould and Lipscomb²⁶. They found, in in vivo experiments in dogs, that resting blood flow was not affected by stenoses of up to 85% occlusion, whereas stenoses of 30% or greater occlusion did limit hyperemic flow. They give plots of their data for quantities they call "coronary flow reserve" and "resistance"; the resistance measure is approximately additive over small to moderate stenoses in series. Using their formulas and approximate formulas fitted to their plots, the measures given in Appendix A were computed. The maximum resistance over the four main coronary vessels is one of the measures included in the data base.

Dr. James R. Hickman, Clinical Sciences Division, SAK, has constructed and collected a variety of other measures of disease severity. Some of these specifically address the prognosis of the angiogram; others are chosen from the scoring systems found in the literature. These are described also in Appendix A. An interesting study, not yet undertaken, would be to define suitable criteria and decide which of the measures are most easily predictable, and whether significant differences in predictability exist. We shall discuss the statistical uses of some of these measures in section VIII.

In addition to the studies reported in this section, some mention should be made of recent articles relating angiographic determination of disease status to post-mortem findings. Schwartz et al.²⁷ report 79% "agreement", with most most errors being underestimated caused by eccentric lesion geometries. Hutchins et al.²⁸ report generally good angiographic assessment of lesions, whereas Vlodaver et al.²⁹ in examining 134 segments from 10 subjects report 33% false negative readings. Overall, based on these and other reports, and on my own viewing of photographs and angiographic films,

I feel that while this source of error is not negligible, it is probably not of greater magnitude than other measurement errors in this problem.

VI. A MULTIVARIATE BINARY/NORMAL DISTRIBUTION:

If it were merely a matter of predicting presence or severity of CAD, ordinary regression, logistic regression, or extensions thereof (see section VIII) would be adequate. However, the missing data structure of our data base will demand that a joint distribution be constructed for the variables involved, in order that the sophisticated missing data procedures to be described in the next section may be implemented. As we will see, treating the predictor variables as random rather than fixed will allow us to write a joint density in the exponential family which has convenient marginal distribution properties.

Multivariate statistical techniques for continuous variables are well studied for only the multivariate normal distribution. Fortunately, our sample is large enough that we may comfortably fit approximate normalizing transformations. Similarly, multivariate categorical variable distributions have been studied extensively, both in their own right, and as part of discrimination problems, often motivated by problems similar to that at hand.^{30,31,32,33,34,35.} Depending on the expected data structure and the intentions of the analyst, different models are used, although the log-linear approach seems as common as any, partly because of certain inherent advantages and partly because of the existence of good, easy-to-use commercially available estimation programs.

For notational simplicity we shall restrict our attention to the case where q binary variables are measured. (See Cox³⁶ for a general discussion of this type of data.)

Some authors reduce this case to one with one multinomial variable taking on 2^c possible values, but this forfeits the inherent relationships between the variables. Most of the categorical variables which are present in our data base are binary, and we will treat the rest in that fashion, with some loss of information.

Joint multivariate binary normal models have received little attention in the literature considering their frequent applicability. Olkin and Tate³⁶ worked out correlation models, with attendant distribution theory, for the location model, where the mean vector for the normal variables is allowed to vary conditionally with the (one) categorical variable, but the (conditional) covariance matrix is fixed; Afifi and Elashoff³⁷ discussed the deficiencies of the usual two-sample T^2 test for this model, and construct information theoretic tests of the hypothesis of equal mean vectors. (The T^2 test is closely related to the usual linear discriminant function.) Chang and Afifi³⁸ study the classification problem, using the same model, with one dichotomous predictor variable and g or $g > 2$ categories for classification. Iremowski³⁹ develops a joint model for the discrimination/classification problem which is very similar to that which we will present below, and compares likelihood ratio discrimination under this model with use of the linear discriminant function. He does not however, exploit the conditional and marginal distribution aspects of his model as we will below.

This distribution is constructed as follows:

Let Y_j^* , $j = 1, \dots, c$ be binary $[0,1]$ variables; one of these could be an indicator variable for presence of CAD. As in (32) and (33), it will be extremely convenient to record these as

$$X_j = 2 \cdot Y_j^* - 1 \dots \quad (3)$$

Let $P(y_1, \dots, y_c) = \text{Prob}(Y_1=y_1, \dots, Y_c=y_c)$; then the log-linear model may be written

$$\log P(y_1, \dots, y_c) = \lambda_0 + \sum_i \lambda_i y_i + \sum_{i \neq j} \sum \lambda_{ij} y_i y_j + \dots + \lambda_{1\dots c} y_1 \dots y_c \quad . \quad (4)$$

(The notation (3) allows for the simple representation (4) rather than the usual cumbersome $\lambda_{y_1 y_2 \dots y_c}^{A_i A_j \dots}$ notation, and emphasizes the similarity between this model and the 2^c factorial linear model with one degree of freedom and, with parsimonious notation, one parameter for each main effect and each interaction term.) Note that if we were to set $y_j = 0$ ($y_j^* = \frac{1}{2}$), all terms in (4) involving effect j or any of its interactions vanish, leaving a model involving only other effects. Unfortunately, the resulting model does not give the same marginal probabilities as does (4), so this does not provide a satisfactory treatment for missing data except, perhaps, as an initial approximation. (This trick does work neatly in linear, as opposed to loglinear, models⁴⁰; however, with those, it is possible for cell probability estimates to be negative.)

Let

$$y' = (1, y_1, \dots, y_c, y_1 y_2, \dots) \quad (5)$$

be the vector of observations and products of observations; y' will be of dimension $m \leq 2^c$, according to the number of interaction terms included, and let

$e' = (\lambda_0, \lambda_1, \dots, \lambda_c, \lambda_{12}, \dots)$ be the corresponding vector of parameters. With this notation,

$$P(y_1, \dots, y_c) = \exp(e'y) \quad . \quad (6)$$

Then, conditioned on Y , $X' = (X_1, \dots, X_p)$ has a multivariate normal ($B'y, \Sigma$) distribution, where B is the matrix of regression coefficients of the X 's on the Y 's. Conditionally this may be viewed as a multivariate 2^q factorial linear model in which interaction terms of the same orders as in the Y distribution are included.

As usual, we write the conditional density of X given that $Y = y$ as

$$f(x|y) = (2\pi)^{-p/2} |\Sigma|^{-1/2} \exp \left(-\frac{1}{2} (x-B'y)' \Sigma^{-1} (x-B'y) \right), \quad (7)$$

with the joint distribution becoming

$$f(x, y) = (2\pi)^{-p/2} |\Sigma|^{-1/2} \exp \left(\theta'y - \frac{1}{2} (x-B'y)' \Sigma^{-1} (x-B'y) \right). \quad (8)$$

The marginal distribution of X will be a finite mixture of normal distributions

$$f(x) = \sum_Y f(x, y), \quad (9)$$

where the summation is over all of the 2^q cells of the Y or Y^* distribution.

Moments are

$$EX = \sum_Y B'y \exp(\theta'y) \quad (10)$$

$$EY^* = \sum_Y y^* \exp(\theta'y) \quad (11)$$

$$\text{Cov } X = \Sigma + B' \left(\sum_Y y y' \exp(\theta'y) \right) B - (EX)(EX)', \quad (12)$$

$$\text{Cov } Y^* = \sum_Y y^* y^{*'} \exp(\theta'y) - (EY^*)(EY^*)', \quad (13)$$

It is of particular interest for this application to examine certain of the marginal and conditional distributions resulting from this distribution. Let $X' = (X_1', X_2')$ and $Y^{*'} = (Y_1^{*'}, Y_2^{*'})$ be partitions of the respective vectors X and Y^* . Then

$$f(y_1^*) = \sum_{y_1^*} \exp(\theta'y) \quad (14)$$

where the summation is over all cells having the given value of y_1^* .

$f(x_1)$ has the same form as $f(x)$, with p replaced by p_1 , the dimension of X_1 ; Z replaced by Z_{11} , and B' replaced by B'_1 , where

$$Z = \begin{bmatrix} z_{11} & z_{12} \\ z_{21} & z_{22} \end{bmatrix} \quad \text{and} \quad B' = \begin{bmatrix} B'_1 \\ B'_2 \end{bmatrix}$$

is partitioned to correspond to the partitioning of X .

$$f(y_1^* | x_1) = \frac{\sum_{y_1^*} \exp(\theta'y + x_1' Z_{11}^{-1} B'_1 y - \frac{1}{2} y' B_1 Z_{11}^{-1} B'_1 y)}{\sum_{y^*} \exp(\theta'y + x_1' Z_{11}^{-1} B'_1 y - \frac{1}{2} y' B_1 Z_{11}^{-1} B'_1 y)} \quad (15)$$

where y^* , y indicate summation over all cells of the Y distribution. $f(y_1^* | x)$ has the same form, with x_1 , B_1 , and Z_{11} replaced by x , B , and Z respectively. Also, $f(y^* | x)$ and $f(y^* | x_1)$ are obtained simply by omitting the summation in the numerator.

Note that that if Y_1^* consists of only one variable, (15) takes the form of a ratio of linear combinations of exponentials of linear combinations of the X_1 or X variables. If the regression coefficients of X_1 on Y_1^* vanish, this will take the form of a logistic risk function. On the other hand, if these coefficients do not vanish, various joint non-linear effects in the X_1 variables may show up; this aspect of the model needs further investigation.

$$f(y_1^* | y_2^*, x) = \frac{\exp(y'B_1 \Sigma^{-1} x_1 - \frac{1}{2} y'B_1 \Sigma^{-1} B_1 y + \theta'y)}{\sum_{y_1^*} \exp(y'B_1 \Sigma^{-1} x_1 - \frac{1}{2} y'B_1 \Sigma^{-1} B_1 y + \theta'y)} ; (16)$$

for $f(y_1^* | y_2^*, x)$ make the usual substitutions in x , B , and Σ . Hence, if Y_1^* is one variable, the conditional distribution of Y_1^* given the rest of the binary variables and any subset of the continuous variables will be of the form of a logistic risk function, with parameters given by B , Σ , and θ .

Thus, it will be possible to compare many of the logistic risk functions appearing in the literature directly with marginal conditional distributions derived from the fitted distribution (8). Alternately, it will be possible to write down the distribution of any variable conditioned on any subset of the rest, in particular, conditioned on the subset recorded for the case at hand! Because of the form of the distribution, maximum likelihood estimation may be done independently for θ and for B and Σ ; the former by iterative proportional fitting or constrained Newton-Raphson algorithms, and the latter in closed form by usual MANOVA procedures.

One problem with the model is the large number of parameters to be fitted. Our large data base will help here; also, one should make all possible efforts to limit the number of interaction terms which enter the model.

This procedure and model are conceptually closer to the discriminant analysis approach than the logistic risk function approach, which is appropriate in view of the normal distributions of our (transformed) variables.^{41,42,43,44.}

VII. MISSING DATA PROCEDURES:

The small proportion of complete records in the USAFSAAM data base make it highly desirable to consider procedures for using incomplete records in estimation. Some authors have suggested using the mean of a variable as replacement for a missing value⁴⁵. A more satisfactory, simple approach is to use regression to predict missing values^{45,46}; this clearly makes use of the correlation between variables, and programs to implement these techniques are commercially available. Such a procedure was used in the analysis described in Section VIII to stand in for the ratio of total cholesterol to HDL. A drawback to the use of these programs is that they use the same set of variables to replace a given variable in all cases, and consequently are most useful where the missing data proportion is small, or where the missing data are confined to one variable or to a few variables which are reasonably uncorrelated with one another.

In the latter circumstance one could also consider using regression formulas developed from data sets taken from similar populations, which have more data present. In this study, HDL cholesterol is a prime candidate for this treatment, in that it is known to be a useful risk factor, but has been recorded at SAM only since December 1977.

The regression approach is useful, in that it allows for the use of standard statistical packages for estimation or analysis after the missing data are replaced. However, it is limited by the missing data pattern as indicated above. Also, one is tempted not to make allowances for the missing data replacement when reporting the precision of one's results; in fact, it is often not clear how this allowance should be done. Furthermore, the procedure is inaccurate for substantially non-normal distributions, particularly for discrete distributions. To overcome these

objections, one can always write down the appropriate marginal likelihood for each record, and then do estimates; clearly this is impossibly tedious.

An intriguing alternative is variously called the Missing Information Principle⁴⁷ or the EM algorithm⁴⁸. As presented by Dempster et al.⁴⁸, the procedure takes the following form in the regular exponential family

$$f(x|\theta) = b(x)\exp(\theta \cdot t(x))/a(\theta), \quad (17)$$

where x represents the complete data, $t(x)$ represents the complete data sufficient statistics, and θ the so-called natural parameters. Let z represent the observed data, i.e., z is y when y is not missing. Initial estimates of θ are obtained (from complete cases only, perhaps). Then, if $\theta^{(p)}$ is the value of θ after p iterations, we perform the following cycle: E-step; estimate the complete data sufficient statistic $t(x)$ by

$$t^{(p)} = E(t(x)|z, \theta^{(p)}) \quad (18)$$

M-step: determine $\theta^{(p+1)}$ by solving

$$E(t(x)|\theta) = t^{(p)} \quad (19)$$

or, if that is not possible, by letting $\theta^{(p+1)}$ be the maximum likelihood estimator (MLE) computed as if $t^{(p)}$ were the actual sufficient statistic. (Note that $t^{(p)}$ from (18) need not correspond to any realisable actual value of $t(x)$; for example, with discrete data, $t(x)$ may be integer-valued, whereas $t^{(p)}$ need not be.) The authors show that a fixed point of this iterative process must be a (local) maximum or fixed point of the likelihood, and give conditions under which a fixed point will be known to be an MLE. Note that the M-step can often be accomplished by standard algorithms, and the E-step bears some resemblance to the regression idea mentioned previously.

The algorithm as stated produces MLE's of the parameters based on available data; the filling in of missing values, as one way of implementing the E-step, is gratuitous. None-the-less, one might consider the fill-in values themselves as MLE's of the unknown observation.

In the distribution proposed in Section VI, the sufficient statistics are sums of binary variables and product thereof corresponding to interaction terms included in the model, and sum of the continuous variables within groups defined by the binary variables, and sum of squares and crossproducts corrected for group means. Therefore the contributions to the E-step can be computed on a case-by-case basis, although the various expectations involved will generally not be gotten by simple data replacement. Also, since the sufficient statistics are not guaranteed to be integers for the binary variables, iterative proportional fitting will not work as an EM algorithm; rather, another numerical iterative method such as Newton-Raphson must be used.

Beale and Little⁴⁷ compare several missing data procedures by simulation in a regression setting, concluding that EM-type procedures are generally preferable. One alternative they suggest is the use of these procedures to fill in the predictor variables (using all variables), then computing the regression using only those cases for which the dependent variable is present. This modification is appropriate to our data set. They also derive a method of weighting cases according to the amount of missing data for the case.

One open question, relevant to our investigation, is that of how many variables to include in the fill computation. Specifically, if one wants to predict Y from, say, no more than k X variables, all with greater or fewer missing

values and all more or less correlated, what rules should be used in deciding when to stop including x variables in the EM algorithm, before producing the desired prediction procedure using the estimated parameters of the joint distribution fitted to all variables?

Another problem is that the missing data procedures presume that the fact that a data value is missing is independent of what that value would have been. In our situation, angiographic determination of CAD status ^{is missing} if the cardiologist thinks it quite unlikely that disease is present based on values of other variables¹⁵. The performance of the EM algorithm should be investigated in this situation, perhaps by simulation.

VIII. THE USE OF CAD SEVERITY MEASURES:

Most of the work which has been done on the risk factor problem has considered only the presence or absence of CAD; see (11) or (12) for exceptions. Making good statistical use of measure of disease severity requires some additional modelling effort.

It is clear that in any population in which any non-negligible proportion of the subjects are disease-free, the severity measure must have a "point mass" at zero. This will do serious damage to the usual regression or linear model structure, regardless of how one transforms disease scores. In the USAFSAI data base described above, about 90% of the subjects have severity scores of zero; this difficulty can not be ignored. One could restrict attention only to those subjects with positive severity scores, for some purposes, but not for the purpose of developing screening procedures.

One can make use of the disease severity measures through more sophisticated modelling. According to Osborne¹⁶ and others, we may consider CAD to have two aspects or phases,

which may be called the "trigger" or "latent" disease stage, when the subject's susceptibility to the disease is established, and the "acute" phase, in which lesions develop and, consequently, cardiac function is impaired. Different mechanisms may contribute to the two phases; different risk factors may be useful in predicting them. In the absence of lesions the latent disease phase is, at this time, a hypothetical entity; none-the-less, such a model may help to "explain" the proportion of subjects who have high values of risk factors, but no clinical evidence of CAD. If such a model fits the available data well, it may also help to define limits on our ability to predict the occurrence of the acute phase of the disease.

The presence or absence of the latent disease state may be adequately modelled by a logistic risk function. To incorporate the severity score into the statistical model, we need a distribution shape for the severity score, which can vary from subject to subject as does the risk. It will be almost necessary that the severity score be discrete or discretized, to avoid problems with a variable being considered to be continuous in some subjects and discrete (zero) in others.

For certain of the scores which have been computed in the UAFSAM data base, such as number of lesions or significant lesions or number of segments affected, the mathematical prerequisites for a Poisson distribution seem approximately satisfied. A "logistic risk function trigger/Poisson disease severity score" model is presented here.

Let T_i be 1 or 0, according to whether or not the "trigger has fired" for the i^{th} subject, and write the logistic risk part of the model as

$$P(T_i = 1) = \frac{e^{\beta'x_{i1}}}{1 + e^{\beta'x_{i1}}} \quad (10)$$

where $\beta'x_{i1} = \exp(\beta'x_{i1})$, x_{i1} being the vector of logistic predictor variables, with $x_{i1} \neq 1$.

Then, of course, $P(T_i = 0) = 1 - p_i$. Let Y_i be the observed severity score for the i^{th} subject. We have

$$P(Y_i = 0 | T_i = 0) = 1 \quad (21)$$

$$P(Y_i = y_i | T_i = 1) = e^{-\lambda_i} \lambda_i^{y_i} / y_i!, \quad y_i = 0, \dots,$$

where $\lambda_i = \exp(\gamma'x_i)$ is the positive mean of the Poisson distribution. Let $d_i = 0$ or 1 according as Y_i is 0 or positive. Since the T_i are not always observed, we write down the marginal distribution of Y_i :

$$P(Y_i = 0) = (a_i + e^{-\lambda_i}) / (1 + a_i) \quad (22)$$

$$P(Y_i = y_i) = e^{-\lambda_i} \lambda_i^{y_i} / ((1 + a_i) y_i!), \quad y_i = 1, \dots$$

The likelihood for the sample may be conveniently written as

$$L = \prod (1+a_i)^{-1} (a_i+e^{-\lambda_i})^{1-d_i} (e^{-\lambda_i} \lambda_i^{y_i}/y_i!)^{d_i}, \quad (23)$$

From which one can derive likelihood equations and compute maximum likelihood estimates by, e.g., the Newton-Raphson algorithm. Starting values for the logistic risk parameters are supplied by the linear discriminant function, using the d_i to designate groups; for the Poisson mean coefficients, values are guessed which give reasonable values for the Poisson means. In trials, the Newton-Raphson algorithm has seemed sensitive to gross inaccuracies in the starting values.

The model and fitting algorithm have only been tested briefly with two predictor variables so far, due to the short time available after completion of the data base. The variables used were age and the ratio of total cholesterol to HDL cholesterol, or a regression-based substitute when HDL was not available. Subjects without angiographic endpoints were given severity scores of zero, and the number of lesions observed was the severity score used. Although it is pre-

nature to give definite findings, it appears that age may be useful in predicting only the trigger, whereas the lipid ratio is useful in predicting both phases of the disease process. By "eyeball" the model seems to fit reasonably well; formal goodness-of-fit procedures have been developed and programmed, but not yet applied here.

As mentioned previously, the advantage inherent in this model is that it allows for a large 0 severity score category consistent with high values for risk factors for the trigger stage of the disease. If the model appears promising, one should attempt to measure the trigger phase through long-term follow-up. (Of 8 subjects who had angiograms repeated at SAH after a negative first test, 3 were positive; depending on feelings about the length of time appropriate between phases, this might be taken as evidence that the three flyers were probably already in the latent disease category the first time.)

III. RECOMMENDATIONS:

The summer's effort has identified several useful approaches to the CAD risk assessment problem. Of these, the appropriate data base which has been constructed will be useful in any future investigation; it requires some clean-up effort.

Initial investigations of the two-stage disease process modelling are promising; this should be continued on a serious scale, and other severity measures should be studied alongside.

Due to the nature of the data set, some provision will have to be made for missing value replacement for at least certain key variables such as HDL cholesterol. It would be interesting and useful to carry out the EM algorithm with the model described in section VI; this seems not to have appeared in the literature, and the problem is certainly not an isolated one.

Certain other questions have come up and been discussed briefly above; all deserve some attention, and it seems reasonable to give them that attention in the context of this investigation.

REFERENCES

1. Ellestad, Fox, Bruce, Dodge, Gensini, Humphries, Kannel, Levy, Mankin, McHenry, Sheffield, and Tavel, "Task Force I: Identification of Ischemic Heart Disease", The American Journal of Cardiology, Vol. 36, pp. 597-608, 1975.
2. J. Truett, J. Cornfield, and W. Kannel, "A Multivariate Analysis of the Risk of Coronary Heart Disease in Framingham", Journal of Chronic Disease, Vol. 20, pp. 511-524, 1967.
3. J. Cornfield, "Joint Dependence of Risk of Coronary Heart Disease on Serum Cholesterol and Systolic Blood Pressure: A Discriminant Function Analysis", Federation Proceedings, Vol. 41, pp. 58-61, 1962.
4. S. J. Rabkin, J. A. L. Mathewson, and R. B. Tate, "Predicting Risk of Ischemic Heart Disease from Systolic and Diastolic Blood Pressures", Annals of Internal Medicine, Vol. 88, pp. 342-345, 1978.
5. R. J. Brand, "An Examination of the Association between A-B Behavior and Coronary Heart Disease Incidence", NHLBI Forum on Coronary Prone Behavior, St. Petersburg, FL, June 1-3, 1977.
6. A. H. Rosencranz, R. J. Brand, R. I. Sholtz, and M. Friedman, "Multivariate Prediction of Coronary Heart Disease During 2.5 Year Follow-up in the Western Collaborative Group Study", The American Journal of Cardiology, Vol. 37, pp. 903-910, 1976.
7. D. R. Holmes, Jr., L. R. Elveback, R. L. Frye, B. A. Kottke, and R. D. Ellefson, "Association of Risk Factor Variables and Coronary Artery Disease Documented with Angiography", Circulation, Vol. 63, pp. 893-899, 1981.
8. M. P. Castelli, J. T. Doyle, T. Gordon, C. G. Hames, E. C. Hjortland, S. B. Hulley, A. Kaplan, and W. J. Zukel, "HDL Cholesterol and Other Lipids in Coronary Artery Disease", Circulation, Vol. 55, pp. 767-771, 1977.
9. H. Joy and D. W. Trump, "Significance of Minor ST Segment and T Wave Changes in the Resting Electrocardiogram of Hypertensive Subjects", British Heart Journal, Vol. 43, pp. 40-45, 1981.

10. K. Balnave, M. E. Scott, P. Morton, and J. G. Murtagh, "Reliable Prediction of Coronary Artery Disease Using Treadmill Exercise Testing", British Medical Journal, 1978.
11. L. D. Fisher, J. W. Kennedy, B. R. Chaitman, T. J. Ryan, C. McCabe, D. Swiner, F. Tristani, M. Schloss, and H. R. Garner, "Diagnostic Quantification of CASS (Coronary Artery Surgery Study) Clinical and Exercise Test Results in Determining Presence and Extent of Coronary Artery Disease", Circulation, Vol. 63, pp. 987-1000, 1981.
12. A. J. Anderson, J. J. Barborick, and A. A. Rimm, "Risk Factors and Angiographically Determined Coronary Occlusion", American Journal of Epidemiology, Vol. 107, pp. 8-14, 1978.
13. J. E. Dimsdale, A. H. Hutter, J. Gilbert, T. P. Hackett, P. C. Block, and D. E. Catanzano, "Predicting Results of Coronary Angiography", American Heart Journal, Vol. 98, pp. 881-886, 1979.
14. V. F. Froelicher, P. Yanowitz, A. J. Thompson, and M. C. Lancaster, Treadmill Exercise Testing at the USAF School of Aerospace Medicine: Physiological Responses in Airmen and the Detection of Latent Coronary Artery Disease, AGARDograph No. 210, Advisory Group for Aerospace Research and Development, North Atlantic Treaty Organization.
15. J. R. Hickman, unpublished communication, 1981.
16. V. F. Froelicher, Jr., M. H. Thomas, C. Pillow, and M. C. Lancaster, "Epidemiologic Study of Asymptomatic Men Screened by Maximal Treadmill Testing for Latent Coronary Artery Disease", The American Journal of Cardiology, Vol. 34, pp. 770-776, 1974.
17. J. R. Hickman, unpublished communication, 1981.
18. M. A. Woodbury, K. G. Manton, and E. Stallard, "Longitudinal Analysis of the Dynamics and Risk of Coronary Heart Disease in the Framingham Study", Biometrics, Vol. 35, pp. 575-585, 1979.
19. E. Cohn, B. Kamm, H. Feteih, N. Brand, and N. Goldschlager, "Use of Treadmill Score to Quantify Ischemic Response and Predict Extent of Coronary Disease", Circulation, Vol. 59, pp. 286-295, 1979.

20. G. A. Diamond, M. Hirsch, J. S. Forrester, H. M. Staniloff, R. Vas, S. W. Halpern, and H. J. C. Swan, "Application of Information Theory to Clinical Diagnostic Testing: The Electrocardiographic Stress Test", Circulation, Vol. 63, pp. 915-921, 1981.
21. G. S. Uhl, T. H. Kay, J. R. Hickman, Jr., E. A. Montgomery, and G. H. McGonahlan, "Detection of Coronary Artery Disease in Asymptomatic Aircrew Members with Thallium-201 Scintigraphy", Aviation, Space and Environmental Medicine, Vol. 51, pp. 1250-1255, 1980.
22. G. R. Osborne, The Incubation Period of Coronary Thrombosis, Butterworths, London, 1963.
23. J. E. Michalek and R. C. Tripathi, "The Effect of Errors in Diagnosis and Measurement on the Estimation of the Probability of an Event", Journal of the American Statistical Association, Vol. 75, pp. 713-721, 1980.
24. J. M. Inzer, J. Kishel, M. E. Kent, J. A. Ronan, Jr., A. M. Ross, and W. C. Roberts, "Accuracy of Angiographic Determination of Left Main Coronary Artery Narrowing", Circulation, Vol. 63, pp. 1056-1064, 1981.
25. J. A. McAlpine, Heart and Coronary Arteries, Springer-Verlag, Berlin, 1975.
26. K. L. Gould and K. Lipscomb, "Effects of Coronary Stenoses on Coronary Flow Reserve and Resistance", The American Journal of Cardiology, Vol. 34, pp. 48-66, 1974.
27. J. N. Schwartz, Y. Kong, G. B. Hackel, and A. G. Bartel, "Comparison of Angiographic and Postmortem Findings in Patients with Coronary Artery Disease", The American Journal of Cardiology, Vol. 40, pp. 174-178, 1975.
28. G. L. Hutchins, B. H. Bullock, R. L. Ridolphi, L. S. C. Griffiths, F. T. Lohr, and E. A. Picolic, "Correlation of Coronary Arteriograms and Left Ventriculograms with Postmortem Studies", Circulation, Vol. 56, pp. 31-37, 1977.
29. J. Vlodaver, R. Breck, R. A. Van Thiel, and J. E. Edwards, "Correlation of the Antemortem Coronary Arteriogram and the Postmortem Specimen", Circulation, Vol. 47, pp. 132-139, 1973.

30. M. Hills, "Discrimination and Allocation with Discrete Data", Applied Statistics, Vol. 16, pp. 237-250, 1967.
31. E. S. Gilbert, "On Discrimination Using Qualitative Variables", Journal of the American Statistical Association, Vol. 63, pp. 1399-1416, 1968.
32. D. R. Cox, "The Analysis of Multivariate Binary Data", Applied Statistics, Vol. 21, pp. 113-120, 1972.
33. D. C. Martin and R. A. Bradley, "Probability Models, Estimation, and Classification for Multivariate Dichotomous Populations", Biometrics, Vol. 28, pp. 203-221, 1972.
34. D. H. Moore, II, "Evaluation of Five Discrimination Procedures for Binary Variables", Journal of the American Statistical Association, Vol. 68, pp. 399-404, 1973.
35. J. Aitchison and C. G. G. Aitken, "Multivariate Binary Discrimination by the Kernel Method", Biometrika, Vol. 63, pp. 413-420, 1976.
36. I. Olkin and R. F. Tate, "Multivariate Correlation Models with Mixed Discrete and Continuous Variables", Annals of Mathematical Statistics, Vol. 32, pp. 448-465, 1961.
37. A. A. Afifi and R. M. Elashoff, "Multivariate Two Sample Tests with Dichotomous and Continuous Variables. I. The Location Model", Annals of Mathematical Statistics, Vol. 40, pp. 290-298, 1969.
38. P. C. Chang and A. A. Afifi, "Classification Based on Dichotomous and Continuous Variables", Journal of the American Statistical Association, Vol. 69, pp. 336-339, 1974.
39. W. J. Krzanowski, "Discrimination and Classification Using Both Binary and Continuous Variables", Journal of the American Statistical Association, Vol. 70, pp. 782-790, 1975.
40. G. G. Koch, P. B. Imbrey, and D. W. Reinfurt, "Linear Model Analysis of Categorical Data with Incomplete Response Vectors", Biometrics, Vol. 28, pp. 663-692, 1972.

41. M. Halperin, W. C. Blackwelder, and J. I. Verter, "Estimation of the Multivariate Logistic Risk Function: A Comparison of the Discriminant Function and Maximum Likelihood Approaches", Journal of Chronic Disease, Vol. 24, pp. 125-158, 1971.
42. D. J. Press and S. Wilson, "Choosing Between Logistic Regression and Discriminant Analysis", Journal of the American Statistical Association, Vol. 78, pp. 697-705, 1973.
43. K. G. Delmotte and J. S. Diebold, unpublished communication, 1981.
44. D. Efron, "The Efficiency of Logistic Regression Compared to Normal Discriminant Analysis", Journal of the American Statistical Association, Vol. 70, pp. 898-898, 1975.
45. R. H. Timm, "The Estimation of Variance, Covariance and Correlation Matrices from Incomplete Data", Psychometrika, Vol. 35, pp. 417-437, 1970.
46. J. W. Franc, "Some Simple Procedures for Handling Missing Data in Multivariate Analysis", Psychometrika, Vol. 41, pp. 409-415, 1976.
47. E. M. L. Beale and R. J. A. Little, "Missing Values in Multivariate Analysis", Journal of the Royal Statistical Society, Series B, Vol. 37, pp. 140-145, 1975.
48. R. I. Dempster, N. R. Laird, and D. B. Rubin, "Maximum Likelihood from Incomplete Data via the EM Algorithm", Journal of the Royal Statistical Society, Series B, Vol. 39, pp. 1-38, 1977. (Discussion, pp. 32-38.)

APPENDIX A

```

*****
*
*      DATE:      8/20/81
*
*      TIME:      11:50
*
*      FINAL SUMMER VERSION
*
*****

```

File description for SAM CARDIAC REFERRAL FILE prepared for
Dr. Charles B. Davis.

DSN = HH.H3H01.B05G054.DAVES.D810812
Number of fields =
Record format = FIXED BLOCK
Record size =
Block size =

Field	Location	Format	Mnemonic	Content	Source
=====	=====	=====	=====	=====	=====
1	1-9	I9	SSAN	Social security number	Cover
2	10-36	6A4,A3	NAME	Name	Cover
3	37-42	A1,I5	CASENR	Case nr. from SAM referral visit	Cover
4	43-48	3I2	DOE	Date of SAM referral visit,yyymmdd	Cover
5	49-54	3I2	DOB	Date of birth,yyymmdd	Cover
6	55-58	I4	CATHSEQ	Catheterization sequence number	Cath
7	59-61	I3	CATHWT	Weight at catheterization	Cath
8	62-63	I2	CATHHT	Height at catheterization	Cath
9	64	A1	FAMILYH	Family history of CVD? (N/Y)	Cath
10	65	A1	HIGHBP	Diagnosed high blood press? (N/Y)	Cath
11	66	A1	EXERCISE	Exercised regularly in the past but no longer? (N/Y)	Cath
12	67	A1	FAT	Regularly eat meat with visible fat or skin? (N/Y)	Cath
13	68-69	I2	REGG	Number of eggs eaten per week	Cath
14	70	A1	CHEESE	Does the subject regularly eat cheese or butter? (N/Y)	Cath
15	71-73	3I1	REFERRAL	Reasons for SAM referral	Cath
16	74-83	5I2	CLINICAL	Clinical reasons for cath	Cath
17	84-97	7I2	ECGRSN	Electrocardiographic reasons for catheterization	Cath
18	98-100	I3	AORTIC+S	Systolic aortic pressure	Cath
19	101-103	I3	AORTIC+D	Diastolic aortic pressure	Cath
20	104-106	I3	AORTIC+M	Mean aortic pressure	Cath
21	107	A1	CACOMP	Coronary angiography done? (N/Y)	Cath
22	108	A1	CORUANG	Angiography (Normal,Abnormal)	Cath
23	109-110	I2	SUMSONE	Sum of 'Sones lesion grades'	Cath
24	111	I1	MAXSONE	Maximum of 'Sones lesion grades'	Cath
25	112-113	I2	VESSEL	Vessel disease score (Thompson?)	Cath
26	114-119	3I2	LABDOE	Date of laboratory examination	Lab
27	120-123	I4	CHOL	Cholesterol (see CHOL+ADJ below)	Lab
28	124	A1	flag1		
29	125	A1	flag2		
30	126-129	I4	TRIGL	Serum triglyceride	Lab
31	130	A1	flag1		
32	131	A1	flag2		
33	132-135	I4	PHOS	Serum phosphorus	Lab
34	136	A1	flag1		
35	137	A1	flag2		

37	141	A1	flag1		
38	142	A1	flag2		
39	143-145	I3	TWOBS	Two hour blood sugar	Lab
40	146	A1	flag1		
41	147	A1	flag2		
42	148-150	I3	URIC	Uric acid	Lab
43	151	A1	flag1		
44	152	A1	flag2		
45	153-158	I6	WBC	white blood count	Lab
46	159	A1	flag1		
47	160	A1	flag2		
48	161-163	I3	FCORT	Fasting cortisol	Lab
49	164	A1	flag1		
50	165-167	I3	.5CORT	Half hour cortisol	Lab
51	168	A1	flag1		
52	169-171	I3	ONECORT	One hour cortisol	Lab
53	172	A1	flag1		
54	173-175	I3	1.5CORT	1.5 hour cortisol	Lab
55	176	A1	flag1		
56	177-179	I3	2CORT	Two hour cortisol	Lab
57	180	A1	flag1		
58	181-183	I3	3CORT	Three hour cortisol	Lab
59	184	A1	flag1		
60	185-187	I3	4CORT	Four hour cortisol	Lab
61	188	A1	flag1		
62	189-191	I3	5CORT	Five hour cortisol	Lab
63	192	A1	flag1		
64	193	A1	flag2		
65	194-199	3I2	TDMDOE	Date of treadmill exam, yymmdd	Tdmill
66	200-203	2I2	T+TIME	Total treadmill time, m:ss	Tdmill
67	204	A1	flag2		
68	205-207	F3.2	MAX+O2	Maximum oxygen consumption, liters	Tdmill
69	208	A1	flag2		
70	209-217	3I3	SUPINE	Supine Sbp, DBP, heart rate	Tdmill
71	218	A1	flag2		
72	219-227	3I3	WALK+INI	walking initial SBP, DBP, HR	Tdmill
73	228	A1	flag2		
74	229-237	3I3	WALK+LST	Last walking SBP, DBP, HR	Tdmill
75	238	A1	flag2		
76	239-241	3I1	TERMIN	Reasons for terminating treadmill	Tdmill
77	242	A1	flag2		
78	243	A1	HYPERS	History of hypertension? (N/Y)	Tdmill
79	244	A1	flag2		
80	245	A1	ANTIHYPER	Using hypertensives? (N/Y)	Tdmill
81	246	A1	flag2		
82	247-252	3I2	ECG+DOE	Date of ECG exam	Ecg
83	253-254	I2	ECGHT	Height at ECG	Ecg
84	255	A1	flag2		
85	256-258	I3	ECGWT	Weight at ECG	Ecg
86	259	A1	flag2		
87	260-280	7I3	DX+CODES	ECG diagnostic codes	Ecg
88	281	A1	flag2		
89	282-287	3I2	PULDOE	Date of pulmonary exam	Pulm
90	288-290	I3	PULHT	Height at pulmonary exam, cm	Pulm
91	291	A1	flag2		
92	292-296	F5.1	PULWT	Weight at pulmonary exam, kg	Pulm
93	297	A1	flag2		
94	298-300	I3	RL+VCPVC	FVC / predicted FVC * 100%	Pulm
95	301	A1	flag2		
96	302-304	I3	B+FEF7PP	MMEF / predicted MMEF * 100%	Pulm
97	305	A1	flag2		
98	306-308	I3	B+FEV1PV	FEV1 / FVC * 100%	Pulm

99	309	A1	flag2		
100	310-312	I3	H+FEV3PV	FEV3 / FVC * 100%	Pulm
101	313	A1	flag2		
102	314-316	I3	DELTA	Nitrogen washout, %	Pulm
103	317	A1	flag2		
104	318	I1	SMOKE+1	Has subject smoked cigarettes for at least one year? 1 = N, 2 = Y	Pulm
105	319	A1	flag2		
106	320	I1	SNOKE+N	Does subject smoke now? 1=N,2=Y	Pulm
107	321	A1	flag2		
108	322-323	I2	YR+STUP	For how many years stopped?	Pulm
109	324	A1	flag2		
110	325-327	F3.1	PACK+DAY	Average number of packs of cigarettes per day (?)	Pulm
111	328	A1	flag2		
112	329	A1	ASTHMA	Ever had asthma? 1 = N, 2 = Y	Pulm
113	330	A1	flag2		
114	331	A1	COUGH	Chronic cough ever? 1 = N, 2 = Y	Pulm
115	332	A1	flag2		
116	333	A1	COLD	Cold recently or now? 1=N,2=Y	Pulm
117	334	A1	flag2		
118	335-340	I12	MEDDOE	Med. date of exam	Coron.
119	341-347	F7.3	MEDWT	Weight Med.use file (. in file)	Coron.
120	348	A1	flag2		
121	349-352	F4.1	PBFAT	% body fat (. in file)	Coron.
122	353	A1	flag2		
123	354-359	A1, I5	LABCASE	Laboratory case number	Lab
124	360-365	A1, I5	TUMCASE	Treadmill case number	Tdmill
125	366-371	A1, I5	ECGCASE	Initial referral case number	Cover
126	372-377	A1, I5	PULCASE	Pulmonary case number	Pulm
127	378-382	F5.1	JASTOT	Total Jenkins Activity Score	Coron.
128	383	A1	flag2		
129	384-388	F5.1	JAS+S	Jenkins Activity Score - S factor	Coron.
130	389	A1	flag2		
131	390-394	F5.1	JAS+J	Jenkins Activity Score - J factor	Coron.
132	395	A1	flag2		
133	396-400	F5.1	JAS+H	Jenkins Activity Score - H factor	Coron.
134	401	A1	flag2		
135	402-403	I2	JASAGE	Age at JAS	Coron.
136	404	A1	flag2		
137	405-410	A1, I5	JASCASE	JAS case number	Coron.
138	411-415	I5	CASERTE	Rating case number	Coron.
139	416-417	A2	THOMAS	Thomas rating	Coron.
140	418	A1	flag2		
141	419-420	A2	ROSEN	Rosenman rating	Coron.
142	421	A1	flag2		
143	422-424	A3	INTERP	Treadmill interpretation	Tdmill
144	425	A1	flag2		
145	426-427	I2	YR+SNOKE	Years smoked	Pulm
146	428-429	I1, A1	flag2		
147	430-435	A1, I5	MEDCASE		Coron.
148	436-438	I3	H+SCORE	Hickman score (?)	Coron.
149	439-441	I3	HDLCHOL	HDL cholesterol	Lab
150	442	A1	flag1		
151	443	A1	flag2		
152	444-449	I12	RATE+DT	Date of rating	Coron.
153	450-455	I13	TDM+ECG	Resting ECG	Tdmill
154	456	A1	flag2		
155	457-459	I3	SQ+SONE	Sum of squared 'Sones grades'	Cath
156	460-463	I4	ADJ+CHOL	Chol. adjusted for meas. technique	Lab*
157	464	A1	flag1		
158	465	A1	flag2		
	466-468	I3			

159	469-498	3A10	REFCODE	Referral diagnostic codes	Cover
160	499	I1	ACT+STAT	Activity status	Tdm11
161	500	A1	flag2		
162	501-505	F5.4	PH+REST	Resting blood pH	Pulm
163	506-510	F5.4	PH+POST	Post-exercise blood pH	Pulm
164	511-516	A1,I5	CATHCASE	Catheterization case number	Cath
165	517-522	3I2	CATHDOE	Date of catheterization	Cath
166	523-572	10A5	LESGRADE	Lesion locations and grades	Hickman
167	573-574	I2	NRLES	Number of lesions observed	Davis
168	575-577	I3	LESVOL	Index of lesion volume	Davis
169	578	I1	NVES	Number of vessels with sig. lesion	Davis
170	579	I1	NVSTRING	Stringent version of NVES	Davis
171	580	I1	NVCASS	CASS version of NVES	Davis
172	581-582	I2	SSH	Sum of Hickman lesion grades	Davis
173	583-584	I2	SSS	Sum of 'Sones' lesion grades	Davis
174	585-586	I2	SSHw	Weighted, adjusted version of SSH	Davis
175	587-588	I2	SSSw	Weighted, adjusted version of SSS	Davis
176	589	I1	NSEG30	Number segments with 30% lesions	Davis
177	590	I1	NSEG50	Number segments with 50% lesions	Davis
178	591	I1	HR1	High risk flag 1	Davis
179	592	I1	HR2	High risk flag 2	Davis
180	593	I1	HR3	High risk flag 3	Davis
181	594-596	I3	VESRES	Maximum vessel resistance index	Davis

Notes:

SSAN, NAME WILL BE DELETED IN COPY OF FILE SUPPLIED TO C.R.D.

The file is sorted by CASENR, including the initial letter of the case number. This sorting is (nearly) chronological within initial letters of the case number.

* in source column means 'derived from'

flag1 is coded as follows

- 1 = abnormal value
- 2 = lab error
- 3 = subject improperly prepped
- 8 = computer detected error
- 9 = comment in association with that field

Codes 1 and 8 are determined as follows:

for each measurement threshold values a,b,c,d are determined, such that for $b < x < c$ the value is considered normal, for $a < x < b$ or $c < x < d$ it is considered abnormal, and for x outside of (a,d) the value is assumed to be in error. For lab data values are given:

Measurement	a	b	c	d
CHOL	50	100	250	1000
TRIGL	20	20	150	3000
PHOS	50	100	300	1000
FBS	30	40	120	600
TWOBS	30	60	220	600
URIC	3	4	8	14
WBC	2000	2900	10000	18000
CORT (all)	0	5	22	99.9
HDLCHOL	++	++	++	++

flag2 - * indicates that the data was collected at a visit previous to the SAM visit; for ECG it indicates that the reading was taken more than 6 months prior to the SAM visit.

Comments on the data base:

Persons are selected from the cover sheet file because of having a referral diagnostic code among those selected as being appropriate to referrals for cardiac problems and/or symptoms, with the provision that the DOE was no earlier than 710201.

W9xxxx case numbers are assigned in the field; these numbers are stored in the variable inappropriately called ECGCASE. Where these persons later visited SAM, the DOE and REFCODE are those of the visit. If they did not visit SAM, the DOE and REFCODE are those from the W9xxxx cover sheet.

ECG DXCODES are from the ECG repository file, not from data collected during the subject's visit to SAM.

CATH file data is included from the first catheterization visit following the referral visit, regardless of intervening time span. Results of subsequent catheterizations, if any, will be included 'by hand'.

Note that PH+REST and PH+POST are available on only 5 and 1 subjects respectively.

A description of the various angiography scores suggested by Hickman and Davis.

- 1. NRLES Number of lesions observed.
- 2. LESVOL An index of the volume of lesion present (Davis).

This is computed as the sum over all lesions present of the quantity

$$\frac{3}{w} * (1 - (1 - D)^C)^{1.5}$$

where w is an average relative diameter for the segment involved (6 for A,B, 5 for N,U, 4 for C,P, 3 for I,S, 2 for K,R1, and 1 for others), D is the observed greatest diameter reduction of the artery, and C = 1.46 has been found to relate diameter to area reasonably well for a variety of common lumen shapes.

- 3. NVES Number of vessels with significant disease.
- 4. NVSTRING Stringent version of NVES.
- 5. NVCASS Less stringent version of NVES, used by CASS.

These scores count a vessel if its greatest lesion is at least as large as the criterion given:

Vessel	Segments	(NVES)	(NVSTRING)	(NVCASS)
LMCA	A,B	30%	30%	50%
LAD	C,F,G,H	50%	30%	70%
LCA	I,K,L	50%	30%	70%
RCA	N,O,P,S,T	50%	30%	70%

- 6. SSH Hickman's sum of segment scores.
- 7. SSS Sum of segment scores (attributed to Sones).
- 8. SSHw weighted and adjusted version of SSH.

9. SSSW Weighted and adjusted version of SSS.

The above scores use the following coding schemes:

%reduction	(0,0)	(0,10)	(10,50)	(50,75)	(75,90)	(90,100)	(100,100)
SSH	0	1	2	3	4	5	6
SSHw							
seg B	0	1	4	6	8	10	12
seg C,I	0	1	2	3	8	10	12
other	0	1	2	3	4	5	6

then add 3 points if all of C,I,O have at least 75% lesions

%reduction	(0,0)	(0,30)	(30,50)	(50,90)	(90,100)	(100,100)
------------	-------	--------	---------	---------	----------	-----------

SSS	0	1	2	3	4	5
SSSw						
seg B	0	1	4	6	8	10
seg C,I	0	1	2	6	8	10
other	0	1	2	3	4	5

then add 3 points if all of C,I,O have at least 50% lesions

10. NSEG30 Number of segments with at least 30% lesions.

11. NSEG50 Number of segments with at least 50% lesions.

12. HR1 High risk flag 1.

1 if A or B has at least 50% lesion, otherwise 0.

13. HR2 High risk flag 2.

1 if C has at least 90% lesion, otherwise 0.

14. HR3 High risk flag 3.

1 if at least 3 of 4 vessels have at least 75% lesions,
0 otherwise.

15. VESRES Vessel resistance index (Davis).

This is a measure of the resistance to blood flow due to the stenoses in the major coronary vessels. It is computed as the maximum over the four vessels of

$$\text{RESISTANCE} = 3.57 + 712. * \exp(-1.69 * \text{CFR}) ,$$

where CFR (coronary flow reserve) is given by

$$\text{CFR} = 4.1 + 0.06 * D - 0.14 * D^2 - 3.5 * D^3 ,$$

D being the proportional greatest diameter reduction due to the stenosis.

A resistance of approximately 135 indicates a hyperemic response of approximately 1; this will be the situation if the flow cannot increase in response to stress. The approximation used will produce a resistance of 299 for a single 100% stenosis; values above that must refer to multiple stenoses. For small and moderate values of resistance, resistance is additive for multiple stenoses.

1981 USAF - SCEEE SUMMER FACULTY RESEARCH PROJECT

Sponsored by the

AIR FORCE OFFICE OF SCIENTIFIC RESEARCH

Conducted by the

SOUTHEASTERN CENTER FOR ELECTRICAL ENGINEERING EDUCATION

FINAL REPORT

A MOLECULAR ORBITAL STUDY OF $\text{NO}_3^- \cdot \text{H}_2\text{O}$, $\text{OH}^- \cdot \text{HNO}_3$, AND

$\text{H}^+(\text{H}_2\text{O})_m(\text{CH}_3\text{CN})_k$ CLUSTER IONS

Prepared by: Dr. Carol A. Deakyne
Academic Rank: Assistant Professor
Department and University: Department of Chemistry
College of the Holy Cross
Research Location: Air Force Geophysics Laboratory, Aeronomy Division,
Atmospheric Structure Branch
USAF Research Colleague: Dr. John F. Paulson
Date: September 14, 1981
Contract No: F49620-79-C-0038

A MOLECULAR ORBITAL STUDY OF $\text{NO}_3^- \cdot \text{H}_2\text{O}$,
 $\text{OH}^- \cdot \text{HNO}_3$, AND $\text{H}^+(\text{H}_2\text{O})_m(\text{CH}_3\text{CN})_k$ CLUSTER IONS

by

Carol A. Deakyne

ABSTRACT

The structure and energetics of $\text{NO}_3^- \cdot \text{H}_2\text{O}$, $\text{OH}^- \cdot \text{HNO}_3$, $\text{H}^+(\text{CH}_3\text{CN})$, $\text{H}^+(\text{H}_2\text{O})(\text{CH}_3\text{CN})$, and $\text{H}^+(\text{CH}_3\text{CN})_2$ have been investigated ab initio at the STO-3G and 4-31G basis set levels. Fully optimized geometries have been obtained for the cations and for several conformations of $\text{OH}^- \cdot \text{HNO}_3$. Partial geometry optimization is shown to be sufficient for $\text{H}^+(\text{H}_2\text{O})(\text{CH}_3\text{CN})$. The hydrogen bond in $\text{H}^+(\text{H}_2\text{O})(\text{CH}_3\text{CN})$ is asymmetric and much of the positive charge is localized on the proton; the hydrogen bond in $\text{H}^+(\text{CH}_3\text{CN})_2$ is symmetric and the positive charge is more delocalized. The data on $\text{H}^+(\text{H}_2\text{O})(\text{CH}_3\text{CN})$ are consistent with a hydrogen bond which is stabilized primarily by an electrostatic interaction. The results for $\text{H}^+(\text{CH}_3\text{CN})_2$ are evidence for predominantly covalent binding in the H-bond in that ion. Calculated proton affinities and bond dissociation energies are in reasonable agreement with experiment, particularly when they are calculated via isodesmic reactions. Suggestions are made for follow-on research in these areas.

ACKNOWLEDGEMENT

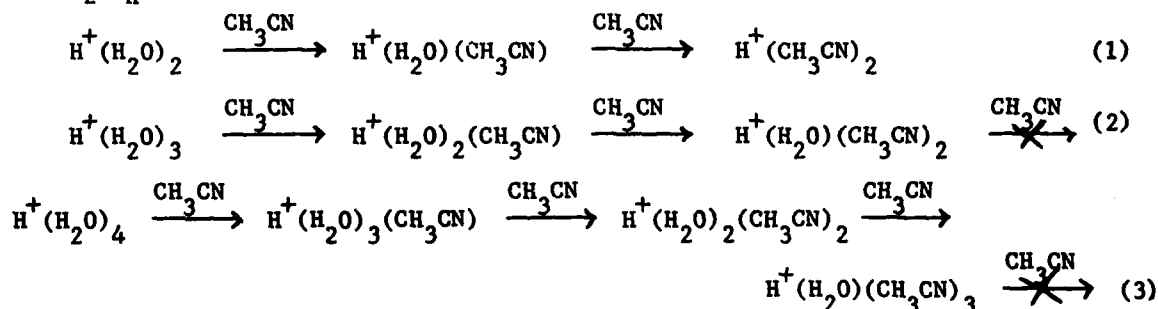
The author would like to thank the Air Force Systems Command, the Air Force Office of Scientific Research, the Southeastern Center for Electrical Engineering Education and the Atmospheric Structure Branch of the Air Force Geophysics Laboratory at Hanscom AFB, MA for enabling her to enjoy a very interesting and productive summer. In particular, the author would like to express her gratitude to Dr. John F. Paulson for suggesting this research project and for his friendly collaboration and helpful comments. She would also like to thank Dr. Steven L. Guberman for many valuable discussions and all the people working at the Atmospheric Structure Branch for their hospitality.

I. INTRODUCTION:

In recent years balloon-borne mass spectrometers have been utilized to determine the ionic composition of the earth's stratosphere.¹⁻⁷ These studies indicate that both the positive and negative ions are clustered species. Two types of positive ions found in the stratosphere are proton hydrates, $H^+(H_2O)_n$, and $H^+(H_2O)_m X_k$ cations, where X has a mass of 41 ± 1 amu and must have a proton affinity greater than 175 kcal/mole and an abundance greater than $7 \times 10^4 \text{ cm}^{-3}$ in order to enter into the ion chemistry.¹⁻⁴ The negative ion content of the stratosphere is dominated by large cluster species of the type $NO_3^-(HNO_3)_n$, $HSO_4^-(H_2SO_4)_n$, $HSO_4^-(HNO_3)_n$, and $HSO_4^-(H_2SO_4)_n(HNO_3)_m$.⁵⁻⁷

The identity of X in the positive cluster ions is still uncertain. Two proposed candidates are $MgOH$ ⁸ and CH_3CN , acetonitrile.² Smith et al⁹ have carried out studies using a selected ion flow tube (SIFT) apparatus which indicate that CH_3CN is indeed a viable candidate for X. In comparison, data on the height variations of the abundance ratios for the $H^+(H_2O)_m X_k$ and $H^+(H_2O)_n$ cations argue against X being $MgOH$.¹⁰

The SIFT experiments⁹ have shown that CH_3CN rapidly replaces H_2O in the cluster ions $H^+(H_2O)_n$ according to the following reactions.

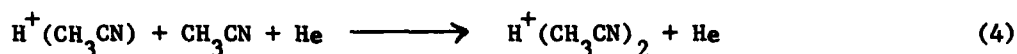


An interesting result is that in reaction sequences (2) and (3) the last H_2O molecule is not replaced.

These experiments demonstrate that the presence of CH_3CN in the stratosphere would lead to the rapid formation of $H^+(H_2O)_m(CH_3CN)_k$ ions and provide support for the hypothesis that X is CH_3CN . Further support for this hypothesis is that ions with masses equivalent to those of various $H^+(H_2O)_m(CH_3CN)_k$ ions are observed in the stratosphere.^{2,3,10} Of course, these results do not prove that CH_3CN is X but they do strongly suggest that it is a likely candidate. Additional evidence would be provided by finding an adequate source of CH_3CN in the stratosphere. Although the kinetic data indicate that the required concentration of CH_3CN is relatively

small ($\leq 10^7$ molecules cm^{-3} at ~ 35 km) no sources of CH_3CN have been identified as yet. Feasible possibilities are reactions of N^+ and N_3^+ with hydrocarbons such as CH_4 and neutral-neutral reactions between nitrogen atoms and carbon-containing molecules.⁹ In addition, CH_3CN may be transported into the stratosphere from below.¹⁰

Smith et al.⁹ also looked at the following reaction:



They found that this reaction proceeds very rapidly but subsequent CH_3CN substitution of $\text{H}^+(\text{CH}_3\text{CN})_2$ proceeds only very slowly. These observations are consistent with the thermodynamic data obtained by Meot-Ner¹¹ which show that bonding of the second CH_3CN to $\text{H}^+(\text{CH}_3\text{CN})$ is relatively weak. Smith et al.⁹ interpret these results as an indication that the $\text{H}^+(\text{CH}_3\text{CN})_2 - \text{H}_2\text{O}$ and $\text{H}^+(\text{CH}_3\text{CN})_3 - \text{H}_2\text{O}$ bonding is significantly stronger than the $\text{H}^+(\text{CH}_3\text{CN})_2 - \text{CH}_3\text{CN}$ and $\text{H}^+(\text{CH}_3\text{CN})_3 - \text{CH}_3\text{CN}$ bonding, respectively. However, they recognize that the relative stabilities of these ions may be critically affected by structural differences.

Cluster ions of NO_3^- are important in the chemistry of the ionosphere as well as that of the stratosphere.^{5-7,12,13} Consequently, cluster ions of NO_3^- with H_2O have been under extensive investigation recently.¹⁴⁻¹⁷ Wu and Tiernan¹⁴ have measured the bond dissociation energies of $\text{NO}_3^- \cdot \text{H}_2\text{O}$ and $\text{OH}^- \cdot \text{HNO}_3$ ions. The cluster ions were generated from reaction mixtures containing various combinations of NO , NO_2 , H_2O , O_2 and O_3 . They find that only one ion with the general formula $\text{OH}^- \cdot \text{HNO}_3$ (bond dissociation energy approximately 75 kcal/mole) is obtained. However, two ions with the general formula $\text{NO}_3^- \cdot \text{H}_2\text{O}$ (bond dissociation energies approximately 10 and 34 kcal/mole) may be formed depending upon the combination of reactants used to generate the cluster ions, i.e. whether or not the reaction mixture contained O_3 .

The results on $\text{OH}^- \cdot \text{HNO}_3$ agree with those obtained by Paulson¹⁵ and Yamdagni and Kebarle.^{16a} In contrast, Payzant et al.^{16b} observe only one $\text{NO}_3^- \cdot \text{H}_2\text{O}$ ion (bond association energy approximately 12 kcal/mole). However, since their experimental procedure generated $\text{NO}_3^- \cdot \text{H}_2\text{O}$ from $\text{C}_2\text{H}_5\text{ONO}_2$, there was no O_3 in the reaction mixture.

The present project is concerned with using ab initio molecular orbital theory to determine: 1) the optimum structures and the solvation enthalpies of the $\text{H}^+(\text{H}_2\text{O})_m (\text{CH}_3\text{CN})_k$ cations observed by Smith et al.⁹, 2) the optimum structure of the $\text{OH}^- \cdot \text{HNO}_3$ ion, and 3) whether there is a second bound structure for $\text{NO}_3^- \cdot \text{H}_2\text{O}$ as reported by Wu and Tiernan.¹⁴ (The structure of one of the $\text{NO}_3^- \cdot \text{H}_2\text{O}$ clusters has already been studied by ab initio techniques.¹⁸) Molecular orbital calculations have been carried out on a number of cluster ion systems recently.¹⁷⁻²³ At the CNDO/2 level,²⁴ studies

include those on the $\text{NO}_3^-(\text{H}_2\text{O})_n$,¹⁷ $\text{NO}_2^-(\text{H}_2\text{O})_n$,¹⁷ $\text{HCO}_3^-(\text{H}_2\text{O})_n$,¹⁹ $\text{H}^+(\text{H}_2\text{O})_n$,²² and $\text{OH}^-(\text{H}_2\text{O})_n$ ions.²² At the *ab initio* level, $\text{H}^+(\text{H}_2\text{O})_n$,^{20,21} $\text{OH}^-(\text{H}_2\text{O})_n$ ²⁰ and $\text{H}^+(\text{CO})_n$ ²³ ions among others have been investigated. These calculations have been found to be of considerable value in interpreting and correlating experimental results and in yielding insight into the bonding, stability and charge distributions of clusters.

Information on the structures of these complexes is of interest for several reasons. First, it will lead to a more complete understanding of the forces between ions and neutral molecules, in particular the role of hydrogen bonding, which is believed to be significant,^{11,17,23} in the solvation of positive and negative ions. Second, it will provide data on the number of solvent molecules which can be accommodated by an ion and on its inner and outer solvation shells. This information is useful since the kinetic properties, mobilities, and products of the ionic recombination reactions of these clusters are believed to be dependent on their sizes.²⁵ Thermodynamic data on clustering reactions is needed in the theoretical development of aerosol formation¹⁷ and of the chemical mechanisms involving negative ions which cause radio and radar blackout, i.e., photodetachment and photodissociation.²⁵ The calculated charge distributions will indicate whether the positive or negative charge is relatively evenly distributed or whether it is localized as assumed in some electrostatic models used to compute bond energies.

II. OBJECTIVES

Our specific objectives were to use *ab initio* molecular orbital (MO) theory to determine the following:

- (1) the optimum structure of both $\text{OH}^- \cdot \text{HNO}_3$ and the postulated $\text{NO}_3^- \cdot \text{H}_2\text{O}$ ion obtained from O_3 ;
- (2) the optimum structures and the calculated solvation enthalpies of the following acetonitrile containing cations: $\text{H}^+(\text{CH}_3\text{CN})_2$, $\text{H}^+(\text{H}_2\text{O})(\text{CH}_3\text{CN})$, $\text{H}^+(\text{CH}_3\text{CN})_3$, $\text{H}^+(\text{CH}_3\text{CN})_2(\text{H}_2\text{O})$, $\text{H}^+(\text{CH}_3\text{CN})(\text{H}_2\text{O})_2$, $\text{H}^+(\text{CH}_3\text{CN})_4$, $\text{H}^+(\text{CH}_3\text{CN})_3(\text{H}_2\text{O})$, $\text{H}^+(\text{CH}_3\text{CN})_2(\text{H}_2\text{O})_2$, and $\text{H}^+(\text{CH}_3\text{CN})(\text{H}_2\text{O})_3$;

(3) the most economical basis set which yields accurate results.

The results obtained will be analyzed to ascertain and elucidate:

- (1) the relative stability of straight-chain, branched, and cyclic structures;
- (2) why the last H_2O molecule in the $\text{H}^+(\text{H}_2\text{O})(\text{CH}_3\text{CN})_n$, $n = 3, 4$, cations is not readily replaced;
- (3) the role of hydrogen bonding in the ion-molecule interactions and the optimum type of hydrogen bond, i.e., linear or bent and symmetric or asymmetric;
- (4) the amount of charge transfer through the hydrogen bonds and the nature of the cooperative interaction between them in the positive cluster ions;
- (5) the number of solvent molecules which can be accommodated in the inner and outer shells of the cations;
- (6) the structural reorganization around the excess proton produced by the addition of solvent molecules and the relationships between structure, charge transfer, and energetics.

III. COMPUTATIONAL DETAILS

The calculations were carried out ab initio using the Gaussian 70 computer program on a DEC VAX 11/780 computer. The closed shell ground state wavefunctions for the species investigated are described by single Slater determinants composed of doubly occupied molecular orbitals. The molecular orbitals are expressed as linear combinations of atomic basis functions. Newton and Ehrenson²⁰ have shown that although reasonable structural data can be obtained for $\text{H}^+(\text{H}_2\text{O})_n$ and $\text{OH}^-(\text{H}_2\text{O})_n$ with the minimal STO-3G s,p basis set,²⁶ the split valence 4-31G s,p basis set²⁷ is required to obtain both reasonable structures and energetics for these ions. Consequently, the 4-31G basis set was utilized in the study of $\text{OH}^- \cdot \text{HNO}_3$ and $\text{NO}_3^- \cdot \text{H}_2\text{O}$. However, the large size of some of the cations led to an attempt to use the STO-3G basis set to compute their optimum structures. This attempt was abandoned for all of the cations other than the $\text{H}^+(\text{CH}_3\text{CN})_n$ ions, $n = 2-4$, since the STO-3G basis set level inverts the relative proton affinities of CH_3CN and H_2O .²⁸ The results for $\text{H}^+(\text{CH}_3\text{CN})_2$ indicate that for both the STO-3G and 4-31G basis sets the proton is centrally located between the two CH_3CN groups. Thus, the STO-3G basis set will be utilized, at least initially, for the $\text{H}^+(\text{CH}_3\text{CN})_n$ cations.

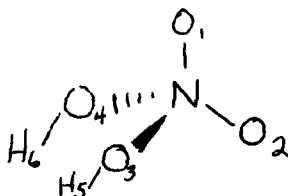
Accurate geometrical structures were obtained via a global optimization (to 0.001 Å and 0.1°) performed by the force relaxation method of Pulay²⁹ using an algorithm developed by Schlegel.³⁰ Initially, a partial and then a complete geometry optimization was carried out for each type of ion to ascertain which coordinates must be optimized for accurate results. The structural parameters used to initiate the optimization procedure for the hydrogen bonded complexes were derived from the optimum geometries of the monomer units. Accurate estimates of the optimum geometries of OH⁻ · HNO₃ and NO₃⁻ · H₂O were required or convergence problems were encountered.

There are some systematic errors, compared to the experimental values, in the geometrical parameters and some other molecular properties computed via the 4-31G and STO-3G basis sets.^{20,31,32} The STO-3G basis often yields bond lengths which are too long and bond angles which are too small.³¹ The 4-31G basis often underestimates bond lengths and overestimates bond angles, particularly those angles involving atoms with lone pair electrons.³¹ In addition, the 4-31G calculated dipole moments are generally too large²⁰ while the STO-3G values are too small.³² Both basis sets often give solvation enthalpies which are too large since no corrections are made for inaccuracies resulting from neglecting changes in zero point energies, electron correlation, and a temperature term. (The calculated enthalpies are for molecules at T = 0 K.) Nevertheless, relative values of these properties along a series of molecules are well reproduced which warrants their use, especially for qualitative comparisons in related systems. Including polarization functions in the basis set and carrying out a configuration interaction and a molecular dynamics study of these species would improve the results.^{17,31} However, this was not feasible for the present study since the required programs were not yet available.

Another procedure for determining more accurate solvation enthalpies, which was employed where possible in this study, is to evaluate them via an isodesmic reaction, i.e., a reaction where the number of bonds of a given type are retained.³³ This method of determining solvation enthalpies is more reliable since it reduces inaccuracies resulting from using single determinant wavefunctions, thereby neglecting electron correlation. Furthermore, zero-point energies are minimized, in general, when balanced chemical reactions are being analyzed.³⁴

IV. RESULTS AND ANALYSIS OF RESULTS

$\text{OH}^- \cdot \text{HNO}_3$ The large magnitude of the experimental bond dissociation energy of $\text{OH}^- \cdot \text{HNO}_3$ ^{14,15,16a} suggests that the OH^- is not hydrogen bonded to the HNO_3 but is covalently bonded to the nitrogen. Thus, the first type of structure examined was the one given below.



Several of the possible conformations of the above species have been investigated; the others remain to be examined. A complete geometry optimization was carried out for each conformer considered, with the exception of the OH bond lengths in conformer III. (Studies reveal that the effect on the total energy of the system of optimizing the OH bond lengths is negligible compared to the effect of the other parameters.) The optimized geometries of those conformers which are local minima on the ground-state singlet surface of this ion are given in Table I. The parameters indicate that all three conformers of $\text{OH}^- \cdot \text{HNO}_3$ have a distorted tetrahedral geometry. The fully optimized geometry of HNO_3 is included in Table I as well. Latajka et al.³⁵ have also carried out a geometry optimization of HNO_3 using the 4-31G basis set. Their values are shown in parentheses. The two sets of parameters differ since Latajka et al.³⁵ constrained the NO_1 and NO_2 bond lengths to be identical.

Table I. Optimized Geometrical Parameters (in Å and degrees)

	$\text{OH}^- \cdot \text{HNO}_3, \text{I}$	$\text{OH}^- \cdot \text{HNO}_3, \text{II}$	$\text{OH}^- \cdot \text{HNO}_3, \text{III}$	HNO_3
$\text{N}-\text{O}_1$	1.343	1.375	1.342	1.219 (1.202) ^c
$\text{N}-\text{O}_2$	1.343	1.314	1.336	1.194 (1.202)
$\text{N}-\text{O}_3$	1.457	1.459	1.455	1.373 (1.421)
$\text{N}-\text{O}_4$	1.457	1.459	1.455	
O_3-H_5	0.957	0.957	0.957	0.961 (0.960)
O_4-H_6	0.957	0.957	0.957	
$\angle \text{O}_1\text{NO}_2$	120.5	119.8	116.9	128.9 (115.2)
$\angle \text{O}_1\text{NO}_3$	109.2	110.9	110.2	116.2 (122.4)
$\angle \text{O}_1\text{NO}_4$	107.1	110.9	110.2	
$\angle \text{NO}_3\text{H}_5$	100.9	100.9	101.1	107.7 (100.0)
$\angle \text{NO}_4\text{H}_6$	101.0	100.9	101.1	
$\angle \text{O}_1\text{O}_2\text{NO}_3^a$	124.5	123.5	126.0	180.0 (180.0)
$\angle \text{O}_1\text{O}_2\text{NO}_4^a$	234.6	236.5	234.0	
$\angle \text{O}_1\text{NO}_3\text{H}_5^b$	-12.5	0.4	59.7	0.0 (0.0)
$\angle \text{O}_1\text{NO}_4\text{H}_6^b$	214.6	-0.4	300.3	

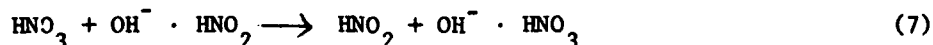
^aAngle between the OON plane and the ONO plane. ^bAngle between the ONO plane and the NOH plane. ^cValues in parentheses are from reference 35.

From the total energies given in Table II, it is evident that the energies of all three conformers are very similar and that I is the most stable structure studied thus far. Using the total energy of I the $\text{OH}^- \cdot \text{HNO}_3$ bond dissociation energy is determined by finding the change in energy for the following reaction.



$$D(\text{OH}^- \cdot \text{HNO}_3) = E(\text{HNO}_3) + E(\text{OH}^-) - E(\text{OH}^- \cdot \text{HNO}_3) \quad (6)$$

The calculated and experimental bond dissociation energies are also included in Table II. The calculated value is low compared to the experimental value as a result of neglecting the terms discussed above in the Computational Details section. The value reported in Table II is the minimum possible calculated bond dissociation energy of $\text{OH}^- \cdot \text{HNO}_3$. If any conformation not yet considered is more stable than I, the magnitude of this calculated energy would increase. However, it is unlikely to increase by as much as 20 kcal. A better estimate of the bond dissociation energy would be obtained by evaluating it isodesmically via the following reaction.



$$\Delta E_{\text{rx}} = D(\text{OH}^- \cdot \text{HNO}_2) - D(\text{OH}^- \cdot \text{HNO}_3) \quad (8)$$

$$\Delta E_{\text{rx}} = E(\text{OH}^- \cdot \text{HNO}_3) + E(\text{HNO}_2) - E(\text{OH}^- \cdot \text{HNO}_2) - E(\text{HNO}_3) \quad (9)$$

Since $D(\text{OH}^- \cdot \text{HNO}_2)$ has been experimentally determined,^{16a} $D(\text{OH}^- \cdot \text{HNO}_3)$ can be found from the above equation provided the energy of each species is known. At this point, the energy of $\text{OH}^- \cdot \text{HNO}_2$ has not been calculated and the isodesmic bond dissociation energy of $\text{OH}^- \cdot \text{HNO}_3$ cannot be evaluated.

Table II. Total Energies (in a.u.) and Bond Dissociation Energies (in kcal)

System	E_{total}	$D(\text{OH}^- \cdot \text{HNO}_3), \text{calc.}$	$D(\text{OH}^- \cdot \text{HNO}_3), \text{obs.}$
$\text{OH}^- \cdot \text{HNO}_3, \text{I}$	-354.30674	53.2 ^c	81 ^d
$\text{OH}^- \cdot \text{HNO}_3, \text{II}$	-354.30377		
$\text{OH}^- \cdot \text{HNO}_3, \text{III}$	-354.30067		
HNO_3	-278.99211(-278.98916) ^a		
OH^-	-75.22979 ^b		

^aReference 35. ^bReference 20. ^cCalculated using $E(\text{HNO}_3) = -278.99211$ a.u.

^dReference 16a.

Atomic charges from population analysis³⁶ are given for $\text{OH}^- \cdot \text{HNO}_3$, I and HNO_3 in Figure I.

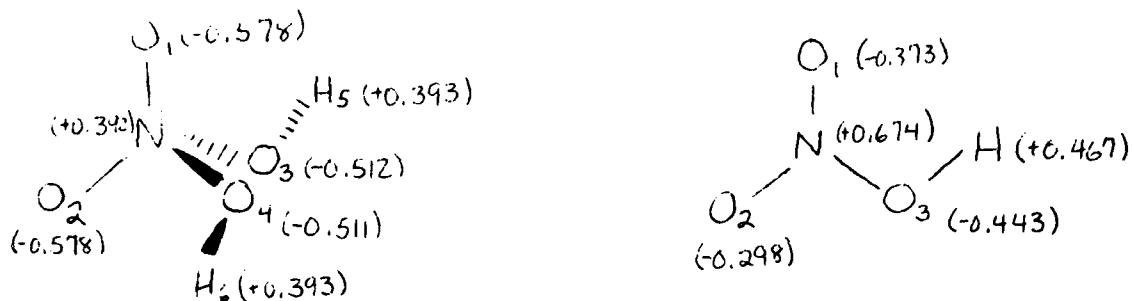
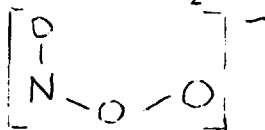


Figure I. Atomic Charges for $\text{OH}^- \cdot \text{HNO}_3$, I and HNO_3 .

Several observations can be made upon examining this figure. (1) 0.882e has been transferred from the OH^- to the HNO_3 group in the ion. (2) The negative charge has been distributed over all of the atoms in the complex; each type of atom is more negative in the ion than it is in HNO_3 . These observations lead to the conclusion that this structure cannot be considered a solvated point charge and that it would be more correctly designated as H_2NO_4^- rather than $\text{OH}^- \cdot \text{HNO}_3$. Several hydrogen bonded systems of this complex ion remain to be treated but they seem unlikely to be as stable as H_2NO_4^- .

The results reported above suggest that it may be necessary to carry out these calculations using a more accurate basis set to obtain reliable energetics. Furthermore, the actual bond dissociation energy most likely represents an average over several contributing structures since the total energies are so similar and the most favorable conformation may not always be easily achieved. To account for this a molecular dynamics³⁷ or Monte Carlo³⁸ approach is required.

$\text{NO}_3^- \cdot \text{H}_2\text{O}$. The fact that the proposed second $\text{NO}_3^- \cdot \text{H}_2\text{O}$ ion is potentially produced from a reaction mixture containing O_3 ¹⁴ suggests that the NO_3^- group has the following atom connectivity and could be written ONO_2^- .



Thus, this structure was examined first. The initial step taken to determine whether the $\text{ONO}_2^- \cdot \text{H}_2\text{O}$ ion is stable with respect to dissociation into ONO_2^- and H_2O and, if so, its bond dissociation energy, was an attempt to find the optimum geometry of ONO_2^- . The next step would have been to use this geometry as the initial guess for the structure of ONO_2^- in the optimization procedure for the complex. Since

AD-A113 708

SOUTHEASTERN CENTER FOR ELECTRICAL ENGINEERING EDUCAT--ETC F/6 5/1
USAF SUMMER FACULTY RESEARCH PROGRAM. 1981 RESEARCH REPORTS. VO--ETC(U)
OCT 81 W D PEELE F49620-79-C-0038

UNCLASSIFIED

AFOSR-TR-82-0227

NL

7-14

4

3-3 '06

convergence problems prevented completion of the first step, the second step was never carried out. This project will be continued when the Gaussian 80 computer program,³⁹ which is known to alleviate such convergence problems and has therefore been sent for, is available at Holy Cross.

$H^+(CH_3CN)$. In order to study the charge redistributions and structure changes which occur upon substitution of the $H^+(H_2O)_n$ ions, it is necessary to know the optimum geometries and atomic charge distributions of CH_3CN , $H^+(CH_3CN)$, $H^+(H_2O)_n$, and H_2O for reference. These molecular properties have already been calculated for H_2O and the $H^+(H_2O)_n$ cations at the 4-31G level^{20,21} and for CH_3CN at the 4-31G⁴⁰ and the STO-3G level.⁴¹ However, no prior calculation of these properties for $H^+(CH_3CN)$ using either basis set is known to me. Kollman and Rothenberg⁴² have studied the proton affinity of CH_3CN but they did not determine the optimum structure of $H^+(CH_3CN)$ or CH_3CN . They used the experimental geometry for CH_3CN ⁴³ and made the following assumptions about the geometry of $H^+(CH_3CN)$: 1) protonation occurs on the nitrogen; 2) the cation is linear; 3) the CH_3CN group has the same bond lengths and bond angles in the neutral and protonated species; 4) the N-H bond length is 1.01Å. To test these assumptions the optimum structure of $H^+(CH_3CN)$ was investigated.

Two objectives of the investigation were to determine whether the proton is bonded to the nitrogen, the carbon, or both (forming a three-center two-electron triangular bond) and whether the cation has a linear or bent shape. The research was initiated by optimizing the geometries of the N-protonated and C-protonated species and selecting a reasonable geometry for the N,C-protonated species at the STO-3G basis set level. This procedure demonstrated that the linear N-protonated system is more stable than the C-protonated and the N,C-protonated cations by 62 and 157 kcal, respectively. The extremely large magnitude of the latter energy difference made it unnecessary to pursue that possibility any further.

Having ascertained the preference for N-protonation, a 4-31G optimization was carried out for that species. The linear structure was again found to be most stable. The 4-31G optimized parameters for the N-protonated species and CH_3CN , the STO-3G values for the N- and C-protonated species and for CH_3CN , and the experimental geometry for CH_3CN are given in Table III. The associated total energies and the calculated, isodesmic, and experimental proton affinities are tabulated in Table IV. The isodesmic proton affinity of CH_3CN is computed via the following equations using the experimental proton affinity of HCN²⁸ as PA(HCN) and the calculated energies of $H^+(HCN)$ and HCN.⁴¹



$$\Delta E_{rx} = E[H^+(HCN)] + E[CH_3CN] - E[H^+(CH_3CN)] - E[HCN] \quad (11)$$

$$\Delta E_{rx} = PA(CH_3CN) - PA(HCN) \quad (12)$$

$$\text{or } PA(CH_3CN) = \Delta E_{rx} + PA(HCN) \quad (13)$$

The calculated proton affinity is obtained from the following equation, where $E[H^+]$ is assumed to be zero.

$$PA(CH_3CN) = -E[H^+(CH_3CN)] - E[CH_3CN] - E[H^+] \quad (14)$$

Table III. Optimized Geometrical Parameters (in Å and degrees)

	C-protonated $H^+(CH_3CN)$ STO-3G ^a	N-protonated $H^+(CH_3CN)$ STO-3G ^a	N-protonated $H^+(CH_3CN)$ 4-31G ^a	CH_3CN STO-3G ^b	CH_3CN 4-31G ^c	CH_3CN expt. ^d
C-N	1.282	1.149	1.130	1.154	1.142	1.157
C-C	1.557	1.505	1.453	1.486	1.455	1.458
C-H	1.090 ^e (1.094) ^f	1.094	1.082	1.088	1.081	1.112
N-H ⁺ (C-H)	1.117	1.038	0.992			
<CCH	110.6 ^e (106.4) ^f	108.1	109.5	109.9	110.3	109.3
<NCC	122.0					
<NCH ⁺	116.3					
<H ⁺ CCH	180.0 ^e					

^aThis work. ^bReference 41. ^cReference 40. ^dReference 43. ^eIn-plane hydrogen.
^fOut-of-plane hydrogens.

Table IV. Total Energies (in a.u.) and Proton Affinities (in kcal).^a STO-3G values are in parentheses.

System	E_{total}	Proton Affinity Calc.	Proton Affinity isodesmic	Proton Affinity expt. ^b
C-protonated $H^+(CH_3CN)$	(-130.52470)			
N-protonated $H^+(CH_3CN)$	-132.04452(-130.62386)			
CH_3CN	-131.72827(-130.27154)	198.6(221.1)	192.3(193.1)	187.0
$H^+(HCN)$	(-91.99783)			
HCN	(-91.67521)	180.8 ^c (202.4) ^d		174.5

^a $E(H^+)$ is assumed to be zero. ^bReference 28. ^cReference 42. ^dReference 41.

A number of observations can be made upon examining Tables III and IV. (1) There is generally very good agreement between the experimental and calculated geometries of CH_3CN , especially for the 4-31G basis. (2) The 4-31G bond lengths are too short and the CCH angle is too large compared to the experimental values following the general trends expected for that basis set.³¹ (3) There is no consistent pattern for the differences in STO-3G and experimental bond lengths. (4) The assumption made by Kollman and Rothenberg⁴¹ that the geometry of the CH_3CN group would remain unchanged upon protonation of acetonitrile was a reasonable assumption. For the 4-31G

results, only the C-N bond length and CCH bond angle are more than negligibly affected by protonation, and those changes are still quite small, i.e. 0.012 Å and 0.8°, respectively. The STO-3G differences are more pronounced. (5) With the exception of the choice for the N-H⁺ bond length, which was slightly too large, their other assumptions were also sound since H⁺(CH₃CN) is N-protonated and linear and the 4-31G calculated and experimental geometries are very similar. (6) The calculated proton affinities are too high for both basis sets used, although the 4-31G value (198.6) is more reasonable than the STO-3G value (221.1). Computed proton affinities are known to be basis set dependent and to improve as the basis is expanded.⁴⁴ Our results agree with this finding. (7) The proton affinities obtained from both basis sets, especially the STO-3G basis, are noticeably improved by computing them isodesmically. Notice that the values are very close for the two basis sets suggesting that the faster, more economical STO-3G basis can be used to study energetics providing isodesmic calculations are performed. (8) The good agreement between these experimental and calculated properties lends credence to the results obtained for the more complex H⁺(CH₃CN)_n and H⁺(H₂O)_m(CH₃CN)_k systems.

The 4-31G atomic charge distributions for H⁺(CH₃CN) and CH₃CN are given in Figure 2.

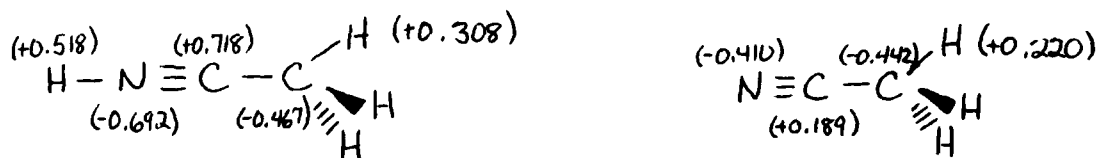


Figure 2. Atomic Charge Distributions for H⁺(CH₃CN) and CH₃CN.

Figure 2 shows that 0.482e has been transferred to the proton from the CH₃CN group, primarily from the cyano carbon and methyl hydrogens. The electron density on the cyano carbon has been decreased further by its being transferred to the nitrogen. This makes the nitrogen more negative in the ion than it is in the neutral molecule and creates a pronounced alternating charge distribution (which is most likely over-emphasized²⁰). This effect has also been observed for protonated azabenzene and may be related to ion stability, i.e. for ions with a wide range of stabilities the greater the charge transfer the more stable they are.⁴⁵

H⁺(H₂O)_m(CH₃CN)_k Ions. One of the reactions observed by Smith et al.⁹ is the following:



To gain some insight into the structure of $\text{H}^+(\text{H}_2\text{O})(\text{CH}_3\text{CN})$ and the thermodynamics of this reaction the optimum geometry of this cation was calculated using the 4-31G basis set. As a preliminary investigation a partial geometry optimization was carried out on several conformations of this ion. In conformation I the acetonitrile backbone and the water molecule are in the same plane. In conformation II the water molecule is in a plane perpendicular to the plane of the acetonitrile backbone. In conformations III and IV the hydrogens in the water molecule are staggered and eclipsed, respectively, with regard to the acetonitrile methyl hydrogens. Conformation I is depicted below in Figure 3.

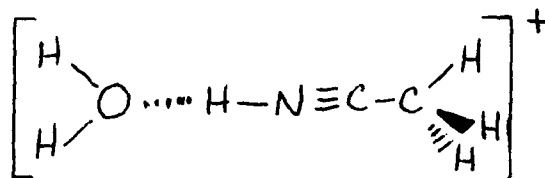


Figure 3. Conformation I of the $\text{H}^+(\text{H}_2\text{O})(\text{CH}_3\text{CN})$ ion.

The partial geometry optimizations were carried out for two reasons. The first was to find out which of the four conformations were reasonable choices and whether I and II as well as III and IV are essentially equivalent as a result of the large distance between the methyl hydrogens and the water hydrogens. The second was to determine whether the common practice^{20,21,41} of fixing the geometries of the monomers, i.e. $\text{H}^+(\text{CH}_3\text{CN})$ and H_2O , at their cationic and neutral structures, respectively, is applicable for this investigation. For this procedure the calculated optimum geometries of $\text{H}^+(\text{CH}_3\text{CN})$ and H_2O are retained in the complex ion and only the $\text{N}\cdots\text{O}$ and N-H distances and the NHO angle are optimized. Carrying this process out for all four conformations is analogous to varying the angle between the symmetry axis of the H_2O molecule and the $\text{O}\cdots\text{H-N}$ bond.

The results from these partial optimizations indicated that the methyl hydrogen-water hydrogen non-bonded interactions are unimportant and make no contribution to the total energy of these systems. Consequently, conformations I and II have identical energies as do III and IV. However, I and III have different energies, so these two conformations were subjected to a full optimization.

The complete geometry optimization showed that conformer I is a local minimum on the potential energy surface for this ion. Conformer III is not since it rotates to I. The fact that I is the most stable conformation of this cation is in line with the tendency of the 4-31G basis set to exaggerate bond angles.³¹

The geometrical parameters obtained from the partial and complete geometry optimizations of conformer I are tabulated in Table V.

Table V. Geometrical Parameters from Partial^a and Complete Optimization (in Å and degrees)

	Partial Optimization	Complete Optimization
O...N	2.509	2.506
N-H	1.081	1.083
N-C	1.130	1.132
C-C	1.453	1.454
C-H	1.082	1.082
O-H	0.950 ^b	0.953
<NHO	90.0	90.0
<NOH	124.4 ^b	123.7
<CCH	109.5	109.7

^aO...N, N-H, and <NHO optimized. ^bReference 20.

A comparison of these parameters, the energies (Table VI) and the charge distributions (Figure 4) of the two systems indicates that using the monomer optimum geometries and carrying out a partial optimization is adequate for this cation. The bond lengths vary by a maximum of 0.003Å and the bond angles by a maximum of 0.7°. Both hydrogen bonds are linear. The energies of the two systems differ by only 0.065 kcal. The charge distributions are essentially equivalent as well. The reason these properties are so similar is that the hydrogen bond is asymmetric and the H has not moved very far toward the O along the hydrogen bond (O...H = 1.423Å, cf. H⁺(CH₃CN) geometry). A larger movement of the H would produce a greater change in geometry which would have to be accounted for in the optimization procedure. Otherwise, a partial geometry optimization will suffice. This conclusion will be particularly useful as the size of the H⁺(H₂O)_m(CH₃CN)_k ions considered increases.

Table VI. Total Energies(a.u.), ΔE_{sub} (kcal/mole), and E_D (kcal/mole)

System	E _{total}	ΔE _{sub} ^a	E _D ^b
H ⁺ (H ₂ O)(CH ₃ CN)	-208.0040		
partial optimization			
H ⁺ (H ₂ O)(CH ₃ CN)	-208.0041	-3.49	-31.97
full optimization			
H ⁺ (H ₂ O) ₂	-152.1791 ^c		-43.6 ^c
H ₂ O	-75.9086 ^c		

^a ΔE_{sub} is the change in energy for reaction 15. ^bE_D is the dimerization energy. ^cReference 20.

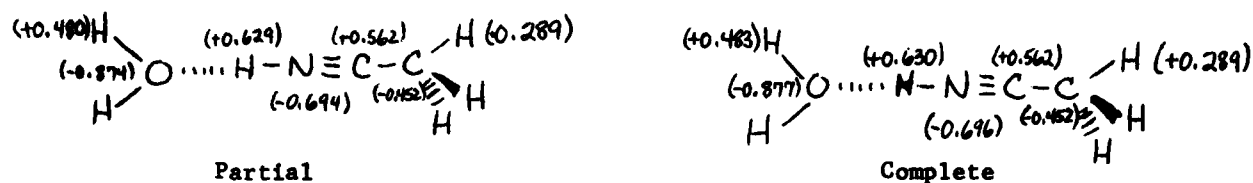


Figure 4. Atomic Charge Distributions for Partially and Completely Optimized $\text{H}^+(\text{H}_2\text{O})(\text{CH}_3\text{CN})$

The proton in $\text{H}^+(\text{H}_2\text{O})(\text{CH}_3\text{CN})$ is associated with the monomer of higher proton affinity (187.0 for CH_3CN vs. 170.3 for H_2O)²⁸ as it is in most of the dimers studied by Desmeules and Allen.⁴⁶ The linear geometry, N-H bond length of 1.083 Å, and value of zero degrees for the angle between the H_2O symmetry axis and $\text{O}\cdots\text{H}-\text{N}$ bond are also consistent with their results. An additional, especially useful result obtained by Desmeules and Allen is that there is a positive, linear correlation between r_2 (i.e. $\text{O}\cdots\text{H}$) and R (i.e. $\text{O}\cdots\text{N}$) dependent only on the row of the proton donor (i.e. N). Our data for $\text{H}^+(\text{H}_2\text{O})(\text{CH}_3\text{CN})$ also falls on the linear portion of their curve indicating that the predominant contributor to the binding in the hydrogen bond in this cation is an electrostatic rather than a covalent interaction.

The dimerization energy or energy of bond formation, E_D (Table VI), for $\text{H}^+(\text{H}_2\text{O})(\text{CH}_3\text{CN})$ is computed using equation 16.

$$E_D = E[\text{H}^+(\text{H}_2\text{O})(\text{CH}_3\text{CN})] - E[\text{H}^+(\text{CH}_3\text{CN})] - E[\text{H}_2\text{O}] \quad (16)$$

The value obtained for this complex, -31.97 kcal/mole, is comparable to the calculated values for $\text{H}^+(\text{NH}_3)_2$, -32.00 kcal/mole,⁴⁶ and $\text{H}^+(\text{H}_2\text{O})(\text{NH}_3)$, -27.72 kcal/mole.⁴⁶ The latter energies as well as the E_D calculated for $\text{H}^+(\text{H}_2\text{O})_2$, -43.6 kcal/mole,²⁰ are all larger than the corresponding experimental ΔH 's by approximately 10 kcal/mole.⁴⁷ These data embolden one to speculate that E_D for $\text{H}^+(\text{H}_2\text{O})(\text{CH}_3\text{CN})$ is also in error by about 10 kcal/mole.

The change in energy which accompanies reaction 15, ΔE_{sub} (Table VI), is found from equation 17 to be -3.49 kcal.

$$\Delta E_{\text{sub}} = E[\text{H}^+(\text{H}_2\text{O})(\text{CH}_3\text{CN})] + E[\text{H}_2\text{O}] - E[\text{H}^+(\text{H}_2\text{O})_2] - E[\text{CH}_3\text{CN}] \quad (17)$$

This figure is in agreement with Smith et al.'s⁹ observation that reaction 15 is a favorable process. ΔE_{sub} and the experimental ΔH are unlikely to have the same magnitude since no correction has been made for zero-point energy, correlation, or temperature effects. However, ΔE_{sub} is an estimation for ΔH and may be a reasonably good one since the correction terms often cancel, at least partially, for balanced chemical reactions.^{34,46}

A comparison of the atomic charge distributions of $H^+(CH_3CN)$ (cf. Figure 2) and $H^+(H_2O)(CH_3CN)$ shows that less electron density is transferred to the proton in the hydrogen-bonded complex (0.370e) than in protonated acetonitrile. Consequently, the positive charge is more localized in $H^+(H_2O)(CH_3CN)$. Most of the 0.370e transferred comes from the cyano carbon and methyl hydrogens. The remainder comes from the water hydrogens. The electron density lost by those atoms is transferred to the nitrogen and oxygen as well as to the proton making the N and O even more negative than they are in $H^+(CH_3CN)$ and H_2O .²⁰ Other groups have also reported examples where both heavy atoms in an H-bond gain charge density upon formation of that bond.^{20,46} All of the above observations are consistent with the conclusion (see above) that much of the stabilization energy of $H^+(H_2O)(CH_3CN)$ results from an electrostatic interaction.

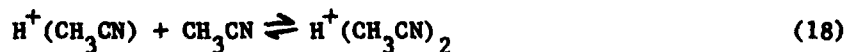
A preliminary investigation of $H^+(H_2O)_2(CH_3CN)$ indicates that the proton is associated with a H_2O molecule in this complex. Elucidation of this result awaits further study of the structure and energetics of this cation.

$H^+(CH_3CN)_n$, $n=1-4$. The STO-3G fully optimized structure of $H^+(CH_3CN)_2$ is tabulated in Table VII. No other ions in the series have been investigated as yet. Only one conformation was considered for $H^+(CH_3CN)_2$ since the results on $H^+(H_2O)(CH_3CN)$ indicated that the total energy would be independent of the methyl hydrogen-methyl hydrogen non-bonded interactions. The possibility that the proton would be located midway between the CH_3CN groups made a complete optimization expedient. A full geometry optimization was also carried out at the 4-31G level to confirm that the two basis sets yield a similar position for the proton. Both calculations predict a linear, symmetric hydrogen bond analogous to the H-bond in $H^+(H_2O)_2$.²⁰ Thus, the STO-3G basis will be utilized to study the $H^+(CH_3CN)_n$, $n=1-4$, ions and only those results are reported here. Not surprisingly the bond lengths and CCH angle in the complex are approximately midway between their values in CH_3CN and $H^+(CH_3CN)$ (cf. Table III).

Table VII. Optimized Geometrical Parameters (in Å and degrees).

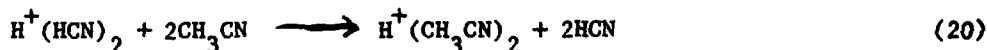
	N...N	N-H	N-C	C-C	C-H	∠CCH
$H^+(CH_3CN)_2$	2.488	1.244	1.149	1.496	1.091	108.8

The total energy of $H^+(CH_3CN)_2$ and the calculated and experimental¹¹ enthalpies of solvation of $H^+(CH_3CN)$ are given in Table VIII. These enthalpies are associated with reaction 18 and the calculated value is computed using equation 19.



$$\Delta H_{calc} = E[H^+(CH_3CN)_2] - E[H^+(CH_3CN)] - E[CH_3CN] \quad (19)$$

The experimental and calculated solvation enthalpies differ by about 16 kcal/mole. A better agreement between them would be obtained by using the experimental solvation enthalpy for $H^+(HCN)_2$ and the energy change for the following isodesmic reaction:



However, since the total energy of $H^+(HCN)_2$ has not yet been calculated, the isodesmic solvation enthalpy cannot be computed.

Table VIII. Total Energy (a.u.) and Solvation Enthalpies (kcal).

	E_{total}	$\Delta H_{calc.}$	$\Delta H_{expt.}$
$H^+(CH_3CN)_2$	-260.96491	-46.5	-30.2 ^a

^aReference 11.

The STO-3G atomic charge distributions for $H^+(CH_3CN)_2$, $H^+(CH_3CN)$, and CH_3CN are displayed in Figure 5. All atoms other than the nitrogens have an atomic charge in the hydrogen-bonded complex which is inbetween its charge in the neutral and protonated monomers. The nitrogens have a greater negative charge in the complex than in either monomer analogous to the result for $H^+(H_2O)(CH_3CN)$ and many other H-bonded systems.⁴⁶ 0.601e was transferred to the proton from the CH_3CN groups in the complex while 0.590e was transferred to it in protonated acetonitrile. This latter observation is not analogous to what was observed for $H^+(H_2O)(CH_3CN)$ and is indicative of the increased covalent character of symmetric H-bonds compared to asymmetric H-bonds, as is the relatively short internuclear separation between the nitrogens in $H^+(CH_3CN)_2$.⁴⁶

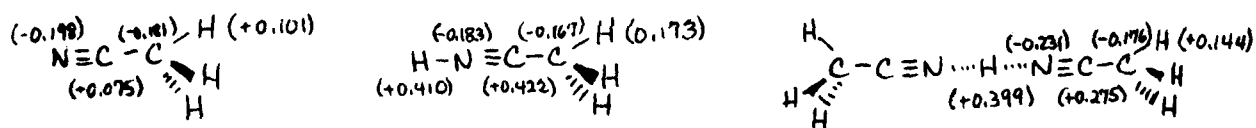


Figure 5. Atomic Charge Distributions for CH_3CN , $H^+(CH_3CN)$, and $H^+(CH_3CN)_2$.

V. RECOMMENDATIONS.

At this point the study of the structures of HNO_3 , $H^+(CH_3CN)$, $H^+(CH_3CN)_2$, and $H^+(H_2O)(CH_3CN)$ are completed at the s,p basis set level. The 4-31G investigation of $OH^- \cdot HNO_3$ is partially finished and that of $NO_3^- \cdot H_2O$ has been initiated. The calculated structures and energetics of all these systems would be bettered by expanding

the basis set, but at present this appears to be necessary only for the negative ions. The energetics would also be improved by computing isodesmic energies and by carrying out Monte Carlo or molecular dynamics calculations. It is proposed that the latter calculations be done for all pertinent systems.

Specific recommendations for follow-on research include:

1) For $\text{OH}^- \cdot \text{HNO}_3$, evaluating other possible conformations and isomers to find the optimum structure of this ion; determining the optimized geometry and energy of $\text{OH}^- \cdot \text{HNO}_2$ for use in computing the isodesmic bond dissociation energy of $\text{OH}^- \cdot \text{HNO}_3$ and in providing more information on the properties of $\text{OH}^- \cdot \text{HNO}_2$ itself.

2) For $\text{NO}_3^- \cdot \text{H}_2\text{O}$, using the Gaussian 80 computer program, which should be available at Holy Cross shortly, to determine whether there are two stable ions with this general formula.

3) For $\text{H}^+(\text{H}_2\text{O})_m(\text{CH}_3\text{CN})_k$, extending the preliminary investigation of $\text{H}^+(\text{H}_2\text{O})_2(\text{CH}_3\text{CN})$ and initiating the study of additional ions of this type to gain some insight into their chemical properties.

4) For $\text{H}^+(\text{CH}_3\text{CN})_n$, continuing the examination of the relationships between structure, charge transfer and energetics for these cations by carrying out calculations on the n=3,4 ions.

REFERENCES

1. Arnold, F., D. Krankowsky, and K.H. Marien, "First Mass Spectrometric Measurements of Positive Ions in the Stratosphere," Nature, Vol. 267, pp. 30-31, 1977.
2. Arnold, F., H. Böhringer, and G. Henschen, "Composition Measurements of Stratospheric Positive Ions," Geophys. Res. Lett., Vol. 5, pp. 653-656.
3. Arijs, E. J. Ingels, and D. Nevejans, "Mass Spectrometric Measurement of the Positive Ion Composition in the Stratosphere," Nature, Vol. 271, pp. 642-644, 1978.
4. Arijs E., D. Nevejans, and J. Ingels, "Unambiguous Mass Determination of Major Stratospheric Positive Ions," Nature, Vol. 288, pp. 684-686, 1980.
5. Arnold, F. and G. Henschen, "First Mass Analysis of Stratospheric Negative Ions," Nature, Vol. 257, pp. 521-522, 1978.
6. Arnold, F. and R. Fabian, "First Measurements of Gas Phase Sulfuric Acid in the Stratosphere," Nature, Vol. 283, pp. 55-57, 1980.
7. Arijs, E., D. Nevejans, P. Frederick, and J. Ingels, Geophys. Res. Letts., 1981, submitted for publication.
8. Ferguson, E., "Sodium Hydroxide Ions in the Stratosphere," Geophys. Res. Letts., Vol. 5, pp. 1035-1038, 1978.
9. Smith, D., N. G. Adams, and E. Alge, "Ion-Ion Mutual Neutralization and Switching Reactions of Some Stratospheric Ions," Planet. Space Sci., Vol. 29, pp. 449-454, 1981.
10. Arnold, F., G. Henschen, and E.E. Ferguson, "Mass Spectrometric Measurements of Fractional Ion Abundances in the Stratosphere - Positive Ions," Planet. Space Sci., Vol. 29, pp. 185-193, 1981.
11. Meot-Ner, M., "Solvation of the Proton by HCN and CH₃CN. Condensation of HCN with Ions in the Gas Phase," J. Am. Chem. Soc., Vol. 100, pp. 4694-4699, 1978.
12. Ferguson, E.E., "Ion-Molecule Reactions in the Atmosphere," NATO Advanced Study Institute Series B, Vol. 40, pp. 377-403, 1979.
13. Fehsenfeld, F.C., C.J. Howard, and A.L. Schmeltekopf, "Gas Phase Ion Chemistry of HNO₃," J. Chem. Phys., Vol. 63, pp. 2835-2841, 1975.
14. Wu, R.L.C. and T.O. Tiernan, "Formation and Thermodynamic Properties of Hydrated NO₃⁻ Ions," 28th Annual Conference on Mass Spectrometry and Allied Topics, May 1980, New York, New York, pp. 145-146.
15. Paulson, J.F., personal communication.
16. a) Yamdagni, R. and P. Kebarle, "Hydrogen-Bonding Energies to Negative Ions from Gas-Phase Measurements of Ionic Equilibria," J. Am. Chem. Soc., Vol. 93, pp. 7139-7143, 1971; b) Payzant, J.D., R. Yamdagni, and P. Kebarle, "Hydration of CN⁻, NO₂⁻, NO₃⁻, and OH⁻ in the Gas Phase," Can. J. Chem., Vol. 49, 3308-3314, 1971.

17. Lee, N., R.G. Keesee, and A.W. Castleman, Jr., "The Properties of Clusters in the Gas Phase. IV. Complexes of H₂O and HNO_x Clustering on NO_x⁻," J. Chem. Phys., Vol. 72, pp. 1089-1094, 1980.
18. Sapse, A.M., G. Snyder and A. El-Kayam, "Ab Initio Molecular Orbital Calculations on Ion-Molecule(s) Clusters," 182nd American Chemical Society National Meeting, August 1981, New York, New York.
19. Keesee, R.G., N. Lee, and A.W. Castleman, Jr., "Properties of Cluster Ions in the Gas Phase. 3. Hydration Complexes of CO₃⁻ and HCO₃⁻," J. Am. Chem. Soc., Vol. 101, pp. 2599-2604, 1979.
20. Newton, M.D. and S. Ehrenson, "Ab Initio Studies on the Structures and Energies of Inner-and Outer-Shell Hydrates of the Proton and Hydroxide Ion," J. Am. Chem. Soc., Vol. 93, pp. 4971-4990, 1971.
21. Newton, M.D., "Ab Initio Studies of the Hydrated H₃O⁺ Ion. II. The Energetics of Proton Motion in Higher Hydrates (n=3-5)," J. Chem. Phys., Vol. 67, 5535-5546, 1977.
22. De Paz, M., S. Ehrenson, and L. Friedman, "Study of the H⁺ and OH⁻ Hydrated Ions by the CNDO/2 Method," J. Chem. Phys., Vol. 52, pp. 3362-3368, 1970.
23. Yamabe, S. and K. Hirao, "A Theoretical Study of the Structure and Stability of H⁺(CO)_n, H⁺(N₂)_n and H⁺(O₂)_n Clusters (n=1-6)," J. Am. Chem. Soc., Vol. 103, pp. 2176-2179, 1981.
24. Pople, J.A. and G.A. Segal, "Approximate Self-Consistent Molecular Orbital Theory. II. Calculations with Complete Neglect of Differential Overlap," J. Chem. Phys., Vol. 43, pp. S136-S149, 1965; Pople, J.A. and G.A. Segal, "Approximate Self-Consistent Molecular Orbital Theory. III. CNDO Results for AB₂ and AB₃ Systems," ibid., Vol. 44, pp. 3289-3296, 1966.
25. Keesee, R.G., N. Lee, and A.W. Castleman, Jr., "Atmospheric Negative Ion Hydration Derived From Laboratory Results and Comparison to Rocket-Borne Measurements in the Lower Ionosphere," J. Geophys. Res., Vol. 84, pp. 3719-3722, 1979.
26. Hehre, W.J., R.F. Stewart, and J.A. Pople, "Self-Consistent Molecular-Orbital Methods. I. Use of Gaussian Expansions of Slater-Type Atomic Orbitals," J. Chem. Phys., Vol. 51, pp. 2657-2664, 1969; Hehre, W.J., R. Ditchfield, R.F. Stewart, and J.A. Pople, "Self-Consistent Molecular Orbital Methods. IV. Use of Gaussian Expansions of Slater-Type Orbitals. Extension to Second-Row Molecules," ibid., Vol. 52, pp. 2769-2773, 1970.
27. Ditchfield, R., W.J. Hehre, and J.A. Pople, "Self-Consistent Molecular-Orbital Methods. IX. An Extended Gaussian-Type Basis for Molecular-Orbital Studies of Organic Molecules," J. Chem. Phys., Vol. 54, pp. 724-728, 1971.
28. Wolf, J.F., R.H. Staley, I. Koppel, M. Taagepera, R.T. McIver, Jr., J. L. Beauchamp, and R.W. Taft, "Gas Phase Basicities and Relative Proton Affinities of Compounds Between Water and Ammonia from Pulsed Ion Cyclotron Resonance Thermal Equilibria Measurements," J. Am. Chem. Soc., Vol. 99, pp. 5417-5429, 1977.
29. Pulay, P., "Ab Initio Calculation of Force Constants and Equilibrium Geometries in Polyatomic Molecules. I. Theory," Molec. Phys., Vol. 17, pp. 197-204, 1969.
30. Schlegel, H.B., Ph.D. Thesis, Queens University, Kingston, Canada, 1975; Schlegel, H.B., S. Wolfe, and F. Bernardi, "Ab Initio Computation of Force Constants. I. The Second and Third Period Hydrides," J. Chem. Phys., Vol. 63, pp. 3632-3638, 1975.

31. Pople, J.A., "A Priori Geometry Predictions," Applications of Electronic Structure Theory, ed. Henry F. Schaefer III, Plenum Press, New York, pp. 1-28, 1977.
32. Hehre, W.J. and J.A. Pople, "Molecular Orbital Theory of the Electronic Structure of Organic Compounds. III. Ab Initio Studies of Charge Distribution Using a Minimal Slater-Type Basis," J. Am. Chem. Soc., Vol. 92, pp. 2191-2197, 1970.
33. Hehre, W.J., R. Ditchfield, L. Randon and J.A. Pople, "Molecular Orbital Theory of the Electronic Structure of Organic Compounds. V. Molecular Theory of Bond Separation," J. Am. Chem. Soc., Vol. 92, pp. 4796-4801, 1970.
34. Radom, L., W.J. Hehre, and J.A. Pople, "Molecular Orbital Theory of the Electronic Structure of Organic Compounds. VII. A Systematic Study of Energies, Conformations, and Bond Interactions," J. Am. Chem. Soc., Vol. 93, pp. 289-300, 1971.
35. Latajka, Z., M.M. Szczesniak, H. Ratajczak, and W.J. Orville-Thomas, "Properties of Strong Hydrogen-Bonded Systems. II. Ab Initio SCF-MO Study of the Hydrogen Bond between Nitric Acid and Ammonia," J. Comput. Chem., Vol. 1, pp. 417-419, 1980.
36. Mulliken, R.S., "Electronic Population Analysis on LCAO-MO Molecular Wave Functions," J. Chem. Phys., Vol. 23, pp. 1833-40, 1955.
37. McGinty, D.J., "Molecular Dynamics Studies of the Properties of Small Clusters of Argon Atoms," J. Chem. Phys., Vol. 58, pp. 4733-4742, 1973.
38. Mruzik, M.R., F.F. Abraham, D.E. Schreiber, and G.M. Pound, "A Monte Carlo Study of Ion-Water Clusters," J. Chem. Phys., Vol. 64, pp. 481-491, 1976.
39. Binkley, J.S., R.A. Whiteside, R. Krishnan, R. Seeger, D.J. DeFrees, H.B. Schlegel, S. Topiol, L.R. Kahn, and J.A. Pople, obtained from Department of Chemistry, Carnegie-Mellon University, Pittsburgh, Pa. 15213.
40. Hopkinson, A.C., M.H. Lien, K. Yates, P.G. Mezey, and I.G. Csizmadia, "A Nonempirical Molecular Orbital Study on the Acidity of the Carbon-Hydrogen Bond," J. Chem. Phys., Vol. 67, pp. 517-523, 1977.
41. Whiteside, R.A., J.S. Binkley, R. Krishnan, D.J. DeFrees, H.B. Schlegel, and J.A. Pople, Carnegie-Mellon Quantum Chemistry Archive, p. 123.
42. Kollman, P. and S. Rothenberg, "Theoretical Studies of Basicity. Proton Affinities, Li^+ Affinities, and H-Bond Affinities of Some Simple Bases," J. Am. Chem. Soc., Vol. 99, pp. 1334-1342, 1977.
43. Thomas, L.F., E.I. Sharrad, and J. Sheridan, "Microwave Spectra of Some Partially Deuterated Methyl Derivatives. I. Methyl Cyanide and Methylacetylene," Trans. Faraday Soc., Vol. 51, pp. 619-625, 1955.
44. Del Bene, J.E., "A Molecular Orbital Study of Protonation. Geometry and Basis Set Dependence of Computed Proton Affinities," Chem. Phys. Letts., Vol. 55, pp. 235-238, 1978.
45. Del Bene, J.E., "A Molecular Orbital Study of Protonation. 2. Pyridine and Diazines," J. Am. Chem. Soc., Vol. 99, pp. 3617-3619, 1977.

46. Desmeules, P.J. and L.C. Allen, "Strong Positive Ion Hydrogen Bonds: The Binary Complexes Formed from NH_3 , OH_2 , FH , PH_3 , SH_2 , and ClH ," J. Chem. Phys., Vol. 72, pp. 4731-4748 (1980).
47. a) Grimsrud, E.P. and P. Kebarle, "Gas Phase Ion Equilibria Studies of the Solvation of the Hydrogen Ion by Methanol, Dimethyl Ether, and Water. Effect of Hydrogen Bonding," J. Am. Chem. Soc., Vol. 95, pp. 7939-7943, 1973;
b) Payzant, J.D., A.J. Cunningham, and P. Kebarle, "Gas Phase Solvation of the Ammonium Ion by Ammonia and Water and Stabilities of Mixed Clusters $\text{NH}_4^+(\text{NH}_3)_n(\text{H}_2\text{O})_w$," Can. J. Chem., Vol. 51, pp. 3242-3249, 1973.

1981 USAF - SCEEE SUMMER FACULTY RESEARCH PROGRAM

Sponsored by the

AIR FORCE OFFICE OF SCIENTIFIC RESEARCH

Conducted by the

SOUTHEASTERN CENTER FOR ELECTRICAL ENGINEERING EDUCATION

FINAL REPORT

ANALYSIS OF SEVERAL SOLID PROPELLANT STABILIZERS

BY DC POLAROGRAPHIC TECHNIQUES

Prepared by: Dr. Donald W. Emerich

Academic Rank: Professor

Department and University: Department of Chemistry
Mississippi State University

Research Location: Air Force Rocket Propulsion Laboratory
Liquid Rocket Division, Chemistry Branch

USAF Research Colleague: Capt. Eldron L. Boehmer

Date: 1 Sept. 1981

Contract No: F49620-79-C-0038

ANALYSIS OF SEVERAL SOLID PROPELLANT STABILIZERS

BY DC POLAROGRAPHIC TECHNIQUES

by

Donald W. Emerich

ABSTRACT

The polarographic reduction of N-Methyl-p-nitroaniline, 2-Nitrodephenylamine (2-NDPA), and 4-Nitrodiphenylamine (4-NDPA), was demonstrated using a Princeton Applied Research (PAR) Model 174A Polarographic Analyzer with Drop Timer. The polarographic cell consisted of the PAR two-piece cell body, dropping mercury electrode, platinum counter electrode, and silver-silver chloride in 0.1 formal sodium chloride in methanol as reference electrode. Solutions of the stabilizers were prepared in methanol containing 0.3 formal lithium perchlorate as supporting electrolyte.

Each compound exhibited a single reduction wave (Sampled DC or Pulse modes) or single peak (Differential Pulse mode). Efficient oxygen removal from the solutions is required to secure satisfactory polarograms. Half-wave potentials observed using the Sampled DC mode (versus the above-mentioned reference electrode) were: -0.97 v. for the N-Methyl-p-nitroaniline, -0.80 v. for the s-Nitrodiphenylamine, and -0.86 v. for the 4-Nitrodiphenylamine. The limiting current (Pulse mode) and the peak current (Differential Pulse mode) is directly proportional to concentration, within the limits of precision obtained, for each of the stabilizer solutions.

An attempt to quantitate the concentration of 4-NDPA in the methanol extract of a solid propellant sample by DC polarography using the Pulse mode and the Differential Pulse mode was not successful due, presumably, to interference by other compounds extracted with the stabilizer that also are reduced at the dropping mercury electrode and at potentials that overlap the wave of the stabilizer. The necessity for separation of the methanol extracted compounds prior to the polarographic quantation of the stabilizer is evident.

Acknowledgements

The author gratefully acknowledges his appointment as a participant in the USAF/-SCEEE Summer Faculty Research Program under the sponsoring of the Air Force Systems Command and the Air Force Office of Scientific Research, and the Air Force Rocket Propulsion Laboratory.

In addition to the helpful suggestions of USAF research colleague, Capt. Eldron L. Boehmer, the author, is sincerely grateful for the assistance received from many Air Force personnel and civilian employees in the Chemistry Branch of the Liquid Rocket Division of the Rocket Propulsion Laboratory. Special thanks are due Mr. John Nakamura, Mr. W.L. Robbs, and Mr. Louis Dee for their assistance in making this research possible. The following should also be cited for their helpfulness and friendly cooperation: Lt. Kevin Wager, Mr. D.B. Cooke, Mr. Herman Martens, Mr. George Shoemaker, Mr. Mel Abrego, Mr. Stephen Terao, Sgt. Robert Searle, Pvt. Galye Angelo, Mr. Tom Owens, Mr. Roy Wurzback, Mr. Curt Chandler, and Ms. Lisa Emmanuel. Also, the following co-operative education students and summer employees gave occasional assistance: Ms. Mary Fiske; and Messrs. Matthew Doyle, Dale Coutu, Steve Smith, Cary David, Brian McPheeters, and George Walker, for which the author is grateful.

I. INTRODUCTION:

Polarography is an electroanalytical technique in which current is measured as a function of applied voltage or potential using a dropping mercury electrode (DME) as working electrode in a 2-electrode cell with a non-polarizable counter electrode, or in a 3-electrode cell in which the additional electrode is a constant potential reference electrode and the potential of the DME versus the reference electrode is the independent variable. Instrumentation permits recording of the cell current as a function of the applied voltage or the DME potential. Classical DC polarography measures current continuously while a constantly increasing voltage or potential is applied. Using modern electronics, additional modes to secure the polarogram of i vs. E or the first derivative of i vs. E , etc. are now available: viz. Sampled DC, Pulse, Differential Pulse, Rapid Scan (Oscillographic), AC, etc.

The measurement of the current, i , versus the voltage or potential E , of a solution containing the electroactive species and a large concentration of an indifferent electrolyte with the DME as working electrode produces a sigmoid curve in which the limiting current corrected for background yields a net (diffusion) current that obeys the Ilkovic equation (DC or Sampled DC modes). The Ilkovic equation is:

$$i_d = 0.67 n D^{1/2} C m^{2/3} t^{1/6} \quad (1)$$

where i_d = ave. current during the lifetime of the mercury drop (microamps), n = no. of electrons transferred per electroactive species, D = the diffusion coefficient (cm^2/sec), C is concentration of the electroactive species (mols/liter), m = the rate of mercury flow at the DME (mg/sec) and t = the drop time of the DME (sec).

The direct proportionality of C and i_d under the conditions of constant mercury flow rate, constant drop time (of the DME), and constant temperature is the basis of the analytical application of the polarographic DC and Sampled DC modes. Similar proportionality of concentration and Pulse mode limiting current, i_l and Differential Pulse mode peak current, i_p is observed when the electrode process is diffusion controlled and often closely approximates a direct proportionality when the electrode process is controlled by a different mechanism.

The optimal concentration range for DC or Sampled DC polarographic modes is from 10^{-2} to 10^{-4} formal. In favorable cases, the lower limit can be extended to 10^{-6} formal, particularly with Pulse or Rapid Scan polarographic modes. Application of polarographic techniques to analysis requires that the species being analyzed be electroactive but that neither the supporting electrolyte nor the solvent undergoes electrode reaction during the potential scan. The potential at which the other electroactive species present in the solution undergo electrochemical change at the DME must be separated by more than 0.1 v. in order to successfully determine the diffusion, limiting, or peak currents of each. Classical polarographic work utilizes buffered aqueous solutions when the rate-controlling step of the electrochemical reaction involves protons. When solubility considerations do not permit an aqueous solvent medium, non-aqueous solutions may be utilized.

II. OBJECTIVES OF THE RESEARCH EFFORT

The original research goals were to survey and establish the feasibility of using the voltammetric electroanalytical technique to the analysis of propellant components: those in present use and those projected for future use.

After surveying propellant components for their potential for analysis by voltammetry (polarography is the DME in the working electrode), it was decided, after consultation with the Air Force research colleague, to focus on analysis of stabilizers used in solid rocket propellants. This decision was based on the chemical functional groups present in these compounds and the fact that the present High Performance Liquid Chromatography (HPLC) procedure in use with these compounds is considered excessively time-consuming due to the necessity for removal of suspended matter by filtration. The possibility of a rapid quantitation by voltammetry, without the lengthy filtration procedure required by HPLC was thus very attractive. Since extraction of stabilizers is made using methanol as solvent, it was decided to investigate the polarography of stabilizers in methanol solvent to determine the feasibility of quantitation of these compounds by this technique.

III. CHEMTRIX MODEL SSP-5A POLAROGRAPHIC SYSTEM

The Chemtrix, Inc. Model SSP-5A Differential Polarographic Analyzer system consisting of Differential Amplifier Type 305, Polarographic Time Base Type 205, Storage Oscilloscope 564B, and Dropping Mercury Electrode (DME) Assembly Type 105, was investigated using a 5×10^{-3} formal cobalt (II) chloride solution in 0.1 formal potassium chloride, aqueous medium. Satisfactory curves at the higher sensitivity settings could not be obtained by this investigator and the system was not utilized further in this study.

IV. PRINCETON APPLIED RESEARCH (PAR) MODEL 174A POLARGRAPHIC ANALYZER WITH DROP TIMER

A 5×10^{-3} formal aqueous solution of cobalt (II) chloride containing 0.1 formal potassium chloride as supporting electrolyte was used to check out the above-mentioned system. Excellent performance and reproducibility was observed with the system and all subsequent studies were made with this instrumentation.

V. THE POLARGRAPHIC CELL

The polarographic cell used throughout these studies consisted of the PAR Model 9300 Cell Top, Model 9301 Cell Bottom, Model 9330 Outgassing Tube, and Model 9361 Reference Electrode Salt Bridge Tube along with the DME, platinum counter electrode and silver-silver chloride in 0.1 formal sodium chloride in methanol reference electrode. A Sargent capillary 8 in. long served as the DME. The counter or auxiliary electrode was fabricated from a 1 in. length of 18 gauge platinum wire and 7 mm o.d. Pyrex tubing. The silver-silver chloride reference electrode was fabricated from 0.5 in. length of 18 gauge platinum fused into a 4 inch length of 7 mm o.d. Pyrex tubing which was subsequently silver plated from a silver nitrate-sodium cyanide aqueous solution using a Beckman Electroscan 30 electrolysis apparatus, then made anodic in a cell with potassium chloride aqueous solution. This treatment yielded a silver chloride coating onto the silver plating. After careful rinsing with distilled water, then methanol, it was kept thereafter in contact with 0.1 formal sodium chloride in methanol solution in the PAR Reference Electrode Salt Bridge. The latter made contact with the polarographic solution surrounding the DME via a short length of inert plastic tubing 3 mm o.d. heat sealed onto a small cylinder of porous Vycor tubing.

VI. STABILIZER SOLUTIONS FOR PRELIMINARY EXPERIMENTS AND CALIBRATION

Solutions of each of the stabilizers investigated were prepared by direct weighing of the compounds as received followed by dissolution in distilled methanol. The N-Methyl-p-nitroaniline was Eastman No. 1248; the 2-Nitrodiphenylamine (2-NDPA) and the 4-Nitrodiphenylamine (4-NDPA) were Aldrich Chemical Co. No. 15717-1 and 10,357-8, respectively. No decomposition of these stock solutions was observed during the several weeks they remained in the laboratory at 70 Deg. F. temperature.

VII. PRELIMINARY STUDIES OF THE POLAROGRAPHIC BEHAVIOR OF METHANOL SOLUTIONS OF N-Methyl-p-nitroaniline, 2-NDPA, and 4-NDPA

Preliminary studies of the polarographic behavior of the above-mentioned stabilizers in methanol were carried out at 1×10^{-4} formal concentration using 0.3 formal lithium perchlorate as the supporting electrolyte (SE). A first scan of the potential range of (up to) 3 volts on the DME cathode relative to the previously mentioned reference electrode after a 30 minute degassing with gaseous nitrogen, the laboratory GN2. Subsequent scans were made with 10 minute degassing periods prior to the scan. It was quite obvious that oxygen removal was not complete by these procedures prior to running the polarogram. It was decided to install a gas washing bottle containing 0.1 F sodium sulfite in the GN2 stream used for degassing, and in series with it two additional gas washing bottles containing technical grade methanol and distilled methanol, respectively. This arrangement was ineffective. A 0.1 formal solution of vanadous chloride prepared according to instructions given by Meites proved very satisfactory. Later, at the suggestion of the Air Force research colleague, a Sargent tube furnace was tried in which the GN2 passed through an 8 in. Pyrex tube of 1 in. o.d. filled with Coleman "Cuprin" copper wire at 510 Deg. C. furnace temperature reading. This procedure proved inadequate. The connectors in the train perhaps permitted diffusion of air into the GN2 stream.

VIII. POLAROGRAPHY OF N-METHYL-p-NITROANILINE IN METHANOL

A 10^{-4} formal solution of this compound in methanol containing 0.3 formal SE was scanned in three of the four modes available with the PAR system. Excellent well-defined polarographic reduction waves were observed with the Sampled DC and Pulse modes and a well-defined peak was obtained in the Differential Pulse mode (Cf. Fig. 1 & 2). Repeat scans gave good reproducibility. Standard deviation for $E_{1/2}$ or E_p values were 2 percent relative for the several modes utilized. The i_d values determined from the Sampled DC mode polarograms showed a standard deviation of 5 percent relative, the i_l values determined from the Sampled DC mode polarograms showed a 6 percent relative standard deviation and the i_p values determined from the Differential Pulse polarograms gave a standard deviation of less than 2 percent relative. Cf. Table I. The $E_{1/2}$ of this compound as measured by the Sampled DC mode polarograms is -0.97 v. vs. the silver-silver chloride in methanol solvent containing 0.1 formal sodium chloride. The $E_{1/2}$ (ave.) observed with the Pulse mode is -1.02 v., slightly more negative than that observed in the Sampled DC mode but this was expected from the work of Parry and Osteryoung. The peak voltage E_p from the Differential Pulse polarogram gave an average value of -0.991 v. More concentrated solutions of the stabilizer were also scanned. The data for i_d , i_l , and i_p as a function of concentration of the N-Methyl-p-nitroaniline are plotted in Fig. 3 & 4. The results indicate that these current parameters closely adhere to a direct proportionality with depolarizer (stabilizer) concentration. The values obtained with the Pulse mode (i_l) and the Differential Pulse mode (i_p) agree better with a direct proportionality than do the i_d values obtained in the Sampled DC mode. The i_l values indicate the expected greater signal response compared with i_d and i_p values. An accuracy of 5% seems to be a reasonable estimate for the technique with this stabilizer. It should be noted that

the solutions polarographed were prepared by addition of 0.01 formal stock solution of the stabilizer to 10 ml of the 0.3 formal solution of the SE so that a slight dilution of the SE resulted. This has been ignored and assumed to have negligible effect within the concentration range under study, 10^{-3} to 10^{-4} formal in stabilizer.

IX. POLAROGRAPHY OF 2-NITRODIPHENYLAMINE, (2-NDPA) IN METHANOL

A 10^{-4} formal solution of this compound in methanol solution containing 0.3 formal lithium perchlorate as SE was scanned starting from 0 volts with a possible scan range of 3 volts (negative) of the DME relative to the reference electrode, in all four modes of the PAR system. The SE solution was scanned in all four modes prior to addition of the 2-NDPA. The scans of the SE solution indicated the incomplete removal of oxygen by the degassing with GN2 from the laboratory supply system. The greatest difficulty was observed in the Differential Pulse mode. Considerable "noise" or anomalous peaks or waves appeared in the scans made in the Sampled DC mode which were made following scans in the other modes. It was then discovered that the binding post for the counter electrode lead at the Drop Timer of the PAR system was loose. After this binding post was tightened, the problem disappeared. It was decided to run scans beginning at -0.5 volts and proceeding to more negative values until electroreduction of the SE commenced, since the wave did not begin until the voltage had gone beyond -0.5 volts. The data obtained for $E_{1/2}$ and E_p as well as values of i_d , i_l , and i_p for the several solution concentrations scanned are listed in Table 2. The ave. $E_{1/2}$ value observed under the experimental conditions used was -0.77 v. in Sampled DC and DC modes. The value in the Pulse mode was -0.80 v. which is slightly more negative as predicted by Parry & Osteryoung. E_p was -0.78 v., very nearly the same as the normal $E_{1/2}$ value. Using the data of Table 2, i_l was plotted against concentration (Fig. 7) and i_p was plotted against concentration (Fig. 8). Quite good agreement was observed for a direct proportionality of these current parameters and concentration. It may be noted that the slope of the i_l vs. concentration curve for N-Methyl-p-nitro-aniline is 12.4 whilst that for 2-NDPA is only 4.8. This is not surprising since the mol. wt. of the first named compound is 152 and that of 2-NDPA is 214. The lighter weight molecule should have a larger diffusion coefficient and the ratio of the slopes of these lines should be equal to the square root of the ratio of the diffusion coefficients if the Ilkovic equation (1) applies.

X. POLAROGRAPHY OF 4-NITRODIPHENYLAMINE, (4-NDPA), IN METHANOL

As was done with the two previous stabilizers, a 1×10^{-4} formal solution of 4-NDPA was prepared in methanol with 0.3 formal lithium perchlorate as SE. This solution was scanned in the Sampled DC, Pulse, and Differential Pulse modes, respectively, after scanning the SE solution in each of these modes. Later, additional 4-NDPA stock solution

was added to the 1×10^{-4} formal solution to make the stabilizer concentration 9.91×10^{-4} formal. The latter solution was then scanned in each of the modes previously mentioned. The resulting data are summarized in Table 3. Polarograms of 4-NDPA solutions using the Sampled DC and Differential Pulse modes, respectively, are shown in Fig. 9 and Fig. 10. The calibration curves plotted from the data of Table 3 for the three modes scanned with these solutions are given in Fig. 11 and Fig. 12. A comparison of the i_1 vs. concentration curves of 2-NDPA and 4-NDPA shows that the slope of the 4-NDPA curve is somewhat greater than that for 2-NDPA. From this we can conclude that the diffusion coefficient of 4-NDPA is slightly greater than that of 2-NDPA in methanol at the temperature of the experiment. This is not surprising since molecule configuration will affect diffusion as well as molecular weight. Using the limited data of Table 3, straight lines were drawn between the data points and there appears to be a direct proportionality between the values of i_d , i_1 and i_p with concentration. Again, the data for i_1 and i_p give better agreement with the direct proportionality with concentration than does i_d . The $E_{1/2}$ observed for 4-NDPA with the Sampled DC mode polarograms was -0.86 v., which is 0.88 volts more negative than the $E_{1/2}$ of 2-NDPA. In methanol solution, 2-NDPA is more readily reduced than is 4-NDPA. It is unclear how this might be related to the activity of these stabilizers in a solid propellant. The $E_{1/2}$ in the Pulse mode was 0.08 v. more negative than the normal $E_{1/2}$ value following the prediction of Parry and Osteryoung for relative values of these properties. Again, the E_p value (-0.88 v.) is only 0.02 v. more negative than the normal $E_{1/2}$.

XI. AN ATTEMPT TO ANALYZE A METHANOL EXTRACT OF A SOLID PROPELLANT SAMPLE FOR 4-NDPA STABILIZER

Mr. Louis Dee supplied a sample of the methanol extract from 0.1155 g. of a solid propellant containing 4-NDPA, i.e. the entire methanol extract from the solid propellant sample was present on the filter paper sample supplied. The filter paper sample was itself extracted with several portions of methanol and diluted to 25.0 ml volume in a volumetric flask. One ml of the resulting solution was added to 10 ml of 0.3 formal lithium perchlorate in methanol and polarographic scans were made in Pulse and Diff. Pulse modes following the same procedures previous used with 4-NDPA and the other stabilizers previously studied. The polarograms obtained are shown in Fig. 13 and Fig. 14. As can be readily observed, it is not possible to deduce the i_1 or the i_p value for the 4-NDPA in the sample from these polarograms, presumably because of interference by other electroactive species that have extracted along with the stabilizer in the solid propellant methanol extract.

XII. RECOMMENDATIONS:

The results of the research reported herein indicate that the stabilizers used with solid propellants can be quantitated by the polarographic technique used in the studies on the individual compounds provided that the stabilizers are the only electroactive species present in solution. As indicated in XI, above, the methanol extract of the solid propellant obviously does contain other electroactive species that interfere in quantitation of the stabilizers; i.e. the $E_{1/2}$ values of these other species overlaps the $E_{1/2}$ of 4-NDPA which was the stabilizer present in the sample examined. Since methanol extracts in which N-Methyl-p-nitroaniline or 2-NDPA were not examined it is not possible to state that the i_1 or i_p values cannot be deduced from polarographic scans of aliquots of the extracts of these last named stabilizers but the probability is not high that this can be done with these compounds, either. It is necessary to conclude on the basis of the evidence available that a prior separation of the compounds present in the methanol extract must be carried out before quantitation of the stabilizer by a polarographic scan. Presumably this would involve thin-layer, paper, or column chromatographic separation of the stabilizer from the other compounds, extraction of the stabilizer (or elution if more practicable) followed by quantitation.

Another possible approach would be to investigate the possibility of a more selective solvent or solvent mixture that could quantitatively extract the stabilizer but extract negligible amounts of the interfering compounds.

Another avenue to explore would be the possible anodic quantitation of the stabilizers employing a glassy or pyrolytic graphite electrode in place of the DME because the stabilizers in this study would be expected to undergo electrooxidation. Perhaps the interferences due to cathodic reactions will be eliminated.

The application of polarography or voltammetry is not narrowly limited to stabilizers in their possible application to the analysis of ordnance, propellants or explosives. The references in the concluding section of this report mention a number of studies on these materials.

Voltammetry employing other solvents for the quantitation always holds the possibility that greater selectivity can be achieved without prior separation, by effectively attenuating the potential spectrum available. The number of systems that could be studied with a given mix of compounds becomes very extensive, indeed.

TABLE 1. Polarographic Study of N-Methyl-p-nitroaniline in methanol

A. Sampled DC

Concn. F	$E_{1/2}$ volts	std. dev.	i_d microamps	std. dev.
1×10^{-4}	-0.94	0.02	4.12	0.21
"	-0.97		4.44	
"	-0.99		4.51	
2×10^{-4}	-0.984	0.02	6.82	0.20
"	-0.96		6.54	

B. Pulse

Concn. F	$E_{1/2}$ volts	std. dev.	i_p microamps	std. dev.
1×10^{-4}	-1.03	0.02	13.0	0.8
"	-1.00		11.9	
"	-1.00		13.5	
2×10^{-4}	-1.03		25.0	

C. Differential Pulse

Concn. F	$E_{1/2}$ volts	std. dev.	i_p microamps	std. dev.
1×10^{-4}	-0.996	0.006	1.36	0.02
"	-0.984		1.33	
"	-0.989		1.32	
2×10^{-4}	-0.996		2.74	

DMG: $m = 0.965$ mg/sec, $t = 2$ sec, drop-timer controlled

SE: 0.3 formal lithium perchlorate (in methanol)

Reference Electrode: silver-silver chloride in methanol containing 0.1 formal sodium chloride

Temperature: 70 Deg. F.

TABLE 2. Polarographic Study of 2-Nitrodiphenylamine 2-NDPA
in Methanol, (1)

A. DC, Sampled DC

Concn. F	$E_{1/2}$ (2) volts	std. dev.	i_d microamps	std. dev.	Notes
1×10^{-4}	-0.768	-	-	-	DC mode
"	-0.71	-	-	-	S.DC "

B. Pulse

Concn. F	$E_{1/2}$ (2) volts	std. dev.	i_1 microamps	std. dev.
1×10^{-4}	-0.80	0.01	3.72	0.06
5.66×10^{-4}	-0.80	0.00	25.4	0.3
9.91×10^{-4}	-0.824	0.003	44.6	0.02

C. Diff. Pulse

Concn. F	E_p (2) volts	std. dev.	i_p microamps	std. dev.
1×10^{-4}	-0.78	-	1.10	0.01
5.66×10^{-4}	-0.78	0.00	6.43	0.01
9.91×10^{-4}	-0.786	0.003	11.0	0.01

(1) See Table 1 for details of DME, SE, Ref. Electrode, Temp.

(2) Average values.

TABLE 3. Polarographic Study of 4-Nitrodiphenylamine (4-NDPA)
in Methanol. (1)

A. Sampled DC

Concn. F	$E_{1/2}$ volts	i_d microamps
1×10^{-4}	-0.86	0.73
9.91×10^{-4}	-0.86	12.5

B. Pulse

Concn. F	$E_{1/2}$ volts	i_d microamps
1×10^{-4}	-0.94	4.00
9.91×10^{-4}	-0.94	53.0

C. Diff. Pulse

Concn. F	$E_{1/2}$ volts	i_d microamps
1×10^{-4}	-0.88	0.839
9.91×10^{-4}	-0.88	8.63

(1) See Table 1 for details of DME, SE, Ref. Electrode, temp.

(2) Average values.

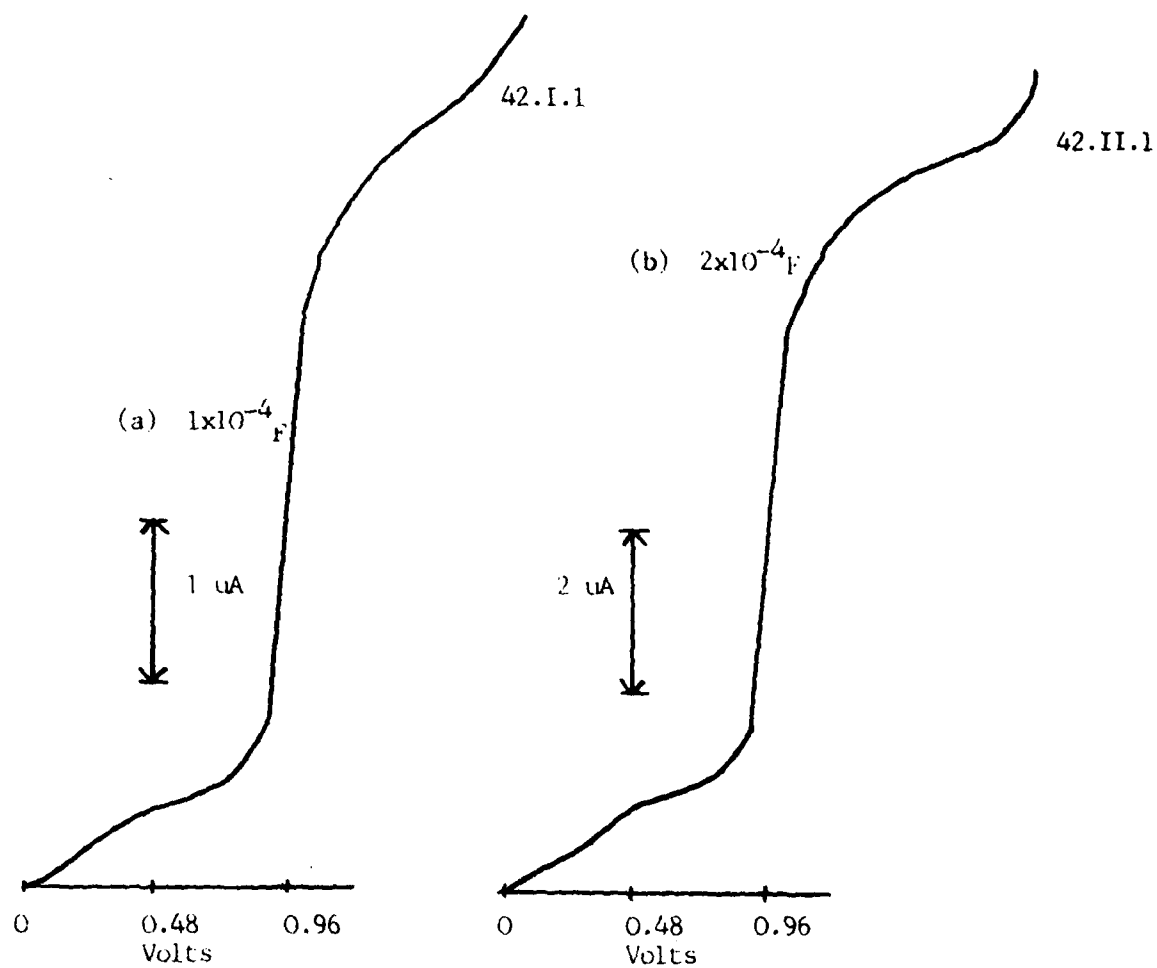


FIG. 1

Polarograms of N-Methyl-p-nitroaniline, Sampled DC Mode.
 Methanol Solvent, 0.3 formal lithium perchlorate as SE,
 silver-silver chloride in 0.1 formal sodium chloride in
 methanol as reference electrode; 70° F.
 DME: $m=0.965$ mg/sec. $t=2$ sec (drop-timer controlled)

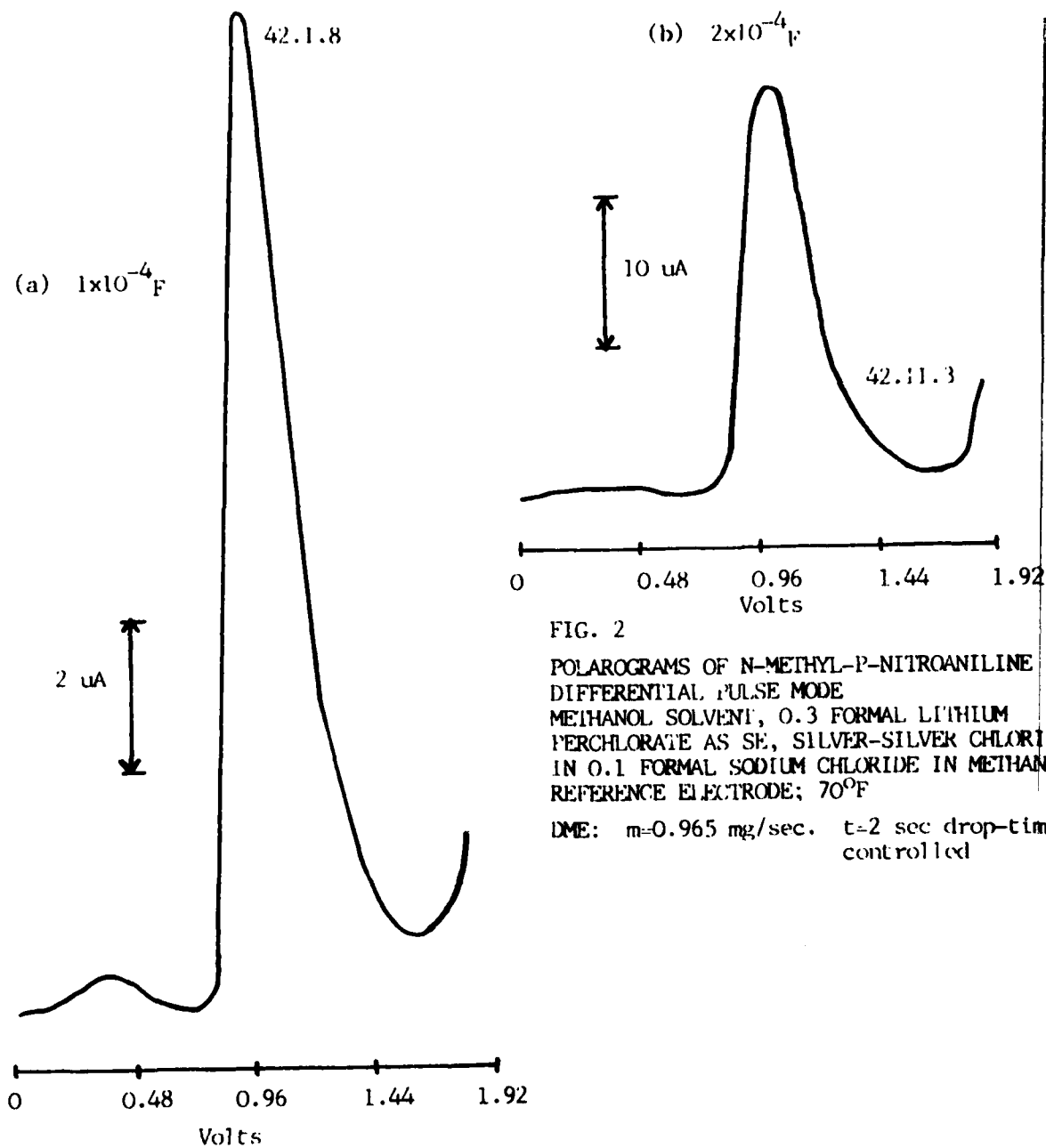


FIG. 2

POLAROGRAMS OF N-METHYL-P-NITROANILINE
DIFFERENTIAL PULSE MODE
METHANOL SOLVENT, 0.3 FORMAL LITHIUM
PERCHLORATE AS SE, SILVER-SILVER CHLORIDE
IN 0.1 FORMAL SODIUM CHLORIDE IN METHANOL
REFERENCE ELECTRODE; 70°F

DME: $m=0.965$ mg/sec. $t=2$ sec drop-time
controlled

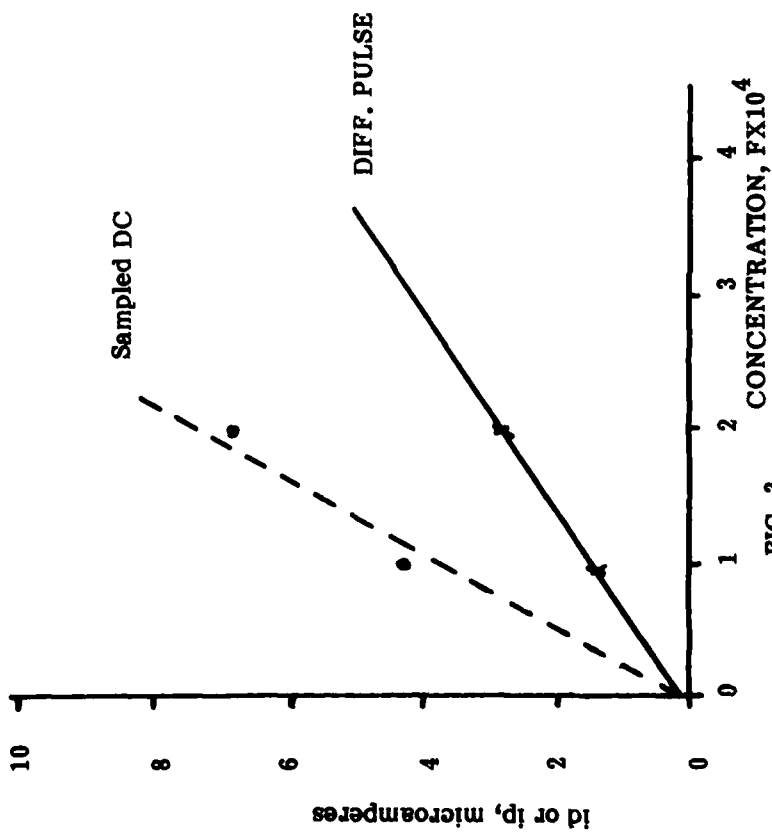


FIG. 3

CALIBRATION CURVES: N-Methyl p-nitroaniline

id vs C, Sampled DC Mode; ip vs C, Diff. Pulse Mode

Supporting Electrolyte: lithium perchlorate,
0.3 F in Methanol Ref. Electrode Silver,
Silver Chloride in 0.1 F NaCl, Methanol Solvent

DME: $m = 0.965$ $t = 7.1$ sec
mg/sec
Temp 70°F

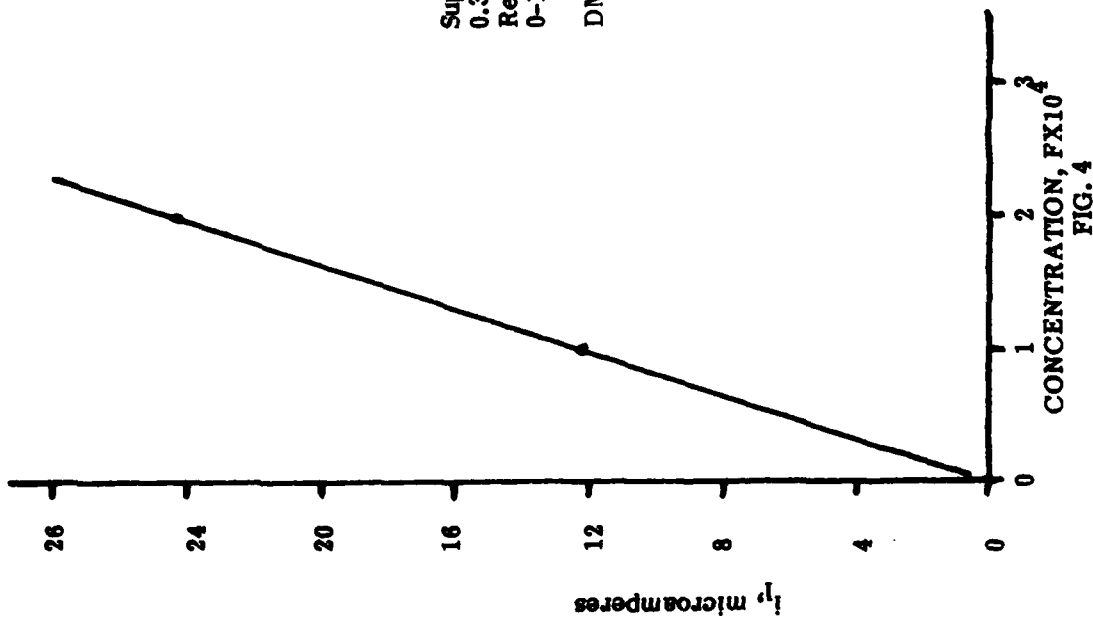


FIG. 4

CALIBRATION CURVE: N-Methyl p-nitroaniline

i_p vs C, Pulse Mode

Supporting Electrolyte: lithium perchlorate
 0.3 F in Methanol
 Ref. Electrode Silver, Silver chloride in
 0-1 F Sodium Chloride, Methanol Solvent

DME: $m=0.965$ mg/sec. $t=7.1$ sec.
 temp 70° F

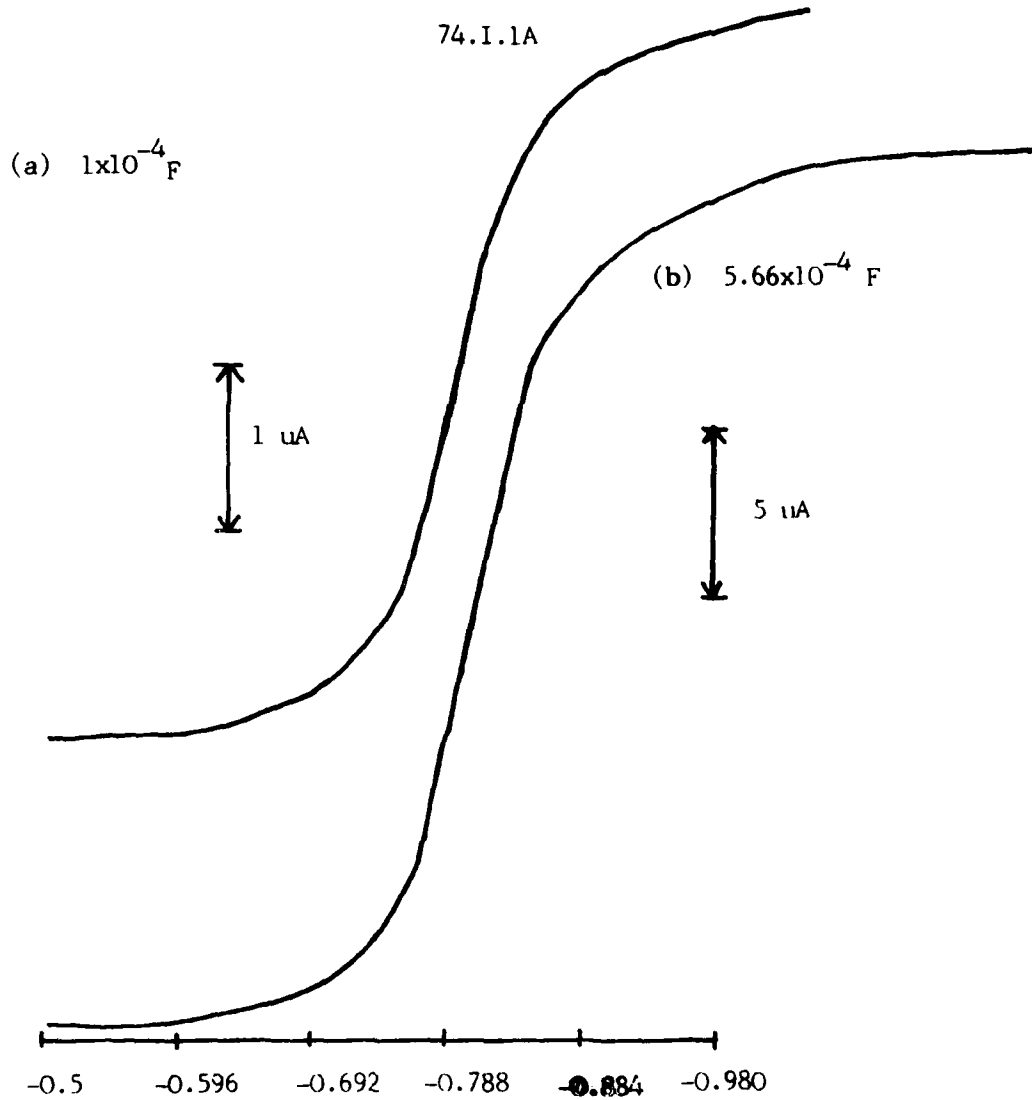


FIG. 5
 POLAROGRAMS OF 2-NDPA PULSE MODE
 SEE FIG. 1 FOR DETAILS

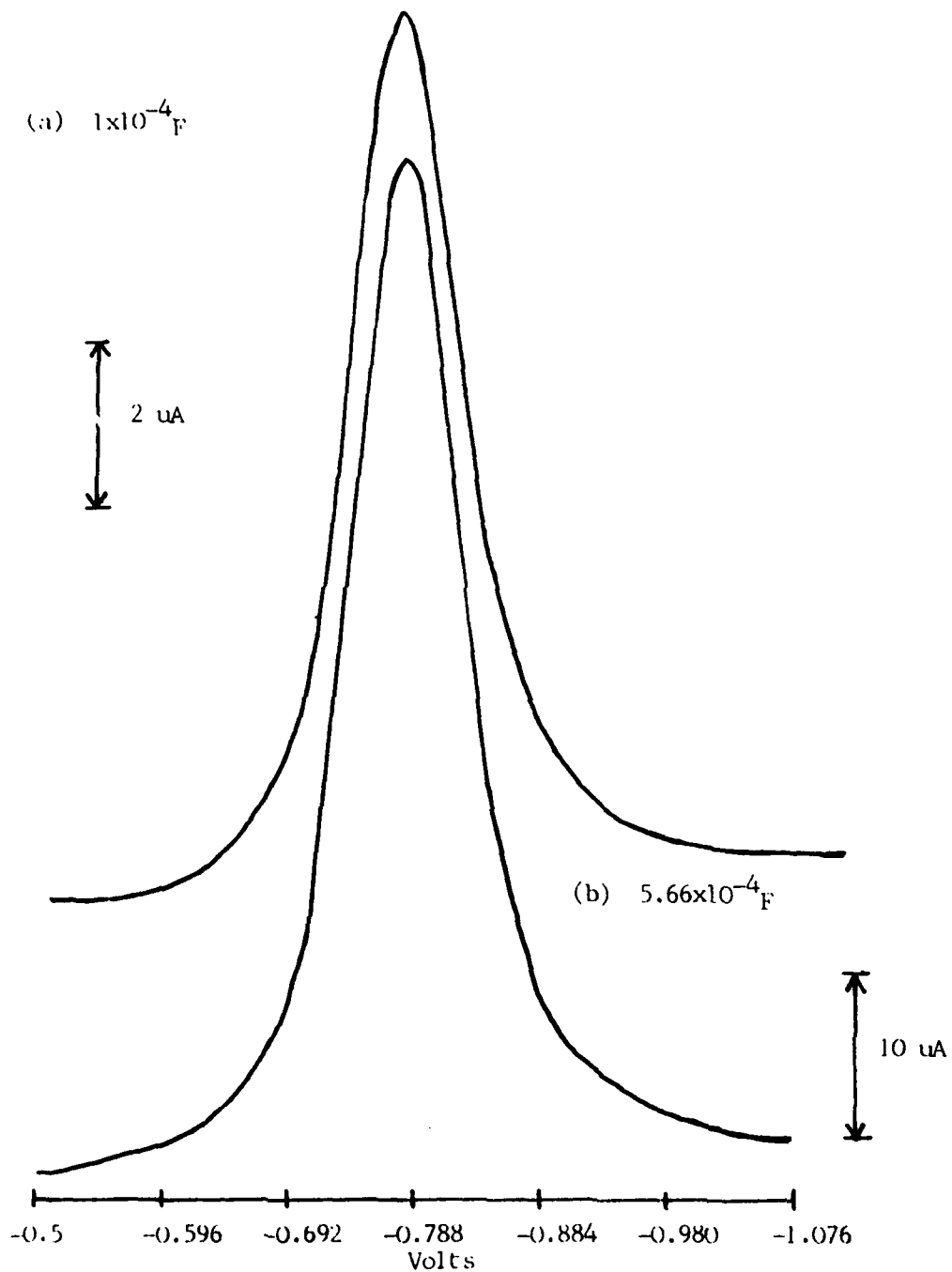


FIG. 6
POLAROGRAMS OF 2-NDPA DIFFERENTIAL PULSE MODE
SEE FIG. 1 FOR DETAILS OF POLAROGRAPHIC CELL & DME

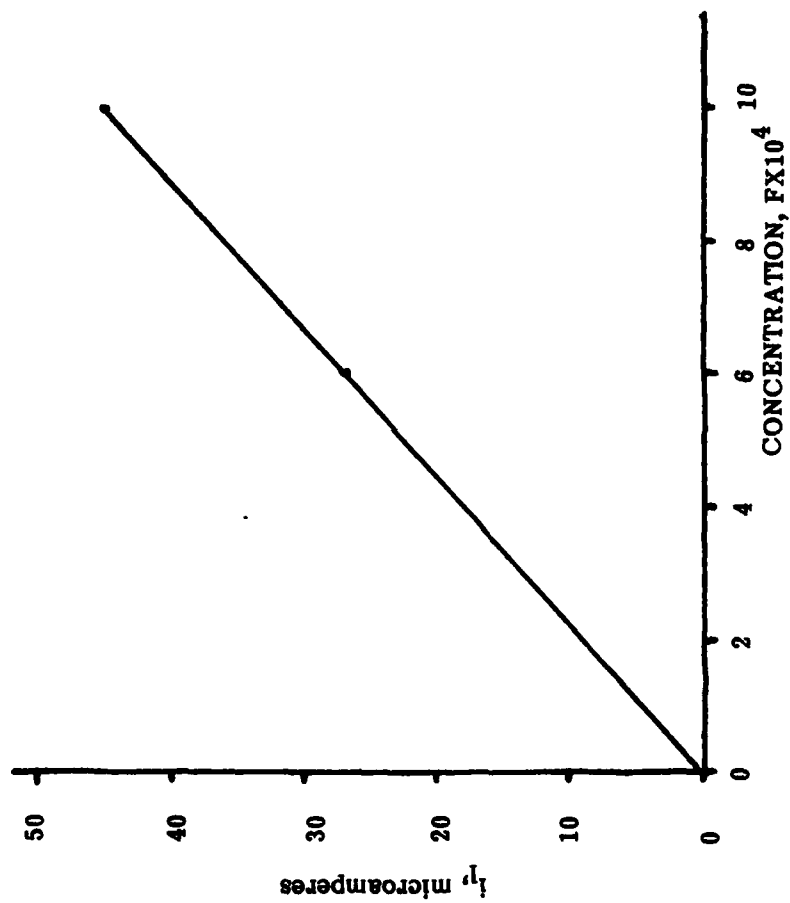


FIG. 7

CALIBRATION CURVE: 2 - NITRODIPHENYLAMINE (2-NDPA)

i_e vs. CONCENTRATION
(PULSE MODE)

SEE FIG. 3 FOR DETAILS OF POLAROGRAPHIC
CELL & DME

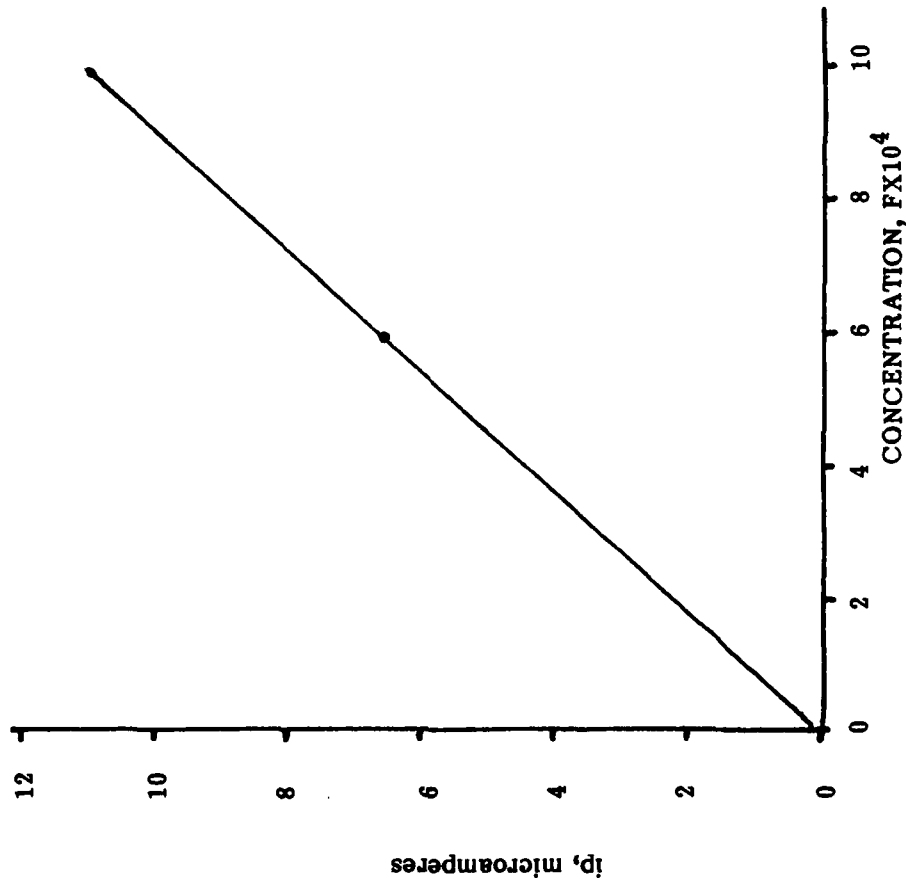


FIG. 8

CALIBRATION CURVE: 2 - NITRODIPHENYLAMINE (2 - NDPA)

ip vs. CONCENTRATION
(DIFFERENTIAL PULSE MODE)

SEE FIG. 3 FOR DETAILS OF

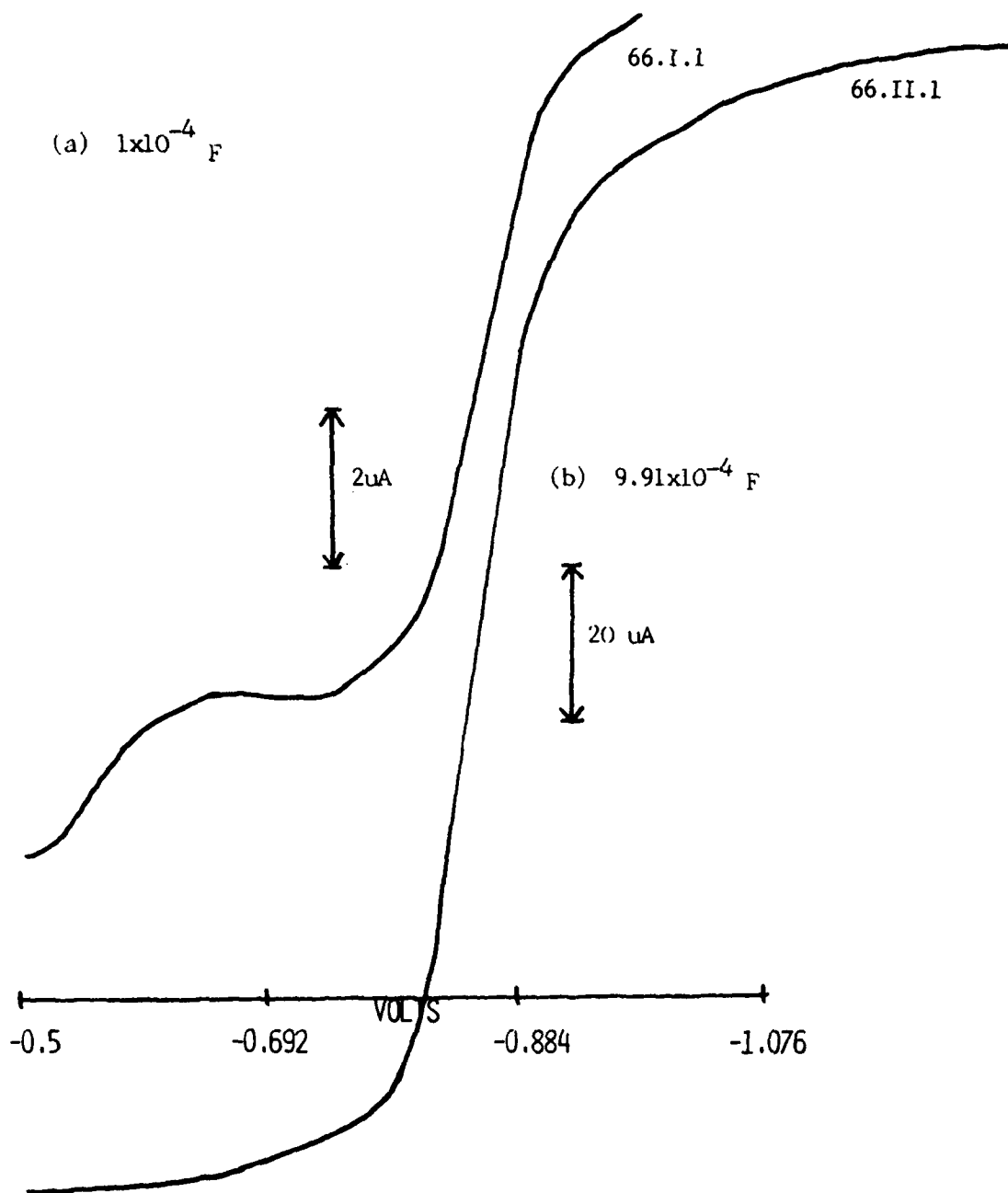


FIG. 9

POLAROGRAMS OF 4-NDPA SAMPLED DC MODE

SEE FIG. 1 FOR DETAILS OF POLAROGRAPHIC CELL & DME

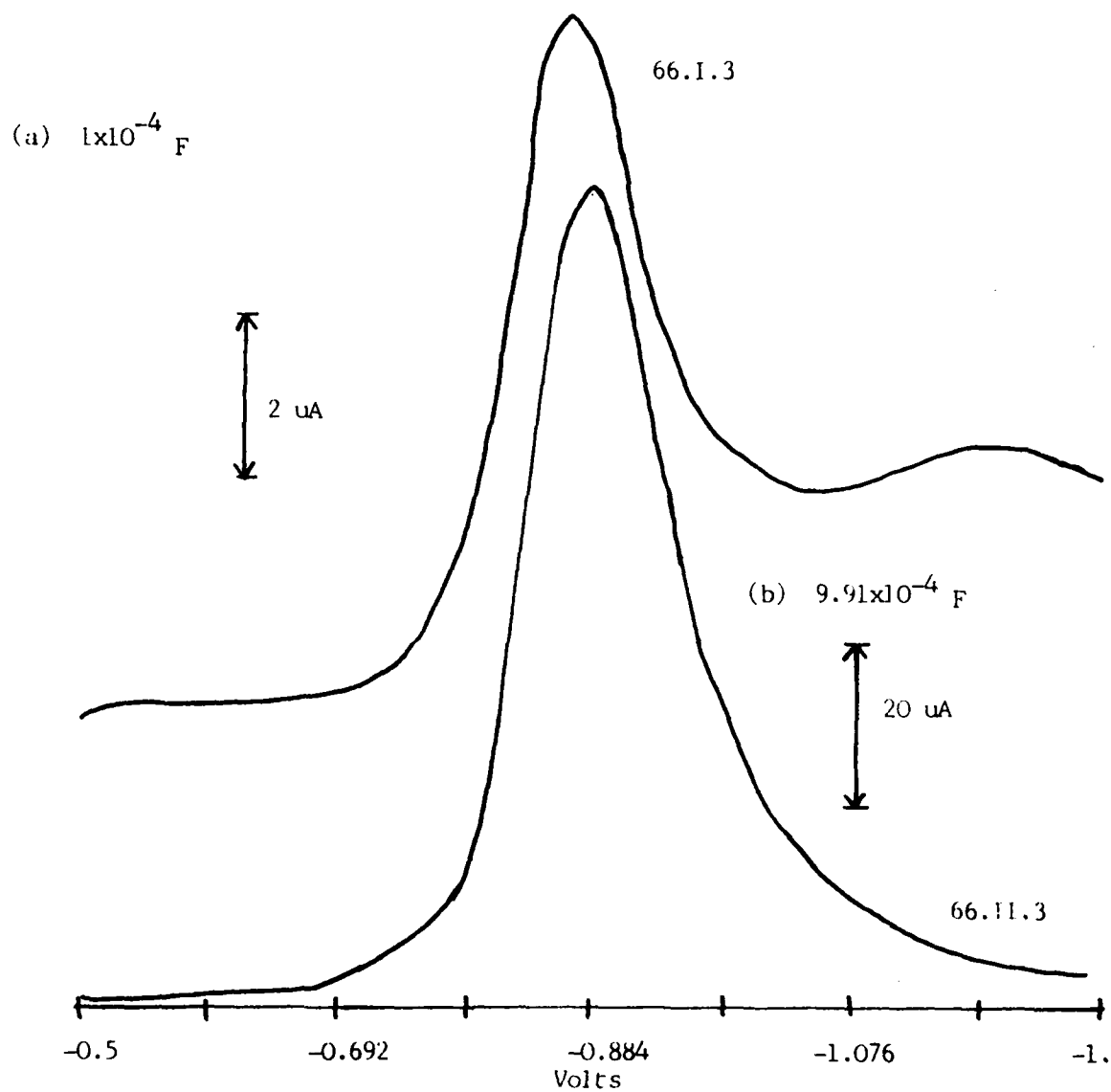


FIG. 10
 POLAROGRAMS OF 4-NDPA DIFFERENTIAL PULSE MODE
 SEE FIG. 1 FOR DETAILS OF POLAROGRAPHIC CELL & DME

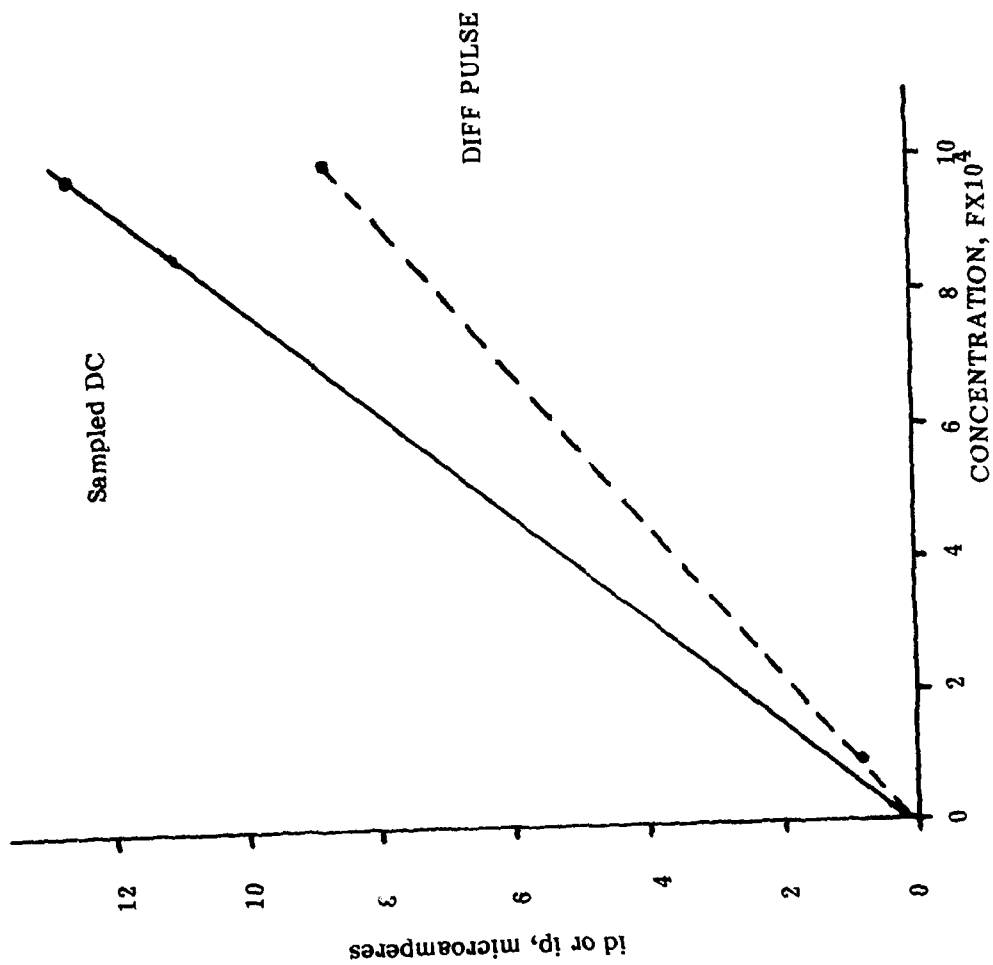


FIG. 11

CALIBRATION CURVES: 4 - NITRODIPHENYLAMINE (4 - NDPA)

id vs. C, SAMPLED DC MODE

ip vs. C, DIFF PULSE MODE

SEE FIG. 3 FOR DETAILS OF POLAROGRAPHIC CELL & DME

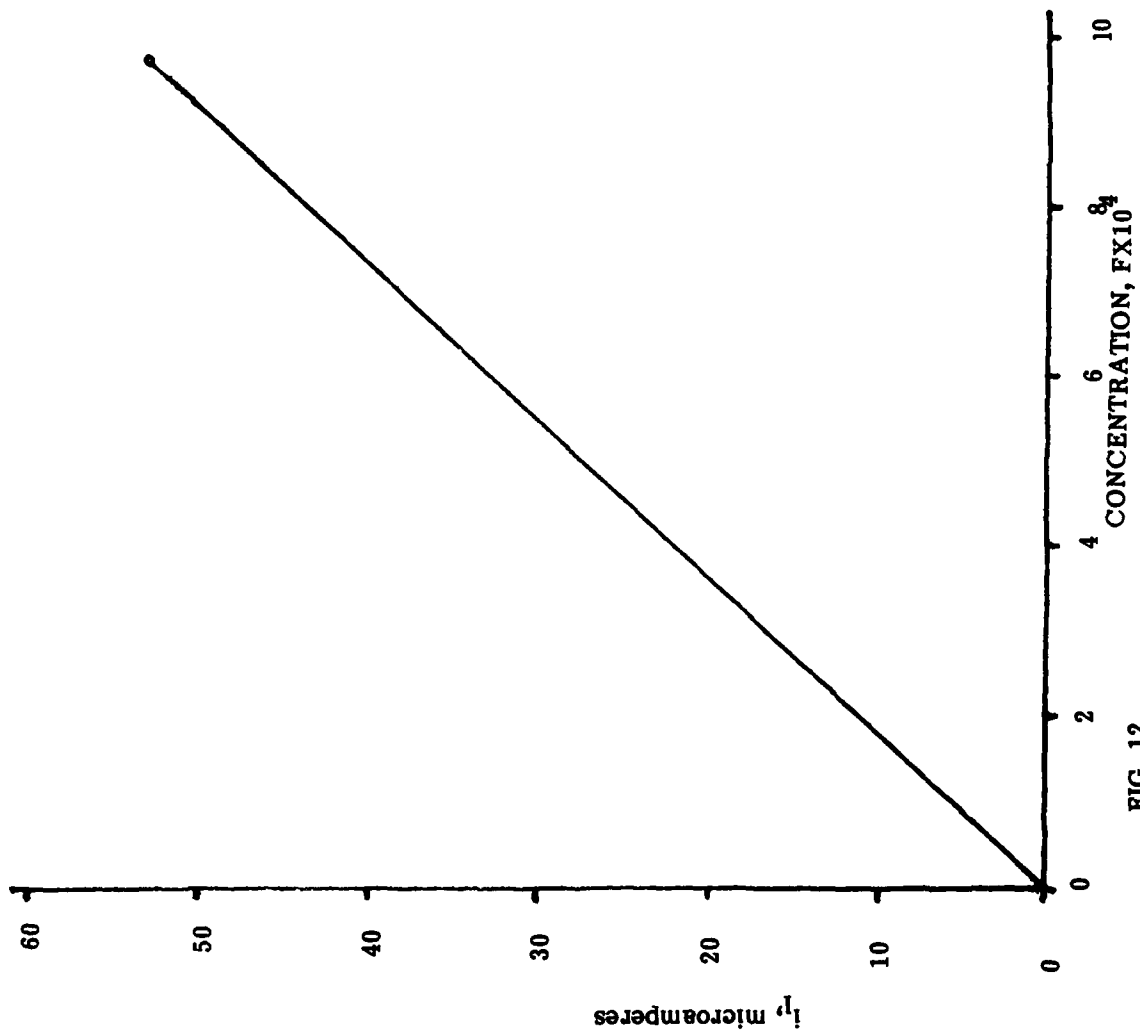


FIG. 12

CALIBRATION CURVE: 4 - NITRODIPHENYLAMINE (4 - NDPA)

i_p vs CONCENTRATION
(PULSE MODE)

0.1155 G
SOLID PROPELLANT SAMPLE. DRY METHANOL
EXTRACT REDISSOLVED IN 25 ML METHANOL.
1 ML OF METHANOL SOLUTION ADDED TO 10 ML
0.3 F LITHIUM PERCHLORATE IN METHANOL
10 GIVE SOLN. POLARO GRAPHED.

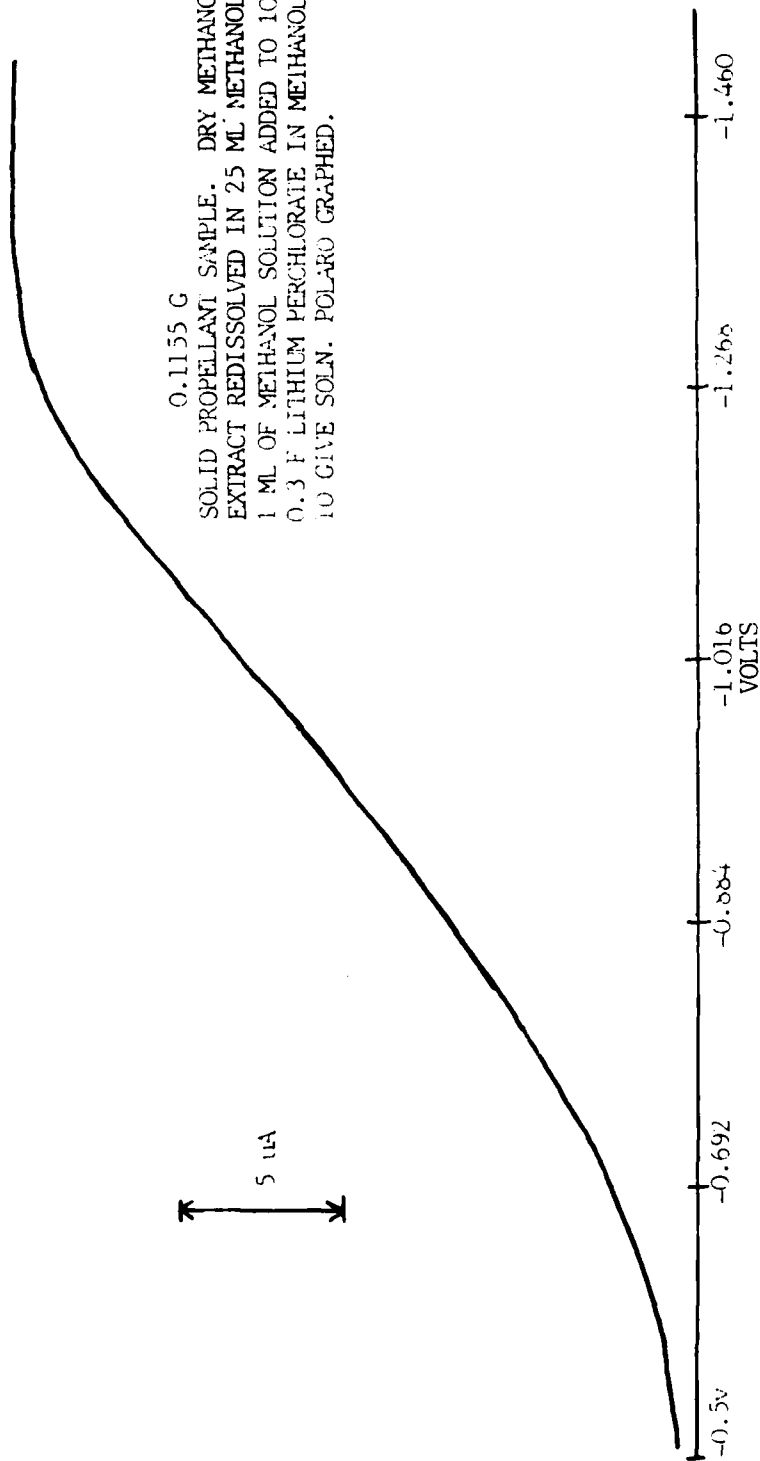


FIG 13

POLAROGRAPH OF METHANOL EXTRACT OF SOLID PROPELLANT CONTAINING 4-NDPA PULSE MODE

SEE FIG 1 FOR DETAILS OF DME & CELL

SEE FIG. 13 FOR DETAILS OF SOLN.
POLAROGRAPHED

- 1 FIRST SCAN
- 2 REPEAT SCAN

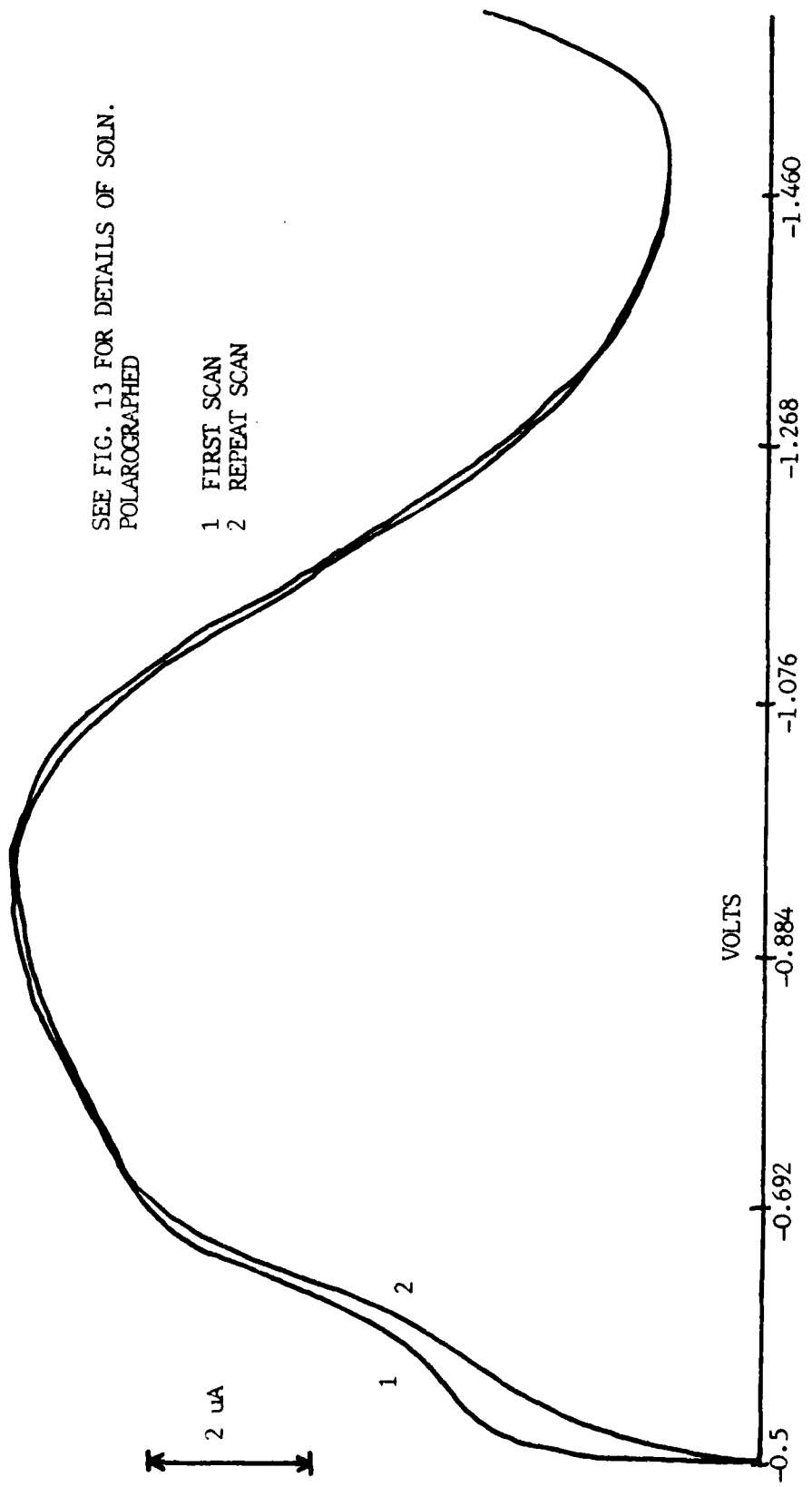


FIG. 14
POLAROGRAM OF METHANOL EXTRACT OF SOLID PROPELLANT CONTAINING 4-NDPA
DIFF PULSE MODE

SEE FIG. 1 FOR DETAILS OF DME AND CELL

REFERENCES

1. Meites, Louis, Polarographic Techniques, New York, N. Y., (Interscience-Wiley, 1965), p. 89.
2. Milner, G. W. C., The Principles & Applications of Polarography," London, Gr. Britain, (Longmans, Green and Co.,1957), p. 106.
3. Kolthoff, I. M., "Rev. Fundamentals of Polarography in Inert Organic Solvents," in Polarography 1964 Vol. I, G. J. Hills, ed., London, Gr. Britain, (MacMillan, 1965), p. 1.
4. Schaap, W. B., "Resistance Compensation in Polarography," Anal. Chem., Vol. 36, pp. 1251-58, 1964.
5. Kumar, G. P., and D. A. Pantony, " A Reference Electrode for Polarography in Organic Solvents," in Polarography 1964 Vol. II, G. J. Hills, ed., London, Gr. Britain, (MacMillan, 1965), p. 1061.
6. Hetman, Johan S., " Polarography of Explosives," Frezenius Z. Anal. Chem., Vol. 264, pp. 159-64, 1973.
7. Hetman, J. S., " Appl. of Cathode Ray Polarograph to Analysis of Explosives III. Simult. Detn. of NG and Dinitroglycol," Talanta, Vol. 5, pp. 267-71, 1950.
8. Hetman, J. S., " Polarog. Behavior of Erythritol Tetranitrate and Mannitol hexanitrate," Anal. Chim. Acta, Vol. 28, pp. 588-90, 1963.
9. Hetman, J. S., " Appl. of Cathode Ray Polarograph to Analysis of Explosives. Detn. of Mercury Fulminate," Talanta, Vol. 3, pp. 127-30, 1959.

10. Hetman, J. S., "Polarographic Behavior of Dinitrochlorohydrin and Diglycerol Tetranitrate," Talanta, Vol. 10, pp. 931-33, 1963.
11. Whitnack, Gerald C., R. D. Weaver, and H. W. Kruse, "Polarographic Behavior and Large Scale Electrolysis of Some Alkylnitrosamines," U. S. Govt. Research Report, Vol. 38, No. 22, pp. 24- , 1963.
12. Yinon, Jehuda, "Anal. of Explosives," Crit. Rev. Anal. Chem., Vol. 7, pp. 1-35, 1977.; Anal. Abstracts, Vol. 34, p. 607, 1978.
13. Bol'shakova, L. N., N. V. Pavelko, A. S. Shevchuk, V. D. Shein, and B. F. Ustovshchikov, "Polarographic Determination of Some Nitroso Compounds Used Industrially," Zh. Anal. Khim., Vol. 34, p. 564- , 1979 ; Anal. Abstracts, Vol. 37, p. 428- , 1979.
14. Wild, A. M., "Polarographic Estimation of Tetracene and Nitro-resorcinates in Single Caps Containing Both Substances," Chem. & Ind., Vol. 20, p. 819- , 1963.
15. Whitnack, G. C., "Determination of TNT in Warhead Exudates by Linear Sweep Polarography," Anal. Chem., Vol. 35, p. 970-73, 1963.
16. Sinha, S. K., and K.R.K. Rao, "Physical Methods in the Analysis of Explosives," J. Sci. Ind. Res. India, Vol. 22, p. 208- , 1963; Anal. Abstracts, Vol. 11, p. 2246- , 1964.
17. Martel, G. and M. Vignaud, "Polarographic Detn. of Explosives," Ind. Chim. Belge, Vol. 32, p. 626- , 1967; Anal. Abstracts, Vol. 15, p. 7114- , 1968.

18. Prestia, John V., "Polarography of Ordnance Compounds,"
U. S. Govt. Report Announce Index, Vol. 79, No. 24, p. 262, 1979.
USNA-EPRD-39.
19. Whitnack, Gerald C., "Applied Polarography for Analysis of
Ordnance Materials. Part 3. Field Test of NWC Digital Polarograph
and Pollution Monitoring System," U. S. Govt. Report Announce. Index,
Vol. 79, No. 13, p. 228, 1979. NWC-TP-5860-PT-3.
20. Whitnack, Gerald C., "Detn. and Monitoring of Some Organic Explosives
in Natural and Effluent Water by Single-Sweep Polarography,"
Conf. Proceedings, North American Chemical Congress 1975, Ann Arbor,
Michigan, (Ann Arbor Science Publishers, 1976) .
21. Whitnack, Gerald C., "Applied Polarography for Analysis of Ordnance
Materials. Part 1. Detn. and Monitoring of 1,2-Propyleneglycoldinitrate
in Effluent Water by Single-Sweep Polarography," U. S. Govt. Report
Announce. Index, Vol. 76, No. 19, p. 174, 1976.
22. Jarrel, James R., and Yvon P. Carignan, "Polarographic Study of
Nitrate Esters. I. Reduction of Pentaerythritol Mononitrate,"
U. S. Govt. Res. Develop. Rep., Vol. 69, No. 19, p. 50, 1969.
23. Frey, Max, "Recent Methods in the Investigation of Propellants.
III. Prediction of the Life of Nitrate Ester Propellants,"
Explosivstoffe, Vol. 15, pp. 97-105, 1967
24. Riganti, V., S. Locchi, and R. Curti, "Oscillopolarography of
Explosive Nitro Derivatives," Rass. Chim, Vol. 21, No. 1, pp. 3-8,
1969.

25. Holland, A. R., and A. G. S. Benahm, " The Continuous Polarographic Determination of Small Amounts of Nitroglycersine in Plant Effluent," Analyst, Vol. 93, pp. 817-820, 1968
26. Parry, E. P., and R. A. Osteryoung, "Evaluation of Analytical Pulse Polarography," Anal. Chem., Vol. 37, pp. 1634-37, 1965.
27. Zuman, Petr, " Some Techniques in Organic Polarography," in Advances in Analytical Chemistry and Instrumentation, Vol. 2, C. N. Reilley, ed., New York, N. Y., (Interscience-Wiley, 1963), pp. 219-53.
28. Fisher, Dale J., "Advances in Instrumentation for DC Polarography and Coulometry," in Advances in Anal. Chem. and Instrumentation, Vol. 10, Electroanalytical Chemistry. H. W. Nurnberg, ed., pp. 1-158, 1974.

1981 USAF - SCEE Summer Faculty Research Program

Sponsored by the

Air Force Office for Scientific Research

Conducted by the

Southeastern Center for Electrical Engineering Education

Final Report

The Impact of Background Characteristics

On OAP Scores:

Developing Baseline Data

Prepared By: Chris W. Eskridge, Ph.D.
Academic Rank: Assistant Professor
Department: Department of Criminal Justice
University: University of Nebraska
Research Location: Leadership and Management Development Center
Directorate of Research and Applications
Maxwell Air Force Base AL 36112
USAF Research Colleague: Major Lawrence O. Short, Ph.D.
Date: August 14, 1981
Contract No: F49620-79-C-0038

THE IMPACT OF BACKGROUND CHARACTERISTICS

ON OAP TEST SCORES:

DEVELOPING BASELINE INFORMATION

by

Chris W. Eskridge, Ph.D.

ABSTRACT

In an attempt to enhance the validity of the Organizational Assessment Package (OAP) as an organizational assessment instrument, this project sought to determine the nature and extent of the variance in OAP scores that could be explained due to the impact of background characteristic variables, and to develop standardized background test score coefficients to control for the impact of such variables. To achieve this end, the data were subjected to a zero order correlation analysis, an eta² analysis, a breakdown analysis of variance, and a multiple classification analysis.

It was found that background characteristic variables accounted for a significant amount of variance in OAP scores. When controlling for the impact of background characteristics, OAP scores tended to decrease slightly in size. It was additionally found that background information variables accounted for a relatively large portion of the variance in period of time change scores. When controlling for such background factors, most OAP scores still increased over time, but at a reduced rate. These findings emphasize the need and usefulness of the standardized background test score coefficients for both consulting and evaluation purposes.

ACKNOWLEDGEMENTS

The author wishes to express his gratitude to the Air Force Systems Command, the Air Force Office of Scientific Research, the Southeastern Center for Electrical Engineering, and the staff of the Research and Analysis Directorate of the Leadership and Management Development Center, Maxwell Air Force Base, Alabama, for a rewarding summer of research activity. Special thanks and appreciation is extended to:

Col Guy H. Winstead, Jr.
Lt Col David Wilkerson
Major Lawrence O. Short
Captain Jeffrey S. Austin
Captain Janice Hightower
Lt Daniel Salvino
CMSgt Frank Branham

CMSgt Judith Vermila
CMSgt Al Snider
SMSgt David W. Hubbard
MSgt Mike Rehberg
TSgt Gerald Wheeler
Sgt George Buchanan
Ms. Alice LaPorte

Mrs. Patsy Beale

TABLE OF CONTENTS

- I. INTRODUCTION
- II. OBJECTIVES
- III. METHODOLOGY
 - Research Design
 - Variables
 - Procedures
 - Sample
- IV. ANALYSIS AND DISCUSSION
 - Correlation Analysis
 - Breakdown Analysis of Variance
 - Eta² Analysis
 - Multiple Classification Analysis
 - Standardized Coefficients
 - Period in Time Trends
 - OAP Score Variance
 - Application of the Standardized Coefficients to the Present Data Set
- V. SUMMARY AND RECOMMENDATIONS
- VI. REFERENCES
- VII. APPENDIX
 - Tables
 - 1 - Background Information Items
 - 2 - Raw Data Dependent Variable Mean Score
 - 3 - Background Item Frequencies
 - 4 - Zero Order Correlations: Pre Test Data
 - 5 - Zero Order Correlations: Post Test Data
 - 6 - Analysis of Variance Summary Table:
 - Pre Test Data - Age
 - 7 - Analysis of Variance Summary Table:
 - Pre Test Data - Gender
 - 8 - Analysis of Variance Summary Table:
 - Pre Test Data - Pay Grade

- 9 - Analysis of Variance Summary Table:
Pre Test Data - Years in the Air Force
- 10 - Analysis of Variance Summary Table:
Pre Test Data - Race
- 11 - Analysis of Variance Summary Table:
Pre Test Data - Level of Education
- 12 - Analysis of Variance Summary Table:
Pre Test Data - NCO PME
- 13 - Analysis of Variance Summary Table:
Pre Test Data - CO PME
- 14 - Analysis of Variance Summary Table:
Pre Test Data - Months at Present Station
- 15 - Analysis of Variance Summary Table:
Pre Test Data - Supervisory Responsibilities
- 16 - Analysis of Variance Summary Table:
Pre Test Data - Supervisor Writes Reports
- 17 - Analysis of Variance Summary Table:
Pre Test Data - Work Group Size
- 18 - Analysis of Variance Summary Table:
Pre Test Data - Usual Work Schedule
- 19 - Analysis of Variance Summary Table:
Pre Test Data - Use of Group Meetings
- 20 - Analysis of Variance Summary Table:
Pre Test Data - Frequency of Group Meetings
- 21 - Analysis of Variance Summary Table:
Post Test Data - Age
- 22 - Analysis of Variance Summary Table:
Post Test Data - Gender
- 23 - Analysis of Variance Summary Table:
Post Test Data - Pay Grade
- 24 - Analysis of Variance Summary Table:
Post Test Data - Years in The Air Force
- 25 - Analysis of Variance Summary Table:
Post Test Data - Race
- 26 - Analysis of Variance Summary Table:
Post Test Data - Level of Education

- 27 - Analysis of Variance Summary Table:
Post Test Data - NCO PME
- 28 - Analysis of Variance Summary Table:
Post Test Data - CO PME
- 29 - Analysis of Variance Summary Table:
Post Test Data - Months At Present Station
- 30 - Analysis of Variance Summary Table:
- Post Test Data - Supervisory Responsibilities
- 31 - Analysis of Variance Summary Table:
Post Test Data - Supervisor Writes Performance Reports
- 32 - Analysis of Variance Summary Table:
Post Test Data - Work Group Size
- 33 - Analysis of Variance Summary Table:
Post Test Data - Usual Work Schedule
- 34 - Analysis of Variance Summary Table:
Post Test Data - Use of Group Meetings
- 35 - Analysis of Variance Summary Table:
Post Test Data - Frequency of Group Meetings
- 36 - Eta Squared Summary Table: Job Enrichment Needs
- 37 - Eta Squared Summary Table: Task Autonomy
- 38 - Eta Squared Summary Table: Advancement/Recognition
- 39 - Eta Squared Summary Table: Perceived Productivity
- 40 - Eta Squared Summary Table: Job Satisfaction
- 41 - Eta Squared Summary Table: Perceived Supervisor Capacity
- 42 - Eta Squared Summary Table: Organizational Climate
- 43 - MCA Coefficient Summary Table: Job Enrichment Needs
- 44 - MCA Coefficient Summary Table: Task Autonomy
- 45 - MCA Coefficient Summary Table: Advancement/Recognition
- 46 - MCA Coefficient Summary Table: Perceived Productivity
- 47 - MCA Coefficient Summary Table: Job Satisfaction
- 48 - MCA Coefficient Summary Table: Perceived Supervisor Capacity
- 49 - MCA Coefficient Summary Table: Organizational Climate
- 50 - Correlation Summary Table: Longitudinal Changes in OAP Scores
- 51 - MCA Summary Table: Composite R Squared
- 52 - Analysis of Variance Summary Table: Eta Squared and MCA Derived
R Squared
- 53 - Corrected Dependent Variable Mean Scores
- 54 - Impact of Standardized Coefficients Upon Present OAP Scores

Figures

- 1 - Within Group Variance: Pre Test Data - Age
- 2 - Within Group Variance: Pre Test Data - Gender
- 3 - Within Group Variance: Pre Test Data - Pay Grade
- 4 - Within Group Variance: Pre Test Data - Years in The AF
- 5 - Within Group Variance: Pre Test Data - Race
- 6 - Within Group Variance: Pre Test Data - Level of Education
- 7 - Within Group Variance: Pre Test Data - NCO PME
- 8 - Within Group Variance: Pre Test Data - CO PME
- 9 - Within Group Variance: Pre Test Data - Months at
Present Station
- 10 - Within Group Variance: Pre Test Data - Supervisor
Responsibilities
- 11 - Within Group Variance: Pre Test Data - Supervisor Writes Reports
- 12 - Within Group Variance: Pre Test Data - Work Group Size
- 13 - Within Group Variance: Pre Test Data - Usual Work Schedule
- 14 - Within Group Variance: Pre Test Data - Use of Group Meetings
- 15 - Within Group Variance: Pre Test Data - Frequency of Group
Meetings

I INTRODUCTION

This research effort drew upon data collected by the United States Air Force Leadership and Management Development Center (LMDC), and particularly its Directorate for Management Consultation (DMC). The mission of DMC is that of a consulting resource for Air Force managers. In particular, managers are encouraged to call upon DMC for background information and assistance in solving organizational problems. Such problems include low levels of productivity and morale, poor communications, organizational conflict, etc. The typical mode of operations is for DMC to deploy a consulting team at the invitation of a commander to a particular location. On the first visit, the consulting team gathers data to identify and diagnose the causes of problems based on two methods. First, the consultants may make personal observations and conduct interviews with key personnel on-site. Second, a diagnostic survey questionnaire called the Organizational Assessment Package (OAP), developed jointly by LMDC and the Human Resources Laboratory (Hendrix and Halverson; 1979) is administered to a sample of personnel in the unit. The consultants then return to LMDC and the data are analyzed. Using the results from the OAP, along with other data sources, the consulting teams develop a provisional diagnosis and plan a return visit to the site usually within 6-8 weeks following the initial visit. During the second visit a number of things may happen. First, the results of the OAP for their work groups are almost always fed back to the supervisors, and to various levels. Occasionally, feedback is presented to entire work groups in a one-on-one group fashion. In addition to data feedback, the consultants work with problem groups and develop management action plans to help solve their problems. In some cases, specific organizational development techniques may be used as deemed necessary by the consultants. Approximately 12 to 24 weeks following this visit, the OAP is again administered as a follow-up in an attempt to determine results of the visit.

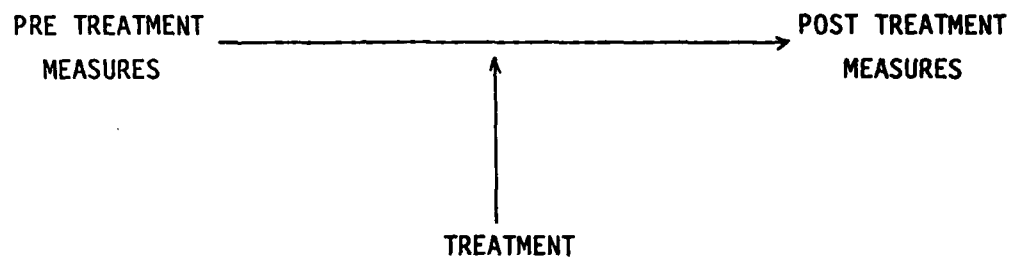
II OBJECTIVES

This research effort sought to identify the nature and extent of the variance in OAP scores that could be explained due to the impact of background characteristics, and to identify types of persons who scored the OAP in certain ways at given points in time, and over a period of time. Types of persons upon whom the DMC consultants appear to have their greatest impact and their least impact were to be identified. With this information, standardized OAP coefficients were to be developed, which, when applied in the future, would enhance the construct validity of the OAP as an organizational assessment instrument.

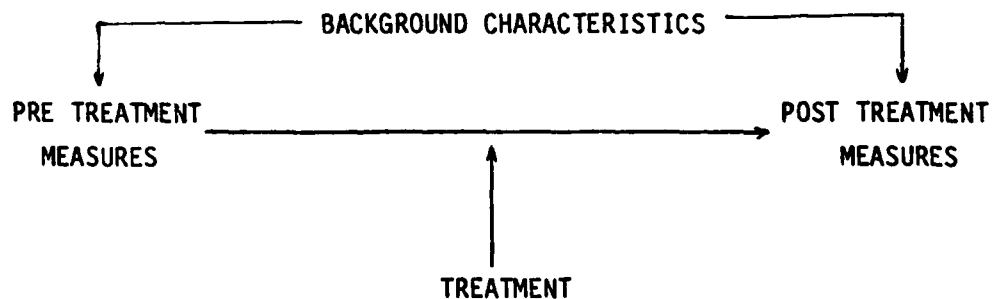
III METHODOLOGY

Research Design and Limitations

As Conlon (1980) has noted, the experimental design implicit in the present data set is a multiple treatment group, panel design model of the following form:



The pre treatment measures in this instance are the pre test OAP scores, the post treatment measures are the post test OAP scores, and the treatment is the DMC consultant efforts. As previously noted, this present study sought to ascertain and isolate the impact of background characteristics upon pre test and post test OAP scores. The panel design would be modified as follows:



Such a design possesses several tenants (Conlon, 1980; Cook and Campbell, 1979; Markus, 1979). In particular, panel designs require uniform treatment. However, such is clearly not the case in this present study. Indeed, it appears as if different consultants use different treatment techniques in different situations with different personnel. Furthermore, there is no guarantee that those who took the post test OAP survey received any treatment at all, perhaps having taken the survey on one of their first days on base. Panel designs require longitudinally constant populations. A panel design does not necessarily mandate a case by case tracking. Indeed, a random selection technique could be used to identify those to take the pre treatment test and the post treatment test, as long as all persons received the same treatment and as long as the population remains constant. Neither was the case in this instance. Consequently, there is no guarantee whatsoever that those who took the pre test OAP survey were of the same group who received the treatment and later took the post test OAP survey. Of even greater concern, as previously noted, is the fact that those who took the post test OAP survey may not have even received the treatment. These are very serious drawbacks, and in the context of a panel design, serve to taint the entire data set.

Many have noted the potential presence of a number of extraneous, intervening situations and circumstances in addition to background characteristics, that may be causing variation in the OAP scores (Campbell and Stanley, 1973). While little can be done in this present effort to control for these intervening variables, their presence must be noted, as follows:

1. The very fact that respondents know they are being tested tends to bias responses.

2. Personal, cyclical situation variables such as family environment, financial position, personal and family health, etc., may serve to bias responses.

3. Local, state, national and international events such as the Iranian hostage crisis, assassination attempts, oil price increases, interest rate hikes, etc., may serve to bias responses.

4. Respondant's knowledge of the fact that DMC consultants are present on the base may serve to bias responses.

5. Respondents' knowledge of the fact that DMC consultants have worked with base personnel may condition respondents and cause them to respond independent of whether an actual change has occurred or not.

6. There may be a tendency on the part of respondents to skew OAP responses in the direction respondents perceive commanding officers' desire.

7. Work group/division/base morale may be a low ebb yet on the verge of improving, independent of consultant team efforts.

8. Changes in OAP scores may be reflective of longitudinal, cyclical morale patterns on which consulting teams have little impact.

9. Changes in OAP scores may be reflective of a general turnover effect, as those with the lower scores are replaced by newer recruits who have not developed derisive attitudes. In other words, it may well be that changes in OAP scores may be reflective of longitudinal turnover patterns upon which consulting teams may have little impact.

10. Changes in OAP scores may be reflective of instrument decay. It can be reasonably assumed that a number of the above, as well as other potential intervening factors, are normally distributed within the sample, thus causing no significant change in the mean scores (i.e., personal situation variables, news events). However, there are other potential intervening factors that, in all likelihood, skew the data in one direction or another.

In summary, given the limitations of this present data set, a more accurate description of the research design in this instance is a descriptive, non-experimental, panel-type design. The design is descriptive in that the present study sought only to identify and clarify the nature and extent of existing relationships, and was not designed to focus upon discussions of causality. It is non-experimental, not only in that random assignment was lacking in the administration of both the pre test and post test measures, but that individuals who took the pre test and individuals who took the post test may have come from totally different populations. Furthermore, individuals who took the post test and individuals who received the treatment may have come from different populations. It is a panel-type design in that there is a semblance of a panel design (i.e., pre treatment measure, treatment, post treatment measure), though several of the basic aspects of the design are violated (i.e., uniform treatment, longitudinally stable populations).

Variables

As previously noted, the purpose of this present research effort was to ascertain the nature and extent of the variance in the OAP scores that can be explained due to the impact of background variables. Background information items served as the independent variables of interest, and were divided into two groups; personal characteristics and organizational characteristics. These groups are clearly articulated in Table 1 along with a breakdown of each independent variable by category. The personal characteristic variables included age, gender, pay grade, years in the Air Force, race, level of education, and level of professional military education. Organizational characteristic variables included months at present station, for how many people do you write performance reports (supervisory responsibilities), does your supervisor write your performance reports (supervisory reports), work requires you to primarily work with how many people (work group size), usual work schedule, group meetings used to solve problems and set goals (use of group meetings), and frequency of group meetings.

In a previous study, twenty-one orthogonally rotated factors were extracted during a factor analysis of the 149 OAP attitudinal items which appear on the OAP assessment instrument (Hendrix and Halverson, 1979). Seven of these factors were selected as dependent variables for the present study, as follows; job enrichment needs, task autonomy, advancement/recognition, perceived productivity, job satisfaction, perceived supervisor capacity, and organizational climate.* These dependent variables were scored on a scale from 1 to 7. A high score would indicate the following.

1. Job Enrichment Needs - the respondent has a high job enrichment need or desire.
2. Task Autonomy - the current work assignment has a highly acceptable level of autonomy or freedom to the respondent.
3. Advancement/Recognition - the respondent feels that advancement and recognition is forthcoming at a highly acceptable pace and rate.
4. Perceived Productivity - the respondent feels that there is a high level of effectiveness or productivity in his work group.

* Two of the dependent variables, perceived supervisor capacity and organizational climate, were actually additive combinations of several of the original factors. Perceived supervisor capacity was the sum of management-supervision plus supervisory communication climate, divided by two. Organizational climate was the sum of organizational communications climate plus general organizational climate, divided by two.

5. Job Satisfaction - the respondent has a high level of job satisfaction.

6. Perceived Supervisor Capacity - the respondent feels that his supervisor has a great capacity for being a supervisor.

7. Organizational Climate - the respondent feels that there is a highly acceptable climate within the organization.

Of particular interest is the fact that OAP scores have tended to increase slightly from pre test to post test, due at least partially, it is thought, to the DMC consultant treatment. As the data in Table 2 indicate, there has been a 3.54% increase in organizational climate scores, a .36% increase in perceived supervisory capacity scores, a 2.68% increase in job satisfaction scores, a 1.37% increase in perceived productivity scores, a 1.73% increase in advancement/recognition scores, and a 4.66% increase in task autonomy scores. The only dependent variable which has decreased from pre test to post test is job enrichment needs, which shows an overall .5% pre to post reduction. This research effort sought to determine how much of this change is due to the impact of background characteristic variables.

Procedure

In an attempt to clarify the nature and extent of the impact of the independent variables (background characteristic items) on the dependent variables (OAP scores), the data were subjected to a three phase analysis.

Phase One involved a point in time identification of the nature and extent of the variability in both pre test and post test OAP scores that may be explained due to the impact of background variables from a zero order linear perspective, as well as a zero order linear plus non linear perspective. Types of persons who score the OAP in certain ways were identified. Phase One involved a zero order correlation analysis followed by a breakdown analysis of variance and an eta² analysis.

Phase Two involved the development of standardized test score coefficients, based on the data generated in Phase One. Through the use of such standardized coefficients, the OAP scores can become more accurate assessments of the organization, and less a measure of demographic variation. In as much as the OAP is designed to assess organizations, the development of standardized test coefficients which help control the impact of demographics on OAP scores, can serve to enhance the construct validity of the OAP as an organizational assessment instrument. Phase Two also involved a point in

time identification of the nature and extent of the variability in both pre test and post test OAP scores that may be explained due to the impact of background variables from a linear perspective, controlling for independent variable interaction. Phase Two involved the use of multiple classification analysis.

Phase Three involved the identification of the nature and extent of the variability in the period of time (pre test to post test) OAP scores that can be explained due to the impact of background variables. Types of persons who tend to score the OAP in certain ways over time were identified. Types of persons upon whom consulting team appear to be having their greatest impact and their least impact were distinguished. Phase Three involved a further extrapolation of the data generated in the multiple classification analysis employed in Phase Two.

Sample

Data were collected by Air Force consultants who administered the OAP at selected Air Force installations to all available personnel. The pre test data set consisted of 77055 cases and the post test data set consisted of 23547 cases. Background information frequencies for both the pre test sample and the post test sample are found in Table 3.

IV ANALYSIS AND DISCUSSION

Correlation Analysis

Zero order correlation analyses were completed on both the pre test and post test data. Due to the large sample size, virtually all non-zero coefficients were found to be statistically significant at the .01 level, and most beyond .0001. The pre test data zero order categorical typologies articulated below are drawn from information in Table 4. Note that these categorical typologies are at the zero order, and consequently do not account for independent variable interaction. For an iteration of each variable, category by category, see Table 1.

1. Persons who possess higher job enrichment needs are more likely to be older ($R = .1561$), white (.1115), females (.0549), who are at a higher pay grade (.1291), with more years in the Air Force (.1693), who possesses a higher level of education (.2448), a higher level of professional military education among NCOs (.1624) and a lower level of professional military education among COs (-.0150), and more months at their present station (.1563), who work in larger work groups (.0561), on stable, day shift hours (-.0827), who supervise more people (.1172), whose own supervisor writes the respondent's performance report (-.0177), and work in organizations where group meetings are held more frequently (.0803), and are more frequently used to solve problems and set goals (.0885), than those persons who possess lower job enrichment needs.

2. Persons who report that their job possesses a higher level of task autonomy are more likely to be older (.3361), white (.0387), females (.0479), who are at a higher pay grade (.2669), with more years in the Air Force (.2687), who possess a higher level of education (.1852), a higher level of professional military education (NCO .2296; CO .0830), and more months at their present station (.1897), who work in smaller work groups (-.0190), and stable, day shift hours (-.2703), who supervise more people (.1563), whose own supervisor writes the respondent's performance report (-.1551), and work in organizations where group meetings are held more frequently (.1520), and are more frequently used to solve problems and set goals (.2280), than those persons who report that their job possesses a lower level of task autonomy.

3. Persons who feel that advancement and recognition are forthcoming at an acceptable rate are more likely to be older (.0347), non-white (-.0181), males (-.0811), who are at a higher pay grade (.0138), with more years in the Air Force (.1281), who possess a higher level of education (.0775), a higher level of professional military education (NCO .2373; CO .0093), and fewer months at their present station (-.0499), who work in larger work groups (.1275), on stable, day shift hours (-.2703), who supervise more people (.2209), whose own supervisor writes the respondent's performance report (-.1766), and work in organizations where group meetings are held more frequently (.2285), and are more frequently used to solve problems and set goals (.3270), than those who feel that advancement and recognition are forthcoming at a less acceptable rate.

4. Persons who possess higher perceptions of work group productivity are more likely to be older (.1798), white (.0251), females (.0231), who are at a higher pay grade (.1037), with more years in the Air Force (.1285), who possess a higher level of education (.0655), a higher level of professional military education (NCO .1369; CO .0170), and more months at their present station (.0936), who work in larger work groups (.0624), on stable, day shift hours (-.1028), who supervise more people (.1000), whose own supervisor writes the respondent's performance report (-.1322), and work in organizations where group meetings are held more frequently (.1751), and are more frequently used to solve problems and set goals (.2669), than those persons who possess lower perceptions of work group effectiveness.

5. Persons who possess higher levels of job satisfaction are more likely to be older (.2811), white (.0329), females (.0591), who are at a higher pay grade (.1783), with more years in the Air Force (.1556), who possess a higher level of education (.0995), a higher level of professional military education (NCO .1880; CO .0850), and more months at their present station (.1019), who work in larger work groups (.0512), on stable, day shift hours (-.2430), who supervise more people (.1077), whose own supervisor writes the respondent's performance report (-.1563), and work in organizations where group meetings are held more frequently (.1941), and are more frequently used to solve problems and set goals (.3020), than those persons who possess lower levels of job satisfaction.

6. Persons who possess higher perception of their supervisor's supervisory capacity are more likely to be older (.0511), non-white (-.0026), females (-.0105), who are at a lower pay grade (-.0385), with fewer years in the Air Force (-.0543), who possess a higher level of education (.0127), a higher level of professional military education (NCO .0970; CO .0372), and fewer months at their present station (-.0872), who work in larger work groups (.0572), on stable, day shift hours (-.0593), who supervise more people (.0608), whose own supervisor writes the respondent's performance report (-.1578), and work in organizations where group meetings are held more frequently (.2518), and are more frequently used to solve problems and set goals (.3789) than those persons who possess lower perceptions of their supervisor's supervisory capacity.

7. Persons who report that their organization has a more acceptable climate are more likely to be older (.2020), non-white (-.0151), females (-.0151), who are at a higher pay grade (.0693), with more years in the Air Force (.0572), who possess a higher level of education (.0654), a higher level of professional military education (NCO .1527; CO .0583), and more months at their present station (.0148), who work in larger work groups (.0459), on stable, day shift hours (-.1248), who supervise more people (.0769), whose own supervisor writes the respondent's performance report (-.0982), and work in organizations where group meetings are held more frequently (.1565), and are more frequently used to solve problems and set goals (.2645) than those who report that their organization has a less acceptable climate.

While the extent of the relationships were found to vary slightly from pre test to post test (compare the correlation coefficients from Table 4 and Table 5), zero order correlations drawn from the post test data revealed the same general typologies as those for the pre test data.* In other words, it appears as if the same types of people with the same background characteristics tend to score the OAP survey in the same general way at any given point in time. It should be noted, however, that while the extent of the relationships were found to be relatively constant, in the absolute sense, the zero order correlations between background characteristics and OAP scores tend to be somewhat larger in the post test data set than in the pre test data set. This would indicate that background characteristics account for a slightly larger amount of the variance in post test scores than in pre test scores.

*The only difference found in the nature of the typologies was in regards to perceived supervisor capacity. In the pre test data, those who possess higher perceptions of their supervisor's supervisory capacity were more likely to be non-whites (-.0026) at a lower pay grade (-.0385), with fewer years in the Air Force (-.0543). On the post test data, those who possess higher perceptions of their supervisor's supervisory capacity were more likely to be whites (.0042), at a higher pay grade (.0597), with more years in the Air Force (.0290).

Breakdown Analysis of Variance

The correlation analysis shed some light on the general nature and extent of the relationships between the background variables and OAP scores. However, the Pearson correlation coefficient can only identify linear relationships. It was felt that many of the independent variables were related to the dependent variables in a curvilinear factor. To test this hypothesis, and to clearly articulate the existence of any such relationship, a breakdown analysis, using an analysis of variance statistical technique to ascertain the significance of the relationship, was used. Figures 1 through 15 are the primary output of the breakdown analysis, with supporting data developed from the analysis of variance detailed in Tables 6 through 20. Figures 1 through 15 utilize only pre test data. Virtually identical figures were developed utilizing the post test data, but were not included in this report to avoid redundancy.*

Figures 1 through 15 clearly illustrate the existence of a multitude of curvilinear relationships. The data in Tables 6 through 20 reveal the fact that statistically, the relationships illustrated in Figures 1-15 are virtually all significant at the .0001 level. In regard to these significant level figures, it should be noted that the F-test used to derive the levels of significance only captured linear relationships. Consequently, they become conservative estimates. If the presence of linear plus non linear relationships were statistically tested, the levels of significance would have been much higher.

A tremendous amount of information is contained in Figures 1 through 15, a complete review of which is beyond the scope of this piece. There are, however, a number of particularly striking findings of interest.

1. From Figure 1 it can be seen that there is a concave, curvilinear relationship between age and perceived supervisor capacity, with the extremes being 20 years of age or less (+.28 above the mean), 51 years of age or more (+.27), and 21 to 25 years of age (-.21). In other words, those

*Post test analysis of variance data tables have been included in the Appendix (Tables 21 through 35) to document the fact that the relationships identified in the pre test data also appear in the post test data. The F scores for post test were smaller than those for the pre test due to the smaller sample size of the post test data base (77055 versus 23547). The levels of significance for each relationship, however, were all virtually identical ($p < .0001$).

who are 20 years of age or less report having the most positive perception of their supervisors capacity, followed by a decline in this perception to the point where those who are 21-25 years of age report having the most negative perception, followed by a general improvement in their perceptions to the point where those 51 years of age or more, report having a very positive perception.

2. From Figure 1 it can be seen that there is a convex, curvilinear relationship between age and advancement/recognition, with the extremes being 20 years of age or less (-.25), 51 years of age or more (-.44), and 36 to 40 years of age. In other words, those who are 20 years of age or less feel that advancement and recognition is not forthcoming at an acceptable rate. This is followed by a general improvement in these feelings to the point where those in the 36 to 40 age category feel that advancement and recognition is forthcoming at an acceptable rate, and then falls off dramatically to the point where those 51 years of age or more, who feel very strongly that advancement and recognition is not forthcoming at an acceptable rate.

3. From Figure 2 it can be seen that there is a direct positive linear relationship between gender and all OAP scores. Males score below the mean and females score above the mean on all OAP items, with the exception of advancement/recognition. In the latter case, males score above the mean (+.10) while females score below the mean (-.25). In other words, males apparently feel that advancement and recognition is forthcoming at a more acceptable rate than do females. On the other hand, females have higher job enrichment needs, report a more acceptable level of task autonomy, have a higher perception of their work group productivity level, a higher level of job satisfaction, a higher perception of their supervisors' capacities, and a more positive perception of the organizational climate than do males.

4. From Figure 4 it can be seen that there is a concave, curvilinear relationship between years in the Air Force and perceived supervisor capacity, with the extremes being less than one year in the Air Force (+1.04), more than eight years in the Air Force (+.08), and three to four years in the Air Force (-.37). In other words, those who have less than one year in the Air Force report having the most positive perception of their supervisors capacity, followed by a general decline in perceptions to the point

where those who have three to four years in the Air Force report having the most negative perception, followed by a general improvement in perceptions to the point where those with eight years or more in the Air Force report having a positive reception.

5. From Figure 4 it can be seen that there is a concave, curvilinear relationship between years in the Air Force and job satisfaction, with the extremes being less than one year in the Air Force (+.03), more than eight years in the Air Force (+.30), and three to four years in the Air Force (-.44). In other words, those who have less than one year in the Air Force report having a high level of job satisfaction, followed by a general decline in perceptions to the point where those who have three to four years in the Air Force report having the lowest level of satisfaction, followed by a general improvement in job satisfaction level to the point where those with eight years or more in the Air Force report having the highest level of job satisfaction.

6. From Figure 4 it can be seen that there is a concave, curvilinear relationship between years in the Air Force and organizational climate, with the extremes being less than one year in the Air Force (+.37), more than eight years in the Air Force (+.22), and three to four years in the Air Force (-.46). In other words, those who have less than one year in the Air Force report having the most positive perception of the organizational climate, followed by a general decline in perceptions to a point where those who have three to four years in the Air Force report having the most negative perception of the organizational climate, followed by a general improvement in perceptions to the point where those with eight years or more in the Air Force report having a very positive perception.

7. From Figure 5 it could be seen that there is a direct positive linear relationship between race and job enrichment needs. Non-whites score below the mean (-.26) while whites score above the mean (+.11) in regards to job enrichment needs. In other words, non-whites apparently have less job enrichment needs than do whites.

8. From Figure 5 it can be seen that there is a direct positive linear relationship between race and job satisfaction. Non-whites score below the mean (-.09) while whites score above the mean (+.05) in regard to job satisfaction. In other words, whites apparently have a higher level of job satisfaction than do non-whites.

9. From Figure 6 it can be seen that there is a concave, curvilinear relationship between level of education and organizational climate, with the extremes being those with less than a high school degree (+.65), those with Doctorates (+.57), and those with less than two years of college (-.17). In other words, those with less than a high school degree report having the most positive perception of the organizational climate, followed by a general decline in perceptions to the point where those with less than two years of college report having the most negative perception of the organizational climate, followed by a general improvement in perceptions to the point where those with Doctorates report having very positive perceptions.

10. From Figure 6 it can be seen that there is a concave, curvilinear relationship between the level of education and perceived supervisor capacity, with the extremes being those with less than a high school degree (+.38), those with Doctorates (+.32), and those with less than two years of college (-.16). In other words, those with less than a high school degree report having the most positive perception of their supervisor's capacity, followed by a general decline in perceptions to a point where those with less than two years of college report having the most negative perception, followed by a general improvement in perceptions to the point where those with Doctorates report having very positive perceptions.

11. From Figure 6 it can be seen that there is a concave, curvilinear relationship between level of education and job satisfaction, with the extremes being those with less than a high school degree (+.36), those with Doctorates (+.63), and those with a high school degree only (-.16). In other words, those with less than a high school degree report having a high level of satisfaction, followed by a general decline in perceptions to the point where those with a high school degree only report having the lowest level of job satisfaction, followed by a general improvement in job satisfaction level to the point where those with Doctorates report having the highest level of job satisfaction.

12. From Figure 6 it can be seen that there is a concave, curvilinear relationship between level of education and task autonomy, with the extremes being those with less than a high school degree (+.20), those with Doctorates (+.98), and those with a high school degree only (-.24). In other words, those with less than a high school degree feel that their present job has a high level of autonomy, followed by a general decline in this feeling

to the point where those with a high school degree only, report having the lowest task autonomy score, followed by a rise in task autonomy feelings to the point where those with Doctorates report having the highest level of task autonomy.

13. From Figure 6 it can be seen that there is a concave, curvilinear relationship between level of education and perceived productivity, with the extremes being those with less than a high school degree (+.04), those with Doctorates (+.29), and those with a high school degree only (-.10). In other words, those with less than a high school degree feel that their work group is relatively productive, followed by a general decline in this feeling to the point where those with a high school degree only report having the lowest perceived productivity score, followed by a rise in perceived productivity level to the point where those with Doctorates report having the highest level of perceived productivity.

14. From Figure 7 it can be seen that there is a direct, positive linear relationship between NCO professional military education and all OAP scores. In other words, generally, the higher the level of NCO professional military education, the higher the job enrichment needs, the more acceptable the level of task autonomy, the stronger the feelings that advancement and recognition is forthcoming at an acceptable rate, the higher the perception of their work group productivity level, the higher the level of job satisfaction, the higher the level of perceived supervisor capacity, and the more positive the perception of the organizational climate.

15. From Figure 8 it can be seen that there is a very clear and distinct reduction in all OAP scores among those CO's who have completed intermediate service school.

16. From Figure 9 it can be seen that there is a concave, curvilinear relationship between months at present station and perceived supervisor capacity, with the extremes being less than one month at the present assignment (+1.13), 36 months or more at the present assignment (-.02), and 18 to 24 months at the present assignment (-.22). In other words, those with less than one month at their present assignment report having the most positive perception of their supervisor's capacity, followed by a decline in perceptions to the point where those with 18 to 24 months at the present assignment report having the most negative perception, followed by a small improvement in perceptions to the point where those with 36 months or more at their present station who still score slightly below the mean.

17. From Figure 9 it can be seen that there is a concave, curvilinear relationship between months at present station and organizational climate, with the extremes being less than one month at the present assignment (+.79), 36 months or more at the present assignment (+.19), and 18 to 24 months at the present assignment (-.29). In other words, those with less than one month at their present assignment report having the most positive perception of the organizational climate, following a general decline in perceptions to the point where those with 18 to 24 months at their present station report having the most negative perception of the organizational climate, followed by a general improvement in perceptions to the point where those with 36 months or more at their present station who report having a positive perception of organizational climate.

18. From Figure 9 it can be seen that there is a concave, curvilinear relationship between months at present station and job satisfaction, with the extremes being less than one month at the present assignment (+.17), 36 months or more at the present assignment (+.34), and 18 to 24 months at the present station (-.21). In other words, those with less than one month at their present assignment report having a high level of job satisfaction, followed by a general decline in perceptions to the point where those with 18 to 24 months at their present station report having the lowest level of job satisfaction, followed by a general improvement in perceptions to the point where those with 36 months or more at their present station report having the highest level of job satisfaction.

19. From Figure 10 it can be seen that there is a general direct, positive linear relationship between supervisory responsibilities and all OAP scores. In other words, generally the greater the supervisory responsibilities, the higher the job enrichment needs, the more acceptable the level of task autonomy, the stronger the feelings that advancement and recognition is forthcoming at an acceptable rate, the higher the perception of their work group productivity level, the higher the level of job satisfaction, the higher the level of perceived supervisory capacity, and the more positive the perception of the organizational climate. Of particular interest is the fact that there is a slight depression in the linear trend along all OAP scores among those who write performance reports for three persons.

20. From Figure 11 it can be seen that there is an inverse linear relationship between supervisor writes performance reports and all OAP scores. In other words, generally the more likely the respondents are aware that

their supervisors write the respondent's own performance report, the higher the job enrichment needs, the more acceptable the level of task autonomy, the stronger the feeling that advancement and recognition is forthcoming at an acceptable rate, the higher the perception of their work group productivity level, the higher the level of job satisfaction, the higher the level of perceived supervisory capacity, and the more positive the perception of the organizational climate.

18. From Figure 9 it can be seen that there is a concave, curvilinear relationship between months at present station and job satisfaction, with the extremes being less than one month at the present assignment (+.17), 36 months or more at the present assignment (+.34), and 18 to 24 months at the present station (-.21). In other words, those with less than one month at their present assignment report having a high level of job satisfaction, followed by a general decline in perceptions to the point where those with 18 to 24 months at their present station report having the lowest level of job satisfaction, followed by a general improvement in perceptions to the point where those with 36 months or more at their present station report having the highest level of job satisfaction.

19. From Figure 10 it can be seen that there is a general direct, positive linear relationship between supervisory responsibilities and all OAP scores. In other words, generally the greater the supervisory responsibilities, the higher the job enrichment needs, the more acceptable the level of task autonomy, the stronger the feelings that advancement and recognition is forthcoming at an acceptable rate, the higher the perception of their work group productivity level, the higher the level of job satisfaction, the higher the level of perceived supervisory capacity, and the more positive the perception of the organizational climate. Of particular interest is the fact that there is a slight depression in the linear trend along all OAP scores among those who write performance reports for three persons.

20. From Figure 11 it can be seen that there is an inverse linear relationship between supervisor writes performance reports and all OAP scores. In other words, generally the more likely the respondents are aware that their supervisors write the respondent's own performance report, the higher the job enrichment needs, the more acceptable the level of task autonomy, the stronger the feeling that advancement and recognition is forthcoming at

an acceptable rate, the higher the perception of their work group productivity level, the higher the level of job satisfaction, the higher the level of perceived supervisory capacity, and the more positive the perception of the organizational climate.

21. From Figure 13 it can be seen that there is an inverse linear relationship between usual work schedule and all OAP scores. In other words, the more likely the respondent works a stable day shift, the higher the job enrichment needs, the more acceptable the level of task autonomy, the stronger the feeling that advancement and recognition is forthcoming at an acceptable rate, the higher the perception of their work group productivity level, the higher the level of job satisfaction, the higher the level of perceived supervisory capacity, and the more positive the perception of the organizational climate.

22. From Figure 14 it can be seen that there is a direct, positive linear relationship between the use of group meetings to solve problems and set goals and all OAP scores. In other words, the more likely group meetings are used to solve problems and set goals, the higher the job enrichment needs, the more acceptable the level of task autonomy, the stronger the feeling that advancement and recognition is forthcoming at an acceptable rate, the higher the perception of their work group productivity level, the higher the level of job satisfaction, the higher the level of perceived supervisory capacity, and the more positive the perception of the organizational climate.

23. From Figure 15 it can be seen that there is a direct, positive linear relationship between frequency of group meetings and all OAP scores, from frequency of group meetings category *never to monthly*, followed by a general leveling of OAP scores. These findings are of interest in as much as they imply that group meetings held on a monthly basis can serve to optimize OAP scores. More frequent group meetings can serve to raise OAP scores, but the increases are so small that the benefits probably do not warrant the cost of the increased number of meetings.

Eta² Analysis

There are several drawbacks with the results from the analysis of variance. As Figures 1-15 demonstrate, many of the relationships are curvilinear, a trait that the traditional analysis of variance (and the Pearson correlation coefficient for that matter) cannot account for nor reveal.

Furthermore, the F-tests in Table 6-35 were virtually all significant, due to the fact that the sample size was so large ($N = 77055; 23547$). Yet the fact that the F-test statistic is significant does not indicate the extent of the variation in the dependent variable that can be explained by the independent variables. Consequently, in an attempt to determine the extent of the linear and non linear variance in OAP scores that can be explained due to the independent variables, an η^2 analysis was undertaken. The η^2 statistic determines the extent of linear and non linear variance at the zero order (ie. not controlling for interaction between the independent variables).

Data from the η^2 analyses are summarized in Tables 36-42, and can be interpreted as follows (again note that these typologies are at the zero order and do not account for independent variable interaction).

1. Of the variation in job enrichment needs scores as noted in the pre test data (see Table 36), age accounts for 4.5%, gender for .3%, pay grade for 2.1%, years in the Air Force for 3.1%, race for 1.2%, level of education for 6.2%, NCO PME for 2.7%, CO PME for 3.7%, months at the present station for .7%, supervisor responsibilities for 1.6%, supervisor writes performance report for .5%, work group size for .8%, usual work schedule for .7%, group meetings used to solve problems and set goals for .8%, and frequency of group meetings for .9%.

2. Of the variance in task autonomy scores as noted in the pre test data (see Table 37), age accounts for 12.2%, gender for .2%, pay grade for 7.9%, years in the Air Force for 8.7%, race for .1%, level of education for 4.0%, NCO PME for 5.4%, CO PME for 4.3%, months at the present station for 4.2%, supervisor responsibilities for 3.0%, supervisor writes performance report for 2.4%, work group size for .9%, usual work schedule for 7.4%, group meetings used to solve problems and set goals for 5.7%, and frequency of group meetings used to solve problems and set goals for 5.7%, and frequency of group meetings for 4.4%.

3. Of the variation in advancement/recognition scores as noted in the pre test data (see Table 38), age accounts for 3.9%, gender for .7%, pay grade for 3.7%, years in the Air Force for 1.2%, months at the present station for .4%, supervisor responsibilities for 5.6%, supervisor writes performance report for 3.1%, work group size for 1.7%, usual work schedule for .5%, group meetings used to solve problems and set goals for 11.5%, and frequency of group meetings for 6.5%.

4. Of the variation in perceived productivity scores as noted in the pre test data (see Table 39), age accounts for 3.6%, gender for .1%, pay grade for 1.9%, years in the Air Force for 2.8%, race for .1%, level of education for .5%, NCO PME for 1.9%, CO PME for .6% months at the present station for 1.2%, supervisor responsibilities for 1.1%, supervisor writes performance report for 1.8%, work group size for .5%, usual work schedule for 1.1%, group meetings used to solve problems and set goals 7.6%, and frequency of group meetings for 3.9%.

5. Of the variation in job satisfaction scores as noted in the pre test data (see Table 40), age accounts for 8.1%, gender for .4%, pay grade for 4.7%, years in the Air Force for 5.2%, race for .1%, level of education for 1.5%, NCO PME for 3.5%, CO PME for 2.1%, months at the present station for 2.6%, supervisor responsibilities for 1.3%, supervisor writes performance report for 2.4%, work group size for .4%, usual work schedule for 5.9%, group meetings used to solve problems and set goals for 10.2%, and frequency of group meetings for 6.1%.

6. Of the variation in the perceived supervisor capacity scores as noted in the pre test data (see Table 41), age accounts for 1.1%, gender for .0%, pay grade for 2.3%, years in the Air Force for 3.6%, race for .0%, level of education for .3%, NCO PME for 1.0%, CO PME for .9%, months at the present station for 2.6%, supervisor responsibilities for .4%, supervisor writes performance report for 2.5%, work group size for .3%, usual work schedule for .4%, group meetings used to solve problems and set goals for 15.5%, and frequency of group meetings for 8.0%.

7. Of the variation in the organizational climate scores as noted in the pre test data (see Table 42), age accounts for 4.4%, gender for .2%, pay grade for 1.8%, years in the Air Force for 2.9%, race for .0%, level of education for 1.3%, NCO PME for 2.4%, CO PME for 1.9%, months at the present station for 1.6%, supervisor responsibilities for .7%, supervisor writes performance report for .9%, work group size for .3%, usual work schedule for 1.6%, group meetings used to solve problems and set goals for 7.5%, and frequency of group meetings for 3.8%.

The η^2 figures for the post test data are virtually the same as those for the pre test data. In only three instances does the amount of

variance explained by any independent variable increase more than one percent from pre test to post test.* This indicates that background variables tend to be relatively constant in terms of their impact upon OAP scores at any given point in time. In other words, it appears as if background items are impacting upon OAP scores in the same general way at any given point in time. This tends to support the zero order correlation findings that the same types of persons score the OAP the same general way at any given point in time. It should be pointed out, however, that the η^2 analysis revealed that background variables do explain, in absolute terms, a slightly larger amount of the variance on the post test scores than in the pre test scores, indicating that background item variables account for a somewhat larger amount of the variance in post test scores than in pre test scores. This was also determined in the zero order correlation analysis. The general results of the two zero order analyses which used linear, and linear plus non linear measures, were virtually identical.

Multiple Classification Analysis

The η^2 statistic possesses two deficiencies as applied to this present data set. It does not control for interaction among the independent variables known to be present in this data set (see Tables 4 and 5), and is a single item statistic. In this present study, it was desired to examine a composite view of the overall impact of personal characteristics and

*Pay grade accounts for 2.3 percent of the variance of the pre test perceived supervisor capacity score, and .8 percent of the post test perceived supervisor capacity score. Years in the Air Force accounts for 3.6 percent of the variance of the pre test perceived supervisor capacity score, and 1.0 percent of the post test perceived supervisor capacity score. Months at present station accounts for 2.6 percent of the variance of the pre test perceived supervisor capacity score, and .4 percent of the post test perceived supervisor capacity score.

organizational characteristics upon OAP scores, controlling for independent variable interaction. Consequently, a multiple classification analysis (MCA) was employed. MCA allows the value of the independent variables to be statistically adjusted to correct for intergroup differences. By utilizing this MCA design, it is possible to examine the effects of certain independent variables upon OAP scores, controlling for all other independent variables. This is accomplished through the calculation of "corrected" scores which indicate what the outcome scores would have been, given no difference between the groups identified by the independent variables of focus. However, such corrected MCA coefficients and accompanying composite R^2 figures reveal only the extent of the linear relationships in the data. The present data set is known to encompass many curvilinear relationships (see Figures 1 through 15). In the future, partial η^2 scores should be run on the data so as to ascertain the composite linear plus non linear impact of the independent variables, controlling for independent variable interaction. The MCA Analysis thus becomes a conservative estimate of the extent of the relationship between background items and OAP scores. Adding the curvilinear relationships to the composite relationship picture, would serve to increase the amount of variance explained. Yet even without the curvilinear data, the MCA analysis reveals the presence of a number of powerful relationships.

Tables 43 through 49 contain a vast array of provocative data, a complete iteration of which is far beyond the scope of this piece. There are, however, some particular findings of interest, as follows.

1. From the data detailed in Table 43, it can be seen that those with Doctorates report a job enrichment need .28 points above the mean on the pre test, yet 1.07 points below the mean on the post test. Given that the mean changed from 5.55 on the pre test to 5.45 on the post test, this is a total absolute drop of 1.45 points from pre test to post test. Those with Doctorates score the post test 24.9% lower than the pre test in regard to job enrichment needs.

2. From the data detailed in Table 44, it can be seen that those who are 20 years of age or less report a task autonomy score .20 points below the mean on the pre test, and .40 points below the mean on the post test. Given that the mean changed from 3.93 on the pre test to 4.04 on the post test, this is a total absolute drop of .09 points from pre test to post test. Those who are 20 years of age or less score the post test 2.4% lower than the pre test in regard to task autonomy.

3. From the data detailed in Table 45, it can be seen that those with Masters' Degrees report an advancement/recognition score .14 points below the mean on the pre test, and .41 points below the mean on the post test. Given that the mean changed from 4.30 on the pre test to 4.34 on the post test, this is a total absolute drop of .23 points from pre test to post test. Those with Masters' Degrees score the post test 5.5% lower than the pre test in regard to advancement/recognition.

4. From the data detailed in Table 45, it can be seen that those who have completed NCO-PME Phase 5 report an advancement/recognition score .46 points above the mean on the pre test, and .36 points above the mean on the post test. Given that the mean changed from 4.30 on the pre test to 4.34 on the post test, this is a total absolute drop of .07 points from pre test to post test. Those who have completed NCO-PME Phase 5 score the post test 1.5% lower than the pre test in regard to advancement/recognition.

5. From the data detailed in Table 46, it can be seen that those who are 20 years of age or less report a perceived productivity score .02 points below the mean on the pre test, and .44 points below the mean on the post test. Given that the mean did not change, this is a total absolute drop of .42 points from pre test to post test. Those who are 20 years of age or less score the post test 7.7% lower than the pre test in regard to perceived productivity.

6. From the data detailed in Table 46, it can be seen that those who are 41-50 years of age report a perceived productivity score .35 points above the mean on the pre test, and .24 points above the mean on the post test. Given that the mean did not change, this is a total absolute drop of .09 points from pre test to post test. Those who are 41-50 years of age score the post test 1.5% lower than the pre test in regard to perceived productivity.

7. From the data detailed in Table 48, it can be seen that those who are 20 years of age or less report a perceived supervisor capacity score .04 points above the mean on the pre test, yet .40 points below the mean on the post test. Given that the mean changed from 4.89 on the pre test to 5.00 on the post test, this is a total absolute drop of .33 points from pre test to post test. Those who are 20 years of age or less score the post test 6.7% lower than the pre test in regard to perceived supervisor capacity.

8. From the data detailed in Table 48, it can be seen that those with Masters' Degrees report a perceived supervisor capacity score .25 points below the mean on the pre test, and .72 points below the mean on the post test. Given that the mean changed from 4.89 on the pre test to 5.00 on the post test, this is an absolute drop of .36 points from pre test to post test. Those with Masters' Degrees score the post test 7.0% lower than the pre test in regard to perceived productivity.

9. From the data detailed in Table 49, it can be seen that those who are 20 years of age or less report an organizational climate score .17 points below the mean on the pre test, and .56 points below the mean on the post test. Given that the mean changed from 4.58 on the pre test to 4.71 on the post test, this is an absolute drop of .26 points from pre test to post test. Those who are 20 years of age or less score the post test 5.9% lower than the pre test in regard to organizational climate.

10. From data detailed in Table 44, it can be seen that those who are 36-40 years of age report a task autonomy score .22 points above the mean on the pre test, and .38 above the mean on the post test. Given that the mean changed from 3.93 on the pre test to 4.04 on the post test, this is an absolute increase of .27 points from pre test to post test. Those who are 36-40 years of age score the post test 6.5% higher than the pre test in regard to task autonomy.

11. From the data detailed in Table 44, it can be seen that those who are 51 years of age or more report a task autonomy score .52 points above the mean on the pre test, and .70 points above the mean on the post test. Given that the mean changed from 3.93 on the pre test to 4.04 on the post test, this is an absolute increase of .29 points from pre test to post test. Those who are 51 years of age or more score the post test 6.5% higher than the pre test in regard to task autonomy.

12. From the data detailed in Table 44, it can be seen that those with Doctorates report a task autonomy score .03 points below the mean on the pre test, and .26 points above the mean on the post test. Given that the mean changed from 3.93 on the pre test to 4.04 on the post test, this is an absolute increase of .34 points from pre test to post test. Those with Doctorates score the post test 8.7% higher than the pre test in regard to task autonomy.

13. From the data detailed in Table 44, it can be seen that those who write performance reports for three persons report a task autonomy score .10 points above the mean on the pre test, and .21 points above the mean on the post test. Given that the mean changed from 3.93 on the pre test to 4.04 on the post test, this is an absolute increase of .37 points from pre test to post test. Those who write performance reports for three persons score the post test 9.0% higher than the pre test in regard to task autonomy.

14. From the data detailed in Table 44, it can be seen that those who write performance reports for three to five persons report a task autonomy score .11 points above the mean on the pre test, and .25 points above the mean on the post test. Given that the mean changed from 3.93 on the pre test to 4.04 on the post test, this is an absolute increase of .40 points from pre test to post test. Those who write performance reports for three to five persons score the post test 9.7% higher than the pre test in regard to task autonomy.

15. From the data detailed in Table 44, it can be seen that those who work primarily with three to five persons report a task autonomy score .10 points below the mean on the pre test, and .07 points below the mean on the post test. Given that the mean changed from 3.93 on the pre test to 4.04 on the post test, this is an absolute increase of .29 points from pre test to post test. Those who work primarily with three to five persons score the post test 7.4% higher than the pre test in regard to task autonomy.

16. From the data detailed in Table 44, it can be seen that those who report that group meetings are never used to solve problems and set goals report a task autonomy score .46 points below the mean on the pre test, and .44 points below the mean on the post test. Given that the mean changed from 3.93 on the pre test to 4.04 on the post test, this is an absolute increase of .28 points from pre test to post test. Those who report that group meetings are never used to solve problems and set goals score the post test 7.8% higher than the pre test in regard to task autonomy.

17. From the data detailed in Table 45, it can be seen that those who are 51 years of age or more report an advancement/recognition score .68 points below the mean on the pre test, and .49 points below the mean on the post test. Given that the mean changed from 4.30 on the pre test to 4.34 on the post test, this is an absolute increase of .23 points from pre test to post test. Those who are 51 years of age or more score the post test 6.4% higher than the pre test in regard to advancement/recognition.

18. From the data detailed in Table 45, it can be seen that those with Doctorates report an advancement/recognition score .67 points below the mean on the pre test, and .42 points below the mean on the post test. Given that the mean changed from 4.30 on the pre test to 4.34 on the post test, this is an absolute increase of .29 points from pre test to post test. Those with Doctorates score the post test 8.0% higher than the pre test in regard to advancement/recognition.

19. From the data detailed in Table 45, it can be seen that those who write performance reports for six to eight persons report an advancement/recognition score .22 points above the mean on the pre test, and .40 points above the mean on the post test. Given that the mean changed from 4.30 on the pre test to 4.34 on the post test, this is an absolute increase of .39 points from pre test to post test. Those who write performance reports on six to eight persons score the post test 8.9% higher than the pre test in regard to advancement/recognition.

20. From the data detailed in Table 45, it can be seen that those who write performance reports for nine or more persons report an advancement/recognition score .16 points above the mean on the pre test, and .35 points above the mean on the post test. Given that the mean changed from 4.30 on the pre test to 4.34 on the post test, this is an absolute increase of .40 points from pre test to post test. Those who write performance reports for nine or more persons score the post test 9.3% higher than the pre test in regard to advancement/recognition.

21. From the data detailed in Table 45, it can be seen that those who generally work alone report an advancement/recognition score .22 points below the mean on the pre test, and .02 points below the mean on the post test. Given that the mean changed from 4.30 on the pre test to 4.34 on the post test, this is an absolute increase of .30 points from pre test to post test. Those who generally work alone score the post test 7.4% higher than the pre test in regard to advancement/recognition.

22. From the data detailed in Table 47, it can be seen that those who have less than a high school education report a job satisfaction score at the mean on the pre test, and .28 points above the mean on the post test. Given that the mean changed from 4.88 on the pre test to 4.98 on the post test, this is an absolute increase of .38 points from pre test to post test. Those who have less than a high school education score the post test 7.8% higher than the pre test in regard to job satisfaction.

23. From the data detailed in Table 48, it can be seen that females report a perceived supervisor capacity score .02 points below the mean on the pre test, and .21 points above the mean on the post test. Given that the mean changed from 4.89 on the pre test to 5.00 on the post test, this is an absolute increase of .34 points from pre test to post test. Females score the post test 7.0% higher than the pre test in regard to perceived supervisor capacity.

24. From the data detailed in Table 49, it can be seen that those who have less than a high school education report an organizational climate score .36 points above the mean on the pre test, and .86 points above the mean on the post test. Given that the mean score changed from 4.58 on the pre test to 4.71 on the post test, this is an absolute increase of .63 points from pre test to post test. Those who have less than a high school education score the post test 12.8% higher than the pre test in regard to organizational climate.

25. From the data detailed in Table 49, it can be seen that those with Doctorates report an organizational climate score .20 points above the mean on the pre test, and .63 points above the mean on the post test. Given that the mean score changed from 4.58 on the pre test to 4.71 on the post test, this is an absolute increase of .56 points from pre test to post test. Those with Doctorates score the post test 11.7% higher than the pre test in regard to organizational climate.

26. From the data detailed in Table 49, it can be seen that those who write performance reports on two persons report an organizational climate score .01 point below the mean on the pre test, and .16 points above the mean on the post test. Given that the mean score changed from 4.58 on the pre test to 4.71 on the post test, this is an absolute increase of .38 points from pre test to post test. Those who write performance reports on two persons score the post test 8.0% higher than the pre test in regard to organizational climate.

27. From the data detailed in Table 49, it can be seen that those who write performance reports on three persons report an organizational climate score .01 point above the mean on the pre test, and .20 points above the mean on the post test. Given that the mean score changed from 4.58 on the pre test to 4.71 on the post test, this is an absolute increase of .40 points from pre test to post test. Those who write performance reports on three persons score the post test 8.4% higher than the pre test in regard to organizational climate.

28. From the data detailed in Table 49, it can be seen that those who write performance reports on six to eight persons report an organizational climate score .22 points above the mean on the pre test, and .47 points above the mean on the post test. Given that the mean score changed from 4.58 on the pre test to 4.71 on the post test, this is an absolute increase of .32 points from pre test to post test. Those who write performance reports on six to eight persons score the post test 8.2% higher than the pre test in regard to organizational climate.

As per the information detailed above, given the number of intervening variables that could be invalidating the perceived relationship between background variables and the dependent variables, there are some tentative indications that the consulting efforts are impacting unfavorably upon those who are 20 years of age or under in regards to task autonomy, perceived productivity, perceived supervisor capacity, and organizational climate. The consulting efforts also appear to be impacting unfavorably upon those with Masters' Degrees in regard to advancement/recognition and perceived supervisory capacity, and unfavorably upon those with Doctorates in regard to job enrichment needs.

On the other hand, consulting efforts appear to be impacting very favorably upon those with Doctorates in regard to task autonomy, advancement/recognition, and organizational climate, and impacting very favorably upon those with less than a high school education in regard to job satisfaction and organizational climate. The consulting efforts also appear to be very favorably impacting upon those who are 51 year of age or older in regard to task autonomy and advancement/recognition, and very favorably upon females in regard to perceived supervisor capacity. The consulting efforts appear to be impacting very favorably upon those who write performance reports for two, three, and six or more persons in regard to organizational climate and

advancement/recognition, and those who write performance reports for three to five persons in regard to task autonomy. The consulting efforts appear to be very favorably impacting upon those who work in groups of three to six persons, and those who never have useful group meetings in regard to task autonomy. The consulting team efforts appear to be very favorably impacting upon those who work alone in regard to advancement/recognition.

The consulting efforts appear to have a more favorable impact upon non whites and females (versus whites and males) in regard to advancement/recognition, job enrichment needs, perceived productivity, job satisfaction, and organizational climate, a more favorable impact upon whites and females (versus non whites and males) in regard to perceived supervisory capacity, and a more favorable impact upon non whites and males (versus white and females) in regard to task autonomy. In summary, the consulting efforts generally impact more favorably upon non whites and females.

Standardized Coefficients

A major contribution of this present study has been the development of standardized test score coefficients designed to control for the impact of background characteristics. By utilizing these coefficients, the OAP becomes more a measure of the organization, and less a measure of background items. The coefficients for the pre test and post test data are found in Tables 43 through 49 under the Pre Test MCA Coefficient and Post Test MCA Coefficient columns respectively.

It must be emphasized that these coefficients represent a type of grand mean for the entire sample. Each of the sub samples which make up the data set possess different coefficients, which in sum total, equal the coefficients determined in Tables 43 through 49. It must also be emphasized that the coefficients are technically valid only when applied to the data set from which they were derived. In other words, the coefficients cannot be applied, from a purely technical standpoint, to a new population. This is a generalizability problem inherent in all predictive models. Furthermore, these coefficients were developed at one point in time, and are, again from a purely technical standpoint, valid only at that particular point in time. However, from a practical standpoint, the coefficients may be applied to future OAP scores with confidence, despite these limitations. For while the application of the coefficients to other data sets will not render a perfectly accurate corrected OAP score (as the above discussion indicates),

their application will serve to increase the level of accuracy. Furthermore, given the relatively large sample size from which the coefficients were derived (N = 77055; 23547), it is felt that they may be applied with a high degree of confidence. However, to avoid a general decay in their predictive capacity, the coefficients must be periodically updated using the techniques developed in this study.

The coefficients may be applied using the following standardization formula:

$$\text{STANDARDIZED SCORE} = \frac{(N\bar{X}) + \sum(f_i a_i)}{N}$$

Where N = Sample Size

\bar{X} = Dependent Variables Mean Score for the Sample

a_i = -(MCA Coefficient) of category i

f_i = Frequency of category i

Consider the following hypothetical case, looking at the dependent variable job satisfaction. A post test OAP is administered at two hypothetical Air Force bases (Base X and Base Y) and is analyzed, with the following results:

	Base X	Base Y
Sample Size	N = 1325	N = 2625
Job Satisfaction Mean Score	\bar{X} = 4.80	\bar{X} = 4.90
Age		
1) 20 or less	362	52
2) 21-25	267	142
3) 26-30	298	220
4) 31-35	181	398
5) 36-40	160	956
6) 41-50	43	597
7) 51 or more	14	260
Gender		
1) Male	1250	975
2) Female	75	1650
Race		
1) Non-white	66	1050
2) White	1259	1575

While it would appear as if Base Y personnel possess a higher job satisfaction score (4.90 > 4.80), the personal background characteristics are very different. From the data in Table 47 (MCA Coefficient Summary Table: Job Satisfaction), it can be seen that personal background characteristics have a significant impact upon job satisfaction scores. To correct the OAP scores for personal background characteristics and obtain a more accurate assessment of true job satisfaction on each base, the standardization formula is employed using the standardized coefficients found in Table 47.

$$\begin{aligned} \text{Standardized Score Base X} = & [(1325 \times 4.80) + (362 \times .27) + (267 \times .18) + \\ & (298 \times .09) + (181 \times -.08) + (160 \times -.24) + \\ & (43 \times -.47) + (14 \times -.69) + (1250 \times .03) + \\ & (75 \times -.31) + (66 \times -.02) + (1259 \times .01)]/1325 \end{aligned}$$

$$\begin{aligned} \text{Standardized Score Base Y} = & [(2625 \times 4.90) + (52 \times .27) + (142 \times .18) + \\ & (220 \times .09) + (398 \times -.08) + (956 \times -.24) + \\ & (597 \times -.47) + (260 \times -.69) + (975 \times .03) + \\ & (1650 \times -.31) + (1050 \times -.02) + (1575 \times .01)]/2625 \end{aligned}$$

The job satisfaction score, standardized for age, gender and race, is 4.89- for Base X and 4.46 for Base Y. Before standardizing the scores, it appeared as if Base Y personnel had a higher level of job satisfaction (4.90 > 4.80). A more accurate assessment was obtained when background item noise erroneously picked up by the instrument (the extent of which was enhanced due to extreme variation in the background characteristics of the two hypothetical sample populations), was controlled. When this was done, it was found that the job satisfaction score for Base X (4.89), was actually much higher than that of Base Y (4.46).

Other background characteristics can be brought into such standardization efforts as desired, as long as category frequencies and standardized coefficients are known. Age, gender and race were chosen merely to illustrate the technique. The larger the number of background items controlled, the more accurate the standardized score.

It is quite clear that the OAP scores in this example contain a significant portion of error derived from the organizational assessment instruments inability to eliminate the inadvertent measurement of background characteristics. In other words, the presence of certain background characteristics in the hypothetical sample populations tended to bias OAP scores. As this examples illustrates, some of the difference in point in time OAP score comparisons (for example, differences in pre test scores between bases), may not necessarily

reflect differences in respondents' actual perceptions of the organization, but rather differences in background characteristics of the respondents, coupled with the fact that the OAP instrument has a tendency to pick up certain pieces of background characteristic data and erroneously report significant portions of them as organizational assessment data. In the future, all OAP scores should be standardized using the technique outlined herein, to control for this dimension of OAP score error. This will make the OAP more a measure of organizational perceptions, and less a measure of individual background characteristics, and thus serve to enhance the validity of the OAP as an organizational assessment instrument. Attempts should also be made to identify and control for other intervening variables that may be biasing OAP scores.

Period in Time Trends

The data detailed in Table 50 serves to summarize the general trends and impacts of the background variable items upon the dependent variables, from a longitudinal perspective. Pearson correlation coefficients were computed between corrected pre test scores and the difference between the corrected post test scores and the corrected pre test scores. The data can be interpreted as follows.

1. Persons who, on the pre test, report of a more acceptable organizational climate ($R = .27$), a higher level of task autonomy (.14), a greater perceived supervisor capacity (.20), and possess a high level job satisfaction (.05), tend to report a larger increase on the post test than those who, on the pre test, apparently possess a lower job satisfaction, report a lower perceived supervisor capacity, a lower level of task autonomy, and a less acceptable organizational climate.

2. Persons who, on the pre test, report a higher level of perceived productivity (-.13) and felt that advancement and recognition was forthcoming at a faster rate (-.07), report a smaller increase on the post test than those who, on the pre test, felt that advancement and recognition was forthcoming at a slower rate and reported of a lower level of perceived productivity.

3. Persons who, on the pre test, report of higher job enrichment needs (-.31), report a larger decrease on the post test than those who, on the pre test, report of lower job enrichment needs.*

*Recall from Table 2 that the job enrichment needs scores decrease from pre test to post test, unlike any of the other six dependent variables, thus necessitating a slightly different interpretation in this instance.

There is a very significant additional element at work here. Previous research conducted on a sub sample of the present data set (Conlon, 1980), found a rather powerful regression toward the mean effect. Such an effect would tend to artificially depress the Pearson correlation coefficient to negative numbers. However, as the positive correlation coefficients in Table 50 reveal, when controlling for interaction among the independent variables, the regression toward the mean effect is either being dissipated or at least overpowered to some degree. The latter appears to be more likely in as much as the presence of regression toward the mean was clearly documented. The correlation coefficients in Table 50 thus become conservative estimates. They should be larger, positive figures, for the regression toward the mean effect is, in all likelihood, depressing them somewhat. Just how much is not known at this time. The dependent variables advancement/recognition and perceived productivity, for example, are both slightly negative. Controlling for regression toward the mean would in all likelihood result in positive correlation coefficients.

It is concluded that, in general, those who score the pre test higher tend to have larger increases from pre test to post test than those who score the post test lower. With or without the regression toward the mean effect, these general conclusions are the same. If, however, regression toward the mean is as powerful as previous studies indicate, these conclusions are strengthened.

OAP Score Variance

From the data detailed in Table 51, and as implied in all of the analyses detailed up to this point, a small, but significant portion of the variance in OAP scores seems to be coming from background characteristics. The data can be interpreted as follows:

1. Personal background characteristics account for 6.2% ($R^2 = .062$) of the variance in job enrichment needs, 8.9% of the variance in task autonomy, 7.8% of the variance in advancement/recognition, 4.1% of the variance in perceived productivity, 6.9% of the variance in job satisfaction, 1.7% of the variance in perceived supervisor capacity, and 4.9% of the variance in organization climate in the pre test data set.

2. Personal background characteristics account for 6.1% of the variance in job enrichment needs, 6.8% of the variance in task autonomy, 7.3% of the variance in advancement/recognition, 3.7% of the variance in productivity,

7.2% of the variance in job satisfaction, 1.9% of the variance in perceived supervisor capacity, and 4.7% of the variance in organizational climate in the post test data set.

3. Organizational background characteristics account for 3.1% of the variance in job enrichment needs, 15.1% of the variance in task autonomy, 18.2% of the variance in advancement/recognition, 9.2% of the variance in productivity, 15.2% of the variance in job satisfaction, 18.9% of the variance in perceived supervisor capacity, and 9.9% of the variance in organizational climate in the pre test data set.

4. Organizational background characteristics account for 4.3% of the variance in job enrichment needs, 15.6% of the variance in task autonomy, 19.5% of the variance in advancement/recognition, 9.8% of the variance in perceived productivity, 19.7% of the variance in job satisfaction, 20.8% of the variance in perceived supervisor capacity, and 11.6% of the variance in organizational climate in the post test data set.

As can be seen, organizational characteristics tend to explain a larger portion of the variance than do personal characteristics.

While some caution must be used in summing the variance explained due to personal characteristics with the variance explained due to organizational characteristics to arrive at an overall variance explained due to background item variation figure due to the fact that these two sets of independent variables are not entirely orthogonal. It may be tentatively concluded from the pre test data, that background characteristics account for at least 9% of the variation in job enrichment needs, 24% of the variation in task autonomy, 26% of the variance in advancement/recognition, 13% of the variance in perceived productivity, 22% of the variance in job satisfaction, 21% of the variance in perceived supervisor capacity, and 15% of the variance in organizational climate. Post test figures are slightly higher. However, there are a number of dimensions that must be considered carefully before accepting these figures.

These R^2 coefficients are the most conservative estimates due to the fact that they only examine linear relationships, and were derived while controlling for independent variable interaction. The η^2 figures articulated previously, are the highest estimate of the extent of the variance explained due to the fact that they examined linear and non linear relationships, and did not control for the known independent variable interaction.

The data in Table 52 illustrate the minimum and maximum variation (R^2 and η^2 respectively) in the dependent variables that can be accounted for due to background characteristics. It is reasonably assumed that the actual variation falls somewhere between those two extremes. Consequently, the pre test data from Table 52 suggests that actually somewhere between 9% and 30% of the variation in job enrichment needs scores can be explained due to variation in background characteristics, between 24% and 71% of the variance in task autonomy scores can be explained due to variation in background characteristics, between 26% and 48% of the variance in advancement/recognition scores can be explained due to variation in background characteristics, between 13% and 28% of the variance perceived productivity scores can be explained due to variation in background characteristics, between 22% and 54% of the variation in job satisfaction scores can be explained due to variation in background characteristics, between 21% and 39% of the variation perceived supervisory capacity scores can be explained due to variation in background characteristics, and between 15% and 32% of the variation in organizational climate scores can be explained due to variation in background characteristics. Roughly the same figures hold true for the post test data, though the post test figures are slightly larger. Overall, at the very least, depending on the dependent variable of interest, from 9% to 27% of the variation in OAP scores can be accounted for due to the impact of background characteristics, and at most, 28% to 73% of the variation in OAP scores can be accounted for due to the impact of background characteristics.

Overall, the data reveal that there is less than .5% of change in the impact of personal characteristics upon OAP scores from pre test to post test. Organizational characteristics, which serve as more powerful factors upon dependent variable variance, are not quite as constant, with changes as high as 4.5% from pre test to post test. It can be seen that background characteristics seem to serve as relatively constant explicative factors, from a longitudinal perspective. In other words, it appears that background variables impact upon OAP scores in the same way at any given point in time. However, it does appear as if background variables do have a slightly greater impact upon post test scores than upon pre test scores. In other words, the amount of variance explained due to background characteristics is higher on the post test than on the pre test. As detailed earlier, when

this does occur, generally those who score the pre test high have larger increases on the post test than those who score the pre test lower. This supports the findings of the zero order correlation analysis and the η^2 analyses.

Application of the Standardized Coefficients to the Present Data Set

The final phase of this research effort involved an attempt to determine, from a broad perspective, the impact of personal background characteristics upon OAP scores, using the existing data base. The standardized coefficients were applied to the pre test and post test data sets, using the dependent-variable mean scores reported in Table 2, and the frequencies reported in Table 3. The data from this analysis are summarized in Tables 53 and 54.

When controlling for personal background characteristics, OAP scores on both the pre test and post test decreased anywhere from .47% (perceived supervisory capacity, post test) to 3.04% (task autonomy, post test). Post test scores experienced a larger decrease than did pre test scores. The one exception was advancement/recognition which, when background variables were controlled, increased 1.57% on the pre test and increased .32% on the post test. In general, however, upon controlling for background characteristics, OAP scores were not as large as the raw data indicated. Indeed, as seen earlier and substantiated again in Tables 53 and 54, OAP scores are being artificially inflated due to the impact of background characteristics. When controlling for the impact of background characteristics, OAP scores tend to decrease in size. In other words, actual OAP scores to date have not been quite as large as the raw data has indicated, due in part to the high level of interaction among the independent variables (see Tables 4 and 5) which has served to artificially inflate the size of OAP scores,* coupled with the fact that the OAP instrument has a tendency to pick up certain pieces of background characteristic data and erroneously report small, but significant portions of them as organizational assessment data. It may well be in this case that most, if not all of the background characteristic information

*Actually, the interaction effect consists of two parts; a compounding effect of the interaction of highly correlated independent variables (especially non-discrete variables) which causes artificial increases in the size of the dependent variable, and a real effect of interaction which may cause either increases or decreases in the size of the dependent variable. Just how each effects the numbers and figures reported in this study is unknown. However, in as much as many of the independent variables in this study are non-discrete, it is felt that a very large proportion of the interaction effect is of the former variety. Path Analysis might be used in the future to attempt to distinguish real from artificial.

being erroneously reported as organizational assessment information arises from the interaction of the intercorrelated independent variables. In other words, just how much of the error in specific point in time OAP scores that is exclusively due to each source is unknown in this instance, though the parameters of their composite effects have been identified in this study. It was additionally found that some of the differences in point in time OAP score comparisons (differences in pre test scores between Air Force bases, for example) may not necessarily reflect differences in respondents' actual perceptions of the organization, but rather interaction among the independent variables, and differences in background characteristics of the respondents, coupled with the fact that the OAP instrument has a tendency to pick up certain pieces of background characteristic data and erroneously report small, but significant portions of them as organizational assessment data.

Of greater interest is the fact that, when controlling for personal background variables, there is a general reduction in the rate of increase from pre test to post test. Indeed, as the data in Table 54 reveal, 37.12% of the increase in task autonomy scores from pre test to post can be accounted for due to variation in personal background variables, 72.25% of the increase in advancement/recognition scores can be accounted for, 4.38% of the increase in perceived productivity scores can be accounted for, 45.15% of the increase in job satisfaction scores can be accounted for, and 27.12% of the increase in organizational climate scores can be accounted for due to variation in personal background variables. In other words, the actual rate of increase in OAP scores from pre test to post test to date is not as great as the raw data indicates,* again due in part to the high level of interaction among the independent variables which has served to artificially inflate the size of OAP scores. This is also due to the fact that there is some degree of variation in the background characteristics of the respondents from pre test to post test, coupled with the fact that the OAP instrument has a tendency to pick up certain pieces of background characteristic data and erroneously report small, but significant portions of them as organizational assessment data and for some reason report more background data as organizational data on the post test than on the pre test. Interestingly, however, in two cases, the personal background variables do serve to mask greater changes in pre test to post test scores than the raw data

*See Table 2 for a review of the raw data OAP score increases.

indicate. The data reveal that 83.33% of the increase in the rate of increase in perceived supervisor capacity scores were masked by personal background characteristics, and 68.00% of the decrease in the rate of decrease in job enrichment need scores were screened out by personal background characteristics. In other words, the actual rate of increase in perceived supervisory capacity from pre test to post test is greater than the raw data indicates, and the actual rate of decrease in job enrichment need from pre test to post test is greater than the raw data indicates.

It should be noted that these figures were derived using standardized coefficients developed in the MCA analysis. Given that the MCA analysis controlled for multicollinearity among the independent variables and examined only linear relationships, the percentages presented above become the most conservative estimate of the impact of background characteristics upon OAP scores. If linear plus non linear percentages were derived, the above figures would be much larger. Just how much larger needs to be determined in any future examination of this data set. Yet even with the present figures, it can be seen that much of the change from pre test to post test can be accounted for due to variation in the background characteristics of the sample, and the fact that the OAP instrument is more sensitive to background information on the post test than the pre test.

V SUMMARY AND RECOMMENDATIONS

This research effort has developed baseline information as to the nature and extent of the impact of background items upon OAP scores. Numerous relationships and associations have been discussed in a descriptive format. While many more were explored in the research effort, they have not all been discussed in this report. To ascertain the nature and extent of other relationships of interest, interested readers can examine the data generated in the present research effort as detailed in the tables and figures found in the appendix.

There are three major contributions of this project: the development of specific standardized OAP coefficients; the development of a technique to refine those coefficients in the future, and; the development of point in time and period of time typologies. The development of specific standardized OAP coefficients is especially noteworthy. However, these coefficients must be updated periodically using the technique developed in this present effort so as to maintain some semblance of validity.

It was found that background information variables account for a significant amount of variation in OAP scores. Depending upon the dependent variable of interest, background characteristics, in sum total, explain at least 9% to 27% of the variance, and perhaps as much as 28% to 73% of the variance in specific point in time OAP scores. Background characteristics were found to account for a larger proportion of the variance in post test scores than in pre test scores. It was found that when controlling for the impact of background variables, there was a small reduction in the pre test OAP scores, and a slightly larger reduction in post test OAP scores. In other words, when controlling for the impact of background characteristics, OAP scores were not quite as large as the raw data indicated. Indeed, it appears that OAP scores are being artificially inflated, to some degree, due to the high level of interaction among the independent variables, and the fact that the OAP instrument has a tendency to pick up certain pieces of background characteristic data and erroneously report small, but significant portions of them as organizational assessment data. With this in mind it becomes apparent that all OAP scores contain a small, but significant portion of error. In addition, in as much as the presence of certain background characteristics in the sample population has been found to bias OAP scores, it appears that some of the differences in point in time OAP score comparisons (differences in pre test scores between bases, for example) may not necessarily reflect differences in respondents' actual perceptions of the organization, but rather interaction among the independent variables,

and differences in background characteristics of the respondents, coupled with the fact, as previously noted, that the OAP instrument has a tendency to pick up certain pieces of background characteristic data and erroneously report small, but significant portions of them as organizational assessment data. In the future, corrected OAP scores (corrected for background characteristic variance, and any and all other intervening variables that can be isolated) should be computed, utilizing the techniques described herein. This will make OAP scores more a measure of organizational perceptions, and less a measure of individual background characteristics, and thus serve to enhance the validity of the OAP as an organizational assessment instrument.

The general nature of the relationships between background information variables and OAP scores was found to be relatively constant at any given point in time. In other words, the same types of persons were found to score the OAP in the same way at any given point in time. The extent or strength of those relationships, however, were found to shift slightly over time. It was generally found that those who scored the pre test higher, had larger increases in their post test scores than those who scored the pre test lower. This seems to suggest that some kind of self fulfilling prophecy may be taking place. The consulting efforts appear to be impacting more favorably upon those who already hold the Air Force in high regard, and vice-versa, they seem to be having less impact, and perhaps even in some instances, a negative impact upon those who possess a lower image of the Air Force.

It was additionally found that much of the general increase in OAP scores that had been seen in the raw data from pre test to post test was due to variations in the background characteristics of the sample populations from pre test to post test, the effect of the interaction among the independent variables, and the fact that the OAP instrument has a tendency to pick up certain pieces of background characteristic data and erroneously report small, but significant portions of them as organizational assessment information, and furthermore appears to be more sensitive to background information on the post test than on the pre test. Specifically it was found, depending on the dependent variable of interest, that from as little as 4% to as much as 72% of the increases in OAP scores from pre test to post test can be accounted for due to the impact of background characteristics.*

*In two instances, however, background variables did serve to reduce the amount of change in pre test to post test scores.

When controlling for such factors, OAP scores were still found to increase from pre test to post test, but at a reduced rate. In other words, the actual rate of increase in OAP scores from pre test to post test to date has not been as great as the raw data has indicated. To determine the rate of change more accurately in the future, corrected OAP scores must be computed. As with point in time comparisons, period of time analyses also demand the calculation of corrected OAP scores so as to render the OAP more a measure of organizational perceptions, and less a measure of individual background characteristics.

The following illustration summarizes some of the causes of OAP score bias, by category. In as much as OAP score categories build upon each other in some ways (the statistical techniques used in period of time reviews are an extrapolation of the techniques used in point in time comparisons; valid specific point in time scores are needed to affect any valid period of time reviews and point in time comparisons), the causes of bias compounded by category, as the pyramid structure illustrated below implies. As noted, specific point in time OAP scores are influenced by level 1 factors, point in time comparisons are influenced by levels 1 through 3, and period of time change scores by levels 1 through 4.

<u>LEVEL</u>	<u>SOURCE OF BIAS</u>	<u>OAP SCORE CATEGORY</u>
4	OAP Instrument Is More Sensitive To Background Characteristics On The Post Test Than On The Pre Test	Period of Time Score Changes
3	Variation In Background Characteristics Between Sample Populations	Point In Time Comparisons
2	OAP Instrument Reports Some Background Characteristics Information As Organizational Assessment Information	Specific Point in Time Scores
1	Interaction of Highly Correlated Independent Variables Artificially Inflates OAP Scores	Specific Point in Time Scores

AD-A113 708

SOUTHEASTERN CENTER FOR ELECTRICAL ENGINEERING EDUCAT--ETC F/6 5/1
USAF SUMMER FACULTY RESEARCH PROGRAM. 1981 RESEARCH REPORTS, V0--ETC(U)
OCT 81 W D PEELE F49620-79-C-0038

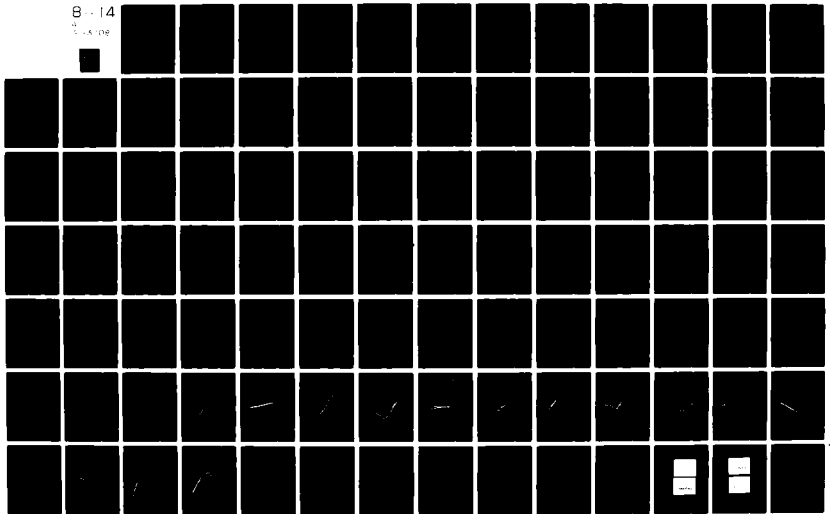
UNCLASSIFIED

AFOSR-TR-82-0227

NL

B-14

1-A-106



From the typologies it was derived that, categorically, older, white, females, who are at a higher pay grade, with more years in the Air Force, who possess a higher level of education, a higher level of professional military education, more months at their present station, who work in smaller work groups, on stable, day shift hours, who supervise more people, whose own supervisor writes the respondent's performance report, and work in organizations where group meetings are held more frequently, and are more frequently used to solve problems and set goals, score the OAP higher on both the pre test and the post test. The greatest positive changes in OAP scores over time occur, categorically, among older, non-white, females, with Doctorates, who supervise six or more persons. The greatest negative changes in OAP scores over time occur among those with Masters' Degrees or are 20 years of age or less.

These conclusions are tendered with some caution. There are a number of extraneous, intervening situations and circumstances, in addition to background characteristics, that may be causing the variation in the OAP scores. Additionally, there are several serious flaws in this present panel-type research design itself, not the least of which is that fact that those who took the post test may not have even received the treatment. This has been a descriptive, non-experimental, panel-type designed research effort, and the results must be viewed from this context.

Of even greater concern has been the less than appropriate application of statistical techniques to this specific data set. For example, a tremendous amount of interaction was found to exist among the independent variables. This was controlled through the use of multiple classification analyses, resulting in a composite variance explained figure. However, it was found that many of the independent variables possess curvilinear relationships with the dependent variables. To identify the extent of the total relationship (linear plus non linear), the η^2 statistic was employed. However, η^2 does not partial out interaction among the independent variables. Future examinations of this data set must employ a partial η^2 or perhaps some type of a polynomial curve that can both account for curvilinear trends in the data, and control for interaction among the independent variables. In addition, efforts will need to be made, perhaps through the use of Path Analysis, to distinguish the artificial compounding impact of highly correlated independent variable interaction upon OAP scores, from any real impact.

VI. REFERENCES

1. Campbell, D.T. and Stanley, J.C., Experimental and Quasi-Experimental Designs for Research Chicago, Illinois: Rand-McNally, 1963.
2. Conlon, E.J. Investigations of Behavioral Consultants in the Air Force Washington, D.C.: USAF/SCEEE Research Reports, Volume I, 1980.
3. Cook, T.D. and Campbell, D.T., Quasi-Experimentation, Chicago, Illinois: Rand-McNally, 1979.
4. Hendrix, W.H. and Halverson, V.B., Organizational Survey Assessment Package for Air Force Organizations Occupation and Manpower Research Division, Brooks AFB, Texas, 1979.
5. Markus, G.B. Analyzing Panel Data. London: Sage Publications, 1979.

VII. APPENDIX

ITEM STATEMENT

Personal Characteristics

Your Age Is:

1. 20 or less
2. 21-25
3. 26-30
4. 31-35
5. 36-40
6. 41-50
7. 51 or more

Gender:

1. Male
2. Female

Your Pay Grade Is:

1. 1-2
2. 3
3. 4
4. 5
5. 6-9
7. 10-12
8. 13-18

Years in the Air Force

1. Less than 1 year
2. More than 1 year, less than 2 years
3. More than 2 years, less than 3 years
4. More than 3 years, less than 4 years
5. More than 4 years, less than 8 years
6. More than 8 years

Your Ethnic Group Is:

1. American Indian or Alaskan Native
2. Asian or Pacific Islander
3. Black, not of Hispanic Origin
4. Hispanic
5. White, not of Hispanic Origin
6. Other

ITEM STATEMENT

Organizational Characteristics

Total Months At This Station:

1. Less than 1 month
2. More than 1 month, less than 6 months
3. More than 6 months, less than 12 months
4. More than 12 months, less than 18 months
5. More than 18 months, less than 24 months
6. More than 24 months, less than 36 months
7. 36 months or more

For How Many People Do You Write Performance Reports?

1. None
2. 1
3. 2
4. 3
5. 4-5
6. 6-8
7. 9 or more

Does Your Supervisor Actually Write Your Performance Report?

1. Yes
2. No
3. Not Sure

Your Work Requires You To Work Primarily:

1. Alone
2. With one or two people
3. As a small work group (3-5)
4. As a large work group (6 or more)

Your Highest Educational Level Obtained Is:

1. Non-high school graduate
2. High school graduate or GED
3. Less than two years of college
4. Two years or more of college
5. Bachelors Degree
6. Masters Degree
7. Doctoral Degree

Highest Level of Professional Military Education:

1. NCO Phase 1 or 2
2. NCO Phase 3
3. NCO Phase 4
4. NCO Phase 5
5. Squadron Officer School
6. Intermediate Service School
7. Senior Service School

What Is Your Usual Work Schedule?

1. Day shift, normally stable hours
2. Swing shift
3. Mid shift
4. Rotating shift schedule
5. Day or shift work, irregular/unstable hours
6. Frequent TDY/travel or frequently on call
7. Crew schedule

How Often Are Group Meetings Used to Solve Problems and Set Goals?

1. Never
2. Occasionally
3. About half the time
4. All of the time

How Often Does Your Supervisor Hold Group Meetings?

1. Never
2. Occasionally
3. Monthly
4. Weekly
5. Daily
6. Continuously

TABLE 1

BACKGROUND INFORMATION ITEMS

Dependent Variable	Pre Test Mean	Post Test Mean	Arithmetic Difference	Proportional Difference
Job Enrichment Needs	5.5327	5.5051	-.0276	-.0050
Task Autonomy	3.9861	4.1719	.1858	.0466
Advancement/Recognition	4.1022	4.1730	.0708	.0173
Perceived Productivity	5.5076	5.5832	.0756	.0137
Job Satisfaction	4.9658	5.0990	.1332	.0268
Perceived Supervisor Capacity	5.0931	5.1112	.0181	.0036
Organizational Climate	4.8059	4.9759	.1700	.0354

TABLE 2
RAW DATA DEPENDENT VARIABLE MEAN SCORES

Item	Pre Test Data		Post Test Data	
	Absolute Frequency	Relative Frequency	Absolute Frequency	Relative Frequency
Sample Population	77055	100.0	23547	100.0
Age:	$\bar{x} = 30.96$		$\bar{x} = 31.67$	
1. 20 or less	9361	12.3	1555	7.0
2. 21-25-	19424	25.6	5886	26.5
3. 26-30	14078	18.6	3986	17.9
4. 31-35	11414	15.1	3482	15.7
5. 36-40	8774	11.6	2831	12.8
6. 41-50	8246	10.8	2807	12.7
7. 51 or more	4533	5.9	1631	7.4
Gender:				
1. Male	63740	83.3	19292	82.5
2. Female	12737	16.7	4100	17.5
Pay Grade:				
1. 1-2	6949	10.2	2141	10.1
2. 3	14661	21.5	4352	20.6
3. 4	13812	20.2	4265	20.1
4. 5	13305	19.5	3937	18.6
5. 6-9	14577	21.4	4430	20.9
6. 10-12	3945	5.8	1565	7.4
7. 13-18	1035	1.5	490	2.3
Years in the Air Force:				
1. 1 or less	6087	8.6	1618	8.0
2. 1-2	7260	10.2	2382	11.8
3. 2-3	6792	9.6	2120	10.5
4. 3-4	6765	9.5	2152	10.6
5. 4-8	13003	18.3	3682	18.2
6. 8 or more	31091	43.8	8284	35.2
Race:				
1. Non-white	18536	24.3	5332	22.8
2. White	57717	75.7	18027	77.2

Item	Pre Test Data		Post Test Data	
	Absolute Frequency	Relative Frequency	Absolute Frequency	Relative Frequency
Level of Education:				
1. Less than H.S.	1831	2.4	432	1.8
2. H.S./GED	29562	38.6	8672	37.0
3. Less than 2 Years college	19876	26.0	5838	24.9
4. More than 2 Years college	10510	13.7	3215	13.7
5. Bachelors Degree	8831	11.5	3277	14.0
6. Masters Degree	5013	6.5	1774	7.6
7. Doctorate	943	1.2	260	1.1
Professional Military Education-NCO:				
1. NCO Phase 1-2	14922	44.7	4164	44.6
2. NCO Phase 3	9551	28.6	2581	27.6
3. NCO Phase 4	6119	18.3	1802	19.3
4. NCO Phase 5	2773	8.3	796	8.5
Professional Military Education-CO:				
1. Squadron Officer School	3352	36.5	1094	36.1
2. Intermediate Service School	4502	49.0	1410	46.5
3. Senior Service School	1342	14.6	529	17.4
Months at Present Station:				
1. 1 or less	1179	1.5	253	1.1
2. 1-6	9287	12.1	2422	10.3
3. 6-12	11822	15.5	3355	14.3
4. 12-18	9465	12.4	2669	11.4
5. 18-24	8535	11.2	2493	10.7
6. 24-36	12393	16.2	3854	16.5
7. 36 or more	23781	31.1	8358	35.7
For How Many People Do You Write Performance Reports?				
1. None	42033	64.5	13531	65.2
2. 1	4645	7.1	1491	7.2
3. 2	4198	6.4	1263	6.1
4. 3	3560	5.5	1142	5.5
5. 4-5	5655	8.7	1750	8.4
6. 6-8	3066	4.7	982	4.7
7. 9 or more	2045	3.1	601	2.9

Item	Pre Test Data		Post Test Data	
	Absolute Frequency	Relative Frequency	Absolute Frequency	Relative Frequency
Does Your Supervisor Write Your Performance Report?				
1. Yes	56165	76.2	17649	76.7
2. No	8856	12.0	2778	12.1
3. Not Sure	8686	11.8	2572	11.2
Work Requires You to Work Primarily:				
1. Alone	5232	18.0	1325	22.6
2. With 1-2 Persons	8710	30.0	1429	24.3
3. With 3-5 Persons	7519	25.9	1762	30.0
4. With 6 or more persons	7553	26.0	1358	23.1
Usual Work Schedule:				
1. Day Shift, Stable	50132	67.2	16615	71.3
2. Swing Shift	3317	4.5	1086	4.7
3. Mid Shift	1668	2.2	463	2.0
4. Rotating Shift Schedule	8092	10.9	1931	8.3
5. Day or Shift, irreg/unstable	6833	9.2	1631	7.0
6. Frequent TDY/travel/ frequent on call	1931	2.6	451	1.9
7. Crew Schedule	2628	3.5	1121	4.8
Group Meetings Used to Solve Problems and Set Goals:				
1. Never	18315	24.9	4720	20.5
2. Occasional	30701	41.7	9629	41.8
3. Almost half the time	11782	16.0	4222	18.3
4. All the time	12884	17.5	4474	19.4
How Often Does Your Supervisor Hold Group Meetings?				
1. Never	11603	15.6	2801	12.0
2. Occasionally	24324	32.7	7003	30.1
3. Monthly	6703	9.0	2436	10.5
4. Weekly	23718	31.8	8619	37.1
5. Daily	6422	8.6	1884	8.1
6. Continuously	1716	2.3	503	2.2

TABLE 3
BACKGROUND ITEM FREQUENCIES

	Age	Gender	Pay Grade	Years in AF	Race*	Level of Education	NCO PME	CO PME	Months at Present Station
Age	.0271								
Gender	-.1000								
Pay Grade	.6731	-.1438	.5721	.0334	.1022	.2327	.0669	.0197	.1177
Years in the Air Force	.6383	-.0092	.0556	.2110	.0133	.1054	.3037	.1891	-.1129
Race*	.0651	-.0673	.1135	.5064	.0028	.0743	-.1129	.0546	.0337
Level of Education	.2305	-.1734	.5473	-.0072	.0578	.1721	.1422	.0126	-.1286
NCO PME	.5666	-.0276	.4325	.4839	.0193	-.0478	-.1331	-.1002	.0022
CO PME	.2510	.0017	.4272	.3866	-.0197	.0872	.1103	.0313	.0139
Months at Present Station	.4352	-.1457	.2519	-.1421	.0072	-.0629	.1322	.0531	.0842
Supervisory Responsibilities	.3060	.0047	-.1238	.1238	.0107	.0498	.1624	-.0150	.1897
Supervisor Writes Reports**	-.1258	-.0521	.0537	-.1461	.0159	.1089	.2296	.0830	.0499
Work Group Size	.1115	-.1321	-.2089	.0408	.0360	.2448	.2373	.0093	.0936
Usual Work Schedule***	-.2545	-.0204	.0216	.0883	.1115	.1852	.0970	.0372	-.0872
Use of Group Meetings	.0676	-.0764	.0554	.1693	.0387	.0775	.1527	.0583	
Frequency of Group Meetings	.0983	-.0549	.1291	.2687	-.0181	.0665			
Job Enrichment Needs	.1561	.0479	.2669	.1281	.0251	.0995			
Task Autonomy	.3361	.0479	.2669	.1281	.0329	.0127			
Advancement/Recognition	.0347	-.0811	.0138	.1285	-.0026	.0654			
Perceived Productivity	.1798	.0231	.1037	.1556	-.0151				
Job Satisfaction	.2811	.0591	.1783	.0543					
Perceived Supervisor Capacity	.0511	.0105	-.0385	.0572					
Organizational Climate	.2020	.0442	.0693						

*Coded non-white/white

**Coded yes/all other

***Coded day shift, stable/all other

TABLE 4 - A
ZERO ORDER CORRELATIONS - PRE TEST DATA

	Supervisor Writes Reports**	Supervisor Reports**	Supervisor Writes Reports**	Work Group Size	Usual Work Schedule***	Use of Group Meetings
Supervisor Writes Reports**	-.0985	-.0313				
Work Group Size	.3056	.0784		.1033		
Usual Work Schedule***	-.0042	-.1380		.0927	-.0616	
Use of Group Meetings	.0945	-.0872		.1060	-.0581	.4946
Frequency of Group Meetings	.1558	-.0117		.0561	-.0827	.0885
Job Enrichment Needs	.1172	-.1551		-.0190	-.2703	.2280
Task Autonomy	.1563	-.1766		.1274	-.0722	.3270
Advancement/Recognition	.2209	-.1322		.0624	-.1028	.2669
Perceived Productivity	.1000	-.1563		.0512	-.2430	.3020
Job Satisfaction	.1077	-.1578		.0572	-.0593	.3789
Perceived Supervisor Capacity	.0608	-.0982		.0459	-.1248	.2645
Organizational Climate	.0769					

*Coded non-white/white

**Coded yes/all other

***Coded day shift, stable/all other

TABLE 4 - B
ZERO ORDER CORRELATIONS - PRE TEST DATA

	Frequency of Group Meetings	J/E Needs	Task Autonomy	Advancement/ Recognition	Perceived Productivity	Job Satisfaction	Perceived Supervisor Capacity
Job Enrichment Needs	.0803	.2800	.3819	.3533	.5123	.4427	.4707
Task Autonomy	.1520	.2093	.2931	.5436	.3970	.5911	
Advancement/Recognition	.2285	.1923	.5052	.4149	.4148		
Perceived Productivity	.1751	.2216	.2732	.4296			
Job Satisfaction	.1941	.0963	.3478				
Perceived Supervisor Capacity	.2518	.1163					
Organizational Climate	.1565						

*Coded non-white/white
 **Coded yes/all other
 ***Coded day shift, stable/all other

TABLE 4 - C
 ZERO ORDER CORRELATIONS - PRE TEST DATA

	Age	Gender	Pay Grade	Years in AF	Race*	Level of Education	NCO PME	CO PME	Months at Present Station
Age	.0278								
Gender	-.1054								
Pay Grade	.6653								
Years in the Air Force	.6305								
Race*	.0649								
Level of Education	.2675								
NCO PME	.5501								
CO PME	.2864								
Months at Present Station	.4175								
Supervisory Responsibilities	.2999								
Supervisor Writes Reports **	-.1419								
Work Group Size	.1165								
Usual Work Schedule***	-.2445								
Use of Group Meetings	.0495								
Frequency of Group Meetings	.0927								
Job Enrichment Needs	.1760								
Task Autonomy	.3436								
Advancement/Recognition	.0374								
Perceived Productivity	.1932								
Job Satisfisfaction	.2819								
Perceived Supervisor Capacity	.1297								
Organizational Climate	.2229								

*Coded non-white/white

**Coded yes/all other

***Coded day shift, stable/all other

TABLE 5 - A
ZERO ORDER CORRELATIONS - POST TEST DATA

	Supervisory Responsibilities	Supervisor Writes Reports**	Work Group Size	Usual Work Schedule***	Use of Group Meetings
Supervisor Writes Reports*	-.0991	-.0264	.0633	-.0572	.4928
Work Group Size	.2771	.0982	.0890	-.0472	.1007
Usual Work Schedule	.0007	-.1444	.1041	-.1006	.2295
Use of Group Meetings	.1009	-.0933	.0560	-.2754	.3480
Frequency of Group Meetings	.1652	-.0843	-.2752	-.0882	.2739
Job Enhancement Needs	.1413	-.1818	.0993	-.1156	.3193
Task Autonomy	.1775	-.1791	.0763	-.2475	.3920
Advancement/Recognition	.2406	-.1634	.0691	-.0821	.2696
Perceived Productivity	.1202	-.1825	.0699	-.1321	
Job Satisfaction	.1311	-.1845	.0468		
Perceived Supervisor Capacity	.0744	-.1234			
Organizational Climate	.0973				

*Coded non-white/white

**Coded yes/all other

***Coded day shift, stable/all other

TABLE 5 - B
ZERO ORDER CORRELATIONS - POST TEST DATA

Job Enrichment Needs	Frequency of Group Meetings	J/E Needs	Task Autonomy	Advancement/Recognition	Perceived Productivity	Job Satisfaction	Perceived Supervisor Cap.
Task Autonomy	.0961	.3152	.4075	.3829	.5493	.4666	.5182
Advancement/Recognition	.1655	.2391	.3320	.5779	.4278	.6054	
Perceived Productivity	.2493	.2332	.5415	.4350	.6061		
Job Satisfaction	.1868	.2709	.3061	.4554			
Perceived Supervisor Capacity	.2056	.1201	.3704				
Organizational Climate	.2613	.1486					
	.1648						

*Coded non-white/white

**Coded yes/all other

***Coded day shift, stable/all other

TABLE 5 - C
ZERO ORDER CORRELATIONS - POST TEST DATA

SOURCE	df	MS	F
JOB ENRICHMENT NEEDS			
Between Groups	6	892.03	567.81*
Within Groups	72445	1.57	
Total	72452		
TASK AUTONOMY			
Between Groups	6	3273.56	1679.72*
Within Groups	72444	1.95	
Total	72451		
ADVANCEMENT/RECOGNITION			
Between Groups	6	746.76	475.57*
Within Groups	70828	1.57	
Total	70835		
PERCEIVED PRODUCTIVITY			
Between Groups	6	705.23	444.25*
Within Groups	71595	1.59	
Total	71602		
JOB SATISFACTION			
Between Groups	6	1465.73	946.80*
Within Groups	64903	1.55	
Total	64910		
PERCEIVED SUPERVISOR CAPACITY			
Between Groups	6	482.01	137.77*
Within Groups	75823	3.50	
Total	75830		
ORGANIZATIONAL CLIMATE			
Between Groups	6	1593.24	583.86*
Within Groups	75823	2.73	
Total	75830		

*Significant at $p < .0001$

TABLE 6
ANALYSIS OF VARIANCE SUMMARY TABLE:
PRE TEST DATA - AGE

SOURCE	df	MS	F
JOB ENRICHMENT NEEDS			
Between Groups	1	363.24	220.82*
Within Groups	73047	1.65	
Total	73049		
TASK AUTONOMY			
Between Groups	1	372.02	167.69*
Within Groups	73052	2.22	
Total	73054		
ADVANCEMENT/RECOGNITION			
Between Groups	1	768.46	472.37*
Within Groups	71425	1.63	
Total	71427		
PERCEIVED PRODUCTIVITY			
Between Groups	1	63.35	38.47*
Within Groups	72207	1.65	
Total	72209		
JOB SATISFACTION			
Between Groups	1	385.18	229.50*
Within Groups	65418	1.68	
Total	65420		
PERCEIVED SUPERVISOR CAPACITY			
Between Groups	1	29.98	8.47**
Within Groups	76475	3.54	
Total	76477		
ORGANIZATIONAL CLIMATE			
Between Groups	1	426.83	149.5*
Within Groups	76475	2.86	
Total	76477		

*Significant at $p < .0001$

**Significant at $p = .004$

TABLE 7
ANALYSIS OF VARIANCE SUMMARY TABLE:
PRE TEST DATA - GENDER

SOURCE	df	MS	F
JOB ENRICHMENT NEEDS			
Between Groups	6	380.77	238.47*
Within Groups	65295	1.59	
Total	65302		
TASK AUTONOMY			
Between Groups	6	1919.85	934.97*
Within Groups	65267	2.05	
Total	65274		
ADVANCEMENT/RECOGNITION			
Between Groups	6	633.56	405.78*
Within Groups	63904	1.56	
Total			
PERCEIVED PRODUCTIVITY			
Between Groups	6	337.56	209.66*
Within Groups	64531	1.61	
Total	64538		
JOB SATISFACTION			
Between Groups	6	765.28	476.13*
Within Groups	58572	1.607	
Total	58579		
PERCEIVED SUPERVISOR CAPACITY			
Between Groups	6	932.94	271.60*
Within Groups	68277	3.44	
Total	68284		
ORGANIZATIONAL CLIMATE			
Between Groups	6	576.82	208.54*
Within Groups	68277	2.77	
Total	68284		

*Significant at $p < .0001$

TABLE 8
ANALYSIS OF VARIANCE SUMMARY TABLE:
PRE TEST DATA - PAY GRADE

SOURCE	df	MS	F
JOB ENRICHMENT NEEDS			
Between Groups	5	697.41	433.43*
Within Groups	67815	1.61	
Total	67821		
TASK AUTONOMY			
Between Groups	5	2633.80	1301.88*
Within Groups	67770	2.02	
Total	67776		
ADVANCEMENT/RECOGNITION			
Between Groups	5	691.35	441.92*
Within Groups	66456	1.56	
Total	66462		
PERCEIVED PRODUCTIVITY			
Between Groups	5	609.14	379.43*
Within Groups	67039	1.61	
Total	67045		
JOB SATISFACTION			
Between Groups	5	1077.93	669.68*
Within Groups	60668	1.61	
Total	60674		
PERCEIVED SUPERVISOR CAPACITY			
Between Groups	5	1831.36	536.46*
Within Groups	70992	3.41	
Total	70998		
ORGANIZATIONAL CLIMATE			
Between Groups	5	1176.51	429.46*
Within Groups	70992	2.74	
Total	70998		

*Significant at $p < .0001$

TABLE 9
ANALYSIS OF VARIANCE SUMMARY TABLE:
PRE TEST DATA - YEARS IN THE AIR FORCE

SOURCE	df	MS	F
JOB ENRICHMENT NEEDS			
Between Groups	1	49.475	17.407*
Within Groups	76251	2.842	
Total	76253		
TASK AUTONOMY			
Between Groups	1	233.96	105.42*
Within Groups	72901	2.22	
Total	72903		
ADVANCEMENT/RECOGNITION			
Between Groups	1	1.788	.51
Within Groups	76251	3.518	
Total	76253		
PERCEIVED PRODUCTIVITY			
Between Groups	1	73.81	44.88*
Within Groups	65314	1.68	
Total	65316		
JOB SATISFACTION			
Between Groups	1	73.81	44.88*
Within Groups	72063	1.65	
Total	72065		
PERCEIVED SUPERVISOR CAPACITY			
Between Groups	1	40.51	24.76*
Within Groups	71294	1.64	
Total	71296		
ORGANIZATIONAL CLIMATE			
Between Groups	1	1492.08	917.41*
Within Groups	72908	1.63	
Total	72910		

*Significant at $p < .0001$

TABLE 10
ANALYSIS OF VARIANCE SUMMARY TABLE:
PRE TEST DATA - RACE

SOURCE	df	MS	F
JOB ENRICHMENT NEEDS			
Between Groups	6	1254.89	811.64*
Within Groups	73188	1.55	
Total	73195		
TASK AUTONOMY			
Between Groups	6	1077.05	504.11*
Within Groups	73181	2.14	
Total	73188		
ADVANCEMENT/RECOGNITION			
Between Groups	6	133.82	82.31*
Within Groups	71566	1.63	
Total	71573		
PERCEIVED PRODUCTIVITY			
Between Groups	6	98.34	60.00*
Within Groups	72333	1.64	
Total	72340		
JOB SATISFACTION			
Between Groups	6	278.58	167.96*
Within Groups	65549	1.66	
Total	65556		
PERCEIVED SUPERVISOR CAPACITY			
Between Groups	6	137.38	39.06*
Within Groups	76559	3.52	
Total	76566		
ORGANIZATIONAL CLIMATE			
Between Groups	6	489.29	173.85*
Within Groups	76559	2.81	
Total	76566		

*Significant at $p < .0001$

TABLE 11
ANALYSIS OF VARIANCE SUMMARY TABLE:
PRE TEST DATA - LEVEL OF EDUCATION

SOURCE	df	MS	F
JOB ENRICHMENT NEEDS			
Between Groups	3	472.39	305.61*
Within Groups	32556	1.56	
Total	32560		
TASK AUTONOMY			
Between Groups	3	1296.27	625.85*
Within Groups	32646	2.07	
Total	32650		
ADVANCEMENT/RECOGNITION			
Between Groups	3	948.24	643.72*
Within Groups	31993	1.47	
Total	31997		
PERCEIVED PRODUCTIVITY			
Between Groups	3	341.34	205.66*
Within Groups	32186	1.66	
Total	32190		
JOB SATISFACTION			
Between Groups	3	594.88	358.84*
Within Groups	29343	1.66	
Total	29347		
PERCEIVED SUPERVISOR CAPACITY			
Between Groups	3	334.73	108.34*
Within Groups	33361	3.09	
Total	33365		
ORGANIZATIONAL CLIMATE			
Between Groups	3	725.78	273.96*
Within Groups	33435	2.65	
Total	33439		

*Significant at $p < .0001$

TABLE 12
ANALYSIS OF VARIANCE SUMMARY TABLE:
PRE TEST DATA - NCO PME

Source	df	MS	F
JOB ENRICHMENT NEEDS			
Between Groups	2	207.95	179.95*
Within Groups	9264	1.16	
Total	9267		
TASK AUTONOMY			
Between Groups	2	418.98	205.03*
Within Groups	9234	2.04	
Total	9237		
ADVANCEMENT/RECOGNITION			
Between Groups	2	84.46	53.52*
Within Groups	9054	1.58	
Total	9057		
PERCEIVED PRODUCTIVITY			
Between Groups	2	38.56	27.29*
Within Groups	9137	1.41	
Total	9140		
JOB SATISFACTION			
Between Groups	2	130.90	83.70*
Within Groups	8431	1.48	
Total	8434		
PERCEIVED SUPERVISOR CAPACITY			
Between Groups	2	111.23	40.10*
Within Groups	9407	2.77	
Total	9410		
ORGANIZATION CLIMATE			
Between Groups	2	210.33	92.25*
Within Groups	9407	2.28	
Total	9410		

* Significant at $p < .0001$

TABLE 13
ANALYSIS OF VARIANCE SUMMARY TABLE:
PRE TEST DATA - CO PME

SOURCE	df	MS	F
JOB ENRICHMENT NEEDS			
Between Groups	6	147.04	89.90*
Within Groups	73079	1.64	
Total	73086		
TASK AUTONOMY			
Between Groups	6	1135.95	533.05*
Within Groups	73076	2.13	
Total	73083		
ADVANCEMENT/RECOGNITION			
Between Groups	6	82.99	50.90*
Within Groups	71458	1.63	
Total	71465		
PERCEIVED PRODUCTIVITY			
Between Groups	6	244.62	150.57*
Within Groups	72232	1.63	
Total	72239		
JOB SATISFACTION			
Between Groups	6	476.69	290.33*
Within Groups	65448	1.64	
Total	65455		
PERCEIVED SUPERVISOR CAPACITY			
Between Groups	6	1173.09	341.52*
Within Groups	76455	3.44	
Total	76462		
ORGANIZATIONAL CLIMATE			
Between Groups	6	583.32	208.32*
Within Groups	76455	2.80	
Total	76462		

*Significant at $p < .0001$

TABLE 14
ANALYSIS OF VARIANCE SUMMARY TABLE:
PRE TEST DATA - MONTHS AT PRESENT STATION

SOURCE	df	MS	F
JOB ENRICHMENT NEEDS			
Between Groups	6	264.12	166.91*
Within Groups	63652	1.58	
Total	63659		
TASK AUTONOMY			
Between Groups	6	710.86	328.77*
Within Groups	63799	2.16	
Total	63806		
ADVANCEMENT/RECOGNITION			
Between Groups	6	951.95	619.20*
Within Groups	62434	1.54	
Total	64441		
PERCEIVED PRODUCTIVITY			
Between Groups	6	182.20	112.75*
Within Groups	62900	1.62	
Total	62907		
JOB SATISFACTION			
Between Groups	6	210.52	126.71*
Within Groups	57165	1.66	
Total	57172		
PERCEIVED SUPERVISOR CAPACITY			
Between Groups	6	135.24	44.09*
Within Groups	65195	3.07	
Total	65202		
ORGANIZATIONAL CLIMATE			
Between Groups	6	216.60	79.66*
Within Groups	65195	2.72	
Total	65202		

*Significant at $p < .0001$

TABLE 15
ANALYSIS OF VARIANCE SUMMARY TABLE:
PRE TEST DATA - SUPERVISORY RESPONSIBILITIES

SOURCE	df	MS	F
JOB ENRICHMENT NEEDS			
Between Groups	1	610.13	372.41*
Within Groups	71982	1.64	
Total	71984		
TASK AUTONOMY			
Between Groups	1	3849.93	1773.27*
Within Groups	71986	2.17	
Total	71988		
ADVANCEMENT/RECOGNITION			
Between Groups	1	3589.64	2265.88*
Within Groups	70423	1.58	
Total	70425		
PERCEIVED PRODUCTIVITY			
Between Groups	1	2044.95	1264.64*
Within Groups	71150	1.62	
Total	71152		
JOB SATISFACTION			
Between Groups	1	2652.81	1615.04*
Within Groups	64460	1.64	
Total	64462		
PERCEIVED SUPERVISOR CAPACITY			
Between Groups	1	5723.97	1886.31*
Within Groups	73847	3.03	
Total	73849		
ORGANIZATIONAL CLIMATE			
Between Groups	1	2002.99	726.90*
Within Groups	74301	2.76	
Total	74303		

*Significant at $p < .0001$

TABLE 16
ANALYSIS OF VARIANCE SUMMARY TABLE:
PRE TEST DATA - SUPERVISOR WRITES REPORTS

SOURCE	df	MS	F
JOB ENRICHMENT NEEDS			
Between Groups	3	117.24	72.99*
Within Groups	28357	1.61	
Total	28361		
TASK AUTONOMY			
Between Groups	3	183.96	84.95*
Within Groups	28348	2.16	
Total	28353		
ADVANCEMENT/RECOGNITION			
Between Groups	3	260.79	157.90*
Within Groups	27711	1.65	
Total	27715		
PERCEIVED PRODUCTIVITY			
Between Groups	3	79.41	50.08*
Within Groups	28002	1.59	
Total	28006		
JOB SATISFACTION			
Between Groups	3	54.23	32.30*
Within Groups	25569	1.68	
Total	25573		
PERCEIVED SUPERVISOR CAPACITY			
Between Groups	3	94.90	30.33*
Within Groups	29010	3.13	
Total	29014		
ORGANIZATIONAL CLIMATE			
Between Groups	3	74.21	27.30*
Within Groups	29010	2.72	
Total	29014		

*Significant at $p < .0001$

TABLE 17
ANALYSIS OF VARIANCE SUMMARY TABLE:
PRE TEST DATA - WORK GROUP SIZE

SOURCE	df	MS	F
JOB ENRICHMENT NEEDS			
Between Groups	1	820.52	500.87*
Within Groups	72670	1.64	
Total	72672		
TASK AUTONOMY			
Between Groups	1	11799.73	5727.83*
Within Groups	72694	2.06	
Total	72696		
ADVANCEMENT/RECOGNITION			
Between Groups	1	606.52	372.33*
Within Groups	71088	1.63	
Total	71090		
PERCEIVED PRODUCTIVITY			
Between Groups	1	1250.18	767.34*
Within Groups	71838	1.63	
Total	71840		
JOB SATISFACTION			
Between Groups	1	6478.50	4083.82*
Within Groups	65082	1.59	
Total	65084		
PERCEIVED SUPERVISOR CAPACITY			
Between Groups	1	818.79	263.03*
Within Groups	74603	3.11	
Total	74605		
ORGANIZATIONAL CLIMATE			
Between Groups	1	3271.60	1186.04*
Within Groups	75063	2.76	
Total	75065		

*Significant at $p < .0001$

TABLE 18
ANALYSIS OF VARIANCE SUMMARY TABLE:
PRE TEST DATA - USUAL WORK SCHEDULE

SOURCE	df	MS	F
JOB ENRICHMENT NEEDS			
Between Groups	3	312.83	192.20*
Within Groups	71841	1.63	
Total	71845		
TASK AUTONOMY			
Between Groups	3	3017.05	1441.05*
Within Groups	71885	2.09	
Total	71889		
ADVANCEMENT/RECOGNITION			
Between Groups	3	4420.38	3049.79*
Within Groups	70321	1.45	
Total	70325		
PERCEIVED PRODUCTIVITY			
Between Groups	3	2961.42	1952.18*
Within Groups	71119	1.52	
Total	71123		
JOB SATISFACTION			
Between Groups	3	2431.33	2431.33*
Within Groups	64434	1.51	
Total	64438		
PERCEIVED SUPERVISOR CAPACITY			
Between Groups	3	11666.74	4512.55*
Within Groups	73678	2.59	
Total	73682		
ORGANIZATIONAL CLIMATE			
Between Groups	3	5074.02	1998.87*
Within Groups	73678	2.54	
Total	73682		

*Significant at $p < .0001$

TABLE 19
ANALYSIS OF VARIANCE SUMMARY TABLE:
PRE TEST DATA - USE OF GROUP MEETINGS

SOURCE	df	MS	F
JOB ENRICHMENT NEEDS			
Between Groups	5	220.31	135.25*
Within Groups	72566	1.63	
Total	72572		
TASK AUTONOMY			
Between Groups	5	1422.84	670.32*
Within Groups	72637	2.12	
Total	72643		
ADVANCEMENT/RECOGNITION			
Between Groups	5	1523.85	993.95*
Within Groups	71029	1.53	
Total	71035		
PERCEIVED PRODUCTIVITY			
Between Groups	5	916.54	580.53*
Within Groups	71822	1.58	
Total	71828		
JOB SATISFACTION			
Between Groups	5	1339.14	847.55*
Within Groups	65048	1.58	
Total	65054		
PERCEIVED SUPERVISOR CAPACITY			
Between Groups	5	3668.12	1293.31*
Within Groups	74480	2.84	
Total	74487		
ORGANIZATIONAL CLIMATE			
Between Groups	5	1569.96	589.07*
Within Groups	74480	2.67	
Total	74486		

*Significant at $p < .0001$

TABLE 20
ANALYSIS OF VARIANCE SUMMARY TABLE:
PRE TEST DATA - FREQUENCY OF GROUP MEETINGS

SOURCE	df	MS	F
JOB ENRICHMENT NEEDS			
Between Groups	6	329.50	208.48*
Within Groups	22379	1.58	
Total	22386		
TASK AUTONOMY			
Between Groups	6	1071.89	546.21*
Within Groups	22425	1.96	
Total	22432		
ADVANCEMENT/RECOGNITION			
Between Groups	6	206.32	125.46*
Within Groups	22103	1.64	
Total	22110		
PERCEIVED PRODUCTIVITY			
Between Groups	6	473.24	315.09*
Within Groups	22365	1.53	
Total	22372		
JOB SATISFACTION			
Between Groups	6	473.24	315.09*
Within Groups	20827	1.50	
Total	20834		
PERCEIVED SUPERVISOR CAPACITY			
Between Groups	6	199.15	69.40*
Within Groups	23171	2.87	
Total	23178		
ORGANIZATIONAL CLIMATE			
Between Groups	6	535.30	209.65*
Within Groups	23171	2.55	
Total	23178		

*Significant at $p < .0001$

TABLE 21
ANALYSIS OF VARIANCE SUMMARY TABLE:
POST TEST DATA - AGE

SOURCE	df	MS	F
JOB ENRICHMENT NEEDS			
Between Groups	1	174.90	105.09*
Within Groups	22585	1.66	
Total	22587		
TASK AUTONOMY			
Between Groups	1	200.77	89.39*
Within Groups	22632	2.25	
Total	22634		
ADVANCEMENT/RECOGNITION			
Between Groups	1	161.21	94.92*
Within Groups	22301	1.70	
Total	22303		
PERCEIVED PRODUCTIVITY			
Between Groups	1	98.24	61.60*
Within Groups	22571	1.59	
Total	22573		
JOB SATISFACTION			
Between Groups	1	254.97	156.61*
Within Groups	21008	1.63	
Total	21010		
PERCEIVED SUPERVISOR CAPACITY			
Between Groups	1	130.69	44.69*
Within Groups	23390	2.93	
Total	23392		
ORGANIZATIONAL CLIMATE			
Between Groups	1	297.18	110.43*
Within Groups	23390	2.69	
Total	23393		

*Significant at $p < .0001$

TABLE 22
ANALYSIS OF VARIANCE SUMMARY TABLE:
POST TEST DATA - GENDER

SOURCE	df	MS	F
JOB ENRICHMENT NEEDS			
Between Groups	6	158.64	99.35*
Within Groups	20612	1.59	
Total	20619		
TASK AUTONOMY			
Between Groups	6	655.63	318.38*
Within Groups	20652	2.06	
Total	20659		
ADVANCEMENT/RECOGNITION			
Between Groups	6	230.23	142.41*
Within Groups	20230	1.62	
Total	20237		
PERCEIVED PRODUCTIVITY			
Between Groups	6	120.68	76.77*
Within Groups	20450	1.57	
Total	20457		
JOB SATISFACTION			
Between Groups	6	264.06	170.27*
Within Groups	19073	1.55	
Total	19080		
PERCEIVED SUPERVISOR CAPACITY			
Between Groups	6	86.45	30.00*
Within Groups	21173	2.88	
Total	21180		
ORGANIZATIONAL CLIMATE			
Between Groups	6	179.43	68.72*
Within Groups	21173	2.61	
Total	21180		

*Significant at $p < .0001$

TABLE 23
ANALYSIS OF VARIANCE SUMMARY TABLE:
POST TEST DATA - PAY GRADE

SOURCE	df	MS	F
JOB ENRICHMENT NEEDS			
Between Groups	5	223.78	136.38*
Within Groups	19615	1.64	
Total	19621		
TASK AUTONOMY			
Between Groups	5	702.54	342.04*
Within Groups	19637	2.05	
Total	19643		
ADVANCEMENT/RECOGNITION			
Between Groups	5	180.38	111.99*
Within Groups	19369	1.61	
Total	19375		
PERCEIVED PRODUCTIVITY			
Between Groups	5	148.12	93.71*
Within Groups	19524	1.58	
Total	19530		
JOB SATISFACTION			
Between Groups	5	116.99	40.60*
Within Groups	18192	1.58	
Total	18198		
PERCEIVED SUPERVISOR CAPACITY			
Between Groups	5	116.99	40.60*
Within Groups	20232	2.88	
Total	20238		
ORGANIZATIONAL CLIMATE			
Between Groups	5	294.22	113.63*
Within Groups	20232	2.59	
Total	20238		

*Significant at $p < .0001$

TABLE 24
ANALYSIS OF VARIANCE SUMMARY TABLE:
POST TEST DATA - YEARS IN THE AIR FORCE

SOURCE	df	MS	F
JOB ENRICHMENT NEEDS			
Between Groups	1	642.67	392.51*
Within Groups	22544	1.64	
Total	22546		
TASK AUTONOMY			
Between Groups	1	66.51	29.59*
Within Groups	22600	2.25	
Total	22602		
ADVANCEMENT/RECOGNITION			
Between Groups	1	12.16	7.14**
Within Groups	22265	1.70	
Total	22267		
PERCEIVED PRODUCTIVITY			
Between Groups	1	38.55	24.12*
Within Groups	22529	1.60	
Total	22531		
JOB SATISFACTION			
Between Groups	1	12.02	7.35***
Within Groups	20979	1.63	
Total	20981		
PERCEIVED SUPERVISOR CAPACITY			
Between Groups	1	1.23	.42
Within Groups	23357	2.93	
Total			
ORGANIZATIONAL CLIMATE			
Between Groups	1	27.03	9.99****
Within Groups	23357	2.71	
Total	23359		

*Significant at $p < .0001$
 **Significant at $p = .0076$
 ***Significant at $p = .0068$

****Significant at $p = .0016$

TABLE 25
 ANALYSIS OF VARIANCE SUMMARY TABLE:
 POST TEST DATA - RACE

SOURCE	df	MS	F
JOB ENRICHMENT NEEDS			
Between Groups	6	414.91	265.68*
Within Groups	22636	1.56	
Total	22643		
TASK AUTONOMY			
Between Groups	6	336.12	155.18*
Within Groups	22694	2.17	
Total	22701		
ADVANCEMENT/RECOGNITION			
Between Groups	6	36.29	21.40*
Within Groups	22357	1.69	
Total	22364		
PERCEIVED PRODUCTIVITY			
Between Groups	6	42.77	26.94*
Within Groups	22624	1.59	
Total	22631		
JOB SATISFACTION			
Between Groups	6	64.09	39.50*
Within Groups	21058	1.62	
Total	21065		
PERCEIVED SUPERVISOR CAPACITY			
Between Groups	6	57.11	19.48*
Within Groups	23461	2.93	
Total	23468		
ORGANIZATIONAL CLIMATE			
Between Groups	6	122.33	45.51*
Within Groups	23461	2.69	
Total	23468		

*Significant at $p < .0001$

TABLE 26
ANALYSIS OF VARIANCE SUMMARY TABLE:
POST TEST DATA - LEVEL OF EDUCATION

SOURCE	df	MS	F
JOB ENRICHMENT NEEDS			
Between Groups	3	143.33	89.59*
Within Groups	9569	1.60	
Total	9573		
TASK AUTONOMY			
Between Groups	3	432.28	208.04*
Within Groups	9626	2.08	
Total	9630		
ADVANCEMENT/RECOGNITION			
Between Groups	3	297.24	194.64*
Within Groups	9419	1.53	
Total	9423		
PERCEIVED PRODUCTIVITY			
Between Groups	3	104.66	64.37*
Within Groups	9494	1.63	
Total	9498		
JOB SATISFACTION			
Between Groups	3	204.56	125.47*
Within Groups	8940	1.63	
Total	8944		
PERCEIVED SUPERVISOR CAPACITY			
Between Groups	3	130.06	44.59*
Within Groups	9837	2.92	
Total	9841		
ORGANIZATIONAL CLIMATE			
Between Groups	3	211.20	80.98*
Within Groups	9837	2.61	
Total	9841		

*Significant at $p < .0001$

TABLE 27
ANALYSIS OF VARIANCE SUMMARY TABLE:
POST TEST DATA - NCO PME

Source	df	MS	F
JOB ENRICHMENT NEEDS			
Between Groups	2	65.46	53.47*
Within Groups	2968	1.22	
Total	2971		
TASK AUTONOMY			
Between Groups	2	136.73	64.56*
Within Groups	2961	2.12	
Total	2964		
ADVANCEMENT/RECOGNITION			
Between Groups	2	13.19	7.80**
Within Groups	2912	1.69	
Total	2915		
PERCEIVED PRODUCTIVITY			
Between Groups	2	10.66	7.70***
Within Groups	2929	1.38	
Total	2932		
JOB SATISFACTION			
Between Groups	2	44.84	30.38*
Within Groups	2783	1.48	
Total	2786		
PERCEIVED SUPERVISOR CAPACITY			
Between Groups	2	9.37	9.75*
Within Groups	3030	.96	
Total	3033		
ORGANIZATION CLIMATE			
Between Groups	2	74.37	32.04*
Within Groups	3030	2.32	
Total	3033		

* Significant at $p < .0001$
 ** Significant at $p = .0004$
 *** Significant at $p = .0005$

TABLE 28

ANALYSIS OF VARIANCE SUMMARY TABLE:
 POST TEST DATA - CO PME

SOURCE	df	MS	F
JOB ENRICHMENT NEEDS			
Between Groups	6	50.83	30.62*
Within Groups	22580	1.66	
Total	22587		
TASK AUTONOMY			
Between Groups	6	345.66	159.69*
Within Groups	22630	2.17	
Total	22637		
ADVANCEMENT/RECOGNITION			
Between Groups	6	30.26	17.82*
Within Groups	22294	1.70	
Total	22301		
PERCEIVED PRODUCTIVITY			
Between Groups	6	72.65	45.96*
Within Groups	22574	1.58	
Total	22581		
JOB SATISFACTION			
Between Groups	6	107.53	66.78*
Within Groups	21009	1.61	
Total	21016		
PERCEIVED SUPERVISOR CAPACITY			
Between Groups	6	42.73	14.54*
Within Groups	23397	2.94	
Total	23404		
ORGANIZATIONAL CLIMATE			
Between Groups	6	127.51	47.52*
Within Groups	23397	2.68	
Total	23404		

*Significant at $p < .0001$

TABLE 29
ANALYSIS OF VARIANCE SUMMARY TABLE:
POST TEST DATA - MONTHS AT PRESENT STATION

SOURCE	df	MS	F
JOB ENRICHMENT NEEDS			
Between Groups	6	116.11	71.92*
Within Groups	20106	1.61	
Total	20113		
TASK AUTONOMY			
Between Groups	6	256.33	118.16*
Within Groups	20131	2.17	
Total	20138		
ADVANCEMENT/RECOGNITION			
Between Groups	6	355.95	224.04*
Within Groups	19881	1.59	
Total	19888		
PERCEIVED PRODUCTIVITY			
Between Groups	6	81.42	51.85*
Within Groups	20056	1.57	
Total	20063		
JOB SATISFACTION			
Between Groups	6	92.72	57.49*
Within Groups	18731	1.61	
Total	18738		
PERCEIVED SUPERVISOR CAPACITY			
Between Groups	6	58.23	20.22*
Within Groups	20753	2.88	
Total	20760		
ORGANIZATIONAL CLIMATE			
Between Groups	6	98.68	37.69*
Within Groups	20753	2.62	
Total	20760		

*Significant at $p < .0001$

TABLE 30
ANALYSIS OF VARIANCE SUMMARY TABLE:
POST TEST DATA - SUPERVISORY RESPONSIBILITIES

SOURCE	df	MS	F
JOB ENRICHMENT NEEDS			
Between Groups	1	265.57	160.31*
Within Groups	22385	1.66	
Total	22387		
TASK AUTONOMY			
Between Groups	1	1670.94	766.49*
Within Groups	22428	2.18	
Total	22430		
ADVANCEMENT/RECOGNITION			
Between Groups	1	1199.75	727.21*
Within Groups	21955	1.65	
Total	21957		
PERCEIVED PRODUCTIVITY			
Between Groups	1	951.21	609.58*
Within Groups	22208	1.56	
Total	22210		
JOB SATISFACTION			
Between Groups	1	1128.84	712.52*
Within Groups	20680	1.58	
Total	20682		
PERCEIVED SUPERVISOR CAPACITY			
Between Groups	1	2277.02	355.63*
Within Groups	22997	2.63	
Total	22999		
ORGANIZATIONAL CLIMATE			
Between Groups	1	936.47	355.63*
Within Groups	22997	2.63	
Total	22999		

*Significant at $p < .0001$

TABLE 31
ANALYSIS OF VARIANCE SUMMARY TABLE:
POST TEST DATA - SUPERVISOR WRITES PERFORMANCE REPORTS

SOURCE	df	MS	F
JOB ENRICHMENT NEEDS			
Between Groups	3	19.79	13.36*
Within Groups	5761	1.48	
Total	5765		
TASK AUTONOMY			
Between Groups	3	23.88	10.73*
Within Groups	5796	2.23	
Total	5800		
ADVANCEMENT/RECOGNITION			
Between Groups	3	39.55	22.91*
Within Groups	5653	1.73	
Total	5657		
PERCEIVED PRODUCTIVITY			
Between Groups	3	16.65	11.39*
Within Groups	5716	1.46	
Total	5720		
JOB SATISFACTION			
Between Groups	3	20.68	12.95*
Within Groups	5395	1.60	
Total	5399		
PERCEIVED SUPERVISOR CAPACITY			
Between Groups	3	26.35	9.65*
Within Groups	5870	2.73	
Total	5874		
ORGANIZATIONAL CLIMATE			
Between Groups	3	18.11	7.45*
Within Groups	5870	2.43	
Total	5874		

*Significant at $p < .0001$

TABLE 32
ANALYSIS OF VARIANCE SUMMARY TABLE:
POST TEST DATA - WORK GROUP SIZE

SOURCE	df	MS	F
JOB ENRICHMENT NEEDS			
Between Groups	1	382.05	231.74*
Within Groups	22645	1.65	
Total	22647		
TASK AUTONOMY			
Between Groups	1	3881.06	1863.76*
Within Groups	22703	2.08	
Total	22705		
ADVANCEMENT/RECOGNITION			
Between Groups	1	294.94	174.27*
Within Groups	22204	1.69	
Total	22206		
PERCEIVED PRODUCTIVITY			
Between Groups	1	479.76	304.62*
Within Groups	22477	1.58	
Total	22479		
JOB SATISFACTION			
Between Groups	1	2099.51	1365.37*
Within Groups	20921	1.54	
Total	20923		
PERCEIVED SUPERVISOR CAPACITY			
Between Groups	1	462.61	158.00*
Within Groups	23296	2.93	
Total	23298		
ORGANIZATIONAL CLIMATE			
Between Groups	1	1104.02	413.75*
Within Groups	23296	2.67	
Total	23298		

*Significant at $p < .0001$

TABLE 33
ANALYSIS OF VARIANCE SUMMARY TABLE:
POST TEST DATA - USUAL WORK SCHEDULE

SOURCE	df	MS	F
JOB ENRICHMENT NEEDS			
Between Groups	3	138.21	83.74*
Within Groups	22261	1.65	
Total	22265		
TASK AUTONOMY			
Between Groups	3	931.15	437.73*
Within Groups	22325	2.13	
Total	22329		
ADVANCEMENT/RECOGNITION			
Between Groups	3	1573.72	1055.91*
Within Groups	22015	1.49	
Total	22019		
PERCEIVED PRODUCTIVITY			
Between Groups	3	937.89	638.44*
Within Groups	22286	1.47	
Total	22290		
JOB SATISFACTION			
Between Groups	3	1237.94	848.57*
Within Groups	20749	1.46	
Total	20753		
PERCEIVED SUPERVISOR CAPACITY			
Between Groups	3	3614.71	1500.71*
Within Groups	23041	2.41	
Total			
ORGANIZATIONAL CLIMATE			
Between Groups	3	1556.86	635.21*
Within Groups	23041	2.45	
Total	23045		

*Significant at $p < .0001$

TABLE 34
ANALYSIS OF VARIANCE SUMMARY TABLE:
POST TEST DATA - USE OF GROUP MEETINGS

SOURCE	df	MS	F
JOB ENRICHMENT NEEDS			
Between Groups	5	101.13	61.46*
Within Groups	22440	1.65	
Total	22446		
TASK AUTONOMY			
Between Groups	5	467.80	217.84*
Within Groups	22508	2.15	
Total	22514		
ADVANCEMENT/RECOGNITION			
Between Groups	5	542.38	342.61*
Within Groups	22182	1.58	
Total	22188		
PERCEIVED PRODUCTIVITY			
Between Groups	5	309.49	202.16*
Within Groups	22459	1.53	
Total	22465		
JOB SATISFACTION			
Between Groups	5	408.84	266.03*
Within Groups	20895	1.54	
Total	20901		
PERCEIVED SUPERVISOR CAPACITY			
Between Groups	5	1070.99	401.34*
Within Groups	23240	2.67	
Total	23246		
ORGANIZATIONAL CLIMATE			
Between Groups	5	435.39	168.18*
Within Groups	23240	2.59	
Total	23246		

*Significant at $p < .0001$

TABLE 35
ANALYSIS OF VARIANCE SUMMARY TABLE:
POST TEST DATA - FREQUENCY OF GROUP MEETINGS

Category	Pre Test η^2	Post Test η^2	Arithmetic Difference	Proportional Difference
Personal Characteristics:				
Age	.0449	.0529	.0080	.1782
Gender	.0030	.0046	.0016	.5333
Pay Grade	.0214	.0281	.0067	.3131
Years in the AF	.0310	.0336	.0026	.0839
Race	.0124	.0171	.0047	.3790
Level of Education	.0624	.0658	.0034	.0545
NCO PME	.0274	.0273	-.0001	-.0036
CO PME	.0374	.0348	-.0026	-.0695
Organizational Characteristics:				
Months at Present Station	.0073	.0081	.0008	.1096
Supervisory Responsibilities	.0155	.0210	.0055	.3548
Supervisor Writes Reports	.0051	.0071	.0020	.3922
Work Group Size	.0077	.0069	-.0008	-.1039
Usual Work Schedule	.0068	.0101	.0033	.4853
Use of Group Meetings	.0080	.0112	.0032	.4000
Frequency of Group Meetings	.0092	.0135	.0043	.4674

TABLE 36

ETA SQUARED SUMMARY TABLE:
JOB ENRICHMENT NEEDS

Category	Pre Test η^2	Post Test η^2	Arithmetic Difference	Proportional Difference
Personal Characteristics:				
Age	.1221	.1275	.0054	.0442
Gender	.0023	.0039	.0016	.6957
Pay Grade	.0791	.0847	.0056	.0708
Years in the AF	.0876	.0801	-.0075	-.0856
Race	.0014	.0013	-.0001	-.0714
Level of Education	.0397	.0394	-.0003	-.0076
NCO PME	.0541	.0609	.0068	.1257
CO PME	.0425	.0418	-.0007	-.0165
Organizational Characteristics:				
Months at Present Station	.0419	.0406	-.0013	.0310
Supervisory Responsibilities	.0300	.0340	.0040	.1333
Supervisor Writes Reports	.0242	.0330	.0088	.3636
Work Group Size	.0089	.0055	-.0034	-.3820
Usual Work Schedule	.0735	.0759	.0024	.0327
Use of Group Meetings	.0567	.0556	-.0011	.0194
Frequency of Group Meetings	.0441	.0462	.0021	.0476

TABLE 37

ETA SQUARED SUMMARY TABLE:
TASK AUTONOMY

Category	Pre Test η^2	Post Test η^2	Arithmetic Difference	Proportional Difference
Personal Characteristics:				
Age	.0387	.0329	-.0058	-.1499
Gender	.0066	.0042	-.0024	-.3636
Pay Grade	.0367	.0405	.0038	.1035
Years in the AF	.0322	.0281	-.0041	-.1273
Race	.0003	.0003	.0000	.0000
Level of Education	.0069	.0057	-.0012	-.1739
NCO PME	.0569	.0584	.0015	.0264
CO PME	.0117	.0053	-.0064	-.5470
Organizational Characteristics:				
Months at Present Station	.0043	.0048	.0005	.1163
Supervisory Responsibilities	.0562	.0633	.0071	.1263
Supervisor Writes Reports	.0312	.0321	.0009	.0288
Work Group Size	.0168	.0120	-.0048	-.3478
Usual Work Schedule	.0052	.0078	.0026	.5000
Use of Group Meetings	.1151	.1258	.0107	.0930
Frequency of Group Meetings	.0654	.0717	.0063	.0963

TABLE 38

ETA SQUARED SUMMARY TABLE:
ADVANCEMENT/RECOGNITION

Category	Pre Test η^2	Post Test η^2	Arithmetic Difference	Proportional Difference
Personal Characteristics:				
Age	.0359	.0408	.0099	.1365
Gender	.0005	.0027	.0022	4.4000
Pay Grade	.0191	.0220	.0029	.1518
Years in the AF	.0275	.0234	-.0041	-.1491
Race	.0006	.0011	.0005	.8333
Level of Education	.0050	.0071	.0021	.4200
NCO PME	.0188	.0199	.0011	.0585
CO PME	.0059	.0052	-.0007	-.1186
Organizational Characteristics:				
Months at Present Station	.0124	.0121	-.0003	-.0242
Supervisory Responsibilities	.0106	.0153	.0047	.4434
Supervisor Writes Reports	.0175	.0267	.0092	.5257
Work Group Size	.0053	.0059	.0006	.1132
Usual Work Schedule	.0106	.0134	.0028	.2642
Use of Group Meetings	.0761	.0791	.0030	.0394
Frequency of Group Meetings	.0388	.0431	.0043	.1108

TABLE 39

ETA SQUARED SUMMARY TABLE:
PERCEIVED PRODUCTIVITY

Category	Pre Test η^2	Post Test η^2	Arithmetic Difference	Proportional Difference
Personal Characteristics:				
Age	.0805	.0832	.0027	.0335
Gender	.0035	.0074	.0039	1.1143
Pay Grade	.0465	.0508	.0043	.0925
Years in the AF	.0523	.0476	-.0047	-.0899
Race	.0011	.0004	.0007	.6364
Level of Education	.0151	.0111	-.0050	-.3311
NCO PME	.0354	.0404	.0050	.1412
CO PME	.0206	.0214	.0008	.0388
Organizational Characteristics:				
Months at Present Station	.0259	.0187	-.0072	-.2780
Supervisory Responsibilities	.0131	.0181	.0050	.3817
Supervisor Writes Reports	.0244	.0333	.0089	.3648
Work Group Size	.0038	.0071	.0033	.8684
Usual Work Schedule	.0590	.0613	.0023	.0390
Use of Group Meetings	.1017	.1093	.0076	.0747
Frequency of Group Meetings	.0612	.0598	-.0014	-.0229

TABLE 40
ETA SQUARED SUMMARY TABLE:
JOB SATISFACTION

Category	Pre Test eta ²	Post Test eta ²	Arithmetic Difference	Proportional Difference
Personal Characteristics:				
Age	.0108	.0177	.0069	.6389
Gender	.0001	.0019	.0018	1800.0000
Pay Grade	.0233	.0084	-.0149	-.6395
Years in the AF	.0364	.0099	-.0265	-.7280
Race	.0000	.0000	.0000	.0000
Level of Education	.0031	.0050	.0019	.6129
NCO PME	.0097	.0134	.0037	.3814
CO PME	.0085	.0057	-.0028	-.3294
Organizational Characteristics:				
Months at Present Station	.0261	.0037	-.0224	-.8582
Supervisory Responsibilities	.0040	.0058	.0018	.4500
Supervisor Writes Reports	.0249	.0340	.0091	.3655
Work Group Size	.0031	.0049	.0018	.5806
Usual Work Schedule	.0035	.0067	.0032	.9143
Use of Group Meetings	.1552	.1635	.0083	.0535
Frequency of Group Meetings	.0799	.0795	-.0004	.0050

TABLE 41

ETA SQUARED SUMMARY TABLE:
PERCEIVED SUPERVISOR CAPACITY

Category	Pre Test eta ²	Post Test eta ²	Arithmetic Difference	Proportional Difference
Personal Characteristics:				
Age	.0442	.0515	.0073	.1652
Gender	.0020	.0047	.0027	1.3500
Pay Grade	.0180	.0191	.0011	.0611
Years in the AF	.0294	.0273	-.0021	-.0714
Race	.0002	.0004	.0002	1.0000
Level of Education	.0134	.0115	-.0019	-.1418
NCO PME	.0240	.0241	.0001	.0042
CO PME	.0192	.0207	.0015	.0781
Organizational Characteristics:				
Months at Present Station	.0161	.0120	-.0041	-.2547
Supervisory Responsibilities	.0073	.0108	.0035	.4795
Supervisor Writes Reports	.0097	.0152	.0055	.5670
Work Group Size	.0028	.0038	.0010	.3571
Usual Work Schedule	.0156	.0175	.0019	.1218
Use of Group Meetings	.0753	.0764	.0011	.0146
Frequency of Group Meetings	.0380	.0349	-.0031	-.0816

TABLE 42

ETA SQUARED SUMMARY TABLE:
ORGANIZATIONAL CLIMATE

Independent Variables	Pre Test MCA Coefficient Adjusted For Independent Variables and Covariates ($\bar{X} = 5.55$)	Post Test MCA Coefficients Adjusted For Independent Variables and Covariates ($\bar{X} = 5.45$)	Post Test Score Minus Pre Test Score	Proportional Difference*
PERSONAL CHARACTERISTICS				
Age				
1) 20 or less	.02	-.01	-.13	-.0233
2) 21 - 25	.02	.00	-.12	-.0215
3) 26 - 30	-.02	-.06	-.14	-.0253
4) 31 - 35	.01	.04	-.07	-.0126
5) 36 - 40	.02	.12	.00	.0000
6) 41 - 50	-.01	.03	-.06	-.0108
7) 51 or more	-.29	-.27	-.08	-.0152
Gender				
1) Male	-.03	-.03	-.10	-.0181
2) Female	.30	.32	-.08	-.0137
Race				
1) Non-white	-.18	-.18	-.10	-.0186
2) White	.07	.06	-.11	-.0196
Level of Education				
1) Less than High School	-.24	-.09	.05	.0094
2) H.S./GED	-.18	-.17	-.09	-.0168
3) Less than 2 Yrs College	.08	.03	-.15	-.0266
4) More than 2 Yrs College	.16	.19	-.07	-.0123
5) Bachelors Degree	.30	.38	-.02	-.0034
6) Masters Degree	.26	.32	-.04	-.0069
7) Doctorate	.28	-1.07	-1.45	-.2487
NCO-PME				
1) NCO Phase 1-2	-.06	-.04	-.08	-.0146
2) NCO Phase 3	-.03	-.01	-.08	-.0145
3) NCO Phase 4	.11	.09	-.12	-.0212
4) NCO Phase 5	.26	.10	-.16	-.0275

Independent Variables	Pre Test MCA Coefficient Adjusted For Independent Variables and Covariates	Post Test MCA Coefficients Adjusted For Independent Variables and Covariates	Post Test Score Minus Pre Test Score	Proportional Difference*
ORGANIZATIONAL CHARACTERISTICS ($\bar{X} = 5.58$)				
For How Many People Do You Write Performance Reports?				
1) None	-.06	-.07	.04	.0072
2) 1	.12	.07	.00	.0000
3) 2	.11	.21	.15	.0264
4) 3	.05	.00	.00	.0000
5) 4-5	.07	.10	-.02	-.0035
6) 6-8	.12	.09	.02	.0035
7) 9 or more	.18	.14	.01	.0017
Your Supervisor Writes Your Performance Report				
1) Yes	.03	.02	.04	.0071
2) No/Not Sure	-.10	-.08	.07	.0128
Your Work Requires You to Work Primarily				
1) Alone	.11	.04	-.02	-.0035
2) With 1-2 persons	-.09	-.06	.08	.0146
3) With 3-5 persons	-.03	-.03	.05	.0090
4) With 6 or more persons	.06	.07	.06	.0106
Usual Work Schedule				
1) Day shift, stable hours	.03	.02	.04	.0071
2) Other	-.06	-.08	.03	.0054
Frequency of Group Meetings				
1) Never	-.01	.02	.08	.0144
2) Occasionally	-.03	-.12	-.04	-.0072
3) Monthly	-.02	.05	.12	.0216
4) Weekly	.05	.06	.16	.0284
5) Daily	-.07	-.01	.11	.0200
6) Continuously	.01	.02	.06	.0107

* (Post Test Mean plus Pre Test MCA Coefficient Category 1) minus Pre Test Score Category 1)
 (Pre Test Mean plus Pre Test MCA Coefficient Category 1)

TABLE 43
 MCA COEFFICIENT SUMMARY TABLE:
 JOB ENRICHMENT NEEDS

Independent Variables	Pre Test MCA Coefficient Adjusted For Independent Variables and Covariates (\bar{X} = 3.93)	Post Test MCA Coefficients Adjusted For Independent Variables and Covariates (\bar{X} = 4.04)	Post Test Score Minus Pre Test Score	Proportional Difference*
PERSONAL CHARACTERISTICS				
Age				
1) 20 or less	-.20	-.40	-.09	-.0241
2) 21 - 25	-.19	-.20	.10	.0267
3) 26 - 30	-.05	-.13	.03	.0077
4) 31 - 35	.06	.10	.15	.0376
5) 36 - 40	.22	.38	.27	.0651
6) 41 - 50	.39	.47	.19	.0440
7) 51 or more	.52	.70	.29	.0652
Gender				
1) Male	-.03	-.04	.18	.0462
2) Female	.32	.37	.16	.0376
Race				
1) Non-white	-.01	.01	.13	.0332
2) White	.00	.00	.11	.0280
Level of Education				
1) Less than High School	-.08	-.13	.06	.0156
2) H.S./GED	-.04	-.01	.14	.0360
3) Less than 2 Yrs College	.01	-.02	.08	.0203
4) More than 2 Yrs College	.03	.02	.10	.0253
5) Bachelors Degree	.14	.12	.09	.0221
6) Masters Degree	.01	.11	.21	.0533
7) Doctorate	-.03	.26	.34	.0872
NCO-PMI				
1) NCO Phase 1-2	-.09	-.11	.09	.0234
2) NCO Phase 3	-.03	.03	.17	.0436
3) NCO Phase 4	.09	.13	.15	.0373
4) NCO Phase 5	.48	.39	.02	.0045

Independent Variables	Pre Test MCA Coefficient Adjusted For Independent Variables and Covariates	Post Test MCA Coefficient Adjusted For Independent Variables and Covariates	Post Test Score Minus Pre Test Score	Proportional Difference*
ORGANIZATIONAL CHARACTERISTICS ($\bar{X} = 4.02$)				
For How Many People Do You Write Performance Reports? ($\bar{X} = 4.28$)				
1) None	-.13	-.18	.21	.0540
2) 1	.31	.23	.18	.0416
3) 2	.28	.17	.15	.0349
4) 3	.10	.21	.37	.0898
5) 4-5	.11	.25	.40	.0969
6) 6-8	.33	.27	.20	.0460
7) 9 or more	.42	.51	.30	.0676
Your Supervisor Writes Your Performance Report				
1) Yes	.07	.06	.25	.0611
2) No/Not Sure	-.24	-.28	.22	.0582
Your Work Requires You to Work Primarily				
1) Alone	.34	.21	.13	.0298
2) With 1-2 persons	-.01	.00	.27	.0673
3) With 3-5 persons	-.10	-.07	.29	.0740
4) With 6 or more persons	-.11	-.10	.27	.0691
Usual Work Schedule				
1) Day shift, stable hours	.21	.20	.25	.0591
2) Other	-.47	-.57	.16	.0451
Group Meetings Used to Solve Problems and Set Goals				
1) Never	-.46	-.44	.28	.0787
2) Occasionally	-.02	-.06	.22	.0618
3) About half the time	.18	.10	.18	.0429
4) All of the time	.45	.41	.22	.0492

* (Post Test Score Category 1 minus Pre Test Score Category 1) / (Pre Test Mean plus Pre Test MCA Coefficient Category 1)

TABLE 44
MCA COEFFICIENT SUMMARY TABLE:
TASK AUTONOMY

Independent Variables	Pre Test MCA Coefficient Adjusted For Independent Variables and Covariates	Post Test MCA Coefficients Adjusted For Independent Variables and Covariates	Post Test Score Minus Pre Test Score	Proportional Difference*
PERSONAL CHARACTERISTICS				
	(\bar{X} = 4.30)	(\bar{X} = 4.34)		
Age				
1) 20 or less	.03	-.01	.00	.0000
2) 21 - 25	-.06	-.08	.02	.0047
3) 36 - 30	.00	-.04	.00	.0000
4) 31 - 35	.10	.13	.07	.0159
5) 36 - 40	.14	.23	.13	.0293
6) 41 - 50	-.09	-.04	.09	.0214
7) 51 or more	-.68	-.49	.23	.0635
Gender				
1) Male	.00	-.01	.03	.0070
2) Female	.04	.08	.08	.0184
Race				
1) Non-white	.05	.06	.05	.0115
2) White	-.02	-.02	.04	.0093
Level of Education				
1) Less than High School	.00	.19	.23	.0535
2) H.S./GED	.02	.02	.04	.0093
3) Less than 2 Yrs College	.00	.00	.04	.0093
4) More than 2 Yrs College	-.05	-.06	.03	.0071
5) Bachelors Degree	.03	.07	.08	.0185
6) Masters Degree	-.14	-.41	-.23	-.0553
7) Doctorate	-.67	-.42	.29	.0799
NCO-PMI				
1) NCO Phase 1-2	-.15	-.15	.04	.0096
2) NCO Phase 3	.01	.05	.08	.0186
3) NCO Phase 4	.21	.25	.08	.0177
4) NCO Phase 5	.46	.36	-.07	-.0147

Independent Variables	Pre Test MCA Coefficient Adjusted For Independent Variables and Covariates	Post Test MCA Coefficients Adjusted For Independent Variables and Covariates	Post Test Score Minus Pre Test Score	Proportional Difference*
ORGANIZATIONAL CHARACTERISTICS (X = 4.14) (X = 4.35)				
For How Many People Do You Write Performance Reports?				
1) None	-.12	-.17	.16	.0398
2) 1	.26	.10	.05	.0114
3) 2	.22	.21	.20	.0459
4) 3	.15	.21	.27	.0629
5) 4-5	.23	.24	.22	.0503
6) 6-8	.22	.40	.39	.0894
7) 9 or more	.16	.35	.40	.0930
Your Supervisor Writes Your Performance Report				
1) Yes	.08	.08	.21	.0498
2) No/Not Sure	-.27	-.39	.09	.0233
Your Work Requires You to Work Primarily				
1) Alone	-.11	-.02	.30	.0744
2) With 1-2 persons	.00	-.03	.18	.0435
3) With 3-5 persons	-.01	.02	.24	.0581
4) With 6 or more persons	.08	.03	.16	.0379
Usual Work Schedule				
1) Day shift, stable hours	.04	.05	.22	.0526
2) Other	-.10	-.14	.17	.0421
Group Meetings Used to Solve Problems and Set Goals				
1) Never	-.52	-.54	.19	.0525
2) Occasionally	-.03	-.09	.15	.0365
3) About half the time	.23	.14	.12	.0275
4) All of the time	.51	.50	.20	.0430

* (Post Test Score Category 1 minus Pre Test Score Category 1) / (Pre Test Mean Plus Pre Test MCA Coefficient Category 1)

TABLE 45

MCA COEFFICIENT SUMMARY TABLE: ADVANCEMENT/RECOGNITION

Independent Variables	Pre Test MCA Coefficient Adjusted For Independent Variables and Covariates ($\bar{X} = 5.48$)	Post Test MCA Coefficients Adjusted For Independent Variables and Covariates ($\bar{X} = 5.48$)	Post Test Score Minus Pre Test Score	Proportional Difference*
PERSONAL CHARACTERISTICS				
Age				
1) 20 or less	-.02	-.44	-.42	-.0769
2) 21 - 25	-.16	-.13	.03	.0056
3) 26 - 30	-.07	-.06	.01	.0018
4) 31 - 35	.08	.09	.01	.0018
5) 36 - 40	.20	.25	.05	.0088
6) 41 - 50	.35	.24	-.09	-.0154
7) 51 or more	.34	.31	-.03	-.0052
Gender				
1) Male	-.01	-.01	.00	.0000
2) Female	.08	.11	.03	.0054
Race				
1) Non-white	-.02	-.06	-.04	.0073
2) White	.01	.02	.01	.0018
Level of Education				
1) Less than High School	-.20	.03	.23	.0436
2) H.S./GED	.01	-.01	-.02	-.0036
3) Less than 2 Yrs College	.03	.00	-.03	-.0054
4) More than 2 Yrs College	-.06	-.01	.05	.0092
5) Bachelors Degree	.01	.12	.11	.0200
6) Masters Degree	-.09	-.02	.07	.0130
7) Doctorate	.30	-.02	-.32	.0554
NCO-PME				
1) NCO Phase 1-2	-.03	-.03	.00	.0000
2) NCO Phase 3	.01	.02	.01	.0018
3) NCO Phase 4	.03	.01	-.02	-.0036
4) NCO Phase 5	.07	.10	.03	.0054

Independent Variables	Pre Test MCA Coefficient Adjusted For Independent Variables and Covariates	Post Test MCA Coefficients Adjusted For Independent Variables and Covariates	Post Test Score Minus Pre Test Score	Proportional Difference*
ORGANIZATIONAL CHARACTERISTICS ($\bar{X} = 5.58$)				
For How Many People Do You Write Performance Reports? ($\bar{X} = 5.71$)				
1) None	-.04	-.08	.09	.0162
2) 1	.01	-.05	-.07	.0125
3) 2	.07	.19	.25	.0442
4) 3	.02	.05	.16	.0286
5) 4-5	.03	.08	.18	.0321
6) 6-8	.11	.20	.22	.0387
7) 9 or more	.22	.28	.19	.0328
Your Supervisor Writes Your Performance Report				
1) Yes	.07	.05	.11	.0195
2) No/Not Sure	-.22	-.25	-.10	.0187
Your Work Requires You to Work Primarily				
1) Alone	-.04	-.08	.09	.0162
2) With 1-2 persons	-.05	-.01	.17	.0307
3) With 3-5 persons	.06	.07	.14	.0248
4) With 6 or more persons	.02	-.01	.10	.0179
Usual Work Schedule				
1) Day shift, stable hours	.05	.04	.12	.0213
2) Other	-.11	-.13	.11	.0201
Group Meetings Used to Solve Problems and Set Goals				
1) Never	-.40	-.44	.09	.0174
2) Occasionally	-.01	-.06	.08	.0144
3) About half the time	.12	.14	.15	.0263
4) All of the time	.42	.37	.08	.0133
*(Post Test Score Category 1 minus Pre Test Score Category 1)				
/ (Pre Test Mean Plus Pre Test MCA Coefficient Category 1)				

TABLE 46

MCA COEFFICIENT SUMMARY TABLE:
PERCEIVED PRODUCTIVITY

Independent Variables	Pre Test MCA Coefficient Adjusted For Independent Variables and Covariates	Post Test MCA Coefficients Adjusted For Independent Variables and Covariates	Post Test Score Minus Pre Test Score	Proportional Difference*
PERSONAL CHARACTERISTICS				
	(\bar{X} = 4.88)	(\bar{X} = 4.98)		
Age				
1) 20 or less	-.29	-.27	.12	.0261
2) 21 - 25	-.20	-.18	.12	.0256
3) 26 - 30	-.07	-.09	.08	.0166
4) 31 - 35	.06	.08	.12	.0243
5) 36 - 40	.19	.24	.15	.0246
6) 41 - 50	.51	.47	.06	.0111
7) 51 or more	.71	.69	.08	.0143
Gender				
1) Male	-.01	-.03	.14	.0287
2) Female	.14	.31	.27	.0538
Race				
1) Non-white	-.03	.02	.15	.0306
2) White	.01	-.01	.08	.0169
Level of Education				
1) Less than High School	.00	.28	.38	.0779
2) H.S./GED	.00	.00	.10	.0205
3) Less than 2 Yrs College	.02	-.02	.06	.0122
4) More than 2 Yrs College	.01	-.03	.06	.0123
5) Bachelors Degree	.13	.18	.15	.0299
6) Masters Degree	-.02	.09	.21	.0432
7) Doctorate	-.15	-.08	.09	.0190
NCO-PME				
1) NCO Phase 1-2	-.07	-.09	.08	.0166
2) NCO Phase 3	.03	.05	.12	.0244
3) NCO Phase 4	.07	.12	.15	.0303
4) NCO Phase 5	.14	.16	.12	.0239

Independent Variables	Pre Test MCA Coefficient Adjusted For Independent Variables and Covariates	Post Test MCA Coefficients Adjusted For Independent Variables and Covariates	Post Test Score Minus Pre Test Score	Proportional Difference*
ORGANIZATIONAL CHARACTERISTICS ($\bar{X} = 5.00$) ($\bar{X} = 5.19$)				
For How Many People Do You Write Performance Reports?				
1) None	-.03	-.07	.15	.0302
2) 1	-.01	-.09	.11	.0220
3) 2	.07	.17	.29	.0572
4) 3	-.02	.11	.32	.0643
5) 4-5	.00	.01	.20	.0400
6) 6-8	.16	.21	.24	.0465
7) 9 or more	.27	.31	.23	.0436
Your Supervisor Writes Your Performance Report				
1) Yes	.08	.07	.18	.0354
2) No/Not Sure	-.26	-.31	.14	.0295
Your Work Requires You to Work Primarily				
1) Alone	-.01	-.03	.17	.0341
2) With 1-2 persons	-.01	-.06	.14	.0281
3) With 3-5 persons	-.02	.02	.23	.0462
4) With 6 or more persons	.04	.06	.21	.0417
Usual Work Schedule				
1) Day shift, stable hours	.17	.17	.19	.0368
2) Other	-.38	-.49	.08	.0173
Group Meetings Used to Solve Problems and Set Goals				
1) Never	-.53	-.60	.12	.0268
2) Occasionally	.00	-.04	.15	.0300
3) About half the time	.21	.13	.11	.0211
4) All of the time	.48	.45	.16	.0292
*(Post Test Score Category 1 minus Pre Test Score Category 1) (Pre Test Mean plus Pre Test MCA Coefficient Category 1)				

TABLE 47

MCA COEFFICIENT SUMMARY TABLE:
JOB SATISFACTION

Independent Variables	Pre Test MCA Coefficient Adjusted For Independent Variables and Covariates (X = 4.89)	Post Test MCA Coefficients Adjusted For Independent Variables and Covariates (X = 5.00)	Post Test Score Minus Pre Test Score	Proportional Difference*
PERSONAL CHARACTERISTICS				
Age				
1) 20 or less	.04	-.40	-.33	-.0669
2) 21 - 25	-.17	-.13	.15	.0318
3) 26 - 30	-.06	-.08	.09	.0186
4) 31 - 35	.06	.07	.12	.0242
5) 36 - 40	.21	.23	.13	.0255
6) 41 - 50	.33	.34	.12	.0230
7) 51 or more	.37	.42	.16	.0304
Gender				
1) Male	.00	-.02	.09	.0184
2) Female	-.02	.21	.34	.0698
Race				
1) Non-white	.03	.01	.09	.0183
2) White	-.01	.00	.12	.0246
Level of Education				
1) Less than High School	.29	.24	.06	.0116
2) H.S./GED	.06	.10	.15	.0303
3) Less than 2 Yrs College	-.04	-.04	.11	.0221
4) More than 2 Yrs College	-.07	-.12	.06	.0124
5) Bachelors Degree	.05	-.01	.05	.0101
6) Masters Degree	-.25	-.72	-.36	-.0700
7) Doctorate	-.02	.05	.18	.0370
NCO-PMI				
1) NCO Phase 1-2	-.06	-.11	.06	.0124
2) NCO Phase 3	.01	.07	.17	.0347
3) NCO Phase 4	.06	.15	.20	.0404
4) NCO Phase 5	.23	.20	.08	.0156

Independent Variables	Pre Test MCA Coefficient Adjusted For Independent Variables and Covariates	Post Test MCA Coefficients Adjusted For Independent Variables and Covariates	Post Test Score Minus Pre Test Score	Proportional Difference*
ORGANIZATIONAL CHARACTERISTICS (X̄ = 4.98) (X̄ = 5.15)				
For How Many People Do You Write Performance Reports?				
1) None	-.01	.03	.21	.0423
2) 1	.00	-.18	-.01	-.0020
3) 2	-.03	-.14	.06	.0121
4) 3	-.02	-.03	.16	.0323
5) 4-5	.04	.04	.17	.0339
6) 6-8	.09	.07	.15	.0296
7) 9 or more	.13	.02	.06	.0117
Your Supervisor Writes Your Performance Report				
1) Yes	.11	.12	.18	.0354
2) No/Not Sure	-.36	-.54	-.01	-.0022
Your Work Requires You to Work Primarily				
1) Alone	-.05	-.07	.15	.0304
2) With 1-2 persons	-.02	.01	.20	.0403
3) With 3-5 persons	.01	.01	.17	.0341
4) With 6 or more persons	.05	.04	.16	.0318
Usual Work Schedule				
1) Day shift, stable hours	.04	.04	.17	.0339
2) Other	-.09	-.11	.15	.0307
Group Meetings Used to Solve Problems and Set Goals				
1) Never	-.97	-1.03	.11	.0274
2) Occasionally	.02	-.12	.03	.0060
3) About half the time	.39	.35	.13	.0242
4) All of the time	.83	.80	.14	.0241

* (Post Test Score Category 1 minus Pre Test Score Category 1) / (Pre Test Mean plus Pre Test MCA Coefficient Category 1)

TABLE 48

MCA COEFFICIENT SUMMARY TABLE:
PERCEIVED SUPERVISOR CAPACITY

Independent Variables	Pre Test MCA Coefficient Adjusted For Independent Variables and Covariates ($\bar{X} = 4.58$)	Post Test MCA Coefficients Adjusted For Independent Variables and Covariates ($\bar{X} = 4.71$)	Post Test Score Minus Pre Test Score	Proportional Difference*
PERSONAL CHARACTERISTICS				
Age				
1) 20 or less	-.17	-.56	-.26	-.0590
2) 21 - 25	-.31	-.30	.14	.0328
3) 26 - 30	-.10	-.10	.13	.0290
4) 31 - 35	.12	.19	.20	.0426
5) 36 - 40	.33	.35	.15	.0305
6) 41 - 50	.67	.64	.10	.0190
7) 51 or more	.77	.90	.26	.0486
Gender				
1) Male	-.01	-.02	.12	.0263
2) Female	.10	.23	.26	.0556
Race				
1) Non-White	.07	.09	.15	.0323
2) White	-.03	-.03	.13	.0286
Level of Education				
1) Less than High School	.36	.86	.63	.1275
2) H.S./GED	.05	.06	.14	.0302
3) Less than 2 Yrs College	-.03	-.03	.13	.0286
4) More than 2 Yrs College	-.09	-.10	.12	.0267
5) Bachelors Degree	.08	.05	.10	.0215
6) Masters Degree	-.08	-.18	.03	.0067
7) Doctorate	.20	.63	.56	.1172
NCO-PME				
1) NCO Phase 1-2	-.07	-.09	.11	.0244
2) NCO Phase 3	.00	.06	.19	.0415
3) NCO Phase 4	.08	.05	.00	.0000
4) NCO Phase 5	.24	.26	.15	.0311

Independent Variables	Pre Test MCA Coefficient Adjusted For Independent Variables and Covariates	Post Test MCA Coefficients Adjusted For Independent Variables and Covariates	Post Test Score Minus Pre Test Score	Proportional Difference*
ORGANIZATIONAL CHARACTERISTICS ($\bar{X} = 4.77$)				
For How Many People Do You Write Performance Reports?				
1) None	-.04	-.13	.12	.0254
2) 1	-.04	.00	.25	.0529
3) 2	-.01	.16	.38	.0798
4) 3	.01	.20	.40	.0840
5) 4-5	.07	.08	.22	.0455
6) 6-8	.22	.42	.41	.0822
7) 9 or more	.36	.47	.32	.0624
Your Supervisor Writes Your Performance Report				
1) Yes	.06	.05	.20	.0414
2) No/Not Sure	-.20	-.23	.18	.0394
Your Work Requires You to Work Primarily				
1) Alone	.02	.00	.19	.0397
2) With 1-2 persons	-.05	-.02	.24	.0508
3) With 3-5 persons	.00	.00	.21	.0440
4) With 6 or more persons	.04	.02	.19	.0395
Usual Work Schedule				
1) Day shift, stable hours	.10	.09	.20	.0411
2) Other	-.23	-.28	.15	.0330
Group Meetings Used to Solve Problems and Set Goals				
1) Never	-.62	-.65	.18	.0434
2) Occasionally	-.01	-.07	.15	.0315
3) About half the time	.24	.19	.16	.0319
4) All of the time	.60	.54	.15	.0279

* (Post Test Score Category 1 minus Pre Test Score Category 1) / (Pre Test Mean plus Pre Test MCA Coefficient Category 1)

TABLE 49

MCA COEFFICIENT SUMMARY TABLE:
ORGANIZATIONAL CLIMATE

	Personal Characteristics	Organizational Characteristics	Personal and Organizational Characteristics
Job Enrichment Needs	*R = -.33	*R = -.24	*R = -.31
Task Autonomy	.35	-.10	.14
Advancement/Recognition	-.50	.16	-.07
Perceived Productivity	-.40	.34	-.13
Job Satisfaction	-.10	.35	.05
Supervisor Capacity	.32	.19	.20
Organizational Climate	.40	.17	.27

*R = Pre Test Score:(Post Test Score - Pre Test Score)

TABLE 50

CORRELATION SUMMARY TABLE:
LONGITUDINAL CHANGES IN OAP SCORES

Dependent Variable	Pre Test R ²	Post Test R ²	Arithmetic Difference	Proportional Difference
Job Enrichment Needs				
Personal Characteristics	.062	.061	-.001	-.0161
Organizational Characteristics	.031	.043	.012	.3871
Task Autonomy				
Personal Characteristics	.089	.088	-.001	-.0112
Organizational Characteristics	.151	.156	.005	.0331
Advancement/Recognition				
Personal Characteristics	.078	.073	-.005	-.0641
Organizational Characteristics	.182	.195	.013	.0714
Perceived Productivity				
Personal Characteristics	.041	.037	-.004	-.0976
Organizational Characteristics	.092	.098	.006	.0652
Job Satisfaction				
Personal Characteristics	.069	.072	.003	.0435
Organizational Characteristics	.152	.197	.045	.2961
Perceived Supervisor Capacity				
Personal Characteristics	.017	.019	.002	.1176
Organizational Characteristics	.189	.208	.019	.1005
Organizational Climate				
Personal Characteristics	.049	.047	-.002	-.0408
Organizational Characteristics	.099	.116	.017	.1717

TABLE 51

MCA SUMMARY TABLE: COMPOSITE R SQUARED

	Pre Test Data		Post Test Data	
	eta ²	R ²	eta ²	R ²
Job Enrichment Needs	30.0%	9.3%	34.2%	10.4%
Personal Characteristics	24.0	6.2	26.4	6.1
Organizational Characteristics	6.0	3.1	7.8	4.3
Task Autonomy	70.8	24.0	73.0	24.4
Personal Characteristics	42.9	8.9	43.9	8.8
Organizational Characteristics	27.9	15.1	29.1	15.6
Advancement/Recognition	48.4	26.0	42.3	26.8
Personal Characteristics	19.0	7.8	17.5	7.3
Organizational Characteristics	29.4	18.2	31.8	19.5
Perceived Productivity	28.5	13.3	31.8	13.5
Personal Characteristics	11.3	4.1	12.2	3.7
Organizational Characteristics	17.2	9.2	19.6	9.8
Job Satisfaction	54.4	22.1	57.0	26.9
Personal Characteristics	25.5	6.9	26.3	7.2
Organizational Characteristics	28.9	15.2	30.7	19.7
Perceived Supervisor Capacity	38.7	20.6	36.0	22.7
Personal Characteristics	9.2	1.7	6.2	1.9
Organizational Characteristics	29.5	18.9	29.8	20.8
Organizational Climate	31.5	14.8	33.0	16.3
Personal Characteristics	15.0	4.9	15.9	4.7
Organizational Characteristics	16.5	9.9	17.1	11.6

TABLE 52

ANALYSIS OF VARIANCE SUMMARY TABLE:
ETA SQUARED AND MCA DERIVED R² SQUARED

Dependent Variable	*Corrected Pre Test Mean	*Corrected Post Test Mean	Arithmetic Difference	Proportional Difference
Job Enrichment Needs	5.4842	5.4380	-.0462	-.0084
Task Autonomy	3.9297	4.0449	.1152	.0293
Advancement/Recognition	4.1666	4.1865	.0199	.0048
Perceived Productivity	5.4655	5.5373	.0718	.0131
Job Satisfaction	4.9032	4.9751	.0719	.0147
Perceived Supervisor Capacity	5.0538	5.0873	.0335	.0066
Organizational Climate	4.7324	4.8545	.1221	.0258

*Corrected for Variation in Personal Background Characteristics

TABLE 53
CORRECTED DEPENDENT VARIABLE MEAN SCORE

Dependent Variables	Pre Test Data			Post Test Data			Pre Test to Post Test		
	Raw Data Mean	Corrected Data Mean	Proportional Difference	Raw Data Mean	Corrected Data Mean	Proportional Difference	Raw Data	Corrected Data	Proportional Difference
Job Enrichment Needs	5.5327	5.4842	-.0088	5.5051	5.4380	-.0671	-.0950	-.0284	-.0034
Task Autonomy	3.9861	3.9297	-.0564	4.1719	4.0449	-.1270	.0466	.0892	.0173
Advancement Recognition	4.1022	4.1666	.0644	4.1730	4.1865	.0135	.0173	.0048	-.0125
Perceived Productivity	5.5076	5.4655	-.0421	5.5832	5.5373	-.0459	.0137	.0131	.0006
Job Satisfaction	4.9558	4.9032	-.0526	5.0990	4.9751	-.1239	.0268	.0147	.0121
Perceived Supervisor Capacity	5.0931	5.0538	-.0393	5.1112	5.0873	-.0239	.0036	.0046	-.0030
Organizational Climate	4.8059	4.7324	-.0735	4.9759	4.8545	-.1214	.0354	.0258	.0096

*Corrected for Variation in Personal Background Characteristics

TABLE 5A
IMPACT OF STANDARDIZED COEFFICIENTS UPON
PRESENT OBP SCORES

FIGURE #1
 WITHIN GROUP VARIANCE:
 PRE-TEST DATA - AGE

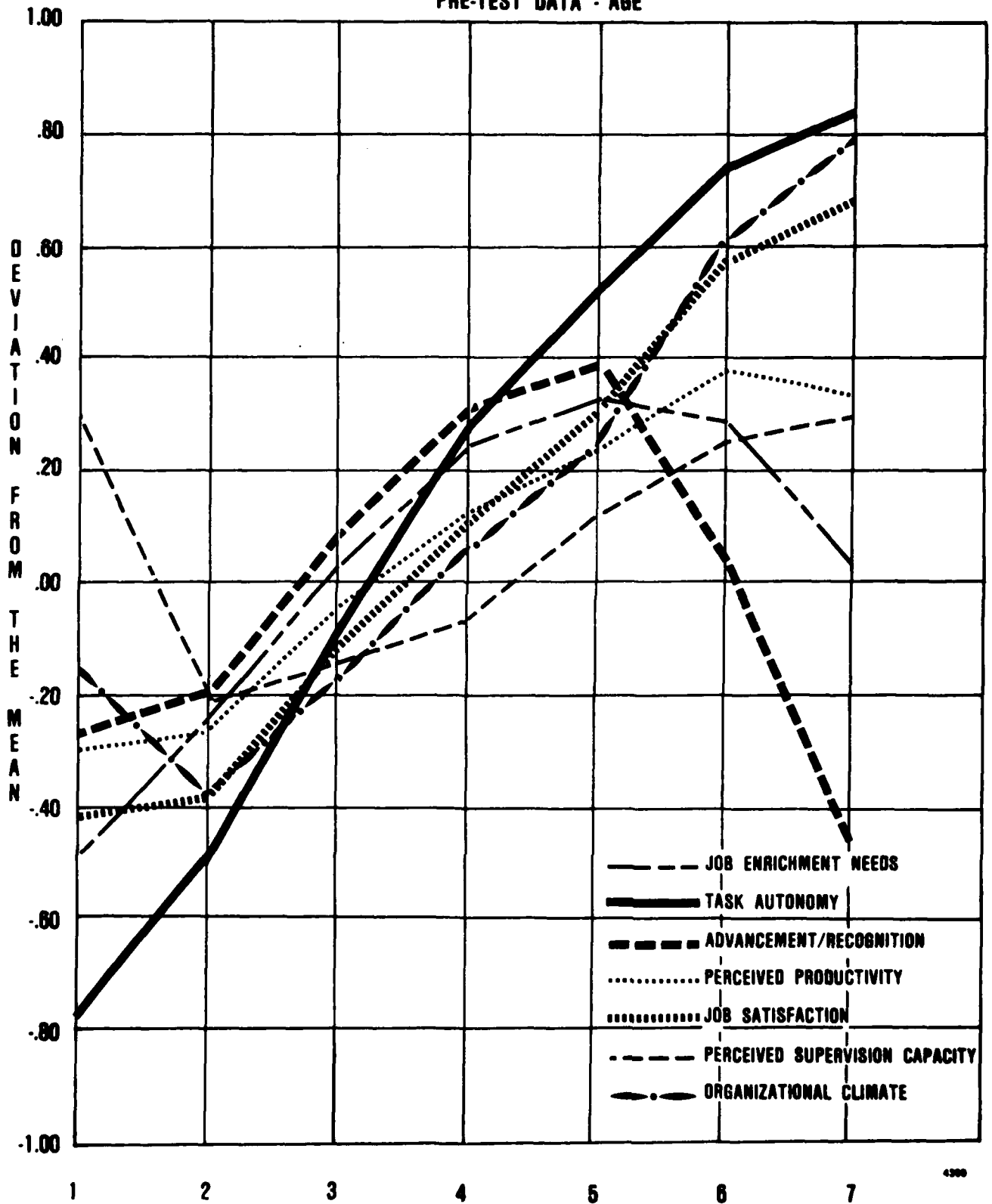


FIGURE #2
 WITHIN GROUP VARIANCE:
 PRE-TEST DATA - GENDER

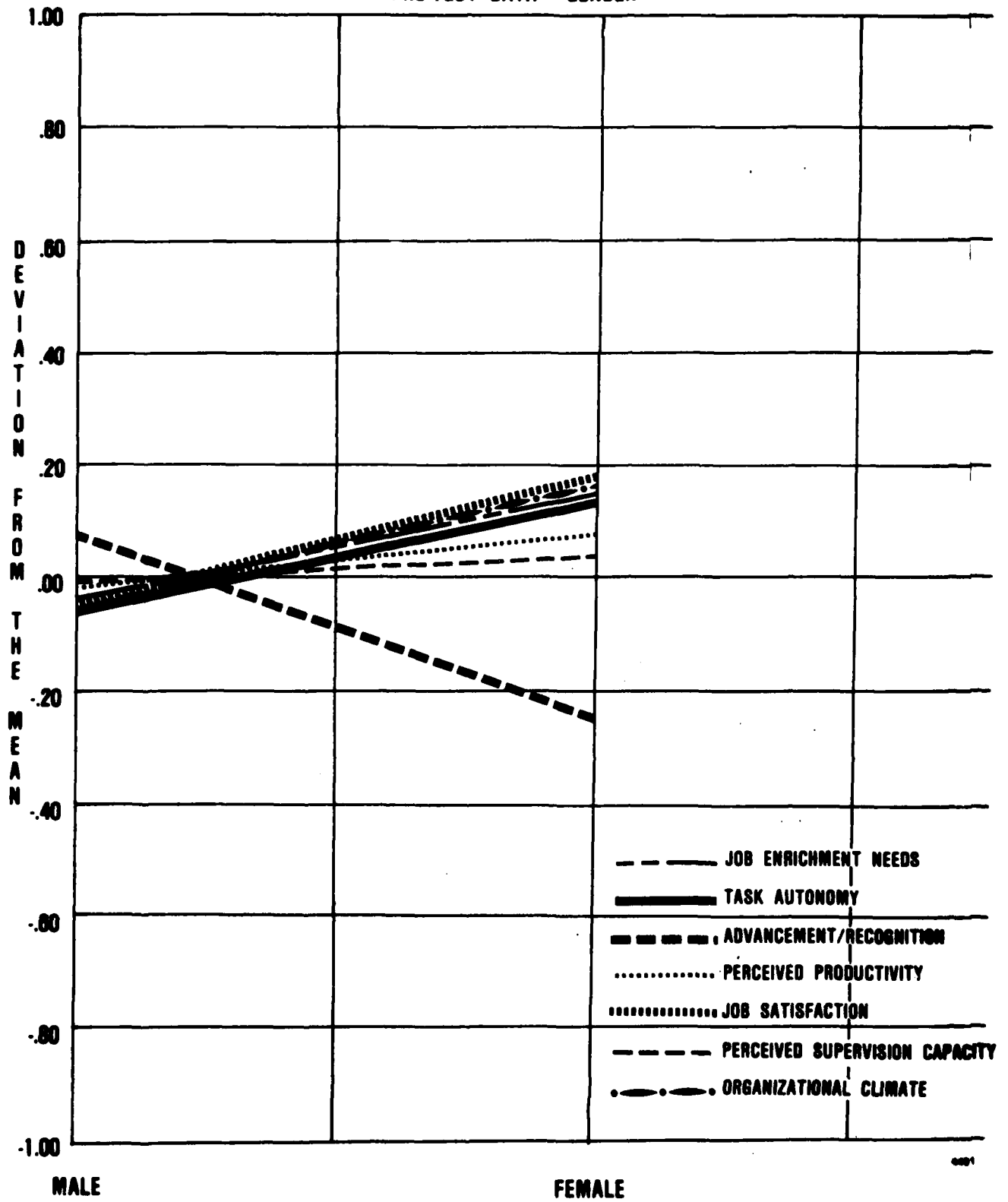


FIGURE #3
WITHIN GROUP VARIANCE:
PRE-TEST DATA - PAY GRADE

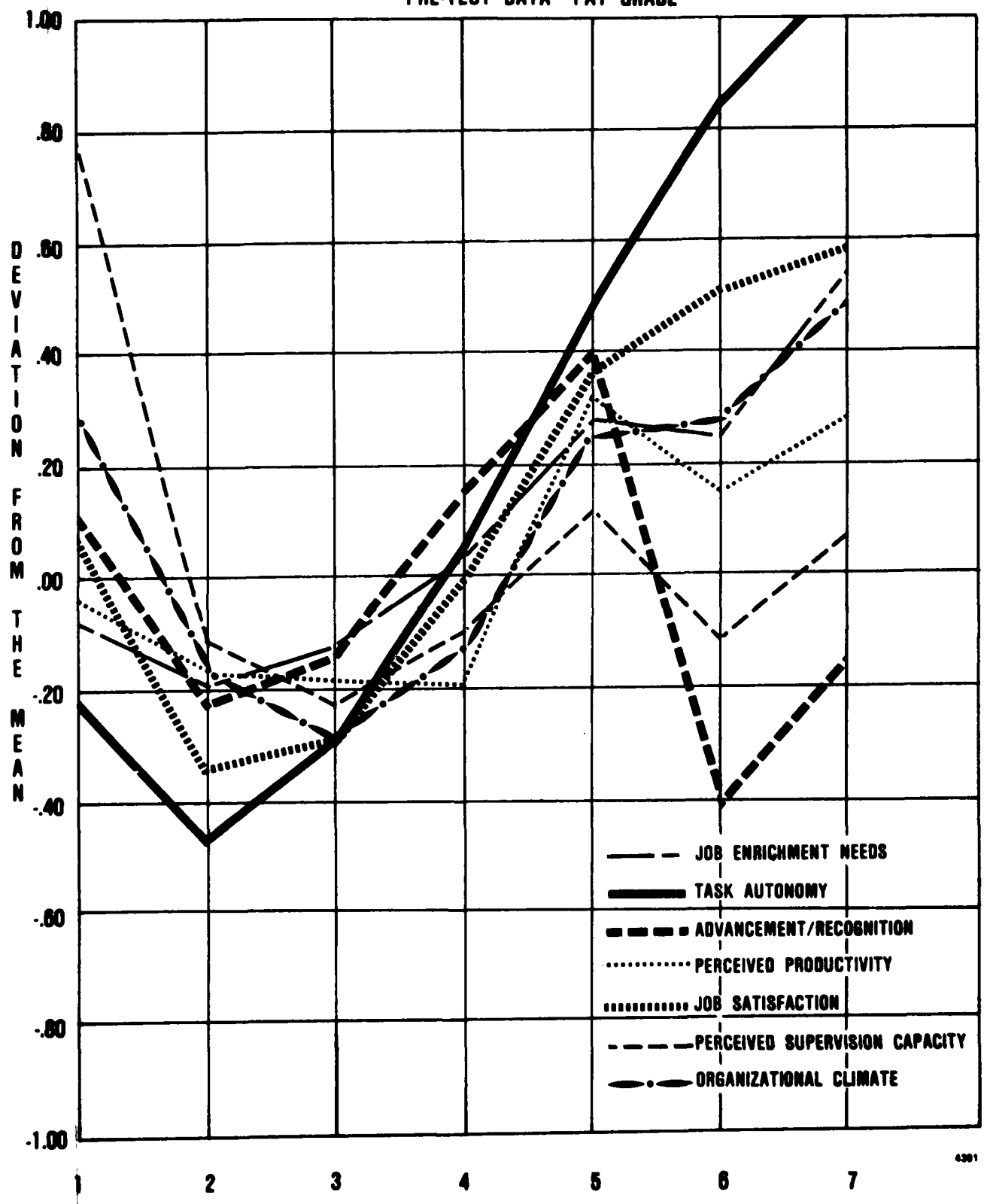
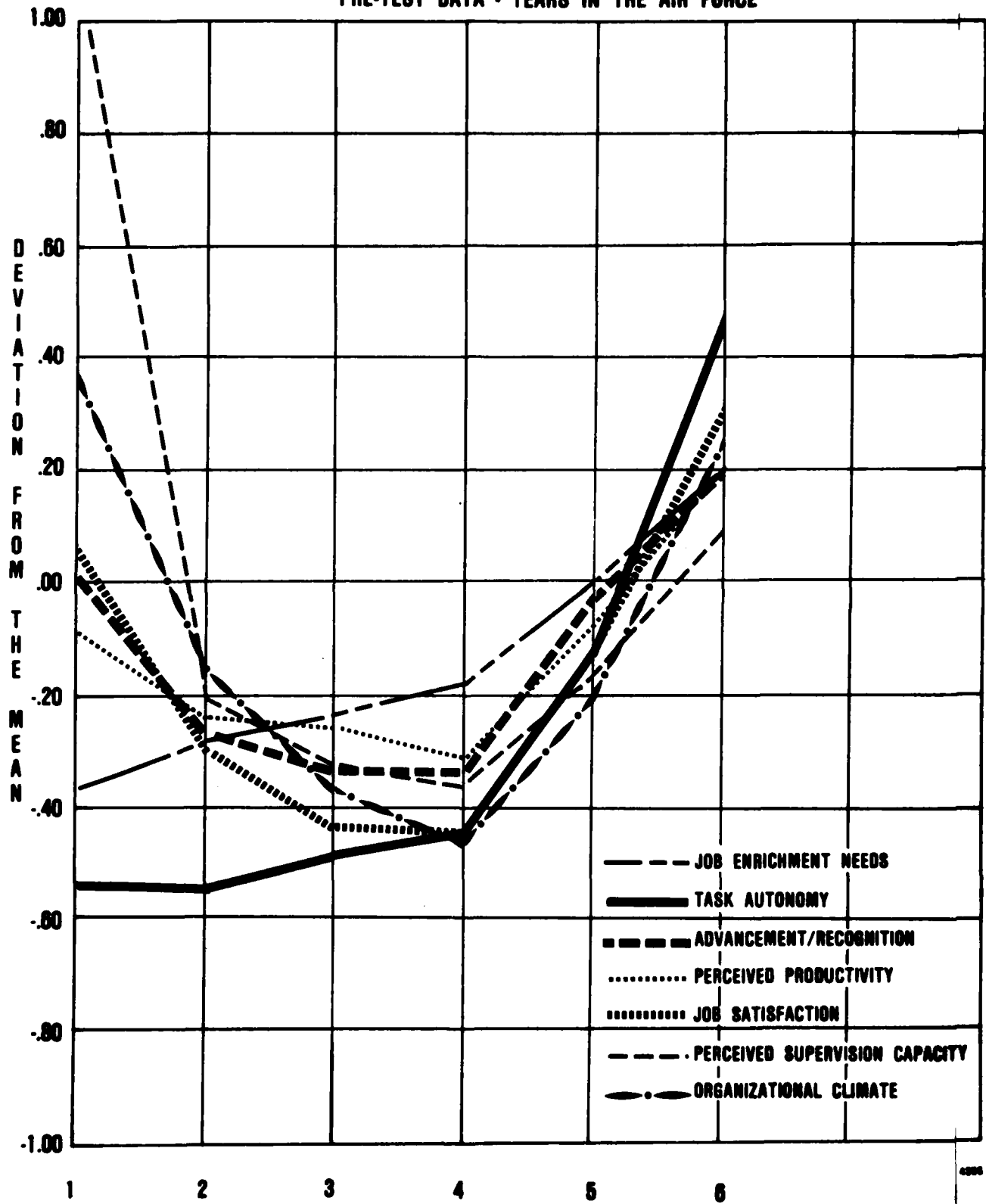


FIGURE #4
WITHIN GROUP VARIANCE:
PRE-TEST DATA - YEARS IN THE AIR FORCE



**FIGURE #5
WITHIN GROUP VARIANCE:
PRE-TEST DATA - RACE**

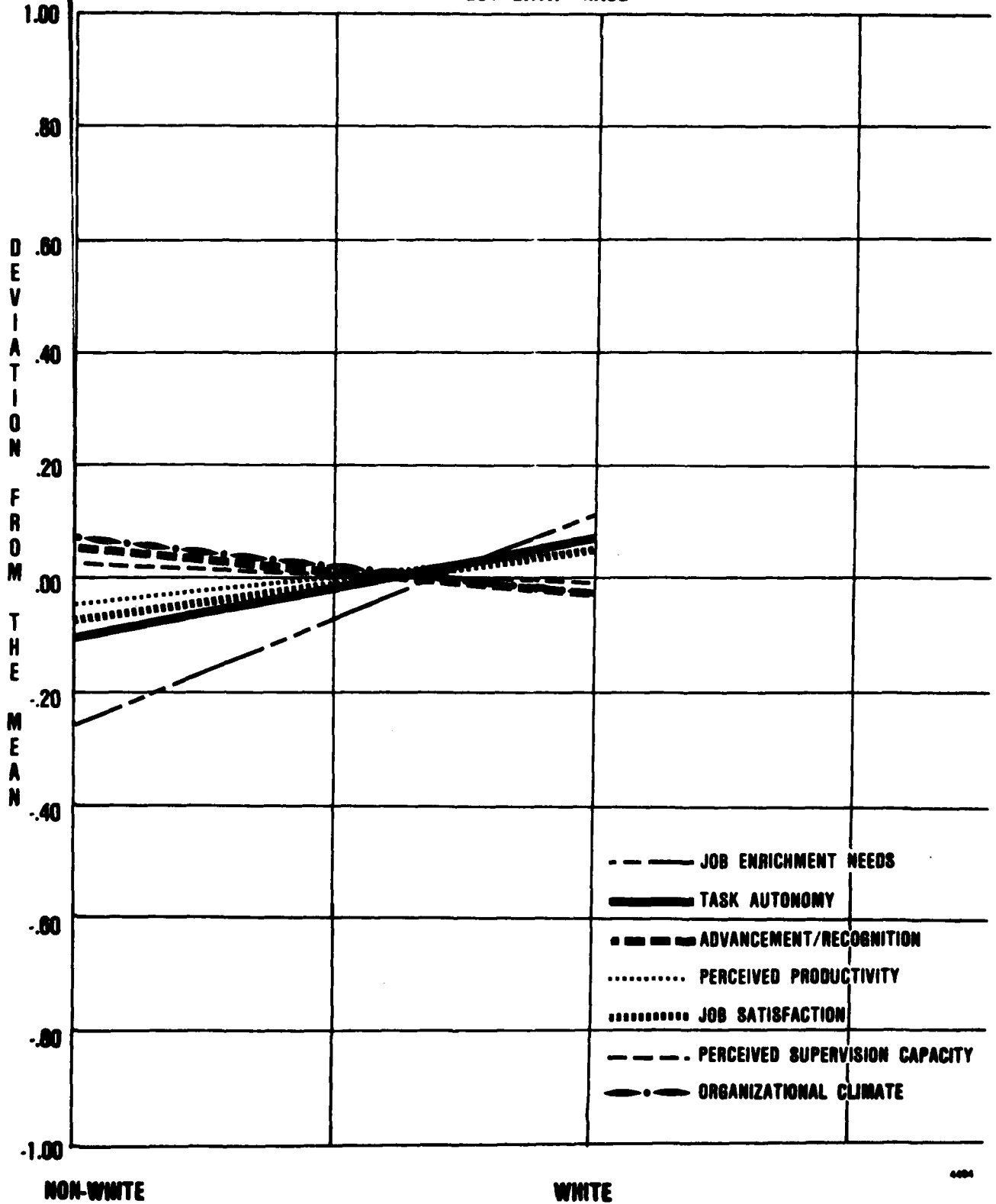


FIGURE #6
 WITHIN GROUP VARIANCE:
 PRE-TEST DATA - LEVEL OF EDUCATION

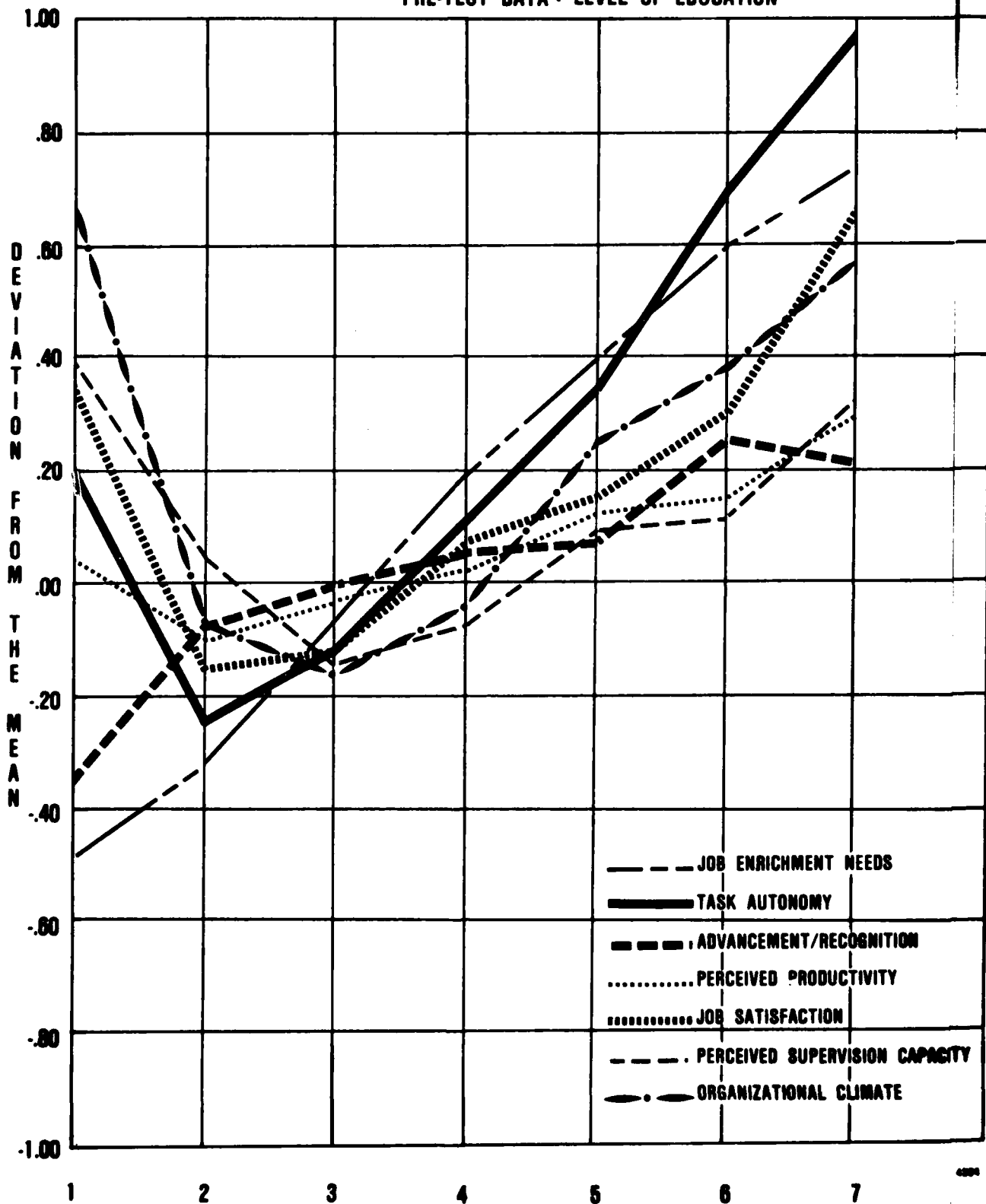
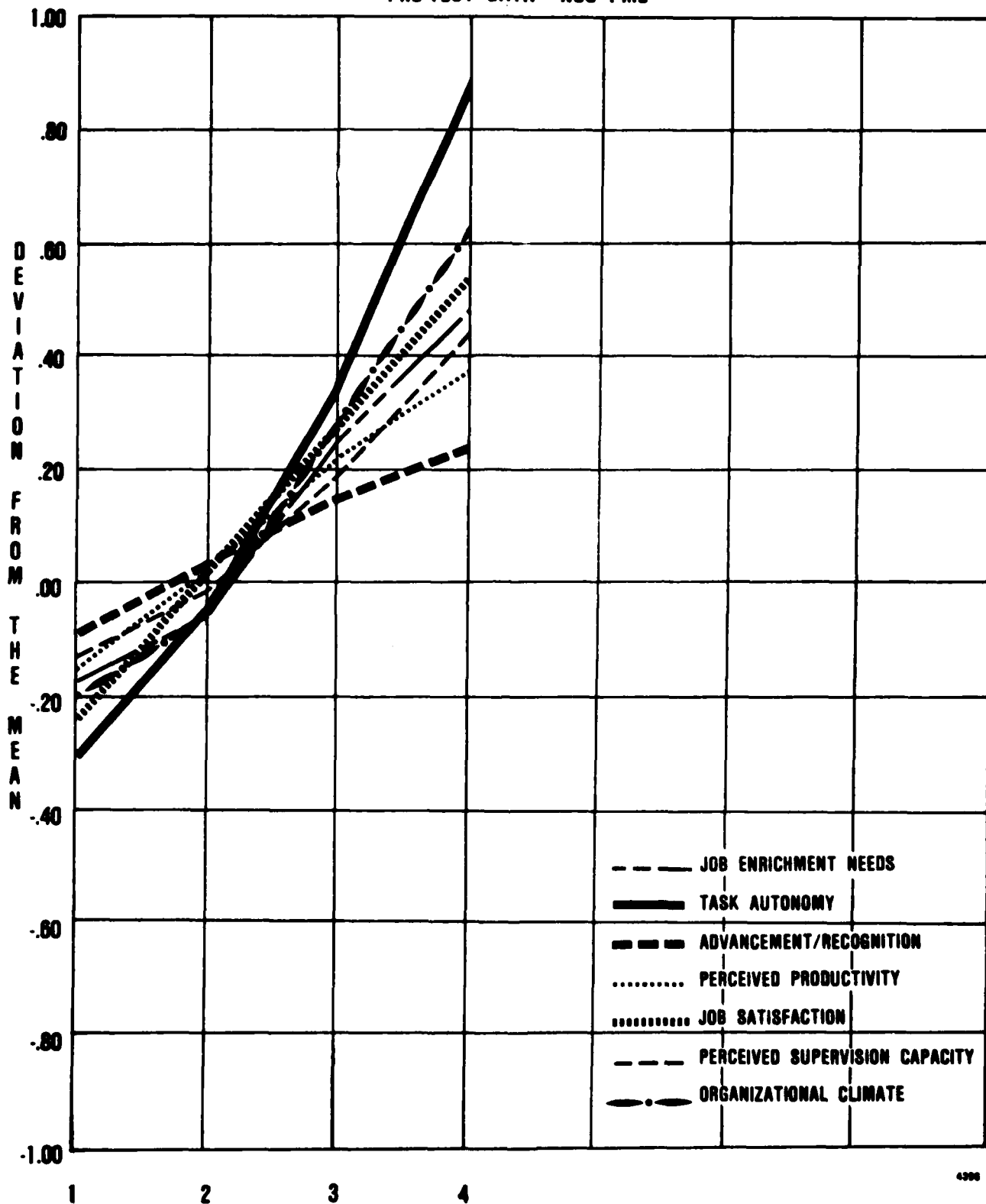


FIGURE #7
WITHIN GROUP VARIANCE:
PRE-TEST DATA - NCO PME



4998

FIGURE #8
 WITHIN GROUP VARIANCE:
 PRE-TEST DATA - CO PME

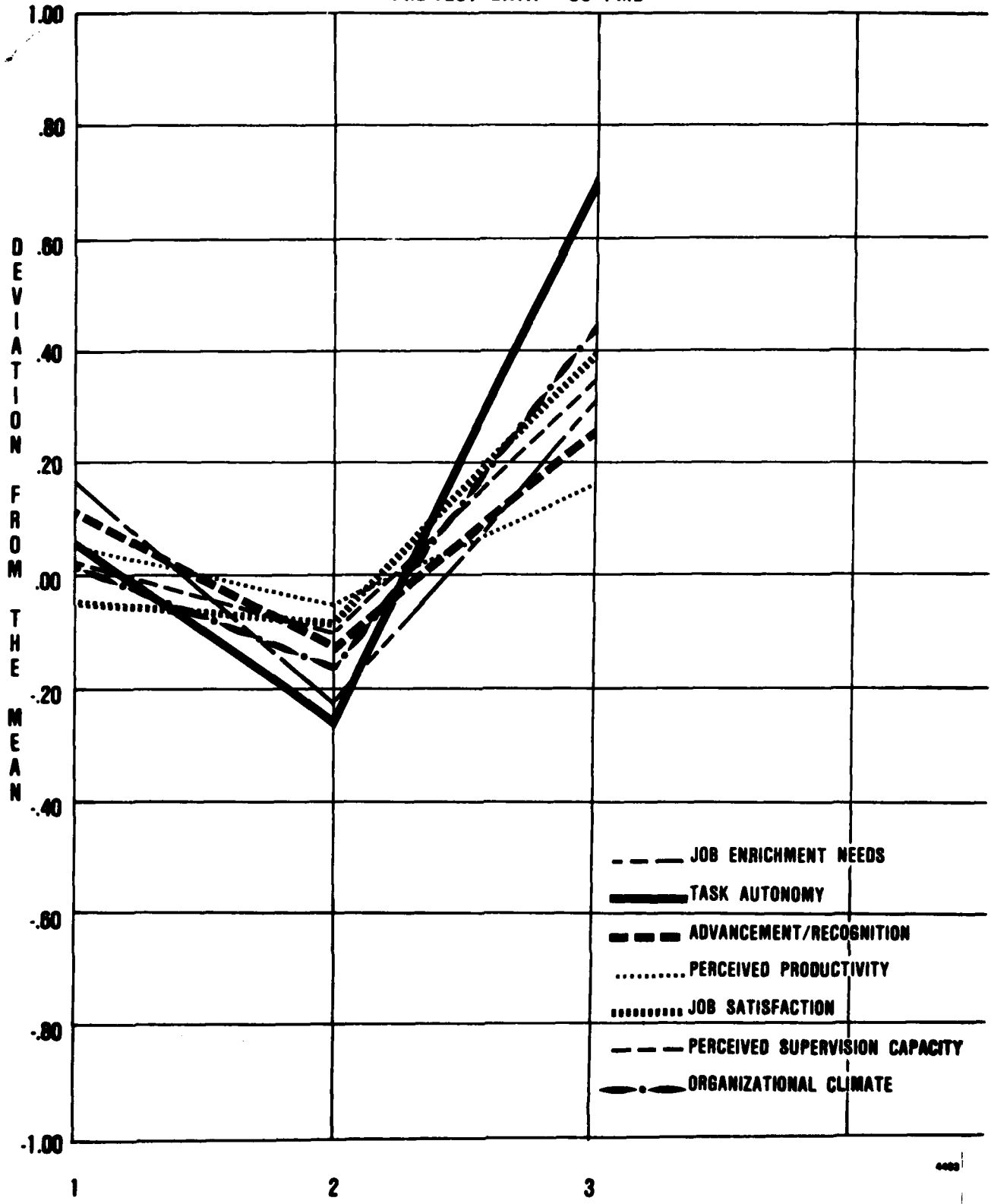


FIGURE #9
WITHIN GROUP VARIANCE:
PRE-TEST DATA - MONTHS AT PRESENT STATION

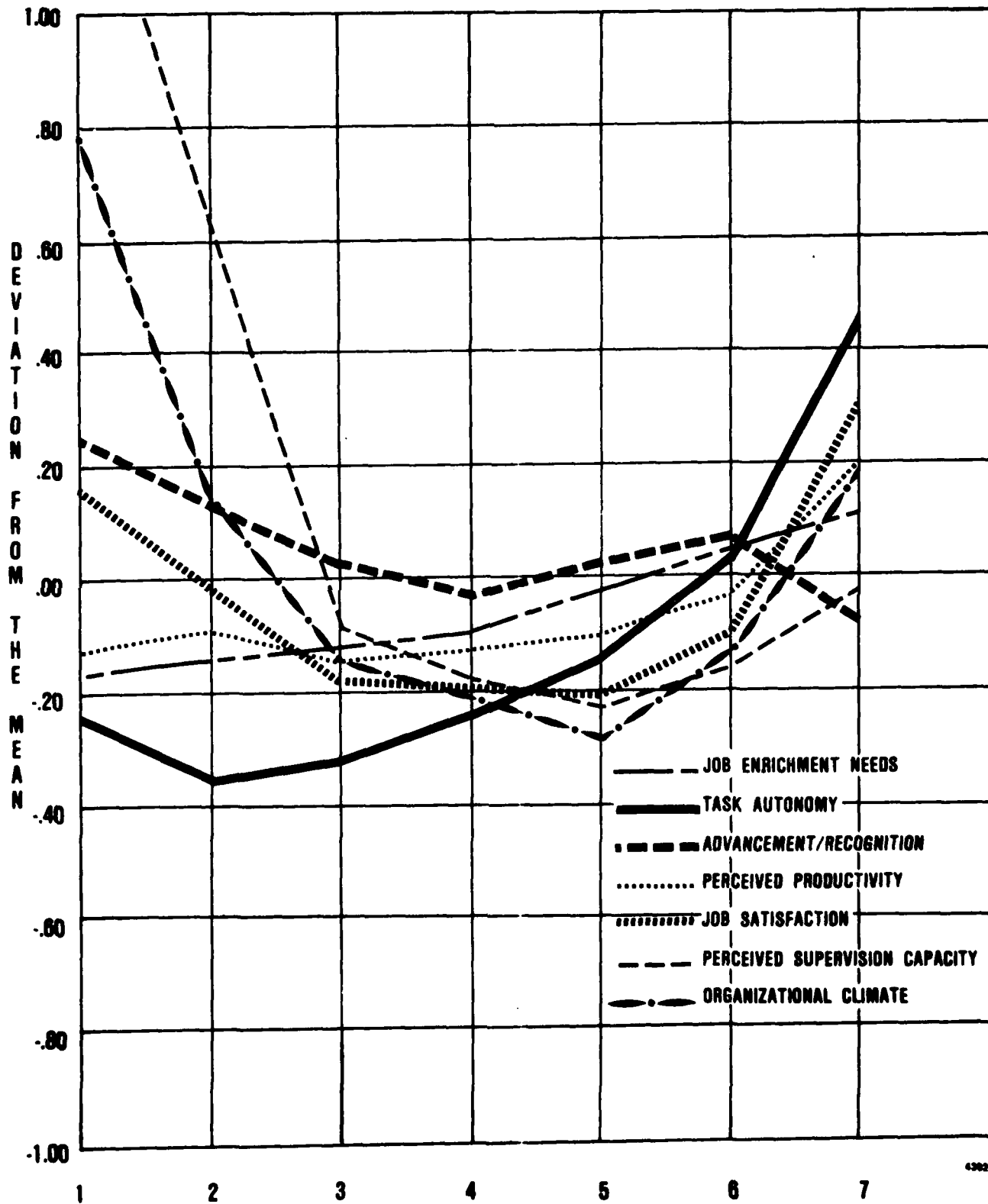


FIGURE #10
 WITHIN GROUP VARIANCE:
 PRE-TEST DATA - SUPERVISORY RESPONSIBILITIES

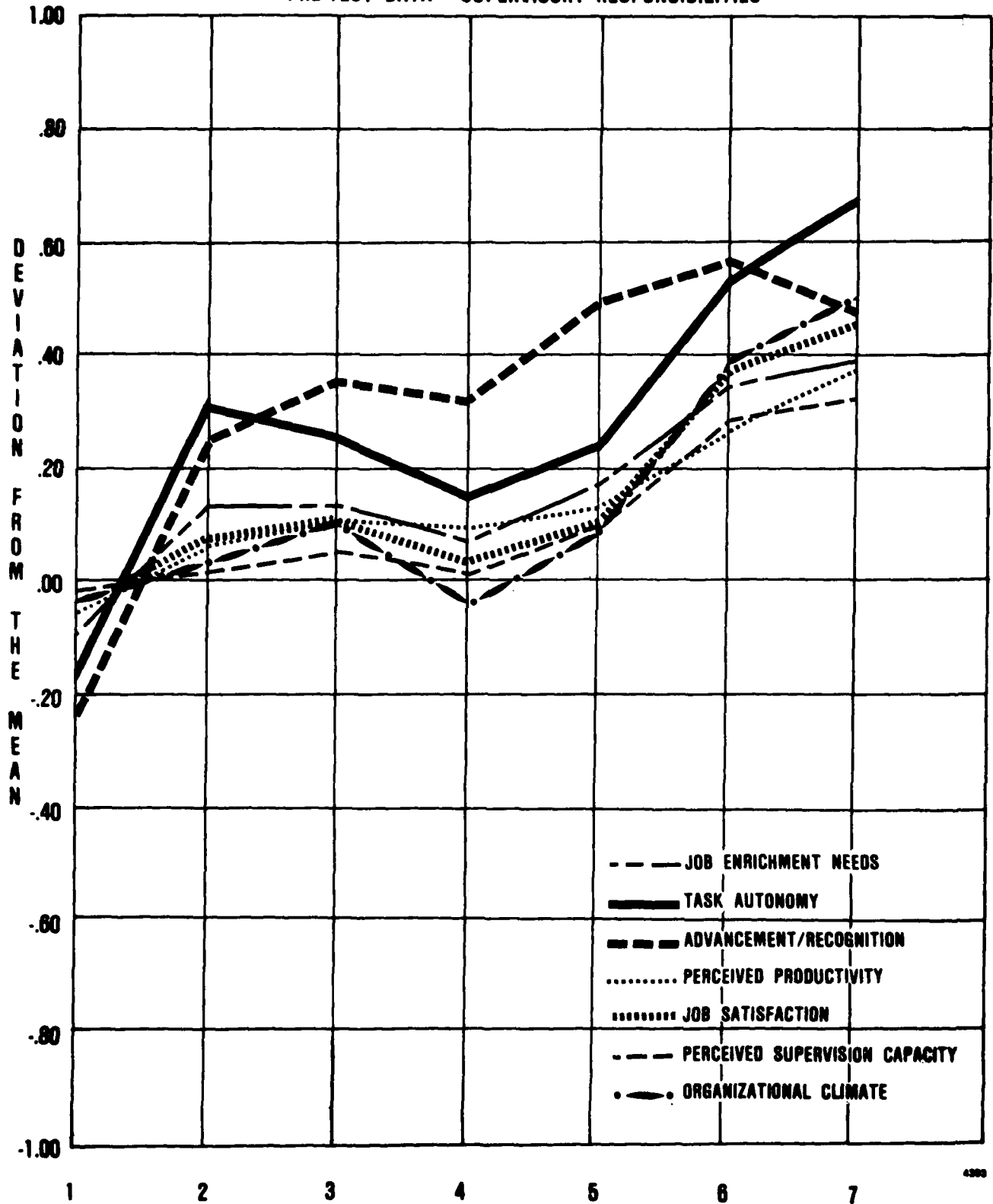
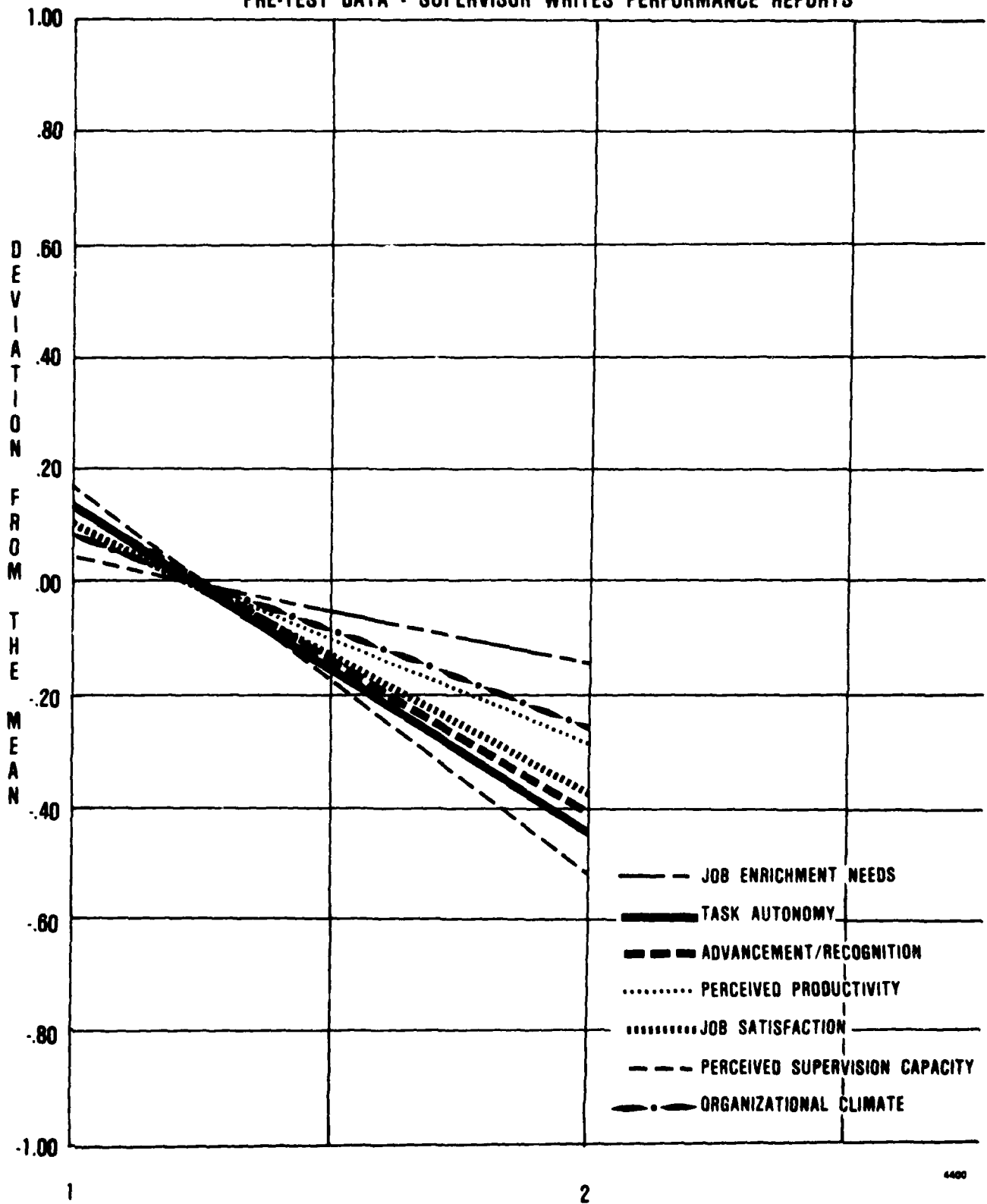


FIGURE #11
WITHIN GROUP VARIANCE:
PRE-TEST DATA - SUPERVISOR WRITES PERFORMANCE REPORTS



4400

FIGURE #12
 WITHIN GROUP VARIANCE:
 PRE-TEST DATA - WORK GROUP SIZE

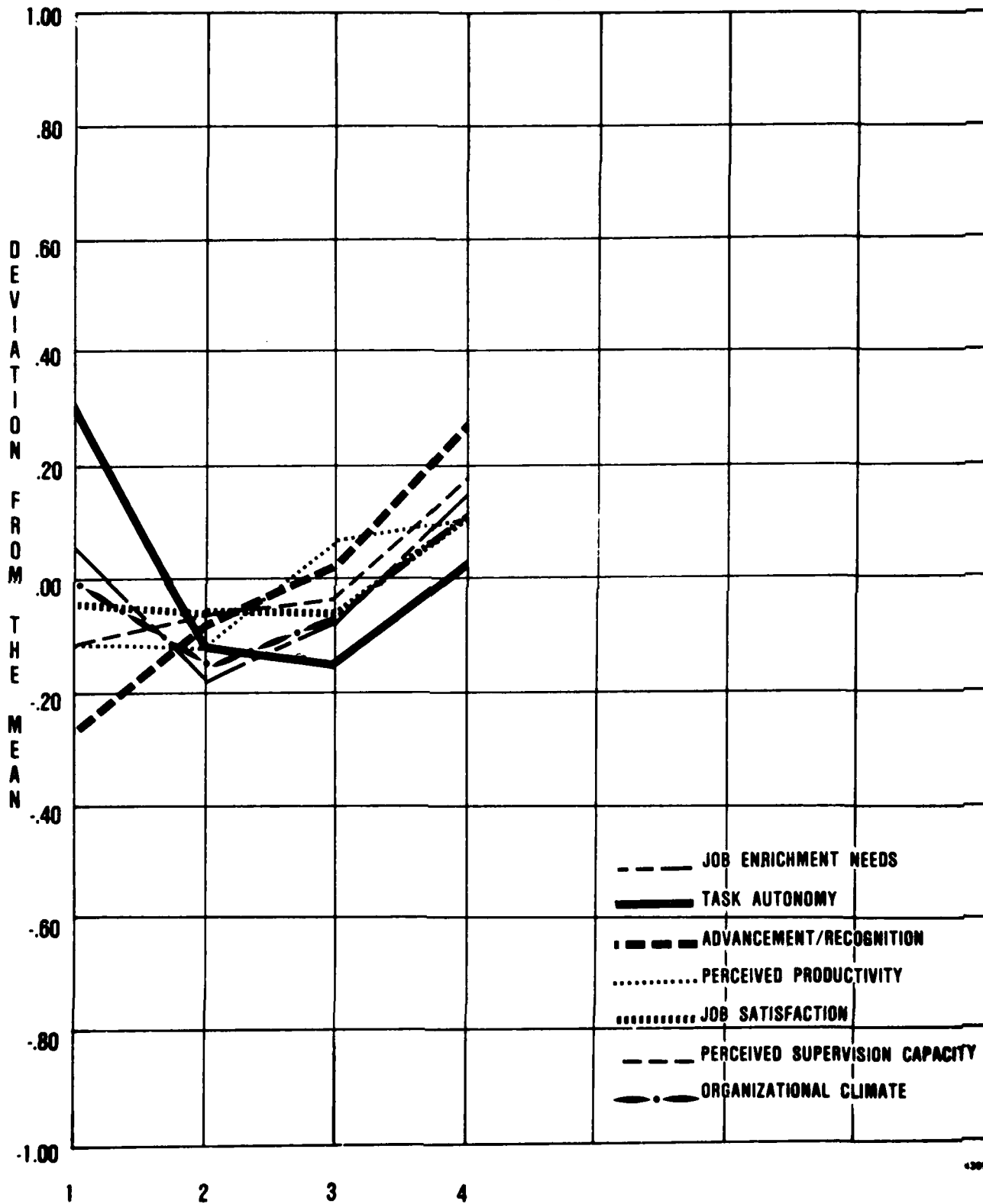
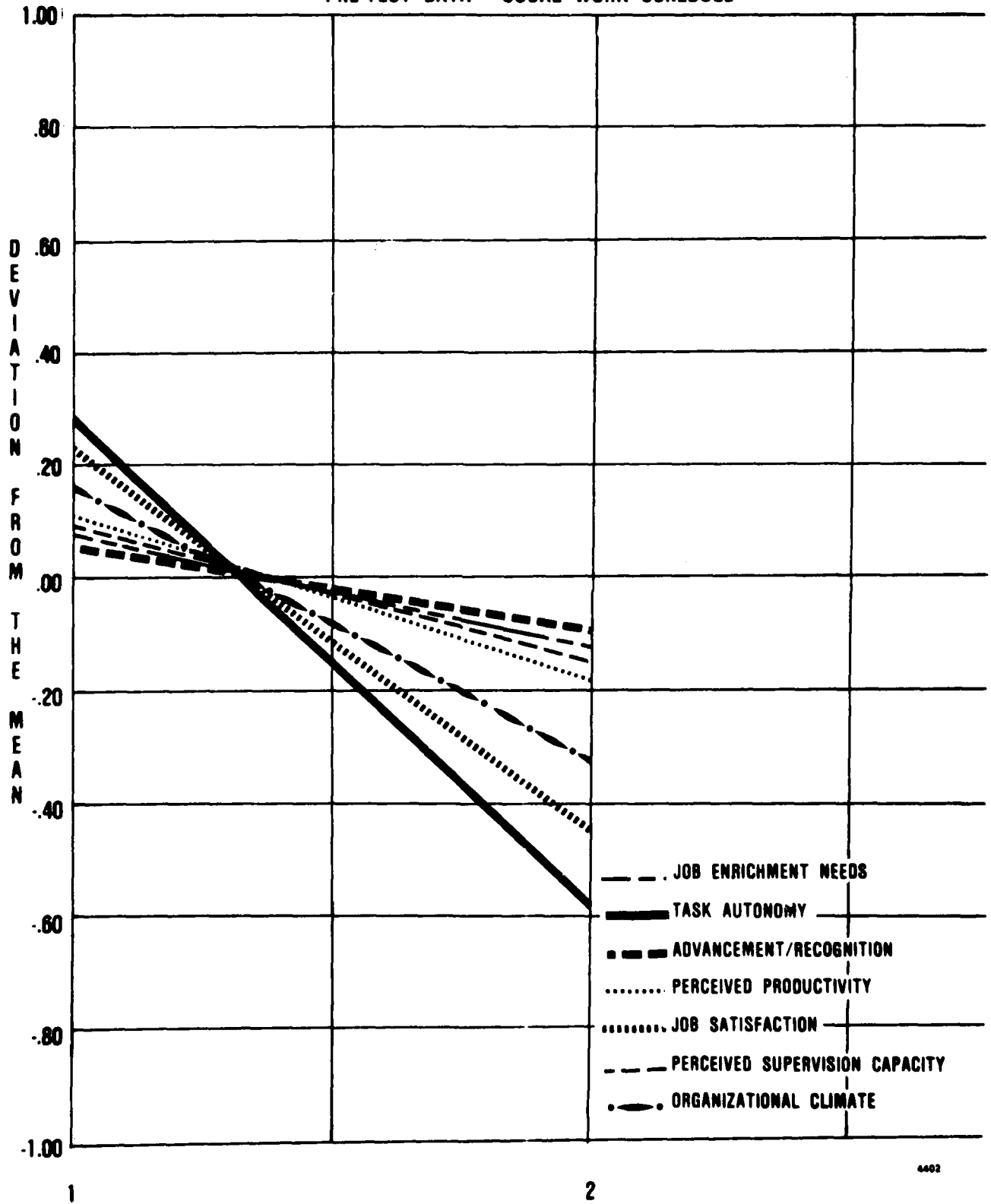
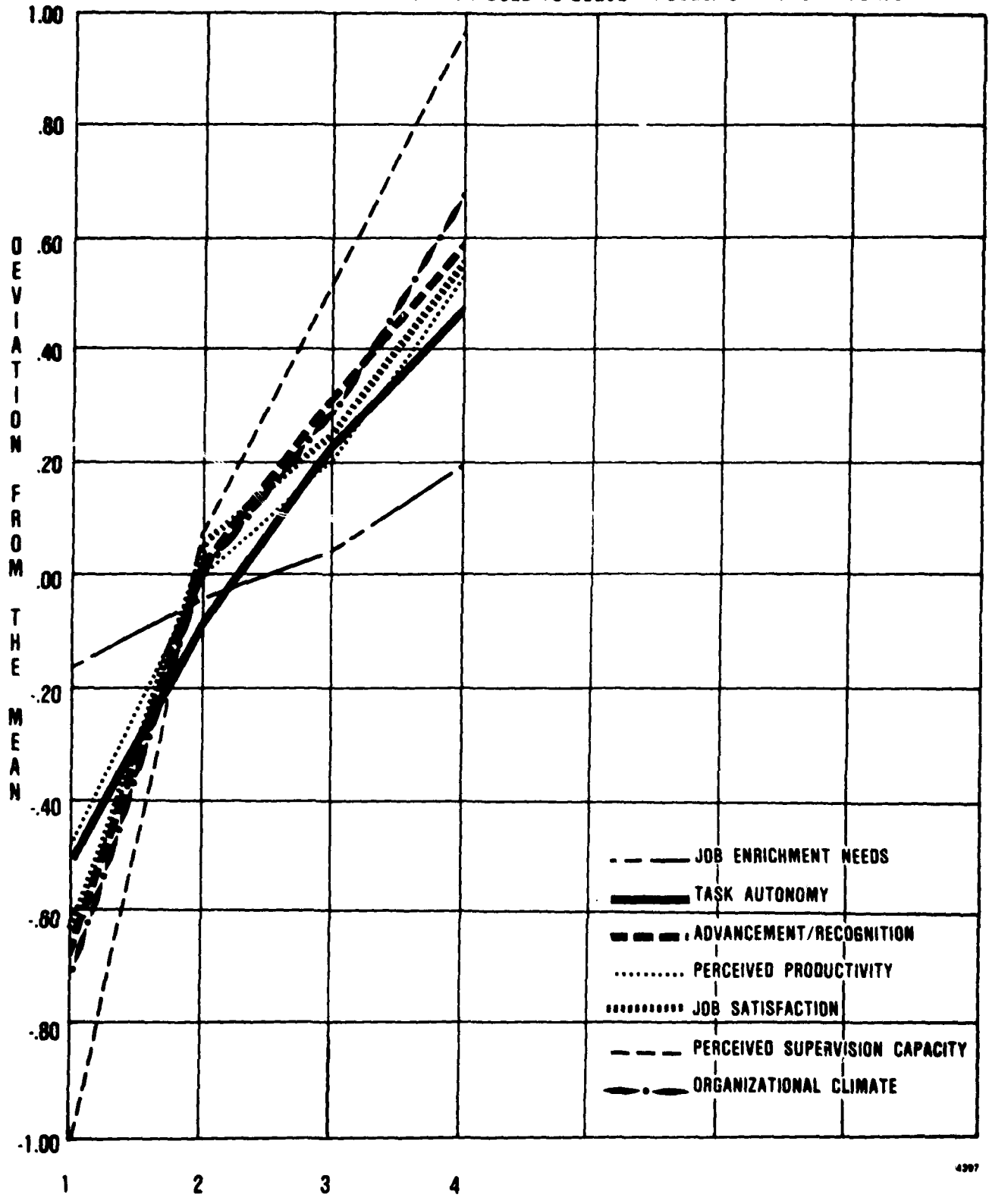


FIGURE #13
 WITHIN GROUP VARIANCE:
 PRE-TEST DATA - USUAL WORK SCHEDULE



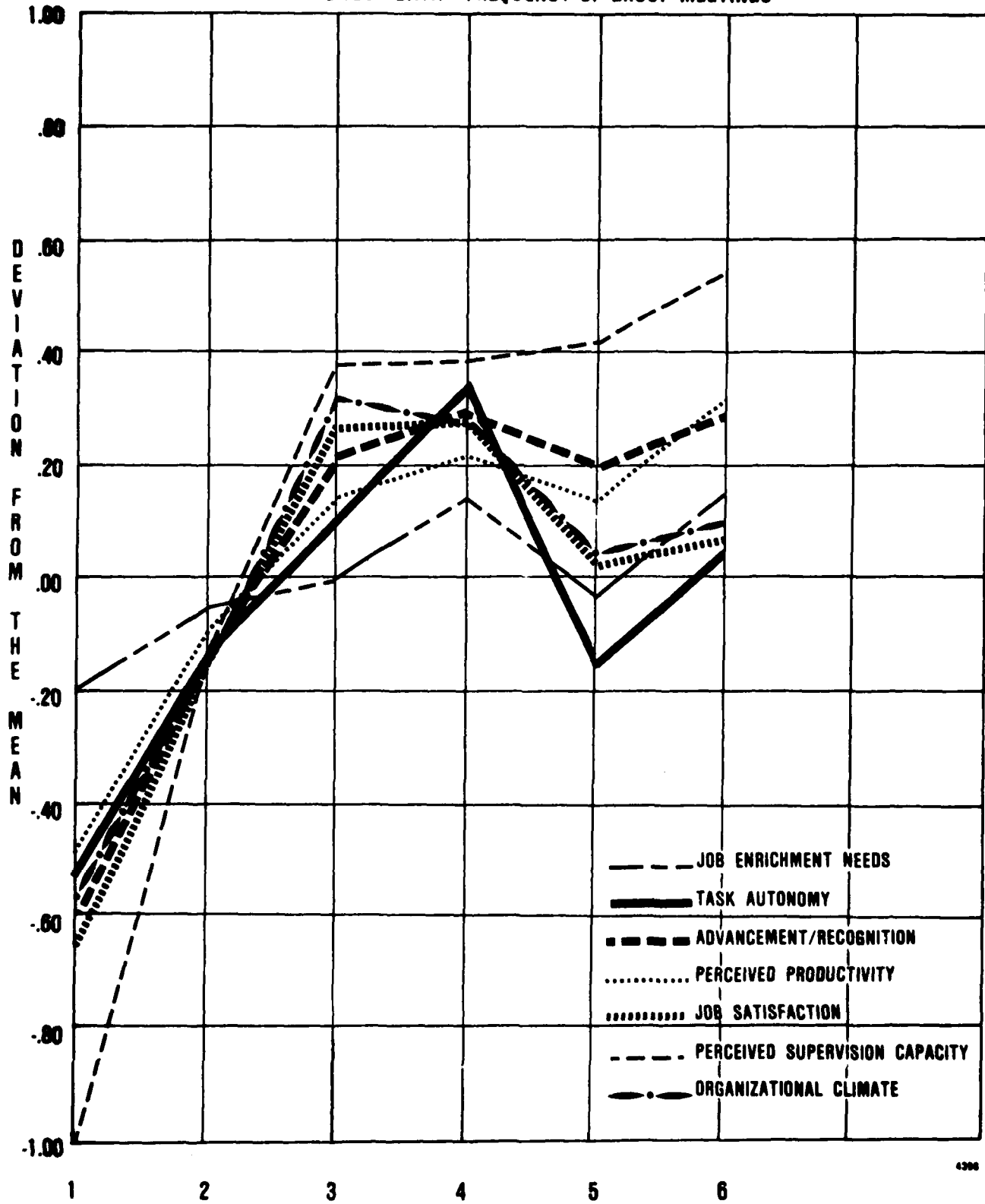
4402

FIGURE #14
WITHIN GROUP VARIANCE:
PRE-TEST DATA - GROUP MEETINGS USED TO SOLVE PROBLEMS AND SET GOALS



4297

FIGURE #15
 WITHIN GROUP VARIANCE:
 PRE-TEST DATA - FREQUENCY OF GROUP MEETINGS



4306

1981 USAF - SCEEE SUMMER FACULTY RESEARCH PROGRAM

Sponsored by the

AIR FORCE OFFICE OF SCIENTIFIC RESEARCH

Conducted by the

SOUTHEASTERN CENTER FOR ELECTRICAL ENGINEERING EDUCATION

FINAL REPORT

RADIATION SIGNATURES FROM A

SPACE POWER SYSTEM

Prepared by: Dr. Glenn E. Fanslow
Academic Rank: Associate Professor
Department and University: Electrical Engineering Department
Iowa State University
Research Location: Air Force Wright Aeropropulsion Laboratory
Aerospace Power Division, Energy Conversion
Branch, Solar/Thermal
USAF Research Colleague: Dr. James F. Holt
Date: July 31, 1981
Contract No: F49620-79-C-0038

RADIATION SIGNATURES FROM A SPACE

POWER SYSTEM

by

GLENN E. FANSLow

ABSTRACT

Magnetic fields produced by the switching currents in the power conditioning circuitry of a space power system are investigated. A theoretical worst-case condition determines the field produced if all of the power available is used to drive a loop antenna. Experimental measurements show that the actual fields radiated from a power system will be much lower than the worst-case condition. It is concluded that the radiation signatures from a space power system would not be easily detectable on the earth.

ACKNOWLEDGEMENTS

The author would like to thank Dr. James F. Holt for suggesting and guiding his efforts on this topic. He would also like to thank the other members of the Solar Energy Conversion group for their help, comments and thoughtful suggestions. Additionally, he would like to thank the Aero Propulsion Laboratory for the support facilities provided and, finally, he would like to thank the Air Force Office of Scientific Research and the Southeastern Center for Electrical Engineering Education for the opportunity to participate in the Summer Faculty Research Program. The experimental data were provided through the help of M.P. Dougherty of the Power Conditioning group.

I. INTRODUCTION:

It is anticipated that future Air Force spacecraft will need higher power at high dc voltage levels. To satisfy this requirement it will be necessary to take low voltage dc from a solar array or battery, convert it to ac by switching, use a transformer to raise the ac to a higher voltage level and then rectify this ac voltage to obtain the high voltage dc. A problem associated with this system is that the switching currents and voltages produced in this power conditioning circuitry are potential sources of electromagnetic radiation that could be used to locate and identify the spacecraft.

II. OBJECTIVES:

The purpose of this study is to investigate the electromagnetic fields from a spacecraft power system and determine the resulting magnitudes of the fields, on the earth, that might be expected from these systems.

III. THE SWITCHING SYSTEM:

The source of switching currents and voltages in a spacecraft power system is the inverter. An example of the circuitry used in this type of equipment is shown in Figure 1.(1) (The system controlling the switching is not shown in this Figure). In operation one half of an ac cycle is produced by

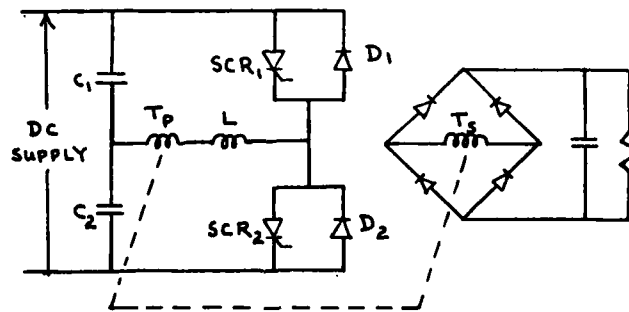


Figure 1

turning SCR 1 and SCR 2 off. This allows current to flow through SCR 1 and in one direction through the primary of the transformer. The other half of the ac cycle is produced by having SCR 2 on and SCR 1 off. Current then flows through SCR 2 and in the opposite direction through the primary of the transformer. The values of the inductors and capacitors in the circuit are selected to provide series resonance conditions. Power output to the load is controlled by adjusting

the times when the SCR's are turned on and off. Diodes D1 and D2 provide paths for capacitor discharging currents to flow when the SCRs are opened.

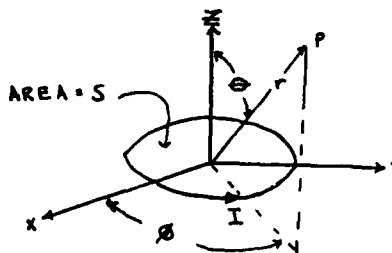
IV. TYPES OF FIELDS TO BE CONSIDERED:

Because there are no switches that are physically opening and closing, most of the magnetic flux would be confined to high permeability core material in the inductors and transformer and the equipment would be enclosed in metallic sheeting, it is not anticipated that there would be much electromagnetic energy radiated. Furthermore it is reasonable to assume that any electric fields that are produced can be reduced to negligible levels by shielding. The problem that remains is the magnetic fields produced by the switching currents. At the frequencies of operation of these systems, ~ 10-20 kHz, these fields are difficult to shield.(2) Thus it is concluded that the problem will be that of quantifying the magnetic fields that will be produced by a spacecraft power system.

V. MAGNETIC FIELD CHARACTERIZATION:

A detailed analysis of the magnetic field sources in a space power system is beyond the scope of this report. Instead the system will be treated as though it could be modeled as a small loop antenna or a superposition of a number of small loop antennas having different currents and orientations.

The fields produced by a loop antenna as shown in Figure 2 (3), will be



$$\vec{E} = j 30 k S I \left(j \frac{k}{r} + \frac{1}{r^2} \right) e^{-jkr} \sin \theta \hat{a}_\theta \quad (1)$$

$$\vec{H} = \left[\frac{SI}{4\pi} \left(j \frac{k}{r^2} + \frac{1}{r^3} \right) e^{-jkr} \cos \theta \right] \hat{a}_r - \left[\frac{SI}{4\pi} \left(\frac{k^2}{r} - j \frac{k}{r^2} - \frac{1}{r^3} \right) e^{-jkr} \right] \hat{a}_\phi \quad (2)$$

Figure 2

For the region near the loop, small r , the most important term in E_θ is that varying as $\frac{1}{r^2}$ and the most important H terms are those varying as $\frac{1}{r^3}$. (These field components are out of time-phase and do not represent an average energy flow). In the far field, large r , the components of interest are those that vary

as $\frac{1}{r}$. (The boundary between near and far field is arbitrarily set at $r = \frac{\lambda}{2\pi}$. $\lambda = \frac{300}{f}$ m with $f =$ frequency in MHz). When the frequencies of operation are 10 to 20kHz, the wavelengths will be 60 and 30km respectively, and near field boundaries will be approximately 10 to 5 km (6 to 3 miles). Thus, for spacecraft operating at 100 to 200 miles above the earth, the fields of interest on the earth would be the far fields

$$E_{\theta} = \frac{120 \pi^2 I S \sin \theta}{r \lambda^2} \quad (3)$$

$$H_{\theta} = \frac{\pi I S \sin \theta}{r \lambda^2} \quad (4)$$

A worst-case condition for radiation to the earth would be to have the maximum current produced in the power system flow through a one-turn loop antenna that is properly directed to provide maximum radiation on the earth. A 10kW - 10kHz power system having a primary current of 100 A through a 1 m² loop, miles above the earth would produce a field of approximately (2) (10⁻¹²) A/m and 8 (10⁻¹⁰) V/m. Although these fields would be higher if the number of turns were increased, the only high-current multi-turn coils in the power system are in the inductor and the transformer and there will be little radiation from these coils because the fields will be contained in the magnetic core material. In fact, because the currents will be flowing through wires in many directions and there are other metals present, as well as the magnetic cores, the external fields produced will be much smaller than those given above.

VI. EXPERIMENTAL:

The following experiments were conducted to obtain measures of the fields produced by the power conditioning equipment:

A 10kW, 10-kHz inverter was operated at nearly full load current conditions by short circuiting the leads that would normally be connected to the primary of the transformer. (This configuration will produce the magnetic fields attributable to the inverter stage of the power conditioning system. It and the primary winding of the transformer are the areas in the system where the highest currents will flow and these will produce the highest magnetic fields

exterior to the system.) The receiving antenna was positioned at a given radius and oriented to obtain maximum signal. For all points around the inverter the maximum voltage was induced when the plane of the loop was normal to a radial vector centered at the inverter. Examples of the results obtained at $r = 2$ and 3m are shown in Figure 3. Approximations of the peak magnetic fields produced may be obtained from the expression for induced voltage e

$$|e| = \frac{d\lambda}{dt} = N \frac{d\phi}{dt} = N B A \omega = N B A 2\pi f \quad (5)$$

where A = area of the loop in m^2
 N = number of turns in the loop
 B = magnetic flux density in W/m^2
 f = frequency in Hertz

for the case when $r = 2\text{m}$, e peak = 25 V this would correspond to a peak B of

$$B \approx \frac{25(10^{-6})}{2\pi(1)(8.66)(10^{-3})(10^4)} = 4.59(10^{-8})\text{ T} \quad (6)$$

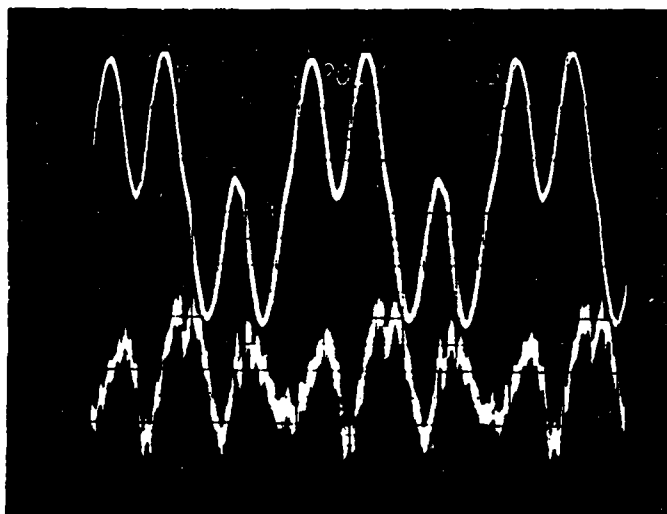
which would correspond to an H field of

$$H = \frac{B}{\mu} = \frac{4.59(10^{-8})}{4\pi(10^{-7})} = 0.0366\text{ A/m} \quad (7)$$

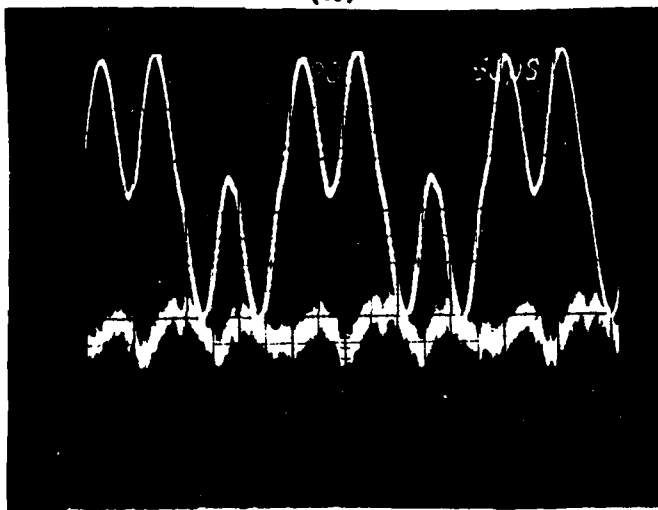
Since the sensing position was so close to the source, the components measured would be near field components normal to the plane of the loop, or \hat{a}_r components. For $H = 0.0366\text{ A/m}$ the magnitude of SI would be approximately

$$\begin{aligned} SI &= H(r^3) 2\pi = (0.0366)(8) 2\pi \\ &= 1.84\text{ A}\cdot\text{m}^2 \text{ (peak)} \end{aligned} \quad (8)$$

This is much lower than the [SI] of 100 A-m^2 that was assumed in part V and it illustrates the fact that a power conditioning system would not be a "good radiator". It should be noted that the peak value of the current in the inverter was $\approx 50 \text{ A}$.



(a)

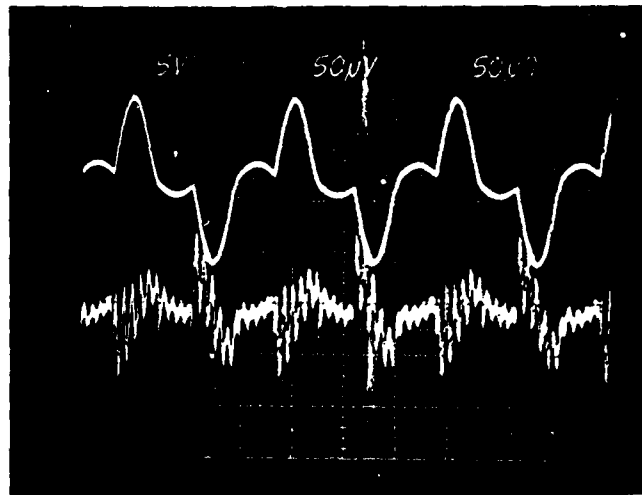


(b)

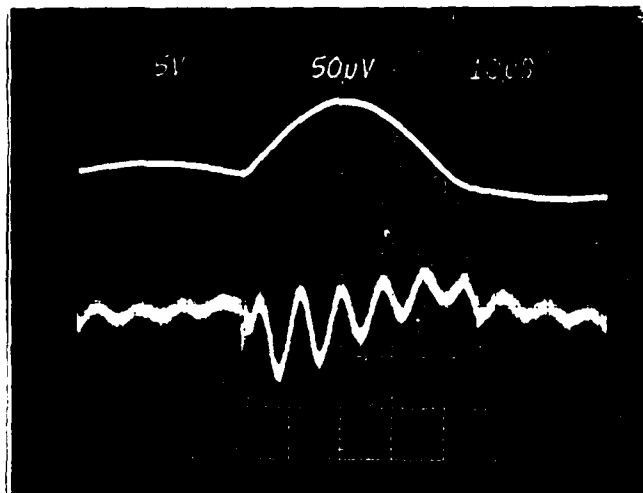
Figure 3

(a) and (b) top curves - inverter current (Vertical - 2V/div)
bottom curves - voltages induced in the antenna (Vertical/ $20\mu\text{V/div}$).
Horizontal - $50 \mu\text{s/div}$. Inverter current was processed through an
instrument transformer having 0.1 V/A .

The experiment was repeated with a complete power conditioning system including a transformer - rectifier and filtered resistive load. The voltage on the secondary was $\sim 7.6\text{kV}$. The results are shown in Figure 4. (Note that the vertical scales in Figures 3 and 4 differ).



(a)



(b)

Figure 4

(a) and (b) top curves inverter current (5V/div) bottom curves - voltage induced in the antenna (50μV/div)

This Figure shows a fundamental that is directly related to the primary current and a transient ringing current that rides on top of this fundamental. Both the magnitude of the fundamental and the magnitude of the transient are approximately $25\mu\text{V}$ - peak. Ringing current frequency is approximately 125 kHz. Peak value of the current in the primary is approximately 80A. The fact that this current produced approximately the same radiated field as the 50A flowing in the first experiment is attributed to changes in the wiring and the presence of the transformer. The results of the experimental measurements show that the magnetic fields radiated to the earth by a space power system would be extremely small. Additionally, the reception of the low frequency signals produced by these systems would require specialized antennas and even then they would be difficult to detect.

VII. RECOMMENDATIONS:

Recommendations for this study would be to investigate the design of the power system to determine wiring configurations and component placements that would reduce exterior magnetic fields to minimal values. Another recommendation would be to investigate the receiving system that would be required to detect the radiation levels that are predicted in this report.

AD-A113 708

SOUTHEASTERN CENTER FOR ELECTRICAL ENGINEERING EDUCAT--ETC F/6 5/1
USAF SUMMER FACULTY RESEARCH PROGRAM. 1981 RESEARCH REPORTS, VO--ETC(U)
OCT 81 W D PEELE F49620-79-C-0038

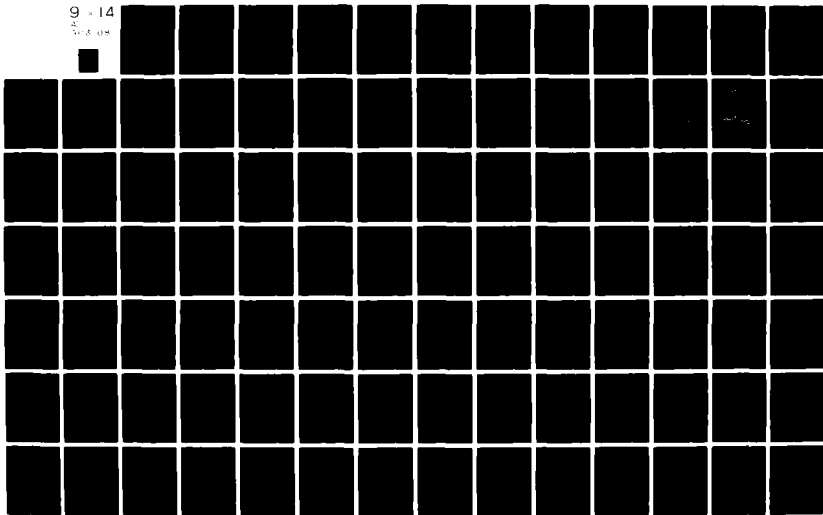
UNCLASSIFIED

AFOSR-TR-82-0227

NL

9 - 14

003 08



REFERENCES

1. Biess, J.J., L.Y Inouye and J.H. Shank, "High Voltage Series Resonant Invertor Ion Engine Screen Supply," Proc. IEEE Power Electronics Specialists Conference, Bell Laboratories, Murray Hill, N.J. June 1974.
2. White, D.R.J., "Electromagnetic Intereference and Compatibility" Vol. 4, Don White Consultants, Germantown, Maryland, 1971.
3. Krauss, J.D., "Antennas," McGraw-Hill Book Company New York 1950.

1981 USAF - SCEEE SUMMER FACULTY RESEARCH PROGRAM

Sponsored by the

AIR FORCE OFFICE OF SCIENTIFIC RESEARCH

Conducted by the

SOUTHEASTERN CENTER FOR ELECTRICAL ENGINEERING EDUCATION

FINAL REPORT

ACETYLENE TERMINATED SYSTEMS: QUINOXALINES AND ISOMERIC SULFONES

Prepared by: Dr. William A. Feld
Academic Rank: Assistant Professor
Department and University: Department of Chemistry
Wright State University
Research Location: Air Force Wright Aeronautical Laboratories
Materials Laboratory, Polymer Branch
USAF Research Colleague: Dr. F. L. Hedberg
Date: September 21, 1981
Contract No: F49620-79-C-0038

ACETYLENE TERMINATED SYSTEMS:
QUINOXALINES AND ISOMERIC SULFONES

by
William A. Feld

ABSTRACT

The use of a 95% m-dibromobenzene: 5% p-dibromobenzene mixture in place of pure m-dibromobenzene in a series of cuprous oxide catalyzed coupling reactions was shown not to affect product distributions. It was also determined that cupric oxide gives identical product distributions to those obtained from cuprous oxide. A new symmetrically substituted quinoxaline, 2,3-bis(4-bromophenoxyphenyl)-quinoxaline was synthesized and fully characterized. A one-pot acetylenic coupling reaction involving iodoaromatics and phenylacetylene was developed. Recommendations for using the results of these projects are offered.

Acknowledgement

The author would like to thank the Air Force Systems Command, the Air Force Office of Scientific Research and the Southeastern Center for Electrical Engineering Education for providing the opportunity to spend a stimulating and enlightening summer at the Materials Laboratory, Wright-Patterson AFB, Ohio. The hospitality and laboratory space provided by the Polymer Branch (AFWAL/MLBP) are especially noted.

The cooperation of Dr. R. L. Van Deusen as Focal Point, the collaboration and guidance of Dr. F. L. Hedberg in defining the projects and many helpful discussions with Dr. F. E. Arnold, Dr. R. C. Evers and Ms. Marilyn Unroe are gratefully acknowledged.

I. INTRODUCTION

The synthesis of polymers for use as high temperature matrix and adhesive resins and the study of their structure-property relationships are of fundamental importance to the long range goals of the Materials Laboratory. To be useful as a matrix or adhesive resin, a polymer must exhibit good thermal oxidative stability as well as moisture insensitivity. Heterocyclic polymers, such as the quinoxalines, exhibit excellent thermal oxidative stability and moisture insensitivity but generally are produced by a condensation reaction in which volatile by-products are evolved giving rise to voids in the cured matrix or adhesive resin. The epoxies have excellent processing, handling and performance characteristics but are not very stable thermally nor do the epoxies or their precursors exhibit an insensitivity to moisture. Significant effort has been directed at the design and synthesis of a resin system that would have good fabrication criteria, i.e. melt processability and room temperature tack and drape, and better thermal oxidative stability and moisture insensitivity than the epoxies. The introduction of acetylene-terminated oligomeric systems¹⁻⁶ which cure by a thermal addition reaction is the state-of-the-art approach to meeting the criteria outlined above.

This project was concerned with (1) the effect of using mixed isomeric reagents in the preparation of an acetylene-terminated sulfone, and (2) the synthesis of a new symmetrically substituted, acetylene-terminated quinoxaline.

II. OBJECTIVES

Our specific objective in the area of acetylene-terminated sulfones was to employ a 95% m-dibromobenzene, 5% p-dibromobenzene mixture in a state-of-the-art copper catalyzed coupling reaction with sulfonyldiphenol. Various dibromobenzene to sulfonyldiphenol ratios were to be investigated to determine their influence on reaction times and monomer to oligomer product ratios.

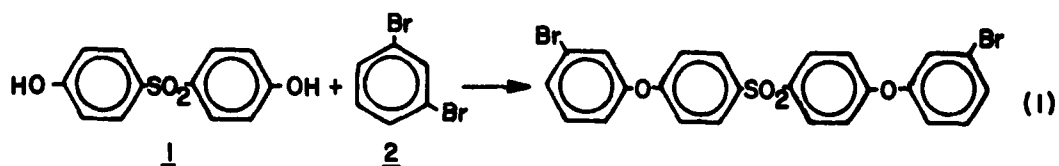
Our objective in the quinoxaline area was to synthesize the unknown symmetrically substituted compound 2,3-bis(4-ethynylphenoxyphenyl)-

quinoxaline as this material would provide a comparison for other unsymmetrically substituted systems.

Our objective concerning follow-on research was to review existing literature pertaining to intramolecular cure (IMC) reactions and propose functionalizations of current systems as well as new potentially useful systems.

III. ACETYLENE TERMINATED SULFONES

A series of cuprous oxide catalyzed coupling reactions involving 4,4'-sulfonyldiphenol (1) and m-dibromobenzene (2) have been carried out⁷. Because of the relatively high cost of m-dibromobenzene as compared to the para isomer and because separation of the isomers in commercial mixtures is prohibitively expensive, a series of cuprous oxide



catalyzed coupling reactions were carried out using 1 and a 95% m-dibromobenzene, 5% p-dibromobenzene mixture. Conditions for the isomeric mixture reactions duplicated those used in the single isomer study cited. Analytical data for these reactions is presented in Table I.

The data in Table I indicate:

- 1) the substitution of an isomeric mixture of dibromobenzenes for a single isomer does not appreciably affect the monomer to oligomer ratio found for a particular dibromobenzene to sulfonyldiphenol ratio.
- 2) Total conversion data is suspect because of the use of several alternate work-up procedures which would be expected to affect overall yield but not monomer to oligomer ratios.
- 3) Cupric oxide can be substituted for cuprous oxide with no change in monomer to oligomer ratio or reaction characteristics.

Table I

Isomeric Dibromobenzene Coupling Reaction Data

Run	DBB/SDP	Yield	Monomer (mmol)	Dimer (mmol)	Trimer (mmol)	DBB	IRatio ^c	SRatio ^d
1	20:1 ^a	6.7g (72%)	5.67g (10)	0.64g (1.5)	-	0.13g	8.9 (6.7)	10.0 (7.5)
2	10:1	5.1g (56%)	3.69g (6.59)	0.79g (1.87)	0.18g (0.45)	0.09g	3.8 (2.8)	3.1 (2.3)
3	6:1	7.5g (78%)	4.5g (8.04)	1.5g (3.55)	0.30g (0.88)	-	2.5 (1.8)	2.4 (1.8)
4	10:1 ^b	6.3g (67%)	5.2g (9.6)	0.59g (1.4)	-	-	8.8 (6.7)	-

a) Dibromobenzene (meta + para) to sulfonyldiphenol ratio.

b) Cupric oxide (CuO) catalyst.

c) IRatio = isomeric ratio = wt monomer/(wt dimer + wt trimer)
(mmol monomer/(mmol dimer + mmol trimer))

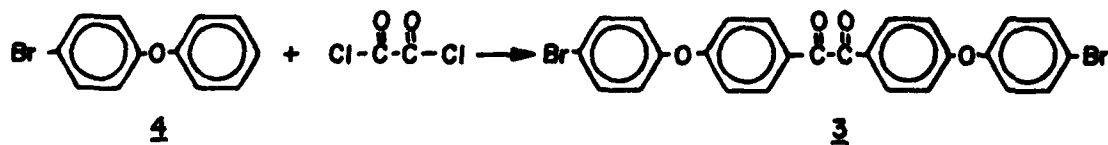
d) SRatio = single isomer ratio determined as in c). See reference 7.

IV. 2,3-BIS(4-ETHYNYLPHENOXYPHENYL)QUINOXALINE

The synthesis and evaluation of several acetylene-terminated quinoxaline systems has been reported.¹⁻³ They exhibit excellent thermal oxidative stability, are moisture insensitive both before and after cure and are excellent candidates for 450-500°F applications. Because these systems are prepared from unsymmetrical starting materials, they exist as mixtures of isomers. It was of interest, therefore, to synthesize a symmetrically substituted, acetylene-terminated quinoxaline system.

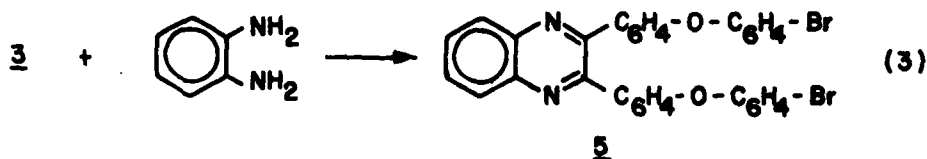
Pertinent data for all new compounds appears in Table 2.

The synthesis of 4,4'-bis(4-bromophenoxy)benzil (3) was accomplished



employing 4-bromodiphenyl ether (4), oxalyl chloride, aluminum chloride

and carbon disulfide as solvent by analogy to the preparation of 4,4'-dimethoxybenzil from anisole.⁸ The diketone 3 was converted into



2,3-bis(4-bromophenoxyphenyl)quinoxaline (5) by reaction with *o*-phenylene diamine in tetrahydrofuran using acetic acid as catalyst. Conversion of

Table 2

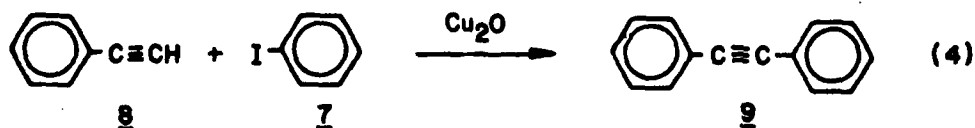
Quinoxaline Analytical Data

Compound	Yield	mp C	C		H		N (Br)	
			Calcd.	Found	Calcd.	Found	Calcd.	Found
3	70%	154-56	56.55	56.65	2.90	2.94	(28.94)	(28.87)
5	90%	127-28	61.52	61.45	3.20	3.04	4.49	4.33

5 to its diethynyl derivative was not complete as of the writing of this report.

V. A ONE-POT CASTRO COUPLING REACTION

As cuprous phenylacetylide is used in an important step⁹ in the synthesis of an intramolecular curing agent, we were especially interested in a recent literature report¹⁰ describing the coupling of phthalimide (6) with bromo- or iodoaromatics. The reaction conditions were applied to



the coupling of iodobenzene (7) and phenylacetylene (8). A 90% yield of

diphenylacetylene (9) was the result. Presumably, cuprous phenylacetylde is formed in-situ at elevated temperatures and reacts with 7. The reaction does not take place in pyridine and does not give good yields when bromobenzene is used in place of 7 in contrast to the reports of Castro and the imide coupling already cited. This new reaction is currently being investigated.

VI. INTRAMOLECULAR CURE (IMC) SYSTEMS

A careful review of existing technical literature pertaining to past and current research in intramolecular cure systems was made. A Mini-grant proposal is currently being prepared for submission to AFOSR concerning new intramolecular cure (IMC) systems.

VII. RECOMMENDATIONS

The results of our investigation of the influence of isomeric mixtures of reagents in the synthesis of acetylene-terminated sulfones indicate that yield and product distributions are affected only slightly. Even the substitution of cupric oxide for cuprous oxide does not change the reaction characteristics. The recommendation, therefore, is that evaluation of acetylene-terminated sulfones be made employing commercially available dibromobenzene mixtures to effectively model scale-up conditions.

Completion of the synthesis and thermal evaluation of 2,3-bis(4-bromophenoxyphenyl)quinoxaline will determine its usefulness. The synthetic sequence represents a simple series of high-yield steps involving readily available starting materials.

REFERENCES

1. Kovar, R. F., G. F. L. Ehlers, and F. E. Arnold, "Thermosetting Acetylene-Terminated Polyphenylquinoxalines," J. Polym. Sci., Poly. Chem. Ed., 15, 1081 (1977).
2. Kovar, R. F. and F. E. Arnold, U.S. Patent 3,975,444 (1976) and U.S. Patent 3,966,729 (1976).
3. Hedberg, F. L., and F. E. Arnold, "Benzil End-Capped Acetylene-Terminated Phenylquinoxalines," Polymer Preprints, 18(1), 826 (1977).
4. Hedberg, F. L., and F. E. Arnold, U.S. Patent 4,098,825 (1978) and U.S. Patent 4,147,868 (1979).
5. Kovar, R. F., G. F. L. Ehlers and F. E. Arnold, "Addition Cured Acetylene-Terminated Polyphenylquinoxaline Oligomers," Polymer Preprints, 16(2), 246 (1975).
6. Hergenrother, P.M., "Linear Polyquinoxalines," J. Macromol. Sci., Rev. Macromol. Chem., C6, 1 (1971).
7. Unroe, M. and F. L. Hedberg, *Personal communication*.
8. Staudinger, H., E. Anthes, and M. Scholler, "Oxalylchloride IV. Ueber die Friedel Craftssche Reaktion mit Oxalylchloride und Oxalylbromide," Berichte, 45, 1594 (1912).
9. Hedberg, F. L. and F. E. Arnold, "Phenylethynyl-Pendent Polyphenylquinoxalines Curable by an Intramolecular Cycloaddition Reaction," J. Polym. Sci., Poly. Chem Ed., 14, 2607 (1976).
10. Sato, M., S. Ebine, and S. Akabori, "Condensation of Halobenzenes and Haloferrocenes with Phthalimide in the Presence of Copper (I) Oxide: A Simplified Gabriel Reaction," Synthesis, 1981, 472.

1981 USAF - SCEEE SUMMER FACULTY RESEARCH PROGRAM

Sponsored by the

AIR FORCE OFFICE OF SCIENTIFIC RESEARCH

Conducted by the

SOUTHEASTERN CENTER FOR ELECTRICAL ENGINEERING EDUCATION

FINAL REPORT

A SIMULATION FRAMEWORK FOR THE EVALUATION OF TERRAIN FOLLOWING AND
TERRAIN AVOIDANCE TECHNIQUES

Prepared by: Dr. John A. Fleming
Academic Rank: Assistant Professor
Department and University: Department of Electrical Engineering
Texas A+M University
Research Location: Avionics Laboratory, Mission Avionics Division,
Applications Branch, System Concepts Group (AFWAL/AART2)
USAF Research Colleague: Stephen K. Gourley, 1Lt, USAF
Date: August 7, 1981
Contract Number: F49620-79-C-0038

A SIMULATION FRAMEWORK FOR THE EVALUATION OF TERRAIN FOLLOWING AND

TERRAIN AVOIDANCE TECHNIQUES

by

John A. Fleming

ABSTRACT

The structure of a simulation for the evaluation of automatic terrain following/terrain avoidance/obstacle avoidance flight is specified. Models for the components of a TF/TA/OA system are proposed. A generator for realistic synthetic terrain is developed and a model for the Digital Land Mass Simulation (DLMS) data base is given and implemented. Finally, a description of the path generation problem is given and research remaining to be done in this area is outlined.

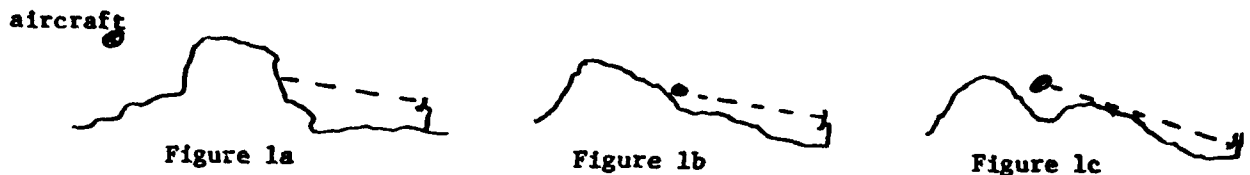
ACKNOWLEDGMENT

The author would like to thank the Air Force Systems Command, the Air Force Office of Scientific Research, and the Southeastern Center for Electrical Engineering Education for providing and administering the program which allowed him to spend a worthwhile ten weeks in research. This period was spent at the Avionics Laboratory of the Air Force Wright Aeronautical Laboratories, located at Wright-Patterson AFB, Ohio. Within the Avionics Laboratory the support of Colonel H. Paskin (Division Chief, Mission Avionics), Mr. M. Spector (Branch Chief, Applications), and A. Duke (Group Leader, System Concepts) is greatly appreciated. Technical discussions with P. Pietrzak of the Flight Dynamics Laboratory, and with D. DeBerry of the radar branch (AARM) proved helpful. The people and working conditions within the Applications Branch (AART) made the author's stay enjoyable as well as worthwhile. Finally, he would like to thank Lieutenant Stephen K. Gourley (AART-2) for suggesting the research topic and for his guidance, encouragement, and expertise throughout the research period.

I. Introduction

Sustained low-level flight is one key to successful penetration into a closely monitored region. By flying close to the ground the probability of detection by ground-based, or air-based, radar sensor systems is substantially reduced due to:

- 1) direct masking of the vehicle by the terrain between it and the source of the illumination. (Fig. 1a)
- 2) indirect masking due to the inability of the radar system to distinguish the vehicle from the ground clutter. (e. g. vehicle and terrain are within the same range or angle resolution cell). (Fig. 1b, 1c)



Even if detection is accomplished, low level flight decreases the probability of a successful track being initiated.

On the other hand, the probability of collision with the ground or with obstacles (houses, towers, transmission lines, etc.) is substantially increased as lower clearance heights are attempted. In order to avoid collision it is necessary that an accurate description of present and upcoming terrain features and obstacles be available to the flight path generator and flight control system so that a safe path can be flown.

In the past the ADLAT program (Ref. 1,2) addressed the terrain following problem.^(*) A radar automatic terrain following system is operational in the Air Force F-111B aircraft. This system is designed for a minimum clearance distance on the order of a few hundred feet.

(*) For the purposes of this report the term "terrain following" refers to vertical maneuvers (go over), while "terrain avoidance" refers to horizontal and vertical maneuvering (go around).

Work is presently underway to address the three-dimensional terrain avoidance problem, with the goal of increased survivability and lower minimum clearance height. (Ref. 3,4). Key to the success of this work will be the necessity to accurately characterize what is ahead and to choose a best path based on this knowledge.

The requirement for obstacle avoidance demands that objects of low radar cross section be detected at sufficient range so that the flight control system can respond and alter the flight path accordingly.

If possible, relative stealth should be maintained. This means that active sensors (radar, laser, altimeter) should only be as powerful as is minimally necessary and these should only operate for the minimum amount of time necessary to accomplish the objective. Scan patterns and scan times should be chosen to obtain the maximum amount of information with a minimum amount of emission. Increased demand for stealthiness leads to incompleteness of sensor information. The tradeoff between stealth and data requirements is an aspect that will need to be addressed. Alternately, "quieter" sensors such as radiometers, passive IR, or millimeter wave might be used.

II. Objectives

The requirement for low probability of detection while preserving low probability of clobber leads to stringent demands on the sensor system of the aircraft. The purpose of this study was to analyze the flow of events for TF/TA/OA flight, to model the various sensors and information sources that might be available to the flight path generator, and to develop a simulation tool that could be used to evaluate probability of detection, probability of clobber, etc., under various sets of sensor parameters, terrain and obstacle features, and threat locations.

Since the purpose of the simulation was to provide a tool for the evaluation of tradeoffs in prescribing the requirements for terrain following/terrain avoidance, the structure of the simulation was chosen so as to be flexible and relatively simple. The models

used for the subsystems were generally chosen in order to provide a reasonable description of the input-output characteristics of the subsystems. There was no attempt to include exact models, in keeping with the expected use of the simulation.

The tasks involved in the work and reported herein were:

- 1) To study the terrain avoidance problem, the performance of candidate sensors, and the approaches being investigated in the area of path generation for terrain avoidance.
- 2) To develop a block diagram which depicts the events, the subsystems and the flow of information within a simulation of terrain avoidance flight.
- 3) To develop models for each of the subsystems that will be used in the simulation package.
- 4) To code the models and specify a set of nominal parameters for each of the models. The coding was done in the FORTRAN IV language and tested on the ASD, CDC Cyber 74 computer system.

III. Background on TF/TA/OA Flight

An approach that has been taken for automatic terrain following is depicted below (Figure 2).



Figure 2.

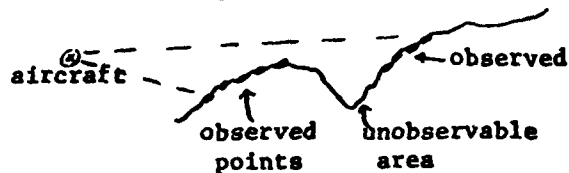
A forward looking radar scans in elevation from an angle θ_1 to θ_2 . The return signal provides range and angle of elevation information of the terrain with respect to the aircraft. A flight path is chosen that will allow clearance of all terrain points by some predetermined height. The development of the algorithm which specifies flight commands based on such information is described in the series of ADLAT studies carried out by CALSPAN (Refs. 1,2).

Unfortunately this type of system exhibits "ballooning" as depicted in Figure 3. The reason for ballooning is that



Figure 3.

the system is unable to see parts of the terrain that are masked from its line of sight (Figure 4).



For terrain following and terrain avoidance a scan in both azimuth and elevation would be used, an algorithm developed to specify flight commands, and then these would be implemented by the flight control system. Terrain masking would remain a problem, and would severely limit side to side maneuvers since ballooning in the horizontal plane could prove disastrous.

Use of the Digital Land Mass Simulation (DLMS) data base from the Defense Mapping Agency has recently been considered as a potential source of information to a terrain following system. The DLMS Level II data base breaks the surface of the earth into approximately 100 foot square grids and provides the smoothed altitude values for each of these grid areas. Incorporation of this data into a terrain following or terrain avoidance system as a stored on-board map allows farther look-ahead and fills in areas that are masked from the sensors. The use of map data in the TF/TA application involves two difficulties. First, an accurate fix of the aircraft position is necessary so that the correct map portion is called down from memory. Second, the DLMS data does not include obstacle information.

An accurate fix of aircraft position might be obtained by periodically updating the inertial navigation system (INS) by either terrain contour correlation (comparison of altimeter data to a stored map) or from the Global Positioning System (GPS). Once the position of the aircraft is known, a section of the DLMS data would be called down and used to augment sensor data in order to provide a "best guess" for the terrain ahead.

Dedicated sensors for obstacle avoidance would be necessary since many obstacles (e. g. electrical or telephone wires) would not be detectable by microwave radar. Candidate sensors for obstacle detection are millimeter wave radar, and infrared or visible lasers.

A depiction of the TF/TA/OA system is shown in Figure 5.

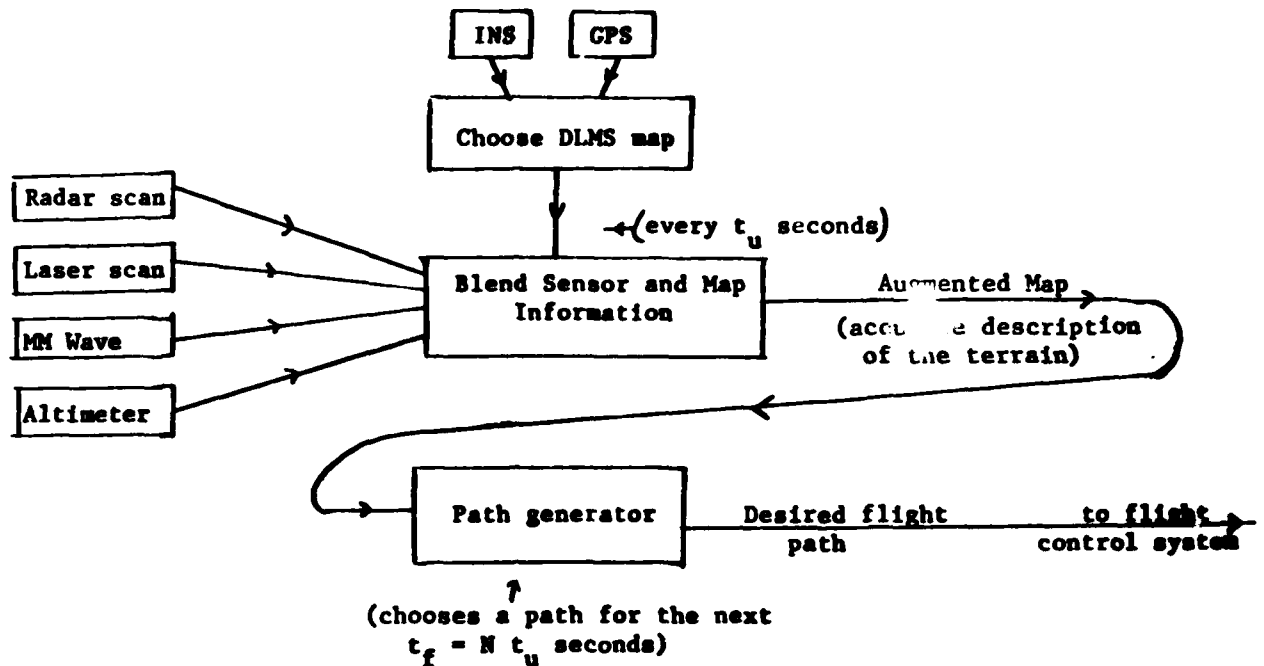


Figure 5.

The path generator is the heart of the system. It searches the augmented map and prescribes a path that attains low altitude flight within the constraints of aircraft performance and crew comfort. The flight control system then provides control signals to the actuators for the aerodynamic surfaces and attempts to follow this path. It is anticipated that the desired flight path would be computed for several segments ahead and recomputed as each segment is flown and new sensor data is obtained. The update time t_u would be determined by factors such as terrain roughness, speed of the aircraft, and range of the sensors.

A mechanism for immediate climb would be added to the system to account for below minimum clearance altitude (as measured by altimeter) and for newly detected obstacles at close range.

IV. Structure of the Simulation

A block diagram of the simulation of TF/TA/OA is shown in Figure 6.

Since the actual flight path and all sensor data will not be exact, it is necessary to distinguish between what is the true position of the aircraft, terrain features, and obstacles, and what the aircraft thinks these locations are. For example, sensors operate from true position and scan true terrain as seen from that position, but return imperfect information. This information is then compared with an estimated position on an imperfect map.

Note: True values are denoted x_T , y_T etc., while estimated values are denoted \hat{x} , \hat{y} , etc.

A description of each of the models shown in the block diagram follows.

A. Terrain Model

Statistical properties of mean, trend removed, actual terrain have been shown to be fairly well characterized as Gaussian distributed, with exponentially decaying correlation among samples. The exponential correlation function is of the form

$$R(\tau) = E \{ Z(x)Z(x+\tau) \} = A \exp(-\tau/Tauc)$$

where the factor Tauc is called the decorrelation distance. Decorrelation distances for typical terrain samples were found to vary from 2500ft. (fairly rough terrain) to 30,000 ft. (fairly smooth terrain). An illustration of the effect of Tauc is given in Figure 7. Both cases would have the same mean value and standard deviation.

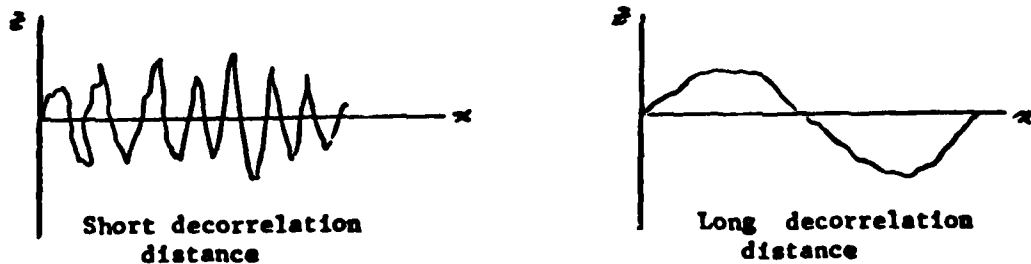


Figure 7.

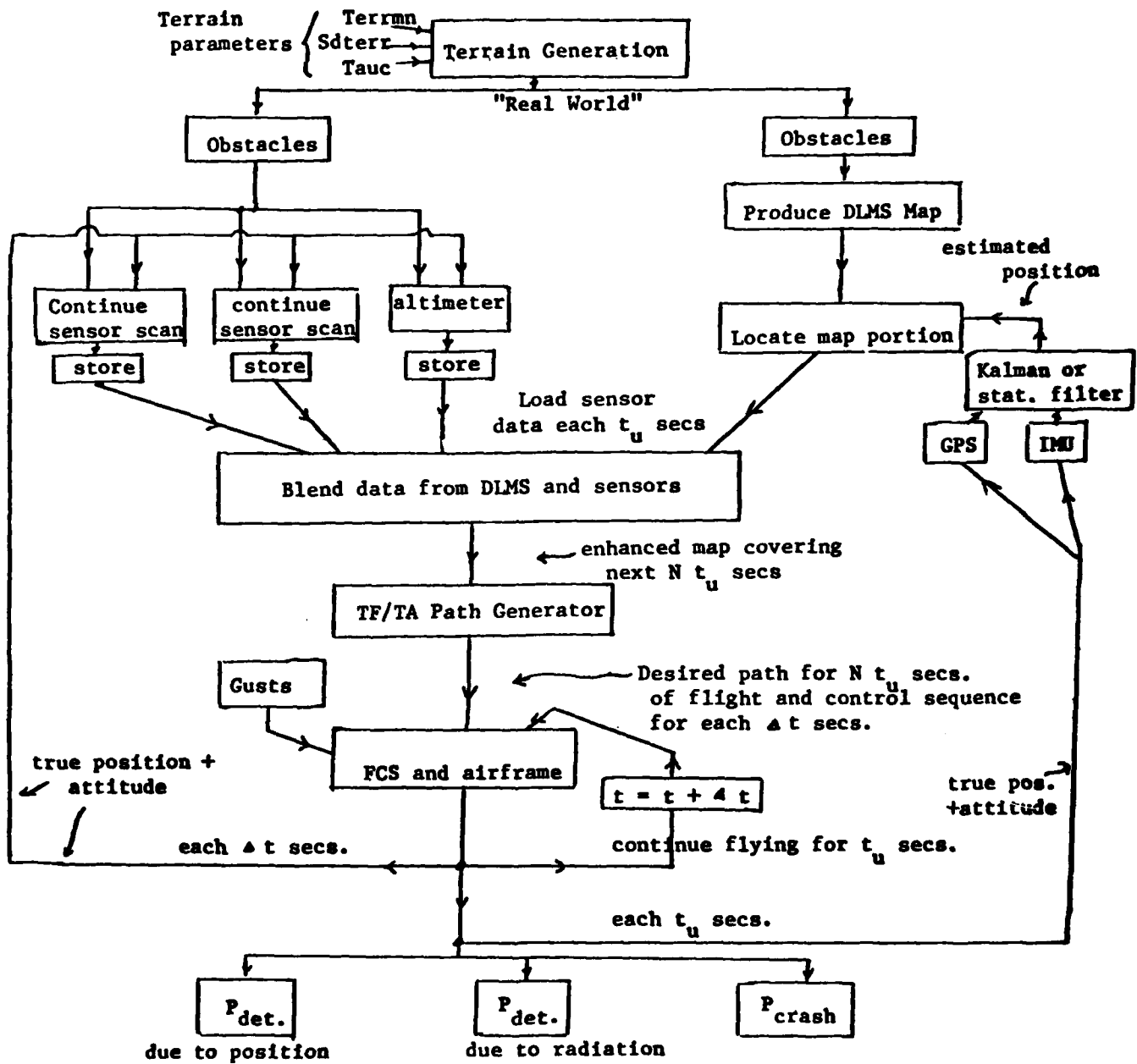


Figure 6. Flow Chart for a Simulation of TF/TA/OA Flight

For the purposes of the simulation package it was decided to produce synthetic terrain as "real world". Therefore it was necessary to develop a procedure to generate points which possessed the desired statistical properties. These properties were:

- 1) Terrain characterized as a two-dimensional stochastic process $Z(x,y)$.
- 2) Heights of the terrain at each (x,y) point Gaussian distributed with mean value $Terrmn$, and standard deviation $Sdterr$.
- 3) Terrain heights correlated in both dimensions with an exponential correlation function. The decorrelation distance was $Tauc$.

Time series analysis provides a mechanism for generating such a process. For the one-dimensional case it is known (Ref. 5) that a first-order autoregressive process of the form

$$Z_t = a Z_{t-1} + \delta + W_{t-1}$$

(where W_t is a zero mean, Gaussian white noise process of standard deviation given by σ_w and δ is a constant trend factor) produces the process, Z_t .

This process is also Gaussian, with a mean value

$$\bar{Z} = \frac{\delta}{1-a}$$

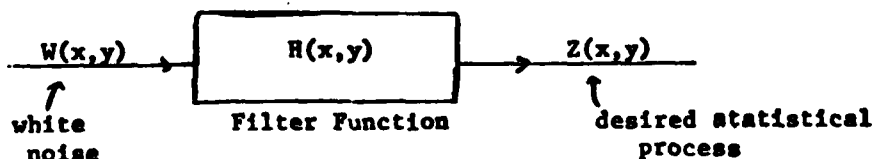
and standard deviation,

$$\sigma_z = \frac{\sigma_w}{\sqrt{1-a^2}}$$

Evaluation of the autocorrelation function for this process shows that

$$R_z(\tau) = A a^\tau.$$

For the case at hand, a generalization to a two-dimensional process must be made.



Consider a general two-dimensional first order discrete autoregressive process of the form

$$Z(x,y) = a_1 Z(x-1,y) + a_2 Z(x,y-1) + a_3 Z(x-1,y-1) + \mathcal{J} + w(x,y) \quad (1)$$

where $w(x,y)$ is a Gaussian white noise process with standard deviation given by σ_w and zero mean.

It is desired to find if constants $a_1, a_2, a_3, \mathcal{J}$, and σ_w exist so that the process $Z(x,y)$ possesses a Gaussian distribution with specified mean, standard deviation, and exponential correlation function of given decorrelation distance. By analogy to the one-dimensional case, and since the correlation in the x and y directions should be the same, we choose $a_1 = a_2 = a$. That is

$$Z(x,y) = a Z(x-1,y) + a Z(x,y-1) + b Z(x-1,y-1) + \mathcal{J} + w(x,y) \quad (2)$$

The autocorrelation function for a two-dimensional discrete process is

$$\gamma_{ij} \triangleq E \{ Z(x,y) \cdot Z(x+i,y+j) \} \quad (3)$$

and we desire that γ_{ij} be of the form

$$\gamma_{ij} = (\text{Sdterr})^2 \cdot \exp(-(i+j)/\text{Tauc}) . \quad (4)$$

Evaluation of the functions $\gamma_{00}, \gamma_{01}, \gamma_{10}$, and γ_{11} , along with algebraic manipulations and the enforcement that $\gamma_{10} = \gamma_{01}$ and $\gamma_{1,-1} = \gamma_{11}$, generates the set of relations

$$\mathcal{J} = \frac{(1 - b - 2a^2) \sigma_w^2}{(1 - b - 4a^2 - 4a^2 b - b^2 + b^3)} \quad (5)$$

$$\gamma_{10} = \gamma_{01} = \left(\frac{a(b+1)}{1 - b - 2a^2} \right) \gamma_{00} \quad (6)$$

$$\gamma_{11} = \left(\frac{2a^2 + b - b^2}{1 - 2a^2 - b} \right) \gamma_{00} . \quad (7)$$

By setting $b = -a^2$ we arrive at the desired relations

$$\gamma_{00} = \frac{\sigma_w^2}{(1 - a^2)^2} \quad (8)$$

$$\gamma_{10} = \gamma_{01} = a\gamma_{00} \quad (9)$$

$$\gamma_{11} = a^2\gamma_{00}, \quad \gamma_{ij} = a^{1+j}\gamma \quad (10)$$

and
$$\bar{z} = \frac{\mathcal{J}}{(1-a)^2} \quad (11)$$

By setting

$$a = \exp(-1/\text{Tauc})$$

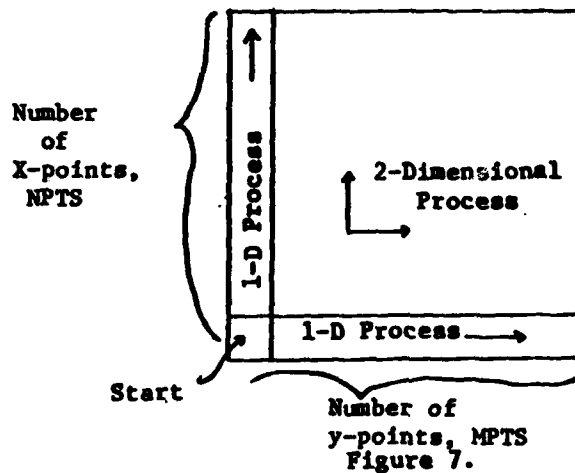
$$\mathcal{J} = \text{Terrm} \cdot (1-a)^2$$

and

$$\sigma_w^2 = (\text{Sdterr})^2 (1-a^2)^2$$

we obtain a two-dimensional stochastic process such that the mean is Terrm, the standard deviation is Sdterr, and the process is exponentially correlated with decorrelation factor, Tauc.

This process needs initial conditions. These are provided as illustrated in Figure 7.



Constants:

$$\mathcal{J}_1 = \text{Terrm} \cdot (1-a)$$

$$\mathcal{J}_3 = \text{Terrm} \cdot (1-a)^2$$

$$w_1 = \text{zero mean, S.D.} = \text{Sdterr} \sqrt{1-a^2}$$

$$w_3 = \text{zero mean, S.D.} = \text{Sdterr}(1-a^2)$$

with $Z(1,1)$ = a Gaussian random variable with standard deviation = Sdterr, and mean = Terrm.

$$Z(1,j) = a Z(1,j-1) + \mathcal{J}_1 + w_1 \quad \text{first row}$$

$$Z(i,1) = a Z(i-1,1) + \mathcal{J}_1 + w_1 \quad \text{first column}$$

$$Z(i,j) = a Z(i-1,j) + a Z(i,j-1) - a^2 Z(i-1,j-1) + \mathcal{J}_3 + w_3.$$

$$i = 2, 3, \dots, \text{NPTS}$$

$$j = 2, 3, \dots, \text{MPTS}$$

Due to the large number of Gaussian random variables that will be generated throughout the simulation a fast procedure to generate such numbers was needed. The procedure chosen was to generate a uniformly distributed random variable in (0,1) and then to refer to a tabulation of the inverse normal distribution function to obtain a Gaussian zero mean, standard deviation = 1, random variable. This value was then multiplied by the desired σ and then added to the desired mean value. This type of procedure is several times faster than the more commonly used procedure of generating and adding a series of uniformly distributed numbers and then relying on the laws of large numbers.

A computer program was written to generate artificial terrain according to the model developed in equations (2) through (11). The input parameters of this program are

- Sdterr = the desired terrain standard deviation in altitude
- Terrmn = the desired terrain mean value of altitude
- Tauc = the decorrelation distance of the terrain sample
(short Tauc = rough, long Tauc = smooth)
- NPTS and MPTS = the number of x and y values to be generated.

The next several figures (T.1 through T.5) show typical terrain maps generated by the terrain generator program. These plots were made using the DISSPLA package of plotting routines. It can be seen from the figures that a wide variety of terrain types can be generated through variation of the input parameters to the procedure.

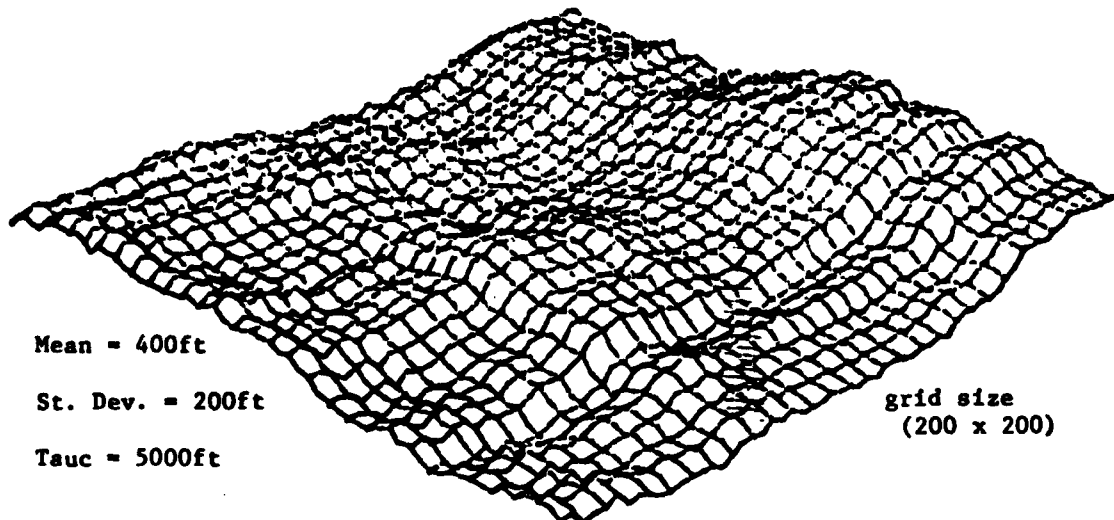


Figure T.1

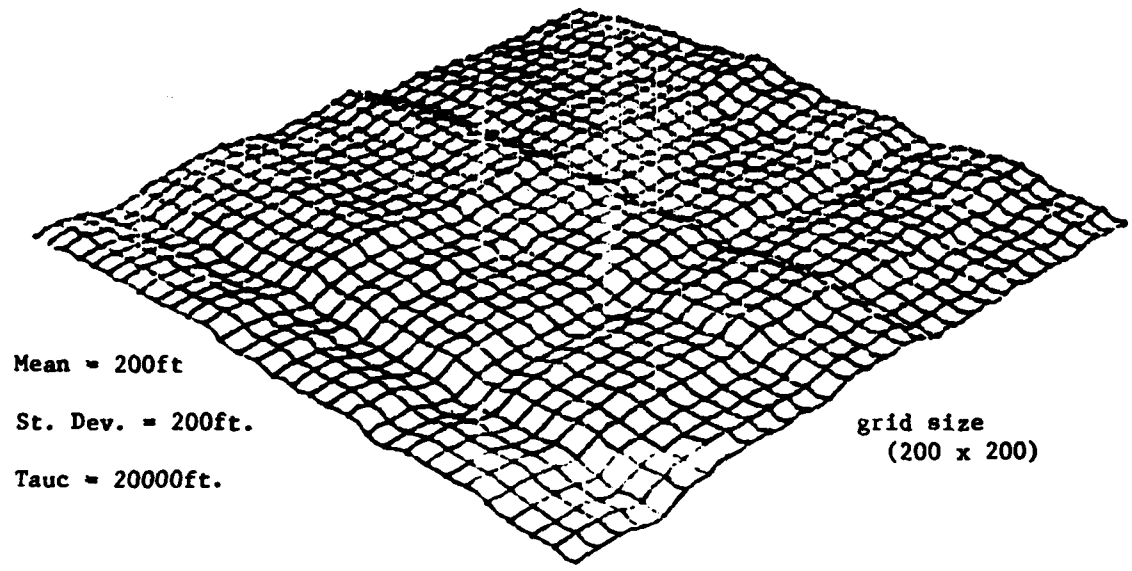


Figure T.2

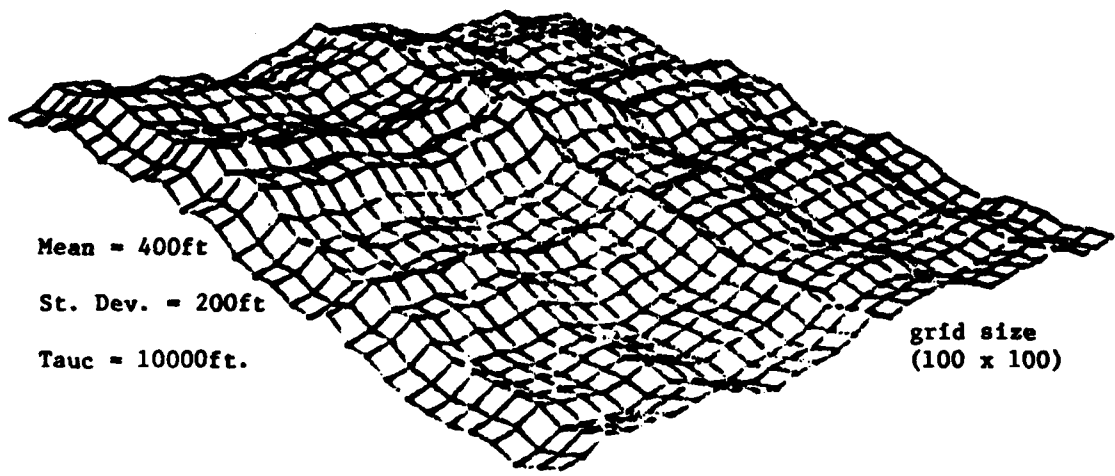


Figure T.3

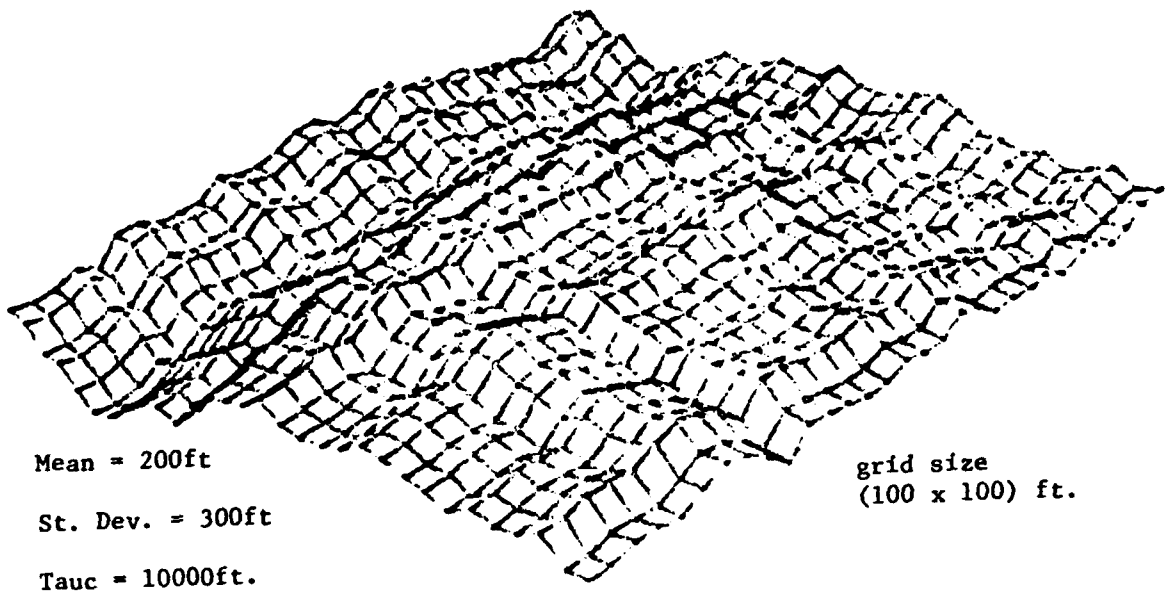


Figure T.4

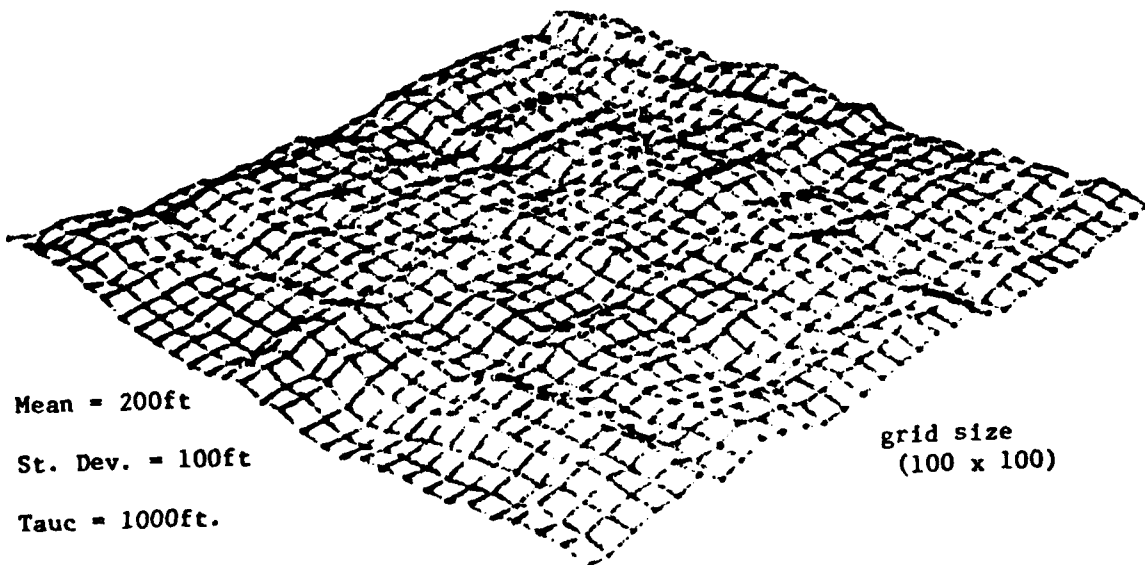


Figure T.5

B. DLMS Data Model

Analysis of the Defense Mapping Agency's DLMS data (Ref. 3) shows that there are biases and random errors which lead to the mislabelling of (x,y) position, and measurement errors that lead to misrepresentation of terrain altitude. That is: DLMS data points must be modeled as

$$DLMS(x,y) = \text{Terrain}(x_1,y_1) + \text{noise in height measurement}$$

where

$$x_1 = x + \text{error in x position}$$

$$y_1 = y + \text{error in y position}.$$

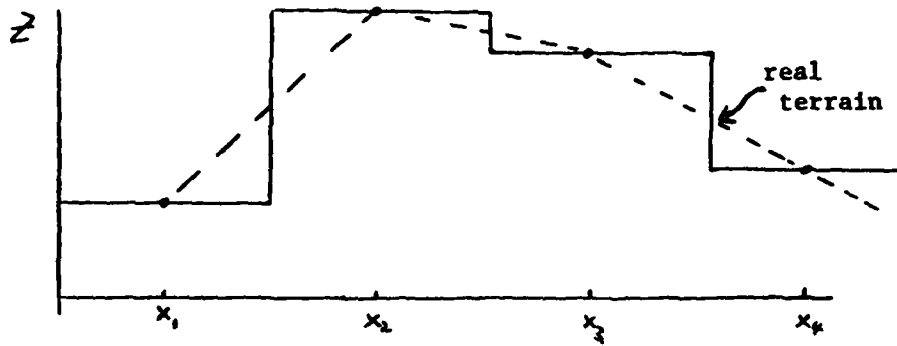
These errors are modeled as biased Gaussian distributed processes. It is likely that the errors are correlated from sample to sample. The errors are also position dependent. Therefore, we model the error processes as two-dimensional autoregressive processes with exponential correlations (as in the terrain generation model).

The procedure for generating the DLMS data, $DLMS(i,j)$, is

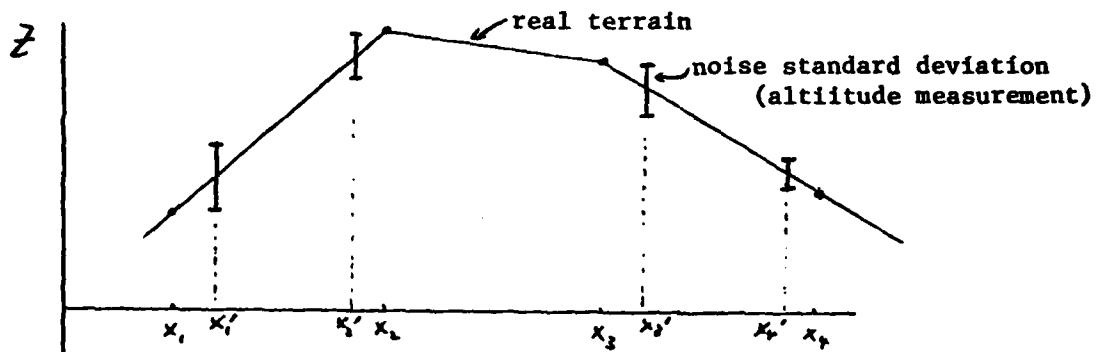
- 1) Form the two-dimensional processes $N_x(x,y)$, $N_y(x,y)$, and $N_z(x,y)$
- 2) Find $X(i,j) = i + N_x(i,j)$
 $Y(i,j) = j + N_y(i,j)$
- 3) Produce $TERRAIN(X(i,j), Y(i,j))$ by linear interpolation of the terrain map
- 4) Add $N_x(i,j)$ to $TERRAIN(X(i,j), Y(i,j))$:
 $DLMS(X(i,j), Y(i,j)) = TERRAIN(X(i,j), Y(i,j)) + N_x(i,j)$
- 5) Back interpolate DLMS points to form $DLMS(i,j)$ for each i,j .

An illustration of the procedure is given in Figure 8. For simplicity a one-dimensional illustration is used, whereas the model is done in two dimensions.

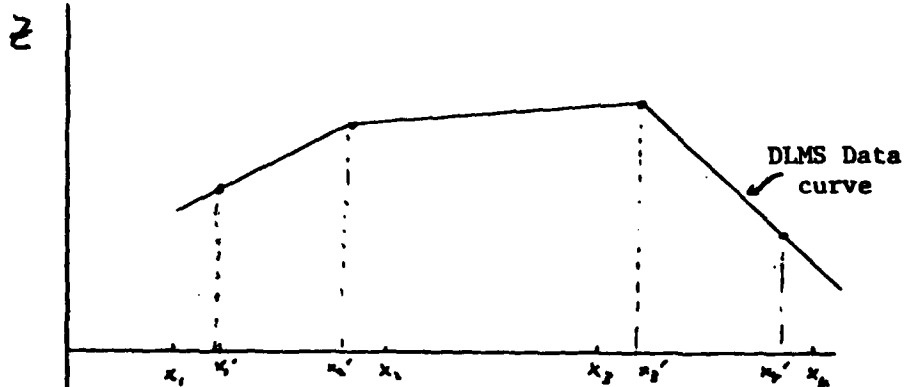
It should be noted that the combination of position errors and height errors leads to a higher standard deviation of the effective (DLMS - True) statistics that is indicated by the height error standard deviation alone. The amount added error is dependent on the slope of the terrain.



$x_1, x_2, x_3,$ and x_4 are the terrain node points



x_1', x_2', x_3' and x_4' are the perturbed node points
(i. e. expected position + noise)



The DLMS terrain is an interpolated version of the noisy altitude measurements.

Figure 8. Illustration of the DLMS Error Model

Nominal parameters for the error sources in DLMS Level 2 data are

Standard deviation (x,y) = 120 ft.

Standard deviation in height = 60ft.

C. Sensor Terrain scans and Information Gathering

The structure of each sensor terrain scan is depicted below.

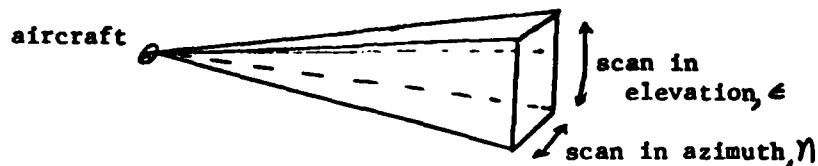


Figure 9

The sensor model takes in true aircraft position (x,y,z) and attitude (roll, pitch, heading) at time t and scans the terrain for Δt seconds starting at the stopping point of the previous scan call. At each angle increment a line of sight is propagated until a terrain point is encountered or until the range is R_{max} . The probability of detection is assumed to be 100% if $R \leq R_{max}$ and 0% if $R > R_{max}$. This assumption is reasonable due to the large cross section of the terrain.

The range and angle reported from the sensor are

$$R = R_t + \text{noise}_R$$

$$\epsilon = \epsilon_t + \text{noise}_\epsilon$$

$$\eta = \eta_t + \text{noise}_\eta$$

where the error terms are described by zero mean, Gaussian, white noise terms of standard deviations given by

$$\sigma_{nR} = \sqrt{(\text{servo noise S. D.})^2 + [(\text{receiver noise S. D.})^2 R^2]^2}$$

$$\sigma_{n\eta} = \sqrt{\left(\frac{(\text{glint noise S. D.})}{R}\right)^2 + (\text{servo noise S. D.})^2 + [(\text{receiver noise S. D.})^2 R^2]^2}$$

$$\sigma_{n\epsilon} = \text{same standard deviation as azimuth errors.}$$

The (x,y,z) position of the terrain point is then calculated by a series of coordinate transformations.

Suppose that the aircraft position is (x_p, y_p, z_p) and the attributes of a target are the triple (R, ϵ, η) (i.e. range, elevation and azimuth) of the target with respect to the aircraft. Also suppose that the attitude of the aircraft is (ψ, θ, ϕ) (i.e. heading angle w.r. to North-East, pitch angle w.r. to horizontal, and roll angle). Then the position of the target in the North, East, Down system is (see Figure 10a)

$$\begin{pmatrix} x \\ y \\ z \end{pmatrix} = \begin{pmatrix} x_p \\ y_p \\ z_p \end{pmatrix} + T_1 T_2 T_3 T_4 T_5 \begin{pmatrix} R \\ 0 \\ 0 \end{pmatrix} .$$

The T_1 through T_5 matrices are coordinate transformations as illustrated in figures 10b through 10e and listed below.

$$T_1 = \begin{pmatrix} \cos \psi & -\sin \psi & 0 \\ \sin \psi & \cos \psi & 0 \\ 0 & 0 & 1 \end{pmatrix}$$

$$T_2 = \begin{pmatrix} \cos \theta & 0 & \sin \theta \\ 0 & 1 & 0 \\ -\sin \theta & 0 & \cos \theta \end{pmatrix}$$

$$T_3 = \begin{pmatrix} 1 & 0 & 0 \\ 0 & \cos \phi & -\sin \phi \\ 0 & \sin \phi & \cos \phi \end{pmatrix}$$

$$T_4 = \begin{pmatrix} \cos \epsilon & 0 & \sin \epsilon \\ 0 & 1 & 0 \\ -\sin \epsilon & 0 & \cos \epsilon \end{pmatrix}$$

$$T_5 = \begin{pmatrix} \cos \eta & -\sin \eta & 0 \\ \sin \eta & \cos \eta & 0 \\ 0 & 0 & 1 \end{pmatrix}$$

and these matrices are orthogonal matrices $(T^{-1} = T^t)$.

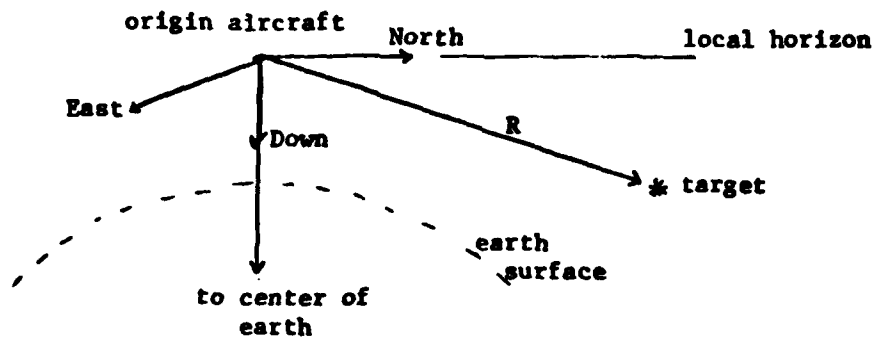


Fig. 10a Aircraft centered inertial coordinate system

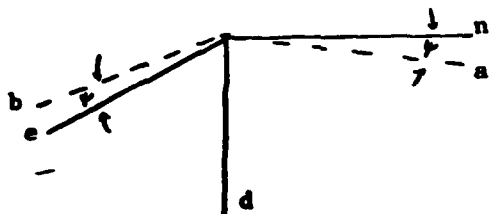


Fig. 10b Transformation through heading angle ψ

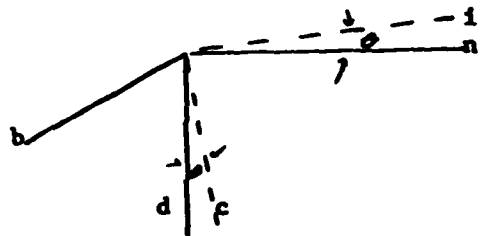


Fig. 10c Transformation through pitch angle θ

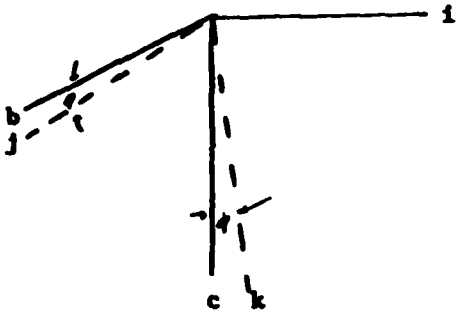


Fig. 10d Transformation through the roll angle ϕ

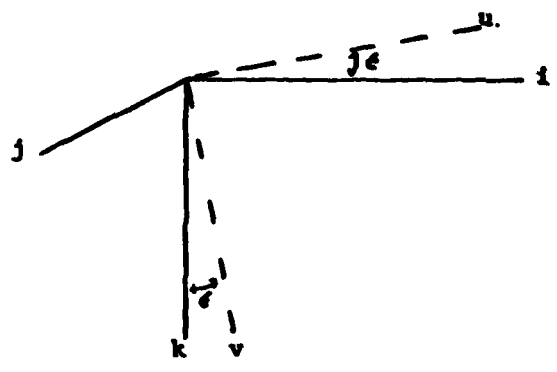


Fig. 10e Transformation through the antenna elevation angle ϵ

D. Obstacle Detection

The procedure used for obstacle detection is somewhat different from that used for terrain mapping in that the cross section of the object and the probability of detection are important factors. It is assumed that the information on obstacle properties is stored in four arrays of size NUMOBST (number of obstacles). It should be noted that the number of obstacles will be much less than the number of terrain points. The arrays are

XOBST(k) - x position of obstacle k

YOBST(k) - y position of obstacle k

ZOBST(k) - height of obstacle k above mean sea level

RCSOBST(k) - radar cross section of obstacle k

For laser or radar sensors the probability of detection depends on the sensitivity of the receiver and the signal to noise ratio (SNR) of the return signal. The SNR can be calculated (see ref. 7) according to

$$\text{SNR}_{\text{radar}} = \frac{P G^2 \lambda^2 \sigma}{(4\pi)^3 R^4 F(kT) B_n}$$

$$\text{SNR}_{\text{laser}} = \frac{P_{\text{av}} e d D^3 \eta_{\text{atm}} \eta_{\text{sys}} \eta}{.088 \lambda R^3 (hf) f_p}$$

where

P = transmitter power
 G = antenna gain
 λ = wavelength
 σ = radar cross section
 R = range
 F = noise figure
 k = Boltzman's constant
 T = temperature ($^{\circ}$ k)
 B_n = noise bandwidth

e = target reflectivity
 d = diameter of obstacle
 D = aperture diameter
 η_{sys} = system efficiency
 η_{atm} = atmospheric attenuation
 η_{ap} = aperture efficiency
 h = Plank's constant
 f = frequency
 f_p = pulse repetition frequency

The model for obstacle detection involves the following steps:

- 1) Find the line of sight from each obstacle to the aircraft
- 2) Determine if there is a terrain point obscuring the obstacle.
(that is, is there a terrain point at closer range and within the same angle, or is there a terrain point above the line of sight?)
- 3) Determine if the obstacle is within the scan limits of the sensor
(that is, find the angle from sensor to obstacle)
- 4) Determine the SNR and the probability of detection P_{det} .
- 5) Generate a uniformly distributed (0,1) random number. If this number is less than P_{det} then the obstacle is correctly detected. If this number is greater than P_{det} then it is not detected.
- 6) Simulate the errors in sensor positioning and range as in the terrain sensor scans.

E. Altimeter

A simple model for the altimeter operation was used (see Ref 7)

$$h_{altimeter} = h_{true} + noise$$

The noise is Gaussian, possibly slightly biased, with a standard deviation given by

$$\sigma = \text{MAX} \{4\text{ft}, 5\% \text{ of } h_t\} .$$

F. GPS Model

The position of the aircraft as determined by a GPS fix was modeled as

$$x_{\text{GPS}} = x_t + \text{noise}_x$$

$$y_{\text{GPS}} = y_t + \text{noise}_y$$

$$z_{\text{GPS}} = z_t + \text{noise}_z$$

where the GPS data errors are nominally (see Ref 3)

$$\sigma_x = 20 \text{ ft.}$$

$$\sigma_y = 20 \text{ ft.}$$

$$\sigma_z = 22 \text{ ft.}$$

G. Inertial Navigation System (INS) and Inertial Measurement Unit(IMU) Model

The aircraft is assumed to be navigated by an on-board inertial navigation system. In general terms this is a system that processes acceleration measurements to obtain position and velocity information. An advantage of an INS is that this system does not rely on any outside measurement or data it is completely self contained. Thus this type of system is non-radiating and is not susceptible to jamming. A disadvantage is that position and velocity information degrades with time.

Errors in inertial systems include (see Ref 16) gyro drifts, accelerometer biases and errors, misalignments, and computer roundoff. Studies indicate that x and y axes errors tend to be independent, Gaussian and zero-mean (Ref 17). The position error increases with time and is cited in reference (3) as

.5 nmi. in position (CEP) per hour
and vertical errors have standard deviation on the order of 83 ft.

If periodic updates of the INS position are performed then the position errors can be lowered since the integration time is decreased. For the purposes of the simulation three options were specified for the inertial system:

- 1) No updating during the flight
- 2) Updating every t_u seconds by a GPS fix
- 3) Updating every t_u seconds with a terrain correlation procedure.

The model chosen for the operation of the inertial navigation system is given by the following relations:

$$x_{INS} = x_t + .5 \left(\frac{6080.2}{3600} \right) \cdot T_u \cdot \cos(\text{angle}) + (\text{old fix error})$$

$$y_{INS} = y_t + .5 \left(\frac{6080.2}{3600} \right) \cdot T_u \cdot \sin(\text{angle}) + (\text{old fix error})$$

$$z_{INS} = y_t + n_z$$

where

Angle = 360° (a uniform (0,1) random variable)

$.5 \left(\frac{6080.2}{3600} \right)$ describes a drift of .5nm/hr

T_u is the update time (= t if no updating is performed)

(old fix error) is the difference between the true position and the sensed GPS (or terrain correlation) estimate at the previous update time. For GPS this error had a standard deviation of 22 ft, while for terrain correlation a value of 90 ft. is used.

n_z is a Gaussian, zero mean random variable of S. D. = 83 ft.

H. Filtering of GPS and INS Data for an Improved Position Estimate

Since a model for the aircraft dynamics can be developed it is possible to propose a Kalman filtering procedure to generate a position and attitude estimate for the aircraft. The measurement vector would consist of the GPS data and the INS data. This aspect of the problem was not studied and is only mentioned here for possible future work.

More typically the inertial system contains its own Kalman filter (based on the model of the IMU dynamics) and provides a filtered

estimate. (See reference 13 for a discussion of the modeling and implementation of such a scheme.) An advantage of this type of approach is that it is likely that the IMU can be modeled fairly accurately.

If the INS data is internally prefiltered then the resulting estimate may be statistically filtered (i. e. weighted sums) with the GPS estimate since these are two independent measurements of the same quantity. This would produce a position estimate that has lower standard deviation than either of the data sources alone, and is very easily implemented.

I. The Sensor Blending Procedure

Since terrain and obstacle information is gathered from several different sources a procedure to evaluate this data is necessary. Although it seems that it might be possible to reduce bias errors through the monitoring of the different data values, no research was performed in this area. Instead, for the purposes of the simulation a baseline conservative approach was taken. This procedure can be stated:

" Choose at each (x,y) point, the highest of all height values sensed, provided that the sensor range for each of the sensors was below some value R_{thr} for which sufficiently low standard deviation of error was expected."

J. The Flight Path Generator and the Flight Control System

The purpose of the path generator is to propose a route and a set of commands that keeps the aircraft close to the terrain, assures safety clearances, and is capable of being flown by the aircraft. The flight control system then accepts the sequence of commands and provides aerodynamic surface deflection commands. These two blocks encompass the particular TF/TA algorithm that is being evaluated. Only the data requirements and position within the computational flow were specified for these blocks.

The inputs to the path generation block include:

- 1) an augmented (best guess) map of the terrain and obstacles covering the area ahead for several segments of update.
- 2) a designated series of way points
- 3) present position, velocity, attitude and attitude rates.

K. Analysis of the Flight - Probability of Detection

A procedure similar (but inverse) to that used for obstacle detection provides a profile of the amount of time the flight was detectable by threats of given capability at specified locations. A variation of the procedure also can be used to examine detection due to the E-M radiation of the aircraft.

V. RECOMMENDATIONS

It is anticipated that the work carried out in this study will be used as a method of studying trade-offs and sensitivities inherent in the terrain avoidance problem. The simulation is designed to be flexible and all performance characteristics of sensors and subsystems are easily modified from their nominal values. Although the modeling is by no means detailed (only gross input-output effects were considered), the simulation package should be useful in providing trend and feasibility information; it cannot be used for definitive analysis, and specific conclusions will not be able to be made without resorting to a much more detailed simulation procedure than was attempted or accomplished here.

Several of the modules described in this report have been coded, tested, and implemented on the ASD CDC Cyber 74 computing system at Wright Patterson AFB. The remaining modules have been specified and flowcharted, but have not yet been implemented or tested. Documentation for the software is being prepared.

In the course of this research into the terrain following/terrain avoidance area, work was exposed that is currently underway to develop path generation algorithms for TF/TA. It appears that a "brute force" approach to this problem will prove to be unreasonable due to the tremendous amount of computation needed to specify the optimal path. In order to assure safe low level flight it will be necessary to use all the terrain information available - which produces a multi-stage dynamic optimization problem over a very large number of constraints. But, this calculation must be performed in an update time of at most one or two seconds.

The author considers the "path generation problem" and other problems

of the same general form a fertile area for future research effort. It appears that there must be a compromise from requiring the solution to a problem, to a position of obtaining a good enough solution, given the time constraints. For example, if the beginning segment of the terrain following trajectory could be found approximately, one may not care if the remaining portions were progressively further from the optimal since only the first segment would be flown.

Most optimization procedures do not exhibit the property that by truncating the optimization procedure before its conclusion the initial portion of the trajectory at that iteration is close to the initial portion of the optimum trajectory. (An example is the dynamic programming procedure wherein one can only find a segment of the optimal trajectory after the complete trajectory has been found). It is the hope of the author that in the next few months he may take a deeper look into this problem area and propose an avenue of promising research.

REFERENCES

1. Asseo, S. J. and P. J. Bronicki, "ADLAT VI Aircraft Control System Studies for Terrain Following/Terrain Avoidance", AFAL -TR-71-134, Air Force Avionics Laboratory, April 1971 (AD-517-289).
2. Bergmann, G. E. and G. L. DeBacker, "Terrain Following Criteria (Final Report). AFFDL - TR-73-135, Air Force Flight Dynamics Laboratory, Wright Patterson AFB, Ohio, June 1974
3. Wendl, M. J., "Advanced Automatic Terrain Following/Terrain Avoidance Control Concepts, Interim Review", McDonnell-Douglas Corp., GP13-0420-1, Wright Patterson AFB, May 1981
4. Wendl, M. J., "Advanced Automatic Terrain Following/Terrain Avoidance Control Concepts, Technical Proposal", McDonnell-Douglas Corp., MDC A6567, June 1980.
5. Nelson, C. R., Applied Time Series Analysis for Managerial Forecasting, Holden Day Inc., San Francisco, 1973.
6. Skolnik, M. I., Introduction to Radar Systems, McGraw Hill, NY 1980.
7. Skolnik, M. I., (Editor), Radar Handbook, McGraw Hill, 1970.
8. Wall, J. and G. Hartman, "Midterm TF/TA Briefing", Honeywell Systems and Research Center, Minneapolis, MN. Presented at the Flight Dynamics Laboratory at Wright Patterson AFB, May 1981.
9. Hovanessian, S. A., Radar Detection and Tracking Systems, Artech House, Dedham, Massachusetts, 1973.
10. Funk, J. E., "Optimal-Path Precision Terrain Following System", AIAA Guidance and Control Conference, Paper 76-1958, San Diego, Cal., August, 1976.
11. Swanson, R. S. and S. A. Musa, "Impact of Terrain Following Requirements on Cruise Missile Design (U)", Institute for Defense Analysis, Report number ADC002591 (DAHC15-73-C0200), January 1975. (SECRET)
12. Swanson, R. S. and S. A. Musa, "Terrain Statistics with Special Reference to Power Spectra (U)", Institute for Defense Analysis, Report number P-1021, May 1974. (CONFIDENTIAL)
13. Farrell, J. L., Integrated Aircraft Navigation, Academic Press, NY, 1976.
14. Oppenheim, A. V. and R. W. Schaffer, Digital Signal Processing, Prentice Hall, Englewood Cliffs, NJ, 1975.
15. Haykin, S., Communication Systems, Wiley, NY, 1978.

16. Kayton, M. and W. R. Fried (Editors), Avionics Navigation Systems, Wiley, NY. 1969.

17. Meyer, D. R. and K. E. Hodge, "Inertial Navigator Flight Testing Experience with the Lockheed F-104", AIAA Journal of Aircraft, May-June, 1964, pp. 141-147.

1981 USAF - SCEEE SUMMER FACULTY RESEARCH PROGRAM

Sponsored by the

AIR FORCE OFFICE OF SCIENTIFIC RESEARCH

Conducted by the

SOUTHEASTERN CENTER FOR ELECTRICAL ENGINEERING EDUCATION

FINAL REPORT

VOLTAMMETRIC STUDIES OF THE LITHIUM/VANADIUM OXIDE ELECTROCHEMICAL CELL

Prepared by: Dr. Dennis R. Flentge
Academic Rank: Assistant Professor
Department and University: Department of Mathematics and Science
Cedarville College
Research Location: Aero Propulsion Laboratory, Power Division,
Battery Laboratory
USAF Research Colleague: Robert Kerr
Date: September 8, 1981
Contract No: F49620-79-C-0038

VOLTAMMETRIC STUDIES OF THE LITHIUM/VANADIUM OXIDE

ELECTROCHEMICAL CELL

by

Dennis R. Flentge

ABSTRACT

The cell composed of a lithium metal anode and a vanadium oxide, V_6O_{13} , cathode has been examined using cyclic voltammetry. The cell was found to discharge in several distinct steps and showed reasonable rechargeability. The cell capacity was found to be 80 Ah/kg V_6O_{13} .

Acknowledgement

The author would like to thank the Air Force Systems Command, the Air Force Office of Scientific Research and the Southeastern Center for Electrical Engineering Education for providing him with an interesting and challenging summer in the Aero Propulsion Lab, Wright-Patterson AFB, OH. He would like to acknowledge the Battery Lab for its excellent facilities and the hospitality shown by the workers there.

He extends special thanks to John Leonard, David Stumpff and S. W. Sexton for their excellent technical assistance.

Finally, he would like to thank Robert Kerr for suggesting this particular research problem and for his collaboration and guidance, and he would like to acknowledge the helpful discussions with Dr. Joseph Maloy.

I. INTRODUCTION

One of the goals in the development of a battery is to achieve the greatest energy output from the smallest weight and volume. Lithium metal is the lightest of all metals and has the largest electrode potential of all metals ($E^{\circ} = 3.045$ volts). Primary lithium batteries have been developed which provide significantly longer useful life than the same size conventional dry cell batteries.

Development of ambient temperature secondary lithium batteries has been somewhat slower. In recent years, however, new solvents, electrolytes and electrode materials have been investigated and production of functional, safe secondary lithium batteries is an achievable goal. A solvent/electrolyte system which shows promise is 2-methyltetrahydrofuran/lithium hexafluoroarsenate (2-Me-THF/LiAsF₆).¹ Holleck, et al., have shown that 100-200 deep discharge cycles are possible in lithium/titanium disulfide cells using 2-Me-THF/LiAsF₆ as the electrolyte system.²

The lithium electrode has a tendency to interact with the solvent. This interaction is moderated by the formation of some type of passivating film on the lithium metal. Some attempts have been made to characterize the surface³ but there has been no detailed work on an electrode which has been cycled extensively. While giving the system some kinetic stability this film also acts to limit the cycling capabilities of a cell.

A useful cathode must be able to reversibly handle lithium. Solid state cathodes which undergo intercalation or topochemical reactions with lithium should adequately meet this need. Transition metal chalcogenides and oxides can be used to provide the cathodic reaction with lithium. One such material is vanadium oxide, V₆O₁₃.⁴ It has a relatively open structure and this should allow movement of lithium cations throughout the material with a minor distortion of the crystal structure.

With these facts in view we felt that a study of the cell composed of a lithium anode, a vanadium oxide cathode and 2-Me-THF/LiAsF₆ electrolyte solution would be valuable.

II. OBJECTIVES

The overall objective of this work was to examine the quality of the Li/V₆O₁₃ cell in 2-Me-THF. Specifically our objectives were:

- (1) To determine the charge and discharge characteristics of the cell.
- (2) To determine the extent of rechargeability of the cell.
- (3) To determine the overall capacity of the cell.

III. CELL PREPARATION AND CONSTRUCTION

Vanadium oxide, V₆O₁₃, was prepared according to the method of Abraham, et al.⁵ The vanadium oxide was then mixed with Shawinigan black (20 weight percent) and Teflon-P powder (10 weight percent). This mixture was pressed onto an expanded nickel grid using a hand press and was heated rapidly to 400°C under a low vacuum (P = 60 microns). The heating process allowed the Teflon-P powder to melt and it gave the electrode mechanical stability when placed into the electrolyte solution. The electrode had an area of one square centimeter per side.

The solvent, 2-methyltetrahydrofuran (2-Me-THF), was distilled under a dry nitrogen atmosphere over calcium hydride. This distilled liquid was then filtered through activated alumina. Lithium hexafluoroarsenate (LiAsF₆) was dissolved in the solvent at temperatures slightly below 0°C. Gradual warming and vigorous stirring were needed to dissolve the last portion of LiAsF₆.

The anode was prepared by pressing one square centimeter of lithium metal (15 mil thickness) into an expanded nickel grid (Exmet Corp., 5N17-4/0). This was then wrapped with a separator. Two of these electrodes were placed into each cell, one on either side of the vanadium oxide cathode.

IV. DISCHARGE CHARACTERISTICS

Figure 1 contains the discharge half cycles for a typical cell. (The charge half cycles which occurred between each of these discharges are shown in Figure 3 and will be discussed below.) The initial discharge of the cell (with voltage limits of 3.0 volts and 1.9 volts) shows three

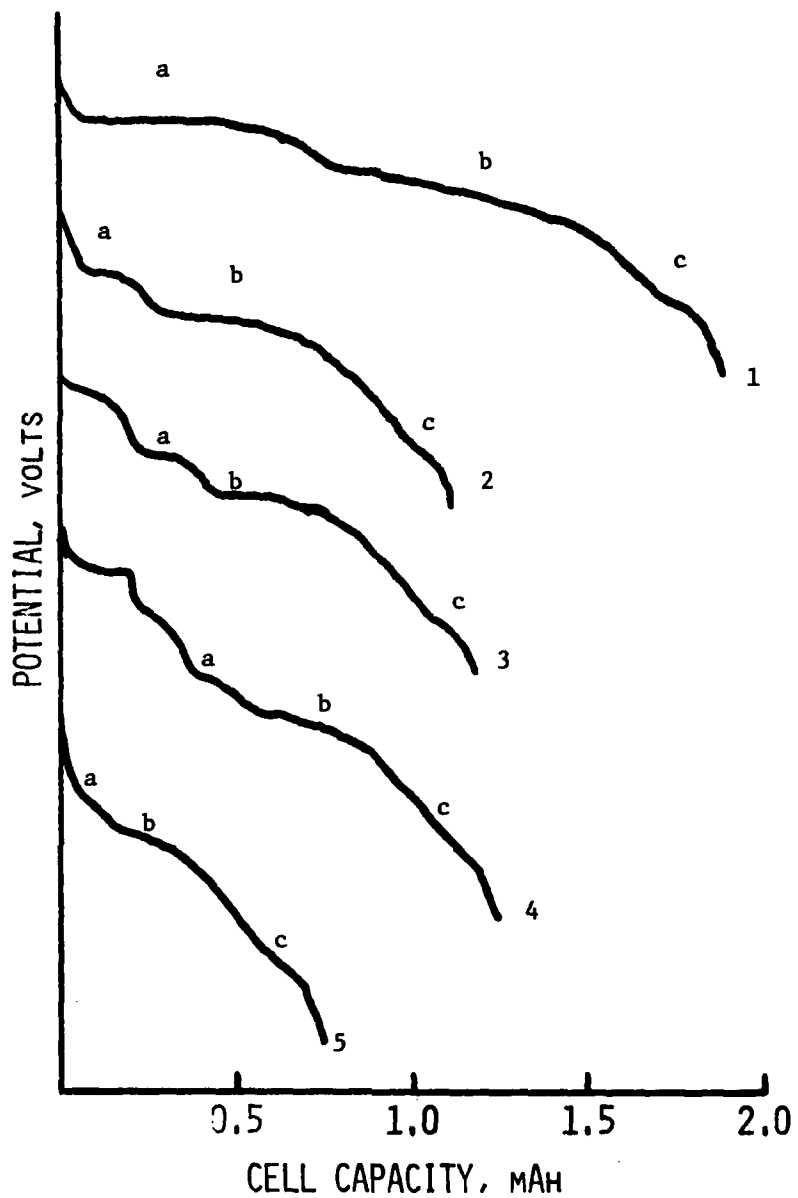


Figure 1. Discharge half cycles showing first five discharges. Current = 0.5 mA. Potential limits for each curve are 2.9 volts and 1.9 volts. Plateaus shown at (a) 2.5 v, (b) 2.3 v and (c) 2.0 v.

distinct plateaus at (a) 2.5 v, (b) 2.3 v and (c) 2.0 v. The plateau at 2.5 v is shortened significantly as the cell proceeds through successive discharge cycles. The plateau at 2.3 v decreases in length but at a slower rate than the 2.5 v plateau. The plateau at 2.0 v changes little throughout the discharge cycles.

The capacity of the cell decreased 42% after the first discharge, remained relatively constant for the next three discharges and then decreased an additional 16% (Figure 2). Instrumental difficulties prevented additional cycling of the cell.

V. CHARGE CHARACTERISTICS

The plot of potential vs. cell capacity for the charge half cycles is shown in Figure 3. Plateaus are seen in the charge curves which correspond to those found in the discharge half cycles. However, the plateaus seen in the charge half cycles do not decrease in length as rapidly as those in the discharge curves. There is also a decrease in the total energy put back into the cell as the number of cycles increases.

VI. CELL CAPACITY

The cell capacity was calculated and was found to be 2.3 mAh when the cathode contained 0.028 g of vanadium oxide. This corresponds to a cell capacity of 80 Ah/kg V_6O_{13} .

VII. CONCLUSIONS AND RECOMMENDATIONS

These studies indicate that the Li/V_6O_{13} electrochemical cell shows a good capacity under low current (0.25 mA/cm^2) discharge. Discharge occurs in several distinct steps. After a sharp initial drop-off in charge acceptance the rechargeability remains constant through several cycles. Improvement in the design of the cell should provide an increase in the number of cycles through which the cell will maintain reasonable rechargeability.

Future cycling studies should be made using varying charge and discharge currents. Variations in the composition of the cathode should be examined.

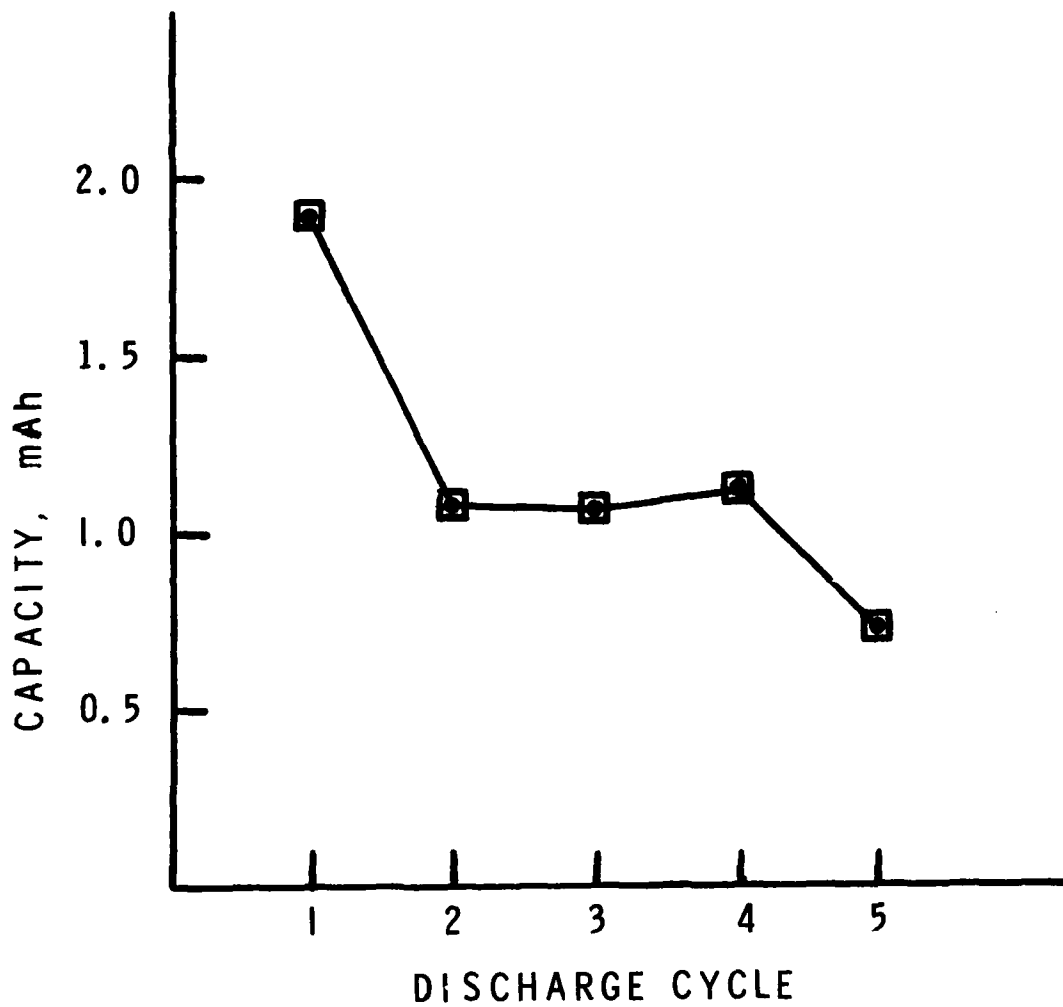


Figure 2. Capacity of the cell vs. cycle number.

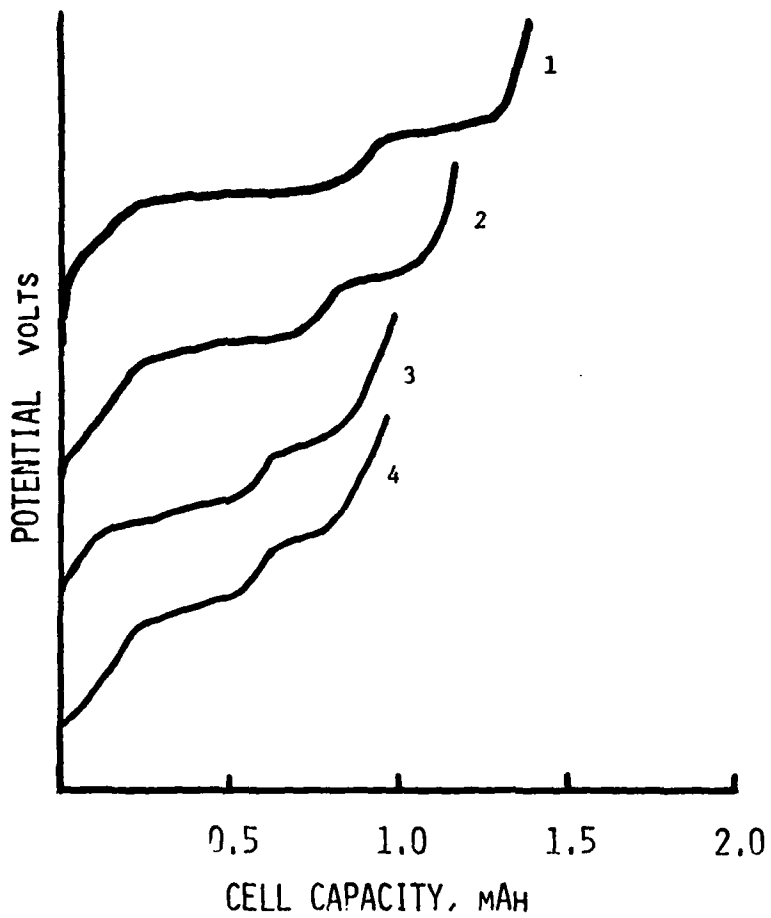


Figure 3. Charge half cycles showing first four charges. Current = 0.5 mA. Potential limits for each charge were 2.0 volts and 3.2 volts.

REFERENCES

1. (a) J. L. Goldman, R. M. Mank, J. H. Young, and V. R. Koch, "Structure and Reactivity Relationships of Methylated Tetrahydrofurans with Lithium," J. Electrochem. Soc., 127, 1461 (1980).
(b) V. R. Koch and Y. H. Young, "2-methyltetrahydrofuran/lithium hexafluoroarsenate: A Superior Electrolyte for the Secondary Lithium Electrode," Science, 204, 499 (1979).
2. G. L. Holleck, K. M. Abraham and S. B. Brummer in Proceedings of the symposium on "Power Sources for Biomedical Implantable Applications; Ambient Temperature Lithium Batteries," B. B. Owens and N. Margalit, eds., The Electrochemical Society, PV80-4, 1980.
3. S. P. S. Yen, D. Shen, R. P. Vasquez, F. J. Grunthaner and R. B. Somoano, "Chemical and Morphological Characteristics of Lithium Electrode Surfaces" J. Electrochem. Soc., 128, 1434 (1981).
4. D. W. Murphy, P. A. Christian, F. J. DiSalvo, and J. N. Carides, "Vanadium Oxide Cathode Materials for Secondary Lithium Cells," J. Electrochem. Soc., 126, 497, (1979).
5. K. M. Abraham, J. L. Goldman, M. D. Dempsey and G. L. Holleck, "Exploratory Development of an Electrically Rechargeable Lithium Battery," Final report prepared for Electronics Technology & Devices Laboratory, October, 1980.

1981 USAF-SCEEE Summer Faculty Research Program

Sponsored by the

Air Force Office of Scientific Research

Conducted by the

Southeastern Center for Electrical Engineering Education

Final Report

Project IMP: Institutionalization Methods and Policies at the
Business Research Management Center

Prepared by: Dr. Harold W. Fox

Academic Rank: Distinguished Professor in Business

Department and Department of Business
University: Ball State University

Research Location: Air Force Business Research Management Center

USAF Research Colleague: Major Robert F. Golden

Date: July 23, 1981

Contract No: F49620-79-C-0038

by:
Dr. Harold Fox

Abstract

"Project IMP: Institutionalization Methods and Policies at the Business Research Management Center" discusses opportunities for translating future research results into action. This report lays out options only. It does not offer recommendations. The principal findings from interviews and secondary sources are:

1. A focus on institutionalization would alter drastically BRMC's methods and procedures. An illustrative set of new procedures appears in the report.

2. Two major premises of such new management methods are: (a) Institutionalization becomes an integral part of every phase of a project, and (b) User involvement in all phases is imperative.

3. BRMC is at a crossroads, and a new articulation of its mission may be in order. Viewed broadly, the articulation includes a decision on the levels of organizational and financial support. The report discusses many possibilities and their ramifications with respect to BRMC's mission, management process, and organization and staffing.

4. Decision makers can select a combination of policies and methods that melds into a cohesive strategy for institutionalization. In the words of two experts on this subject, referenced in the report, "It would be reckless to suggest that there exists a technique or research style which could force or guarantee implementation success."

PROJECT IMP: INSTITUTIONALIZATION METHODS AND POLICIES
AT THE BUSINESS RESEARCH MANAGEMENT CENTER

Harold W. Fox

"How can we assure that research results are translated into action?" This question, posed by Colonel William Cheney, is the point of departure for the following confidential report to Colonel Ronald Deep. The purposes of this report are to:

1. Inform Col Deep about all my findings on this subject
2. Present a tentative draft
3. Serve as platform for extracting a briefing of the Advisory Board, a required report to SCEE, a memo to BRMC personnel, and a set of comments for the survey respondents who requested a copy.

It will be assumed that all research-related activities at BRMC are classifiable as either "A" applied or "B" basic. This paper deals only with "A"-type projects. After a brief elaboration on the nature of the subject matter, this report will discuss institutionalization methods and institutionalization policies, in turn. Methodology is in an appendix.

This report reflects (1) responses from more than 30 interviewees especially selected for their relevant experience and knowledge, (2) secondary sources on this topic, and (3) impressions that I gleaned during 5 weeks of exposure. Because of my lack of Air Force experience, I make no recommendations, but try to spell out various options.

Introduction

Gaining acceptance of something new has long plagued all human enterprise. "There is nothing more difficult to take in hand, more perilous to conduct, or more uncertain in its success, than to take the lead in the introduction of a new order of things."¹ This insight was penned 350 years ago. The situation has not changed much since. In 1981, Deputy Defense Secretary Frank C. Carlucci noted:

The acquisition process has been studied many times by many organizations. . . . However, few of the recommendations have been implemented. . . . A difficulty with implementing recommendations regarding the acquisition process is the great number of players involved to make implementation succeed. This requires persistent, intensive follow-up effort to make sure that the recommendations really do take hold. The most common reason for non-implementation is simply that relentless action on the part of top management is not taken to insure that recommendations are, indeed, implemented. . . .²

At BRMC, the common difficulty of implementation has been exacerbated by vacillating goals, uneven quality of contractor's output, and adverse perceptions of both the support for BRMC as well as BRMC's expertise. Hence institutionalization has burgeoned into major issues of methods and policies affecting DCS officers, BRMC, potential users, and contractors. But this report ignores past successes and possible mistakes or missed opportunities. It discusses options to help operational objectives materialize in the future.

Although activities on BRMC's 1977 EOQ project are indicative of success potentials, there is no single pattern that separates projects that managers use from those they ignore. "It would be reckless to suggest that there exists a technique or research style which could force or guarantee implementation success."³

It is manifest, however, that institutionalization of BRMC-managed projects will require flexibility, cooperation, tolerance, and strenuous efforts from all participants. BRMC's research officers, in particular, will have to exercise ingenuity and inoffensive persistence. The next two sections make these lofty sentiments concrete.

BRMC methods will be discussed first, followed by BRMC policies. The line between procedures and policies is admittedly arbitrary. But it seemed useful to consider first management methods that can be considered and adopted more quickly than policies and, indeed, independent of policies. The methods section delineates how BRMC could manage applied research with a focus on institutionalization.

BRMC Methods

A focus on institutionalization would alter drastically BRMC's methods and procedures. BRMC's research officers seem to be quite willing to make the necessary changes in their work. In fact, they suggested almost all of the activities enumerated on Exhibit 1 and the supporting work descriptions.

The basic concept is that institutionalization is not an afterthought following completion of research but an integral part of every phase of a project. On Exhibit 1, projects are divided into nine phases:

1. Identification of need
2. Prioritization of requests
3. Preparation of Statement of Work
4. Selection of researcher
5. Administration of the contract (research in progress)
6. Receipt of the research report
7. Implementation of findings
8. Feedback of results
9. Dissemination of facts about the project

To assure that research results will be translated into action, the DCS level, BRMC, User(s), and Contractor must contribute. Exhibit 1 gives an overview of their roles at each of the nine phases. The supporting work descriptions itemize the specifics.

This plan is flexible. Inappropriate items can be dropped. Necessary activities that were omitted should be added. An attempt has been made to compromise between excessive detail and insufficient depth. The ideal view of Exhibit 1 is as a work creed - a total commitment to institutionalization of applied research.

Although 46 of the 87 entries on Exhibit 1 devolve upon BRMC, the itemized contributions of DCS, User(s), and Contractor also are essential. In particular, the basic philosophy is User involvement in all phases.

How could such a program of implementation methods be implemented? I suggest that, after review and revision by the executive director, this program be circulated among the research officers. A meeting for the airing of comments and suggestions should follow. In some cases, approvals outside BRMC may be necessary. In due course, a new tentative version should emerge.

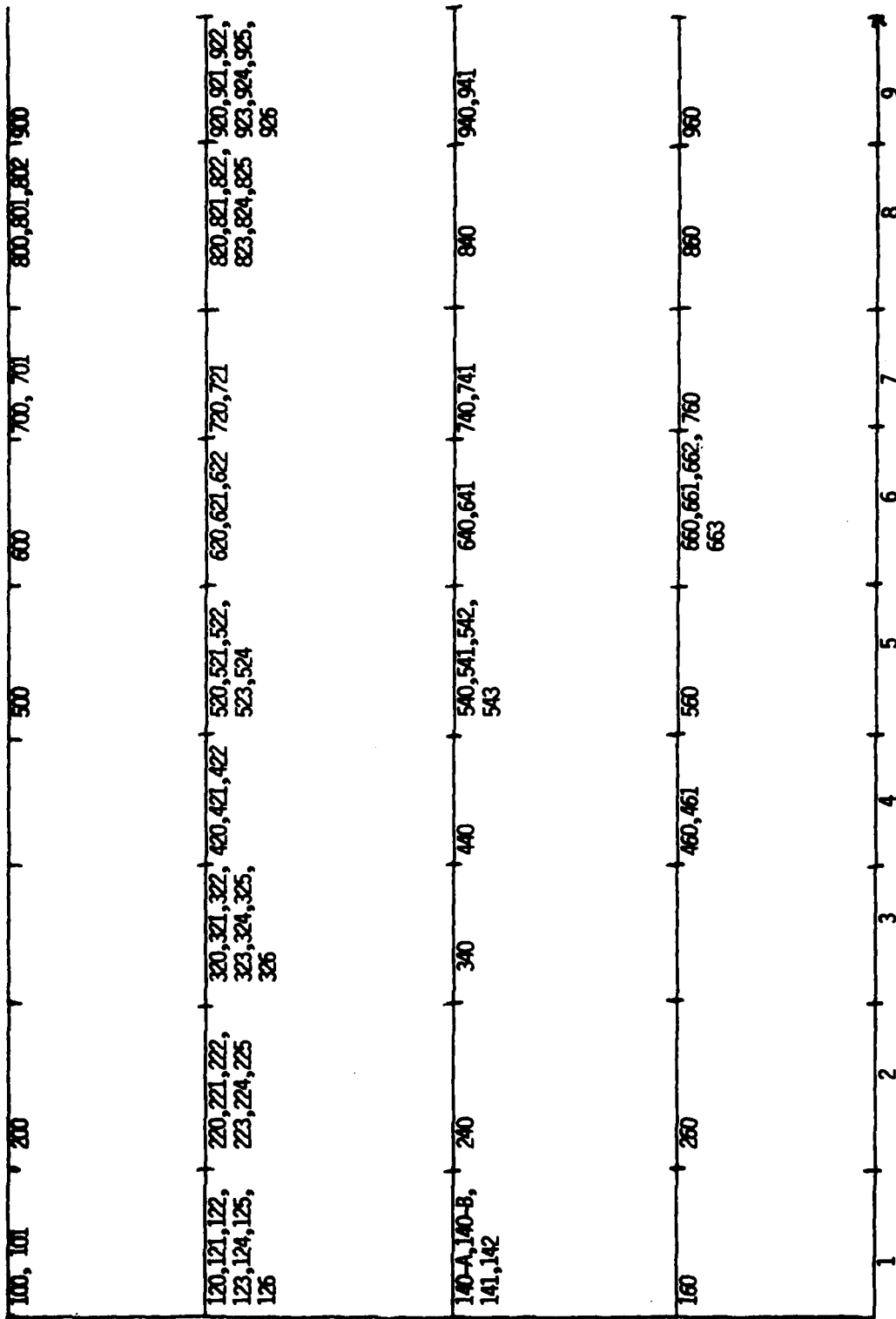
This tentative version serves as a guide and checklist on selected projects. Perhaps each research officer should control at least one project according to this tentative implementation program. The accumulated experience can later serve as input for another version that must be used on all applied research projects.

I offer for consideration a program of the type enumerated in Exhibit 1 because I believe that it could advance institutionalization of research. If so, it would also promote professional growth of the staff and enhance the image of BRMC. But, realistically, there is a limit to what BRMC can, in present circumstances, accomplish toward institutionalization. Implementation has escalated into a policy matter. Some policy matters will be discussed next.

POLICIES

The following discussion of policy options relating to institutionalization of BRMC-managed projects has two sections: DCS level and BRMC level. Both sections discuss separately the BRMC Mission, Management Process, and Organization and Staffing.

Need Ident. Prioritizing SDW Selection Administration Report Implementation Feedback Dissemination



DCS Level

BANC

User/s

Contractor

Management Phase

Exhibit 1

(1) IDENTIFICATION OF NEED

DCS Level:

- 100. Legitimizes the stated need and study objective
- 101. Designates units where results are likely to be used

BRMC

- 120. Classifies requests, proposals, etc. either "A" (applied) or "B" (basic) research. This checklist pertains only to "A" projects.
- 121. BRMC investigates stated need and with intended user(s), redefines it to reflect the "real" problem and its importance.
- 122. BRMC surveys military and civilian literature on this topic as well as ongoing studies elsewhere to find either a workable substitute for research or an adequate stopgap until research can be completed, and conveys this information to user(s).
- 123. A Gantt-type of chart helps in planning and control of all needs. Processing is streamlined. BRMC advises requester about decision dates and keeps requester informed about developments. Every six months, BRMC verifies that the need is still valid.
- 124. BRMC elicits needs directly from program managers.
- 125. Tries to position the need into a reasonable context. The scope should be comprehensive, self-contained, and traceable, not grandiose.
- 126. Looks for other units that may have same need and may be willing to share sponsorship.

Exhibit 1 (cont'd)

User(s)

140-A Requester should provide all or part of the research funds.

140-B If 140-A is not feasible, get in some other way a user's commitment to the project's success.

141 Estimate (and subsequently refine) all costs and ramifications of implementation.

142 Estimate (and subsequently refine) all costs and ramifications of implementation.

Contractor

160. Unsolicited proposal shows detailed steps of institutionalization (what, where, when, why, how)

(2) PRIORITIZING OF REQUESTS

DCS Level:

200. High likelihood of implementation is a necessary factor for a high priority.

BRMC

220. BRMC investigates and explains likelihood of implementation, including DCS support, user commitment, others affected, and regulatory barriers.

221. BRMC modularizes projects so that DCS considers only stages completable within one calendar year.

222. Verifies apparent benefits; e.g., pretest, devil's advocate session.

223. Anticipates human, technological, and structural obstacles to implementation. Develops implementation strategy, together with intended user.

224. Apprises DCS of major risks.

225. Uses the following guide for promotion of needs that are equally important, costly, etc:

Likelihood of Technical Completion	High	Freebees Only	Go-go!
	Low	Donate to other research area	Second Choice
		Low	High

Likelihood of Implementation

User(s)

240. Intended users participate in planning the implementation or other disposition of foreseeable results.

Contractor

260. Proposal shows separate quotations and payments for research and for implementation.

(3) PREPARATION OF STATEMENT OF WORK

DCS Level:

BRMC

- 320 Clear beforehand likely needs for policy changes, formally or informally, with DCS concerned
- 321 SOW specifics (a) liaison with user during the research project, (b) flexibility in methods subject to BRMC approval, (c) course of implementation
- 322 Focus on prospective operating benefits, not on research report
- 323 Certify that serviceable information is not available
- 324 Divide payments into (a) acceptance of report and (b) completion of implementation. Part (b) might be results-based; e.g., cost plus incentive
- 325 Project design must aim for turn-key results
- 326 The study should get involvement of the people who will actually do the job of implementing and operating the new system

User(s)

- 340 Intended user(s) must participate in SOW and approve the purpose, general research approach, and implementation plan

Contractor

(4) SELECTION OF RESEARCHER

DCS Level

BRMC

420 High likelihood of implementation warrants preference for a proposer

421 Seek practical (workable) results, not theoretical breakthroughs

422 Seek flexibility to deal with unanticipated developments

User(s)

440 Intended user approves researcher selection (time limit, 2 weeks).
(Users have a choice. Irreconcilable conflicts are resolved by the
Executive Director of BRMC).

Contractor

460 Must have technical and institutional qualifications for research and
implementation.

461 Implementation plan, approved by BRMC and user(s), is essential

(5) CONTRACT ADMINISTRATION OF RESEARCH IN PROGRESS

DCS Level

500 As a last resort, DCS concerned is asked to help if some change makes implementation doubtful.

BRMC

520 Ensure liaison between BRMC, contractor, and user

521 Disseminate in a periodic newsletter: (a) project and purpose, (b) interim results, (c) invitations to potential users

522 BRMC monitors changes at user(s) or in environment that could inhibit implementation, and takes appropriate action. Examples: Get commitment from a new program manager at user, negotiate a necessary change with contractor.

523 Executive Director is responsible for smooth transition of all pending projects from any departing research manager to successor

524 Executive Director controls implementation schedule.

User(s)

540 User designates a high-level officer as project "champion" for liaison with contractor and BRMC

541 User's personnel participate in the research or the planning of implementation

542 Employ contractor-user team organization, if feasible

543 User notifies BRMC promptly of any development that casts doubt on implementation or expected benefits

Contractor

560 Emphasize consulting instead of research approach

(6) RECEIPT OF RESEARCH REPORT

DCS Level

600 Briefings are mainly a basis for refining implementation plans

BRMC

620 Briefings are mainly a basis for refining implementation plans

621 Consider as a milestone toward implementation

622 BRMC assists with testing, as necessary

User

640 Briefings are mainly a basis for refining implementation plans

641 Liaison officer starts testing or partial implementation promptly

Contractor

660 Briefings are mainly a basis for refining implementation plans

661 Focus on benefits from implementation. Relegate methodology to an appendix

662 Research results are presented in the same frame and upon the same knowledge base as the original problem definition

663 Report must be indexed for easy reference by other potential users

(7) INSTITUTIONALIZATION OF FINDINGS

DCS Level

700 Actively supports implementation, if results warrant

701 Requires explanation from intended user(s) why implementation would not be beneficial

BRMC

720 Helps with implementation till pre-arranged cutoff

721 Helps refine implementation monitoring so that benefits and detriments can be quantified or otherwise communicated

User(s)

740 Liaison officer or program manager proceeds to implement results

741 Non-use requires permission from DCS concerned

Contractor

760 Proceeds to assist with implementation, including necessary supplemental research, per contract

(8) FEEDBACK OF RESULTS

DCS Level

- 800 Have an implementation audit, perhaps by AFISC/SAMI
- 801 DCS assesses whether purpose of research has been achieved
- 802 DCS commends user on benefits achieved

BRMC

- 820 Gathers implementation evidence first-hand
- 821 Administers implementation contests for contractors and users
- 822 Discusses first results with user and contractor to plan improvements
- 823 Considers necessary add-on research
- 824 Reports implementation results to DCS
- 825 Seeks uses of older reports

User(s)

- 840 Gets incentive for accomplishment of intended results. Examples: commendation, award, promotion, increase in budget

Contractor

- 860 Suggests steps to increase benefits

(9) DISSEMINATION

DCS Level

900 Informs the Congress and others of major accomplishment in its command

BRMC

920 Publishes periodical newsletter, lauding users for their accomplishments

921 Publishes articles in magazines and journals

922 Uses other tools such as seminars, briefings, etc.

923 Does not disseminate studies that misfired

924 States apparent limitations

925 Conducts a "marketing" effort toward other potential users

926 Tailors reports to level and interests of recipients

User

940 Give testimonials

941 Share experience with others

Contractor

960 Encourage contractor to publicize the benefits

DCS Level

BRMC Mission

The basic question about BRMC confronting DCS is whether the BRMC organization should continue or not. Related questions are: Could existing military research management organizations perform BRMC's mission more effectively? Is BRMC's purpose only windowdressing for nominal fulfillment of a congressional mandate?

If policymakers decide to continue BRMC and increase the likelihood of use of its managed projects, new policies merit consideration, along with the institutionalization procedures itemized above. Of course, BRMC cannot institutionalize anything. At best it can assist management.⁴ Moreover, high-level support for implementation is essential.

In any organization the top echelon circumscribes a unit's efficacy. Suppose general management gives directions about a unit's mission that are not entirely clear to the unit's incumbents as well as to the executives with whom they interact. Further, suppose general management assigns personnel that lack requisite qualifications. Surely, such actions would set off a cycle as if the unit were programmed to fail. Unqualified personnel with ambiguous direction, although doing the best they can, do not satisfy top management. As a consequence, promotions and other rewards are withheld. Careers are aborted. Morale sags. Qualified candidates avoid assignment to such a unit. Interacting officers disdain it. They do not provide essential data. Respect and cooperation erode. The unit's effectiveness plummets. In turn, top management cuts the unit's budget and support. And matters continually grow worse. Any unit, including BRMC, always faces the danger of such a self-accelerating downward cycle.

BRMC's mission needs new articulation and support, in operating terms, for the direction of incumbents and helpful guidance of pertinent outsiders. The 1980s will experience a substantial rise in Air Force acquisition expenditures. Astute defense management directly helps improve America's preparedness and economy. A new operating platform could launch BRMC's contributions under these new conditions.

BRMC should understand the desired mix of long-term and short-term projects as well as their respective criteria of effectiveness. Second, target segments of intended users should be identified. Some program managers are most likely to implement research results. Some programs need more help than others. Third, prioritization of subject matter will need periodic review. Perhaps BRMC should explicitly specialize in a few areas of top priority, instead of encouraging outsiders to expect that it covers the entire spectrum of the acquisition process. Fourth is specific direction of the desired mix of sources. Among present sources are: AFIT students, academic institutions, Beltway Bandits and other civilian contractors, and Air Force reservists. Each type of source has separate capabilities and limitations. BRMC needs to adapt itself--primarily to its intended users and secondarily to its suppliers.

At what level should BRMC be funded? Some respondents believe that BRMC should have no money to let for applied research. Potential users should defray the expense of projects in their behalf, thus giving them a strong financial stake in the usefulness--i.e., implementation--of research results.

The other extreme advocates a much larger budget than the current \$350,000. An appropriation of say, \$15 million would defray 150 manyears of professional research. The same time in-house would cost about one-half of this amount.

The present budget level limits the scope and depth of contracted research. One could ask whether many meaningful changes in operations can reasonably be expected from efforts at this low level of funding. Subdivision of the small budget into various mixes -- different commands and different time horizons -- leaves very little for the production of substance. Moreover, the requirement to return budgeted funds if contracts have not been let by a fiscal deadline can induce dysfunctional spending pressures. BRMC should spend its budget promptly on worthy projects.

Perhaps implementation of projects would be more likely if top management allowed or even promoted closer liaison between BRMC and potential users. Such a policy may require extra travel money for that purpose. It would

also require other changes that are noted throughout this report. Both the respondents and the applicable literature⁵ insist that deliberate involvement of intended users at every stage of a research process is imperative for useful results that can be implemented.

Management Process

A selection of needs at a high level tends to emphasize rational and political criteria. These are valid for research projects. Institutionalization, however, depends more on the atmosphere at users. Operating units are more apt to use results traceable to a need that they identified, research they helped to design and control, and reports in a format they helped prescribe. Hence DCS should encourage heavy contact between BRMC and program managers.

If requesters know the priority and funding criteria and if they also take sufficient time to identify and justify serious needs, BRMC will have a substantive selection base. Some users want a voice in the selection of research projects for funding. They know best, they argue, the nature of problems and whether proposed solutions are likely to be institutionalized.

A related argument for DCS' encouraging closer contact between BRMC and potential users is the fact that lower echelons are not always aggressive in exposing their problems to higher authority. Altogether, controlled delegation of user involvement at every phase from identification of needs to dissemination of results could promote commitment, pinpoint responsibility, and provide incentives for institutionalization where it is supposed to occur. DCS would, of course, continue to press subunits for implementation of useful research. Along with decentralizing user relations somewhat, DCS could also consider strengthening BRMC's organization.

Organization and Staffing

Every organizational unit needs a reasonably permanent director and staff. Perhaps a colonel for administration and liaison plus a Ph.D. civilian for research expertise could serve as executive director and deputy.

Some respondents have the impression that BRMC has not been a fast-track racecourse of opportunity for incumbents. One suggestion is to put the commanding general's protege in charge. He should be given specific directions, objectives, and support. Upon success, he should be promoted or transferred to an assignment of high potential. Career paths could also be inaugurated to increase the wanted contributions of BRMC research officers. Guidance and incentives motivate good performance. If BRMC is a vital contributor to Air Force effectiveness, DCS could make it a necessary stage in an officer's upward career path. BRMC could help earn a bigger role by adopting some of the policies that are discussed next.

BRMC Level

BRMC Mission

The advent of new leadership at BRMC is an ideal occasion to formulate and execute new policies that will foster institutionalization of projects. To raise BRMC's credibility with its outside publics, perhaps the most urgent need is a series of successes. A review of all ongoing and new projects seems to be in order. Those that can be oriented toward dramatic performance or cost results should receive continued support.

In future selections, a new BRMC policy could insist, high likelihood of implementation is a major criterion. The executive director can schedule a flow of results so that at all times some achievements will be current. Ultimately, BRMC should have a budget of scheduled performance improvements and cost savings. Budgetary control would lead into variance analyses at Phase 8 of research management, feedback of results.

Meantime, should completed work that serves solely research purposes be publicized widely? Lengthy studies whose applicability to currently pressing problems is not obvious to a reader can damage BRMC's image and discourage attention to other, more immediately relevant, reports. Perhaps a one-page summary including an applications assessment would suffice. Let interested readers ask for details.

BRMC could more actively market its services. For example, a contract officer who has been at Wright-Patterson for 20 years heard of BRMC for the first time only recently. This is not an isolated case. Along with marketing, BRMC might benefit from a structured public relations program. A systematic program would be more purposive and disciplined than sporadic briefings and publications. Its cornerstone should be an attractive monthly or quarterly newsletter. A discussion of the arcane arts of marketing and public relations had best be reserved for a separate report, if interest warrants.

The new executive director can further raise BRMC's stature by increasing the amount of liaison with decision makers in Washington. Perhaps BRMC should work on problems at high-level instead of operating units.

In any event, structural conflicts in BRMC's orientation should be resolved. BRMC reports to policymakers who typically want broad studies of durable significance, at a robust quality that precludes adverse ramifications. But BRMC's present clients, the operating units, require specific satisficing solutions to local needs. Temperamentally, regulation-bound Pentagon mores contrast with the relatively freewheeling program managers. BRMC may be buffeted from both sides, impairing its ability to press for institutionalization.

If BRMC is transferred to AFIT, sooner or later its role will change. The case for this transfer has been presented elsewhere. If implementation is a criterion, however, the issue is not clearcut. AFIT's mission of education should favor valid research methodology over practical usable results.

Other options on the most effective placement of BRMC have been suggested. For example, if BRMC's research budget remains miniscule, perhaps the unit should join Systems or Logistics, and specialize in one of these. The important point is that wherever a unit is located organizationally, guidance and support from its superior are necessary to make its management process effective.

Management Process

In mid-1981 BRMC is monitoring 39 projects, of which 21 are funded. The present total is down almost 50% from the level of several years ago.

The new executive director and his staff may wish to review BRMC's policies on acquisition research management. Perhaps formal implementation plans should be part of every "A" (applied type) of project. The implementation plan could specify: (1) User's name and location, (2) Command level, (3) Expected benefits, (4) Likely impact, (5) Method of implementation, (6) Time schedule, (7) Resources for implementation, (8) Justification, (9) Responsibilities, (10) Project milestones (in terms of performance), (11) Feedback, and (12) Measurement criteria.

BRMC should not initiate "A" type of studies unless a committed user or sponsor has been found. Instead, acting as implementation catalyst, BRMC should nurture a climate of acceptance at the intended user. This includes preclearance with all affected jurisdictions. At the user itself, the commitment to implementation must be verified on several levels: technical, psychological, organizational, financial, and temporal. Users must be willing to overcome setbacks and resistance to change.

One practice that requires a new policy because of new regulations is sole sourcing. The requirement of competition can be dysfunctional if used merely to buy at the cheapest quotation. But competition could lead to more usable results if the efficacy of implementation is central to the competitive contest.

Sole sourcing harbors the danger that a coterie of small firms will provide a full service, from generating research ideas to delivery of reports. Its attraction is reduction of management burdens. A policy of screening rivals for research quality and implementation plans as well as for cost might bring more usable output.

In particular, BRMC could require turn-key work. Each project or module should be self-contained, including drafts of necessary regulations and of an implementation strategy that has been precleared with the user.

Organization and Staffing

Major changes in a unit's mission and management lead to new policies on organization and staffing. At a minimum, the personnel has to accept the unit's new thrust psychologically and learn the requirements technically. A different set of qualifications may become necessary for future candidates.

If enough officers with acquisition-related experience are not available, BRMC could seek personnel with a high determination to master this field. In addition to interpersonal skills, a research officer should understand user operations, research technology, and business practices. Nobody is always up-to-date in all of these areas, yet an evident lack of knowledge is a quick way to lose respect and credibility. BRMC needs personnel who pursue this requisite knowledge on their own as avidly as some people follow sports, ecology, or some other outside interest. Guidance should be available from BRMC; DCS should provide incentives.

Such a self-learning program would also enhance the incumbent's ability to service inquiries through secondary data. Further, each incumbent should spend much time with different program managers, to learn their problems and suggest remedies.

Incumbents might advance to implementation specialist. The implementation specialist serves on a series of task forces, along with user and contractor personnel, making research results operational.

Conversely, perhaps field officers should serve temporarily with BRMC. Mutual understanding and rapport could deepen. Another suggestion from a respondent is to hire an expert in operations research or allied field for defining of problems in quantitative terms.

Evidently, personnel turnover has been rapid in the past. It is likely to continue. BRMC could use an orientation program for newcomers and perhaps also for reserve officers and SCEE contractors. The main orientation aid would be a current description of BRMC, its mission, personnel, budget, etc. It should fit the newcomer into the organization as a productive member. Jointly, a qualified mentor and the newcomer should develop a work plan. The mentor should provide detailed instructions.

Implementation

How can new implementation policies be implemented? The executive director and research managers should first develop a set of desired policies that are likely to receive necessary approvals. Some policies may need no or only perfunctory clearance. Gaining approval of the balance requires a strategy tailored to the approving officer and the situation.

METHODOLOGY

This report developed from a two-day orientation visit plus five weeks of full-time library research and personal interviews. Library research included selections from civilian and military retrieval services, perusal of many books, and reading of numerous speeches and special studies related to BRMC, implementation, or change agents.

A creativity session (Exhibits 2 and 3) at BRMC elicited most of the ideas in the section on Methods. Further, I talked with civilian contractors, users, and research directors, rapped with reservists, and interfaced with Air Force officers. These interviews were based on specialized schedules (Exhibits 4, 5, 6). Tabulations are not feasible. The schedules served to initiate unstructured discussions and elicit observations in confidence.

A complete list of respondents follows.

Dr. Paul Arvis, APRO
Col William Cheney, ASD/RWS
Mr. Bruce Clodfelter, ASD/TAK and staff
Col Ronald Deep, AFBRMC
Dr. Richard DeMong, Univ of Virginia
Mr. Jacques Gansler, TASC
Mr. Dick Gilbertson, ARINC
Major Robert Golden, AFBRMC
Lt Col Michael Goldstein and staff, ASD/PMF
Mr. Bob Guyton, Universal Technology

Lt Col Ed Karnasiewicz, AFCOLR
Lt Col David Krahenbuhl, ASD/YPK
Mr. John Kunsemiller, AFSC/PMC
Major Lyle Lockwood, ASD/YPM
Mrs. Linda McLaughlin, AFBRMC
Lt Joseph Peck, AFBRMC
Mr. Peter Perkowski
Mr. Don Robinson, ASD/PMH
Dr. Richard Sapp, NASA
Mr. J. Schaeffer, ASD/PM
Col Cass Schichtle, AFSC/SDX
Maj Frederick Smith, AFBRMC
Dr. Dan Strayer, NCR
Capt Michael Tankersley, AFBRMC
Dr. Tom Varley, ONR
Maj James Weber, AFBRMC
Mr. Robert Williams, APRO
Dr. George Worm, Clemson University
Mr. Fred Wynn, Advanced Technology

Everybody was very helpful. Especially appreciated is the guidance that I received from BRMC personnel. The interpretation of the findings is mine.

THE IDEA TRIGGER SESSION (c)
Creativity Exercise for New-Product Ideas

The Idea Trigger Session, developed and copyrighted by George H. Muller, is a structured process for spurring creativity. You will make an effort to generate ideas for new products.

Eight individuals of diverse backgrounds form a central panel. Three other persons act as recorders. All others participate by doing the same as the central panelists.

At the outset you panelists and other participants must interpret and accept the problem, delimitations, etc. the same way.

Upon signal from the instructor, you concentrate intensely on generating relevant ideas. Dismiss all other thoughts from your mind; don't look at your watch; just itemize in the first column of your tabulation sheet a few key words for each idea. Write down as many ideas, even if "far-out," as possible. Don't evaluate.

After 2 minutes the instructor calls a halt. Thereupon, as each panel member states an idea,

- (1) the three recorders, in turn, commit it to paper.
(Summarize on one line.)
- (2) all others cross out identical or closely similar ideas.
- (3) all try to note related or entirely new ideas in the second column of the tabulation sheet.

State ideas concisely. Each panelist announces only the remaining ideas from his or her first column. Do NOT repeat what somebody else said, even though the same thought was original with you.

Second and third excursions, as time permits, repeat the foregoing procedure. During the second ideation period, add to the second column as many previously not-mentioned ideas as possible. The ideas will be announced and recorded, and they will trigger new thoughts in others. Then write the additional ideas in the third column. This time the panelist who before was last in line will be first.

At the end of the Trigger Session (c), write the number of originals, duplicates, and totals on your tabulation sheet. These numbers will be recorded on the blackboard.

Exhibit 3

THE IDEA TRIGGER SESSION (c)

Contributor _____

Use key words only. Move swiftly from one idea to the next.

First	Second	Third

Originals _____

Duplicates _____

Totals _____

FINDINGS IMPLEMENTED

H. W. Fox

Respondent _____

1. Basic purpose: Discover a pattern that distinguishes studies which are used from studies which are not used.

2. A number of factors contribute to a decision to implement a report. I'm asking for your comments on this partial list and also for additional factors.

a. Credibility of promised benefits

b. Apparent need in your unit

c. Validity of research methods

d. Timeliness

e. Contact between researcher and user; specific adaptations for user's needs

f. Format of report

g. Other

3. What problems have you encountered in the course of implementation?

a. Quality of research

b. Internal (in your unit)

4. How could these problems be prevented or reduced?

5. What could the BRMC do to foster the use of the research it administers?

6. What other suggestions can you offer to help get research findings implemented?

FINDINGS NOT IMPLEMENTED

H. W. Fox

Respondent _____

1. Basic purpose: Discover a pattern that distinguishes studies which are used from studies which are not applied.

2. Why was the study proposed?

3. How much time elapsed between proposal and report delivery?

4. What conditions, pertinent to this study, changed between proposal and report delivery?

5. When did the critical change first become evident?

6. Who outside the proposer's unit could have detected this critical change?

7. What are the deficiencies of the research report, in the following dimensions?

a. technical (substance)

b. timing

c. format

d. other

8. Why were the findings not implemented thus far?

9. What could the BRMC do to foster the use of the research that it administers?

10. What other suggestions can you offer to help get research findings implemented?

Exhibit 6

Policy Questions

H. W. Fox

1. Basic purpose: Discover a pattern that distinguishes BRMC-managed studies which are used operationally from studies which are not used.

2. What is your view of the function of BRMC?

3. How well does BRMC perform this function?

4. What could BRMC do to foster greater use of the research it administers?

5. Is there anything inherent in the BRMC structure that inhibits implementation?

6. What are your suggestions to strengthen the effectiveness of BRMC?

Footnotes

1. Niccolo Machiavelli, The Prince (1532), Ch. 6
2. "Defense Department's Plan for Improving the Acquisition Process," Recommendation 23, reported by the Bureau of National Affairs, Washington, D.C. (May 4, 1981), FCR 880, p. H-10.
3. Peter W. House and David W. Jones, Getting It Off The Shelf (Boulder, CO: Westview Press, n.d.), p. 259.
4. AFR 20-5, par. 2-d (29 June 1973)
5. See, for example, W. L. Wilkie and D. M. Gardner, "The Role of Marketing Research in Public Policy Decision Making," Journal of Marketing (January 1974), p. 46. Also BG (P) James W. Stansberry, "DOD Project Policy--Implementing Procurement Research Results" in Proceedings of the Sixth Annual Department of Defense Procurement Research Symposium (Fort Lee, VA: Army Procurement Research Office, 1977), p.7.

1981 USAF - SCEEE SUMMER FACULTY RESEARCH PROGRAM

Sponsored by the

AIR FORCE OFFICE OF SCIENTIFIC RESEARCH

Conducted by the

SOUTHEASTERN CENTER FOR ELECTRICAL ENGINEERING EDUCATION

FINAL REPORT

SOME PROBLEMS OF LASER VELOCIMETRY AND UNSTEADY AERODYNAMICS
OF CURRENT INTEREST TO THE F. J. SEILER RESEARCH LABORATORY

Prepared by: Dr. Peter Freymuth

Academic Rank: Professor

Department and University: Department of Aerospace Engineering Sciences
University of Colorado

Research Location: Frank J. Seiler Research Laboratory, USAF Academy,
Colorado

USAF Research Colleague: Dr. J. Retelle

Date: 24 July 1981

Contract No: F49620-79-0038

SOME PROBLEMS OF LASER VELOCIMETRY AND UNSTEADY AERODYNAMICS OF
CURRENT INTEREST TO THE F.J. SEILER RESEARCH LABORATORY

by

Peter Freymuth

ABSTRACT

The following problems of current interest have been addressed:

- a. The velocity range of the dual beam TSI anemometer has been considered.
- b. The error in velocity measurement due to noise has been considered for the dual beam TSI anemometer as well as for its proposed three-velocity five beam system.
- c. The possible retrieval of a Doppler burst from noise by means of a digital frequency analyzer has been considered.
- d. The use of plexiglass for optical windows of the laser beam system has been explored for practical purposes.
- e. Toward an investigation of the vortical development for a uniformly accelerated airfoil.

Acknowledgement

This author is grateful for the summer research support provided by the Air Force Systems Command, the Air Force Office of Scientific Research and the Southeastern Center for Electrical Engineering Education at the Frank J. Seiler Research Laboratory, USAF Academy, Colorado. The hospitality by the personnel at the Frank J. Seiler Laboratory is gratefully acknowledged. The author is glad to acknowledge the encouragement and the many discussions with Dr. John P. Retelle and Dr. David Quam who initiated the topics on which the author worked during the summer, based on their experience of the state of laser anemometry for unsteady aerodynamic research.

I. INTRODUCTION:

The importance of laser-velocimetry to the measurement of dynamic stall of moving airfoils has been recognized by workers at the F.J. Seiler Laboratory since 1977 as several reports attest to (1,2,3). A laser velocimeter system has been acquired by the Seiler Lab and is now in working condition and a considerable body of experimental data on dynamic stall behind an oscillating airfoil have been acquired. To fully realise the potential of the anemometer, it has been found of interest to consider the limits of the instrument mainly as a consequence of always present electronic noise. Considerations of effects of noise, retrieval of data from noise and improvement of the current system will form the content of this report. Since the basic laser system has been described in great detail by reports 1-3, it seems appropriate to rapidly move into specific topics. As general background information, on laser velocimetry references 4-6 may serve. The laser anemometer is extensively used in the measurement of the vortical development in unsteady flow over airfoils and for this investigation, its study has served to obtain an insight into this field of aerodynamics. Some time has been spent by this author to study the possibility of an unsteady flow experiment over an airfoil which compliments the work done at the Seiler Laboratory and which is reported in Section VII.

II. OBJECTIVES:

The objective of this work is to identify any limitations of the anemometer due to noise and to suggest ideas for improvement and other routes of data evaluation. An additional objective has been to propose an experiment which complements and augments the work done at the Seiler Laboratory in the field of unsteady aerodynamics over an airfoil.

III. VELOCITY RANGE FOR THE TSI DUAL BEAM ANEMOMETER AS USED IN THE SEILER LAB:

The focal length of the lens is 600 mm. According to the TSI poster, the fringe spacing is of order $d_f = 6.3 \text{ mm}$ (green $\lambda = 514.5 \text{ nm}$; blue $\lambda = 488 \text{ nm}$ are the wavelengths of the most prominent spectral lines).

The maximum velocity can be measured if the system is used without Bragg cell. The velocity then is:

$$V_{\max} = d_f f_{\max} \quad (1)$$

Assuming a maximum frequency of 100 MHz, which can still be processed by the counter, we get

$$V_{\max} = 6.3 \cdot 10^{-6} \text{ m} \cdot 100 \cdot 10^6 \text{ sec}^{-1} = 630 \frac{\text{m}}{\text{sec}}$$

The maximum velocity far exceeds the need and is supersonic. This result for V_{\max} assumes that no Bragg cell is used. Restrictions due to the use of a Bragg cell are discussed at the end of this section.

Let us next estimate the minimum velocity which can be measured and which is negative if a Bragg cell is used. The frequency shift of the Bragg cell is 40 MHz, but can be mixed down to $f_{\text{shift}} = 10 \text{ KHz}, 20 \text{ KHz}, 50 \text{ KHz}$, and factors of 10 up to 20 MHz. A particle at zero velocity has a "virtual velocity" as measured of $V_{\text{virtual}} = d_f f_{\text{shift}}$ such that the most negative velocity which can be measured is

$$V_{\min} = -d_f f_{\text{shift}} \quad (2)$$

Examples: $f_{\text{shift}} = (0.5 \text{ MHz}, 1 \text{ MHz}, 2 \text{ MHz})$ corresponding to
 $V_{\min} = (-3 \text{ m/sec}, -5 \text{ m/sec}, -12 \text{ m/sec})$

There exists ample flexibility in selecting a minimum velocity to be measured.

Use of a Bragg cell and downmixing combine to restrict the maximum frequency which can be measured and thus the maximum velocity.

Example: downshifting from 40 MHz to 1 MHz. This necessitates a downmix frequency of 39 MHz and creates at the minimum velocity a frequency

addition signal of $2 \times 39 = 78$ MHz which must be filtered out. The velocity corresponding to 78 MHz is still very large, however.

Example: downshift from 40 MHz to 20 MHz. This necessitates a downmix frequency of 20 MHz. A 2×20 MHz = 40 MHz filter is needed to get rid of the addition frequency corresponding to the case that the maximum velocity equals the minimum velocity, i.e.

$$V_{\max} = V_{\min} = d_f \cdot 20 \text{ MHz} = 126 \text{ m/sec.}$$

This worst case still appears very adequate for the tunnel used.

A voluntary limit on maximum velocity is usually set by an upper-band limit from a low pass filter for the purpose of minimizing noise.

Example 1: Upper band limit = 5 MHz
downshift to 1 MHz

upper limit is set by $5-1 = 4$ MHz corresponding to a velocity of 25 m/sec.

Example 2: Upper limit = 2 MHz
downshift to 1/2 MHz

leaves 1.5 MHz = 9 m/sec for maximum velocity.

As a reference: the wind tunnel is typically run at 12 m/sec.

IV. PERCENT ERROR IN VELOCITY CAUSED BY NOISE AND FOR A UNIFORM FLOW.

We consider the velocity to be derived from a single Doppler burst. The number of zero crossings taken into account is N and it is assumed that the maximum noise is $1/5$ of the smallest amplitude of the Doppler burst still counted (corresponding to the ratio of threshold levels of the Doppler burst counter).

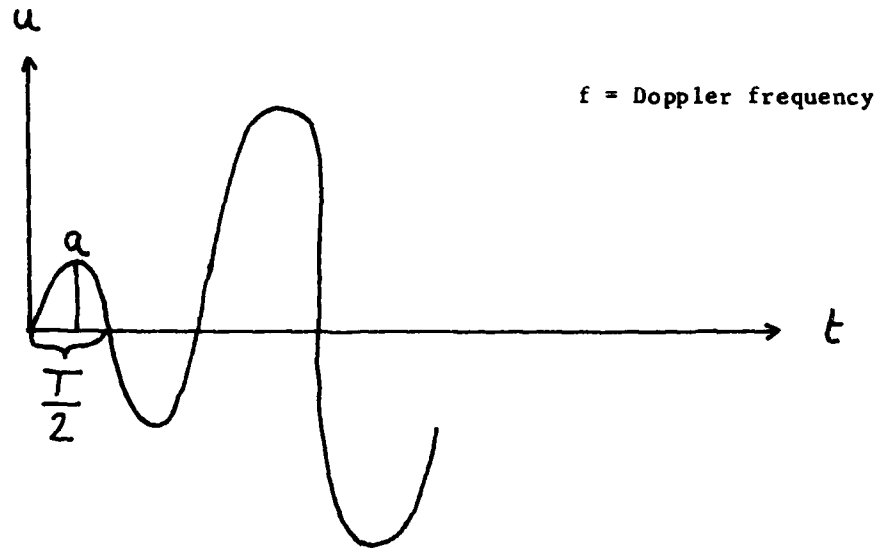


FIGURE 1. INITIAL PART OF A COUNTED DOPPLER BURST

The noise then can shift the time of the initial and final zero crossing by an amount Δt which gives rise to a velocity error.

Linearised treatment: assume for the first zero crossing

$$u = a \sin \omega t \approx a 2\pi f t \quad (3)$$

for small t . If we add a noise signal $a/5$ then $u = \frac{a}{5} + a 2\pi f t = 0$ at zero crossing. This yields a

$$t = \Delta t = \pm \frac{1}{10\pi f} \quad (4)$$

The same shift occurs at the other side of the Doppler burst in the worst case such that

$$\Delta t_{\max} = \pm \frac{1}{5\pi f} \quad (5)$$

If the counter counts N zero crossings, the time that passes in between is

$$t_N = (N-1) \frac{T}{2} = (N-1) \frac{1}{2f} \quad (6)$$

AD-A113 708

SOUTHEASTERN CENTER FOR ELECTRICAL ENGINEERING EDUCAT--ETC F/6 5/1
USAF SUMMER FACULTY RESEARCH PROGRAM. 1981 RESEARCH REPORTS, VO--ETC(U)
OCT 81 W D PEELE F49620-79-C-0038

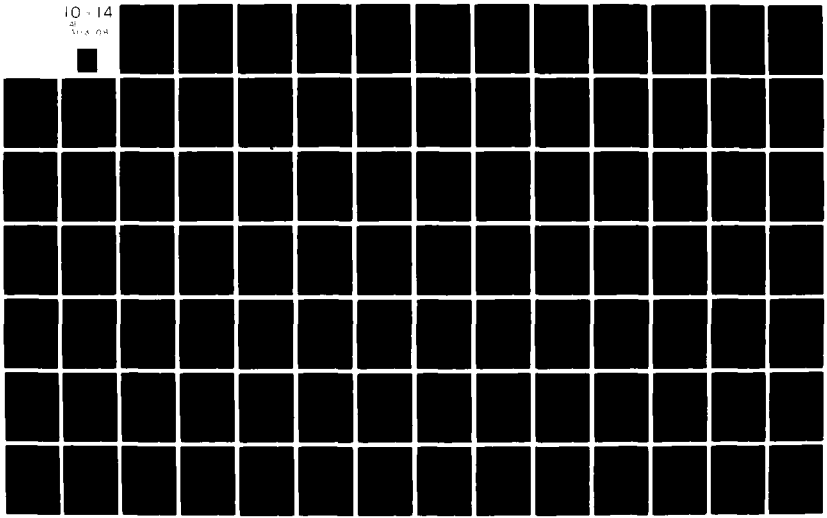
UNCLASSIFIED

AFOSR-TR-82-0227

NL

10-14

30X 04



$$\text{or } f = \frac{N-1}{2} c_N^{-1} \quad (7)$$

$$\Delta f_{\max} = -\frac{N-1}{2} \frac{\Delta c_{\max}}{c_N} = -\frac{N-1}{2} \cdot \frac{4f^2}{(N-1)^2} \cdot \left(\frac{1}{5\pi f} \right) = -\frac{2}{5\pi} \frac{f}{N-1} \quad (8)$$

$$\Delta V_{\max} = d_f \Delta f_{\max} \quad (9)$$

$$V_{\max} = \pm d_f f \frac{2}{5\pi} \frac{1}{N-1} \quad (10)$$

With Bragg shifting the velocity is

$$V = d_f (f - f_{\text{Bragg}}) \quad d_f f_{\text{Bragg}} = V_{\text{Bragg}}$$

$$\text{or } d_f f = V + V_{\text{Bragg}}$$

Therefore

$$\frac{\Delta V_{\max}}{V} = \pm \frac{2}{5\pi} \frac{1}{N-1} \cdot \frac{V + V_{\text{Bragg}}}{V} \quad (11)$$

Examples:

$$1. \quad N = 8 \quad V \gg V_{\text{Bragg}}$$

$$\frac{\Delta V_{\max}}{V} = \pm \frac{2}{5\pi} \frac{1}{7} = \pm 1.8\%$$

2. $V \rightarrow 0$ a very high relative error is incurred and it is best to consider the absolute error $\Delta V_{\max} = \pm \frac{2}{5\pi} \frac{1}{N-1} V_{\text{Bragg}}$.

$$3. \quad \text{at } V = V_{\text{Bragg}} \quad N = 8 \quad \frac{\Delta V_{\max}}{V} = \pm 3.6\%$$

4. for $V \rightarrow -V_{\text{Bragg}}$ the relative velocity error becomes very small.

It should be mentioned at this point that if measurements can be repeated many times and then averaged, the probable error becomes very small, i.e. $\sim \frac{1}{M}$ where M is the number of repeats of the measurements. (See 7, p.11).

Relative velocity error due to additional zero crossings caused by noise.

Noise is capable of reversing the slope near a zero crossing if

$$\frac{d \text{ noise}}{dt} > \frac{d \text{ signal}}{dt} \quad (12)$$

or for the highest amplitude of noise $a/5$ we consider

$$a/5 f \text{ noise} > a f$$

$$f \text{ noise} > 5 f \quad (13)$$

For lower frequencies (small velocity) this appears to limit the dynamic range of the anemometer. However, using a threshold detector before counting can eliminate this menace since the noise signal has a low level compared to the Doppler signal.

Error estimation for the proposed 5 beam TSI system.

Only the velocity component in direction of the optical axis needs special consideration which is extracted from a 3-beam arrangement.

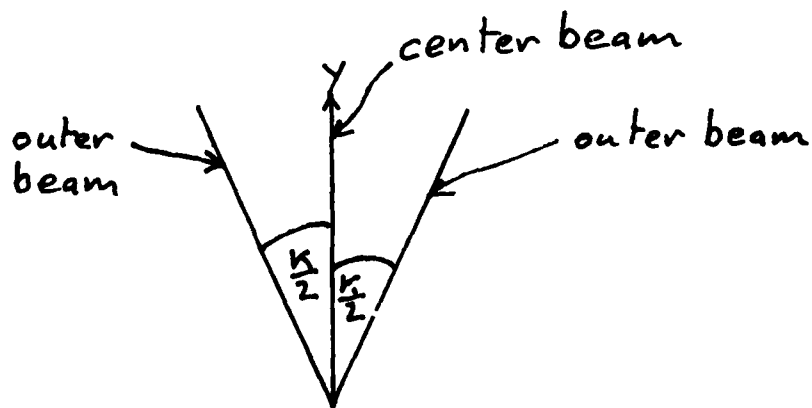


FIGURE 2. ORIENTATION OF THE THREE BEAMS

The center beam forms two fringe systems with the 2 outer beams from which velocities u_1 and u_2 can be measured. These allow the extraction of the velocity component in the optical axis direction y as follows.

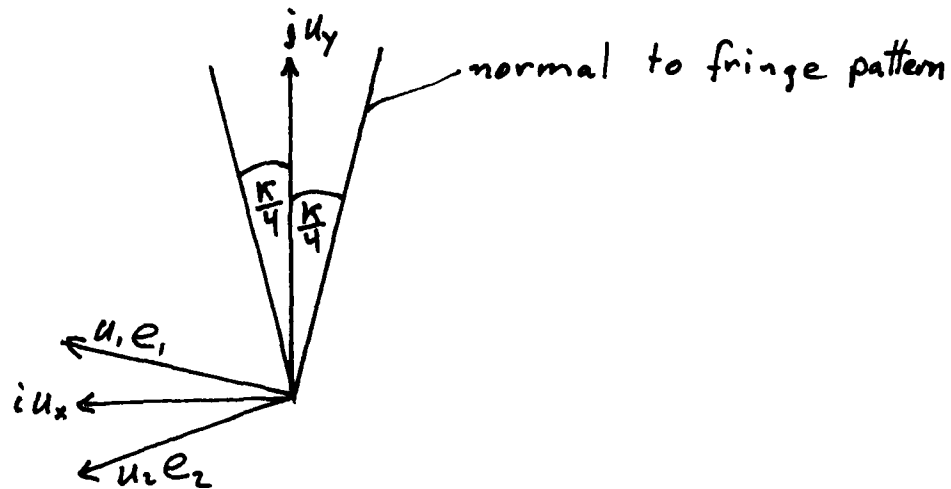


FIGURE 3. ORIENTATION OF UNIT VECTORS i, j, e_1 AND e_2

$$\vec{u} = i u_x + j u_y$$

$$u_1 = e_1 \vec{u} \quad u_2 = e_2 \vec{u}$$

$$u_1 = (e_1 i) u_x + (e_1 j) u_y = \left(\cos \frac{k}{4}\right) u_x + \left(\sin \frac{k}{4}\right) u_y$$

$$u_2 = (e_2 i) u_x + (e_2 j) u_y = \left(\cos \frac{k}{4}\right) u_x - \left(\sin \frac{k}{4}\right) u_y$$

$$u_1 + u_2 = u_x 2 \cos \frac{k}{4} \quad u_1 - u_2 = 2 \sin \frac{k}{4} u_y$$

$$u_x = \frac{u_1 + u_2}{2 \cos \frac{k}{4}} \approx \frac{u_1 + u_2}{2}$$

$$u_y = \frac{u_1 - u_2}{2 \sin \frac{k}{4}} = \frac{u_1 - u_2}{k/2}$$

(14)

The conclusion is that if u_y is of the same order as u_x then the difference in the velocity components $u_1 - u_2$ is very small, i.e. of order $\frac{k}{2} u_x$.

Thus, the relative error is amplified by a factor $\frac{2}{\kappa}$ (and by another factor 2 in the worst case if 2 photomultipliers would be employed because u_1 as well as u_2 are having a maximum error which in the worst case add up). The relative error is increased by a factor $\frac{2}{\kappa}$ relative to the usual arrangement of 2 beams with an angle κ between them if one photomultiplier is used as is proposed by TSI.

Example from the TSI proposal - center beam distance = 140 mm
focal length = 450 mm

$$\kappa \cong \tan \kappa = \frac{140}{450} = 0.3111$$

The error amplification factor thus is:

$$\frac{2}{\kappa} = 6.4$$

If the flow is essentially 2d the component u_y may be much smaller than u_x compounding the problem further.

V. DIGITAL FREQUENCY ANALYSIS OF A DOPPLER BURST IN THE PRESENCE OF NOISE - A FEASIBILITY STUDY.

A. INTRODUCTION:

If a Doppler burst from a laser Doppler anemometer is getting "buried" in electronic noise such that normal counting techniques become unfeasible, there exist still the possibility of retrieving the signal by means of frequency analysis and, in particular, on a digital basis. The quantity which needs to be determined is the Doppler frequency. In a Fourier analysis of a Doppler burst, the Doppler frequency will stand out of the noise if the noise energy and the energy within the Doppler burst are comparable. Digital frequency analysis which allows use of the fast Fourier transform is feasible with proper data handling techniques. In what follows, a Doppler burst will be analyzed followed by recommendations for digital analysis and followed by conclusions.

B. FOURIER TRANSFORM OF THE DOPPLER BURST AND COMPARISON TO NOISE.

When a particle passes thru the test volume, its brightness can be represented as follows:

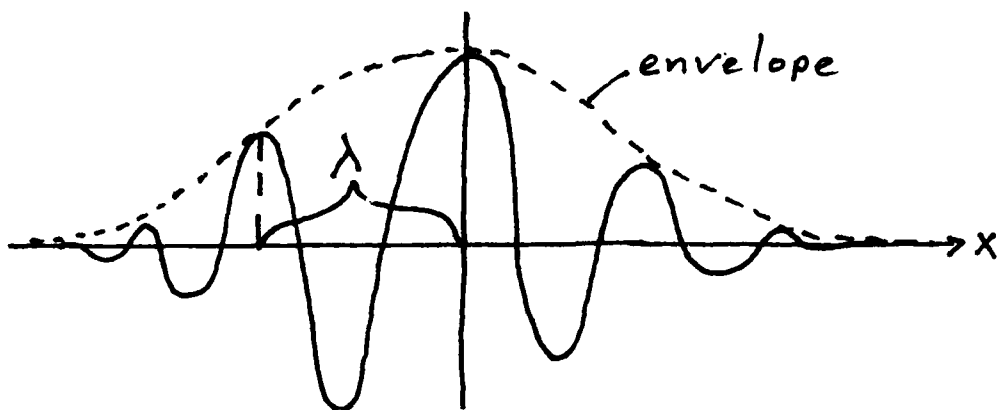


FIGURE 4. SKETCH OF DOPPLER BURST WITH PEDESTAL REMOVAL where the envelope has the form $e^{-(x/b)^2}$ and the fluctuations are of the form $\cos(2\pi x/\lambda)$ such that the Doppler burst normalized to a value 1 at $x=0$ has the form

$e^{-(x/b)^2} \cos(2\pi x/\lambda)$. The probe length d_m is $d_m = 2\sqrt{2}b$. According to reference 8, p.386, the Fourier transform of

$$f(x) = e^{-\pi x^2} \quad \text{is} \quad F(s) = e^{-\pi s^2}$$

According to the similiarity theorem, Reference 8, p.101, for

$$f(x) = e^{-\pi \left(\frac{x}{\sqrt{\pi}b}\right)^2} = e^{-(x/b)^2} \quad \text{we have}$$

$$F(s) = \sqrt{\pi}b e^{-\pi(\sqrt{\pi}bs)^2} = \sqrt{\pi}b e^{-\pi^2 b^2 s^2}$$

According to the modulation theorem, Reference 8, p.108

$$\text{for} \quad f(x) = \cos\left(\frac{2\pi}{\lambda}x\right) e^{-(x/b)^2}$$

$$\text{we have} \quad F(s) = 1/2\sqrt{\pi}b \left[e^{-\pi^2 b^2 (s-1/\lambda)^2} + e^{-\pi^2 b^2 (s+1/\lambda)^2} \right] \quad (15)$$

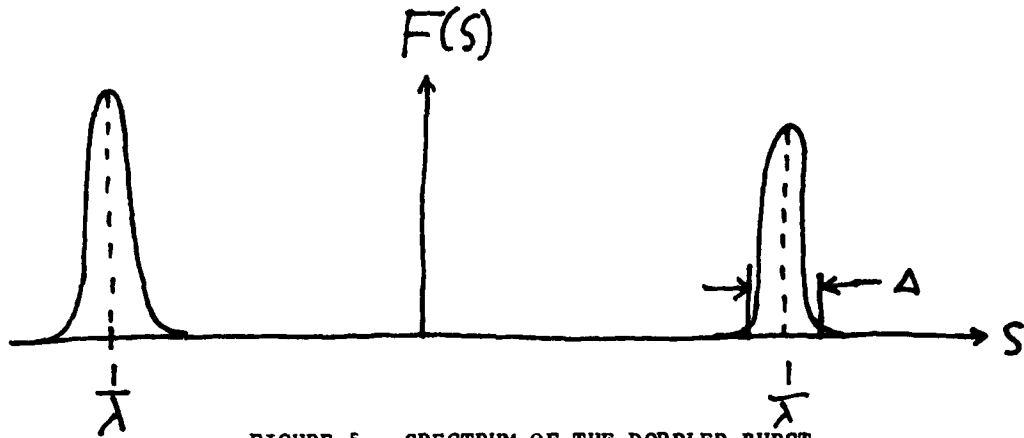


FIGURE 5. SPECTRUM OF THE DOPPLER BURST

width of the spectral spikes:

$$e^{-\pi^2 b^2 (s-1/\lambda)^2} \text{ down to } e^{-2} \text{ at } \pi^2 b^2 \left(\frac{\Delta}{2}\right)^2 = 2$$

$$\Delta = \frac{2\sqrt{2}}{\pi b} = \frac{8}{\pi} \frac{1}{d_m}$$

While the signal is concentrated in a small frequency band Δ the noise is assumed to be distributed from nearly zero frequency to several times (l times) the Doppler frequency, i.e. in a band l/λ .

If the total energy of the noise equals the energy of the Doppler burst, then the signal to noise ratio on an energy basis is:

$$\text{SNR} = \frac{l/\lambda}{\Delta} = \frac{l\pi}{8} \frac{d_m}{\lambda} = \frac{l\pi}{8} N$$

Where N = number of rings.

If the trace which is analyzed exceeds the length of the Doppler burst by a factor K , the noise energy is a factor K larger. i.e. our equation is:

$$\text{SNR} = \frac{\pi}{8} \frac{lN}{K}$$

The above result represents the SNR averaged over the length of the burst; the maximum signal is, however, larger than the average by a factor $\frac{\pi}{2\sqrt{2}}$, which can be seen as follows:

$$\int_{-\infty}^{\infty} e^{-\pi^2 b^2 g^2} dg = \overline{SN} \cdot \Delta = \overline{SN} \frac{2\sqrt{2}}{\pi b} = \frac{1}{\pi b} \int_{-\infty}^{\infty} e^{-n^2} dn = \frac{\sqrt{\pi}}{\pi b}$$

$$\overline{SN} = \frac{\sqrt{\pi}}{2\sqrt{2}}$$

maximum is

whereas the true spectral

$$e^{-\pi^2 b^2 g^2} (g=0) = 1$$

Thus, the maximum signal $SN_{\max} = \frac{2\sqrt{2}}{\sqrt{\pi}} \overline{SN}$ and thus

$$\boxed{SNR_{\max} = \frac{\pi}{2} \frac{\rho N}{K}} \quad (16)$$

Example: $N = 23, K = 1, \rho = 1.$

$$SNR_{\max} = 14.4$$

on an energy basis.

C. CONSIDERATION FOR THE DISCRETE FOURIER TRANSFORM.

For sufficient accuracy in Doppler frequency determination, we require that the Doppler frequency can be determined within 1%. This implies that the step between frequencies Δf must be $f_{\text{Doppler}}/100$. To avoid aliasing problems we require an analysis up to 10 times the Doppler frequency. This implies that we have to subdivide the total run time into 1000 steps. Furthermore, the total run time relates to the frequency step by

$$\Delta f = \frac{1}{T_{\text{run}}} = \frac{f_{\text{Doppler}}}{100}$$

$$\text{Thus, } T_{\text{run}} = \frac{100}{f_{\text{Doppler}}} = 100 T_{\text{Doppler}}$$

Assuming that the length of a Doppler burst is of order 20 times the length of the fringe spacing we find that the total run time needs to be about 5

times the length of a Doppler burst. To avoid the noise problem associated with such a long run, we take only a run of length of the Doppler burst and then add a zero signal for 4 times the length of the Doppler burst.

Basically, we have to be prepared for the longest burst (lowest velocities) and this determines our initial run time for the analysis. We then can enhance the signal to noise ratio by analyzing shorter segments of the run especially when the actual Doppler signal starts to show up allowing proper estimate of the best run time.

In the analysis, in order to not miss any burst, we have to proceed in steps of 1 or 2 fringe spacings between consecutive runs. Analysis is probably best done using the fast Fourier transform.

VI. USE OF PLEXIGLASS AS ACOUSTICAL WINDOW IN LASER VELOCITY.

The transmission of light through plexiglass is of particular interest since it would be a good material for the endplates used for the oscillating airfoil. The transmission of the laser beams through various glasses was measured with the Lexel power meter by measuring the beam power before and after the glass.

For the blue beam we obtained:

$$\text{For window glass} = \frac{112 \text{ mW}}{125 \text{ mW}}$$

$$\text{For "optical glass" window} = \frac{110 \text{ mW}}{125 \text{ mW}}$$

$$\text{For plexiglass (1/8" thick)} = \frac{115 \text{ mW}}{125 \text{ mW}}$$

For the green beam we obtained:

$$\text{Window glass} = \frac{42 \text{ mW}}{46 \text{ mW}}$$

$$\text{Optical glass} = \frac{40 \text{ mW}}{46 \text{ mW}}$$

$$\text{Plexiglass} = \frac{43 \text{ mW}}{46 \text{ mW}}$$

Plexiglass seems to be particularly suited.

Another question is how reflective plexiglass is compared to other glasses. This question could not be answered because the Lexel power meter was not sensitive enough for the reflected beam. High reflectance means an increase in noise at the photodetector of the laser velocimeter although this effect should be very weak when the plexiglass is used as end plate because of the distance from the optical system.

VII. TOWARD AN EXPERIMENTAL INVESTIGATION OF THE VORTICAL DEVELOPMENT AROUND A UNIFORMLY ACCELERATED AIRFOIL.

A. INTRODUCTION.

The aim of research at the Seiler Laboratory in the unsteady aerodynamics area is to learn as much as possible about the flow around airfoils in unsteady motion relative to the flow. Any instrumentation development is only a necessary step toward that ultimate goal. This investigator has been strongly encouraged to look beyond a study of laser velocimetry and assess possible contributions to the broader area of unsteady aerodynamics which augment, complement, and broaden the experimental work at the Seiler Laboratory as well as at the Aerospace Engineering Sciences Department at the University of Colorado. This author spent considerable time in reviewing the unsteady aerodynamics work at the Seiler Laboratory and elsewhere and subsequently has tried to come up with some ideas of how the above mentioned goal can be reached. In the following paragraphs these ideas are spelled out and, hopefully, the author will have the opportunity in the future to put these ideas into practice.

B. REVIEW OF ONGOING WORK AND IDEAS FOR COMPLEMENTING WORK.

The investigation of unsteady flow around an airfoil has been stimulated by practical experiences in helicopter aerodynamics and by the desire to gain additional lift from an airfoil prior to stall. Consequently, rather complicated but realistic configurations like airfoils with oscillating angle of attack (9, 10) and airfoils executing a prescribed flap or spoiler motion have received most attention; in particular, the latter case

is under investigation at the Seiler Laboratory and the former at the University of Colorado. An airfoil in a longitudinally oscillating flow was investigated by Retelle (11) and also showed lift augmentation. While the above experiments are relatively close to aeronautical applications, it also seems desirable to conduct experiments of lesser conceptual complexity which lend themselves to basic insight into the effects of unsteady aerodynamics. The thrust of this study is to come up with some of the kinematically and dynamically simplest configurations for the study of unsteady dynamic effects around airfoils. Such studies can serve as "reference points" for a comparison with other more complex configurations.

C. SIMPLE UNSTEADY CONFIGURATION.

There are two conceptually simple configurations this author suggests: The impulsively started airfoil and the airfoil at constant acceleration started from rest. The first configuration is difficult to achieve experimentally and will, therefore, be deemphasized, at least initially. To the knowledge of this author, the constantly accelerating airfoil has not received attention thus far and he believes that this configuration can become a "reference point" to which more complicated unsteady flow configurations can be compared to for contrast or similarity.

D. CHARACTERISTIC QUALITIES OF THE FLOW CONFIGURATION.

Aside from dimensionless characteristics like the geometrical shape of the airfoil and its angle of attack, there are the following dimensional scales which characterize the flow: the chord length c of the 2-dimensional airfoil, the airfoil acceleration and the kinematic viscosity of the fluid surrounding the airfoil. From the given dimensional quantities, $c, a,$ and ν characteristic scales of velocity and time can be derived. i.e. inviscid scales of velocity and time $V_0 = \sqrt{ac}$ and $T_0 = \sqrt{\frac{c}{a}}$. A

Reynolds number can be defined as

$$Re = \frac{V_0 c}{\nu} = \frac{a^{1/2} c^{3/2}}{\nu}$$

It is hoped that most features of the flow are in essence Reynolds number independent for large Reynolds numbers, i.e. the development of lift

buildup and decay for large angles of attack, for instance. Estimation of achieving a Reynolds number of 10^4 with a chord length of 1 ft =

$$Re = 10^4 = \frac{a^{1/2} \cdot 1 \text{ ft}^{3/2}}{160 \cdot 10^{-6} \text{ ft}^2 / \text{sec}}$$

Thus, $a = 2.6 \text{ ft/sec}^2$, representing 8% of the acceleration of gravity. The speed reached after 5 sec is $V = at = 13 \text{ ft/sec}$ and the distance covered is $s = \frac{a}{2} t^2 = 32 \text{ ft}$ which is envisioned as towing length for the accelerating airfoil. The towing force will be provided by a weight being lowered from a roller by means of gravity.

E. FLOW PHENOMENA TO BE INVESTIGATED.

In this initial phase, it should be established that unsteady lift increase can be obtained by this experiment and whether this lift increase is reasonably independent of Reynolds number like in other experiments performed under AFOSR sponsorship. Once these questions have been answered, more detailed work should be done, in particular one should look for evidence of vortices shed from the forward upper part of the airfoil and how this relates to trailing edge vortex shedding. The study will be by pressure measurement at the airfoil surface and by flow visualization using "smoke tubes" (supplied by Auergerellschaft, GMBH, Germany) towed with the airfoil and using high speed photography. Since the equipment is in essence available, it is hoped that this can be accomplished within the time period of a minigrant.

F. FACILITIES.

At the University of Colorado, Department of Aerospace Engineering Sciences, a long hall (100 ft) is available for the towing experiment. A machinist and an electronic technician can help with the design. A more detailed analysis will be offered within the framework of a minigrant proposal.

VIII. CONCLUSIONS AND RECOMMENDATIONS.

The present laser velocimeter has the operating range which is needed for the intended experiments. Use of plexiglass for airfoil endplates may be helpful in the design of the experiment. Problems with noise can basically be overcome by means of a frequency analyzer, but the realization of such a system needs much design work. This author proposes an unsteady flow experiment which can be a valuable supplement to other unsteady flow experiments under AFOSR sponsorship.

REFERENCES

1. G.W. Sparks and M.S. Francis, "A Laser Doppler Velocimeter for the USAFA Subsonic and Insonic Wind Tunnels. A Feasibility Study", Frank J. Seiler Research Laboratory Report SRL-TM-2307-77-1, October 1977.
2. R.A. Kadlec, "The Application of Laser Doppler Velocimetry to the Study of Vortex Formation and Propagation in Unsteady Separated Flows". 1978 USAF-ASEE Summer Faculty Research Program Final Report, Frank J. Seiler Research Laboratory, August 1978.
3. R.A. Kadlec, G.W. Sparks, and M.S. Francis, "The Development of a Laser Doppler Velocimetry System for Unsteady Separated Flow Research - Preliminary Results", Interim Report SRL-TR-78-0010, October 1978.
4. F. Durst, A. Melling, and J.H. Whitelaw, Principles and Practice of Laser Doppler Velocimetry, Academic Press, 1976.
5. R.J. Adrian and L.M. Fingerson, "Laser Anemometry Theory and Applications", TSI Incorporated, 1978.
6. W.J. Yanta, "The Use of Laser Doppler Velocimeter in Aerodynamic Facilities", AIAA 11th Aerodynamic Testing Conference, March 18-10, 1980. Paper AIAA-80-0435-CP.
7. W.H. Westphal, Physikalisches Praktikum, Vieweg and Sohn, 1955.
8. R.N. Bracewell, The Fourier Transform and its Applications, McGraw Hill, 1978.
9. McCroskey, W.J., 1977, "Some Current Research in Unsteady Fluid Dynamics", J. Fluids Engineering, 99, 8-38.
10. Francis, M., 1978, "Water Tunnel Measurements of Unsteady Separation", F.J. Seiler Report, SRL-TR-0011.
11. Retelle, J.P., 1978, "Unsteady Boundary Layer Flow Reversal in a Longitudinally Oscillating Flow", F.J. Seiler Report, SRL-TR-0006.

1981 USAF-SCEEE SUMMER FACULTY RESEARCH PROGRAM

Sponsored by the

AIR FORCE OFFICE OF SCIENTIFIC RESEARCH

Conducted by the

SOUTHEASTERN CENTER FOR ELECTRICAL ENGINEERING EDUCATION

FINAL REPORT

EFFECTS OF CLOTH SUBSTRATE AND
FINISH ON THE NITROGEN CURE OF
ACETYLENE TERMINATED SULFONE (ATS)
BY TORSION IMPREGNATED CLOTH
ANALYSIS (TICA)

Prepared by: Dr. Joel R. Fried

Academic Rank: Assistant Professor

Department and University: Chemical and Nuclear Engineering
University of Cincinnati

Research Location: Polymer Branch
Non-Metallic Division
Materials Laboratory
Wright-Patterson AFB, Dayton

USAF Research Colleagues: Dr. Ivan J. Goldfarb (EFP)
Dr. Charles Y-C. Lee

Date: September 15, 1981

Contract No. F49620-79-C-0038

EFFECTS OF CLOTH SUBSTRATE AND FINISH ON THE
NITROGEN CURE OF ACETYLENE TERMINATED SULFONE (ATS)
BY TORSION IMPREGNATED CLOTH ANALYSIS (TICA)

by

Joel R. Fried

ABSTRACT

Temperature scans (0-350°C) of acetylene terminated sulfone (ATS) in nitrogen were obtained by torsion impregnated cloth analysis (TICA) using a variety of standard finished and unfinished cloths including quartz, glass, and graphite fabrics. Comparison of results with those obtained by ATS/unfinished glass TICA indicate that the appearance of the highest temperature peak in the loss curve of the unfinished glass sample is not a result of an anomalous curing process but arises from degradation of a cloth impurity, probably an organic binder used in the weaving process. The degradation products are believed to act as a temporary plasticizer for the curing resin. Thermogravimetric analysis and cloth heat treatment experiments support this conclusion. Unfinished quartz has been found to be a superior substrate for TICA applications both for ATS cure studies and as a TICA matrix to study the sub- T_g and T_{ll} transitions of four high temperature engineering thermoplastics.

ACKNOWLEDGEMENTS

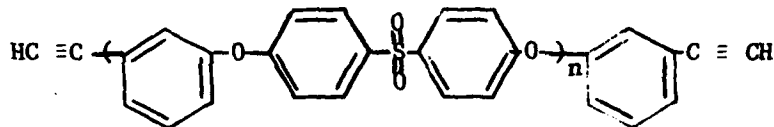
The author wishes to thank the Air Force Systems Command, the Air Force Office of Scientific Research, and the Southeastern Center for Electrical Engineering Education for the opportunity to spend an interesting and productive summer at the Materials Laboratory of Wright Patterson Air Force Base, Dayton, Ohio. Particular appreciation is extended to the Polymer Branch of the Non-Metallic Division for their hospitality and for the opportunity to extend my professional interests.

Especially, the author would like to thank Drs. Ivan J. Goldfarb and Charles Y.-C. Lee for their suggestion of this area of investigation and for their valuable guidance and helpful suggestions during the course of this research. Finally, appreciation is offered to Mr. Jack Henes, Mr. Edward J. Soloski, and Dr. Ching-Chi Kuo for their significant technical input.

I. INTRODUCTION

Torsion Impregnated Cloth Analysis or TICA is a new technique by which the dynamic mechanical properties of thermoset and thermoplastic polymers may be measured. The method, which has been described in detail elsewhere,^{1,2} uses a glass cloth impregnated with the polymer under study. Unlike torsional braid analysis (TBA),^{3,4} TICA is a forced vibrational technique by which the phase difference between torsional stress and strain can be measured while the TICA sample undergoes a time dependent (e.g. sinusoidal) strain. In addition, both loss and storage shear moduli, which correspond qualitatively to G'' and G' in traditional dynamic shear experiments, can be determined as a function of frequency and temperature.

TICA is particularly useful in the study of thermoset polymers for which the complete curing history may be documented. Recently, TICA has been applied in the study of thermal curing of a variety of acetylene terminated oligomers⁵ which are of interest to the Air Force for their potential as high temperature, moisture resistant structural resins and adhesives. Of particular interest is acetylene terminated sulfone (ATS) or 4,4'-bis(3-ethynyl-phenoxy) diphenylsulfone^{6,7}



which is currently being evaluated as a 350°F matrix resin.

TICA temperature scans (0 to 350°C) of an ATS impregnated (unfinished) glass cloth in nitrogen reveal three peaks in the loss ("b" component) curve. The lowest temperature peak (-30°C) corresponds to the glass transition of the uncured oligomer while the two high temperature peaks (210-265°C) are believed to be associated with the vitrification of the curing resin. Similar observations have been made for TICA temperature scans of an acetylene terminated quinoxaline (BA-DAB-BA).^{8,9} In these cases, the appearance of the two high temperature peaks was explained by proposing two curing reactions with different activation energies. Recent studies of BA-DAB-BA TICA have shown that the second peak is absent if a finished quartz cloth is used as a substitute for the traditional glass cloth.¹⁰ It was suggested that the finish of the quartz cloth was responsible for suppressing the higher temperature peak.

II. OBJECTIVES

A project was proposed to study the effects of different cloths and different finishes on the TICA temperature scan of the ATS cure process. The objective was to determine the reason for the absence of the second high temperature peak when finished quartz was used as a TICA substrate. Suggested substrates for this study were unfinished quartz and a variety of finished glass and graphite fabrics.

III. ATS/GLASS TICA

A series of standard TICA samples were prepared by impregnating an unfinished glass cloth with an ATS¹¹ methylene chloride solution by procedures outlined elsewhere.^{1,2} Each cloth was dried in a hood for 24 hours and further dried in vacuum at room temperature for different times to determine the effect of solvent concentrations on the loss ("b") peaks. Results are illustrated in Fig. 1 and summarized in Table I. They show that short drying times have an insignificant effect on the T_g of uncured ATS. Hood drying alone appears to give a higher T_g than additional vacuum drying for one day. The small effect may be due to absorbed water during the open air period. Nine additional days of drying in vacuum results in only a 4°C increase in T_g . By comparison, the two high temperature peaks are more affected by short drying time. The onset of the first high temperature peak decreases in temperature with increasing drying time but its peak temperature (T_1) is unaffected. Residual solvent also acts to increase slightly the peak temperature of the highest temperature peak (T_2).

TABLE I
Effects of Drying Time on the Loss Peaks of
ATS/Unfinished Glass

<u>Days*</u>	<u>Sample No.</u>	<u>RMS No.</u>	<u>T_g (°C)</u>	<u>T_1 (°C)</u>	<u>T_2 (°C)</u>
0	A012-K1	81-111	31	211	271
1	A012-K2	81-112	29	210	266
10	A012-K11	81-126	33	211	263

* days of vacuum drying

Glass cloths with four different finishes were also prepared for ATS TICA. Because these cloths were different in thickness compared to the standard unfinished glass cloth, a different TICA sample preparation was used as outlined in the Appendix. Identifications of finishes are given in Table II.

TABLE II

Hexcel* Glass Finishes

<u>Designation</u>	<u>Type</u>	<u>Chemical Structure</u>
B	primary amine	$\begin{array}{c} \text{OH} \\ \\ \text{HO-Si}-(\text{CH}_2)_3-\text{NH}_2 \\ \\ \text{OH} \end{array}$
C	methacryloxy	$\begin{array}{c} \text{OH} \\ \\ \text{HO-Si}-(\text{CH}_2)_3-\text{C} \begin{array}{l} \text{O} \\ \parallel \end{array} \text{C} \begin{array}{l} \text{CH}_3 \\ \diagup \end{array} = \text{CH}_2 \\ \\ \text{OH} \end{array}$
D	epoxy	$\begin{array}{c} \text{OH} \\ \\ \text{HO-Si}-(\text{CH}_2)_3-\text{O}-\text{CH} \begin{array}{l} \diagup \text{O} \\ \diagdown \end{array} -\text{CH}_2 \\ \\ \text{OH} \end{array}$
E	vinyl-amine	$\begin{array}{c} \text{OH} \\ \\ \text{HO-Si}-(\text{CH}_2)_3-\text{NH}-\text{C}_6\text{H}_4-\text{CH}=\text{CH}_2 \\ \\ \text{OH} \end{array}$

*Hexcel, 11711 Dublin Blvd., Dublin, Ca. 94566

Results of the effect of finish on the ATS nitrogen TICA temperature scans are illustrated by the plots of loss ("b") and storage ("a") moduli in Figs. 2 and 3, respectively. Results of loss peak assignments are given in Table III.

TABLE III

Effects of Glass Finish on the Loss Peak
Assignments of ATS TICA

<u>Finish</u>	<u>Sample No.</u>	<u>RMS No.</u>	<u>T_g (°C)</u>	<u>T₁ (°C)</u>
B	A012-H	81-114	38	212
C	A012-I	81-116	35	205
D	A012-G	81-113	33	209
E	A012-J	81-117	33	210

The principal difference between loss curves of the finished (Fig. 2) and unfinished glass TICA samples is the absence of the T₂ peak in agreement with previous observations of BA-DAB-BA TICA when finished quartz was used as the substrate.¹⁰ Finish B (amine end group) results in a slightly higher T_g of the uncured ATS and sub-cure lossiness than the other finishes. An attempt was made to determine to what extent the finish may contribute to the observed loss curve of the ATS TICA sample. Prior to ATS impregnation, the B cloth was soaked in methylene chloride for nearly five days, rinsed in methanol, and hung to dry in a hood for about one hour. The cloth was then impregnated by ATS/methylene chloride solution and dried according to previous procedures. Comparison of loss curves are shown in Fig. 4 and results are summarized in Table IV.

TABLE IV

Effect of Cloth Treatment on the Loss Peaks of
ATS/Hexcel B Glass Cloth

<u>Treatment</u>	<u>Sample No.</u>	<u>RMS No.</u>	<u>T_g (°C)</u>	<u>T₁ (°C)</u>
none	A012-H	81-114	38	212
methylene chloride/methanol	A012-L	81-118	33	205

Comparison of the washed and unwashed B TICA curves indicates a slight lowering of both the T_g (°C) of uncured ATS and the T₁ peak temperature. These observations may be attributed to either the presence of residual methanol not removed by the standard vacuum drying procedure or partial removal of the finish by methylene chloride extraction.

An additional experiment was performed to see if the finish alone could be detected by TICA of an unimpregnated B cloth. Results of two temperature scans are shown in Fig. 4. On a first heating from 0 to 100°C, the cloth showed high lossiness and evidence for a broad peak centered below 0°C and one near 75°C. The sample was quenched to -65°C and rerun to investigate the lower temperature peak; however, on second heating lossiness decreased and the peaks were diminished. This observation may be attributed to degradation of the finish; however, thermogravimetric analysis (TGA) of the unimpregnated cloth (2° min⁻¹ in helium) indicated no weight loss in the low temperature range and only a 0.27 % wt. loss up to 400°C. An alternate explanation may be offered based on redistribution of the finish along the cloth surface during heating. Further study of untreated finished glass TICA appears warranted.

IV. ATS/QUARTZ TICA

TICA samples of both finished and unfinished quartz cloths were prepared according to procedures outlined in the Appendix. Results of the effects of finish and Air or Nitrogen cure on the b and a curves of ATS TICA are illustrated in Figs. 5 and 6, respectively, while loss (b) peak positions are given in Table V.

TABLE V
Effects of Finish and Cure Atmosphere on the
Loss Peaks of ATS/Quartz TICA

<u>Finish</u>	<u>Cure</u>	<u>Sample No.</u>	<u>RMS No.</u>	<u>T_g (°C)</u>	<u>T₁ (°C)</u>	<u>T₂ (°C)</u>
none	N ₂	A012-F	81-107	40	209	none
none	air	A012-F	81-121	35	214	284
9073*	N ₂	A012-C*	81-101	33	205	none

* Astroquartz, lot no. 24001, style 581/38 (J. P. Stevens and Co., Inc., Glass Fabrics Division, Slater Plant, Slater, South Carolina)

Results of finished quartz TICA are very similar to those of finished glass. In both cases, the T₂ peak is absent. The unexpected result was that the T₂ peak was also absent for the N₂ cure of the unfinished quartz; however, a significant broad T₂ peak with a maximum at 284°C was present

when the unfinished quartz TICA sample was air cured. This latter result suggests a different curing process in air. The N₂ cure results for the unfinished quartz TICA at first suggested that the different chemical compositions of glass and quartz affected the N₂ curing process differently. One additional difference was observed in the color of the two cured TICA samples. The unfinished quartz (as well as all the finished glass) TICA samples were golden yellow after N₂ cure while that of the unfinished glass was deep brown in color. These color differences initially were thought to result from ATS degradation which did not occur when a finish or a quartz substrate was used.

V. TGA AND CLOTH TREATMENT OF UNFINISHED GLASS

To test the degradation hypothesis, TGA of five samples was performed* in an inert atmosphere (helium) and at the same heating rate (2°min⁻¹) as used in the TICA temperature scans. Total TGA weight losses for cloths heated up to 400°C are given in Table VI.

TABLE VI

TGA Weight Losses

<u>Cloth</u>	<u>Wt. Loss (%) at 400°C</u>
B Glass	0.27
ATS/B Glass	0.47
ATS/unfinished quartz	0.55
unfinished glass	2.15
ATS/unfinished glass	2.15

The unexpected result from the TGA measurements was the observation of a significant weight loss for the unfinished glass cloth whether or not it was impregnated with ATS. A comparison of TGA (ATS/glass) and TICA scans is shown in Fig. 7. Weight loss is gradual from between 50 and about 250°C. Above 250°C, significant weight loss begins at a temperature corresponding with the momentary modulus drop and loss peak associated with

* Dupont 951 TGA through the courtesy of Mr. Edward J. Soloski.

the T_2 process. These results are interpreted to indicate that the T_2 process is a result of degradation of unknown surface impurities present on the unfinished glass. As they are liberated and diffuse through the curing resin, the degradation products apparently act as temporary plasticizers which lower modulus and cause a peak in the loss curve.

The nature of the unfinished glass impurities remains unknown; however, results of additional experiments suggests one good possibility as indicated below. Effects of two different cloth preparation procedures on TICA of ATS/unfinished glass are illustrated in Fig. 8 and summarized in Table VII. Results show that washing the cloth for several days in methylene chloride and rinsing in methanol has no effect on the presence of the T_2 degradation peak. Although the T_g of the uncured ATS is unchanged, washing does lower the peak positions of both T_1 and T_2 . This may be attributed to residual methanol in the sample as a similar lowering of T_1 was observed when F-40 finished glass was washed according to the same procedure (Fig. 4) before ATS impregnation. Apparently, the fabric impurity is not soluble in common organic solvents.

TABLE VII

Effects of Cloth Treatment on the Loss Peaks of
ATS/Unfinished Quartz

<u>Treatment</u>	<u>Sample No.</u>	<u>RMS No.</u>	<u>T_g (°C)</u>	<u>T_1 (°C)</u>	<u>T_2 (°C)</u>
none	A012-K11	81-126	33	211	263
methylene chloride/ methanol	A013-F	81-120	30	195	251
vacuum 300°C	A014-E	81-125	31	210	none

The conclusive test that degradation of a cloth impurity is responsible for the T_2 peak observed during nitrogen cure is the effect of vacuum heat treatment of the unfinished glass cloth on the TICA scan. The cloth was heated to 300°C (maximum oven temperature), held at 300°C for approximately three hours, and cooled-all in vacuum. The cloth turned from white to an olive-tan color following this thermal treatment. This cloth was then impregnated with ATS/methylene chloride solution and dried according to standard procedures. Results of the N_2 TICA scan (Fig. 8 and Table VII) show an absence of the T_2 peak while the temperature assignments of the T_g and T_1 peaks remain unchanged. These observations suggest that the

impurity may be binder. When binder is partially removed by heat treatment, glass cloth is reported to have a light tan color (apparently the case when heated to 300°C); when fully removed, the resulting fabric is white.¹² Normally, commercial removal of the binder requires heating the cloth to above 350°C in a furnace. Apparently, the cloth which was believed to be fully heat cleaned and unfinished was actually untreated (greige or loom state).

VI. GRAPHITE AND OTHER CLOTHS

In addition to the finished glass and quartz fabrics, several finished graphite and glass filled graphite cloths were tried as possible TICA substrates. Comparisons of the loss (b) and storage (a) modulus curves of a variety of ATS impregnated glass, quartz, and graphite fabrics are shown in Figs. 9 and 10, respectively. Comparison of loss peak assignments is made in Table VIII.

TABLE VIII

Effect of Cloth and Finish on the Loss Peaks of
ATS TICA

<u>Cloth</u>	<u>Finish</u>	<u>Sample No.</u>	<u>RMS No.</u>	<u>T_g (°C)</u>	<u>T₁ (°C)</u>
glass	epoxy	A012-G	81-113	33	209
graphite- glass	epoxy	A012-D	81-102	37	213
graphite	phenoxy	A012-E	81-103	43	216
quartz	none	A012-F	81-107	40	209

As shown, different cloths and different finishes have insignificant effect on the temperature assignments of uncured ATS T_g and T₁. At most, temperature differences are within 10°C. The graphite fabrics used tend to give smaller and broader transitions than the quartz or finished glass samples. The ease of TICA sample preparation and the sharply defined transitions afforded by the unfinished quartz would indicate it to be an excellent choice for future TICA studies.

VII TICA OF ENGINEERING THERMOPLASTICS

TICA samples of four high temperature thermoplastics were prepared by impregnating a piece of unfinished quartz cloth (3.95" x 1.90") with a concentrated polymer solution (1.5 gms/15 ml solution) using either methylene chloride or chloroform as a solvent. Sample identifications are given below in Table IX. The samples were dried for about 1.5 hrs. in a hood and folded as shown in the Appendix. Ends were taped and the strips were placed in a vacuum oven and heated to 45°C under house vacuum for four days. The oven temperature was then raised to 112°C and full vacuum was applied for an additional seven days.

TABLE IX

Identification of Thermoplastic TICA Samples

<u>Polymer</u>	<u>Source</u>	<u>Solvent</u>
bisphenol A polysulfone (PSF)	UC* Udel ^R P-1700	methylene chloride
bisphenol A polycarbonate (PC)	Aldrich	chloroform
poly(2,6-dimethyl-1,4-phenylene oxide)	GE PPO ^R	chloroform
polyphenylsulfone	UC* Radel ^R	methylene chloride

*Union Carbide Corporation

Each TICA sample was initially heated from 0 or 20°C to about 70°C above its T_g in the RMS. It was then quenched to -150°C and reheated to near its T_{ll} . Results of TICA temperature scans at 11 Hz are shown in Figs. 11 and 12. Assignments of T_g (loss maximum) and the liquid-liquid transition (T_{ll}) are given in Table X.

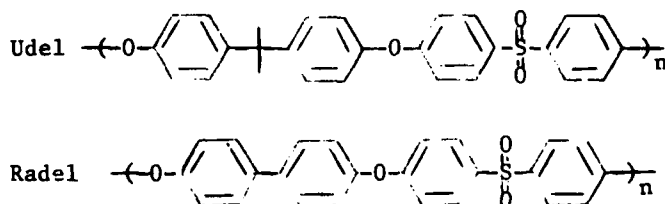
TABLE X

TICA Loss Assignments

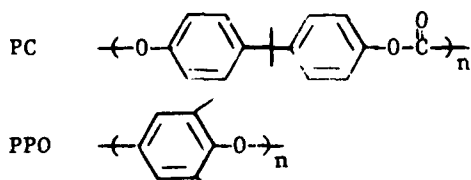
<u>Polymer</u>	<u>Sample No.</u>	<u>RMS No.</u>	<u>T_g (°C)</u>	<u>T_{ll} (°C)</u>	<u>T_{ll}/T_g (°K/°K)</u>
Radel	A014-I	81-130	232	318	1.18
Udel	A014-F	81-131	196	288	1.20
PC	A014-G	81-132	158	223	1.15
PPO	A014-H	81-133	228	302	1.15

As shown for Radel in the right side of Fig. 13, the magnitude of the modulus drop and loss peak marking the glass transition increases upon the second heating. This is a probable consequence of melt impregnation of the tight knit quartz cloth during the initial melting. T_g 's recorded after first and subsequent heatings are unchanged and there are no unassignable loss peaks that would suggest the presence of solvent retained after the drying period.

Inspection of the sub- T_g loss region indicates a γ relaxation centered near -60°C for both Udel and Radel whose related structures are shown below.



These are slightly higher than reported previously for Radel TICA^{1,2,13} and Udel Rheovibron measurements at comparable frequencies. Results for PC and PPO, whose structures are given below, indicate a weak γ



relaxation near -60°C for PC and a very broad, shallow β relaxation near 20°C and the end of a strong γ relaxation below -150°C for PPO in approximate agreement with published Rheovibron results at 11 Hz.¹⁴

Preliminary studies of the effect of different thermal histories on the sub- T_g relaxations of these polymers indicate that liquid structure frozen by quenching the TICA samples rapidly below T_g from T_{ll} may result in changes in the sub- T_g relaxations. This is most clearly shown for Radel whose low temperature TICA scan is shown in the left side of Fig. 13. In this case quenching from above T_{ll} causes a suppression of the γ relaxation

of Radel and an increase in modulus. If secondary relaxations involve limited chain movements in defect regions of the polymer, then the freezing of different liquid structures (i.e. by quenching from above T_R or above $T_{\ell\ell}$) should affect these relaxation processes (and mechanical properties such as impact strength) differently. These very tentative observations may have great significance as to the selection of processing temperatures to optimize mechanical performance. Additional experiments will be proposed in a forthcoming mini-grant proposal to verify these conclusions.

VIII RECOMMENDATIONS

The results of this ten week study suggests several areas of additional experiments:

1. O₂ Cure Experiments - oxygen temperature TICA scans of ATS/finished quartz and finished glass should be performed to compare with the unfinished quartz results. In addition, TGA of ATS/unfinished quartz, unfinished quartz, "unfinished" glass, and several isothermally cured ATS TICA samples should be run in air.
2. Additional Resins - TICA of BAD-DAB-BA on an unfinished quartz cloth (isothermal cure and N₂/air temperature scans) should be performed for comparison with the ATS results.
3. Unfinished Glass - TICA of ATS on a properly heat cleaned Hexcel glass cloth should be obtained for comparison with the finished glass and unfinished quartz TICA results and for evaluation as a future general purpose TICA substrate. Also suggested would be to request Hexcel to heat clean our standard "unfinished" glass cloth by their procedures providing their unfinished glass performs as expected.
4. Additional Cloths - ATS TICA using a Broadgoods cloth (FM 5064) used by Rockwell International.
5. Finish Effects - the sensitivity of TICA in detecting the presence of finish should be explored by performing temperature scans on the four unimpregnated Hexcel finished cloths and Stevens finished quartz cloth.
6. TGA/Mass Spectroscopy - suggested is a study of products liberated during heating of the standard "unfinished" glass to identify the degradation products and determine the nature of the impurity.

REFERENCES

1. Lee, C.Y.-C., and Goldfarb, I.J., "Torsion Impregnated Cloth Analysis (TICA)," AFWAL-TR-80-4159, WPAFB, Oh.
2. Lee, C.Y.-C., and Goldfarb, I.J., "Torsion Impregnated Cloth Analysis (TICA): A Forced Torsion Technique to Study Resins Supported by Inert Substrates," Polym. Eng. Sci., Vol. 21, pp.390-397, 1981.
3. Gillham, J.K., and Schwenker, R.F., Jr., "Thermomechanical and Thermal Analysis of Fiber-Forming Polymers," Appl. Polym. Symp., Vol. 2, pp.59-75, 1966.
4. Gillham, J.K., "Characterization of Thermosetting Materials by Torsional Braid Analysis," Polym. Eng. Sci., Vol. 16, pp.353-356, 1976.
5. Hergenrother, P.M., "Acetylene-Containing Precursor Polymers," J Macromol. Sci., Rev. Macromol. Chem., Vol. 19, pp.1-34, 1980.
6. Loughran, G.A., and Arnold, F.E., "Synthesis and Properties of Acetylene Terminated Sulfone (ATS)," AFWAL-TR-80-4011, WPAFB, Oh.
7. Loughran, G.A., and Arnold, F.E., "Synthesis and Properties of an Acetylene Containing Aryl-Sulfone Resin," Polym. Prepr., Am. Chem. Soc., Div. Polym. Chem., Vol. 21, pp.199=200, 1980.
8. Lee, C.Y.-C., and Henes, J.D., "Effects of Air/Nitrogen Cure on an Acetylene Terminated Quinoxaline Thermoset System," AFWAL-TR-81-4012, WPAFB, Oh.
9. Lee, C.Y.-C., "Dynamic Mechanical Properties of an Acetylene Terminated Quinoxaline System under Air/Nitrogen Cure," submitted to J. Appl. Polym. Sci.
10. Kuo, Ching-Chi, private communication.
11. ATS prepared by Gulf Chemical Co. (Lot No. C-001).
12. J. P. Stevens technical brochure, "Industrial Glass Fabrics".
13. Lee, C.Y.-C., "Dynamic Mechanical Measurement of Polyphenylsulfone (Radel)," AFWAL-TR-79-4062, WPAFB, Oh.
14. Fried, J.R., Kalkanoglu, H., and Yuan, J.-Y., "Heterogeneous Polymer Blends of Poly(2,6-dimethyl-1,4-phenylene oxide): I. DSC, Density, and Dynamic Mechanical Studies". Polym. Eng. Sci. (submitted).

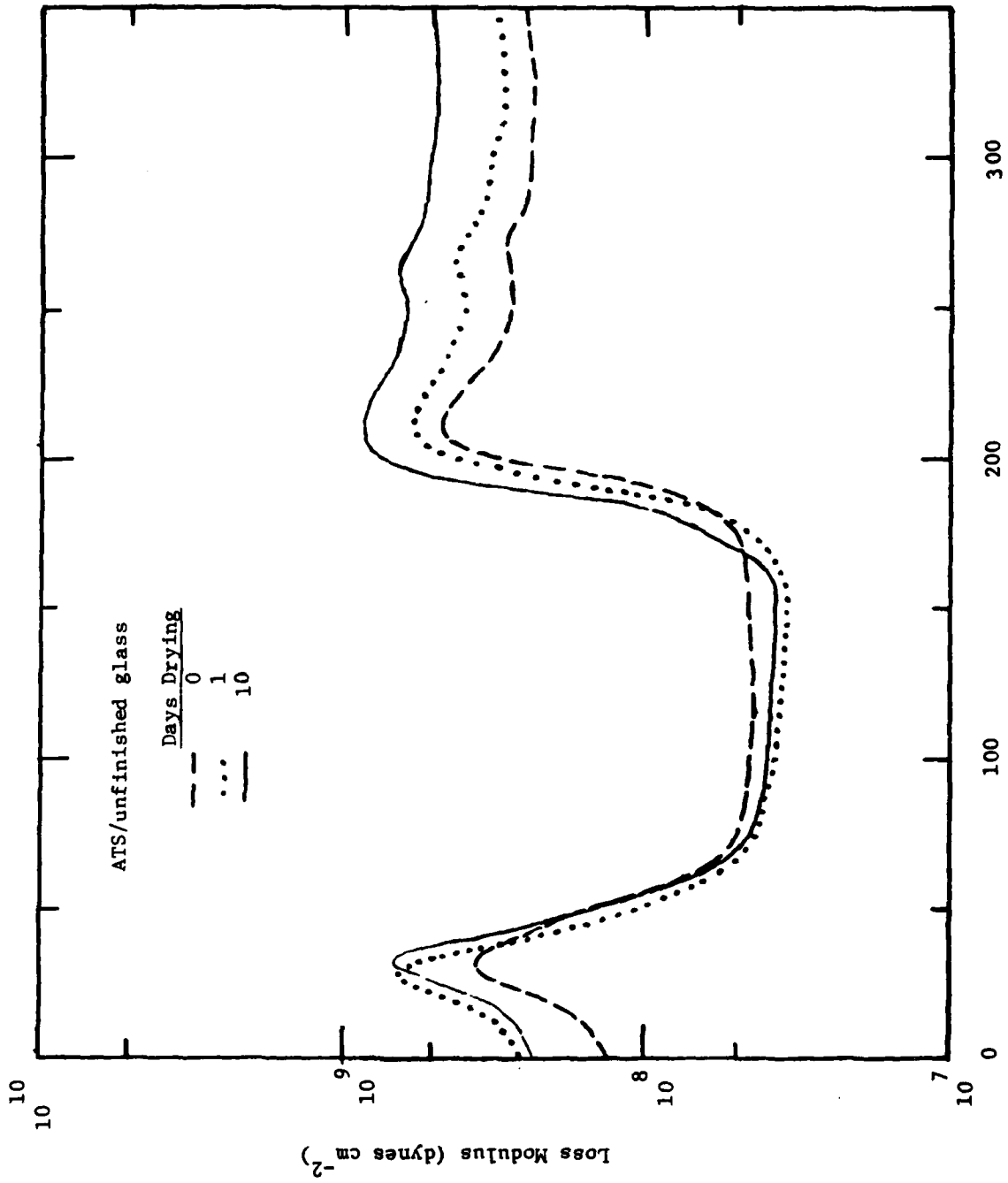


FIGURE 1.

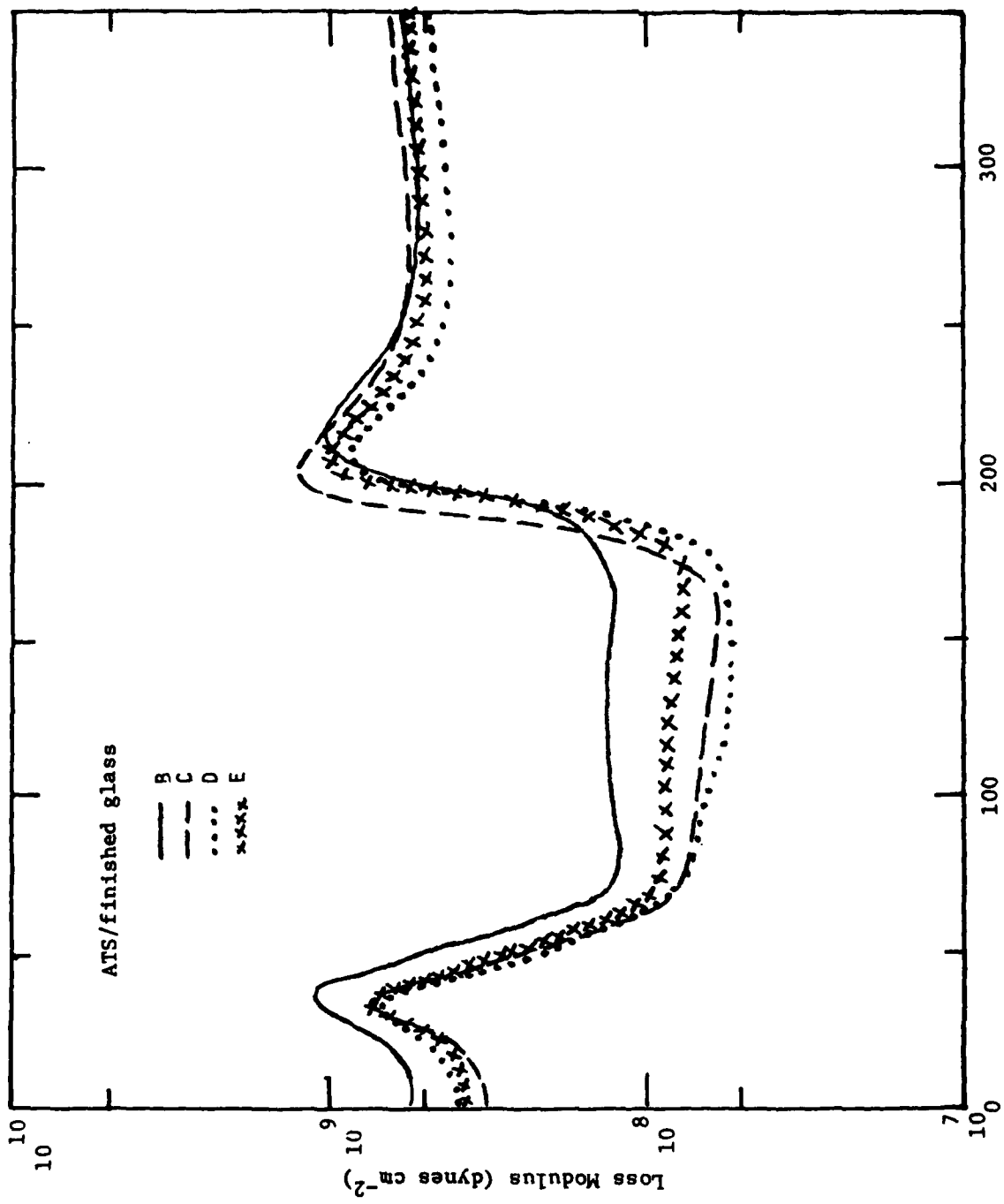


FIGURE 2.

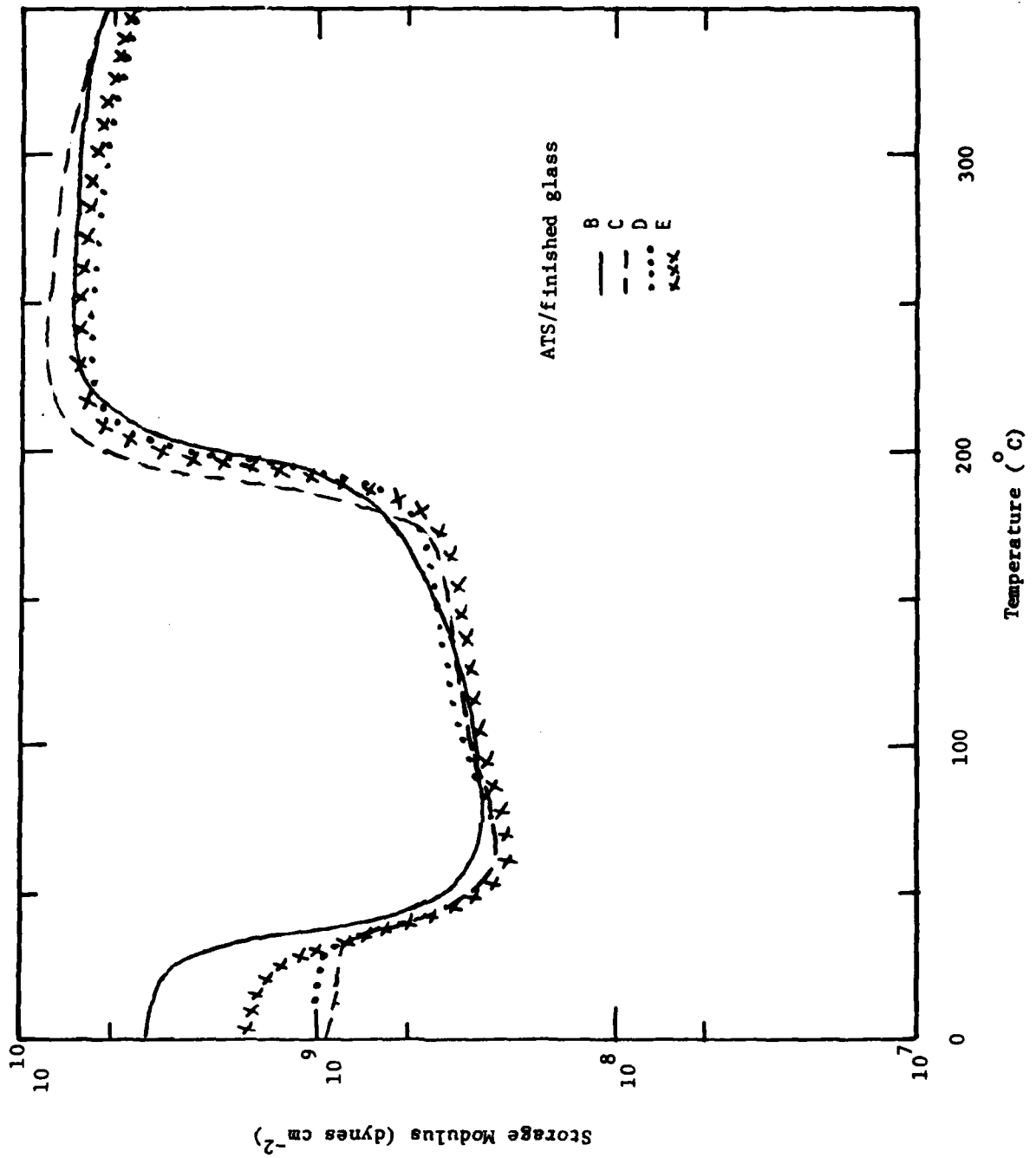


FIGURE 3.

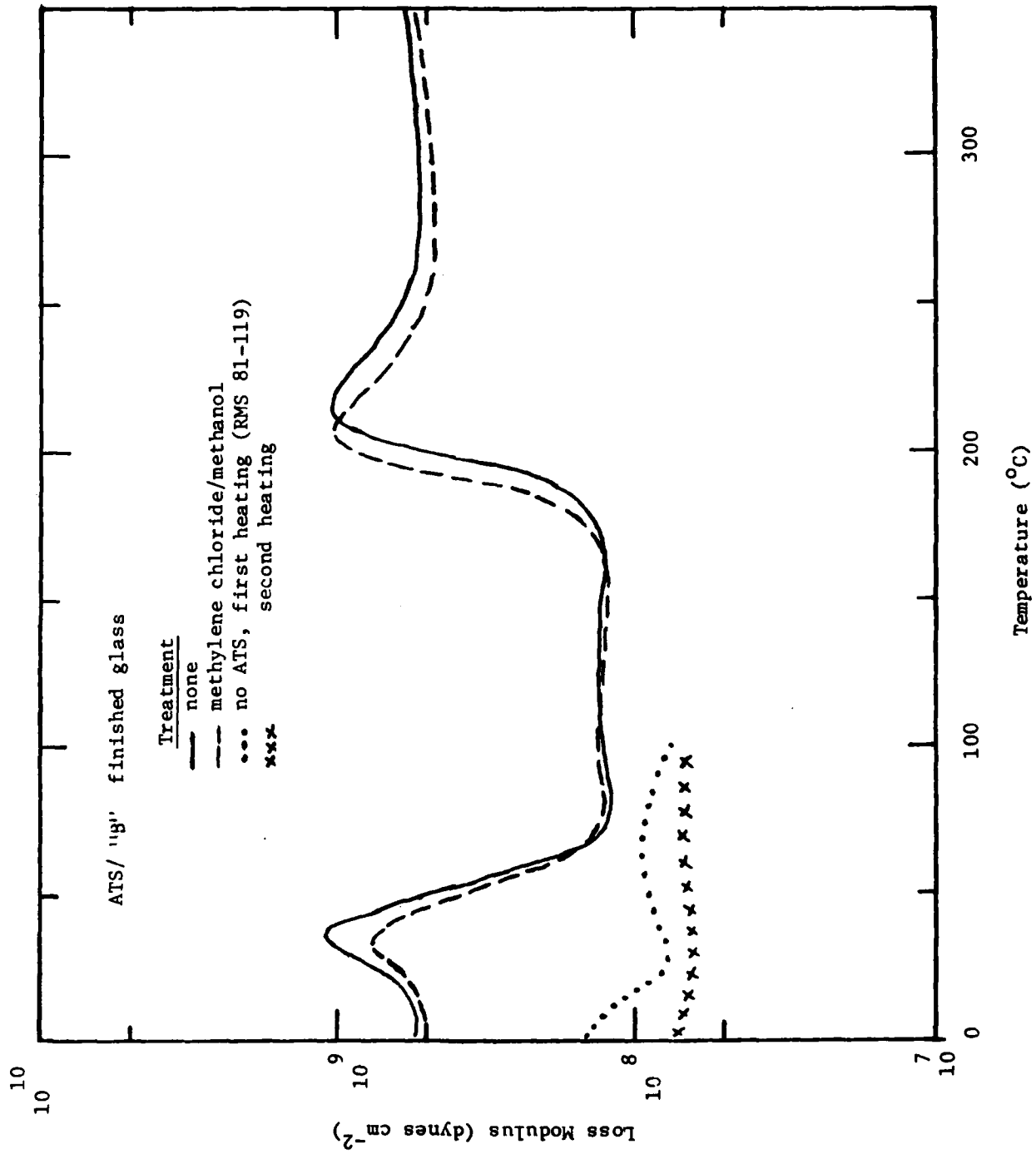


FIGURE 4.

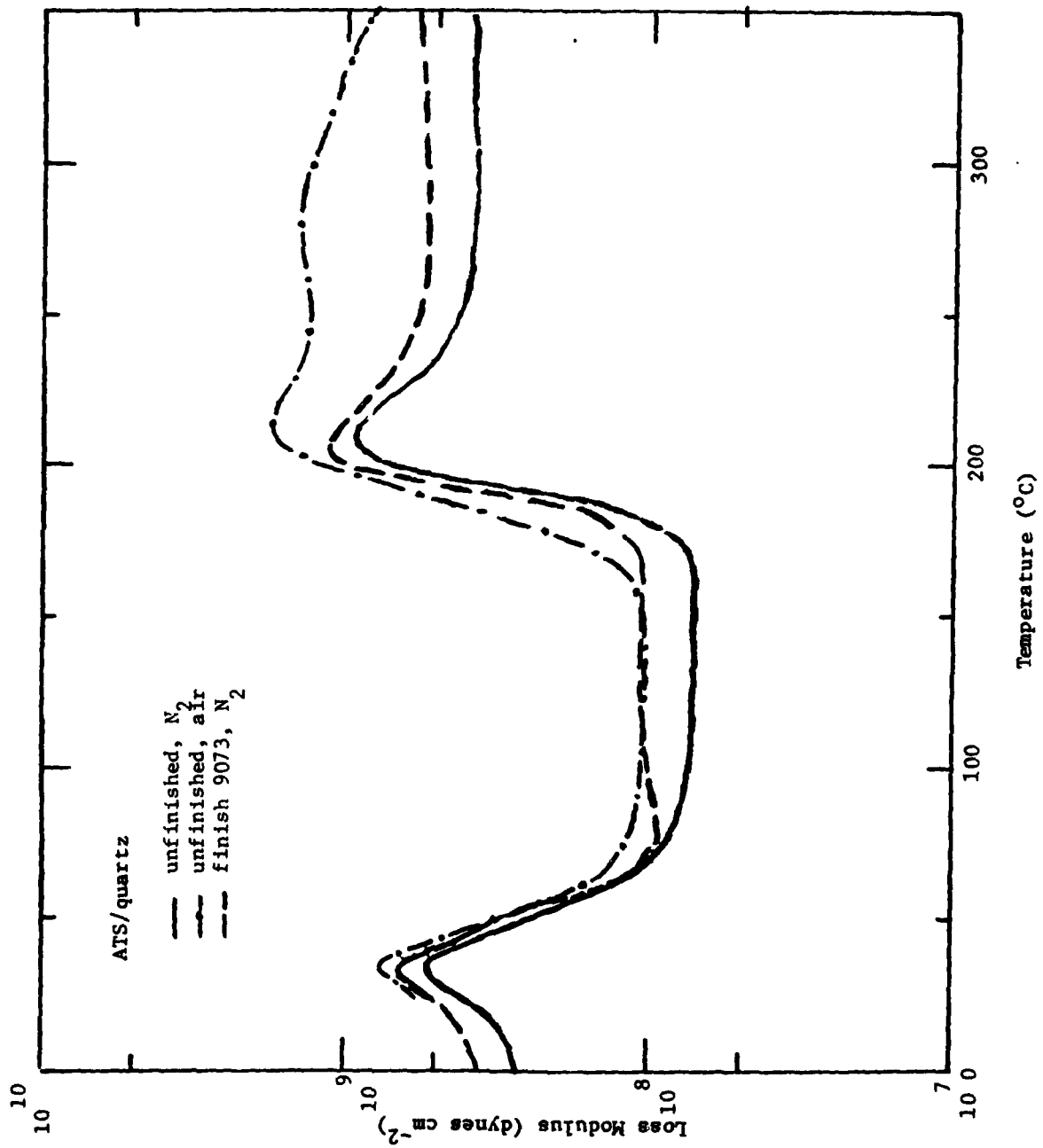


FIGURE 5.

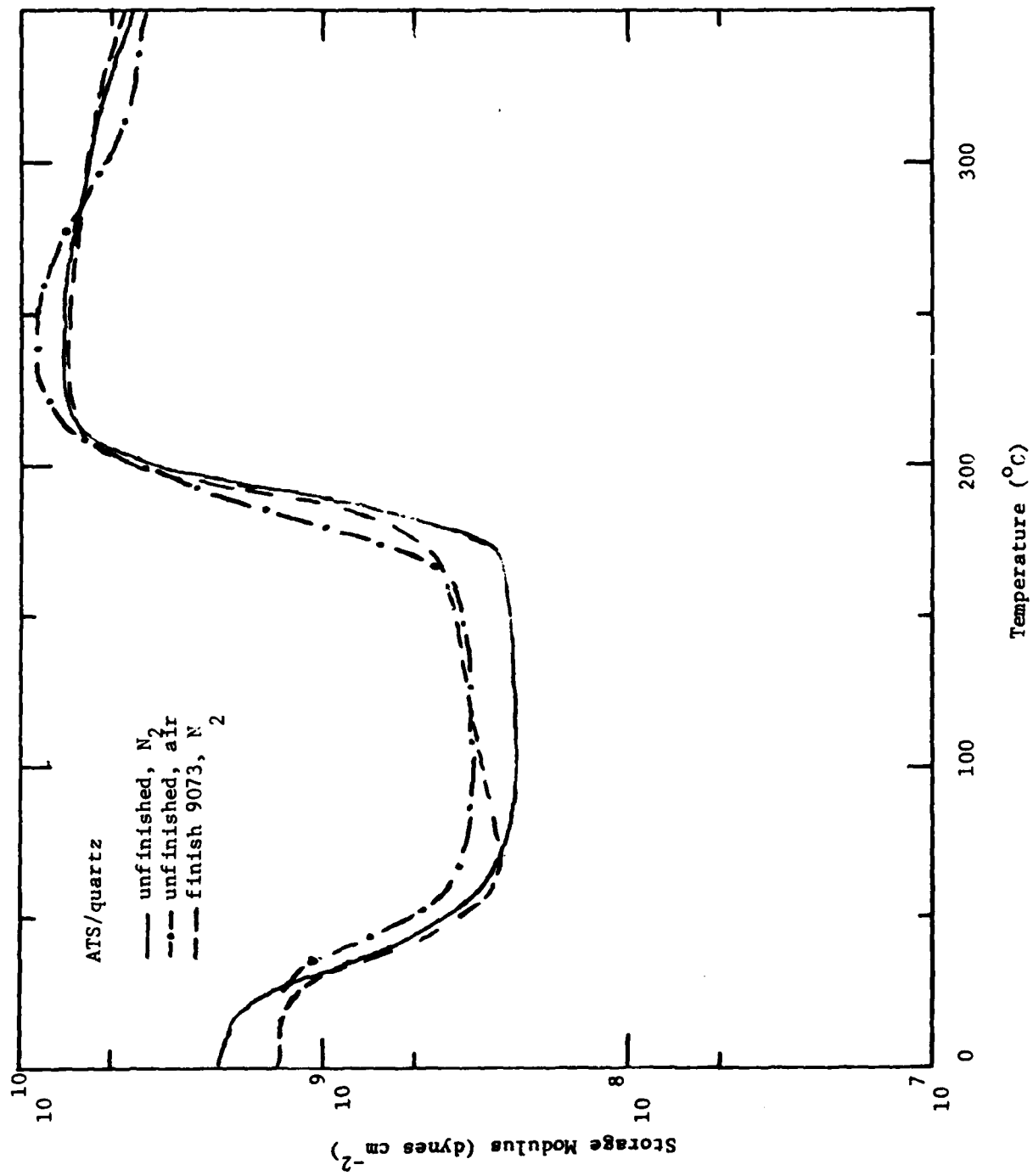


FIGURE 6.

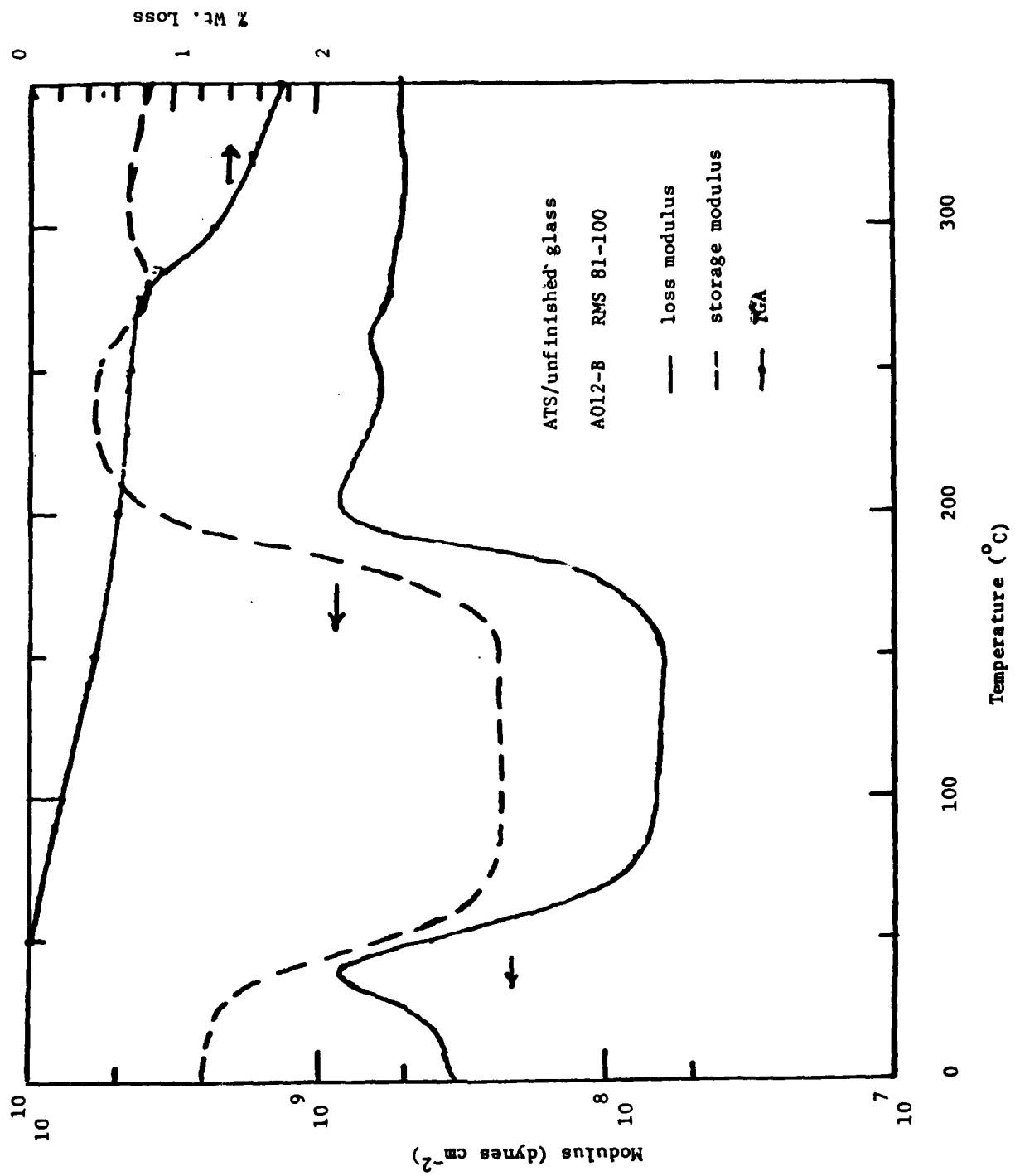


FIGURE 7.

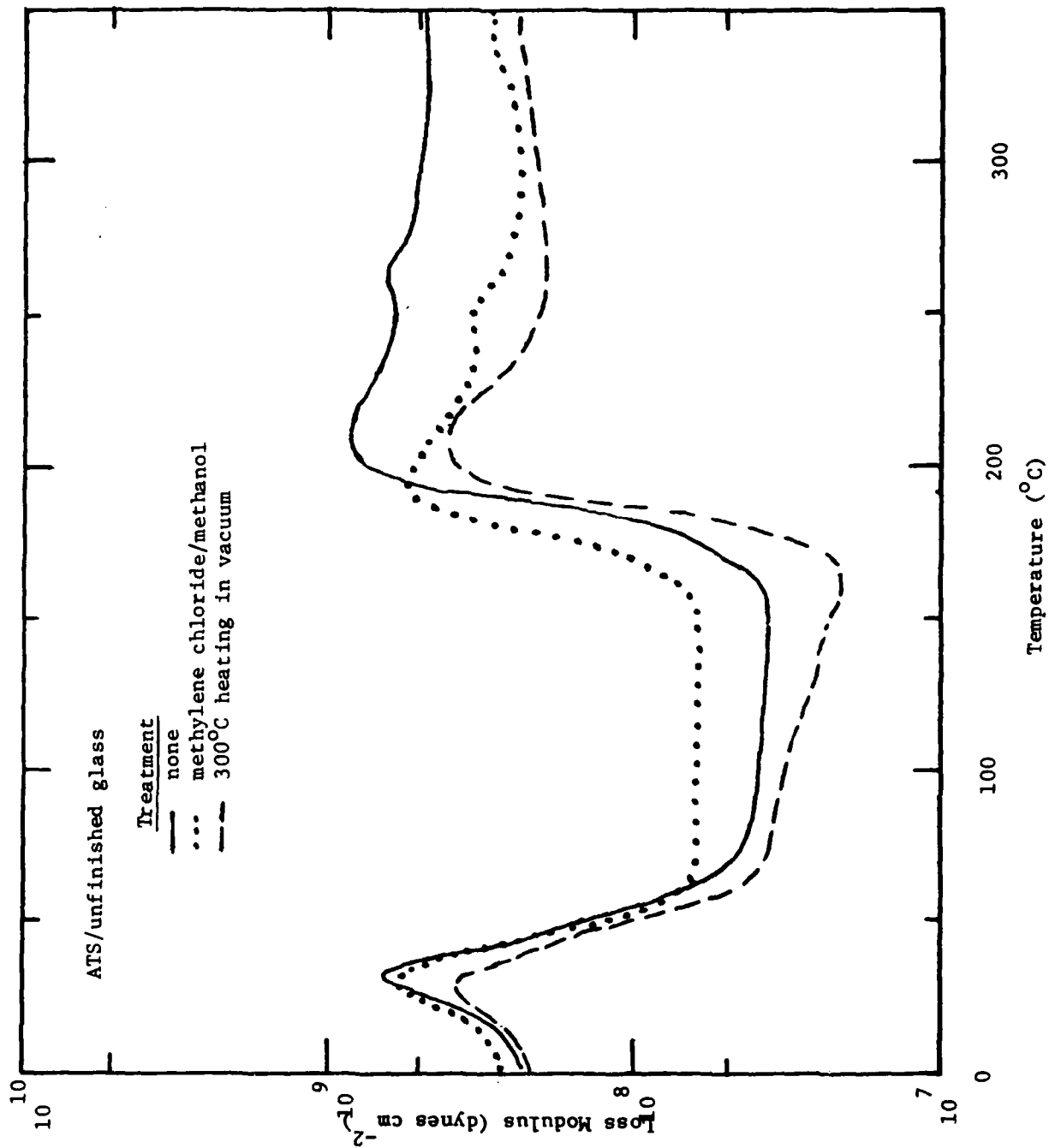


FIGURE 8.

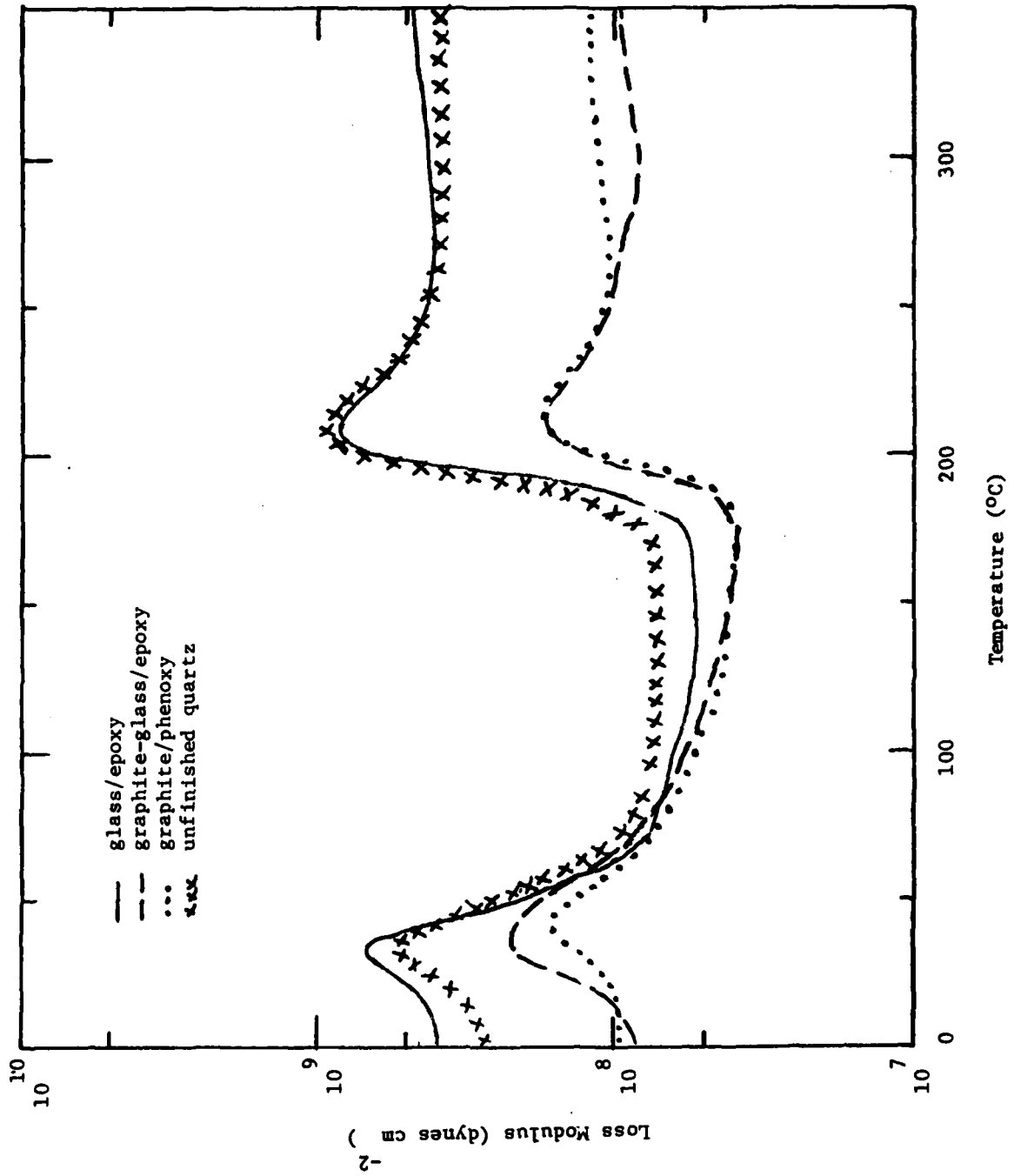


FIGURE 9.

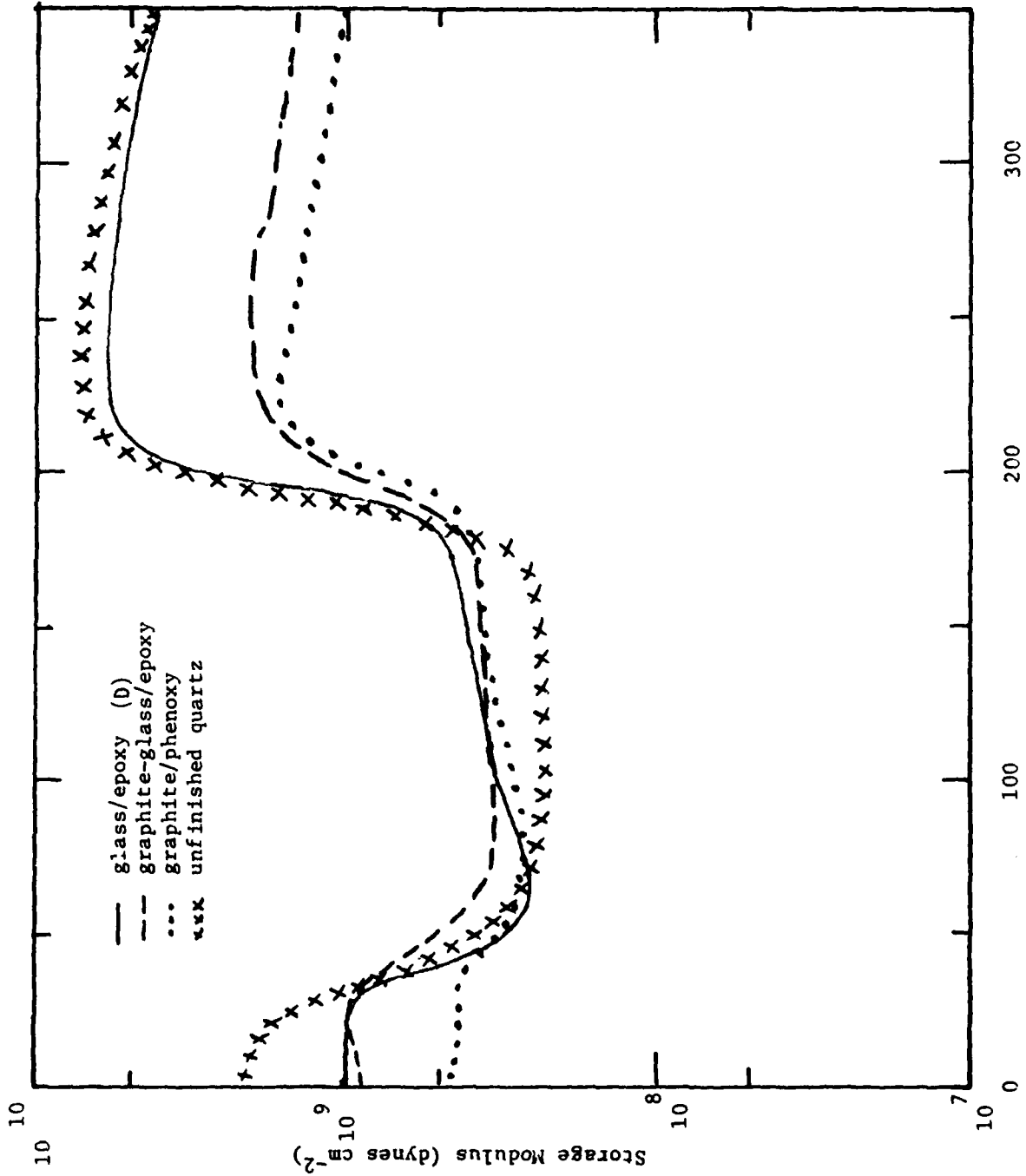


FIGURE 10.

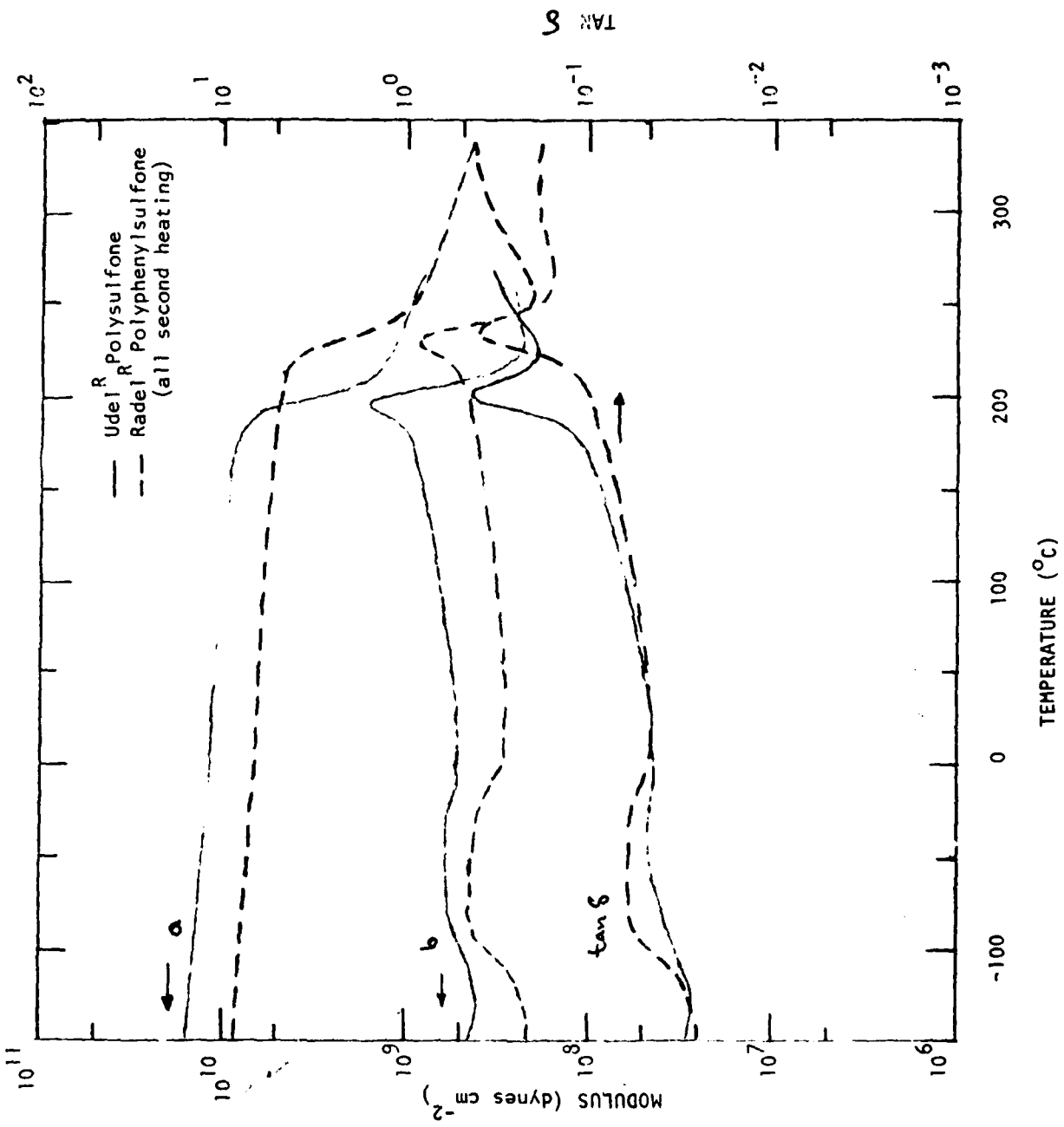


FIGURE 11.

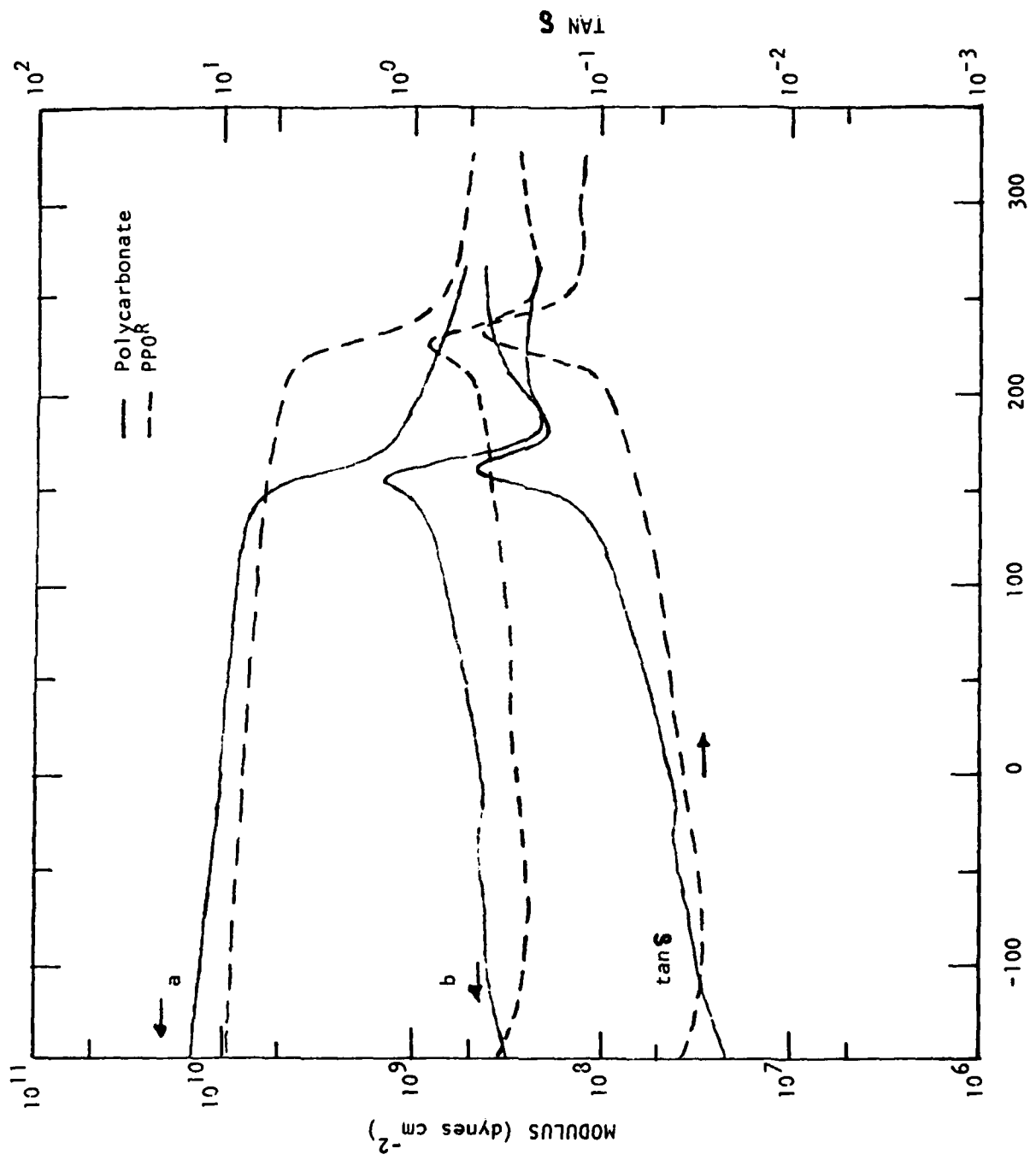
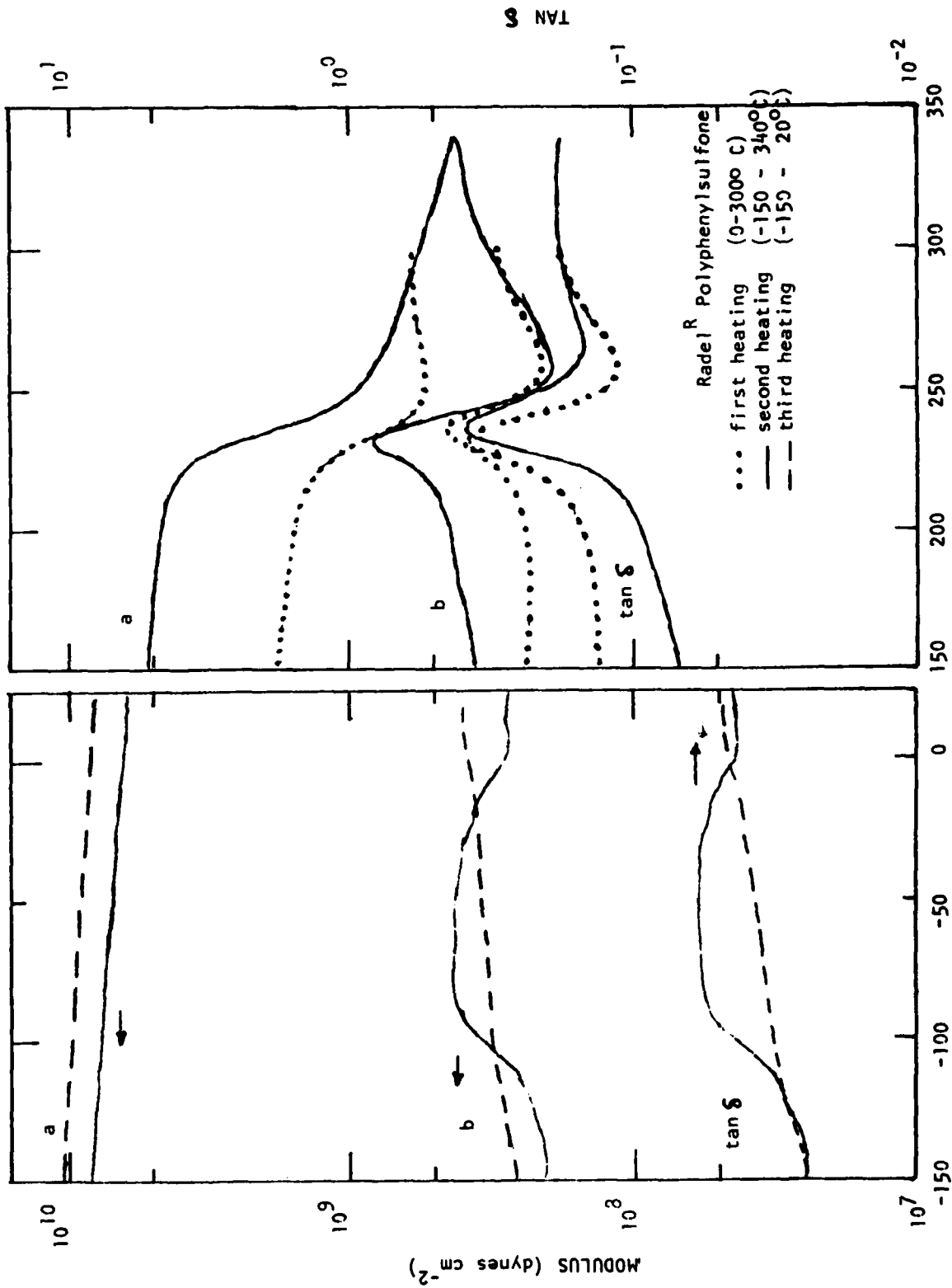


FIGURE 12.

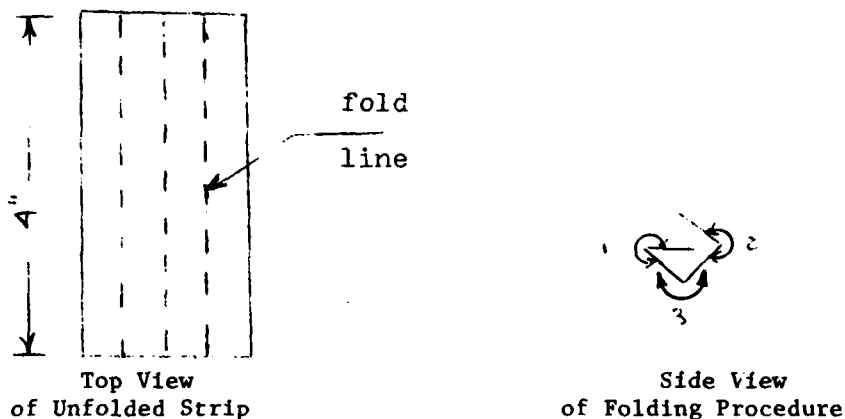


TEMPERATURE (°C)
FIGURE 13.

APPENDIX

TICA Sample Procedure

Rectangular strips of dimensions 4" x 1.90" were cut from ATS (or polymer solution) impregnated cloth and were folded three times as indicated below. In some cases fibers were removed from the center to facilitate folding of stiff cloths.



Two or three strips were sandwiched together in the standard TICA form with either an aluminum shim or piece of foil placed on both sides of each end. Sample preparation procedures for each cloth are given below in Table A1.

TABLE A1

<u>Cloth</u>	<u>ATS/TICA Sample Procedure</u>		<u>Foil or Shim</u>	<u>Comments</u>
	<u>No. Fibers Removed</u>	<u>No. Strips Used</u>		
unfinished quartz	none	3*	foil	cloth was <u>ca.</u> 0.009 in. thick
finished quartz	5	2	foil	cloth was <u>ca.</u> 0.017 in. thick
finished glass	4	2	shim	cloth was <u>ca.</u> 0.0010 in. thick
graphite/ phenoxy	3**	1	shim	Thornell 300 (8 harness satin); thick pliable cloth
graphite-glass / epoxy***	none	2	foil	cloth was <u>ca.</u> 0.014 in. thick

* two strips were used for the polymer TICA samples

** removed after impregnated cloth was dried to prevent unravelling of cloth

*** folded along principal graphite fiber direction

1981 USAF - SCEE SUMMER FACULTY RESEARCH PROGRAM

Sponsored by the

AIR FORCE OFFICE OF SCIENTIFIC RESEARCH

Conducted by the

SOUTHEASTERN CENTER FOR ELECTRICAL ENGINEERING EDUCATION

FINAL REPORT

APPLICATION OF CONJOINT MEASUREMENT THEORY TO

THE QUANTIFICATION OF SUBJECTIVE RATINGS

Prepared by: Dr. David E. Greene
Academic Rank: Assistant Professor
Department and University: Department of Industrial Engineering
Texas A. and M. University
Research Location: Air Force School of Aerospace Medicine, Crew
Technology Division, Crew Performance Branch
USAF Research Colleague: Dr. John F. Courtright
Date: September 7, 1981
Contract No: F49620-79-C-0038

APPLICATION OF CONJOINT MEASUREMENT THEORY
TO THE QUANTIFICATION OF SUBJECTIVE RATINGS

by

David E. Greene

ABSTRACT

Conjoint measurement theory, as applied to the quantification of subjective ratings, is introduced and evaluated through a prototype example in which measures of aircraft quality are used to compare a new fighter aircraft with other classes of fighter aircraft. An ordinal scale of aircraft quality is determined through pilot rank orderings of cells in a two factor rating matrix. Conjoint measurement theory is used to convert this ordinal scale to one with interval properties. The relationship of additive conjoint measurement with the analysis of variance is noted. Two conjoint measurement methods are considered: monotone analysis of variance MONANOVA and delta-scaling. Additive conjoint measurement in this application has two primary problems. First, unless there are many levels in each factor, slight changes in the rank orderings produce major changes in the measurement scale. Second, it is difficult to determine whether the measurement scale is a true improvement over the ordinal scale. Conjoint measurement theory appears to be especially useful in scaling the factors and in modeling the factor relationships.

ACKNOWLEDGEMENT

The author would like to thank the Air Force Systems Command, the Air Force Office of Scientific Research and the Southeastern Center for Electrical Engineering Education for providing him with the opportunity to spend a very worthwhile and interesting summer at the Air Force School of Aerospace Medicine, Brooks AFB, Texas. He would like to acknowledge the laboratory, in particular the Crew Performance Branch, for its hospitality and excellent working conditions.

Finally, he would like to thank Dr. John F. Courtright for suggesting this area of research and for his collaboration and guidance, and he would like to acknowledge many helpful discussions with Dr. Stephen M. Rokicki, Dr. James C. Miller and Capt. Daniel C. Boone.

I. INTRODUCTION

Subjective assessments are important indicators of pilot performance and weapon system effectiveness. The Cooper-Harper¹ subjective rating scale, for example, has been widely used to assess the overall handling quality of a piloted aircraft. Using this rating scale, which has verbal descriptions that range from "excellent" to "major deficiencies," the pilot rates the handling quality from 1 to 10. This rating scale is imprecise in that it expresses only an order relationship; it provides an ordinal measure.

One would like to determine if it is possible to quantify subjective ratings in such a way as to have more precise measures than ordinal measures; that is, to have measures with interval properties. Further, one would like to know if models can be found that explicitly represent the overall measure as a function of basic factors. To these ends, conjoint measurement theory is examined.

The Crew Technology Division at the School of Aerospace Medicine and the Human Engineering Division at the Air Force Aerospace Medical Research Laboratory have general interests in quantifying subjective ratings and specific interests in using conjoint measurement theory to represent workload as a function of subjectively rated factors. Their approach in workload assessment is based upon the monotone analysis of variance method (MONANOVA).² The U.S. Navy has applied conjoint measurement theory, using the delta-scaling method,³ in its mission operability assessment technique (MOAT)⁴ and its simple operability measurement algorithm (SOMA).⁵ These U.S. Navy programs have been used to assess the operability of the Navy F/A-18, A-7E, F-14 and the Air Force F-16 aircraft.

Conjoint measurement theory might best be described as a general scaling and modeling approach.^{6,7,8,9,10,11} This approach produces measurement scales with interval properties, but one is not certain whether these scales can be relied upon. Conjoint measurement theory is fairly abstract; it is usually presented in the literature through axioms and theorems. There are few published applications of this theory to practical real-world problems.

The present paper departs from the usual theoretical presentations and introduces and evaluates conjoint measurement theory through a prototype example.

II. OBJECTIVES

The primary objective is to investigate whether conjoint measurement theory can be used to improve the quantification of subjective ratings. The mathematical foundations of conjoint measurement theory are examined and its relationship with the analysis of variance noted. The measurement scales produced by MONANOVA and delta-scaling are compared. A sensitivity analysis is made of additive conjoint measurement to determine how changes in the rating standards change the measurement scales.

III. PROTOTYPE EXAMPLE

A new fighter aircraft has been developed. We would like to quantify a test pilot's subjective ratings in order to compare this aircraft with other classes of fighter aircraft and to identify strengths and weaknesses. Early identification of problems is important to keep the production costs down and to ensure that a well-designed aircraft is produced on schedule.

Suppose that the aircraft is to be subjectively rated on two different factors: factor A and factor B. Factor A might be workload and factor B might be subsystem effectiveness. Let factor A have verbal descriptive levels a_1 , a_2 and a_3 and factor B have verbal description levels b_1 , b_2 and b_3 .

IV. FACTOR BY FACTOR COMPARISON

Four basic steps are required to convert subjective ratings into meaningful ordinal numbers so that factor by factor comparisons between fighter aircraft can be made.

First, rating standards must be established by a group of fighter pilots to which the test pilot belongs. Each pilot in the group is asked to rank order the cells in the rating matrices for factors A and B in Figure 1, using the integers 1, 2 or 3. Suppose, for the purpose of discussion, that all pilots in the group decide upon a rank ordering for both factors given by the matrix M_0

$$M_0 = (1, 2, 3). \quad (1)$$

Thus, a_3 is preferred over a_2 and b_3 is preferred over b_2 , etc. Matrix M_0

defines a transformation from the verbal descriptive levels a_i or b_i to the ordinal numbers. The rank orderings must be reasonably agreed upon by the pilots in the group before they can be used as standards. (The rank orderings may be obvious if the verbal descriptions are properly written. If this is the case, the pilots need not provide rank orderings.)

Second, after having flown the new aircraft, the test pilot is asked to give subjective ratings for factors A and B. Suppose his ratings are those indicated by x in Figure 2.

Third, the test pilot's subjective ratings are converted to ordinal numbers using the transformations determined in the first step. In this case, the subjective ratings are transformed to a 2 for factor A and a 3 for factor B.

Fourth, the ordinal numbers must be interpreted. The new aircraft is as good (provided "preferred" in fact means "good"), within the resolution of the verbal descriptions, in factor A as another fighter aircraft with a 2 and as good in factor B as another fighter aircraft with a 3. Further, the new aircraft is better, in a consideration of the two factors, than another with a 1 in factor A and a 3 in factor B. However, the new aircraft, in an absolute sense, might be less effective than another with a 3 in factor A and a 2 in factor B.

There are two disadvantages in this factor by factor comparison. First, it treats each factor as having equal importance, when in reality one factor may be much more important than another. Second, it may not be meaningful to compare sets of ordinal numbers for different aircraft.

This factor by factor comparison, however, is simple and it specifically indicates strengths and weaknesses of an aircraft.

V. COMPOSITE MULTIFACTOR COMPARISON

Our objective is to convert each subjective rating pair (a rating on factor A and a rating on factor B) into an ordinal number that represents the overall quality of the aircraft. We will develop ordinal scales of aircraft quality. We proceed as in the factor by factor comparison, but with certain essential modifications.

First, a rating standard must be established by a group of fighter pilots to which the test pilot belongs. Each pilot in the group is asked to rank order the cells (a_i, b_j) in the rating matrix for factors A and B

in Figure 3, using the integers 1 through 9. (The row-column arrangement in the rating matrix, i is the row and j is the column, is for mathematical convenience.) Suppose, for the purpose of discussion, that all pilots in the group decide upon the rank ordering given by the matrix M_1

$$M_1 = \begin{bmatrix} 1 & 3 & 6 \\ 2 & 5 & 8 \\ 4 & 7 & 9 \end{bmatrix} \quad (2)$$

Thus, (a_3, b_3) is the most preferred and (a_1, b_1) is the least preferred. It is noted that rank ordering is a weak mathematical description: while (a_3, b_3) is preferred over (a_2, b_3) , it is not known by how much. However, there is more information in M_1 than in M_0 , for in M_1 the pilot is expressing a preference in which he weighs the importance of one factor with another. Matrix M_1 defines a transformation in which each verbal description pair (a_i, b_j) is mapped to a unique ordinal number; it thus produces an ordinal scale of aircraft quality.

Second, after having flown the new aircraft, the test pilot is asked to give subjective ratings for factors A and B. Suppose his ratings are again those indicated by x in Figure 2.

Third, the test pilot's subjective ratings are converted to a single ordinal number using the transformation determined in the first step. Thus, by the transformation M_1 , the aircraft is an 8.

Fourth, the ordinal number must be interpreted. This, of course, is much simpler than in the factor by factor comparison. The new aircraft is better than another fighter aircraft with a 7, but is less effective than another with a 9.

Our first concern is with the transformation M_1 . Does it vary considerably across subjects? How does it change with changes in the verbal descriptions? Is it reasonable to compute means and variances across subjects? Basic agreement across subjects is required if a specific rank ordering is to be used as a standard by which comparisons can be made.

Our second concern is whether the test pilot gives subjective ratings that are in conformance with the group rating standard. It may be necessary to analyze the subjective ratings of several test pilots.

There are a number of disadvantages in this approach. First, it may be difficult to design a questionnaire such that there is general agreement in the pilot group on the rank ordering. Second, it may not be possible for the human to intelligently rank order several factors, each with a number of levels. Third, an aircraft may have a lower ordinal rating than another, but it is not immediately known which factor contributed most to the problem. Fourth, the ordinal numbers provide only a qualitative measure.

However, the composite multifactor approach, provided the questionnaire is properly designed and the transformation is generally agreed upon, can be expected to give a meaningful ordinal number by which aircraft can be simply and directly compared.

VI. INTRODUCTION TO CONJOINT MEASUREMENT

We would like to convert the subjective rating pairs on factors A and B into numbers that have greater preciseness than the ordinal numbers produced in the composite multifactor comparison. We will develop scales of aircraft quality that have interval properties. In this analysis we will, in addition, prescribe numbers to verbal descriptions (that is, scale these descriptions) and model the aircraft quality as functions of the given factors. We will introduce conjoint measurement theory.

Conjoint measurement theory has a subtle relationship with the analysis of variance. We begin by examining the underlying model for the analysis of variance. Our intention is to proceed from the familiar to the not-so-familiar.

We will assume in our initial analysis that the integers assigned to the cells of the rating matrix have precise mathematical meaning (rather than only expressing an ordering). Thus, matrix M_1 in (2) can be considered as data from a two factor experiment.

We consider the underlying (deterministic) model for an analysis of variance of a two factor experiment with three levels for each factor, no replication effects, and no random effects in the data. This model is given by

$$y_{ij} = \mu + \alpha_i + \beta_j + (\alpha\beta)_{ij}, \quad (3)$$

where y_{ij} is the observation taken at the i th level of factor A and the j th

level of factor B, μ is the grand mean, α_i is the effect of the i th level of factor A, β_j is the effect of the j th level of factor B and $(\alpha\beta)_{ij}$ is the interaction of the i th level of factor A and the j th level of factor B.

The model is further specified by

$$\sum_{i=1}^3 \alpha_i = \sum_{j=1}^3 \beta_j = \sum_{i=1}^3 (\alpha\beta)_{ij} = \sum_{j=1}^3 (\alpha\beta)_{ij} = 0. \quad (4)$$

We identify y_{ij} with the elements of M_1 in (2) and solve for the parameters in (3). The relationships in (3) and (4) provide seventeen equations that uniquely define the sixteen parameters. The parameters are

$$\begin{aligned} \mu &= 5 \\ (\alpha_1, \alpha_2, \alpha_3) &= (-5/3, 0, 5/3) \\ (\beta_1, \beta_2, \beta_3) &= (-8/3, 0, 8/3) \end{aligned} \quad (5)$$

$$(\alpha\beta)_{ij} = \begin{bmatrix} 1/3 & -1/3 & 0 \\ -1/3 & 0 & 1/3 \\ 0 & 1/3 & -1/3 \end{bmatrix}$$

We make two observations. First, according to the model there are interactive effects. Second, the model has assigned numbers α_i and β_j to the verbal descriptive levels a_i and b_j . These numbers give an indication of how close or how far apart the verbal descriptive levels are.

We illustrate what the model does. Suppose the interactive effects were identically zero, then the data would be represented by

$$y_{ij} = \mu + \alpha_i + \beta_j. \quad (6)$$

This equation is the discrete version of the equation of a plane

$$y = \mu + \alpha + \beta \quad (7)$$

defined on the α and β axes. Thus, the model assigns numerical values to the levels of the factors A and B in such a way that the data values lie in

the plane defined by (7). If there are interactive terms, then not all of the data values can be placed in this plane.

Suppose we drop the interactive terms in our representation of M_1 in (3). We then have a new set of numbers \hat{y}_{ij} , which in general are different from the data values y_{ij} , defined by

$$\hat{y}_{ij} = \mu + \alpha_i + \beta_j, \quad (8)$$

with μ , α_i and β_j given in (5). We make the transformations

$$\alpha_i = \hat{\alpha}_i - 5/3, \quad (9)$$

$$\beta_j = \hat{\beta}_j - 8/3, \quad (10)$$

and introduce

$$\hat{\hat{y}}_{ij} = \hat{y}_{ij} - 2/3, \quad (11)$$

in (8) to obtain

$$\hat{\hat{y}}_{ij} = \hat{\alpha}_i + \hat{\beta}_j. \quad (12)$$

We denote the set of values $\hat{\hat{y}}_{ij}$ by \hat{M}_1 . Matrix \hat{M}_1 is given by

$$\hat{M}_1 = \begin{bmatrix} .00 & 2.67 & 5.33 \\ 1.67 & 4.33 & 7.00 \\ 3.33 & 6.00 & 8.67 \end{bmatrix} \quad (13)$$

Compare this matrix with M_1 in (2). Observe that while the matrix elements in \hat{M}_1 are somewhat different from those in M_1 , the rank ordering of the elements has been preserved.

We have in effect transformed the data in M_1 to new data in \hat{M}_1 in such a way that the rank ordering is preserved and the new data satisfies an additive model. This transformation of data is illustrated in Figure 4. Note that numbers have been assigned to the verbal descriptive levels

(that is, they have been scaled) and each cell value in the new data matrix is the sum of the row and column scales.

What we have done is the essence of conjoint measurement: we have found a transformation of the data that preserves the rank ordering and such that a model (in this case, an additive model) holds. Through the transformation we have produced a scale of aircraft quality that has interval properties (the elements of \hat{M}_1 have precise numerical values while the elements of M_1 , as originally defined, express only a rank ordering). We have, in addition, scaled the verbal description levels of each factor.

One may question whether the interval scale of aircraft quality is more meaningful than the ordinal scale. This requires careful study. The implicit assumption in the conjoint measurement analysis is that the model reflects the true world and through the use of the model more precise measures are obtained.

One may question further whether it is proper to transform the data in order to fit a model. It is pointed out that the original data was imprecise (it was a rank ordering). Slight transformations of this data should not change the essential character of the data.

Aside from producing a measure of aircraft quality, this approach has important scaling and modeling aspects. In the scaling of the factors, numbers were assigned to the verbal descriptions. This quantification is useful in the design of questionnaires where one would like the verbal descriptions to be suitably spaced over an interval of interest. Variations in the scale values across subjects may define distributions of the meaning of the verbal descriptions. The model provides a simple law: the measure of aircraft quality is the sum of the two scaled factors.

We transformed the data by neglecting the interaction terms in the deterministic model for the analysis of variance. The general approach in additive conjoint measurement, however, is to systematically search for the order preserving transformation such that the interactive effects are best reduced in the transformed data. Two conjoint measurement methods are considered in this report: monotone analysis of variance (MONANOVA)² and delta-scaling.³

VII. MONANOVA

MONANOVA is an algorithm that seeks the monotone (hence, order preserving) transformation of the data such the transformed data best fit an assumed linear model.² It employs a gradient search. The degree to which the transformed data fit the model is indicated by a number called the stress.

We apply MCNANOVA to our subjective rating problem. The data are given by M_1 in (2). In an additive model, the MONANOVA computer program produces,

with zero stress, the transformed data given by \hat{M}_1

$$\hat{M}_1 = \begin{bmatrix} .00 & 1.47 & 2.94 \\ .92 & 2.39 & 3.86 \\ 1.84 & 3.32 & 4.77 \end{bmatrix}. \quad (14)$$

Scales for factor A and factor B are given in \hat{M}_1 by the first column and first row, respectively. Each element in \hat{M}_1 is the sum of the corresponding row and column scales.

Compare \hat{M}_1 with \hat{M}_1 in (13). Note that each element in \hat{M}_1 is a constant multiple (.55) of the corresponding element in \hat{M}_1 . Recall that \hat{M}_1 was obtained by neglecting the interactive terms in the deterministic model for the analysis of variance.

The representations \hat{M}_1 and \hat{M}_1 are equivalent in the sense that they are related by a linear transformation. Observe that if \tilde{y}_{ij}

$$\tilde{y}_{ij} = \tilde{\alpha}_i + \tilde{\beta}_j \quad (15)$$

is an order preserving additive representation, then so are \tilde{y}_{ij} and \tilde{y}_{ij} defined by

$$\tilde{y}_{ij} = \tilde{y}_{ij} + c_1 = \tilde{\alpha}_i + \tilde{\beta}_j + c_1 = \tilde{\alpha}_i + \tilde{\beta}_j \quad (16)$$

and

$$\tilde{y}_{ij} = c_2 \tilde{y}_{ij} = c_2 \tilde{\alpha}_i + c_2 \tilde{\beta}_j = \tilde{\alpha}_i + \tilde{\beta}_j \quad (17)$$

where $c_2 > 0$. In specifying that the first row first column element in

\hat{M}_1 in (14) was .0, we prescribed the constant c_1 in (16).

Since \hat{M}_1 and \hat{M}_1 are equivalent in the sense given above, it may be more direct to compute \hat{M}_1 rather than \hat{M}_1 . One possible difficulty is that \hat{M}_1 may not always preserve the rank ordering.

VIII. DELTA METHOD

The delta method is an algorithm for converting the ordinal measures on the cells of a matrix to a scale with interval properties satisfying the conditions of additive conjoint measurement.³ In this approach an additive representation is sought that satisfies inequalities specified by the rank ordering of the cells in the matrix. Solution may be found using linear programming methods.

We apply the delta scaling method to our subjective rating problem. The ordinal data is given by M_1 in (2). We use the tally sheet procedure given in reference 4, set all constant "d"s equal to unity, and obtain the

transformed data given by \hat{M}_1 .

$$\hat{M}_1 = \begin{bmatrix} 0. & 7. & 14. \\ 5. & 12. & 19. \\ 9. & 16. & 23. \end{bmatrix}. \quad (18)$$

As in \hat{M}_1 , each element in \hat{M}_1 is the sum of the corresponding row and column

scales. Each element in \hat{M}_1 is approximately 2.65 times the value of the corresponding element in M_1 .

It is fairly tedious to use by hand the delta method. The MONANOVA computer program will be used in the analysis in the next section.

IX. SENSITIVITY ANALYSIS

Through conjoint measurement we have converted an ordinal scale of aircraft quality to one that has interval properties. In this section we will consider how the interval scale values change when there are small

perturbations in the rank orderings.

We use as the unperturbed state the rank ordering in M_1

$$M_1 = \begin{bmatrix} 1 & 3 & 6 \\ 2 & 5 & 8 \\ 4 & 7 & 9 \end{bmatrix} \quad (19)$$

and as perturbed states M_1'

$$M_1' = \begin{bmatrix} 1 & 3 & 5 \\ 2 & 6 & 8 \\ 4 & 7 & 9 \end{bmatrix}, \quad (20)$$

and M_1''

$$M_1'' = \begin{bmatrix} 1 & 3 & 6 \\ 2 & 6 & 8 \\ 5 & 7 & 9 \end{bmatrix}. \quad (21)$$

Matrices M_1' and M_1'' are obtained from M_1 by interchanging two elements. The rank orderings in M_1 , M_1' and M_1'' are reasonable; they are not pathological cases.

Recall that we prescribed the constant c_1 in (16). We now prescribe the constant c_2 in (17). We do this by making the largest interval scale value 100. Thus, the interval scale values will range from 0. to 100.

One would hope that the perturbations in the rank orderings would cause only local effects in the interval scale values. But this is not the case, as may be seen in Figure 5. The perturbation given by M_1' caused a shift of the interval scale values to the right and the perturbation given by M_1'' caused a shift of the interval scale values to the left.

These general shifts make it difficult to interpret the interval scale values. Even though the cell with the ordinal 8 was not perturbed, it was mapped through conjoint measurement to 80.9, 84.6 and 73.1 for M_1 , M_1' and M_1'' , respectively. Suppose it was believed that 75. was a passing score. Then a 8 or 9 would be passing if M_1 was the standard; a 7, 8 or 9 would be

passing if M_1' was the standard; and only 9 would be passing if M_1'' was the standard.

We examine the perturbation effects when the number of levels is increased. We assume four levels for each factor.

We define the unperturbed state by M_2

$$M_2 = \begin{bmatrix} 1 & 3 & 6 & 10 \\ 2 & 5 & 9 & 13 \\ 4 & 8 & 12 & 15 \\ 7 & 11 & 14 & 16 \end{bmatrix} \quad (22)$$

and the perturbed states by M_2'

$$M_2' = \begin{bmatrix} 1 & 3 & 6 & 9 \\ 2 & 5 & 10 & 13 \\ 4 & 8 & 12 & 15 \\ 7 & 11 & 14 & 16 \end{bmatrix}, \quad (23)$$

and M_2''

$$M_2'' = \begin{bmatrix} 1 & 3 & 6 & 10 \\ 2 & 5 & 9 & 13 \\ 4 & 7 & 12 & 15 \\ 8 & 11 & 14 & 16 \end{bmatrix}. \quad (24)$$

The interval scale values determined through conjoint measurement for the ordinal data in M_2 , M_2' and M_2'' are given in Figure 6. While the perturbations still cause shifts in the interval scale values, they are not as pronounced as in the three-level case.

X. SUMMARY COMMENTS ON CONJOINT MEASUREMENT

In our prototype example, our objective was to quantify the test pilot's subjective ratings on the new fighter aircraft so that it could be compared with other classes of fighter aircraft and evaluated. We first developed an ordinal scale of aircraft quality that was based upon a group rating standard. We then used conjoint measurement methods to convert the ordinal scale to one that had interval properties.

The usefulness of these measurement scales of aircraft quality depends on whether there is a generally agreed upon rating standard and whether the test pilot's subjective ratings conform to the standard. These issues must be considered in any subjective rating method.

We have shown that slight changes in the rank orderings can cause major changes in the interval scale values, but that this situation is improved when the number of factor levels is increased. However, when the number of levels is increased, it becomes more difficult for the human to rank order the cells in the rating matrix, and this problem is compounded if there are several factors.

In our prototype example, the test pilot gave the subjective ratings indicated in Figure 2. These ratings were transformed by the rating standard matrix in (2) to an ordinal 8 that was in turn transformed through conjoint measurement to the number 80.9.

We have not answered the question of whether the number 80.9 is a better measure of aircraft quality than the ordinal 8. In the sense that the ordinal 8 expresses only an order of preference, the number 80.9 is more precise (providing the model assumed in the conjoint measurement analysis enhances the measure). However, if the ordinal numbers are interpreted as exact numbers or if they are considered in relation to others (as, for example, 8 out of 9), then they may provide measures that are comparable to the interval scale values.

Conjoint measurement analysis appears to be especially useful in scaling the factors and in modeling. Through scaling, numbers are assigned to the verbal descriptions and this is useful in the design of questionnaires where one would like the verbal descriptions to be suitably spaced over an interval of interest. Variations in the scale values across subjects may define distributions of the meaning of the verbal descriptions. The models exhibit how the different factors contribute to the overall measure.

XI. RECOMMENDATIONS

The concept of a rating standard matrix that transforms subjective ratings on multiple factors into ordinal measures has much promise. The rating standard matrix provides simple and direct quantification of subjective ratings. Its usefulness, however, depends on whether there is a generally agreed upon rating standard.

Further research is needed to determine if there are group rating standards. Effort should be given to the design of questionnaires to promote agreement. If there is considerable variability across subjects in determining the standard, then consideration should be given to whether it is meaningful to average the rank orderings across subjects.

An investigation should be made to determine if the human can effectively provide scalar ratings on the cells of the rating matrix, thus directly establishing interval scales of measurement. It may be possible to mathematically assist the human in assigning numerical values to the cells of the rating matrix (in particular, to rank order them) when there are several factors. For example, enough information to determine a complete rank ordering may be provided by sets of two-factor rank orderings along with a rank ordering of the factors themselves.

Conjoint measurement theory can contribute to the quantification of subjective ratings. It appears to be especially useful in scaling the factors and modeling the factor relationships. Through scaling, numbers are assigned to verbal descriptions and this is useful in the design of questionnaires. The models explicitly show how the factors contribute to the overall measure.

Further research is needed to determine if the measurement scale, produced through conjoint measurement analysis, is a true improvement over the ordinal scale. Analytical and experimental studies should be carried out to determine if the models (for example, an additive model) used in conjoint measurement analysis, in fact, enhance the measure. Systematic ways of choosing the models and evaluating them are needed.

	a_1	a_2	a_3
FACTOR A			
	b_1	b_2	b_3
FACTOR B			

FIGURE 1. RATING MATRICES FOR SINGLE FACTOR ORDERING.

	a_1	a_2	a_3
FACTOR A		X	
	b_1	b_2	b_3
FACTOR B			X

FIGURE 2. EXAMPLE SUBJECTIVE RATINGS FOR NEW AIRCRAFT.

		FACTOR B		
		b_1	b_2	b_3
FACTOR A	a_1			
	a_2			
	a_3			

FIGURE 3. RATING MATRIX FOR TWO FACTOR ORDERING.

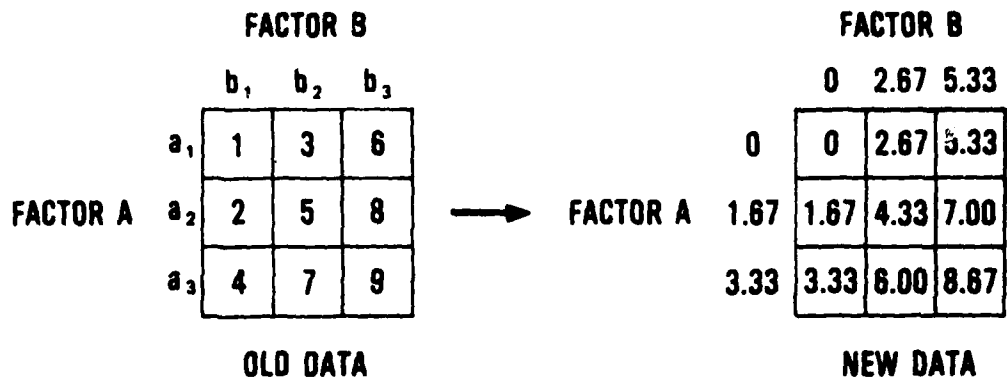


FIGURE 4. OLD DATA AND NEW SCALED ADDITIVE DATA.

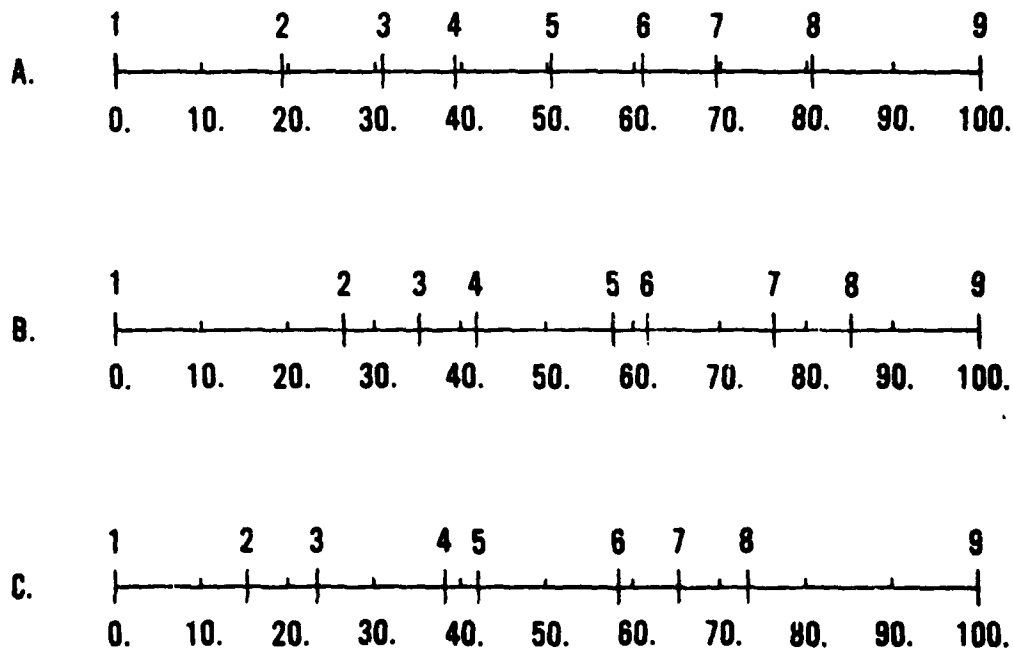


FIGURE 5. INTERVAL SCALE VALUES DETERMINED THROUGH CONJOINT MEASUREMENT FOR ORDINAL DATA IN A. M., B. M., AND C. M.

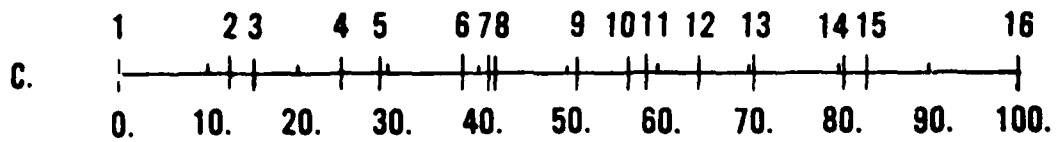
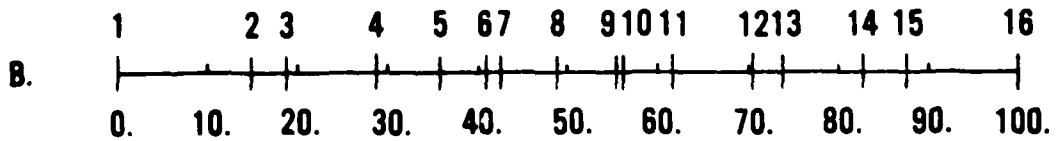
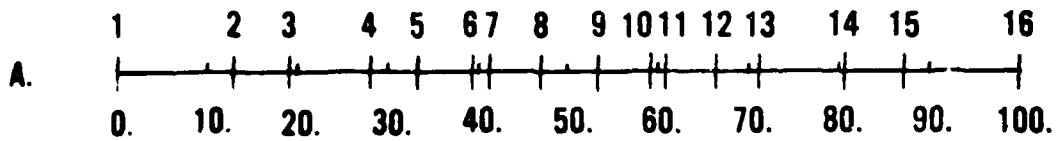


FIGURE 6. INTERVAL SCALE VALUES DETERMINED THROUGH CONJOINT MEASUREMENT FOR ORDINAL DATA IN A. M_2 , B. M_2^1 , AND C. M_2^{11} .

REFERENCES

1. Cooper, G. E. and Harper, R. P., Jr., "The Use of Pilot Rating in the Evaluation of Aircraft Handling Qualities," NASA, TN D-5153, 1969.
2. Kruskal, J. B., "Analysis of Factorial Experiments by Estimating Monotone Transformations of the Beta," J. Royal Stat. Soc., Vol. 27, pp. 251-263, 1965.
3. Coombs, C. H., Dawes, R. M. and Tversky, A., Mathematical Psychology, Englewood Cliffs, New Jersey, Prentice-Hall, 1970.
4. Helm, W. R. and Donnell, M. L., "Mission Operability Assessment Technique: A System Evaluation Methodology," Pacific Missile Test Center, TP-79-31, 1979.
5. Donnell, M. L., Adelman, L. and Patterson, J. F., "A System Operability Measurement Algorithm (SOMA): Applications, Validation, and Extensions," Pacific Missile Test Center, PR 81-11-156, 1981.
6. Shepard, R. N., "The Analysis of Proximities: Multidimensional Scaling with an Unknown Distance Function I," Psychometrika, Vol. 27, pp. 125-140, 1962.
7. Shepard, R. N., "The Analysis of Proximities: Multidimensional Scaling with an Unknown Distance Function II," Psychometrika, Vol. 27, pp. 219-246, 1962.
8. Kruskal, J. B., "Multidimensional Scaling by Optimizing Goodness of Fit to a Nonmetric Hypothesis," Psychometrika, Vol. 29, pp. 1-27, 1964.
9. Kruskal, J. B., "Nonmetric Multidimensional Scaling: A Numerical Method," Psychometrika, Vol. 29, pp. 115-129, 1964.
10. Krantz, D. H. and Tversky, A., "Conjoint Measurement Analysis of Composition Rules in Psychology," Psychological Review, Vol. 78, pp. 151-169, 1971.
11. Baird, J. C. and Noma, E. Fundamentals of Scaling and Psychophysics, New York, New York, John Wiley and Sons, 1978.

1981 USAF - SCEEE SUMMER FACULTY RESEARCH PROGRAM

Sponsored by the

AIR FORCE OFFICE OF SCIENTIFIC RESEARCH

Conducted by the

SOUTHEASTERN CENTER FOR ELECTRICAL ENGINEERING EDUCATION

FINAL REPORT

SENSOR NOISE AND KALMAN FILTER FOR AIDED
INERTIAL NAVIGATION SYSTEM

Prepared by: Dr. Gurmohan S. Grewal
Academic Rank: Professor
Department and University: Electrical Engineering
Southern University
Research Location: Air Force Avionics Laboratory, System
Avionics Division
USAF Research Colleague: Capt Nicholas Drobot
Date: July 31, 1981
Contract No: F49620-79-C-0038

SENSOR NOISE AND KALMAN FILTER FOR AIDED

INERTIAL NAVIGATION SYSTEM

by

Gurmohan S. Grewal

ABSTRACT

Inertial Navigation System, barometric altimeter, TACAN, and ILS are used to achieve a synergistic combination of the outputs of individual subsystems. Kalman filter is used to provide an ideal method for data processing in this multisensor navigation system. The filter design begins with the development of mathematical and statistical error models to describe the truth system. The truth model is simplified and reduced, in steps, to lower the computation burden on the on-board computer. The covariance analysis and the Monte Carlo methods of testing the performance of the Kalman filters based on reduced and simplified system models are discussed. Suggestions for further research in the area of fault detection and isolation are offered.

Acknowledgement

The author would like to thank the Air Force Systems Command, the Air Force Office of Scientific Research, and the Southeastern Center for Electrical Engineering Education for providing him with the opportunity to spend a very worthwhile and interesting summer at the Air Force Avionics Laboratory, Wright-Patterson AFB, Ohio.

Finally, he would like to thank Capt Nick Drobot for suggesting this area of research and for his assistance and guidance.

I. INTRODUCTION

Inertial Navigation Systems (INS) and non-inertial navigation aids such as TACAN, ILS, Loran, OMEGA, navigation satellites, etc., have been used in a number of multisensor-based navigation systems. Outputs of the individual subsystems are combined synergistically. The software accomplishes this combination ideally utilizing the data from the subsystems to yield much more accurate results than these subsystems can provide unaided. Data processing algorithm, called Kalman filter, provides a systemic and logical method of weighing various sources of information to produce a best estimate of the quantities of interest.

This research is concerned with the development of a Kalman filter that combines the data from a baro-inertial navigation with the range and bearing measurements of a TACAN system during the cruise portion of the flight and the measurements from an ILS system during the descent and the final approach phase of a flight (Ref 1). The resulting filter provides the position and the attitude of the aircraft.

The performance of a Kalman filter is dependent upon adequate mathematical and statistical models to describe the true system including system and measurement dynamics, system disturbances and measurement errors, and initial condition information. These models are formulated in the state space. There are two approaches available for the state space formulation of the models: the "total" state space models and the "error" state space models. In the total state space formulation, position, velocity, and attitude are among the state variables, and the measurements include accelerometer outputs and signals from TACAN or ILS. The resulting vehicle dynamics equations are nonlinear, high frequency, and are not adequately developed for use in the Kalman filter. In the error state space formulation, the errors in the inertial navigation system position, velocity, and attitude values are among the state variables, and measurements are composed of the differences between the inertial and the external source data. The resultant vehicle dynamics equations for the error state space formulation are low frequency, linear, and fairly well developed for use in the Kalman filter (Ref 2, 3, 4). Consequently, the error state space formulation, which is also called "indirect" filter, is adopted. Further, the indirect filter can be implemented in two ways: feedforward and feedback. In the case of feedforward,

the output of the filter, which is the optimal estimates of the errors between the inertial system outputs and the true values, is subtracted from the inertial system outputs to obtain the best available estimate of the vehicle position, velocity, and attitude. The inertial system is unaware of the existence of the Kalman filter. The inertial system is free to drift with unbounded errors. As these errors get large, the adopted model of the inertial system becomes invalid, resulting in filter "divergence." On the other hand, in the feedback configuration, the output of the filter, which is the error between the true values and the inertial values, is fed back to the inertial system to obtain a set of corrected inertial outputs. Thus the inertial system errors are not allowed to grow unbounded. Moreover, the filter need not propagate the estimates of the error state variables. Hence, the feedback configuration is preferred.

If the comprehensive truth models are used in the development of Kalman filter, the resulting filter will require extensive memory and computation time, making it impractical for the limited on-board computer to handle the problem. The computation load is approximately proportional to the third power of the number of states required for modelling the system dynamics. Therefore, simplified models, rather than the truth models, are used in the filter development. The models simplification will result in performance degradation. In order to make intelligent approximations and assumptions necessary to obtain workable models, it is important to thoroughly understand the laws governing the involved system. Resulting performance degradation can be analyzed using covariance analysis and the Monte Carlo methods. The Air Force has fully developed, unclassified, transportable software packages for vehicle trajectory generation (Ref 5), covariance analysis (Ref 6), Monte Carlo analysis (Ref 7), and for plotting the results of Monte Carlo analysis (Ref 8), specifically to aid the testing and evaluation of the Kalman filter.

II. OBJECTIVES

The effort involved for this Summer Faculty Program had two main objectives:

- (1) To provide an option for the injection of random errors into the outputs of the INS, TACAN, and air data sensor models of the Digital Avionics Information System (DAIS). Each of these random error sources is to be capable of interruption by the setting of an appropriate flag bit in a control word.

- (2) After a detailed study of the available comprehensive TACAN/ILS-aided baro-inertial navigation system models (Ref 2, 3, 4, 9), develop reduced states simplified models in order to obtain a workable Kalman filter. The simplifications and the reductions are to be implemented in steps in order that the Kalman filter resulting from each approximation can be tested for the performance sensitivity to that particular approximation. There will not be enough time to complete the performance analysis, but the strategy for the step-by-step models simplification is to be well established by the end of this ten-week summer period.

III. RANDOM ERRORS INJECTION INTO DAIS SENSOR MODELS

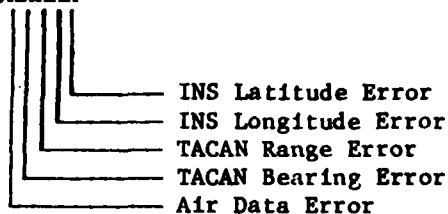
In order to simulate various error conditions, a control word is defined with the following bit assignments:

Control Word Bit Assignments

Error Model	Signal	Bit No 1=ON, 0=OF	Default Value
INS	Actual Latitude	1	1
	1 Lat. Error	2	0
	5 Lat. Error	3	0
	Actual Longitude	4	1
	1 Long. Error	5	0
	5 Long. Error	6	0
TACAN	Actual Range	7	1
	1 Range Error	8	0
	5 Range Error	9	0
	Actual Bearing	10	1
	1 Bearing Error	11	0
	5 Bearing Error	12	0
Air Data	Actual TAS	13	1
	1 TAS Error	14	0
	5 TAS Error	15	0
	Not Used	16	0

The DEC-10 FORTRAN statement for the control word is inserted in the SCEN subroutine of DAIS:

IERROR = "OXXXXX



Default value IERROR = "011111

Octal Digit Values = 1 , NO Noise
 2 , 1σ Noise
 4 , 5σ Noise

The control word is set by the operator at the beginning of the simulation run.

3.1 Random Noise Model

A normally distributed random variable N of zero mean and unit variance is obtained from two independent samples U_1 and U_2 of uniform distribution between zero and one by the following equation:

$$N = (-2 \ln(u_1))^{1/2} \sin(2\pi u_2)$$

A second normally distributed is obtained from the above equation by changing the SIN to COS:

$$N = (-2 \ln(u_1))^{1/2} \cos(2\pi u_2)$$

The time correlation is introduced as follows:

$$X_n = \exp(-\Delta t/\tau) X_{n-1} + (1 - \exp(-2\Delta t/\tau))^{1/2} N_n$$

where

n = nth iteration
 Δt = iteration interval
 τ = correlation time

The error e_n of mean M and standard deviation σ is obtained by the following equation:

$$e_n = \sigma X_n + M$$

Since this random noise is used repeatedly, a subroutine called RNOISE is generated for it. FORTRAN coding for this subroutine is as follows:

```
      SUBROUTINE RNOISE(XLAST,DELT,TAU,SIGMA,ERR,XCUR)
      DOUBLE PRECISION X,X1,X2,RHO,ERR,XCUR,XLAST,PI2
      IF(X2.EQ.0.) GO TO 5
      X=X2
      X2=0.
      GO TO 10
5     CALL RDN(U1)
      CALL RDN(U2)
      PI2=6.28318530717958648D0
      X1=DSQRT(-2.DO*ALOG(U1))*DCOS(PI2*U2)
      X2=DSQRT(-2.DO*ALOG(U1))*DSIN(PI2*U2)
      X=X1
10    RHO=DEXP(-DELT/TAU)
      XCUR=RHO*XLAST+DSQRT(1-RHO**2)*X
      ERR=SIGMA*XCUR
      RETURN
      END
```

The variable X2 needs to be zeroed at the beginning of the simulation.

3.2 INS Error Model

The INS error model introduces errors into the horizontal navigation channels. These errors have the following parameters:

Velocity Error Standard Deviation = 0.707 n.m./hr. per axis
Velocity Error Mean Error = 0 per axis
Velocity Error Correlation Time = 30 min. per axis

Since the INS model does not integrate velocity, the velocity error is integrated to form position errors to be added to INS position outputs. First, two velocity errors δV_N and δV_E are derived. These velocity errors are integrated to obtain the latitude error $\delta \lambda$ and the longitude error $\delta \phi$,

$$\begin{aligned}\delta \lambda &= \delta \lambda + (\delta V_N / R_0) \Delta t \\ \delta \phi &= \delta \phi + (\delta V_E / R_0 \cos \lambda) \Delta t\end{aligned}$$

where R_0 is the radius of the earth. Then the noise-corrupted direction cosines, longitude, and velocity outputs are:

$$\begin{aligned}C_{XK} &= C_{XK} - \cos \alpha \sin \lambda \delta \lambda \\ C_{XY} &= C_{XY} + \sin \alpha \sin \lambda \delta \lambda \\ C_{XZ} &= C_{XZ} + \cos \lambda \delta \lambda \\ \phi &= \phi + \delta \phi \\ V_N &= V_N + \delta V_N \\ V_E &= V_E + \delta V_E\end{aligned}$$

where α is the wander angle. The following codes are inserted at the end of INSIN and INSNAV, respectively:

Code To Be Inserted In INUIN Subroutine

```
DOUBLE PRECISION XLINVE,XLINVN,DLINVE,DLINVN,PI2
PI2=6.28318530717958648D0
CALL RDN(U1)
CALL RDN(U2)
XLINVE=DSQRT(-2.DO*ALOG(U1))*COS(PI2*U2)
XLINVN=DSQRT(-2.DO*ALOG(U1))*SIN(PI2*U2)
DELLAT=0.
DELLNG=0.
SDINVE=(SQRT(2.)/2.)/(3600.*FPSKTS)
TAUINV=1800.
SDINVN=SDINVE
IF((IERROR.AND."000007").EQ."000001) SDINVN=0.
IF((IERROR.AND."000007").EQ."000004) SDINVN=5*SDINVN
IF((IERROR.AND."000070").EQ."000010) SDINVE=0
IF((IERROR.AND."000070").EQ."000040) SDINVE=5*SDINVE
```

Code To Be Inserted In INUNAV Subroutine

```
DOUBLE PRECISION XCINVE,XCINVN
IF((IERROR.AND."000077").EQ."000011) GO TO 100
CALL RNOISE(XLINVE,DTINUS,TAUINV,SDINVE,DLINVN,XCINVN)
CALL RNOISE(XLINVN,DTINUS,TAUINV,SDINVN,DLINVE,XCINVE)
XLINVE=XCINVE
XLINVN=XCINVN
VELEFS=VELEFS+DLINVE
VELNFS=VELNFS+DLINVN
DELLAT=DELLAT+(DLINVN/EARADF)*DTINUS
DELLNG=DELLNG+(DLINVE/(EARADF*COS(ANLATR)))*DTINUS
FLNGOR=FLNGOR+DELLNG
CXDIR=CXDIR-COS(WANDER)*SIN(ANLATR)*DELLAT
CYDIR=CYDIR+SIN(WANDER)*SIN(ANLATR)*DELLAT
CXZDIR=CXZDIR+COS(ANLATR)*DELLAT
100 CONTINUE
```

3.3 TACAN Error Model

Random, time-correlated errors, having the following characteristics, are added to the TACAN range and bearing measurements:

Range Bias Error Standard Deviation	= 2000 ft.
Bearing Bias Error Standard Deviation	= 2 deg.
Range and Bearing Correlation Time	= 5 sec.
Range and Bearing Mean Error	= 0

The following code is inserted into the TACAN and CHNTAC subroutines of DAIS.

Code To Be Inserted Into TACAN Subroutine

```
DOUBLE PRECISION XLTACR,XLTACB,PI2
CALL RDN(U1)
CALL RDN(U2)
XLTACR=DSQRT(-2.DO*ALOG(U1))*DCOS(PI2*U2)
XLTACB=DSQRT(-2.DO*ALOG(U1))*DSIN(PI2*U2)
```

```

SDTACR=2000.
SDTACB=2./DEGPRR
TAUTAC=5.
IF((IERROR.AND."000700").EQ."000100) SDTACR=0.
IF((IERROR.AND."000700").EQ."000400) SDTACR=5.*SDTACR
IF((IERROR.AND."007000").EQ."001000) SDTACB=0.
IF((IERROR.AND."007000").EQ."004000) SDTACB=5.*SDTACB
DTTACS=DELTIM*(8./ITRATE(MODELN))

```

Code To Be Inserted Into CHNTAC Subroutine

```

DOUBLE PRECISION XCTACR,XCTACB
IF((IERROR.AND."007700").EQ."001100) GO TO 100
CALL RNOISE (XLTACR,DTTACS,TAUTAC,SDTACR,DLTACR,XCTACR)
CALL RNOISE (XLTACB,DTTACS,TAUTAC,SDTACB,DLTACB,XCTACB)
XLTACR=XCTACR
XLTACB=XCTACB
CRANGF=CRANGF+DLTACR
CAZMTR=CAZMTR+DLTACB
100  CONTINUE

```

3.4 Air Data Error Model

In order to corrupt true air speed (TAS) without disturbing the calculation of altitude, the temperature output from the air data sensor model is perturbed. The sensitivity of the TAS to changes in the temperature is related as follows:

$$\frac{dT_R}{T_R} = 2 \frac{dTAS}{TAS}$$

where T_R is the temperature in deg.R. A percentage error in the TAS of $k\%$, is:

$$T_R = T_R (1 + 2k/100)$$

where R is a random, time-correlated variable with the following parameters:

Percentage Error in TAS = 3%, 16
Correlation Time = 3 min.

The following code is inserted in the ADCIN and ADC subroutines to achieve the required temperature corruption.

To Be Inserted In ADCIN Subroutine

```
DOUBLE PRECISION XLADCT
CALL RDN(U1)
CALL RDN(U2)
XLADCT=DSQRT(-2.D0*ALOG(U1))*COS(PI2*U2)
SDADCT=3.
TAUADC=180.
IF((IERROR.AND."070000").EQ."010000) SDADCT=0.
IF((IERROR.AND."070000").EQ."040000) SDADCT=5.*SDADCT
DTADCS=DELTIM*(64./ITRATE(MODELN))
```

To Be Inserted Into ADC Subroutine

```
DOUBLE PRECISION XCADCT
IF((IERROR.AND."070000").EQ."010000) GO TO 100
CALL RNOISE(XLADCT,DTADCT,TAUADC,SDADCT,DLADCT,XCADCT)
XLADCT=XCADCT
TMALTR=TMALTR*(1.+2.*DLADCT/100.)
100 CONTINUE
```

IV. THE FUNDAMENTAL STRUCTURE OF KALMAN FILTER

The system state is described by:

$$\underline{X}(k+1) = \underline{\Phi}(k+1, k)\underline{X}(k) + \underline{B}(k)\underline{U}(k) + \underline{G}(k)\underline{W}(k)$$

and the measurements are described by

$$\underline{Z}(k) = \underline{H}(k)\underline{X}(k) + \underline{V}(k)$$

where,

$\underline{X}(k)$ = n-by-1 state vector at time t_k
 $\underline{U}(k)$ = r-by-1 deterministic input vector
 $\underline{W}(k)$ = s-by-1 driving noise vector
 $\underline{Z}(k)$ = m-by-1 measurement vector

$\underline{V}(k)$ = m-by-1 measurement noise vector
 $\Phi(k+1, k)$ = n-by-n state transition matrix
 $\underline{B}(k)$ = n-by-r deterministic input matrix
 $\underline{G}(k)$ = n-by-s noise input matrix
 $\underline{H}(k)$ = m-by-n measurement matrix

and, $W(k)$ and $V(k)$ are zero mean white noise sequences with known covariance:

$$E[\underline{W}(j)\underline{W}(k)^T] = \begin{cases} \underline{Q}(k) & j = k \\ \underline{0} & j \neq k \end{cases}$$

$$E[\underline{V}(j)\underline{V}(k)^T] = \begin{cases} \underline{R}(k) & j = k \\ \underline{0} & j \neq k \end{cases}$$

$$E[\underline{W}(j)\underline{V}(k)^T] = \underline{0}$$

The Kalman filter updates the state estimate $\underline{X}(k)$ and error covariance $\underline{P}(k)$ at the measurement time t_k by:

$$\hat{\underline{X}}(k) = \hat{\underline{X}}(k^-) + \underline{K}(k)\underline{V}(k)$$

$$\underline{P}(k) = \underline{P}(k^-) - \underline{K}(k)\underline{H}(k)\underline{P}(k^-)$$

From one measurement to the next, the state and error covariance are extrapolated as follows:

$$\hat{\underline{X}}(k^-) = \underline{\Phi}(k, k-1)\hat{\underline{X}}(k-1) + \underline{B}(k-1)\underline{U}(k-1)$$

$$\underline{P}(k^-) = \underline{\Phi}(k, k-1)\underline{P}(k-1)\underline{\Phi}(k, k-1)^T + \underline{G}(k-1)\underline{Q}(k-1)\underline{G}(k-1)^T$$

where $\underline{K}(k)$ is the Kalman filter gain and $\underline{V}(k)$ is the innovation process,

$$\underline{K}(k) = \underline{P}(k^-)\underline{H}(k)^T\underline{V}(k)^{-1}$$

$$\underline{V}(k) = \underline{Z}(k) - \underline{H}(k)\hat{\underline{X}}(k^-)$$

and

$$\begin{aligned}\underline{V}(k) &= E[\underline{V}(k) \underline{Y}(k)^T] \\ &= \underline{H}(k) \underline{P}(k) \underline{H}(k)^T + \underline{R}(k)\end{aligned}$$

The above recursive relations are initiated by a priori knowledge of the state and the error covariance at time . Thus,

$$\begin{aligned}\hat{\underline{X}}(0) &= \hat{\underline{X}}_0 \\ \underline{P}(0) &= \underline{P}_0\end{aligned}$$

V. FULL-SCALE STATE SPACE ERROR MODELS

The comprehensive error models, which are the departing point of the models simplifications, are presented in this section (Ref 1).

5.1 Inertial System Error Model

With the latitude-longitude mechanization (x: level east, y: level north, z: up) of the platform orientation, the full-scale inertial system errors model is developed in terms of the following state variables:

- (1) Position errors ($\delta R_e, \delta R_n, \delta R_u$) defined as the computed values minus the true values,
- (2) Velocity errors ($\delta V_e, \delta V_n, \delta V_u$) defined similarly,
- (3) Misalignment angles (ψ_e, ψ_n, ψ_u) defined as angles from the computer axis to the platform axes,
- (4) Accelerometer errors ($\alpha_e, \alpha_n, \alpha_u$)
- (5) Platform drift errors ($\epsilon_e, \epsilon_n, \epsilon_u$).

Because of the limited cross-feed between the vertical loop and the level loop and due to the fact that the vertical loop needs to be stabilized by the barometer altimeter measurement of the altitude, the vertical and the level loops are decoupled.

5.1.1 Inertial System Level Loop State Equations

$$\begin{aligned}
 \delta \dot{R}_e &= ((v_e/R) \tan L) \delta R_n + \delta v_e \\
 \delta \dot{R}_n &= ((v_e/R) \tan L) \delta R_e + \delta v_n \\
 \delta \dot{v}_e &= -\omega_s^2 \delta R_e + (2\omega_{ie} \sin L + (v_e/R) \tan L) \delta v_n - a_u \psi_n + a_n \psi_u + v_e + \xi_e \\
 \delta \dot{v}_n &= -\omega_s^2 \delta R_n - (2\omega_{ie} \sin L + (v_e/R) \tan L) \delta v_e - a_e \psi_u + a_u \psi_e + v_n + \xi_n \\
 \dot{\psi}_e &= \omega_u \psi_n - \omega_n \psi_u + \epsilon_e \\
 \dot{\psi}_n &= -\omega_u \psi_e + \omega_e \psi_u + \epsilon_n \\
 \dot{\psi}_u &= \omega_n \psi_e - \omega_e \psi_n + \epsilon_u \\
 \dot{\alpha}_e &= -(1/T_{ae}) \alpha_e + (1/T_{ae}) \eta_{ae} \\
 \dot{\alpha}_n &= -(1/T_{an}) \alpha_n + (1/T_{an}) \eta_{an} \\
 \dot{\epsilon}_e &= -(1/T_{ee}) \epsilon_e + (1/T_{ee}) \eta_{ee} \\
 \dot{\epsilon}_n &= -(1/T_{en}) \epsilon_n + (1/T_{en}) \eta_{en} \\
 \dot{\epsilon}_u &= -(1/T_{eu}) \epsilon_u + (1/T_{eu}) \eta_{eu}
 \end{aligned}$$

where

- R = radius of the earth
- L = latitude
- ω_s = Schuler frequency
- ω_{ie} = earth rotation rate
- a_i = accelerometer outputs, $i=e, n, u$
- ω_i = gyro outputs, $i=e, n, u$
- T = correlation times
- η = white zero-mean Gaussian noises
- ξ = errors in the gravity vector, $i=e, n$

5.1.2 Baro-Inertial Vertical Loop State Equations

The vertical state equations are:

$$\begin{aligned}
 \delta \dot{x}_1 &= -c_1 \delta x_1 + (1 + c_1 c_4) \delta x_2 + c_2 \delta h_B \\
 \delta \dot{x}_2 &= (2\omega_s^2 - c_2) \delta x_1 + c_2 c_4 \delta x_2 - \delta x_3 + \delta h_B + \delta(a_n - g) \\
 \delta \dot{x}_3 &= c_3 \delta x_1 - c_3 c_4 \delta x_2 - c_3 \delta(a_n - g)
 \end{aligned}$$

where

$$\delta x_1 = \delta R_2$$

$$\delta x_2 = \delta V_2$$

$$\delta x_3 = C_3 (\delta R_2 - C_4 \delta V_2 - \delta h_B)$$

The C_1 values are selected to obtain a desired vertical loop time constant.

5.2.1 Measurement Error Model For TACAN (Ref 1)

The bearing and the range error measurements are:

$$\begin{aligned}\delta \beta &= \beta_{INS} - \beta_{TACAN} \\ &= (y/A) \delta R_e - (x/A) \delta R_n - b_\beta + \eta_\beta\end{aligned}$$

$$\begin{aligned}\delta \rho &= \rho_{INS} - \rho_{TACAN} \\ &= (x/B) \delta R_e + (y/B) \delta R_n - b_\rho + \eta_\rho\end{aligned}$$

where

$$x = R \cos L_{AIC} (L_{AIC} - L_{TACAN ST.})$$

$$y = R (L_{AIC} - L_{TACAN ST.})$$

$$z = h_{AIC} - h_{TACAN ST.}$$

$$A = x^2 + y^2$$

$$B = (x^2 + y^2 + z^2)^{1/2}$$

$$\beta_{TACAN} = \beta_{TRUE} + b_\beta - \eta_\beta$$

$$\beta_{INS} = \beta_{TRUE} + (\partial \beta / \partial x)_{INS} \delta R_e + (\partial \beta / \partial y)_{INS} \delta R_n$$

$$\rho_{TACAN} = \rho_{TRUE} + b_\rho - \eta_\rho$$

$$\rho_{INS} = \rho_{TRUE} + (\partial \rho / \partial x)_{INS} \delta R_e + (\partial \rho / \partial y)_{INS} \delta R_n$$

The TACAN measurement biases b_β and b_ρ are represented as state variables,

$$\dot{b}_\beta = \eta_{b_\beta}$$

$$\dot{b}_\rho = \eta_{b_\rho}$$

5.2.2 Measurement Error Model For ILS (Ref 1)

The localizer measurement λ and the glidescope measurement S are modelled as follows:

$$\begin{aligned}\lambda &= \lambda_{\text{TRUE}} + \delta\lambda - V_\lambda \\ S &= S_{\text{TRUE}} + \delta S - V_S\end{aligned}$$

where V_λ, V_S are zero mean white noise, and $\delta\lambda, \delta S$ are zero mean exponentially correlated variables which will produce two extra state variables. The measurement errors to be used are:

$$\begin{aligned}\delta z_\lambda &= \lambda_{\text{INS}} - \lambda_{\text{ILS}} \\ &= (y/A)\delta R_e - (x/A)\delta R_n - \delta\lambda + V_\lambda \\ \delta z_S &= S_{\text{INS}} - S_{\text{ILS}} \\ &= (B/(A+z)^2)\delta R_u - \delta S + V_S\end{aligned}$$

where

$$\begin{aligned}x &= R \cos L_{A/C} (L_{A/C} - L_{\text{ILS ST.}}) \\ y &= R (L_{A/C} - L_{\text{ILS ST.}}) \\ z &= h_{A/C} - h_{\text{ILS ST.}} \\ A &= x^2 + y^2 \\ B &= (A)^{1/2}\end{aligned}$$

5.3 Simplified Models (Ref 1)

A Kalman filter based on the comprehensive models of the previous section is impractical because of the excessive computation burden on the on-board computer. In order to develop a workable Kalman filter, the underlying models must be simplified. These simplifications will result in the filter performance degradation. Some of these simplifications may result in an unacceptable loss in the performance of the resultant filter. Thus, it is essential that the performance sensitivity to each simplification be evaluated. The rest of this section outlines some of the feasible simplifications.

5.3.1 Simplified Inertial Level Loop

The step-by-step simplifications are performed in the following order:

- Step 1 All the terms in the comprehensive state equations which are of the order of magnitude of w_{1e} are ignored, resulting in removal of the weak coupling between the states. The result will not be the reduction of the number of states, but will make the state transition matrix sparse.
- Step 2 Model the accelerometer output uncertainties by a white noise of appropriate power. This will result in reducing the number of states by two.
- Step 3 The three states modelling the gyro drift rates are removed by replacing the gyro drift by a white noise of appropriate intensity.

After the above three-step simplification, the state equations become:

$$\begin{aligned}\dot{\delta R}_e &= \delta V_e \\ \dot{\delta R}_n &= \delta V_n \\ \dot{\delta V}_e &= -w_s^2 \delta R_e - a_u \psi_n + a_n \psi_u + \epsilon_e + \xi_e \\ \dot{\delta V}_n &= -w_s^2 \delta R_n - a_u \psi_e - a_e \psi_u + \alpha_n + \xi_n \\ \dot{\psi}_e &= w_u \psi_n - w_n \psi_u + \epsilon_e \\ \dot{\psi}_n &= -w_u \psi_e + w_e \psi_u + \epsilon_n \\ \dot{\psi}_u &= w_n \psi_e - w_e \psi_n + \epsilon_u\end{aligned}$$

5.3.2 Simplified Vertical Loop

Although the undamped vertical loop is unstable for the short period during approach and landing, the Kalman filter can be developed using the undamped vertical loop dynamics.

$$\begin{aligned}\dot{\delta h} &= \delta V_u \\ \dot{\delta V}_u &= \alpha_u + \eta_u\end{aligned}$$

where η_u is a white noise representing the term $(-a_u \psi_e + a_e \psi_n)$

5.3.3 Simplified TACAN Model

The state due to the TACAN range bias is removed.

VI. RECOMMENDATIONS

1) All the approximations and reductions which are proposed to achieve simplified models are based on intuition and a thorough knowledge of the laws governing the system. The eventual justification of any simplification must be based on the effect it has on the performance of the resultant filter. This perform analysis was not undertaken during these ten weeks due to the shortage of time. The Air Force Avionics Laboratory has four fully developed, unclassified, transportable software packages:

GCAP

PROFGEN

SOFE

SOFEPL

which are specifically designed to test and evaluate suboptimal Kalman filters. It is recommended that the Kalman filter obtained after each simplification be tested using these four software programs.

2) If the aided inertial navigation system is operating properly, the innovation process of the Kalman filter is a white, zero mean, Gaussian sequence of known covariance. The innovation process can be used to detect and isolate a fault in the navigation system. There are two important methods available for this purpose:

- 1) The multiple model technique.
- 2) The generalized likelihood ratio method.

It is recommended that, using these two methods, software algorithms be developed for the fault detection and isolation for the aided inertial navigation system.

REFERENCES

1. P. S. Mayback, "Filter Design for a TACAN-Aided Baro-Inertial System with ILS Smoothing Capability," AFFDL-TM-7U-52, May 1974.
2. W. G. Heller, "Free Inertial and Damped Inertial Navigation Mechanization and Error Equations," The Analytic Science Corp., Report No. TR-312-2, October 1974.
3. W. G. Heller, "Covariance Propagation Equations for Optimal and Suboptimal Kalman Filter for Integrated Multisensor Inertial Systems," The Analytic Science Corp., Report No. TR-312-1, July 1974.
4. W. G. Heller, "Models for Aided Inertial Navigation System Sensor Errors," The Analytic Science Corp., Report No. TR-312-3, February 1975.
5. S. H. Musick, "A Computer Program for Generating Flight Profile," AFAL-TR-76-247, 1976.
6. E. L. Hamilton, G. Chitwood, and R. M. Revees, "The General Covariance Analysis Program (GCAP), An Efficient Implementation of the Covariance Analysis Equations," Air Force Avionics Laboratory, WPAFB.
7. S. H. Musick, "SOFE: A Generalized Digital Simulation for Optimal Filter Evaluation User's Manual," AFWAL-TR-80-1108, October 1980.
8. R. E. Feldman, S. H. Musick, "SOFEPL: A Plotting Postprocessor for 'SOFE', User's Manual," AFWAL-TR-80-1109, to be published.
9. J. C. Pinson, "Inertial Guidance for Cruise Vehicles," in C. T. Leondes Ed., Guidance and Control of Aerospace Vehicles, McGraw-Hill Book Company, New York, 1963.
10. R. L. Blanchard, "A New Algorithm for Computing Inertial Altitude and Vertical Velocity," IEEE Transactions on Aerospace and Electronic Systems, Vol AES-7, No. 6, November 1971.

1981 USAF - SCEE SUMMER FACULTY RESEARCH PROGRAM

Sponsored by the

AIR FORCE OFFICE OF SCIENTIFIC RESEARCH

Conducted by the

SOUTHEASTERN CENTER FOR ELECTRICAL ENGINEERING EDUCATION

FINAL REPORT

CALIBRATION OF WIDEBAND OPTICAL SIGNAL PROCESSOR (WOSP)

Prepared by: Paul B. Griesacker, Ph.D.
Academic Rank: Associate Professor
Department and University: Department of Physics
Gannon University
Research Location: Rome Air Development Center/IRAP
USAF Research Colleague: Albert A. Jamberdino
Date: August 10, 1981
Contract No.: F49620-79-C-0038

CALIBRATION OF WIDEBAND OPTICAL
SIGNAL PROCESSOR (WOSP)

by

Paul B. Griesacker

ABSTRACT

The physical principles of the operation of an electro-optical signal processor using the Coherent Light Valve to modulate the optical wave and a high resolution vidicon TV camera as the output transducer are discussed. System characteristics are presented. System start up and shut down procedures are suggested and system diagnostics are explained. The results of initial calibration and resolution measurements are presented and an exhaustive list of recommendations relative to future development of the WOSP system are listed.

Research sponsored by the Air Force Office of Scientific Research/AFSC, United States Air Force, under Contract F49620-79-C-0038. The United States Government is authorized to reproduce and distribute reprints for governmental purposes notwithstanding any copyright notation hereon. This manuscript is submitted for publication with the understanding that the United States Government is authorized to reproduce and distribute reprints for government purposes. Further, any news releases, interviews, and all other public statements referring to research sponsored by AFOSR will acknowledge as the supporting agency the Air Force Office of Scientific Research/Air Force Systems Command, United States Air Force.

Acknowledgements

Many thanks are due to the Air Force Systems Command, the Air Force Office of Scientific Research and the Southeastern Center for Electrical Engineering Education for providing the opportunity for the author to spend a very interesting and valuable summer at the Rome Air Development Center, Griffiss AFB NY. The author would also like to acknowledge the Development Center, and in particular the Recording and Analysis Section for its hospitality and excellent working conditions.

Furthermore, he would like to thank Mr. A. A. Jamberdino for suggesting this topic for investigation and for his assistance and leadership throughout the period of the effort. The author also acknowledges many helpful discussions with J. D. Petruzelli and M. Heffron and finally he would like to thank M. F. Lowry for the many hours of invaluable assistance in the laboratory and his numerous useful suggestions.

CALIBRATION OF WIDEBAND OPTICAL SIGNAL PROCESSOR (WOSP)

I. INTRODUCTION

In the past few decades the beginning of a long and lasting union has been in the making between the field of physics known as optics and the field of engineering known as communications. This is understandable since both disciplines encompass the study and design of systems that transmit and analyze information that is carried by waves. In electronics the information is generally of a temporal nature while in the optical case, the information is of a spatial nature. The basis for this union lies in the common analytical approach of Fourier analysis which lends itself naturally to both fields. Much convenience, simplicity and insight is gained by decomposing the information carried by waves into its corresponding frequency spectrum. The Fourier Transform, a well known mathematical operation, becomes an invaluable tool in both disciplines. It yields the temporal frequency spectra of electrical signals and the spacial frequency spectra of optical images. For years the optical scientists have had a simple optical system for empirically generating the two dimensional spatial frequency spectra of two dimensional spatial images, while the communications community have had to devise complicated, expensive and marginally adequate electrical systems to measure the one dimensional temporal frequency spectra of temporal signals. In optics it is the simple converging lens that performs this operation. The converging lens focuses incident parallel rays to a point in its focal plane, as shown in Figure I. Position in the focal plane now is related to direction on the incident wave front. It is well known^{1,2,3} that if the complex field distribution of a wave front across any plane is Fourier Analyzed, the resulting spectrum of spatial Fourier components can be interpreted as plane waves traveling in different directions. One can then see how the converging lens forms the Fourier Transform of an incident wave front in its focal plane. An equivalent statement of the above is that the Fraunhofer diffraction pattern of any object will be imaged in the back focal plane of a

converging lens. Phase is important in this process, therefore the radiation must be coherent for the Fourier Transform in the focal plane to be measureable.

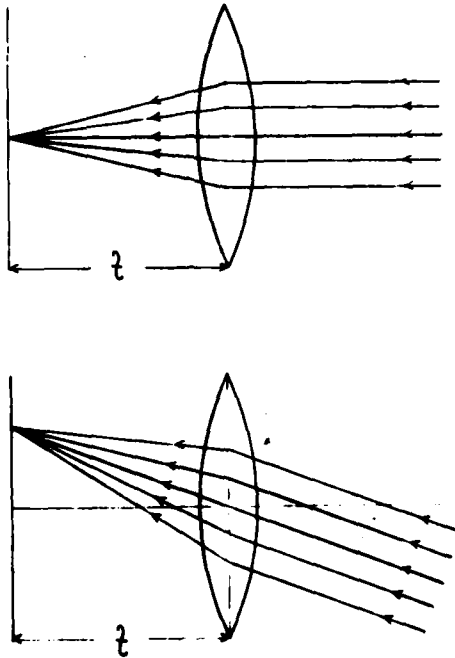


Figure 1. Converging Parallel Rays

The ability to take the Fourier Transform of an electrical signal by optical means, requires that the information carried on the electrical wave be transferred to an optical wave. Then the optical

radiation can be passed through a transforming lens. There are at this time three methods of achieving the above: the Bragg cell^{4,5}, the Hughes Liquid Cristal Light Valve⁶, and the General Electric Coherent Light Valve^{7,8}. This report deals exclusively with the last of these.

Figure 2, shows the essentials of the Coherent Light Valve (CLV). It consists of a rotating glass disc which is continually recoated with a uniform film of transparent dielectric fluid. The fluid is written upon by an electron gun. The charge placed on the surface of the fluid deforms the surface by electrostatic forces and turns the fluid film into a variable thickness transparent layer or a phase object. That is, the film modulates the phase of the transmitted light more than it modulates the amplitude. Without an input signal, the electron gun writes a raster compatible with conventional TV format, have 525 horizontal lines per frame, two fields per frame interlaced at a rate of 60 fields per second. This yields 15,750 lines per second at 63.5 μ s per horizontal line.

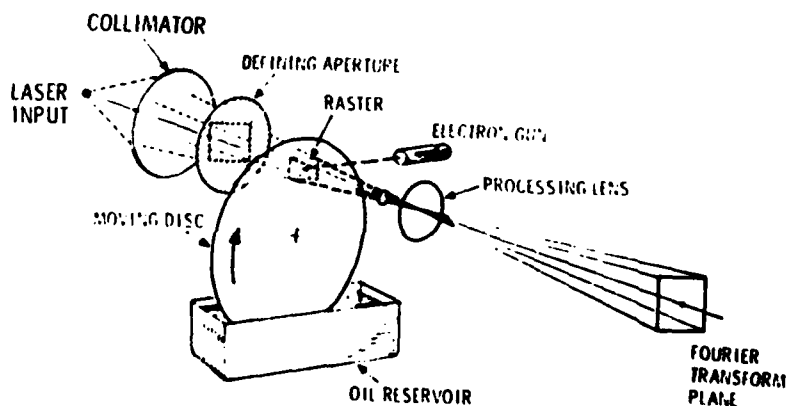


Figure 2. Coherent Light Valve

When an electrical signal is introduced to the input of the CLV the electron gun sweep rate is varied in such a way that the amplitude of deformation of the fluid film is directly related to the amplitude of the input electrical signal. Therefore, the horizontal raster lines, which used to constitute a uniform horizontal phase grating, are modulated by this electrical signal. The modulation continues successively from line to line and introduces a vertical component to the phase grating. The physical properties of the vertical component of the grating are determined by the input electrical signal. Thus, modulation of the incident light by the vertical component of the grating is the method of introducing information in the electrical signal onto the coherent optical radiation. The modulated light then propagates to the processing lens and has its Fourier Transform displayed in the focal plane of the lens, sometime referred to as the Fourier Transform plane.

The raster or grating in the CLV has variation in two orthogonal directions, which in the general case would lead to a situation where the incident light could be scattered to any position in the Fourier Transform plane, but in this case the horizontal spacing of the grating is fixed and only the vertical component of the grating varies. This limits the possible locations in the transform plane where the incident light can be scattered. In fact, the frequency output is configured along locus lines similar to a raster and is referred to as a folded or two dimensional spectrum. Figure 3 demonstrates the configuration of the folded spectrum locus lines.

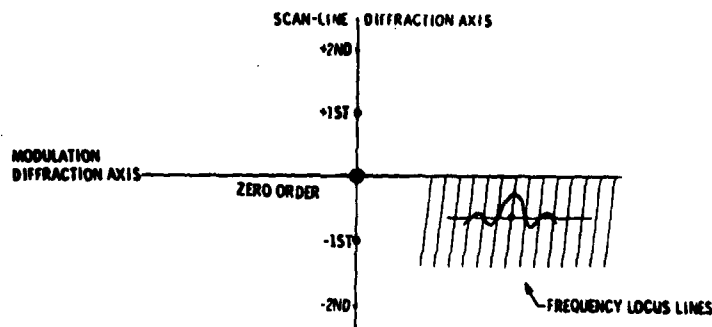


Figure 3. Locus Lines

If a pure tone or a single unmodulated frequency is input to the CLV, the modulation of the horizontal raster lines introduces a vertical component to the grating. If the input frequency is an integral multiple of the sweep rate there will be an equal number of cycles on each horizontal line and the vertical component of the grating can be orthogonal, relative to the horizontal component. In this case the incident beam of coherent light would not only be scattered in a vertical plane by the horizontal component of the grating as described above, but each of these scattered beams would also be scattered, in a horizontal plane by the vertical component of the grating, corresponding to the various orders of the positive and negative spatial frequencies of the vertical component of the grating. This multiplicity of spots will fill the focal plane. However, the information content is redundant from order to order so we restrict ourselves to that portion of the first order which falls in a rectangular area of the fourth quadrant of the focal plane adjacent to the origin of the focal plane, which lies on the optical axis of the system as shown in Figure 3.

These single frequency beam spots or spatial frequency loci are not infinitely small but are actually Fraunhofer diffraction patterns of the illuminated portion of the grating in the CLV raster. Their shape or amplitude distribution then is the Fourier Transform of the illuminated portion of the raster. Since this illuminated portion is rectangular, these single frequency beam spots have the shape of a two dimensional sinc function^{1,2,3,8}. The shape of the sinc function $\frac{\sin x}{x}$ is shown in Figure 4. The distribution of energy in the focal plane for the single frequency beam spot will be proportional to the square of the two dimensional sinc function. Thus, we can see that the energy of a single frequency will be spread all over the focal plane. However, the sinc function damps out quickly and most of the energy in the higher order maxima will be below the detection threshold of any real detector. Note that the zeros of the sinc function are the zeros of the sinusoid in the numerator and are equally spaced, excepting at the origin where the sinc

function has its maximum. There will be a vertical sync function related to the vertical size of the raster and a horizontal sync function related to the horizontal size of the raster.

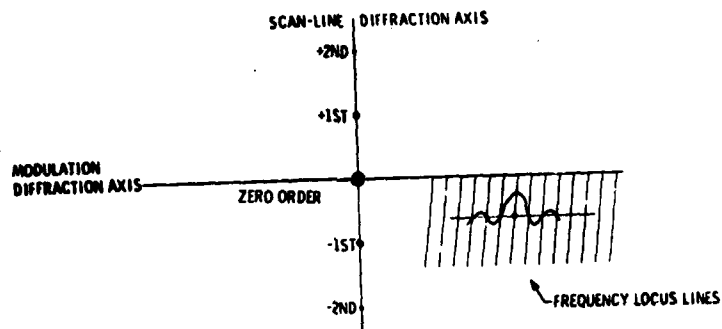


Figure 4. Sync Function

An important consideration in the application of the folded or two dimensional spectrum is the avoidance of the circumstance where a signal falling on one locus line will also fall on adjacent locus lines. This problem is referred to as coarse frequency resolution or interlocus isolation. The ideal case occurs when the central maximum of the sync function falls on one locus line and the zeros fall on all the other locus lines as is shown in Figure 4. Five frequency resolution is

The raster-like configuration of the spectrum locus lines lends itself to detection by a TV camera if the size and orientation of the spectrum locus lines are coincident with the camera raster. This coincidence is insured by imaging the spectrum locus lines in the transform plane onto the raster lines of the active area of a vidicon, by a telecentric lens system^{9,10}. Now frequency which corresponds to position in the transform plane corresponds to time on a horizontal line of the output of the vidicon, and intensity at a position in the transform plane is recorded as the signal amplitude at the corresponding time on a horizontal line of the vidicon output.

The system described above takes the Fourier Transform of an electrical signal by optical means. It is herein referred to as a Wide-band Optical Signal Processor (WOSP).

Without an input signal the CLV will write uniform horizontal raster lines on the fluid film. The collimated beam of laser light is then diffracted into many beams by this uniform horizontal phase grating and beams of light are scattered in directions corresponding to the angles determined by the interference effects of the grating. These directions are determined only by the ratio of the wavelength of the laser light to the grating spacing. In the present case a series of beams would be scattered in a vertical plane, both above and below the unscattered portion of the incident beam leaving the grating. These rays correspond to the various orders of the interface pattern. The scattered beams resemble limited wave fronts traveling in different directions and the processing lens focuses them at different points in its back focal plane as shown in Figure 1. At each of these points in the focal plane will appear an image of the Fraunhofer diffraction pattern of the illuminated portion of the grating. If this diffraction pattern is relatively small the images will appear as points of light in the focal plane.

related to the vertical sync function and the vertical size of the raster.

If the frequency of the signal input to the CLV is not a harmonic of the CLV sweep frequency, the vertical component of the raster cannot be in perfect vertical register and will then not be orthogonal with the horizontal component. Now the scattered beams will not lie in a perfectly horizontal plane and they will be scattered diagonally. As the frequency increases, the scattering will be more diagonal until the frequency again becomes a harmonic of the CLV sweep frequency. The locus lines are diagonal and equally spaced as shown in Figure 3. The image of the radiation in the focal plane is then magnified and imaged on the target of the vidicon camera. And opaque chrome film with an array of parallel slits on the vidicon faceplate, helps improve the interlocus isolation.

An exploratory development model of the WOSP system described above was recently delivered to RADC and the goal of this effort was the calibration of that system.

II. OBJECTIVES

The objective of this effort was to calibrate the exploratory development model of a WOSP system described above which was recently delivered by General Electric to RADC. Stable and reliable operation of a system is a pre-requisite of calibration. Therefore, insuring stable and reliable operation of the system became a primary goal. Given the ubiquitous perversity of large and complicated systems of this nature and the time available for the effort, an optimal approach was undertaken. The specific objectives chosen were:

- a) To bring the WOSP to stable and reliable operation in its new location at RADC and at the same time determine the proper operating conditions of each subsystem.
- b) To determine the proper turn on and shut down procedures for reliable operation by inexperienced personnel.

- c) To identify any unexpected system characteristics.
- d) To identify any improvements that would make the system more reliable and bring it closer to the status for an advanced development model.
- e) To initiate a calibration relative to fine frequency resolution, course frequency resolution or interlocus isolation, and amplitude resolution.

Complete absolute calibration and correlation studies will be left for future investigations.

III. SYSTEM DESCRIPTION

A schematic of the WOSP system is given in Figure 5, where the correlation technique is also shown. This investigation did not attempt any correlation experiments. The block diagram of the WOSP system in Figure 6 shows the wiring layout for the subsystems. All cable here is 75 ohm coaxial cable excepting the ones carrying the correction signals ΔV and ΔH . They are recommended⁹ to be low-capacitance 93 ohm coaxial cable. Referring to Figures 5 and 6 throughout the following discussion will be helpful to the reader. Much of the detail contained in references 8 and 9 is not repeated in this report.

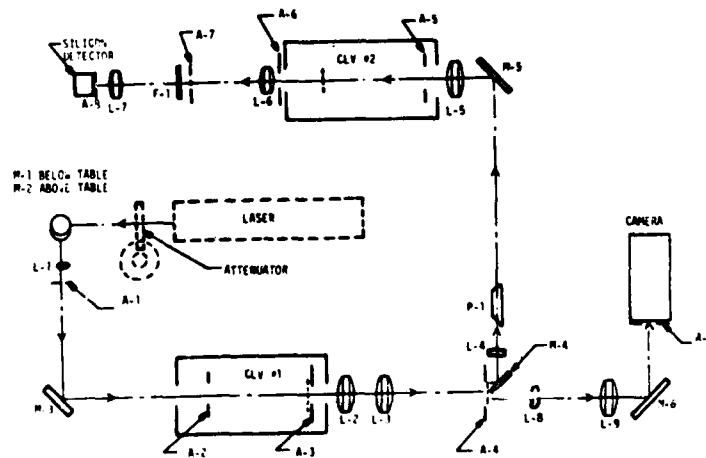


Figure 5. WOSP

AD-A113 708

SOUTHEASTERN CENTER FOR ELECTRICAL ENGINEERING EDUCAT--ETC F/6 S/1
USAF SUMMER FACULTY RESEARCH PROGRAM. 1981 RESEARCH REPORTS, VO--ETC(U)
OCT 81 W D PEELE F49620-79-C-0038

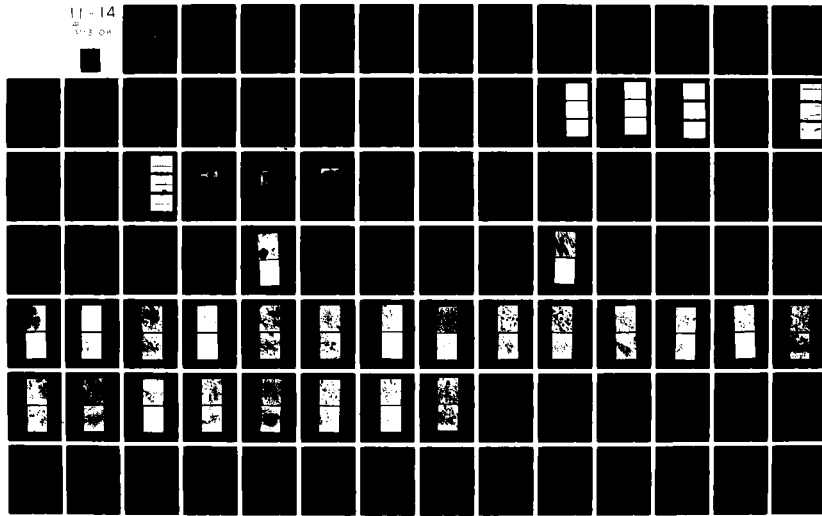
UNCLASSIFIED

AFOSR-TR-82-0227

NL

11-14

103 04



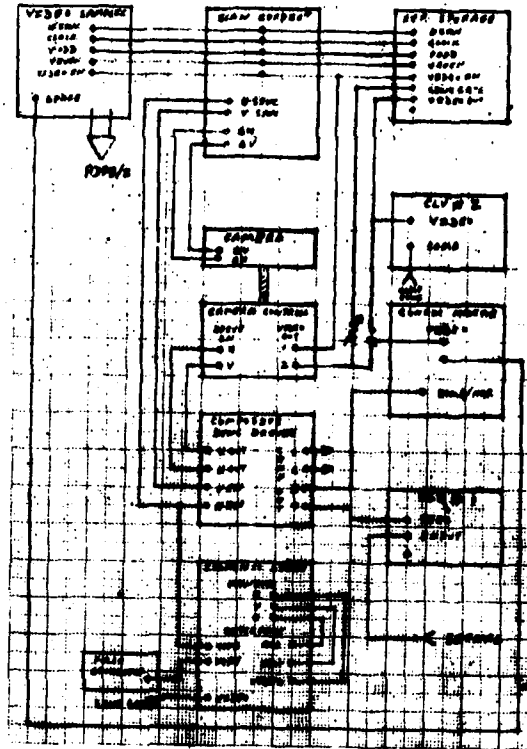


Figure 6. WOSP System

THE LASER

The source of coherent radiation used in this investigation was a Lexcel Model 75(argon-ion) Laser. It was found that when the three phase line voltage to the laser measured approximately 129V per phase, the

laser power supply sustained damage to some components. Voltage measured at the designated test points listed in the laser operating manual were at least ten per cent different than those listed in the manual and most were lower than recommended. Laser current could not be reduced below 11A. Maximum laser current was approximately 15A.

When the line voltage was reduced to approximately 122V per phase, the laser power supply operated properly. The measured voltages at the designated test points were normal and laser current could be adjusted at the CURRENT control from approximately 5A to 15A.

The zener diode Z1 in the laser power supply was replaced by some equivalent components during this investigation.

These components should be removed and replaced by a 1N2997B which was purchased for that purpose. Also, after the microswitch on relay K2 was replaced, the delay time between pressing the POWER ON switch and the lighting of the READY indicator is measured at 20 seconds. This delay is supposed to be 30 seconds, to enable the laser cathode to come to operating temperature.

When starting the laser, the recommended procedure in the laser manual suggests setting the CURRENT control to maximum current before depressing the LASER START switch. This starts the laser at maximum power and a beamstop should be inserted somewhere between the laser and the vidicon camera until the laser has started and the current can be reduced to normal operating levels (between 6A and 8A). This procedure will protect the vidicon target from excessively high light levels which could damage the effected area and possibly change the vidicons response in that region of its target area. A convenient location for insertion of a beamstop is between the laser and the Jodan VBA-200 attenuator immediately following it as shown in Figure 5.

In this investigation the laser was found to operate for hours with little detectable power level drift. However, the amplitude of the information is dependent both on the amplitude of the input signal at the CLV and the laser power, so a beam splitter and laser power monitor should be inserted in the system to monitor any variation of laser power

during periods of data collection.

The system was usually operated with the laser current set at 6A and Jordan VBA-200 variable optical attenuator immediately following the laser in Figure 5 was set at one half its full range.

The optics between the laser and the CLV are well described in Reference 10.

THE COHERENT LIGHT VALVE

The next important component in the WOSP system is the CLV. The theory of the operation and characteristics of Coherent Light Valves are described in detail in References 7 and 8. Operation of this CLV, a PJ-7000 series projector, is discussed in Reference 10 and in the CLV operator's manual. The CLV is the heart of the WOSP system. It modulates the optical wave with the information in the electronic input signal. The CLV raster determines the size and spacing of the grating discussed above. The stability and uniformity of this grating determine the stability and resolution of the WOSP system.

Stability and uniformity of the raster depend on the properties of the dielectric fluid which are strongly dependent on temperature. It is recommended⁸ that the heater never be turned off, (The heater was on throughout the entire period of this investigation) excepting for long periods of storage. In addition, there is a waiting period of about one hour after the ON switch (located at the rear corner of the CLV housing) is turned on, before the COLD/READY indicator on the remote control box indicates a READY condition. After the READY condition is indicated the OPERATE switch may be depressed and the raster can be seen to build up slowly. It has been noticed during this investigation and previously¹¹ that the raster reaches its most stable operating conditions approximately four or five hours after the OPERATE switch is activated. It was also noticed during this study that sometimes between three and five hours after the OPERATE switch had been activated, the raster would disappear and return one or more times over a period of less than one hour, implying that either the current to the electron gun in the CLV

was disrupted or the voltage applied to the deflection plates was sweeping the electron beam out of the field of view. This problem was intermittent and never occurred with enough regularity to permit a study of its cause. Often, the CLV would operate in a stable manner for many hours after this occurrence. For a few days, the CLV was isolated from the power line by an isolation transformer and a variac. The system seemed to be especially stable during that period of time. This took place shortly after the Drive Inverter Board was damaged by the high line voltage.

Heat generated at the CLV causes convection currents in the surrounding air. These currents present a varying index of refraction for the coherent beams of laser radiation entering and leaving the CLV. The result of this is seen as a slow wandering of the scattered beams of light reaching the focal plane and then the vidicon. This beam wander is random and effects both the fine frequency position and coarse frequency position as viewed on the Conrac TV monitor, the Isometric Display, or by viewing the video out of the vidicon on a time delayed oscilloscope. It can be minimized to the point where it will not be noticed from these qualitative measurements, by placing tubing inclosures for the beam path both before and after the CLV. These tubings were constructed of rolled paper and should be sealed with tape to the CLV body around the input and output window. Care must be taken not to burn one's finger on the CLV body, since it is approximately 75°C when at operating temperature. If the tubing is only about 30 cm long, the ends away from the CLV should be masked to achieve the best results.

When the quantitative measurements were attempted, it was discovered that the beam spot for a single frequency input signal appeared on more than one frequency locus line. Noting that the illuminated portion of the CLV raster was not large enough to give the proper sync function as shown in Figure 4, a rectangular mask at the input of the CLV was removed and replaced by a larger mask which illuminated almost the entire raster. The result was that instead of

the beam spot being seen on four or five locus lines, it now could be seen on approximately twenty locus lines. Further investigation showed that when viewing the CLV raster through the output window, a distortion of the raster can be clearly seen in its upper left hand corner. This distortion is always present. It is larger when the OPERATE switch is first activated but its area never gets smaller than approximately 15 per cent of the raster. If masking of the incident laser beam is done in such a manner that this distortion is avoided, the interlocus spreading can be reduced to approximately five locus lines. The input mask should be as close to the input window as possible for best results. Another mask at the output window of the CLV will give a small additional improvement in reducing the size of the beam spot. The shaping and positioning of these masks is very tedious and time consuming. It is helpful to have more than one person doing the shaping and positioning and having a high resolution TV monitor near the CLV is invaluable during this operation. The tubing mentioned above should be removed for this task and replaced afterwards without disturbing the masks. These phenomena have been noticed previously¹¹.

To improve the interlocus isolation, several suggestions were made. The first was to attempt to use the other CLV used in previous correlation studies¹⁰, but use of this older design tube was not advised¹¹. Another suggestion of apodization at the input mask will reduce the amplitude of the secondary maxima of the sync function, but it will also increase the distance between the two zeros of the central maximum, a result also found in the process of windowing¹² of antenna apertures. Another suggestion¹¹ was to reduce the speed of the rotating disc in the CLV and then possibly reduce the amount of the distortion in the raster. Another suggestion was the use of a lens to magnify the uniform portion of the raster by a factor of two and double the number of horizontal lines by using the 1024 line potential of the CLV and changes the sweep rate in an appropriate manner. There was not enough time to try either of the last two suggestions.

The transfer optics between the CLV and the vidicon are described in detail in reference 10. This is the region of the Fourier Transform plane, and the location where the transfer optics to the second CLV are located to perform correlation experiments as shown in Figure 5. They are also described in reference 10.

THE FOCAL PLANE OUTPUT TRANSDUCER

The detector that measures the Fourier Transform of the input signal or the unit that records the intensity of radiation as a function of position in the focal plane is a high-resolution vidicon camera. A General Electric TE31A-CCTV Camera system, coupled with horizontal and vertical scan correction circuits, converts the optical Fourier Transform into video form for further processing and is referred to as a Focal Plane Output Transducer (FPOT or a Scan Corrected Output Transducer⁹). In this system horizontal and vertical spatial reference filters are made an integral part of the vidicon tube to yield reference signals for the scan correction circuits as described in reference 9.

The video output from the vidicon can be monitored visually by a Convac RQA-14 high resolution TV monitor⁷ and an Isometric Display^{7,8}. The Isometric Display consists of an HP1300A electrostatic deflection TV monitor with an Interface Unit that produces a pseudo three-dimensional display. For stable operation of the Isometric Display the vertical sync pulses to the Interface Unit are taken from a Systron-Donner 106A Data Pulse pulse generator. The pulse from the 106A is approximately 2V negative, about 180 μ s long, triggered by the V-OUT sync pulse from the Composite Sync Driver and delayed by approximately 180 μ s. Both the delay and the width here are about the time length of three horizontal sweeps. The horizontal sync for the Interface Unit is taken from H-OUT on the Composite Sync Driver.

From Figure 6 one can see that the Scan Correct Unit not only supplies the entire WOSP system with clock and sync pulses, but also supplies the horizontal and vertical sweep corrections ΔH and ΔV to the vidicon. These corrections should compensate for any sweep errors that

might be present in the camera. During this investigation the automatic correction procedures did not seem to improve the camera's response to uniform illumination of the vidicon target. This conclusion was based on the assumption that uniform illumination of the vidicon target should yield uniform video output on each horizontal line.

The video output of any single scan line may be readily observed by using the Isometric Display and the reticle generated by Reference Storage Unit¹⁰. The Reference Storage Unit¹⁰ is used in correlation studies to store the Fourier Transform of any signal of interest, for later use in correlation experiments¹⁰. The Reference Storage Unit generates a reticle consisting of one brightened scan line from the vidicon. The identity of this particular scan line is determined by the LINE SELECT control. The video of the brightened scan line is available at the LINE GATE output of the Reference Storage Unit. Viewed on the Conrac, the reticle appears as one line which is brighter than the others. Viewed on the Isometric Display, the reticle stands out above all the other scan lines in the apparent Z direction. In this manner the video level of any scan line can be examined.

Since the Scan Correct procedures⁹ did not give a uniform video level on all scan lines for uniform illumination of the vidicon target, another procedure was used in this investigation. With uniform illumination incident on the vidicon target, almost uniform video, as registered on the Isometric Display, was obtained by manually adjusting the vidicon position and orientation¹⁰ and adjusting the horizontal and vertical CENTER and SIZE controls on the Sweep and Align circuit board of the Camera Control Unit (Figure 6).

Before these adjustments are made, the manual and automatic corrections from the Scan Correction Unit should be zeroed. The automatic corrections are zeroed by operation of the H-ZERO and V-ZERO controls. The manual corrections are zeroed by viewing the ΔH and ΔV outputs of the Scan Correction Unit with an oscilloscope and zeroing these by adjusting the CENTER, SIZE and SCEW controls for both vertical and horizontal corrections.

The Isometric Display^{7,8} consists of an HP1300A electrostatic deflection display with an Interface Unit that produces a pseudo three-dimensional display. This type of display^{7,8} is very useful for examining the alignment of the vidicon. Since the signal level across each horizontal scan can be examined while a uniform illumination of the vidicon is being displayed. The Line Select cursor from the Reference Storage Unit will offset each horizontal sweep for individual examination. Any deviation of a flat response across the horizontal line will indicate a misalignment of the vidicon horizontal sweep relative to the Spatial Reference Filter mask⁹ on the vidicon faceplate.

If the Isometric Display gives an indication that the vidicon tube should be rotated in its yoke, the high voltage should be turned off during any manual manipulation of the tube. It is also important to note that the tube is clamped by a rubberlike retaining ring near the faceplate end. Manual rotations are accompanied by an immediate springing back, which removes part of the manual rotation and a gradual creeping back toward the original orientation that lasts for more than one day. Precise horizontal sweep alignment relative to the Spatial Filter Mask will take several days. This alignment should be coupled with adjustment of the VERTICAL CENTER control and VERTICAL SIZE control on the Sweep and Align circuit board in the Camera Control Unit. Some adjustment of the HORIZONTAL CENTER and HORIZONTAL SIZE control on the same board will be necessary also. It seems that these H and V controls do not behave in an orthogonal manner.

THE VIDEO SAMPLING UNIT

The Video Sampling Unit^{9,10} contains a fast analog-to-digital converter and a limited memory. It strobos data into its memory from one TV frame and transfers these data to the digital computer's memory through the computer's interface unit. It transfers a maximum of 2048 binary words per sample from a given TV frame. The location of the sample from the frame is operator controlled by input parameters at the computer terminal. The Video Sampling Unit divides each video line into

32 cells and will assign the average value of the video level in each of 16 samples per cell to the respective sample. These values are represented in the software unit range from 0 to 255 (saturation). A total of 16 samples in each of 32 cells per video line with 480 active lines implies a possible 245,760 samples per frame. The maximum sample size available with this unit is 2048 or 0.83 per cent of the data available in one frame. It takes the PDP8/I approximately five minutes to print out the sample data for one sample. At this rate, it would take more than ten hours to get a hard copy of an entire frame if the present system is used. In practice only a limited bandwidth of the output will be of interest. However, for a full bandwidth calibration this system would be too slow.

Since each locus line or video line contains a frequency band of 15750HZ, the 16 samples per cell for 32 cells per line implies a band of 30.76 HZ per sample which appears to be adequate considering the system's reported^{8,9} fine frequency resolution of somewhat less than 150HZ.

The Display Module Unit in the Video Sampling Unit permits monitoring⁹ the video input to the Video Sampling Unit and this same video input to the A/D converter with its horizontal sync pulses removed. There are also VIDEO GAIN and DC LEVEL controls on the Display Module which are used to add gain up to a maximum of a factor of three and to adjust the minimum signal level that will be sent to the A/D converter. While monitoring the input to the A/D converter⁹, the two controls above should be adjusted so that the maximum video at the A/D converter is not more than 1.0 volt and the minimum video is not less than 0 volts. Excursions outside this range will be clipped by the A/D converter. For reliable operation, the video input to the Video Sampling Unit should not be more than 1.0 volt peak to peak. A typical single horizontal line of video signal from a CW tone input at the CLV is shown in Figure 7-a.

For this signal, the peak to peak amplitude has been determined mainly by the laser power level, the amplitude of the CW input to the CLV, and the MANUAL ADJ. control on the Camera Control Unit. It can be seen that less than 60 per cent of the peak to peak value of the video is useful signal information. This adjustment should be set for the largest expected input signal in any given application since larger signals would lead to saturation at the Video Sampling Unit.

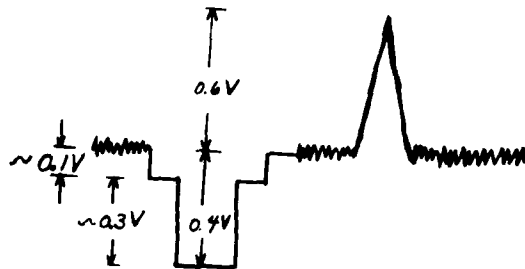


Figure 7-a. CW Tone Input



Figure 7-b. Typical Output

An example of a typical output from the Display Module Unit is presented in Figure 7-b, where the noise level is close to zero and the signal level is less than 1.0 volts. A signal of 1.0 volt or above is saturated (255 SU) and the noise should be about 1 to 5 SU for reliable recording of data. Reducing the noise to zero SU with the DC LEVEL control on the Display Module Unit can lead to misinterpretation of some data.

The digital circuits of the Video Sampling Unit and the PDP8/I software for processing the data transferred are discussed in reference 9. A pair of vertical cursors which identify the sample of data chosen by the operator at the computer terminal can be displayed on the Conrac TV monitor and the Isometric Display as a visual reference for the operator. The cursor is available from the output jack on the Video Sampling Unit marked SPARE as shown in Figure 6. During this investigation, the cursors which were originally thin vertical lines, as shown in reference 9, became broad vertical bars approximately one cell wide. There was not sufficient time during this effort to determine the cause of this problem.

IV. DIAGNOSTICS

Any attempt to take meaningful data raises questions about current system reliability. For this reason, some recommended operating procedures and system reliability checks are included in this section. Many of these suggestions will be specific to the actual laboratory conditions during this investigation.

Before initiating the recommended start-up sequence presented below, the inter system cable connections in Figure 6 should be verified and all power connections to the system should be made to the same column. The latter will avoid ground fault problems encountered early in this investigation. Since the Laser has no electrical connection to the rest of the system at this time, it need not be included in the latter suggestion above. If, however, in the future, the laser power

supply is connected to the rest of the system by some form of AGC feedback circuit, the above suggestion would apply. Before start-up, all subsystem power switches should be in the OFF mode. Their circuit breakers 12, 14, 15, 16, 17, and 18 on the service panel of column 7 may be closed. Circuit breaker 10 of that panel is never turned off, so that power will always be supplied to CLV heater circuit as mentioned in Section III. After appropriate adjustments have been made to the laboratory temperature control system, the following procedures¹⁰ may be started.

START-UP SEQUENCE

- 1) Turn on the CLV's ON/OFF switch (located at the rear corner of the CLV). Wait for the COLD/READY indicator on the CLV's remote control box to show a READY condition. This takes a little less than one hour. During this period the rest of the start-up sequence may be completed.
- 2) Depress the ON/OFF toggle on the Camera Control Unit to the ON position.
- 3) Turn ON the power switches of the TV monitors, the Isometric Interface Unit, the Systron-Donner pulse generator, the CRT's and the reference signal generators. The signal generators need not be connected to the input of the CLV until it is in the OPERATE mode.
- 4) Depress to the ON position, the power switches on the Reference Storage Unit, the Scan Correction Unit and the Video Sampling Unit.
- 5) If desired, the PDP8/I may now be turned on by this sequence:
 - a) Depress the POWER key.
 - b) Mount the tapes on the Tape Unit by setting the LOCAL/OFF/REMOTE switches to LOCAL and manually winding at least ten feet of tape on both take-up reels. Set the LOCAL/OFF/REMOTE switches to REMOTE.
 - c) Register the decimal number 7605 on the console. Depress the LOAD ADD key then depress the START key.
 - d) Type EXE ILOOP4 at the terminal and depress the CARRIAGE RETURN

key.

If the bootstrap has been previously entered into the PDP8/I the machine will spend approximately five minutes cycling through the tapes before printing out the prompt TYPE IN FIRST ROW. If the bootstrap is not in memory, the computer will not respond to the CARRIAGE RETURN key. Instructions for entering the bootstrap are taped to the PDP8/I console.

- 6) Shortly before laser power is desired, the Laser may be started. The Laser has a finite lifetime and needs no more than about one half hour of operation to stabilize, to an operating condition where laser power drift is not noticeable. The following sequence is partly¹⁰ recommended in the laser operators manual.
 - a) Turn on the Laser's cooling water supply. Change the water filter if it is plugged and restricts the flow rate.
 - b) Insert a beam stop in the WOSP system between the Laser and the vidicon target to prevent burning of the target, since the Laser starts at maximum beam current. When placing a beamstop between the Laser and the JODON attenuator, shown in Figure 5, do not reflect the laser beam directly back on itself and back into the laser cavity.
 - c) Turn on the Laser's main power switch located on the service panel of column 9. Notice the indicator lights on the Laser Power Supply and refer to the instruction in the operator's manual.
 - d) If a ready condition is indicated, depress the POWER ON switch and wait until the READY indicator lights. Turn the CURRENT control to maximum current (full clockwise) then depress the LASER START switch. The green laser beam should appear immediately indicating that the Laser has started. Now turn the current down to approximately 6A and remove the beamstop when laser radiation is desired into the system.
- 7) When the COLD/READY indicator on the CLV remote control box shows a READY condition, depress the OPERATE switch and observe the buildup

of the CLV raster. The signal generator and or other input sources can now be connected to the CLV input. Use the attenuator if input signals greater than 0dbm are expected.

The scan correction procedure recommended in Section III can be performed without the Laser or the CLV. A source of uniform illumination for the vidicon target can be made from a naked light bulb and a piece of diffusing material like a piece of milk glass or ground glass. This light source can conveniently be inserted between L-3 and A-4 of Figure 5.

The system shut-down sequence is not exactly the opposite of the start-up procedure. Therefore, the sequence suggested from this investigation is given below.

SHUT-DOWN SEQUENCE

- 1) Disconnect all inputs to the CLV or increase the attenuators in that circuit to maximum attenuation. The input units and signal generators may now be turned off.
- 2) It is now a good time to put a beamstop at the output of the Laser before the Jodon attenuator in Figure 5. Since the Laser is operating, one can see where the reflected beam will fall. It is suggested¹¹ that the reflected beam be positioned on the housing of the Laser head, but not back into the laser cavity. The Laser may be turned off by pushing the POWER OFF switch. The POWER and READY indicators will go off the and Laser is de-energized. The LINE and FUSE indicators will remain lighted until the circuit breaker in the service panel on column 9 is opened.

N.B. Allow cooling water to flow for 5 minutes after POWER OFF switch has been pressed. If the Laser is not being operated, the cooling water should be turned off to prevent excessive condensation in the Laser head and power supply.

- 3) Depress the STAND BY switch on the remote control box of the CLV to the STAND BY condition. The ON/OFF switch (located at the rear of the CLV) may now be turned to OFF.

- 4) If the PDP8/I is on, the turn-off sequence is recommended as follows:
 - a) Depress the STOP switch.
 - b) Remove the tapes from the Tape Unit by setting the LOCAL/OFF/REMOTE switches to LOCAL and manually rewinding the tapes from the take-up reels. Set the LOCAL/OFF/REMOTE switches to REMOTE.
 - c) Turn the POWER key to the OFF position. Now circuit breaker 14 on the service panel of column 7 may be opened.
- 5) Turn off the ON/OFF switches of the TV monitors, the Systron-Donner pulse generator, the Isometric Display Interface Unit, the Reference Storage Unit and the Scan Correction Unit.
- 6) Turn the power ON/OFF switch of the Camera Control Unit to the OFF position.
- 7) After a check of all ON/OFF switches to make certain they are all in the OFF mode, circuit breakers 12, 14, 15, 16, 17, and 18 on the service panel of column 7 may be opened and the circuit breaker on the service panel of column 9 may be opened to remove power from the Laser. Circuit breaker 10 on column 7 is never opened. It supplies power to the heater circuit of the CLV.

Remember not to let the laser cooling water run for more than 5 minutes after the laser POWER OFF switch has been pressed.

SYSTEM CHECKS

Before a signal is input to the CLV or the Laser is turned on, the Conrac monitor and Isometric Display can give some indications of system performance. With no illumination of the vidicon target, the rasters of both monitors should appear much like commercial TV screens with no signal at the antenna, displaying a stable uniform raster of uniform brightness. There are, however, two obvious artifacts due to uneven response of the vidicon target. One is a thin circular arc of brighter than normal video in the upper right quadrant of the TV screen, and the other is a pair of broad bars which appear brighter than normal video in

the lower left quadrant of the screen. They can also be seen on the Isometric Display and appear as in Figures 14, 15, 21, 23, and 25 of reference 9. These artifacts were not able to be removed by any scan correct procedure tried during this investigation.

The Isometric Display will not present a stable display unless the vertical sync is stretched and delayed as described earlier in Section III. A schematic of the Interface Unit of the Isometric Display appears on page 26 of reference 8.

After stable and normal response of the monitors is realized, it is informative to examine the raster of the CLV. The initial examination should be done with the Laser off or with the beamstop inserted. The CLV raster should appear uniform, rectangular and stable when viewed through the output window of the CLV. The raster appears as a blue fluorescence on a dark background. There is one artifact apparent in the CLV raster which appears as a thin bright circular arc in the upper left quadrant of the raster as shown in Figure 8-a. This artifact has always been present in this CLV¹¹ and a recommendation¹¹ to slow down the rotation rate of the rotating disc may improve the situation but was not attempted during this investigation and is not expected to remove the problem entirely. As mentioned above, the CLV raster reaches its most stable condition after about four hours of operation. When the Laser beam is introduced through the input window of the CLV, the Laser illuminated portion of the raster can be seen through the output window. This observation carries with it the potential of eye damage to the observer; all necessary precautions should be taken during this observation. The line of sight used should make the largest possible angle with the direction of the unscattered Laser beam. The intersection of the Laser beam and the CLV raster will not be easily discernable unless the Laser beam current is at least 9A or more, with the Jodon attenuator set at one half its full range. For this observation, a beamstop should be placed somewhere between L-3 and the vidicon window A-9 shown in Figure 5. A convenient place for the

beamstop is near A-4 in Figure 5. For best results, the illuminated portion of the CLV raster should avoid the edges and the artifact mentioned above as described in Section III and shown in Figure 8-b. The input mask discussed in Section III determines the position and size of this illuminated portion of the CLV raster. This observation need not be done unless there is indication that there might be a related problem. It is a most useful observation when adjusting the input mask at the input window of the CLV.



Figure 8-a. CLV Raster

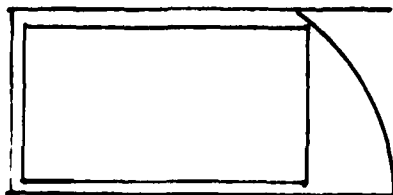


Figure 8-b. Recommended Illuminated Area

When the Laser beam is incident on the CLV raster, no Laser light should be scattered to the target of the vidicon unless there is a signal applied at the input of the CLV. This is so because the zero order unscattered beam is stopped by the beam splitter M-4 in Figure 5. Also, mask A-4 stops all scattered Laser light except that falling in the region of interest in the fourth quadrant of the focal plane is shown in Figure 3. There should be very little change noticed on the monitors when the Laser is turned on with no input signal at the CLV. Under these conditions, a vertical row of small bright beamspots should be seen on the edge of the beam splitter M-4.

TEST MODES

Test signals that are useful for system alignment and reliability checks are well described in reference 10. These four test modes were found to be quite valuable during this investigation for doing qualitative frequency calibrations as are done in reference 10 and evaluating long term drift and stability of the system. It was noticed that drift was minimized and stability was maximized after about four hours of operation of the CLV. Small adjustments in the spatial size and position of the test modes can be made by adjustments to the H-SIZE and V-SIZE controls on the CLV.

When viewing the test modes on the monitors do not forget that there is a 90° rotation of the vidicon involved so that the frequency locus lines are parallel to the scan lines of the camera. Information that is located at the top of the aperture A-4 from left to right as viewed from L-3, appears along the left edge of the Convac monitor from bottom to top. The focal plane information at the bottom of the aperture in A-4 appears at the right side of the Conrac monitor. The format of the Isometric Display is quite variable by manipulation of the Jog-Stick on the Isometric Interface Unit, but the relative orientation of the test modes can be correlated with the orientation of the vidicon artifacts in the Isometric Display raster, as mentioned above.

SYMPTOMS

Some details to look for when observing the test modes are: beam

spot size, beam spot position, beam spot wander and beam spot jitter. Beam spot size was discussed in Section III and the best that was possible during this investigation was to reduce the beam spot distribution to five video lines. This condition is not new¹¹ for this CLV as is apparent from Figures 46 and 51 of reference 9. If the beam spot size is larger than this, the masking at the CLV discussed in Section III should be checked. Beam spot position for the various test modes can be compared with the results in reference 10. Small changes can be made by adjusting the H-SIZE and V-SIZE controls on the CLV. Rotating and translating the vidicon also determines the beam spot position, but this is a tedious adjustment and need not be done unless the system has been physically disturbed. Beam spot wander, a slow drift of the beam spot in random directions as viewed on the monitors is usually corrected by enclosing the beam path in tubing that isolates the air in the beam path from air currents. This is especially true close to the CLV, since it is a source of heat. Beam spot jitter, a very erratic and quick random motion of the beam spot about some average position, is probably not caused by distortions in the CLV from mechanical causes like wobble of the rotating disc or improper flow of the dielectric fluid, since there would tend to vary slowly. However, electronic noise could cause the raster to be written in an erratic manner from improper horizontal or vertical sync or improper operation of the Cathode Current or Grid Drive circuits of the CLV. The jitter could be caused by improper horizontal or vertical sync in either the CLV, the vidicon, or the monitors.

During this investigation, there were times when jitter was not observed and there were times when it was observed. Always there were more serious problems to address and a detailed study of this problem was not possible in the time available. However, monitoring of various signals in the system by adding a tee and running a cable to one of the oscilloscopes introduces impedances mismatches with the resulting loading down of some circuits and unwanted reflections in others. The

last time jitter was observed was at the end of this investigation when there were many tees and many multiple connections for which the system was not designed. It is suspected that this condition may be at least part of the jitter problem. Furthermore, when the system was demonstrated for the new IR Division Chief, all extraneous connections had been removed and jitter was not observed.

The few times that the CLV raster disappeared while the system was operating, as described in Section III, the beam spot was observed to move quickly off the monitor screen by following its video line to the left edge of the screen, which corresponds to the high frequency side of the spatial frequency locus line. The beamspot then did not reappear on the screen even at higher frequencies. The beamspot would return to approximately its former position when the CLV raster automatically built back up. The CLV raster usually built back up to its former operating condition within a few minutes. The cause of this phenomena was not discovered during the course of this investigation.

SYNC PULSES

It is apparent from Figure 6, that the Scan Correction Unit is the source of sync and clock pulses for the entire WOSP system. On the back panel of the Scan Correction Unit, as seen in Figure 13 of reference 9, there are two sets of output jacks, one set for the Camera and one set for the Video Sample Unit. These sync signals are presented here for future reference.

The odd vertical sync from the Scan Correction Unit (SCU) to the Video Sample Unit is compared to the vertical sync from the SCU for the Camera in Figure 9-a. The scale for both signals is 2V/DIV. Both signals are almost 2 volts positive with the blanking pulse going to zero. Note that the blanking pulses start in perfect time register but the Video Sample Unit blanking pulse is about 20 μ s longer. Figure 9-b compares the horizontal sync from the SCU to the Video Sample Unit to the horizontal sync from the SCU for the camera. The scale for both signals is 2V/DIV. Both signals are positive with the blanking pulse

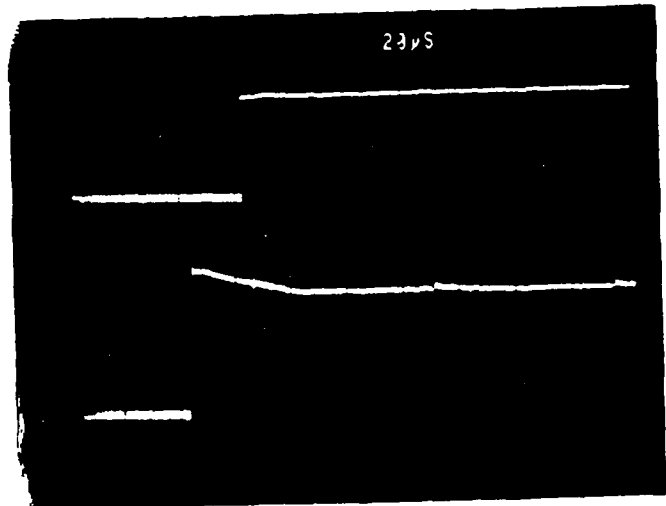
going to zero. It is suspected that the overshoot and ringing is due to impedance mismatches caused by adding tees at the output of the SCU and attaching the oscilloscope cables without attempting to match impedance. Figure 9-c, which displays the same information as Figure 9-b but with a different time scale, shows that the blanking pulses differ in duration by at least a factor of three and blanking pulse to the Video Sample Unit starts about 5 μ s later than the blanking pulse for the Camera. Note the high frequency artifact in horizontal sync signal for the Camera.

The sync signals from the SCU for the Camera go first to the Composite Sync Driver Unit as shown in Figure 6. In Figure 10 some of the inputs and outputs of the Composite Sync Driver are shown. In Figure 10-a, the vertical sync for the camera (V-IN) to the Composite Sync Driver with V-OUT from the Composite Sync Driver to the Camera Control Unit. The scale for both signals is 2V/DIV. Both signals are positive with the blanking pulse going to zero. Both blanking pulses are in perfect time register. Figure 10-b compares the horizontal sync signal for the Camera (H-IN) to the Composite Sync Driver to the Camera Control Unit. The scale of both signals is 2V/DIV. Both signals are positive with the blanking pulses going to zero. Both blanking pulses are in perfect time register. Figure 9-c displays the same information but with a different time scale. Note the high frequency artifact in the horizontal sync signal for the Camera. It is suspected that the overshoot and ringing in H-OUT from the Composite Sync Driver is due to impedance mismatching.

In Figures 11-a and 11-b the composite sync signal from the Composite Sync Driver is compared to the vertical sync for the camera (V-IN) and the horizontal sync for the camera (H-IN). The scale for all these signals is 2V/DIV. As above, the V-IN and H-IN signals are positive at 2V with the blanking pulses going to zero. However, the composite sync signal is positive at about 4V with the blanking pulse going to zero. Both the vertical and horizontal pairs of blanking

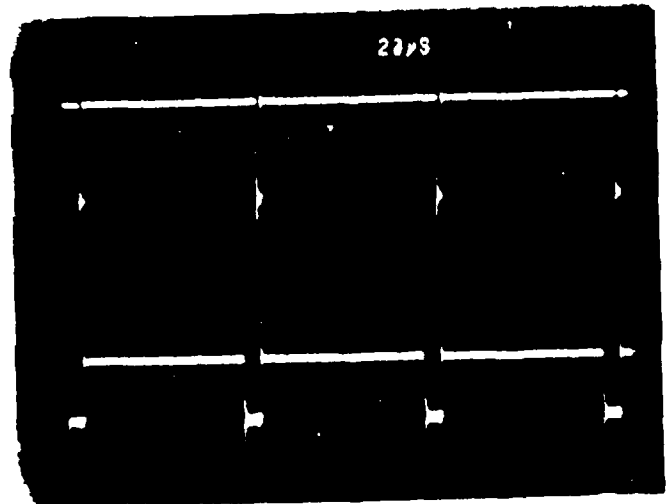
9-a) Vertical sync to the Video
Sample Unit (odd)

Vertical sync for the Camera



9-b) Horizontal sync to the Video
Sample Unit

Horizontal sync for the Camera



9-c) Horizontal sync to the Video
Sample Unit

Horizontal sync for the Camera

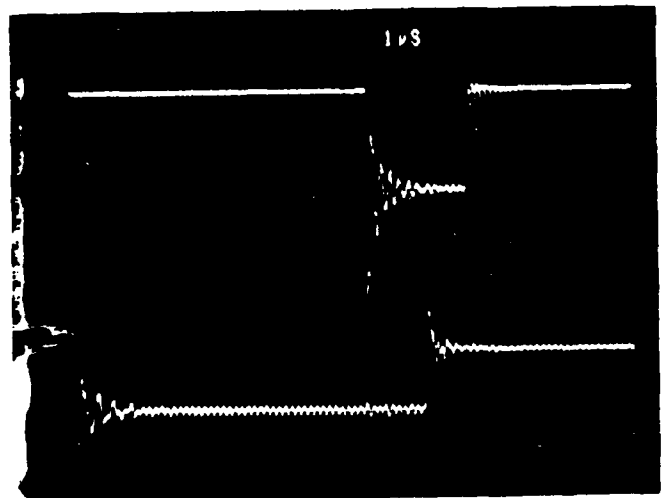
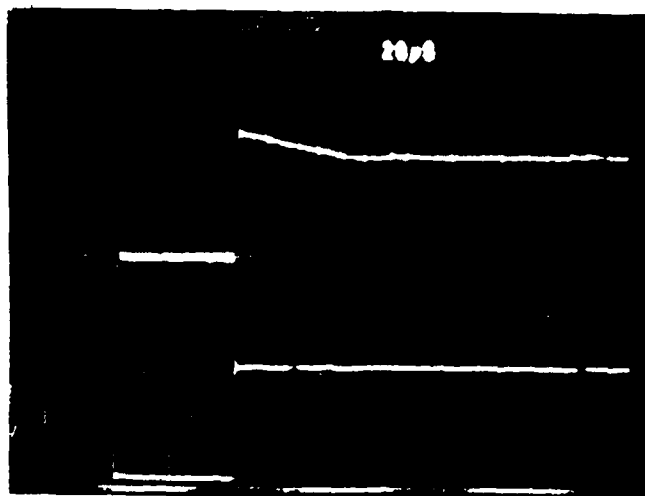


Figure 9. Horizontal and Vertical
Sync Signals

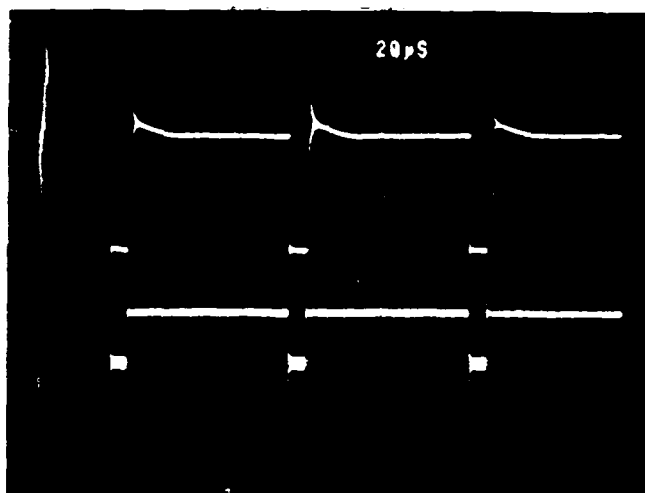
10-a) Vertical sync for the Camera
(V-IN)

V-OUT from the Composite
Sync Driver



10-b) H-OUT from the Composite
Sync Driver

Horizontal sync for the
Camera (H-IN)



10-c) H-OUT from the Composite
Sync Driver

Horizontal sync for the
Camera (H-IN)

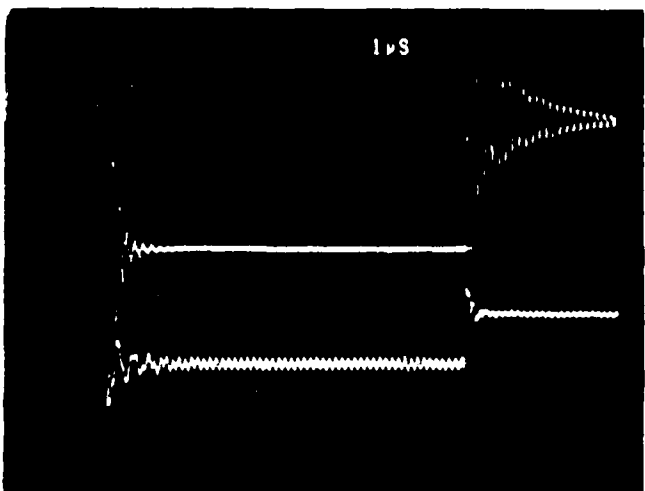
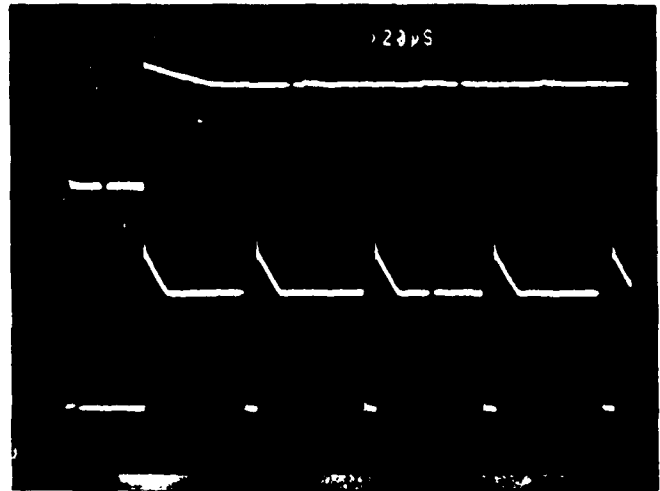


Figure 10. Horizontal and Vertical Sync Signals

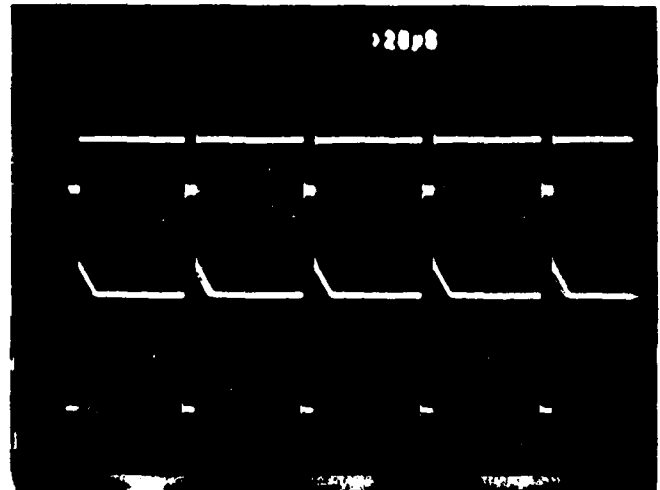
11-a) Vertical sync for the
Camera (V-IN)

The composite sync signal
from the Composite Sync
Driver



11-b) Horizontal sync for the
Camera (H-IN)

The composite sync signal
from the Composite Sync
Driver



11-c) CLOCK from the Scan Correct
Unit

Horizontal sync signal for
the Camera

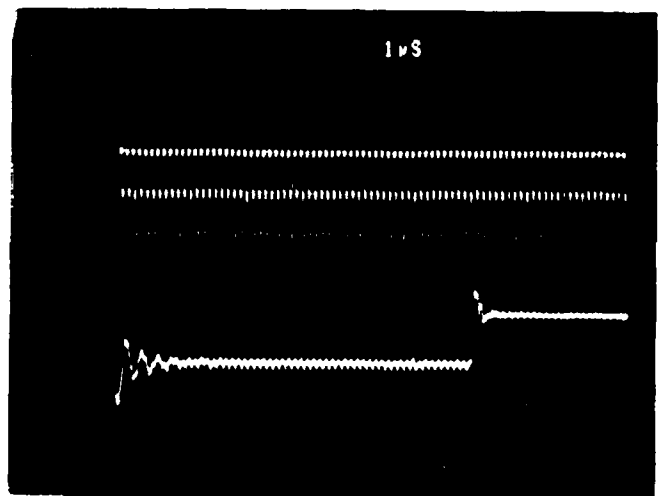


Figure 11. Composite Sync Pulse

pulses are in perfect time register. The purpose of the 5V peaks on the composite sync signal was not determined during this investigation. Figure 11-b compares the CLOCK signal from the SCU with the horizontal sync signal for the Camera. The horizontal sync signal for the camera is displayed at a scale of 2V/DIV as before and the CLOCK signal is displayed at 5V/DIV. This figure identifies the artifact in the horizontal sync signal to the camera as being from the CLOCK signal.

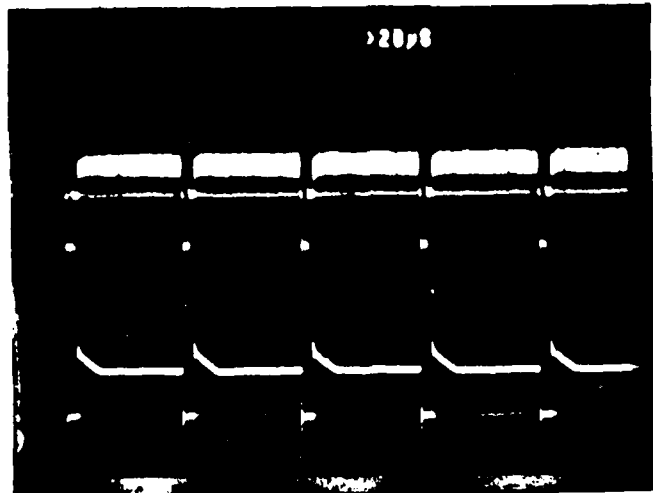
In Figure 12 some characteristics of the video from the Camera Control Unit are shown. In Figure 12-a VIDEO OUT #1 from output jack J4 on the Camera Control Unit is compared to the composite sync signal. The scale of the VIDEO OUT #1 signal is 0.2V/DIV and the scale of the composite sync signal is 5V/DIV. The VIDEO OUT #1 signal is a negative pulse with maximum negative of -4V at the bottom of the blanking pulse. In Figure 12-b VIDEO OUT #1 and VIDEO OUT #2 from output jack J5 on the Camera Control Unit are compared. The scale for both signals is 0.1V/DIV. Both signals are in perfect time register. The CLOCK signal seems to be present in VIDEO OUT #2 but not detectable in VIDEO OUT #1. During this investigation, VIDEO OUT #1 was sent to the Video Sample Unit to avoid any problems that might arise from the CLOCK signal in VIDEO OUT #2. Figure 12-c displays VIDEO OUT #1 from the Camera Control Unit with a different time scale. The scale of this signal is 0.2V/DIV as above. Here it is clear the video out of the camera has $18\frac{1}{2}$ blank lines per frame. Which for the standard 525 lines per field and $262\frac{1}{2}$ lines per frame, $18\frac{1}{2}$ blanklines per frame implies a possible maximum of 244 active lines per frame or 488 possible active lines per field. However, it is stated on page 107 of reference 9 that there are 240 active lines per field and the Video Sampling Unit only reads a maximum of 240 scan lines from each frame.

V. RESULTS

The results of some measurements are presented in this section. They constitute an attempt to begin calibration of the WOSP system. However, much of the time spent with the system during this

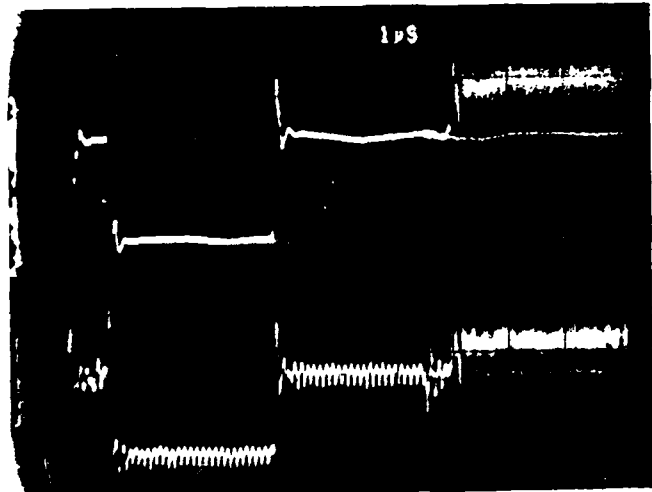
12-a) VIDEO OUT #1 from Camera Control Unit

Composite sync signal



12-b) VIDEO OUT #1 from Camera Control Unit

VIDEO OUT #2 from Camera Control Unit



12-c) VIDEO OUT #1 from Camera Control Unit

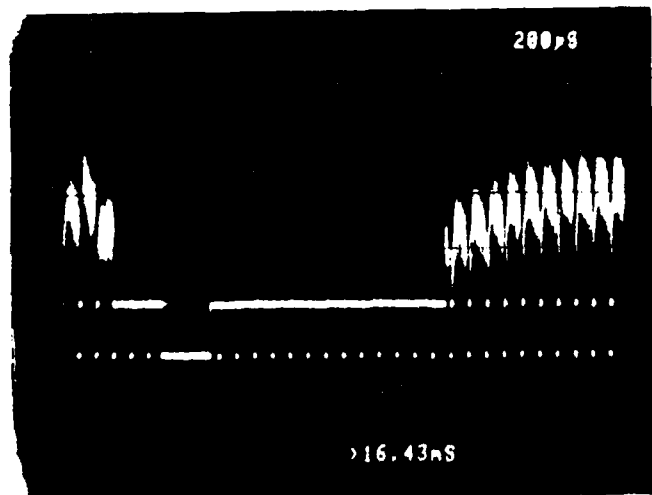


Figure 12. Video Signals

investigation was devoted to bringing the system to a state of stable and reliable operation. The largest blocks of time were consumed solving the line voltage problems mentioned earlier and the associated equipment repairs. Some time was spent solving a ground fault problem and finding the proper sync signal for the Isometric Display Interface Unit. A large portion of time was spent aligning the optics, adjusting the masks mentioned earlier and attempting to get the previously⁹ recommended scan correct procedures to give reliable results.

When the system was brought to a state of stable and reliable operation and a reliable scan correct procedure was determined, there was little time left to collect data. A decision was made at this time to attempt the initial steps in a calibration procedure. The results of this approach are presented herein. Since these measurements were only attempted once, they have not yet been shown to be repeatable. The results of these measurements should then be considered qualitative rather than quantitative. It is the opinion of the author that the system is now ready for a more quantitative calibration.

EXPERIMENTAL APPROACH

For these measurements, the WOSP system was configured as is shown in Figure 5 and 6. However, the correlation option was not used and a TEKTRONIX oscilloscope main frame with a 7A18N dual trace vertical amplifier and a 7B85 delaying time base was connected to the jack marked as A/D OUT on the Display Module of the Video Sample Unit. The oscilloscope lead was put on a tee with a 75 Ω termination as recommended⁹ and the external trigger was connected by a tee to V SYNC for the Camera from the Scan Correct Unit. These connections may have influenced the results somewhat, but the effect is not considered a serious problem for this qualitative study.

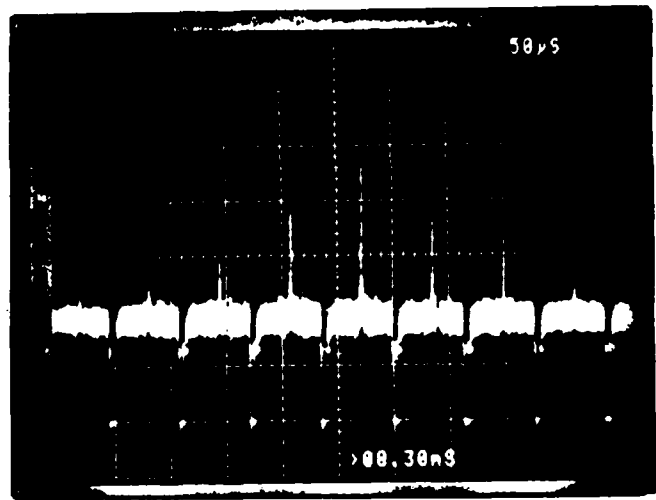
The reference signals used were taken from a Hewlett Packard 8640-B Signal Generator, and the AM modulating signals were taken from a Hewlett Packard 3300A Function Generator with a 3304A Sweep/Offset plug-in. The frequency was checked by a Hewlett Packard 5245L Electronic

Counter. The output amplitude of the Signal Generator was measured to have very little variation in amplitude over the frequency range used in this investigation.

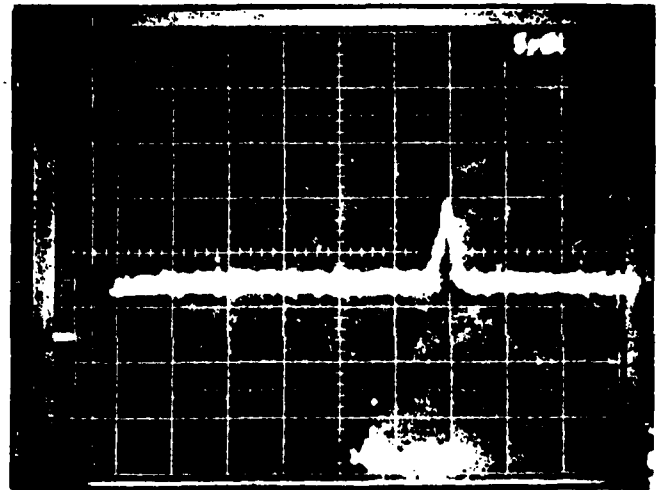
A preliminary investigation was done monitoring the signal entering the Coherent Light Valve from the Signal Generator by monitoring it with an oscilloscope teed at the input of the CLV. There was found to be large reflections in the line and the amplitude of both the signal, and reflections changed significantly as the input signal was varied from approximately 3MHz to 12MHz. The indication is that the input circuit of the CLV is frequency dependent. The frequency response of the WOSP system will then be affected accordingly. A detailed study of this response was not attempted during this investigation.

A pure CW tone of 7.8962MHz with an amplitude of 0.1V was used in the following experiments since it produced a frequency response approximately in the center ¹⁰ of the screen on the Conrac Monitor, and therefore in the center of the 'region of interest' in the spatial frequency plane mentioned above. The Laser current was set at 7.0A. The resulting beamspot as viewed on the monitor exhibited no beam wander as described in Section IV, but it did exhibit 'jitter'. The size of the beamspot can be determined from Figure 13-a where the signal is seen on at least eight horizontal lines. Since these lines are from only one frame in the field, it can be assumed that the signal appears in at least sixteen horizontal lines. The scale of Figure 13-a is 0.2V/DIV and the bottom of the horizontal sync pulses is at 0.6V negative. When AM modulation was added to the above input signal, the results were recorded in Figures 13-b at 200Hz and 13-c at 400Hz. In both figures the scale is 0.2V/DIV and the time base is 5 μ s/DIV. In the oscilloscope trace, the 400Hz modulations are clearly resolved, but the 200Hz modulation was clearly resolved both on the Conrac monitor and the Isometric Display monitor. Also Figure 16 shows a plot of the data from the PDP8/I for this 200Hz modulation. The signals are somewhat resolved but not to the extent that would have been expected from viewing the

13-a) WOSP output from 7.8962MHz CW input showing signal on many spatial frequency locus lines.



13-b) WOSP output form 7.8962MHz carrier amplitude modulated with 200Hz modulation. The sum and difference signals here can be recorded.



13-c) WOSP output form 7.8962MHz carrier amplitude modulated with 400Hz modulation showing sum and difference signals fully resolved.

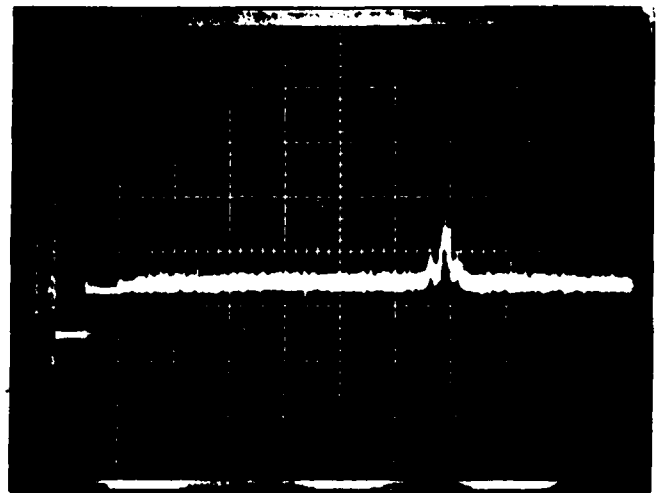


Figure 13. Output Signals

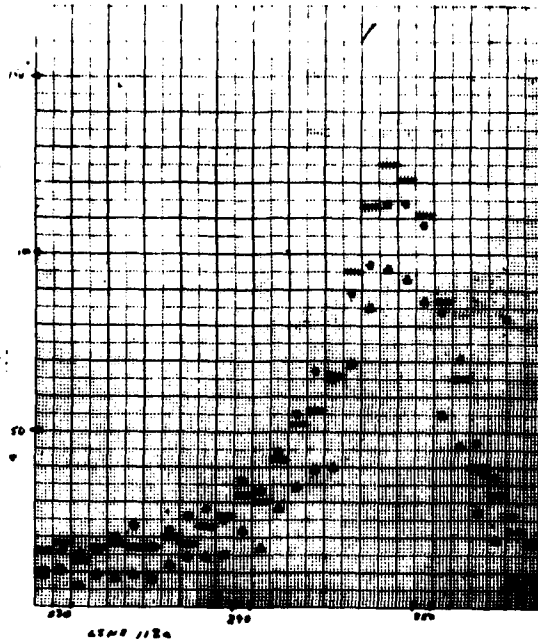


Figure 14. Signal Peaks

In Figure 15-b, the output seems to be near saturation at input signal levels above 0.3V, at least for the existing settings of other fixed parameters mentioned above. All these measurements were made with an input of 7.8962MHz at 0.1V and excepting where specified otherwise, the laser beam current was 7.0A. Since the PDP8/I output did not exceed 255 software units as shown in Figure 14, it may be surmised that the saturation did not take place in the A/D converter but at some place prior to that.

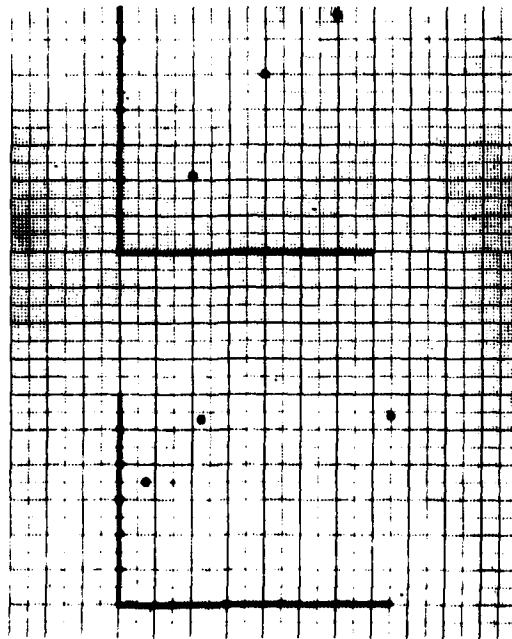


Figure 15- a,b. Output Energy

Fine frequency resolution was discussed previously and shown in

Figures 13-b and 13-c. Figure 16 is a plot of the PDP8/I output for the 0.1V signal at 7.8962MHz with 200Hz AM modulation. The laser beam current was 7.0A for this measurement. The 200Hz modulation signals are just resolved in this computer output, but as viewed on the Conrac and Isometric Display monitor, the 200Hz modulation signals were completely resolved. Note that on the oscilloscope trace of Figure 13-b, the 200Hz signals are hardly resolvable.

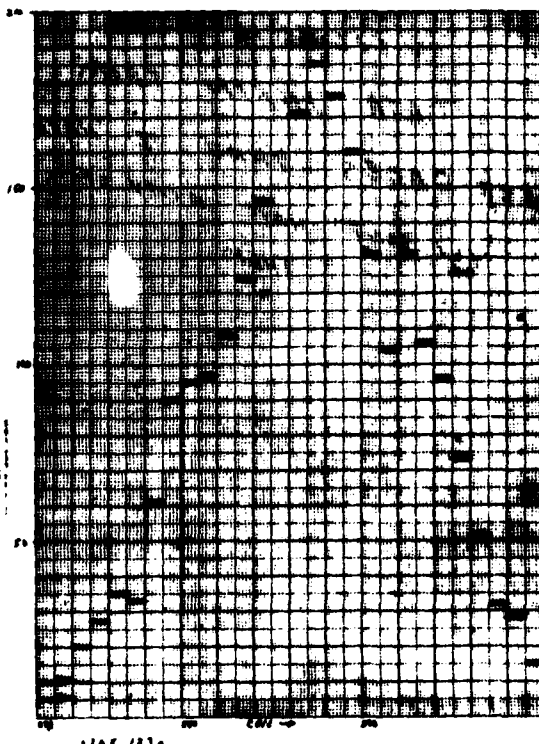


Figure 16. PDP8/I Output

A definition of resolution used in experimental spectroscopy is given by the full width of the signal peak at half of its maximum value divided by the location of the peak on the frequency axis and this ratio is multiplied by 100 per cent. For the 0.1V signal at 7.8962MHz and with a laser beam current of 7.0A, the signals peaks were about ten samples wide at half the maximum. With each sample corresponding to 30.76Hz the fine frequency resolution as defined above is about 3.9×10^{-3} .

To test the coarse frequency resolution the 7.8962MHz carrier amplitude modulated with 15750Hz. This would place the sum and difference spatial frequencies directly above and below the spatial

frequency of the carrier on adjacent locus lines. The result was an input where the signals were not resolved on the Conrac and Isometric Display monitors nor in the output of the PDP81/I. Next, the 7.8962MHz carries was amplitude modulated with $5 \times 15750\text{Hz}$ or $78,750\text{Hz}$, which would place the sum and difference spatial frequencies five lines directly above and below the carries spatial frequency. These signals were completely resolved on the Conrac and Isometric Display monitors and in the output of the PDP8/I as shown in Figure 17.

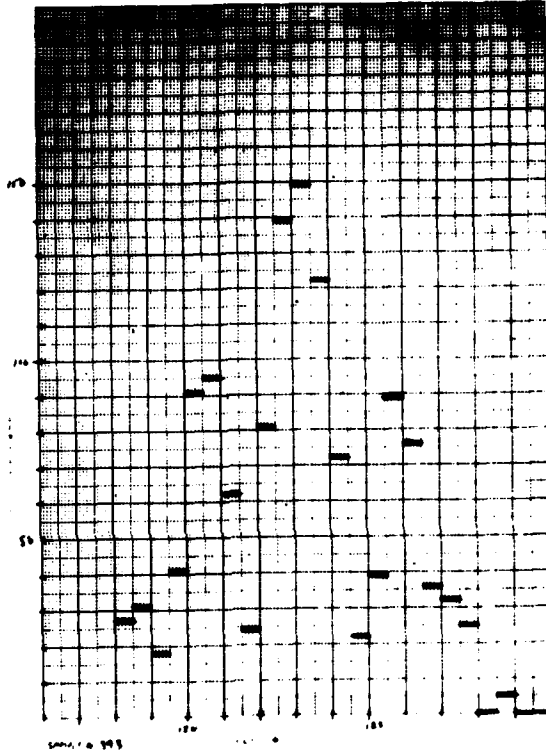


Figure 17. PDP8/I

Due to limitations in time, no further data could be taken, but as one can see from the data above, there are many interesting questions that should be resolved by further investigation. The coarse frequency resolution as defined above is measured at approximately 1.59. This coarse frequency resolution problem lies in the size of the useful part

of the CLV raster and in the spacing of the spatial frequency locus lines in the Fourier Transform plane. It is expected by the author that eventually this problem will be solved.

VI. RECOMMENDATIONS

The large number of recommendations included in this section should not be construed as a criticism of the system or system design but should be recognized as evidence that the author is favorably impressed with the WOSP idea and is convinced that the electro-optical signal processor is an idea whose time has come. Studying electrical signals via the Fourier Transform can be an invaluable tool to scientists and academicians. It should be predictable that every serious laboratory will eventually have an electro-optical processor. With the ability to do correlations in a consistent and reliable manner and in real time, this system will have many useful applications in all areas of science including generation of the Ambiguity Function^{13,14} for RADAR system design. There are also frequency filtering capabilities that are not available electronically.

In short, it is the hope of the author that the recommendations will help reduce the time to that day when this system will attain the status of advanced development model.

In addition to the recommendations listed below, there is a list of valuable recommendations on page 88 and 89 of reference 10. The author agrees with each of them and did not repeat them all here, simply to keep the size of this document manageable.

The recommendations resulting from the present investigation are listed below:

1. There should be a full time staff member assigned to the WOSP system to hasten its evolution from the status of exploratory model to the status of advanced development model in a reasonable period of time. This staff member should be an experienced electrical engineer. He should be supported by somebody with a background in

physical and/or Fourier optics.

2. The entire WOSP system should be protected from transients and line voltage drift by isolation transformers and voltage levelers.
3. The optical bench should be electrically grounded and the Coherent Light Valve should be grounded to the table.
4. The Zener diode in the laser power supply mentioned in Section III should be replaced by the recommended component. The time delay between pressing the POWER ON switch and the lighting of the READY indicator should be corrected to prevent damage to the laser cathode.
5. The masks at the CLV and in the Fourier Transform Plane are made of paper. They should be replaced by permanent apertures. It would be wise to make these apertures position and size adjustable with micrometer drives. They should be made of black metal or some other non-reflecting material.
6. Tubing inclosures around all optical beam paths should be introduced to isolate the laser beam from air currents and thermal disturbances. This should be done in particular immediately before and after the Coherent Light Valve. The tubing adjacent to the light valve should be sealed against the CLV body around the input and output windows.
7. The power cable from the Camera Control Unit to the Camera Head should be supported in a horizontal attitude and clamped in such a manner that no force or torque is transmitted to the Camera Head.
8. Since the use of tees, to monitor signals of interest, during trouble shooting gave evidence of causing the loading down of some circuits and reflections in the line leading to others, all outputs of all units in the WOSP system should be equipped with distribution amplifiers. This will be necessary if reasonable advances are to be made with this exploratory development model.
9. Two additional high resolution TV monitors, one near the Coherent Light Valve and the other near the Video Sampling Unit will be

extremely valuable for making fine adjustments in the CLV raster and the Display Module. These monitors should be capable of displaying the cursors from the Reference Storage Unit and the Video Sampling Unit.

10. A very useful tool for trouble shooting, alignment and calibration would be the ability of the operator to identify the line number of the cursor from the Reference Storage Unit. Possibly an indicator on the control panel of the Reference Storage Unit would be satisfactory.
11. The cursor from the Video Sampling Unit is about 15 volts. A permanent variable attenuator would be useful at the output jack which is designated LINE GATE.
12. As mentioned in Section III, the Coherent Light Valve raster reaches its most stable operating condition approximately four or five hours after the OPERATE switch is depressed. The Light Valve should be put on a timer. The ON switch should be activated approximately five hours before the beginning of the laboratory day and the OPERATE switch should be activated approximately one hour later providing that the COLD/READY indicator is indicating the READY condition. Remember that the heater circuit for the CLV should never be turned off excepting for shipping and long periods of storage.
13. The vidicon camera tube gave some indication that its horizontal sweep was not perfectly aligned with the reference mask on its face. A very small rotation of the tube in its yoke should be attempted. This will be a very slight adjustment and should be accompanied by adjusting the SIZE and CENTER controls on the Sweep and Align Board of the Camera Control Unit. This should follow the procedure recommended in Section III. The alignment will probably take several days.
14. The operation of the Scan Correct Unit should be checked, preferably by the designer. Distribution amplifiers should be

- added to all of its outputs.
15. Until the operation of the Scan Correct Unit has been checked out, the scan correction procedures recommended in Section III should be used.
 16. A beam-splitter and power monitor should be placed in the laser beam before the Jodon attenuator. The power monitor should drive a feed-back circuit to the Laser Power Supply to hold laser power constant. This will prevent laser power drift from affecting amplitude calibration of the WOSP system.
 17. A feedback loop should be supplied to keep the raster of the CLV from drifting in vertical size, horizontal size and contrast. This could be accomplished by continuously feeding a reference signal to the input of the CLV whose frequency would be such that its associated beamspot in Fourier Transform plane would fall far from the 'region of interest' mentioned in Section I. Monitoring the position and intensity of this reference beam could supply the necessary feedback signals for the CLV raster control circuits.
 18. A study should be made of the apparent amplitude variation of the vidicon response of a CW tone input to the CLV as the tones frequency is varied. As the output signal moves across a horizontal line, its amplitude seem to vary periodically modulo 60Hz. This occurs even though the amplitude of the input signal is kept constant as its frequency is varied.
 19. An attempt should be made to operate the rotating disc in the Coherent Light Valve at lower speeds in an attempt to reduce the amount of distortion in the CLV raster.
 20. An investigation should be made into the suggestion from Section III to magnify the CLV raster optically by a factor of 2 and use 1,023 lines per field. Some adjustment will probably be needed for the horizontal size. The goal here is to keep the spacing length of the spatial frequency locus lines the same as they are now, but reduce the size of the beam spot by increasing the apparent size of

the grating.

21. If recommendation 20 is not possible or practical, an attempt should be made to obtain a Coherent Light Valve with a raster that has a usable area of larger size. CLV #2 of this system is not recommended for this purpose since it is of an earlier design than CLV #1.
22. Frequency response of the system can be made more uniform by adding input amplifiers whose frequency response compliments the frequency response of the system.
23. Computer interface provisions should be made to speed the collection and analysis of data. The present system is quite primitive.
24. If the gain and frequency response of the system cannot be stabilized in a satisfactory manner, provision should be made to introduce reference signals with the unknown input. The software can then recalibrate when gain or frequency drifting is detected.
25. Software should be developed to read data and read reference signals then interpolate both the frequency and energy of the spectrum in the data sample.

REFERENCES

1. Goodman, Joseph, W., Introduction to Fourier Optics, San Francisco, California, McGraw-Hill Book Company, 1968.
2. Shulman, Arnold, R., Optical Data Processing, New York, New York, John Wiley & Sons Inc., 1970.
3. Kline, Miles, V., Optics, New York, New York, John Wiley & Sons Inc., 1970.
4. Kirchner, E.K., Yeager, J.R., "Today's Capabilities of Microwave Acousto-Optic Devices," SPIE Vol. 90, 1976, pp. 4-11.
5. Coppock, R.A., Croce, R.F., and Woodman, D.P., "Optical Channelized Receiver Application to Radar," SPIE, Vol. 128, Sept. 1977, pp. 234-237.
6. Grinberg, J. et.al., "Liquid Crystal Electro-Optical Modulators for Optical Processing of Two-Dimensional Data," SPIE, Vol. 128, 1977, pp. 253-266.
7. Noble, M.L., and Hoefler, W.G., Coherent Light Valve Processor, An Unsolicited Proposal Submitted to: Rome Air Development Center, September, 1974.
8. Noble, M.L., RADC Laboratory CLV Processor, A Final Report Prepared for Rome Air Development Center, March, 1976.
9. Noble, M.L., Optical Transducer for WOSP, An Operating Manual Prepared for Rome Air Development Center, December, 1978.
10. Lowry, M.F., Noble, M.L., and Hoefler, W., Optical Correlation Techniques, RADC-TR-81-20 Final Technical Report, March, 1981.
11. Lowry, M.F., Private Communication.
12. Oppenheim, Alan, V., and Schaffer, Ronald, W., Digital Signal Processing, Englewood Cliffs, New Jersey, Prentice-Hall, Inc., 1975.
13. Papoulis, A., Signal Analysis, New York, New York, McGraw-Hill Book Company, 1977.
14. Srinath, M.D., and Rajaseraran, P.K., An Introduction to Statistical Signal Processing with Applications, New York, New York, John Wiley & Sons Inc., 1979.

1981 USAF - SCEE SUMMER FACULTY RESEARCH PROGRAM

Sponsored by the

AIR FORCE OFFICE OF SCIENTIFIC RESEARCH

Conducted by the

SOUTHEASTERN CENTER FOR ELECTRICAL ENGINEERING EDUCATION

FINAL REPORT

CORROSION STUDIES OF CALCIUM/THIONYL CHLORIDE ELECTROLYTE SYSTEMS

Prepared by: Dr. Vijay K. Gupta
Academic Rank: Assistant Professor
Department and University : Department of Chemistry
Central State University
Research Location: Aero-Propulsion Laboratory, Wright Patterson
Air Force Base, Dayton, Ohio 45433
USAF Research Colleague: Mr. Robert L. Kerr
Date: September 15; 1981
Contract No: F49620-79-C-0038

CORROSION STUDIES OF CALCIUM-THIONYL CHLORIDE

ELECTROLYTE SYSTEMS

by

Vijay K. Gupta

ABSTRACT

The Calcium-thionyl chloride battery system is very attractive from the point of view of combining high energy density with a high degree of system safety. The most pressing problem in this system is the high self discharge rate of Calcium (corrosion). In order to understand the problem of calcium corrosion, the corrosion studies of calcium in thionyl chloride and different electrolytes have been carried out as function of time and temperature. The present study has indicated that calcium metal surface can be effectively cleaned and polished and the metal is highly sensitive to air and moisture. High purity of solvent and electrolytes and the moisture content of chemicals are very significant as far as the corrosion of calcium metal is concerned. Pure thionyl chloride causes less corrosion as compared to lithium or calcium electrolytes. The amount of corrosion increases with the passage of time and the rate of corrosion is significantly affected by the increase in temperature. Further studies incorporating different additives to the electrolyte have been suggested for further work. The use of calcium alloys rather than pure calcium has also been suggested as a possible direction of further research to achieve high energy density and safe battery systems.

Acknowledgments

The author would like to thank the Air Force Systems Command, the Air Force Office of Scientific Research, and the Southeastern Center for Electrical Engineering Education for providing him with this exciting opportunity to spend a very worthwhile summer at the Aero-Propulsion Laboratory, WPAFB, Dayton, Ohio. He would like to acknowledge the laboratory, in particular the Battery Research Laboratory, for its hospitality and excellent working conditions.

In addition, he would like to thank Mr. John F. Leonard and Mr. James W. Logsdon for providing valuable technical assistance in carrying out this project. Finally he would like to express his appreciation and thanks to Dr. David H. Fritts, Mr. Robert L. Kerr, and Mr. James S. Cloyd for suggesting this area of research and for their helpful suggestions and criticism.

I. INTRODUCTION

High energy density batteries play an important role in various military applications as power sources (1). During the past few years, various lithium battery systems have been developed to fulfill the need for long shelf-life high energy density batteries. One of which is Lithium-Thionyl Chloride battery system. The lithium-thionyl chloride system has exhibited the capability of providing the highest energy of all the lithium systems, but it has experienced the problems of voltage delay and safety. Certain lithium properties, the low melting point (180°C), the ignition temperature (190°C in O_2) (2,3), high heat of combustion (71 Kcal/eq) present serious safety problems: burning and molten lithium may also be hazardous. A recent explosion of a large (approximately 42 kw-hr) lithium-thionyl chloride battery claimed one life and two injuries (4) (4th of August 1976, Ogden Utah). Thus lithium batteries have not reached the general public and their use has been restricted mostly to military applications.

The above problems have resulted in the development of an alternative(5-9) system based on thionyl chloride using an anode other than lithium which might show an improved voltage response after storage and better safety features. The anode chosen for this purpose is calcium. The main incentive for using calcium in place of lithium is that calcium anodes have the prospect of higher temperature operation as compared to lithium anodes. A comparison of the calculated theoretical energy densities of lithium and calcium-thionyl chloride cells (6,8) is given below assuming reaction products of SO_2 , S, and either LiCl or CaCl_2 .

	<u>Cell Potential(V)</u>	<u>Energy Density w-hr/cm³</u>	<u>Specific Energy Density w-hr/kg.</u>	<u>Melting Point</u>
Li	3.65	2.00	1474	180 C
Ca	3.64	1.97	1230	839 C

The above values indicate that the energy densities of calcium-thionyl chloride system compare favorably with lithium-thionyl chloride system.

In addition, Calcium is more abundant and cheaper than lithium and has higher electronic conductivity than lithium. The disparity between melting points of the two metals is of special interest since the 839° C temperature required for the calcium to melt would not likely be reached by any internally driven cell condition, thus precluding the thermal runaway so often seen in the lithium-thionyl chloride cells. Therefore Calcium-thionyl chloride battery system is very attractive from the point of view of combining high energy density with high degree of safety (the latter remains to be fully established). This system requires additional research before it can be deemed practical for many applications.

II. OBJECTIVES

The main objective of this ten week project was to investigate the most pressing problem of high self discharge rate of the calcium metal (corrosion) in the calcium-thionyl chloride battery system. Since this is a primary battery, it is necessary for the self discharge rates to be very small if practical storage batteries are to be achieved. The purpose of the program was to define qualitatively and quantitatively the self discharge rate and to determine if this rate can be significantly altered by changes in the electrolyte composition, the surface condition of the electrode, and the change in temperature. In order to understand the corrosion phenomena of the calcium metal, the corrosion studies of the calcium metal when exposed to thionyl chloride and/or thionyl chloride electrolyte systems as a function of time and temperature have been performed.

III. EXPERIMENTAL

This section deals with the chemicals and equipment used, cleaning and preparation of the calcium metal surface, the preparation of the electrolytes, and the procedures used to pack the samples into appropriate glass ampules.

Calcium Metal: Calcium was supplied by Eagle-Pitcher Industries (EPI) obtained from P.M.F. Alloys in the form of 0.05 inch thick metal sheet. It was packed in mineral oil in Argon atmosphere. Calcium sheets were taken out and washed three times with reagent grade n-hexane to remove mineral oil

and were stored under n-hexane. The metal sheets had greyish and black spots. In order to determine the quality of the calcium metal surface as received, the Scanning Electron Microscope (SEM) photomicrograph was taken as shown in figure 1 (a). From the photograph it appears that the surface is corroded, and the film could be due to the formation of oxide and hydroxide on the metal surface. Thus it was decided to clean the surface chemically or mechanically. The clean sample was exposed to the laboratory environment for 64 hours and looked at again under SEM as shown in figure 1(b). The surface had developed heavy corrosive spots. It was therefore, decided to store and clean the calcium metal in air and moisture free environment (dry box), before exposing the calcium metal surface to solvent or electrolytes.

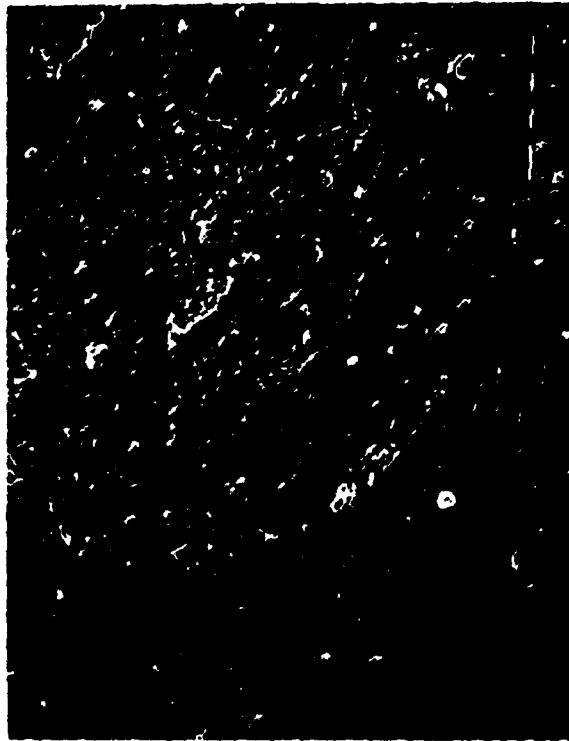
Dry Box: A dry box (10) was used to provide the dry and oxygen free environment to store calcium metal. All the cleaning processes of the calcium metal surface were also carried out in the dry box. The major components of the dry box system shown in figure 2 are:

1. a provision for an inert atmosphere (helium was used);
2. a recirculating pump for continual removal of any gaseous impurities such as water vapor from the helium (by pumping through the molecular sieve columns);
3. a provision for maintaining a continuous positive pressure;
4. an isolation or transfer compartment (which allows chemicals and equipment to be introduced into the box without contaminating the box environment with air or/and water vapor);
5. a provision for regeneration of the molecular sieves; and
6. a relative humidity and oxygen sensor to enable constant monitoring of the water vapor and oxygen level in the dry box. A dew point of about -78°C (≤ 2 ppm water vapor) and ≤ 2 ppm oxygen was maintained for the duration of the work.

Thionyl Chloride: This material was supplied by GTE-Sylvania and was originally prepared by Mobay Chemical Company. Thionyl chloride was water white in appearance. Analysis by GTE showed less than 50 ppm of water in



b) 50 X



a) 50 X

Figure 1. SEM Photomicrographs of Ca Metal (a) As-Received from GTE (b) Exposed to Laboratory Environment for 64 Hours.

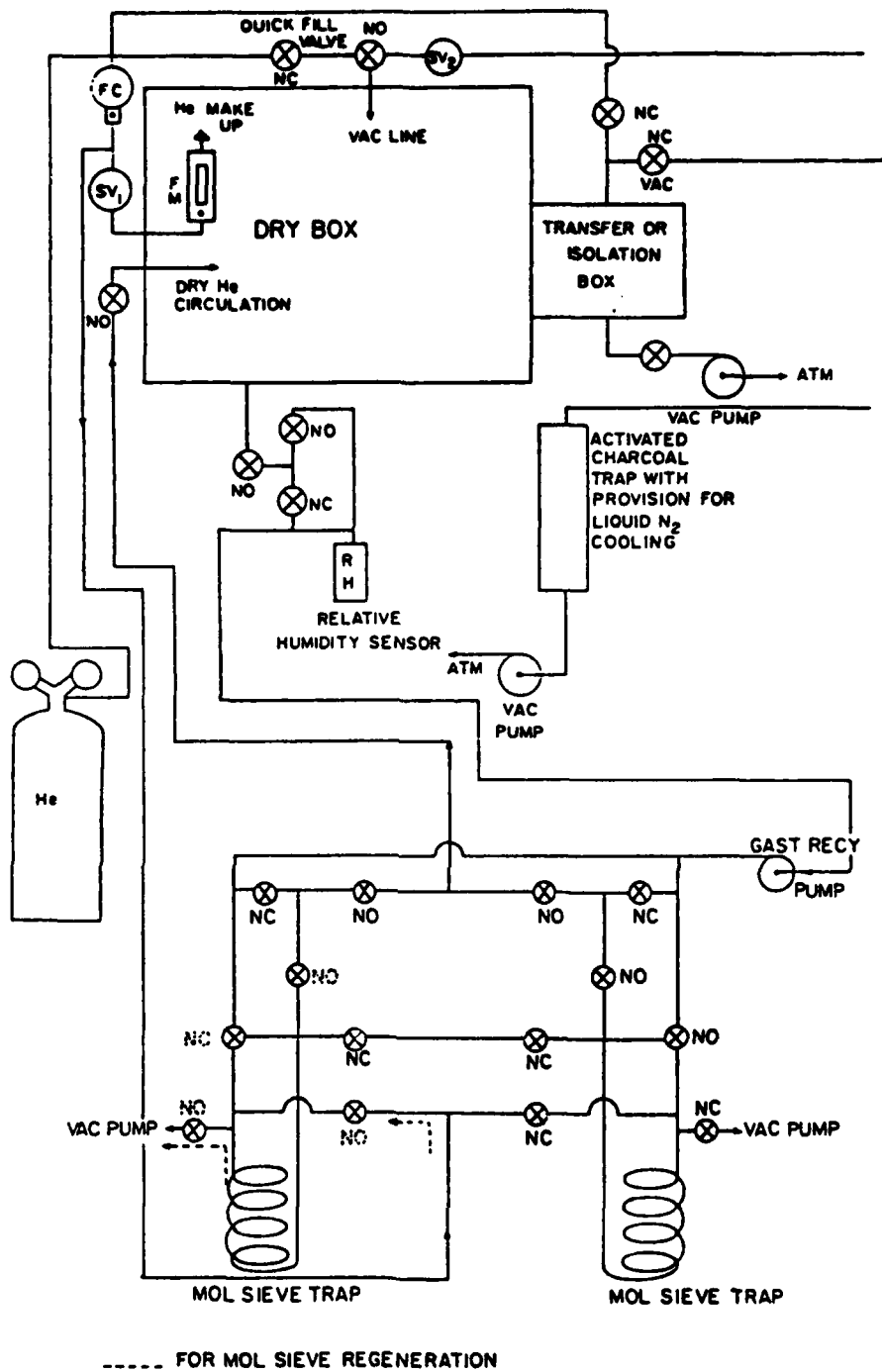


Figure 2 . Block Diagram of Helium Dry Box and Purification System.

TABLE I

THIONYL CHLORIDE COMPOSITION

<u>Component</u>	<u>Weight % Typical</u>
Sulfuryl Chloride	< 0.009%
Sulfur Chlorides	< 0.1%
Sulfur Dioxide	< 0.3%
Residue on Evaporation	< 0.1%
Nickel	5 ppm
Iron	5 ppm
Lead	5 ppm
Copper	1 ppm
Zinc	1 ppm
Other Metals	10 ppm
Water	< 50 ppm
Organics	Not Detected

the thionyl chloride. The analysis of the thionyl chloride is given in table I (10). The experiments with thionyl chloride and electrolytes were handled in glove bag rather than dry box. This glove bag was purged with helium several times in order to assure the glove bag environment free of air and moisture. The glove bag was set up under the hood due to the corrosive and toxic nature of thionyl chloride.

Lithium Electrolyte: Two samples of LiAlCl_4 in SOCl_2 were obtained. One sample provided by GTE-Sylvania was 1.8 M lithium tetrachloro aluminate in thionyl chloride (L-0099) and was clear but slightly colored. The other sample was provided by Eagle-Pitcher Industries obtained from Apache Chemicals. This electrolyte was 1.5 M LiAlCl_4 in SOCl_2 and was of brown color.

Calcium Electrolyte: It was prepared by taking 50 ml of GTE supplied thionyl chloride in a ground glass stoppered flask, and adding to it 13.35 g of anhydrous AlCl_3 (reagent grade obtained from Allied Chemicals) and 5.80 g of anhydrous CaCl_2 (reagent grade obtained from Mallinckrodt). The mixture was repeatedly shaken and stored in the glove bag for 24 hours. It was observed that all of the AlCl_3 went into the solution but some CaCl_2 was left undissolved, thus giving Al/Ca ratio of greater than 2. The solution was filtered and used for experiments.

Lithium-Calcium Electrolyte: This electrolyte was prepared by mixing 25 ml of the GTE supplied lithium electrolyte and 25 ml of the internally prepared calcium electrolyte. The mixture will be referred as Mix electrolyte.

Preparation of the Calcium Metal Surface: As pointed out earlier the metal surface did need cleaning in order to assure the clean surface to begin with. It was decided to try two approaches to cleaning process either chemically or mechanically.

Chemical Cleaning: The calcium metal strip was placed in the china crucible and heated to 750°C in tube furnace in 5% H_2 and 95% He environment for two hours. The metal sample was heavily coated with greyish white oxide film. The process was repeated again but there was no improvement. It was felt

probably the environment was not completely free from air and moisture and the metal is very sensitive to air and moisture specifically so at 750° C. An alternative approach was taken by placing a small furnace in the dry box, and the metal sample heated at 850° C for two hours in helium environment. The treatment resulted in the formation of heavy oxide film of amorphous nature, so chemical cleaning was discarded.

Mechanical Cleaning: Several approaches to this cleaning method were tried. Initially the metal surface was hand cleaned using an emery paper in the dry box, but the process was too slow and ineffective and left scratches on the surface. Then a belt sander was installed in the dry box but its operation was difficult due to the design of the sander. Finally an instrument known as Dremel High Speed Rotor Tool with rubber backed circular rotating disc was used to polish the surface. A circular piece of sanding paper of the size of the circular disc was cut and mounted on the rubber-backed circular disc. The metal surface was polished with three different grades of polishing paper. First it was polished with 220 Grit Aluminium Oxide and then with 150 Grit Aluminium Oxide, and finally with jewellers Crystal Bay Crocus cloth. The treatment resulted in a very shiny, smooth and clean surface. SEM photomicrographs of the clean surface are shown in figure 3. The surface condition was considered acceptable and reasonably clean from the point of view of corrosion studies.

Sample Packing: Calcium metal sheets were cut into small pieces of the size 0.75"x0.2"x0.05" (these sizes are approximate only). The samples were packed into 56 glass serum bottles and were sealed using neoprene seals and aluminium caps in Helium atmosphere in the dry box. The sealed samples were then transferred to the glove bag purged with helium and were filled with solvent and electrolytes as detailed below:

six samples were used as blanks.

ten samples were filled with GTE-Sylvania[™] SOCl₂.

ten samples were filled with lithium electrolyte 1.8 M (GTE).

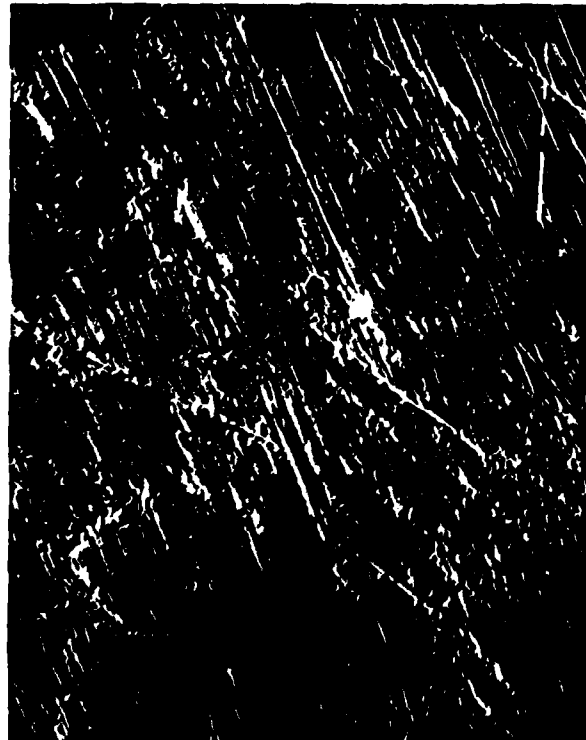
ten samples were filled with calcium electrolyte 1.0 M (prepared internally).

ten samples were filled with mix electrolyte.

ten samples were filled with lithium electrolyte 1.5 M (EPI).



b) 1000 X



a) 100 X

Figure 3. SEM Photomicrographs of Ca Metal Surface Cleaned and Polished in the Dry Box.

The glass syringe alongwith stainless needle was used to inject the electrolyte through the neoprene septum. The process was quite tedious due to the solidification of the electrolyte in the needle and blocking the needle, so needles had to be replaced frequently. Half of the samples of each kind were stored at room temperature (22^o C) in a dessicator and the other half were stored in an oven maintained at 55^o C. After a period of three days it was observed that neoprene washers were reacting with thionyl chloride, so all the samples were transferred back to the glove bag and all the neoprene seals were replaced with teflon seals which did seal the samples effectively except the samples stored at 55^o C experienced loss of some solvent in some cases after about ten days. This may have been caused due to the high vapor pressure of thionyl chloride at 55^o C. The samples were observed for corrosion on the Calcium metal surface both visually and using SEM. The results are described in the next section.

IV. RESULTS AND DISCUSSION

The corrosion data resulting from visual examination of the samples is described in Tables 2 and 3. Table 2 describes the data for different systems as a function of time at room temperature (22^o C) and table 3 contains the data at 55^o C. The information so obtained is rather qualitative in nature, however, it is apparent that corrosion on Calcium metal surface is increasing as the storage time is increasing. Increase in temperature has also led to higher rate of corrosion. Among the electrolytes Ca-electrolyte caused maximum corrosion where as thionyl chloride caused least corrosion. Between the two Li-electrolytes GTE electrolyte caused lesser degree of corrosion as compared to EPI electrolyte. The rate of corrosion was also much slower in case of GTE electrolyte as compared to EPI electrolyte. Mix electrolyte's behaviour was in between GTE Li-electrolyte and Ca-electrolyte. All the electrolytes experienced change in color from light color to dark brown or black but EPI electrolyte which was originally brown in color changed to light color after being subjected to Calcium metal. It may be concluded that calcium metal has helped cleaning the EPI electrolyte.

TABLE 2
 RELATIVE CORROSION OF CALCIUM METAL IN DIFFERENT SYSTEMS AT ROOM TEMPERATURE (22° C)

Solvent/Electrolyte	24 Hours	7 Days	14 Days	30 Days
Helium	no change	no change	no change	no change
Pure SOCl_2	no change	black spots near the edges surface still shining	few black spots on the surface and surface turning slightly grey in color	surface completely grey and the electrolyte turns dark black in color
Li-Electrolyte (GTE)	no change	surface turning grey black spots on surface and near the edge and electrolyte changing brown	surface complete grey electrolyte turning darker in color more black spots	surface completely grey electrolyte becomes dark in color black spots on the surface and edges
Ca-Electrolyte	few black spots on the edges surface still shining	black spots on edges and surface and color of surface turns grey electrolyte turns brown in color	black spots all over surface grey electrolyte turns black	more and larger black spots all over surface dark grey electrolyte black and viscous
Mix-Electrolyte	few black spots on the edges surface still shining	black spots on edges and surface and surface color grey and electrolyte brown	more black spots on edges and surface electrolyte turns dark brown	black spots all over the surface electrolyte turns black and surface completely grey
Li-Electrolyte (EPI)	black spots on edges electrolyte becomes clear	black spots all over surface grey	black spots grow in size and surface grey in color	

TABLE 3
 NEGATIVE CORROSION OF CALCIUM METAL IN DIFFERENT SYSTEMS AT 55° C

Solvent/Electrolyte	24 Hours	7 Days	14 Days
Helium*	no change	no change	slight greyish color on surface
Pure SOCl ₂ *	black spots on the surface and surface turning grey	more black spots on the surface and surface turning darker grey loss of electrolyte observed	more black spots on surface and edges surface dark grey half of the electrolyte lost
Li-Electrolyte* (GTE)	surface completely grey electrolyte turning darker in color more black spots	surface completely grey electrolyte becomes dark black more black spots on the surface and edges	surface completely grey and electrolyte becomes dark black more black spots on the surface and edges and loss of electrolyte observed
Ca-Electrolyte*	black spots all over grey surface electrolyte turns black	more and larger black spots all over surface dark grey electrolyte turns black and viscous	more black spots on the edges and surface and surface dark grey some of the metal eaten up electrolyte black and viscous
Mix-Electrolyte*	more black spots on edges and surface electrolyte turns dark brown	black spots all over the surface and edges electrolyte turns black and surface grey in color	black spots all over the surface and edges electrolyte turns black and viscous and surface grey in color
Li-Electrolyte (EPI)	black spots on edges and surface electrolyte becomes clear	black spots all over the surface getting dark grey	black spots all over the surface and getting larger in size and surface dark grey

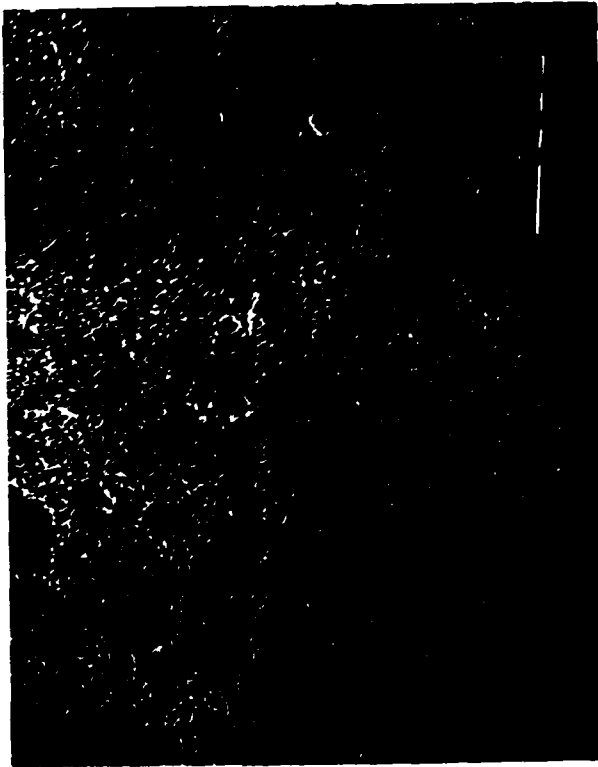
* These systems were stored at room temperature for 13 days before they were subjected to 55° C.

The extent of corrosion and rate of corrosion was observed by examining Ca samples at different time intervals using SEM. The packed samples were transferred to glove bag which was free from air and moisture. The seals were removed, the Ca sample was removed from the serum bottle and wiped dry with paper towel to get rid of the loose material and the electrolyte on the metal surface and the sample was transferred into the zip-lock polyethylene bag and sealed in the bag in order to avoid atmospheric exposure. The polyethylene bags were transferred to the transfer chamber of the dry box and were subjected to vacuum and helium three times before they were taken into the dry box. In the dry box individual samples were mounted on a circular brass disc using a silver containing paint as glue. Samples were then transferred from the dry box to the SEM room in zip-lock polyethylene bag so as to minimize ambient atmosphere induced degradation of the sample.

SEM photomicrographs of Ca exposed to thionyl chloride at different time intervals are given in figures 4-6, figures 7 and 8 are at 55° C. As one looks at figures 4-6, it appears that extent of corrosion increases with the passage of time, and figures 7 and 8 indicate that increasing the temperature has increased the rate of corrosion, resulting in thicker film of LiCl of non-conducting nature. Figures 9-11 are for Ca metal exposed to GTE 1.8 M LiAlCl₄ in SOCl₂ at room temperature as a function of time and figures 12 and 13 are at 55° C. The extent of corrosion increased as a function of time and the rate of corrosion increased with increase in temperature. Time and temperature had similar kind of effect for other systems also the data for Ca metal exposed to Ca(AlCl₄)₂ in SOCl₂ is given in figures 14-18, and data for Ca exposed to Mix-electrolyte is given in figures 19-23. and the data for Ca exposed to LiAlCl₄ in SOCl₂ (EPI) is given in figures 24 and 25. If the photomicrographs from figures 6, 11, 16, and 21 are compared with each other, it appears that most corrosion is caused in case of figure 16, and the least corrosion is caused in case of figure 6. Figure 16 belongs to Ca-electrolyte and figure 6 belongs to thionyl chloride system. The SEM observations are in agreement with the observation made in case of visual examination. Li-electrolyte from GTE caused more corrosion than thionyl chloride system but less than



b) 1000 X

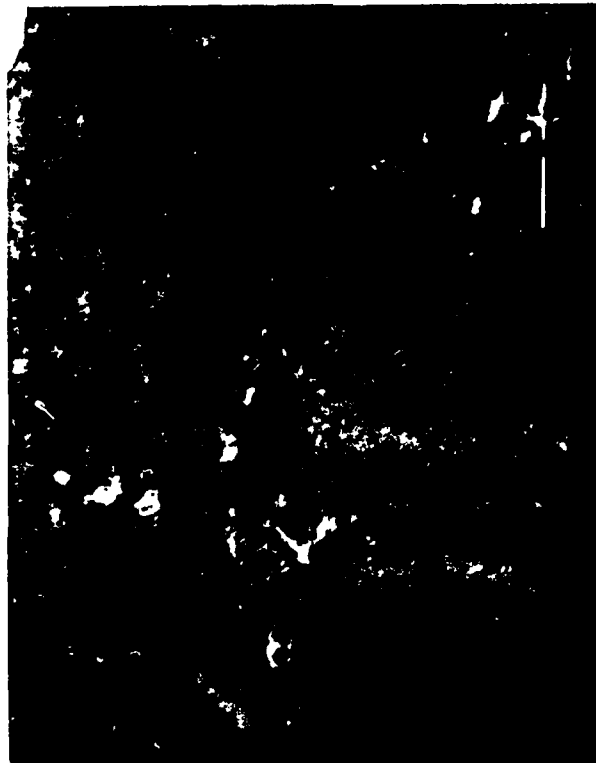


a) 100 X

Figure 4. SEM Photomicrographs of Ca Metal Exposed to Pure Thionyl Chloride for 13 Days at Room Temperature (22° C).



a) 100 X



b) 1000 X

Figure 5. SEM Photomicrographs of Ca Metal Exposed to Pure Thionyl Chloride for 20 Days at Room Temperature (22° C).

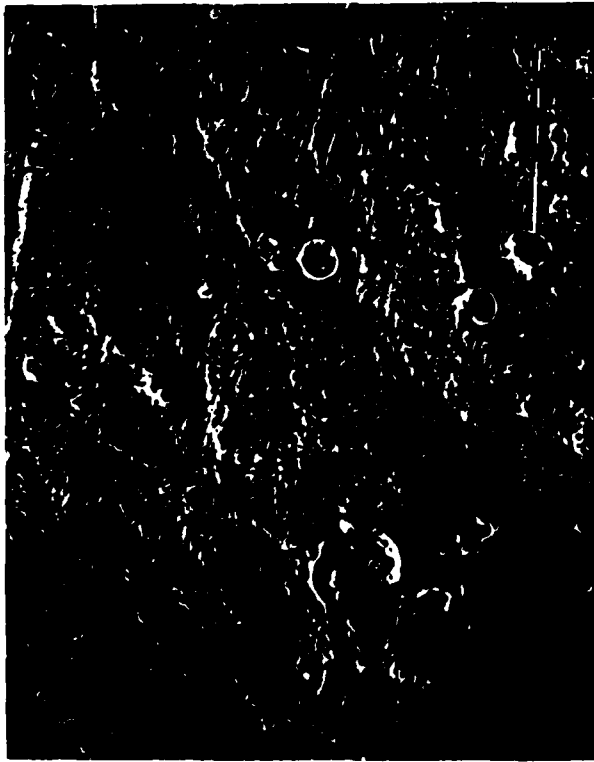


b) 1000 X



a) 100 X

Figure 6. SEM Photomicrographs of Ca Metal Exposed to Pure Thionyl Chloride for 30 Days at Room Temperature (22° C).

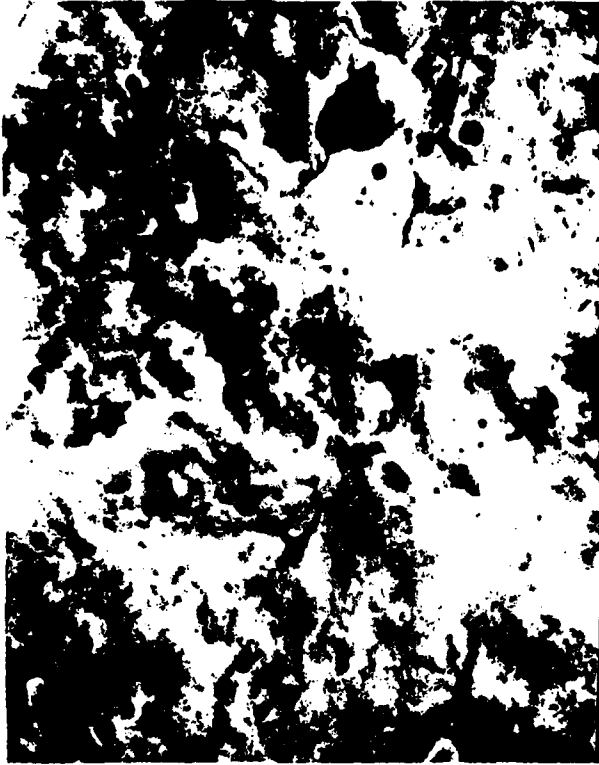


a) 100 X

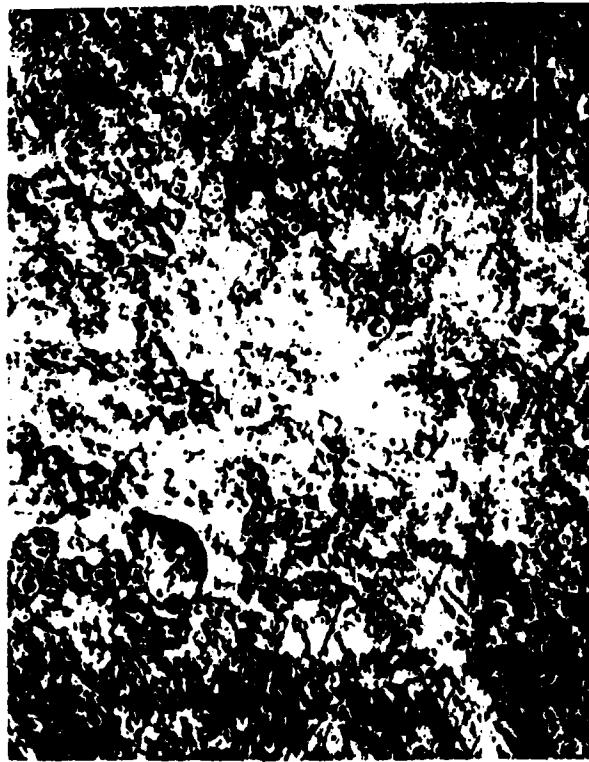


b) 1000 X

Figure 7. SEM Photomicrographs of Ca Metal Exposed to Pure Thionyl Chloride for 13 Days at Room Temperature (22° C) and 7 Days at 550 C.

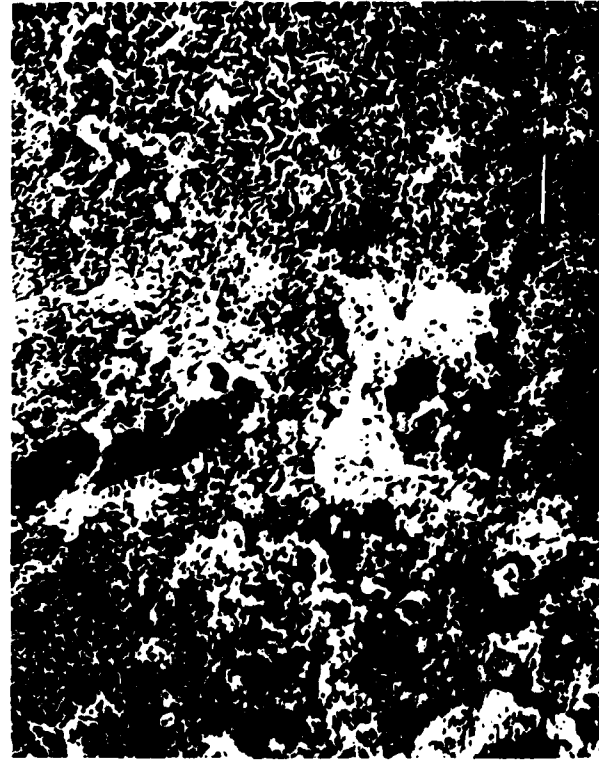


b) 1000 X

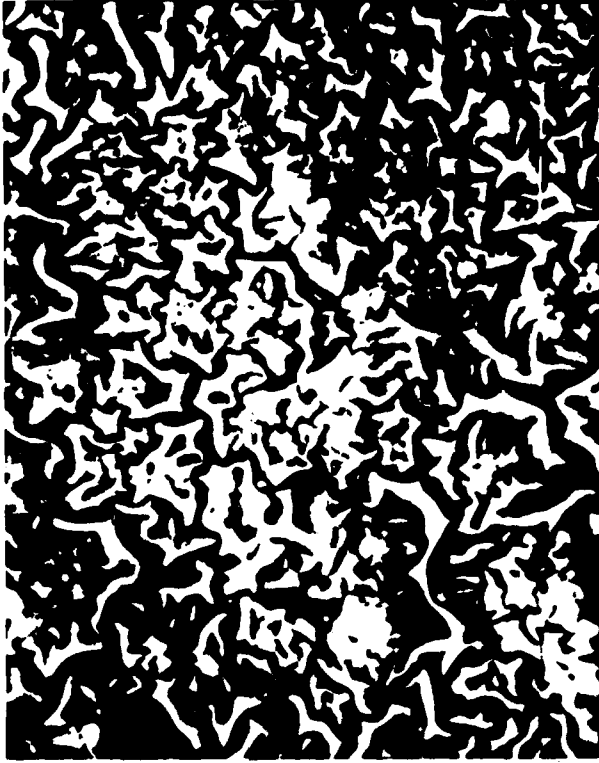


a) 100 X

Figure 8. SEM Photomicrographs of Ca Metal Exposed to Pure Thionyl Chloride for 13 Days at Room Temperature (22° C) and 17 Days at 55° C.



a) 100 X



b) 1000 X

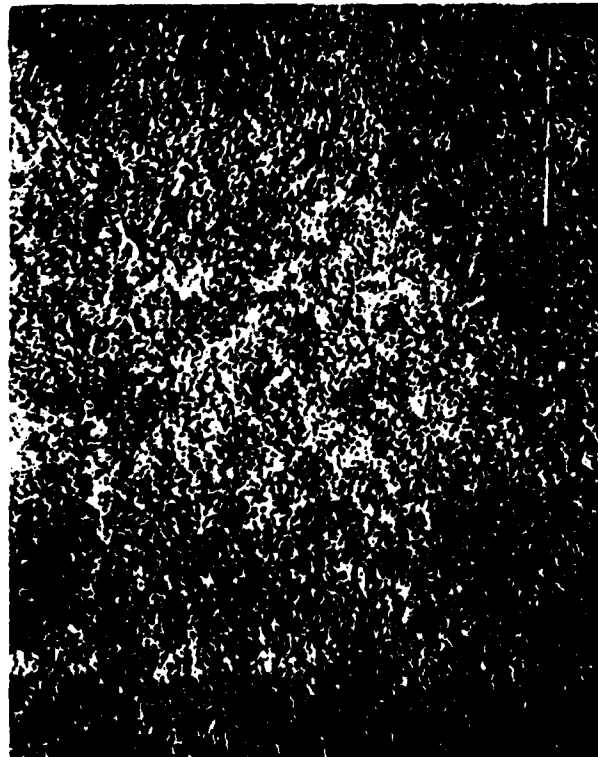
Figure 9. SEM Photomicrographs of Ca Metal Exposed to GTE Li-Electrolyte for 13 Days at Room Temperature (22° C).



a) 100 X



b) 1000 X
Figure 10. SEM Photomicrographs of Ca Metal Exposed to GTE Li- Electrolyte for 20 Days at Room Temperature (22° C).



a) 100 X



b) 1000 X

Figure 11. SEM Photomicrographs of Ca Metal Exposed to GTE Li- Electrolyte for 30 Days at Room Temperature (22° C).

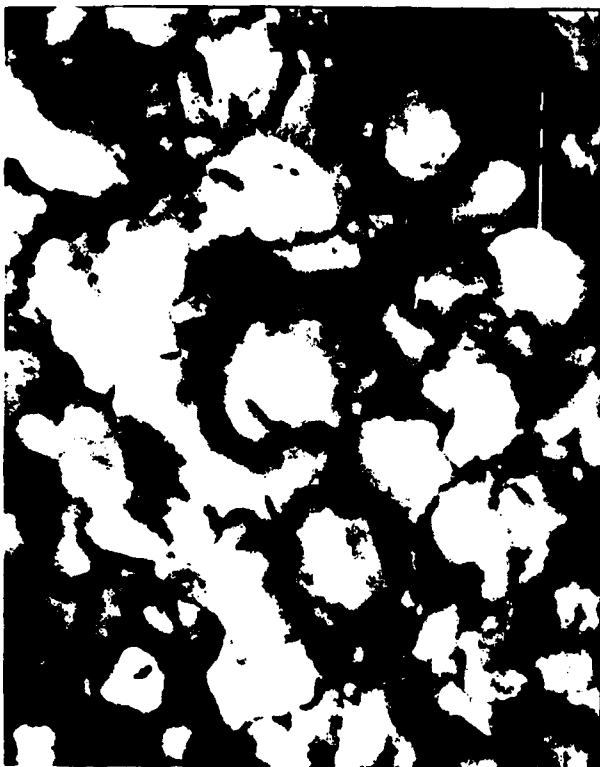


a) 100 X



b) 1000 X

Figure 12. SEM Photomicrographs of Ca Metal Exposed to GTE Li- Electrolyte for 13 Days at Room Temperature (22° C) and 7 Days at 55° C.

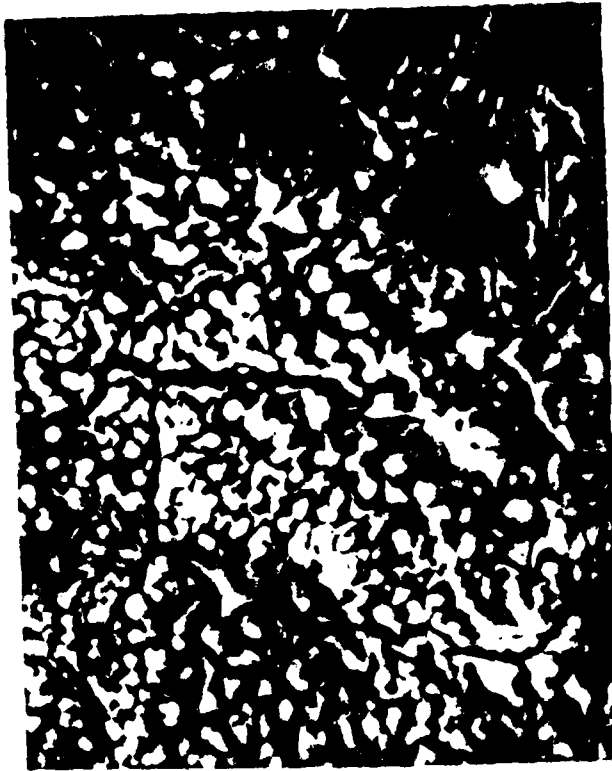


b) 1000 X



a) 100 X

Figure 13. SEM Photomicrographs of Ca Metal Exposed to GTE Li-Electrolyte for 13 Days at Room Temperature (22° C) and 17 Days at 55° C.



b) 1000 X

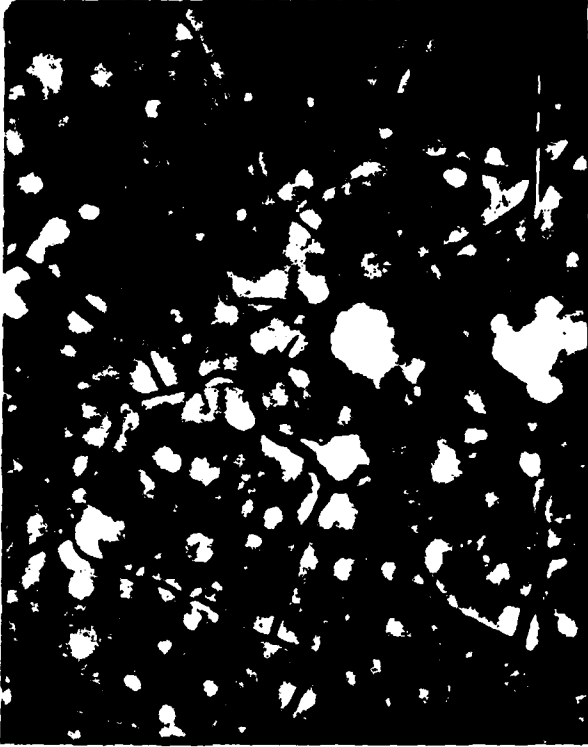


a) 100 X

Figure 14. SEM Photomicrographs of Ca Metal Exposed to Ca-Electrolyte for 13 Days at Room Temperature (22° C).

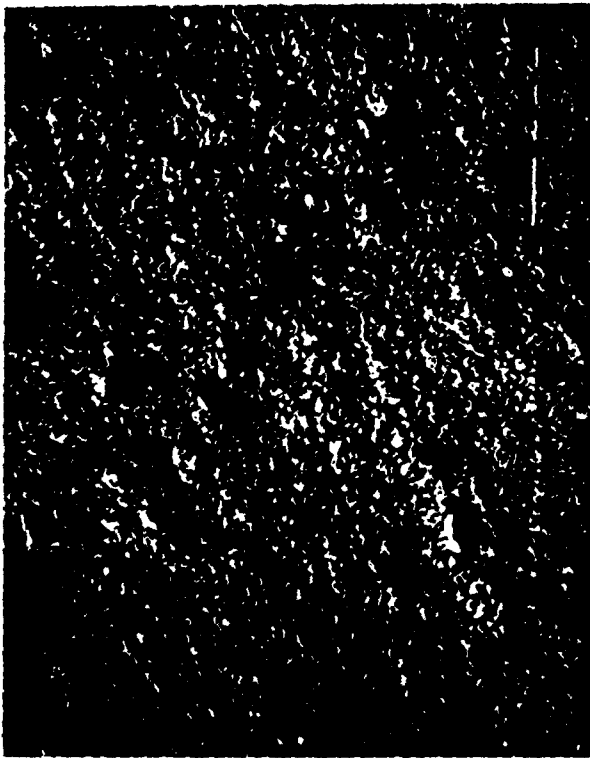


a) 100 X



b) 1000 X

Figure 15. SEM Photomicrographs of Ca Metal Exposed to Ca-Electrolyte for 20 Days at Room Temperature (22° C).

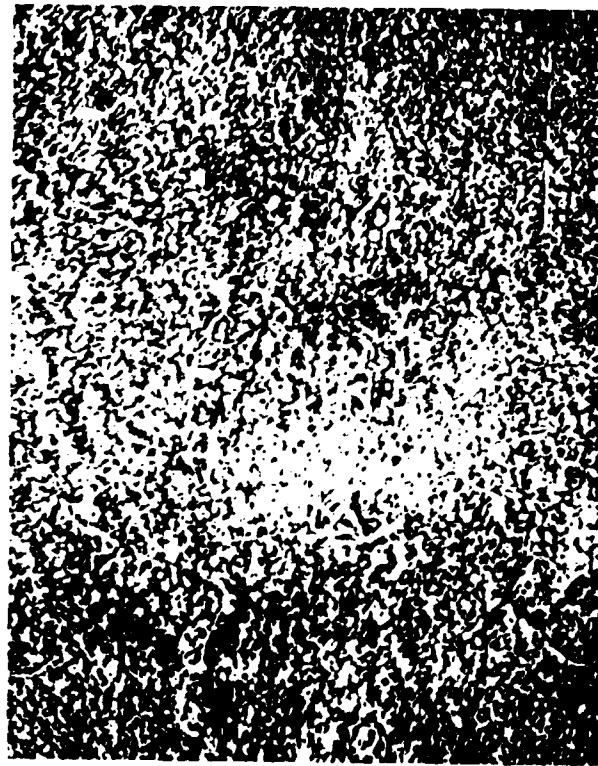


a) 100 X

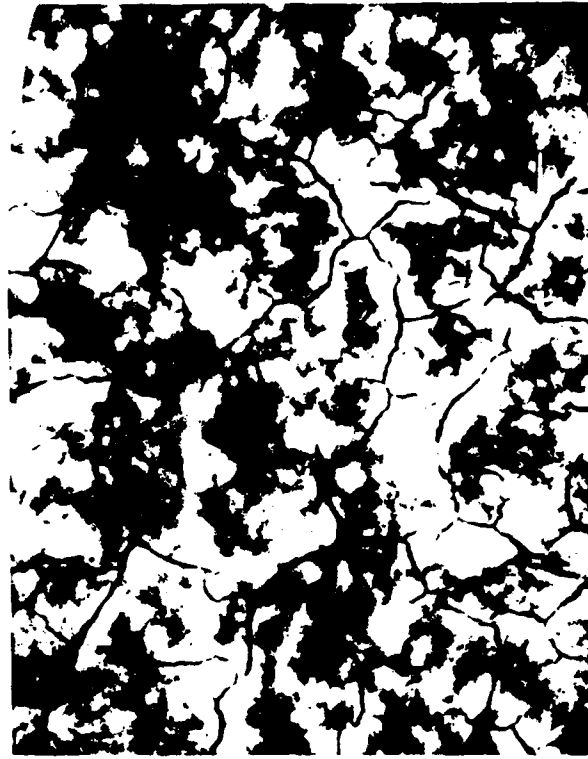


b) 1000 X

Figure 16. SEM Photomicrographs of Ca Metal Exposed to Ca- Electrolyte for 30 Days at Room Temperature (22° C).



a) 100 X



b) 1000 X

Figure 17. SEM Photomicrographs of Ca Metal Exposed to Ca-Electrolyte for 13 Days at Room Temperature (22° C) and 7 Days at 55° C.

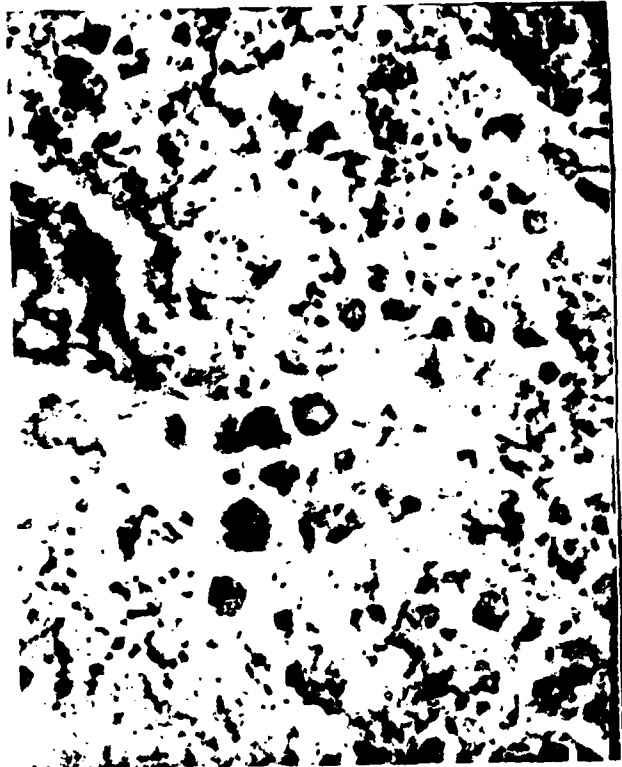


a) 100 X



b) 1000 X

Figure 18. SEM Photomicrographs of Ca Metal Exposed to Ca-Electrolyte for 13 Days at Room Temperature (22° C) and 17 Days at 55° C.

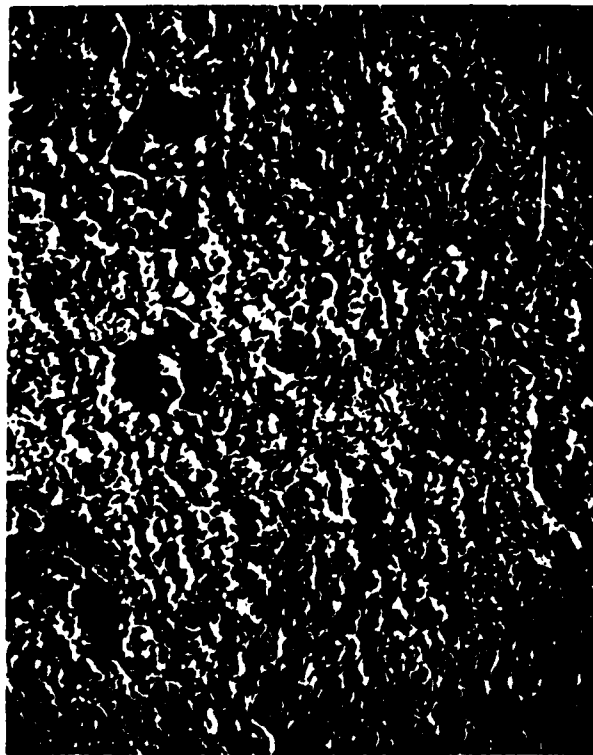


b) 1000 X



a) 100 X

Figure 19. SEM Photomicrographs of Ca Metal Exposed to Mix-Electrolyte for 13 Days at Room Temperature (22° C).



a) 100 X



b) 1000 X

Figure 20. SEM Photomicrographs of Ca Metal Exposed to Mix-Electrolyte for 20 Days at Room Temperature (22° C).

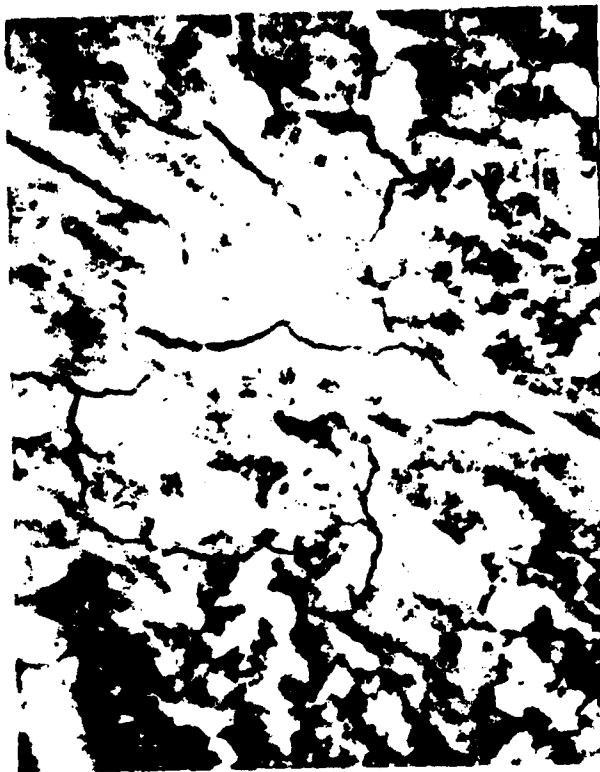


a) 100 X

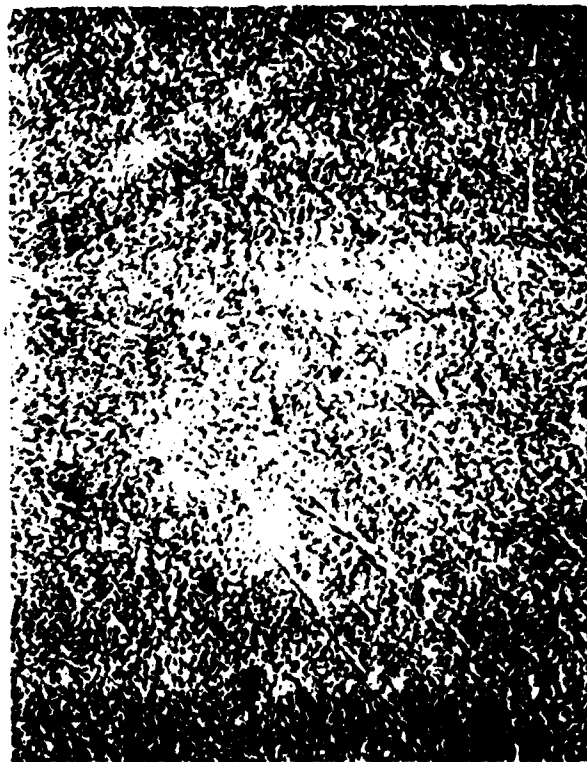


b) 1000 X

Figure 21. SEM Photomicrographs of Ca Metal Exposed to Mix-Electrolyte for 30 Days at Room Temperature (22° C).



b) 1000 X



a) 100 X

Figure 22. SEM Photomicrographs of Ca Metal Exposed to Mix-Electrolyte for 13 Days at Room Temperature (22° C) and 7 Days at 55° C.

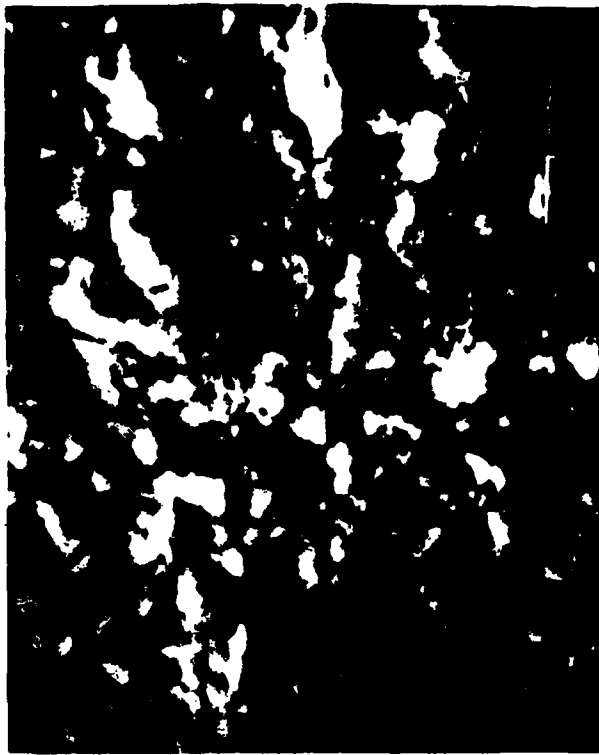


a) 100 X

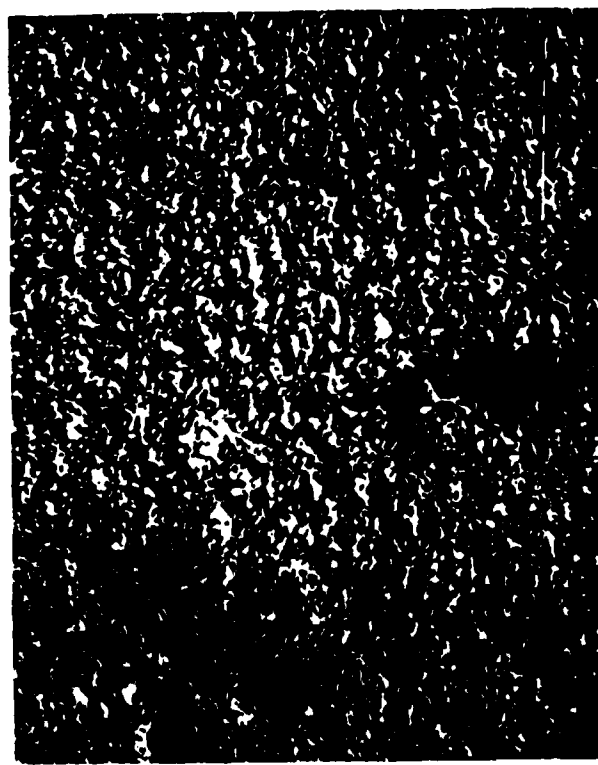


b) 1000 X

Figure 23. SEM Photomicrographs of Ca Metal Exposed to Mix-Electrolyte for 13 Days at Room Temperature (22° C) and 17 Days at 55° C.



b) 1000 X

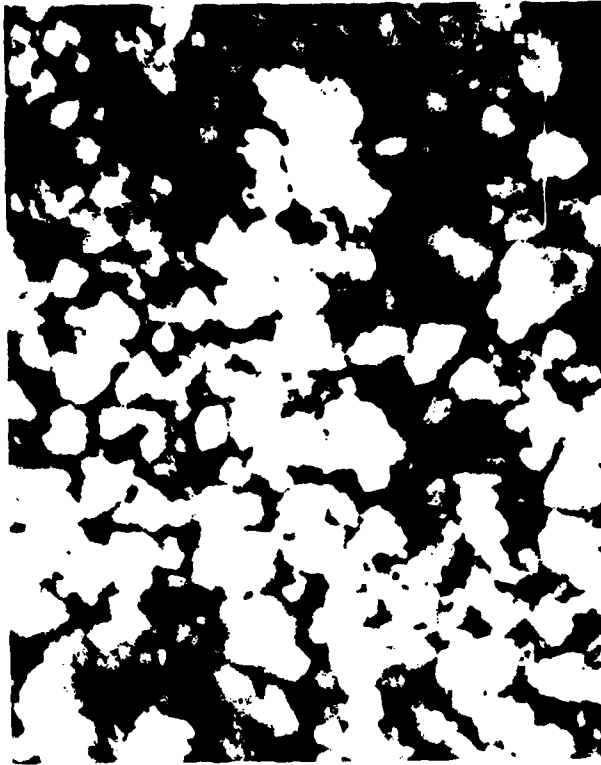


a) 100 X

Figure 24. SEM Photomicrographs of Ca Metal Exposed to EPI Li- Electrolyte for 14 Days at Room Temperature (22° C).



a) 100 X



b) 1000 X

Figure 25. SEM Photomicrographs of Ca Metal Exposed to EPI Li- Electrolyte for 14 Days at 55° C.

Mix-electrolyte and Ca-electrolyte in the same time period. If figures 11 and 24 are compared it is noticed that the extent of corrosion is more in figure 24 as compared to figure 11. Figure 24 belongs to Li-electrolyte (EPI) and figure 11 belongs to Li-electrolyte (GTE). It appears that EPI electrolyte has caused the same level of corrosion, if not more, as compared to GTE electrolyte in half the time.

If one were to sketch this data in the form of a graph, of a qualitative nature, the result would be as shown in figure 26. This graph presents the relative corrosion rates of Calcium metal in different systems. As indicated in figure 26 a slight amount of corrosion was observed for Ca metal sealed and stored in the helium environment at the 55° C. This may have been caused due to the fact that all samples had been stored in the same chamber so some air or thionyl chloride vapor might have leaked into these samples since the aluminium caps were slightly corroded, and at the same time some loss of thionyl chloride was observed in other samples. It appears that with the passage of time seals were not holding too well, especially at 55° C. In order to assure that teflon seals are inert to thionyl chloride, several seals were examined after removing the samples from the bottles. The teflon seals did not indicate any damage or rough surface, thus it may be concluded that teflon is not affected by thionyl chloride under the experimental conditions investigated.

V. SUMMARY AND CONCLUSIONS

In addition, to the above general discussion of calcium corrosion, the salient results of this investigation are:

1. Ca metal can be reasonably cleaned and polished using the mechanical cleaning methods as described earlier.
2. Suitable electrolytes such as LiAlCl_4 and $\text{Ca}(\text{AlCl}_4)_2$ can be prepared if attention is paid to the purity of the materials used and water is kept out of the system.
3. The corrosion of Ca metal is a significant problem in the systems investigated. The corrosion occurs during storage and more rapidly at 55° C.

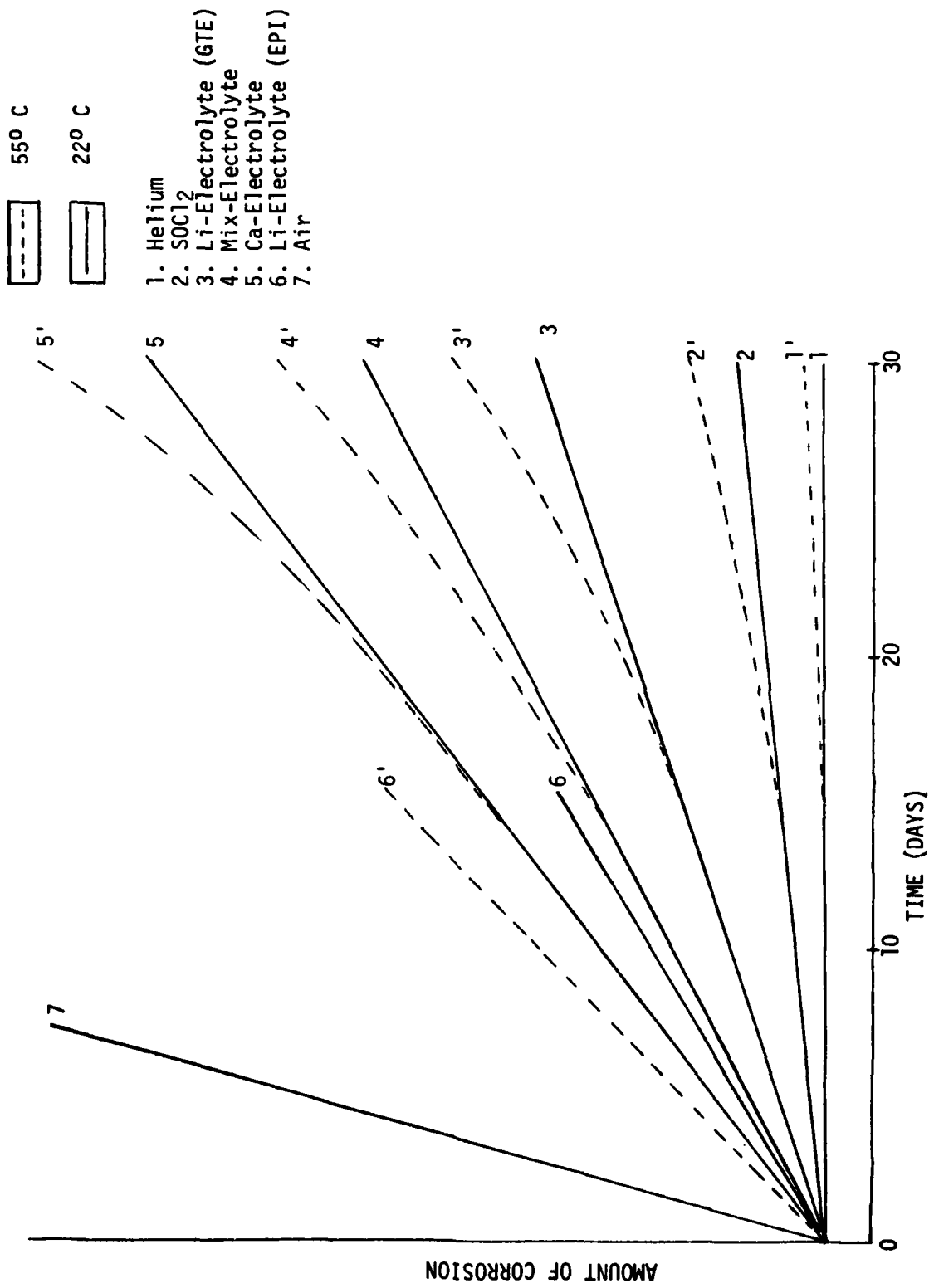
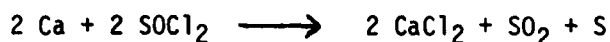


Figure 26. Relative Corrosion Rates of Calcium Metal in Different Systems.

4. Both SO_2 and CaCl_2 appear to be the likely products. The formation of SO_2 can be explained by the fact that pressure was developed in the samples. CaCl_2 formation may be supported by the amorphous and non-conducting nature of the film formed on the metal surface. Thus the corrosion reaction may be written as



A similar reaction has also been suggested by Staniewicz (8).

VI. RECOMMENDATIONS AND SUGGESTIONS FOR FURTHER WORK

At this point of investigation, if the results are to be put in practical perspective, following recommendations may be worth carrying out:

1. Calcium metal should be cleaned and polished before using in the battery.
2. Since moisture and air effect the metal surface significantly, the cells should be packed in the dry box environment.
3. High purity of electrolytes and solvents free from moisture should be used to prepare electrolytes.

In view of further suggestions for work, the work done by Dey (11) suggests that lowering the electrolyte concentration of LiAlCl_4 in SOCl_2 reduces the rate of LiCl film formation on lithium surface, thus a similar investigation in case of calcium system will be worthwhile. The work reported by Gabano (12) suggests that altering the electrolyte with polyhedral anions such as $\text{B}_{10}\text{Cl}_{10}$ and with $\text{AlCl}_3/\text{Li}_2\text{O}$ significantly improves voltage delay, thus incorporating these or similar ions into the electrolyte for calcium batteries may also result in reduced voltage delay and reduced level of corrosion. Driscoll and co-workers (13) have suggested that addition of PCl_5 to the electrolyte reduces the cell passivation during storage, similar investigation in the calcium battery system will be worth the effort. Driscoll has investigated performance of several lithium alloys and some of the alloys such as Lithium alloyed with Ag, Cd, Mg, or Si have displayed better recovery rate and better anode utilization than pure lithium. In view of Driscoll's findings it is suggested that alloys of calcium with different metals such as Li, Mg, Cd, Ag, or Si should also be investigated as alternates to pure calcium for these high energy density battery systems.

REFERENCES

1. J.F. McCartney, W.H. Shipman, C.R. Gundersen, 'Development of Lithium Inorganic Batteries for Navy Applications.' NUCTV 1618 (1975).
2. A.V. Gross, and J.B. Conway; Ind. Eng. Chem. 50, 663 (1958).
3. W.C. Reynolds, 'Investigations of Ignition Temperatures of Solid Metals,' NASA TNS-182 (1959).
4. 'Hill Top News,' (Hill AFB Newspaper) 6th August(1976).
5. R. Higgins, and L. Elliot, 'Calcium Inorganic Electrolyte Battery Development,' AFAPL-TR-79-2044 (1979).
6. R.L. Higgins, 'Development of the Ca/SOCl₂ System,' Power Sources Conference, Atlantic City, NJ, June (1980).
7. R.L. Higgins, 'Calcium Inorganic Electrolyte Battery Development,' AFAPL-TR-79-2044 (1981).
8. R.J. Staniewicz, 'A Study of the Calcium-Thionyl Chloride Electro-chemical System,' Journal of The Electrochemical Society, 127 782-789 (1980).
9. J.G. Becsey, 'Studies of Various Anodes Replacing Lithium in High Energy Density Batteries,' Report submitted to AFAPL (1978).
10. R.G. Keil, W.E. Moddeman, T.N. Wittberg, J.R. Hoenigman, P.S. Zaidain, and J.A. Peters, 'Non-Aqueous Electrode Research,' AFWAL-TR-80-2094 (1980).
11. A.N. Dey, 'Lithium-Solvent Interactions in Li/SOCl₂ and Li/SO₂ Battery Systems,' Proceedings of The Electrochemical Society, Vol 80-7 83-97(1980).
12. J.P. Gabano, 'Lithium Passivation in Liquid Cathode Battery Systems,' Proceedings of The Electrochemical Society, Vol 80-7 98-114 (1980).
13. J.R. Driscoll, S.B. Brummer, P. Gudrais, G.L. Holleck, D.E. Tolland, and M.L. Turchan, 'Lithium-Inorganic Electrolyte Batteries,' Research and Development Technical Report ECOM-74-0030-F, March (1978).

1981 USAF - SCEEE SUMMER FACULTY RESEARCH PROGRAM

Sponsored by the

AIR FORCE OFFICE OF SCIENTIFIC RESEARCH

Conducted by the

SOUTHEASTERN CENTER FOR ELECTRICAL ENGINEERING EDUCATION

FINAL REPORT

AN INVESTIGATION INTO STATE ESTIMATION FOR AIR-TO-AIR MISSILES

Prepared by: Dr. Kenneth R. Hall
Academic Rank: Associate Professor
Department and University: Department of Aerospace Engineering
Mississippi State University
Research Location: Air Force Armament Laboratory
Guided Weapons Division
Systems Analysis and Simulation Branch
USAF Research Colleague: P. L. Vergez, 1Lt, USAF
Date: July 24, 1981
Contract No. F49620-79-C-0038

AN INVESTIGATION INTO STATE ESTIMATION FOR AIR-TO-AIR MISSILES

by

Kenneth R. Hall

ABSTRACT

The use of modern control theory in the development of the guidance algorithms for homing missiles requires full knowledge of the state vector for producing the optimal control law. In the majority of situations encountered, this state information is not available directly from the measurements but must be deduced from the actual measurements. The process of obtaining the desired state information from the measurements is known as state estimation and is the subject of this study. The estimation procedure requires that a model of the state vector propagation be created, and the output of the model is used to construct estimates of the measurements. As the measurements are made, the discrepancy between the actual measurements and the estimated measurements is used to adjust the state estimates of the model. This study will address the creation of an estimation algorithm (the extended Kalman filter), the application of the theory to the missile control problem, and then discuss the use of the available information in allowing the filter algorithm to adapt to the noise characteristics of the problem. Numerical results are obtained and compared to information from other sources. Suggestions for further research are offered.

ACKNOWLEDGEMENT

The author would like to express his appreciation to the Air Force Systems Command, the Air Force Office of Scientific Research and the Southeastern Center for Electrical Engineering Education for providing him with the opportunity to spend a very worthwhile and interesting ten weeks at the Air Force Armament Laboratory, Eglin Air Force Base, FL. In particular, the systems analysis and simulation branch provided excellent working conditions and hospitality during this period. Lastly, the author would like to thank 1Lt. Paul Vergez, the research colleague, and his associates, 1Lt. Jim McClendon and Maj. Paul Torrey, for the interesting discussions and for the personal friendship which was exhibited throughout the study.

OBJECTIVES

The use of modern optimal control theory in developing the guidance law for an air-to-air missile pursuing a maneuvering target frequently leads to the need for state variable measurements which are not measurable by the sensor complement of the missile. Kalman filtering and, specifically, extended Kalman filtering is the estimation technique used to extract the desired state variable quantities from the available measured quantities. The objective of this study was to place the guidance algorithm and the estimation algorithm on a firm mathematical footing, to explain some of the discrepancies which appear between theory and application, and to investigate means of improving the estimation algorithm for the air-to-air missile problem. The mathematical development will include the development of the guidance law from linear quadratic control theory assuming full availability of state variable information and the development of the extended Kalman filter estimation algorithm to provide the needed state variable information from the missile sensor complement which features a passive seeker. The improvements in the filter development will take the form of numerical integration by quadratures, numerical generation of the state transition matrix, improvements in the filter algorithm, and studies in the use of adaptive filtering for improved accuracy.

I. INTRODUCTION:

The problem of guiding an airborne missile to achieve a target objective originated in Germany during World War II. The German scientists employed various guidance schemes for the missiles which ranged from open loop preprogrammed commands to elementary inertial guidance systems. The rest of the world rapidly assimilated the airborne missile into their weaponry and also inherited the problem of guiding the missile to the designated target. Two missile systems which are currently in widespread use by the United States for air-to-air combat are the AIM-7 (Sparrow) and the AIM-9 (Sidewinder). Both of these missiles employ some form of proportional navigation (pro-nav) in their guidance algorithms. Guidance systems employing pro-nav were developed during the 1950s for use with analog devices, and while providing excellent service in the use for which they were intended, cannot perform as well as modern guidance systems which are developed around current digital technology. The introduction of modern technology in the form of minicomputers and microcomputers allows the application of modern optimal control techniques to the guidance of these airborne missiles. Adaptive control systems with variable gains and onboard processing capability provide the potential for increased performance and versatility for these weapons with small investment. The price for the increased potential is the need for development of the optimal control law and the accompanying estimation algorithm for processing the sensor measurements for the control system.

The sensor complement employed on air-to-air missiles is usually composed of rate gyros and accelerometers for determining information about the missile and a seeker of some form for determining information about the target. The missile sensors typically provide noisy measurements of the missile data and the seeker provides noisy information about the target. The seeker information can be composed of measurements of line-of-sight data only (passive seeker) or measurements of line-of-sight data and range data (active seeker). The active seekers typically use some form of onboard radar to obtain the range data and are more complex than the passive seekers. This study will consider passive seekers only.

The missile employed in the this study is an extension of the current missile technology in that the missile has short aerodynamic surfaces (wings) which can generate large aerodynamic forces in the pitch plane of the missile. For steering, the missile rolls to orient the pitch plane in the direction of the desired control force and uses the lift force as the control force. This type of missile is known as a bank-to-turn (BTT) missile as opposed to those missiles which do not employ lift and are called skid-to-turn (STT) missiles. The particular BTT missile employed in this study can typically attain accelerations of 20 to 30 Gs due to thrust and is limited structurally to a maximum acceleration of 100 Gs. The thrusting period is approximately 2.5 seconds, and the missile is not allowed to maneuver during the first 0.4 seconds while clearing the launching aircraft. This information is given to furnish background for the control law development.

The development of the control law follows the form known as the deterministic linear quadratic optimal control problem in which the control is assumed to be composed of a linear combination of the state variables and the control system is supposed to minimize some quadratic measure of the performance known as the performance index. The assumption that the states are measured and available is not true so an algorithm must be derived which will furnish the information about the states to the control law from the measurements which are available. For noisy measurements, one must employ elements of statistical (stochastic) analysis to determine the needed information. For problems governed by linear differential equations with linear state-measurement relationships, the optimal estimator is the Kalman filter algorithm. For nonlinear problems where the differential equations are nonlinear or the state-measurement relations are nonlinear, or both, the estimation algorithm is the extended Kalman filter. This study is concerned with linear differential equations with nonlinear state-measurement relations, so the extended Kalman filter will be used. One section of this report deals with the development of the extended Kalman filter and the logic which is employed in the development.

The Kalman filter employs a model of the state propagation process to determine estimated state values at a point in time. These estimated states are used to construct an estimated measurement vector at that time. The difference between the actual measurement and the estimated measurement is then used to update the state estimates to a more correct value.

The usual practice when constructing a Kalman filter algorithm is to assume some constant parameters for the noise characteristics which are specific to the particular problem configuration. The filter is therefore "tuned" for a certain operating condition. One of the contributions of this study is to show the way to let a filter compute its own noise characteristics and therefore tune itself to the problem configuration. There is no problem in adapting to the noise characteristics of the measurements as the measurement residuals themselves furnish the desired information. The procedure of adapting to the process noise, the noise associated with the state propagation process, is not so straightforward and no clearly correct procedure of accomplishing this adaptation is apparent.

II. PROBLEM DEVELOPMENT

The differential equations governing the motion of an air-to-air missile pursuing a maneuvering target are developed in this section of the paper. The control for the problem will be the acceleration vector for the missile. The problem could be expressed in terms of the target's inertial position, velocity and acceleration vectors and the missile's inertial position, velocity and acceleration vectors. This formulation of the problem would involve fifteen state variables and three controls. An alternate expression of the problem is in the form of the target's position and velocity vectors relative to the missile, and the target's and missile's inertial acceleration vectors. This last form requires only nine state variables and three controls while providing the same problem information and will be the form of the equations chosen for this study.

A set of inertial axes is established at the instant of missile launch and will be the axes for the problem analysis. The inertial axes are established with the x-axis in the direction of the initial velocity vector of the missile projected into the horizontal plane, the z-axis vertically downward, and the y-axis completes the right-handed system (Figure 1). From this time onward, all position, velocity and acceleration vectors will be described in terms of components along these coordinate axes.

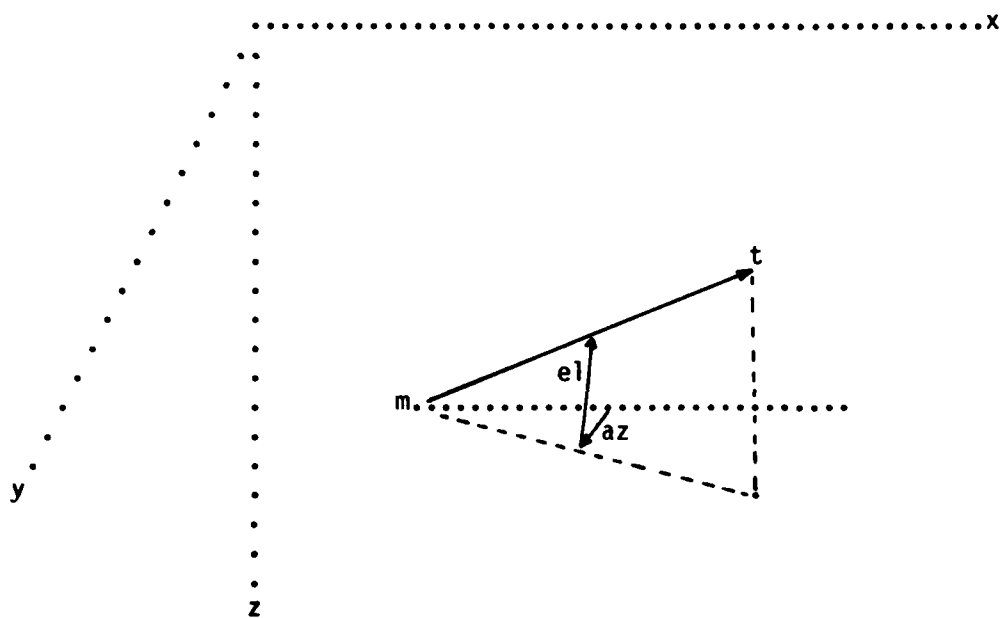


Figure 1. Missile-Target Engagement Geometry

Let $\underline{R}_T, \underline{V}_T, \underline{A}_T$ be the symbols for the target's inertial position, velocity and acceleration vectors, respectively. Let $\underline{R}_M, \underline{V}_M, \underline{A}_M$ be the symbols for the missile's inertial position, velocity and acceleration vectors, respectively. Let $\underline{R}, \underline{V}$ be the symbols for the target's position and velocity vectors relative to the missile and the differential equations governing the state variables of the problem may be written in the following form.

$$\dot{\underline{R}} = \underline{V}_T - \underline{V}_M = \underline{V}$$

$$\dot{\underline{V}} = \underline{A}_T - \underline{A}_M$$

$$\dot{\underline{A}}_T = \underline{J}_T$$

The symbol \underline{J}_T in the equation above represents the time derivative of the inertial acceleration vector of the target. If a non-zero value is used for this time derivative, then the equations will predict the future actions of the target when, in reality, The future actions of the target are a random quantity to the missile control system. Since these equations are being developed for use by the missile control system, the time derivative of target acceleration will be set equal to zero. It should be noted that this does not preclude target accelerations or maneuvers but merely furnishes a model to the control system which uses the current acceleration vector of the target as a constant in control computations.

Define the scalar components of the nine-element state vector and the three element control vector by the following symbols:

X_1, X_4, X_7	x, y, z components of relative position
X_2, X_5, X_8	x, y, z components of relative velocity
X_3, X_6, X_9	x, y, z components of target acceleration
U_1, U_2, U_3	x, y, z components of missile acceleration

The state variable differential equations may now be written in the standard form for linear problems as follows.

$$\frac{d}{dt} X = A X + B U$$

$$\frac{d}{dt} \begin{bmatrix} X1 \\ X2 \\ X3 \\ X4 \\ X5 \\ X6 \\ X7 \\ X8 \\ X9 \end{bmatrix} = \begin{bmatrix} 0 & 1 & 0 & 0 & 0 & 0 & 0 & 0 & 0 \\ 0 & 0 & 1 & 0 & 0 & 0 & 0 & 0 & 0 \\ 0 & 0 & 0 & 0 & 0 & 0 & 0 & 0 & 0 \\ 0 & 0 & 0 & 0 & 1 & 0 & 0 & 0 & 0 \\ 0 & 0 & 0 & 0 & 0 & 1 & 0 & 0 & 0 \\ 0 & 0 & 0 & 0 & 0 & 0 & 0 & 0 & 0 \\ 0 & 0 & 0 & 0 & 0 & 0 & 0 & 1 & 0 \\ 0 & 0 & 0 & 0 & 0 & 0 & 0 & 0 & 1 \\ 0 & 0 & 0 & 0 & 0 & 0 & 0 & 0 & 0 \end{bmatrix} \begin{bmatrix} X1 \\ X2 \\ X3 \\ X4 \\ X5 \\ X6 \\ X7 \\ X8 \\ X9 \end{bmatrix} + \begin{bmatrix} 0 & 0 & 0 \\ -1 & 0 & 0 \\ 0 & 0 & 0 \\ 0 & 0 & 0 \\ 0 & -1 & 0 \\ 0 & 0 & 0 \\ 0 & 0 & 0 \\ 0 & 0 & -1 \\ 0 & 0 & 0 \end{bmatrix} \begin{bmatrix} U1 \\ U2 \\ U3 \end{bmatrix}$$

Note the natural division of the full nine-state differential equation into three independent three-state differential equations.

$$\frac{d}{dt} \begin{bmatrix} X1 \\ X2 \\ X3 \end{bmatrix} = \begin{bmatrix} 0 & 1 & 0 \\ 0 & 0 & 1 \\ 0 & 0 & 0 \end{bmatrix} \begin{bmatrix} X1 \\ X2 \\ X3 \end{bmatrix} + \begin{bmatrix} 0 \\ -1 \\ 0 \end{bmatrix} U1$$

$$\frac{d}{dt} \begin{bmatrix} X4 \\ X5 \\ X6 \end{bmatrix} = \begin{bmatrix} 0 & 1 & 0 \\ 0 & 0 & 1 \\ 0 & 0 & 0 \end{bmatrix} \begin{bmatrix} X4 \\ X5 \\ X6 \end{bmatrix} + \begin{bmatrix} 0 \\ -1 \\ 0 \end{bmatrix} U2$$

$$\frac{d}{dt} \begin{bmatrix} X7 \\ X8 \\ X9 \end{bmatrix} = \begin{bmatrix} 0 & 1 & 0 \\ 0 & 0 & 1 \\ 0 & 0 & 0 \end{bmatrix} \begin{bmatrix} X7 \\ X8 \\ X9 \end{bmatrix} + \begin{bmatrix} 0 \\ -1 \\ 0 \end{bmatrix} U3$$

The state variable differential equations can be written in the standard form whether they represent the full nine-state system or one of the three three-state systems. The standard form is a linear, non-homogenous vector differential equation for which standard solution techniques involving the state transition matrix can be applied.

$$X(TF) = F(TF, T) X(T) + \int_T^{TF} F(TF, t) B(t) U(t) dt$$

$$\dot{F} = A F$$

$$F(T, T) = I, \text{ the identity matrix}$$

If the full nine-state system is described, then the state transition matrix is a 9x9 matrix. If, however, one of the three-state systems is described, then the state transition matrix is a 3x3 matrix. From the equation above, the knowledge of the current state, in combination with an analytical solution to the state transition matrix and a time history of the control, will allow the determination of the final state value. This property will be employed in the development of the optimal control law.

III. CONTROL LAW DEVELOPMENT

The optimal control law for an air-to-air missile pursuing a maneuvering target is derived in this section. The optimum result for this problem is the minimization of the final miss distance while maintaining acceptable levels of control along the missile trajectory. The control vector is the acceleration vector for the missile, and, in the absence of foreknowledge of target maneuvers, the target acceleration will be assumed constant. The performance index for the problem is given by the expression below.

$$J = \frac{1}{2} X^t(TF) S(TF) X(TF) + \int_T^{TF} \frac{1}{2} U^t(t) W U(t) dt$$
$$S(TF) = \begin{bmatrix} S1 & 0 & 0 \\ 0 & S1 & 0 \\ 0 & 0 & S1 \end{bmatrix}; \quad S1 = \begin{bmatrix} 1 & 0 & 0 \\ 0 & 0 & 0 \\ 0 & 0 & 0 \end{bmatrix}; \quad W = \begin{bmatrix} w & 0 & 0 \\ 0 & w & 0 \\ 0 & 0 & w \end{bmatrix}$$

The definition of the control weighting matrix as a diagonal matrix and the natural diagonal form of the final state weighting matrix allows the performance index for the nine-state problem to be written as the sum of three independent performance indices, one for each independent coordinate axis. This should have been expected, as the state differential equations also decomposed into three independent sets. Using similarity, one may solve one of the independent three-state problems and use the result to infer the solution to the full nine-state problem. This is the approach which is taken in the following analysis.

Choose the x-axis for the three-state problem direction chosen for analysis, and use the following definitions.

$$X = [X_1, X_2, X_3]^t$$

$$J = \frac{1}{2} X(T)^t S_1 X(T)^t + \int_T^{TF} \frac{1}{2} U_1^t(t) w U_1(t) dt$$

The symbols S_1 and w have the same meaning given to them on the previous page. The problem is now to minimize the above performance index subject to the set of differential constraints represented by the differential equations.

$$\dot{X} = A X + B U_1$$

$$A = \begin{bmatrix} 0 & 1 & 0 \\ 0 & 0 & 1 \\ 0 & 0 & 0 \end{bmatrix}; \quad B = \begin{bmatrix} 0 \\ -1 \\ 0 \end{bmatrix}$$

An augmented performance index is formed by appending the differential equations to the original performance index using the costate variables.

$$P = [P_1, P_2, P_3]^t$$

$$J = \frac{1}{2} X(T)^t S_1 X(T)^t + \int_T^{TF} \left(\frac{1}{2} U_1^t w U_1 + P^t (A X + B U_1 - \dot{X}) \right) dt$$

$$H = \frac{1}{2} U_1^t w U_1 + P^t (A X + B U_1)$$

The numerical Hamiltonian defined by the last equation is purely for notation, in that the expressions arising from the optimization procedure may be expressed in terms of the numerical Hamiltonian.

The minimization of the augmented performance index with no constraints is equivalent to the minimization of the original performance index with the differential equation constraints.

Set the first variation of the augmented performance index equal to zero and obtain the conditions necessary to produce a minimum of the augmented performance index, and a minimum of the original performance index. Note that the original performance index was a quadratic form with a positive definite weighting matrix, so only a minimum exists for the problem. Setting the first variation of the augmented performance index equal to zero produces the following conditions.

$$\text{Boundary: } (X^t(TF) S1 - P^t(TF)) d(X(TF)) + (H(TF)) d(TF) = 0.$$

$$\text{State: } \dot{X} = A X + B U1$$

$$\text{Costate: } \dot{P} = -A P$$

$$\text{Optimality: } U1 = -\frac{1}{W} B P$$

The boundary condition furnishes a final value for the costate variable in terms of the final value of the state variable. For now, the final time will be considered fixed. If the optimality condition is used to eliminate the control from the state and costate differential equations, a classic two point boundary value problem will result with the initial values of the states known and the final values of the costates known. Most problems of this nature must be solved by an iterative procedure, but this particular problem possesses an analytical solution.

Consider now the integration of the costate equations which are linear homogenous differential equations with constant coefficients.

$$\dot{P} = -A P ; \text{ and } P(TF) = S1 X(TF)$$

$$\frac{d}{dt} \begin{bmatrix} P1 \\ P2 \\ P3 \end{bmatrix} = - \begin{bmatrix} 0 & 0 & 0 \\ 1 & 0 & 0 \\ 0 & 1 & 0 \end{bmatrix} \begin{bmatrix} P1 \\ P2 \\ P3 \end{bmatrix} ; \begin{bmatrix} P1(TF) \\ P2(TF) \\ P3(TF) \end{bmatrix} = \begin{bmatrix} X1F \\ 0 \\ 0 \end{bmatrix}$$

$$P1 = X1F$$

$$P2 = X1F (TF-T)$$

$$P3 = X1F \frac{(TF-T)^2}{2}$$

The analytical solutions for the costate differential equations are in terms of the unknown parameters of final position and final time. While these parameters are not yet known, they are not variables but constants to be determined. Using the optimality condition, express the optimal control in terms of these unknown parameters as follows.

$$U1 = - \frac{1}{w} B P$$

$$U1 = \frac{1}{w} X1F (TF-T)$$

The optimal control is now known in terms of the parameters and time. This will allow us to use the state transition matrix solution to the state differential equations as the integral term can now be evaluated.

$$X(TF) = F(TF, T) X(T) + \int_T^{TF} F(TF, t) B U_1(t) dt$$

As the state transition matrix is required for the actual integration, the following determination of the state transition matrix will be advantageous.

$$\dot{F} = A F ; F(T, T) = I , \text{ the identity matrix}$$

$$F = \begin{bmatrix} 1 & (TF-T) & \frac{(TF-T)^2}{2} \\ 0 & 1 & (TF-T) \\ 0 & 0 & 1 \end{bmatrix}$$

The expression for the state transition matrix may be used in the state variable equation above to yield the following expression for X_1F .

$$X_1F = X_1 + X_2 (TF-T) + X_3 \frac{(TF-T)^2}{2} - X_1F \frac{(TF-T)^3}{3w}$$

Solving for the value of X_1F from this equation will allow the elimination of one of the unknown parameters which appear in the optimal control.

For shorthand notation define the symbol for the time-to-go, ($TTG=TF-T$).

$$X_1F = \frac{3w}{3w + TTG} \begin{bmatrix} 1, TTG, \frac{TTG^2}{2} \end{bmatrix} \begin{bmatrix} X_1 \\ X_2 \\ X_3 \end{bmatrix}$$

$$U_1 = \frac{3TTG}{3w + TTG} \begin{bmatrix} 1, TTG, \frac{TTG^2}{2} \end{bmatrix} \begin{bmatrix} X_1 \\ X_2 \\ X_3 \end{bmatrix}$$

Using similarity, the expression for the optimal control in one dimension can be expanded to all three dimensions. The full optimal control vector in component form is produced as follows:

$$GN = \frac{3 \text{ TTG}}{3 w + \text{TTG}}$$

$$U_1 = GN \left(X_1 + X_2 \text{ TTG} + X_3 \frac{\text{TTG}^2}{2} \right)$$

$$U_2 = GN \left(X_4 + X_5 \text{ TTG} + X_6 \frac{\text{TTG}^2}{2} \right)$$

$$U_3 = GN \left(X_7 + X_8 \text{ TTG} + X_9 \frac{\text{TTG}^2}{2} \right)$$

Note that this optimal control is a one parameter family of solutions for the problem. Until TTG has been assigned a value, there is no value for the control. The specification of TTG will provide a unique value for the optimal control.

If one component of the missile acceleration (the control) were known, then the equation for TTG could be solved in that direction and the result used to specify the control components in the other two directions. One component of missile acceleration which is known is the thrust acceleration. The solution technique for TTG will be to determine the projection of the optimal control onto the thrust axis, equate this projection to the thrust acceleration and solve the resulting equation for the value of TTG. For simplification, the missile thrust acceleration vector is assumed to be colinear with the missile velocity vector and both vectors are assumed to be available.

Let \underline{AMV} denote the thrust acceleration vector for the missile which is assumed to be along the velocity vector. Obtain the equation for determining TTG from the following inner product of these two vectors.

$$\begin{aligned} \underline{AMV} \cdot \underline{VM} &= \underline{AM} \cdot \underline{VM} = U_1 VM_1 + U_2 VM_2 + U_3 VM_3 \\ &= GN \underline{VM} \left(\underline{R} + \underline{V} TTG + \underline{AT} \frac{TTG^2}{2} \right) \end{aligned}$$

Replacing GN with the expression involving TTG will allow the development of a cubic equation for TTG.

$$C_1 + C_2 TTG + C_3 TTG^2 + C_4 TTG^3 = 0.$$

$$C_1 = 3 \underline{w} \underline{VM} \underline{AMV}$$

$$C_2 = 3 \underline{VM} \underline{R}$$

$$C_3 = 3 \underline{VM} \underline{V}$$

$$C_4 = \underline{VM} \left(\frac{3}{2} \underline{AT} - \underline{AM} \right)$$

With the assumption that that all the information regarding the state variables is available the cubic equation can be solved for TTG. Note that the value of TTG obtained is valid for the information used to obtain TTG. Changes in the thrust acceleration of the missile or changes in the target acceleration will cause discontinuities in the calculation of TTG. One major discontinuity occurs when the missile exhausts its fuel supply and the thrust force

drops immediately to zero. When that occurs, the equation for TTG collapses into a quadratic equation in TTG when the zero roots are eliminated. With C1 equal to zero, the quadratic equation for the solution of TTG will be:

$$C2 + C3 TTG + C4 TTG^2 = 0.$$

The determination of TTG from the quadratic is straightforward. One point of interest -- when the radical term which naturally results from the quadratic equation is expanded to first order terms only, the common TTG of the pro-nav guidance systems reappears.

With the determination of a value for TTG, the optimal control law is completely specified in terms of the current state vector information. One should remember the assumptions which were made in the development of the guidance law and in the determination of the parameters which provide a unique control.

IV. ESTIMATION ALGORITHM DEVELOPMENT

An estimation algorithm is a computational technique for extracting desired information from available information. In the previous section, the optimal control was determined in terms of the state vector and the estimation algorithm is the means of furnishing the state vector information to the control law. Ideally, enough sensors of sufficient complexity would be employed to directly measure the state information needed by the control law. Due to technology limitations and budgetary restrictions, the more common practice is to use simple, reliable, available sensors and attempt to extract the desired information from the sensed information by using estimation techniques.

For the control of an air-to-air missile with a passive seeker, the available sensors measure the inertial acceleration of the missile and the angles defining the line-of-sight direction from the missile to the target. All measurements are corrupted by some form of additive noise and there is uncertainty in the conditions used to initialize the filter model. From these measurements, the estimation algorithm should determine the target's position and velocity relative to the missile, and the inertial acceleration of the target -- the full state vector. This section of the report will deal with the development of the estimation algorithm, the extended Kalman filter, and apply the algorithm to the missile problem.

An estimation algorithm relies upon a model of the process by which the state vector describing the system is propagated in time. This problem is described by a linear model and we will assume that the actual state vector follows the same linear model plus an extra term to account for any unmodeled terms, incorrectly modeled terms, integration inaccuracies and any other errors which we will lump together into the category called "process noise". The true state vector propagation is represented by the linear vector differential equation given below.

$$\dot{X} = A X + B U + C$$

Where:

- X is an N-state vector
- A is an NxN matrix of constants
- B is an NxM matrix of constants
- U is an M-control vector
- C is an N-vector of coefficients

The integration of these linear differential equations by utilizing the state transition matrix provides a recursive propagation equation as given below.

$$X(k+1) = F X(k) + G U(k) + q(k)$$

Where:

- X(k) is the state vector at the k-th time point
- F is the NxN state transition matrix
- G is the NxM control transition matrix
- q is an N-vector of noise terms

One should note at this point in the discussion that if the exact form of the differential equation were known, if the exact value of the initial state vector were known, if the exact value of the control were known, and if the integration procedure were exact, there would be an exact model of the process and there would be no need for estimation. The only input required to produce the state vector would be the time for which the state vector is desired. The fault with this line of reasoning is that there are no exact quantities in the real world. For problem solution in the real world, one must make a "best guess" or estimate of the initial state vector, obtain a control vector based upon the estimated state vector, and propagate the state estimate to a new time based upon an "assumed form" or model of the state propagation relationships. As new information arrives in the form of measurements, the propagated state estimate is "corrected" or updated to conform to the measurement information. In the estimation world, the terms "propagate" and "update" are of paramount importance.

Let X denote the true value of the state vector, let XH denote the best estimate of X using all available information, and let XB denote the propagated state vector before correction for the latest measurement.

$$X(k+1) = F X(k) + G U(k) + q(k)$$

$$XB(k+1) = F XH(k) + G U(k)$$

Note that the true state is unknown, and that all we have is an estimate of the state propagated by an assumed model of the propagation process.

An error propagation equation can be obtained by subtracting the true state propagation equation from the estimated state propagation equation. Define the following terms in the error propagation equations:

$$XBe = XB - X$$

$$XHe = XH - X$$

Where $XBe(k+1) = F XHe(k) - q(k)$

The error equations are not used to propagate errors as we would remove the errors if we knew about them. The error equations are useful for propagating error bounds which can be established. Define the covariance matrix PB as the expected value of the outer product of the propagated estimation error bound (XBe) with itself. In a similar fashion, define the covariance matrix PH for the estimation error bound (XHe).

$$PB = E(XBe XBe^t)$$

$$PH = E(XHe XHe^t)$$

The use of the covariance matrix relieves us from having to guess the signs of the initial estimation errors as the diagonal terms of the covariance matrices are the squares of the estimation error bounds. Assuming that the initial estimation error bounds are uncorrelated with zero expected values allows us to set the off-diagonal terms in the covariance matrix equal to zero. The estimation error covariance matrix provides a measure of the relative confidence which can be placed in the validity of the state

estimate as shown by the growth or decline of the estimation error bounds. The equation governing the propagation of the estimation error covariance matrix may be obtained from the propagation equation for the estimation error.

$$XBe(k+1) = F XHe(k) - q(k)$$

$$\begin{aligned} PB(k+1) &= E(XBe(k+1) XBe^t(k+1)) \\ &= E((F XHe(k) - q(k)) (F XHe(k) - q(k))^t) \end{aligned}$$

Expanding the indicated product of the last equation into simple products and assuming that the state estimation error on the k-th step and the state propagation process error during the k-th step are uncorrelated with zero expected product allows us to write the propagation equation for the estimation error covariance as follows:

$$PB(k+1) = F PH(k) F^t + Q(k)$$

The last equation makes use of the following expected values and definitions.

$$E(F XHe XHe^t F^t) = F PH F^t$$

$$E(F XHe q^t) = 0.$$

$$E(q XHe^t F^t) = 0.$$

$$E(q q^t) = Q, \text{ the process error covariance matrix}$$

Now, the initial state vector can be estimated and the estimation model used to propagate the state vector to a new point in time. At the same time, the initial state estimate error bound can be established and used to initialize the estimation error covariance matrix. The estimation error covariance matrix may then be propagated to the new point in time along with the state estimate. One requirement for being able to propagate the estimation error covariance matrix is the definition of the process error covariance matrix, Q , which is due to the propagation process error. An estimate must be made of the difference between the model used to propagate the state estimates and the real world, and this estimated process error bound used to generate the process error covariance matrix. Note that the process error will always increase the estimation error covariance. A summary of the estimation procedure to this point is presented below.

Initialize: XH, PH, Q

Propagate: $XB(k+1) = F XH(k) + G U(k)$

$$PB(k+1) = F PH(k) F^t + Q(k)$$

Once the estimate of the state vector is propagated to the new time, a model of the relationship of the state vector to the measurement vector can be used to estimate the measurement vector. Let Z denote the true measurement vector, let ZB denote the estimated measurement vector, and

let the following equation represent the nonlinear relationship between the state vector and the measurement vector.

$$Z = h(X) + r$$

$$ZB = h(XB)$$

The additional term, r , in the true measurement relation is to accommodate any error sources between the measurement model and the real world. The term, r , is known as the measurement error. The difference between the true measurement and the estimated measurement can be determined from $ZBe = ZB - Z$, and will be given the name of measurement residual.

$$\begin{aligned} ZBe &= ZB - Z \\ &= h(XB) - h(X) - r \end{aligned}$$

Expand $h(X)$ about XB as we know the value of XB and we do not know the value of X . This will give an equation relating the measurement residual to the propagated state estimate error, and, while we cannot use the equation for computing the error, we will use it for obtaining the update relation. Define H as the matrix of partial derivatives of h with respect to the state evaluated at the state estimate and obtain:

$$ZBe = H XBe - r$$

Note that this last equation is a linear equation, even though the original relationship between the state and the measurement was nonlinear.

For completeness, define the covariance matrix for the measurement residual as CZ, and obtain the following equation.

$$\begin{aligned}
 CZ &= E(ZBe ZBe^t) \\
 &= E((H XB - r) (H XB - r)^t) \\
 &= H PB H + R
 \end{aligned}$$

In the equation above, the measurement error and propagated state estimation error are assumed uncorrelated with zero expected product, and $R = E(r r^t)$ is defined as the measurement error covariance matrix. The characteristics of the measurement process may be summarized below.

Estimate: $ZB = h(XB)$
 Measure: $ZBe = Z - ZB$
 Obtain: R
 $CZ = H PB H + R$

The incorporation of the measurement data into the estimation process will allow the correction or updating of the state estimate to make the estimated measurement more closely correspond to the true measurements. In order to accomplish the updating, some relationship must be established between the updated state estimate and the measurement. For obtaining a linear, unbiased state estimate, the updated state estimate will be formed from a linear combination of the propagated state estimate and the measurement residual. The updated state estimate, XH, the updated estimation error, XHe, and the updated estimation error covariance

matrix, PH, are given by the following equations.

$$\begin{aligned} XH &= XB - K (ZB - Z) \\ XHe &= XBe - K ZBe \\ &= (I - K H) XBe - K r \\ PH &= (I - K H) PB (I - K H)^t + K R K^t \end{aligned}$$

Note the introduction of the gain matrix K which is the Kalman gain matrix. At this time the value of the matrix is unknown. The equations above are therefore relations until the value of K is specified; then the equations can be used for updating the state estimate and the estimation error covariance.

The way in which the gain matrix is obtained specifies the type of estimation which is being used. If K is chosen to minimize the estimation error in some way, then the resulting estimator will be a minimum error estimator. If K is chosen to minimize the estimation error covariance in some way, then the resulting estimator will be a minimum variance estimator. This study will develop and use the minimum variance type of estimator.

Set the first variation of the updated estimation error covariance matrix expression above to zero and solve for the value of K which would produce this result. The value obtained in this manner is given below.

$$K = PB H^t (H^t PB H^t + R)^{-1}$$

Note that K depends only on the propagated values and the measurement error covariance, which is a pleasing result (no iteration required).

The insertion of this value of K into the equation for PH will considerably simplify the equation to the following form to be used for updating.

$$PH = (I - K H) PB$$

The entire update procedure may now be summarized as follows.

$$\begin{aligned} \text{Obtain: } K &= PB H^t (H^t PB H^t + R)^{-1} \\ \text{Update: } XH &= XB - K (ZB - Z) \\ PH &= (I - K H) PB \end{aligned}$$

The composite estimation procedure for the extended Kalman filter may now be summarized in the following table. Note that the same notation is employed as was used in the development and that the timepoint identification has been added to all the terms. The one unresolved difficulty with the filter is that the process error covariance and the measurement error covariance matrices are not determined in the process but are prespecified.

$$\begin{aligned} \text{Initialize: } & XH, PH, Q, R \\ \text{Propagate: } & XB(k+1) = F XH(k) + G U(k) \\ & PB(k+1) = F^t PH(k) F + Q(k) \\ \text{Measure: } & Z(k+1) \\ & ZB(k+1) = h(XB(k+1)) \\ & ZBe(k+1) = ZB(k+1) - Z(k+1) \\ & CZ(k+1) = H(k+1) PB(k+1) H^t(k+1) + R(k+1) \\ \text{Update: } & K(k+1) = PB(k+1) H^t(k+1) CZ^{-1}(k+1) \\ & XH(k+1) = XB(k+1) - K(k+1) ZBe(k+1) \\ & PH(k+1) = (I - K(k+1) H(k+1)) PB(k+1) \end{aligned}$$

V. ADAPTIVE ESTIMATION

In the development of the extended Kalman filter for estimation, it was noted that a potential difficulty existed in the manner of specifying the process error covariance matrix, Q , and the measurement error covariance matrix, R . This section of the paper will deal with computational methods for allowing the estimation algorithm to compute the unknown covariance matrices as part of the estimation procedure. Ideally, the adaptive filtering would permit the estimation algorithm to account for nonlinearities, for error sources not included in the model, and for all forms of noise. Practically, we cannot hope to accomplish this, but we can attempt to improve the filter operation and obtain an improvement in the estimation of the states.

The measurement residuals provide a source of information for estimating the measurement error covariance matrix. A moving window sample of measurement residuals will be used to create an unbiased estimate of the measurement error covariance matrix. The relationships for computing the characteristics of the measurement error are summarized in the table below.

$$\text{Measure: } ZBe(k) = ZB(k) - Z(k)$$

$$\text{Determine: } ZBem(nm) = \frac{1}{nm} \sum_{i=1}^{nm} ZBe(k)$$

$$CZ(nm) = \frac{1}{nm-1} \sum_{i=1}^{nm} (ZBe(i) - ZBem(nm))(ZBe(i) - ZBem(nm))^t$$

$$R = CZ - H P B H^t$$

The process error does not have any convenient residuals from which to calculate statistics. One could use the difference between the propagated state estimate and the updated state estimate as a residual and form a covariance matrix for this residual. The equations corresponding to this procedure are given below.

$$\text{Propagate: } XBe(k) = F XHe(k-1) - q(k-1)$$

$$\text{Update: } XHe(k) = F XHe(k-1) - q(k)$$

$$q(k) = XHe(k) - F XHe(k-1)$$

$$qm(nm) = \frac{1}{nm} \sum_{i=1}^{nm} q(i)$$

$$CQ(nm) = \frac{1}{nm-1} \sum_{i=1}^{nm} (q(i) - qm(nm))(q(i) - qm(nm))^t$$

$$Q = CQ$$

The procedure indicated above should be explored in more depth as the limited amount of time for this study precluded the rigorous investigation of estimation techniques. It was important to try the various parts of the theoretical analysis, but if there was no definite improvement in the simulated missile performance, the attempt was discarded. Also, attempts which failed for any reason were not analyzed in depth.

VI. NUMERICAL RESULTS

The theory developed in the previous sections was placed into practice in the simulation of a bank-to-turn missile launched at a maneuvering target. The performance of the estimation algorithm was tested by using the estimator to supply state vector information to the control system of the missile during the engagement. All launches took place at a common altitude of ten thousand feet and a common speed of Mach 0.9. A variety of launch ranges and geometries were utilized to illustrate various operating conditions for the missile. The target was a "smart target" in that it performed evasive maneuvers at accelerations of up to 9 Gs. The simulation of the missile and target are resident on the computer system at Eglin AFB, and is a very complete simulation for evaluation of the estimation algorithms. The table below summarizes the launches.

Engagement	Range(ft)	Aspect Angle(deg)	Off-Boresight Angle(deg)
1	8000	0	0
2	13000	90	0
3	26000	180	0
4	7500	0	40
5	11000	90	40
6	24000	180	40
7	1000	45	0
8	3000	135	0
9	1000	45	40
10	3500	135	40

Testing of the estimation algorithms is accomplished by running a series of Monte Carlo runs for each launch condition and using the mean miss distance of the series as an indicator of missile performance. A comparison of the estimation algorithm with and without the measurement error adaptation is given in the table below.

Engagement	Regular EKF	Adaptive EKF
	Miss (ft)	Miss (ft)
1	5.73	2.45
2	7.00	3.73
3	4.81	33.0
4	13.1	3.60
5	7.85	5.93
6	3.00	20.0
7	3.55	4.87
8	11.6	9.38
9	2.01	1.42
10	4.61	4.17

As can be seen from the table above, the adaptive filter improves the terminal miss distance for almost all of the engagements. The two notable exceptions are engagements 3 and 6 which are for launches in the 24000 to 26000 feet range. The reason for the poor performance of the filter on these two engagements is not apparent, but it seems that the filter should not be allowed to process data which is inside the noise band as are long-distance angular measurements.

Stability problems were encountered with the estimation algorithms which tried to adaptively estimate the process error covariance matrix. The reason for the stability problems was thought to be due to the lack of enough information to estimate both measurement statistics and process statistics when only measurement information is incoming to the system. At any rate, the time span allocated for the study precluded any in-depth analysis of this problem. Literature searches indicate that this is a common complaint--that the estimation of the process error statistics leads to an unstable algorithm. After encountering the stability problem with the process error covariance adaptation, a constant process error covariance matrix was employed for the rest of the study. Some attempt was made to empirically adapt to the process error statistics, but no conclusive results were attained.

VII. CONCLUSIONS AND RECOMMENDATIONS

This study has produced a composite mathematical analysis of the control system design of an air-to-air missile with bank-to-turn control. Detailed development of the control law from the linear quadratic control theory produced a control law as a function of the current state vector and the time-to-go parameter. Suggested ways of determining time-to-go include simplifications to the point that an analytical solution is possible, iterative solution of the cubic equation which was developed in Section III of this paper, and iterative solution of the two point boundary value problem for a minimum time intercept. The state vector information for the control law is obtained from an estimation algorithm which processes noisy measurement data in an optimal manner to produce state information. A detailed discussion of the development of estimation algorithms of the extended Kalman filter variety is provided with a great deal of discussion about why certain practices are followed. The concept of adaptive filtering is explored with the promise of improving the operation of the estimation process by allowing the filter to "tune" itself to the given scenario. Numerical results are provided which indicate the improvements in performance due to the adaptation by the filter. Lastly, a verbal and written description of why all this theory works provides a long needed aid to understanding the

the complimentary roles played by modern applied optimal control and by modern applied optimal estimation.

The concept of adaptive filters should be explored in depth as the adaptability feature would allow the decrease in time for creating estimators for given problems and would also allow an increase in the performance and capabilities of the filter operation. The concept of filters with internal safeguards for preventing filter divergence should be explored more thoroughly. Kalman filters are the optimal linear filters, but the concept of nonlinear filters should be explored for nonlinear problem application. In addition, the concept of suboptimal filters which possess increased stability or speed of adaptability is a subject for research.

The use of miss distance as a measure of performance for the estimation algorithms may be misleading if it is the only criteria used in selecting or discarding filters. The control system and the estimation algorithm must be a complementary pair or the best estimation algorithm will perform poorly with a poorly designed control law.

More emphasis should be placed upon the research into control systems which are not just derivatives of the linear quadratic regulator. More complex performance indices may provide increased capabilities and a performance index which is a composite of other performance indices may provide the best performance of all.

REFERENCES

1. Arthur Gelb, Ed., Applied Optimal Estimation, The M.I.T. Press, Cambridge, Mass., 1977.
2. Arthur E. Bryson, and Yu-Chi Ho, Applied Optimal Control, Blaisdell Publishing Company, Waltham, Mass., 1969.
3. J.R. McClendon and P.L. Vergez, "Application of Modern Control and Estimation Theory to the Guidance of Tactical Air To Air Missiles", Proceedings of the Second Meeting of the Coordinating Group on Modern Control Theory, 1980.
4. J.M. Sammons, S. Balakrishnan, J.L. Speyer, and D.G. Hull, Development and Comparison of Optimal Filters, AFATL-TR-79-87, Eglin AFB, 1979.
5. K.A. Myers, Filtering Theory Methods and Applications to the Orbit Determination Problem for Near-Earth Satellites, AMRL 1058, University of Texas, Austin, Tx, 1973.

APPENDIX

FORTRAN LISTING OF ESTIMATION ALGORITHM SUBROUTINE

```

L 510,1000
SUBROUTINE EXTKAL(TIM,MM,XX,X)
ADAPTIVE EXTENDED KALMAN FILTER -- 0 STATES
COMMON/IREL/DXI,DYI,DZI,DVXI,DVYI,DVZI
COMMON/TACC/ATX,ATY,ATZ
COMMON/FILTER/PI(0,0),TFIL,IFIL,IFIL,SAMP,ILOPT,APX1,AMY1,ANZI,
AZ,EL,RMC,RMCDOT
DIMENSION X(0),XB(0),PI(0,0),PB(0,0),PHI(3,3),Q(0,0)
DIMENSION RES(2),R(2,2),M(2,0),CK(0,2)
DIMENSION S1(3,3),S3(2,2)
DIMENSION SR1(2,30),SRM(2)
DIMENSION SQ(0,30),SQM(0)
GAUSSIAN QUADRATURE VEICHTS (CV) AND LOCATIONS (CX)
DIMENSION CV(0),CX(0)
DATA CV/2 17132440,2* 36870157,2* 40701303/
DATA CX/ 9324051, - 9324051, - 66120039, 66120039,
- 66120039, 23861919, - 23861919/
DATA TOL,TOL2/1.0E-10,1.0E-20/
DATA NMS,NMST,RNMS,RNMSI/20,10,20,10./
IF(TIM,GT,TOL) GO TO 200
INITIALIZATION
X(1)-DXI
X(2)-DVXI
X(3)-0
X(4)-DYI
X(5)-DVYI
X(6)-0
X(7)-DZI
X(8)-DVZI
X(9)-0
TL=0.3
QM=150
TFIL=0
OTS=1/SAMP
MOT=5*OTS
OT2=OTS*HOT
DO 100 J=1,9
DO 100 J=1,9
PI(J)-PI(I,J)
1000-100

```

```

L,1010,1500
1010- DO 104 J=1,3
1020- DO 104 J=1,3
1030- Q11,J=0
1040-104 S11,J=0
1050- Q12,21-Q1
1060- Q13,31-Q1
1070- DO 100 I=1,0
1080- DT=HOTSCX(I)*HOT
1090- TEM=EXPI-TL*DT
1100- PH11,11=1
1110- PH11,21=DT
1120- PH11,31=(TEM+TL*DT-1)/(TL*TL)
1130- PH12,11=0
1140- PH12,21=1-TEM+1/TL
1150- PH12,31=1-TEM+1/TL
1160- PH13,11=0
1170- PH13,21=TEM
1180- PH13,31=TEM
1190- DO 100 J=1,3
1200- DO 100 K=1,3
1210- TEM=0
1220- DO 105 K1=1,3
1230- DO 105 K2=1,3
1240-105 TEM=TEMPHI(J,K1)SQ(K1,K2)*PHI(K,K2)
1250-106 S11,J,K1-S11,J,K1+HOTSCX(I)*TEM
1260-C**** SI CONTAINS THE INTEGRAL OF PHI*PHIT -- 3X3
1270-C****
1280-C****
1290- TEM=EXPI-TL*DT
1300- PH11,11=1
1310- PH11,21=DT
1320- PH11,31=(TEM+TL*DT-1)/(TL*TL)
1330- PH12,11=0
1340- PH12,21=1-TEM+1/TL
1350- PH12,31=1-TEM+1/TL
1360- PH13,11=0
1370- PH13,21=TEM
1380- PH13,31=TEM
1390-C****
1400-C****
1410-C****
1420- DO 115 I=1,2
1430- DO 110 J=1,30
1440-110 SR11,J=0
1450- SRM11=0
1460- DO 115 J=1,2
1470-115 R11,J=0
1480-C****
1490- DO 125 I=1,9
1500- DO 120 J=1,30

```

L,1510,2000

1510-120 S0(1,J)-0
1520- SOM(1)-0
1530- DO 125 J-1,0
1540- O(1,J)-0
1550- DO 120 I-1,3
1560- DO 120 J-1,3
1570- O(1,J)-S(1,J)
1580- O(1,3,J)-S(1,J)
1590-120 O(1,6,J)-S(1,J)
1600- RETURN

1610-Cxxxx
1620-Cxxxx
1630-Cxxxx
1640-200

OPERATION

CALL SECOND(1)
XB(1)-X(1)+DTSX(2)+PHI(1,3)X(3)-DT2AMX
XB(1)-X(1)+DTSX(5)+PHI(1,3)X(6)-DT2AMY
XB(1)-X(1)+DTSX(8)+PHI(1,3)X(9)-DT2AMZ
XB(2)-X(2)+PHI(2,3)X(13)-DTSAMX
XB(5)-X(5)+PHI(2,3)X(16)-DTSAMY
XB(8)-X(8)+PHI(2,3)X(19)-DTSAMZ
XB(13)-PHI(3,3)X(13)
XB(16)-PHI(3,3)X(16)
XB(19)-PHI(3,3)X(19)

1740-Cxxxx
1750-Cxxxx
1760-Cxxxx
1770-
1780-
1790-220

XB CONTAINS PREDICTED STATE -- 0X1

DO 220 I-1,0
DO 220 J-1,0
PB(1,J)-0
DO 230 I-1,3
DO 230 J-1,3
DO 230 K1-1,3
DO 230 K2-1,3
PB(1,J)-PB(1,J)+PHI(1,K1)X(1,K1)+PHI(1,K2)X(1,K2)
PB(1,J)-PB(1,J)+PHI(1,K1)X(1,K1)+PHI(1,K2)X(1,K2)+PHI(1,K3)X(1,K3)
PB(1,3,J)-PB(1,3,J)+PHI(1,K1)X(1,K1)+PHI(1,K2)X(1,K2)+PHI(1,K3)X(1,K3)
PB(1,3,J)-PB(1,3,J)+PHI(1,K1)X(1,K1)+PHI(1,K2)X(1,K2)+PHI(1,K3)X(1,K3)+PHI(1,K4)X(1,K4)
PB(1,6,J)-PB(1,6,J)+PHI(1,K1)X(1,K1)+PHI(1,K2)X(1,K2)+PHI(1,K3)X(1,K3)+PHI(1,K4)X(1,K4)+PHI(1,K5)X(1,K5)
PB(1,6,J)-PB(1,6,J)+PHI(1,K1)X(1,K1)+PHI(1,K2)X(1,K2)+PHI(1,K3)X(1,K3)+PHI(1,K4)X(1,K4)+PHI(1,K5)X(1,K5)+PHI(1,K6)X(1,K6)

1830-
1840-
1850-
1860-
1870-
1880-
1890-
1900-
1910-
1920-230
1930-Cxxxx
1940-Cxxxx
1950-Cxxxx
1960-
1970-
1980-240
1990-Cxxxx
2000-Cxxxx

PB CONTAINS PHIPSPHIT -- 0X0
DO 240 I-1,0
DO 240 J-1,0
PB(1,J)-PB(1,J)+Q(1,J)

PB CONTAINS PREDICTED STATE ERROR COVARIANCE -- 0X0

```

L 2010 2500
2010-Cxxxx
2020-
2030-
2040-250
2050-
2060-
2070-
2080-
2090-
2100-
2110-
2120-
2130-
2140-
2150-
2160-
2170-Cxxxx
2180-Cxxxx
2190-Cxxxx
2200-Cxxxx
2210-Cxxxx
2220-Cxxxx
2230-Cxxxx
2240-
2250-
2260-310
2270-
2280-
2290-
2300-
2310-
2320-
2330-
2340-
2350-320
2360-325
2370-Cxxxx
2380-Cxxxx
2390-Cxxxx
2400-
2410-
2420-
2430-
2440-
2450-200
2460-Cxxxx
2470-
2480-205
2490-Cxxxx
2500-Cxxxx

DO 250 I=1,2
DO 250 J=1,0
H11,J)=0
RXYZ-XB11)X2+XB(4)X2
RXYZ-XB17)X2
RXY-SORT(RXY2)
RXYZ-SORT(RXYZ2)
RES11)-EL-ATAN2(-XB(7),RXY)
RES12)-AZ-ATAN2(XB(4),XB(1))
H11,1)-XB(1)X(7)/(RXYRXYZ2)
H11,4)-XB(4)X(7)/(RXYRXYZ2)
H11,7)-RXY/RXYZ2
H12,1)-XB(4)/RXY2
H12,4)-XB(1)/RXY2
H12,7)-0

H CONTAINS MEASUREMENT PARTIALS -- 2X0
R(1,1)-R(2,2)-(5.025E-07)*25/RXYZ2)
FILTER MEASUREMENT NOISE ADAPTATION
DO 310 I=1,2
DO 310 J=1,MMS1
SR11,J)-SR11,J)+1)
SR12,MMS1)-RES(1)
SRM11)-ISR11,MMS1)*RMS1)*SRM111)/RMS
SRM12)-ISR12,MMS1)*RMS1)*SRM121)/RMS
DO 325 I=1,2
DO 325 J=1,2
TEM=0
DO 320 K=1,MMS
TEM-TEM+ISR11,K)-SRM111)*SR(J,K)-SRM(J))
R(I,J)-TEM/RMS1
R CONTAINS MEASUREMENT ERROR COVARIANCE -- 2X2
DO 265 I=1,2
DO 265 J=1,2
S311,J)=0
DO 268 K1=1,0
DO 268 K2=1,0
S311,J)-S311,J)+H11,K1)*PB(K1,K2)*H(J,K2)
R(I,J)-R(I,J)-FMMS1)*S311,J))/RMS
S311,J)-S311,J)+R(I,J)
S3 CONTAINS MPPBMT+R -- 2X2

```

```

L 2510 ,3000
2510-C****
2520-   DET-S3(I,I)*S3(2,2)-S3(2,1)*S3(1,2)
2530-   TEM-TOL2
2540-   IF (DET.LT.0.1) TEM=-TOL2
2550-   IF (ABS(DET).LT.TOL2) DET=TEM
2560-   TEM-S3(I,I)
2570-   S3(I,I)-S3(2,2)/DET
2580-   S3(2,2)-TEM/DET
2590-   S3(1,2)-S3(1,2)/DET
2600-   S3(2,1)-S3(2,1)/DET
2610-C****
2620-C****
2630-C****
2640-   DO 270 J=1,9
2650-   CK(I,J)=0
2660-   DO 270 K1=1,9
2670-   DO 270 K2=1,2
2680-   CK(I,J)=CK(I,J)+PB(I,K1)*S3(K2,J)
2690-270
2700-C****
2710-C****
2720-C****
2730-   CK IS THE KALMAN GAIN MATRIX -- 9X2
2740-   DO 280 I=1,9
2750-   X(I)=XB(I)
2760-   X(I)=X(I)+CK(I,J)*RES(I)
2770-C****
2780-C****
2790-C****
2800-
2810-   DO 295 I=1,9
2820-   P(I,J)=0
2830-   DO 298 K1=1,2
2840-   DO 298 K2=1,9
2850-   P(I,J)=P(I,J)+CK(I,K1)*S3(K2,J)
2860-295
2870-C****
2880-C****
2890-C****
2900-   P CONTAINS (I-CK)*PB -- 9X9
2910-   RETURN
2920-C****
2930-C****
2940-C****
2950-   FILTER PROCESS NOISE ADAPTATION
2960-   DO 330 J=1,9
2970-   SQ(I,J)=SQ(I,J+1)
2980-330
2990-   DO 340 I=1,9
3000-   SQ(I)=SQ(I)+RMSI*RMSI/SQ(I)/RMSI
3010-340

```



```

L.3010.3300
3010-
3020- DO 355 J=1,9
3030- DO 355 J=1,9
3040- TEM=0
3050- DO 350 K=1,NMS
3060-350 TEM=TEM+ISO(I,K)-SOM(I)*((SQ(J,K)-SOM(J)))
3070-355 O(I,J)=TEM/RNMSI
3080-C###
3090-C### FILTER TIME CALCULATION
3100-C###
3110- CALL SECOND(T2)
3120- TFIL=TFIL+T2-T1
3130- RETURN
3140- ENO
3150-#C,NE,VRG
3160-#C,NE,VRG
3170-2000 2 2 0 3 2
3180-188
3190-0
3200-10000 100 0 4 1 0 0 0 0.0000 1.
3210-10 10 20000 10. 10. 20000 10. 10. 20000.
3220-#EOR
3230-#EOF

```

1981 USAF - SCEEE SUMMER FACULTY RESEARCH PROGRAM

Sponsored by the
AIR FORCE OFFICE OF SCIENTIFIC RESEARCH

Conducted by the
SOUTHEASTERN CENTER FOR ELECTRICAL ENGINEERING EDUCATION

FINAL REPORT

OPTIMAL RECOVERY FROM CRATERING ATTACK

ON AIRBASE PREPARED SURFACES

Prepared by: Dr R. Michael Harnett
Academic Rank: Associate Professor
Department and University: Electrical and Computer Engineering
Clemson University
Research Location: Air Force Armament Laboratory, Analysis
Division, Weapon Evaluation Branch
USAF Research Colleague: Mr Joel B. Knight
Date: August 7, 1981
Contract No: F49620-79-C-0038

OPTIMAL RECOVERY FROM CRATERING ATTACKS
ON AIRBASE PREPARED SURFACES

by

R. Michael Harnett

ABSTRACT

The problem of locating minimum-repair areas on airbase prepared surfaces which meet operational requirements is addressed. Both runways and taxiways are considered. An algorithm is described which achieves exact optimal solutions for the runway problem recognizing variation in crater repair difficulty. The algorithm is shown through computational experiments to feature increased computational efficiency compared to existing solution methods. An algorithm is described which achieves exact optimal solutions for the taxiway problem recognizing variation in crater repair difficulty. Computer codes for the algorithms are provided. Suggestions for further research in this area are offered.

ACKNOWLEDGMENTS

The author would like to thank the Air Force Systems Command, the Air Force Office of Scientific Research and the Southeastern Center for Electrical Engineering Education for providing the opportunity to spend a stimulating summer at the Air Force Armament Laboratory, Eglin AFB FL. In particular he would like to acknowledge the Weapon Evaluation Branch of the Analysis Division for its hospitality and excellent working conditions. A special thanks is owed Mr Joel B. Knight for his help in coordinating the summer program and Messrs Daniel A. McInnis and Jerry P. Bass for their many helpful discussions. Finally, he would like to acknowledge the assistance of Mrs Malinda S. Brewer in the preparation of this report.

I. INTRODUCTION

Under combat conditions both US and enemy Air Force operations require the use of resources that may be battle damaged. Primary examples of such resources are cratered runways and taxiways. The objective of launching sorties as rapidly as possible after an airbase attack necessitates an analysis of the pattern and size of craters imposed on operating surfaces to determine the minimum-repair strategy for obtaining minimum operational requirements. These operational requirements are generally stated in terms of the minimum clear width and length required for takeoff and the minimum clear width required for maneuvering among craters on taxiway surfaces to gain access to the runway.

The capability to determine optimal responses to airbase prepared-surface attacks is important in an offensive context (blue-on-red) as well as a defensive one (red-on-blue). In evaluating the effectiveness of a postulated attack on the prepared surfaces of a red airbase, it is important to consider the best possible response that an intelligent opposition could mount. Only in this way is the real effectiveness of the postulated attack learned. This usage requires that a computer-based methodology be developed, for solving these problems, which is in a form suitable to be imbedded within elaborate airbase attack models.

In the red-on-blue context, the runway search problem can be solved by operational personnel using graphical representations of runway craters and a template corresponding to minimum takeoff requirements. The taxiway search is inherently more difficult when craters are clustered because of the great flexibility that exists in maneuvering among them. Furthermore, both the runway and the taxiway search problems are very difficult to optimize by graphical techniques when significant variation in crater size exists and especially when the relationship between crater repair difficulty and crater radius is not linear. Computer-based numerical techniques should be capable of producing more accurate solutions to these problems than can be produced by operational personnel and should require less time.

II. OBJECTIVES OF THE RESEARCH EFFORT

The numerical technique in use, at the inception of this research, for solving the runway search problem is structured for applications in which all craters are equally difficult to repair. Specifically, it is formulated to find the runway area that contains the smallest number of craters. Additionally, it employs an exhaustive enumeration scheme and, as a result, may be considered computationally inefficient. The numerical techniques available, at the inception of this research, for solving the taxiway search problem may be described as heuristic approximations. They are essentially untested although they have been observed variously to produce infeasible and/or non-optimal results. No method was available for obtaining exact solutions for taxiway search problems and, therefore, rigorous validation of any heuristic was impractical.

The objectives of this research were twofold. First, it was desired that a numerical technique for solving runway search problems be developed which would feature increased computational efficiency. The intent in improving computational efficiency was to facilitate the exercising of large-scale airbase attack models in evaluating various blue-on-red weapons/tactics. Associated with this objective was the desire that the resulting technique be able to accommodate problems exhibiting variation in crater repair difficulty. The second major objective of this effort was to develop a numerical technique for obtaining exact solutions to taxiway search problems, again recognizing variation in crater repair difficulty. The intent was to provide a basis for empirically validating computationally efficient heuristic methods for the taxiway search problem.

III. RUNWAY SEARCH ALGORITHMS

Background

This section describes two algorithms that were developed for solving the runway search problem. The runway search problem is to find the area on a runway, that has been cratered by bomb attack, which can be repaired in the minimum amount of time. In this effort the following simplifications were imposed upon the problem.

1. The objective was established to minimize the number of craters impinging upon the runway area to be used.
2. Craters were characterized as having square areas with varying side lengths and center coordinates.
3. Access to any runway area selected for use was assumed to be available.
4. Only areas oriented parallel to the overall runway will be considered as feasible solutions to the runway search problem.

Approach

The general approach employed by the runway search algorithms may be characterized as implicit enumeration. The solution process is accelerated, as compared to explicit (exhaustive) enumeration, to achieve improvements in computational efficiency. Differences in the bases for accelerating the search distinguish the two implicit enumeration algorithms described in this section.

The basis for the enumeration of solutions is common to the implicit enumeration algorithms developed in this research as well as the explicit enumeration algorithm used as a standard of comparison. This basis is an examination of sequential solutions down the length of the runway (x-direction) with the same lateral positioning (y-direction). This will be termed a "sweep" of the runway. The initial solution (frame) examined has a corner at $(x,y)=(0,0)$. Improvement in this frame is first sought by translating it in the x direction. For an adjacent frame to be a better solution it must exclude at least one crater that the initial frame contained. Therefore the next solution is enumerated by placing the trailing edge (least x coordinate) of the frame at the leading edge (greatest x coordinate) of the crater, contained in the first sweep, which

has the smallest leading edge x coordinate (first one excluded as the frame is translated down the sweep area). By repeatedly advancing the frame down the sweep by the minimum distance required to wholly exclude one new crater, each possible integer-valued solution (in terms of the number of craters impinging upon the frame) is examined. All such solutions on the runway can be enumerated by applying this enumeration scheme to all possible sweep areas. These may be determined by "indexing" the sweep area across the runway so as to sequentially eliminate one crater from each previous sweep.

The basis for the two implicit enumeration algorithms developed in this research is the acceleration of the enumeration in both the x direction (down the sweep) and the y direction (indexing of the sweep area across the runway). The scheme for accelerating in x is shared by the two algorithms. They are distinguished by the methods used to accelerate the search in the y direction (index the sweep area across the runway).

Algorithms

The algorithms, called UPONE and UPMANY, are described in the following flow diagrams. These diagrams are presented in terms of variable names which were taken from the computer code listings presented in appendices to this report. The input variables (which are common to both algorithms) are defined as follows:

INPUT VARIABLES:

LL	= length of runway
WW	= width of runway
L	= minimum clear length
W	= minimum clear width
N	= number of craters
X(J)	= x coordinate of center of crater J
Y(J)	= y coordinate of center of crater J
R(J)	= radius of crater J
CRMAX	= maximum crater radius

The internally-defined variables that are common to both algorithms are defined as follows:

COMMON VARIABLES:

TSYL = lower y coordinate of sweep area
TSYU = upper y coordinate of sweep area
= TSYL + W
TSXL = lower x coordinate of a frame in sweep area
TSXU = upper x coordinate of a frame in sweep area
= TSXL + L
JX = number of craters impinging upon sweep area
ISORT(J) = number of crater, impinging upon sweep area, which has J th smallest leading edge (X(J)+R(J))
ICC = number of craters impinging upon a particular frame
ICSTAR = smallest value of ICC encountered
XSTAR = value of TSXL for frame associated with ICSTAR solution
YSTAR = value of TSYL for frame associated with ICSTAR solution
IDP = the number of craters to be excluded in a single move of the frame down the sweep area
ISTART = position of last crater in ISORT vector to be expelled by moving the frame down the sweep area

The variables peculiar to UPONE are defined as follows:

UPONE VARIABLES:

MINY = number of the crater, impinging upon the total sweep area, with the minimum value of Y(J)+R(J). This will be the next crater excluded by indexing the sweep area across the runway
TL = upper limit (on TSXU) for a sweep following the indexing of the sweep area. Frames with TSXU >TL could not be benefited by indexing the sweep area to exclude the last crater excluded
= Min {LL, X(MINY)+R(MINY)+L}

NOTE: TXSL functions as the lower limit counterpart for TL since the sweep begins with a frame whose lower edge is at TSXL and progresses in the direction of increasing X values. After the first sweep it is initialized as $TXSL = \text{Max} \{0, X(\text{MINY}) - R(\text{MINY}) - L\}$.

The variables peculiar to UPMANY are defined as follows:

UPMANY VARIABLES:

SORT(J) = top edge of crater, impinging upon sweep area,
which has J th smallest top edge ($Y(J) + R(J)$)
ISWEP = best frame count observed in the current sweep
JDP = the number of craters to be excluded in indexing
the sweep area across the runway

The UPONE and UPMANY algorithms are shown in Figures 1 and 2 respectively. The algorithms may be seen to conduct the sweep in the same way. Each time a frame count is obtained it is used to determine the minimum amount by which the frame must be moved in order to obtain improvement over the best frame count observed during the search. With ICSTAR = the best frame count observed at some point during a search and ICC = the crater count for the current frame, it is known that the frame must be advanced at least far enough to exclude $IDP = ICC - ICSTAR + 1$ craters in order to find a solution better than ICSTAR. When $IDP > 1$ the search is accelerated and the enumeration scheme becomes implicit rather than explicit, since all possible solutions will not need to be enumerated to be assured of finding the optimal solution.

The algorithms may be seen to be different in the ways in which they index the sweep area and restrict the range of the subsequent sweep. UPONE always indexes the sweep area to exclude one crater which impinged upon it. Since the resulting new sweep area can be improved over the previous one only in the vicinity of the expelled crater, the search of the new sweep area may be restricted to this neighborhood. The bounds on a frame in the new sweep area which may be improved by the absence of the crater excluded by indexing the sweep area are as follows. Its lower extremity must satisfy $TSXL > X(J) - R(J) - L$ and also $TSXL > 0$, where J = the number of the crater excluded in indexing the sweep area. Its upper extremity must

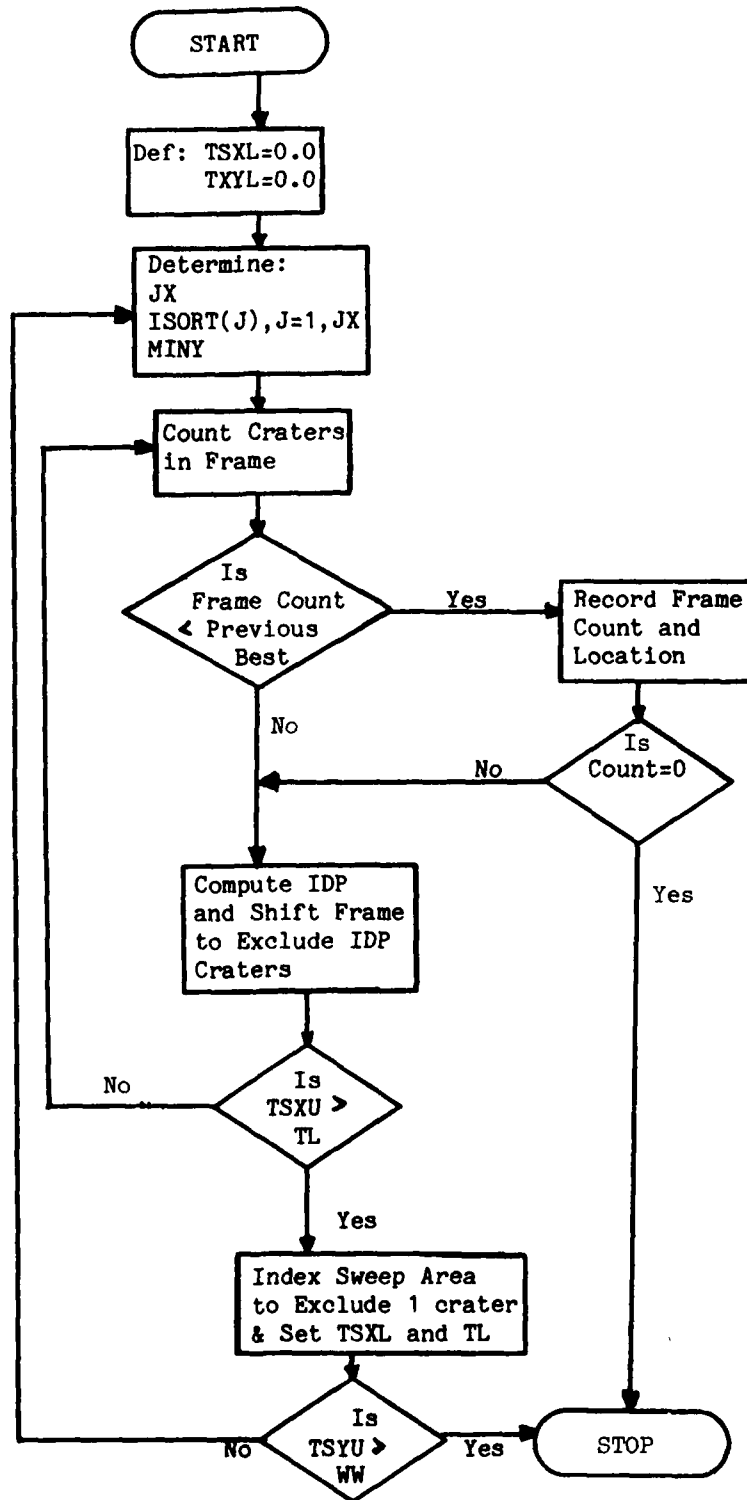


FIGURE 1. UPONE Algorithm

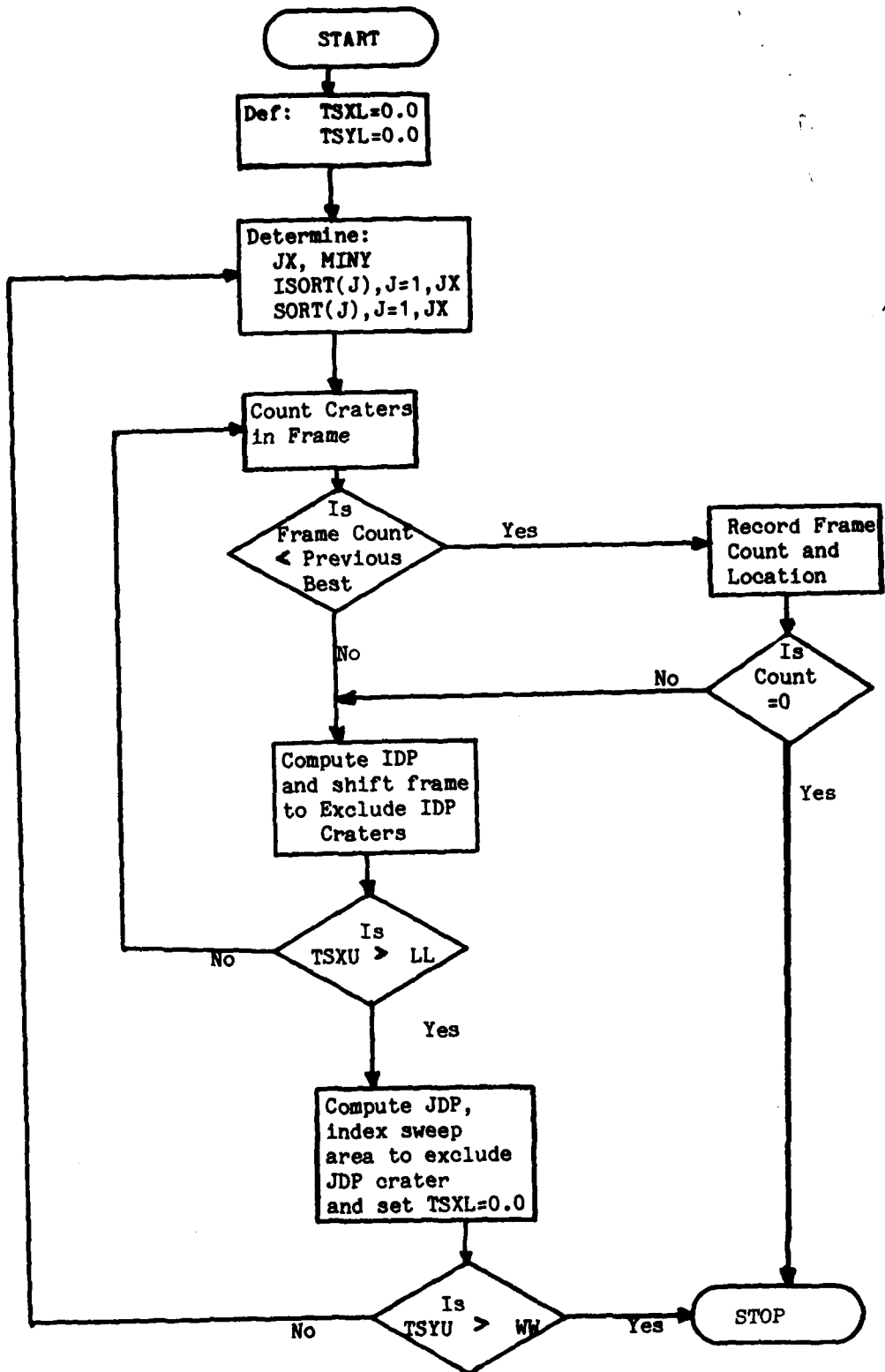


FIGURE 2. UPMANY Algorithm

satisfy $TSXU \leq X(J)+R(J)+L$ and also $TSXU \leq LL$. Therefore, the sweep is initiated with $TSXL = \text{Max} \{0, X(J)-R(J)-L\}$ and the frames upper extremity ($TSXU$) is limited not to exceed $TL = \text{Min} \{X(J)+R(J)+L, LL\}$

UPMANY seeks acceleration of the search by speeding the indexing of the sweep area across the runway. It determines the minimum number of craters (JDP) that must be excluded from the sweep area in order for the subsequent sweep area to contain a frame that is better than the best one yet found in the search. This is determined from $JDP = ISWEP - ICSTAR + 1$.

Results

Because these two algorithms contain both advantages and disadvantages relative to each other it is not possible to conclude analytically which is superior. Therefore, an empirical comparison of computer code execution times was conducted for selected test problems. The results of this study are summarized in Table 1.

TABLE 1

<u>Problem</u>	Algorithm Execution Times (m sec)				
	<u>N</u>	<u>Cuts</u>	<u>CLSTRP</u>	<u>UPONE</u>	<u>UPMANY</u>
1	20	2	24	16	20
2	40	2	49	29	19
3	60	3	164	45	34
4	60	30	94	48	52

Problems 1 and 2 involve Gaussian-distributed craters in 2 runway cuts. Problem 3 involves Gaussian-distributed craters in 3 runway cuts. Problem 4 involves uniformly distributed craters in 2 slanted rows down the runway. Algorithm execution times are given (in milliseconds) for the two implicit enumeration algorithms developed in this research and an explicit enumeration algorithm (CLSTRP). Table 2 shows this execution time data for UPONE and UPMANY restated in terms of percentages of the corresponding time for CLSTRP.

TABLE 2
Percent of CLSTRP Execution Time

<u>Problem</u>	<u>N</u>	<u>Cuts</u>	<u>UPONE</u>	<u>UPMANY</u>
1	20	2	67	83
2	40	2	59	39
3	60	3	27	21
4	60	30	51	55

These data indicate the following:

1. The uniform distribution (Problem 4) is considered to be a worst case for the implicit enumeration algorithms. Therefore, they are thought to be generally advantageous with respect to explicit enumeration. This case is of little practical importance.

2. Problems 1, 2, and 3 show UPONE to be more efficient than UPMANY only for very small problems.

3. Problem 3 shows the computational advantage of UPMANY to be very significant for larger problems.

Recommendation

Based on this brief computational experiment it is recommended that the UPMANY runway search algorithm be substituted for CLSTRP in all applicable computer models. This will increase execution efficiency of the models. Algorithm UPONE could be used but it offers less computational advantage than UPMANY. Additionally, UPONE entails a logic sensitivity to data that is undesirable. In case of an exact tie in the y-coordinate of the upper edge of multiple craters, UPONE could miss an optimal solution. No such logic sensitivity is inherent in UPMANY.

IV. TAXIWAY SEARCH ALGORITHM

Background

This section describes an algorithm developed to solve the taxiway search problem. This problem is to find the set of craters on a taxiway that can be repaired with minimum effort to permit successful negotiation of the taxiway. This solution would include the repair of no craters if it is possible to maneuver around all of them and traverse the taxiway. Taxiing is presumed to occur at very low velocities permitting great maneuvering flexibility. Maneuvers are restricted only by the minimum clear width associated with the aircraft.

The following simplifications were imposed upon the problem formulation.

1. The objective was established to minimize the total difficulty associated with repairing craters on the taxiway.
2. Craters to be repaired must be repaired in their entirety.
3. The difficulty of repairing two overlapping craters is the sum of their individual difficulties.

Approach

The first step in the solution of the taxiway search problem is its decomposition into a sequence of "subproblems" the results of which are additive. Subproblems are determined by identifying clear strips across the taxiway whose width are at least the minimum clear width required for maneuvering among craters. The optimum total crater repair is the sum of the minima from the subproblems.

The general approach employed by the taxiway search algorithm, in solving each subproblem, may be classified as implicit enumeration. Specifically, a "branch and bound" technique is used with trinary crater repair variables defined as follows:

$$IN(J) = \begin{cases} 1 & \text{if crater J is to be repaired} \\ 0 & \text{if crater J is not to be repaired} \\ -1 & \text{if no decision has been made for crater J (this} \\ & \text{variable is "free")} \end{cases}$$

Trial solutions (in terms of these variables) are postulated using the following branching rule. Branching is performed by enumerating the possible values for the free variable with the smallest x-coordinate of its center. Each such postulated trial solution is termed a "node". Enumerating the possible values for a variable creates 2 nodes from 1 which existed previously.

Each time a new node is established, a lower bound on the total repair area for the node is computed. This bounding is done by summing the repair difficulties for all craters (J) corresponding to variable values $IN(J)=1$ for the node. Branching is always done from the untruncated node with the smallest lower bound value.

Nodes may be terminated in any of the following three ways:

1. When it becomes "feasible".
2. When it becomes "infeasible".
3. When its lower bound value exceeds the value of the best

feasible solution.

A node is classified as feasible when repair of only the craters associated with variable values $IN(J)=1$ at the node is sufficient to permit traversing the taxiway. A node is classified as infeasible when repair of all craters associated with variable values of $IN(J)\neq 0$ is insufficient to permit traversing the taxiway. It is important to note that, under these definitions, a node may be neither feasible nor infeasible.

The overall flow of the branch and bound algorithm is shown in Figure 3. The most difficult step is the determination of feasibility or infeasibility. This is accomplished by ignoring all craters that would be repaired and determining if it is possible to maneuver among the remaining craters and traverse the taxiway. This determination is made by a kind of "backtracking" algorithm that works with the remaining craters in pairs that have consecutive x-coordinates of their centers.

The backtracking algorithm is shown in Figure 4. Two types of terminations are shown. STOP 1 is a termination after finding that it is impossible to maneuver around the JT craters remaining on the taxiway after currently-projected repairs. STOP 2 is a termination after finding that it is possible to traverse the taxiway around the JT craters. The backtrack-

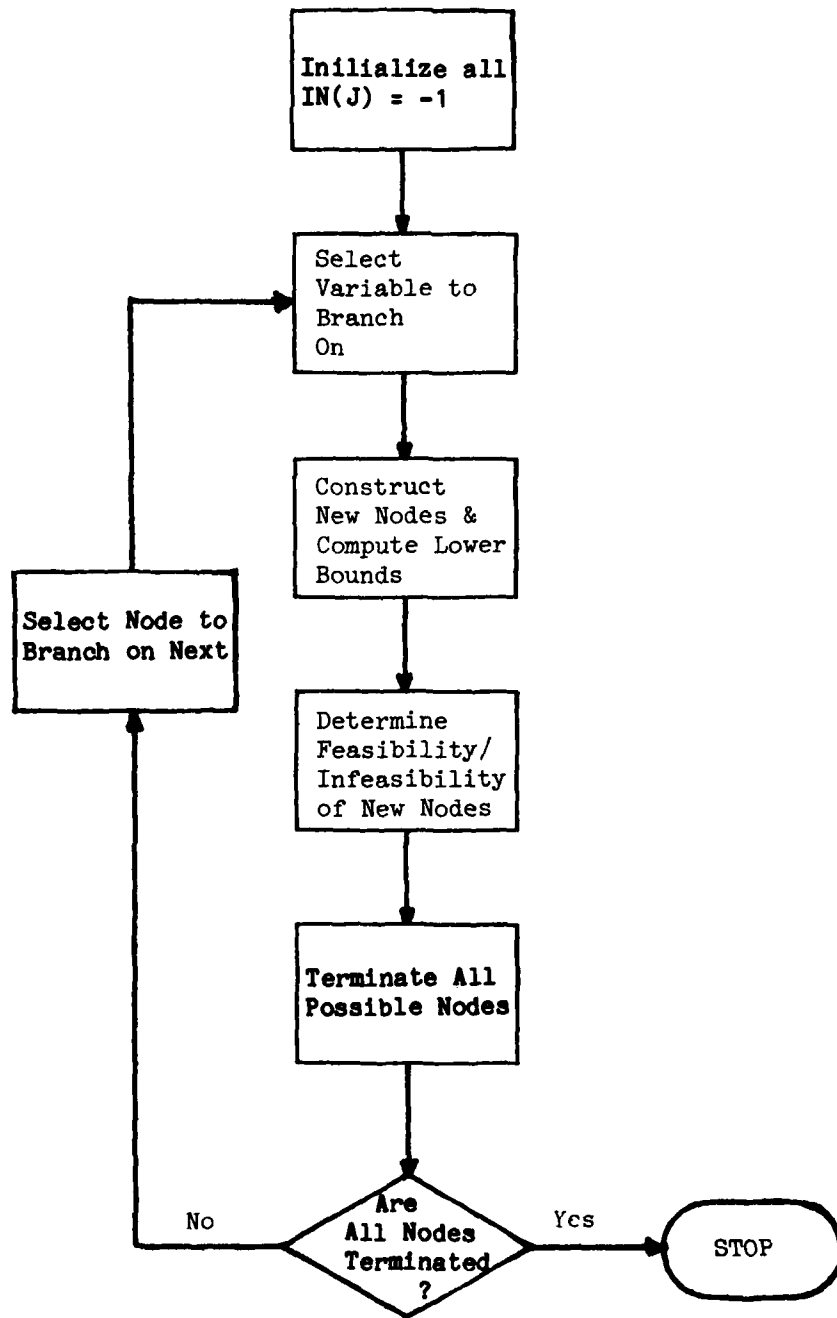


FIGURE 3. Taxiway Branch and Bound Algorithm

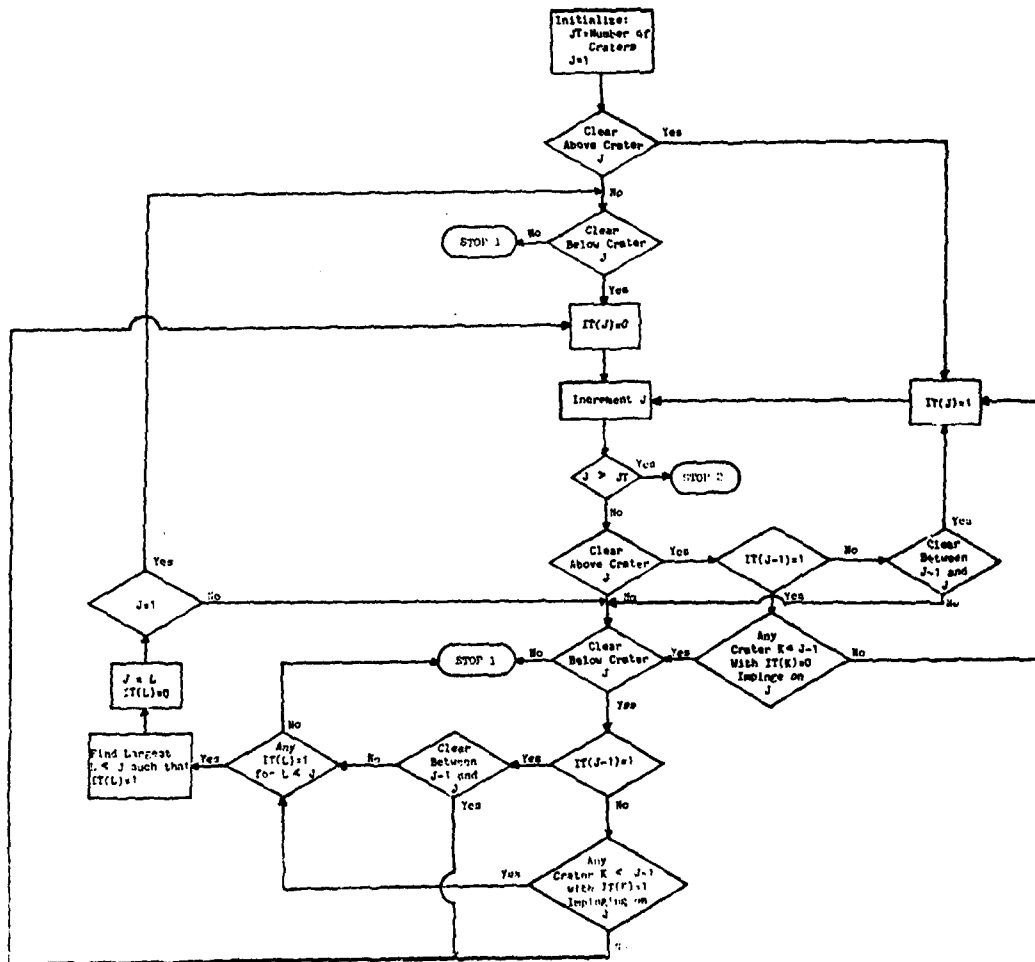


FIGURE 4. Backtracking Algorithm For Determining Clear Path

ing algorithm gives preference to paths around the top (large y-direction) of craters by attempting first to assign the path to pass "above" each crater (IT(J)=1). If this can't be done the "below" assignment (IT(J)=0) is considered. According to this "above-first" convention, backtracking will be done to the last "above crater" assignment.

Determinations of "clear above" ("clear below") are made by examining the clearance, if any, between the top (bottom) edge of the crater and the top (bottom) of the taxiway. If it is determined that we can clear above (below) 2 consecutive craters, the possibility of interference, with this passage, by previous craters is checked by determining if any previous crater labeled for passage below (above) "impinges" upon crater J. A crater is said to impinge upon crater J if the distance between their closest edges is less than the minimum clear width required for maneuvering between craters. If it is desired that a passage be made above crater J-1 and below crater J (or below crater J-1 and above crater J) a check is made to determine if clearance exists between craters J-1 and J.

Determination of clearance between two craters is a complicated process. This clearance can be impeded in a number of ways. The process used to determine the existence of this clearance is shown in Figure 5. This process is sensitive to the distinction between (1) an attempt to pass above J-1 and below J versus (2) passing below J-1 and above J. For convenience in Figure 5 a flag (C) is set to indicate which case we are concerned with.

The two bases for terminating the process, STOP 1 and STOP 2, correspond to finding blockage between the craters and finding clearance between them, respectively. The process involves numerous checks to determine if one crater impinges upon another. As before, this "direct impingement" is taken to mean that the minimum clear width for taxiing does not exist between their closest edges. The process in Figure 5 also involves determining "indirect" impingement between two craters. Indirect impingement (say between craters A and B) indicates that while A does not impinge on B, it does impinge upon a third crater (C) which impinges upon B. Thus because of the existence of C, clearance does not exist between A

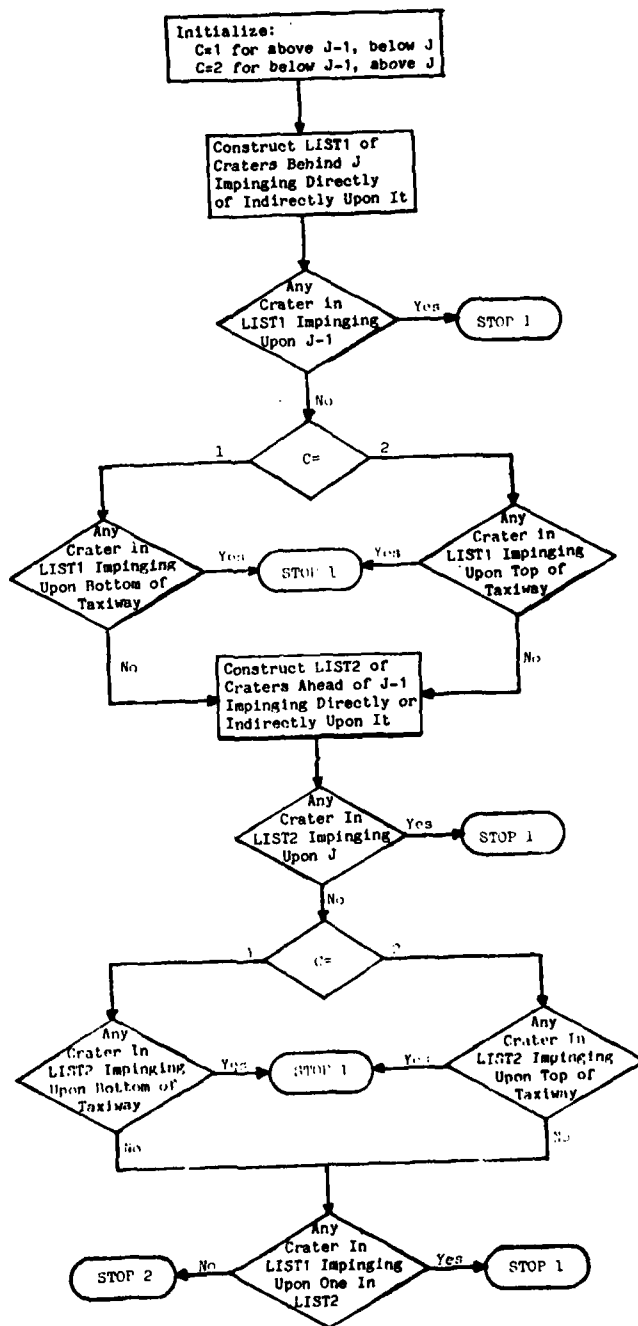


FIGURE 5. Logic for Determining Clearance Between Craters

and B. In fact any number of craters could be involved in the indirect impingement of A upon B. The example in the following table illustrates the full range of possibilities.

<u>Crater</u>	<u>Impinges Directly Upon Crater(s)</u>
A	B,C,D
B	A,C,E
C	A,B,E
D	A
E	B,C,F
F	E

Crater D would be said to impinge indirectly upon crater F through the direct chains: D,A,B,E,F and D,A,C,E,F.

Computer Code

A computer code for the taxiway search algorithm is presented in an appendix to this report. The code involves a main routine (TAXIWAY) and two subroutines (CHECK and BETWN). TAXIWAY implements the logic shown in Figure 3 while CHECK and BETWN implement the procedures shown in Figures 4 and 5, respectively.

The input variables for TAXIWAY are the following:

Input Variables:

N = number of craters
 WW = taxiway width
 W = minimum clear width for taxiway
 X(J) = x-coordinate of crater J
 Y(J) = y-coordinate of crater J
 R(J) = radius of crater J

In addition the following parameter must be defined in the FORTRAN source code as shown in the listing of TAXIWAY.

NNSD = number of nodes provided for in dimension statement

The following variables are determined in the various routines:

TAXIWAY Variables:

ATOTAL = total area repaired in optimal solution to problem

A(J) = difficulty of repairing crater J (shown as crater area in code listing)

CRMAX = radius of largest crater

NREP = number of craters to be repaired in optimal solution to problem

IREP(I) = number of I th crater to be repaired in optimal solution to problem (I=1,2,...,NREP)

NSUB = number of subproblems in problem

ISTART(I)= first crater in subproblem I (I=1,2,...,NSUB)

BFEAS = total repair difficulty in best feasible solution of subproblem

IBEST = number of node corresponding to best feasible solution of subproblem

NODE(I,J)= value of I th variable in node J

NBR = number of next node to branch on

NEXT = number of next node to be created

BL(J) = lower bound of node J

ITERF(J) = indicate feasibility of node J
+1 \Rightarrow feasible
-1 \Rightarrow infeasible
0 \Rightarrow undetermined

NC = number of craters in subproblem

CHECK Variables:

IN(I) = NODE(I,J) for a particular node, J, to be checked

JT = number of craters remaining unrepaired in node being examined

WX(K) = x-coordinate of K th crater remaining in current node (K=1,2,...,JT)

WY(K) = y-coordinate of K th crater remaining in current node (K=1,2,...,JT)

WR(K) = radius of K th crater remaining in current node
(K=1,2,...,JT)

BETWN Variables:

NL1 = number of craters in LIST1
NL2 = number of craters in LIST2
LIST1(J) } see discussion of Figure 5
LIST2(J) }
XMIN = minimum x-coordinate of a crater which could reach
LIST1
XMAX = maximum x-coordinate of a crater which could reach
LIST2

Results

The performance of the TAXIWAY algorithm is illustrated by the 21 crater example shown in Figure 6. The craters are distributed on a 70 by 280 foot taxiway with centers, radii and repair difficulties (indicated by crater areas) as shown in Table 3. The crater distribution may be seen in Figure 6 to present three independent subproblems.

The minimal-repair results from TAXIWAY are shown in Table 4 for 4 cases differing only in the minimum clear width (W) required for maneuvering. It is interesting to note the change in the results for subproblem 1 as W increases from 15 to 20 feet. TAXIWAY recognizes that the distance between the closest edges of craters 1 and 2 (19 feet) does not meet the minimum clear width requirement with the result that the craters recommended for repair switch from 4 and 5 to 1 and 7.

Similarly, the algorithm recognizes that the clearance between craters 11 and 13 (10.6 ft) is sufficient to permit passage (W=10) with only crater 14 repaired, but when W is increased to 15 this clear passage doesn't exist. Then when W is increased from 20 to 25 feet the clearance above crater 12 is no longer sufficient to permit taxiing above it with only the repair of crater 10. The algorithm recognizes the adequacy of the clearance between craters 11 and 15 (25.2 ft) to permit taxiing with only the repair of craters 13 and 14.

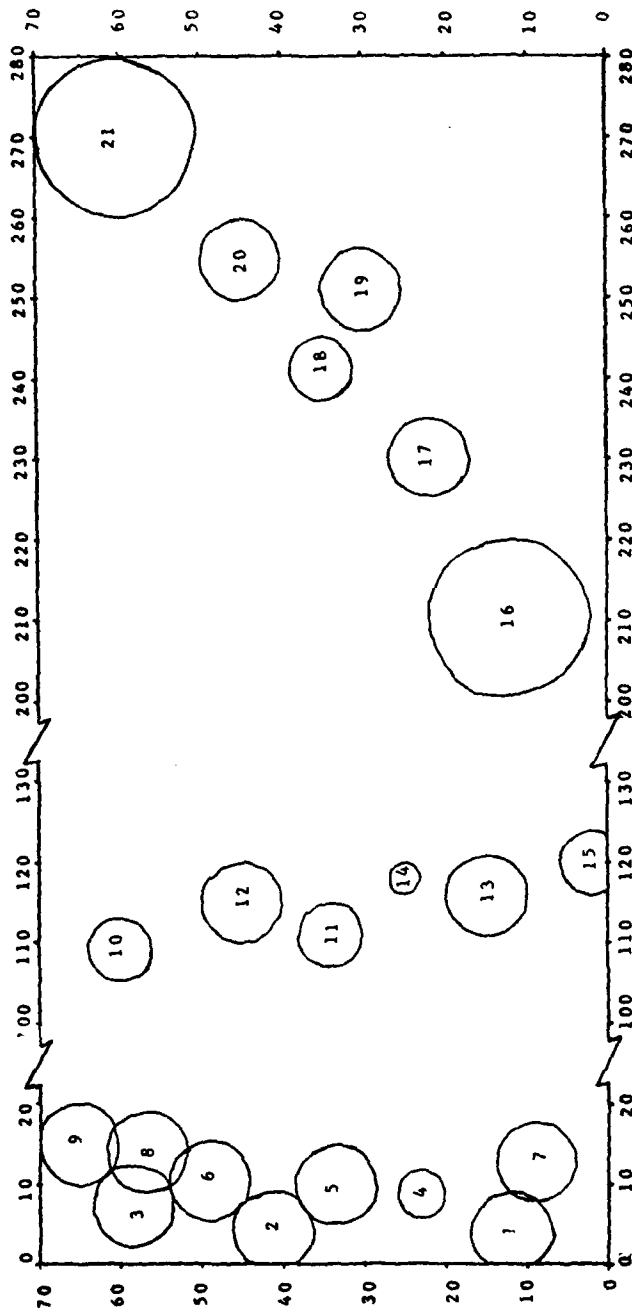


FIGURE 6. TAXIWAY Test Problem

TABLE 3
TAXIWAY Example Data

<u>J</u>	<u>X(J)</u>	<u>Y(J)</u>	<u>R(J)</u>	<u>A(J)</u>
1	4	12	5	78.5
2	5	41	5	78.5
3	7	58	5	78.5
4	9	23	3	28.3
5	10	33	5	78.5
6	11	49	5	78.5
7	13	9	5	78.5
8	14	57	5	78.5
9	15	65	5	78.5
10	109	60	4	50.3
11	111	34	4	50.3
12	115	45	5	78.5
13	116	15	5	78.5
14	118	25	2	12.6
15	120	2	4	50.3
16	210	12	10	314.2
17	230	22	5	78.5
18	241	35	4	50.3
19	251	30	5	78.5
20	255	45	5	78.5
21	270	60	10	314.2

TABLE 4
TAXIWAY Results

<u>Problem</u>	<u>W(ft)</u>	<u>Crater Selected for Subproblem:</u>			<u>Repair Area (ft²)</u>
		<u>1</u>	<u>2</u>	<u>3</u>	
1	10	4	14	18	91.1
2	15	4,5	10	17	235.6
3	20	1,7	10	17	285.9
4	25	1,4,7	13,14	17,18	405.3

In subproblem 3 with $W=10$ the algorithm recognizes the adequacy of the clearance between crater 17 and 19 (12.5 ft) and the deficiency of the clearance between 17 and 18 (8 ft). The optimal solution is determined to be the repair of crater 18 (the smallest one in subproblem 3). The adequacy of the clearance between 16 and 18 (24.6 ft) is recognized for $W=15$ and $W=20$. However, for $W=25$ the necessity is recognized of repairing 18 in addition to 17 to utilize the clearance between craters 16 and 19 (29.8 ft) and below crater 19 (25 ft).

It was recognized at the time TAXIWAY was developed that, while it would generate exact optimal solutions, its "branch and bound" approach could present serious computational difficulties regarding memory requirements. This arises from the requirement to provide storage for the value of each variable associated with each node that is enumerated in the process of solving each subproblem. The number of nodes which will be enumerated can not be predicted exactly. It is only known to be less than or equal to 2^C , where C = the number of craters in the subproblem. The node requirements for 12 random test problems are summarized in Table 5.

TABLE 5
MEMORY SUMMARY FOR TEST PROBLEMS

C	3	4	5	7	10
	75	50	12	8	7
Node	38	31	10		3
Percents	38	31			
	38				
Means	47	37	11	8	5

This table shows the maximum number of nodes required for each problem as a percentage of the maximum number of nodes possible for the corresponding subproblem (2^C). The mean values of these percentages is shown to be a decreasing function of subproblem size.

Summary

The dimensioned memory requirement (decimal words) for TAXIWAY is indicated by the polynomial $5N+S+6C+CM+2M+1$, where

- N = number of craters in problem
- S = number of subproblems $\leq N$
- C = maximum number of craters in a subproblem $\leq N$
- M = maximum number of nodes to be enumerated in a subproblem.

This dimensioned memory requirement is a strong function of C and M. Therefore the solution of practical problems with the TAXIWAY algorithm will necessitate particular emphasis on estimation of these parameters. The test results with TAXIWAY revealed that M will probably be a percent of 2^C that declines as C increases. The estimation of M for large values of N will be difficult and will require extensive test results.

Failure to provide sufficient dimensioned storage for nodes will lead to termination of the execution and probable loss of all useful information generated. Because of the catastrophic nature of this result, TAXIWAY should be used only for problems sufficiently small to achieve a high confidence of not exceeding dimensioned storage. In this regard, TAXIWAY may not be practical for use within other complex models.

The obvious advantage of the TAXIWAY algorithm over previously-existing algorithms is its capacity to develop exact optimal solutions to the repair-minimization problem. This suggests a role for which TAXIWAY is clearly suitable. It can be used as a vehicle for empirically validating heuristic techniques. A number of such approximations could be developed to require minimal computing resources. The performance of these techniques could be determined by comparing their results to those of TAXIWAY for representative test problems.

V. MODIFIED RUNWAY SEARCH ALGORITHM

Background

An important characteristic of the runway search algorithms described in Section III of this report is that they pursue the objective of minimizing the number of craters impinging upon the runway area to be used. This objective is naive in that it attaches no significance to the variation in repair difficulty that would accompany variation in the sizes of the craters to be repaired. A more realistic formulation of the problem would minimize the total time required to repair craters impinging upon the runway area to be used. This section describes a modified runway search algorithm which permits the minimization of any selected measure of crater repair difficulty.

UPMANY-A Algorithm

Because of the inherent superiority of the UPMANY runway search algorithm, as compared to UPONE (see Section III), the development of a modification to minimize repair difficulty proceeded as a departure from UPMANY. The basic structure of the algorithm is as shown in Figure 2. However, the following important differences should be noted.

The initialization includes the definition of the difficulty involved in repairing each crater. In the listing of UPMANY-A, shown in an appendix to this report, the difficulty of repairing crater J, represented by $A(J)$, is computed to be the area of the circular crater which has radius $R(J)$. For purposes of testing the computer code, crater area was taken as the measure of repair difficulty.

Rather than evaluating a frame by counting the craters which impinge upon it, UPMANY-A sums the difficulty measures for these craters. Subsequently, the algorithm accelerates its search by moving the frame far enough to exclude, wholly, the minimum number of craters which collectively entail at least the desired crater repair difficulty. This desired difficulty is given by the difference between the total measure for the current frame and the minimum total measure observed thus far in the search. This convention is consistent with the assumption that any crater impinging upon the runway area to be used would have to be repaired in its entirety.

The basis for accelerating the indexing of the sweep area across the runway is another distinction between UPMANY and UPMANY-A. The difference between the minimum frame repair difficulty observed in the last sweep and the minimum frame repair difficulty observed thus far in the search is used by UPMANY-A as the minimum amount of repair difficulty which will be excluded from the sweep area in indexing it across the runway. The sweep area is indexed only far enough to exclude, wholly, the minimum number of craters possible and yet exclude the desired minimum amount of repair difficulty.

It is interesting to note that under special conditions the objectives of UPMANY and UPMANY-A are identical. When all craters present equal difficulty of repair, then the minimization of repair difficulty is the same as minimization of the number of craters to be repaired. Furthermore, the minimization of the number of craters repaired can be achieved with UPMANY-A, even when crater sizes vary, by defining all crater difficulties, $A(J)$, to be the same positive quantity.

Input variables and computed variables in the computer code for UPMANY-A are largely the same as for UPMANY. Exceptions are as follows:

COMPUTED VARIABLES:

$A(J)$ = difficulty of repairing crater J
AICC = total difficulty of repairing craters impinging upon a particular frame
CSTAR = smallest value of AICC encountered
JSORT(J) = number of crater, impinging upon the sweep area, which has J th smallest top edge ($Y(J)+R(J)$)
SWEP = smallest value of AICC observed in a particular sweep

VI. RECOMMENDATIONS

The UPMANY-A algorithm should be incorporated in all appropriate airbase-attack models. This will provide immediate improvements in computational efficiency. It will also provide the capability to address problems involving variation in crater repair difficulty.

The UPMANY-A and TAXIWAY algorithms should be distributed to organizations tasked with responsibilities relating to runway and taxiway repair. They should be informed of the capabilities of these algorithms when used in a red-on-blue context.

An empirical study of the performance of heuristic algorithms currently in use for the taxiway search problem should be conducted. The TAXIWAY algorithm can provide a basis for determining the accuracy of these heuristics. If, at the conclusion of this investigation, it is determined that existing heuristics are inadequate, an effort aimed at the development of improved heuristics should be initiated. The TAXIWAY algorithm can also provide a basis for validating any new developments.

The runway and taxiway search problems represent portions of the overall problem of determining optimal responses to airbase attack. The taxiway search addresses only a single segment of taxiway. In reality taxiways exist in a network configuration linking various aircraft shelters to various runway access points. Both the runway and taxiway problems consider only cratered surfaces with no restrictions on access. In reality, airbase attacks may be expected to include area-denial munitions (mines) in some combination with cratering devices, greatly complicating the recovery process. In addition to these complications a potential disparity exists between the static repair-minimization objective of these search problems and the dynamic sortie-maximization objective which motivates the pursuit of optimum approaches to the recovery from airbase attacks. Research should be initiated to develop prescriptive methods for addressing the dynamic sortie-maximization objective. The goal of determining optimum time-phased responses to airbase attacks should be adopted. Success in this ambitious undertaking would eliminate error due to the formulation attributes described above. It would contribute materially to developing a capability to determine the effectiveness of postulated changes in weapons and tactics and to manage optimally the recovery from red-on-blue attacks.

APPENDIX

Listings of Computer Codes

```

C ***** LIST OF CODE FOR UPONE ALGORITHM *****
C
      REAL L,LL
      TSXL=0.0
      TSYL=L.0
      TSXU=L
      TSYU=W
      TSYL=L.0
      TL=LL
      ICSTAR=N
C ***** SET UP FOR SWEEP *****
C ***** DETERMINE MINY, JX, AND ISORT(J) FOR J=1,JX *****
25 MINY = -1
   ISTART = 0
   JX=0
   DO 11 J=1,N
     IF(Y(J)+R(J).LE.TSYL) GO TO 11
     IF(Y(J)-R(J).GE.TSYU) GO TO 11
     IF(MINY.LT.0) MINY = J
     IF(Y(J)+R(J).LT.Y(MINY)+R(MINY)) MINY=J
     IF(X(J)-R(J).GE.TL) GO TO 11
     IF(X(J)+R(J).LE.TSXL) GO TO 11
     IF(JX.GT.0) GO TO 5
     JX = J
     ISORT(1) = J
     GO TO 11
5   IT=JX
   JX=JX+1
17  JZ = ISORT(IT)
   IF (X(J)+R(J).GE.X(JZ)+R(JZ)) GO TO 19
   ISORT(IT+1) = ISORT(IT)
   IT = IT - 1
   IF(IT.GT.0) GO TO 17
   ISORT(1) = J
   GO TO 11
18  ISORT(IT+1)=J
11  CONTINUE
C ***** EXECUTE SWEEP *****
C ***** COUNT CRATERS IN FRAME *****
19  IX = ISTART + 1
   ICC = 0
30  IF (IX.GT.JX) GO TO 6
   JM = ISORT(IX)
   IF(X(JM) - R(JM).GE.TSXU) GO TO 32
   ICC = ICC+1
31  IX=IX+1
   GO TO 30
32  IF(X(JM)-CRMAX.LT.TSXU) GO TO 31
C ***** COMPARE FRAME COUNT *****
6   IF(ICSTAR.LE.ICC) GO TO 16
   ICSTAR=ICC
   XSTAR=TSXL
   YSTAR=TSYL
C ***** MOVE FRAME *****
16  IUP=ICC-ICSTAR+1
   ISTART = ISTART + IUP
   IF(ISTART.GT.JX) GO TO 20
   KTMP=ISORT(ISTART)
   TSXU=X(KTMP)+R(KTMP)+L + 0.00000001
   IF(TSXU.GT.TL) GO TO 20
   TSXL=TSXU-L
   GO TO 10
C ***** SWEEP FINISHED *****
20  TSYU=Y(MINY)+R(MINY)+W + 0.00000001
   IF(TSYU.GT.W) GO TO 10
   TSYL=TSYU-W
   TSXL=X(MINY)-R(MINY)-L
   IF(TSXL.LT.0.0) TSXL=0.0
   TSXU = TSXL + L
   TL=X(MINY)+R(MINY)+L
   IF(TL.GT.LL) TL=LL
   GO TO 25
100 STOP

```



```

C ***** LIST OF CODE FOR UP MANY ALGORITHM *****
C
REAL L,LL
TSXL=J.0
TSYL=L.0
TSXU=L
TSYU=W
ICSTAR= N
C ***** SET UP FOR SWEEP *****
25 JX=0
   ISTART = 0
   ISWEP = N
   DO 11 J=1,N
   IF (Y(J)+R(J).LE.TSYL) GO TO 11
   IF (Y(J)-R(J).GE.TSYU) GO TO 11
14 IF (JX.GT.0) GO TO 5
   JX = J
   ISORT(1) = J
   SORT(1) = Y(J) + R(J)
   GO TO 11
5 IT=JX
  JX=JX + 1
17 JZ= ISORT(IT)
  IF (X(J)+R(J).GE.X(JZ)+R(JZ)) GO TO 18
  ISORT(IT+1) = ISORT(IT)
  IT = IT - 1
  IF (IT.GT.0) GO TO 17
  ISORT(1) = J
  GO TO 16
18 ISORT(IT+1)=J
119 IT = JX - 1
117 IF (Y(J) + R(J).GE.SORT(IT)) GO TO 118
  SORT(IT+1) = SORT(IT)
  IT = IT - 1
  IF (IT.GT.0) GO TO 117
  SORT(1) = Y(J) + R(J)
  GO TO 11
118 SORT(IT+1) = Y(J) + R(J)
11 CONTINUE
C ***** EXECUTE SWEEP *****
C *** COUNT CRATERS IN FRAME ***
10 IX = ISTART + 1
   ICC = 0
30 IF (IX.GT.JX) GO TO 6
   JM = ISORT(IX)
   IF (X(JM) - R(JM).GE.TSXU) GO TO 32
   ICC = ICC+1
31 IX=IX+1
   GO TO 30
32 IF (X(JM)-CRMAX.LT.TSXU) GO TO 31
C *** COMPARE FRAME COUNT ***
6 IF (ICSTAR.LE.ICC) GO TO 16
  ICSTAR=ICC
  XSTAR=TSXL
  YSTAR=TSYL
  IF (ICSTAR.EQ.0) GO TO 100
C *** MOVE FRAME ***
16 IOP=ICC-ICSTAR+1
  IF (ISWEP.GT.ICC) ISWEP = ICC
  ISTART = ISTART + IOP
  IF (ISTART.GT.JX) GO TO 20
  KTMP=ISORT(ISTART)
  TSYU=X(KTMP)+R(KTMP)+L + 1.00000001
  IF (TSXU.GT.LL) GO TO 20
  TSXL=TSXU-L
  GO TO 10
C ***** SWEEP FINISHED *****
20 JUP = ISWEP - ICSTAR + 1
  TSYU = SORT(JUP) + W + 1.00000001
  IF (TSYU.GT.WH) GO TO 100
  TSYL = TSYU - W
  TSXL = J.0
  TSXU = L
  GO TO 25
100 STOP

```

```

C ***** LIST OF CODE FOR UP MANY-A ALGORITHM *****
C
  DIMENSION X(N),Y(N),R(N),A(N),ISORT(N),JSORT(N)
  REAL L,LL
  TSYL=0.0
  TSYL=0.0
  TSXU=L
  TSYU=W
  CSTAR= 10.0E15
C ***** DEFINE A(J) = DIFFICULTY OF REPAIRING CRATER J *****
  DO 24 J=1,N
24 A(J) = 3.14159*R(J)*R(J)
C ***** SET UP FOR SWEEP *****
25 JX=0
  ISTART = 0
  SWEP = 10.E15
  DO 11 J=1,N
  IF (Y(J)+R(J).LE.TSYL) GO TO 11
  IF (Y(J)-R(J).GE.TSYU) GO TO 11
14 IF (JX.GT.0) GO TO 5
  JZ = 1
  ISORT(1) = J
  JSORT(1) = J
  GO TO 11
  5 JX=JX + 1
  JZ= ISORT(IT)
17 IF (X(J)+R(J).GE.X(JZ)+R(JZ)) GO TO 18
  ISORT(IT+1) = ISORT(IT)
  IT = IT - 1
  IF (IT.GT.0) GO TO 17
  ISORT(1) = J
  GO TO 116
18 ISORT(IT+1)=J
116 IT = JX - 1
117 JR=JSORT(IT)
  IF (Y(J) + R(J).GE.Y(JR) + R(JR)) GO TO 118
  JSORT(IT+1) = JSORT(IT)
  IT = IT - 1
  IF (IT.GT.0) GO TO 117
  JSORT(1) = J
  GO TO 11
118 JSORT(IT+1) = J
C ***** EXECUTE SWEEP *****
C ***** DETERMINE DIFFICULTY OF REPAIRING CRATERS TOUCHING FRAME ***
10 IX = ISTART + 1
  AICC = 0.0
30 IF (IX.GT.JX) GO TO 6
  JH = ISORT(IX)
  IF (X(JH) - R(JH).GE.TSXU) GO TO 32
  AICC = AICC + A(JH)
31 IX=IX+1
  GO TO 30
32 IF (X(JH)-CRMAX.LT.TSXU) GO TO 31
C ***** COMPARE REPAIR DIFFICULTY FOR FRAME ***
  6 IF (CSTAR.LE.AICC) GO TO 16
  CSTAR=AICC
  XSTAR=TSXL
  YSTAR=TSYL
  IF (CSTAR.LE.0.00000001) GO TO 100
C ***** MOVE FRAME *****
16 TEMP = AICC - CSTAR
  ISTART = ISTART + 1
41 IF (ISTART.GT.JX) GO TO 28
  IS = ISORT(ISTART)
  IF (TEMP.LE.A(IS)) GO TO 998
  TEMP = TEMP - A(IS)
  GO TO 41
998 IF (SWEP.GT.AICC) SWEP=AICC
  TSXU = X(IS) + R(IS) + L + 0.000000001
  IF (TSXU.GT.LL) GO TO 28
  TSXL=TSXU-L
  GO TO 10
C ***** SWEEP FINISHED *****
20 TEMP = SWEP - CSTAR
  JDP = 0
46 JDP = JDP + 1
  IF (JDP.GT.JX) GO TO 100
  JS = JSORT(JDP)
  IF (TEMP.LE.A(JS)) GO TO 45
  TEMP = TEMP - A(JS)
  GO TO 46
45 TSYU = Y(JS) + R(JS) + W + 0.000000001
  IF (TSYU.GT.WM) GO TO 100
  TSYL = TSYU - W
  TSXL = 0.0
  TSXU = L
  GO TO 25
100 STOP

```

```

CCCCC ***** LIST OF CODE FOR TAXIWAY ALGORITHM *****
CCCCC
CCCCC P000000 TAXIWAY (INPUT, OUTPUT, TAPE5=INPUT, TAPE6=OUTPUT)
CCCCC DIMENSION NODE(100), I(100), R(100), ISTART(100), A(100), X(100)
CCCCC , R(1), N(1), LIST1(100), LIST2(100), I(100), MX(100), MY(100), WR(100), IREP(100)
CCCCC NC = MAX NUMBER OF CRATERS IN A SUBPROBLEM
CCCCC NNSJ = MAX NUMBER OF NODES NEEDED IN A SUBPROBLEM
CCCCC NSUB = MAX NUMBER OF SUBPROBLEMS TO BE SOLVED
CCCCC N = NUMBER OF CRATERS IN ENTIRE PROBLEM
CCCCC DIMENSION NODE(20, 20), I(20), R(100), ISTART(11), A(40), X(40),
CCCCC , R(1), Y(1), LIST1(12), LIST2(20), I(20), WK(20), WY(20), WR(20),
CCCCC IREP(20)
CCCCC COMMON NFM, NF, NL, CRMAX, WM, W
CCCCC
CCCCC DEFINE NNSJ = NUMBER OF NODES PROVIDED FOR IN DIMENSION STATEMENT
CCCCC
CCCCC NNSJ = 100
CCCCC READ (5, 800) N, WM, W
CCCCC 800 FORMAT (I5, 3F1, 0)
CCCCC DO 801 J = 1, N
CCCCC 801 READ (5, 802) X(J), Y(J), R(J)
CCCCC 802 FORMAT (3F5, 0)
CCCCC CRMAX = 0
CCCCC DO 803 J = 1, N
CCCCC IF (CRMAX.LT.R(J)) CRMAX = R(J)
CCCCC 100 A(J) = X(J) * R(J) * 3.14159
CCCCC WRITE (6, 903) N, WM, W, CRMAX
CCCCC 803 FORMAT (6H1 N = , I5, 7H WM = , F5, J, 6H W = , F4, 0, 13H CRMAX = ,
CCCCC , F4, J, // 20H J X(J) Y(J) R(J) /)
CCCCC DO 804 J = 1, N
CCCCC 804 WRITE (6, 904) J, X(J), Y(J), R(J)
CCCCC 805 FORMAT (15, 3F5, 0)
CCCCC NMAX = 0
CCCCC IREP = 0
CCCCC ATOTAL = 0.0
CCCCC
CCCCC *** SEARCH FOR SUBPROBLEMS ***
CCCCC
CCCCC ISTART(1) = 1
CCCCC NSUB = 1
CCCCC NFM = N - 1
CCCCC DO 100 J = 1, NFM
CCCCC JP = J + 1
CCCCC JM = J
CCCCC EL = X(J) + R(J)
CCCCC EU = X(JP) - R(JP)
CCCCC IF (EL.LT.EU) GO TO 103
CCCCC 101 JM = JM + 1
CCCCC IF (X(JM) + R(JM).GT.EL) EL = X(JM) + R(JM)
CCCCC IF (X(JM) + CRMAX.LE.EU) GO TO 103
CCCCC GO TO 101
CCCCC 102 JP = JP + 1
CCCCC IF (JP.GT.N) GO TO 105
CCCCC IF (EU.GT.X(JP) - R(JP)) EU = X(JP) - R(JP)
CCCCC 105 IF (EL.LT.EU) GO TO 103
CCCCC NSUB = NSUB + 1
CCCCC ISTART(NSUB) = J + 1
CCCCC CONTINUE
CCCCC ISTART(NSUB + 1) = N + 1
CCCCC 804 WRITE (6, 904) NSUB
CCCCC 804 FORMAT (7, // 7H NSUB = , I5, 24H STARTING CRATERS FOLLOW, /)
CCCCC 805 WRITE (6, 905) (ISTART(I), I = 1, NSUB)
CCCCC 805 FORMAT (24I5)
CCCCC
CCCCC *** SOLVE SUBPROBLEMS ***
CCCCC
CCCCC DO 100 JS = 1, NSUB
CCCCC NF = ISTART(JS)
CCCCC NL = ISTART(JS + 1) - 1
CCCCC NFM = NF - 1
CCCCC CRMAX = 0
CCCCC DO 101 JNF = NF, NL
CCCCC IF (CRMAX.LT.R(J)) CRMAX = R(J)
CCCCC 5 CONTINUE
CCCCC NC = NL - NFM
CCCCC WRITE (6, 932) JS, NC, ISTART(JS), CRMAX
CCCCC 802 FORMAT (7, // 11H SUBPROBLEM , I3, 4H FAS, I3, 27H CRATERS STARTING AT NUMB
CCCCC , F4, I3, 14H MAX RADIUS = , F5, 1)
CCCCC IF (NC.GT.2) GO TO 1
CCCCC IFAS = 0
CCCCC IF = IF + 1
CCCCC IF (Y(NF) + R(NF).LE.WM - W) GO TO 112
CCCCC IF (Y(NF) - R(NF).GE.W) GO TO 122
CCCCC IFAS = IFAS + A(NF)
CCCCC IREP = IREP + 1
CCCCC IREP(NREP) = NF
CCCCC ATOTAL = ATOTAL + A(NF)
CCCCC IF (X(NF) + R(NF).LE.WM - W) GO TO 220
CCCCC IF (Y(NF) - R(NF).GE.W) GO TO 220
CCCCC IF (X(NF) - R(NF).LE.W) GO TO 220
CCCCC IF (Y(NF) + R(NF).GE.W) GO TO 114
CCCCC IFAS = IFAS + A(NF)
CCCCC IREP = IREP + 1
CCCCC IREP(NREP) = NF
CCCCC ATOTAL = ATOTAL + A(NF)
CCCCC GO TO 220
CCCCC 112 IF (X(NF) + R(NF).LE.WM - W) GO TO 220
CCCCC IF (Y(NF) - R(NF).GE.W) GO TO 220
CCCCC 113 ATOTAL = ATOTAL + A(NF)
CCCCC IFAS = IFAS + A(NF)
CCCCC IREP = IREP + 1
CCCCC IREP(NREP) = NF
CCCCC GO TO 220

```

```

114 X0 = X(NF) - X(NP)
    Y0 = Y(NF) - Y(NP)
    LIST = SQRT (X0 * X0 + Y0 * Y0) - R(NF) - R(NP)
    IF (LIST.GE.W) GO TO 222
    IF (Y(NF)-R(NF).GE.W.AND. Y(NP)-R(NP).GE.W) GO TO 222
    AMI = A(NF)
    ISAVE = NP
    IF (A(NF).GT.A(NP)) ISAVE = NP
    IF (A(NF).GT.A(NP)) APIN = A(NP)
    ATOTAL = ATOTAL + A*IN
    NREP = NREP + 1
    IMS = (IMS) = ISAVE
    BFEAS = BFEAS + AMIN
    GO TO 222
122 IF (NCL-1) GO TO 222
    IF (Y(NP) - R(NP).GE.W) GO TO 222
    IF (Y(NP) + R(NP).LE.W - W) GO TO 114
    GO TO 113

*** CHECK CLEAR PATH ***
1 DO 2 J = 1,NC
2 NODE (J,1) = 0
  CALL CHECK (NODE,IFLAG,X,Y,R,WX,MY,MR,NC,LIST1,LIST2,IT)
  IF (IFLAG.LE.J) GO TO 3
  BFEAS = J*0
  IBEST = J
  GO TO 2J0

*** BRANCH AND BOUND FOR SUBPROBLEM JS ***
*** INITIALIZATION FOR BRANCH AND BOUND ***
3 NEXT = 2
  NBR = 1
  BFEAS = 10E15
  IBEST = -1
  DO 4 I = 1,NCSD
  JL(I) = 0.0
  ITRF(I) = 0
  DO 5 J = 1,NC
  4 NODE (J,I) = -1

*** BRANCH ***
10 J = 0
21 J = J + 1
  IF (NODE(J,NBR).LT.1) GO TO 22
  NODE(J,NEXT) = NODE(J,NBR)
  GO TO 20
22 NODE (J,NBR) = 0
  NODE (J,NEXT) = 1

*** COMPUTE BOUNDS ***
BL(NEXT) = BL(NBR) + A(NF + J)

*** CHECK FEASIBLE COMPLETIONS ***
IF (J.EQ.NC) GO TO 40
  JP = J + 1
  DO 31 JT = JP,NC
3J NODE (JT,NEXT) = 0
  CALL CHECK (NODE(J,NEXT),IFLAG,X,Y,R,WX,MY,MR,NC,LIST1,LIST2,IT)
  IF (IFLAG.LE.J) GO TO 31
  ITRF(NEXT) = 1
  IF (BL(NEXT).GE.BFEAS) GO TO 31
  BFEAS = BL(NEXT)
  IBEST = NEXT
31 DO 32 JT = JP,NC
  NODE (JT,NEXT) = -1
32 NODE (JT,NBR) = 1
  CALL CHECK (NODE(J,NBR),IFLAG,X,Y,R,WX,MY,MR,NC,LIST1,LIST2,IT)
  IF (IFLAG.LE.J) ITRF(NBR) = -1
34 NODE (JT,NBR) = -1
  GO TO 4
  ITRF(NBR) = -1
  ITRF(NEXT) = 1
  IF (BL(NEXT).GE.BFEAS) GO TO 43
  BFEAS = BL(NEXT)
  IBEST = NEXT
  GO TO 43

*** TERMINATE ALL POSSIBLE NODES ***
41 IF (IBEST.LE.J) GO TO 50
43 DO 44 JT = 1,NEXT
  IF (ITRF(JT).NE.1) GO TO 42
  IF (BL(JT).GE.BFEAS) ITRF(JT) = -1
42 CONTINUE
51 CONTINUE

*** DETERMINE NEXT NODE TO BRANCH ON ***
NBR = -1
DO 61 JT = 1,NEXT
  IF (ITRF(JT).NE.0) GO TO 60
  IF (NBR.GT.J) GO TO 52
  NBR = JT
60 J = BL(JT)
  GO TO 61
52 IF (BL(JT).GE.G07J) GO TO 60
  GO 7 J = BL(JT)
  NBR = JT
61 CONTINUE

```

```

IF (N1K,LE,J) GO TO 79
NEXT = NEXT + 1
IF (NEXT,LE,NMSD) GO TO 11
WRITE (6,22)
822 FORMAT (/26H *** TERMINATING DUE TO INSUFFICIENT STORAGE FOR NC
      LUES ***
COC
*** WRITE FEASIBLE SOLUTIONS ***
NMX = NEXT - 1
DO 2/5 J = 1,NMX
IF (ITERF(J),LE,J) GO TO 823
WRITE (6,22) BL(J)
822 FORMAT (/26H FEASIBLE SOLUTION VALUE =,F16.1,254 REPAIR DECISIONS
      1 FOLLOW,/)
WRITE (6,23) (NOCE(I,J),I=1,NC)
823 FORMAT (60I2)
825 CONTINUE
STOP
7J ATOTAL = ATOTAL + DFEAS
20J CONTINUE
IF (BFEAS,LE,0,J) GO TO 22J
DO 21J I = 1,NC
IF (NOCE(I,INEST),LE,J) GO TO 211
NREP = NREP + 1
IREP(NREP) = NFM + I
21J CONTINUE
22J CONTINUE
IF (NEXT,LE,NMAX) GO TO 23J
NMAX = NEXT
NCMAX = NC
23J CONTINUE
WRITE (6,24) ATOTAL,NREP,(IREP(I),I=1,NREP)
84J FORMAT(/25H OPTIMAL SOLUTION VALUE =,F10.0,/,21H REPAIR THE FOLLOW
      1ING,14,8H CRATERS,/,J2I4)
WRITE (6,25) NMAX,NCMAX
84J FORMAT(/,23H MAXIMUM NUMBER OF NODES STORED =,I5,4H FOR,14,
      18H CRATERS)
STOP
SUBROUTINE CHECK (IN,IFLAG,X,Y,R,MX,MY,MR,NC,LIST1,LIST2,IT)
DIMENSION IN(NC),IT(NC),MX(NC),MY(NC),MR(NC),X(NC),Y(NC),
      R(NC),LIST1(NC),LIST2(NC)
COMMON NFM,NP,NL,CRMAX,WM,W
IFLAG = 1
JT = 0
DO 5 JX = 1,NC
IF (IN(JX),GE,1) GO TO 5
JT = JT + 1
JJ = NFM + JX
MX(JT) = X(JX)
MY(JT) = Y(JX)
MR(JT) = R(JX)
6 CONTINUE
IF (JT,LE,J) RETURN
IT(1) = 1
IF (MY(1) - MR(1),GE,W) IT(1) = 0
IF (MY(1) + MR(1),LE,W - W) IT(1) = 1
IF (IT(1),LT,6) GO TO 999
JX = 1
10 JX = JX + 1
JX4 = JX - 1
IF (JX,GT,JT) RETURN
COC
*** CAN WE GET OVER JX ? ***
IF (MY(JX) + MR(JX),GT,W - W) GO TO 12
IF (IT(JX),LE,J) GO TO 11
COC
*** DO AN 'OVER - OVER' ***
XMI4 = MX(JX) - MR(JX) - CRMAX - W
COC
*** CHECK BACK ***
JTEMP = JXM
13 JTEMP = JTEMP - 1
IF (JTEMP,LE,J) GO TO 16
COC
*** DOES AN 'UNDER' IMPINGE UPON JX ? ***
XD = MX(JX) - MX(JTEMP)
YD = MY(JX) - MY(JTEMP)
DIF = SQRT (XD * XD + YD * YD) - MR(JX) - MR(JTEMP)
IF (DIF,GE,W) GO TO 15
IF (IT(JTEMP),LE,J) GO TO 12
15 IF (MX(JTEMP),GE,XMIN) GO TO 13
16 IT(JX) = 1
GO TO 10
COC
*** TRY FOR 'UNDER - OVER' ***
11 JFLAG = 1
CALL BETWN (JXM,JX,JT,JFLAG,MX,MY,MR,LIST1,LIST2)
IF (JFLAG,LE,0) GO TO 12
IT(JX) = 1
GO TO 10
COC
*** CAN WE GET UNDER JX ? ***
12 IF (MY(JX) - MR(JX),LT,6) GO TO 999
2J IF (IT(JXM),GE,1) GO TO 14
COC
*** DO AN 'UNDER - UNDER' ***
XMI4 = MX(JX) - MR(JX) - CRMAX - W

```

```

C000 *** DOES AN 'OVER' IMPINGE UPON JX ? ***
C000 JTEMP = JXM
C000 17 JTEMP = JTEMP - 1
C000 IF (JTEMP.LE.0) GO TO 15
C000 X0 = MX(JX) - MX(JTEMP)
C000 Y0 = MY(JX) - MY(JTEMP)
C000 DIS = SQRT (X0 * X0 + Y0 * Y0) - MR(JX) - MR(JTEMP)
C000 IF (DIS.GE.4) GO TO 15
C000 IF (DIS.GE.3) GO TO 500
C000 18 IF (MX(JTEMP).GE.XMIN) GO TO 17
C000 IT(JX) = 0
C000 GO TO 10
C000 *** TRY FOR 'OVER - UNDER' ***
C000 14 JFLAG = 2
C000 CALL SETM (JXM,JX,JT,JFLAG,MX,MY,MR,LIST1,LIST2)
C000 IF (JFLAG.LE.1) GO TO 511
C000 IT(JX) = 0
C000 GO TO 10
C000 *** BACKTRACK ***
C000 511 JI = JX
C000 512 JI = JI - 1
C000 IF (JI.LT.1) GO TO 999
C000 IF (IT(JI).LE.0) GO TO 511
C000 JX = JI
C000 JXM = JX - 1
C000 IF (JXM.LE.0) GO TO 501
C000 IF (MY(JX) - MR(JX).GE.W) GO TO 20
C000 GO TO 512
C000 512 IF (MY(JI) - MR(JI).LT.W) GO TO 999
C000 IT(JI) = 0
C000 GO TO 11
C000 999 JFLAG = 1
C000 RETURN
C000 END
C000 SUBROUTINE SETM (JXM,JX,JT,JFLAG,MX,MY,MR,LIST1,LIST2)
C000 DIMENSION MX(JT),MY(JT),MR(JT),LIST1(JT),LIST2(JT)
C000 COMMON NFN,NP,NL,CRMAX,W,M
C000 *** JFLAG .LE. 1 IMPLIES 'UNDER - OVER' ***
C000 *** JFLAG .GE. 2 IMPLIES 'OVER - UNDER' ***
C000 KFLAG = 1
C000 NL = 1
C000 LIST1 (1) = JX
C000 NL = 1
C000 K = JX
C000 XMI = MX(JX) - MR(JX) - CRMAX - W
C000 *** CONSTRUCT 'LIST1' OF CRATERS BEHIND JX IMPINGING
C000 DIRECTLY OR INDIRECTLY UPON IT ***
C000 1 KM = JXM
C000 *** DETERMINE IF KM IMPINGES UPON K ***
C000 2 IF (MX(KM).LT.XMIN) GO TO 4
C000 DO -3 IX = 1,NL1
C000 IF (KM.EQ.LIST1(IX)) GO TO 3
C000 13 CONTINUE
C000 X0 = MX(K) - MX(KM)
C000 Y0 = MY(K) - MY(KM)
C000 DIS = SQRT (X0 * X0 + Y0 * Y0) - MR(KM) - MR(K)
C000 IF (DIS.LT.W) GO TO 3
C000 IF (JFLAG.LE.1.AND.MY(KM) + MR(KM).GT.W - W) GO TO 999
C000 IF (JFLAG.GE.2.AND.MY(KM) - MR(KM).LT.W) GO TO 999
C000 *** DETERMINE IF KM IMPINGES UPON JX ***
C000 X0 = MX(KM) - MX(JX)
C000 Y0 = MY(KM) - MY(JX)
C000 DIS = SQRT (X0 * X0 + Y0 * Y0) - MR(KM) - MR(JX)
C000 IF (DIS.LT.W) GO TO 999
C000 TEMP = MX(KM) - MR(KM) - CRMAX - W
C000 IF (XMIN.GT.TEMP) XMIN = TEMP
C000 NL = NL + 1
C000 LIST1 (NL) = KM
C000 3 KM = KM - 1
C000 IF (KM.GT.0) GO TO 2
C000 4 NL = NL + 1
C000 IF (NL.GT.NL2) GO TO 5
C000 K = LIST1(NL)
C000 GO TO 1
C000 *** CONSTRUCT 'LIST2' OF CRATERS AHEAD OF JX IMPINGING
C000 DIRECTLY OR INDIRECTLY UPON IT ***
C000 5 NL2 = 1
C000 LIST2(1) = JX
C000 NL = 1
C000 K = JX
C000 XMAX = MX(K) + MR(K) + CRMAX + W
C000 *** DETERMINE IF KP IMPINGES UPON K ***
C000 7 KP = JX
C000 8 IF (MX(KP).GT.XMAX) GO TO 10
C000 DO -3 IX = 1,NL2
C000 IF (KP.EQ.LIST2(IX)) GO TO 9
C000 11 CONTINUE

```

```

XD = MX(K) - MX(KP)
YD = MY(K) - MY(KP)
DIS = SQRT ( XD * XC + YD * YD) - WR(KP) - WR(K)
IF (DIS.GE.W) GO TO 9
IF (JFLAG.LE.1.AND.MY(KP) - WR(KP).LT.W) GO TO 999
IF (JFLAG.GE.2.AND.MY(KP) + WR(KP).GT.W - W) GO TO 999
CCC *** DETERMINE IF KP IMPINGES UPON JX ***
XD = MX(KP) - MX(JX)
YD = MY(KP) - MY(JX)
DIS = SQRT (XD * XD + YD * YD) - WR(KP) - WR(JX)
IF (DIS.LT.W) GO TO 399
TEMP = MX(KP) + WR(KP) + CQMAX * W
IF (XMAX.LT.TEMP) XMAX = TEMP
NL2 = NL2 + 1
LIST2(NL2) = KP
9 KP = KP + 1
IF (KP.LE.JT) GO TO 5
1J NL1 = NL1 + 1
IF (NL1.GT.NL2) GO TO 1333
K = LIST2(NL1)
GO TO 7
CCC *** DETERMINE IF LIST1 IMPINGES UPON LIST2 ***
100J DO 3J K1=1,NL1
L1=LIST1(K1)
DO 3J K2=1,NL2
L2=LIST2(K2)
DX=MX(L1) - MX(L2)
DY=MY(L1) - MY(L2)
J1=SQRT(DX*DX + DY*DY) - WR(L1) - WR(L2)
IF (J1.LT.W) GO TO 399
3J CONTINUE
GO TO 23J0
999 KFLAG = 0
200J JFLAG = KFLAG
RETURN
END

```

1981 USAF - SCEE SUMMER FACULTY RESEARCH PROGRAM

Sponsored by the

AIR FORCE OFFICE OF SCIENTIFIC RESEARCH

Conducted by the

SOUTHEASTERN CENTER FOR ELECTRICAL ENGINEERING EDUCATION

FINAL REPORT

INFRARED CLUTTER: EFFECTS OF AIR MOTION PRODUCED BY AURORAL ZONE JOULE HEATING

Prepared by: Dr. Ronney D. Harris
Academic Rank: Professor
Department and University: Department of Electrical Engineering and
Center for Atmospheric and Space Science
Utah State University
Research Location: Air Force Geophysical Laboratory
Optical Physics Division
Radiation Effects Branch
USAF Research Colleague: Dr. J. P. Kennealy
Date: August 14, 1981
Contract No: F49620-79-C-0038

INFRARED CLUTTER: EFFECTS OF AIR MOTION
PRODUCED BY AURORAL ZONE JOULE HEATING

by

Ronney D. Harris

ABSTRACT

Irregularities, or clutter, in the earth's infrared profile may cause problems in Air Force infrared surveillance systems. One such irregularity may be produced by particle precipitation and Joule heating in the auroral zone. Vertical air motion induced by this heating can carry infrared active molecules above the dissociation level resulting in patches of enhanced infrared radiation scattering. A two-dimensional self-consistent model of the neutral gas motion has been developed. The problems associated with a general numerical solution of the Navier-Stokes equations for compressible gases have been discussed, and a specific scheme to solve these equations for our model are outlined.

Acknowledgement

The author would like to thank the Air Force Systems Command, the Air Force Office of Scientific Research, the Air Force Geophysical Laboratories, and the Southeastern Center for Electrical Engineering Education for the opportunity to spend a very profitable ten weeks at the Air Force Geophysical Laboratories, Hancomb AFB, Bedford, Mass. The Radiation Effects Branch kindly provided working space and interaction with many distinguished scientists. Special thanks are due to Drs. A. T. Stair and J. P. Kennealy for a portion of their busy time and for their interest in this project.

I. INTRODUCTION:

The heat balance of the earth's environment is an equality between the absorption of solar radiation and emission of infrared radiation (or heat) to outer space. The largest infrared energy source is the near earth atmosphere. Minor atmospheric gases such as CO_2 , H_2O , O_3 and nitrogen compounds form the infrared emitters. If these molecules are uniformly distributed in latitude and longitude, infrared radiation should be uniform. If on the other hand there is spatial variation in these molecules or their temperatures, then irregularities should be expected in the earth's infrared signature. Thus, we might define infrared clutter as irregularities in the background infrared radiation. Clutter was a term that was used in Radar technology to indicate spurious echos, i.e. echos from waves, hills, birds, buildings, etc. that were not of primary interest to the radar operation. In other words - noise. The term can also be used with regard to infrared sunveillance systems to signify radiation from natural or non-man made events.

Until global measurements of infrared radiations are made, it is not possible to put a quantitative measurement to the infrared clutter. However, it is interesting to conjecture on causes and strengths of possible infrared clutter sources. One of the largest perturbations of the earth's atmosphere is the aurora, and many measurements have shown the aurora's effect on the global distribution of composition, temperature and winds at high altitudes.^{13,14,15,16} Dramatic changes also occur in the direct auroral infrared radiations. It is with these facts in mind that we set out to model an auroral event and investigate any change that might occur in the upper altitude infrared radiations.

The calculation of infrared inhomogenities by auroral joule heating and energetic particle precipitation requires a multilevel calculation. First, it is necessary to calculate the charged particle motion in the ionospheric regions due to the high latitude electric field which has its source in the magnetosphere. The electric fields are conducted into the atmosphere by the equipotential geomagnetic field lines. These electric fields are primarily horizontal and drive charged particles across horizontal planes. In the F region the motion of both ions and electrons is $\bar{E} \times \bar{B}/B^2$, but lower down in the E region the motion of ions and electrons is somewhat different because of the altitude dependence of the collision rates. The motion of the ions and

electrons is impeded through collisions with the more numerous neutral gas molecules. This collision process from the point of view of the neutral gas acts as a source of horizontal momentum and heat energy. The second level of calculation is then the determination of the neutral gas motion, as driven by the charged particles, particularly vertical movement near the 100 km level which can redistribute the molecular composition. The 100 km level is important because above this altitude many important infrared emitters such as CO_2 and H_2O are dissociated by the solar ultraviolet radiation. If the aurora creates a new spatial distribution of the infrared emitting molecules, we should then expect to calculate a new infrared radiation distribution. In this way we can calculate the deviations from the normal, quiet background values that are produced by the aurora. This last level of the model is the direct calculation of infrared radiation transport.

II. OBJECTIVES

The most difficult portion of the infrared modeling process described above is the calculation of neutral gas motion. The non-linear equations of mass, momentum and energy conservation applicable to the high altitudes on a rotating sphere must be solved simultaneously. A most formidable task. The goals then of this research were the following:

- (1) Define a model that would incorporate the essential features of the high altitude neutral atmosphere. This model would be used to calculate flow patterns (winds) and temperatures produced by the auroral particles and electric fields described above.
- (2) Review models used by other investigators to weigh their approximations against their results. What can we expect to lose by using approximations to the conservation equations?
- (3) Assimilate some of the numerical techniques that have been successfully used by others on similar problems.

III CONSERVATION EQUATIONS

The Navier-Stokes equations for fluid dynamical motion¹⁷ can be found from the moments of the Boltzman equation:¹

$$\frac{\partial \rho}{\partial t} + \nabla \cdot (\rho \bar{U}) = 0$$

$$\rho \frac{D\bar{U}}{Dt} = -\nabla \cdot \bar{\tau} - \rho \bar{g} + \frac{\delta m}{\delta t} \quad (1)$$

$$\frac{3}{2} \frac{DP}{Dt} = - \frac{3}{2} \rho (\nabla \cdot \bar{U}) + \nabla \cdot \bar{q} + \bar{\tau} : \nabla \bar{U} + \frac{\delta E}{\delta t}$$

(Refer to the Appendix for definitions of the variables and vector operators.)

The above equations are derived with the assumption of collision dominated expressions for the stress tensor and heat flow vector¹. The quantities $\delta M/\delta t$ and $\delta E/\delta t$ are changes in neutral gas momentum and energy due to collisions with different gases. In our problem, the only other gases are the charged particles. The following expressions result for the collision integrals².

$$\frac{\delta M}{\delta t} = - \sum_i \rho v_{ni} (\bar{U} - \bar{V}_i) + \sum_i \frac{v_{ni} Z_{ni} \mu_{ni}}{kT_{ni}} (\bar{q} - \frac{\rho}{\rho_i} \bar{q}_i) \quad (2)$$

$$\frac{\delta E}{\delta t} = - \sum_i \frac{\rho v_{ni}}{m_n + m_i} 3k(T - T_i) - \sum_i \frac{\rho m_i}{m_n + m_i} v_{ni} |\bar{U} - \bar{V}_i|^2$$

Since the lifetime of the charged particles is much less than the time constant of the motions of interest, we do not calculate in a self consistent manner the state of the ion or electron gases. (This just means we ignore the internal energy of the ion and electron gases.) Thus, the ion and electron temperatures are assumed to be the same as the neutral gas; i.e. in (2) $T - T_i = 0$ and $\bar{q}_i = 0$. The resulting momentum and energy terms are due solely to the relative velocity between neutral molecules and charged particles. Heat conduction from the electron gas, which can attain very high temperatures in electron precipitation events, will be investigated later.

Since we are interested in infrared structure, and the greatest variability in the auroral zone is in the latitudinal (north-south) direction, we need to examine motion in the north-south-vertical plane. The equations of motion on a horizontal plane tangent to a spherical rotating earth have been given by Haurwitz³.

$$\begin{aligned} \frac{Du}{Dt} - 2 \Omega (v \sin \phi - w \cos \phi) &= \frac{F_x}{m} \\ \frac{Dv}{Dt} + 2 \Omega u \sin \phi &= \frac{F_y}{m} \\ \frac{Dw}{Dt} - 2 \Omega u \cos \phi &= \frac{F_z}{m} \end{aligned} \quad (3)$$

where Ω is the angular rotation rate of the earth, ϕ is latitude of the tangent plane and u, v, w are the east, north and upward velocities respectively. The centrifugal acceleration terms have been lumped into the gravity vector for an ellipsoidal earth. One can show that the coriolis force, $f = 2\Omega \sin\phi$ is called the coriolis coefficient, acts perpendicular to both the earth's axis and the fluid motion. Hence, it is a deflecting force and cannot change the energy of the velocity, only the direction. A coriolis force must be added to the Navier-Stokes equations of (1) to complete the mathematical specification.

Hardly anybody uses these completely general, non-linear equations to solve geophysical problems.⁵ The reason is that the complete set of conservation equations describe motions whose time constants may vary over a range as large as 10^4 ; i.e. motion that includes high frequency sound waves as well as low frequency planetary waves. In many geophysical problems the vertical acceleration is perhaps only 10^{-4} times as large as the gravitational and vertical pressure gradient forces. Hence, a very accurate calculation is required to determine the vertical velocity. There is often a near balance between the horizontal pressure gradient and coriolis forces. These factors require an unrealistic accuracy requirement on numerical computations. Under the circumstances, it is usual practice to compromise and use only approximate mathematical formulations. Because of the near perfect balance between gravitational and vertical pressure gradient terms, the most common simplification is to replace the vertical equation of motion by the hydrostatic equation⁵

$$\frac{\partial P}{\partial z} = -\rho g$$

This approximation simplifies the vertical motion expression and at the same time eliminates sound waves from the remaining system of equations. The resulting expressions are known by meteorologists⁵ as the "primitive equations". Whereas, the original conservation equations (1) were all prognostic, i.e. each one has a time variation, the hydrostatic equation is not time dependent. The hydrostatic equation clearly requires the ratio of the vertical pressure gradient and the density to be constant. This sort of an identity expression is called a "diagnostic equation". Since we are forcing our flow to have hydrostatic stability, another useful simplification is to use pressure as the vertical coordinate. As a side benefit in this new coordinate system, the

continuity equation takes on a very simple form and the density doesn't appear in the continuity equation. In the regular cartesian coordinate system the convective derivative can be written

$$\frac{D}{Dt} = \frac{\partial}{\partial t} + u \frac{\partial}{\partial x} + v \frac{\partial}{\partial y} + w \frac{\partial}{\partial z}$$

where t,x,y, and z are independent variables. In a pressure coordinate system, the independent variables are t,x,y, and p. Since the lowest level in our model will be p_0 we choose a slightly different variable which has a linear variation in an exponential atmosphere

$$Z = \ln (p_0/p)$$

This leaves the convective derivative in the form

$$\frac{D}{Dt} = \frac{\partial}{\partial t} + u \frac{\partial}{\partial x} + v \frac{\partial}{\partial y} + w \frac{\partial}{\partial Z}$$

where $W = DZ/Dt$. By the chain rule of differentiation we also find

$$\frac{\partial f}{\partial z} = \frac{\partial f}{\partial Z} \frac{\partial Z}{\partial z} = \frac{1}{H} \frac{\partial f}{\partial Z}$$

where $H = g/RT$ defined as the scale height, and f is any dependent variable.

The horizontal derivative takes the form

$$\frac{\partial f}{\partial x} \Big|_z = \frac{\partial f}{\partial x} \Big|_Z - \frac{\partial f}{\partial Z} \left(\frac{\partial Z}{\partial x} \right) \frac{\partial z}{\partial x} \Big|_Z$$

The subscripts z and Z mean at constant z (altitude) or on a constant Z (pressure) surface. Utilizing these new variables in (1) and after considerable operational calculus we get the approximate conservation equations in pressure coordinates.

$$\nabla_H \cdot \bar{U}_H + \frac{\partial w}{\partial Z} - w = 0$$

$$\frac{\partial h}{\partial Z} = RT/g$$

$$\rho \frac{D\bar{U}_H}{Dt} = \nabla_H \cdot \bar{\tau} - 2(\bar{\omega} \times \bar{U})_H + \frac{\delta M}{\delta t}$$

(4)

$$\frac{3}{2} \frac{DP}{Dt} = - \frac{3}{2} p(\nabla \cdot \bar{u}) + \nabla \cdot \bar{q} + \bar{\tau} : \nabla \bar{u} + \frac{\delta E}{\delta T}$$

where the horizontal and convective derivatives apply on surfaces of constant Z (pressure). The subscript H means the horizontal components. There are many specialized forms for the heat equation. We leave it in the general form until we get to specific applications. The symbol h has been used to represent the height of a constant Z surface above a constant height surface z. If calculations start from a static atmosphere, the constant Z surfaces are horizontal and correspond to certain constant heights. The dependent variables are the horizontal velocities $\bar{U}_H = u\hat{i} + v\hat{j}$, the vertical motion of a pressure surface W, the temperature T, the height of a pressure surface h, and the pressure p. But p is related to Z and W. So we have 6 unknowns and six relationships, 5 equations in (4) and $W = DZ/Dt$.

Now that we have the equations which most conveniently and most simply described our problem, it is necessary to decide exactly what auroral model we ought to analyze. As mentioned earlier, we desire to calculate the motion in a north-south-vertical plane. This may be done by allowing a zonal (east-west) velocity which has no zonal variation ($\partial/\partial x = 0$). Our coordinate system would be rectangular with x (east), y (north) and $Z = \ln(p_0/p)$ upward. This model might be considered a 2 1/2 dimensional flow. The appeal of this model is that the zonal (eastward) velocity will be the largest velocity, perhaps several hundred meters per second. The easterly velocity would be the only velocity large enough to measure, hence provide a possible check on the calculations. The negative aspect of this model is a numerical one. The large eastward velocity couples via the coriolis force into the north-south motion equation. This term which is several orders of magnitude larger than the other terms must be balanced by the north-south pressure gradient. These two large terms that appear in the y equation, swamp out the smaller forces which actually drive the y directed motion. In our initial calculations it seems wise to ignore completely the zonal flow and only calculate motion in the north-south-vertical plane. Zonal velocities can then be estimated with the decoupled x equation alone. Mathematically we must set $u = 0$ and $\partial/\partial x = 0$.

There is a second consideration with regard to the model. It is obvious that the momentum and energy equations are highly non-linear. If the equations could be linearized, the necessary calculations would be much simplified. This

can be done by assuming the dependent variables have a basic or steady value plus a perturbed value. For example, we might write

$$\begin{aligned}V_T &= V_o + V \\W_T &= W_o + W \\T_T &= T_o + T \\h_T &= h_o + h\end{aligned}$$

where the subscript T means total and o is basic state. The normal assumption is that the perturbed value is much less than the basic state value, e.g. $T \ll T_o$. Normally for a resting atmosphere $V_o = W_o = h_o = 0$. If the total values are substituted into (4) and the products of perturbed values are neglected compared to linear perturbation terms, then a set of linear equations is developed. One can also neglect the adjective terms at this level of approximation. The resulting linear model will not yield exact results, but should give the overall flow pattern and reasonable estimates of the flow magnitudes. This model might be satisfactory for some applications, especially if the numerical calculations are more easily accomplished.

IV NUMERICAL TECHNIQUES

This brings us to the consideration of the numerical methods that are available to solve systems of partial differential equations like (4). Basically there are two time stepping techniques, explicit and implicit. The explicit method utilizes information at time step n to advance the calculations to time step n + 1. Simply written

$$\frac{u^{n+1} - u^n}{\Delta t} = Lu^n$$

where u is the vector of dependent variables and L is a non-linear operator accounting for all terms except $\partial u / \partial t$. For the simple diffusion equation it can be shown that the explicit scheme is convergent and stable if and only if $\Delta t / \Delta z^2 < .5$, where Δz is the size of the spatical steps. This restriction forces very small time steps with concomitant large computer run times to achieve accurate answers. The implicit scheme can be summarized by the expression

$$\frac{u^{n+1} - u^n}{\Delta t} = \theta (Lu^{n+1}) + (1-\theta)Lu^n$$

where $.5 \leq \theta \leq 1$ guarantees convergence and stability for all values of Δt . When $\theta = 1/2$ the values of u at time step n are equally weighted with the values of u at time $n+1$. This weighting is called the Crank-Nicolson scheme.⁴ The only problem with the implicit scheme is that Lu has to be expressed so that it can be evaluated at time step $n+1$. For linear functions of L , and perhaps for simple non-linear features, the implicit scheme is surely the method to use because of the stability characteristics. However, the fully non-linear equations of (4) preclude the use of the implicit scheme.

The explicit time stepping scheme can be made more accurate by utilizing the "leap frog" method^{11,12} or the n cycle method of Lorenz.^{9,10} This leap frog scheme is simply a central differencing scheme for time integration. If all variables are known at time step n and also $n-1$, then we step forward by the expression

$$\frac{u^{n+1} - u^{n-1}}{2\Delta t} = Lu^n$$

It has been found that after a few tens of steps forward in time the u^{even} and u^{odd} decouple.¹² To correct this problem it is only necessary to average the even and odd time step values every so often. This may be done by using the regular explicit form

$$\frac{u^{n+1} - u^n}{\Delta t} = Lu^n$$

once every 30 steps or so. Another trick to help stability is to evaluate any diffusion type terms, i.e. terms having second order spatial derivatives, at the backward time step, time $n-1$.^{11,12}

An element that has some impact on the numerical scheme to be used is the way in which spatial variations are handled. Basically, one either uses a finite number of grid points at which the variables are evaluated or an expansion of orthogonal functions to approximate the motion variables. The global circulation model developed at the National Center for Atmospheric Research (NCAR) uses a finite discrete grid in both the horizontal and vertical (pressure). The global stratospheric model developed at MIT used a finite grid in the vertical but described the horizontal variations by spherical harmonic functions. Both models appear to function adequately. For the case of spectral harmonics in the horizontal and finite differences in the vertical, each

variable is expanded into a series of sines and cosine terms. For example, the temperature might be written

$$T = \sum_m A_m \cos\left(\frac{m\pi y}{L}\right) + \sum_m B_m \sin\left(\frac{m\pi y}{L}\right)$$

Equating all the cosine terms and sine terms results in a series of equations like (4) at each altitude expressing the relationships between the harmonic amplitudes. This technique eliminates the horizontal derivatives, leaving partial derivatives in time and height. Enough harmonics must be used so that horizontal variations can be described by the harmonic series. The source functions must also be expanded into harmonic series to complete the method. For a linear set of equations the process is especially simple. For nonlinear equations, cross terms in the series add to the complexity of the problem. There does not seem to be much appreciable difference in the numerical complexity between the spectral or finite difference schemes for the leap frog technique in our 2-dimensional model. This is because the derivatives needed for the method are evaluated at the previous time step and thus can be easily found.

Using an implicit scheme where the primitive equations have been linearized and the horizontal variations described by harmonic functions is a rather straight forward procedure. However, if the horizontal variations are to be described by finite differences, a rather different integration scheme is required. Following the method of Peaceman and Rachford⁶ we let ψ equal the vector of dependent variables. The first time step we use the expression

$$\frac{\psi^{n+1} - \psi^n}{\Delta t} = A \frac{\partial^2 \psi^{n+1}}{\partial Z^2} + B \frac{\partial \psi^{n+1}}{\partial Z} + \frac{1}{2} (C\psi^{n+1} + F^{n+1}) + D \frac{\partial^2 \psi^n}{\partial y^2} + E \frac{\partial \psi^n}{\partial y} \quad (5)$$

where A, B, C, D, E and F are coefficient matrices. Since the value of ψ^n is known, we are effectively evaluating only the Z variation at time $n + 1$. The first and second spatial derivatives would be formed by the central differences

$$\frac{\partial^2 \psi_j}{\partial Z^2} = \frac{\psi_{j+1} - 2\psi_j + \psi_{j-1}}{\Delta Z^2} \qquad \frac{\partial \psi_j}{\partial Z} = \frac{\psi_{j+1} - \psi_{j-1}}{2\Delta Z}$$

where j is the altitude index. Since only three unknown values are contained in

(5), the system for all altitudes forms a block tridiagonal matrix which can be solved by straight forward methods. The next step in time is written

$$\frac{\psi^{n+2} - \psi^{n+1}}{\Delta t} = \frac{\partial^2 \psi^{n+2}}{\partial y^2} + E \frac{\partial \psi^{n+2}}{\partial y} + \frac{1}{2} (C\psi^{n+2} + F^{n+2}) + A \frac{\partial^2 \psi^{n+1}}{\partial Z^2} + B \frac{\partial \psi^{n+1}}{\partial Z}$$

Again if we use central differences in the y direction the equations form a tridiagonal system since ψ^{n+1} is known. By alternating the evaluation of the Z and y variations in the way shown, it is possible to solve the system of algebraic equations that result from finite differences by straight forward methods. If both the y and Z derivatives are attempted simultaneously, a set of algebraic equations is generated where the whole coefficient matrix is filled with non-zero elements. These equations are much more difficult to solve simultaneously than the tri-diagonal set formed by the alternate Z and y differences. Since the implicit method is both convergent and stable for all Δt , one can step forward with large time steps.

The final concept in the numerical simulation is the boundary conditions. Meteorology problems generally consider only a small part of the atmosphere. This means that at least part of the boundary is open so mass can flow into and out of the region. For our proposed model to calculate infrared clutter, all boundaries are open. However, extensive flow in and out of the region will only occur at the top boundary. A number of people have studied the problem of open boundaries with respect to the specification of the variables on the boundaries.^{7,8} Necessary and sufficient conditions for the primitive equations are not yet known, but with care not to over specify the boundary conditions progress can be successfully made. As an example, let us consider the boundary conditions that are necessary to solve (4). The heat and momentum sources vary with altitude. At 90km the sources are essentially zero. At 300 km the source is almost independent of altitude. This characteristic of the driving source suggests that we can specify u, v, W, T and h to be zero at the lower boundary. The pressure and density would have the basic state values. At the upper boundary the viscous forces are the dominant terms and tend to smooth out any vertical variations. By placing the top boundary at the appropriate level, the vertical gradients of u, v, W and T can be set at zero. The value of W at the top boundary is found from the continuity equation. The pressure level height h is found by integrating the hydrostatic equation from the bottom upwards. This gives us ten boundary conditions for the six variables.

VI RECOMMENDATIONS

We have attempted in the above paragraphs to briefly describe the problems associated with a numerical solution to the "primitive equations" of meteorology. These considerations plus the advice of other scientists lead to a fairly clean conclusion; the greatest probability for success lies with the leap frog method for time integration. Because this is an explicit scheme, due care must be exercised to assure numerical stability and convergence. The question whether to describe the horizontal variations with a spectral device or finite differences is still not clear for our 2-dimensional model. With these caviats in mind, we propose the following plan to model the motion produced by auroral processes:

1. Form the linearized conservation equations utilizing the leap frog method for time integration, the spectral decomposition for the horizontal variations of the 2-dimensional motion and finite differences in the vertical pressure coordinate. The equations that result from linearizing (4) and neglecting advection terms are given below.

$$\frac{\partial T}{\partial t} = -W \chi_0 + \left(\frac{\lambda}{\rho_0 c p}\right) \frac{\partial^2 T}{\partial y^2} + \left(\frac{\lambda}{\rho_0 c p H^2}\right) \frac{\partial^2 T}{\partial z^2} + \frac{\delta H}{\rho_0 c p \delta t} \quad (6)$$

$$\frac{\partial v}{\partial t} = g \frac{\partial h}{\partial y} + \frac{\mu}{\rho_0} \frac{\partial^2 v}{\partial y^2} + \left(\frac{\mu}{\rho_0 H^2}\right) \frac{\partial^2 v}{\partial z^2} + \frac{\delta M}{\rho_0 \delta t}$$

$$0 = \frac{\partial u}{\partial y} + \frac{\partial W}{\partial z} - W$$

$$0 = \frac{\partial h}{\partial z} - \frac{RT}{g}$$

$$\chi_0 = \frac{\partial T_0}{\partial z} + \frac{RT_0}{cp}$$

the quantity χ_0 is called the static stability and is a measure of the resistance of the atmosphere to overturning. The equations will be solved sequentially at each time step. Solve for T, then integrate the hydrostatic equation from bottom to top to find h, then find v and finally integrate downward from top to bottom to

evaluate W . In each step we use updated values, i.e. like h^{n+1} to find v^{n+1} rather than h^n . This process has been found to yield more stable results.¹² Boundary conditions will be

$$v = T = W = h = 0 \quad \text{Lower boundary}$$

$$\frac{\partial v}{\partial z} = \frac{\partial T}{\partial z} = \frac{\partial W}{\partial z} = 0 \quad \text{Upper boundary}$$

The spectral representation for horizontal variations leads to an assumption of periodic boundary conditions at the sides. About twenty harmonics will be used initially to describe the horizontal variations. Diffusion terms will be evaluated at the backward time step. This also is a stability consideration. Because these equations are linear and because the heat source is symmetric and momentum source antisymmetric with respect to the center of the region, we find that (6) breaks into two sets of equations, with symmetric variations and antisymmetric variations. The sum of the two solutions is the total solution.

2. The linearized approximation to the motion will be solved to give us experience and to indicate flow patterns. As we evaluate the motion predicted by the linear equation (6), we will begin to code the non-linear equations (4) into the computer. A moment's thought will reveal that the leap-frog time scheme will handle non-linear terms very effectively. The experience gained by running the linear model should give us valuable insight into the effects of non-linear terms on the motion and the numerical tricks useful to get good results.

Appendix - Symbol Definitions

- ρ = mass density (kg/m^3)
 \vec{U} = vector velocity (m/s) = $u\hat{i} + v\hat{j} + w\hat{k}$
 t = time (seconds)
 T = temperature ($^{\circ}\text{K}$)
 p = isotropic pressure (kg/m^2)
 \vec{p} = Pressure tensor (kg/m^2)
 $\vec{\tau}$ = Stress tensor = $\vec{p} - pI$ (kg/m^2)
 \vec{q} = Heat flow vector ($\text{joules/m} - \text{s}$) = $\lambda \nabla T$
 g = acceleration of gravity (km/s^2)
 ν = collision frequency (s^{-1})
 k = Boltzmann Constant
 m = mass per particle (kg)
 η = $5p/6\nu$ = viscosity coefficient (kg/m-s)
 λ = $25/8$ (kp/mv) = heat conduction coefficient ($\text{joules/m-s-}^{\circ}\text{K}$)
 μ_{ni} = $m_n m_i / m_n + m_i$ = reduced mass
 T_{ni} = $(m_i T_n + m_n T_i) / m_n m_i$ = reduced temperature
 Z_{ni} = constant (see Schunk, 1977)
 D = $\frac{\partial}{\partial t} + \vec{U} \cdot \nabla$ = convective derivative
 $\vec{\tau}$ = $\eta [\nabla \cdot \vec{U} + (\nabla \cdot \vec{U})^T - 2/3 (\nabla \cdot \vec{U})]$ stress tensor
 \vec{V}_i = vector ion velocity

$$\nabla \vec{u} = \begin{bmatrix} \partial u / \partial x & \partial v / \partial x & \partial w / \partial x \\ \partial u / \partial y & \partial u / \partial y & \partial w / \partial y \\ \partial u / \partial z & \partial u / \partial z & \partial v / \partial z \end{bmatrix}$$

$$\vec{P} : \vec{\tau} = \begin{bmatrix} P_{xx} & P_{xy} & P_{xz} \\ P_{yx} & P_{yy} & P_{yz} \\ P_{zx} & P_{zy} & P_{zz} \end{bmatrix} \times \begin{bmatrix} \tau_{xx} & \tau_{xy} & \tau_{xz} \\ \tau_{yx} & \tau_{yy} & \tau_{yz} \\ \tau_{zx} & \tau_{zy} & \tau_{zz} \end{bmatrix} = \text{tensor product}$$

REFERENCES

1. R.W. Schunk, "Mathematical Structure of Transport Equations for Multispecies Flows", Rev. Geophys and Spa. Sci., vol 15, pp 429-445, 1977
2. B.S. Tanenbaum, "Transport Equations for a Gas Mixture", Phys. of Fluids, vol 8, pp 683-686, 1965
3. B. Haurwitz, Dynamic Meteorology, (McGraw Hill, New York, 1941) pp 127
4. J.H. Smith, Numerical Solution of Partial Differential Equations, (Oxford Univ. Press, 1965) Chapter 2
5. J.R. Holton, An Introduction to Dynamic Meteorology, (Academic Press, New York, 1972) pp 149
6. D.W. Peaceman and H. H. Rachford Jr. "The Numerical Solution of Parabolic and Elliptic Differential Equations", J. Soc. Indust. Appl. Math., vol 3, pp 28-41, 1955
7. E.N.. Lorenz, "Energy and Numerical Weather Prediction", tellus, vol 12, pp 364-373, 1960
8. J. Olinger and A. Sundström, "Theoretical and Practical Aspects of some Initial Boundary Value Problems in Fluid Dynamics", SIAM J Appl. Math., vol 35, pp 419-446, 1978
9. E.N. Lorenz, "An N-Cycle Time Differencing Structure for Stepwise Numerical Integration", Mon. Wea. Rev. vol 99, pp 644-648, 1971
10. M. Israeli and D. Gottlieb, "On the Stability of the N Cycle Scheme of Lorenz", Mon Wea Rev, vol 102, pp 2540-2556, 1974
11. E.C. Riddley - private communication, 1980
12. R. Aiken - private communication, 1980

13. H.G. Mayr and I Harris, "Some Characteristics of Electric Field Momentum Coupling with the Neutral Atmosphere", J. Geophys. Res., vol 83, pp 3327-3336, 1978
14. R.G. Roble, R.E. Dickinson and E.C. Ridley, "Thermospheric Response to the November 8-9, 1969, Magnetic Disturbances", J. Geophys. Res., vol 84, pp 4209-4216, 1979
15. J.M. Straus and M. Schutz, "Magnetospheric Convection and Upper Atmospheric Dynamics", J. Geophys. Res., vol 81, pp 5822-5831, 1976
16. M.R. Schoeberl and D.F. Strobel, "The Zonally Averaged Circulation of the Middle Atmosphere", J. Atmos. Sci., vol 35, pp 577-591, 1978
17. H. Lamb, Hydrodynamics, (Dover Pub, New York, 1932) pp 577

1981 USAF - SCEEE SUMMER FACULTY RESEARCH PROGRAM

Sponsored by the

AIR FORCE OFFICE OF SCIENTIFIC RESEARCH

Conducted by the

SOUTHEASTERN CENTER FOR ELECTRICAL ENGINEERING EDUCATION

FINAL REPORT

CATABOLISM OF TOLUENE IN THE BLUEGILL SUNFISH

Prepared by: Dr. Franklin D. Hill

Academic Rank: Professor

Department and University: Department of Chemistry
Grambling State University

Research Location: Aerospace Medical Research Laboratory, Toxic Hazards
Division, Environmental Quality Branch

USAF Research Colleague: Major James M. Livingston

Date: September 11, 1981

Contract No: F49620-79-C-0038

CATABOLISM OF TOLUENE IN THE BLUEGILL SUNFISH

by

Franklin D. Hill

ABSTRACT

The catabolism of toluene by bluegill sunfish exposed to a high, non-lethal, aqueous concentration of the non-labelled hydrocarbon is investigated. No catabolic product of toluene could be identified in fish bile following hydrocarbon exposure. The inability to identify certain expected catabolic products is discussed. Suggestions for further research in this area are offered.

Acknowledgement

The author would like to thank the Air Force Systems Command, the Air Force Office of Scientific Research and the Southeastern Center for Electrical Engineering Education for the opportunity to spend an interesting and worthwhile summer at the Aerospace Medical Research Laboratory, Wright-Patterson AFB, OH. He would like to commend the Toxic Hazards Division for its hospitality and excellent working conditions.

The author thanks Major James M. Livingston for suggesting this area of research and for his collaboration and guidance. Finally, he would like to acknowledge helpful discussions with Lt Col Roger Inman and Mr. Jeffrey Fisher.

I. INTRODUCTION

Aromatic hydrocarbons are known to be toxic to mammals and aquatic organisms.^{1,2,3} These compounds are the main water soluble components of petroleum based fuels such as gasoline and jet fuels. The aircraft industry alone, including the US Air Force, uses several hundred thousand gallons of jet fuel daily. Large quantities of these compounds are also used as industrial solvents. The production, storage, transport, and use of such large amounts of these fuels and solvents pose a threat to aquatic organisms from water contamination by accidental spillage. The accumulation of these chemicals by aquatic organisms might be harmful not only to these organisms but to humans who consume them.

Aromatic hydrocarbons, being among the most toxic compounds in petroleum, have received considerable attention in recent years. Several studies have been performed on their effects upon living organisms, especially aquatic organisms. Polycyclic aromatics have received particular attention because some are carcinogenic. They exhibit low volatility at laboratory conditions and are therefore easier to investigate than monocyclics.

Although several articles have reported the fate and toxicity of aromatic compounds in aquatic and terrestrial animals, few articles have been concerned with the bioconversion of aromatics in living systems. This is particularly true in the case of the monocyclic hydrocarbons. These represent a large proportion of the water soluble fraction of petroleum fuels and are also the most toxic.

An understanding of the catabolism of the monocyclics is important in understanding their toxic effects upon cells and living organisms.

The present project was undertaken to determine if toluene, a main monocyclic aromatic component of petroleum fuels, is catabolized in aquatic organisms. As a large consumer of petroleum based jet fuel (JP-4), the US Air Force is concerned about the toxic effects of this major component, including its catabolic products, upon living organisms.

II. OBJECTIVES

The main objective of this project is to investigate the catabolism of the main monocyclic aromatic hydrocarbons in aquatic organisms. The specific objectives were:

1. To determine if the toluene is catabolized in the bluegill sunfish, and if so
2. To isolate and identify catabolic products formed, and
3. To postulate the mechanism of catabolism.

Toluene was selected for the study because of its high concentration in the water soluble fraction of jet fuel (JP-4) and its relatively high toxicity to mammals.

III. EXPERIMENTAL

The bluegills Lepomis macrochirus used in this investigation were obtained from Fender's Fish Hatchery, Baltic, Ohio. They were 9-14 cm in length and had a mean net weight of 14.49 ± 3.54 g. Fish were maintained in the laboratory in an aquarium containing water with a temperature of 19-21°C, pH of 7.2 to 7.6, dissolved oxygen 9-9.8, and a hardness of about 150 mg CaCO₃/liter.

Fish were exposed to 8.7 ppm toluene solution for 48 hours in an aquarium containing about 5 liters solution per fish. The water was stirred to mix the toluene evenly before exposure but was not oxygenated during exposure. However, the fish were transferred to fresh toluene water following 8, 24, and 30 hours of exposure.

A control group of fish was maintained under similar conditions except that no toluene was added to their aquarium.

After 48 hours of exposure, the fish were removed from experimental solutions and the gall bladders removed. Organs were pooled and frozen until analysis by thin layer chromatography (TLC).

For TLC, bile from pooled tissue was applied to 20 x 20 cm Analabs OF plates. The plates were developed in p-dioxane:benzene:acetic acid (25:90:4; v:v:v:System A) until the eluent front had reached 12 cm. A second sample of bile was applied to 20 x 20 cm Applied Science Absorbosil 5 plates. Development was with the upper solvent phase of 1-butanol:concentrated ammonium hydroxide:water (40:10:50; v:v:v:System B).

Standards were chromatographed under similar conditions and located colorimetrically by spraying with 50% aqueous H_2SO_4 containing 10% $K_2Cr_2O_7$ at ambient temperature. Available standards included benzoic acid, benzyl alcohol, hippuric acid, o-cresol, m-cresol, and p-cresol.

After evaporation of eluting solvent, 1 cm bands were scraped from the plates, pooled, and extracted with ethyl ether to remove nonconjugated derivatives. The extracts were concentrated under a stream of nitrogen.

The TLC scrapings were extracted again with dichloromethane:isopropyl alcohol:water (75:25:2: v:v:v) to remove conjugated hydrocarbon derivatives. These extracts were concentrated under reduced pressure. Extracts were analyzed by both gas liquid chromatography (GLC) and gas chromatography-Mass Spectrometry (GC-MS).

GLC was performed on a Varian Aerograph, Model 274010-20, equipped with a flame ionization detector and a 6 feet, 1/8 inch diameter stainless steel column packed with 10% SE-30 on 80/100 mesh chromosorb W using helium carrier gas, flow rate 30 ml/min. Analysis were carried out with an injector temperature of 230°C, detector temperature 260°C, and column temperature from 30°C to 240°C programmed at 10° per minute.

GC-MS analyses of extracts were carried out with an automated Hewlett-Packard Model 5985 GC-MS with a 7906 Disc Drive and 5945 Gauge Controller. The instrument was programmed to perform a library search and list probable compounds from matching spectra. Sample separation was on a SE-30 column from 30°C to 240°C with a 10°/min increase.

IV. RESULTS AND DISCUSSION

Bluegill sunfish exposed to 8.7 ppm aqueous toluene at ambient temperature showed no abnormal behavior. All fish survived the 48 hour exposure, substantiating the sublethal nature of this toluene concentration. However, an accidental exposure to 10.4 ppm toluene during the investigation caused the fish to become highly irritable and to lose their equilibrium. This observation implies that the toluene LC₅₀ value for bluegills is less than

10 ppm³, considerably less than was reported in an earlier publication.⁴

Fish placed in experimental water with 8.7 ppm toluene at temperatures more than two degrees below ambient temperature showed the same response as they did at 10.4 ppm toluene. Evidently tolerance to toluene is temperature dependent. Additional studies are needed to determine the LC₅₀ at various temperatures.

TLC plates of cresol standards gave brown colors when sprayed with 50% aqueous H₂SO₄ containing 10% potassium dichromate. Benzyl alcohol, benzoic acid and hippuric acid did not form distinctive colors but were located on the plates by differences in appearance along the line of migration. R_f values of standards are given in Table 1.

TABLE 1
R_f VALUES OF STANDARDS ON TLC PLATES

COMPOUND	SYSTEM A	SYSTEM B
	p-dioxane:benzene:acetic acid (25:90:4; v:v:v) OF PLATES	1-butanol:conc. NH ₄ OH:H ₂ O (40:10:50; v:v:v) ADSORBOSIL 5 PLATES
o-cresol	.90	.93
m-cresol	.86	.93
p-cresol	.85	.92
benzyl alcohol	.81	.92
benzoic acid	.86	.63
hippuric acid	.24	.48

As indicated by R_f values neither system was effective in separating the cresols and benzyl alcohol, all of which migrated close to the eluent front.

Both system separated hippuric acid from the nonconjugated standards, and the Adsorbosil plates with basic eluent (System B) gave adequate separation of benzoic acid from the remaining standards.

The TLC systems were not the most desirable for separating potential toluene metabolites or the metabolites of other small monocyclic aromatics which would be volatile. In addition to poor separation of nonconjugated standards eluent evaporation was slow. Time required for the eluent to evaporate from the plates after development undoubtedly resulted in considerable loss of volatile catabolites. Although the eluting mixtures have been used successfully for separating metabolites of polycyclic aromatics^{5,6} their low volatility is a disadvantage with highly volatile compounds. Such solvents could also be used with radioactive substrates where location of metabolites is most important and GLC and GC-MS analyses would not follow. When TLC extracts are to be used for these additional analyses a more volatile eluent would be desirable. At least the inclusion of eluent in the extract should not give peaks which overlap those of the metabolites. TLC scraping should be done immediately without extended time for eluent evaporation when separating volatile compounds.

GLC analysis of extracts of pooled 1 cm scrapings from the TLC plates of bile from control fish gave chromatograms similar to that of bile from fish exposed to toluene. No qualitative differences were observed in any of the chromatograms. Similar analyses of solutions of standard compounds gave satisfactory chromatograms for the cresols only and m-cresol was not separated from p-cresol. Retention times of standards were benzyl alcohol, 8.7 min (117°); o-cresol, 9.3 min (123°); p-cresol, 9.7 min (127°); and m-

cresol, 9.8 min (128°). Benzyl alcohol required an unexpectedly high concentration to give an observable peak. Benzoic acid and hippuric acid did not form the usual peaks, indicating that the column and operating parameters were not the most suitable for determining small amounts of these potential metabolites.

GC-MS analyses of TLC extracts expected to contain the nonconjugated toluene metabolites were not positive. None of the expected oxidized metabolites, i.e., benzyl alcohol or the cresols, were suggested from the library search of spectra programmed into the automated instrument. Benzyl alcohol and the cresols were not present in bile extracts from fish exposed to 8.7 ppm toluene. Either these catabolites are not produced from toluene in bluegills or they are produced in such minute amounts that they can not be identified by chromatographic methods used in this investigation.

Available time did not allow detailed examinations of all TLC extracts. The fractions expected to contain the conjugated derivatives were not analyzed. GC analysis indicated that hippuric acid did not give a normal peak but probably decomposed at high temperature. Liquid chromatography would probably be more desirable than GC for separating and identifying conjugated metabolites sensitive to high temperature. Conjugated metabolites could have been present in the extracts but not indicated using the GC conditions employed. Additional investigations on these fractions are needed.

Ring labelled C¹⁴ toluene was not available for the present investigation. Its use could have made the isolation and identification much more definitive. Catabolites produced from the radiolabelled compound could have been located on TLC plates by scintillation counting of extracts of TLC scrapings. Once

located, emphasis could have been placed on similar extracts from plates with nonlabelled toluene.

V. RECOMMENDATIONS

Results reported in the current investigation do not positively eliminate the presence of any of the oxidation products suspected. It does emphasize the difficulty in isolating and identifying extremely small quantities of catabolites without using radiolabeled substrates. This investigation should be continued and extended to include other components in the water soluble fractions of petroleum products such as JP-4 fuel.

I plan to continue this investigation with ring labeled C-14 toluene. It is highly desirable that substrates labelled with carbon-14 or tritium be employed where possible. It is much more convenient to locate a labeled catabolite than spend long, useless hours working with fractions most of which do not contain compounds of interest.

It is also desirable to incorporate high performance liquid chromatography (HPLC) into the separation of temperature sensitive compounds as at least one standard appeared to be in this investigation.

The determination of metabolites of volatile, monocyclic aromatic compounds is a tedious and delicate operation. Volatilization of products should be carefully controlled in performing laboratory operations or considerable loss of volatile products could occur.

Catabolic studies of monocyclic aromatics in fish should involve the gallbladder or its contents since this organ has been shown to be a major accumulation site in studies with aqueous radioactive toluene.⁷ Oxidized substrates are believed to be stored in the gallbladder for excretion.

REFERENCES

1. M. Windholz, The Merck Index, 9th Ed., (Merck & Company Publishers, Rahway, N.J., 1976)
2. D. C. Malins, Effects of Petroleum on Arctic and Subarctic Environments and Organisms, Volume 2. (Academic Press, New York, N.Y., 1977)
3. P. E. Benville Jr., and S. Korn, "The Acute Toxicity of Six Monocyclic Aromatic Crude Oil Componentes to Striped Bass (Morone Saxatilis) and Bay Shrimp (Crago Fanciscorum)", California Fish and Game, Vol. 63, pp. 204-209, 1977.
4. Q. H. Pickering and C. Henderson, "Acute Toxicity of Some Important Petrochemicals to Fish", Water Polut. Control Fed. Four., Vol. 38, pp. 1419-1429, 1966.
5. D. C. Malins, T. K. Collier, L. C. Thomas and W. T. Roubal, "Metabolic Fate of Aromatic Hydrocarbons in Aquatic Organism: Analyses of Metabolites by Thin-Layer Chromatography and High-Pressure Liquid Chromatography", Int. J. Environ. Anal. Chem., Vol. 6, pp 55-66, 1979.
6. W. T. Roubal, T. K. Collier, and D. C. Malins, "Accumulation and Metabolism of Carbon-14 Labelled Benzene, Naphthalene, and Anthracene by Young Coho Salmon (Oncorhynchus Kisutch)", Arch. Environ. Contam. Toxicol., Vol. 5, pp. 513-529, 1977.
7. W. O. Berry, "A Comparative Study of the Uptake of Toluene by Bluegill Sunfish Lepomis Macrochirus and Crayfish Orconectes Rusticus", Environ. Pollut. Ser. A., Vol. 21, pp. 109-119, 1980

1981 USAF - SCEEE SUMMER FACULTY RESEARCH PROGRAM

Sponsored by the

AIR FORCE OFFICE OF SCIENTIFIC RESEARCH

Conducted by the

SOUTHEASTERN CENTER FOR ELECTRICAL ENGINEERING EDUCATION

FINAL REPORT

STUDIES OF THE ENGINEERING DESIGN PROCESS:

DESIGN OF EXPLOSIVELY DRIVEN GENERATORS; HUMAN

FACTORS IN HAZARDOUS ACTIVITIES

Prepared by: Dr. Francis J. Jankowski, P.E.

Academic Rank: Professor

Department and University: Department of Engineering
Wright State University

Research Locations: Air Force Weapons Laboratory
Advanced Concepts Branch (NTYP)
Applied Physics Division
and
Surety Branch (NTSSA)
Nuclear Systems Engineering Division

USAF Research Colleagues: Dr. Robert E. Reinovsky (NTYP)
Mr. Andrew J. Smith (NTSSA)

Date: 18 September 1981

Contract No. F49620-79-C-0038

STUDIES OF THE ENGINEERING DESIGN PROCESS:
DESIGN OF EXPLOSIVELY DRIVEN GENERATORS; HUMAN
FACTORS IN HAZARDOUS ACTIVITIES

by

Francis J. Jankowski

ABSTRACT

This study looks at two design problem areas for insights into developing better engineering design methods. An examination of current practice in explosively driven magnetic compression generators shows a need for emphasizing the systems approach, with attention to efficiency, safety factors and constraints, and evaluating alternative approaches. Conservative and "forgiving" design approaches are proposed for initial engineering designs.

The application of human factors to improving safety in hazardous activities is examined. A study of accident statistics suggests that other countries, particularly Japan, may have a better safety record than the U.S.A. Japanese business and management practices are reviewed; these may have application to safety. Several stress and stress-related factors are examined. Reducing high stress will improve safety. A systems approach to the application of human factors to the improvement of safety appears essential.

Suggestions for the execution of engineering design and for further research are offered.

ACKNOWLEDGEMENTS

The author would like to thank the Air Force Systems Command, the Air Force Office of Scientific Research and the Southeastern Center for Electrical Engineering Education for providing the opportunity for him to undertake this ten week study at the Air Force Weapons Laboratory, Kirtland Air Force Base, New Mexico.

He wishes to thank Robert E. Reinovsky for suggesting several areas of research in the pulsed energy field, for his support and for many helpful discussions and suggestions; he further expresses his appreciation for interesting and helpful discussions with several individuals in the group, in particular William L. Baker, James H. Degnan, and Paul Levi.

He wishes to thank Andrew J. Smith for suggesting problems and providing guidance in the human factors area.

In addition he wishes to acknowledge the helpful discussions, reference publications provided or suggested, and other aids given by many individuals, including:

C. Max Fowler

Robert Caird

James Goforth

all of the Los Alamos Scientific Laboratory, for a tour of their facility and helpful discussions of pulsed energy experiments.

Robert R. Rehder, of the Robert O. Anderson Graduate School of Management, University of New Mexico for his discussions of the Japanese methods of management and the Japanese culture.

Alan D. Swain, Sandia Laboratories, for discussions of safety, human factors, and hazardous activities.

Richard Holladay

Robert Cerc

of the Air Force Weapons Laboratory, for helpful discussions, and making data file searches.

Alexander Cohen, NIOSH, Department of Health, Education and Welfare.

Joel R. Buchanan, Nuclear Safety Information Center, Oak Ridge National Laboratory.

John Inzano, Bureau of Labor Statistics, Department of Labor.

William Reynard, Aviation Safety Reporting System Office, NASA.

William Collins, FAA, Department of Transportation.

Alan Diehl, FAA, Department of Transportation.

Malcolm L. Ritchie, FAA, Department of Transportation and Wright
State University.

He wishes to further thank the following groups for aid in locating
and obtaining materials for this study:

Research librarian staffs at:

Technical Library, Air Force Weapons Laboratory.

Zimmerman Library, University of New Mexico.

Parish Memorial Library, Anderson Schools of Management, University
of New Mexico.

Medical Center Library, University of New Mexico.

Staffs at:

National Safety Council, Statistics Office, Chicago.

United Nations, Demographic Statistics Office.

EG & G Idaho, Inc.

Finally he would like to thank John J. Ungvarsky of the Director's
Office and Arthur H. Guenther, Chief Scientist, Air Force Weapons labora-
tory, for their support and aid in the performance of this summer program.

I. INTRODUCTION:

The Air Force is extremely dependent on technology. The effectiveness of the Air Force can be increased if: the equipment procured is better designed to give improved performance, more reliability and/or lower cost; if the combination of design and operation is planned so as to give maximum performance with a minimum of accidents. These two factors are quite different, the first having to do with the physical characteristics and functioning of the equipment and the second having to do with its operation by people.

The engineering design process can favorably influence all of the above factors. The initial need is to identify as many factors as possible which will influence design. Further steps include increasing the awareness and capability for the engineering establishment to include the pertinent factors in the design process, and to create the environment and motivation to accomplish it. The increasing of awareness and capability is primarily an educational process. It is done most effectively at the university in training new engineers, but is also accomplished by continuing education courses, workshops, conferences, and professional society meetings.

Creating a favorable environment and motivation to promote effective engineering design is partly a task of writing specs and contract requirements. However, this is also an educational task. Contractors, engineers, and user personnel must be convinced that these are worthwhile factors to be incorporated into the process.

In the investigations reported here, two tasks were studied. The first was the design of explosively driven magnetic compression generators (MCG). A survey of these generators show a very low energy efficiency and a very high unit cost. It is also evident that constructing a generator has been treated as a scientific experiment rather than an engineering design problem. Applying the principles and methods of engineering design should give considerable improvement in cost-effectiveness of generator construction.

The second task studied was that of applying human factors to the planning and carrying out of hazardous activities. In this study, the hazardous activities were not specified; hazardous Air Force activities could include aircraft flights and the handling of munitions, conventional

and nuclear.

It was a surprising result (at least to the investigator) that a large fraction of military aircraft accidents are being attributed to "pilot error." Recent nuclear and space accidents, as well as aircraft flight experience, show that safety is system dependent. The design of the physical equipment, the selection and training of operators, the organization structure of the institution, and the communication between groups will all influence the safety of the activity.

In this investigation, aircraft flight experiences, nuclear experience, and industrial accident statistics, domestic and foreign, were studied for leads to means of improving safety.

II. OBJECTIVES:

The overriding objectives, the ones which gave direction to the formulating of the research program, are those having to do with engineering design as a process which can be taught, applied, and improved. The research was carried out via two separate research tasks. Each of these tasks had its sub-set of objectives.

The primary objective was to study the engineering design process, to identify factors important to the process, and to learn how these factors can best be presented to and implemented by engineers.

Engineering design is taken in a systems context. It includes conceptual and detailed design of the physical equipment, specifying how it is to be operated and maintained, and how it is to interface with other equipment and with the mission of the user organization.

The sub-set of objectives within the two tasks studied are presented within the discussion of the separate tasks, below.

III. TASK A: MAGNETIC COMPRESSION GENERATOR (MCG) DESIGN

A-I. INTRODUCTION

Magnetic Compression Generators (MCG's; also called Magneto-Cumulative Generators, and several similar names) are used to obtain short, intense pulses of electric energy. The most common primary energy source to drive MCG's is the chemical energy released by the detonation of high explosive (HE). Other primary sources have included compressed gases and the kinetic energy of moving masses.

Tables A-1 and A-2 give data on MCG machines which are reported in published, unclassified literature. Publications usually give only the generator parameters needed to make the points the authors wish to communicate. Many of the parameters given in Tables A-1 and A-2 have been derived from the given data; in several cases, certain parameters had to be estimated, applying principles of common practice, scaling off drawings, etc.

One fact emerging from Table A-1 is the generally low efficiency of generators. Efficiencies for conversion of chemical to electrical energy run from a small fraction of a percent to approximately four percent for the USA machines. The Soviets apparently put more emphasis on efficiency, with values approaching twenty percent.

If the published data is examined in more detail, e.g., References 1a, 4 and 7, a further point which stands out is the variability, and often unreliability of the functioning of generators. The Soviets may have done more toward designing for reliability, Pavlovskii¹¹ reports that several tens of experiments give energy deviations within a 10 percent experimental error (note that current deviations would be approximately half of this value). USA experience has been 50 percent variations in current outputs.

While costs of MCG units are not reported in published literature, the costs of individual units are reputed to be comparable to the cost of individual automobiles. Depending on size and construction, an MCG can be as cheap as a stripped down compact car, or as expensive as a Cadillac.

The general conclusion, particularly in the USA, is that producing an MCG has been a scientific experiment, not an engineering design task.

A-II. OBJECTIVES OF THIS TASK

The objective of this task is to arrive at a program, or guidelines for formulating a program, to develop a magnetic compression generator (or

TABLE A-1 - SUMMARY OF MCG's REPORTED IN REPORTS & PUBLICATIONS

TYPE	MACHINE	REF.	$L_c, \mu\text{H}$	$L_s, \mu\text{H}$	L_c/L_s	$T, \mu\text{s}$	I_0, mA	V_0, kJ	I_p, MA	W_p, kJ	I_p/I_0	W_p/W_0	λ	HE, MG	EFFICIENCY
S	LASER ARRAYS	13	0.114	0.0335	3.4	4.3	0.37	10	1.26	28	3.4	2.8	0.83		
S	DETACHMENT	13	0.242	0.011	22	92	0.61	45	5.38	159	8.8	3.4	0.89	4.0 DETAS	12
S	LASER CENTER STATIONS OUTSIDE	12	0.725	0.075	9.7	93	0.65	169	4.01	603	6.2	3.6	0.77	10-85% EST	36
S	IN SERIES	12	0.725	0.0375	19.4	94	0.58	178	7.13	953	12.3	7.4	0.83		
S	FORMING	5	0.005 - 0.05 EST	0.0094	10	36	0.0095 EST	0.0035 EST	0.034-0.045 EST	0.016	7.0	4.4 EST	0.84	0.52 DETAS	7.6
S	SOVIET M-41	16	0.540 EST	0.005-0.005 EST	~120	60	0.360 EST	35	5	50-45	14	1.4 - 1.8 EST	0.54	~1.1 PLASTIC	~5.5
S	SOVIET M-48, M-49	16	0.440 EST	0.005 EST	92	60	0.380 EST	33	11.6	460	35	14	0.79	~1.8 PLASTIC	~4.8
P	LASER	13	0.0335	0.0015	22	6	1.3	30	10	74	7.7	2.5	0.64	2.5 MG 9404	13.4
P	LASER	11	0.051	0.0048	11	3	4.85 EST	600	9.57 EST	220	2	0.37	0.28	25 - 9404	134
P	SPRINT	7	0.194 EST	0.006	32	5 - 8 EST	0.48 EST	11	3.85	45	8	4	0.59	12 - 9404 EST	65.2
P	BUTLER-DUGGIN	14													
H	BEAMER 88	4	45	0.015	3000	30	6×10^{-5}	8×10^{-5}	0.0057	2.4×10^{-6}	95	3	0.57	0.26	1.59×10^{-5}
H	BEAMER 88	4	45	0.015	3000	30	0.031	27	0.37	1.02	12	0.05	0.31	0.26	1.59
H	BEAMER 812	4	25	0.045	555	36	0.0145	2.6	1.3	38	90	14	0.71	0.32	1.7
H	BEAMER 818	4	725	0.11	6500	124	0.007	18	10	5500	1428	310	0.83	25.7	138
H	BEAMER 810	4	46	0.08	575	80-100	0.05	58	2.6	3740	180	56	0.82	80	420
H	BEAMER 810	4	46	0.20	230	80-100	0.05	58	2.6	676	52	12	0.73	80	420
H	BEAMER 84	4	0.65	0.024	27	22	0.18	10.5	2.6	81	14	7.7	0.80	0.82	4.4
H	BEAMER 85	4	4.5	0.17	26	62	0.16	58	1.5	191	9.4	3.3	0.68	2.0	11
H	MODEL 106	3	4.35 EST	0.06	73	27	0.12	31	2.6	270	22	8.7	0.72	2.3 - 9404	12.3
H	106 SWITCHED LOAD	3	4.35 EST	0.06	73	27	0.12	31	2.6	270	22	8.7	0.72	2.3 - 9404	12.3
H	MODEL 169	3	10.8 EST	0.07	154	44	0.12	78	5.8	1177	48	15	0.77	7.7	41.3
HC	SOVIET C-40	14		0.002		38 EST		2	15	200		100		0.27 EST	~1.1
	C-40 Mod. Sec.			0.016				2	2.5	50				.16	0.7
	C-40 Coax. Sec.		0.016	0.002	8		2.5	50	15	200	5.2	4	0.79	.08	0.4
HC	SOVIET C-168	14		0.008		180 EST			58	9000				8 EST	~20
	Mod. Sec.			0.004					9.7	3000					
	Coax. Sec.		0.004	0.008	8		9.7	5000	54	9000	5.2	3	0.79		
HC	SOVIET C-328	14	16	0.20	80	E-FOLD 2-160	0.35	1000	12.5	16000	36	16	0.82	30	150
HC	SOVIET C-328	14	16	0.10	160	E-FOLD 2-160	0.25	500	14	10000	56	20	0.79	30	150
HC	SOVIET C-328M	14	4	0.10	40	E-FOLD 2-100	0.81	1500	22.4	25000	28	19	0.90	60	300

* S = Strip P = Plate H = Helical H-C = Helical Coaxial
 Note: Published Data Was Often Incomplete; Many Entries In This Table Are Estimated, Scaled From Drawings, etc.

TABLE A-2 - MCG ARMATURE DATA; EXPERIMENTAL RESULTS.

TYPE	REFERENCE	H.E. THICKNESS OR RADIUS	ARMATURE		MASS RATIO ARMATURE TO H.E.	ARMATURE VELOCITY MM/US	EFFICIENCY % CHEM TO KIN. ENG. ELECTRICAL
			MATERIAL	THICKNESS			
STRIP GENERATORS							
SOVIET #4-1	1G	0.6	CU	0.2	3.70	1.14	42 ~1.0
SOVIET #4-8, 49	1G	1.0	CU	0.3	3.34	1.18	41 ~4.8
SOVIET	1B		CU	0.2	(2.35) ⁺		40
SOVIET	1B		CU	0.2	(1.15) ⁺	1.9	36
SOVIET	1B		CU	0.1	(0.90) ⁺	2.1	35
SOVIET	1B		CU	0.3	(3.10) ⁺	1.23	41
LASL 0.6M 2-SIDE	12	3.2	CU	0.16	0.75	2.97 (2.34) ^{***}	30/59 ^{***} 1.3
PLATE GENERATORS							
LASL 2.5 KG HE	13	7.6	CU	0.16	0.103	4.03	15 0.6
LASL 2.5 KG HE	13	7.5	AL	0.32	0.0628	4.35	10
LASL 15. KG HE	11	5.08 ^{***}	AL	0.32	0.0944	4.09	14 0.2
SANDIA	7,14	7.5	AL	0.313	0.0626	4.35	4-5.2 10 0.07
HELICAL GENERATORS							
LLL #8	4	1.27	CU	0.3175	3.38	1.41	60 ~0.1
LLL #18	4	6.35	CU	0.635	1.14	2.26	51 4.0
LLL #10	4	13.86	CU	0.635	0.487	3.05	40 0.8
LLL #4	4	2.54	CU	0.3175	1.47	2.03	53 1.8
SANDIA #106	3	6.98	AL	0.635	0.186	3.5	20/9 2.2
SANDIA #129, 169	3	8.6	AL	1.02	0.173	3.57	19 2.8
HELICAL - COAXIAL							
SOVIET C-160	1H	3.2	CU	0.32	1.19	2.2	50 ~20
SOVIET C-320	1H	6.6	CU	0.80	1.20	2.2	51 7

* For Two Armatures With H,E, Sandwiched Between, The Combined Mass Of The Two Armatures Are Reported In This Table.

** Estimated From Given Angle Of Driven Armature.

*** H.E. Taken To Be 9404 Or Equivalent

† Estimated From Given Armature Mass And Velocity.

magneto-cumulative generator; MCG) with an electrical pulse of 0.5 to 1.0 magajoules. The generator is to be:

RELIABLE and REPEATABLE. After a development period, the generators should produce an output pulse within specified limits on a high percentage of trials, e.g., a specified energy pulse 20 percent, on more than 90 percent of the trials might be specified.

COST EFFICIENT. The materials, particularly the generator coil and the explosive (HE), should be of reasonably priced and available materials. The physical design should be such that extensive machining and extremely tight tolerances will not be required. These requirements, combined with the energy efficiency specified below, will result in better cost efficiency than generally obtained.

ENERGY EFFICIENT. This requirement will keep the mass of HE at a minimum. Problems of confinement, waste heat rejection and debris removal or collection will be minimized, should they be important. Energy efficiency will also generally work toward cost efficiency.

To attain the objectives stated above, a systems approach is indicated. Alternatives in geometry, materials, pulse shaping, etc., should be evaluated in light of their impact on the entire device. The final result should be an overall optimization.

A-III. TYPES OF MCG's

All MCG's incorporate a magnetic coil, often one turn, sometimes multi-turn, a means of energizing the magnetic circuit, a moving armature, and a source of energy (HE) to drive the armature against the resistance of the magnetic field. Electrical conductors to introduce the energizing current and conductors to take the generated energy to the load, switches, insulation, and other details complete the generator.

Several geometries are used. The more common ones are described briefly below.

STRIP, OR BELLOWS GENERATOR (Single Armature). An open sandwich of HE and metal plate form the driver and armature. A fixed metal plate, the stator, is positioned a distance from the armature plate. The energizing circuit is connected to the armature and stator at one end; the load is connected across the armature and stator at the other end. The HE is detonated at the end most distant from the load. The first motion of the armature crowbars the energizing

circuit out of the generating circuit. The armature, stator and load then constitute a single loop electrical circuit. The HE progressively drives the armature into the stator, compressing the magnetic flux into the load (a coil) and reducing the inductance of the circuit. To a first-order approximation, the product of current and inductance is a constant. The decreasing inductance results in increasing current, and increasing energy delivered to the load.

STRIP OR BELLOWS GENERATOR (Two armatures). A single sheet (plate or slab) of HE may have armatures and stators on both sides. This arrangement is shown in Figure A-1. Operation is similar to that described above.

An alternate two-armature design is to do away with the stator and drive two armatures together¹³. The load is connected to the ends of the two armatures. This design has been operated but is not commonly used.

PLATE GENERATOR. The geometry of the plate generator appears similar to that of the strip generator, except that the load is connected at the stator. The main difference is in operation. The strip generator detonation is end initiated (or end edge); the plate generator detonation is surface initiated so that the entire armature is driven at the same instant towards the stator. At future times the position of the armature is parallel to its rest position.

An alternate design is to drive two armatures together¹¹. Experimental trials have never operated consistently.

HELICAL GENERATOR. The stator of the helical generator is a spiral of wire (or of multiple parallel wires, or of a flat strip). The armature is a metal cylinder, with the HE filling this cylinder. The energizing current passes through the spiral, through the load, and returns, often through the armature. The magnetic flux is excluded from the interior of the armature by the eddy currents generated in the armature. The HE is initiated at the end (away from the load). The expanding armature contacts the spiral coil, first at the end, and progressively along the length of the coil. The inductance is decreased in two ways: the expanding cylinder reduces the volume occupied by the magnetic flux, and; the expanding armature progressively shorts out the turns of the coil, reducing the turns to zero.

COAXIAL GENERATORS. In its simplest form, the coaxial generator consists of two tubes, the outer being the stator and the inner, filled with HE, being the armature. Another way of picturing is to take the drawings of Figure A-1 as

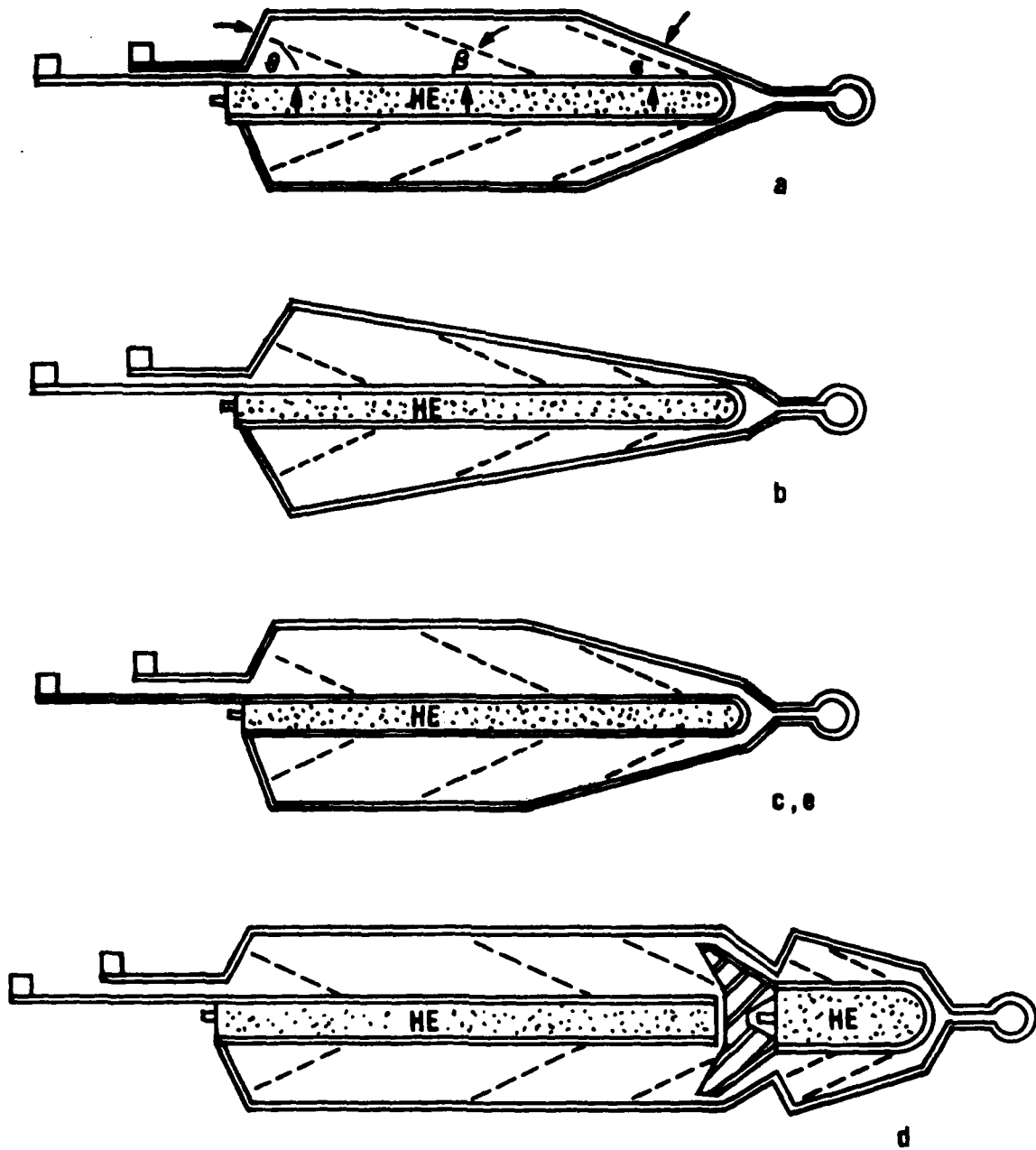


FIGURE A-1. BELLOWS (STRIP) GENERATOR GEOMETRIES

cross-sections and develop cylinders by revolving these cross-sections about the centerlines of the HE. The load is connected to the two cylinders at one end and the energizing circuit at the other. In this arrangement the current is axial and the magnetic flux azimuthal. If the HE detonation is end initiated, the expanding armature progressively compresses the flux toward the load end, giving a long pulse. If the HE detonation is centerline initiated, the armature expands outward, compressing the flux along the entire length and producing a shorter pulse. This short pulse condition is also obtained by shaping the stator to match the expansion cone of the armature with end initiation of the HE.

OTHER. Other geometries include imploding coaxial cylinders, double-ended (center load) helical and coaxial, and spherical².

A-IV. DESIGN PROCESS

DESIGN APPROACH. In most cases, in the USA-MCG development, the devices have been designed to emphasize a single particular characteristic. Typical characteristics as design objectives have been to obtain a short pulse, such as two microseconds directly from the generator, or to maximize the energy gain, thus minimizing the demands on the energizing devices (usually a capacitor bank). This procedure often (usually) led to further problems, which would be addressed one at a time, and possibly never satisfactorily solved.

COMPUTER CODES. Computer codes, in MCG work, have been used primarily to analyze and understand the operation of the device, and, to a lesser extent, to identify design weaknesses and predict the effects of design changes. Computer codes have practically always been written for a particular type device. As time has progressed, codes have become more complex and more complete, but they still depend on empirical data, estimates, and approximations. They are useful for the reasons stated above, but are not being used to initiate a design.

Some codes reported in unclassified literature, in chronological order, are:

CHEG (Calculation of High Explosion Generator), Shearer et al⁴ (1968). This code analyzed the behavior of a coaxial generator. The deceleration of the armature by the magnetic field was included, but acceleration by detonation product pressure was not. Armature increments were assigned initial velocities and times at which they would start to move.

Crawford and Damerow³ (1968). This code is written for a helical generator. A framing camera was used to obtain the shape of an armature driven

by HE. Shapes, at various times in the operation, were duplicated with static models. The inductance and resistance of each model was measured with inductance and resistance bridges. These data provided input for the computer code.

Butler and Duggin⁷ (1975). For plate generators, this code was a simple one-dimension model. The inductance was determined as a function of time by measurements of a mockup using an inductance bridge.

Caird and Turchi⁹ (1975). For a plate generator, this code analyzed the performance of the generator which was already in existence.

SWL, Tucker^{1e} (1975). A helical generator code. Experimental data from the operation of the generator being modeled is needed to set two constants. Skin resistance and proximity effects are accounted for by multiplying the resistance by a constant. The ratio of the lost flux to the coupled flux is assumed to be of the form $C_1 + C_2\phi$ (ϕ being the total magnetic flux).

COMAG-III, McGlaun, Thompson and Freeman^{1c} (1979), (COMAG-1, 1977). This is a two dimensional helical generator code. It allows six sections of turn splitting and/or changes in wire diameter. This code uses Hydrocode CSQ-II in its treatment of materials; up to ten materials and layered armatures and HE are permitted. One empirical adjustment made to the code is to force the HE to burn at an artificially low temperature in order to arrive at the correct electrical resistance. The authors comment, "too cumbersome and expensive to be used as a design tool for parameter studies".

COMPUTER CODE IMPORTANCE. While computer codes are not available to design new generators, codes are valuable to understanding their operation, predicting the effects of design modifications, and helping to identify weak points and problem areas in a design. The engineering design of a new MCG is still a development effort, and a parallel code analysis is very useful to producing a satisfactory generator.

MCG THEORY. The theory and principles of MCG operation is covered in many places^{2, 1h, others} and will not be covered here except as needed.

A-V. ARMATURE DESIGN

In the generator, the chemical energy of the HE is converted to kinetic energy in the moving armature. The material, thickness, and geometry all affect the efficiency with which this energy conversion takes place.

MATERIALS. In MCG's reported in the literature, 75 percent use copper armatures; see Table 2. Commercial grade copper sheet appears to be satisfactory for strip and plate generators. Cylindrical armatures are generally machined; it is not clear whether commercial grade tubing or pipe might be used for this purpose.

The second material used for armatures is soft, annealed aluminum. Typical is 6061 aluminum annealed to T0 condition. As with copper, stock rolled sheet is used for flat armatures, machined cylinders for cylindrical armatures.

ARMATURE GEOMETRY. Armatures are generally flat or cylindrical. Tapered cylinders (conical) have also been used^{1h}. Sphericals have been proposed²; spherical appears to be a particularly attractive geometry for nuclear explosive sources. No spherical generator experiments have been reported in the open literature.

In analyzing armature velocity and efficiency, the Gurney method⁶ was used. Gurney, in 1943, applied momentum and energy relations to analyze the velocity of fragments from shells and grenades of a range of sizes. Kennedy reviewed the method and applied it to a number of cases of interest in generator design.

The Gurney method introduces a quantity, $\sqrt{2E}$, the Gurney velocity, where E is the kinetic energy of the detonation products in the direction of plate motion. The Gurney velocity is a characteristic of each type of HE. The ratio, $v/\sqrt{2E}$, v being the plate velocity, is a dimensionless velocity of the driven material.

Kennedy uses the Gurney analysis to obtain the value of $v/\sqrt{2E}$ as a function of M/C, the ratio of armature mass to HE mass, and of N/C, the tamper mass to HE mass ratio for tampered cases.

The efficiency of energy conversion, chemical to kinetic, is readily obtained as

$$\epsilon = \left(\frac{v}{\sqrt{2E}} \right)^2 \cdot \left(\frac{M}{C} \right) \cdot \left(\frac{E}{\Delta H_d} \right) \quad (1)$$

ΔH_d is the chemical energy of the explosive. The other terms are defined above. This relation reduces to

$$\epsilon = \frac{\frac{1}{2} MV^2}{C \Delta H_d} \quad (2)$$

which is the ratio of total kinetic energy of the armature to total chemical energy (if M and C refer to entire generator).

The ratio, $E/\Delta H_d$ is a characteristic of the HE being used, but is always close to 0.7. The value 0.7 can be used for conceptual designs with no significant loss to accuracy.

Flat, open sandwich type armatures are single flat plates driven by the HE. The HE can be initiated on an edge, as in strip generators, or on a surface, as in plate generators. Since the HE generates pressures and detonation product momentum in two directions, the chemical energy is poorly utilized. The maximum conversion of chemical to kinetic energy is approximately 25 percent; see Figures A-2 and A-3.

The efficiency of the open sandwich type armature can be increased by placing a tamper (ballast or reflector mass) on the open side of the HE. Table A-3 compares some tampered cases to other possible armature geometries.

TABLE A-3
EFFICIENCY OF TAMPERED AND OTHER GEOMETRY ARMATURE - HE ARRANGEMENTS

CASE NO	TYPE	M C	N C	v $\frac{mm}{\mu S}$	ϵ PERCENT
1	Open Sandwich	0.68	0	2.0	24
2	Tampered Open Sandwich	1.0	1.0	1.9	32
3	Tampered Open Sandwich	1.0	4.35	2.24	44
4	Tampered Open Sandwich	1.0	20	2.44	52
5	Symetrical Sandwich	1.8	0	2.0	63
6	Cylindrical	1.6	0	2.0	56

M = Mass of Armature

N = Mass of Tamper

C = Mass of HE

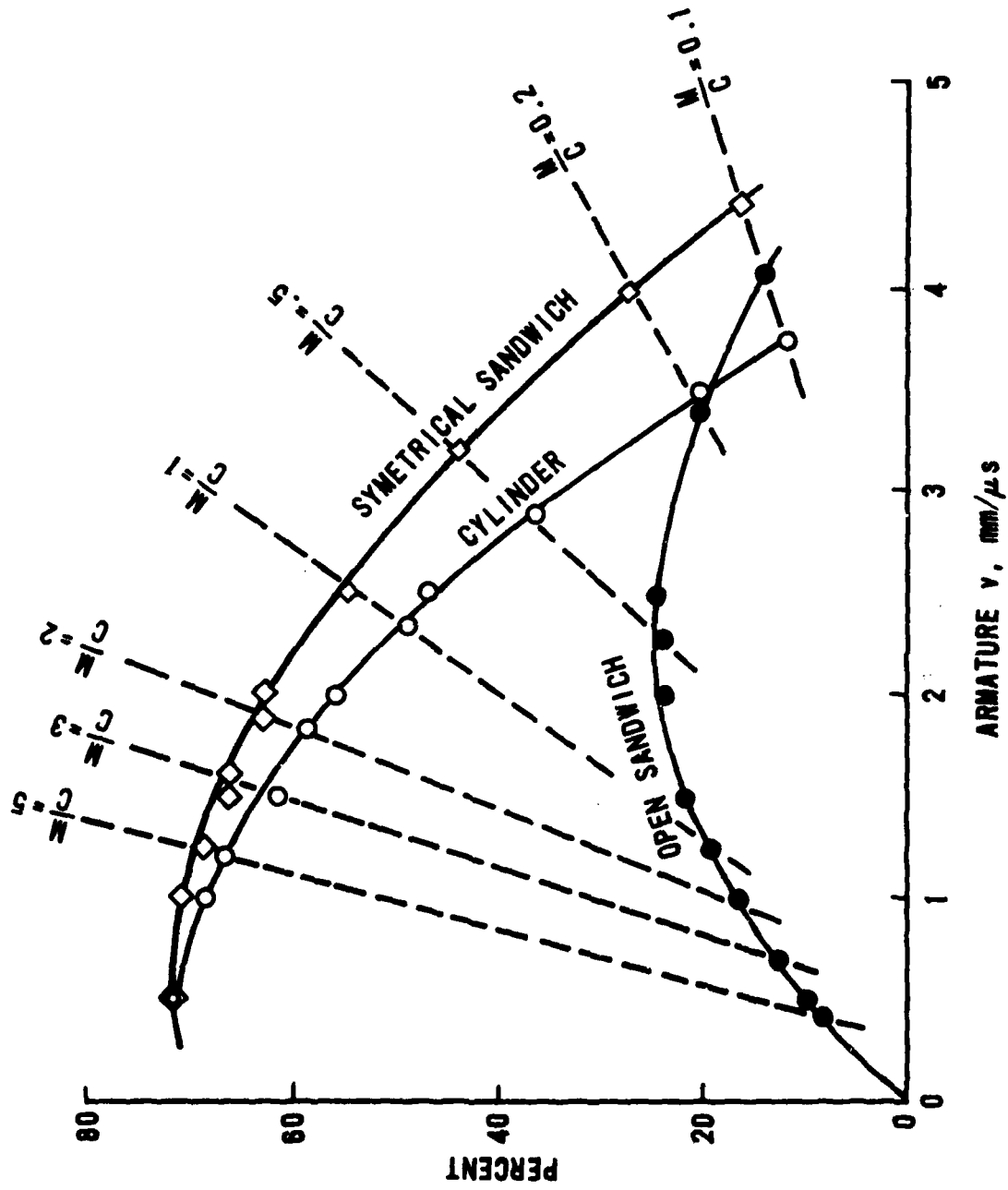


FIGURE A-2. MCG EFFICIENCY, CHEMICAL TO KINETIC ENERGY
(USING THE GURNEY METHOD⁶)

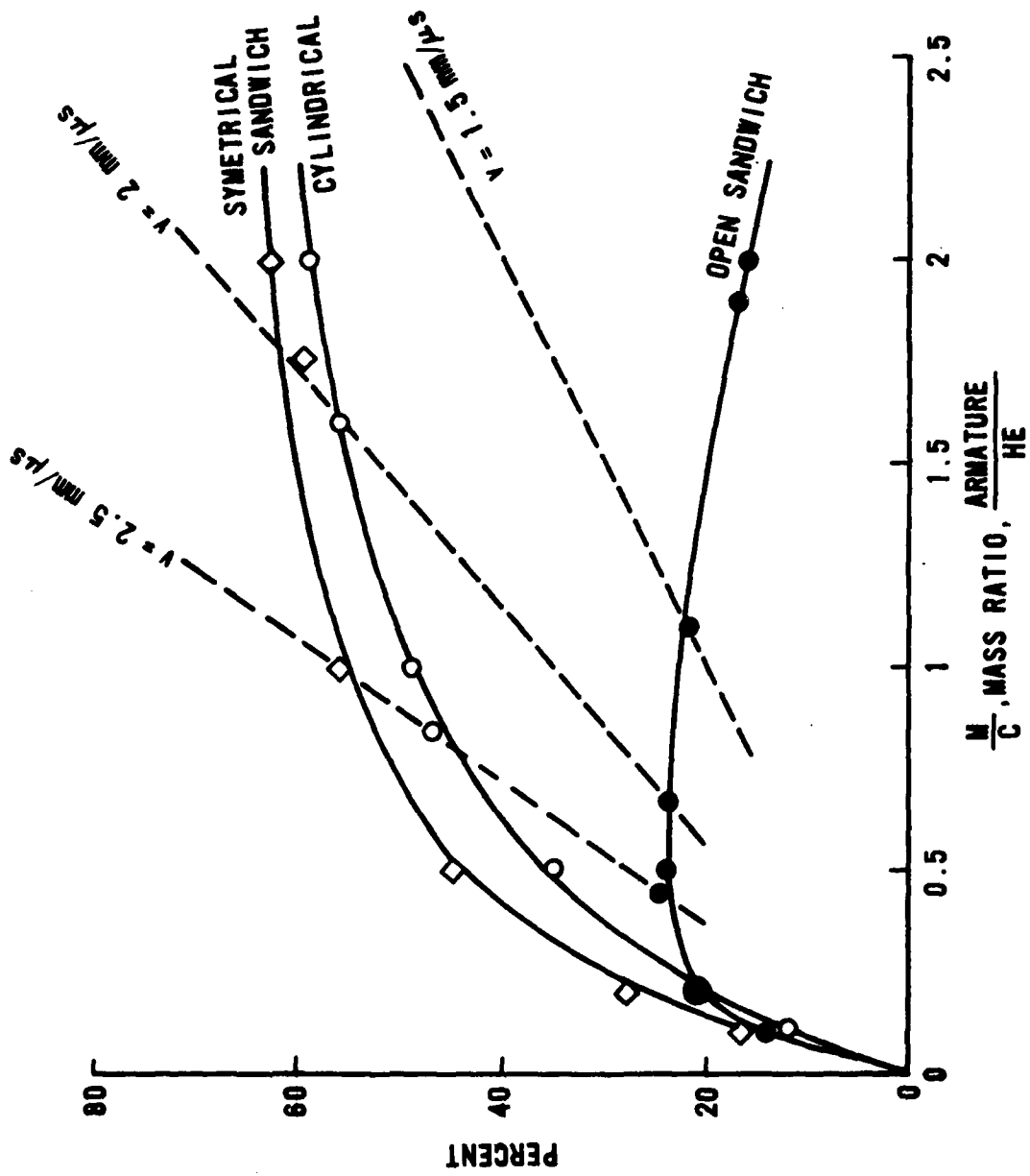


FIGURE A-3. MCG EFFICIENCY, CHEMICAL TO KINETIC ENERGY (USING THE GURNEY METHOD⁶)

Symmetrical sandwich armature arrangement places the HE between two equal mass armatures. The efficiency of this arrangement, as compared to the open sandwich, gains in two ways. The energy which would be lost to open space is now used to drive another armature; further, each armature acts as a tamper for the other giving another increase in efficiency. Conversion efficiencies of the order of 60 percent are readily obtained.

Cylindrical armatures benefit from using the full expansion of the detonation products, but suffer from the circumferential expansion with increasing radius. As a result, cylindrical armatures approach the symmetrical sandwich in efficiency at larger M/C ratios, but drop well below at lower M/C ratios.

Cylindrical imploding armatures have been used to obtain high magnetic fields, and, experimentally, to drive coaxial generators. One complication is that to be effective, initiation must take place at many points around the circumference at the same moment. A disadvantage is that much of the energy is carried off by outward flowing detonation products without contributing to the output. It is inefficient.

ARMATURE MASS. Figure A-4 shows the M/C (armature to HE mass ratio) for several USA and Soviet generators. There is but a small overlap of the efforts of the two groups, the Soviets having an average M/C of 2.1, while the USA average is 0.67. These averages are not meaningful, except, as an indicator of the trends and the area in which each group is working. These differences undoubtedly arose from differing objectives, the lower mass armature giving a shorter pulse while the heavy armature produces higher efficiency.

An extremely low mass ratio is inefficient because a large fraction of the chemical energy goes into accelerating the detonation products. A large ratio is efficient because in a dynamic reaction the momentum is conserved, and a larger mass is given a larger momentum, but less energy compared to a lower mass with a higher velocity. Pavlovskii^{1h} also suggests that in the large mass armatures, plastic flow absorbs energy, reducing the kinetic energy.

Pavlovskii^{1h} also suggests, for maximum efficiency, the armature velocity should be 1.5 to 2.0 mm/ μ s; then again, in the same paper, he states that for maximum efficiency the M/C should be 3. This last M/C value is consistent with the 1.5 mm/ μ s for cylinder and symmetrical sandwich armatures.

It might be noted that the very low values of M/C used in many USA generators are both in a region of low efficiency, and in a region of high

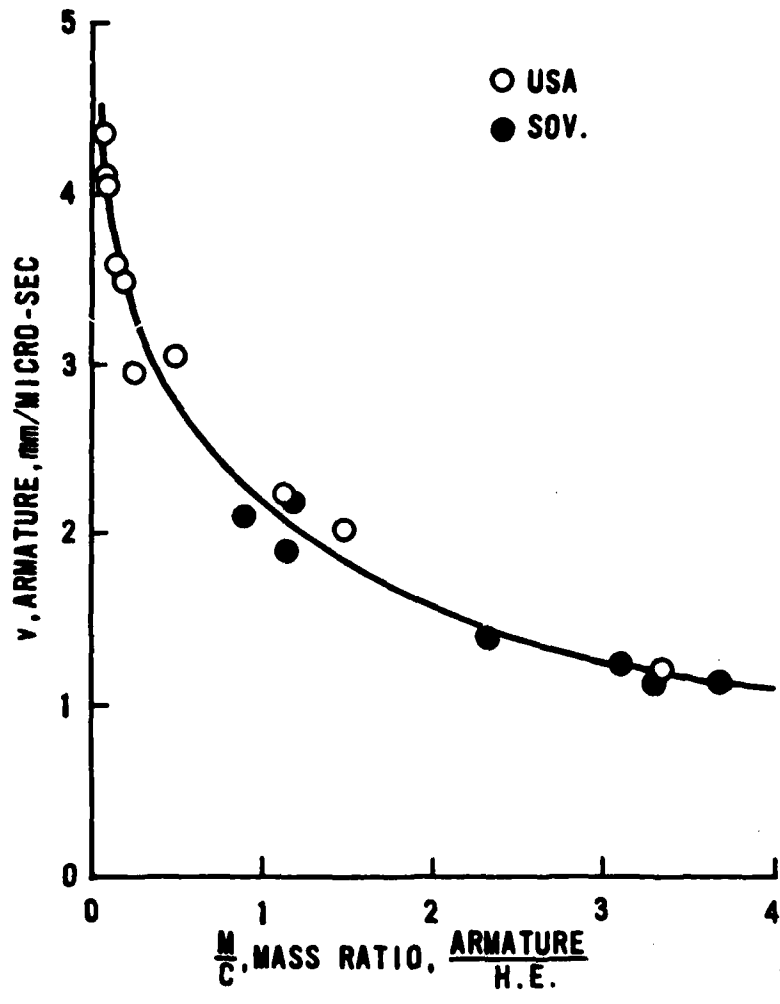


FIGURE A-4. ARMATURE VELOCITIES. POINTS DERIVED FROM REPORTED DATA AND THE APPLICATION OF THE GURNEY METHOD . THE GURNEY METHOD IS NOT RELIABLE FOR $\frac{M}{C} < 0.2$.

efficiency gradient. Small changes in construction or performance of HE and other materials might lead to large variations in output.

Higher M/C values, with lower armature velocities, give higher efficiencies for the cylinder and symmetrical sandwich types. The open sandwich peaks at M/C of about 0.5, but if tampered, this peak would move to higher values of M/C. With a tamper-to-HE mass ratio of 10 and a M/C of 1.0, the conversion efficiency is over 30 percent, and goes to approximately 40 percent for M/C = 5. At this last condition, the armature velocity will be approximately 1.0 mm/ μ s. compared to 0.42 mm/ μ s for the untampered case.

EDGE AND END EFFECTS. If the L/D ratio (length to diameter of a cylinder; width to thickness of the HE in a sandwich) is too low, losses from the ends and edges will reduce energy conversion below the values given by the Gurney method. No definitive work has been published on this problem, but Kennedy⁶ states that if the L/D is less than six, the velocities can be 10 to 20 percent less than predicted. This would translate to 20 to 35 percent loss in energy. The L/D = 6 might be taken as a lower limit for an efficient generator.

STABILITY OF THE ARMATURE. Occasional comments in the literature suggest that M/C too small or armature throw distances too large may result in unstable armature behavior, e.g., Grover, et.al.^{1a}, stated that armatures of smaller radius than that of their standard test generator showed rippling and breakup before the generation was complete (page 173). However, there is little published on armature stability. One might expect that thin armatures, flat plates or cylinders, would exhibit instabilities similar to that observed on imploding thin shells.

Using moderate values of M/C, say 2 to 3, not only gives favorable energy conversion efficiencies, it is also likely to result in stable armature behavior.

CURRENT LIMITATIONS. High current densities can lead to high local magnetic field densities, distortion of metal parts, melting of surfaces, and other problems. These problems are more likely to be encountered in helical generators where the spiral conductor must carry the entire current. Other type generators usually have relatively larger conductors which reduce the severity of the problem.

Fowler² suggests an upper limit of one megampere per cm of conductor width.

A-VI. STATOR DESIGN

The stator is the fixed part of the generator against which the armature is driven. The stator may be a helical coil, a cylinder, or an arrangement of flat plates. Figure A-1 illustrates some of the stator geometries possible with a bellows-type generator. Table A-4 gives the parameter values used to obtain the results shown in Figure A-5. This shows how the stator shape can affect the output pulse shape.

TABLE A-4
BELLOWS TYPE GENERATOR PARAMETERS DESCRIBED IN FIGURES A-1 AND A-5

CASE	β	α	θ	RELATIVE LENGTH	RELATIVE HEIGHT*
a	15	15	75	ℓ	0.0833 ℓ
b	15	8.2	75	ℓ	0.139 ℓ
c	15	8.44	75	1.0850 ℓ	0.0904 ℓ
d	15	75	75	ℓ	0.0708 ℓ
e	15	10	75	ℓ	0.098 ℓ

$$L_g = 250 \text{ Units}$$

$$L_L = 8.33 \text{ Units}$$

* Perpendicular distance from armature to most distant point of stator.

In addition to having low electrical resistance, the stator must be designed to stay below some limiting current density (Fowler suggests a maximum of 1 MA/cm; Caird and Turchi⁹ give limits of 1.4 MA/cm and higher), and must be restrained so as to maintain the required geometry during the charging and generation phases of the operation.

The restraining of the stator is handled in a number of ways. The inertia of the stator is one important method. Pavlovskii^{1h} suggests a rule-of-thumb that the ratio of the mass of the stator to that of the HE should be 10 or greater. Fowler¹⁵ suggests using steel plates or bars to back up, or act as tamper to the stator. Shearer⁴ casts the coil of their Helical Generator Model 10 in epoxy resin. Pavlovskii^{1h} casts the coils of his helical generators in cement. In illustrations, Crawford and Damerow³ show their Models 106 and 129

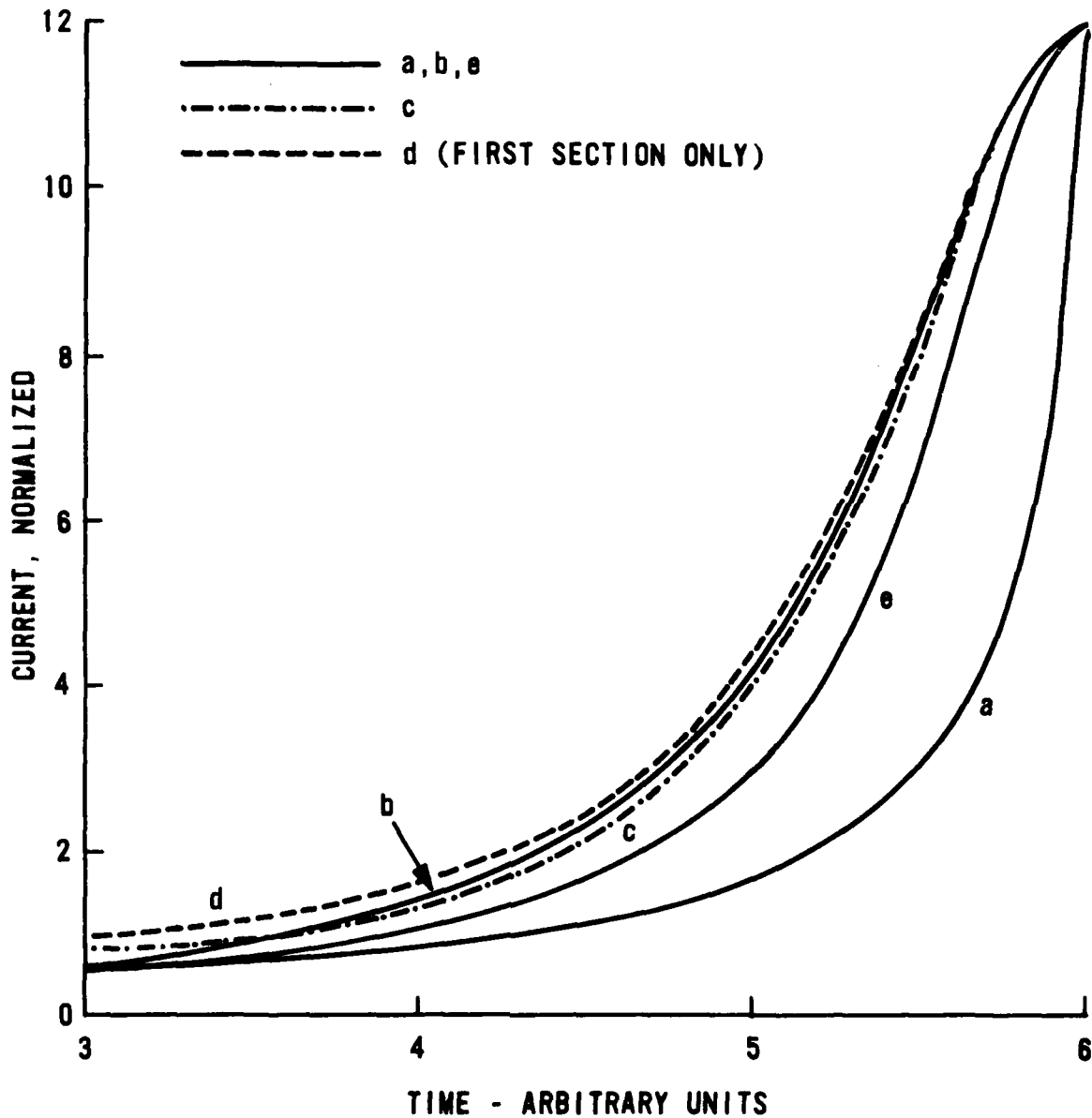


FIGURE A-5. CALCULATED GENERATOR CURRENT HISTORY FOR BELLOWS TYPE GENERATORS OF FIGURE A-1.

helical generators with coils cast in some unspecified material. Others, e.g., Fowler¹², calculate the inertial effects and find the motion acceptable for that particular case.

The force tending to move a stator develops from the pressure of the magnetic fields. This pressure exists and grows from the start of the energizing phase through to the completion of the generation phase. The distortion of the stator near the end of the generation is particularly serious. It can change the angle at which the armature meets the stator, resulting in a changed pulse shape. (See Figures A-1 and A-5 and Table A-4). The stator distortion can leave pockets of flux at the completion of the generation, giving a lower output current than planned.

The stator must be restricted in its motion, either by inertia of the stator itself, or by the inertia of the stator and backing material (tamper or ballast) .

A-VII. ENERGIZING THE GENERATOR

The initial energizing of a generator or a system of coupled generators is practically always done with a capacitor bank. (Storage batteries have been used; see Shearer⁴). The capacitor bank is switched into the generator circuit by a quick acting closing switch. The HE is detonated at approximately maximum current. The action of the HE crowbars the capacitor bank out of the generator circuit.

In this energizing operation; some of the energy stored in the bank is lost in I R losses in the circuit; larger amounts are lost to the generator because energy is stored in the inductance of the lines from the bank to the generator and in the inductance of the capacitors. Fowler¹² reports 37 to 55 percent of the stored energy delivered to the generator. Other investigators appear to experience similar transfer efficiency, e.g., Crawford and Damerow³ deliver 31 kJ to a generator from 90 kJ stored in a capacitor bank.

In principle, increasing the energizing current (and energy) should produce an increase in output current and energy. That there is a practical limit, beyond which increasing the energizing current gives no further increase in output current, has been observed by many investigators. Pavlovskii^{1h}, in their Model C-40 generator, found 30-40 kJ to be the maximum effective input. Shearer reports a maximum effective input of 1 k A for their Model 8 generator into a 15 nH load. Crawford and Damerow³ report maximum outputs of 3 MA and

6.6 MA for their Models 106 and 169 generators, respectively. Bitshenkov and Lobanov^{1b} found that increasing the energizing current above 300 kA produced no further increase in output current (maximum of 2.6 MA) in their bellows-type generator. Fowler¹⁵ reports that one of their generators works fine with energizing fields of 300 - 350 kG but fails with energizing fields of 500 kG.

The reasons for this limiting effect is not understood, but increasing resistance effects are suspected by some investigators.

The practical limit in energizing current is found by experiment. The limiting field intensities reported by Fowler¹⁵ might be used as a guide in planning the experiments.

A-VIII. PULSE SHAPING

Pulse shaping involves controlling the total time to maximum current, the, rate of rise (especially during the last 80 percent of the current rise), the total time to maximum current delivered to the load, and the general shape of the pulse up to the peak value. Several methods are used to affect the pulse shape, including generator design, crowbar switching the output to load, explosive closing switch to load, and the use of non-linear elements (fuses) in the output circuit. Most efforts at pulse shaping are directed toward shortening the pulse to the load and decreasing the rise time of the pulse to the load.

PULSE SHAPING BY GENERATOR DESIGN. Pulses can be made long or short, within limits, by suitable generator design. A long helical, bellows, or strip generator will give long pulses, determined by the length of the generator and the detonation velocity of the HE. Detonation velocities are 6 to 9 mm/ μ s. Generators are a few cm to the order of a meter in size. This produces pulse lengths of a few microseconds to approximately 100 microseconds. The final current rise time and pulse shape depends on the shape of the generator elements (see Figures A-1 and A-5 and Table A-4).

Short pulses can be obtained by designing the generator so that the generation phase is completed in a short time. Plane initiated plate generators, center-line initiated coaxial generators, surface initiated imploding coaxial generators, and end initiated shaped stator coaxial generators all produce pulse lengths that are dependent on the closing time of the armature and stator. This depends on the gap size and the armature velocity. Gaps are typically 2-10 cm; velocities are 2-5 mm/ μ s. Thus, pulses can be obtained as short as 4 microseconds.

The generators listed in the paragraph above are all low inductance machines. They will not produce large current or energy multiplications. Therefore, they are frequently combined with other generators which supply the energizing currents. A coaxial generator is made as an integral part of a helical generator, or a plate generator follows a bellows generator. In coupled or cascade generators, the total pulse length will be the time of operation of the entire system, unless some method of switching is incorporated.

PULSE SHAPING BY SWITCHING. Generators which produce long pulses generally have a long period at low current, with the major part of the current rise in a relatively short period at the end. In the cases shown in Figures A-1 and A-5, Case (a) has the last half of the current rise in the last 3 percent of the generation period, while the broadest curve of the group takes but 13 percent of the time for the last 50 percent of the rise. With coupled generators, this rise might take a still shorter fraction of the total generation time. Thus, the pulse to the load can be shortened by switching the load into the circuit at a late time. There are a number of ways to do this.

One method to sharpen the pulse to the load is to transformer couple the generator to the load. During the energizing and early part of the generation cycle, the transformer secondary can be open. The inductance of the transformer primary is the load on the generator. Shortly before the generation is complete, the load is switched into the transformer secondary circuit. There appears to be no published reports on experimental trials of this procedure.

Another method to sharpen the pulse to the load is to have a ballast inductive load connected in parallel with the load. Initially, the load circuit is open and the ballast absorbs the entire generator output. At the desired time, late in the generation cycle, the load is switched into the circuit. If the load is of lower inductance than the ballast, most of the energy will flow to the load.

If the ballast inductance is comparable to or less than the load inductance, an opening switch is needed to remove the ballast from the system as the load is being connected. The most direct way to do this is to use a fuse as the ballast, and a spark gap or dielectric switch for connecting the load. Initially, the current flows through the fuse. At the design current, the fuse will increase in resistance by vaporizing or by increasing substantially in temperature. This results in a voltage increase which causes the switch to the

load to close. Wires can be used as fuse elements for lower level currents, up to a few megamperes. Crawford and Damerow³ used 26 No. 22 copper wires as a fuse that opened at slightly over 2 MA; the current to the load reached 90 percent of its final value of 2.7 MA in 1.2 microseconds. A 35 kV dielectric switch connected the load to the circuit.

Pavlovskii^{1j} reports using an explosively driven opening switch which produced a current rise time of 0.5 microsecond.

Higher currents, several megamperes, require large numbers of wires. Foils may be more attractive as opening switches. Reinovsky and Smith^{16,1m} have reported a 190 ns rise time for switching 7 MA into a load.

A further variation, used by Caird, et.al.¹¹, is to use a ballast load on the final generator stage, with a built-in crowbar switch to connect the load into the generating circuit. In this scheme, the load is not connected during the energizing storage.

A-IX. COUPLING OF GENERATOR TO LOAD

The generator may be direct coupled to the load, or may be switched in after the generation is underway (see above) or may be transformer coupled. Transformer coupling has been discussed by several investigators (References 1f, 1k, 1l, 2); autotransformer coupling is also described (References 1j, 5).

The use of transformer coupling allows MCG's to be used to provide pulsed energy to resistive and capacitive loads, and to inductive loads which are of greater inductance than the generator. Fowler² points out that in a first order approach to transformer coupling, the energy transferred to the load is independent of the load inductance and that the required transformer secondary inductance has a very broad, flat maximum; thus, the energy transferred is relatively insensitive to the transformer secondary inductance.

The problems with transformer coupling are the practical problems of geometry, construction, insulation and primary-secondary coupling.

A-X. GAS SHOCK PROBLEM

The armature of the MCG is driven at high speed, up to 5 mm/microsecond. It is possible that shock waves in the gas volume would precede the armature. The shock wave will raise the temperature of the gas, possibly into the electrical conducting region. If this occurs, the conducting gas will short out the generating coil, leading to premature termination of the generating cycle.

Helium, Freon, and air have been used as filler gases. Problems are most often observed in the generators with the very low M/C ratio (armature mass to HE mass). Using M/C values greater than unity will reduce the possibility of shock problems in air. Atmospheres other than air should not be necessary.

Vacuum would be ideal, but problems of sealing occur with the many electrical conductor penetrations required.

A-XI. SERIES - PARALLEL MCG's

MCG units have been operated in series or in parallel to increase the output. In the system design, the jitter in the detonation and in the burning of the HE need be considered in designing the output pulse shape. The output of individual units should be broad enough (in time) to ensure that the peaks will overlap, and add in the desired way.

A-XII. RECOMMENDATIONS: MCG DESIGN

1. Use a conservative approach; under-design; apply safety factors or their equivalent. This approach will produce greater reliability and will permit relaxation of tolerances and material specifications.

2. Use "forgiving" designs; designs which will still deliver an output when tolerances are not quite correct, or when timing is off, etc. This is equivalent to designing inherent stability into an aircraft, which will "forgive" mis-handling of the controls.

3. Design for efficient use of HE; this will give greater freedom in making other design compromises; the efficiency may be desirable to reduce shock, debris, and waste heat.

4. Emphasize efficiency and reliability; compromise (at least initially) on pulse shape.

5. Do final pulse shaping with fuses and switches; a final MCG stage can sharpen the pulse, but appears to be a less desirable approach.

6. Consider staging, i.e., one MCG energizing the next in series. Consider both direct and transformer coupling.

7. Consider using a number of MCG units in series to obtain a desired current output.

8. Develop a computer modeling program in parallel with the experimental effort.

9. For efficient use of HE:

(a) Double sided bellows or strip generator (one sheet or plate of HE drives two armatures).

(b) Helical generator, end detonated.

(c) Coaxial generator, end detonated.

(d) Consider a short strip generator, end edge detonated, with the stator shaped and positioned to give an output like a plate generator.

10. For "forgiving" type generators; have closing angle between armature and stator 5 degrees or greater, but not less than one degree (plate and coaxial generators). In helical generators, a 5 degree helix angle is desirable; two degrees may be satisfactory.

11. Avoid if possible:

(a) Large plate generators.

(b) Generators having two armatures driven together by separate pieces of HE.

(c) Implosion type cylindrical generators.

(d) Closely spaced turns (small helical angle) helical generators.

IV. TASK B: HUMAN FACTORS IN HAZARDOUS OPERATIONS:

B-I. INTRODUCTION

Table B-1 gives accident fatality rates for four industrialized countries. Two things stand out in this table: first, industry safety is better than the safety of the nation as a whole. Industrial fatality rates are 5 to 15 per cent of fatality rates from all causes.

A second point noted in Table B-1 is that the USA is not the safest in the world. In fact, of the four countries listed, the USA has the poorest record. (There are countries, as shown below, with poorer safety records.) This second point suggests that an evaluation of the safety practices, policies and customs of other countries may suggest new ways to promote and improve safety in the USA.

TABLE B-1
ACCIDENT FATALITY RATE
(Latest Year Reported)

Country	Industrial Fatalities ¹ per 1000 Workers Per Year	Accident Fatalities ² per 1000 Population, per year, all causes
Holland	0.02 (1978)	0.373 (1977)
United Kingdom	0.03 (1979)	0.306* (1976)
Japan	0.04 (1979)	0.266 (1977)
USA	0.06 (1978)	0.469 (1976)

Rates, Normalized to Lowest in Table

Holland	1	1.4
United Kingdom	1.5	1.2*
Japan	2	1
USA	3	1.8

* England and Wales

TABLE B-2
 Reported Causes of Aircraft Accidents 1970-1980
 (Survey of Abstracts of 46 Reports and Publications)

Major Cause	Per Cent Reports
Pilot error	37
System deficiency	43
Undetermined	20

Some insight on safety of hazardous operations can be obtained by evaluating the causes of accidents. For example, in the early 1940's most aircraft accidents were attributed to "pilot error." Then people began to recognize that changes in the design, location, and display of aircraft controls and instruments, and a revision of procedures could greatly reduce the errors made by pilots; design was recognized as a principle cause of many accidents that previously had been listed as pilot error. Now it appears we have made the circle. The more obvious, easily made design changes have been made, and future advances in product safety will be in small increments and at greater time intervals. People are once again attributing aircraft accidents to "pilot error." Table B-2 shows the results of a survey of 46 abstracts of publications and reports on aviation safety.

Thirty seven per cent of the abstracts identify pilot error as the major cause of accidents; if those abstracts not classifiable are omitted, the fraction goes to 46 per cent. In 1974, one report³ states "the 10 leading causal citations (for aircraft accidents) all involve pilot failure." In 1980, a group from the U.S. Army Agency for Aviation Safety wrote,⁴ "Human error is the largest cause of U.S. Army aircraft accidents."

The next great advance improving safety will come from the application of human factors to the system. In aviation, the system includes the aircraft, communications, navigation, maintenance, terminals, procedures, organizational structures, policies, personnel selection and training, and all the other factors impinging on flights.

The importance of applying human factors to the system is seen from the reports on the Three-Mile-Island nuclear accident. The

President's Commission on the Accident stated "our investigation has revealed problems with the 'system' that manufactures, operates, and regulates nuclear power plants. There are structural problems in the various organizations, there are deficiencies in various processes, and there is a lack of communications, among key individuals and groups . . . we found problems with the human beings who operate the plant, with the management that runs the key organization, and with the agency that is charged with assuring the safety of nuclear power plants. . . . within the NRC . . . no one was specifically concerned with human factors engineering."⁵

In a review article on human factors in nuclear power, Hagen and Mays state, "However, a distinction must be made between operator error that is directly attributable to operator actions or inactions and the aspect of human error that results from deficient training, inadequate procedures, and deficiencies in control-room design and display of information."⁶ This statement reinforces the Kemeny statement on the importance of the system to safety.

This point of view is further confirmed by the investigators' report on the fatal NASA accident of March 19, 1981.⁷ This report states the cause of the accident to be not any hardware malfunction, but a string of communications breakdowns, improperly followed procedures and inadequate safety checks.

In aviation the importance of human factors applied to the system is being recognized. E. I. Wiener writes, "A review of the major accidents in U.S. commercial aviation leads to the conclusions that FCIT (controlled flight into terrain) accidents are the result of system-induced errors, and that these errors will continue to be generated by the unwieldy system of vehicles, traffic control, and terminals"⁸ Gerathwohl states, "If the cockpit is properly designed and the pilot fully integrated into the system, the workload, strain, and other stress -- producing factors can be kept at a minimum."⁹

"Stress-producing factors" mentioned by Gerathwohl appear frequently in the analysis and discussion of aircraft accidents, but was not considered to be a factor in the Three-Mile-Island accident. Stress-producing factors certainly are related to systems design and systems safety. As is seen in the TMI discussion, the system influencing safety

TABLE B-3
FATALITY RATES FROM ACCIDENTS

Country	Fatalities per 1000 Workers per Year		Fatalities per 100 Population Per Year		All Accidents Except Auto ²
	Manufacturing ¹	Mining ¹	All Accidents ²	Auto Accidents ²	
Holland	0.02 1978	0.14 1977	0.373 1977	0.186 1977	0.187 1977
United Kingdom**	0.03 1979	0.29 1979	0.306 1976	0.123 1976	0.183 1976
Japan	0.04 1979	0.48 1979	0.266 1977	0.106 1977	0.160 1977
United States	0.06 1978	0.54 1979	0.496 1976	0.219 1979	0.250 1976
Sweden	0.06* 1977	0.44* 1977	0.480 1975	0.151 1975	0.329 1975
France	0.08* 1978	0.43 1978	0.748 1970	0.235 1970	0.513 1970
Fed. Rep. Germany	0.13* 1979	0.52* 1979	0.515 1976	0.235 1976	0.280 1976
India	0.13 1977	0.80 1977	0.195 1973	0.071 1973	0.124 1973
Kenya	0.49 1978	0.80* 1973	0.062 1970	0.010 1970	0.052 1970

37-34

* Number of compensated fatalities. All others are number of reported fatalities

** Manufacturing and Mining -- United Kingdom. All and Auto Accidents -- England and Wales

includes not only the engineering design and the operation of that device or machine, but also the organizational structure, the management methods and policies, the communications between the various groups, the regulation of the activity, and interfacing with the public with government, etc. The handling and implementation of these issues can strongly influence stress factors and overall safety.

In evaluating hazardous operations in regard to human factors and systems safety, an examination of techniques and methods in other countries may be productive, particularly if these other countries have a good safety record. Japan is one such country. The Japanese safety record appears better than ours, Japanese management techniques are widely studied by U.S. managers, and Japanese products enjoy a good reputation for their construction, finish, and operation.

This study emphasizes the factors brought out above, the importance of reducing stress and stress-related factors, the importance of the systems approach, including organization, management, procedures and engineering design in the system, and finally, the possibility of utilizing approaches used by other countries to promote greater safety.

B-II. OBJECTIVES OF THIS TASK

The primary objective in this task is to examine Human Factors in hazardous operations in several areas, in several countries, and in detail, and to evaluate the various discoveries as to value and potential for reducing accidents.

The task was carried out on a general basis. Accident potential, stress, and human factor problems occur in all hazardous operations. Useful safety measures in one area of activity may find application in other areas.

For the Air Force, improved safety will be of value in practically all areas of its operations: aircraft flights, operations in adverse environments, storage, transporting, and handling of conventional and nuclear munitions, operating sophisticated equipment employing high power, and others.

Because of time and resource limitations, this Task was limited to search and preliminary evaluation, with the intent to identify areas where further investigations might be fruitful.

It is possible, and hoped, that some of the areas for potential study have already been studied and reported on, and some may become subjects of study at other laboratories and institutions.

B-III. ACCIDENT STATISTICS.

Statistics on accidents other than automobile, and other than USA, are difficult to obtain. The difficulty is reflected by the comment made by the editor of the International Labor Organization's Year Book of Labour Statistics:¹ "data on non-fatal accidents do not lend themselves easily to international comparison and have therefore been excluded from these tables." Even fatal-accident data is not free of ambiguities. Some ways fatalities are reported include:

Number reported per 10^6 worker-hours.

Number reported per 1000 workers per year.

Number reported per 1000 worker-years of 300 days each.

Number of compensated cases per 10^6 worker-hours.

Number of compensated cases per 1000 worker-years of 300 days each.

Further, a worker who dies from complications of an accident suffered at an earlier date may have his death attributed to the immediate cause rather than to the accident.

The statistics reported below were adjusted in the following ways: the 10^6 worker-hours were treated as consisting of workers working 2000 hours per year; the 1000 worker-years of 300 days each were treated as 1000 worker-years, the 300 days being ignored (this may result in equating 2000 and 2400 hour work-years, not serious considering the variability of reporting and uncertainty in the data); no attempt was made to adjust "compensated" vs "reported" cases.

Table B-3 presents fatality data for several countries for the most recent year reported. As might be anticipated, the fatal accident rate in industry is higher in the less developed and the developing countries, while the total accident rates are lower in these same countries.

Several countries have lower accident fatality rates than the USA, both in industry and in the total accident categories. What appears surprising is the high fatality rate in France for all accidents, and the relatively high rate for manufacturing.

With one exception there appears to be no data on non-USA non-fatal accident rates readily available. The one exception is that prior to 1969, Japan published extensive statistics using categories and units practically identical to those used by the US Bureau of Labor Statistics. Table B-4 and Figures B-1 and B-2 present the most recent Japanese data (located in this study) compared to the USA data of the same period. These data give the frequency and severity of lost-time accidents (one day or more lost) and includes fatalities (a very small part of the total). In frequency, in the ten categories included in Table B-4. Japan has a lower accident rate in all but ordnance. This is shown graphically in Figure B-1; accident rates identical in the two countries would lie on the 45 degree line. The dash line gives an approximate fit to the data; this gives a value of 5/3 for the ratio of accident rates in the USA to that in Japan.

Table B-4 and Figure B-2 show that in severity of accidents (as measured by total days lost per 10^6 employee-hours), USA and Japan are approximately equal.

Tables B-5 and B-6, and Figures B-3, B-4 and B-5 illustrate some of the variables which create uncertainties and difficulties in making comparisons and drawing conclusions from accident statistics.

Table B-5 gives some data on distributions of size of establishments. Note that in Table B-4 and Figures B-1 and B-2 only establishments of 100 or more employees were included in the Japan data, while the USA data included all establishments (2 or more employees). Table B-5 shows that in 1960, approximately midway through the reporting period, only 47 per cent of the Japanese establishments were included in the data presented in Table B-4 and the accompanying figures. It also shows the number of small establishments in Japan is declining.

TABLE B-4
 LOST-TIME INDUSTRIAL ACCIDENT RATES^{10, 11}
 USA* AND JAPAN**

USA data, 10 year average, 1958 - 1967.

Japan data, 13 year average, 1955 - 1967.

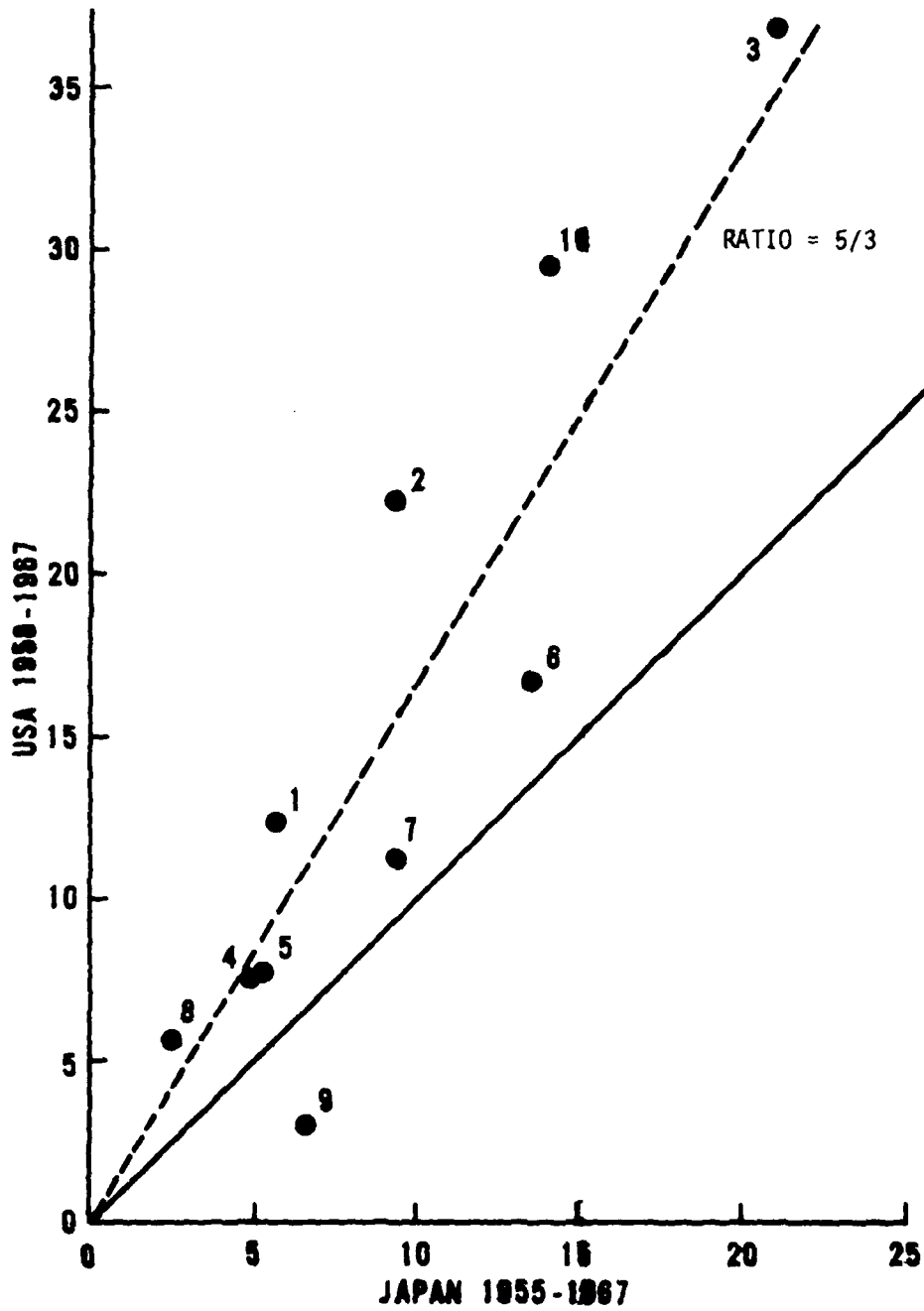
<u>Activity</u>	<u>Frequency</u>		<u>Severity</u>	
	Number per		Days lost per	
	10 ⁶ Employee-Hours		10 ⁶ Employee Hours	
	<u>USA</u>	<u>Japan</u>	<u>USA</u>	<u>Japan</u>
1. Manufacturing	12.4	6.61	717	650
2. Food Processing	22.3	9.24	1006	540
3. Lumber	37.0	21.0	2966	2090
4. Chemicals	7.6	4.83	629	550
5. Petroleum	7.8	5.16	862	540
6. Fabricated Metal Products	16.8	13.47	905	1370
7. Machines, non-electric	11.3	9.43	576	640
8. Electrical and Electronic	5.7	2.44	273	250
9. Ordnance	3.0	6.69	289	610
10. Construction	29.6	13.93	2376	2760

* Survey covered 50,000 establishments including approximately 50 per cent of all manufacturing employees; all size establishments except self-employed individuals were included

** Survey covered all public and private establishments employing 100 or more.

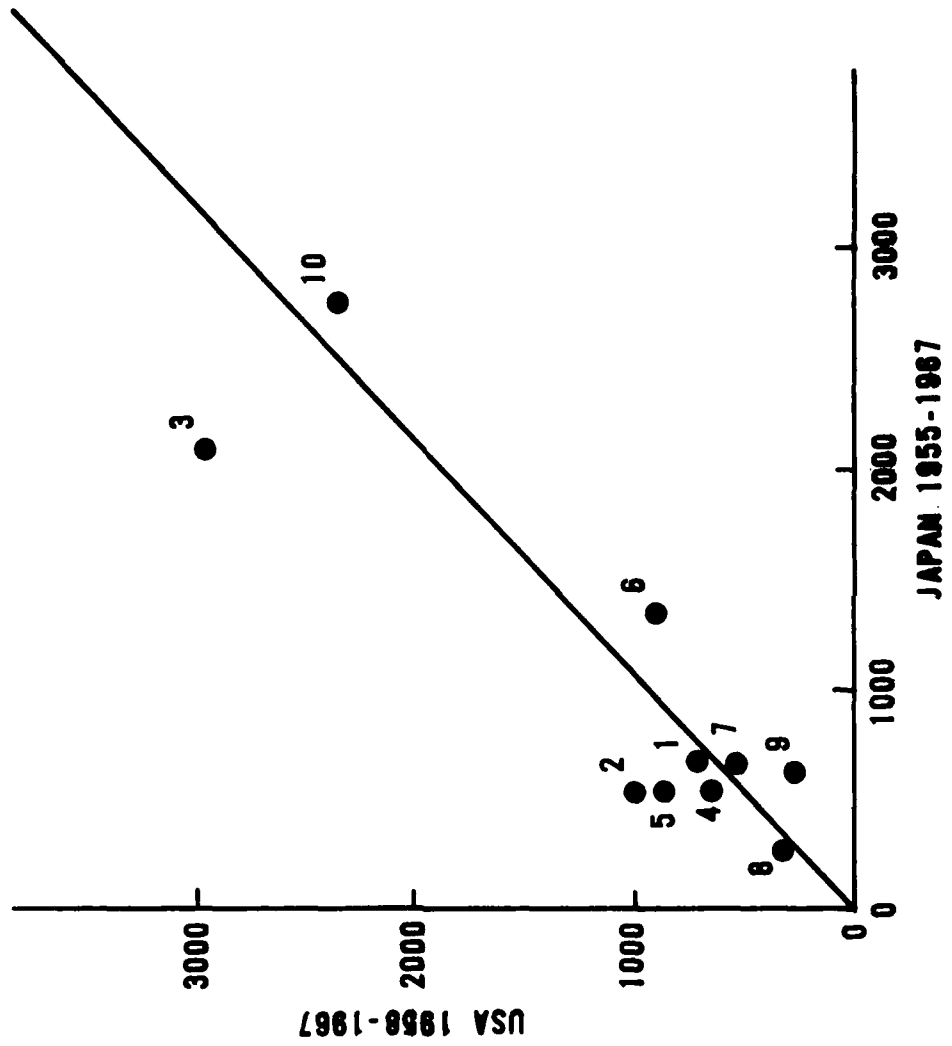
FIGURE B-1

INDUSTRIAL ACCIDENT FREQUENCY PER 10^6 EMPLOYEE-HOURS



For identification of numbered points, see Table B-4

FIGURE B-2
 INDUSTRIAL ACCIDENT SEVERITY RATE
 DAYS LOST PER 10⁶ EMPLOYEE-HOURS



For identification of numbered points, see Table B-4

TABLE B-5
 STATISTICS ON SIZE OF MANUFACTURING ESTABLISHMENTS¹²

<u>Country</u>	<u>Per Cent Manufacturing Establishments with <100 Employees</u>	<u>Per Cent Manufacturing Employees in Organizations of <10 Employees</u>	
		1954	1967
	1960		
Japan	52.8	23	16
United States	27		3
United Kingdom	20.3		
Denmark	47.2		

TABLE B-6
 INDUSTRIAL ACCIDENTS AND ILLNESSES
 IN U.S. MANUFACTURING, 1979¹³

<u>Size of Organization, Number of Employees</u>	<u>Total Nr Accident and Illness cases per 100 employees per year (lost time and non-lost time cases)</u>
1-19	8.3
20-49	14.5
50-99	17.7
100-249	17.8
250-499	15.4
500-999	12.3
1000-2499	9.2
2500-	6.6
Average	13.3

Table B-6 gives, for the USA only, the industrial accident and illness rates (97 per cent accidents) as a function of establishment size. In general, larger establishments have lower accident rates. In this table, the smaller organizations also appear to have lower accident rates. This latter is likely to be a true trend because in smaller organizations, employees may feel a stronger dedication to and a greater "ownership" of the enterprise, and thus may be more careful workers. However, this data on small establishments may be misleading; in the small organizations, workers may be less well covered by workmen's compensation and/or may be driven by a profit incentive, so that time may not be taken off for accidents which, in a larger establishment, would become a lost-time accident. This last effect is also suggested by the data shown in Figure B-4 below.

Figure B-3 shows the trends in lost-time accident rates in the USA in several industries. One observation is that the accident rates are increasing in every case. This trend will be discussed in connection with Figure B-4.

Another observation of Figure B-3 is that various occupations have widely different accident rates, and that occupations generally considered hazardous have the better safety record. This is a true effect; in the hazardous occupations, everyone, from workers through management, are safety conscious and puts effort and resources into preventing accidents.

The variations in accident rates in various occupations suggests that the fatality rates reported in Tables B-1 and B-3 may not be as directly comparable as they appear. Possibly the low fatality rate reported by Holland is due to the nature of the industry in Holland more than it is to safe practices by Dutch workers and management. For meaningful comparisons of safety, it may be necessary to apply weighting factors to the reported data, or obtain more detailed or specific data.

Another factor that may perturb the data, making international comparisons difficult, is the productivity, or exposure factor.¹⁴ An official of the shipbuilding industry reports¹⁵ that a frigate requiring 1.6 million man-hours in the USA would require 5 million man-hours in Britian. If accident rates were equal based on equal outputs; the reported British rate would be one-third the USA rate, based on worker-hours. Accident statistics are reported on the basis of worker-hours, but it might be reasonable to

FIGURE B-3
 LOST TIME INJURY AND INDUSTRIAL ILLNESS RATES¹³
 NOTE: In 1979, injuries accounted for 92-100%

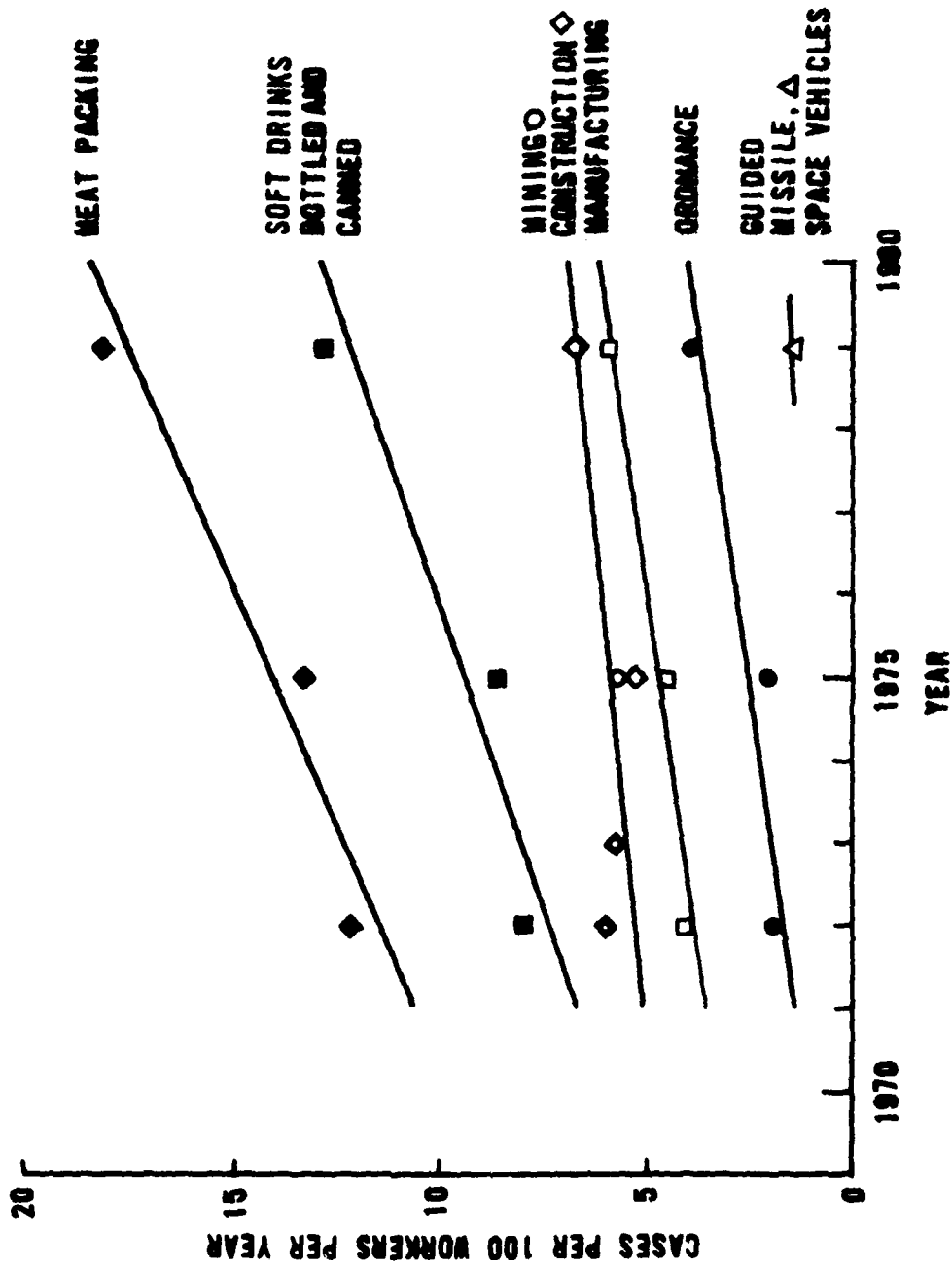
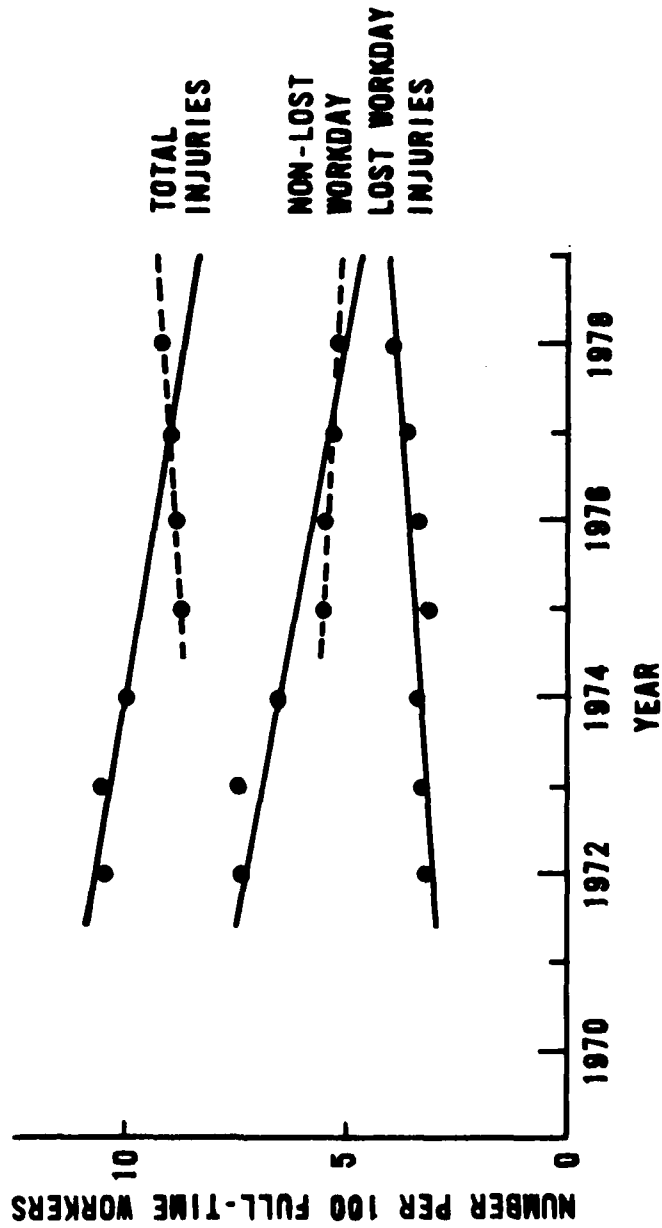


FIGURE B-4
 OCCUPATIONAL INJURY INCIDENCE RATES, USA 16



expect accident rates to be related to the amount of work done, which determines how much the worker is exposed to hazardous situations.

Figure B-4 shows recently published data illustrating the trends in accident rates in the USA. Here the lost-time accidents are seen to be increasing while the non-lost-time accidents have been decreasing. The total accident rate, over the long term, has been decreasing also. One interpretation of this data is that changes in workmen's compensation has encouraged workers to take time off on borderline cases that previously might have been non-lost-time accidents. The Bureau of Labor Statistics feels that industrial safety has continued to improve over this time period ¹⁷

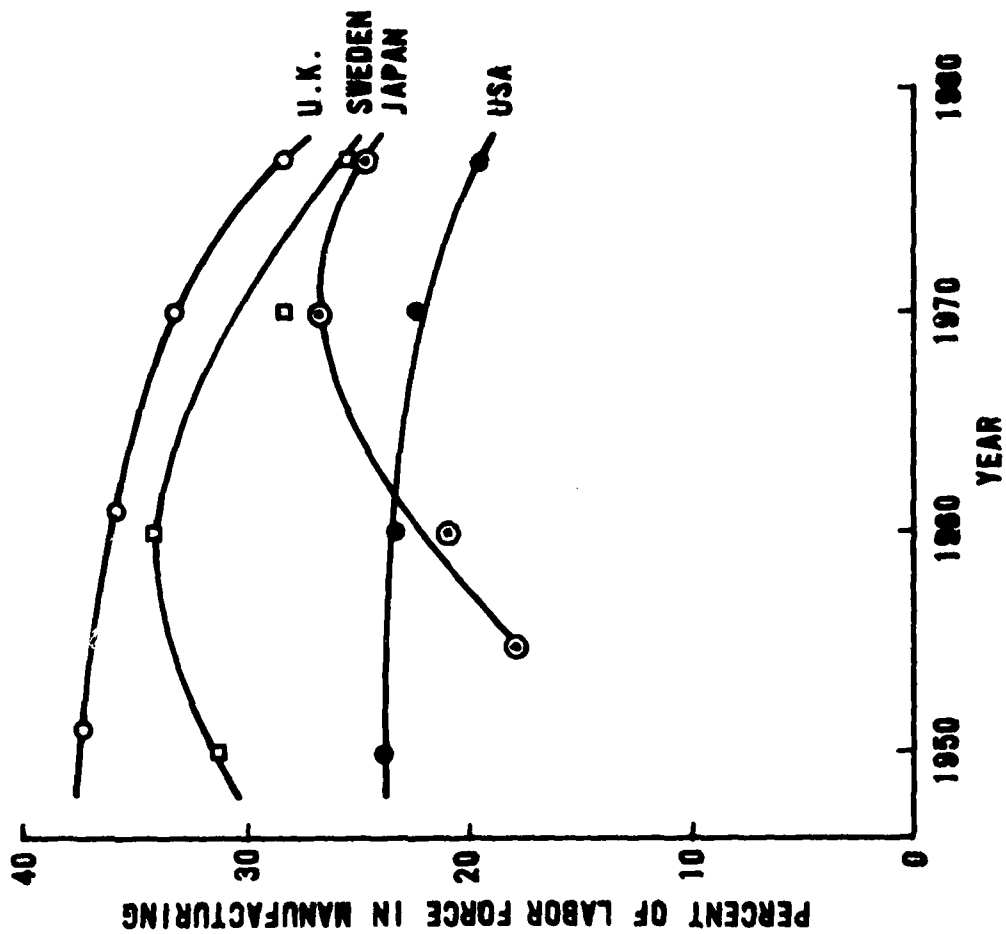
Figure B-5 shows the per cent of the labor force which is engaged in manufacturing for four countries. The steep decline in the past decade is due primarily to the increase in automation permitted by computers, and in particular to the introduction of robots in manufacturing. In speculating how low this percentage might go, one might recall that 200 years ago agriculture required the labors of 80 to 90 per cent of our work force. Today, less than four per cent of our work force is engaged in agriculture.

The trends shown above, the decrease in workers in manufacturing, the increased use of robots, the decrease in the number of small manufacturing establishments, and other changes will all have an impact on accident rates and on accident prevention. More detailed information and a careful evaluation of safety accomplishments are needed to determine if one country has a better, safer operation than another, and whether changes that could be made would be worthwhile.

B-IV. THE JAPANESE EXPERIENCE

Several countries appear to be candidates for further study on accident rates, and the means used (or not used) to control them. Tables B-1 and B-3 show that Holland, the U.K., and Japan all have lower accident rates than the USA, in manufacturing, mining, and in total rates. A more complete list may show others. In the other direction, France shows an unusually high accident rate, particularly in non-industrial. The factors responsible for very low and very high accident rates may suggest further means of reducing the rates in the USA.

FIGURE B-5
PERCENT OF LABOR FORCE IN MANUFACTURING¹⁸



Japan was chosen for an initial study. The low accident rates relative to the USA are shown in Tables B-1, B-3, and B-4, and Figure B-1. Japanese products are generally considered to be well designed and well made. Japanese-built automobiles rate quite highly, particularly in regard to "fits and finishes"; this is accomplished with one-half the inspectors in the factory compared to the USA practice.¹⁹ The factors which make inspectors more effective or less needed may have implications toward improving of safety in hazardous operations in the USA.

Another striking example is that in 1980, Hewlett Packard reported a failure rate in memory chips of:¹⁹

Japanese made, 0.01-0.019%, and
USA made, 0.059-0.267%.

Quality of performance and safety are closely related; factors increasing one may positively affect both.

Japan has only recently evolved as a major industrial nation; Figure B-5 shows how the industrial employment grew in the 50's and 60's while that of the USA and UK was static or declining. The growth of industry within a nation with a culture very different from the Western nations makes an interesting study.

This rapid growth of industry in Japan is also causing changes in Japanese society. As an example, unity is a basic concept in Japanese society. That hierarchies exist in society and in business has been looked upon as essential, and that the interdependence between levels is part of the unity. Hierarchy and unity are inseparable concepts.

A recent, democratic movement in Japan is challenging these concepts. This movement is demanding equality first, as a prerequisite to accepting unity. However, at the present time, the old values and concepts appear to be the stronger and more influential factors.

Another change is the growth of large businesses and the decline in the number of small establishments. (See Table B-5.) This means that more workers travel farther from home to work. The trend is toward the weakening of the family as the center of Japanese society.

This dynamic social climate in Japan makes analysis and the drawing of conclusions more difficult and less positive. Even with this dynamism, the value systems and cultural characteristics of Japan show through and exert a major influence on Japanese business and social life. The uniqueness

of the Japanese culture, their low accident rates, and their good product record makes this a good subject for initial investigation.

In addition to the statistical sources already quoted, references 12, 19, 20, 21, 22 and 23 were the sources for most of the following material.

Japanese Employment Status. In Japanese business there are three classes of workers:

1. Key employees, or members. These are permanently employed.
2. Mid-term employees are employed on a regular basis. They have fewer fringe benefits and can be laid off.
3. Temporary workers are hired on a short term basis, which is renewable. Most women are in this category. In this category some employees work full-time for many years.

The first class, the "members" of the organization are permanently employed. In a business downturn, temporary workers and mid-term employees are let go, stockholders dividends are cut, and management takes a salary cut before the key employees are affected.

In the larger companies, the key employees, or members, are only hired at entrance level employment, directly out of high school or college. Employees are preferred with a good general education. Extensive on-the-job training is given to all new permanent employees. This on-the-job training often includes living at the school and taking physical education, as well as training in their assignment and indoctrination into company policies.

Workers leaving a position can only find employment in a smaller company.

Except for a small number of upper level managers, retirement at 55 is compulsory. However, in a survey,²¹ only 26 per cent of retirees went directly into retirement. The rest continued working, 33 per cent with the same company and 41 per cent at a different company. Often a "retired" worker will continue at the same job at a substantially reduced salary.

The permanent employment of key²² workers has advantages and disadvantages. The advantages are:

It fits into the Japanese desire for security and order in their lives.

Recruitment costs are reduced.

On-the-job training benefits are retained.

Resistance to change (e.g., introduction of robots) is reduced.

Resistance to job reassignment is reduced.

Some of the disadvantages are:

Unsatisfactory performance must be tolerated.

It is a cause of overstaffing.

There is a preoccupation with group solidarity at the expense of technical competence.

Informal cliques cut across organization charts, creating rivalries and complicating the decision process.

Management Methods. Over the past several years, many USA companies have been studying Japanese business and management methods, and adapting some of these methods for domestic operations. An example is the Quality Control Circle which is effective in Japan and is being tried extensively in the USA.

Rehder²⁰ states that many of the techniques which USA management is so interested in are actually Japanese adaptations of principles developed in the US since the Hawthorne Experiment, but previously rejected by US business. Now, with increased international competition and domestic inflation and unemployment, US business is pressed to improve production. Rather than accept principles formerly rejected, management is looking to Japan for "new" ideas that may be effective.

The emphasis in Japanese business is on harmony and unity. Conflict and confrontation are avoided. Decisions are made by consensus; there is considerable amount of behind-the-scenes checking and consulting before a decision or a proposal is presented. Most communications are oral. Written communications are generally confirmations of decisions made.

This mode of operation makes it difficult to get clarification or further information on a decision. The emphasis is on group action, norms, and responsibilities. The method precludes fixing responsibilities and giving rewards.

There are benefits to this group method of operation. Workers have a line of communication through a group which engenders a feeling of belonging and of participation. There exists a mutual trust between an individual and the group which carries over to a trust between levels of the organization. If there is a separation between "us and them," it is between the organization and competing organizations or between the organization and the world external to the organization. The us-them feeling is never applied to labor vs management.

A further benefit from the emphasis on the group rather than the individual is that individuals will suggest ideas that will benefit other than their own task. The individual recognition may be absent, but anything that benefits the company is a benefit to every individual in the company. and if the suggestion fails, the group takes the responsibility.

This group action is implemented in Quality Control Circles (sometimes referred to as Quality Circles). The Q.C. Circle includes the workers from one assembly line or from one section of a factory. Supervisors and possibly management representatives are included. Anyone can present a problem and anyone can offer solutions to problems.

The Q.C. Circle is being used in the USA, but the operation differs from the Japanese in its reward structure. In the USA, savings from suggestions are documented, and awards are made on the basis of the savings. Such awards can be substantial, several thousands of dollars. In contrast, monetary awards in Japan are for token amounts. However, the circle is given broad recognition, including stories in the company's publications, and company paid trips to regional and national conferences where they can present their suggestion to a wider audience. It was a Q.C. Circle visiting a Lockheed plant while on a world tour, a reward for their group performance, that introduced the Q.C. Circle idea to the USA.

There are several additional consequences of this group management approach. Goals are shared and communicated. Middle managers frequently are participants in the formulation of strategic goals. Proposals usually are generated at a lower level, giving the advantage of employee participation, but the disadvantages of formulating proposals at a level where there is lesser understanding of long-range company objectives. This also creates a situation where top executives have little authority to reject proposals.

Middle managers usually resolve conflicts informally. There is no reference to an organization chart to find a line of authority. Organization charts are for external use, to show titles and positions to those outside the organization. The organization chart is not followed inside the organization.

Society-Business-Government Relations. The company is the major social institution. Workers are first loyal to the company. Relatives and friends are enlisted to support the company.

This first loyalty to the company may appear to be a built-in cause of conflict. It is not because the Japanese understand their society in terms of an organic unity. All levels, individual, family, company, government, are interdependent, mutually trustful and mutually supportive. The goals of the government are substantially incorporated into the goals of the company. The futures of the employee and of the employer are intertwined. In the Japanese concept of society, there is no conflict between levels.

There are feelings of moral obligations on the part of individuals and of institutions to fulfill established roles in society. These roles include an implied company responsibility to care for the employee, and an implied government responsibility to care for the company. Thus, the government will take steps to control production and trade levels and to provide assistance, or to restrict the availability of resources, to attain the balance in industry which appears best and healthy for everyone concerned. In the USA this would be considered governmental interference which would not be welcomed. These factors all increase the unity between levels of society.

Japanese firms have stockholders, but generating dividends for stockholders is not a primary objective. Operations and decisions are based on the principle that a company morally belongs to all employees. Employees are looked upon as the most valuable asset of the company. Protecting the employees has a high priority. Further guiding rules are seen in the first two "principles" of a large Japanese Bank,²² the first being service to their customers, and the second is to contribute to the public welfare. The prosperity and growth of the bank is in "principle" number four; a profit on the financial statement is not mentioned.

Goals and Motivations. The importance of the employees to the company is discussed above. Conserving human resources is of high priority in a company.

Companies have economic goals, but the profit motive is never high. Continuity and growth are more important and are greater motivating factors. It is noted¹² that maximizing continuity and growth rather than profit results in a greater rate of reinvestment, but little change in utilization of resources.

Companies also are motivated by the desire to develop a common direction and meaning (harmony and unity), and to enhance the satisfaction of work. These are further emphasis on conserving human resources.

USA Management Response to Needs and to Japanese Procedures.¹⁹

USA industry has needs to be more productive and more competitive. Of the responses listed below, some are derived directly from the Japanese experience, some are influenced by the Japanese approach, and others have been developed in other ways. These responses are listed without comment.

Upper Level Responses

- Matrix Organization
- Project Teams
- Task Forces
- Management Development Programs

Lower Level Responses

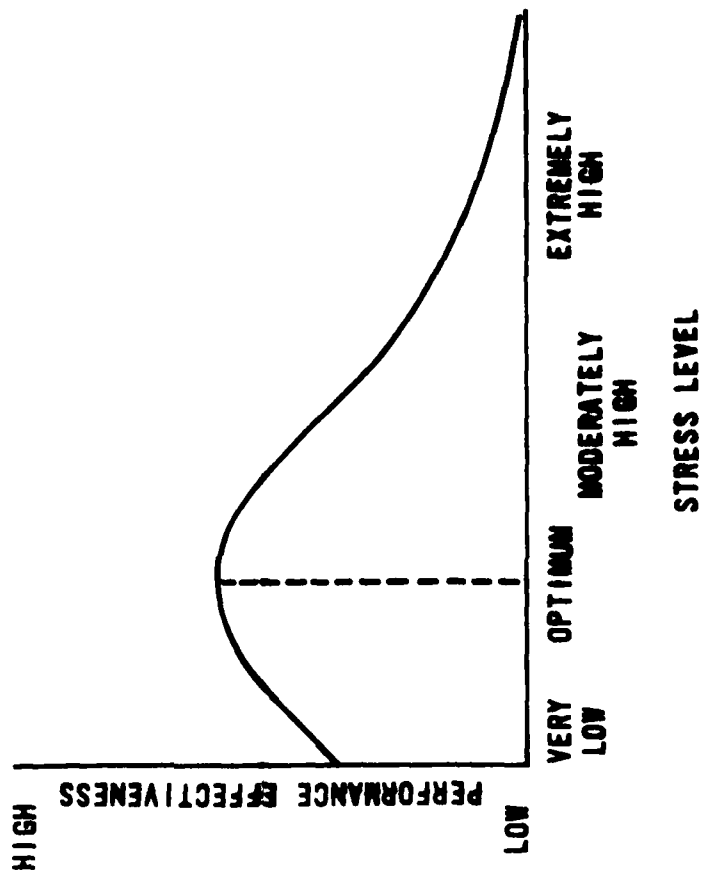
- Quality of Work-Life Improvement
- Job Enlargement
- Autonomous Work Groups
- Ombudsman
- Liaison Individuals
- Facilitators
- Quality Control Circles
- Training Programs.

B-V STRESS

The importance of controlling stress levels in hazardous operations is introduced in Section B-I, above. Swain²⁴ points out the importance of an optimum stress level in graphical form, reproduced here in Figure B-6. Very low stress levels occur in long, uneventful aircraft flights, monitoring attack-warning radar, guarding installations, operating power plants, and others. High stress levels occur in emergency situations, unanticipated events, infrequent activities, etc.

Swain²⁴ quotes examples of the degradation of performance in high stress situations. In extremely high stress flight situations, 15 per cent (360 out of 2450) of the aircraft commanders actions either worsened or did not improve the situation. This estimate is believed to be low as

FIGURE B-6
HYPOTHETICAL RELATIONSHIP BETWEEN PERFORMANCE AND STRESS



non-survivors could not be interviewed and are not included in the results. When the actions of the entire aircrew were studied, 37 per cent (457 out of 1229) actions were ineffective or worsening.

Swain²⁴ further states that in extremely high stress situations, if the first attempted corrective action fails, the probability of error on the next trial doubles, and doubles again on each successive trial. Four unsuccessful attempts can result in complete disorganization of the individual. Observation of carrier landings leads to the belief that this doubling rule also applies to moderately high stress situations.

Stress, too high or too low, will increase the probability of human error. The occurrence of a human error can create a situation which generates stress, reducing the probability of proper corrective action. Human errors can also result from fatigue (unrelieved stress), from inattention (too low stress level), distraction, mistakes and other cases of poor human performance. Further causes of human error may be due to engineering design weaknesses, inadequate or inappropriate training, communication errors or weaknesses, poor supervision and other organizational type problems.

Another important cause of human error in stressful situations is that of the attitude or mindset of the individual. Misinterpretation of the indicators of the emergency can occur. This is particularly likely to happen in the occurrence of low probability events, and in emergencies following long periods of low stress operations.

It is difficult to estimate the importance, quantitatively, of stress levels to safety, because practically all experiments have been laboratory experiments, with assurances that there will be no catastrophic outcome. One interesting attempt to measure stress and adaptation to stress in more realistic situations is a Soviet experiment²⁵ analyzing voice recordings made during free fall parachute jumps. The full report on this work has not been seen by this investigator.

Below is discussed some of the findings on stress and related factors coming out of this Task effort.

Distraction. Distraction has been described as an important cause of mishaps and a potential cause of accidents.^{26, 27} A NASA study (Ref. 27; the original study was not available to this author at the time this work was done) analyzed 169 reported cases of aircraft flight mishaps involving distractions. Activities causing distractions included paperwork,

P.A. announcements, conversation, flight service (to passengers), company radio communications, weather avoidance, checklists, malfunctions, traffic watch, ATC communications, new crew members, searching for the airport, plus a miscellaneous group. Some interesting points were noted. In every case (22 cases) involving checklists, the checklist accomplishment was given priority over ATC (Air Traffic Control) requirements, and in every case, there was a potential or actual violation of an ATC rule or regulation.

Malfunctions in the aircraft, and radar controller's point-out of other traffic were two situations which drew the complete crew attention, to the neglect of other duties, such as monitoring the flight path of the aircraft and the watching for other traffic. These discoveries might suggest changes in procedures, in crew instruction, or in crew training to further reduce the probability of accidents.

Altitude Alert System. The altitude alert system is not a major cause of mishaps; a total of 32 cases were reported in 6511 event reports. 28 However, there are some interesting observations which may be useful in applying human factors to other problems.

The alert system produces a visual and an aural alarm. It was originally installed as a backup system. It is being used as a primary system. The aural indicator is liked by long haul operators who have long periods of low workload. Short haul operators are less enthusiastic about the visual and aural warnings. Some say there are too many signals in the cockpit.

A proposal has been made to permit the removal of the aural signal alarm on reaching altitude, but to keep it as an alarm warning of deviations from altitude.

Inspections. The concern is sometimes expressed that the formal, "big show" military inspections may be counterproductive. In the effort to make a good showing, equipment may be put into service which might not be fully prepared for service; further the preparation for and the conduction of the inspection may raise the stress level on the participants to a level that may increase accident possibilities, or the after-effects may result in a more accident-likely condition.

Whether the above concerns are real or serious is not known. Possibly such concerns have been reinforced by stories in fiction and in Hollywood movies.

Countering these negative factors are several positive factors. A good showing is a source of pride to those being inspected, a positive morale factor. The preparation and the inspection promotes unity in the organization. It may be an interruption to the monotony and boredom which routine may generate. It is likely to give fresh definition to organization objectives and tasks, and strengthen the ties and interaction with the larger organization or the society in which it exists. All of these factors are likely to be positive in improving performance and decreasing accidents.

Activities which evolve over many decades have a way of adapting to the psychological needs of the participants and to the culture of which it is a part. This may be the case with the formal "big show" military inspection.

There still may be a value in studying the safety elements in inspections. Our society has seen great changes in recent decades, in our technology, our relative position to other nations, our world-wide commitments, and in value systems within our society. Customs, such as the inspection, change slowly. Customs which met 19th Century or early 20th Century needs may not meet the current and future needs. Some changes may be beneficial to promoting safety, such as greater recognition of participants, redefinition of criteria, the expectations and rewards regarding the inspectors, etc. Appendix A gives an outline of some of the factors which might be considered in a study of inspections for the purpose of increasing safety.

Proficiency Maintenance. Safety can be enhanced if the operators involved in an activity perform at optimum proficiency. Swain²⁴ shows how proficiency drops off following a period of training, and discusses the importance and frequency requirements for retraining.

Both pilots and air traffic control tower operators are highly trained and are in positions where mistakes could lead to hazardous situations. It is interesting to note that pilots have to take periodic proficiency checks,²⁹ but air traffic controllers do not.³⁰ It is the controllers who complain most about the stress level of their work. Is it possible that periodic proficiency checks for controllers would confirm their capability and serve as a milestone in their career, and thus reduce the stress level that they feel they are subjected to? It does not seem likely that both systems, proficiency checks for pilots, no checks for controllers, could be optimum.

B-VI. RECOMMENDATIONS

This Human Factors study, to date, suggests more areas to investigate than it does conclusions and actions to take. Some suggested continuing efforts are:

1. Extend the study of accident rates in other countries. Additional data might be obtained through various industrial and trade associations, such as Shipbuilder's Council of America, the American Institute of Steel Construction, and the American Iron and Steel Institute. Professional Societies may be sources of data also. Airline, shipping, and transportation safety records could give further comparisons of USA and non-USA safety records. These data should be analyzed, normalized, weighted, and compared.

2. Based on the Japanese manufacturing performance record and on the accident statistics presented here, Sections B-I and B-III, there is a strong feeling that the differences of safety records of Japan and USA are real. If the study proposed in paragraph 1 above confirms this and/or if other differences, e.g., with Holland, United Kingdom, France, are real, then a search should be conducted for reasons for the differences. A final step would be an evaluation of any differences found to see if methods in other countries could be applied here to improve the safety record in the USA.

3. A comparison and an evaluation could be made on qualifications, training, performance, and safety records of USA and foreign, military and civilian control tower operators. There appear to be differences in qualifications and training. Are these significant, and do they relate to safety and performance?

4. The NASA Aviation Safety Reporting System has many thousand event reports related to civilian aviation. The USAF Directorate of Aerospace Safety has a similar bank of data in its Hazardous Air Traffic Reports. The NASA group has used its data bank to produce a report on the effects of fatigue on safety (requested, but not available for this study), but has not done one on stress. Studies, such as the effect of stress on safety, and the factors causing stress, might be done with the help of the two organizations mentioned above. The civilian results should be of interest and of value to the military and vice-versa.

5. A study of the Japanese Nuclear Power safety experience could prove informative and useful. Japanese Nuclear Power Plant operators submit but one per cent as many event reports (per reactor) as do USA operators.³¹ This difference is undoubtedly attributable to differences in reporting methods and standards. A study of publications in professional journals, particularly proceedings of national and international meetings may yield some safety comparisons. Also, many Japanese Nuclear Plant operators are trained in the USA. To what extent do USA procedures influence Japanese procedures? How are the Japanese customs of group norms and group responsibilities carried over into nuclear operations? Again, a study of the professional publications might be a good starting point.

6. Inspections, particularly the formal inspections of the military and of the nuclear power industry, may affect safety, and might be used to improve safety. See Section B-V and the Appendix for a discussion of this topic.

7. As a supplement to inspection and supervision, a study might be made of the feasibility and value of building more monitoring capability into machines (airplanes, etc.). Currently, monitors sound alarms if potentially hazardous situations develop. Monitors might be extended in scope and operation to monitor, inform (real time) and record, not only malfunctions, but also show superior performance. This monitoring could be applied to both the machine performance and to the operator performance. This, if properly applied, could be a source of encouragement and challenge to the operator, and would be a supplement to the formal inspection (the recording showing the performance).

V. RECOMMENDATIONS:

Recommendations specific to each of the two tasks are given in Sections A-XII and B-VI above. Here only more general recommendations will be presented. These are two in number.

1. Importance of the systems approach. In application of human factors to improve safety, it is quite apparent, in the TMI accident, in NASA space work, and in flight safety, that applying human factors to the designing of the man-machine interface, or the operator environment, is not sufficient. The design of the procedures, the management, the regulation, the inspection methods, the communications, the operator training, and many other factors must be integrated to optimize safety. The entire system must be optimized for performance and safety.

Likewise, the design of pulsed generators will benefit from a systems approach. Selection of design specs, performing trade studies on alternatives, recognizing constraints, and applying safety factors or equivalent will all lead to more effective designs.

The systems approach is applicable in practically all endeavors and problem solving efforts. It should be developed and utilized fully.

2. The principle of "forgiving" designs is likely to become a useful concept. The principle is already used in designing aircraft, watercraft, and nuclear reactors which are inherently stable; a small error in control or a small perturbation will cause only a momentary disturbance from equilibrium; the system will quickly return to a stable condition. Also, the redundancy built into many control and communication systems results in "forgiving" designs. Errors in operation or component failure will be tolerated and the system will continue operating. However, the idea of developing a "forgiving" design as a design objective or as a basic design principle is not common.

Application of the principle of a "forgiving" design is likely to be cost effective. In the long term there will be fewer major failures, fewer accidents, and greater percentage of missions completed. These results will compensate for the additional cost or the reduced performance which may result from this approach.

In human factors and safety, the "forgiving" design approach may be essential. Human error can be reduced by training, but can never be completely eliminated. This puts a limit on safety accomplished by

reducing human error. Safety can be improved beyond this limit (and accidents reduced) by designs following the "forgiving" concept. The system can be designed to accept some human error without resulting in accidents or loss of mission. It should be possible to design a "forgiving" system which will inform operators of errors, thus performing a training function during regular operation.

The concept of "forgiving" design is one which needs further development. Various ways of stating the principle, various ways of applying it, means of quantifying or identifying the degree of "forgiving", the trade-off of "forgiveness" against cost, performance, and other factors, could all be investigated further. The concept needs further clarification, development, and exposure to the engineering design community.

In the recent past, engineering design has gone through several phases--"design to specs"; "design-to-cost", and "design-to-life-cycle-cost". "Forgiving design" may be a next step.

References: TASK A, MCG DESIGN

1. Megagauss Physics and Technology, P. J. Turchi, Editor, Plenum Press (1979)

Individual papers from reference 1 which are cited:

1a. J. E. Grover et al., Small Helical Flux Compression Generators, *ibid*, pp 163-180.

1b. E. I. Bitshenkov and V. A. Lobanov, Energy Capabilities and Magnetic Flux Losses in "Bellows" - Type Explosive Generators, *ibid* pp 181-191.

1c. J. H. McGlaun et al., COMAG-III: a 2-D MHD Code for Helical CMF Generators, *ibid* pp 193-203.

1d. J. R. Freeman, et al., Numerical Studies of Helical CMF Generators, *ibid* pp 205-218.

1e. T. J. Tucker, A Finite - Element Model of Compressed Magnetic Field Current Generators, *ibid*, pp 265-273.

1f. C. M. Fowler, et al., Pulse Transformer Operation in Megagauss Fields, *ibid*, pp 275-285.

1g. E. I. Bitshenkov, et al., Investigation of Capabilities of Magneto - Cumulative Megagauss Magnetic Field Generation, *ibid*, pp 471-477.

1h. A. I. Pavlovskii, et al., Magnetic Cumulation Generator Parameters and Means to Improve Them, *ibid*, pp 557-583.

1i. A. I. Pavlovskii, et al., A Multiwire Helical Magnetic Cumulation Generator, *ibid*, pp 585-593.

1j. A. I. Pavlovskii, et al., Formation and Transmission of Magnetic Cumulation Generators Electromagnetic Energy Pulses, *ibid*, pp 595-609.

1k. A. I. Pavlovskii, et al., Transformer Energy Output Magnetic Cumulation Generators, *ibid*, pp 611-626.

1l. B. D. Khristoforov, et al., Experimental Research on Explosive -Driven Magnetic Generator Performance with Resistive-inductive Load, *ibid*, pp 527-532

1m. D. L. Smith, R. P. Henderson, and R. E. Reinovsky, Inductively Driven Imploding Plasma System of X-Ray Generation, *ibid*, pp 337-349.

2. C. M. Fowler, et al., An Introduction to Explosive Magnetic Flux Compression Generators, LA-5890-MS, NTIS (1975).

3. J. C. Crawford and R. A. Damerow, Explosively Driven High-Energy Generators, J. App. Phys., Vol. 39, No. 11, pp 5224-5231 (October 1968).

4. J. W. Shearer, et al., Explosively - Driven Magnetic - Field Compression Generators, J. App. Phys., Vol. 39, No. 4, pp 2102-2116 (March 1968).
5. D. B. Cummings, Cascading Explosive Generators with Autotransformer Coupling, J. App. Phys., Vol. 40, No. 10, pp 4146-4150 (September 1969).
6. J. E. Kennedy, Gurney Energy of Explosives: Estimation of the Velocity and Impulse Imparted to Driven Metal, Sandia Laboratories Report SC-RR- 70-790, (December 1970).
7. R. I. Butler and B. W. Duggin, Explosive Generator Development for the SHIVA Program, SAND 75-0562, NTIS, (January 1976).
8. R. S. Caird, SHIVA Explosives Generator Development, LASL Report M-6-35 (Technical Progress Report, R-087) (September 1973).
9. R. S. Caird and P. J. Turchi, Use of High Energy, Short Pulse Explosive Generators to Drive Electromagnetic Implosions, AFWL-TR-74-222 (Originally LASL Report M-6-36) (April 1975).
10. R. S. Caird, SHIVA Explosives Generator Development, LASL Report M-6-42 (November 1973).
11. R. S. Caird, et al., Explosive Generators for SHIVA, LASL Report M-6-121 (July 1975).
12. C. M. Fowler, et al., Explosive Generators for SHIVA, LASL Report M-6-122 (July 1975).
13. R. S. Caird, et al., Explosive Generators for SHIVA, LASL Report M-6-155 (February 1976).
14. R. I. Butler to W. Baker, Private Communication March 28, 1975.
15. C. M. Fowler, Private Communication.
16. R. E. Reinovsky and D. L. Smith, Fuse Switches for High Current Inductive Pulse Compression Systems, Final Report on Workshop on Repetitive Opening Switches, Texas Tech University, January 28-30, 1981, pp 259-268.

REFERENCES: TASK B, HUMAN FACTORS

1. Year Book of Labour Statistics, 1980, International Labour Office, Geneva (1980).
2. Demographic Yearbook 1978, United Nations, NY (1979).
3. M.K. Strickler (FAA, Washington, D.C.) and J.J. Eggspuehler (Ohio State University), AIAA Student Journal, vol. 12, Winter 1974-75, pp. 8-12.
4. D.S. Ricketson, W.R. Brown and I.N. Graham (U.S. Army Agency for Aviation Safety), Aviation, Space, and Environmental Medicine, vol. 51, September 1980, pp. 1036-1042.
5. J.G. Kemeny, et. al., Report of the President's Commission on the Accident at Three Mile Island--The Need for Change: The Legacy of TMI, GPO, October 1979.
6. E.W. Hagen and G.T. Mays, Nuclear Safety, vol. 22, No. 3, pp. 337-346, May-June 1981.
7. Science News, vol. 120, p. 23, July 11, 1981.
8. E.L. Wiener, Proceedings of the 19th Annual Meeting of the Human Factors Society, Dallas, Texas, 1975, pp. 95-101.
9. S.J. Gerathwohl, Revue de Medecine Aeronautique et Spatiale, vol. 13, 1st Quarter, 1974, pp. 76-80.
10. Japan Statistical Yearbook, 1968.
11. Handbook of Labor Statistics 1969, U.S. Department of Labor, Bureau of Labor Statistics, Bulletin 1630, July 1969.
12. R.E. Caves and M. Uekusa, Industrial Organization in Japan, The Brookings Institute (1976).
13. Occupational Injuries and Illnesses in 1979: Summary, U.S. Department of Labor, Bureau of Labor Statistics, Bulletin 2097, April 1981.
14. Suggested by A.D. Swain, private communication.
15. Christian Science Monitor, July 23, 1981, pp. 12-13.
16. Occupational Injuries and Illnesses in the United States by Industry, 1978, U.S. Department of Labor, Bureau of Labor Statistics, Bulletin 2078, August 1980.
17. Private communication, John Ingano, Bureau of Labor Statistics, Washington, D.C.
18. Handbook of Labor Statistics 1978, U.S. Department of Labor, Bureau of Labor Statistics, Bulletin.

19. R.R. Rehder, "What American and Japanese Managers are Learning From Each Other", Business Horizons, No. 81212, pp. 63-70, March 1981.
20. Private communication, Dr. Robert R. Rehder, Professor, Robert O. Anderson Graduate School of Management, The University of New Mexico.
21. S.P. Sethi, Japanese Business and Social Conflict, Ballinger Publishing Co. (1975).
22. T.P. Rohlen, For Harmony and Strength: Japanese White-Collar Organization in Anthropological Perspective, U. Calif. Press (1974).
23. Y. Tsurumi, Japanese Business: A Research Guide with Annotated Bibliography, Praeger Publishers (1978).
24. A.D. Swain, Handbook of Human Reliability Analysis with Emphasis on Nuclear Power, NUREG-CR-1278, October 1980.
25. N.V. Krylova, Institute of Psychology, Moscow, reported at the 29th Congress of the International Astronautical Foundation, at Dubrovnik, Yugoslavia, October 1978.
26. R.L. Jacks, Flying Safety, March 1981, pp. 22-24.
27. Flying Safety, June 1981, pp. 25-27.
28. "Human Factors Associated with Altitude Alert Systems", NASA Aviation Safety Reporting System, Quarterly Report No. 6, pp. 25-37, July 1978. (NASA TM 78511).
29. Code of Federal Regulations, Title 14, Part 61.58.
30. Code of Federal Regulations, Title 14, Part 65.
31. Private communication, J.R. Buchanan, Nuclear Safety Information Center.
32. A. Cohen, M. Smith, and H.H. Cohen, Safety Program Practices in High Versus Low Accident Rate Companies--An Interim Report (Questionnaire Phase), U.S. Department of Health, Education, and Welfare, GPO, June 1975.
33. R. Cleveland, H.H. Cohen, M.J. Smith, and A. Cohen, Safety Program Practices in Record-Holding Plants, U.S. Department of Health, Education, and Welfare, DHEW (NIOSH) Publication No. 79-136, March 1979.

APPENDIX: INSPECTIONS IMPACT ON SAFETY, A STUDY OUTLINE.

As pointed out in the text, Section B-V, inspections have both positive and negative impacts. The study proposed here is not to balance the positive against the negative, or to evaluate the worthiness or need of inspections. The purpose is to examine the process with the objective of proposing changes which may improve inspections in regard to promoting safety.

The objectives of the inspection should be identified. Is the inspection the best vehicle for accomplishing these objectives? Are there other means of accomplishing these objectives? Are there safety implications in the procedure used?

Some possible objectives of inspections are:

Objectives of those instituting inspection.

1. Evaluation: performance, management, training, equipment, etc.
2. Control: a means of administrative control of performance, procedures, etc.
3. Training: a practice and demonstration of operations.
4. Maximize positive performance.
5. Identify corrective actions needed.
6. Identify and reward superior performance.

Objectives of those being inspected.

1. All or several of the above.
2. Measure self-performance.
3. Leverage to get changes, equipment.
4. Competitive, with other units.
5. Minimize interruption of on-going function.

Objectives of those doing the inspecting.

1. To do a superior, complete job.
2. To report completely, positively and/or negatively.

Types of inspections cover a broad spectrum. The Nuclear Regulatory Commission in particular has utilized a variety of inspections. A study of the impact on safety would be informative.

Inspections may be unannounced, announced and on a regular or periodic schedule, or may be announced on an irregular schedule.

The scope of the inspections also may vary greatly, including:

1. General, comprehensive.
2. Specific, limited to certain operations, phases of activities, or particular equipment.
3. Audit, a check of records, record keeping, and special materials; may be general or specific.
4. Observation and/or review of operations. May be general, specific, or of specified or requested operations.

In the evaluation of inspections in regard to effect on safety, some of the areas to be looked at are:

1. Effect on operations. Interruption of routine; possible delays in normal mission schedule; pre- and post-inspection effects, performance, etc.
2. Accomplishment of objectives of the inspection.
3. Performance of inspection. Completeness, fairness, accuracy, interaction with the operation being inspected.
4. Criteria used in judging. Is it known by all? Is it reasonable and attainable?
5. Design of inspection. Who performed by, how, who reported to, what are the feedback channels?

A search should be made for studies and evaluations of inspections and safety. Some NIOSH reports include parts on inspections and safety, but not in great depth^{32,33}.

Many operations, particularly the more hazardous ones, include inspections. Some of these operations are:

Nuclear Power Plants
Nuclear Fuel Fabrication
Nuclear Waste Processing
Chemical Explosive Manufacturing
Munitions Manufacturing
Fireworks Manufacturing
Mining
Aircraft Flight Operations
Shipping - Water

Auto Vehicle Operations

LPG and LNG

Railroad Operations

Biological and Genetic Research

Chemical Warfare

Military Maneuvers

Construction Industry

A study of inspections related to safety and impact on safety in some of these fields may be fruitful.

1981 USAF - SCEEE SUMMER FACULTY RESEARCH PROGRAM

Sponsored by the

AIR FORCE OFFICE OF SCIENTIFIC RESEARCH

Conducted by the

SOUTHEASTERN CENTER FOR ELECTRICAL ENGINEERING EDUCATION

FINAL REPORT

IMPACT OF CYLINDRICAL RODS ON RIGID BOUNDARIES

Prepared by: Dr Stanley E. Jones
Academic Rank: Associate Professor
Department and University: Department of Engineering Mechanics
University of Kentucky
Research Location: Air Force Armament Laboratory, Munitions
Division, Bombs and Warheads Branch
USAF Research Colleague: Mr William W. Dyess, Jr.
Date: July 31, 1981
Contract No.: F49620-79-C-0038

IMPACT OF CYLINDRICAL RODS ON RIGID BOUNDARIES

by

Stanley E. Jones

ABSTRACT

A new formulation of the normal rod impact problem is given. The rod is divided into two regions: that which is undergoing plastic deformation and that which is not. The material formulation in the plastic zone is discussed in detail, along with an application to the rigid/perfectly plastic rod. Conclusions and recommendations are given in the last section of the report.

Acknowledgement

The author would like to thank the Air Force Armament Laboratory for the opportunity to work and study at Eglin Air Force Base. Special thanks are due to Mr William Dyess, Jr. and Dr Joseph C. Foster, Jr. for their time and encouragement during the course of this work.

I. INTRODUCTION

The problem of describing the deformation process in a rod normally impacting a rigid boundary is relatively easy to solve if the impact velocity is low, the rod behaves elastically, and the rod aspect ratio (length/diameter) is fairly high. The problem remains tractable even when the last assumption is relaxed, provided that the first two assumptions are preserved. In fact, the solution of the thick, elastic rod was given by Pochhammer^{29*} and Chree³⁰ (see also Love²⁸) almost a hundred years ago.

The current interest in this problem centers on the range of impact speeds for which large strains are possible. In other words, suppose that the impact speed is high enough to produce permanent or plastic deformation in the rod. Now the problem becomes fairly complex and an engineering theory describing the event has not been found.

II. OBJECTIVES

The ultimate objective of this project is to develop an engineering theory to describe the process of long rod penetration into targets of various materials. The analysis presented in this report simply refers to the rod impacting a rigid boundary, a model for what has become known as the Taylor Test⁸. The philosophy behind the model is this: if an engineering theory based on the principles of mechanics can be found, which correlates well with the "Taylor Anvil Experiment," then, by suitable adjustment in the boundary conditions, the analysis can be adopted to the penetration problem. The first step toward a penetrator model is an accurate impact model. The primary objective of this report is to provide the impact model.

*Numbers in superscript refer to references found at the end of the report.

III. FORMULATION OF THE PROBLEM

Consider a rod of initial length L and radius R . Suppose that the rod impacts (normally) a rigid wall with impact speed V_0 . If V_0 is sufficiently large, then the subsequent deformation field can be divided into two separate categories: that which is undergoing plastic deformation and that which is not. Suppose that we identify the material in the plastic deformation zone by region B and the material outside of the plastic deformation zone as region A. Regions A and B are assumed to be separated by a limiting plane interface which is strictly time dependent, but in general depends on the impact speed V_0 , the material characteristics of the rod, and the rod aspect ratio (length/diameter). Let $l(t)$ locate the position of the plastic interface in the original configuration of the rod. Obviously, $l(0) = L$ and as $l(t)$ decreases, the extent of region B, the material deforming plastically, increases. The diagram below describes the situation.

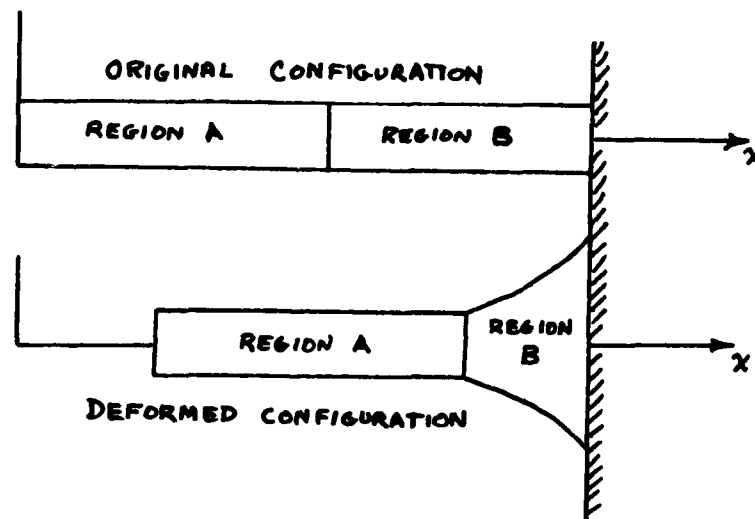


Fig. 1

The conditions which exist at the plane, plastic interface vary with the behavior assumed for region A of the rod. In general, these conditions may be described in terms of interface displacement and velocity, the conditions for strain and strain-rate, and an energy relation between the two regions. For example, if region A is assumed to behave as a rigid rod of current length $l(t)$, then the conditions at the plastic interface reduce to a displacement and velocity match, along with zero strain and strain-rate at $x=l(t)$ (measured in the original configuration of the rod). The zero strain-rate condition is equivalent to saying that the velocity gradient is zero in this case, at the rigid/plastic interface. More detail will follow the sections on analysis of the plastic deformation zone.

IV. DEFORMATION IN THE PLASTIC ZONE

In region B, the rod material undergoes plastic deformation. In general, the strains and strain rates will be very high when compared to their elastic component. It will be assumed that elastic effects are entirely negligible in the plastic deformation zone. It is further assumed that the rod impact is perfectly normal and that the impact will produce an axi-symmetric plastic deformation field. In this symmetric field, x is assumed to be the axis of the rod and r, θ the radial and circumferential positions, relative to the axis.

Under the aforementioned conditions, the strain-displacement relations become:

$$\epsilon_x = \frac{\partial u_x}{\partial x} \quad (4.1)$$

$$\epsilon_r = \frac{\partial u_r}{\partial r} \quad (4.2)$$

$$\epsilon_{\theta} = \frac{u_r}{r} \quad (4.3)$$

$$2\gamma_{rx} = 2\gamma = \frac{\partial u_r}{\partial x} + \frac{\partial u_x}{\partial r} \quad (4.4)$$

where $\epsilon_x, \epsilon_r, \epsilon_{\theta}$ are the normal strains, γ is the only nonzero shear strain and u_x, u_r are the longitudinal and radial displacement components.

The momentum balance on a material element leads to:

$$\rho \frac{\partial^2 u_x}{\partial t^2} = \frac{\partial \sigma_x}{\partial x} + \frac{\partial \tau}{\partial r} + \frac{\tau}{r} \quad (4.5)$$

$$\rho \frac{\partial^2 u_r}{\partial t^2} = \frac{\partial \tau}{\partial x} + \frac{\partial \sigma_r}{\partial r} + \frac{\sigma_r - \sigma_{\theta}}{r} \quad (4.6)$$

where ρ is the rod density (assumed constant) and $\sigma_x, \sigma_r, \sigma_{\theta}, \tau = \sigma_{rx}$ are the axial, radial, hoop and shear stress components.

Equations (4.1) - (4.6) are valid for all material states, elastic or plastic. However, they must be supplemented by a set of relations which strictly apply to plastic deformation. To make the distinction temporarily clear, all plastic deformation variables are denoted by "superscript p ." It is assumed that the following relations apply to the dynamic state of the material.

The material relation is a general work-hardening, rate-sensitive law given by

$$\bar{\sigma} = f(\bar{\epsilon}^P, \dot{\bar{\epsilon}}^P) \quad (4.7)$$

where $\bar{\sigma}$ is the measure of effective stress after yielding, $\bar{\epsilon}^P$ and $\dot{\bar{\epsilon}}^P$ are the measures of effective plastic strain and strain-rate.

The stress components are related to the effective stress (after yielding) through the Von Mises Yield Criterion (see Hill⁵; P. 20), which in this case assumes the form:

$$2\bar{\sigma}^2 = 6\tau^2 + (\sigma_r - \sigma_\theta)^2 + (\sigma_\theta - \sigma_x)^2 + (\sigma_r - \sigma_x)^2 \quad (4.8)$$

Finally, the formulation is made complete with the addition of the Lévy-Mises Flow Law (see Hill⁵; P. 38), governing the strain rates. Again, it is assumed that these relations are valid for a dynamic situation. In this case, they assume the form:

$$\dot{\epsilon}_x = (2\sigma_x - \sigma_r - \sigma_\theta) \frac{\dot{\bar{\epsilon}}^P}{2\bar{\sigma}} \quad (4.9)$$

$$\dot{\epsilon}_r = (2\sigma_r - \sigma_x - \sigma_\theta) \frac{\dot{\bar{\epsilon}}^P}{2\bar{\sigma}} \quad (4.10)$$

$$\dot{\epsilon}_\theta = (2\sigma_\theta - \sigma_x - \sigma_r) \frac{\dot{\bar{\epsilon}}^P}{2\bar{\sigma}} \quad (4.11)$$

$$\dot{\gamma}^P = \dot{\gamma}_{rx}^P = 6 \sigma_{rx} \frac{\dot{\epsilon}^P}{2\bar{\sigma}} = 3\tau \frac{\dot{\epsilon}^P}{\bar{\sigma}} \quad (4.12)$$

Inherent in equations (4.9) - (4.12) are the statement of material isotropy and incompressibility. Material isotropy can be inferred from the normality of the strain increment vector to the yield surface. Although there is disagreement on this point, there is strong evidence to support the contention that flow normality and isotropy are equivalent (Jones and Gillis²⁵). The incompressibility conclusion stems from the addition of equations (4.9), (4.10), and (4.11). Their sum delivers the relation

$$\dot{\epsilon}_x^P + \dot{\epsilon}_r^P + \dot{\epsilon}_\theta^P = 0 \quad (4.13)$$

from which it follows that the sum of the normal plastic strains is zero.

$$\epsilon_x^P + \epsilon_r^P + \epsilon_\theta^P = 0 \quad (4.14)$$

Equation (3.14) is the statement for incompressibility of the material in the plastic state.

With all plastic strain variables replaced by total strains, equations (3.1) through (3.12) form a system of twelve equations in the twelve unknown functions $\bar{\epsilon}, \epsilon_x, \epsilon_r, \epsilon_\theta, \gamma, u_x, u_r, \bar{\sigma}, \sigma_x, \sigma_r, \sigma_\theta, \tau$. In general, this system is not manageable except by numerical approximation (e.g. Chang and Horie²⁷). The next section is devoted to reduction of the system.

V. REDUCTION OF THE SYSTEM - PLANE WAVE THEORY

As pointed out at the end of section 4, the complete system of plastic deformation relations (4.1) - (4.12) offers no prospect for a solution as it stands. The system does, however, offer the basis for an engineering theory from which the relationship between key physical parameters can be determined. We begin by assuming that, in the first approximation, the axial displacement component u_x is independent of r . This means that plane cross sections remain plane and that the effects due to "warping" of the cross sections are negligible[†]. Eliminating the strains in (4.14) by means of (4.1) - (4.3), results in the fundamental relation for the Plane Wave Theory (PWT).

$$\frac{\partial u_x}{\partial x} + \frac{\partial u_r}{\partial r} + \frac{u_r}{r} = 0 \quad (5.1)$$

Since $u_r = 0$ when $r = 0$ and u_x is independent of r , integration of (5.1) gives the relationship between the radial and axial displacement components.

$$u_r = -\frac{1}{2} r \frac{\partial u_x}{\partial x} \quad (5.2)$$

Equation (5.2) indicates immediately that

$$\epsilon_r = \epsilon_\theta = -\frac{1}{2} \epsilon_x \quad (5.3)$$

which is a key conclusion of Bridgeman¹ (P. 13) in his analysis of necking in round bars under quasistatic conditions. Using (5.3) in (4.10) and (4.11) delivers another important consequence of the PWT.

$$\sigma_r = \sigma_\theta \quad (5.4)$$

[†]A second-order theory which accounts for "warping" is certainly possible, but it will not be pursued in this report.

The reader is reminded of the assumption regarding elastic strains in the plastic zone which stipulates that $\epsilon_x \approx \epsilon_x^p$, $\epsilon_r \approx \epsilon_r^p$, etc.

Again, we observe that (5.4) is one of Bridgeman's Classic Assumptions¹ (P.15).

When (5.4) is applied to the yield function (4.8), a vastly simpler expression results.

$$\bar{\sigma}^2 = 3\tau^2 + (\sigma_x - \sigma_r)^2 \quad (5.5)$$

For specimens whose aspect ratios are not too small, the term $3\tau^2$ will generally be small when compared to $(\sigma_x - \sigma_r)^2$ (see Jones, Gillis and Shalaby¹²). With this rationale, $\bar{\sigma}$ can be approximated by the dominant term in (5.5).

$$\bar{\sigma} = \sigma_x - \sigma_r \quad (5.6)$$

In the PWT, $\bar{\sigma}$ will be approximately uniform at any cross-section.

Now, the momentum equations (4.5) and (4.6) can be substantially manipulated to yield a tractable system. For convenience, these equations are given here.

$$\rho \frac{\partial^2 u_x}{\partial t^2} = \frac{\partial \sigma_x}{\partial x} + \frac{\partial \tau}{\partial r} + \frac{\tau}{r} \quad (5.7)$$

$$\rho \frac{\partial^2 u_r}{\partial t^2} = \frac{\partial \tau}{\partial x} + \frac{\partial \sigma_r}{\partial r} \quad (5.8)$$

Where the term involving $\sigma_r - \sigma_\theta$ has been neglected according to (5.4). Using (5.2) and (5.4) in (5.7) and (5.8), while treating $\bar{\sigma}$ as radially independent, allows the following two equations to be written.

$$\rho r \frac{\partial^3 u_x}{\partial x \partial t^2} = r \frac{\partial^2 \bar{\sigma}}{\partial x^2} + r \frac{\partial^2 \sigma_r}{\partial x^2} + \frac{\partial^2 (r\tau)}{\partial x \partial r} \quad (5.9)$$

$$\rho r \frac{\partial^3 u_x}{\partial x \partial t^2} = - \frac{\partial^2 (r\tau)}{\partial x \partial r} - \frac{\partial}{\partial r} \left(r \frac{\partial \sigma_r}{\partial r} \right) \quad (5.10)$$

By adding (5.9) and (5.10), an equation with no dependence on the shear stress τ results.

$$2\rho r \frac{\partial^3 u_x}{\partial x \partial t^2} = r \frac{\partial^2 \bar{\sigma}}{\partial x^2} + r \frac{\partial^2 \sigma_r}{\partial x^2} - \frac{\partial}{\partial r} \left(r \frac{\partial \sigma_r}{\partial r} \right) \quad (5.11)$$

To estimate the radial stress component, one can use (5.8), with the assumption that the shear gradient does not contribute substantially to in a first order theory. This gives the following result for σ_r :

$$\sigma_r = \sigma_{r0} - \frac{\rho r^2}{4} \frac{\partial^3 u_x}{\partial x \partial t^2} \quad (5.12)$$

where σ_{r0} is the value of σ_r at $r = 0$. This function can be determined from the free boundary condition at the rod radius $r = R$, i.e.

$$\sigma_{r0} = \frac{\rho R^2}{4} \frac{\partial^3 u_x}{\partial x \partial t^2} \quad (5.13)$$

Now, using (5.12) and (5.13) to eliminate σ_r from (5.11) yields the fundamental effective stress and axial displacement relation.

$$\rho \frac{\partial^3 u_x}{\partial x \partial t^2} = \frac{\partial^2 \bar{\sigma}}{\partial x^2} + \frac{\rho R^2}{4} \frac{\partial^5 u_x}{\partial x^3 \partial t^2} - \frac{\rho r^2}{4} \frac{\partial^5 u_x}{\partial x^3 \partial t^2} \quad (5.14)$$

Quite obviously, the last term in (5.14) is r dependent while all others in the equation are independent of r . It is apparent that this term corresponds to some higher order approximation. It could be neglected entirely. However, a better approach would be to incorporate it into the analysis by averaging with respect to r over each cross section. The result is:

$$\rho \frac{\partial^3 u_x}{\partial x \partial t^2} = \frac{\partial^2 \bar{\sigma}}{\partial x^2} + \frac{\rho R^2}{8} \frac{\partial^5 u_x}{\partial x^3 \partial t^2} \quad (5.15)$$

Without loss, (5.15) can be integrated once with respect to x and the arbitrary time function discarded to achieve the final stress/displacement relation.

$$\rho \frac{\partial^2 u_x}{\partial t^2} = \frac{\partial \bar{\sigma}}{\partial x} + \frac{\rho R^2}{8} \frac{\partial^4 u_x}{\partial x^2 \partial t^2} \quad (5.16)$$

This is the result of Kolsky and Douch¹⁰ in 1962. They indicate that Love²⁸ has also used (5.16) to as a fundamental relationship for elastic rods.

Equation (5.16) connects the axial displacement to the effective stress, including some lateral inertia effects. As the rod radius R tends to zero, it can be observed that the one-dimensional momentum equation is recovered. The effect due to rod thickness is solely represented by the last term of equation (5.16), in this analysis.

In order to complete the PWT, one must observe that a reasonable consequence of uniform effective stress at each cross section in the plastic zone is also uniform strain and strain-rate. The formulation is then complete if

$$\bar{\epsilon} = \bar{\epsilon}^P = \frac{\partial u_x}{\partial x} \quad \left(\dot{\bar{\epsilon}} = \dot{\bar{\epsilon}}^P = \frac{\partial^2 u_x}{\partial x \partial t} \right) \quad (5.17)$$

and (4.7) is used to connect $\bar{\sigma}$ and $\bar{\epsilon}$. For then, (5.16), (5.17) and (4.7) constitute a system of three equations in the three unknown functions u_x , $\bar{\sigma}$ and $\bar{\epsilon}$. This system, along with the boundary conditions mentioned in section 3, comprize the basis for solution of impact problems by the PWT.

VI. THE RIGID/PERFECTLY PLASTIC ROD

In the rigid/perfectly plastic rod, it is assumed that the effective stress gradient in the plastic zone is zero, i. e. the material constitutive law has a graph of the form shown below (Fig 2).

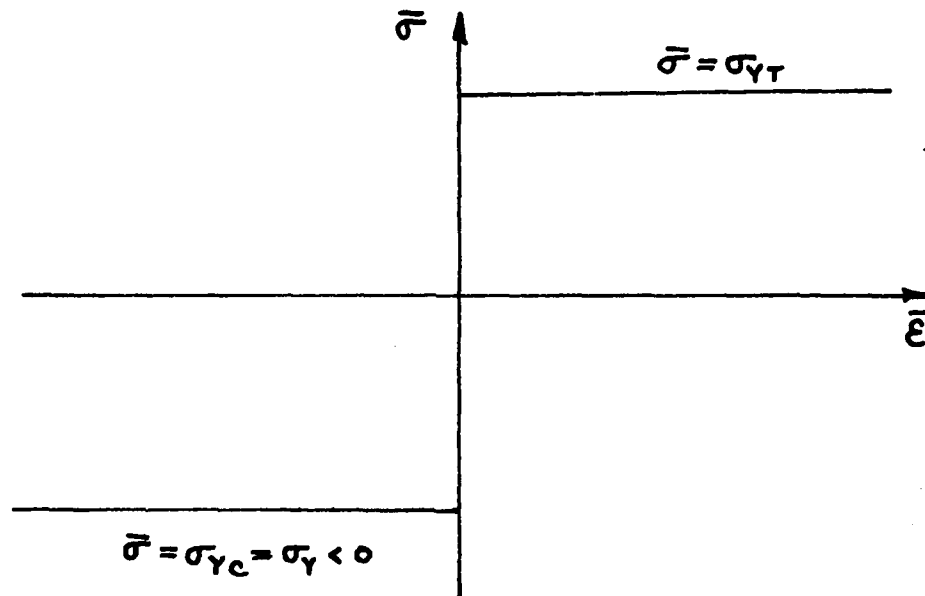


Fig. 2

σ_{YT} is the yield stress in tension and $\sigma_{YC} = \sigma_Y$ is the yield stress in compression. Although σ_{YT} and σ_{YC} are assumed to be constants, they may be velocity dependent.

Such an ideal material response model can often be used to qualify the critical parameters in the deformation process. In this case, the fact that $\bar{\sigma} = \sigma_{YC} = \sigma_Y$ throughout the plastic zone, leads to the important conclusion that

$$\frac{\partial \bar{\sigma}}{\partial x} = 0 \quad (6.1)$$

in equation (5.16). This greatly reduces the complexity of (5.16) and allows the fundamental equation governing axial displacement to assume the form:

$$\frac{\partial^2 u_x}{\partial t^2} = \frac{R^2}{8} \frac{\partial^4 u_x}{\partial x^2 \partial t^2} \quad (6.2)$$

Equation (6.2) is to be solved subject to the boundary conditions at the rigid wall $x=L$ and at the rigid/plastic interface $l(t)$. At the rigid boundary $x=L$, quite obviously, there should be no axial displacement and the axial velocity component should be zero. These conditions are expressed as:

$$u_x = 0 \quad \text{and} \quad \frac{\partial u_x}{\partial t} = 0 \quad \text{when} \quad x = L \quad (6.3)$$

At the rigid/plastic interface $x=l(t)$, the conditions of zero effective strain and strain-rate must be met. These two conditions are expressed as:

$$\frac{\partial u_x}{\partial x} = 0 \quad \text{and} \quad \frac{\partial^2 u_x}{\partial x \partial t} = 0 \quad \text{when} \quad x = l(t) \quad (6.4)$$

Now, the remaining interface conditions are not so apparent as (6.3) and (6.4). They must be determined from the Equation of Motion for the rigid section of the rod, region A, and the restrictions on the available energy in the system.

The current state of the rigid rod section can be determined from a free body diagram. The impulse-momentum equation is:

$$\frac{d}{dt} (\rho \pi R^2 l(t) V_B) = \pi R^2 \sigma_Y \quad (6.5)$$

Where V_B is the current velocity for the rigid rod section, ρ is the rod density, and $\sigma_Y = \sigma_{Yc} < 0$ is the compressive yield stress for the impact velocity V_0 . Equation (6.6) can be integrated to give the velocity-length relationship:

$$\int l(t) V_B = \sigma_Y t + \rho L V_0 \quad (6.6)$$

where $l(0) = L$ and $V_B(0) = V_0$. Note that (6.6) offers a time limitation on the event $0 \leq t \leq t_f = -\frac{\rho L V_0}{\sigma_Y}$. If x_B denotes the displacement of the back end of the rod, then

$$\frac{dx_B}{dt} = V_B \quad (6.7)$$

and

$$x_B = \int_0^t \frac{\sigma_Y t + \rho L V_0}{\rho l(t)} dt \quad (6.8)$$

determines the current displacement of all cross-sections of the rigid rod section. If the conditions for velocity and displacement at the rigid/plastic interface are to agree with (6.6) and (6.8), then it follows that

$$u_x = x_B \text{ and } \frac{\partial u_x}{\partial t} = v_B \text{ when } x = l(t) \quad (6.9)$$

The formulation is not complete with only the boundary conditions (6.3), (6.4) and (6.9). It should be pointed out that the six conditions expressed through (6.3), (6.4) and (6.9) are not independent. In fact, only four of the six boundary conditions are independent. The general solution to (6.2) involves four arbitrary functions. Since, only four independent boundary conditions have been determined, the motion of the free boundary $l(t)$ cannot be evaluated, in addition to the general solution of (6.2). This situation can be resolved with the addition of an available energy restriction.** At any time, the total energy in the system must equal the kinetic energy of the rod on impact. The relation expressing this fact is:

$$\underbrace{\frac{1}{2} \rho \pi R^2 L v_0^2}_{\text{TOTAL ENERGY}} = \underbrace{\frac{1}{2} \rho \pi R^2 l v_B^2}_{\text{KINETIC ENERGY of the RIGID Rod Section}} + \underbrace{\int_{V_P} \int_0^{\bar{E}} \bar{\sigma} d\bar{E} dV}_{\text{PLASTIC WORK}} + \underbrace{\frac{1}{2} \rho \int_{V_P} (v_r^2 + v_x^2) dV}_{\text{KINETIC ENERGY of the PLASTIC MATERIAL}} \quad (6.10)$$

where $v_r = \frac{\partial u_r}{\partial t}$ and $v_x = \frac{\partial u_x}{\partial t}$ are the velocity components in the plastic zone in the radial and axial directions and V_P is the current volume of the plastic zone. For the perfectly plastic material, the plastic work term can be easily reduced.

$$\int_{V_P} \int_0^{\bar{E}} \bar{\sigma} d\bar{E} dV = -\pi R^2 \sigma_Y u_x(l, t) \quad (6.11)$$

** The author is indebted to Dr Joseph C. Foster, Jr. for this observation and the subsequent energy equation.

Replacing the plastic work term in (6.10) by its equivalent (6.11), yields the energy expression:

$$\frac{1}{2} \rho \pi R^2 L V_0^2 = \frac{1}{2} \rho \pi R^2 l V_B^2 - \pi R^2 \sigma_Y u_x(l, t) + \frac{1}{2} \rho \int_{V_p} (v_r^2 + v_z^2) dV \quad (6.12)$$

This result compares with that given by Wilkins and Guinan¹¹ for the final displacement of the rigid rod section. To see this, set $t = t_f$ and observe that all time dependent terms are zero. Thus,

$$u_x(l, t_f) = - \frac{\rho L V_0^2}{2 \sigma_Y} = X_R(t_f) \quad (6.13)$$

which estimates the terminal position of the rigid rod section. If the true strain measure (logarithmic) for axial strain is used, then (6.13) will be precisely the result of Wilkins and Guinan.¹¹

The addition of (6.12) completes the formulation. Equation (6.2) is to be solved subject to (6.3), (6.4), (6.9) and (6.12). Displacements in the plastic zone, as well as the motion of the plastic interface $l(t)$, are determined in the final result.

One of the fortunate aspects of the perfectly plastic material model is that the general solution of (6.2) is available:

$$u_x = C_1(t) e^{\frac{\sqrt{R} x}{R}} + C_2(t) e^{-\frac{\sqrt{R} x}{R}} + a(x) t + b(x) \quad (6.14)$$

In equation (6.14), $C_1(t)$ and $C_2(t)$ are arbitrary functions of time, while $a(x)$ and $b(x)$ are arbitrary functions of x . These four functions, along with $l(t)$, are to be determined from the boundary conditions (6.3), (6.4), and (6.9) and (6.12). There are precisely enough conditions to evaluate the five functions in question. The details will be given in another report.

VII. CONCLUSIONS AND RECOMMENDATIONS

The formulation of the problem given in sections 3-5 offers versatility and promise for solutions not achieved to date. There is really no question that the application presented in section 6 will be completed. Only the restriction of time prevented that work from being included in this report. So, the prospect of giving solutions to the rod impact problem in terms of material strength parameters, impact speed, and lateral inertia effects appears to be excellent. The author recommends that the formulation be used for the following:

- (i) completion of the application to the rigid/perfectly plastic rod in section VI.
- (ii) a study of the effects of work hardening and rate sensitivity on the plastic deformation field.
- (iii) development of numerical techniques for the solution of free boundary (plastic interface) problems for some sophisticated material models.
- (iv) modification of the boundary conditions at the rigid boundary to accommodate the rod as a penetrator.
- (v) development of numerical techniques for the solution of the free boundary/target penetration problem.

REFERENCES

1. P. W. Bridgman, Studies in Large Plastic Flow and Fracture, McGraw-Hill, New York (1952).
2. A. Nadai, Theory of Flow and Fracture of Solids, McGraw-Hill, New York (1950).
3. N. Cristescu, Dynamic Plasticity, North-Holland, Amsterdam (1967).
4. H. J. Plass, Jr., "A Theory of Longitudinal Plastic Waves in Rods of Strain-Rate Dependent Material, Including Effects of Lateral Inertia and Shear," Plasticity, Proc. 2nd Symp. on Naval Structural Mechanics, (E. H. Lee and P. S. Symonds, eds.), Pergamon, New York (1960).
5. R. Hill, The Mathematical Theory of Plasticity Clarendon Press, Oxford (1971).
6. J. S. Rinehart and J. Pearson, Behavior of Metals under Impulsive Loads, Dover Publications, New York (1965).
7. F. Helie, "Traite de Balistique Experimentale," Dumaine, Paris (1884).
8. G. I. Taylor, "The Use of Flat-Ended Projectiles for Determining Dynamic Yield Stress," Proc. R. Soc. A, Vol 194, P. 289 (1948).
9. T. Von Karman and P. Dunez, "The Propagation of Plastic Deformation in Solids," J. Appl. Phys. Vol. 21, P. 987 (1950).
10. H. Kolsky and L. S. Douch, "Experimental Studies in Plastic Wave Propagation," J. Mech. Phys. Solids, Vol. 10, PP. 195-223 (1962).

11. M. L. Wilkins and M. W. Guinan, "Impact of Cylinders on a Rigid Boundary," J. Appl. Phys. Vol. 44, No. 3, PP. 1200-1206 (1973).
12. S. E. Jones, P. P. Gillis and A. H. Shalaby, "Stress Distributions in the Vicinity of a Neck," J. Appl. Phys. Vol. 50, No. 5, PP. 3168-3173 (1979).
13. L. E. Malvern, "Plastic Wave Propagation in a Bar of Material Exhibiting a Strain Rate Effect," Quarterly of Appl. Math. Vol. 8, PP. 405-411 (1951).
14. H. Kolsky, Stress Waves in Solids, Dover Publications, New York.
15. J. N. Goodier and P. G. Hodge, Jr., Elastic and Plasticity, Wiley, New York (1958).
16. E. R. Wood and A. Phillips, "On the Theory of Plastic Wave Propagation in a Bar," J. Mech. Phys. Solids Vol. 15, PP. 241-254 (1967).
17. A. Tate, "A Theory for the Deceleration of Long Rods after Impact," J. Mech. Phys. Solids Vol. 15, PP. 387-399 (1967).
18. A. Tate, "Further Results in the Theory of Long Rod Penetration," J. Mech. Phys. of Solids, Vol. 17, PP. 141-150 (1969).
19. A. Tate, "A Simple Hydrodynamic Model for the Strain Field Produced in a Target by the Penetration of a High Speed Long Rod Projectile," Int. J. Eng. Sci. Vol. 16, PP. 845-858 (1978).
20. R. F. Recht, "Taylor Ballistic Impact Modelling Applied to Deformation and Mass Loss Determinations," Int. J. Eng. Sci.
21. G. I. Barenblatt, Similarity, Self-Similarity, and Intermediate Asymptotics Consultants Bureau, New York (1979).

22. F. G. Tricomi, Integral Equations Interscience, New York (1957).
23. T. C. T. Ting and P. S. Symonds, "Longitudinal Impact on Viscoplastic Rods - Linear Stress - Strain Law," J. Appl. Mech., Vol. 31, PP. 199-207 (1964).
24. T. C. T. Ting and P. S. Symonds, "Impact on Rods of Non-Linear Viscoplastic Material - Numerical and Approximate Solutions," Int. J. Solids Structures, Vol. 3, PP. 587 - 605 (1967).
25. S. E. Jones and P. P. Gillis, "A Generalized Quadratic Flow Law for Sheet Metals" (submitted for publication).
26. W. A. Allen and J. W. Rogers, J. Franklin Inst. , 272, P. 275 (1961).
27. H. L. Chang and Y. Horie, "Two-Dimensional Stress Waves Resulting from Axisymmetric Impact of Finite-Length Rods," Technical Report AD-754 119, Nat. Tech. Info. Serv., U. S. Dept. of Commerce (1973).
28. A. E. H. Love, The Mathematical Theory of Elasticity Cambridge University Press (1927).
29. L. Pochhammer, J. Reine Angew. Math. (Crelle) 81, 324 (1876).
30. C. Chree, Trans. Camb. Phil. Soc. 14, 250 (1889).

1981 USAF - SCEEE SUMMER FACULTY RESEARCH PROGRAM

Sponsored by the

Air Force Office of Scientific Research

Conducted by the

Southeastern Center for Electrical Engineering Education

FINAL REPORT

An Information-Theoretic Approach
To Target Estimation of a Conical Scan Controlled
Laser Radar Tracking System

Prepared by: Dr. Paul Kalata
Department and University: Dept. of Electrical and Computer Engineering
Research Location: Weapons Laboratory - Kirtland AFB, NM 87117
Contract Number: F49620-C-79-0038

An Information-Theoretic Approach To Target Estimation
of a Conical Scan Controlled Laser Radar Tracking System

by:

Dr. Paul Kalata

ABSTRACT

High energy laser systems with highly accurate measurements as target tracking sensors use a conical scan process to obtain a target capture and tracking within the narrow beamwidth. This searching process and the target tracking algorithm are major factors in the performance of the laser radar/target tracking system. The summer research results presented in this paper use information-theoretic concepts in establishing laser radar/target tracking performance bound independent of the filtering algorithm. A computer program was developed to calculate the lower bound of the estimation error variation due to a dithered signal, non-linear gaussian glint measurement process.

Acknowledgements

This work was funded by the Air Force Summer Faculty Research Program (SFRP), administered by the Southeastern Center for Electrical Engineering Education (SCEEE) under contract F49620-79-C-0038.

An Information-Theoretic Approach
To Target Estimation of a Conical Scan Controlled
Laser Radar Tracking System

Dr. Paul R. Kalata
Department of Electrical and Computer Engineering
Drexel University
Philadelphia, Pennsylvania
19104

Abstract

High energy laser systems with highly accurate measurements as target tracking sensors use a conical scan process to obtain a target capture and tracking within the narrow beamwidth. This searching process and the target tracking algorithm are major factors in the performance of the laser radar/target tracking system. The summer research results presented in this paper use information-theoretic concepts in establishing laser radar/target tracking performance bound independent of the filtering algorithm. A computer program was developed to calculate the lower bound of the estimation error variation due to a dithered signal, non-linear gaussian glint measurement process.

I. Introduction

A. Radar/Target Tracking Process

Conical beam scanning for target capture and tracking is a common procedure used in microwave radar systems [1,2]. The conical scan process, with appropriate system modifications, can also be used in laser radar systems [3]. With the near-ultimate limit in measurement accuracy obtainable with the laser, tracking system performance in terms of beam steering variations or jitter should be correspondingly achievable. Microwave and laser based radar/target tracking systems illustrated by Figure 1 operate in similar ways.

The sequence of events for an active tracking process is:

- i) The transmitter directs a signal in space which reflects off the target.
- ii) The receiver senses the return, correlates it with the transmitted signal and generates track measurements.

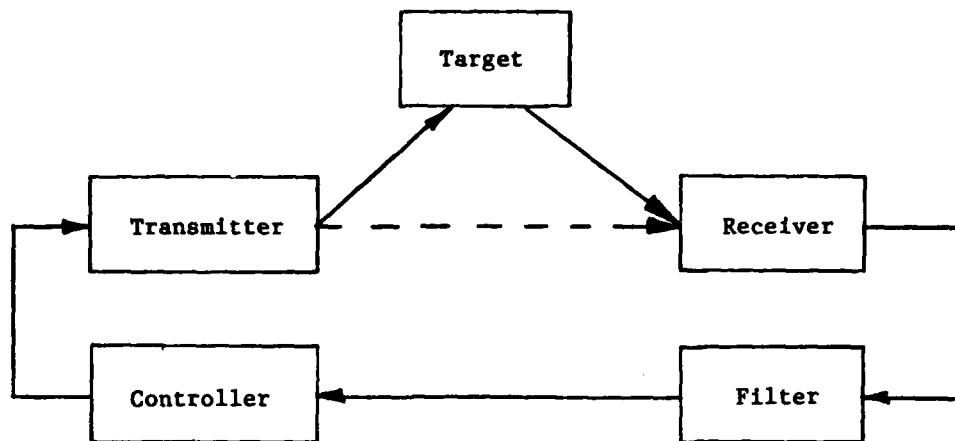


Figure 1: Basic Elements of a Radar/Target Tracking System

- iii) The measurements are then passed through a filter, producing track estimates and the controller predicts the target's position for the next sequence and steers the beam accordingly.

The successful operation of a tracking system is obviously dependent on the ability of its hardware to secure track measurements and has a key role in determining tracking parameters and the entire system performance. The measurement accuracy is also involved in determining the optimal filtering parameters as well as the resulting radar/target tracking system performance. Although laser radar measurements are extremely accurate, the small beamwidth makes target capture difficult. The search necessary to secure a laser radar measurement is the key process in the laser radar operation.

B. Statement of the Problem

The objective of the laser radar beam steering controller is to quickly capture the target with minimal fluctuations or jitter. One source of jitter is due to the resulting noise within the target estimation process, and there is a natural limit to what filtering can do to minimizing this jitter component. The summer research effort was to investigate this limit through the information-theoretic approach. To this end, the problem can be stated:

Given a laser/target tracking system with a conical scan, dithered measurement process, evaluate the information-theoretic estimation lower performance bound of the system.

Once the problem is information-theoretically cast and bounds established, many useful results can be obtained such as:

1. compare present tracking performance to its theoretical limit,
2. determine the tracking parameters which will improve the theoretical performance limit, and
3. compare the resulting error variance performance of an "optimal" filtering algorithm to its theoretical limit.

C. Information-Theoretic Performance Bound

The method which will be used to establish the laser radar/target tracking performance bound will be the use of Information Theory. The original use of Information Theory was to establish a performance bound on communication systems with minimal analysis [4]. The derived communication performance bound is independent of the implemented encoding/decoding process and simply states that reliable communication is possible if the transmission rate R is less than the channel capacity C , i.e., $R < C$, a function of the system.

Recently, Information Theory was shown to be useful in establishing performance bounds for the general estimation problem [5,6] in that the estimation error entropy $H(\tilde{x})$ is bounded by the system equivocation $H(x|z)$ with conditional probability density function $p(x|z)$, i.e.,

$$H(\tilde{x}) > H(x|z) \triangleq E(-\ln(p(x|z)))$$

which is only a function of the system and independent of the implemented estimation process. Based on the error entropy criterion, various estimation techniques, including non-linear non-gaussian estimation [7], system identification [8], and prediction, filtering, and smoothing [6,9] have not only complimented modern mean-square-error results, but also provided specific performance bounds for estimation convergence. As a by-product of the information-theoretic analysis of the estimation problem, an important design concept was derived in that a mean-square-error (MSE) estimate is a minimax error entropy estimate, i.e.

$$\min \max H(\tilde{x}) \Leftrightarrow \min ||V(\tilde{x})||.$$

For the normal estimation problem, the derived optimal error entropy estimation process is the Kalman filter and the error covariance matrix is identical to the system conditional covariance matrix, i.e.,

$$V(\tilde{x}) = V(x|z).$$

II. Laser/Target Tracking System Model

A. Mathematical Model

In general, non-linear stochastic systems can be modeled by continuous time differential vector state equations

$$\dot{x}(t) = f(t, x, w, u) \quad (1)$$

$$z(t) = g(t, x, n, u) \quad (2)$$

where

$x(t)$ is an n -dimensional state vector,
 $z(t)$ is the m -dimensional measurement vector,
 $u(t)$ is the p -dimensional input control vector,
 $w(t)$ is the q -dimensional system noise vector, and
 $n(t)$ is the r -dimensional measurement noise vector.

For a radar/target tracking system, the vector system function $f(\cdot)$ would include and describe both the target as well as the beam steering dynamics. The

vector function $g(\cdot)$ describes how the physical state vector x is being observed. Figure 2 illustrates the conical scan dithered stochastic control [10] for one angle of the laser radar system.

1. Glint Measurement Process

The glint measurement process can be modeled by the deterministic gaussian function

$$z(t) = I_0 \exp(-y^2/2\sigma^2) + n(t) \quad (3)$$

where $y(t)$ is the target/beam center angular error,
 σ is a parameter of the glint return,
 I_0 is the reflected intensity for zero error, and
 $n(t)$ a zero mean white noise process with variance σ_n^2 .

2. Conical Scan, Dither Control

To achieve a target capture, the laser beam conically scans space and obtains target/beam boresighting [3] using a returned energy increasing controller. To generate target tracking measurements, the beam center is nutated and the returned signal is correlated with that transmitted.

Of particular interest is the applied dither signal in the beam control resulting in a target angular error

$$y(t) = x + X_b + A \sin(\omega t) \quad (4)$$

where x is the reference angle uncertainty of the target,
 X_b is the beam center offset bias of the glint measurement process, and
 $A \sin(\omega t)$ is the supplied dither signal.

Illustrated by Figure 2 is the dither signal applied to the beam, the glint measurement, and the target correlation and filtering processes.

E. Estimation Error Lower Bound

The estimation process uses the measurements $z(t)$ to reconstruct the state vector by an estimate $\hat{x}(t|t)$ i.e.,

$$\hat{x}(t|t) = \hat{x}(t, z(t))$$

and a measure of the estimation accuracy is given by some norm of the error

$$\tilde{x}(t|t) = x(t) - \hat{x}(t|t)$$

such as the mean-square error MSE measure

$$e(t) = E(x(t|\tilde{t}) \tilde{x}'(t|t)).$$

For the scalar system, the continuous time error entropy lower bound is the system equivocation [5,6,11]

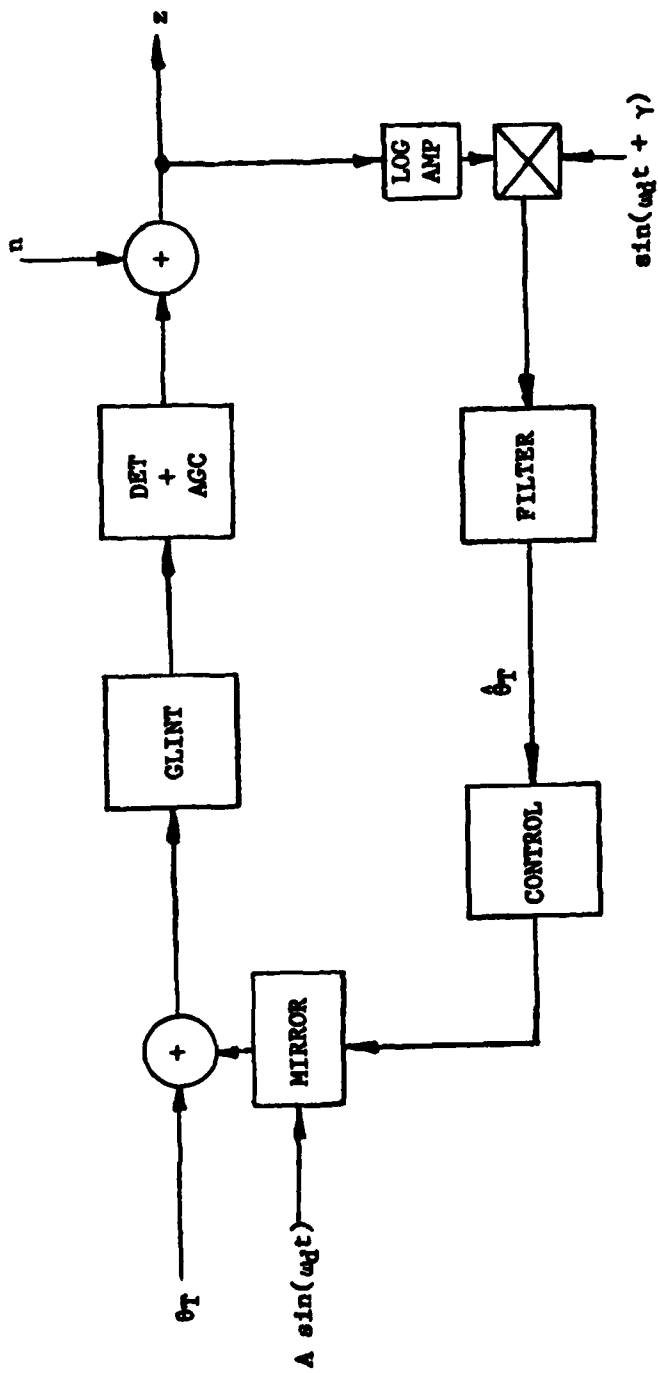


Figure 2: Conical Scan, Dithered Radar/Target Tracking Stochastic Control System

$$H(\tilde{x}(t)) > H(x(t)|z).$$

The error variance/entropy inequality [6] is given by

$$1/2 \ln(2\pi e \sigma_{\tilde{x}}^2) > H(\tilde{x})$$

which results in the error variance lower bound

$$\sigma_{\tilde{x}}^2 > \frac{1}{2\pi e} \exp(2H(x|z)). \quad (5)$$

Using information-theoretic relationships [6], the system equivocation can be expressed as

$$\begin{aligned} H(x|z) &= H(x) - I(x; z) \\ &= H(x) - H(z) + H(z|x) \end{aligned} \quad (6)$$

and substituting the above into Eq. (4) yields

$$\sigma_{\tilde{x}}^2 > \frac{1}{2\pi e} \exp(2H(x)) \exp(2H(z|x)) / \exp(2H(z)).$$

The conditional entropy $H(z|x)$ can be bounded from below [12] by

$$H(z|x) > N_1(t) = 1/2 \int_0^t E(g^2(\tau)/\sigma_n^2) d\tau \quad (7)$$

and the entropy $H(z)$ is bounded from above by

$$H(z) < N_2(t) = \sum_{r=0,2,\dots}^{\infty} \sum_{n=r}^{\infty} \frac{t^{k-1}}{(r/2)!(n-r)!2^k} \int_0^t E(g^2(\tau)/\sigma_n^2)^k d\tau \quad (8)$$

where $k = n-r/2$ and the error variance lower bound becomes

$$\sigma_{\tilde{x}}^2 > \frac{1}{2\pi e} \exp(2H(x)) \exp(2N_1(t)) / \exp(2N_2(t)). \quad (9)$$

For the glint measurement process with a gaussian distribution for the unknown angle x , Eq. (7) becomes

$$N_1(t) = \frac{1}{2} \int_0^t \int_{-\infty}^{\infty} \frac{1}{\sqrt{2\pi}\sigma_x} \exp(-x^2/2\sigma_x^2) dx \frac{I_0}{\sigma_n^2} \exp(-y^2/\sigma^2) d\tau. \quad (10)$$

With the biased dither of Eq. (4), Eq. (10) can be rewritten as

$$\begin{aligned} N_1(t) &= \frac{1}{2} \frac{1}{\sqrt{2\pi}} \frac{I_0}{\sigma_n^2} \int_0^t \exp(-(X_b + A \sin(\omega\tau))^2 / (2\sigma_x^2 + \sigma^2)) d\tau \\ &\quad \cdot \int_{-\infty}^{\infty} \exp(-(x-a)^2 / 2\sigma_b^2) dx \end{aligned}$$

where $a = 2\sigma_b^2 (X_b + A \sin(\omega t)) / \sigma^2$

$$\sigma_b^2 = \sigma_x^2 \sigma^2 / (2\sigma_x^2 + \sigma^2)$$

Using the mathematical identity of unity for the integral of a gaussian function, the above becomes

$$N_1(t) = \frac{I_0^2}{\sigma_n^2} \frac{\sigma_b}{\sigma_x} \frac{1}{2} \int_0^t \exp(-(X_b + A \sin(\omega\tau))^2 / (2\sigma_b^2 + \sigma^2)) d\tau \quad (11)$$

which requires a numerical integration. Since the integrand is periodic, then for any integer n,

$$\int_0^{nt_p} f(\cdot) = n \int_0^{t_p} f(\cdot)$$

where an evaluation of $N_1(t = nt_p)$ can be made at periodic points in time.

Evaluation of $N_2(t)$ of Eq. (8) requires an integration of

$$\int_0^t E \left[\frac{I_0^2}{\sigma_n^2} \exp(-y^2 / 2\sigma^2) \right] k d\tau$$

which reduces to

$$\left[\frac{I_0^2}{\sigma_n^2} \frac{\sigma_c}{\sigma_x} \right] k \int_0^t \exp(-(X_b + A \sin(\omega\tau))^2 / (2\sigma_c^2 + \sigma^2)) d\tau \quad (12)$$

where $\sigma_c = \sigma / \sqrt{k}$. The same condition on the periodicity of the integrand holds for the above and integer values of $N_2(t = nt_p)$ can be made with one complete, periodic numerical integration. Note that both Eq. (11) and (12) contain the signal to noise ratio I_0 / σ_n and the system performance should improve accordingly.

C. Numerical Example

The above integrals were numerically evaluated using the computer program PRK08A (see Appendix A) which also calculates the information reduction factors and the error entropy lower bound. Consider the following example of a stationary target with parameters:

A = 5 normalized units
 ω : f = 300 Hz
 $\sigma = 10$
 $\sigma_x = 10$
 I_0 / σ_n : variable
 X_b : variable

For a signal to noise ratio of unity, $I_0 / \sigma_n = 1.0$, Figure 3 illustrates the various elements needed to determine the lower bound for a zero bias, $X_b = 0$.

Figure 3a is the one period biased dither average and numerical integration.
Figure 3b is $N_1(t)$ and the information reduction factor.
Figure 3c is the resulting error variance lower bound.
Figure 4 is the same conditions as above for $X_b = 2.5$.
Figure 5 is for $X_b = 5.0$.
Figure 6 is for $X_b = 10.0$.

The 10 second order of magnitude to settle down is for the case $I_0/\sigma_n = 1.0$ which is not the nominal operating condition. Doubling the signal-to-noise, results in a faster responding lower bound as illustrated by Figure 7, $\{X_b = 0, 2.5, 5.0, 10\}$. Noticed that as the bias X_b becomes much larger than the glint σ , the performance deteriorates.

IV. Conclusion

A. Summary

The lower bound to the angle estimation error with the laser radar dither measurement glint process was formulated and an analytical/numerical algorithm developed for evaluation. The error variance reduction factor due to information in the measurements is shown to be proportional to the signal-to-noise ratio I_0/σ_n . The resulting algorithm was programmed using the VAX digital computer and initial test cases made. Preliminary results indicate that similar performance bounds exist anywhere near the measurement glint null.

B. Extensions

There are some readily apparent extensions that can be made to this summer research investigation:

1. Vary design parameters such as I_0/σ_n , σ/σ_k , A , and X_b using the existing program and derive optimal tracking operating conditions.
2. Calculate the actual angular error variation lower bound for a field test case and compare the measured and lower bound results.
3. Evaluate the resulting estimation performance with the Kalman estimation process (see Appendix B).
4. Extend the target model to include motion and maneuverability.
5. Calculate the effects of the jitter from the feedback controller.

C. Acknowledgements

This work was funded by the Air Force Summer Faculty Research Program (SFRP), administered by the Southeastern Center for Electrical Engineering Education (SCEEE) under contract F49620-79-C-0038.

Reference

1. Berkowitz, R.S., Modern Radar, Analysis, Evaluation and System Design, Wiley, New York, 1965.
2. Skolnik, M.I., Radar Handbook, McGraw Hill, New York, 1970.
3. Erteza, A., "Boresighting a Gaussian Beam on a Specular Target Point: A Method Using Conical Scan", Applied Optics, Vol. 15, March 1976.
4. Shannon, C.E., "A Mathematical Theory of Communication - I and II" The Bell System Tech. J., Vol. 27, July and Oct. 1948.
5. Kalata, P.R., "An Information-Theoretic Approach to Estimation in Discrete Time Systems", Ph. D. Dissertation, Illinois Institute of Technology, May 1974.
6. Kalata, P. and Priemer, R., "Linear Prediction, Filtering and Smoothing: An Information-Theoretic Approach", Information Sciences, Feb. 1979.
7. Kalata, P. and Priemer, R., "On Minimal Error Entropy Stochastic Approximation", Int. J. Systems Science, Vol. 5, Sept. 1974.
8. Kalata, P. and Priemer, R., "On System Identification With and Without Certainty", J. Cybernetics, Vol. 8, 1978.
9. Kalata, P. and Priemer, R., "When Should Smoothing Cease?", Proc. IEEE, Vol. 62, Sept. 1974.
10. Dillow, J., James, N. and Loos, G., "A Control Model for a Conical Scan Tracking System," AFWL-TR-76-131, Kirtland AFB.
11. Zakai, M., and Ziv, J., "Lower and Upper Bounds on the Optimal Filtering Error of Certain Diffusion Processes," IEEE Trans. Information Theory, Vol. IT-18, May 1972.
12. Galdos, J., "A Lower Bound on Filtering Error with Application to Phase Demodulation," IEEE Trans. Information Theory, Vol. IT-25, July 1979.
13. Sage, A., and Melsa, J., Estimation Theory with Applications to Communication and Control, McGraw Hill, 1971.

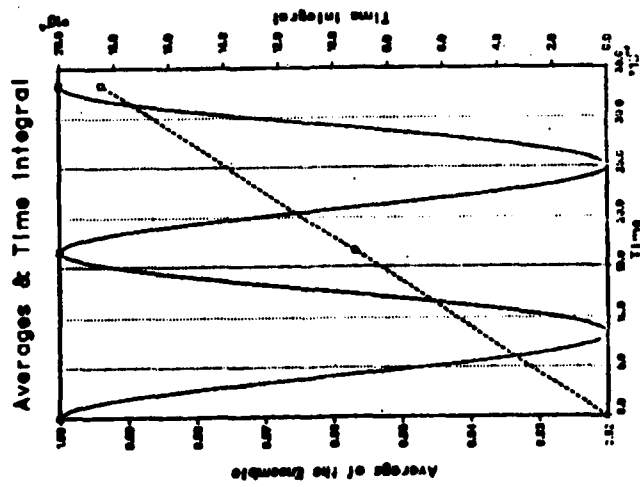


Figure 3a)

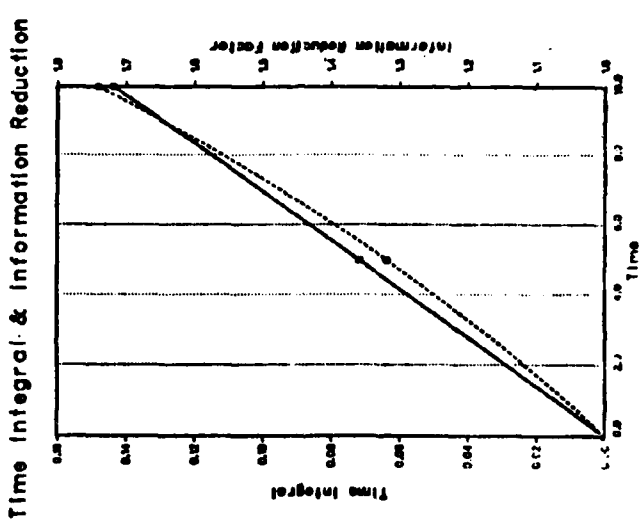


Figure 3b)

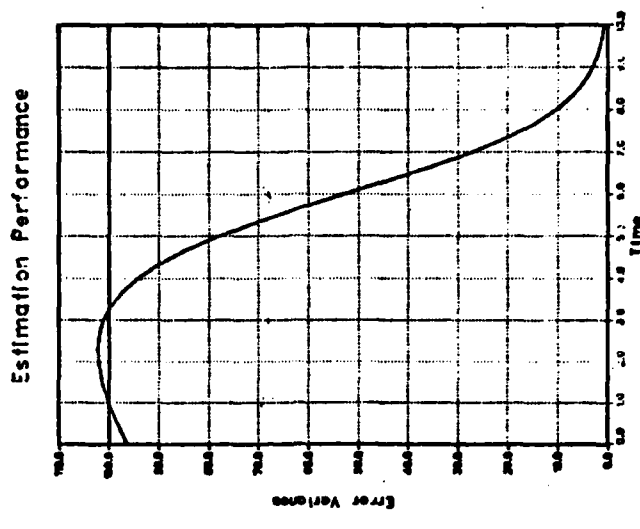


Figure 3c)

Figure 3: Lower Bound Results for $I_0/\sigma_n = 1.0$ and $X_b = 0$

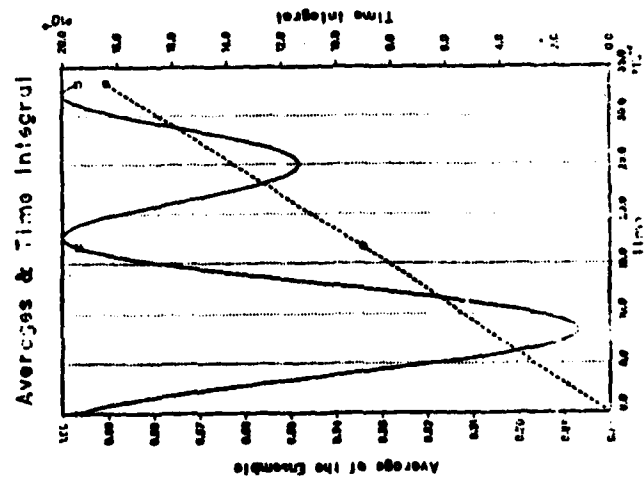
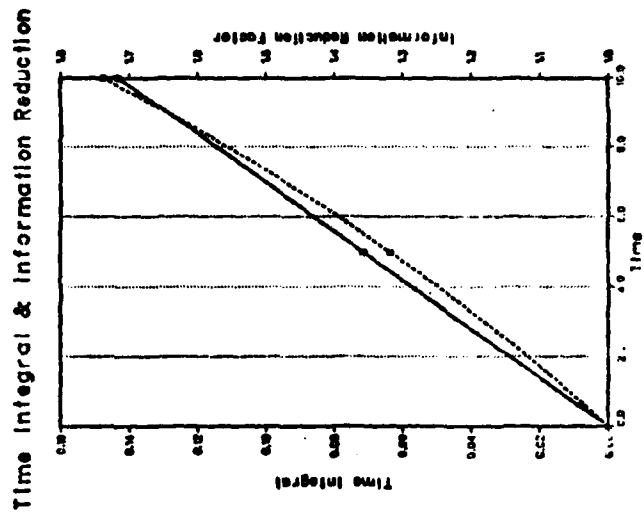
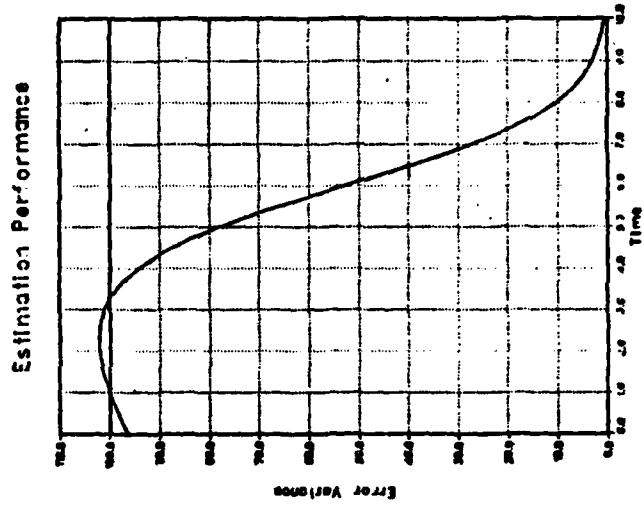


Figure 4: Lower Bound Results for $I_0/\sigma_n = 1.0$ and $X_b = 2.5$

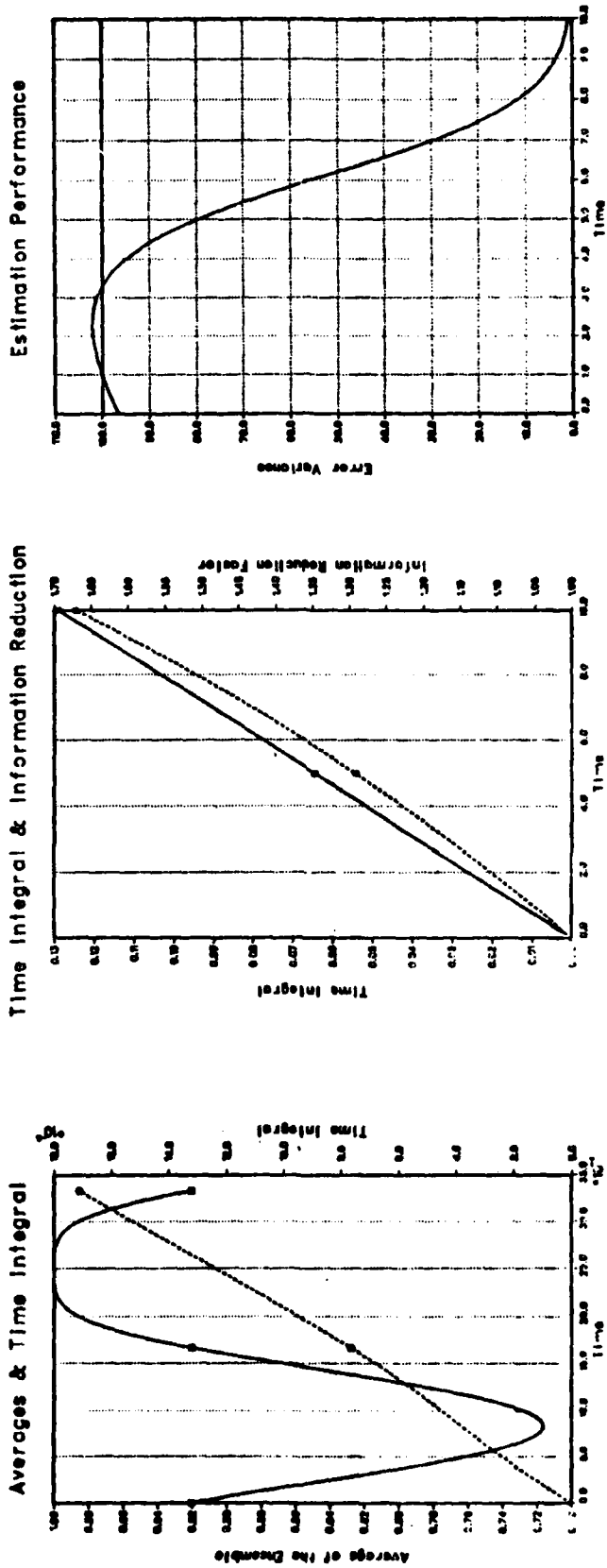


Figure 5: Lower Bound Results for $I_0/c_n = 1.0$ and $X_b = 5.0$

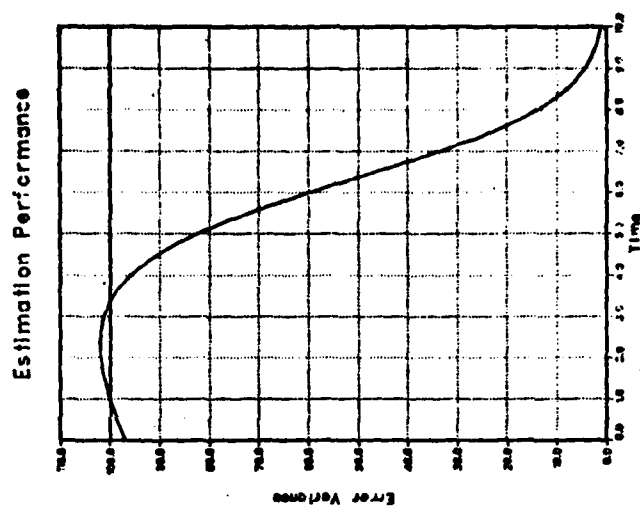
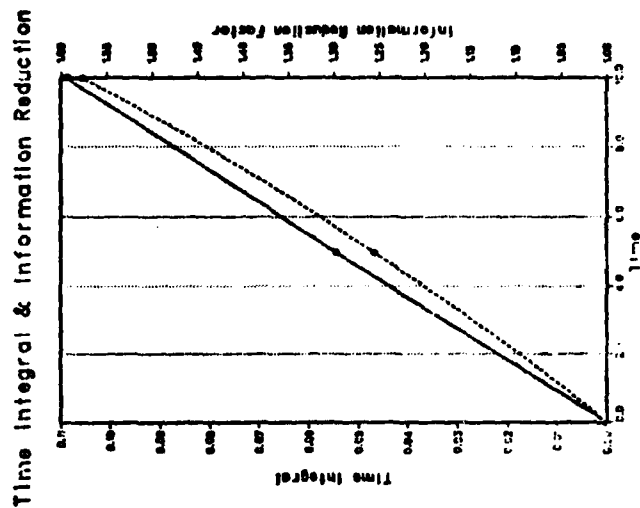
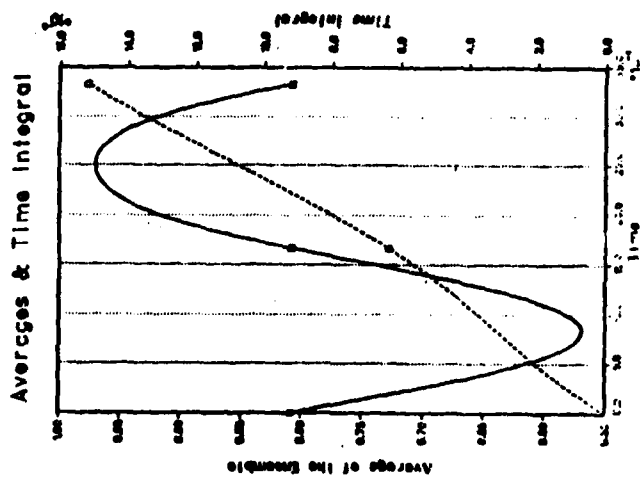
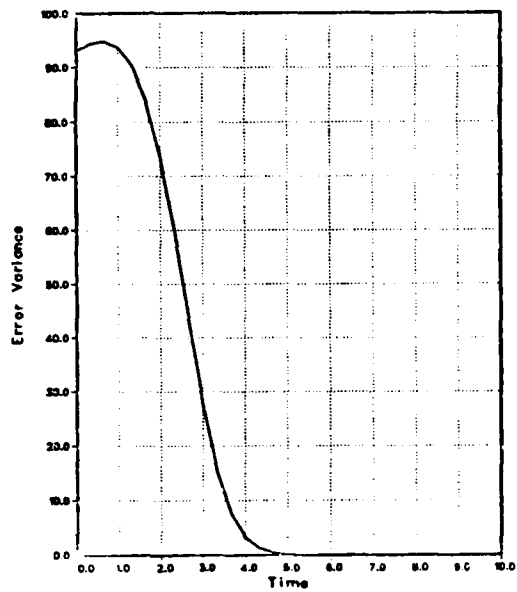


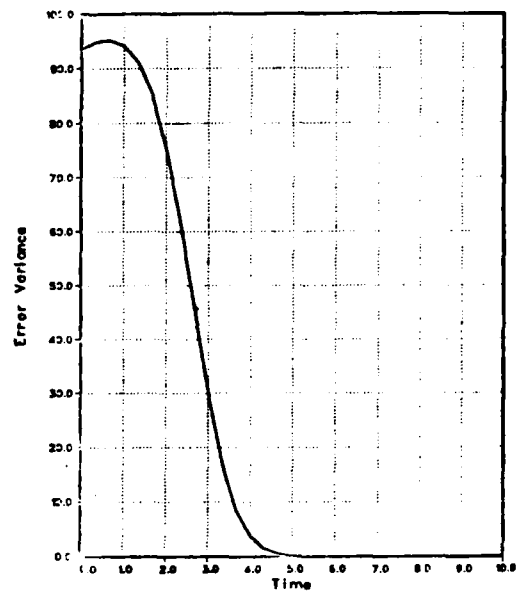
Figure 6: Lower Bound Results for $I_0/\sigma_n = 1.0$ and $X_b = 10.0$

Estimation Performance



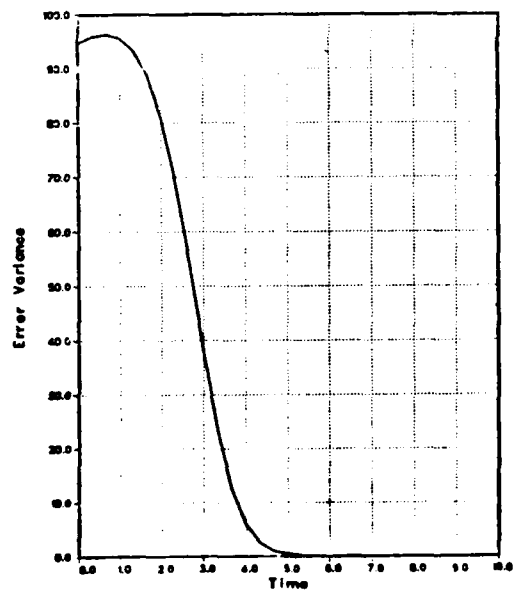
$X_b = 0.0$

Estimation Performance



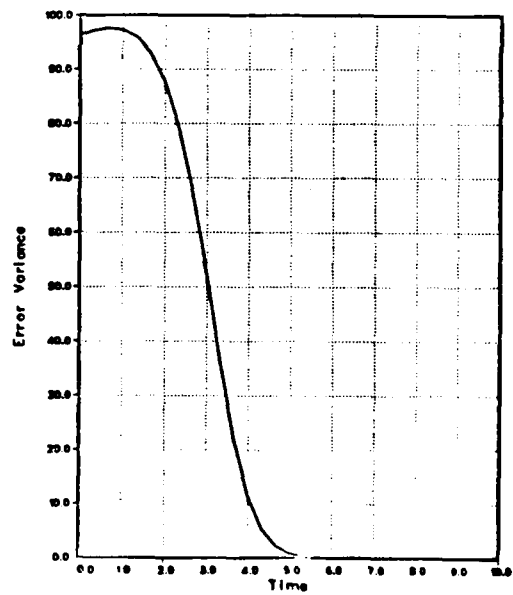
$X_b = 2.5$

Estimation Performance



$X_b = 5.0$

Estimation Performance



$X_b = 10.0$

Figure 7: Lower Bound Results for $I_0/\sigma_n = \sqrt{2}$ and $X_b = 0, 2.5, 5.0,$ and 10.0 .

Appendix A

Computer Program PRK08A Used to Calculate the Estimation Error
Variance Lower Bound

PRK08A Program

```

* EXIT
*TYPE PRK08A.COM
*TYPE PRK08A.COM
*TYPE PRK08A.FOR
*TYPE PRK09A.FOR
*LINK PRK08A, PRK09A, PLOT/LIB, 'IMSL', 'DISSPLA'
*RUN PRK08A
*EXIT
*TYPE PRK08A.FOR
PROGRAM PRK08A
DIMENSION T(101), VALUE(101, 21), AREAP(101, 21)
DIMENSION AREAPP(101)
DIMENSION VALUEP(101)
DIMENSION AN2UB(101)
DIMENSION AINF(21, 21), IINF(21, 21)
DIMENSION H6VAR(101), AAA(101), TIMET(101), AREATF(101), AREAT(101)
DATA PI, E/3.141529265, 2.718281828/
DATA TU, TL, XB, A, SIG, W0/10., -10., 10., 5., 10., 300. /
DATA SIGX, SIGN, AIO/10., 1., 1. /
III=21
CALL INFCN(AINF, IINF, III)
IPL0T=1
IPL0T=0
IPRINT=1
IF(IPL0T.EQ.1) GO TO 11
C
CALL COMPRS           ! Initialize DISSPLA graphics package
C
CALL VS11
C
11 CONTINUE
N=101
ITIME=100
C
ITIME=1000
C
NTIME=31
C
ITIME=1
XB=5.
C
XB=1.0
C
READ(5, *) XB
DO 202 IKK=1, 11
XB=IKK-1
WRITE(6, 27) XB
27 FORMAT(/, ' GLINT BIAS = ', F10.5)
N1=N-1
TP=1./W0
W=W0*2.*PI
WRITE(6, 45) TP, W0
DT=TP/100.
DO 333 K=1, III
WRITE(6, 33) K
33 FORMAT(1H0, ' K = ', I5)
AK=K
CON1=1.
CON2=SIG/2./TU
CON3=1./2./PI/E

```

Appendix A

PRK08A Program

PRK08A.LUG:8

25-AUG-1981 17:27:10.46

Page 2

```

SIGX2=SIGX*SIGX
SIG=10.
SIG=SIG/SQRT(AK)
SIG2=SIG*SIG
SIGN2=SIGN*SIGN
SIGB=SQRT((SIGX2*SIG2)/(2.*SIGX2+SIG2))
CON4=(A10*A10/SIGN2)**K*SIGB/SIGX
WRITE(6,35) CON4
35  FORMAT(' INTEGRATION CONSTANT =',F14.5)
AREA=0.0
45  FORMAT(1H1,' TIME PERIOD = ',F10.5,' SECONDS',/
1' ANGULAR FREQUENCY = ',F14.2,' RADIANS/SECOND')
WRITE(6,78)
DO 75 J=1,N
T(J)=TP*(J-1)/N1
VALUEP(J)=EXP(-(XB+A*SIN(W*T(J)))*2/(2.*SIGX2+SIG2))
VALUE(J,K)=CON4*VALUEP(J)
IF(J.EQ.1) GO TO 74
AREA=AREA+.5*DT*(VALUE(J,K)+VALUE(J-1,K))
74  CONTINUE
AREAP(J,K)=AREA
AREAPP(J)=AREA
VPAST=VALUE(J,K)
C   IF(IPRINT.EQ.1 .AND. K.NE.1) GO TO 75
IF(IPRINT.EQ.1) GO TO 75
WRITE(6,79) J,T(J),VALUEP(J),AREAP(J,K)
75  CONTINUE
WRITE(6,79) N,T(N),VALUEP(N),AREAP(N,K)
ACYCLE=AREA
78  FORMAT(' J TIME VALUE AREA')
79  FORMAT(15,7E14.5)
98  FORMAT(//,' I TIME CYCLE AREA AREA')
99  FORMAT(//,' I TIME AREA SOURCE VARIANCE
1 ' INCREASE REDUCTION ERROR VARIANCE ',/
2 39X,'(ENTROPY) (INFORMATION) (LOWER BOUND)')
IF(K.GT.1 .AND. K.LT.III) GO TO 100
IF(IPL0T.EQ.1) GO TO 100
C   CALL TWOAXIS(T,VALUEP,T,AREAPP,N,
1 ' (A)VERAGES & (T)IME (I)NTEGRAL $',
2 ' (T)IME$',
3 ' (A)VERAGE OF THE (E)NSEMBLE $',
4 ' (T)IME (I)NTEGRAL $')
100 CONTINUE
333 CONTINUE
141 FORMAT(1H1' TIME INCREMENTS ARE : '.15.' & '.15)
DO 202 JJ=1,1
IF(JJ.EQ.1) ITIME=100
IF(JJ.EQ.2) ITIME=500
IF(JJ.EQ.3) ITIME=1000
WRITE(6,141) ITIME,NTIME
WRITE(6,181)
DO 179 I=1,NTIME
WRITE(6,*)
C   AN2UB(I)=1.0/AINF(1,1)
AN2UB(I)=1.0/AINF(1,1)
T(I)=ITIME*(I-1)*TP
DO 175 IR=1,III,2

```

Appendix A

PRK08A Program

```

IF(K.LE.1) GO TO 171
TVALUE=T(I)**(K-1)
171 CONTINUE

C AN2UB(I)=AN2UB(I)+T(I)**K*VALUE(I,K)
C
AN2UB(I)=AN2UB(I)+TVALUE*ITIME*AREAP(N,K)/AINF(IR,IN)
C
174 CONTINUE
IF(IPRINT.EQ.1) GO TO 175
WRITE(6,180)I,IR,IN,K,T(I),AN2UB(I),AREAP(N,K),AINF(IR,IN)
C
175 CONTINUE
C WRITE(6,180) I,III,III,K,T(I),AN2UB(I),AREAP(N,K),AINF(IR,IN)
C
179 CONTINUE
180 FORMAT(4I5,3E13.5,F30.0)
C
181 FORMAT(1H0,' I R+1 N+1 K TIME SUMMATION AREA(
IN,K) AINF(R,N)')
C
C ENTROPY OF SOURCE
H6=.5*LOG(12.*(TU*TU/3.))
H6=.5*LOG(SIGX2/CON3)
H6VAR=CON3*EXP(2.*H6)
C
WRITE(6,185) SIGX2
185 FORMAT(1H1,/' INITIAL VARIANCE OF THE STATE =',F14.3)
WRITE(6,99)
DO 101 J=1,NTIME
TIMET(J)=ITIME*(J-1)*TP
AREAT(J)=ITIME*(J-1)*ACYCLE
AREATF(J)=EXP(+0.5*ITIME*(J-1)*AREAP(N,1))**2
H6VAR(J)=H6VAR
AN2UB(J)=AN2UB(J)**2
AAA(J)=H6VAR(J)*AREATF(J)/AN2UB(J)
C IF(IPRINT.EQ.1) GO TO 101
WRITE(6,779) J,TIMET(J),AREAT(J),H6VAR(J),AREATF(J),AN2UB(J),AAA(J)
779 FORMAT(I5,4F14.4,E14.5,F14.4)
101 CONTINUE
WRITE(6,779) NTIME,TIMET(NTIME),AREAT(NTIME),H6VAR(NTIME),AREATF(NTIME)
1,AN2UB(NTIME),AAA(NTIME)
IF(IPL0T.EQ.1) GO TO 201
CALL TWOAXIS(TIMET,AREAT,TIMET,AREATF,NTIME,
1 '(T)IME (I)NTEGRAL & (I)NFORMATION (R)EDUCTION *',
2 '(T)IME*',
3 '(T)IME (I)NTEGRAL*',
4 '(I)NFORMATION (R)EDUCTION (F)ACTOR*')
C
CALL XYLIN2(TIMET,H6VAR,TIMET,AAA,NTIME,
1 '(E)STIMATION (P)ERFORMANCE*',
2 '(T)IME*',
3 '(E)RROR (V)ARIANCE*')

201 CONTINUE
202 CONTINUE
IF(IPL0T.EQ.1) GO TO 401
CALL DONEPL ! All plotting completed

```

Appendix A

PRK08A Program

```

      END
*TYPE PRK09A. FOR
C      PROGRAM PRK09A
      SUBROUTINE INFCON(V, IV, NT)
      DIMENSION V(NT, NT), IV(NT, NT)
      REAL IFN, IFR
C      NT=10
      DO 101 I=1, NT
      DO 101 J=1, NT
      V(I, J)=0.0
      IV(I, J)=0
101     CONTINUE
      NT1=NT+1
      DO 201 IR=1, NT, 2
      IRO=IR-1
      DO 201 IN=IR, NT
      INO=IN-1
      IFR=1
      IEND=IRO/2
      IF(IEND.EQ.0) GO TO 152
      DO 151 I=1, IEND
      IFR=I+IFR
151     CONTINUE
152     CONTINUE
      IFN=1
      IEND=INO-IRO
      IF(IEND.EQ.0) GO TO 172
      DO 171 I=1, IEND
      IFN=I+IFN
171     CONTINUE
172     CONTINUE
C      WRITE(6, 185) IRO, IFR, INO, IFN
185     FORMAT(/' R+1 =', I4, ' (R/2)! =', I5,
1 /, ' N+1 =', I4, ' (N - R)! =', I12)
C      IV(IR, IN)=IFR*IFN*2** (INO-IRO/2)
      V(IR, IN)=IFR*IFN*2. ** (INO-IRO/2)
201     CONTINUE
C      WRITE(6, 205)
205     FORMAT(1H1, ' R+1  N+1  2** (N-R/2) ')
      DO 301 I=1, NT
      DO 301 J=1, NT
C      WRITE(6, 306) I, J, IV(I, J)
301     CONTINUE
305     FORMAT (10I7)
306     FORMAT(2I5, I10)
      WRITE(6, 406)
      DO 401 N=1, NT
C      WRITE(6, 405) N, (IV(IR, N), IR=1, NT)
      WRITE(6, 404) N, (V(IR, N), IR=1, NT, 2)
401     CONTINUE
404     FORMAT(I4, 12E10. 2)
405     FORMAT(I4, 10I11)
406     FORMAT(1H1, ' N+1  R+1=  1          2          3          4          5
15          6          7          8          9          10          11'./)
C      STOP
      RETURN
      END

```

APPENDIX A

PRK08A Output (typical)

OLINT BIAS = 0.00000

INITIAL VARIANCE OF THE STATE = 100.000

I	TIME	AREA	SOURCE VARIANCE (ENTROPY)	INCREASE (INFORMATION)	REDUCTION	ERROR VARIANCE (LOWER BOUND)
1	0.0000	0.0000	100.0000	1.0000	0.10373E+01	96.4063
2	0.3333	0.0048	100.0000	1.0186	0.10426E+01	97.7031
3	0.6667	0.0096	100.0000	1.0376	0.10490E+01	98.9113
4	1.0000	0.0144	100.0000	1.0570	0.10570E+01	100.0006
5	1.3333	0.0191	100.0000	1.0767	0.10667E+01	100.9330
6	1.6667	0.0239	100.0000	1.0967	0.10788E+01	101.6606
7	2.0000	0.0287	100.0000	1.1172	0.10939E+01	102.1237
8	2.3333	0.0335	100.0000	1.1380	0.11130E+01	102.2493
9	2.6667	0.0383	100.0000	1.1592	0.11371E+01	101.9483
10	3.0000	0.0431	100.0000	1.1808	0.11678E+01	101.1162
11	3.3333	0.0479	100.0000	1.2028	0.12073E+01	99.6320
12	3.6667	0.0527	100.0000	1.2252	0.12584E+01	97.3641
13	4.0000	0.0574	100.0000	1.2481	0.13253E+01	94.1773
14	4.3333	0.0622	100.0000	1.2713	0.14134E+01	89.9499
15	4.6667	0.0670	100.0000	1.2950	0.15309E+01	84.5942
16	5.0000	0.0718	100.0000	1.3192	0.16893E+01	78.0891
17	5.3333	0.0766	100.0000	1.3438	0.19058E+01	70.5100
18	5.6667	0.0814	100.0000	1.3688	0.22058E+01	62.0557
19	6.0000	0.0862	100.0000	1.3943	0.26282E+01	53.0527
20	6.3333	0.0909	100.0000	1.4203	0.32332E+01	43.9294
21	6.6667	0.0957	100.0000	1.4468	0.41153E+01	35.1565
22	7.0000	0.1005	100.0000	1.4738	0.54252E+01	27.1653
23	7.3333	0.1053	100.0000	1.5012	0.74057E+01	20.2713
24	7.6667	0.1101	100.0000	1.5292	0.10452E+02	14.6303
25	8.0000	0.1149	100.0000	1.5577	0.15214E+02	10.2389
26	8.3333	0.1197	100.0000	1.5868	0.22759E+02	6.9719
27	8.6667	0.1245	100.0000	1.6163	0.34858E+02	4.6369
28	9.0000	0.1292	100.0000	1.6465	0.54443E+02	3.0242
29	9.3333	0.1340	100.0000	1.6771	0.86377E+02	1.9417
30	9.6667	0.1388	100.0000	1.7084	0.13871E+03	1.2316
31	10.0000	0.1436	100.0000	1.7402	0.22476E+03	0.7743

Appendix B

Extended Kalman Filter for the Laser Radar Target Estimation

A straight-forward design of a Kalman Filter [13] for target tracking yields the following set of equations to be implemented.

$$\dot{\hat{x}}_b = K(t)[z(t) - g(\hat{y}, t)]$$

$$y(t) = \hat{x}_b + A \sin(\omega t)$$

$$g(y, t) = I_0 \exp(-y^2/2\sigma^2)$$

$$K(t) = -\frac{V_{\hat{x}}}{\sigma_n^2} \frac{\hat{y}}{\sigma^2} g(\hat{y}, t)$$

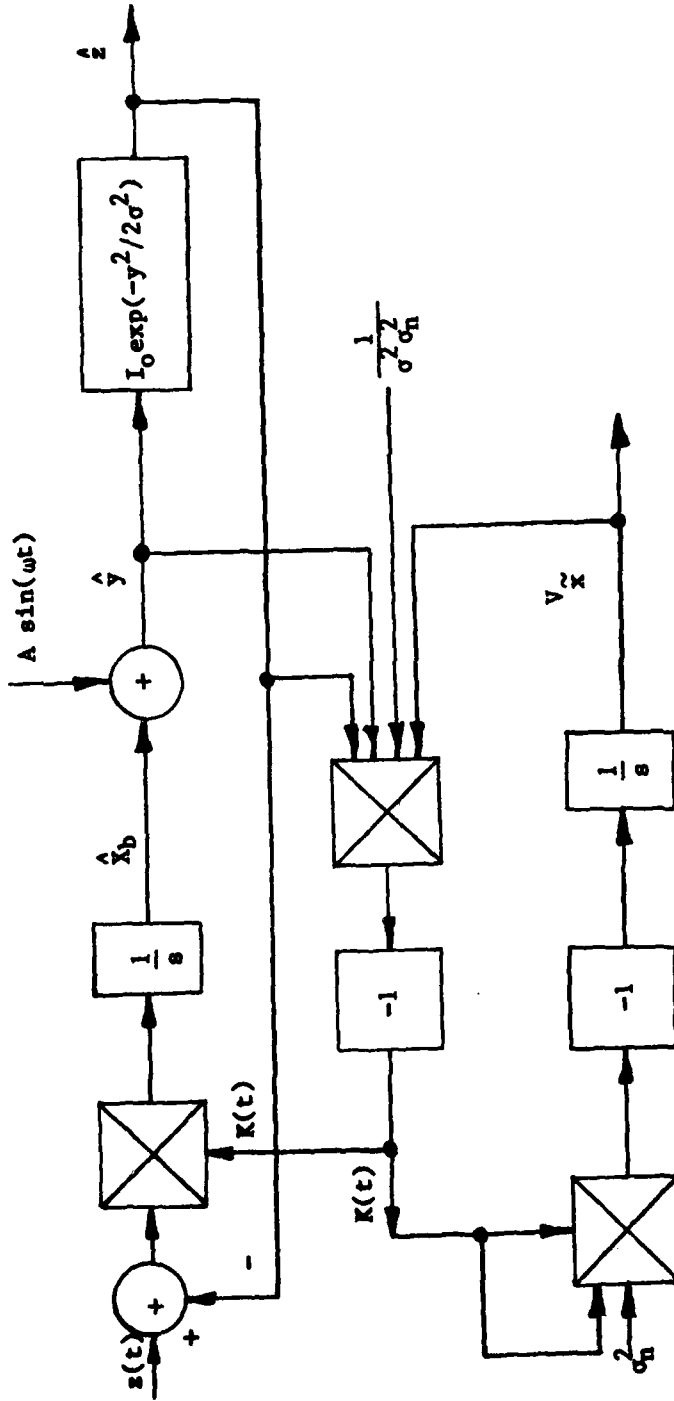
$$\dot{V}_{\hat{x}} = -\frac{V_{\hat{x}}^2}{\sigma_n^2} \frac{\hat{y}^2}{\sigma^4} g^2(\hat{y}, t)$$

Note that:

$$\dot{V}_{\hat{x}} = -K^2(t)\sigma_n^2$$

The following is a block diagram for the above filtering process.

APPENDIX B



Extend Kalman Filter for the Laser Radar Tracking Process

1981 USAF - SCEEE SUMMER FACULTY RESEARCH PROGRAM

Sponsored by the

AIR FORCE OFFICE OF SCIENTIFIC RESEARCH

Conducted by the

SOUTHEASTERN CENTER FOR ELECTRICAL ENGINEERING EDUCATION

FINAL REPORT

ELECTRICAL CHARACTERIZATION OF ION IMPLANTATION IN GaAs

Prepared by: Dr. Richard Y. Kwor
Academic Rank: Assistant Professor
Department and University: Department of Electrical Engineering
University of Notre Dame
Resear Location: Air Force Avionics Laboratory,
Electronics Branch
USAF Research Colleague: Dr. Y. S. Park
Date: August 7, 1981
Contract No: F49620-79-C-0038

ELECTRICAL CHARACTERIZATION

OF ION IMPLANTATION IN GaAs

by

Richard Kwor

ABSTRACT

Two separate projects are reported. The first is the study of the effect of two-stage annealing of sulfur-implanted GaAs. Electrical activations for samples annealed at 900 °C for 15 min. are compared with samples annealed at 700 °C for 15 min. and then 900 °C for 15 min. The results show a slight improvement of mobility and activation for two-stage annealed samples. Further research in this area is suggested. The second part is the fabrication and testing of Se-ion implanted MESFETs made from GaAs substrates obtained from various suppliers. The FET performances are used in a study of the correlation between device characteristics and substrate properties.

Acknowledgement

The author would like to thank the Air Force Systems Command, the Air Force Office of Scientific Research and the Southeastern Center for Electrical Engineering Education for providing him with the opportunity to spend a very worthwhile summer at the Air Force Avionics Laboratories, Wright-Patterson AFB, OH. He would like to acknowledge the laboratories, in particular the Electronics Research Branch, for its hospitality and excellent working conditions.

He would specially like to express his appreciation to Dr. Y. S. Park for his collaboration and guidance in the project. Finally, he would like to acknowledge many helpful discussions with Dr. Y. K. Yeo and Dr. F. Pedrotti, and to thank Mr. J. Ehret and Mr. C. Geesner for their technical support.

I. INTRODUCTION:

GaAs has received much attention in the past decade. Many new GaAs devices promise to offer better performance than their Si counterparts. GaAs technology has reached the level now that it is possible to fabricate medium and large scale integrated circuits with the material. Among various technologies used, ion implantation is considered to be a key to future complex GaAs circuits. Indeed, GaAs integrated logic circuits with 1000 logic gates have been made using selective ion implantation. However, many basic material and processing problems still remain and fundamental studies of the ion implanted GaAs are much needed.

The present project is centered around the research of ion implanted GaAs and is divided into two separate parts. The first is to study the effect of two-stage annealing (two consecutive annealings of the implanted substrate at different temperatures) of sulfur-implanted GaAs substrates. The second--the fabrication and testing of GaAs MESFETs -- is part of a large scale study on semi-insulating GaAs substrates. This study is aimed to find possible correlation of impurity content and impurity diffusion with conversion propensity and MESFET performance.

This report contains two major sections. In the first section, experiments on two-stage annealing of sulfur-implanted GaAs are reported along with some preliminary results. In the second, a detail account of GaAs MESFET fabrication and testing processes are given.

II. OBJECTIVES

The two main objectives of this project are:

- (1) To initiate and conduct the two-stage annealing experiments for sulfur-implanted GaAs; and from the preliminary results to evaluate the effect of such an annealing process on the activation of the implanted substrates.

(2) To set up the necessary equipments for GaAs MESFET fabrication at the Electronics Branch, to make and test MESFETs using substrates from different sources; and to search for correlations between the FET characteristics and the substrate material properties.

III. TWO-STAGE ANNEALING

Thermal annealing is now generally adopted as a standard process to remove implantation damages and to activate the implanted dopants. The temperature used varies between 850 °C and 950 °C, while the annealing time ranges from 15 min. to 30 min. Using thermal annealing, good electrical activation can be achieved for the common dopants S, Se, Si, Te, Be, Mg, and Zn. However, because of the high temperature used there is always some dopant redistribution during annealing. Being a light element, sulfur exhibits a pronounced diffusion tail after 15 min. anneal at temperatures above 800 °C.¹ Such a diffusion tail is undesirable in many device applications. Its existence limits the usefulness of S as an n-type dopant in GaAs. The formation of this tail results from the high temperature used in the annealing, and is possibly enhanced by the radiation induced damages. Even though most of the implantation damages in GaAs can be removed at anneal temperatures below 700 °C², good electrical activation requires anneal temperatures above 850 °C. Thus temperatures higher than 850 °C must be used in one-stage annealing of sulfur implants. And the highest reported activation efficiency for this energy is about 60 %.³ For two-stage annealing, lower temperature is first used to remove most of the crystal damages and higher temperature is then used to achieve good electrical activity. In this way, undesirable damage-enhanced diffusion may be reduced. To test the validity of this assumption, a set of experiments were conducted to study the effect of two-stage annealing. They are described below.

A. Two-Stage Annealing Experiments

The substrate materials used were $\langle 100 \rangle$ oriented Cr-doped semi-insulating GaAs from Crystal Specialties, Inc. and undoped semi-insulating GaAs from Metals Research, Inc. Prior to implantation, the samples were cleaned with organic solvents and subsequently free-etched with an $\text{H}_2\text{SO}_4; 30\% \text{H}_2\text{O}_2; \text{H}_2\text{O}$ solution in a 3:1:1 ratio by volume for 60 sec. to remove the polishing damages. Sulfur ions were implanted at 120 keV to doses ranging from $1 \times 10^{13} \text{ cm}^{-2}$ to $1 \times 10^{14} \text{ cm}^{-2}$. After implantation the samples were capped with $\sim 1000 \text{ \AA}$ of pyrolytically deposited Si_3N_4 and annealed at various temperatures in flowing hydrogen gas. Then the encapsulants were removed with HF and indium ohmic contacts were made on the surface of the samples. Hall-effect/sheet-resistivity measurements for the samples were made using the standard van der Pauw technique. The results are shown in Table 1 and Table 2.

B. Discussions

Table 1 shows the results from surface Hall measurement on S-implanted GaAs annealed under various conditions. It is seen that the undoped substrates have lower activation efficiency than the Cr-doped substrates implanted and annealed under identical conditions. Moreover, for dose of 1×10^{13} the two-stage annealing improves both the mobility and activation efficiency. For the dose of $1 \times 10^{14} \text{ cm}^{-2}$ the improvement becomes less noticeable. This is probably due to the activation limitation at high doses resulting from precipitation. To further investigate the effect of two-stage annealing, sulfur was implanted into Cr-doped substrate (from the same wafer used in Table 1) to doses of 1×10^{13} , 3×10^{13} and $6 \times 10^{13} \text{ cm}^{-2}$. The results of Hall measurements are shown in Table 2. Here as expected, because of the higher doses, two-stage annealing results in very little change of activation even though it does increase the mobility slightly. An interesting result is that a very high activation efficiency has been obtained — 82 % for dose of $3 \times 10^{13} \text{ cm}^{-2}$ and 54 % for dose of $6 \times 10^{13} \text{ cm}^{-2}$. This is the highest activation

Sample No.	Substrate	Dose (cm^{-2})	Anneal condition	Average mobility	Average sheet concentration	Activation efficiency
CR13PY90	Cr-doped	1×10^{13}	900° (15min)	3880	4.6×10^{12}	46.4 %
CR13PY7090	Cr-doped	1×10^{13}	700° (15min) 900° (15min)	3764	5.2×10^{12}	51.5 %
CR14PY90	Cr-doped	1×10^{14}	900° (15min)	2328	1.5×10^{13}	14.8 %
CR14PY7090	Cr-doped	1×10^{14}	700° (15min) 900° (15min)	2431	1.5×10^{13}	14.6 %
US13PY90	Undoped	1×10^{13}	900° (15min)	4450	3.5×10^{12}	35.0 %
US13PY7090	Undoped	1×10^{13}	700° (15min) 900° (15min)	3904	4.7×10^{12}	47.7 %
US14PY90	Undoped	1×10^{14}	900° (15min)	2538	1.3×10^{13}	12.7 %
US14PY7090	Undoped	1×10^{14}	700° (15min) 900° (15min)	2229	1.3×10^{13}	13.4 %

Table 1. Surface Hall Measurement Results for one- and two-stage Annealing of S-implants in GaAs

Sample No.	Substrate	Dose (cm^{-2})	Anneal condition	Average mobility	Average sheet concentration	Activation efficiency
CR13PY90B	Cr-doped	1×10^{13}	900° (15min)	3389	5.98×10^{12}	59.8 %
CR13PY7090B	Cr-doped	1×10^{13}	700° (15min) 900° (15min)	3512	5.90×10^{12}	59.0 %
CR313PY90B	Cr-doped	3×10^{13}	900° (15min)	2719	2.46×10^{13}	82.0 %
CR313PY7090B	Cr-doped	3×10^{13}	700° (15min) 900° (15min)	2964	2.30×10^{13}	76.0 %
CR613PY90B	Cr-doped	6×10^{13}	900° (15min)	2191	3.19×10^{13}	53.0 %
CR613PY7090B	Cr-doped	6×10^{13}	700° (15min) 900° (15min)	2242	3.25×10^{13}	54.0 %

Table 2. Surface Hall Measurement Results for one- and two-stage Annealing of S-implants in GaAs.

efficiency of S implants in Cr-doped GaAs at this energy (120 keV) ever reported.

IV. RECOMMENDATIONS I

From the surface Hall measurement results, it is apparent that for medium dose levels two-stage annealing improves the mobility and activation of S-implants. To complete the study, it is recommended that experiments be conducted for lower doses (between 10^{12} and 10^{13} cm^{-2}). The mobility and activation for each dose should be measured. Furthermore, the profiling for these S-implants needs to be done so that the effect of two-stage annealing on diffusion tails can be investigated. Also, study on the implants with very high activation should be carried out.

V. CORRELATION OF GaAs SUBSTRATE PROPERTIES AND FET PERFORMANCE

The performance of GaAs MESFETs is closely related to the properties of the substrates. Factors such as mobility and Cr doping concentration in the substrate, etc. have profound effects on the devices. A systematic study is carried out such that a detail characterization of GaAs substrates (both Cr-doped and undoped semi-insulating) from various sources is done using various techniques listed in Table 3. MESFETs were fabricated from these substrates and were tested to find possible correlations of impurity content and impurity diffusion with conversion propensity and FET performance. This is a joint effort undertaken by many researchers in the Electronics Research Branch of WPAFB Avionics Laboratories. In this report, GaAs MESFET fabrication techniques and testing procedures are described. Informations regarding other aspects of the study can be found elsewhere.⁴

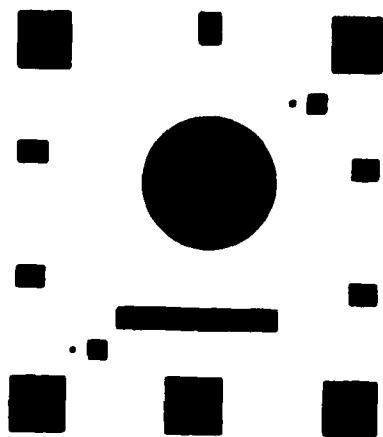
A. MESFET Fabrication

GaAs MESFETs were made with the procedures described below:

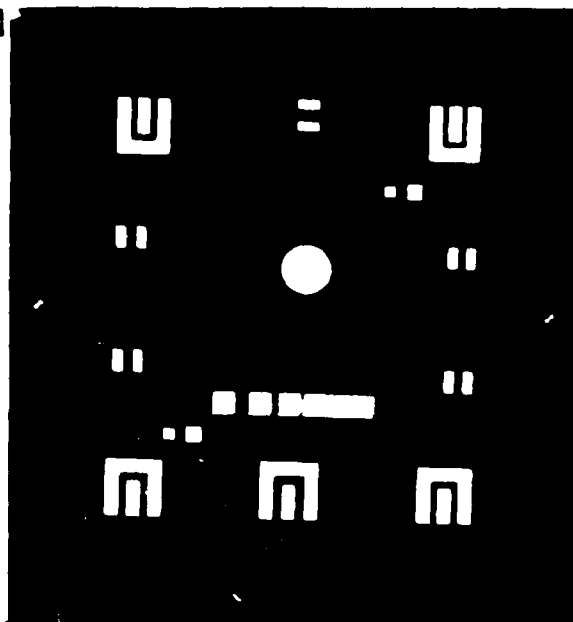
CHARACTERIZATION	METHODS
Defect Analysis	Etch-pit density TEM
Topography	X-ray Analysis Photoluminescence (PL) SEM
Impurity Content	Spark Source (SSMS) OEM SIMS Fourier Transform Infra Red PL Photoconductivity (PC) Photo Hall (PH) Temperature-dependent Hall
Impurity Diffusion	SIMS Differential Hall PIX (Proton induced X-ray) PL RBS
Electrical Conversion	Differential Hall Temperature-dependent Hall Resistivity
Active Layer Characterization	PL Hall DLTS SIMS

Table 3. GaAs Substrate Material Characterization

- (1) Sample preparation and cleaning:
Wafers of $\frac{1}{2}$ " x $\frac{1}{2}$ " size are cut from selected substrates, cleaned with organic solvents and then etched in 3:1:1 $\text{H}_2\text{SO}_4:\text{H}_2\text{O}_2:\text{H}_2\text{O}$ for 1 min. to remove polishing damages.
- (2) Ion implantation:
 Se^+ ions are implanted into the samples at 120 keV to a dose of $5 \times 10^{12} \text{ cm}^{-2}$.
- (3) Annealing:
The wafers are capped with $\sim 1000 \text{ \AA}$ of Si_3N_4 and annealed in flowing H_2 at 900°C for 15 min. The encapsulation is then removed with HF.
- (4) Mesa etching:
The wafers are coated with AZ 1350J positive photoresist using a spinner. After the photoresist is dried in an oven at 95°C for 25 min., the wafers are loaded into a photomaskaligner and exposed UV light for 30 sec. through mask No. 1 (Fig. 1). The mesa patterns are developed in AZ developer solution (2 parts of DI water to 1 part of AZ developer) for $1\frac{1}{2}$ min. Then the wafers are postbaked at 140°C for 25 min. before they are etched in NaOH (0.5 M) + H_2O_2 (4%) for 3 min. The etched depth is about 2500 \AA . After a thorough rinse, the photoresist covering the mesas are removed using acetone.
- (5) Ohmic contact formation:
Drain and source patterns are defined on the wafers using photolithography and mask No. 2. Au-Ge-Ni is then evaporated onto the wafers. The photoresist is lifted off leaving drain and source covered with Au-Ge-Ni. A layer of $\sim 3000 \text{ \AA}$ of Si_3N_4 is RF sputtered onto the wafers which are then annealed at 425°C for 2 min. to alloy the Au-Ge-Ni, forming ohmic contact.
- (6) Gate formation:
Gate patterns are defined using photolithography and mask No. 3. The Si_3N_4 film in the gate, source and drain regions is plasma-etched away. Al is then evaporated onto the wafer. Again the



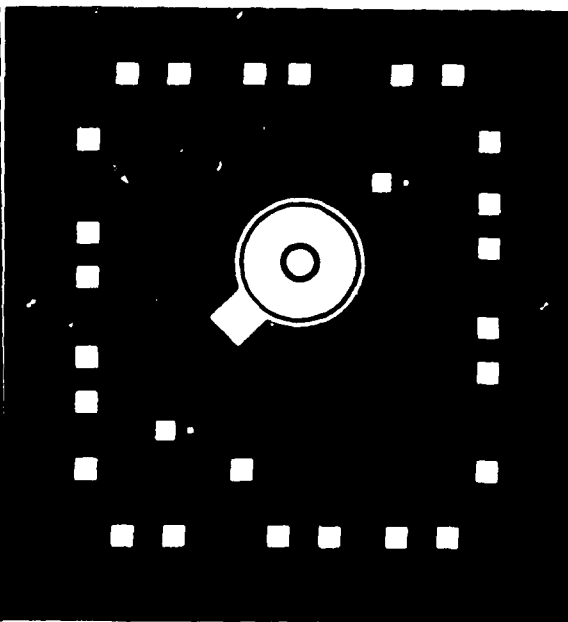
No. 1



No. 2

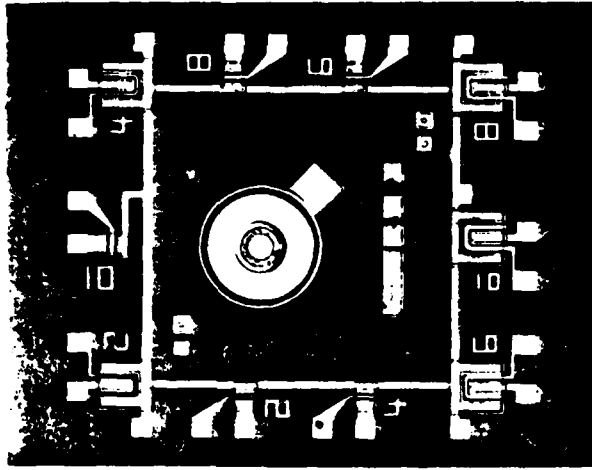


No. 3

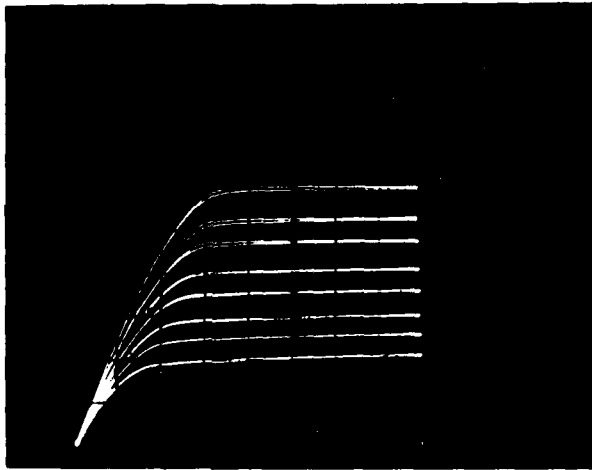


No. 4

Fig. 1. MESFET Masks



(a)



(b)

Fig. 2. (a) Photograph of a Finished MESFET Test Pattern

(b) Typical I_D vs. V_{DS} Characteristics

Vertical Scale 1 mA/div.
Horiz. Scale 1 V/div.
Step -.2 V

lift-off technique is used for the metalization.

(7) Contact pad formation:

Mask No. 4 and lift-off technique are used to put $\sim 5000 \text{ \AA}$ of Au for contact pads.

The MESFET fabrication process is largely completed. Dices can be cut and bonded to a header for testing. For simple I-V characteristics, no bonding is necessary, a micromanipulator is used instead. It is known that intermetallics sometimes form between Au-based and Al-based metalizations. They are avoided in commercial devices by using barrier metals. However, for our project, the above described simple process should be sufficient.

B. Test Procedures

I_D vs. V_{DS} characteristics for the devices are recorded using a curve tracer. The pinchoff voltage V_0 and the corresponding transconductance g_m are calculated. Then from the known quantities of the MESFET (built-in voltage V_b , gate length L , and gate width W) the effective values of mobility μ , channel height a and channel dopant concentration N can be determined using the methods outlined in ref. 5. These values will then be correlated with the substrate material data from other characterization techniques. The test results for the first 10 samples are shown in Table 4.

C. Discussions

The results in Table 4 show a wide spread of peak concentration, channel height and mobility for various substrates. Several substrates have very high activation efficiency, with peak carrier concentration near or over $1 \times 10^{18} \text{ cm}^{-3}$. Since the LSS theory only predicts a peak of $1 \times 10^{18} \text{ cm}^{-3}$ for Se implants at a dose of $5 \times 10^{12} \text{ cm}^{-2}$ and energy of 120 keV (Fig. 3) there is a possibility that more than $5 \times 10^{12} \text{ cm}^{-2}$ dose has been implanted. Because of the high carrier concentrations,

SAMPLE NO.	SUBSTRATE NO.	MOBILITY ($\text{cm}^2/\text{V-sec}$)	EFFECTIVE CH. HEIGHT a (micron)	EFFECTIVE CONC. N (/cu. cm)
1.	μw C42 T-9-15	520	0.1	8×10^{17}
2.	Cominco 30(117)	1200	0.14	4×10^{17}
3.	CS C-324-24	early breakdown		
4.	Cominco 30(9)	4400	0.2	2×10^{17}
5.	CS E199-30	800	0.09	1×10^{18}
6.	μw C40 T-8-19	2700	0.07	1.3×10^{18}
7.	CS 4890-4	early breakdown		
8.	MRC A64/M-1	870	0.09	1×10^{18}
9.	μw C32 T-26-65	1100	0.12	7×10^{17}
10.	μw C42 T-7-13	early breakdown		

Table 4. MESFET Characteristics for Cr-doped Semi-Insulating Substrates Implanted with 5×10^{12} cm^{-2} of Se at 120 keV.

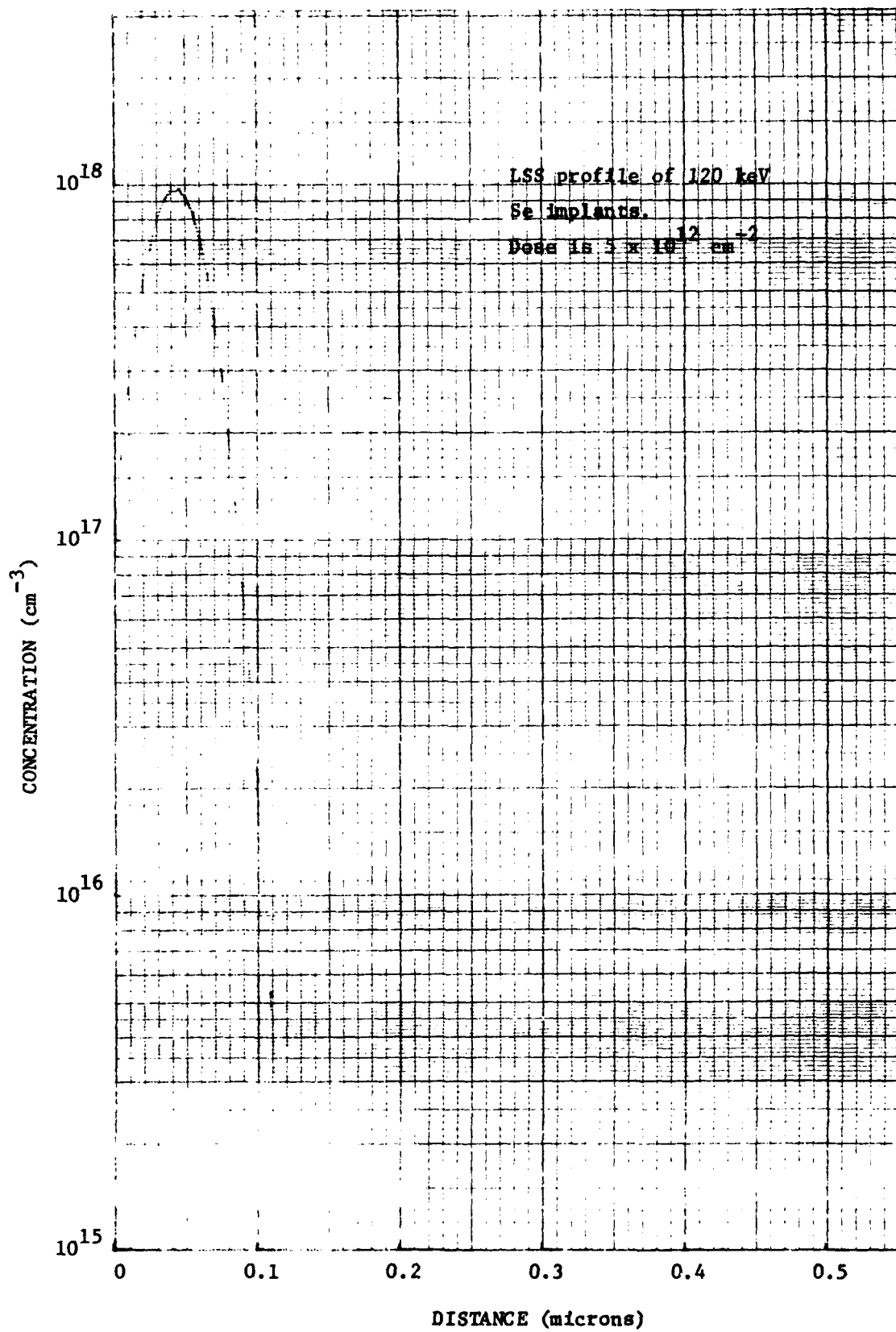


Fig. 3. LSS Profile for $5 \times 10^{12} \text{ cm}^{-2}$ Se Implants

the MESFETs made from these substrates all show early breakdown. Under these circumstances, it is no longer possible to accurately calculate the FET parameters.

VI. RECOMMENDATIONS II

In order to obtain more accurate results for the MESFET characterization, a lower dose of ion implantation must be used. However, it must not be too low as to cause difficulty in Hall measurement. A dose of $3 \times 10^{12} \text{ cm}^{-2}$ for Se implant at 120 keV will be a good choice. It is recommended that further experiments to be carried out with the substrates implanted to doses of $3 \times 10^{12} \text{ cm}^{-2}$ and device characterization be made and correlated to the material data obtained from other techniques.

REFERENCES

1. Y. K. Yeo, Y. S. Park, R. Kwor, "Correlation of Electrical with SIMS Atomic Profile of S Implants in GaAs," submitted to Appl. Phys. Letters. 1981.
2. J. S. William and H. B. Harrison, "Transient and Furnace Annealing of Ion Implanted Gallium Arsenide," in Laser and Electron-beam Solid Interaction and Materials Processing, Vol. 1, Ed. J. F. Gibbons et al. North-Holland, 1981.
3. R. Kwor, Y. K. Yeo, Y. S. Park, "Electrical Activation and Depth Profiles of S-implants in GaAs," in preparation to be submitted to J. of Appl. Phys. 1981.
4. D. Look, WPAFB Avionics Lab. private communication.
5. K. Lehovec, R. Zuleeg, "Voltage-Current Characteristics of GaAs J-FET's in the Hot Electron Range," Sol. State Electr. Vol. 13, pp. 1415-1426, 1970.

1981 USAF - SCEEE SUMMER FACULTY RESEARCH PROGRAM

Sponsored by the

AIR FORCE OFFICE OF SCIENTIFIC RESEARCH

Conducted by the

SOUTHEASTERN CENTER FOR ELECTRICAL ENGINEERING EDUCATION

FINAL REPORT

A REVIEW OF CURRENT DATA BASE SYSTEMS

FOR FLEXIBLE MANUFACTURING

Prepared by: Dr. C. Richard Liu
Academic Rank: Associate Professor
Department and University: School of Industrial Engineering
Purdue University
Research Location: Air Force Wright Aeronautical Laboratory
WPAFB, OH
USAF Research Colleague: Rosann M. Stach
Date: October 6, 1981
Contract No.: F49620-79-C-0038

A REVIEW OF CURRENT DATA BASE SYSTEMS FOR FLEXIBLE MANUFACTURING

by

Dr. Richard Liu

ABSTRACT

Three different data base models; namely, hierarchical, relational and network, are reviewed. Related data base schema designs are discussed.

ACKNOWLEDGEMENT

The author would like to express his deepest appreciation to Ms. Rosann Stach for her assistance and support through the SCEE summer program in which he has gained invaluable experience. He is also very grateful for the friendship offered by his colleagues at the Materials Laboratory, AFWAL.

Introduction

1. As the role of computer in modern industry becomes more and more important, the evolution of information handling has progressed from file management to data base management. Unfortunately, a principal impediment to the more widespread use of data base management has been the absence of understanding of what a data base system is, in the technical sense.
2. In this report, an overall review of the study of data base system is presented. Generally, "data base" simply refers to a collection of data. The difference between a primitive file and a sophisticated data base is that a "file" consists of many records of some given record types, while a "data base" consists of many records of many different record types. Such that a file management information system may use many separate files. And a "data base" management system needs only a single organized structure in which all important records are interrelated and maintained. The data processing is done rather by finding desired records in the data base, than by tediously merging of separate file. A data base system is a software package. By itself, this software is not an information system, but it can be used to build an information system for some application (e.g., interactive manufacturing data base, order processing, inventory management, payroll, etc). A data base system is generally in the sense that it is not oriented toward any specific application. It provides facilities for defining the logical structure to which records will be organized in a data base. It also provides the activities of record creation, insertion deletion, modification, data extraction, and finding records. All of these activities

were known as the manipulation of data records.

Data base system can be classified on the basis of the logical structuring facilities that they provide for building information system. These include three data models such as 1) hierarchical 2) relational 3) network structures. In the following section, each of these models will be discussed using a representative system.

The Three Data Models

The hierarchical, relational, and network data models employ different terminologies for defining the logical structure of a data base. The presentation was based on the definitions given by CODASYL DATA BASE TASK GROUP REPORT of 1971 [4]. An example is shown in Figure 1. The correspondence among the three terminologies are illustrated in Figure 1a. The distinctions among the three kinds of logical structures are evident from examining the example logical structures of Figures 1b-d. A rectangle represents a record type (segment types, relation scheme). A directed arc represents a set (parent-child relationship) parting from the owner record type (parent segment type) to the member record type (child segment type).

Each of these three approaches gives a different way for organizing one's viewing or modeling the real world: as a network, as a tree(s), or as a collection of tables. These differences result in different data manipulation facilities. The hierarchical and network models represent relationships among record types and data manipulation is accomplished in terms of those relationships, with the relational model there are only tables. Data manipulation is therefore accomplished in terms of

combining tables on the basis of common attributes and extracting data from tables. In the following section, the representative data base systems for each of the three data models, namely, IMS for the hierarchical model, system R for the relational model, and MDBS for the network model, are presented. Certain distinctive features are emphasized.

IMS

1. Overview

IMS (IBM's Information Management System) is based on the hierarchical data model [15]. There are two kinds of data base: physical and logical data base. In IMS, one can have physical data base without logical data base, but not vice versa. The major difference between them is that for a physical data base one of several special storage techniques must be selected, while the logical data base does not require. Also the physical data base consists of only the physical parent-child relationship, but the logical data base can contain both the physical and logical relationships.

It is illustrated in Figure 2 to manifest the physical and logical relationships of the two different data bases. The logical relationship is usually established between physical data bases. This function allows IMS to support forms of networking and leads to a reduction in redundancy.

2. Physical Storage Organizations

In IMS, a user is required to specify a physical storage organization for each physical data base. Four types of storage organizations are allowed: HSAM, HISAM, HDAM, and HIDAM. Each denotes a different method for mapping segments to storage and accessing a "data base record." An IMS data record consists of a root segment and all of its descendant segments. Figure 3b shows two data base records for the hierarchy chart of Figure 3a. The storage organizations are described briefly in Figures 4, 5, and 6. In general, there are four types:

- A) HSAM - the hierarchical sequential access method: The segments of a data base record are related by physical adjacency and the data base records are sequentially organized.
- B) HISAM - the hierarchical indexed sequential access method: The data base record are stored sequentially in a primary storage area and the extra segments are allocated in an overflow area. A pointer is used to link the records in two areas.
- C) HDAM - the hierarchical direct access method: The segments within a data base record are linked by pointers with two options: hierarchical chaining or physical child/physical twin chaining. The records are accessed on the basis of a key value in its root segment.
- D) HIDAM - the hierarchical indexed direct access method: An index is used to accomplish direct accessing of data base records

3. Formal Specification of a Data Base

The critical data base design issues for IMS users involve the following decisions: 1) the constitution of the hierarchy charts for data bases, 2) the usage of logical relationships, 3) the choice of the physical storage organizations, and 4) the fields of the sequencing keys for each segment type. The major kinds of statements used in IMS Data Base Description Language are 1) DBD, 2) DATASET, 3) SEGM, 4) FIELD, 5) LCHILD, and 6) DBDGEN, FINISH, END. Such that a data base can be defined by these statements.

Once data base hierarchies have been defined, subhierarchies must be formally defined. Each subhierarchy is called a PCB (Program Communication Block). In IMS, a PSB (Program Specification Block - which is a named

collection of PCBs) is used to allocate and manage a buffer area between the data bases and to execute an application program. The PSB is defined in terms of several statements: 1) PCB, 2) SENS GG, 3) PSB GEN, and 4) END.

4. Data Manipulation Language

The data manipulation language of IMS is called Data Language/1 CDL/1, which can be based on existing PL/1, COBOL or assembler host languages. DL/1 commands are executed with respect to a particular PCB hierarchy existing in the program's PSB. Arguments for a DL/1 can include an argument count, the name of a DL/1 command, the name of the PCB, the name of an I/O area, and Segment Search Arguments (SSAs). Several basic DL/1 commands are listed such as 1) GET UNIQUE(GU), 2) GET NEXT (GN), 3) GET NEXT WITHIN PARENT (GNP), 4) GET HOLD (GHU, GHN, GHNP), 5) INSERT (ISRT), and 6) DELETE (DLET) and REPLACE (REPL).

SYSTEM R

1. The Relational Data Model

The relational data model was proposed by Codd in 1970 [9]. A relational data base can be expressed by a group of two-dimensional tables called relations. The columns are known as the attributes (fields) that constitute the relation's schema. The row is known as tuple consists of data values for the attributes. Each tuple has an unique identification key value.

Codd proposed two languages for manipulating the data within the tables: relational algebra and relational calculus. In general, the relational algebra combines several tables into a derivative table (file). The relational calculus is used to define a relation derived from existing relations.

2. Overview of System R

System R supports a relational data base view and provides a calculus oriented language (SEQUEL) for data manipulation. The system has two components: the Relational Data System (RDS) and the Relational Storage System (RSS). RDS compiles SEQUEL statements and generates the answer for the requests. It also maintains a catalog of external names and provides security. RSS performs simple, record-at-a-time operations and provides data recovery, transaction management and data definition facilities. The system structure is shown in Figure 7. Also an example for System R is given as Figure 8 by showing the schemas of three relational tables.

3. Table Definition

A relation is defined or dropped from a relational schema through the SEQUEL commands CREATE TABLE or DROP TABLE, respectively. Two kinds of accessing methods can be specified with CREATE or DROP commands: index and link. Indexing allows a tuple to be either directly or sequentially accessed based on the attributes of the relation. The link access provides access path links from tuples of different relations.

4. Data Manipulation

As mentioned in previous section, SEQUEL is used in System R for data manipulation, which can be used as a stand-alone or together with PL/1 or COBOL programs. The basic structure of a SEQUEL statement involves: SELECT, FROM, and WHERE clauses. In a PL/1 or COBOL program, these statements must be prefixed with a \$ sign and a LET/OPEN command. The main features of SEQUEL are demonstrated by the examples given in Figure 9.

MDBS

1. Overview

The Micro Data Base System (MDBS) [16] is specially available on microcomputers. Not only for network model, MDBS supports logical structuring features that are unavailable in other data base system. The basic functions of MDBS are illustrated in Figure 10. They are used to support different types of schemas such as 1) Network, 2) N=M Set, 3) Artificial Record Type, 4) Two Member Record Types, 5) Recursive Set, and 6) System.

2. Data Description Language

The MDBS data description language is used to specify the data item types, record types and set types in an MDBS logical structure. The general statements include: 1) RECORD, 2) ITEM, 3) SET, and 4) OWNER, MEMBER. There exist some set orders to access the data record: 1) FIFO, 2) LIFO, 3) SORTED, and 4) IMMAT. Besides the above statements, every schema must contain a special record type called SYSTEM. The MDBS DDL specification for the supplier-part schema of Figure 10f is shown in Figure 11.

3. Data Manipulation

The MDBS data manipulation language (DML) provides the user to manipulate the data base even defined with the DDL. The DML routines can be called from BASIC, FORTRAN, COBOL, PL/1, PASCAL and machine language host programs. The generic form of a DML call is shown as

EO = CALL (A, "routine name,arguments", host language variables)

where A = A DMS entry point address
 Routine name = Name of DML routine
 Arguments = The list of arguments
 EO = A variable in the application program.

In network systems, data manipulation is based on currency indicators include:

- 1) The current record occurrence (CRO) of a record type.
- 2) The current owner (CO) of a set or N=M set.
- 3) The current number (CM) of a set or N=M set.
- 4) The current of the run unit (CRU)

Several of the most commonly used MDDBS DML commands are listed as follows: LO DEFINE, 2) CRS, 3) AMS, 4) FMSK, 5) FFM, 6) FNM, 7) GETM, 8) FGO, 9) SOM, and 10) SMM. All of these and other commands are detailed in the MDDBS User's Manual [16]. A sample example is given in Figure 12 showing the conjunction of the DML commands.

Query Interface

As it required, the user of DML must be a programmer. However, MDDBS provides a query language for nonprogrammers. An MDDBS query has the following generic format:

<COMMAND><FIND CLAUSE><CONDITIONAL CLAUSE><PATH CLAUSE>

The features of the MDDBS query system are detailed in [17].

Dynamic Restructuring of a Schema

The Dynamic Restructuring System (DRS) [18] allows any MDDBS schema to be altered after data has already been located. There are many kinds

of schema alternations performed by DRS: 1) ADI (Add Data Item), 2) ART (Add Record Type), 3) AST (Add Set Type), 4) DDI (Delete Data Item), 5) DRT, and 6) DST. By using DRS, it speeds the accessing of data manipulation.

DATA BASE SCHEMA DESIGN

1. Overview

Regardless of which kind of data base system is used, the schema is designed to establish a user's view of world and used as the basis for data manipulation. Prior to designing the data base schema, the designer must preserve real world data relationships, through whatever mechanisms are available in the data model being used. Four relationships are concerned -- many-to-many, many-to-one, one-to-many, and one-to-one. After the relationship preservation, structural anomalies are considered for the consistency and redundancy problems that may arise from certain schema designs. These are some sample anomaly problems as follows: 1) Redundancy anomalies, 2) Update anomalies, 3) Insertion anomalies, and 4) Deletion anomalies. Usually, anomalies can be completely eliminated in a network model. On the contrary, in the relational model, anomalies are happed in record types. Therefore, there are two approaches for designing the data base schema for these two models.

2. An Approach to Relational Schema Design

In the relational model, data base design is based on the notion of normal forms. The procedure used to derive normal forms is called normalization.

3. An Approach to Network Schema Design

There is a useful procedure for designing a network schema, which is summarized in Figure 13. This design strategy has been adopted from [13]. To use this procedure, the user must have the concepts of relationship preservation and structural anomalies mentioned previously.

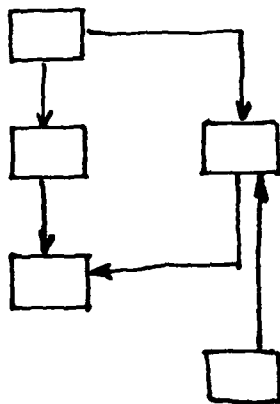
CONCLUSIONS

Several conclusions have been made from the previous short description of the data base management system includes three data models.

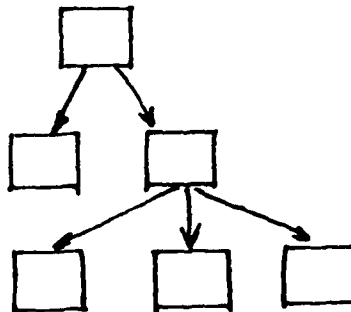
1. There can be substantial differences among the data base management systems even based on the same data model. Among three data models, hierarchical systems are known to have the most differences. Based on CODASYL DBTG, network systems have the least differences.
2. The choice of a data base system is influenced by the modeler's view of the world. Also the model can be chosen by its performance.
3. It is expected to merge these various data models to be a general data base system.
4. The automation of schema design is another important development in the future of data base management systems.
5. Although file management is still widely used, data base management systems will become more available for the people. It is hoped that this DBMS will interface with a decision support systems and turn eventually to respond to nonprogramming user's requests.

Network (MDS)	Hierarchical (IMS)	Tabular/Relationship (System R)
data item type	field	attribute
item occurrence	field value	attribute value
record type	segment type	relation schema
record occurrence (record)	segment	tuple
set type (set)	parent-child relationship	--
set occurrence	--	--

a. Terminological Correspondences



b. Example Network

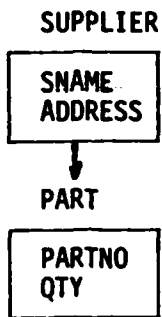


c. Example Hierarchy

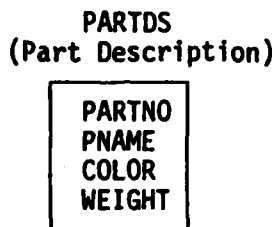


d. Example of Relations

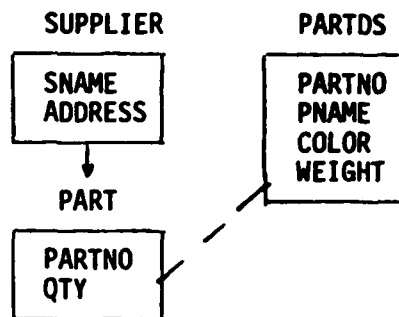
Figure 1



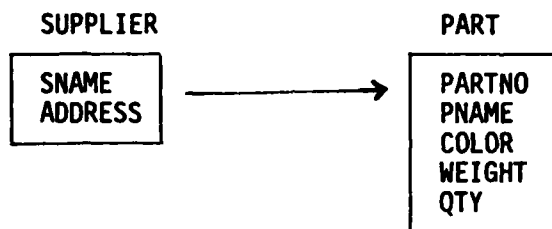
a. The SUPPDB Data Base



b. The PARTDSDB Data Base



c. Logical Relationship between two segment types



d. User View Based on Logical Relationship

Figure 2

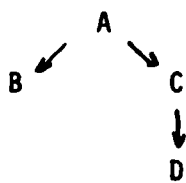


Figure 3a

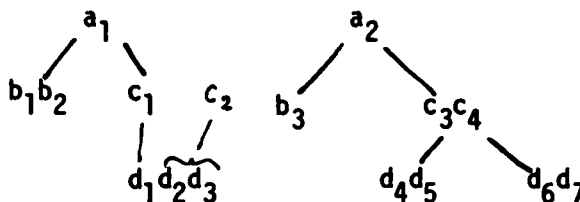


Figure 3b

a₁b₁b₂c₁d₁c₂d₂d₃a₂b₃c₃d₄d₅c₄d₆d₇ ...

Figure 4

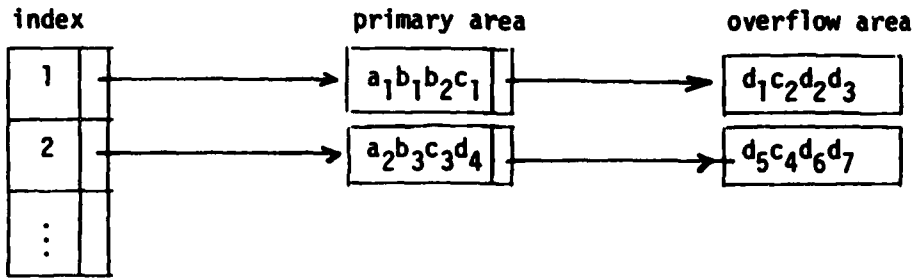
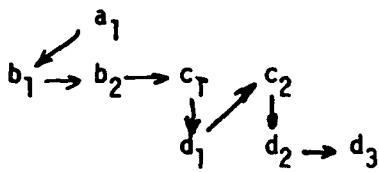
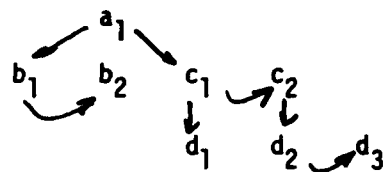


Figure 5



a. Hierarchical Chaining



b. Physical Child/Physical Twin Chaining

Figure 6

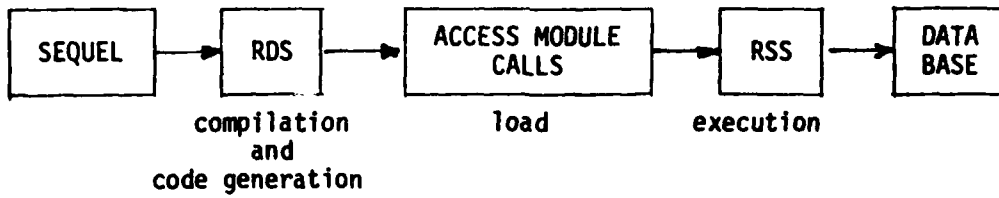


Figure 7

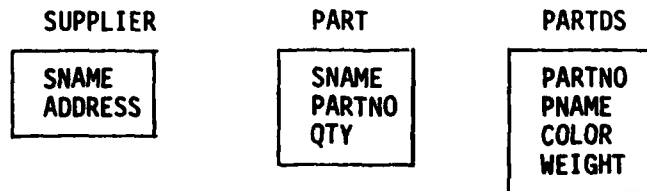


Figure 8

PART		
SNAME	PARTNO	QTY
SA	#101	200
SB	#102	300
SC	#103	500

PARTDS (PART DESCRIPTION)			
PARTNO	PNAME	WEIGHT	COLOR
#101	NUT	10	WHITE
#102	BOLT	20	RED
#103	WASHER	15	BLUE

Figure 9a

2. Print the suppliers that supply at least one white part.

```

SELECT [UNIQUE] SNAME
FROM      PART
WHERE     PART IN
          (
            SELECT PARTNO
            FROM    PARTDS
            WHERE   COLOR = 'WHITE'
          )
          or
SELECT UNIQUE SNAME
FROM    PART, PARTDS
WHERE   PART.PARTNO = PARTDS.PARTNO
        AND COLOR = 'WHITE'

```

'UNIQUE' is used to eliminate duplicate supplier names.

Figure 9b

5. Insert a new supplier in the PART relation, then delete all tuples in PART for the 'SA' supplier.

```
INSERT INTO PART (SNAME, PARTNO)
<SD, # 104>;
DELETE PART
WHERE SNAME = 'SA';
```

Figure 9c

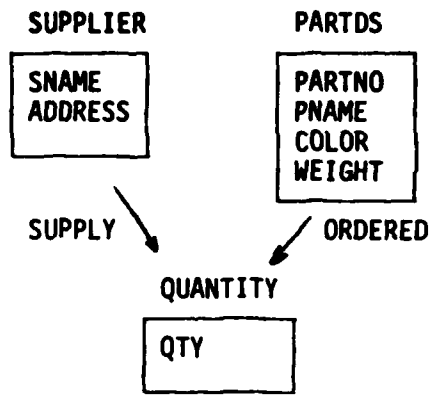
6. Update the weight of part '101' in PARTDS.

```
UPDATE PARTDS
SET WEIGHT = 50
WHERE PART = '101'.
```

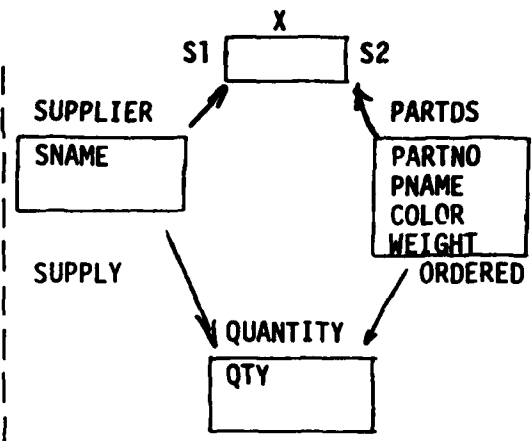
Figure 9d

```
$ LET S BE
SELECT SNAME
INTO $X
FROM SUPPLIER
WHERE PARTNO = $Y
$ OPEN S;
$ FETCH S;
$ CLOSE S;
```

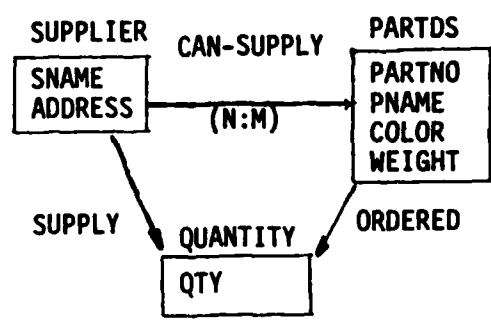
Figure 9e



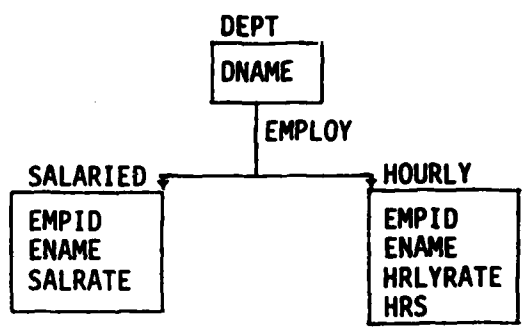
a. Supplier-Part Network Schema



b. Representing a Many-to-Many Relationship with an Artificial Record Type



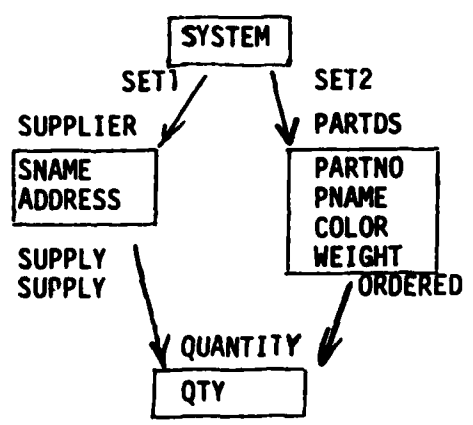
c. Representing a Many-to-Many Relationship with an N:M Set



d. A Set with Two Member Record Types



e. Recursive Use of a Set



f. Schema with SYSTEM

Figure 10

RECORD	SUPPLIER					
ITEM	SNAME	CHAR	20			
ITEM	ADDRESS	CHAR	30			
RECORDS	PARTDS					
ITEM	PARTNO	INT				
ITEM	PNAME	CHAR	20			
ITEM	COLOR	CHAR	10			
ITEM	WEIGHT	REAL				
RECORD	QUANTITY					
ITEM	QUANTITY	REAL				
SET	SET1	AUTO		1:N		
					SORTED	SNAME
OWNER	SYSTEM					
MEMBER	SUPPLIER					
SET	SET2	AUTO		1:N		
					SORTED	PARTNO
OWNER	SYSTEM					
MEMBER	PARTDS					
SET	SUPPLY	MAN		1:N		
					FIFO	
OWNER	SUPPLIER					
MEMBER	QUANTITY					
SET	ORDERED	MAN		1:N		
					IMMAT	
OWNER	PARTDS					
MEMBER	QUANTITY					
END						

Figure 11

```
EO = CALL (A1, "DEFINE, SUP", A2, A3)
EO = CALL (A1, "DEFINE, QTY", N)
EO = CALL (A1, "DEFINE, NAME", A4)
NAME = 'LEHR'
```

```
EO = CALL (A0, "FMSK, SET1, NAME")
EO = CALL (A0, "GETM, SET1, SUP")
```

```
PRINT A2, A3
```

```
EO = CALL (A0, "SOM, SUPPLY, SET1")
10 EO = CALL (A0, "GETM, SUPPLY, QTY")
EO = CALL (A0, "SMM, ORDERED, SUPPLY")
EO = CALL (A0, "GFO, PNAME, ORDERED, NAME")
```

```
PRINT A4, N
```

```
EO = CALL (A0, "FNM, SUPPLY")
```

```
IF EO.EQ.0 GO TO 10
```

(*A9, A1, A2, A3, A4, N,
EO are program variables*)

Figure 12

The 7-Step Procedure for Network Schema Design:

Step 1: List all data item types.

List data item types.

Step 2: If there is a 1-to- relationship between two data item types, then aggregate them into the same record type.

Find all 1-1 relationships and aggregate accordingly.

Step 3: For each data item that has not been put into a record type, declare a new record type to contain it alone.

Create record type for any unaggregated data item type.

Step 4: If a 1-to-N relationship exists between two record types draw in the appropriate set.

For each 1-to-N relationship create a set.

Step 5: Remove the sets of any transitive 1-to-N relationship (i.e., change

Remove transivities.

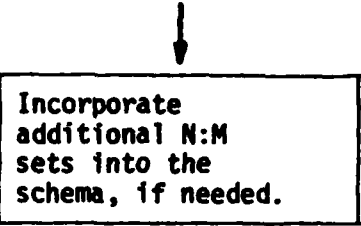


Step 6: For each unattached record type (i.e., not yet participating in a set) find the attached record type that, conceptually, seems to be the most closely related to it. Create an N:M set between these record types, arbitrarily calling one the owner and the other the member

Create any needed N:M sets to integrate unattached record types into the network schema.

Figure 13

Step 7. For each record type, ask the question: does the concept represented by this record type have a N:M relationship to any other record type, a relationship that you want to have incorporated into the schema. If it does and if that relationship is not already represented in the schema, then add an N:M set to represent this relationship. Begin by considering those record types that are not owners of sets; then recursively consider those record types that own already-considered record types.



Incorporate additional N:M sets into the schema, if needed.

Figure 13 (continued)

References

- [1] CODASYL Systems Committee. Data Base Task Group Report, ACM, April, 1971
- [2] IBM, IMS/VS publications, GH20-1260 (General Information), SH20-9025 (System/Application Design Guide), SH20-9026 (Application Programming Reference Manual) and SH20-9027 (Systems Programming Reference Manual), IBM, White Plains, NY, 1978.
- [3] Codd, E. F., "A Relational Model for Large Shared Data Banks," Comm. ACM 13: 6, pp. 377-387, June 1970.
- [4] MDBS, "User's Manual MDBS.DMS, MDBS.DDL", Micro Data Base System, Inc., Lafayette, IN, 1979.
- [5] MDBS, "MDBS, QRS Query System/Report Writer," Micro Data Base System, Inc., Lafayette, IN, 1980.
- [6] MDBS, "MDBS.DRS User's Guide," Micro Data Base System, Inc., Lafayette, IN, 1980.
- [7] Holsapple, C. W., "Data Description and Manipulation Languages for Microcomputer Data Bases," Computer Age, December, 1980.